MATERIALS CENTRAL TECHNICAL LIBRARY
OFFICIAL FILE COPY

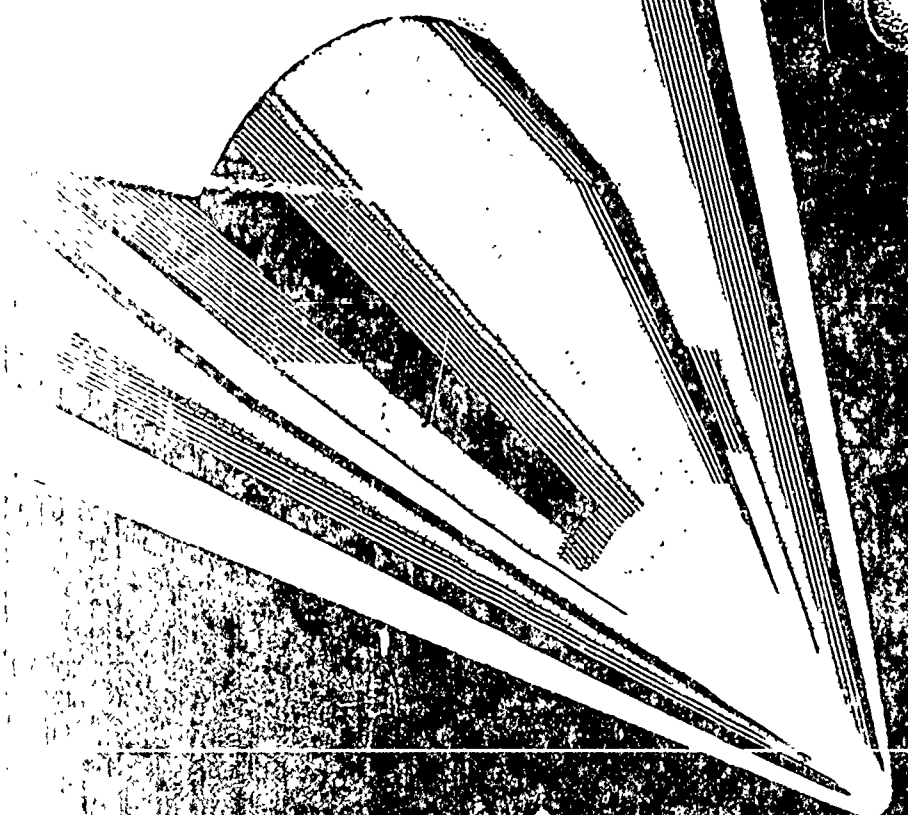
N

ASD Technical Report 61-645

AD-271529

PROCEEDINGS OF SYMPOSIUM ON AEROTHERMOELASTICITY

AD-271529



30, 31 October 1961
and
1 November 1961

AERONAUTICAL SYSTEMS DIVISION

AFSC

ASD TECHNICAL REPORT 61-645

PROCEEDINGS OF SYMPOSIUM ON AEROTHERMOELASTICITY

30-31 October and
1 November 1961

AERONAUTICAL SYSTEMS DIVISION
AIR FORCE SYSTEMS COMMAND
UNITED STATES AIR FORCE
WRIGHT-PATTERSON AIR FORCE BASE, OHIO

800 - February 1962 - 21-889

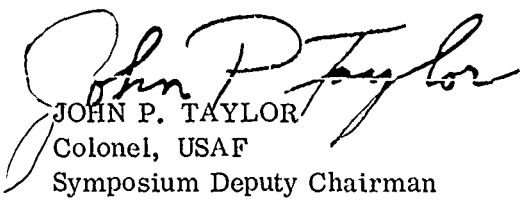
PREFACE

The first USAF Symposium on Aerothermoelasticity, sponsored by the Air Force Systems Command, was held under the auspices of the Aeronautical Systems Division in Dayton, Ohio, 30-31 October and 1 November 1961. The purposes of the symposium were to: (a) stimulate thinking and technical discussion by presenting challenging new aerothermoelastic problems expected in the design of future aerospace vehicles; (b) provide a platform for presenting bold, new research objectives essential to advancing the aerothermoelastic state-of-the-art rapidly and effectively; and (c) distribute symposium proceedings delineating these research goals and problem areas for more effective utilization of total technical resources at all levels. The program was designed to aid those individuals and groups who work daily with the problems of kinetic heating, thermodynamics, thermoelasticity, steady and unsteady aerodynamics, and control system dynamics involved in advanced flight vehicle design and development.

The proceedings are set forth in this report in the same order as presented during the symposium. The technical papers are grouped by subject into basic sessions: Aerothermoelasticity, Flight Control, Aerothermodynamics, and Structures. The name of the speaker and his affiliation are given at the beginning of each paper.

Every effort has been made to keep the errors and omissions of this report to a minimum and still publish the vital technical information for timely distribution to the symposium attendees. If serious errors or omissions are noted, they should be brought to the attention of Mr. W. J. Mykytow, ASRMDD, Aeronatucal Systems Division, Wright-Patterson Air Force Base, Ohio. Necessary errata sheets will be prepared and distributed.

The timely publication of this report is primarily due to the fine contributions of the speakers, session chairmen, and authors of technical papers. The Symposium Technical Committees gratefully acknowledge these contributions and express their appreciation.



JOHN P. TAYLOR
Colonel, USAF
Symposium Deputy Chairman

NOTICES

When Government drawings, specifications, or other data are used for any purpose other than in connection with a definitely related Government procurement operation, the United States Government thereby incurs no responsibility nor any obligation whatsoever; and the fact that the Government may have formulated, furnished, or in any way supplied the said drawings, specifications, or other data, is not to be regarded by implication or otherwise as in any manner licensing the holder or any other person or corporation, or conveying any rights or permission to manufacture, use, or sell any patented invention that may in any way be related thereto.

Qualified requesters may obtain copies of this report from the Armed Services Technical Information Agency, (ASTIA), Arlington Hall Station, Arlington 12, Virginia.

This report has been released to the Office of Technical Services, U. S. Department of Commerce, Washington 25, D. C., for sale to the general public.

Copies of ASD Technical Reports and Technical Notes should not be returned to the Aeronautical Systems Division unless return is required by security considerations, contractual obligations, or notice on a specific document.

ABSTRACT

The Proceedings of the Aeronautical Systems Division Symposium on Aerothermoelasticity are presented in this report.

The potential impact of aerodynamic heating resulting from high-speed flight on flight vehicle design has been recognized for some time. Many agencies have been conducting research to determine the effects of aerodynamic heating on the various separate disciplines comprising the engineering and scientific aspects of modern and future flight vehicle design. A more integrated approach has been considered in the field of aerothermoelasticity - - the area that includes thermodynamics, aerodynamics, structures, stability and control, and dynamics. A symposium on Aerothermoelasticity was held to present the latest significant developments in each scientific area and engineering area that comprise the component parts of this technology. To help the symposium attendee evolve an integrated position of the entire state-of-the-art, new and significant contributions were presented in four technical areas consisting of dynamic aerothermoelasticity (flutter), stability and control, thermodynamics and aerodynamics (or aerothermodynamics), and structures including material and construction concepts. Categories important and significant to each technical area are discussed state-of-the-art wise. In addition, separate papers are given on items of special importance.

PUBLICATION REVIEW

The publication of this report does not constitute approval by the Air Force of the findings or conclusions contained herein. It is published only for the exchange and stimulation of ideas.



DAVID M. JONES
Brigadier General, USAF
Symposium Chairman

TABLE OF CONTENTS

	PAGE
INTRODUCTION	1
OPENING REMARKS AND WELCOME ADDRESS - Brigadier General David M. Jones	5
KEYNOTE ADDRESS - Major General Don R. Ostrander	8
SESSION I	
DYNAMIC AEROTHERMOELASTICITY	11
Chairman: Dr. R. L. Bisplinghoff, Massachusetts Institute of Technology	
PROBLEMS AND DEVELOPMENTS IN AEROTHERMOELASTICITY - I. E. Garrick and Herbert J. Cunningham	12
PROGRESS IN AEROTHERMOELASTICITY OUTSIDE THE UNITED STATES - Dr. Peter A. Castruccio and Milton Rogers	61
FUTURE DYNAMIC AEROTHERMOELASTIC CONSIDERATIONS FROM A VEHICLE REQUIREMENTS VIEWPOINT - 1/Lt Thor M. Snaring and 1/Lt Donald J. Ketter	91
POTENTIAL AEROTHERMOELASTIC PROBLEMS ASSOCIATED WITH ADVANCED VEHICLE DESIGN - Dr. W. R. Laidlaw and John H. Wykes	120
THEORETICAL HYPERVELOCITY UNSTEADY AERODYNAMICS - Dr. Holt Ashley and Garabed Zartarian	161
PREDICTION OF STIFFNESS AND VIBRATION CHARACTERISTICS OF TRUSSES, MULTI-STAGE CYLINDERS, AND CLUSTERED CYLINDERS - Dr. Francis C. S. Hung and Donald J. Stone	219
A CONSIDERATION OF THE SIMILARITY REQUIREMENTS FOR AERO-THERMOELASTIC TESTS ON REDUCED SCALE MODELS - W. G. Molyneux	290
SESSION II	
FLIGHT CONTROL	341
Chairman: Professor Bernard Etkin, University of Toronto	
FLIGHT CONTROL OF AEROTHERMOELASTICALLY AFFECTED VEHICLES - M. B. Zisfein	342

PAGE

THE AERODYNAMICS OF DISTORTED SURFACES - Dr. Eugene E. Covert 369

NONLINEAR HYPERSONIC THERMOELASTIC STABILITY AND CONTROL DERIVATIVES - Vincent Donato, James R. Batt, and Joseph Padlog 407

FLIGHT CONTROL OF HYPERSONIC VEHICLES WITH A TEMPERATURE SENSING LOOP - Daniel Dommasch 468

FUTURE CONTROL SYSTEMS FOR VEHICLES WITH LARGE AEROTHERMO-ELASTIC EFFECTS - P. C. Gregory and H. M. Davis 498

SESSION III

AEROTHERMODYNAMICS 529

Chairman: Dr. Alfred J. Eggers, Jr.
Ames Research Center, NASA

HEATING PROBLEMS OF ENTRY INTO PLANETARY ATMOSPHERES FROM SUPERCIRCULAR ORBITING VELOCITIES - Dr. Sinclaire M. Scala 530

HEAT TRANSFER DUE TO THE INTERACTION BETWEEN A SWEPT PLANAR SHOCK WAVE AND A LAMINAR BOUNDARY LAYER
- Anthony Martellucci and Dr. Paul A. Libby 593

DETERMINATION OF HYPERSONIC AERODYNAMIC LOADS AND DERIVATIVES ON RE-ENTRY GLIDE VEHICLES - Frank S. Malvestuto, Jr. 641

A CRITICAL REVIEW OF PREDICTION TECHNIQUES APPLICABLE TO RE-ENTRY VEHICLES - Richard D. Neumann and 2/Lt Edward T. Meleason 678

TURBULENT BOUNDARY LAYERS ON HIGHLY COOLED SURFACES AT HIGH MACH NUMBERS - Andrew F. Burke 704

THE VISCOUS BLUNT-BODY PROBLEM - H. Hoshizaki 742

SESSION IV

STRUCTURES 775

Chairman: Mr. Martin Goland
Southwest Research Institute

A SURVEY OF STRUCTURAL DESIGN PROBLEMS IN A COMBINED THERMAL AND LOAD ENVIRONMENT
- Dr. Robert S. Levy, Harold Switzky, Dr. Marvin Forray, Malcolm Newman, and Claus J. Meissner 776

PAGE

MATERIALS AND CONSTRUCTION CONCEPTS FOR STRUCTURES SUBJECTED TO SEVERE KINETIC HEATING
- Charles J. Cosenza, Robert D. Guyton, and M/Sgt Jesse C. Ingram, Jr. 847

MATRIX STRUCTURAL ANALYSIS OF HEATED AIRFRAMES
- Richard H. Gallagher 879

TRANSIENT STRUCTURAL PERFORMANCE UNDER AN INTERMITTENT LOAD-TEMPERATURE-TIME ENVIRONMENT - Dr. Pao C. Huang 918

METHODS AND ANALYSIS OF HEAT TRANSFER - Peter E. Grafton 962

WING LEADING EDGE OPTIMIZATION FOR GLIDE RE-ENTRY VEHICLES - Wilbur L. Hankey and Captain Richard E. Russell 994

CLOSING REMARKS - Colonel A. L. Wallace, Jr. 1014

SYMPOSIUM COMMITTEE ORGANIZATION

Symposia Director for ASD: Dr. John E. Keto	ASGS
Symposium Chairman: Brigadier General David M. Jones	ASGV
Symposium Deputy Chairman: Colonel John P. Taylor	ASRM

Technical Committee:

W. J. Mykytow, Chairman	ASRMDD
H. M. Davis, Co-chairman	ASRMCM
A. C. Draper	ASRMDF
P. A. Parmley	ASRMDS
1/Lt R. L. Swaim	ASRMCM
1/Lt T. M. Snaring	ASRMDD
G. E. Maddux	ASRMDS
R. D. Neumann	ASRMDF
Colonel W. C. Nielson, Advisor	ASRMD
Lt Colonel George M. Manning, Advisor	ASRMC
H. A. Magrath, Advisor	ASRMD
C. R. Bryan, Jr., Advisor	ASRMC

AFSC Coordinator: Major W. R. Hipple	SCTA

Arrangements Committee:

A. J. Cannon, Executive Manager	ASOOS
W. E. Stitz, Co-manager	ASRMDD
I. L. Schwartz, Protocol	ASGDP
R. Maltby, Publicity	ASEP
C. High, Press Relations	ASNVPI
Mrs. Gladys Luse, Technical Publications	ASAPTS
C. E. Sondergelt, Printing	ASAPP
Mrs. Sallie Dykman, Recorder	EWJ
H. C. Hoffman, Visual Communications	ASAV
S/Sgt C. R. Knifley, Chief Projectionist	ASGDM
R. Hendricks, Transportation	ASTST
Captain R. I. Erb, Senior Escort Officer	ASRMDF

INTRODUCTION

The technical field of aerothermoelasticity results from the combination of three component sciences: aerodynamics, thermodynamics, and dynamics. In considering deformable structures, one tends to break dynamics down into two characteristics, inertia and elasticity. Hence, aerothermoelasticity is generally discussed as being made up of four parts: aerodynamic, thermodynamic, elastic, and inertia effects. The symposium symbol of four line-connected spheres suggests the four parts of aerothermoelasticity and their interactions. In some cases, the interaction or coupling between parts is strong and in other cases it is weak. Aerospace phenomena which fall under the jurisdiction of aero-thermo-elasticity include, as Mr. Garrick will point out in his paper, mechanical vibration, stability, aerothermodynamics, thermoelasticity, vibration and heat, aeroelasticity, stability and heat, static aeroelasticity, and dynamic aeroelasticity.

Perhaps the major effect of the thermodynamic aspects of high-speed flight on dynamic aeroelasticity is the reduction in stiffness due to increased temperature and thermal stresses caused by thermal gradients. An important part of future efforts, therefore, will be to accurately compute the thermoelastic properties of advanced structures. Methods for accurate prediction of the heat flux input must be available, particularly for positions away from the stagnation point. The unsteady aerodynamic theories must provide data for new types of configurations having much lower aspect ratios and higher leading sweep angles. Methods must realistically account for blunt leading edges, strong shocks, high angles of attack, wing-body interference, body aerodynamics, etc.

The first session of the symposium concerns dynamic aerothermoelasticity or flutter. There are two main purposes to this session. One is to discuss the state-of-the-art in various areas, and the other is to estimate potential problem areas. The first paper does both by delineating problem areas significant to various missions and by indicating the current design and analysis background. The second paper makes an attempt to estimate the state of the aerothermoelastic art outside the United States so as to provide a relative estimation of position. Potential problem areas are then suggested based on estimated vehicle requirements and needed research areas are indicated. A review and an evaluation are also made from the aerospace vehicle designers viewpoint. Particular and important parts of the art are then discussed in the last three papers. The review of the status of unsteady aerodynamics concerns the hypervelocity range. Since new forms of structural configurations have emerged for aerospace vehicles, the status of thermo-elastic analysis procedures for trusses, multi-stage cylinders, and clustered cylinders or boosters is evaluated. The session concludes with a treatise on similarity requirements for reduced-scale, aerothermoelastic models.

Manuscript released on 15 November 1961 for publication as an ASD Technical Report.

Aerothermoelasticity affects flight control system design and analysis in a number of complicating ways. The dynamic characteristics of the controlled element (vehicle) along with the controlling element gain can be drastically altered. Frequently, the control data signal-to-noise ratio becomes critical. In the face of degraded information, declining control power, and adverse shifts in system dynamic characteristics, the control system designer frequently will have cause to change the airframe' s structural design criteria.

We can usually build control systems for stable aerothermoelastic systems. In a limited number of cases, mild instabilities can be stabilized; however, the state-of-the-art is based on our ability to analyze the problem. If the problem is linear, an answer can usually be found. Coefficients for the linear equations can also be generated with some confidence. It is the nonlinear descriptive functions for aerodynamics, structures and control system components, and the overall analytic framework that form the present ragged edge of the state-of-the-art in aerothermoelastic flight control analysis. A hypersonic flight condition will automatically place the analyst at the edge of present capabilities. It is hoped that at this symposium some of the borders of our present technical capability will be defined and some of the possibilities offered by advanced control systems and methods will be considered.

The first flight control paper introduces the subject of aerothermoelastic flight control analysis with a broad survey of the current state-of-the-art and the relationship of this topic to the other sessions. This is followed by a penetrating analysis of pressure redistributions due to distortions. This problem has been one of the keys to the success of present day linear supersonic analyses. When speeds extend into the hypersonic range, the linear techniques on which we have relied are inadequate. A nonlinear repetitive solution technique is then described that will provide a method for arriving at static aerothermoelastic corrections to hypersonic stability and control derivatives.

The next paper describes a system designed to successfully cope with the variations experienced in the re-entry flight control problem due to atmospheric and vehicle characteristic uncertainties. Finally, the last paper considers the tremendous design potential inherent in the new adaptive control system technique applied to aerothermoelastically affected vehicles.

The aerothermodynamics session has been planned to present and advance the state-of-the-art on all fronts of lifting entry - - from orbit and near space. Aerodynamic heating estimates may be performed on the more simple geometries with an accuracy of 15 to 20 percent. Work to date has been confined generally to the sub-orbital flight regime with a limited "order of magnitude approach" in the super-orbital regime. Analyses of complex lifting bodies and/or swept delta shapes have been confined to those regions where geometric symmetry exists. More sophisticated procedures are currently being devised; these are not, however, generally amenable to design applications and require tedious calculations for correct application. Particular papers have been selected to discuss the low density flows, boundary layer - - shock wave interaction and super-orbital entry problems. Two basic accomplishments are sought after. These are: (1) a technical

exposition of new work in aerothermodynamics and (2) a timely discussion of aerothermodynamic procedures that will enable the entire field of aerothermoelasticity to develop.

In the initiation of any new vehicle design, the first iteration of the structure is in the care of the structures engineer, although later structural iterations may be strongly influenced by the elastician, the aerodynamicist, or the flight control engineer. It is the structures engineer who defines the structural configuration within the constraints of external and internal volumetric requirements and provides the deflection and strength characteristics. The design objectives of providing a structure which has integrity throughout its life, an adequate life span, maximum reusability through the minimum need for refurbishing or replacing of parts, a high structural weight efficiency, and a design cycle accomplished in a reasonable time have always existed. They have never been more challenging than they are today when applied to the design of high speed vehicles and the attendant imposition of aerodynamic heating.

The need for structural weight efficiency was never more critical than that required for aerospace systems. Weight may well be a prime go or no-go feasibility factor for advanced systems. It may often be the restricting element in the selection of the launch system and in the launched vehicle's mission performance. Weight will certainly have an impact on the economics of putting payloads in space. Heating of structures is not conducive to structural efficiency. The ability to gain improved weight efficiency will depend on our capability to define accurately the load and temperature environment throughout the vehicle's life, to accurately analyze the structure and its response, and to devise means to obviate the thermal input or its effects. Fortunately, the development of computer technology is providing for analytical sophistication and one of the means back to structural efficiency.

The effect of structural heating on achieving these objectives, the new and complex design problems that it has created, means for alleviating or minimizing its effect, and the methodology used to account for heating will be covered in the structures section.

The following, then, may be listed as specific objectives of the Aeronautical Systems Division Symposium on Aerothermoelasticity:

1. To suggest potential aerothermoelastic problems that may occur on future aerospace vehicles,

2. To stimulate interest and thinking on aerothermoelastic problems,

3. To present and evaluate the general state-of-the-art,

4. To describe research needed to fill gaps in the state-of-the-art,

5. To foster exchange of technical information and procedures between experts in the specific technical areas comprising aerothermoelasticity, and

6. To encourage coordination of related technical efforts by interested groups.

The Air Force needs the whole-hearted assistance, participation, and support of the entire scientific and engineering community to accomplish the tremendous progress necessary to avoid the many severe problems that are possible.

OPENING REMARKS

AND

WELCOME ADDRESS

by

Brigadier General David M. Jones

Vice Commander, Aeronautical Systems Division

Good morning, gentlemen. I am indeed gratified to see such a large attendance. I notice that we planned very well - - we opened our meeting with the first day of winter. Those of you who were not here won't believe it, but we had a very beautiful October. We don't know if we should accuse our visitors of bringing this weather, or perhaps our planning people just wanted you to feel at home as you probably remember Dayton. At any rate, welcome. I am David M. Jones, Vice Commander of Aeronautical Systems Division. It is my great pleasure to welcome you officially to our Symposium on Aerothermoelasticity. I have been practicing that word for only six months! It is significant that this symposium is being held in Dayton, of course, for reasons that are manifold and obvious, and since Dayton is the birthplace of aviation, we feel it is a good one; we use it every chance we get. We at Wright Field are proud of our heritage and the work that has been done here in the past, and which we know will continue in the future. Under the present day AFSC organization, we expect ASD to continue contributing to the over-all Air Force posture. To do this, however, we need help. We have these meetings whenever we can, and we beg, borrow, or try to convince people they should attend because we need help wherever we can get it. Certainly we in the Air Force have no monopoly on knowledge. We are willing to listen to anyone who can help us. In fact, we have even listened to those who can't help us!

The difficult and tricky problems which have always been our lot in the past appear to have become almost hopelessly complex. We use the word "hopelessly" guardedly, of course, because no one really believes these problems are hopeless; however, we certainly agree they are complex and must be attacked in spite of their formidability. It is important not only because of the progress we've made and will continue to make going further into space, but from an ASD point of view, plain old safety of flight. We still have people integrated into the machine and we are concerned about their safety.

Aerothermoelasticity - - and that's the last time I'm going to say it, from now on it is ATE - - is the more familiar aeroelastic problem complicated by the effects of aerodynamic heating. Aeroelastic problems were born when it was realized that elastic deflections and the susceptibility of aircraft structures to various oscillations and vibrations were impeding the safety and effectiveness of military aircraft.

Great progress has been made on this problem and over this same span of time, equal progress has been made on the contemporary problems of flutter, structural divergence, dynamic loads, and so forth.

Today these same problems are present with the added complication of the effects of kinetic heating. This complicating factor together with the new vehicle concepts will require the development of increasingly accurate theories for predicting both aerodynamic heating rates and the resultant structural strength necessary for both static and dynamic loadings. The flight control system must help in this regard by reducing loads, must be adaptive over a wide range of performance variables, and must cope with stability problems. Structures heated to 2,000°F may reduce structural rigidities by at least 30 percent. These aspects of aerospace technology are becoming so important that we at ASD felt it valuable to survey this total problem with you.

We planned this symposium with three things in mind: to stimulate thinking and to obtain technical discussion by presenting challenging new ATE problems expected in the design of future flight vehicles; to provide a platform for presenting new, bold research objectives essential to advancing the ATE state-of-the-art rapidly and effectively; and to distribute widely the proceedings of our symposium to secure more effective utilization of total technical resources at all operating levels.

As you know, within the past few years. several technical meetings and conferences have been held in which various technical aspects of flight control, structures, and aerothermodynamics have been examined separately. However, to my knowledge, this is the first time that a select group of experts has been assembled from the academic, industrial, and government agencies to discuss interdisciplinary aspects of these important problems. It is by such coordinated efforts that we can best meet and overcome the challenges we face in aeronautics and astronautics.

We must be particularly aware of the needs of basic and applied research. The research accomplished will be a vital prerequisite not only for aircraft but also for aerospace vehicles. It is essential that we now determine to build a firm technological foundation of basic and applied research and upon such a base our future weapon systems can be built with confidence.

Our program here has been designed to review the requirements for this technological foundation, particularly in the ATE area. I am particularly pleased to have here such outstanding spokesmen from both the management and technical sides of our house.

Before I introduce our keynote speaker, I would like to make a small point. You will notice on this wall a small profile. You have probably determined that it has to do with the profile of one of our pet projects here at ASD - - that of Dyna Soar. Since we are all assembled here on this problem - - ATE - - most of us probably know that things get a little warm when you re-enter the earth's atmosphere from space. It turns out that as of this morning, this profile is classified; therefore, we have not displayed the Dyna Soar models which might show graphically the effects of this heating. We hope before the symposium is over that we can convince somebody that this profile is not classified and can display this very pretty picture.

At any rate with this brief and heartfelt welcome, I would like to introduce our keynote speaker for the symposium. He is the Vice Commander of the Ballistic Systems Division of the Air Force Systems Command, a post which he assumed a month ago. Prior to this assignment, he was Director of Launch Vehicles for the National Aeronautics and Space Administration, in charge of NASA booster development and rocket launching operations.

A long, long time before that, as a 1937 graduate of West Point, he served at Fort Bliss, Texas, where he was a horse artillery man and I was a cavalryman. He still is an artillery man but the size and range of his weapons are a far cry from the 37-millimeter howitzer he dealt with in those days! He is a graduate of the Command General Staff School at Fort Leavenworth and the Industrial College of the Armed Forces at Washington, D. C.

In 1947 he was assigned to the Air Material Command, now the Air Force Logistics Command, at Wright-Patterson. He was also Commander of the Holloman Air Development Center; Director of Development at Headquarters ARDC, now AFSC; and Assistant for Guided Missiles Production with the NATO Assistant Secretary General in Paris, France.

I take great pleasure in introducing Major General Don R. Ostrander.

KEYNOTE ADDRESS

by

Major General Don R. Ostrander

Vice Commander, Ballistic Systems Division

General Jones, gentlemen, I am particularly delighted to be able to open this symposium, not because I pretend to be an expert in this field but because I have had some fairly direct, and I might add not particularly welcome, experience with some of the problems in this field, both in my present assignment and in my last one in NASA. I though I would take a very few minutes this morning to sort of recap a little of the history of some of our past headaches in this field, and then to say just a few words about the vital importance of this work, not only to you as symposium guests, but I think to the entire aerospace community.

Incidentally, I am delighted to notice the degree to which this symposium integrates a number of technical disciplines as already mentioned by General Jones. I think that this approach is extremely important and I think it is vital to the overall evolution of our aerospace systems. I believe this kind of coordination among specialists in different technical disciplines will improve our ability to evaluate and to integrate the separate research results both in this country and in other countries, whose combined products are necessary for any real "breakthrough" in this area.

Now historically, as you gentlemen know much better than I, our present knowledge in this field can be traced I think into two separate disciplines. Aerothermoelasticity is, of course, the name given to the technical area that involves both kinetic heating and aeroelasticity. You will probably remember that we first encountered the effects of flexibility on static structural loads somewhere around 1952 on the F-89. On this airplane, flexible wing effects caused a bending moment at the wing root which was some 35 percent higher than we had expected. Today these aeroelastic effects are, of course, very carefully and very routinely accounted for in a structural design, and the predicted effects are quite systematically checked by a flight-load survey program, which is an integral part of the overall structural integrity program for all high performance aircraft.

Aeroelastic effects on stability and control occurred with the introduction of high aspect ratio swept wing aircraft. You will probably remember that the B-47 encountered aileron reversal in 1948. Thereafter, ailerons on swept aircraft were moved inboard to correct this condition. Coupling of interactions between control system equipment and low frequency vibration modes of the structure occurred on the B-36, on the B-52, and on the Snark. More complex control systems, such as adaptive control, even further complicate this general problem area. This same phenomenon is, of course, an extremely important aspect of ballistic missile and space launch vehicle design, which is where I have most recently been involved in the problem.

Prior to about 1950, the flutter engineers' major problem was with control surface and tab flutter and the solution was relatively simple and straightforward, enough properly located weight was usually sufficient to lick the problem. However, since 1950 there obviously have been such major aerodynamic and propulsive advances that the dynamic pressures to which aircraft and, of course, ballistic missiles are exposed have increased tremendously. As a consequence, sufficient stiffness has had to be incorporated as a fundamental design feature to insure prevention of flutter.

Thus, you might say that the dynamics and the aeroelastic problems began to focus somewhere around 1948 to 1950. However, at about the same time another bugaboo began to emerge. This was the kinetic or the aerothermodynamic heating problem. Fundamental laws of thermodynamics were obviously well known back before 1900, and hypersonic theories were developed before 1945. Then by 1950 or thereabouts, supersonic flights had occurred and recognition of the "thermal barrier" - - as we knew it then - - caused the evolution of what we know today as aerothermodynamics.

By 1955, the magnitude and importance of the heating problem had become pretty widely recognized. It lent impetus to the development of new materials, new theories, and new design construction procedures, led to the blunt nose ablation technique, and finally culminated in the first successful re-entry in 1958.

I know that most of you are more familiar than I am with this capsule history of the subject, but I thought it might be worthwhile to summarize the background against which we can view the purpose of this meeting.

We meet here for the next three days to discuss the variety of problems that occur in today's hypersonic speed regime as a result of the impact of kinetic heating on aerodynamics, on structural design, on stability and control, and on flutter. Future aircraft and spacecraft are going to encounter increasingly severe conditions, and the allowable weight is going to have to be more stringently held to a minimum. In view of these unavoidable structural flexibilities and the severe environments that we are going to encounter, design conditions are going to be significantly more severe and more exacting.

It is claimed to be absolutely essential for us to recognize new problems well in advance in a weapons system and to define them quantitatively as well as qualitatively. It is for this reason that we feel that it is necessary at this time to have met together and to evaluate the state-of-the-art and try to arrive at some creative new research objectives. This, of course, is the fundamental purpose of this symposium.

The Air Force is committed to contribute to this aerothermoelastic state-of-the-art on a high priority basis. New methods of obtaining data are going to be required. For example, increased free flight experiments with rocket boosted models are going to be essential to overcome the limitations of ground facilities. We hope to obtain significant information by testing hypersonic glide vehicles which will be boosted to high speeds and altitudes by the Blue Scout.

We have established what is known as Project Asset, and I am a little bit like General Jones in that I can understand why this one has been abbreviated, because it stands for aerothermodynamic/elastic, structural systems environment test. This program, we hope, will provide us with information on materials, on structural construction methods, on static and dynamic loads, and on aerothermodynamics for future aerospace designs. The speed range involved in Mach Number 4 to Mach Number 22 with corresponding velocities of 4,200 feet per second at 110,000 feet altitude to 20,000 feet per second at 245,000 feet.

The need to extend the state-of-the-art in this field is critical and the teamwork of the entire aerospace community is going to be required if we are going to obtain the information we need on a timely basis. It is quite obvious that the Air Force alone cannot solve the really thorny problems that have been facing us. Industry, universities, NASA, and research institutes, all are going to have to give their participation and support if we are to develop the aerospace vehicles that are so necessary for our military superiority as well as for our national prestige. We in the Air Force need your help and your cooperation and we know that we can count on it just as we have so many times in the past. Thank you.

SESSION I

DYNAMIC AEROTHERMOELASTICITY

Chairman: Dr. R. L. Bisplinghoff
Massachusetts Institute of Technology

PROBLEMS AND DEVELOPMENTS IN AEROTHERMOELASTICITY

by

I. E. Garrick* and Herbert J. Cunningham**

Langley Research Center, NASA

ABSTRACT

The paper aims first to delineate problem areas significant to various flight vehicles and missions, and to indicate the current technological background of significance for design and analysis. It is noted that both designing to live with thermal stresses and designing to avoid thermal stresses may lead to types of dynamic problems to be overcome. The second part consists of a selection of recent results and findings, both experimental and analytical, which show effects of high temperatures and of transient heating rates on vibration and flutter characteristics of lifting surfaces and panel coverings. Also included is mention of some useful experimental facilities.

* Chief, Dynamic Loads Division, NASA-Langley Research Center

**Aerospace Technologist, NASA-Langley Research Center

PROBLEMS AND DEVELOPMENTS IN AEROTHERMOELASTICITY

INTRODUCTION

This paper aims to discuss briefly and selectively the "state of the union" of several technologies which combine to make up aerothermoelasticity - a field of ever emerging significance for high velocity flight vehicles, from supersonic aircraft to reentry vehicles. It is proposed to deal first with this hybrid field in a general way, to indicate the technological disciplines involved and the types of vehicles of concern. Following this general discussion, which it is hoped will also serve partly as a background for subsequent papers of this symposium, there will be given more specific illustrations or applications taken mainly from recent work of NASA.

As will be discussed, we are basically concerned herein with the field of aeroelasticity, as modified, extended, and influenced by aerodynamic thermal effects. These thermal effects are associated with the friction and compression of air molecules being slowed down from hypersonic and from supersonic speeds in the neighborhood of stagnation points, along boundary layers, and near shock fronts. Aeroelasticity itself, the consequences of static and dynamic deformations of components of flight vehicles, interacting with sources of flow energy, or with sources of internal energy, has reached in the past decade a prime position in the aircraft design office. Its prime role in design for space vehicle flight is often hidden in the systems analysis approaches. One may take it as an axiom that, as the performance goals of preliminary design are attempted to be realized in practice and as space flight vehicles develop further, the aeroelastic hard facts-of-life will present themselves at subsequent more mature stages of design. If the lessons of experience of aircraft are valid indications, the solution of some of these problems will require every means at our disposal including the use of prototypes in flight.

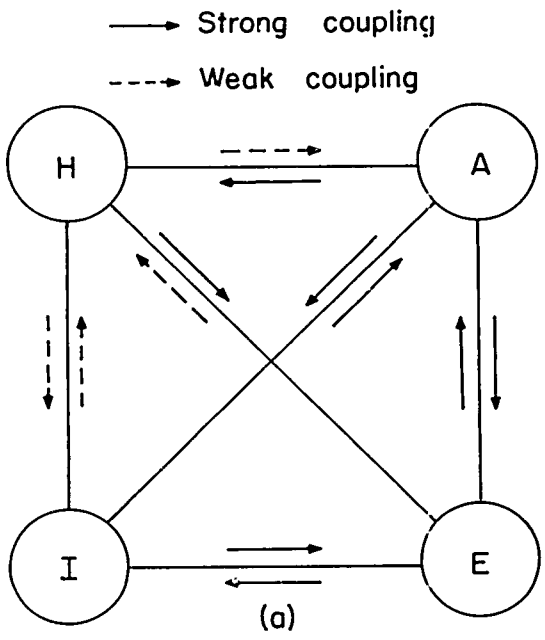
It would be unrealistic and presumptuous to attempt the task of providing an adequate survey without allowing the selected general references as well as the separate contributed papers of this symposium to ease and to take over the task. This is the purpose of many of the

references provided. The Wright Brothers lecture of Bisplinghoff (ref. 1) of some five years ago, for example, has already set a classic stage for the subject to which the present paper can only add in a minor way.

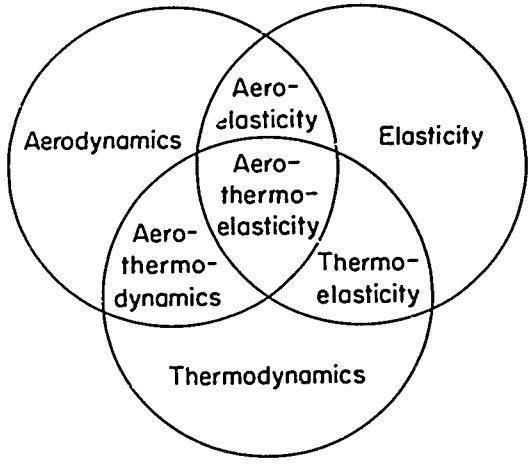
General disciplines involved.- Some 15 years ago, with a view mainly towards transonic and lower supersonic speed problems of aircraft, A. R. Collar prophetically described the expanding domain of aeroelasticity with the aid of his well-known aeroelastic triangle. It will help in a general way to survey the disciplines of aerothermoelasticity with a topological extension to the triangle. Professor Bisplinghoff (ref. 2) has already done this in an illuminating way with the use of a rectangular diagram. (See figure 1(a).) Rogers (ref. 3) has utilized a descriptive intersection of three circles (figure 1(b)); however, a more descriptive diagram makes use of four circles as in figure 1(c); interrelationships represented by the overlapping regions are indicated. Still another diagram of interest is that shown in figure 2.

In his triangle, shown shaded as one face of the tetrahedron in figure 2, Collar sought to indicate the separate and combined fields of aeroelasticity. Thus, he considered, for example, the whole field of mechanical vibrations as represented by the link (E)(I). The link (A)(I) includes most of the aircraft stability and control field, that of (A)(E) the field of static aeroelasticity due to deformations and airloads. Within the shaded triangle there are placed those areas involving interactions of the separate disciplines, for example, dynamic aeroelasticity or flutter, buffeting, and dynamic response.

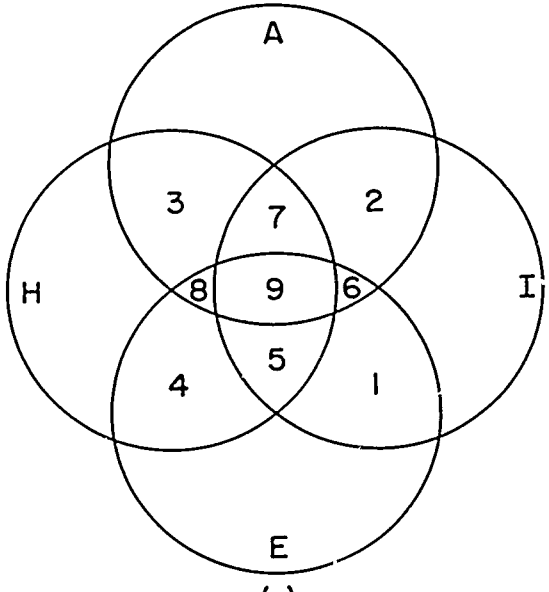
The base triangle (H)(E)(I) would herein represent, for example, the mechanical vibration field modified by the added dimension of heat or elevated temperatures. In an expanded sense the base triangle must rest on or be associated with engineering materials and their physical properties, not only in the sense of the determination of these properties for given materials, but also in the more fundamental sense of developing materials of desired strength and elastic properties. The role of the solid state physicist and of advanced materials research, and of other technologies, e.g. those of high temperature engines and nuclear reactors, is evident. One need only mention the words fatigue and fatigue at elevated temperatures (thermoelasticity on a molecular or crystalline scale) to recognize how vast an area is embraced in the base triangle and how far we have yet to go in its mastery.



(a)



(b)



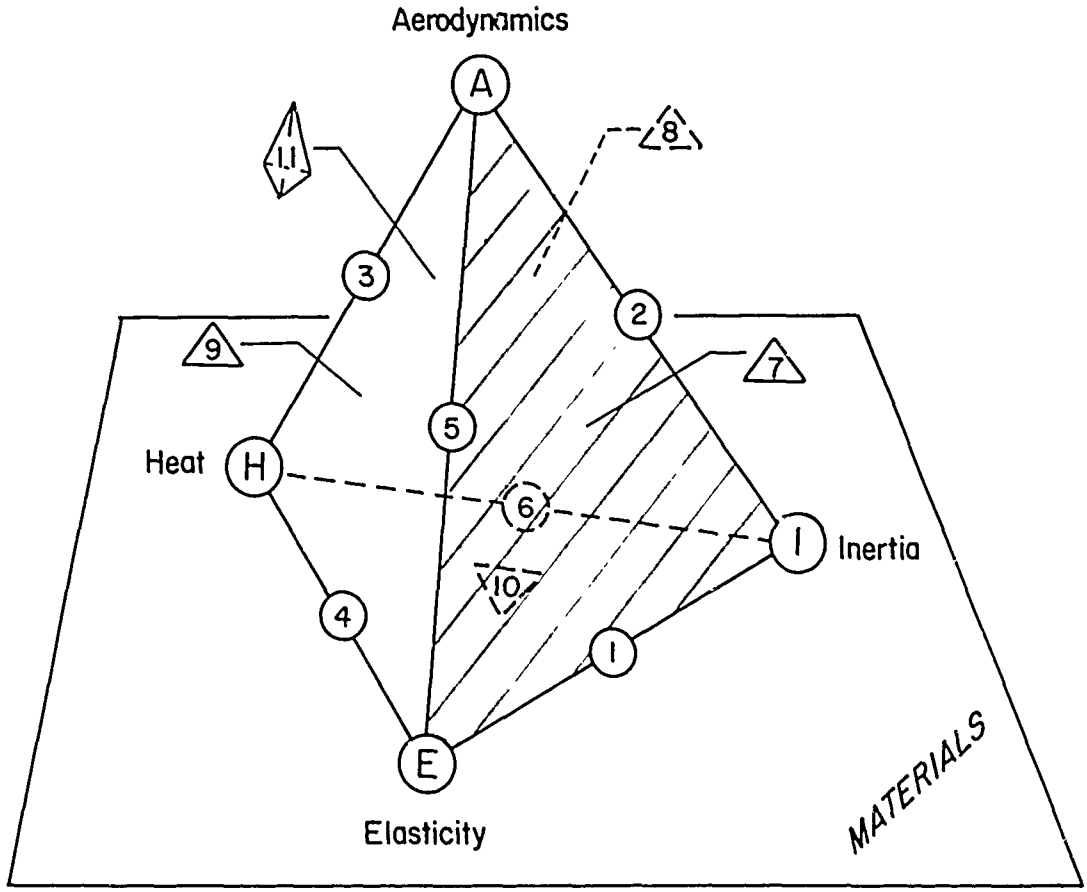
(c)

A Aerodynamics
E Elasticity
I Inertia
H Heat

1 Mechanical vibration
2 Stability
3 Aerothermodynamics
4 Thermoelasticity
5 Vibration and heat
6 Aeroelasticity
7 Stability and heat
8 Aerothermoelasticity, static
9 Aerothermoelasticity, dynamic

NASA

Figure 1.- Interrelationships of aerothermoelasticity.



I	Vibration	7	Aeroelasticity, dynamic
2	Stability	8	Stability & heat
3	Aerothermodynamics	9	Aerothermoelasticity, static
4	Thermoelasticity	10	Vibration & heat
5	Aeroelasticity, static	11	Aerothermoelasticity, dynamic
6	Thermal molecular processes		

NASA

Figure 2.- Aerothermoelastic tetrahedron.

The link (H)(E) by itself may be considered to represent the fundamental technology of thermoelasticity; some of the basic equations of this area go back to the Nineteenth Century and are associated with the classical work of Duhamel, Lord Kelvin, and others; more recently it has again been the subject of much active work, notably by Biot, and many others. (See list of references in ref. 4.) This area includes the determination of thermal stresses, thermoelastic damping, and heat transfer in the material; the phenomena of buckling and behavior during post buckling exhibit the overriding importance of considerations of nonlinearities. It is also pertinent to note that the link (H)(I) in a macroscopic sense is weak, although for molecular processes it can be strong.

The link (H)(A) represents the entire domain of aerothermodynamics. Elements of this domain are the effects of shock waves, the determination of the atmospheric heat inputs arising from the conversion of translational energy into internal degrees of freedom, the chemical effects of dissociation and ionization at high temperatures, the estimation of heat transfer to the vehicle for laminar or turbulent flows, and considering air as a continuum, as dissociated, or in free molecular flow, and whether in a state of equilibrium or nonequilibrium. Within the triangular face (A)(H)(E) are such subjects as ablation, surface reactions, static aerothermoelasticity, e.g., warping and associated loads. Within the tetrahedron itself lies the domain of dynamic aerothermoelasticity. It appears on the basis of the various time factors in this domain, as discussed by Bisplinghoff, that problems which arise can generally be treated sequentially, since the time constants of the thermoelastic processes are usually considerably greater than those for the aerothermal and aeroelastic processes. Indeed, the designer has strong motivation to design the structure to separate as far as possible the severest regions of these three processes; those responsible for selection of flight missions, and operators who fly vehicles, must also aim at alleviation and not compounding of effects. It should be pointed out that not enough experience has been accumulated in this regard, and problems that would involve true interaction effects can be visualized and expected. Illustrations of these are the interaction of heating and stability in reentry, or that of heating and aerodynamic effects of warping, certain regions of flutter, and adverse combinations of elevated temperature, high structural loads and unsteady environment.

In a later section of the paper on aerothermoelastic research facilities the capabilities of some of these facilities and possible procedures for exploring the various domains indicated by the tetrahedron are discussed.

FLIGHT CORRIDORS FOR VARIOUS VEHICLES

Some of the operating conditions for which aerothermoelastic problems are of practical concern for various classes of vehicles are illustrated in figure 3. Contours of constant dynamic pressure q and radiation equilibrium temperature T_E for a point one foot behind the leading edge are shown as functions of altitude and speed. Operating regions of interest for several types of vehicles are indicated in an approximate way by the various shaded portions. Our supersonic military airplanes are pushing into these new problem areas, and aerothermoelastic considerations will play an important role in the development of commercial supersonic transports. The X-15 research airplane has pioneered in flight measurements in the aerothermal field and much has been learned about associated aeroelastic effects of direct application to both supersonic aircraft and reentry vehicles; a few brief items of interest are mentioned in the section of the paper which follows. The anti-missiles and ICBM reentry bodies must function under extreme combinations of dynamic pressure and temperature. The small dark area indicated in the transonic region represents, as is known, a potentially troublesome design area for all these vehicles. The combinations of thermal environment and dynamic pressure for winged or manned reentry vehicles are not as extreme for their normal reentry conditions depicted here, as they could be for an abort condition.

Thus, normal reentry trajectories do not always represent the most critical design conditions as indicated in figure 4, where the design curves of dynamic pressure versus Mach number for the Mercury vehicle are shown. Early in the development of Mercury it was realized that normal reentry from orbit did not produce as severe an aerothermoelastic environment as did the abort conditions. The figure indicates that the dynamic pressures reached during escape from an aborted launch are nearly three times as high as those encountered during normal reentry. The temperatures and accelerations associated with abort also are much higher. A similar situation has evolved in the development of the Dyna-Soar winged reentry vehicle. In addition to conditions produced by the abort action, designing to take advantage of the winged vehicle's maneuverability brings additional severity to the aerothermoelastic environment.

SOME FLUTTER AND LOADS CONSIDERATIONS FOR THE X-15 AIRPLANE

The X-15 airplane, as referred to earlier, was designed as a research aircraft to explore and pioneer in flight regions wherein aerothermal effects were becoming important. It is of interest to indicate herein one or two highlights of the aeroelastic regime. Detailed technical information is naturally to be found in classified documents or special conference reports.

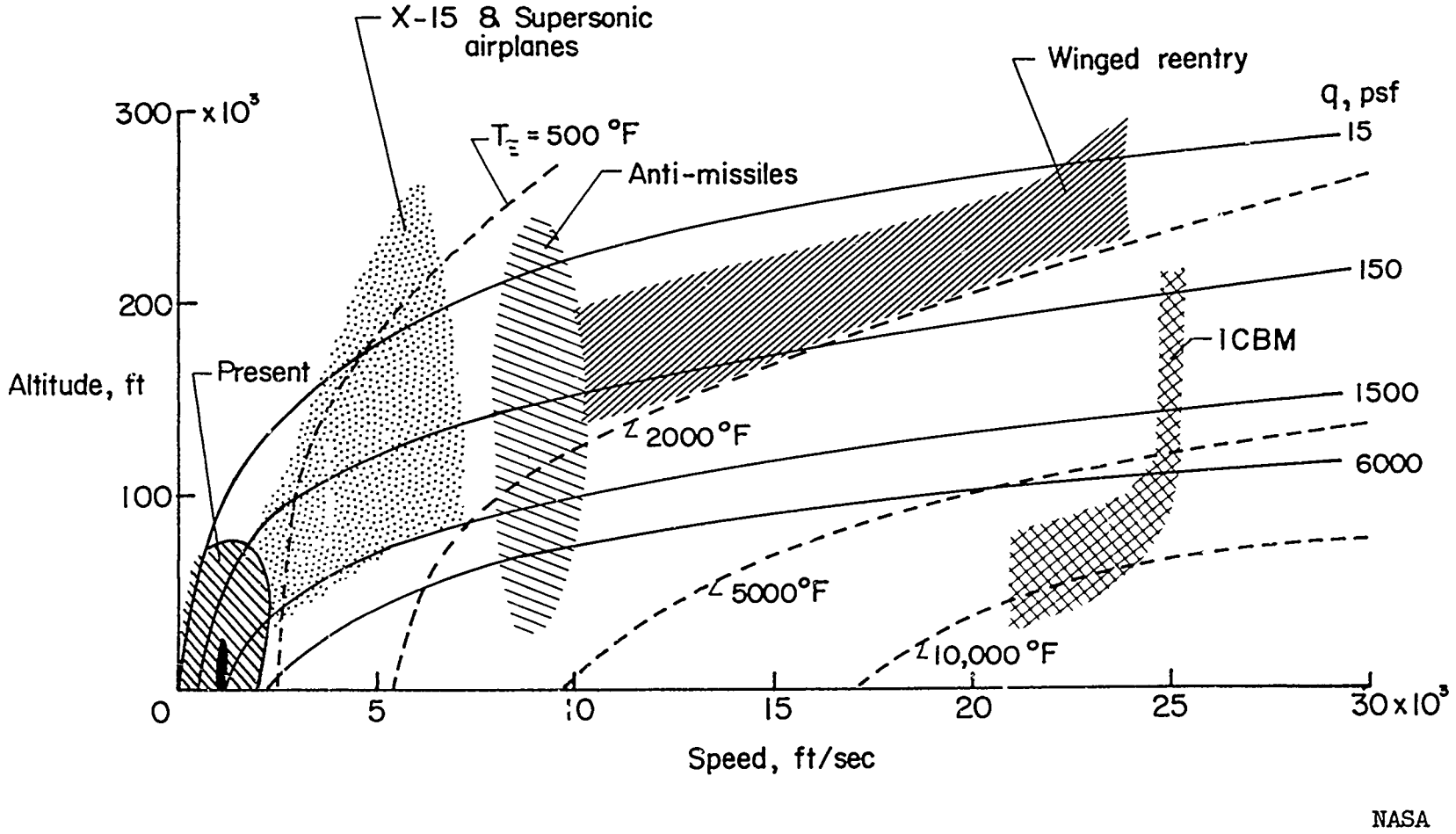


Figure 3.- Flight corridors for various vehicles.

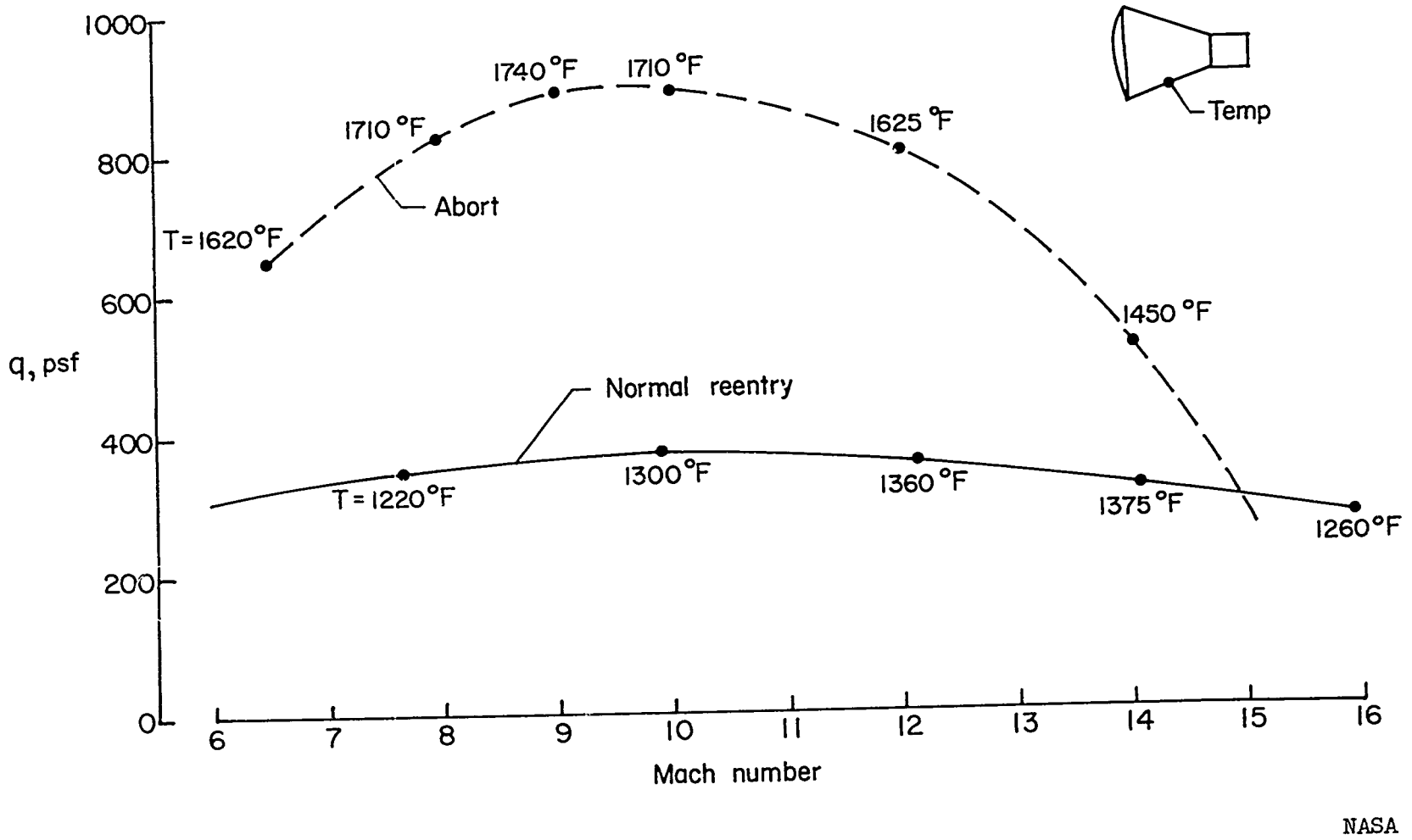


Figure 4.- Normal reentry and abort conditions for the Mercury vehicle.

Figure 5 shows shaded parts of the aircraft that have been affected and modified by considerations of flutter. Large parts of the fuselage and tail surfaces consist of various types of corrugated panels aimed at providing proper stiffness and thermal stress alleviation. It was found, as higher dynamic pressures were explored in flight, that many of these panels had to be reinforced. Panels with corrugations normal to the flow were especially prone to flutter. The figure shows a typical corrugated panel which was later stiffened by a center strip, and also shown are flight measurements of the relative amplitude of panel vibrations. Rather high frequencies were involved in these vibrations. The stiffened panels eliminated the indications of panel flutter and reduced the level of vibratory response to the background level of aerodynamic noise. It is of interest to note that the problem was compounded by thermal stresses that were induced on some of the panels by their proximity to the liquid oxygen tank. A further discussion of panel flutter is given in a later section of this paper.

The horizontal stabilizer, an all-moving control surface, presents several instructive points arising from its design to be free of flutter. We will let the project report speak for itself (ref. 5).

> "A rather extensive program was conducted both experimentally and analytically to demonstrate the freedom of this surface from flutter. Several conditions of stiffness as affected by temperature were considered although particular attention was directed toward the maximum-temperature, buckled-skin configuration.
>
> "Originally the horizontal stabilizer weighed 179 lbs. with 0.035-in. Inconel-X skins and a heavy I-beam running along the 57 percent chord and two smaller channel beams near the leading edge and at the trailing edge. The ribs were 0.050-in. titanium oriented perpendicular to the main beam. As the design progressed, it was noted that the structural torsional stiffness deteriorated more rapidly with temperature than had been anticipated. For this reason, the internal structure of the stabilizer was modified twice. First, the main beam was beefed up and the rib spacing was reduced to produce a lesser depth of skin buckle and yield what was thought at the time to be a sufficiently high stiffness in the 1200° F buckled-skin condition. This modification resulted in a 197.35-lb. surface. Subsequent studies indicated this was not sufficient for a partially loaded surface at temperature where the skin buckles were neither compression (from temperature) or diagonal tension (from load), but effectively floating from one to the other buckle condition. The final structure was a result of increasing the skin gage from 0.037-in. to 0.050-in. Inconel-X and replacing the 0.050-in. titanium ribs forward of the main beam with 0.040-in. Inconel-X ribs yielding a 227.5-lb. surface."

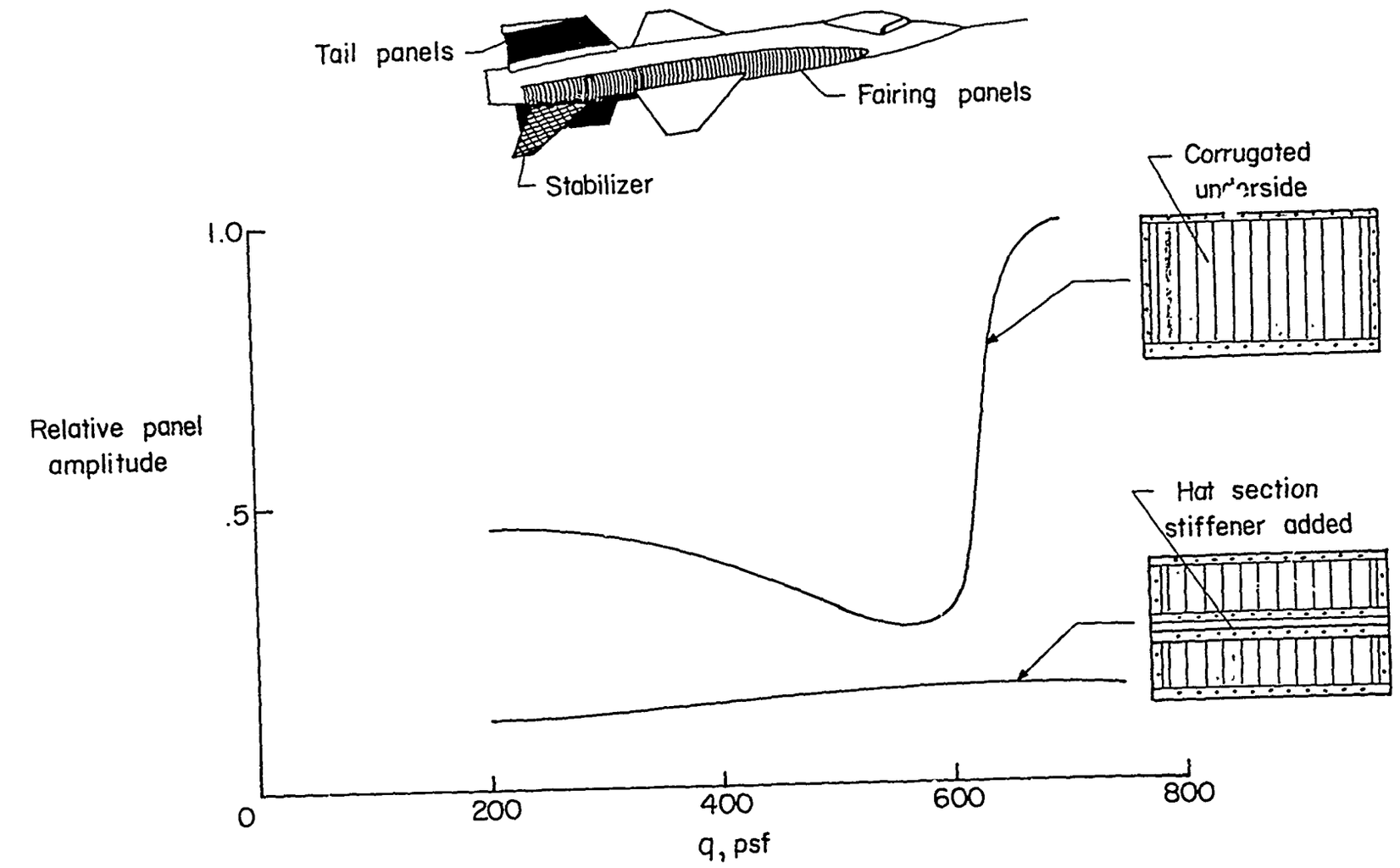


Figure 5.- Regions of X-15 airplane modified by considerations of flutter.

Similarly the all-movable control surface generally, which is a basic component of most guided missiles and of nearly all high-speed aircraft, can present very troublesome design problems in order to be free of flutter in a high temperature environment. It is of additional interest to note that proposed lifting and maneuverable configurations (see, e.g., ref. 6) for reentry from space will depend on control surfaces of various types, and hence present similar problem areas.

The highly transient conditions along the trajectories for a typical X-15 flight lead to considerable lag in thermal equilibrium. The thermal stresses that arise and the time varying environments pose added dimensions to the basic design envelopes which usually make use of V-n (speed-load factor) diagrams. The following pertinent observations are made in reference 7:

> "Familiar velocity-load factor (V-n) diagrams, which define the allowable maneuver load factor versus speed at a given altitude, do not appear to lend themselves to a modification which includes the effects of temperature on the structure. These temperature effects on the X-15 type structure are two-fold. One, the temperature differences that exist from one part of the structure to another can induce stresses which may add or subtract from the stresses due to air loads. Second, extremely high temperatures have the effect of reducing the ultimate load carrying ability of the structure. The real complication arises from the fact that neither the temperature levels nor the differences can be directly associated with a specified velocity, altitude, and load condition. The history of the portion of the flight preceding this condition can strongly affect the temperatures."

PARAMETERS OF AEROTHERMOELASTICITY

The basic partial differential equations of thermoelasticity were formulated many years ago. Very few explicit solutions of the numerous equations were feasible, however, except for the simplest structural elements and for special boundary conditions. The large-scale high-speed computing of the past decade has entirely changed the outlook. With the aid of methods of idealizing structures into component elements and utilizing influence coefficients and matrix methods, it has been possible to develop practical numerical schemes and programs for deflection and stress analysis of heated structures. Variational methods employing direct energy or complementary energy relations in combination with iteration procedures have also found considerable application. Some discussion of these methods is to be found in reference 8 by Turner and others at Boeing, in reference 9 by Gallagher and others at Bell Aerosystems, in reference 10 by Agyris, in

reference 11 by Lansing and others at Grumman, and in reference 12 by Mar, Pian, and Dugundji at M.I.T. Houbolt (ref. 13) has indicated the practical use of difference-equation methods which also permit the convenient handling of boundary conditions. It is of interest to mention that the comprehensive and elegant methods of analysis of heat flow, thermoelasticity, and viscoelasticity of Biot (see, for example, reference 14 and the bibliography therein) of the past few years are being summarized by him in a monograph being prepared for the Air Force Office of Scientific Research.

The field of aeroelasticity in the past half dozen years has seen the addition of the valuable books by Fung and by Bisplinghoff, Ashley, and Halfman (refs. 15 and 16). Being prepared for publication is the comprehensive six-volume collection, the AGARD "Manual on Aeroelasticity," under the editorship of W. P. Jones. In the aerodynamics of high-speed flight, the material on unsteady supersonic and hypersonic flow by Miles (refs. 17 and 18), that of Probstein and Hayes on hypersonic flow (ref. 19), and the recent article, reference 20, may be singled out for mention. Of special interest for high-speed aeroelasticity is the use of quasi-steady flow considerations, for example, those of piston theory to allow for thickness effects, in combination with Newtonian theory to allow for bluntness effects. The evaluation of proper bounds of application, however, remains a problem.

It is the purpose here, after some general remarks on nondimensional parameters, to do little more than list some of these nondimensional parameters of importance in the various areas and to indicate their relevance for the manifold scaling problems that need to be looked at.

It is well to recall that in the final analysis it is the physical phenomena that determine the nondimensional parameters of significance. Insofar as systems of mathematical equations have been developed in a given area and have withstood the test of time as to their relevance for prediction, they can be directly used. Caution must be employed in extending their use to new phenomena or for combined effects. Navier-Stokes equations in aerodynamics, for example, are not valid in free molecular flow nor are equations of elasticity of Lamé in plastic flow. The Buckingham pi theorem, another way of developing nondimensional parameters, enables only good guesses to be made after proper choice of physical parameters. Engineering criteria, which develop by accumulated observation and experience in application, play an important role in simplifying parameters still further, for often criteria can be fortuitously simple despite the complicated physical behavior that can take place.

It is well known that, even disregarding heat inputs, it is no simple or ready matter to scale models for aeroelastic effects; already compromises are required which can be based on a separation of problem areas. For any given prototype, different kinds of models may be required for transonic- and supersonic-speed testing, for early or late design stages, and which must be tailored to the capabilities and characteristics of the available wind tunnels. For classical flutter of an all-movable control, for example, the proper range of dynamic pressure is significant, and the advantages of variable dynamic pressure or variable density testing are well known in that trend data can be provided instead of isolated point data. For stall flutter or buffeting, the Reynolds number and flow separation strongly enter the picture, and detailed flow correlation as well as detailed damping considerations can be significant for analysis of stresses.

The compromises and trade-offs with regard to thermal duplication or heat simulation provide major study areas in themselves. Should heat effects be calculated in advance and a cold model employed with a reduced stiffness range to allow for it? This is one recognized procedure and, in fact, hypersonic wind tunnels with helium as a medium have been justified as one type of major attack on entry speed aeroelastic problems. There are additional compromises involved in the use of helium in wind tunnels, since the flow near blunt stagnation regions of the body and for the streamwise regions are affected differently by the change in the adiabatic index. These questions will not be pursued here, although additional remarks on the use of facilities are given in the last section of the paper.

Discussion of aerothermoelastic scaling has been given in several places; a comprehensive one has been given by Calligeros and Dugundji (ref. 21). The point of view taken for development of the nondimensional parameters is that based on the general aerodynamic equations for the subsonic and supersonic speed areas and separately for the hypersonic areas. Also, use is made of the equations of elasticity, governing the stresses and deflections of a heated elastic isotropic body, and allowing for large structural deflections. Conduction of heat in the body is considered to be governed by Fourier's classical heat-conduction equation. Similarity of boundary conditions for the flow and for the elastic restraints is also imposed. A prime conclusion, which had been arrived at also by others, is that correct scaling between a model and a prototype for all these areas is possible only for a scale ratio of unity. Molyneux (ref. 22) uses the method of selecting pertinent variables in advance and arrives at a similar conclusion. This result is rather discouraging for the scaling of prototypes in small-scale facilities; even compromises utilizing different materials and media do not permit much deviation from the scale ratio of unity.

For descriptive purposes, a list of nondimensional quantities (as in reference 21), which is essentially applicable to the flow about an elastic body of a nondissociated gas considered as a continuum, is given:

1.	$M = V/a$	Mach number
2.	$Re = \rho VL/\mu$	Reynold's number
3.	q/E_0	ratio of dynamic pressure $\rho V^2/2$ to reference elastic modulus
4.	ρ_B/ρ_∞	ratio of body density to free-stream density
5.	Vt_0/L	unsteady flow parameter (reduced wavelength)
6.	k_∞/K_0	ratio of heat conductivity of gas to that of body
7.	$\alpha_0 T_0$	body thermal expansion
8.	T_0/T_∞	ratio of reference temperature to free-stream temperature
9.	$\varkappa_0 t_1/L^2$	thermal diffusivity time constant
10.	u_0/L	reference measure of deflection
11.	σ_0/E_0	reference measure of stress
12.	p_F/E_0	nonaerodynamic force distribution
13.	$\varepsilon_0 \sigma T_0^3 L/K_0$	surface emissivity or radiation
14.	$V/\sqrt{gL}$	Froude number (gravitational effects)
15.	$Pr = \mu c_p/k$	Prandtl number (heat transfer effects)
16.	$\gamma = c_p/c_v$	adiabatic index, ratio of specific heats

In addition there are several quantity ratios which are unity, if the same model and prototype materials are tested at the same temperature in the same gas, and these can be listed as: modulus of elasticity E/E_0, Poisson ratio υ/υ_0, thermal expansion α/α_0, body heat conductivity K/K_0, body specific heat C/C_0, body emissivity ϵ/ϵ_0, gas specific heat $c_p/c_{p\infty}$, gas heat conductivity k/k_∞, and gas viscosity μ/μ_0.

Combinations of these quantities can, of course, bring in many other well-known nondimensional quantities. The significant parameters for classical flutter without consideration of heat are usually the first five of the above list, except for disregard of any quantitative satisfying of the Reynolds number. It is the satisfying of the Reynolds number, arising through the thermal requirements that greatly increases the severity of the scaling problem. There are naturally many special cases involving, for example, assumed restricted flow conditions and structural representations that greatly reduce the number of parameters to be satisfied. Some of the cases to be discussed in subsequent sections represent such applications.

INDICATED MAGNITUDE OF THE REENTRY HEAT PROBLEM

Methods of calculation of heat inputs are in the general literature, e.g. references 23 and 24, and are the subject of several papers to be presented; they will not be described herein. In general, these methods for the determination of the convective heat transfer rates have been well established for moderate heating reentry conditions. An interesting and useful correlation of temperatures at an index point (a reference location) of the X-15 with the total energy (kinetic plus potential) of the vehicle at its flight apogee has been given in reference 7. (See figure 8, therein.) For the higher speed conditions, a good deal of further work is necessary and desirable as very complex aerothermochemical processes exist. An indication of the increasing importance of radiation from the glowing gas and of radiative heat transfer to the structure for vehicles entering at very high speeds is given in the following significant calculations made by L. Roberts (ref. 25), in which the concept of total entry energy is a basic consideration. The table indicates relative convective and radiative heating quantities Q_c and Q_r for a nonlifting vehicle of about the size of the Mercury capsule $\left(\frac{Mg}{C_D A} = 50 \text{ lb/sq.ft.}, R = 10 \text{ ft.}, G_{max} = 10\right)$ for reentry from a circular, lunar, and a Mars orbit, respectively.

TABLE

Return from -	V_i, ft/sec	Q_c, Btu/sq.ft.	Q_r, Btu/sq.ft.
Circular orbit	26,000	6,400	53
Moon	36,000	16,900	2,500
Mars	46,000	23,200	120,000

While Q_r is negligible for a circular orbit, and is only about 15 percent of Q_c for a return from a lunar orbit, it can be the overwhelmingly overriding quantity for a return from a Mars orbit. For a partly lifting vehicle these quantities, particularly Q_c, can be considerably increased.

STRUCTURAL CONCEPTS FOR WINGED REENTRY VEHICLES

One means of alleviating problems arising from the aerothermoelastic interactions is to evolve structural concepts which separate the effects of the environment. An example of this approach is the so-called "cold" or protected primary structure, i.e., a design wherein the main load carrying structure is maintained at relatively low temperatures by an insulating outer shield. The weight and availability of suitable insulating materials and the requirement for active cooling systems in regions of high heat input are serious problems associated with this approach. A discussion of design factors for protected structures is given by Heldenfels in reference 26.

Another concept which is being considered in the design of the Dyna-Soar vehicle is the radiation cooled "hot" structure where the primary load carrying members are designed to function at relatively high temperatures. In this approach, thermal stresses are minimized by the use of pin-jointed determinate trusses for the primary structure. The air loads are transmitted to the trusses by outer panels which are attached to each other by suitable joints to permit thermal expansion. Although this arrangement greatly alleviates thermal problems for the primary structure, the aerothermoelastic environment imposed on the lightly loaded outer panels is very severe and, in fact, stiffness requirements for the prevention of panel flutter are dictating, to a large extent, the design of these panels. An extended proposed concept, a multiple layer heat shield, combines features of the "hot" and "cold" structure. It involves a sandwich-

type construction of multiple layers of waffled or dimpled sheets attached to each other, wherein each layer would restrict radiative and convective passage of heat. For any given concept, the number of detail designs to yield efficient structures and to be studied with available and advanced materials is appallingly large. There are many other requirements imposed on these panels including resistance to acoustic fatigue and alleviation of thermally induced stresses. Efficient designs which will meet all requirements will require a great deal of ingenuity and inventiveness on the part of the designer.

Boost-glide heat-shield temperature time-history study.- In figure 6 there is shown for a particular reentry study a calculated temperature-time history curve for a point on the underside and some 5 feet from the nose of a boost-glide vehicle. The temperature time-history was produced in the structures laboratory at the Langley Research Center by program-controlled arrays of quartz lamps, radiating to a heat shield about 2 feet square. The shield weighed about 1 lb/ft^2; its panel cover was a refractory corrugated metal attached with U-clips to the protected structure, and the interspace was filled with a layer of 0.4 in. of quartz-fibre insulation. Shown in the figure also are the temperatures on the protected side of the structure; temperature differences of about 1000° F are noted to exist. It is considered that the technique for producing the desired heating program is well in hand. It may be observed that the temperature of the protected structure develops very gradually (except for the power-failure interval indicated). Heat shields of comparable design, as a matter of interest, have successfully withstood airflow at M = 3 having a dynamic pressure of 3000 lbs/sq.ft., and stagnation temperatures up to around 660° F. These radiative heating techniques provide a feasible way of simulating aerodynamic heating environments for stiffness and vibration testing of structures.

EFFECT OF HIGH TEMPERATURE ON THE STATIC AND DYNAMIC MODULUS OF ELASTICITY OF METALS

The structural concepts discussed in the previous section imply all sorts of new structural materials to cope with high temperatures. Furthermore, a much wider range of the physical and even the chemical properties of the materials has become important. Only a few years ago the emissivity, resistance to meteoritic impact, and behavior in the presence of a white-hot ionized atmosphere, as examples, were of little or no concern. Today, these and many other material properties (see, for example, ref. 27) are being studied intensively.

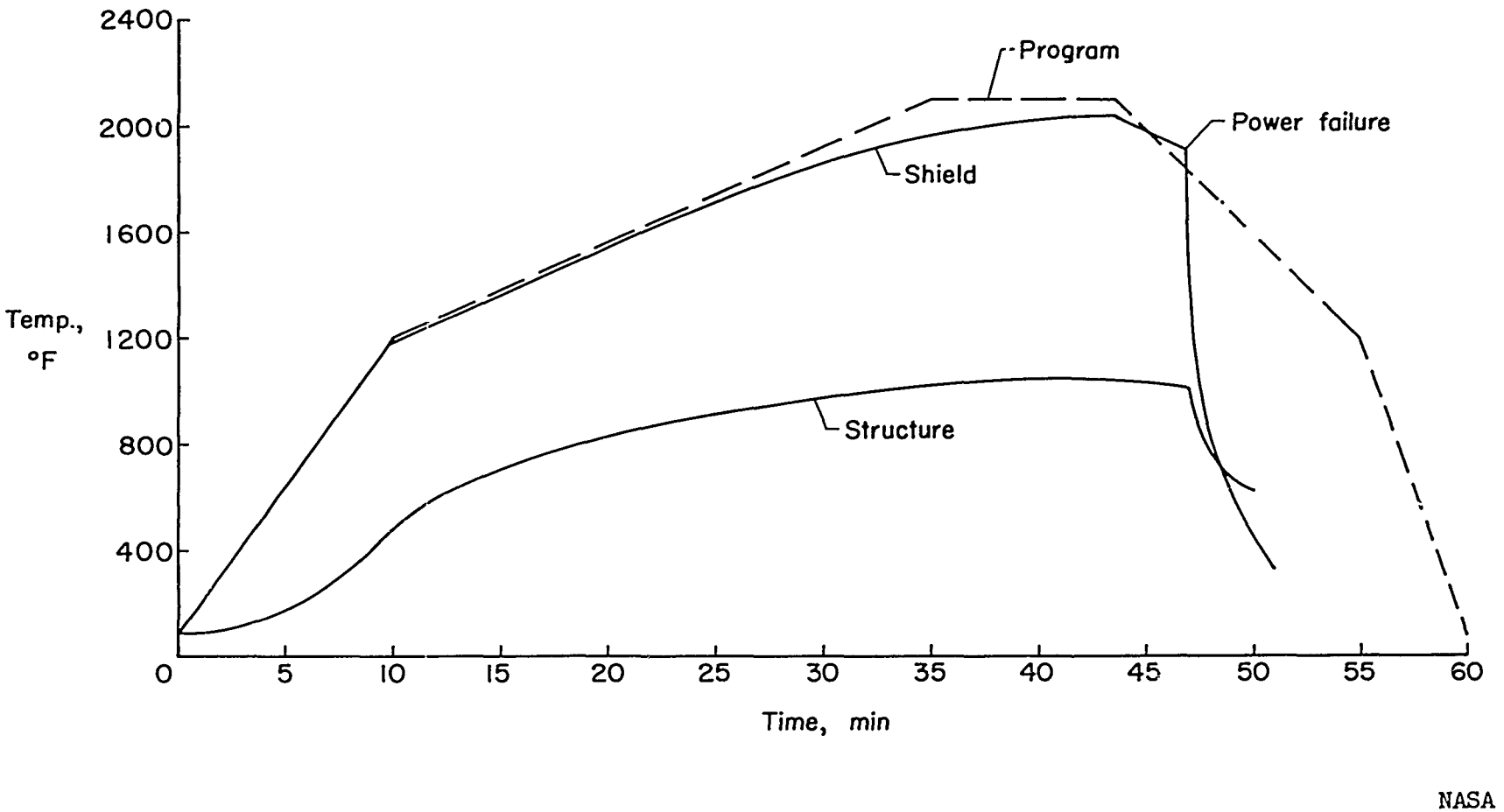


Figure 6.- Heat-shield temperature time history.

The present purpose is to discuss a particular physical property that is always important and is perhaps of the most direct concern in the field of aerothermoelasticity; namely, the modulus of elasticity, and the effect of heat upon it. As a metal is heated above room temperatures, its modulus begins to decrease gradually, then more rapidly as higher temperatures are reached. Furthermore, the measured modulus differs in value according to the method of measurement, whether static or dynamic.

Figure 7 (from ref. 28) shows the variation of the modulus E with temperature found experimentally for steel, a titanium alloy, an aluminum alloy, and a magnesium alloy over a range of temperature. The statically measured E are shown by the dashed lines faired through the square symbols. The dynamically measured E are given for two sets of experiments by the solid lines and the circular symbols. The more rapid increase of downward slope of the static measurements as compared to the dynamic measurements is obvious for the magnesium, aluminum, and titanium alloys. There is little difference of slope for the steel up to 1000° F. In explaining the differences between dynamic and static moduli, it is concluded in reference 28 that these differences are due to various internal-friction mechanisms, of which anelastic effects appear to be predominant, and cannot be attributed to the influence of creep on static stress-strain measurements.

The analogy between the static and dynamic moduli in the field of thermoelasticity, and the static and dynamic slope of the lift-curve slope in the field of aerodynamics may be of some interest. As is well known, the dynamic C_{L_α} is usually greater than the static value and its effect superimposed on the static loading level can lead to complex unsteady-flow phenomena such as stall flutter and buffeting. Similarly, in thermoelasticity one might expect complex vibrational characteristics of structures that are subjected to combined high temperatures and large static loadings. However, an important alleviating factor seems to be that in meeting static strength requirements at high temperatures, additional structure would be available for satisfying stiffness as well.

Figure 7 gives results for four metals and extends only to 1000° F. Additional information, mostly on dynamic modulus, is to be found in various references. Reference 29, for example, presents elevated-temperature dynamic moduli of elasticity of 40 commercial metals and alloys at temperatures up to 1800° F obtained by a longitudinal resonance technique. Reference 30 consists of five reports which discuss several techniques of measuring both static and dynamic moduli and include some data. An ultrasonic pulse-echo technique for measurement of the dynamic elastic modulus is described in reference 31, and gives some measured values for temperatures up to 2000° F. The necessity for data from many more materials, and extending to much higher temperatures is obvious.

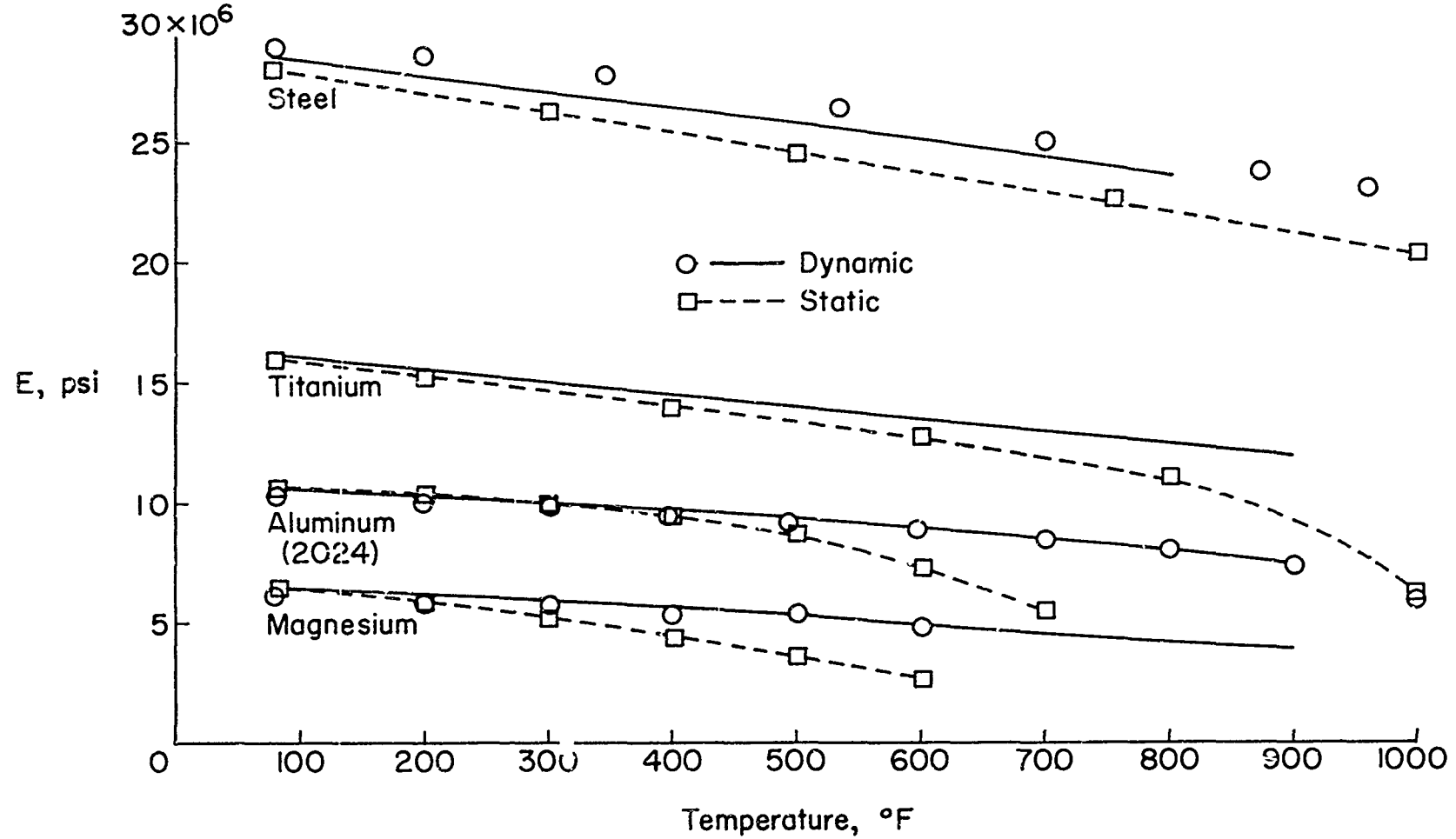
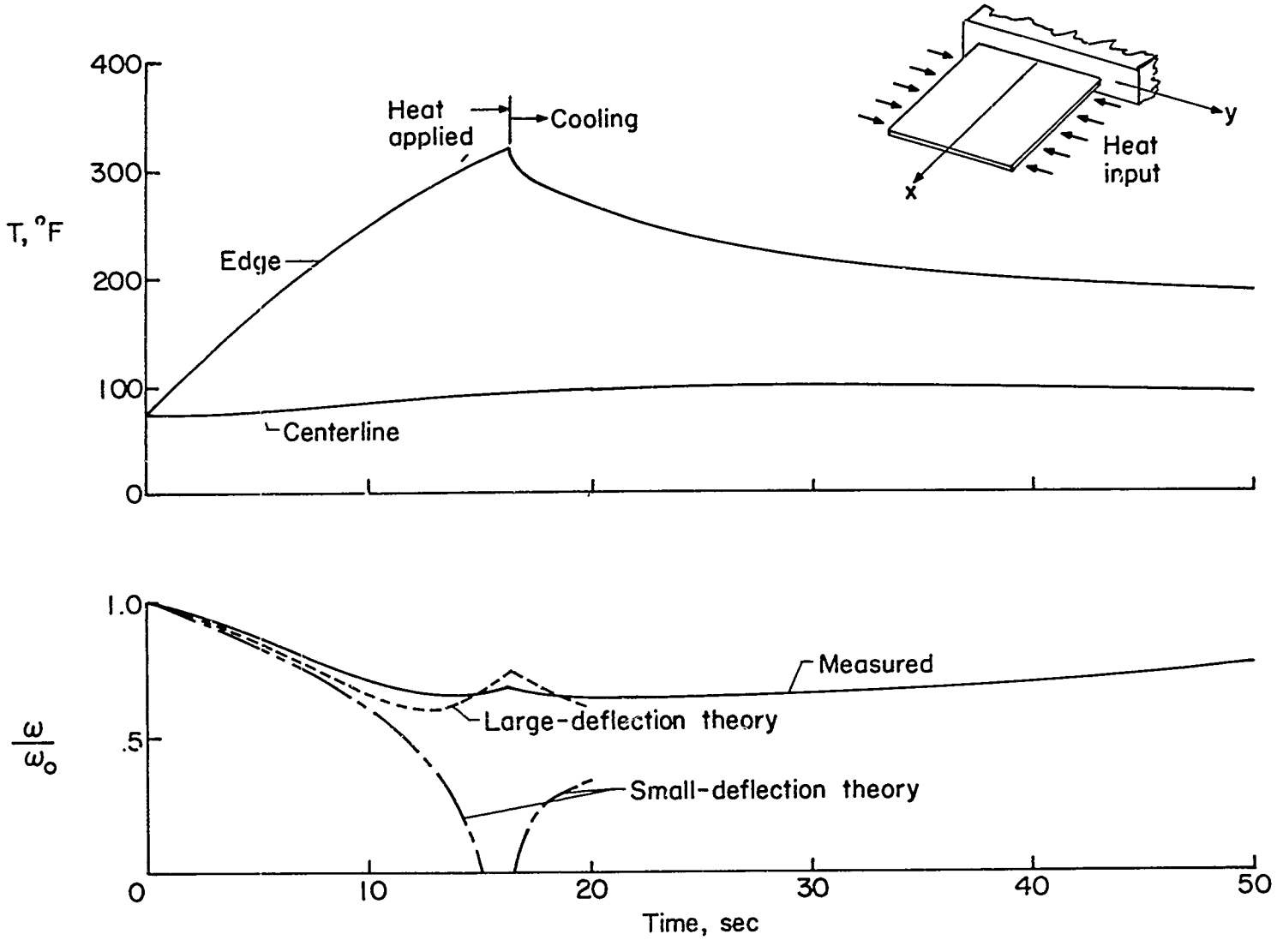


Figure 7.- Variation of dynamic and static modulus with temperature.

EFFECT OF TRANSIENT HEATING ON VIBRATION FREQUENCIES

In addition to the undesirable effects of high temperatures on the modulus of elasticity discussed above, there is another effect of heat which can be very important even at moderate temperatures, the effect of internal thermal stresses. Thermal stresses can arise from rapidly changing conditions of heat input where time lags are involved or also from equilibrium conditions where thermal gradients occur, as for example, between the leading edge and points farther aft on a wing. Thermal gradients result in incremental tension and compression stresses in the different regions of a structure. Commonly, but by no means inevitably, the thermally stressed structure has a lessened net stiffness available to resist both static loads and the inertia loadings associated with vibrations. The latter condition is manifested by lowering of natural frequencies and considerable attention has been given to determining such effects.

The analysis of these thermal effects based on small-deflection theory has been recognized for some time to be inadequate when initial deflections are present, especially near buckling conditions. Considerable improvement is obtained with the large-deflection theory which is nonlinear and which couples the deflections and the midplane stresses. Some comparisons of thermal gradient effects on torsional stiffness as obtained by experiment and by theoretical analysis are presented in reference 32, and may be used as a basis for discussion. The sketch on figure 8 represents the uniformly thick rectangular cantilever plate with heat input at the two edges. The analysis involved an approximate solution of the von Kármán large-deflection differential equations modified to include effects of initial deflections or imperfections and of nonuniform temperature distributions. Figure 8 shows at the top the temperature time-history of the plate centerline and of the edges; as indicated, the plate was heated for about 16 seconds, then the heat supply was shut off. The lower part of the figure shows the time-history of the first torsion frequency ω divided by its initial value ω_0. The solid line shows the experimentally measured frequency and the line of short dashes the result calculated from large-deflection theory using the small measured initial twist of 0.35° at the tip of the plate. Also shown are the results calculated from small-deflection theory (if the plate were exactly flat, large-deflection theory would give the same result for the prebuckling state). The intersection with the zero-frequency line means that a theoretically perfect flat plate would have reached a marginal condition of torsional buckling due to thermal stresses. The large-deflection theory provides a good comparison with the measured result, whereas it is obvious from the figure that in this case small-deflection theory is not adequate when even very small initial deflections exist in the presence of an appreciable thermal stress loading.



NASA

Figure 8.- Effect of transient heating on torsional frequency.

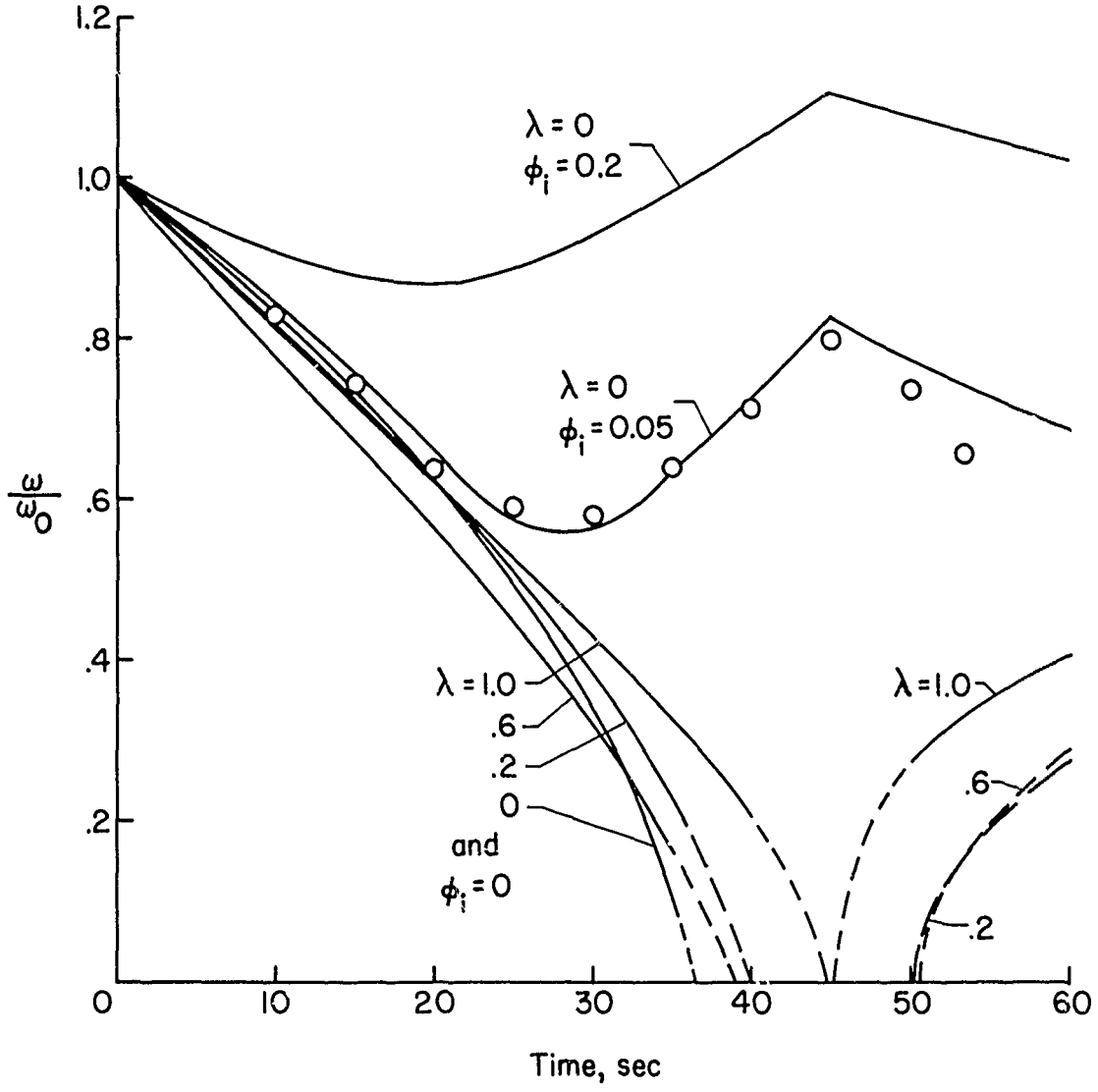
Some recent unpublished work done at Purdue University by C. Bailey is of interest in that it supplements the rectangular flat-plate work to include effects of taper. The effect on the torsional frequency of heating a plate rapidly at its edges was studied both theoretically and experimentally for plates having an aspect ratio $A = 5/3$ and four different taper ratios $\lambda = 1.0$ (rectangular), $\lambda = 0.6$, 0.2 and 0 (triangular). The theoretical results were obtained on the basis of large-deflection theory. The ratios ω/ω_0 of the torsion frequencies to their unheated values are plotted as functions of time in figure 9. The four clustered theoretical curves which slope down to intersect the horizontal axis are for assumed perfect flat plates which experience the respective heating rates used in the experiments. For the present purpose, the experimental results for the triangular plate only are presented as the circles. The theoretical curve that closely follows the experiments was obtained using a chosen initial deflection of the triangular plate, and the uppermost curve was calculated using four times that initial deflection. The two higher curves on figure 9 which show effects of initial deflection (φ_i) again make clear that such effects can be important even though the deflection is physically small and, fortunately, the results are beneficial in comparison with those of small-deflection theory.

The effect of thermal gradients on natural frequencies, in particular torsional as just discussed, has been illustrated by results on solid metal plates. On wings of the more normal built-up type of construction effects of thermal gradients on stiffness, and therefore on natural frequencies, are less pronounced but harder to calculate. Some wing vibration modes can even experience a modest increase as the wing is heated rapidly. See, for example, reference 33.

FLUTTER OF A RAPIDLY HEATED SOLID WING

An interesting case history study of the effect of aerodynamic heating on the bending-torsion flutter of a rectangular wing at a Mach number of 2 has been made by Runyan (ref. 34). The wing was of solid aluminum-alloy construction and had a thin biconvex-like section. When exposed to air at 300° in a blowdown jet at $M = 2$ it did not flutter, whereas exposed to air heated to 800°, it experienced severe flutter for about two seconds and then stopped. The calculated loss in torsional stiffness as a function of time, corresponding to the calculated temperature distributions, is shown in figure 10. This calculation was made in accordance with the small-deflection analysis (which turns out to be adequate for the purpose) given by Budiansky and Mayers (ref. 35), and based on the equation

$$(GJ)_{eff} = (GJ)_i + \int_A \sigma_y r^2 \, dA$$



NASA

Figure 9.- Effect of transient heating on torsional frequency of flat plates with tapered planform.

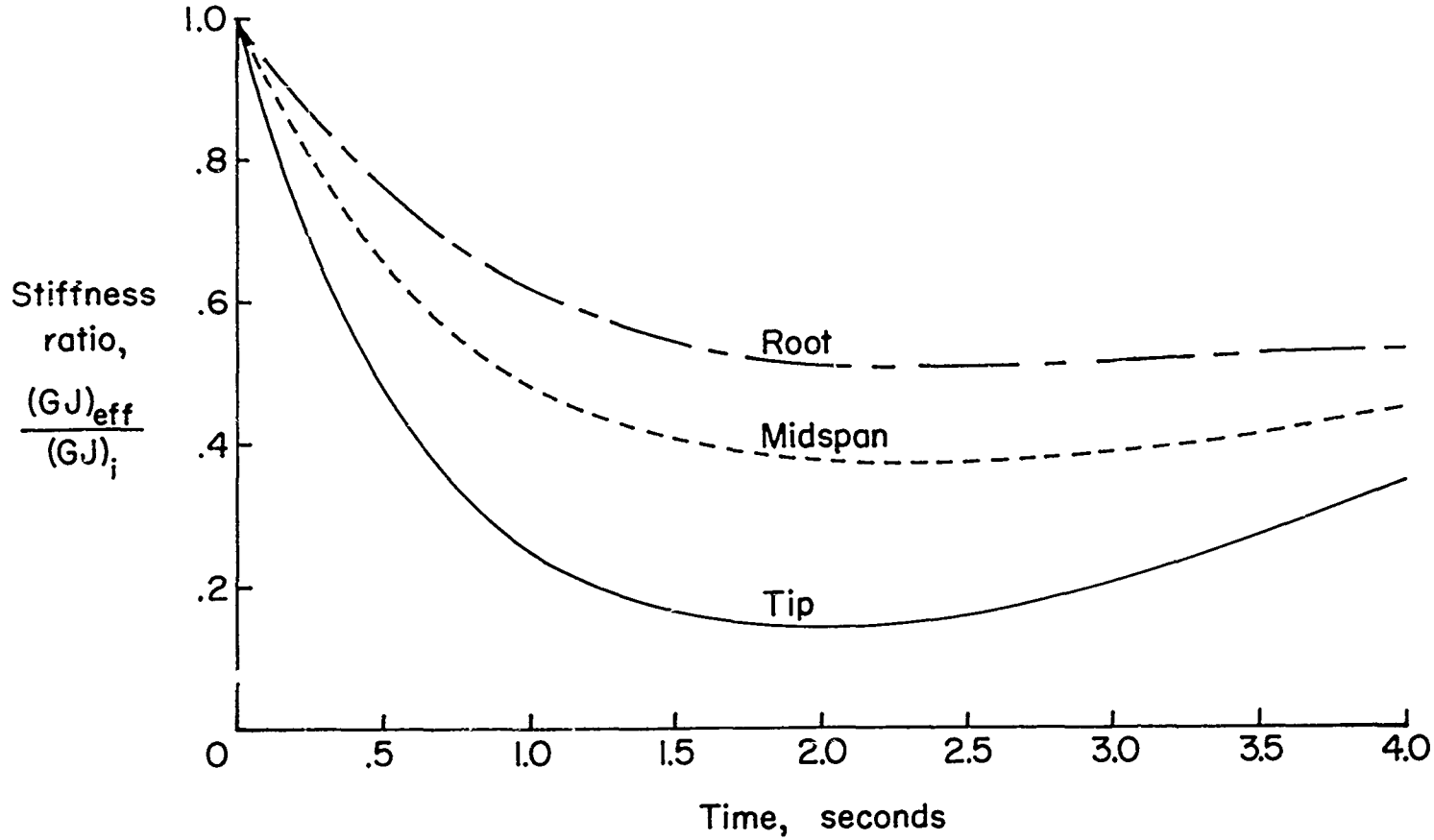
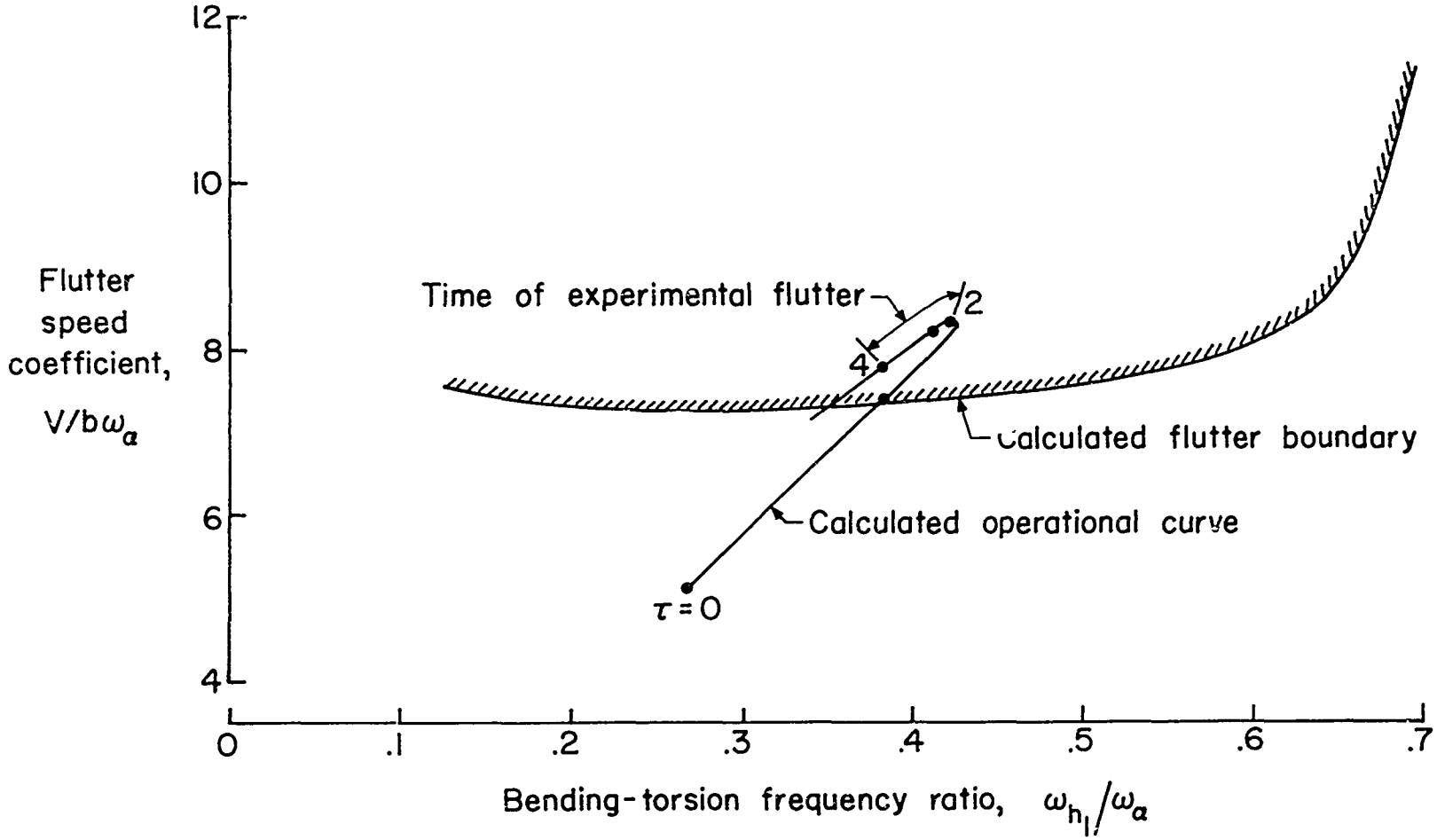


Figure 10.- Calculated loss in torsional stiffness as a function of time for test wing.

where the integral term accounts for the loss in torsional stiffness associated with the thermal stresses (σ_y is negative for compression) and is associated with the induced compression effect along the hotter leading and trailing edges. Figure 11 shows the flutter results plotted as a flutter speed coefficient against the bending-torsion frequency ratio. The calculated flutter boundary and the operational time-history curves are shown and indicate reasonable correspondence with the flutter phenomena that did occur. The thermal-stress effects on the solid wing are greater than those that would occur on a built-up wing of more normal construction. However, fins of many guided missiles are frequently made solid, and may be exposed to high dynamic pressures and rapid heating simultaneously. The case is also illustrative of prediction techniques in research, for it is important to recognize, as discussed briefly in the next item, that many of our research tools may also be subject to the coloring of their data results by aerothermoelastic effects.

EFFECT OF THERMAL GRADIENT ON FLUTTER OF A THIN LOW-ASPECT-RATIO PLATE

During the course of a study of flutter trends for supersonic speeds for a series of low-aspect-ratio wings (ref. 36), a marked sensitivity of low-aspect-ratio thin plates to small thermal gradients was encountered. Although these data were not included in reference 36 because the thermal effects were not analyzed, they are presented here as an illustration of transient thermal effects possible on certain models. The small blowdown-type wind tunnel used for this investigation operates with an ambient temperature air storage tank, but due to transient heat transfer effects the stagnation temperature in the test section is sometimes as much as 100° F above ambient temperature. Since the tunnel runs are of only a few seconds duration, the model does not have sufficient time to reach an equilibrium temperature and there usually is a small temperature difference between the leading edge and trailing edge of the model. The effect of this thermal gradient on the flutter characteristics of a thin low-aspect-ratio constant-thickness plate is illustrated in figure 12 where the flutter velocity index is plotted as a function of the time from the start of the various tunnel runs until flutter occurred. Actually, the temperature difference between the leading edge and trailing edge of the model might have been a more significant parameter for plotting the data; however, this quantity was not determined for all the points. A typical variation of the flutter index with time is shown by the dashed lines where the arrows indicate the manner in which the flutter point was approached. (V is speed, b is reference half-chord, ω_α is torsional frequency, μ is plate/air density parameter.) At a given Mach number and stagnation



NASA

Figure 11.- Effect of aerodynamic heating on flutter of solid wing at M = 2.0.

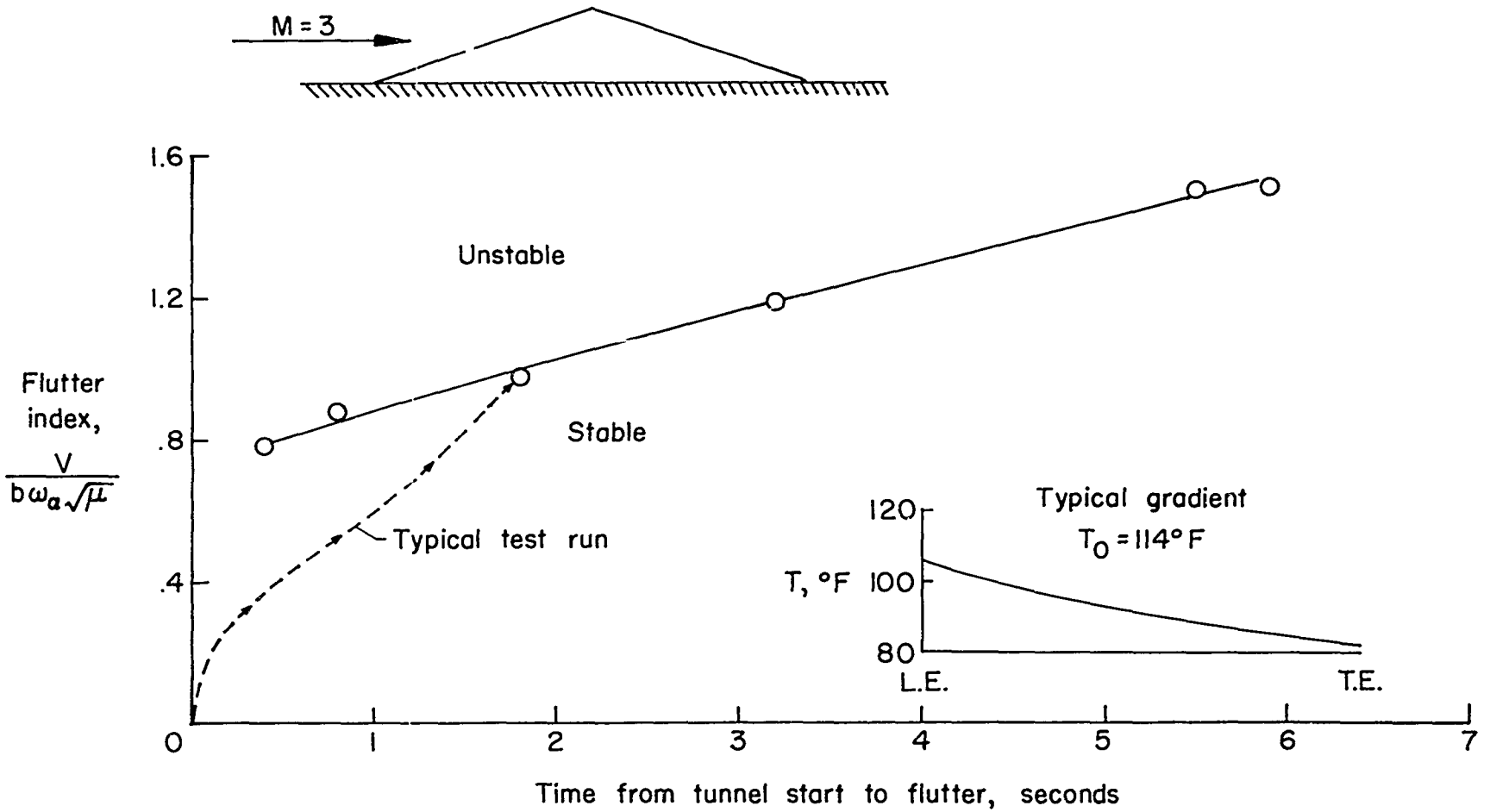


Figure 12.- Effect of thermal gradient on flutter of thin low-aspect-ratio plate.

temperature the air density could be increased rapidly or slowly, and the flutter occurs at a value of the flutter index depending on the effect of the thermal gradient on the effective stiffness of the plate. Typical temperatures measured on the model for one of the runs are shown on the figure and indicate that at a stagnation temperature of 114° F a temperature difference of only 24° F existed between the leading and trailing edge. The flutter data indicate that for even such small temperature differences, large flutter speed variations are possible. These large effects are believed to be associated with the increased importance for this low-aspect-ratio structure of the clamped root restraint on the thermally induced stresses. Tests on models of somewhat higher aspect ratio indicated greatly reduced sensitivity to these thermal effects. It is possible that the effect of the mass ratio parameter is also intertwined in the results since this has not been analyzed herein.

CAMBER FLUTTER

The increased importance of camber modes (sometimes inappropriately termed chordwise modes) as additional factors to the beam-type modes in the flutter analysis of low-aspect-ratio wings has been known for some time. One current way of taking the camber flexibility into account is by use of flexibility influence coefficients for the whole surface. A significant contribution to the analysis of twisting and bending of heated lifting surfaces involving camber flexibility is given by Bisplinghoff in reference 37. A series of experimental studies with ribless multiweb wings was conducted several years ago in the heated supersonic preflight jet at Wallops Station, and also more recently in the Langley 9- by 6-foot thermal structures tunnel. The range of stagnation temperature was from about 300° F to 670° F. When flutter was obtained, it clearly involved large relative amounts of "flag-waving" or camber-bending motion and was usually destructive to the model.

Analysis which did not take into account the details of the camber deformations was not successful in predicting the experimental results. Recent work of Kruszewski and Thomson (as yet unpublished) at Langley Research Center has improved the determination of the camber modes and has resulted in improved correlation with experiment. Figure 13 shows at the top the diagrammatic representation of the wing cross-section, employed in a representative-section analysis. The wing section was analyzed as two bent beams (or plates) which are joined at leading and trailing edges at a fixed angle. When the section deforms the chordwise distribution of thickness of the airfoil is assumed to be maintained unchanged by the presence of the multiwebs. The external spring supports at leading and trailing edges are proportioned in accordance with the measured first-torsion frequency of a given test wing. The modes shown are: mode 1, rigid vertical translation; mode 2, first torsion with appreciable camber; mode 3, a symmetric camber; mode 4, an antisymmetric camber.

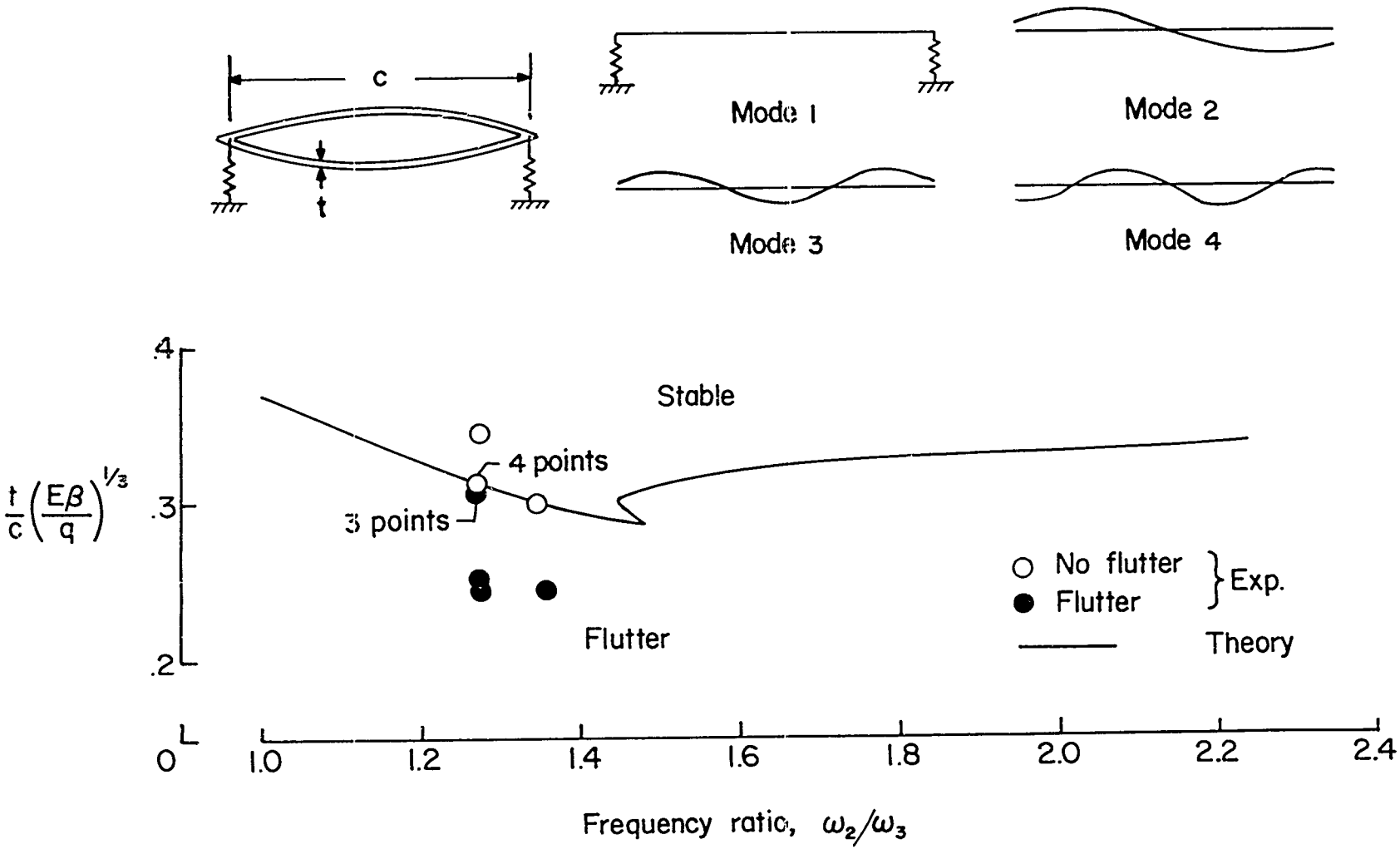


Figure 13.- Camber flutter, experiment and analysis.

Figure 13 shows the results of a Galerkin modal analysis which employed these four modes and aerodynamic forces from a modified piston theory (modified by use of pressures proportional to $1/\beta$ rather than to $1/M$ where $\beta = \sqrt{M^2-1}$). The ordinate is an often used panel flutter parameter involving skin thickness t, chord length c, modulus of elasticity E, Mach number quantity β, and dynamic pressure q. The abscissa is the ratio of the frequencies of mode 2 and mode 3. The flutter region is below the solid curve. A number of test points is shown, the open circles denoting no flutter and the solid circles the flutter points obtained on multiweb wings of aspect ratio 1.0 at Mach numbers 2 and 3. Good agreement of analysis and experiment is apparent. One can in retrospect view this type of flutter as a combination of classical wing flutter and panel flutter.

PANEL FLUTTER

Panels are natural structural elements for both aircraft and space vehicles. It would appear that the problem of saving weight would dictate that large parts of space vehicles will utilize panels and therefore may be designed by panel flutter considerations. Some panel flutter experience of the X-15 airplane was discussed in an earlier section. There is a large number of parameters and factors which affects panel flutter, such as, thickness, aspect ratio, material properties, curvature, edge supports and restraints, operating environment, pressure differences, etc. Both the experimental and analytical phases of the subject have to be pursued much further. A timely review of the analytical work and of the available experimental work was given by Fung early in 1960 (ref. 38). Some additional experimental data are given in references 39, 40, and 41. It is the purpose here to indicate some engineering criteria which include flutter data for corrugated panels designed to alleviate thermal stresses, and to present some information on effects of transient heating obtained analytically and experimentally.

Figure 14 (from reference 39) gives a summary of experimental results for a variety of panels, including some corrugated panels. Despite the many factors and parameters affecting flutter which are not shown explicitly, this rather simple plot suggested by theoretical consideration has proven to be useful for engineering design purposes. The ordinate is a commonly used panel flutter parameter which is directly proportional to the thickness required to prevent flutter. (It is the same as the ordinate used in figure 13, and involves the Mach number M, modulus of elasticity E, dynamic pressure q, thickness t, and length ℓ of the panel.) The abscissa is the length to width ratio of the panel. This summary plot contains results for panels of different sizes and materials, for Mach numbers from 1.6 to 6, at different temperatures, and with different midplane compressive

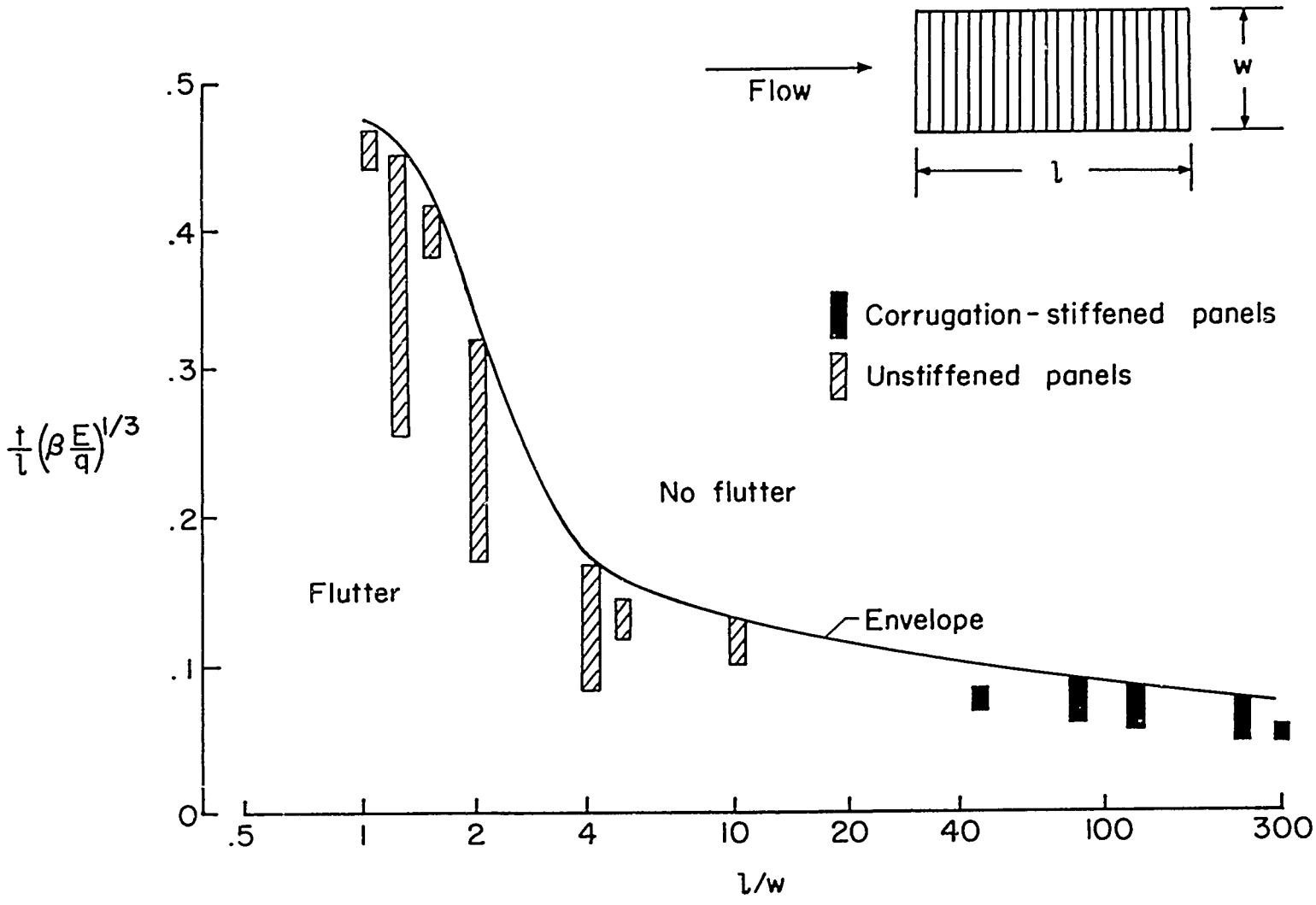


Figure 14.- Experimental summary for flutter of rectangular panels.

loadings and amounts of buckling. The panels were restrained on all four edges to a degree that was intermediate between tightly clamped and simply supported. The shaded bands are results obtained from unstiffened panels. The dark bands were obtained from corrugation-stiffened panels for which the corrugations of the stiffening undersurface were oriented normal to flow direction. For the corrugation-stiffened panels the determination of an effective thickness and width (effective in a structural sense as explained in reference 39) permits a logical inclusion of both types of panels on one plot. The upper envelope boundary specifies the thickness required to prevent flutter under the severest combination of test conditions for a given ratio of l/w. It is to be noted, however, that swept or yawed panels appear to require further study (ref. 41). Although the criterion type of plot is very useful for initial design studies, many refinements in the data will be required to assure allowable weight savings.

The condition under which panels seem to be generally most susceptible to a flutter instability is for the panel to be nearly or marginally buckled by a compressive edge loading. A common way for a panel to become buckled is by thermal expansion induced by aerodynamic heating. Some of the recent work in the Langley thermal structures tunnel has investigated the effect of transient heating on panel flutter. The interesting phenomenon has been observed that not only can a panel start fluttering as it is gradually heated by the airflow, but it can also stop and become stable again in a buckled condition, though the dynamic pressure and stagnation temperature of the airflow are held constant. Some experimental results of "start-stop" flutter are presented in references 39 and 40, and some of the data from the latter are shown in figure 15.

The figure shows results obtained on a flat aluminum-alloy panel which was divided by heavy stringers into bays, each of which had a length-to-width ratio of 10. The ordinate is the same as that of the previous figure. The abscissa is a measure of thermal stress and involves the coefficient α of thermal expansion, the amount of temperature increase ΔT of the center of a panel bay measured from the beginning of the test run, and the thickness to width ratio t/w. The plot shows for a large number of experimental tests, the start of flutter by the open circles and the cessation of flutter by the solid circles. A line has been faired through the experiments. A test time history that would exemplify many of the tests would be a straight horizontal line across the plot passing from the stable, flat-panel region, through the flutter region, and emerging into the stable buckled-panel region.

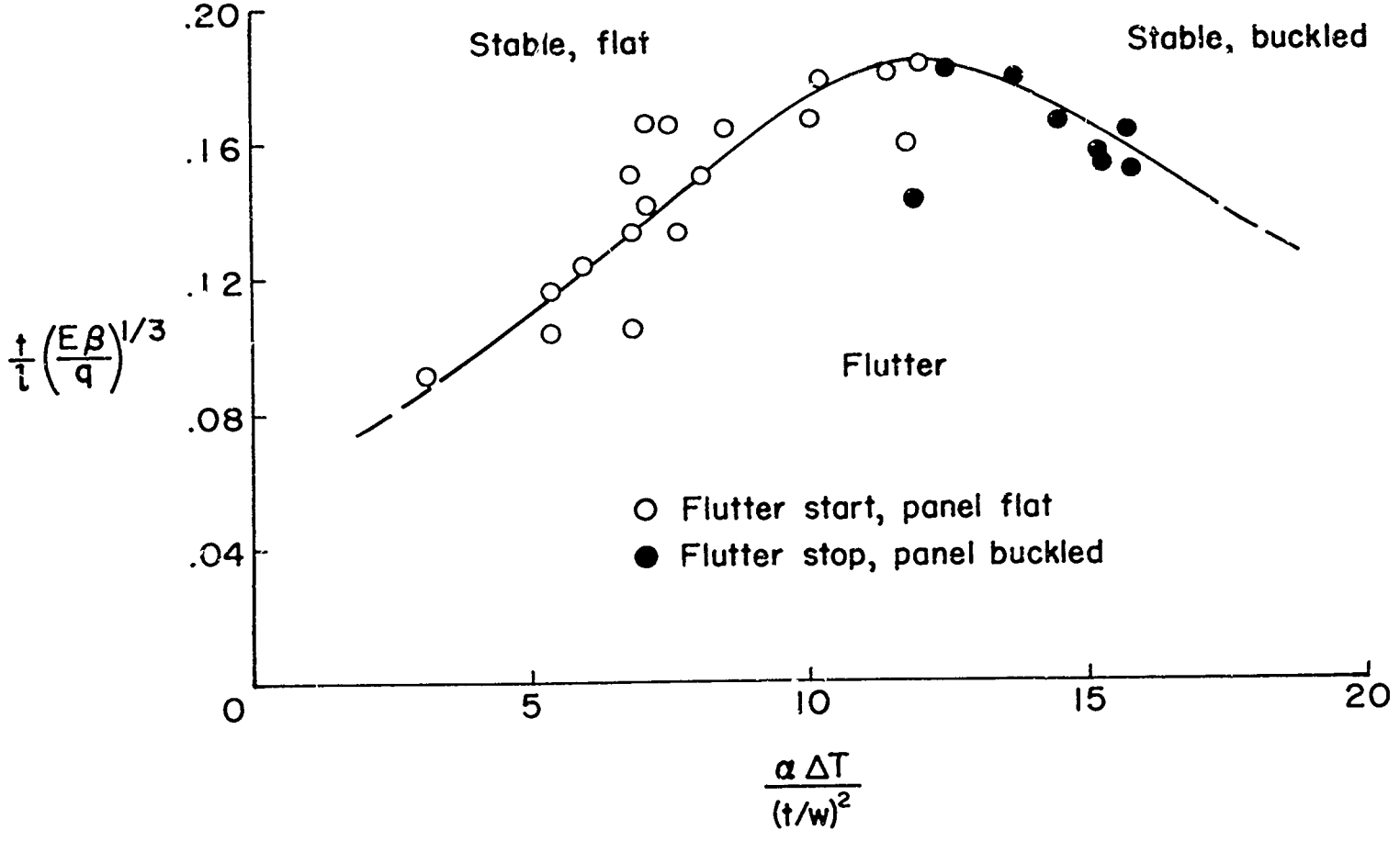


Figure 15.- Effects of aerodynamic heating on panel flutter.

In seeking a theoretical explanation of the start-stop flutter phenomenon involving buckling, it is of interest to examine the stability of buckled panels. For two-dimensional panels such a theoretical analysis was made by Fung in reference 42 for simply supported panels, and by Eisley in reference 43 for clamped-edge panels which are buckled by midplane compression loading. (Also, see discussion in reference 44.)

Some theoretical results are shown in figure 16 for isotropic square panels which are flat when unstressed. (These results are from yet unpublished work by R. W. Fralich of Langley Research Center for rectangular panels.) The edges of the panel are simply supported but are rigidly restrained from expanding outward as the panel heats up. The heating is assumed to yield a uniformly distributed temperature increase ΔT; the assumed edge restraint is associated with the compressive edge loadings P_x and P_y. The ordinate Q, found convenient by several previous investigators, is proportional to the cube of the inverse of the ordinate of the previous figure, but also includes the Poisson-ratio function $(1 - \nu^2)$. For the abscissa Fralich has used a parameter that is proportional to the amount by which the panel would expand due to ΔT, if it were free to do so (rather than the buckle height used by some previous investigators).

The figure applies to an initially unstressed panel, that is, $P_x = P_y = 0$ when $\Delta T = 0$. The dashed curve rising from the horizontal axis separates the region on the left where the panel is flat and stable, from the region on the right where the panel is stable in its primary buckling mode. Above the solid curves is the flutter region. The right-hand portion of the solid-line boundary was obtained on the basis of the von Kármán large-deflection plate theory and linearized static aerodynamic strip theory. A Galerkin modal solution was employed which made use of the first two static buckled modes. The left-hand solid-line boundary was obtained on the basis of small-deflection theory and using the first two vibration modes of the flat panel in a prebuckling condition.

The flutter boundaries on figure 16 may provide an explanation of the "start-stop" flutter phenomenon that has been found experimentally. A possible panel time-history for which the dynamic pressure q is constant and for which ΔT increases is shown by the horizontal dotted line ABCD. Between points A and B the plate is unbuckled and dynamically stable. From B to C it flutters. At C the plate stops fluttering and becomes stable in its first buckling mode, and the depth of the buckle continues to increase toward D. It is also of interest that Fralich has found that the slope of the right-hand portion of the flutter boundary can be increased or decreased by varying the initial edge compressive loadings P_x and P_y independently.

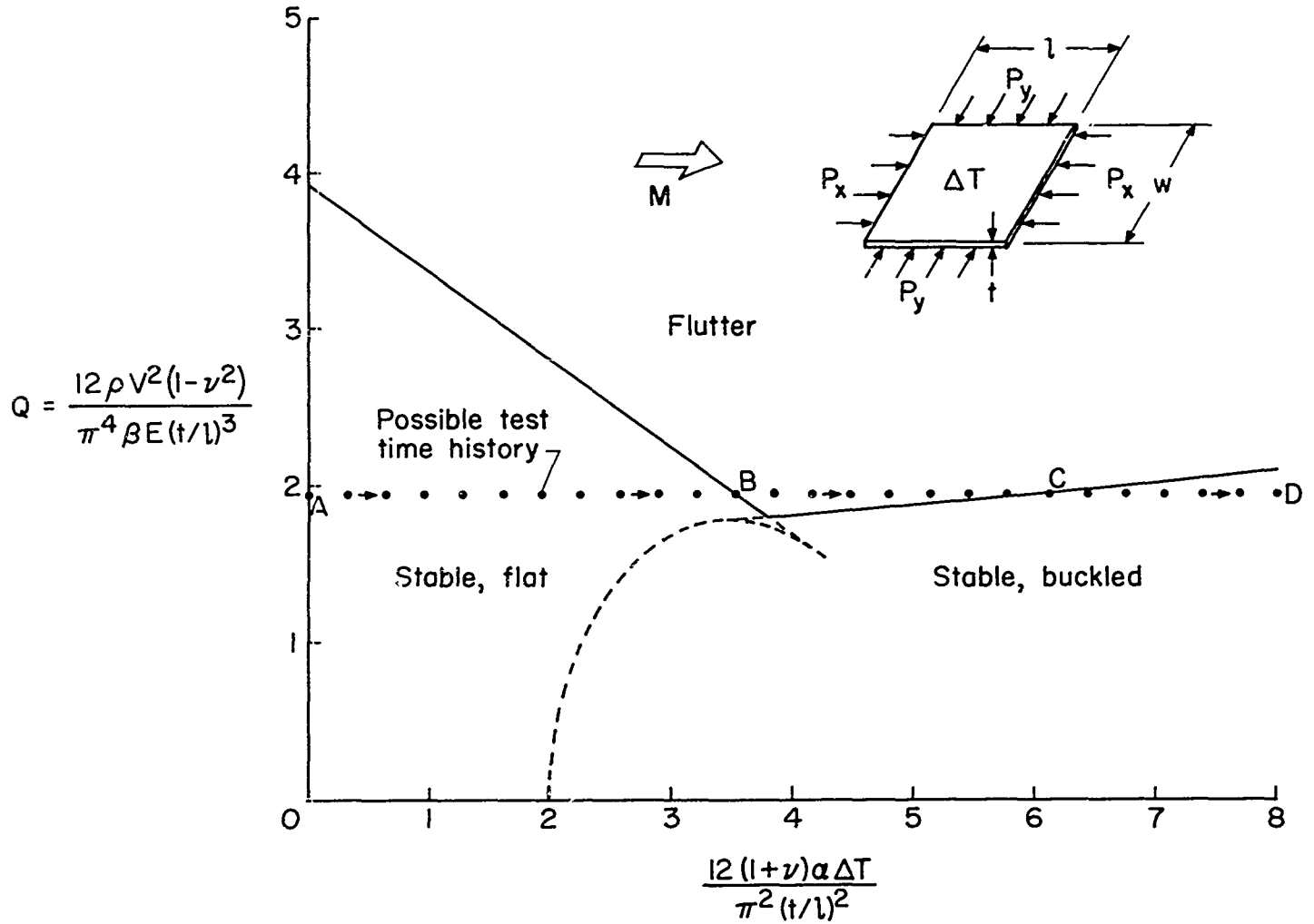


Figure 16.- Flutter boundary for a simply supported square plate with a uniform temperature increase.

The indications are that panel flutter will continue to be an important area for theoretical and experimental work, and one in which the thermal effects need careful resolution. Moreover, the closely associated phenomena of structural response to aerodynamic noise and buffeting for lightly damped panels or shells are also in the picture and need additional resolution.

AEROTHERMOELASTIC RESEARCH FACILITIES

There are few facilities that are suitable for experimental research on combined dynamic aerothermoelastic problems. The requirements are very severe for a facility that will produce the correct aerodynamic forces, aerothermal input, and provide sufficient range in dynamic pressures with adequate running times. It was mentioned earlier that correct scaling of model tests for all the significant parameters is possible only at a scale factor of 1.0. Thus, a full-scale test is generally desirable but obviously requires a very large wind tunnel, even for component testing. For most wind tunnels scale factors substantially different from 1.0 must be used, and it is necessary that the scaling laws for one or more of the significant parameters be compromised. Judicious selection of parameters and test procedures combined with analytical approaches, however, permit extrapolation to full-scale values with some degree of confidence.

With such a combined approach in mind, it is evident that a facility is useful even if it is capable of successfully isolating the effect of only a few parameters. For example, the heat input can be evaluated with a rigid model in a facility which achieves only the correct heat transfer characteristics; that is, with reference to figure 2 the aerothermal interaction line (H)(A) is studied. With the correct heat load determined, the change in structural properties can be evaluated by analysis or by a static heat test on a full-scale component or scaled model. Thus, the thermoelastic interaction line (H)(E) of figure 2 is considered. Finally, a wind-tunnel facility can be employed which correctly simulates only the aerodynamic inputs for testing a number of dynamic models scaled structurally to represent different critical conditions of temperature and dynamic pressure. In this way, the aerothermoelastic tetrahedron of figure 2 can be brought into the domain of the aeroelastic triangle (A)(E)(I).

Several facilities will be briefly mentioned that have contributed to the solution of dynamic aerothermoelastic problems. The dynamic pressure-Mach number range of wind tunnels frequently used for aeroelastic testing at Langley are shown on figure 17. It is emphasized that this list is not complete, as no attempt has been made to include herein other available wind tunnels or shock tube facilities. Also shown here are nominal boundaries for several launch vehicles. The

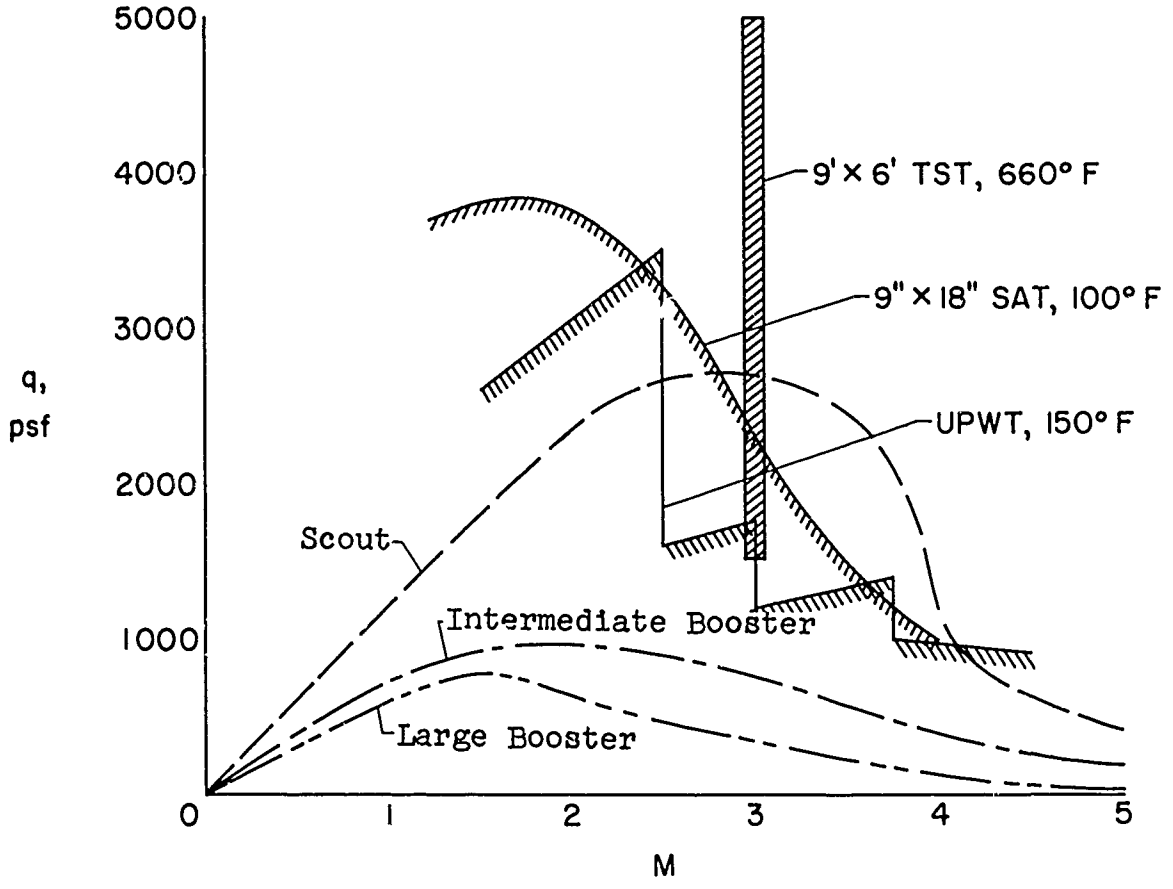
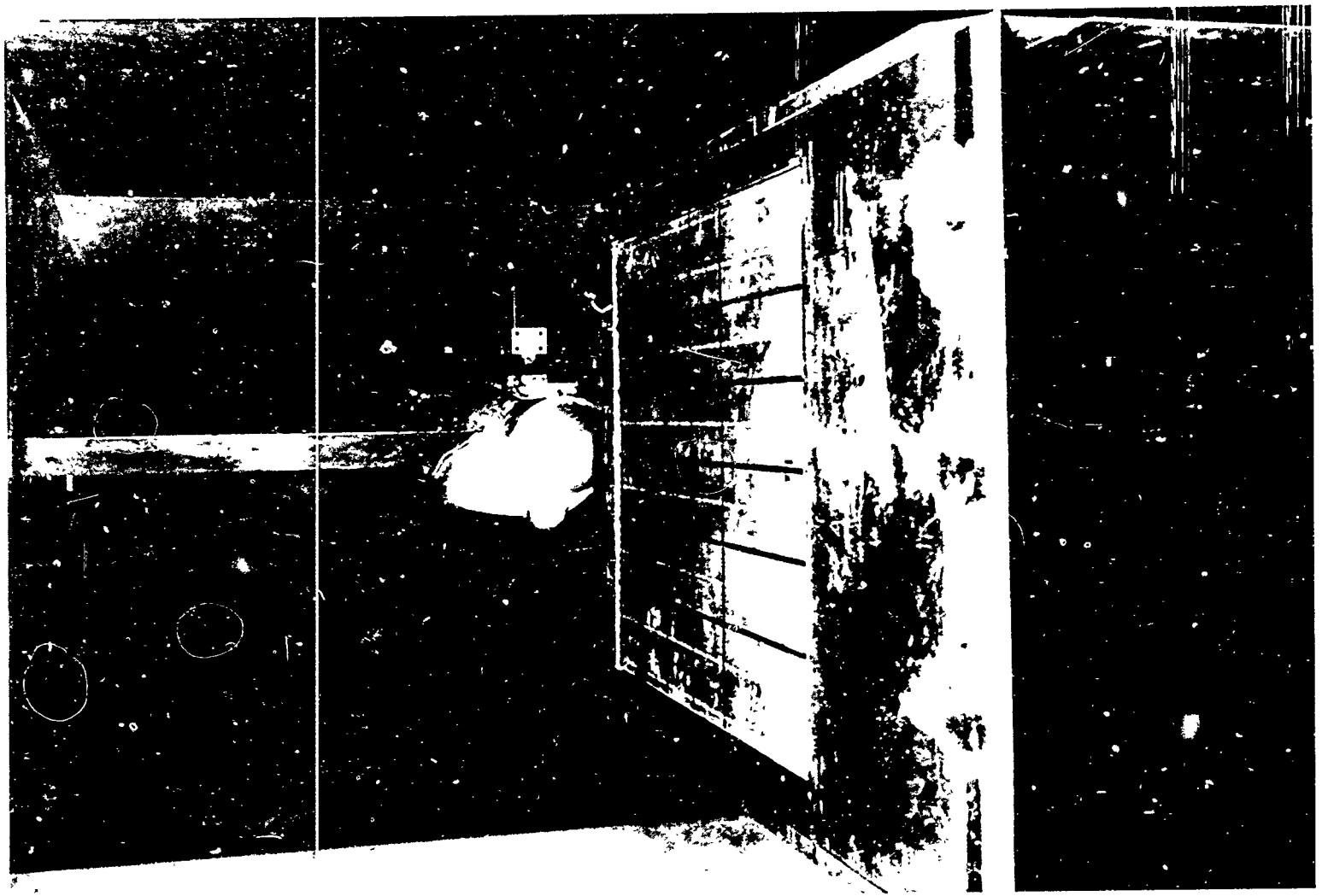


Figure 17.- Dynamic pressure Mach number ranges for three NASA-Langley wind tunnels useful for aerothermoelastic research.

9- by 18-inch supersonic aeroelasticity tunnel (SAT) operates at ambient stagnation temperature and is used for evaluating aerodynamic inputs and for testing aeroelastic models. Although ambient stagnation temperatures are used, some effects of transient heating have been obtained in this facility. The unitary plan wind tunnel (UPWT) indicated on figure 17 is basically an ambient temperature facility and is used to evaluate aerodynamic inputs and aeroelastic interactions. However, it has also been used to simulate temperature effects in the case of panel flutter. Figure 18 illustrates a panel flutter installation. The panel for the test shown is mounted on a splitter plate which removes the panel from the thick wall boundary layer. For tests wherein temperature effects are simulated, the splitter plate assembly is reversed, and the panel is heated by a bank of quartz radiative heat lamps. Thus, certain temperature effects are simulated without large stagnation temperatures in the test medium. The thermal structures tunnel (TST) indicated in figure 17 attains stagnation temperatures to 660° F. The large (9- by 6-foot) test section, large dynamic-pressure range, and running times of over one-half minute permit simulation of aerothermoelastic effects. The facility correctly simulates the aerodynamic and temperature conditions for $M = 3$ flight, and is frequently used for testing a wide variety of full-scale components. Figure 19 shows a full-scale vertical tail of the X-15 airplane installed in the test section of the thermal structures tunnel. This wind tunnel is thus seen to be an impo tant research tool in the field of aerothermoelasticity, and it plays a special role for supersonic aircraft research.

In figure 20 are shown several hypersonic facilities in operation and under construction. Shock tunnels, low-dynamic-pressure facilities and wind tunnels with very short running times are not included on this figure, although these facilities are required to study aerothermal aspects. The solid bars indicate facilities in operation that are used for aeroelasticity tests while the open bars represent facilities under construction that will contribute to the solution of aerothermoelastic problems. The wind tunnels shown fall into two classes, those for study of aeroelasticity problems and those for conduct of aerothermal research. Also shown are approximate boundaries for an anti-missile and for a lunar reentry vehicle. The facilities are seen to provide a good degree of coverage of dynamic pressure and Mach numbers for the trajectories shown.

There are other facilities, notably the wind tunnels at Tullahoma that simulate high temperatures and Mach numbers and are large enough to conduct tests of full-scale components. A flight test bed has also been proposed whereby a missile reentry nose cone of a large booster will be fitted with models to study aerodynamic forces, heat transfer, and aerothermoelasticity phenomena at reentry Mach numbers and under very high heating rates. Scaled models must be used, hence complete aerothermoelastic simulation is not achieved. Such tests are very expensive.



NASA
L-59-7228

Figure 18.- Installation in Unitary Plan wind tunnel for panel flutter study.

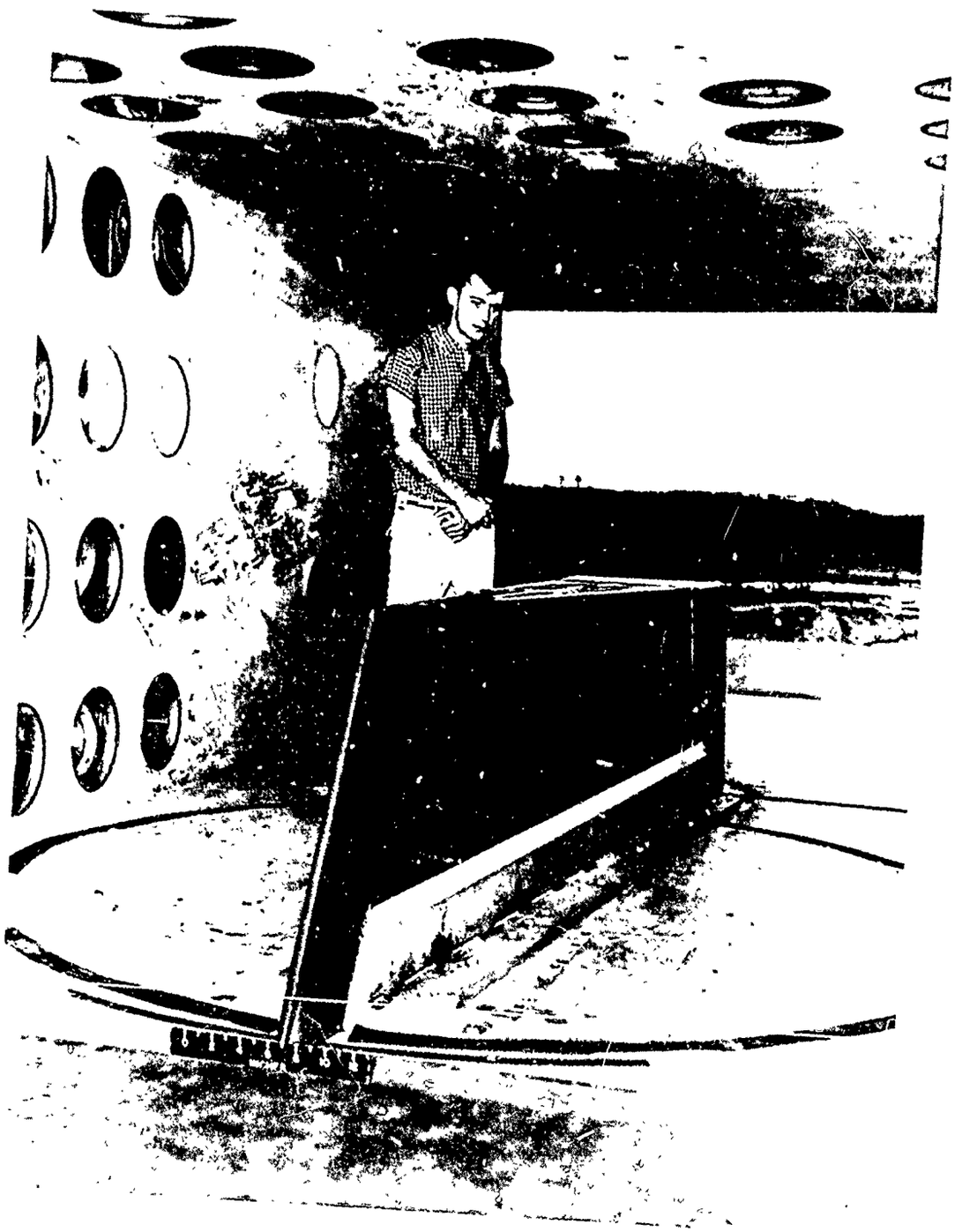
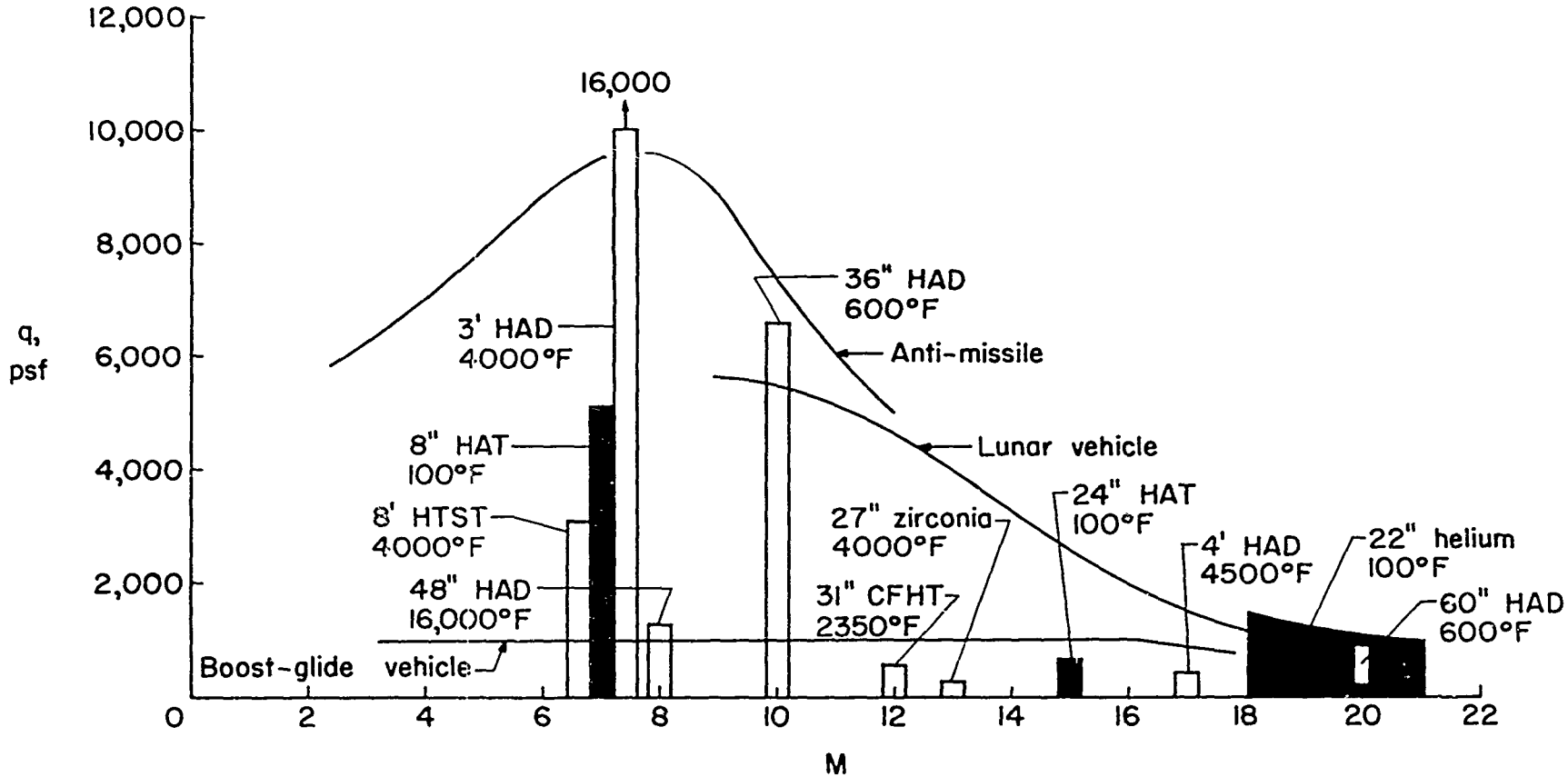


Figure 19.- Vertical tail of X-15 airplane in the 9- by 6-foot thermal structures tunnel.

NASA
L-59-5208



NASA

Figure 20.- Characteristics of several NASA-Langley hypersonic facilities, in operation and under construction, useful for aerothermoelastic research. HAD - hypersonic aerothermal dynamics facility; HAT - hypersonic aeroelasticity tunnel; HTST - high-temperature structures tunnel; CFHT - continuous-flow hypersonic tunnel.

It is thus seen that facilities are available for aeroelastic research over the Mach number range of significance, but the combined test facilities which include thermal effects are restricted to the medium supersonic range. At higher Mach numbers the aeroelastic and thermoelastic contributions are generally studied separately although some partial simulation is possible.

CONCLUDING REMARKS

The foregoing brief survey of developments in aerothermoelasticity has intentionally been partly general and also partly specific. The interrelationship of the various technological disciplines has been stressed and illustrated by several applications. There are both purely scientific aspects aimed at prediction and understanding, and engineering or technological aspects aimed at simplified criteria, reliability, safety, and structural efficiency and integrity. Both aspects naturally interact and in research there is the need to pursue them both; on the one hand, with simple laboratory models, with analysis, and controlled experiments; on the other hand, with specific component testing, with environmental studies and with large-scale facilities. The aerothermoelastic field will clearly continue to offer problems and challenges for many years to come for both science and technology.

In closing, the kind assistance of A. G. Rainey, D. J. Martin, and of Miss Vera Huckel in the preparation of material and figures for some of the sections is acknowledged.

REFERENCES*

1. Bisplinghoff, R. L., Some Structural and Aeroelastic Considerations of High-Speed Flight (Nineteenth Wright Brothers Lecture), Jour. Aero. Sci., Vol. 23, No. 4, pp. 289-321, April 1956

2. Bisplinghoff, R. L., and Dugundji, John, Influence of Aerodynamic Heating on Aeroelastic Phenomena, Chapter 14 of High Temperature Effects in Aircraft Structures, AGARDograph No. 28, editor Nicholas John Hoff, Pergamon Press, 1958. pp. 288-312.

3. Rogers, Milton, Aerothermoelasticity, Aerospace Engineering, Vol. 17, No. 10, October 1958. pp. 34-43.

4. Chadwick, P., Thermoelasticity, The Dynamical Theory, Chapter VI of Progress in Solid Mechanics, Vol. I, edited by I. N. Sneddon and R. Hill, North-Holland Publishing Co., Amsterdam, 1960

5. Many authors, Final Flutter Analyses, X-15 Airplane, North American Aviation, Inc., Rep. No. NA-60-1334, June 30, 1961. pp. 10-11.

6. Becker, John V., Re-entry from Space, Scientific American, Vol. 204, No. 1, January 1961. pp. 49-57.

7. Johnston, E. W., and Johnson, R. N., Analysis of Sub-Orbital Vehicle Reentry Constraints, North American Aviation, Inc., Rep. No. NA-61-167, February 3, 1961, paper presented at American Rocket Soc., Lifting Reentry Vehicles: Structures, Materials and Design Conf., Palm Springs, Calif., April 4-6, 1961

8. Turner, M. J., Dill, E. H., Martin, H. C., and Melosh, R. J., Large Deflections of Structures Subjected to Heating and External Loads, Jour. Aero Sci., Vol. 27, No. 2, February 1960. pp. 97-106.
   and
   Turner, M. J., The Direct Stiffness Method of Structural Analysis, Boeing Airplane Co., presented at the Structures and Materials Panel of AGARD, Aachen, Germany, September 17, 1959

---

* Many appropriate additional references are to be found in the bibliographies of the cited references.

9. Gallagher, R. H., Quinn, J. F., and Padlog, J., Deformational Response Determinations for Practical Heated Wing Structures, Bell Aerosystem Co., presented at Symposium on Structural Dynamics of High-Speed Flight, Los Angeles, Calif., April 24-26, 1961
and
Gallagher, R. H., Quinn, J. F., and Turrentine, Donald, Thermal Effects on Static Aeroelastic Stability and Control, Part III - Experimental and Analytical Methods for the Determination of Thermally-Affected Wing Deflectional Behavior, WADC Technical Report 58-378, December 1959

10. Argyris, J. H., and Kelsey, S., Energy Theorems and Structural Analysis, Butterworths Scientific Publications, London, England, 1960, (originally in Aircraft Engineering, October 1954 to May 1955)

11. Lansing, W., Jones, I. W., and Ratner, P., A Matrix Force Method for Analyzing Heated Wings, Including Large Deflections, Grumman Aircraft Engineering Corp., Report No. ADR 04-03b-61.1, May 1961, also presented at Symposium on Structural Dynamics of High Speed Flight, Los Angeles, Calif., April 24-26, 1961

12. Mar, J. W., and Pian, T. H. H., Structural Developments of New Interest to the Aeroelastician, Chapter 2 of Aeroelasticity - Notes for a Special Summer Program, Mass. Inst. of Tech , June 23-July 3, 1958
and
Mar, J. W., and Dugundji, John, Aerodynamic Heating Effects on Aeroelasticity, Chapter 4, same reference.

13. Houbolt, John C., A Study of Several Aerothermoelastic Problems of Aircraft Structures in High-Speed Flight, Mitteilungen aus dem Institut für Flugzeugstatik und Leichtbau an der ETH, Zürich, Nr. 5, Verlag Leemann, Zürich, 1958

14. Biot, M. A., New Thermomechanical Reciprocity Relations with Application to Thermal Stress Analysis, Jour. Aero. Sci., Vol. 26, No. 7, July 1959. pp. 401-408

15. Fung, Y. C., An Introduction to the Theory of Aeroelasticity, John Wiley and Sons, 1955

16. Bisplinghoff, R. L., Ashley, H., and Halfman, R. L., Aeroelasticity, Addison-Wesley Pub. Co., Cambridge, Mass., 1955

17. Miles, J. W., The Potential Theory of Unsteady Supersonic Flow, Cambridge University Press, 1959

18. Miles, J. W., Unsteady Flow at Hypersonic Speeds, Proceedings of the Eleventh Symposium of the Colston Research Society, University of Bristol, April 6-8, 1959, pp. 185-201, Butterworths Scientific Publications (London)

19. Hayes, Wallace D., and Probstein, Ronald F., Hypersonic Flow Theory, Academic Press, Inc., New York, 1959

20. Zartarian, Garabed, Hsu, Pao Tan, and Ashley, Holt, Dynamic Airloads and Aeroelastic Problems at Entry Mach Numbers, Jour. Aero. Sci., Vol. 28, No. 3, March 1961. pp. 209-222.

21. Calligeros, John M., and Dugundji, John, Similarity Laws Required for Experimental Aerothermoelastic Studies, M.I.T. ASRL Tech. Rep. 75-1 for ONR, May 1959; also Part 2 - Hypersonic Speeds, M.I.T. ASRL Tech. Rep. 75-2 for ONR, February 1961

22. Molyneux, W. G., Scale Models for Thermoaeroelastic Research, RAE Technical Note No.: Structures 294, March 1961

23. Fay, J. A., and Riddell, F. R., Theory of Stagnation Point Heat Transfer in Dissociated Air, Jour. Aero. Sci., Vol. 25, No. 2, February 1958. pp. 73-85, 121.

24. Lees, Lester, Laminar Heat Transfer over Blunt Nosed Bodies at Hypersonic Flight Speeds, Jet Propulsion, Vol. 26, No. 4, April 1956. pp. 259-269.

25. Roberts, Leonard, Ablation and Atmospheric Entry, NASA Langley Research Center, presented to the Structures and Materials Panel of AGARD, Paris, France, May 22-26, 1961

26. Heldenfels, Richard R., Frontiers of Flight Structures Design, pp. 29-51 of Aeronautics and Astronautics, Proceedings of the Durand Centennial Conference held at Stanford University, August 5-8, 1959, edited by N. J. Hoff and W. G. Vicenti, Pergamon Press, Inc., 1960

27. Rhode, Richard V., and Houbolt, John C., The Impact of Space Technology on Research and Development - Structures and Materials, NASA, presented before the General Assembly of AGARD, Copenhagen, Denmark, October 20-29, 1958

28. Vosteen, Louis F., Effect of Temperature on Dynamic Modulus of Elasticity of Some Structural Alloys, NACA TN 4348, August 1958

29. Hill, W. H., Shimmin, K. D., and Wilcox, B. A., Elevated-Temperature Dynamic Moduli of Metallic Materials, American Society for Testing Materials, Preprint No. 74, 1961

30. Many authors, Symposium on Determination of Elastic Constants, American Society for Testing Materials, Special Technical Publication No. 129, 1952

31. Levitt, A. P., and Martin, A. G., Ultrasonic Determination of Elastic Constants of Metals at Elevated Temperatures, Watertown Arsenal Laboratories Technical Report No. WAL TR 143/34, September 1959

32. Heldenfels, Richard R., and Vosteen, Louis F., Approximate Analysis of Effects of Large Deflections and Initial Twist on Torsional Stiffness of a Cantilever Plate Subjected to Thermal Stresses, NACA Report 1361, 1958

33. McWithey, Robert R., and Vosteen, Louis F., Effects of Transient Heating on the Vibration Frequencies of a Prototype of the X-15 Wing, NASA TN D-362, May 1960

34. Runyan, Harry L., and Jones, Nan H., Effect of Aerodynamic Heating on the Flutter of a Rectangular Wing at a Mach Number of 2, NASA TN D-460, June 1960

35. Budiansky, Bernard, and Mayers, J., Influence of Aerodynamic Heating on the Effective Torsional Stiffness of Thin Wings, Jour. Aero. Sci., Vol. 23, No. 12, December 1956, pp. 1081-1093, 1108.

36. Hanson, Perry W., and Levey, Gilbert M., Experimental and Calculated Results of a Flutter Investigation of Some Very Low Aspect-Ratio Flat-Plate Surfaces at Mach Numbers from 0.62 to 3.00, NASA TM X-53, August 1959 (Report confidential, title unclassified)

37. Bisplinghoff, Raymond R., The Finite Twisting and Bending of Heated Elastic Lifting Surfaces, Mitteilungen aus dem Institut für Flugzeugstatik und Leichtbau an der ETH Zürich, Nr. 4, Verlag Leeman, Zürich, 1957

38. Fung, Y. C. B., A Summary of the Theories and Experiments on Panel Flutter, AFOSR TN 60-224, Calif. Inst. of Tech., May 1960

39. Kordes, Eldon E., Tuovila, Weimer J., and Guy, Lawrence D., Flutter Research on Skin Panels, NASA TN D-451, September 1960

40. Dixon, Sidney C., Griffith, George E., and Bohon, Herman L., Experimental Investigation at Mach Number 3 of Effects of Thermal Stress and Buckling on the Flutter of 4-Bay, Aluminum-Alloy Panels with Length-Width Ratios of 10, NASA TN D-921, 1961

41. Kordes, Eldon E., and Noll, Richard B., Flight Experience of Panel Flutter, NASA TN D-1058, 1961, also presented at Amer. Rocket Soc. Lifting Reentry Vehicles: Structures, Materials, and Design Conf., Palm Springs, Calif., April 4-6, 1961

42. Fung, Y. C., The Flutter of a Buckled Plate in a Supersonic Flow, AFOSR TN 55-237, Calif. Inst. of Tech., July 1955

43. Eisley, J. G., The Flutter of a Two-Dimensional Buckled Plate with Clamped Edges in a Supersonic Flow, AFOSR TN 56-296, Calif. Inst. of Tech., July 1956

44. Garrick, I. E., Some Concepts and Problem Areas in Aircraft Flutter (The 1957 Minta Martin Aeronautical Lecture at Mass. Inst. of Tech), S.M.F. Fund Paper No. FF-15, Inst. of the Aero. Sci., March 1957

PROGRESS IN AEROTHERMOELASTICITY OUTSIDE THE UNITED STATES

by

Peter A. Castruccio*

Aeronca Manufacturing Corporation

and

Milton Rogers**

Air Force Office of Scientific Research

ABSTRACT

A synthesis of the foreign unclassified literature in Aerothermoelasticity is presented. The field of Aerothermoelasticity is classified by salient subordinate disciplines, and the principal theoretical and experimental design and verification tools for each discipline are listed and briefly described. Within this framework of classification, essential characteristics of foreign efforts, particularly Soviet, as gleaned and deduced from the literature, are described and discussed.

* Director of Research, Aeronca Manufacturing Corporation
**Chief, Mechanics Division, Air Force Office of Scientific Research

PROGRESS IN AEROTHERMOELASTICITY OUTSIDE THE UNITED STATES

INTRODUCTION

Aerothermoelasticity is a young science. As such, the interpretation of its content and purpose and of its subdivisional branches varies somewhat from country to country.

To achieve a uniform understanding, or, as the mathematicians would say "to normalize the meaning", a brief review and a statement of definitions is important.

Consider a solid body moving in a uniform compressible fluid. If this body be considered rigid, the study of the interaction between the fluid and the solid constitutes the science of classical Aerodynamics.

This science, which yielded satisfactory results in the early days of aircraft design, is based upon an assumption which is only partially valid. As in all things scientific, design predictions are based upon a "model" or "models" which the scientist attempts to cast as closely as possible in adherence to nature. Soon after the establishment of any model, the state of the art pushes onward and one finds that the model becomes progressively less adequate. Thus the model is successively refined and each major refinement leads to a more comprehensive reformulation of the science employing a new model which encompasses the last one as a special case. This evolutionary process stems basically from the inability of the human mind to visualize at once all the variables and their potential relationships. This process is typical of the evolution of early aerodynamics into aerothermoelasticity. The first step in the evolution came about with the discovery of the phenomena of divergence and later flutter. This led to the realization that, in practice, solid bodies, and particularly airframes, cannot be considered rigid but rather must be viewed as elastic, meaning that

they are endowed with the property of deforming under the loads caused by the fluid. More generally, elasticity implies capability of storing energy. The interaction of a solid body considered elastic, with a fluid forms the domain of Static Aeroelasticity; which deals with the deformations and induced stresses in elastic structures interacting with a moving fluid.

As the speed of aircraft has increased, aeroelastic considerations have assumed increasing importance in the design of airframes. In fact, today they impose very significant design bounds on the structural analyst.

In addition to elasticity, real bodies in motion possess the property of inertia, which provides another form of energy storage. The interaction between inertia and elasticity gives rise to a class of phenomena which forms the realm of a rather specialized branch of technology dealing with vibrations.

The interaction between a structure possessing elasticity and inertia and a moving fluid constitutes the domain of Dynamic Aeroelasticity, which includes: the transient response of structures to gusts and other non-uniform perturbations in the fluid (buffeting); the response of the structure to the unsteady motion of the fluid (flutter). In some ways, dynamic aeroelasticity is analogous to the transient response of circuits, familiar to the electrical engineer.

The models corresponding to the definitions above have proven adequate for the design of high-performance structures up to speeds in the moderate supersonic region. As speeds increase beyond Mach 3 or 5, the passage of the structure through the fluid causes an appreciable temperature increase within the fluid due to molecular impact and viscous friction effects. This temperature increase in the gas stream transfers heat to the structure and causes a new series of phenomena, to wit:

1. Deformation of the structure, caused either by uniform temperature increases acting on restrained structures, dissimilar materials, or by temperature gradients across the structure.

2. Changes in the elastic moduli of the materials comprising the structure. These affect the vibrational, deflectional, and stress-strain characteristics of the structure.

3. Changes in the stress characteristics. These affect the yield point and therefore the integrity of the structure.

4. Changes in the properties of the fluid itself. Up to the lower hypersonic velocities, these changes occur primarily in the parameters of density, viscosity, and thermodynamical properties of the fluid.

The study of the behavior of an elastic structure under the influence of heat constitutes the domain of Thermoelasticity. The motion of an elastic, inertial structure through a fluid at sufficiently high speeds to generate important thermal effects forms the domain of Aerothermoelasticity. As aeroelastic considerations have been a dominant factor in the design of modern high speed airframes, it is likely that aerothermoelastic considerations may assume increasing importance as we enter the hypersonic era.

As speeds increase towards the Mach 25 region (Aerospace plane et similia) the temperature rises to a point where substantial ionization of the fluid may occur. A mixture of fluid and plasma may surround the moving structure. When the plasma effects become appreciable or can be utilized for specific purposes, can a new branch of the science be expected to arise: Aerothermomagnetoelasticity?

The research effort in Aerothermoelasticity has concerned itself with fluids closely resembling the composition of the earth's atmosphere. The advent of planetary exploration in depth will require extending our model to fluids of radically different composition, such as can be anticipated for Venus and eventually for the giant planets. These investigations will probably give rise to anotner branch of the science: Planetary Atmothermo(magneto)elasticity, which can be expected to acquire significant importance when the go-and-return interplanetary vehicle becomes reality. This vehicle will have to withstand the environment of different atmospheres and must be designed accordingly. Table I recapitulates these definitions.

Aerothermoelasticity is fundamental to the design of all high performance vehicles, whether US or foreign, which move through the atmosphere, from supersonic transports to glide re-entry vehicles. It should be noted in passing, that the full exploitation of this branch of science is important only if advanced, efficient designs are sought. Because of present propulsive power limitations, efficient structural designs are essential and thus an appreciable period of growth can be forecast for this science.

TABLE I

DEFINITIONS AND MODELS IN AEROTHERMOELASTICITY

DISCIPLINE	MODEL	
	FLUID	STRUCTURE
AERODYNAMICS	Cold (air)	Rigid
STATIC AEROELASTICITY	Cold (air)	Elastic
DYNAMIC AEROELASTICITY	Cold (air)	Elastic-inertial
AEROTHERMODYNAMICS	Hot (air)	Rigid
THERMOELASTICITY	-	Elastic-hot
AEROTHERMOELASTICITY	Hot (air)	Elastic-hot inertial
AEROTHERMOMAGNETOELASTICITY	Plasma-air	Elastic-hot inertial
ATMOTHERMO(MAGNETO)ELASTICITY	Plasma-planetary atmosphere	Elastic-hot inertial

For purposes of orientation, the principal trends in the United States which today underlie aerothermoelastic design and experimentation are briefly reviewed. The dominant theme in the field, as far as design is concerned, is to divide the total analysis into separate investigations of the aeroelastic and the aerothermal behavior of the structure. The results achieved by the two concurrent methods are then matched by successively converging approximations until the total design results.

Modern advanced research efforts consist of attempting to recognize when the aeroelastic and the aerothermal problems can be uncoupled and when the uncoupling is not sufficiently realistic for the purpose at hand.

In general, the approaches used in the US today are primarily semi-empirical in nature, meaning that they serve as design confirmation. No comprehensive synthesis approach, from which the structure can be designed directly from knowledge of the problem, is as yet available.

ELEMENTS OF AEROTHERMOELASTICITY

The principal subdivisions of Aerothermoelasticity and the design tools currently employed in each are:

A. Theoretical Tools

1. Aeroelasticity

a. Static aeroelasticity

(1) Structural divergence

Concerns itself with the determination of elastic structural deflections caused by the fluid flow. Its purpose is the elimination deflections, such as may cause control reversal or structural failure.

(2) Stress analysis

Concerns itself with the determination of safety limits. Its purpose is to ensure the structural integrity of the vehicle.

The principal theoretical and design tools employed in static aeroelasticity are:

(a) Tabulation schemes employing numerical computation.

(b) Methods based upon structural influence coefficients, employing numerical computation. The influence coefficients are either measured experimentally or calculated.

(c) Methods based upon aerodynamic influence coefficients, either measured or calculated. These methods are applied via numerical computations.

(d) Modal methods which are partially numerical and partially analytical.

(e) Closed form mathematical analysis.

(3) Static stability and control

Concerns itself with the interaction between the airstream and the vehicle considered as a system. The principal tools employed here, in addition to static ae oelasticity, are those of aerodynamic equilibrium of forces and moments.

Of these, preferred today in the United States are the numerical methods in which the structure is subdivided into boxes or volume quanta, with the inputs also quantized, and with the computation performed on computing machines.

b. Dynamic aeroelasticity

(1) Steady state stability (flutter)

Concerns itself with the determination of the critical speed and/or critical structural parameters which give rise to a dynamic aeroelastic condition wherein the flexible airframe interacts with the airstream to cause a sustained oscillation which may grow to destructive amplitude. At present, no attempt is made to control this. Its effects are avoided by placing the speed at which flutter occurs above the maximum design speed of the vehicle.

(2) Stress analysis

Concerns itself with determining transient loads and stresses resulting from the application of forces such as wind gusts, or from accelerations of the vehicle.

Both peak and fatigue stresses are of interest. As discussed before, flutter analysis can be considered a special case of the total transient behavior, although for practical reasons it is emphasized separately.

The basic theoretical design tools employed in dynamic aeroelasticity are the following:

(a) Flutter analysis, which employs analytical vibration theory in conjunction with aerodynamic theory.

(b) Modal methods, employing time-dependent forcing functions.

(c) Numerical tabulation schemes. Paramount under these is the total unified approach in which the influence coefficients and tabulation schemes of static aeroelasticity are used with the addition of inertial terms.

(3) Dynamic stability and control including autopilot

Concerns itself with the dynamic control problem of the vehicle. Principal theoretical tools are servo analysis and linear and non linear control system synthesis.

2. Aerothermodynamics

a. Fluid dynamics

Investigates the energy content in the fluid stream under dynamic conditions. For our problem, the energy content in the fluid layers adjacent to the body is controlling. For flows without such an adjacent layer (e.g. free-molecule flow), the direct transfer of energy to the structure due to molecular motion may be used.

The principal theoretical tools are:

(1) The Navier-Stokes equations and various corollaries and simplifications thereof.

(2) The momentum transfer equations, and collaries and simplifications thereof.

(3) Numerical methods derived from the analytical tools above.

b. Heat transfer

Is concerned with the transfer of heat from the fluid to the structure and with the flow of heat and the distribution of temperature within the structure.

The principal theoretical tool is heat transfer theory and various numerical methods derived therefrom.

c. Aerothermochemistry

Is concerned with the chemical changes in the fluid caused by temperature and their effects upon the properties of the fluid. Included in this category are also investigations of the changes in physico-chemical properties of the material composing the structure, which cause such phenomena as sputtering, oxidation and ablation.

The basic tool of this science is physical chemistry.

3. Thermoelasticity

a. Effect of heat upon properties of materials

Concerns the changes in elastic properties of materials, such as degradation of Young's modulus, change of yield point, etc. caused by heat.

b. Thermostress analysis

Investigates the behavior of structures under the simultaneous occurrence of thermal loads and structural loads.

The principal tools employed to study the effects of elevated temperatures upon the properties of materials are yet experimental. With additional progress in the science of solid state physics, analytical tools for accurate prediction of thermoelastic changes should come to the foreground.

4. Aerothermoelasticity

Is concerned with the total interaction of the environment and the structure. Its object is the design prediction of structural performance under the simultaneous application of airloads and thermal loads. Its theoretical and design tools are as yet confined to the verification by successive approximations of the results achieved by the aeroelastic, aerothermodynamic, and thermoelastic analyses.

The theoretical design tools are recapitulated in Table II.

B. Experimental Tools

Experimental tools are of major importance in the substantiation of design criteria and in the verification of structures in the aeroelastic and aerothermoelastic regime.

These are:

1. Ground tests

a. Ground vibration resonance survey

Performed upon the full-scale vehicle, suspended in simulated flight conditions, by means of special vibrating units and special transducers.

b. Static tests

Performed by applying static forces to the full-scale structure, and measuring corresponding deflections. Thermal effects are produced by means of heat lamps, heat blankets, etc.

2. In-flight tests

a. Stick-bang, rudder-kick, explosive charge techniques

TABLE II

THEORETICAL DESIGN TOOLS IN AEROTHERMOELASTICITY

DISCIPLINE	THEORETICAL DESIGN TOOLS
STATIC AEROELASTICITY	Tabulation schemes Structural influence coefficients Aerodynamic influence coefficients Modal methods Closed form analysis
DYNAMIC AEROELASTICITY	Flutter analysis Modal methods Unified numerical approach Serve analysis
AEROTHERMODYNAMICS	
Fluid Dynamics	Navier-Stokes equations and corollaries Momentum transfer equations and corollaries Numerical methods
Heat Transfer	Thermodynamic theory
Aerothermochemistry	Physical chemistry
THERMOELASTICITY	Experimental Solid state physics Statics
AEROTHERMOELASTICITY	Successive checks from aeroelastic, thermoelastic, and aerothermodynamic computations

Artificial perturbations to the control surfaces applied by man or by mechanical programmers. They are generally useful only if a previous theoretical analysis has been performed.

b. Steady-state excitation techniques

Performed either by causing periodic control modulation or by vibrating the entire structure by means of a vibration exciter.

The measurement technqiue consists of noting the decay rates and frequency changes.

c. Impulsive testing

With impulsive testing, the structure is excited by ballistic devices (such as rotating rockets on the wing tips). Measurement is performed by noting characteristic frequency changes and mode decays.

In-flight testing is inherently dangerous and safety measures such as controllable mass changes during flight are sought to assure safety.

3. Model testing

a. Wind tunnels

Useful for correlations between models and full-size structures.

b. Free-fall model testing

c. Rocket-power model testing

Can be applied in two distinct modes:

(1) With ground sleds

(2) With rocket boosters.

The experimental tools currently employed are recapitulated in Table III.

TABLE III

EXPERIMENTAL TOOLS IN AEROTHERMOELASTICITY

GROUND TESTS

Vibration resonance survey

Static tests

FLIGHT TESTS

Stick-bang technique

Steady-state excitation

Impulsive testing

MODEL TESTS

Wind tunnel

Free fall

Rocket power, by ground sled or by rocket boost

PHASES OF TECHNOLOGICAL ACTIVITY

At this point it is well to regain our perspective. In the remainder of this paper an attempt will be made to estimate the adequacy of the current understanding of, and applications of, Aerothermoelasticity to the design of efficient, high-performance airframes; either on the board today or projected for the foreseeable future.

From the perspective of practical engineering design of a structure, the state-of-the-art in the U.S. and the Free World vis-a vis that of the U.S.S.R. and of the Communist World will be compared. Possible gaps in our state-of-the-art will be indicated and methods hopefully will be suggested for swinging the balance of technology in our favor.

It is difficult at best to assess the state-of-the-art in structural design as it is actually practiced by only reviewing and analyzing published literature. The reasons for this are to be found in the manner in which practical structural design is performed.

Following are the basic steps which bridge the gap from initial conception to final embodiment of any high-performance structure.

1. Establishment of the Mathematical Model

   The first step after the structure has been visualized is the construction of a simplified mathematical model, which is generally a degenerated form of the equations of classical mathematical physics so chosen as to include no more and no less than the phenomena of importance in the problem under consideration.

2. Experimental Data

   These may be required before the model can be completed. In particular, experimental data supply necessary information on properties of materials and constitute useful guides in deciding what to include and what to exclude in the categories of magnitude of deformation, shape, motion, and loading.

3. Solution of Mathematical Equations

   Next, the attempt is made to solve the degenerate equations which govern the selected model. These are carried out if possible with sufficient generality and also sufficient detail to make possible an understanding of the essential action of the mathematical model and to permit experimental testing of the results. This phase often requires the development of new mathematical techniques.

4. Experimental Tests

Next, certain critical experiments are performed to test the full adequacy of the mathematical model and the validity of any approximations made in the course of the mathematical solution.

5. Development of New Experimental Methods

In several cases the problem cannot be handled by familiar mathematical methods but answers are nevertheless required without delay. Such problems can often be resolved by devising new experimental methods. A typical example is the extension of the field of photo-elasticity to three dimensions, and various methods of determining residual stresses.

6. Design Methods

The above five steps, which can broadly be considered as research, cannot advance the practical side of the state of the art until their results have been interpreted in terms useful to the design engineer. This role devolves upon the so-called methods engineer who absorbs, digests and integrates the results of the research, and then compiles and promulages the "Design Manual" which becomes the "Bible" to be used by the design engineer.

7. Design

This is performed by the "pick and shovel" analysts via day-by-day detailed analysis of each and every structural component of an assembly using the design manual as a guide.

8. Empirical Testing

Experiments are performed with the primary objective of obtaining confirmatory answers with highly valuable results for specific development projects.

The op[illegible]erature furnishes information only upon the first five phases [illegible]sted above. Nothing is ever said, not even in the U.S., about the real key to the structural design, namely the "design manual". Nay, even in a free society such as ours, design manuals constitute jealously guarded information proprietary to each industrial complex. Thus, truly, it is the methods engineers which are the final artificers of the state-of-the-art and who constitute, in one

of Khrushschev's flowery phrases, part of the corps of "unsung heroes" of the State.

It appears clearly that evaluating the true practical state-of-the-art from the open literature exclusively is therefore like trying to evaluate the size of an iceberg from only visual observation of that portion protruding above water.

Nevertheless, certain strategic indicators can be used. First we observe that by necessity research paces technological achievements. The transfer from the results of research to the final embodiment is subject to a delay which depends upon the technological flexibility of the industrial machine and upon the interest on the part of the end user.

For example, in the U.S. a task force approach was used in the development of the ballistic missile. To achieve the end result quickly, stringent restraints were imposed upon deviations from the main goal by the scientific and technological community; so that, for example, the topic of aerothermoelasticity, which is possibly of crucial importance to lifting hypersonic vehicles, was essentially ignored, by direction, by the technologists working on the ballistic missile. It is interesting to note that the task force approach as used by the US in the development of the ballistic missile is closely analogous to the method used by the USSR in picking a technological problem to exploit, and concentrating upon it. Thus, it can be conjectured that although the USSR is very active in fields such as thermal stress, vibrations, theory of thin shells, etc., they may be essentially unprepared technologically to take advantage of the potential benefits from these studies in other fields of hardware development which deviate from the manufacturing and development requirements of their current main fields.

One of the strengths which arises from the so-called inefficiency of the U. S. system is the fact that many of the "out" companies not directly participating at any one moment in major programs spend considerable in-house effort to devise ways and means of providing alternate answers to National technological problems, which in many cases bring into reality the results of research not used in programs under way. Thus, inherent in the U.S. system is a healthy flexibility which ultimately results in the ability to take advantage technologically of research results and thereby to move rapidly, efficiently, and surely into new and effective military hardware.

In the USSR there exist no "out" companies or groups able to operate freely. The Soviet emphasis on a completely planned, "wasteless" environment, has within it an inflexibility which can

cause long delays in the embodiment of new technologies, since the working levels may not have had occasion to acquire the know-how to fully exploit the new technology.

The research-embodiment gap is recognized in the USSR. In this context a quote by the Russian editor, I. M. Rabinovich, in the introduction to a recent survey on "Structural Mechanics in the U.S.S.R. - 1917 to 1957" is enlightening: ..... "An analysis of the contents..... will allow the reader to observe the existence of a reciprocal influence of.....technology (of the USSR) and structural mechanics, the aid which.....science provides to technology as well as the significance .....in formulating and solving with success engineering problems in our Country. In certain areas, structural mechanics in the USSR is ahead of structural practice..... At the same time, the development of structural mechanics lags in certain areas behind the requirements of construction. ..... This lag of course is not a result of stagnation in science. On the contrary, in all these areas .....in the USSR there is.....considerable and sometimes outstanding progress."

Research, which can thus be considered only as a necessary but not sufficient indicator of technological achievement, is nevertheless a powerful index of the relative strength of nations in specific technological areas.

It should be pointed out on the other hand that once the theoretical result is published, the state of the art for that particular item is substantially equalized throughout the world, countering to a great extent any advantage in potential a Nation may have acquired through its research accomplishments.

Because research is the root of the technological tree, and since it is the most readily available indicator of state of the art, this paper will concentrate on analyzing the relative strengths of the US and USSR through the medium of the published research, keeping in mind the ability to apply such knowledge, as gleaned from the meager references on the state of the art in practice.

WORLD PROGRESS IN AEROTHERMOELASTICITY

The principal national centers of activity in Aerothermoelasticity are shown in Table IV. Since very few papers directly concerned with

TABLE IV

NATIONAL RANK IN AEROTHERMOELASTICITY
BASED ON INTEGRATED OUTPUT OF SCIENTIFIC PAPERS

US

USSR

UK

EUROPE: West Germany, France, Italy, Sweden, Austria, Benelux, Spain, Portugal, Switzerland

JAPAN

EUROPEAN COMMUNIST STATES: Poland, Hungary, Rumania, Czechoslovakia

OTHERS: India, South America, China, Israel

Aerothermoelasticity could be found in the open literature, it was decided to concentrate on looking into that literature dealing with closely contributing outfields, such as aeroelasticity, viscoelasticity, plasticity, aerothermodynamics, plate and shell theory, thermal stresses, etc., to form subjective opinions as to the potential capabilities and interest of the various nations in the problem. The countries mentioned individually in Table IV are those found to be most active in the field, or in closely related subfields. The group labeled "Others" encompasses nations which publish substantially less than those of the other groups.

If one attempts to rate these national groups, the ranking order shown in Table IV appears to be approximately correct. The criteria used in rating were output and depth and originality of the material with weight given to the surmised applicability of the published material to practical pending national aerospace problems.

Several interesting differences appear in the output of the various national groups. The published literature of the USSR and of the European Communist States deals almost exclusively with theoretical studies without mention of applications. For instance, in the area of hypersonics, aerodynamics, and aerothermodynamics, these groups concentrate on the theoretical analysis of the interaction of a fluid with a large variety of geometrical shapes, with nary a word as to the ultimate or possible utility of these studies. By contrast, the U.S. and free world literature is replete with allusions to particular applications and even with articles entirely devoted to applications. While in the U.S. literature one reads frequent discussions of specific applications to vehicles such as Dyna Soar, X-15, etc., and in the Western European literature one frequently finds discussions of thermoelastic problems applied to specific classes of airplanes, this content is almost totally lacking in the Communist literature. A notable exception exists in the case of flutter, in which the Communist literature occasionally concedes that the theoretical results have applications to airplanes and hypersonic vehicles; even here, however, no mention is ever made of specific vehicles.

In attempting to understand the meaning of this lack of practical implications in the published USSR literature, and the almost overemphasis on application in the US literature, one major difference between the US and the USSR methods of supporting and reporting research must be considered. In the USSR, a practical objective is dictated

somewhere in the highest echelons of planning; research to accomplish this objective is then directed. Thus, in reporting his research, the Soviet scientist is under no compulsion (in fact, quite the contrary) to indicate the application or implication of the research in his published papers.

In the US on the other hand, the research scientist, to get support for his ideas, has to appeal through the medium of only published literature to a rather vast pragmatically inclined audience which is unprepared for his activity: above all, the American audience is motivated by the desire to know the end application of the idea before investing in its support. Moreover, since research is a continuing activity, published papers often reflect only a stepping stone to further work and implicit in these papers is the plea for continued support which again is based on pointing out possible and useful applications of the research. Some of our papers in fact prepare the ground for the support of research by discussing only the applications of specific proposed research work.

From a practical viewpoint, the objective of Aerothermoelasticity is to predict with reasonable certainty the conditions under which structural failure in a high temperature environment will occur. The means of prediction are mathematical or empirical, and rest ultimately upon experiment, since we are dealing with new forces and new environments where we cannot even be sure of the parameters of importance. For reasons of economy in the long run, progress in the field of Aerothermoelasticity depends essentially on bringing an ever-larger body of physical phenomena within the range of mathematical treatment.

The USSR and European trend appears to be aimed at gaining a basic understanding of the phenomena by means of the more sophisticated analytical tools. In the US, although analytical articles are not lacking, the general spirit seems to be aimed at achieving quick results, by whatever means are available, towards hardware embodiments satisfying practical needs. One gets the general impression that Russians and Europeans would like to understand first, and construct next, with maximum economy; while Americans would prefer to build first, if at all possible, with understanding as a secondary issue, almost in the category of a necessary but not-too-welcome stumbling block.

COMPARISON BETWEEN US AND USSR

A comparison of three typical fields contributing to Aerothemoelasticity yields the results in Table V.

From these comparisons, the following general conclusions can be drawn:

1. The US and USSR are about even in state-of-the-art in this discipline. However, the US has the edge at the moment if it chooses to use it because of its more intensive use of experimental research and its greater flexibility and technological case in application.

2. To fully exploit this labile edge requires substantial additional investment in advanced large experimental tools.

More specifically, Table V shows that:

1. The US is ahead in the area of thermal response of flight structures.

2. That although the USSR is ahead in the theoretical development of vibration theory and dynamic response of structures, the US is well ahead in applications. This can be attributed in part to our knowledge of Soviet theory, coupled with our practical interest in the field and with our resources and skills in experimental facilities.

3. The USSR is well ahead in the theory, and probably in the application of thin wall structures since both nations have developed large aeroballistic boosters, with the Soviets developing the capability of launching larger payloads.

The preference of the Soviets for analytical solutions is exemplified in their excellent schools of applied mathematics, particularly in the area of functional analysis (Kantorovich, Krassovski), which is a compact, modern conceptual tool for formulating mathematico-physical models in a unified mathematical framework. The pioneering work of Muskhelishvili and his school in continuum mechanics as well as the excellence of men like Hovozhilov (shell theory and non-linear elasticity),

TABLE V

COMPARISON OF OUTPUT BETWEEN US AND USSR
IN THREE SUBFIELDS OF AEROTHERMOELASTICITY

VIBRATIONS AND DYNAMIC RESPONSE OF STRUCTURES	US	USSR
1. Stability of motion		++
2. Nonlinear vibrations		++
3. Experimental research	++	
4. Applications to flight structures	++	
THERMAL RESPONSE OF FLIGHT STRUCTURES		
1. Thermal stress	-	-
2. Thermal shock	++	
3. Ultrahigh thermal effects	+	
4. Creep and strength at high temperatures	++	
THIN-WALLED STRUCTURAL ELEMENTS		
1. Mathematical foundation		+
2. Thermal problems	+	
3. Layered shells		++
4. Experimental research	++	
5. Nonlinear theories and effects		++
6. Thin-walled shafts		+
7. Recent books and monographs		+
	12+	11+

Keldish (aerodynamics), Sedov (similarity laws), Ilyushin (plasticity), etc., evidences the basic theoretical strength of the USSR for the advanced design of structures at elevated temperatures.

As regards aeroelastic analysis, particularly flutter, the trend is projected in the book by Zubov: "The Methods of A. M. Liapunov and their Applications", namely the use of Liapunov's Direct Method in the framework of functional analysis for study of the stability of solutions of partial differential equations. It should be noted, however, that the direct stability theory is merely a part of the more general subject of topological dynamics. Recently U. S. scientists have obtained results concerning stability in aerodynamics and magneto-hydrodynamics by Liapunov's Direct Method and have suggested consequently that the combination of topological dynamics and functional analysis would provide a more powerful mathematical machinery for the solution of aerothermoelastic problems.

Let us mention in passing the outstanding work in the Navier-Stokes equations performed by Ladyzhenskaya and Kiselev, and in thermoelastic equilibrium theory by Lur'e.

As an assist in assessing the true aims of Soviet research regardless of official statements, the following conjecture is offered: namely, that Soviet scientists are under strong motivation to publish, for reasons of scientific self-expression and for career advancement. However, work on certain problems cannot be published as such; therefore, it must be published as either purely theoretical research or, when the problem is too applied, camouflaged under the guise of some other practical problem, having no military implication, that also fits the conceptual theoretical model. Thus, for example, work on the aeroelastic behavior of chimneys could well conceal an underlying problem of the interaction between winds and slender cylindrical bodies, suggestive of missiles or rocket boosters on the launch pad.

With reference to the theoretical design tools employed, it is clear that the USSR takes advantage of its analytical excellence; however, no evidence exists that as yet their analytical tools are directly applicable to the synthesis of specific structures. It is conjectured that their ultimate design tool still consists of numerical methods, although greatly aided by analytical insight.

Numerical tools in aerothermoelastic design depend heavily upon the mathematical tool of numerical analysis, and upon the practical tool of computer technology. In the theoretical aspects of numerical analysis, the Soviets do not appear to be ahead of the US, notwithstanding their rich tradition in this field. Computer technology is composed of two distinct segments, which could be called the "software" and the "hardware" segments, respectively. The software aspect concerns itself with the formulation of algorithms and the coding of the machine. From a practical standpoint, it is not as important to create sophisticated algorithms and codes as it is to generate algorithms and codes adequate for the machines on hand. In this regard, the difference in outlook between Soviet, European and US mathematicians is evident: thus while the younger American mathematician appears concerned with the search for workable machine algorithms with adequate codes, the European or Soviet mathematicians generally attempt to devise ingenious algorithms without too much regard for whether or not they can solve practical problems. However, it is interesting to note when using machines for analysis, the Soviet scientist tends to be more brute force in his approach than his American counterpart.

As regards Soviet computer technology, the evidence points to great concentration upon the development of large, fast, and reliable digital machines. Since 1956, a number of Soviet digital computers have appeared such as the BESM, the STRELA, the URAL, the POGODA, the KRISTALL. Although it appears that these machines are not available in the large quantities that are found in the US, indications are strong that their use is rapidly becoming more widespread.

The Soviets are concentrating considerable effort in the areas intermediate between science and engineering such as control theory thermoelasticity and so forth. This concentration upon the more abstract aspects of engineering is usually attributed in this country to the generally higher mathematical training of the Soviet engineer in comparison to his US colleague... However, it may be well due to a great extent to necessity, caused by the scarcity of experimental tools, such as was and is still to a lesser degree the case in Europe. Also, it is interesting to note that the theoretical engineer, when faced with tackling a practical problem being aware of the assumptions and idealizations made in his derivations, is generally psychologically uneasy at the thought of experimentation, which may prove him wrong.

In an engineering science such as Aerothermoelasticity, theory and experiment go hand in hand, each providing balance and support to the other. As in a world of all males or all females, an engineering science which is either all experiment or all theory is essentially sterile, soon losing touch with reality and dooming itself to extinction.

EXPERIMENTAL STATE OF THE ART

It is therefore important also to look at Soviet experimental methods, procedures and facilities: unfortunately, the open literature is not rich in this field. However, the following conclusions can be drawn from what material is available:

1. The Soviets appear active in wind-tunnel research in flutter. Particularly, there seems to be evidence of considerable experimental work in panel flutter.

2. European communist literature (e.g. Czechoslovakian) discusses research in similarity laws between models and full-scale vehicles.

3. New and sophisticated experimental facilities are known to exist at Moscow University for the purpose of establishing plastic stress-strain relations for a three-dimensional state of stress. These facilities are unique in the world.

4. Considerable effort in experimental testing of structures and materials at elevated temperatures is known to have been expended at the new Siberian research center.

From the foregoing, it is obvious that the USSR is developing a capability to perform experimental research and development. This is natural and to be expected as the country comes of age technologically. It can be expected in fact, that as time goes on, the Soviets will rely more and more on their own experimental data as compared to the situation which has prevailed in the past, wherein Soviets have relied massively upon US experimental results.

Experimental research in Aerothermoelasticity has taxed, is taxing and will increasingly tax our economy, even though we can take advantage of an already existing base of facility components such as

the existing 100-million dollar Steam Plant at Tullahoma which can be used to exhaust the test section of an aerothermoelastic wind tunnel, or the existing pumps, compressors, etc., at Wright Field, Langley Field, and other installations throughout the country. Also, our GNP of roughly 500 billion per year can absorb more easily the necessary expenditure to augment our experimental capability in this field; whereas the USSR with a GNP of roughly one-third that of the US is faced with the problem of installing these facilities virtually from scratch, with therefore a net cost per equivalent facility twice or triple the cost to us.

These high costs arise from the requirement of testing large structural samples under simulated thermal inputs as high as 1000 to 2000 BTU/sq. ft. /sec for periods of time which are measured in signif cant fractions of an hour. Even if it were possible to separate the aerothermoelastic problem into the two relatively independent aerothermal and thermoelastic problems, the experimental methods presently used for structural test would be inadequate. In fact, radiant heat facilities can supply only on the order of 100 BTU/sq. ft. /sec.; induction heating methods can perhaps augment this capability by a factor of two or at the most three. This is a far cry from the factor of ten which will ultimately be required for the full aerothermoelastic simulation of superorbital reentry with a lifting vehicle.

Gas dynamic means offer a possible solution to this problem of heat input: however, no matter what means are used to provide the laboratory simulation, the cost and complexity of these facilities will be great. It is therefore not to be excluded that the Soviets may attempt to circumvent the need for depth in Aerothermoelasticity, as they have already done in their Vostok.

However, military necessity may well dictate weapons and flight vehicles where Aerothermoelastic considerations are very important. The U.S. has already attacked the problem head on. For example, we have flown the X-15 airplane, the fastest airplane on record, and have made public our progress in design of a recoverable, controllable, landable, winged manned orbital vehicle, namely Dyna Soar. Morever, we have publicized as an accomplishment the development of the B-70, a moderately high supersonic Mach number bomber. We have also indicated interest in developing a supersonic transport. All of these designs involve Aerothermoelastic considerations. On the other hand,

the Russians have not to date revealed a design in the B-70 class, nor a vehicle of a Dyna Soar type, nor have they given any indication of developing a supersonic transport: this latter would be more useful for them with their vast sprawling domain of interest covering some half the circumference of the globe than to us with our more limited territory. This again may indicate a lack of depth in the practice of Aerothermoelastic engineering which is in contrast to their quantitative and qualitative output in thermoelasticity and Aerothermodynamics in the open literature.

This is not to say that the Soviets, even should they decide to continuously circumvent the Aerothermoelastic problem in practice will shelve their current research effort in those subfields of Aerothermoelasticity in which they have already demonstrated technological competence. They may use this research effort as a psychological weapon to be unsheathed at international symposia and in the arena of scientific literature.

CONCLUSIONS

The theoretical foundations upon which the applied science of Aerothermoelasticity is based are the classical concepts of mathematical physics: in particular, mechanics of continua. Continuum mechanics yields the laws, in mathematical form; however, these laws are dependent upon certain coefficients and certain functions which relate to the physical properties of materials.

If there were at hand an all-inclusive description of such physical properties of materials, the solution of every problem of mechanics could be in principle obtained from the general solution of a universal set of governing equations.

Such an approach is not feasible at present, since the requisite mathematical description of materials properties is not available, and further the mathematical tools for a general solution are not sufficiently developed.

Therefore, practical progress in this field depends heavily upon experimental observations albeit tempered with a strong theoretical effort. For the US to economically exploit the advantage it now has through its vast complex of experimental facilities and manufacturing know-how it will be necessary to strengthen the analytical ability of

its structural team. Thus we should move closer towards that happy norm which lies between our extreme dependence on experiment and the USSR's overly mathematical bent.

However, this is a long-term effort starting from the high school and continuing through the higher levels of professional training. In the short term, it will be necessary to rely as before on a heavy experimental program and steps must be taken to insure that adequate tools are available, regardless of their seemingly high onus upon the economy. At this time, economizing on facilities is putting the brakes on progress and perhaps yielding the fragile cup of technological advantage to the USSR who is growing up technologically and can therefore be expected to become more and more active and proficient in experimental activity.

In comparing the state of the art, certain general conclusions can be drawn:

1. The Soviet Bloc has a potential advantage in their concentration on theoretical development and their use of sophisticated mathematical techniques. However, this potential advantage will not become a real advantage until the theory is tested and proven either in practice or more importantly in laboratory experiments. To date the USSR has relied heavily on experimental data released by the US and in some cases Western European nations such as the United Kingdom. This reliance on externally provided experimental data can be expected to wane as the Soviet Bloc develops adequate experimental tools for its scientific and technological community.

The major obstacle towards the USSR acquiring such an experimental capability is the cost of the facilities.

2. Although the US has been active in subfields of Aerothermoelasticity and actually leads the world in the total field of Aerothermoelasticity, it appears from an examination of published literature and conversations with design engineers, that our knowledge at the moment is only marginally adequate for the design of vehicles such as the B-70 or Dyna Soar. Our knowledge is as yet inadequate for future lifting vehicles such as an advanced Dyna Soar, an Aerospace Plane, a lifting Apollo, and so forth. Luckily, the USSR through publishing its theoretical findings in the scientific literature, supplies a valuable

fountain of material which should be taken advantage of by government supported translation services on a more expanded and timely basis than is currently the practice. Moreover, Federally sponsored courses in Russian should be instituted, perhaps even as on the job training for scientists and engineers.

3. Although the Soviets appear to have circumvented the need for depth in Aerothermoelastic design, and may continue to do so in the future because of a lack of experimental facilities, this should not be interpreted as an indication that they will stop or minimize their research effort in the sub fields of Aerothermoelasticity. In fact, it can be expected that they will increase their activity in research in this field, utilizing their publications as a psychological weapon, within the international contest for man's opinion and regard.

This renders all the more important that we take advantage of this possible deluge of valuable knowledge by implementing the recommendations made in 2. above, with regard to translation services and augmenting the ability of the American engineering community. It is worthy of note that the Soviets have found it economical to provide such translating services for their scientists and engineers, and it is a fair surmise that more Russian methods engineers can read English than American methods engineers can read Russian.

REFERENCES

1. Rogers, M., Aerothermoelasticity, Aero/Space Engineering, October 1958, pp. 34-43.

2. Bisplinghoff, R. L., Ashley, H., and Halfman, R. L., Aeroelasticity, Addison-Wesley Publishing Co., Cambridge, Mass., 1955.

3. Fung, Y. C., An Introduction to the Theory of Aeroelasticity, John Wiley & Sons, New York, 1955.

4. International Aerospace Abstracts, The Institute of the Aerospace Sciences, Inc., Phillipsburg, N. J., Vol. 1, Nos. 1-5

5. Trilling, L., Soviet Aeronautical Scientists: How They Work and Where They Publish, Aero/Space Engineering, July 1961.

6. Rabinovich, I. M., Structural Mechanics in the USSR, 1917-1957, Pergamon Press, New York, 1960.

7. Hermann, G., Unpublished AFOSR Source Material, 1958.

8. Second International Congress on Aeronautical Sciences, Zurich, Switzerland, Sept. 12-16, 1960 (ICAS).

9. Applied Mechanics Reviews, published by the American Society of Mechanical Engineers, Easton, Pa., Vols. 5 through 14, No. 9, 1952 - September 1961.

FUTURE DYNAMIC AEROTHERMOELASTIC CONSIDERATIONS FROM A VEHICLE REQUIREMENTS VIEWPOINT

Thor M. Snaring, 1/Lt, USAF
Donald J. Ketter, 1/Lt, USAF
Flight Dynamics Laboratory
Aeronautical Systems Division

ABSTRACT

This paper is concerned with a discussion of dynamic aerothermoelasticity on the basis of estimated future system requirements. Aerothermoelastic problem areas are identified and discussed with regard to their possible scope and complexity. Limitations of current aerothermoelastic technology as well as potential research gaps resulting from future requirements are also discussed. The paper is generally aimed at dynamic aerothermoelastic phenomena; however, some static aerothermoelastic problem areas are indicated, and new phenomena peculiar to space dynamics are identified.

FUTURE DYNAMIC AEROTHERMOELASTIC CONSIDERATIONS FROM A VEHICLE REQUIREMENTS VIEWPOINT

INTRODUCTION

The term "aerothermoelasticity" identifies that branch of flight mechanics which involves the mutual interaction between aerodynamic, inertial, and elastic forces on flight structures subjected to a thermal environment. It has been recognized in the past that elevated temperatures associated with aerodynamic heating at high supersonic and hypersonic Mach numbers can produce limitations in the allowable velocities and dynamic pressures of aircraft and missiles, and many of the effects of elevated temperatures on flight structures fall within the purview of aerothermoelasticity.

Flight vehicle technology in the aerothermoelastic area has advanced significantly since the introduction of three dimensional subsonic incompressible flow theories in the early 1940's. However, many shortcomings and uncertainties still exist. Prediction methods for aerothermoelastic phenomena are generally limited with respect to accuracy from a quantitative viewpoint in all speed regimes, and for certain configurations and environments, even limited in a qualitative sense. Although a great deal of knowledge exists in the subsonic and supersonic speed regimes, a completely suitable transonic unsteady aerodynamic theory is still lacking. In regions where thermal effects are significant, there are no generally available methods for conducting scaled wind tunnel testing or vibration testing under conditions which require relatively complete aerothermoelastic or thermoelastic simulation. Techniques of flight-flutter testing, although adequate for present day vehicles, may have to be revised for future designs where thermal effects are significant and the onset of flutter will be dependent on the vehicle's past environment. Applied research on aerothermoelasticity may very well be the key to the successful development of future aerospace vehicles.

This paper attempts to forecast some dynamic aerothermoelastic problems which may be important in the design of future aerospace vehicles. Potential problem areas are identified and discussed with regard to their possible scope and complexity. In addition, the need for and value of additional research is indicated for those areas where gaps in the current state-of-the-art exist because of new vehicle

requirements. The discussion is generally limited to dynamic aerothermoelastic phenomena; however, some static aerothermoelastic problem areas and new phenomena peculiar to space dynamics are identified.

SECTION I: ANALYSES OF FUTURE SYSTEM REQUIREMENTS FROM AN AEROTHERMOELASTIC PERSPECTIVE

Forecasting aerothermoelastic phenomena for future system requirements is a difficult task in view of the wide variety of vehicles and associated operating environments that might be contemplated for future development. Some requirements may involve vehicles which will operate solely within the earth's atmosphere while others could possibly involve space vehicles for interplanetary travel. In view of this wide range of operating environment, future flight vehicles will vary greatly in configuration, construction, materials, control, guidance, etc., and aerothermoelastic phenomena common to one system may be absent altogether in another.

The following discussion presents future aerothermoelastic considerations for two basic types of flight vehicles. These are: (a) those vehicles whose primary mode of operation is within the earth's atmosphere, hereafter referred to as atmospheric vehicles; and (b) those vehicles whose primary mode of operation is out of the earth's atmosphere, hereafter referred to as space vehicles. The distinction between these two types of vehicles is arbitrarily chosen as follows: atmospheric vehicles are defined as those which operate between altitudes from sea level to 150,000 feet at speeds from subsonic through hypersonic; and, space vehicles are defined as those which leave the earth's atmosphere, perform some space mission, and/or re-enter the earth's atmosphere.

A. ATMOSPHERIC VEHICLES

The next decade will undoubtedly witness further development of atmospheric vehicles whose primary mode of operation is within the earth's atmosphere. These vehicles may be manned or unmanned and may be required to perform missions such as short range logistics, low

altitude offense and defense, and tactical operations. Inasmuch as their mode of operation will be within the earth's atmosphere, it is quite likely that aerodynamic surfaces will be utilized to provide lift, control and stability. Therefore, this type of vehicle will encounter aerothermoelastic phenomena of a varying degree depending on configuration and operating environment.

Aeroelastic problems, such as fixed surface bending-torsion flutter, T-tail flutter, flutter of wings with external stores, buzz, aeroservoelastic coupling, buffeting, all movable control surface flutter, panel flutter, dynamic loads, etc. will continue to be important considerations in the design of atmospheric vehicles. These problems will be complicated due to the effects of aerodynamic heating, aerodynamic and structural nonlinearities, accelerated flow conditions (at least for anti-ICBM type vehicles), and rapidly varying inertia or mass conditions. Some aspects and implications of these problems as well as some recent developments are discussed in the following paragraphs.

Panel flutter has been a problem of particular concern in the design of modern day aircraft and missiles, and is expected to become more severe with the current trend toward thinner gage structures. In the past, the occurrence of panel flutter was seldom catastrophic and simple fixes were available. In the future, however, it is entirely possible that the application of "fixes" may defeat the purpose of some designs where structural weight must be at an absolute minimum. The current status of the panel flutter problem leaves much to be desired in the way of adequate prediction methods and design criteria. Fung's[1] recent work gives a comprehensive review of various theories, and a summary of the panel thickness requirements, based on both theoretical and experimental studies, for the prevention of panel flutter under various conditions. The large discrepancies between experiment and theory have been partially explained by Voss[2] in a recent paper. Most of the panel flutter work to date, however, has been for simple panels and boundary conditions with idealized aerodynamic inputs. New types of panel construction such as those exhibiting orthotropic and anisotropic properties could make realistic solutions much more difficult to obtain. In addition, aerothermodynamic effects arising from boundary layer viscosity, angle of attack, sweep, and heating will be important and must be delineated.

Other aspects of aerothermoelastic phenomena which could be important in the design of future atmospheric vehicles are the effects of flight acceleration and rapidly changing ambient conditions. Some recent work in this area by MIT[3] and CEA[7] under ASD sponsorship has led to several interesting conclusions for low accelerations (of the order 10 to 15 g's). These are: the main effect of acceleration on the aeroelastic response of high speed vehicles is to cause the aerodynamic

coefficients to be explicit functions of time. The direct effects of acceleration are probably negligible in most practical situations; the transonic region is the flight regime where the effects of time-varying coefficients are the largest because of rapid and significant changes in aerodynamic coefficients associated with the transition from high subsonic to supersonic flow; in binary flutter the envelope of free response in accelerated flight can be simply predicted with satisfactory accuracy from the quasi-static q versus M and ω versus M curves for the flutter root; and, for a system in which the natural frequency varies with time the shape of the envelope of response to continuous sinusoidal excitation is strongly dependent on the frequency of excitation.

However, consideration of highly accelerating anti-missile missiles and boost glide vehicles operating in a high speed, high temperature environment raises serious questions as to the validity of these conclusions and to the applicability of linear constant coefficient analysis, since it is easy to envision either large deflection motions due to combinations of high dynamic pressure and large transient stiffness losses, and/or large rates of change of mass, stiffness, and ambient conditions.

Consider the hypothetical case of an anti-missile missile with both a high and low altitude capability. Possible flight paths for such a vehicle are presented in Figure 1. This system could have a body or fuselage of fairly high fineness ratio, fixed surfaces for aerodynamic stability, and all-movable surfaces for aerodynamic control. The control surfaces might possibly be of the canard type. The anti-missile missile would, by virtue of its mission, be characterized by very high accelerations and rapid maneuverability. The former could be as high as 100 to 200 g's and the total flight time from launch to target may be a matter of only a few minutes. For the sea level to high altitude flight path shown in Figure 1, ambient conditions would vary quite rapidly from M = 0 at sea level to M = 10.0 at altitude, while the low altitude flight path would be characterized by high dynamic pressures and rapidly changing aerodynamic coefficients. Also, the mass distribution of the vehicle would be changing rather rapidly due to the expenditure of fuel. The resultant aeroelastic equations of motion for such a system in either flight path would contain highly time-dependent coefficients and strong nonlinearities, and the analyst may have to resort to a variable coefficient analysis applicable for strong nonlinearities in order to expect reasonable results. This situation leads to a very interesting question. How does one define flutter under such conditions? The ordinary concepts of aeroelastic stability would not apply since it is entirely possible that the dynamic response for such a system would be characterized by a period of instability (increasing amplitude of oscillations) followed by a period of stability

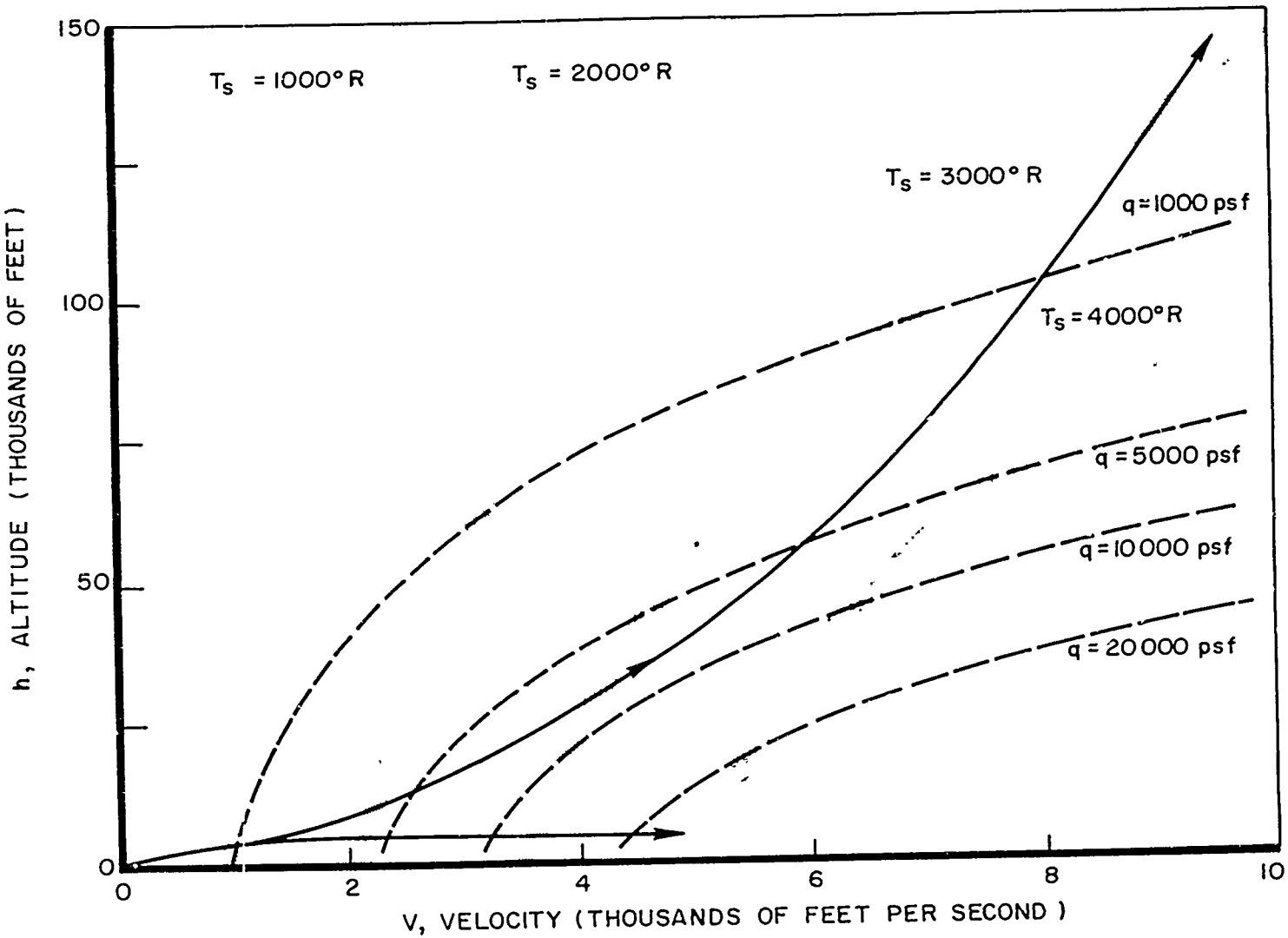


Figure 1. High/Low Altitude Defensive Vehicle Trajectories

(neutral or decreasing amplitude of oscillation) and so on. Such response could be either destructive or non-destructive depending on maximum amplitudes of oscillation achieved and the strength of the vehicle's structure. Combined with this is the fatigue aspect of the problem. Should the vehicle be subjected to repetitive oscillations of the type described above, even though the amplitude of the oscillations during a single occurrence is not large enough to cause catastrophic failure, the structure might be weakened due to creep and fatigue to the point where destructive flutter would occur.

A most important aeroelastic consideration in the design of future winged atmospheric vehicles will be the detailed delineation of the effects of aerodynamic heating and past heating history. CIT[8] conducted some studies in this area and showed that neglecting the effects of heating and past heating history may lead to unconservative results. Consider, for example, the case of a low altitude penetration aircraft. A possible flight trajectory for such a vehicle is illustrated in Figure 2 with the penetration accomplished as follows: (a) cruise at M = 5.0 at an altitude of 50,000 feet; (b) when penetration is to be initiated, decelerate at constant altitude to a Mach number of 1.5; (c) reduce altitude from 50,000 feet to near sea level at constant Mach number; (d) accelerate at constant altitude to a Mach number of 3.0; and (e) maintain this altitude and Mach number to target. Inasmuch as the time factor involved is extremely important in specifying equilibrium temperatures, let us arbitrarily assume that the final condition is reached ten minutes after penetration is initiated, i.e., it takes ten minutes to achieve the condition specified in (e) from the condition specified in (a). Depending on the configuration involved, the equilibrium stagnation temperatures for the high altitude cruise portion of the flight could be as high as 3,000° F, and the vehicle would be in the "soaked" temperature condition with reduced stiffness due to the static reduction in the elastic modulus of the material. As penetration is accomplished, temperatures and temperature distributions will be continuously changing until finally the "soaked" condition of the low altitude - low Mach number condition is achieved, where equilibrium temperatures may be of the same order as the high altitude - high Mach number condition. In the interim, inplane thermal stresses due to transient cooling and heating would be introduced which would increase and decrease, respectively, the relative stiffness possibly to the extent where flutter could occur. The point to be made here is that the occurrence of flutter can be dependent on the past thermal history of the vehicle as well as on instantaneous conditions. The implications of this hypothesis could have far-reaching effects with respect to the normal procedures and techniques associated with the aerothermoelastic design of new flight vehicles. Extensive flutter analysis, model tests,

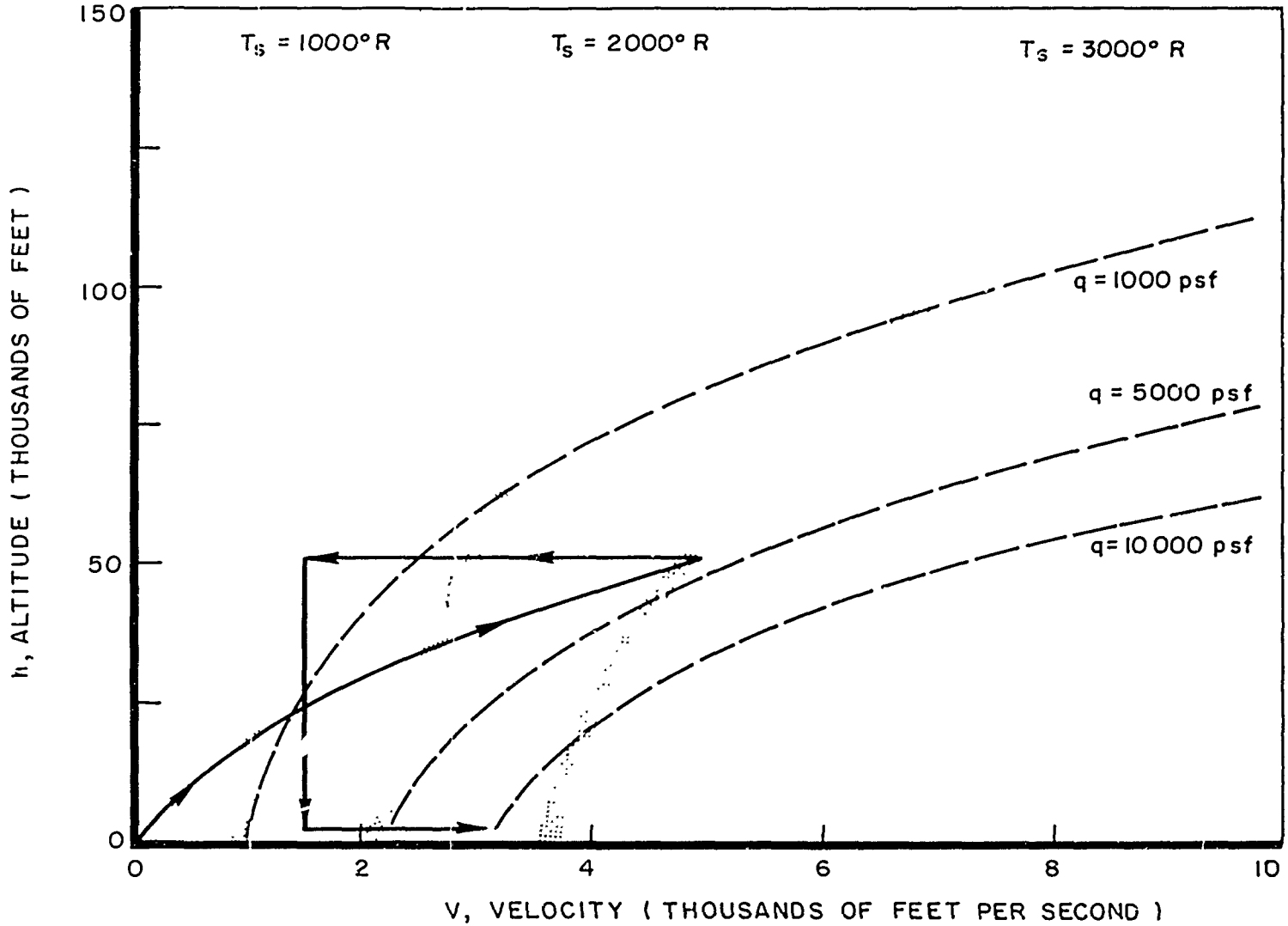


Figure 2. Low Level Penetration Aircraft Flight Path

ground vibration tests, and flight flutter tests for conditions encountered over a wide variety of maneuvers within the flight envelope would have to be conducted to completely insure the safety of the design. Inasmuch as this would be impractical from a cost and time standpoint, the aerothermoelastician must be judicious in selecting critical flight paths for analyses and test programs. Also, it may be necessary to revise current procedures of flight flutter testing since the onset of flutter will be dependent on the vehicle's past environment, and hence, an infinite number of flight paths would have to be undertaken to validate the vehicle's aerothermoelastic integrity.

One of the most difficult tasks in aerothermoelastic analyses is the evaluation of the aerodynamic influence coefficients. Although the subsonic and supersonic speed ranges are relatively well covered in this respect, a completely suitable transonic theory is still lacking. The development of quasi-steady and indicial aerodynamic procedures have alleviated this situation somewhat, and the ASD is currently sponsoring research to further the development and establish the validity of these methods, covering not only the transonic speed range, but the supersonic and hypersonic speed ranges as well. The development of piston theory and other supersonic unsteady aerodynamic theories have contributed significantly to the state-of-the-art, however, there is still room for improvement, particularly to overcome current limitations and extend their applicability to new configurations. In the hypersonic speed range, the extended shock expansion and variational theories (References 10, 11) have been formulated and successfully applied to not-so-simple configurations. These cover the range of the hypersonic similarity parameter, $M\delta$, where M is the Mach number and δ either the fineness ratio for bodies or the maximum thickness for airfoils. Areas requiring further research include the delineation of the effects of wing-body interference and nonlinearities due to airfoil shape, blunt leading edges, thickness, and angle of attack. Real gas phenomena including boundary layer and viscous effects, ionization and dissociation may be significant at the higher hypersonic speeds. However, Miles[9] suggests that such features as dissociation, ionization, slip-flow, and interaction with magnetic fields will be of only minor importance for problems in flutter and transient loading except for their influence on the downstream steady flow field.

Other aerothermoelastic conditions which may be important since they affect the relative stiffness of the vehicle are the effects of creep, fatigue, and secondary structural damage. These problems could be particularly important in the design of future manned systems where the flight vehicle will be utilized many times over.

B. SPACE VEHICLES

The 1965-1975 time period will see the development of many unique and unusual systems which must perform their primary mode of operation in a space environment and must be capable of exit from and re-entry into planetary atmospheres. These systems will be designed to perform one or more functions including offensive, defensive, reconnaissance, logistics, and experimental missions. Occurrence of some "classical" aerothermoelastic problems on space systems is still a possibility while the vehicle is within the earth's atmosphere because of stringent design criteria such as minimum weight, reliability, target accuracy, stability, performance, etc. These and other design criteria which result from system requirements will not necessarily eliminate the susceptability of new systems to old problems, but will likely provide new twists to old problems. A good example of this is the HTOL space vehicle which is discussed in more detail later. In the following sections, dynamic aerothermoelastic considerations, and phenomena peculiar to space dynamics resulting from possible requirements for vehicles to perform a military mission in space, are discussed with respect to various Launch, Exit, Space Operation, and Re-entry, and Recovery requirements.

LAUNCH

Requirements may call for space vehicles which are capable of either a conventional aircraft type take-off or of being launched vertically with large boosters of either the liquid or solid propellant type from surface or sub-surface launch sites. Certain dynamic aeroelastic considerations are attendant to each specific requirement.

Vehicles using horizontal take-off techniques (HTOL vehicles), and yet capable of space operations, require low structural to gross weight ratios with enormous fuel requirements and, as a result of structural strength efficiency, will be quite flexible. In terms of physical dimensions, HTOL space vehicles will be quite large and could consist of a long slender body with low aspect ratio wings. Such a vehicle might be re-usable, thus necessitating consideration of the structural fatigue problem. This will be influenced by repeated taxi, take-off, and landing loads resulting from runway roughness. Loads resulting from landing impact will also represent a critical design condition. With regard to predicting the dynamic response characteristics of this flexible structure to shock, impact, and other transient loadings, fuel slosh degrees of freedom for various dynamic loading conditions must be included in the equations of motion for the overall structural response.

The following paragraphs present a brief discussion of considerations which will result from requirements for vertically boosted vehicles. Such vehicles will have increasingly low structural to gross weight ratios and very large payloads. Payload weight requirements for the future will probably necessitate use of boosters in the 1.5 to 12 million pound thrust class for all types of missions. These boosters could consist of clusters of smaller rockets which may be attached in varying numbers - say, for example, from 3 to 8. Clusters of this type will present formidable difficulties to the prediction of their free vibrational response in terms of accounting for various items which influence the vehicles stiffness characteristics; such as joint shear properties, internal pressure, discontinuities, cut-outs, and nonlinearities due to large deformations. Other considerations include a definition of transient buckling loads for unsymmetrical thrust build-up (due to engine failures), tie-down release loads, and control system interaction with the structure including fuel slosh dynamics for liquid fueled boosters. Requirements for sub-surface launching generate special dynamic aerothermoelastic considerations. Underground silo launchings may cause traveling shock waves between the booster and silo wall during ignite and subsequent pressure pulses on the booster body during lift-off within the silo. These unsteady forces or transient loading conditions could produce local panel failures or complete booster failures due to exceeding design bending moments.

For vertically boosted vehicles with winged or lifting body payloads, prelaunch dynamic loads and aeroelastic instabilities become a primary consideration. Vehicles exposed to ground wind loads on the launch pad may experience either torsional or lateral bending oscillations which are induced by Karman Vortex shedding. When combined with large steady state drag loads this may produce critical design base bending moments.

EXIT

Basically, one can envision two modes of exit from the sensible atmosphere to the space environment. The first mode involves transition through the flight corridor to increasing altitudes and velocities utilizing a lifting configuration of low thrust to weight ratio. The second mode, and possibly the one to be used most frequently, consists of rapid vertical boost using very large boosters of high thrust to weight ratios. Again, certain considerations are common to each mode of exit and other considerations (at least for the vertical boost mode) are peculiar to the specific mission for which a requirement exists.

For example, assume there exists a requirement for manned orbital flight at low altitudes (less than 100 n.m.), and that the orbital condition is to be achieved with a horizontal take-off vehicle which ascends the flight corridor. As previously mentioned, such a vehicle (HTOL) will be quite flexible. Figure 3 shows that the aerodynamic heating for this type of exit is of the same order of magnitude

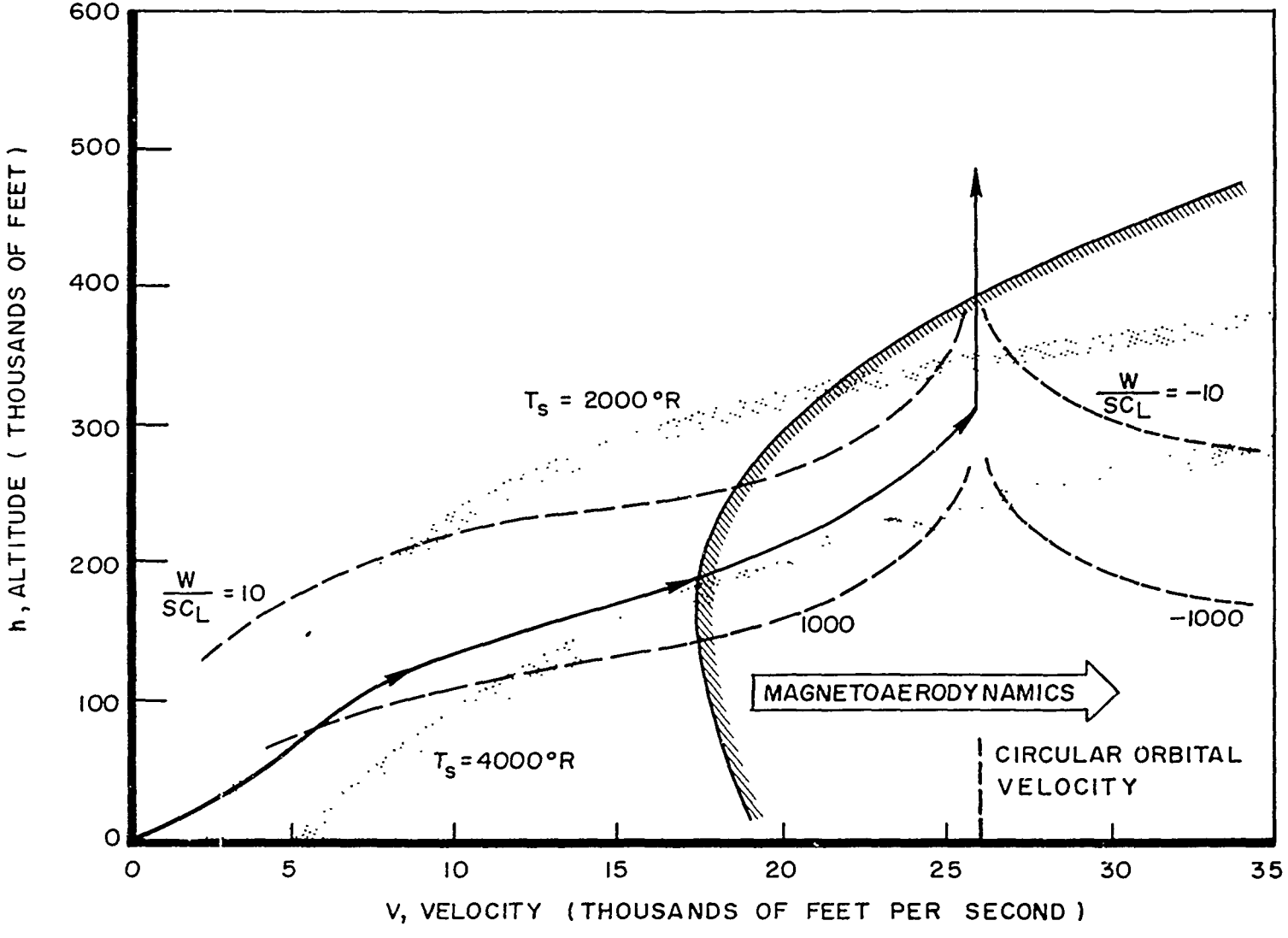


Figure 3. Lifting Exit Trajectory

(stagnation equilibrium temperatures of 3500 to 4000° R) as experienced by re-entry vehicles. The Mach number and dynamic pressure (1000 psf) attained by lifting exit vehicles within the lower atmosphere will generally be greater than those experienced by medium and low W/SC_L lifting re-entry vehicles. Thus, aerothermoelastic problems will be an important consideration in the design of lifting exit vehicles. If such a vehicle employs aerodynamic control - possibly canards - consideration must be given to all-movable surface flutter, buzz, and buffeting. Unusual fuels, fuel tank configurations, and fuel tank locations could be employed, thus causing difficulties in the prediction of the structural-control system interaction and the determination of fuel slosh dynamics. Adaptive control systems which deliberately take advantage of the nonlinear and time-varying character of the response of the structure may be utilized. Since adaptive control systems require the detailed knowledge of elastic vibration characteristics, a problem of fundamental importance will be the accurate determination of thermal effects on the normal modes and frequencies of the structure. The prediction of the dynamic characteristics of new materials and design concepts begins to assume a great deal of importance for this mode of exit. For example, use of a radiation cooled structure with orthotropic materials and nonhomogenous (composite) panels will make panel flutter solutions much more difficult to obtain. Both the prediction of panel flutter and free vibrations will be affected by possible use of combinations of elastic, viscoelastic, and inelastic materials throughout the structure. Consideration must also be given to the prediction of dynamic response to random excitations, such as atmospheric turbulence, aerodynamic noise, and mechanically induced vibrationsin a changing thermal environment.

In addition to the time-varying effects of high temperatures on lifting exit vehicles, advanced propulsion techniques which involve both expenditure and accumulation of fuel while in flight may magnify the effects of changing center of gravity, mass distribution, and moments of inertia. Also, the prediction of unsteady aerodynamic loads at high velocities (greater than 18,000 fps) within the atmosphere (below 300,000 ft.) may require consideration of hypersonic flow features such as dissociation, ionization, chemical non-equilibrium, slip-flow, free-molecular flow, and boundary layer electrical interactions with magnetic fields. This is shown by the area designated "magnetoaerodynamics" which covers a large portion of the re-entry corridor in Figure 3. It is thus evident that a requirement for the lifting exit vehicle would constitute a challenge to both the designer and the analyst in attempting to insure the vehicle's structural integrity from an aerothermoelastic viewpoint.

The following remarks are directed toward some considerations which will be peculiar to vertical boost vehicles and to the mission for which their payload is designed. On the one extreme payloads may be winged gliders, and on the other extreme they may be only instrument packages with shell casings or shroud coverings. Payloads of the later type have been used extensively in the past and aerothermoelastic problems associated with boosters carrying these types of payloads have not been too severe. However, since boosters in the 1.5 to 12 million pound class are being planned and long (interplanetary) or orbital (recoverable) missions are contemplated, this picture may change considerably.

Either liquid or solid boosters in this class will have very large fuel consumption rates and thus the time-varying effects of changes in mass distribution, center of gravity, and moment of inertia will again require consideration. In contrast to lifting exit vehicles, the accompanying time-variant ambient conditions will also dominate the picture. Although temperature effects will not be so extreme for the boost mode, dynamic pressures in excess of 3000 psf can occur at supersonic speeds, which will make the vehicle susceptible to nose divergence, body bending-control system coupling instabilities, classical bending-torsion flutter, all-movable control surface flutter, and panel flutter.

Requirements may call for many different types of control ranging from pure aerodynamic to pure reaction jet systems. Aerodynamic control introduces free-play considerations, along with possible divergence, flutter, and aeroservoelastic-body bending instabilities. The latter problem is also common to thrust vector control using gimballed engine nozzles. Single degree of freedom flutter for blunt nose surfaces must be considered for control by use of vanes submerged in the rocket exhaust. Reaction jet control requirements introduce the possibility of coupling between alternating thrust forces and body bending degrees of freedom.

Another critical problem area for the vertical mode of exit concerns the dynamic loads on the booster associated with large wind shear gradients and sharp edged gusts. This problem is of particular importance since peak dynamic pressures are often reached between 30,000 and 40,000 feet altitudes. Buffeting loads will continue to be important for vertically boosted vehicles, particularly in the transonic region due to the fluctuating forces generated by shock formation.

There is one more consideration for exit which results from requirements for manned space flight. This concerns the ability of the man to withstand the dynamic loads to which he will be subjected during exit. The heat, stress, and vibratory (frequency, amplitude, and acceleration) tolerances of the human body will surely become design

conditions for many parts of the vehicle and portions of the flight path.

SPACE

Space flight requirements imply considerations which involve the elastic and inertia properties of the structure, magnetic forces, gravity forces, radiation forces, temperature, and flight path characteristics. These considerations will depend upon whether the flight path is to be a circular orbit or an elliptical orbit, whether it is to be near or far, or whether it involves escape from and re-entry of the earth's gravitational field.

As in the case of exit flight, specific mission requirements will influence the scope and complexity of the dynamic considerations of space flight. For instance, an orbital reconnaissance vehicle, whether manned or unmanned, would probably have high stability and orientation control requirements. However, the configuration and construction will depend a great deal on the presence or absence of a crew.

Consider the unmanned reconnaissance vehicle which moves in a far elliptical orbit varying in altitude from 100 to 3000 nautical miles. Such a vehicle could be very large and flexible and might require internal pressurization. Periodically varying radiation and gravity forces would affect the stability of the flight path and might excite very low frequency structural vibrations. The internal damping of such a structure would be an important consideration from the standpoint of reliable equipment operation. Limit amplitude or periodic oscillations could be induced by interactions of cyclic thermal stresses due to solar heating, varying centripetal accelerations and coriolis accelerations. Again, stability augmentation might be satisfied by imparting a rotational velocity to the vehicle. Here, techniques for predicting the dynamics of a rotating structure might have to account for the effects of fuel slosh under near zero gravity conditions, unsymmetrical inertia, and gyroscopic forces due to rotating machinery, etc. Furthermore, the effects of structural damage due to meteoric impact must be considered.

The manned reconnaissance vehicle (at least versions in the 1970-1975 time period) would probably be capable of maneuvering in orbit. The effects of fluctuating propulsion forces (maybe from a shock generating propulsion device) on the dynamic response of such a structure might have to be taken into consideration, particularly if the vehicle was a permanent reconnaissance space station which must be maneuvered in orbit. Other considerations for this system include a precise definition of the dynamic environment to which the crew will be exposed.

Extended space operations may imply a requirement for orbiting fuel tankers for use by manned vehicles in order to simplify operations. Of particular importance to the successful employment of this concept with regard to liquid fuel is the dynamics of fuel sloshing including the elasticity and inertia of the structure under both transient and periodic excitations. For both liquid and solid fuel tankers, rendezvous and grappling loads must be taken into consideration.

One can envision orbital vehicles with a single bombardment capability (i.e., the vehicle itself would perform the offensive or defensive action), or one can conceive of a platform with a multiple bombardment capability. The platform itself (or portions thereof) could be recoverable and, therefore, might resemble a winged glider or a lifting body rather than a vehicle designed solely for space functions.

Recent history of the development of weapon systems shows a trend for the employment of experimental systems to pave the way for subsequent development of an operational capability. It seems reasonable to expect this trend to continue and even to intensify as man enters the space age. For instance, the development of a moon-based outpost might be preceded by the use of unmanned systems which would survey the moon environment from orbit, soft land large payloads on the moon, and return lunar samples to the earth. Manned travel to the moon and return would follow and it might then be possible to establish a permanent moon based military station. This same concept could be extended to interplanetary exploration and the development of a capability to perform military operations in deep space.

It does not necessarily follow that operation of a vehicle solely in a space environment (travel between the earth, moon, mars, etc.) precludes consideration of dynamic problems. Dynamic response and instabilities (catastrophic failures) must still be taken into consideration in terms of trajectory dynamics, mechanically induced vibrations, and flow induced excitation due to propulsion system operation. Electromagnetic disturbances, both natural and artificial (induced) could present considerations to the dynamics analyst. Meteorite impact and penetration and the effects of either primary or secondary structural damage due to micrometeorite bombardment are additional problems to be analyzed. ASD is currently sponsoring studies to determine the effects of meteoric impact on various types of panels. The structural concepts being studied include multi-wall construction of various materials with different core designs. This program involves both analytical and experimental effort.

But perhaps the most critical and most complex considerations facing the aerothermoelastician are the problems attendant to the requirements for successful re-entry and recovery of low structural weight/gross weight space vehicles. These are discussed in the following section.

RE-ENTRY AND RECOVERY (LANDING)

Both static and dynamic aerothermoelastic considerations during re-entry of the earth's atmosphere (and other planetary atmospheres for that matter) cover a wide range of important parameters such as configuration, density, velocity, dynamic pressure, temperature, heating rate, angle of attack, etc. It is a foregone conclusion that re-entry and recovery requirements will exist for future military space vehicles. It is equally obvious that the mode of re-entry and recovery which is employed will be strongly influenced by the vehicle's mission and the presence or absence of a crew.

The use of extremely light weight inflatable or expandable structures for orbital reconnaissance missions, satellite maintenance and servicing missions, crew ferrying missions, etc. appears attractive in principle. An estimated trajectory for this type of structure is shown in Figure 4. Such structures could be composed of extremely light weight, flexible materials, possibly even temperature resistant fabrics, rubber, or filament wound structures. W/SC_L will be of the order of 1.0 psf to 5.0 psf, wing loadings will range from 2 to 10 psf, and temperatures will be between 1000° R and 2000° R with heating rates between 70 and 100 Btu/ft^2/sec. Vehicles such as a "para-glider" and "Rogallo wing" fall into this class. Requirements for such a re-entry generate consideration for panel flutter, flag waving flutter, large amplitude oscillations, and the influence of elastic degrees of freedom on dynamic stability. In the area of unsteady aerodynamics, consideration must be given to the prediction of forces and moments in regions of frozen flow, free-molecular flow, transition flow, and continuum flow for blunt nose bodies, large leading edge radii, and curved panels. Recent in-house research at ASD indicates that previous estimates for the region of 90 to 100% frozen flow may actually extend down to 200,000 feet instead of rising to 300,000 feet as shown in Figure 4. Panel response predictions must account for the effects of pressure differential, curvature, in-plane stresses, flexible boundaries, and inelastic materials. Furthermore, unique methods of control for this type of re-entry could impose additional problems in the aeroservoelastic area.

A variation on the present method of recovery of payload packages from orbit is the ballistic re-entry of vehicles from super-orbital velocities at 35,000 fps (a typical example is contained in Figure 5) by 1970 and possibly 100,000 fps by 1975. The severity of the dynamic pressure and heating rates encountered by vehicles re-entering from super-orbital velocities is a function of their re-entry velocity, flight

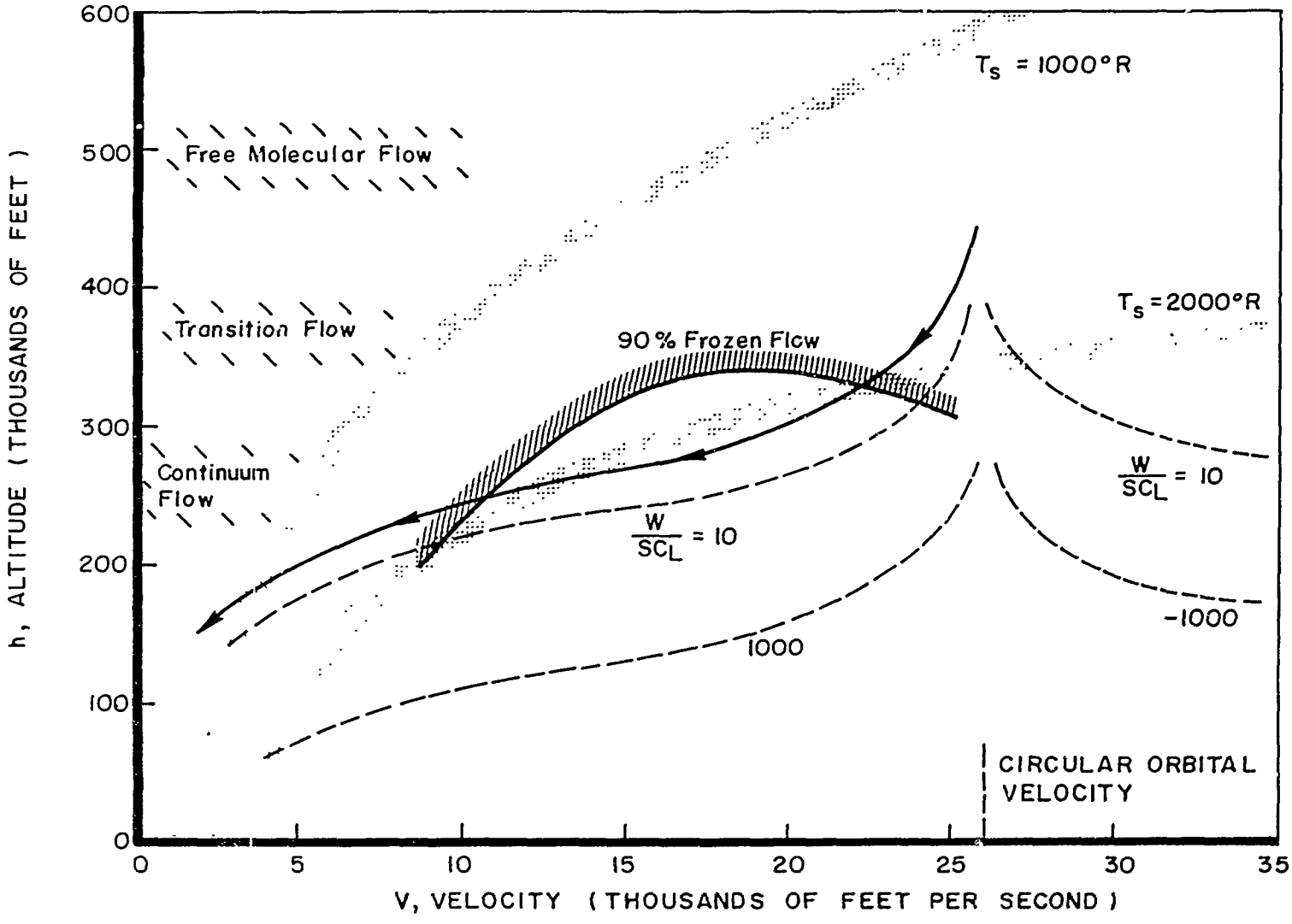


Figure 4. Expandable Structure Lifting Re-entry Trajectory

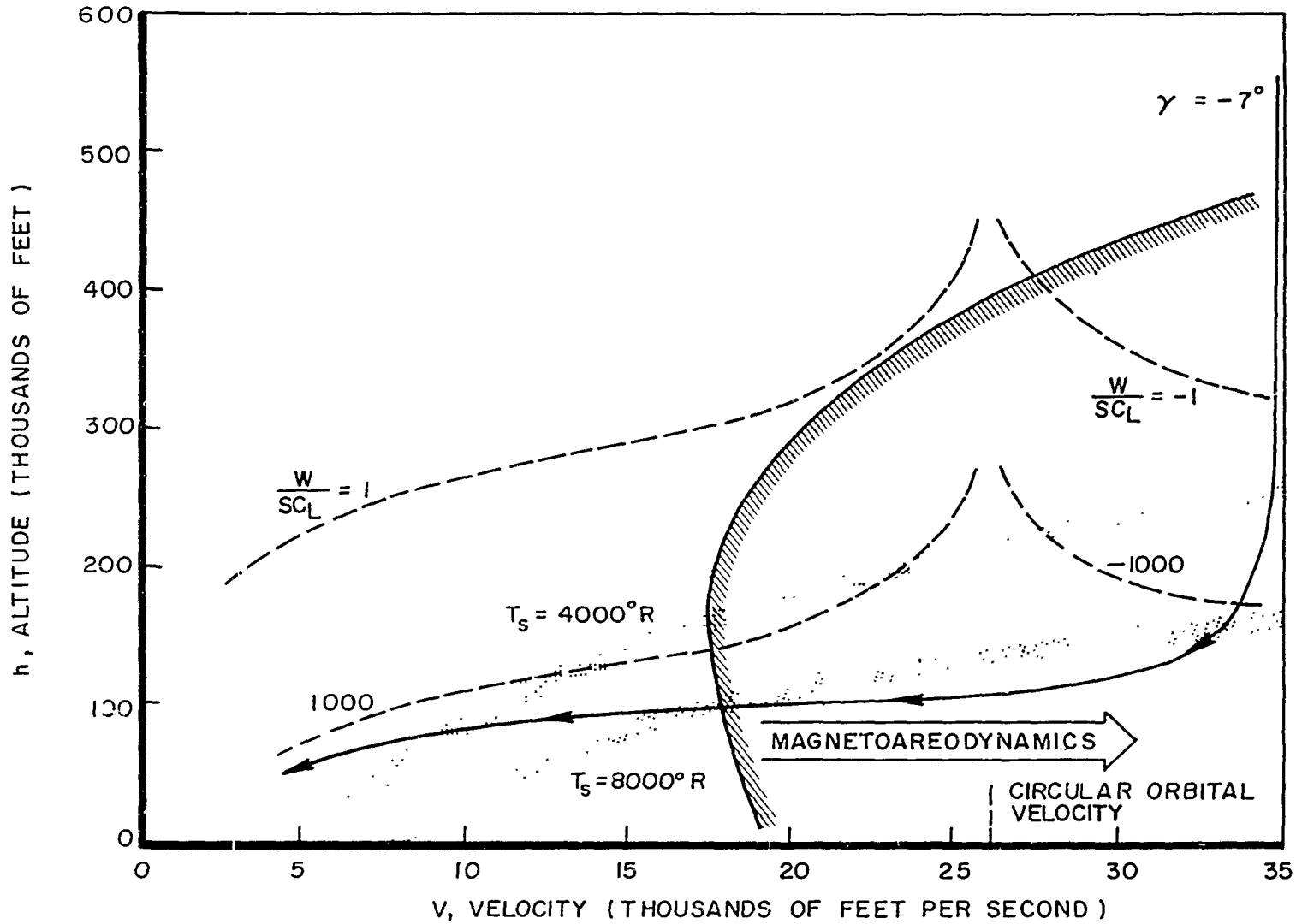


Figure 5. Supercircular Ballistic Re-entry Trajectory

path angle, and configuration. However, for re-entry from 35,000 fps stagnation heating rates in excess of 10,000 Btu/ft^2/sec. and dynamic pressures in excess of 1000 psf could easily occur for ballistic or low L/D vehicles (L/D less than 0.5).

For the case of ballistic re-entry consideration must be given to the prediction of flutter for curved panels and shells of various design concepts including heat sink designs, composite structures, and ablative structures, while accounting for the effects of unsteady magnetoaerodynamic flow. Requirements may arise for some type of aerodynamic control, thus necessitating consideration of control effects on aerothermoelastic phenomena. Requirements for extremely large payloads may yield a vehicle which would be many times the size of present day nose cones. Therefore, due to the relatively high dynamic pressures and temperatures (as far as re-entry is concerned) possible problems with regard to nose divergence and thermal effects on structural stiffness must be investigated. The aeroelastic stability characteristics and buffeting response of blunt nosed bodies is a matter of further concern. Also, various drag devices such as balloons, parachutes, or plate-like drag brakes may impose additional considerations in the areas of buzz, buffeting, and separated flow effects.

Present day effort seems to be concentrated on the possibility of satisfying possible future requirements for re-entry and recovery with glide lifting re-entry vehicles. Glide flight paths could be used by high L/D lifting bodies (L/D $\sim$ 3.0) and by wing-body combinations. Large re-entry vehicles will probably traverse the flight corridor at W/SC_L's ranging from 50 psf to 1000 psf as shown in Figure 6. Re-entry from super-orbital conditions (35,000 fps) with a controlled pull up will present the most severe heating environment in the 1970 time period and by 1975 interest might be focused on lunar and interplanetary vehicles re-entering at 100,000 fps and capable of similar maneuvers.

The structural approach to be employed on lifting re-entry vehicle will greatly depend on the presence or lack of a crew, whether a lifting body or a winged glider is used, the time required for re-entry, the equilibrium W/SC_L, weight and volume requirements, etc. For short time re-entry (less than 10 minutes), transient heating effects on stiffness and vibration characteristics must be considered. i.e., peak heating during the typical pull-up maneuver illustrated in Figure 6 will be in the order of 700 to 800 Btu/ft^2/sec. On the other hand, long time re-entry (greater than 30 minutes) requirements, particularly for re-usable structures, impose consideration for the effects of creep and permanent thermal distortions on stiffness, vibration, and flutter characteristics.

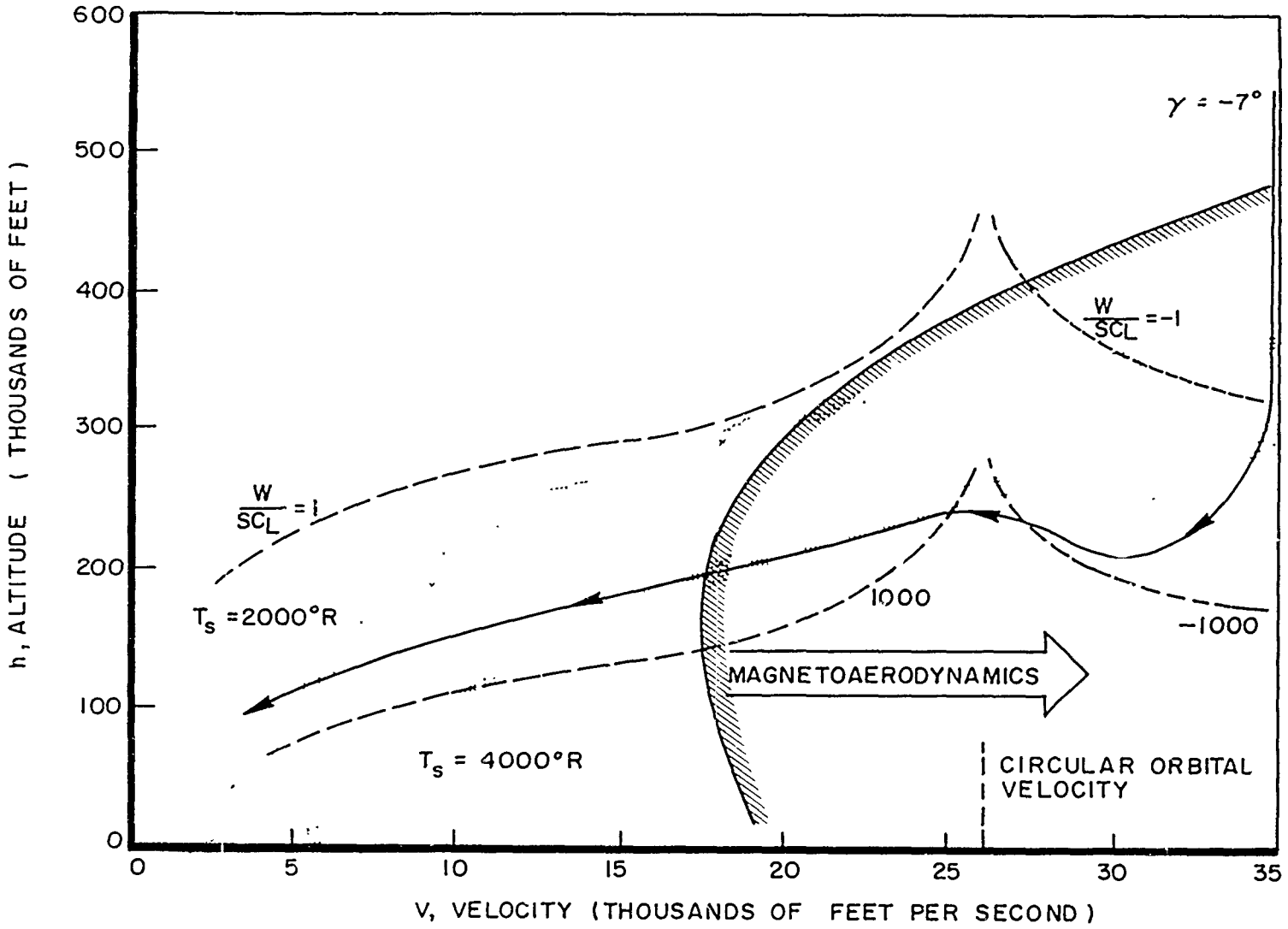


Figure 6. Supercircular Lifting Re-entry Trajectory

A limited flight test program under ASD contract is being conducted to partially investigate the effects of a suborbital lifting re-entry environment on stiffness, vibration, and flutter. The overall purpose of these aerothermoelastic experiments is to assess the accuracy of analytical methods for predicting thermal effects on structural dynamic characteristics and aeroelastic instabilities. Two recoverable glide re-entry vehicles will be boosted by Air Force's Blue Scout Booster to an initial altitude and velocity of approximately 180,000 ft at 12,000 fps and 155,000 ft at 11,000 fps with W/SC_L's of approximately 150 and 220, respectively. On board instrumentation will gather data on skin temperatures, structural strains, surface static pressures, and other structural and aerothermodynamic data. Additional instrumentation will sense dynamic data due to artificial excitation including natural frequencies and mode shapes, oscillatory local pressures and unsteady aerodynamic hinge moments on a simulated control surface, and flutter frequency and mode shape. All measured data will be compared with predicted results.

The nonlinear effects of angle of attack, leading edge bluntness, and thickness must be accounted for with regard to both static and dynamic aerothermoelastic problems. The effects of thick boundary layers, viscosity, and shock-boundary layer interaction will require detailed treatment. Inertia loads due to pull-ups and abrupt maneuvers at high W/SC_L's is a consideration common to both low and high L/D vehicles.

Certainly future system requirements will demand successful recovery of crews, payload packages, and possibly even boosters. Additional specifications for re-usability of the structure will impose limitations on the manner in which recovery is accomplished; for example, "air-snatch" techniques vs water impact vs conventional landing. Primary considerations in the recovery sequence lie in the area of dynamic loads and response. For example, consider the requirement for soft landing a heavy, long slender vehicle on the moon. One method consists of entering the moon's atmosphere backwards, decreasing velocity by means of rocket thrust, and attenuating impact loads by means of crushable or deformable structures or a tripod arrangement of strut-oleo combinations. Many necessary considerations are similar to launching from the earth in the vertical boost mode. However, much more serious problems are concerned with the impact load attenuation, shock transmission, and the coupled response of the attenuation device and the structure.

It is also conceivable that some vehicles could be recovered by either vertical or horizontal landing on water. Horizontal landings on both the water and land will occur at relatively high speeds and will cause both impact and dynamic load problems in view of minimum weight design requirements.

SECTION II: GENERAL REMARKS AND RECOMMENDED RESEARCH

This Section discusses the status of current flight vehicle aerothermoelastic technology with the principal objective of indicating those areas where a concentrated effort is required to insure the timely progression and availability of the state-of-the-art. Although the technology in this area is reasonably well abreast of current vehicle design requirements, there exists a need for new analytical tools, new ground test facilities, new flight test techniques and new environmental data to improve the understanding of and ability to either avoid or control aerothermoelastic and astroelastic phenomena. This is not meant to imply the need for major breakthroughs in the aerothermoelastic area, but rather to stimulate a realization that the current state-of-the-art leaves much to be desired in the way of adequate prediction methods, testing facilities and procedures, and design criteria.

A most important problem area and one in which much research is required is the delineation of the effects of aerodynamic heating and heating rates on stiffness and vibration characteristics. Analytical procedures are required for the accurate prediction of thermoelastic phenomena associated with new structural configurations such as composite, anisotropic and orthotropic types, particularly for superorbital reentry environments. An advancement is necessary in the technology (i.e., new methods and techniques) for scaled wind tunnel testing or vibration testing under conditions which require relatively complete aerothermoelastic or thermoelastic simulation.

It has been mentioned previously that panel flutter is a problem requiring immediate attention. Design criteria and trend data are required for anisotropic and orthotropic panels and heat shields, including the effects of aerodynamic and structural nonlinearities such as large amplitude motion, viscous and boundary layer effects, angle of attack, sweep, etc.

The detailed and accurate definition of unsteady aerodynamic pressure distributions associated with the various aerothermoelastic problems is another area in which much research is required, particularly in the always troublesome transonic regime and also the hypersonic speed range. Hypersonic unsteady theories must be validated by experiments and extended to higher Mach numbers. Recently observed differences between the experimental and theoretical flutter trends with Mach number for cantilevered and semi-rigid models at hypersonic Mach numbers are probably due to real gas effects (i.e., thick boundary layers, viscosity) and indicates the need for methods which account for these

features. Also, methods are required for predicting unsteady airloads including the effects of aerodynamic and structural nonlinearities, such as large amplitude motion and rapidly varying ambient conditions.

Although a large backlog of experience exists on flutter, the hypersonic speed range is relatively unexplored. The effects of chordwise flexibility, wing-body interference, blunt leading edges and angle of attack on flutter characteristics for low aspect ratio, highly swept configurations over the entire speed range require investigation and the establishment of design criteria.

With the trend toward larger boosters for space oriented missions, aeroservoelastic problems could be an important design consideration. Coupling between the elastic vibration modes and control system dynamics, particularly the higher order modes, requires detailed knowledge of both the structure and control system characteristics. In this regard, the development of an accurate method to predict the natural frequencies and mode shapes of many clustered cylinders under conditions of time-varying mass, inertia, damping, and stiffness would have immense value in the design of 1.5 to 12 or even 20 million pound thrust boosters. Methods are needed for calculating joint and attachment stiffnesses, and also stiffness characteristics of thin shelled structures.

Other analytical tools which are needed include methods which describe the nonlinear behavior of structures and mathematical techniques for approximating solutions to strongly nonlinear equations having rapidly varying coefficients. Methods are also needed which will both qualitatively and quantitatively describe new force fields which influence astroelastic phenomena for areas in which space vehicles must operate. Such methods will have value in satisfying stiffness requirements to meet design criteria such as minimum weight, reliability, and safety. Lastly, there exists a need to devise prediction methods for treating both static and dynamic aerothermoelastic phenomena including real gas effects in the velocity range from 15,000 fps through 35,000 fps. The value of these methods lies in optimizing the design of re-entry structures from a stiffness, rather than a strength, viewpoint.

It was pointed out earlier that present day methods of aerothermoelastic analyses oftentimes yield results which are not sufficiently accurate, thus necessitating lengthy and costly ground vibration tests, wind tunnel tests, and flight tests to check predictions for the aerodynamic, stiffness, and inertia characteristics of flight vehicles. Nor is there any hope of escape from this situation, for both in the past and in the future, the analytical description of an aerothermoelastic system is subject to the abilities of the analyst in selecting the theories to be used, the degrees of freedom to be included, the method of solution, and the interpretation of results.

It is imperative that future vehicles be subjected to ground tests under closely simulated conditions. Structures should be subjected to both space and re-entry environments in either duplication or simulation tests, insofar as possible. Adequate dynamic testing laboratories and wind-tunnel facilities should be constructed (if possible and practical) and utilized in both developmental programs and applied research programs in order to insure timely and progressive advancement in the aerothermoelastic and astroelastic state-of-the-art. The need for these two types of facilities is adequately demonstrated by the implications of future requirements, and the value of ground testing as an alternate approach (in contrast with theoretical analyses) to the advancement of technology is quite significant.

Although ground testing serves an essential role in the qualification of a vehicle for flight and in applied research on aerothermoelastic and astroelastic phenomena, it has certain limitations which demand the use of a third approach to the advancement of technology. For instance, the degree of duplication or simulation attainable in a ground facility is often limited by available funds, space and power requirements, safety hazards, etc. Also, ground facility tests often demand use of small scale models which must bear similarity to the prototype; and this similarity is sometimes difficult, if not impossible to obtain except for 1:1 scale ratios. Some progress has been made by MIT under an ONR contract to investigate the theoretical aspects of "restricted" purpose models. This approach shows some promise for limited investigations, but does of necessity neglect certain parameters and similarity conditions. Therefore, it is sometimes necessary to resort to flight testing techniques, which are of value for research purposes in assessing the accuracy of prediction methods, in checking the validity of ground test results, and in gathering environmental data (for which there is a dire need). Therefore, suborbital, orbital, and superorbital flight tests may also serve as a means for "filling the gap" in technology between the present and the time when adequate ground facilities become available. Besides providing opportunity for research testing in the real environment, development flight tests can be used to pave the way for and accelerate the attainment of an operational capability.

In connection with experimental approaches to the advancement of technology in the aerothermoelastic and astroelastic areas, there is a critical need for radically new instrumentation techniques in order to accurately obtain desired data. Consideration should be given to the development of photoelectric or radio isotope techniques for gathering oscillatory acceleration, velocity, and displacement data, both on the ground and in flight. High frequency vibration and internal and external noise pickups which can operate at high temperatures are required along with lightweight, in flight data reduction devices.

Lastly, in view of the desirability and necessity for conducting ground tests and flight tests to meet future requirements and the extremely high cost of full scale tests, there exists an urgent need for a practical resolution of the problem of aerothermoelastic modeling, a need for studies of astroelastic modeling, the construction of adequate ground vibration test facilities which either simulate or duplicate expected space and re-entry environments, and the construction of hypervelocity thermal wind tunnels with large test sections.

SUMMARY

In summary, this paper has presented a discussion of many of the considerations which must be faced by the dynamicist who will be concerned with the design of future atmospheric and space vehicles. The implications, problem areas, and technological advances which have been presented must be boldly faced to insure the timely development of operational capabilities for all types of missions. The considerations which have been presented in this paper are summarized in Table I which shows in condensed form some of the unsteady aerothermodynamic, thermoelastic, inertia, and aerothermoelastic problems which may occur.

To satisfy estimated future system requirements in the 1965-1975 time period, continued applied research effort must be expended to produce solutions to anticipated problems and to re-orient design philosophy which must be employed throughout the developmental stage of future vehicles. In particular, it can be safely stated that the impact of minimum weight design criteria, adverse thermal effects on structural dynamic characteristics, and anticipated operating environments (both steady and unsteady) have elevated the importance of stiffness aspects of structural design. Although present design concepts give adequate consideration to the attainment of acceptable overall vehicle stiffness properties, problems dependent on local joint and panel stiffness levels have begun to appear and need increased attention. It is anticipated that the stiffness aspect of both atmospheric and space structures' design will soon be the most important of all basic design considerations.

Table 1. Summary of Critical Problem Areas

Unsteady Aerothermodynamics	Transonic coefficients Transient (indicial) aerodynamics Nonlinear effects of airfoil or body shape, thickness, angle of attack, and large amplitude oscillations Effects of shock wave interaction and separated flow Time variant ambient effects Low density-high velocity flows Effects of boundary layer and viscosity Wing-body interference Measurements - correlation with theory
Thermoelasticity	Heating effects on stiffness and vibration characteristics Nonlinear effects of vibration amplitudes - shells, membranes, and panels Stiffness and vibration characteristics of staged and clustered bodies Nonlinear effects of large deflections, plasticity, viscoelasticity Modeling techniques Vibration testing techniques Flight flutter testing techniques High temperature gradients/high thermal stresses Buckling and creep effects

Table 1. (Continued)

Thermoelasticity (Con't.)	Vibration and stiffness characteristics of expandable structures, Rogallo wings, etc. Vibration and stiffness characteristics of sandwich, anisotropic, and filament wound structures. Vibration characteristics of orthotropic panels
Inertia	Large rates of change of mass Fuel slosh, swirl
Aerothermoelastic Phenomena	Divergence Buffeting Buzz Panel and shell flutter Control surface flutter Aeroelastic effects on dynamic stability Aeroservoelastic coupling Effects of heating and past heating history on flutter Dynamic response - impact landing/alighting Ground wind induced oscillations Chordwise flexibility effects on flutter Sail plane/Rogallo wing flutter Dynamic buckling Accurate noise and vibration prediction

REFERENCES

1. Fung, Y. C., A Summary of the Theories and Experiments on Panel Flutter, AFOSR TN 60-224, May 1960.

2. Voss, H. M., The Effect of Some Practical Complications on the Flutter of Rectangular Panels, Presented at AIA Symposium on Structural Dynamics of High Speed Flight, April 1961.

3. Brunelle, E. J. Jr., Transient and Nonlinear Effects on High Speed, Vibratory Thermoelastic Instability Phenomena, Part I - Theoretical Considerations, WADD TR 60-484, July 1960

4. Bisplinghoff, R. L., Some Structural and Aeroelastic Considerations of High Speed Flight, J. Aero. Sci., April 1956.

5. Runyan, H. L. and Morgan, H. G., Flutter at Very High Speeds, NACA RM L57D16a, June 1957.

6. Rogers, J., Aerothermoelasticity, Aero/Space Eng'g, October 1958

7. MacNeal, R. H., Hill, J. H., and Mazelsky, B., The Effects of Time Varying Aerodynamic Coefficients on Aeroelastic Response, WADD TR 60-390, April 1960.

8. Harder, R. L., Lock, K., McCann, D.G., Wilts, C.H., Royce, W. W., Supersonic Flutter Analysis Including Aerodynamic Heating Effects, WADC TR 59-559, February 1960.

9. Miles, J. W., Unsteady Flow at Hypersonic Speeds, Proceedings of the Eleventh Symposium of the Colston Research Society, University of Bristol, April 6 - 8, 1959, pp. 185-201, Butterworths Scientific Publications (London).

10. Zartarian, G., Unsteady Airloads on Pointed Airfoils and Slender Bodies at High Mach Numbers, WADC TR 59-583, December 1959

11. Zartarian, G. and Hsu, P. T., Theoretical and Experimental Studies on Airloads Related to Hypersonic Aeroelastic Problems of General Slender Pointed Configurations, ASD TR 61-7, April 1961.

POTENTIAL AEROTHERMOELASTIC PROBLEMS ASSOCIATED WITH ADVANCED VEHICLE DESIGN

W. R. Laidlaw
John H. Wykes

North American Aviation, Inc.

ABSTRACT

Several classes of aerospace vehicles are defined according to a generalized breakdown of flight regimes and mission requirements. Within each class, typical vehicle configurations and design requirements are discussed. Particular emphasis is placed on the nature of the conflicting design requirements and the methods of resolving these conflicts as they influence or determine the solutions to critical aerothermoelastic problems. In the discussion of aerothermoelasticity, the relative influence of the problem on the final design and configuration of the vehicle is indicated.

POTENTIAL AEROTHERMOELASTIC PROBLEMS ASSOCIATED WITH ADVANCED VEHICLE DESIGN

1. INTRODUCTION

With the ever widening flight regimes and mission requirements of aerospace vehicles, the classical areas of vehicle dynamics and aeroelasticity have been steadily broadening to include thermodynamics in such an intimate manner as to make feasible the definition of a generalized problem class - Aerothermoelasticity.

In general, the individual component problems of this field are familiar. It is, however, the nature of their complex interrelationships and the subsequent incorporation of their solutions into the design of advanced aerospace craft configurations that forms the basis of the present discussion.

It is not the purpose of this paper to present methodology; but rather to establish a base from which the nature of the problems may be viewed in consonance with the many classes of vehicles and missions contemplated in future atmospheric and space operations. The view will be that of the designer who in performing his task must attempt to resolve continually the many conflicting requirements of specialist doctrines with the goal of achieving a final result which is acceptable, although probably not optimum, from the point of view of each participating discipline.

The discussion is introduced by identifying several basic classes of aerospace vehicles. Wherever possible, the characteristic missions associated with each class, or a combination of classes, are indicated. This is followed by an identification of the principal component problems associated with the field of Aerothermoelasticity. As noted above, none of these problems or considerations are in themselves new. They are, however, included here in order to completely define Aerothermoelasticity in terms of the sum of its parts; and to enable a systematic discussion of design interrelationships in the light of the selected vehicle classifications. In effect, therefore,

a "vehicle class-problem type" matrix is constructed to serve as the basis of the design presentation wherein the problems assume their individual personalities and priorities as a function of the vehicle class to which they apply.

2. BASIC AEROSPACE VEHICLE CLASSIFICATION

The aerospace vehicles and missions to be discussed below are by no means exhaustive. They are believed, however, to be sufficiently representative to encompass the majority of design problems to be encountered in considering Aerothermoelasticity. We will eliminate from discussion aircraft designed to perform subsonic missions. This is done not because they have unimportant or uninteresting problems but because they have had the benefit of considerable attention in the past. The following aerospace vehicle classes will be defined for the purposes of the present discussion:

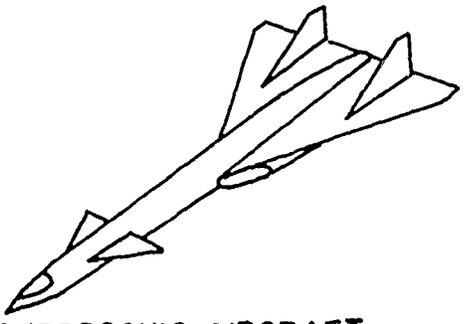
Supersonic aircraft
Hypersonic aircraft
High L/D re-entry spacecraft
Low L/D re-entry spacecraft
Manned spacecraft
Unmanned spacecraft
Spacecraft launch vehicles

Configurations representative of these typical vehicle classes are shown in Figure 1.

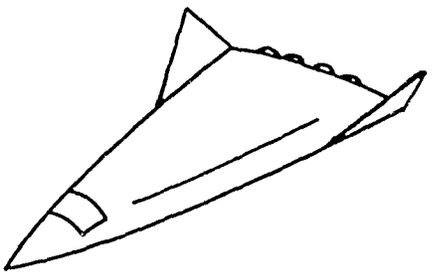
Supersonic Aircraft

Aircraft in this category are powered by turbojet or turbofan engines using JP fuel. They are winged with relatively high L/D (approximately 7.0); and have conventional monocoque or semi-monocoque structure of steel and/or titanium. Cruise speeds lie in the Mach number region from 2.0 to 4.0 with altitudes ranging up to approximately 100,000 Ft. Structures will be subjected to steady state temperatures in the vicinity of 600° to 800° F during cruising flight; and the design dynamic pressure may be a high as 2000 P.S.F. depending on the mission altitude. Examples of this class of aircraft are:

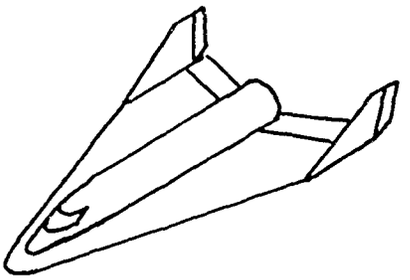
a) Supersonic transport
b) Supersonic bombers (high and low altitude)
c) Early version of the recoverable booster system



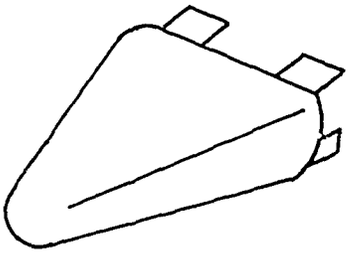
SUPERSONIC AIRCRAFT



HYPERSONIC AIRCRAFT



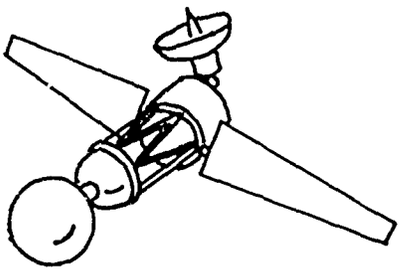
HIGH L/D RE-ENTRY SPACECRAFT



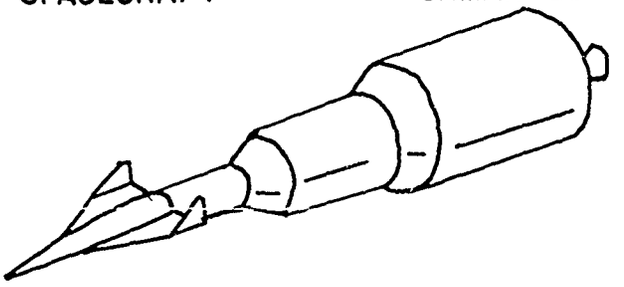
LOW L/D RE-ENTRY SPACECRAFT



MANNED SPACECRAFT



UNMANNED SPACECRAFT



SPACECRAFT LAUNCH VEHICLE

FIGURE 1 AEROSPACE VEHICLE CLASSES

Hypersonic Aircraft

These aircraft are powered by turbojets, rockets, turboramjets, or other hybrid engines using cryogenic fuel (i.e. hydrogen). They will be winged with moderate L/D (approximately 4.0). By virtue of the extremely low fuel density, they will require high volume and a heat protected or insulated structure. Maximum speeds will be in the vicinity of M = 12.0 at altitudes up to 250,000 Ft. At these conditions, however, the flight time will be relatively short. Steady state and transient temperatures of approximately 1500° to 2000° F may be expected although the dynamic pressures at the high temperature design point will be less than 1000 P.S.F. At lower altitudes and temperatures, the dynamic pressure limit will be approximately 2500 P.S.F. Typical examples of this type of vehicle are:

a) Advanced recoverable booster
b) Hypersonic bomber

High L/D Re-Entry Spacecraft

These vehicles have no propulsive equipment save for small retrorockets for re-entry initiation. They will have relatively low wing loadings with an L/D in the vicinity of 2.0. It is possible that variable aerodynamic geometry will be employed; and external drag devices may serve in conjunction with reaction and aerodynamic controls as a primary means of re-entry flight path correction. The structure may be of the truss-heat protected type, forced cooling, or hot refractory metal configuration. For satellite velocity re-entries, a maneuvering, maximum heating load (as opposed to a maximum heating rate) trajectory will be flown with maximum temperatures near 3000° F in local regions such as leading edges, nose, etc. Design dynamic pressures will be of the order of 1000 to 1500 P.S.F. Boost-glide vehicles are typical of this class.

Low L/D Re-Entry Spacecraft

Vehicles of this type have no wings but nevertheless achieve a limited lifting capacity ($L/D \approx 0.5$) from the basic body shape. The structure is heat protected either by means of heat sinks or ablative materials. Either reaction controls or combined aerodynamic-reaction controls are used to provide limited maneuverability. The re-entry

trajectory is determined primarily by re-entry conditions and the ballistic coefficient $\left(\frac{W/S}{C_D}\right)$. These vehicles will be utilized primarily for "deep space" or "long time" missions where the relative inefficiency of the re-entry is offset by the volumetric efficiency of the unwinged aerodynamic shape. Re-entry trajectories will result in high heating rates and critical temperatures of the order of 5000° F with dynamic pressures of approximately 2000 P.S.F. Current examples of this type of spacecraft are:

a) Mercury
b) Apollo

Manned Spacecraft

These vehicles are wingless and may or may not have provisions for re-entering planetary atmospheres. The basic shape of the vehicle is largely determined by the heavy emphasis on life support and power systems which require pressurized crew enclosures and meteoroid and radiation shielding. Conventional or inflatable structure may be used. Rocket or nuclear propulsion will be employed. Reaction controls are used for maneuvering. Operative speeds will be satellitic or super-satellitic at altitudes beyond 500,000 Ft. The temperature in space will depend on the vehicle's relative rates of absorption and radiation. A vehicle of this type spending any time on the moon would have to consider a lunar day-night temperature cycle of +250° F to -250° F. Space stations are typical of this class of spacecraft.

Unmanned Spacecraft

Spacecraft of this type are wingless and, for the most part, have simple truss or basic unpressurized structure. The design is influenced by a heavy emphasis on electronics and associated sensors. Rocket propulsion, and reaction controls will be used for maneuvering. It may be desirable, in some instances, to provide landing capabilities. The temperature environment will depend on the vehicle's relative absorption and radiation characteristics in space. Illustrative examples of spacecraft of this type are:

a) Surveyor
b) Prospector

c) Ranger
d) Explorer

Spacecraft Launch Vehicles

The design of this type of unmanned vehicle is dominated by the large liquid or solid rocket propulsion system. The structure is either free standing or pressure stabilized. Control is obtained with reaction controls or vectored thrust using command control/inertial guidance. Lifting surfaces may be needed for aerodynamic stability. The maximum altitude is in the vicinity of 500,000 Ft.; the design dynamic pressure, approximately 1000 P.S.F.; and the design temperature approximately 400° to 500° F. Wind shear and pad loads are of particular importance in the design of these vehicles. Examples of this class are:

a) Atlas
b) Saturn
c) Nova

3. MISSIONS

In the foregoing classification it has been necessary to grossly oversimplify the presentation in order to achieve an identification of several basic vehicle types. In actual practice, specific spacecraft are tailored to the demands of a particular mission; and, in most cases, combine the features of two or more of the basic classes. Accordingly, the following section will indicate, in a general manner, the nature of some of the more common combinations. We will eliminate from the discussion those examples wherein the basic classification implies the mission directly (e.g. supersonic aircraft-supersonic transport).

Ballistic Missile

The mission objective is to place a warhead on a predetermined target within a selected or defined error. The system combines a suitable launch vehicle with a low L/D re-entry body. In this case, the re-entry vehicle is unmanned and may frequently operate ballistically (i.e. L/D = 0).

Recoverable Booster

The principal objective of this mission is to enable a significant reduction of launch cost of orbital payloads through the mechanism of recovery and reuse of launch vehicles. Under certain conditions this could imply the unmanned recovery of one or more stages of a vertical launch booster system (i.e. by means of parachute or paraglider systems). For the most part, however, it implies a manned, winged, lower stage vehicle transporting nonrecoverable upper stages which are launched along ballistic trajectories. Accordingly, such a recoverable booster system would be comprised of a supersonic or hypersonic aircraft combined with a typical unmanned launch system. It should be noted that at the "drop point" a steep pull-up of the first stage is required in order to minimize the maneuvering loads and conserve fuel in the subsequent unmanned stages.

Aerospace Plane

The aerospace plane type system is really an extension

of the recoverable booster concept. In this case, however, the performance of the lower stage is so increased as to permit an orbital flight capability: thus, in effect, yielding a manned, winged, one-stage-to-orbit recoverable vehicle. Intermediate versions could utilize "piggy back" arrangements wherein a multistage approach is used involving individual, manned, recoverable stages. Obviously, therefore, the aerospace plane is a compounding of a hypersonic aircraft with a high L/D re-entry spacecraft in a single vehicle. The multi-stage version would in effect combine these same classes through the assemblage of several distinct vehicles or stages.

Orbital Reconnaissance or Bombardment

This system requires a suitable launch vehicle of either the manned or unmanned type in conjunction with a recoverable orbital vehicle. The orbital mission itself dictates the use of a large number of complex sensors in combination with suitable computers, data and command links. Accordingly, as mission time is extended, the maintainance requirement normally dictates the use of a manned vehicle. Whether manned or unmanned, however, a strong requirement for landing accuracy and flexibility of landing site and landing time exists. This latter consideration prompts the use of a high L/D winged vehicle with its attendant re-entry maneuvering capability. Since the vehicle will, in most cases, be confined to earth orbital operations, the structural weight penalties associated with the use of wings in combination with parabolic re-entry velocities will not be experienced to any great extent.

Deep Space Operations

Here, again, a suitable earth escape booster is called for. Since, however, escape velocities are required, the launch vehicle will normally be of the multi-stage, vertical launch, non-recoverable type. At the present time, the spacecraft themselves are of the unmanned variety; and in only a few cases are provided with re-entry capability. In the future, however, as booster systems increase in performance and reliability, it is logical to expect that these systems will be manned. The manned system must, of course, be recoverable; and, in addition, may be designed for an extended mission time by virtue of its "in-flight"

maintenance capability. Since re-entries from parabolic velocity are called for and since the mission time will be long, the structural efficiency must be maximized. This normally calls for the use of an unwinged, low L/D re-entry, spacecraft configuration. In addition to the earth landing capability, certain missions will require landings on other planets or celestial bodies. In the event that a planetary atmosphere exists, the landing technique will be similar to that employed for earth return. In many cases, however, a landing in the absence of an atmosphere must be effected (i.e. lunar) in which event a propulsive technique will be necessary.

Space Logistics

A space logistic vehicle's characteristics will vary considerably as a function of the particular mission requirement. In the earth-space-earth case, the logistic system will be similar to the aerospace place or recoverable booster system; whereas for space-space missions, manned or unmanned spacecraft will be employed. In all cases, the logistic spacecraft must be capable of accurate rendezvous, followed by suitable docking and systems interconnection with the parent craft. It should be noted that certain other military missions require similar capabilities (e.g. satellite inspection).

4. AEROTHERMOELASTIC PROBLEMS

In the previous sections several basic classes of aerospace vehicles and missions have been identified. In a similar manner, the present section will delineate the principal component problems of the overall field of Aerothermoelasticity. In several instances the items named are not problems in the strictest sense, but rather critical design considerations. For purposes of completeness, however, they will be listed here in order to aid in a comprehensive view of Aerothermoelasticity.

Classical Flutter

This problem may be identified as an aerodynamic-structural vibratory instability of lifting surfaces involving several structural and/or rigid body degrees of freedom. As shown in Figure (2), it typically figures in the design process in establishing basic structural stiffness levels as functions of Mach number and altitude (or "q"). Often it determines gross mass distribution characteristics, particularly for hinged or rotating surfaces, or for situations where large concentrated masses are involved. Infrequently it is a determinant of basic aerodynamic shape or control system characteristics.

Panel Flutter

This problem is characterized by a high frequency, aerodynamic-structural instability of local panels or areas of a vehicle's surface. It figures in the design process as a detail design consideration in establishing panel thickness, edge restraint, geometry, and stiffener location. The problem is difficult to predict accurately except in rather idealized situations and frequently requires use of empirical or test data such as that used to establish the criteria of Figure (3).

Forced Vibration

Generally, this problem is involved in the design process from the standpoint of dynamic stress resulting from structural vibration; that is, excitation of one or more structural modes. The character of the problem varies

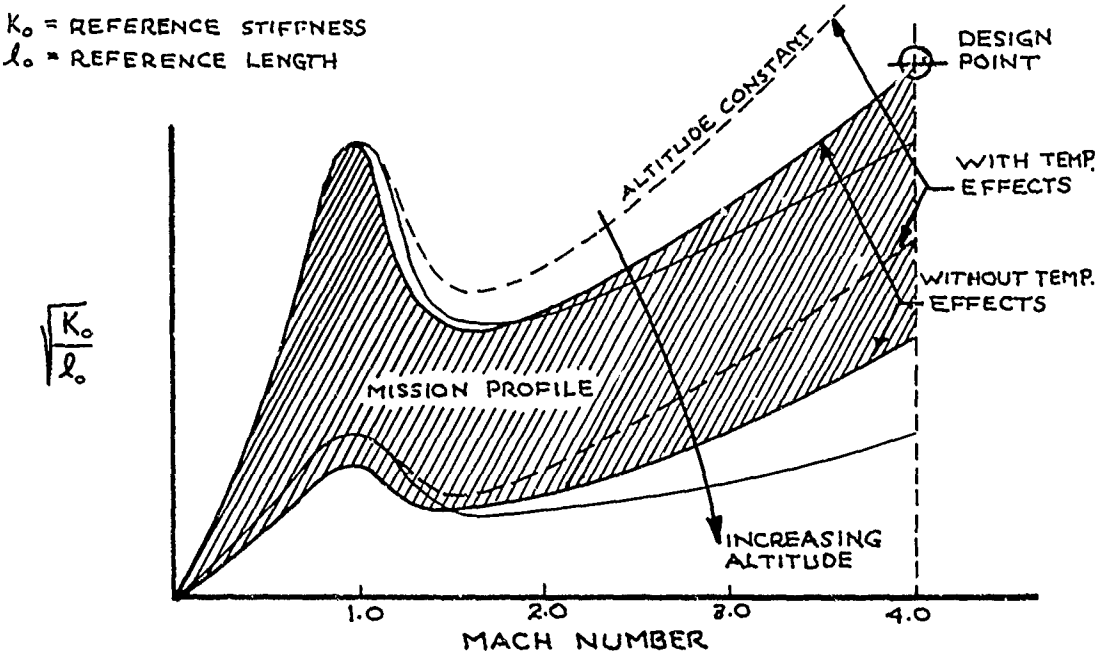


FIGURE 2 LIFTING SURFACE FLUTTER STIFFNESS REQUIREMENT

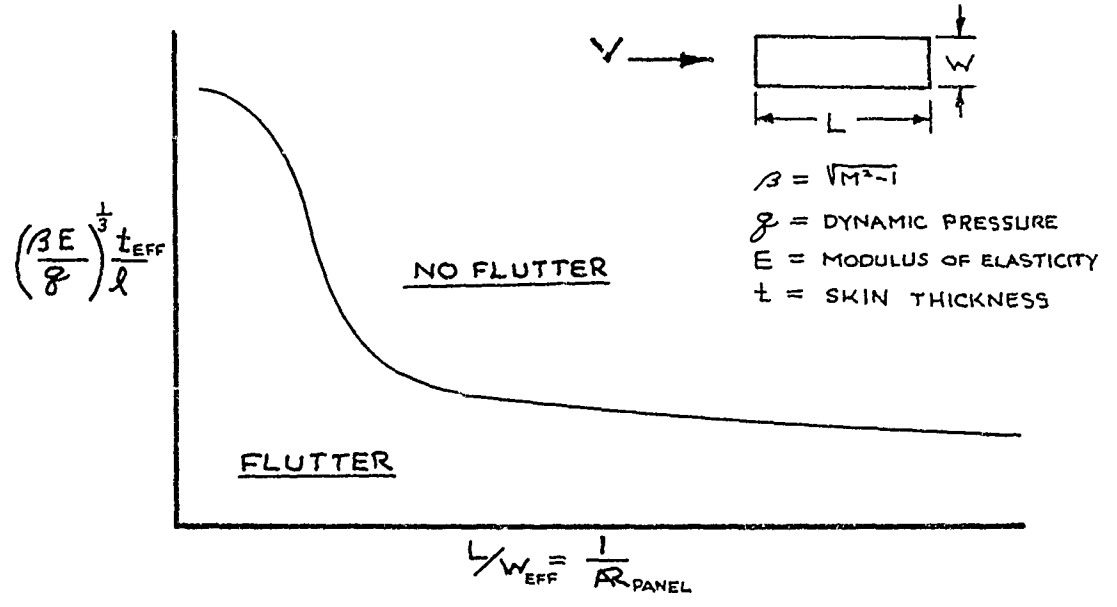


FIGURE 3 PANEL FLUTTER STIFFNESS REQUIREMENT

widely as a function of the forcing function and degree of dependence on aerodynamics. Examples include landing, taxiing, abrupt control motions, release of external stores, and in-flight impact with foreign bodies. It is an extremely important consideration in stress analysis and fatigue analysis of flexible airframes.

Acoustics

The acoustics problem is a variation of the forced response problem where the excitation has a broad band harmonic content arising from acoustic sources such as boundary layer turbulence, engines (see Figure (4)) and high velocity internal flows. It is usually treated in a manner similar to panel flutter with the principal consequences affecting the fatigue life of local structural regions. Even though the stress levels may be relatively lower than other fatigue-causing excitations, the stress cycle rate is extremely high. As indicated in Figure (5), the acoustic fatigue mode could become more critical than the lower frequency load cycles.

Buffet

Buffet is a problem similar in many respects to acoustic excitation, forced vibration, and gust phenomena. In this case, the nature of the forcing function is again random and in many respects similar to boundary layer turbulence but for the turbulence scale. The problem is usually associated with major flow discontinuities or separations and the response involves both rigid and flexible airframe degrees of freedom. In addition to the obvious load and fatigue considerations, the problems of maneuvering limitations and crew comfort must be considered. Unlike the acoustic problem, the overall structural response may be dependent on significant aerodynamic coupling and even involve instabilities such as stall flutter.

Static Aeroelasticity

The static aeroelastic problem is associated with the "static" interaction between aerodynamic or inertia loads and structural deformation. In addition to the obvious influence and modification of the design loads, the changes in basic stability derivatives such as shown in Figure (6) are fundamental considerations in elementary dynamic and

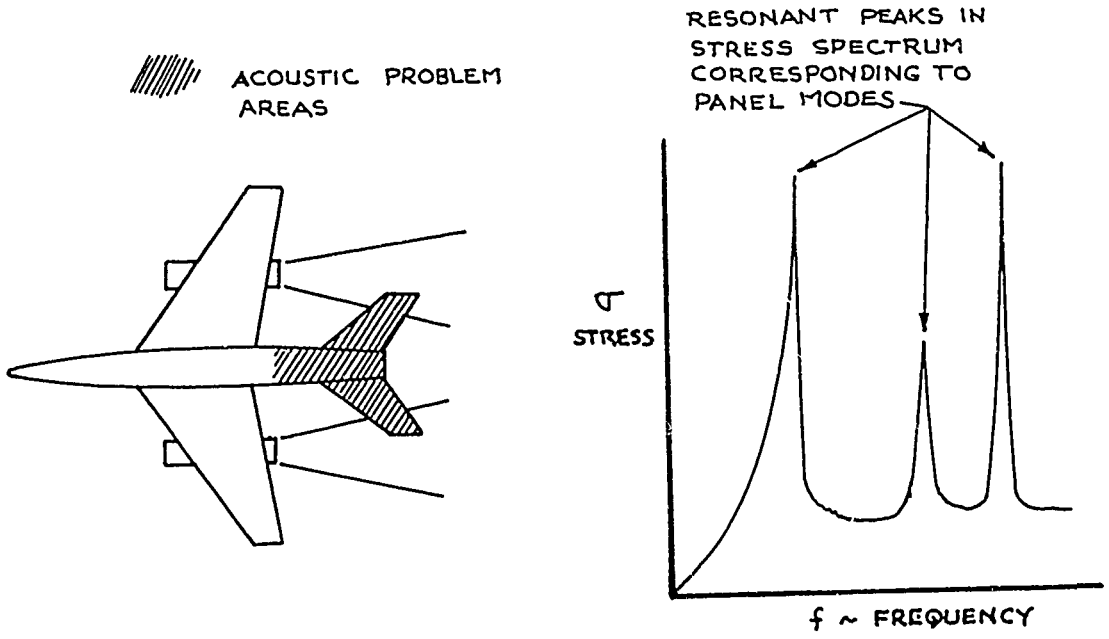


FIGURE 4 EFFECT OF ACOUSTICS ON STRESS

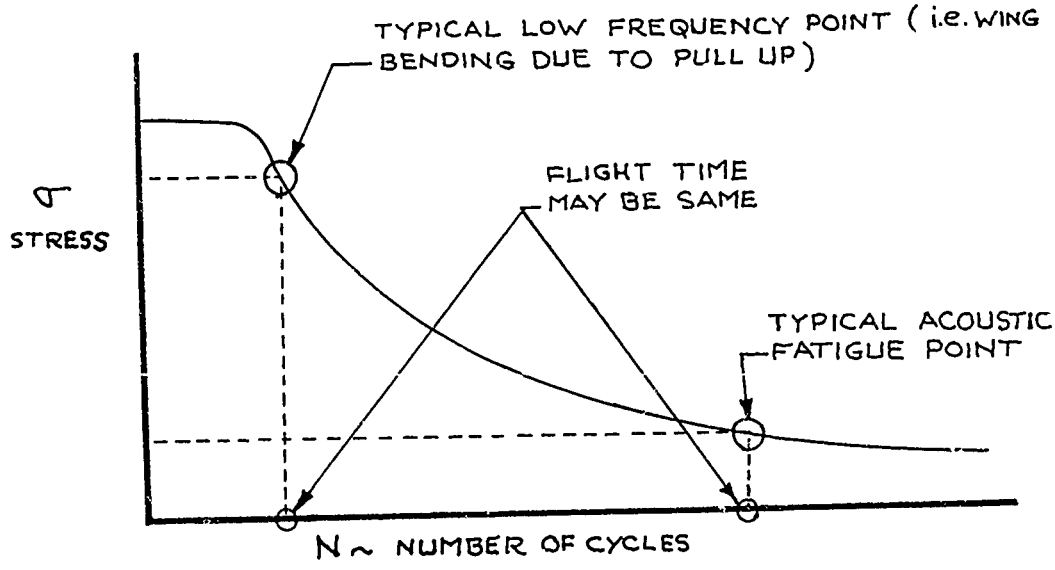


FIGURE 5 EFFECT OF STRESS RATE ON FATIGUE LIFE

performance analyses in which structural dynamics, per se, are insignificant. As in the case of flutter, the principal control is through the medium of structural stiffness and the major determining flight parameter is the dynamic pressure.

Temperature

Steady state temperatures resulting from thermal equilibrium at sustained high Mach number flight conditions are a basic consideration in all aerothermoelastic analyses. Usually the problem results from the heat transfer characteristics of the flow field in conjunction with the "heat sink" capacity of the airframe. Similar problems are encountered, however, in the vicinity of engines and other concentrated heat sources.

The basic problem involves the temperature deterioration of structural properties such as the stiffness moduli and allowable stresses. In addition, the creep rate increases with increasing temperature thus leading to important permanent deformation considerations. The basic temperature levels may drastically influence the choice of structural materials, alter design load and fatigue criteria, and determine internal cooling systems requirements. Furthermore, thermal cycling due to repeated mission performance may reduce the useful life of the vehicle from a combination of creep effects and permanent changes in material properties.

Thermal Stress

Thermal stress problems result from the differential expansion of structural components usually associated with the existence of temperature gradients throughout the airframe. These conditions, in turn, usually occur in conjunction with transient flight conditions while moving from one state of thermal equilibrium to another (Figure (7)). The problem is extremely important in stress analysis and must be taken together with maneuvering stress conditions. Stress duration and time history are dependent on the thermodynamics of the structure, flight time history, structural plasticity, and structural arrangement. Thermal stresses may affect critically the stiffness characteristics of built up structures; and, in this manner, lead to serious consequences in such stiffness dependent problem areas as flutter and static aeroelasticity. Also, they may on occasion produce sufficient structural deformation to affect

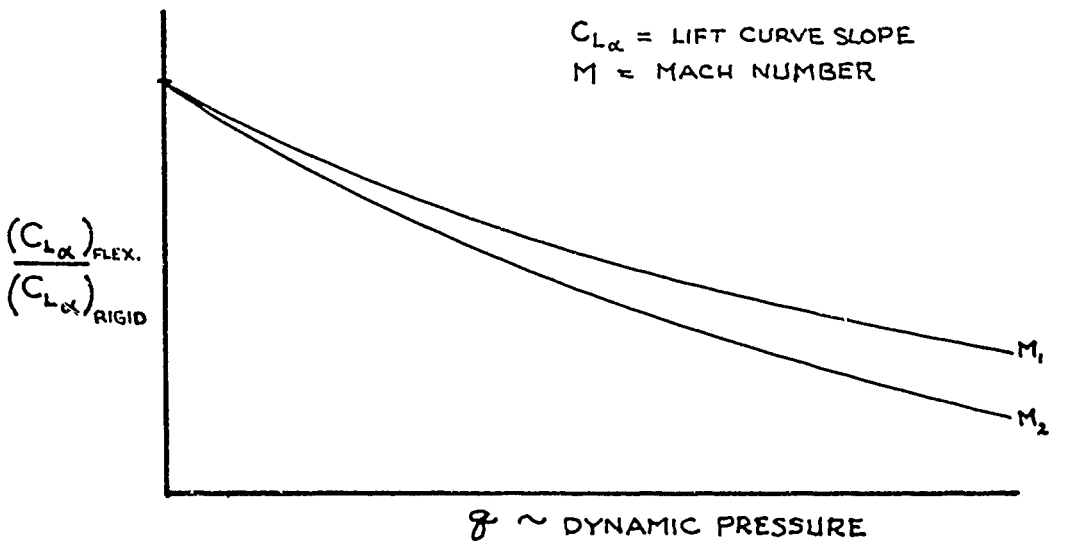


FIGURE 6 LIFT CURVE FLEXIBLE TO RIGID RATIO AS INFLUENCED BY DYNAMIC PRESSURE

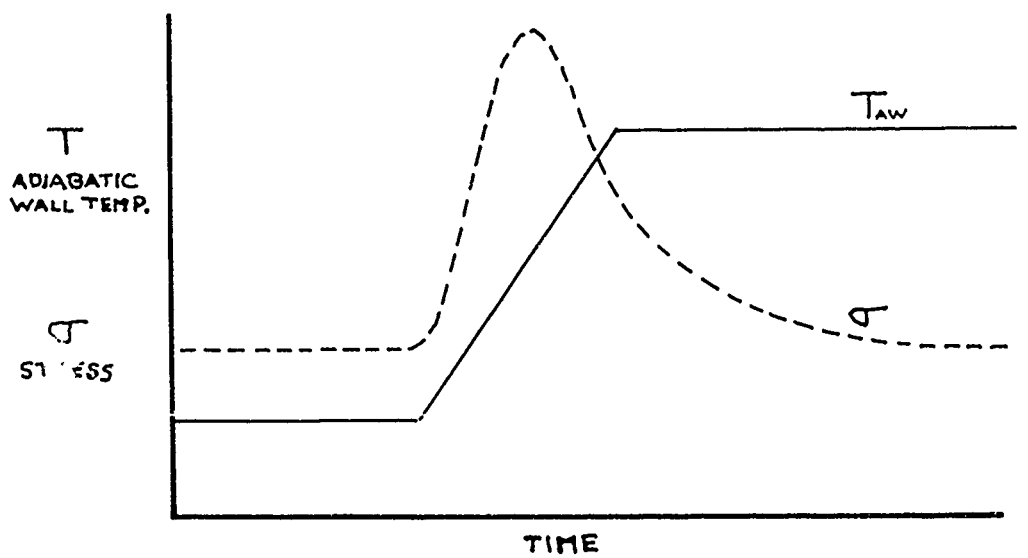


FIGURE 7 TRANSIENT THERMAL STRESS

external aerodynamics and associated loadings as in the case of leading edge "curling".

Materials

Materials considerations usually result from analyses of specific problem combinations in a particular design situation. Weight, cost, produceability, and fabrication requirements are paramount in addition to the obvious requirements on stiffness, strength, creep, and fatigue life. Most new structural materials have been selected on the basis of their capabilities in high or very low temperature environments. Such refractories as molybdenum, columbium, and beryllium have been considered in addition to steel and titanium as primary structural components. Besides load carrying materials, heat absorbtive, insulative, and ablative materials are also basic needs of a variety of vehicle types. Oxidation and the coating materials required to prevent it constitute one of the major high temperature materials research problems.

Rigid Body Instabilities

Typically this problem involves the major mass and inertia characteristics of the vehicle in combination with its basic external and sometimes internal aerodynamics (i.e. duct inlets, etc.). In many cases, where unusual vehicle shapes are involved, all six basic degrees of freedom may be non-linearly coupled inertially and aerodynamically. Figure (8) shows the familiar roll-inertia coupled stability problem. Undesirable situations may occur as a result of (or in combination with) forced or free body motions; that is to say, basic transients may become unstable or forcing inputs may produce unacceptable motions from the flying qualities point of view. Considerations relating to this problem are usually basic to the choice of the external aerodynamic configuration.

Fuel Sloshing

Primarily, the fuel sloshing problem is associated with high mass ratio vehicles exposed to missions or environments which may produce significant and rapidly varying loads. The effects manifest themselves in the form of inertia coupling between airframe and fuel motions. Major changes in vehicle dynamics frequently occur both as a

result of the additional non-linear fuel degrees of freedom and the rapidly varying fuel mass as illustrated in Figure (9). Problems of this type may also involve airframe - control system dynamic coupling and internal structural loads. Often the consequences result in major changes in fuel tankage and baffling, fuel sequencing, and structural and/or control system configuration.

Inertia Cross Coupling

Inertia cross coupling is a generalized problem classification of which certain rigid body and fuel slosh problems represent particular examples. Many situations exist in which high angular rates in inertial space give rise to coupling type phenomena involving both rigid and flexible degrees of freedom. Very often, however, the coupling terms are non-linear and non-Eulerian. The consequences of these problems are many and they frequently involve major design load and control system requirement changes. The problem invariably occurs in consonance with unusual geometric configurations, large concentrated masses, and a general lack of inherent system damping.

Control System Instabilities

Control system instabilities are usually related to problems involving rigid body and/or structural degrees of freedom. Typically, the requirements on control system performance have increased as a result of more demanding missions. This has led to considerations or requirements for both stability augmentation and automatic flight equipment. Problem consequences usually involve sensor locations, structural characteristics, major modifications (and sometimes compromises) in the open loop performance characteristics. Usually the problem is initiated by an inertial sensor such as an accelerometer or rate gyro and is subsequently augmented through an incompatible set of airframe dynamics for the flight condition or vehicle configuration in question. Figure (10) depicts a typical effect of structural flexibility on sensor location.

Gust Response

The gust response problem is closely related to the rigid body and forced vibration problem areas. In this case, the forcing function is primarily aerodynamic in the

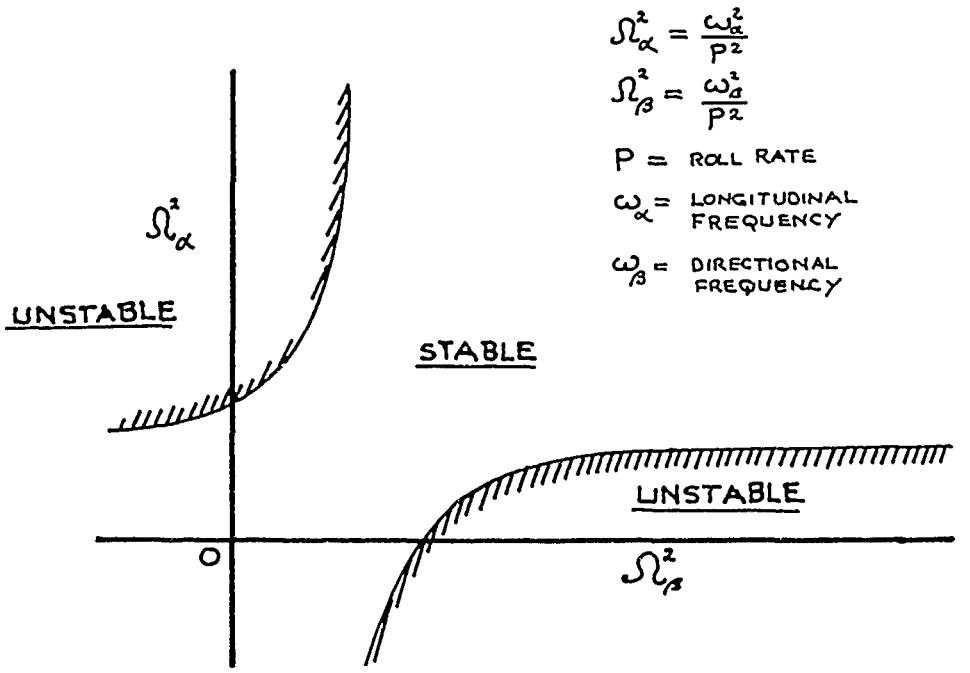


FIGURE 8 RIGID BODY STABILITY FOR STEADY ROLL RATES

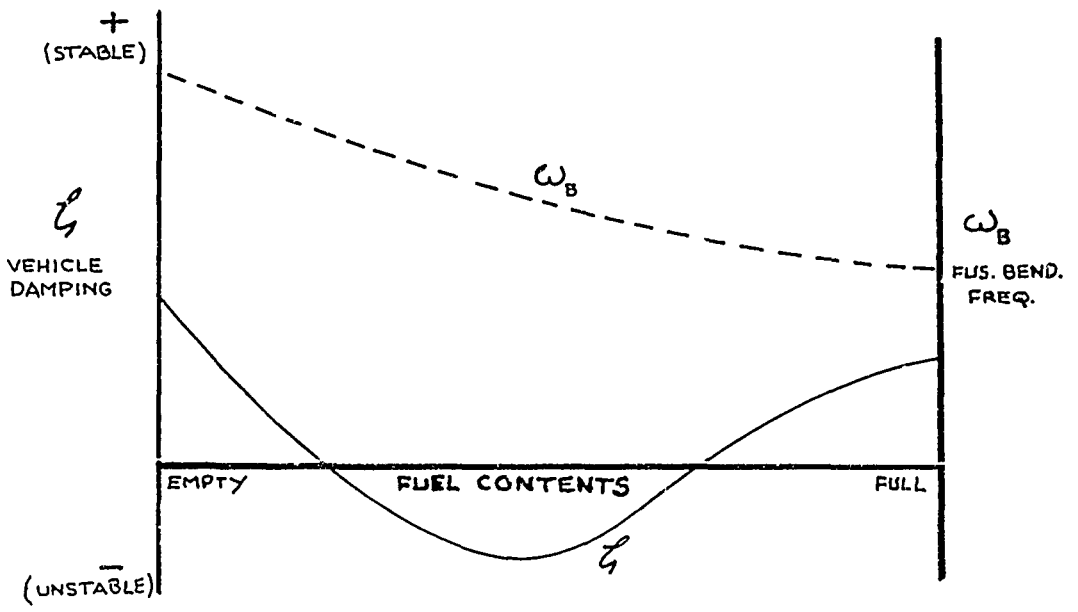


FIGURE 9 VEHICLE DAMPING DUE TO FUEL SLOSH-AUTOPILOT COUPLING

form of a tri-axial wind shear distribution. In a realistic situation the loads are random with a relatively broad band spectrum. The consequences relate directly to structural loads, fatigue, and (in extreme cases) crew performance degradation. Figure (11) depicts a typical gust bending moment power spectrum. The severity of the problem is a function of the flight condition, inertial characteristics, and aerodynamic configuration.

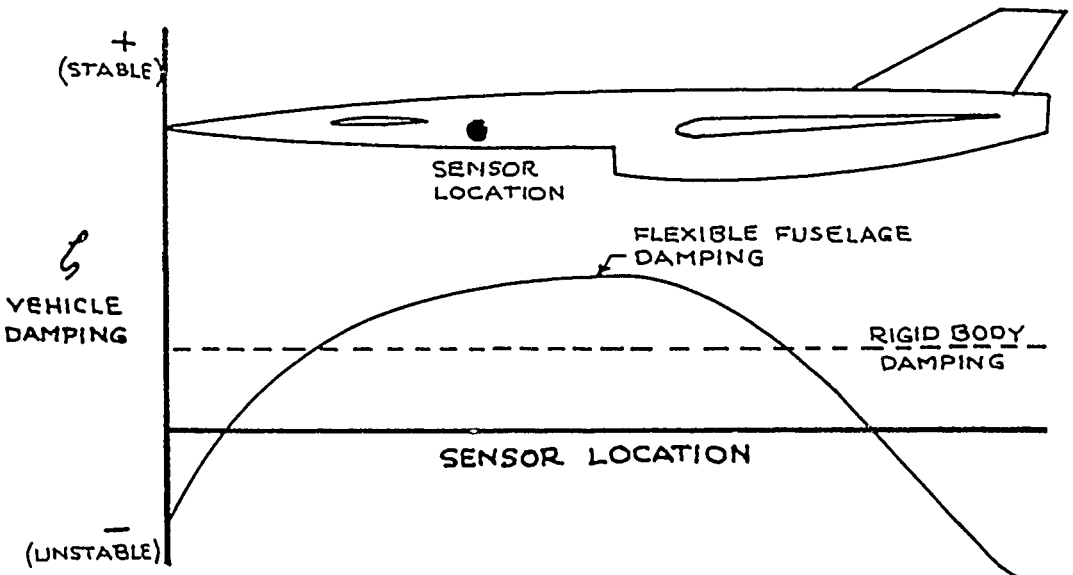


FIGURE 10 VEHICLE DAMPING DUE TO AUGMENTATION AS INFLUENCED BY SENSOR LOCATION ON A FLEXIBLE FUSELAGE

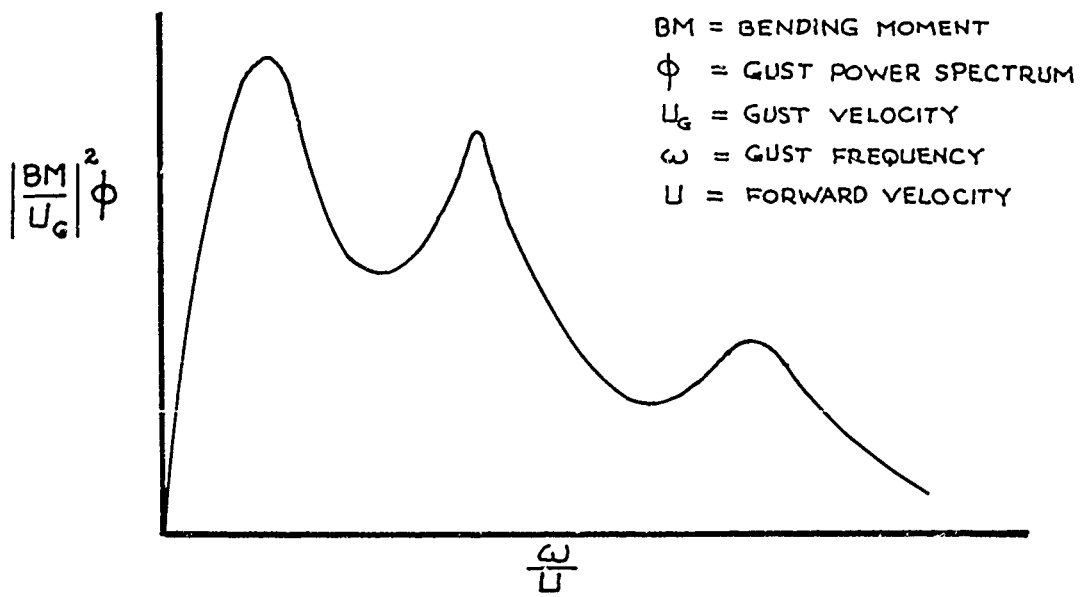


FIGURE 11 BENDING MOMENT POWER SPECTRUM GUST RESPONSE

5. DESIGN CONSIDERATIONS

In the following section, the design influences of Aerothermoelasticity will be examined in accordance with the individual vehicle classifications previously defined. It will be noted that the critical emphasis on individual problems varies considerably with the vehicle type. Only those problems or considerations which are of a critical nature in the design process will be examined in detail.

Supersonic Aircraft

As examples of supersonic aircraft of interest from the aerothermoelastic point of view, consider the supersonic transport or bomber. The basic mission requirement of these vehicles is to transport a payload over long distances rapidly and economically. These goals immediately dictate the general size of the vehicle as well as a winged configuration with, in all probability, a high volume fuselage (more so for the transport than the bomber). The wing will have a high L/D at the design lift coefficient for range; and will most probably have a high sweep angle, low aspect ratio, and a low thickness ratio to minimize the supersonic drag. The fuselage volume is determined by the payload and equipment to be carried, but its fineness ratio is set by supersonic drag considerations. To achieve fuel economy, the cruise altitude will be high and will, in turn, be a major factor in setting the wing size. For a given design (or cruise) Mach number, the cruise altitude establishes the dynamic pressure which, in turn, dictates the wing loading required for operation at (L/D)max. It should be noted that as the design altitude at a fixed Mach number is reduced the required wing loading increases. This will normally be effected by reducing the wing size.

Classically, wing flutter considerations have dictated structural stiffness levels. In so far as the wing itself is concerned, this situation will still exist. It is significant, however, that the stiffness requirement is based on flight at the maximum Mach number rather than the transonic condition which has frequently, in the past, constituted the critical case. Figure (2) clearly illustrates the reasons for this shift to the higher Mach number stiffness design point. In effect, the combination of temperature

and increasing Mach number lead to requirements over and beyond those dictated by the lower altitude transonic condition. It will be noted from Figure (2) that as the altitude at the design Mach number is reduced the required stiffness increases. This may be attributed directly to the increasing dynamic pressure. For a wing of fixed size, the structural weight to prevent flutter would increase significantly were it not for the fact that the overall wing size must be reduced to maintain optimum cruise lift coefficient. Figure (12) demonstrates the effect of selected cruise altitude on the overall wing weight fraction. It will be noted that as the design altitude is reduced the wing weight reduces to a point where the increasing weight for flutter prevention offsets further weight reductions due to decreasing wing size.

When the temperature impact on design is examined, it is found that the effect is primarily a steady state one. Generally the vehicle accelerates sufficiently slowly that nearly equilibrium structural temperatures are maintained at all times. The maximum temperature at the design Mach number and altitude is large enough, however, that its effect must be included in the flutter analysis. In general, the temperature effect enters the analysis through its impact on the elastic moduli of the material. The principal considerations relating to thermal stresses occur during the deceleration phase where the vehicle may slow at a high rate while at the same time encountering increased loads and dynamic pressures associated with lower altitude flight. In this case not only the stiffness effects on flutter require consideration but also the combined effects of maneuvering and thermal stresses.

In order to reduce surface temperatures, it is expedient to utilize the heat sink capacity of the JP fuel. This process is obviously time and range limited but may result in a significant cooling effect for "dash" missions.

Designing for optimum performance at high Mach number and altitude has produced configurations which, in many cases, cannot meet the low speed wing loading requirements dictated by runway length. One solution to this problem receiving serious consideration is a variable geometry (swept) wing. The various wing configurations must be examined for flutter in the intermediate flight regime; and much attention must be devoted to the stiffness requirements on pivots, actuators, and local backup structure.

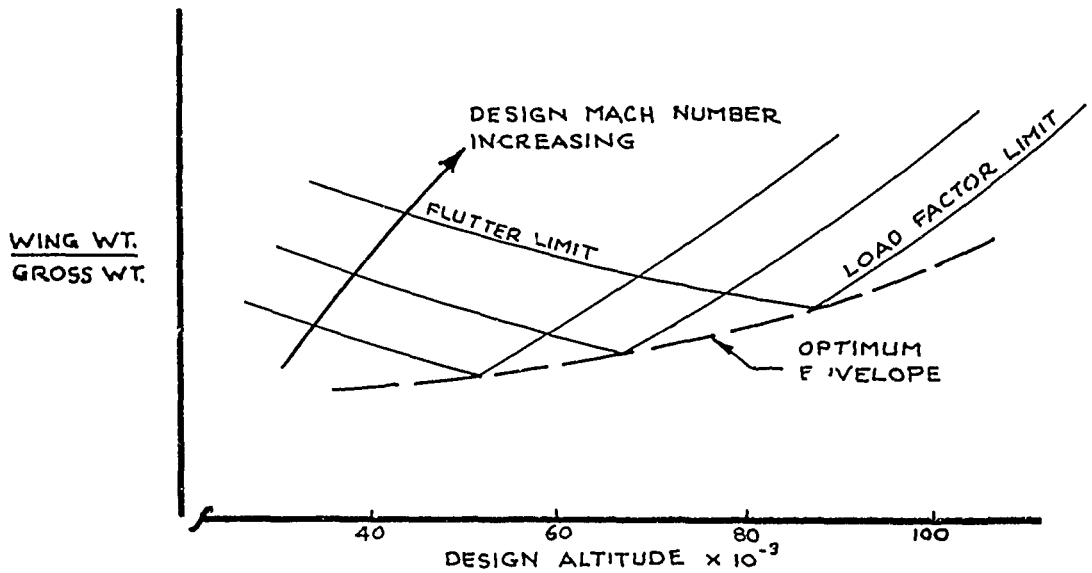


FIGURE 12 WING WEIGHT - ALTITUDE OPTIMIZATION

Panel flutter traditionally becomes more serious as the operating dynamic pressure increases at supersonic Mach numbers. It is evident, therefore, that panel flutter including the effects of elevated temperature must be considered in a supersonic aircraft design. The problem is frequently difficult to separate from acoustic fatigue because the failure modes are very similar and both are aggravated by high Mach number and dynamic pressure. The problem is somewhat alleviated by the use of honeycomb structure which has been shown to be desirable from a temperature and structural efficiency standpoint.

In view of the high fineness ratio fuselage required, fuselage bending now becomes a primary design problem. This characteristic, when taken together with the fact that a low aspect ratio wing is utilized, leads to flutter modes of low frequency involving wing chordwise and fuselage bending. Also, many configurations require a canard surface for trim drag reasons, thus leading to flutter problems involving symmetric and antisymmetric fuselage modes coupled with canard degrees of freedom. The fuselage bending situation is aggravated in the supersonic transport by virtue of the requirement for an unobstructed fuselage shell with many window cut-outs which reduce the shear carrying capability of the structure.

In addition to these problems, the low frequency fuselage bending characteristics will be a major factor in control system design. Over and beyond an aggravated deflection problem associated with the mechanical elements, several important dynamic considerations are involved. Inertial sensors (accelerometers, gyros) will pick up flexible structural motions thus leading to a consideration of servo-elastic instabilities.

Gusts encountered during low altitude bombing or attack missions will be a major factor in determining structural loads and may limit the performance through an application of structural fatigue and crew tolerance criteria. In so far as "rigid body" gust response at low altitude is concerned, high wing loadings and low aspect ratio wings constitute relieving factors. Structural response, however, increases directly with speed. In dealing with these problems, a full consideration must be given to using the flight control system as a gust alleviator and to using both natural and artifical structural

damping techniques.

Static aeroelastic problems will require consideration directly proportional to dynamic pressure and structural efficiency. As in the flutter case, major problem emphasis will be on wing chordwise and fuselage bending. Static aeroelasticity, as always, will dictate final aerodynamic parameters and steady state load characteristics. Basic dynamic stability will involve, in roughly equal parts, consideration of rigid body, and low frequency structural degrees of freedom. It is significant that the "uncoupled" rigid body stability frequencies tend to be of the same magnitude as the lower structural frequencies.

Hypersonic Aircraft

As performance requirements increase above Mach number 4 to 5, cryogenic fuels must be utilized to achieve increases in specific impulse (or reductions in specific fuel consumption). These fuels must be used in air-breathing or non-air-breathing propulsion systems; but air-breathing systems are preferred for fuel consumption reasons. This change over from JP to cryogenic fuels dictates major changes in vehicle aerodynamic and structural configuration. Since cryogenic fuels have approximately 7 percent of the density of conventional fuel, internal volume and physical size must increase enormously. A decrease in vehicle density therefore results. The net effect is the selection of configurations with high volumetric efficiency and a trend toward flying wing or lifting body shapes.

Since the fuel must be maintained in a liquid state at temperatures near absolute zero, extremely demanding insulation requirements exist. These are made more stringent since high external temperatures resulting from high Mach number flight also exist. The structure, therefore, must be adequate to take external temperature and yet minimize inward heat conduction. A major consequence of inward heat conduction is fuel "boil off". As the inward heat flow increases, fuel vapor is vented overboard at a higher rate. This fuel loss may be charged off as a performance degradation. At a fixed performance level (i.e. mission requirement) the fuel weight lost due to "boil off" may be balanced against an increased insulation weight. It should be noted that in addition to fuel weight one must consider seriously the increased weight and volume of structure

required to contain excessive takeoff fuel. The effect of insulation thickness is shown in Figure (13).

Obviously, a serious potential thermal stress problem occurs even under steady state flight conditions. Solutions include the use of an efficient external radiating heat shield in combination with an inner insulated load carrying shell. To the maximum extent possible, the external loads must be transferred to the inner structure through a minimum number of mechanical connections to minimize heat conduction through the structural path. The demands on vehicle performance are in many aspects similar to those of a conventional booster and dictate an extremely low mass fraction (i.e. ratio of empty weight to gross weight). In order to improve structural efficiency, therefore, serious consideration must be given to the use of structural fuel tanks, thus integrating the function of the internal structure (see Figure (14)).

Structure of the type needed to meet the volume, temperature, and insulation requirements will be subject to serious panel flutter problems. Classical flutter, however, will be associated primarily with chordwise bending of the entire vehicle and be literally inseparable from dynamic stability and servo-elastic considerations.

Acoustic problems arising from the propulsion system will be somewhat diminished by locating the high energy sources at the base end of the vehicle, although the boundary layer effects will be comparable to the supersonic aircraft.

A major problem arises in the design of the inlets on air breathing configurations. A large capture area with extremely high recovery efficiency is dictated; and, accordingly, high local heat rates are obtained on sharp duct edges and throat regions. Structural instability on duct lips and internal variable geometry sections will be prime considerations. These instabilities will be similar to leading edge instabilities and panel flutter, respectively.

Hypersonic aircraft currently under consideration will spend a relatively short time at the maximum Mach number condition and the balance of the time accelerating to or decelerating from this flight regime. Accordingly, the vehicle will be subjected to extreme thermal stress

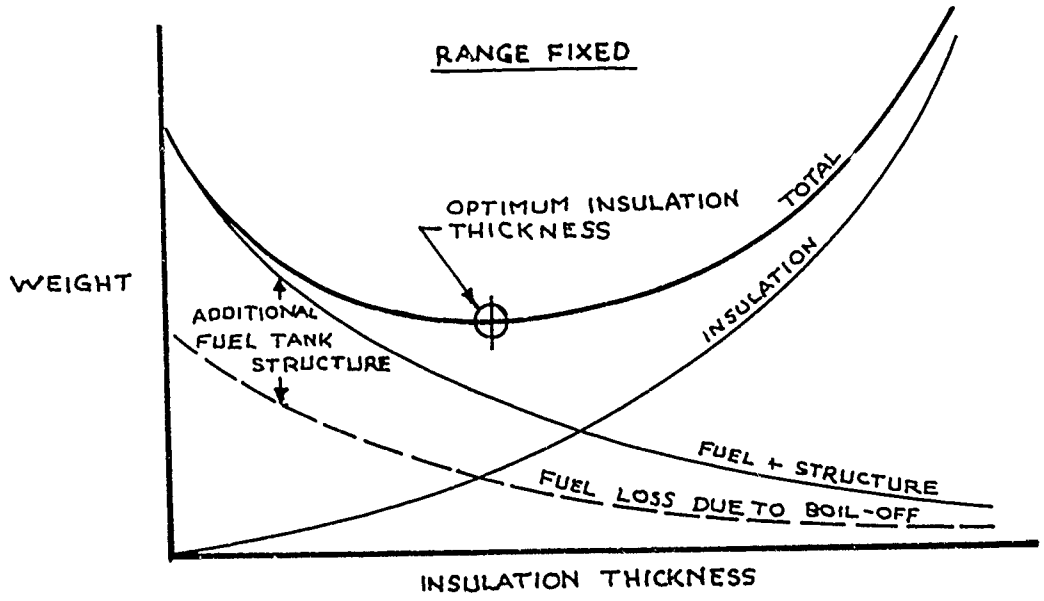


FIGURE 13 INSULATION — FUEL TANK STRUCTURE WEIGHT OPTIMIZATION

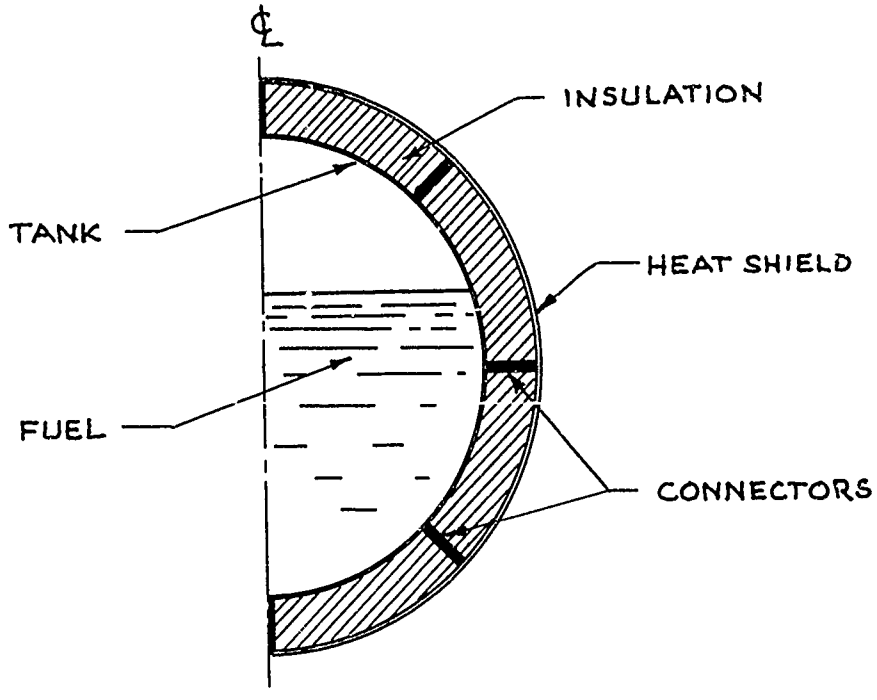


FIGURE 14 TYPICAL INTEGRAL CRYOGENIC STRUCTURE

environments. These thermal stresses will develop not only because of the aforementioned acceleration-deceleration flight profile, but also because of the strong inside-outside temperature gradients.

Generally speaking, gust problems will be most severe during the return portion of flight at low wing loadings. The aerodynamic gust loads will not necessarily exceed those associated with the higher weight climb-out condition, but the accelerations encountered will expose fixed equipment items and crew to a more severe environment.

Static and dynamic stability will be dependent, as always, on the overall aerodynamic characteristics. These, in turn, will be highly oriented to the achievement of a maximum lift-drag ratio. In hypersonic flight this frequently requires the use of "positive interference" techniques such as droop tips and inlet duct "shadowing". Although desirable from the performance standpoint, such approaches frequently lead to complex aerodynamic nonlinearities which must be accounted for in the many necessary dynamic analyses.

High L/D Re-Entry Spacecraft

This type of vehicle will normally be employed only on sub-orbital or orbital re-entry missions. The weight penalty paid for wings on vehicles re-entering from super-satellitic speeds is very great due to the greatly increased cooling requirements. Also super-satellitic missions are normally of much longer duration, with the landing requirements taking on a different emphasis in competition with other mission requirements. The winged, low wing loading vehicle is chosen for re-entry because it will permit a wide variety of trajectories. The normal design trend is to utilize maneuvering to minimize heating rate and heat load; trading, thereby,heat protection material for wing weight. A highly swept leading edge is employed on the wing to further reduce the heating rate.

Structures for vehicles in this class are normally a combination of separate external, insulated "shingles" and an interior truss arrangement to minimize thermal stresses. Other alternate arrangements include cooled structure (either forced or radiative cooling) and monocoque or semi-monocoque construction or refractory metals with

corrugated webs for thermal stress reduction. Truss type structure is normally used with relatively thick wings and deep bodies. As the vehicle thickness reduces, the joint weight of trusses become exorbitant and recourse must be made to monocoque or semi-monocoque techniques utilizing either radiation cooling or a refractory metal configuration. Since non-redundant structures such as the truss-type tend to minimize thermal stresses, the stress problem grows in proportion to the degree of redundancy and becomes more severe as the monocoque approach is introduced.

Panel flutter will represent the most basic form of structural instability. The analytical and test investigations must account for thermal buckling, thermal deterioration of material properties, and stress induced by maneuvers and thermal gradients. This is illustrated in Figure (15) where it will be noted that re-entries at higher wing loadings involve higher combinations of temperature and dynamic pressure.

Classical flutter will still be a problem for monocoque and semi-monocoque wings of relatively small thickness ratio and requires detailed investigation as the wing loading increases (i.e. reducing the altitude of the equilibrium re-entry trajectory. For thick wing configurations, classical flutter will be somewhat alleviated due to the inherently higher stiffness levels and the lower heating rates associated with the lower curvature surfaces.

During recoveries from aborted boost trajectories (normally sub-orbital) it is frequently necessary to simultaneously maximize the lift and drag coefficients. This gives rise to a requirement for extensible drag brakes which under the re-entry conditions are subjected to extremely high loads and heating rates. The possibility of instabilities similar to transonic "buzz" is very high and frequently dictates structural stiffness levels and actuator characteristics.

The requirement for maneuverability opens up the necessity of considering a number of combined rigid body and structural dynamic problems. The techniques of affecting proper control over re-entry trajectories involve maneuvering in roll at high angles of attack, thus giving rise to potential non-linear cross coupling dynamics. This, in turn, establishes stringent control requirements. Also,

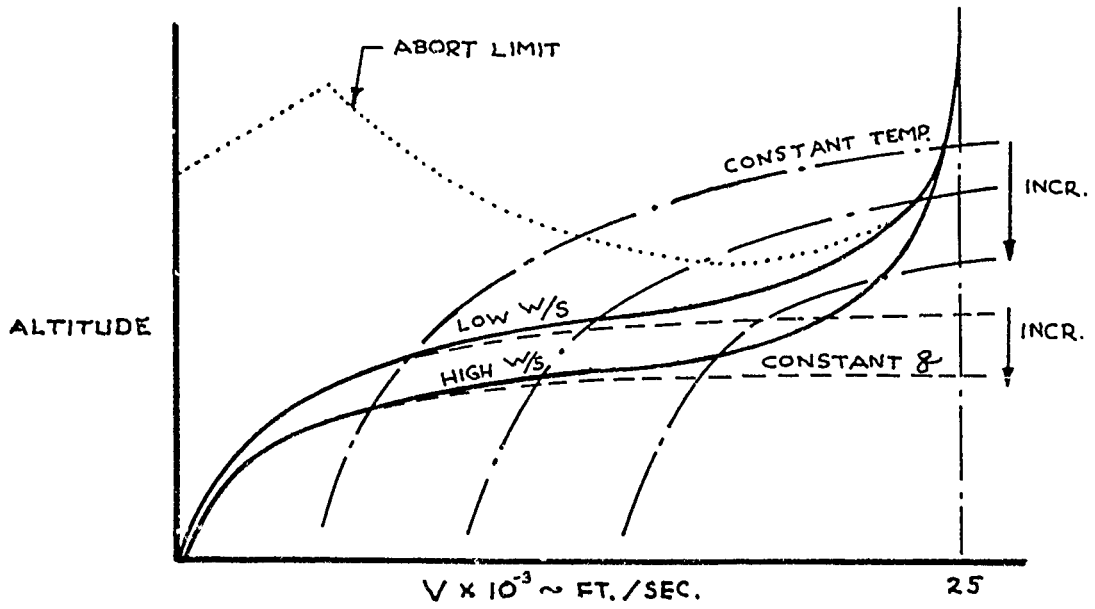


FIGURE 15 EFFECT OF WING LOADING ON RE-ENTRY TRAJECTORY

these maneuvers expose the vehicle to a wide variety of combined temperature-aerodynamic loadings which require investigation to determine design loads and operating limits. Buffet problems will be severe due to maneuvering at high angles of attack adding to flight control and structural fatigue problems.

One principal advantage of the winged vehicle is its capability to maneuver and to use fairly long glide ranges to make available a large number of landing sites. The ability to predict, however, touch down site and to determine before hand an optimum flight schedule is a difficult and exacting computation problem. Therefore, careful attention must be paid to on-board computer and sensor equipment together with the autopilot tie-in. The autopilot loop is consequently quite elaborate and must be subjected to careful analysis under all anticipated flight conditions to avoid rigid body and structural instabilities.

Material problems are in direct proportion to the nature of the chosen structural configuration. For the heat shielded or externally insulated structure, the external surface characteristics are extremely important; and much attention must be paid to surface finish, heat transfer characteristics, protective coatings, and fabrication techniques. The interior structure, on the other hand, may be fabricated from a relatively low temperature, easily worked material. Hot refractory structures, however, are extremely critical throughout; and although offering potential weight advantages when used on relatively thin surfaces, they require an extreme effort in fabrication.

Low L/D Re-Entry Spacecraft

Vehicles of the low L/D type will be utilized for deep space missions and, accordingly, will be required to re-enter at speeds up to escape velocity. With but limited maneuver capabilities, an essentially ballistic trajectory will be followed with attendant high heating rates and heat loads.

The structure of this type of vehicle will invariably consist of an integral load carrying monocoque shell heat protected externally by suitable ablative material. Figure (16) indicates the general nature of the heat shield optimization process. It will be noted that as the heat shield

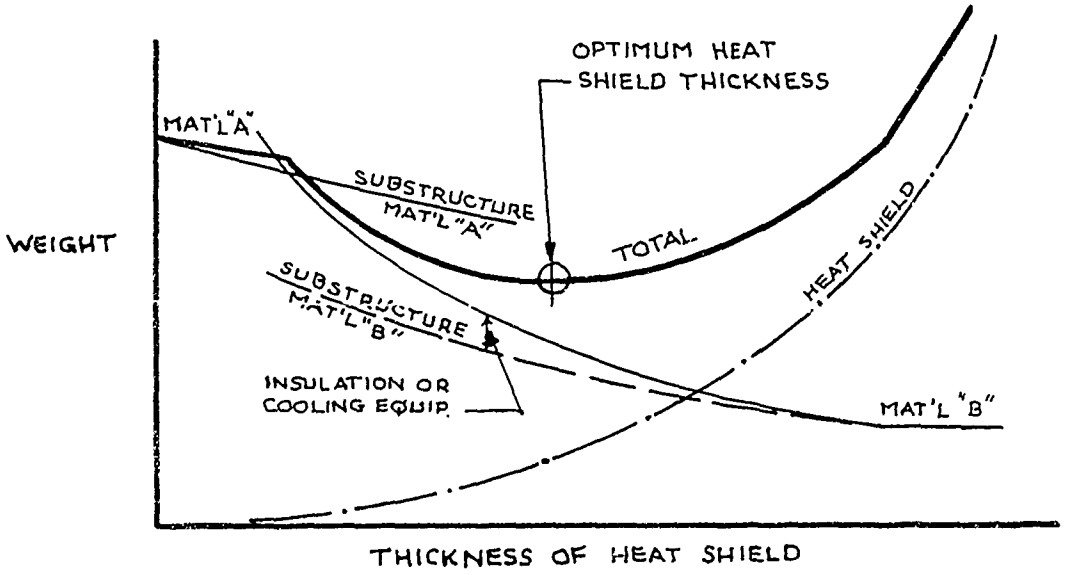


FIGURE 16 HEAT SHIELD — SUBSTRUCTURE WEIGHT OPTIMIZATION

thickness increases the weight of the substructure and insulation material is reduced until it approaches an asymptotic value corresponding to a "cold" design. The effect on total spacecraft weight of using refractory metal substructure (material "A") in conjunction with a thin ablative coating is also shown. The principal problem will be associated with the characteristics and attachment techniques of the ablative material itself. In addition, panel flutter problems will exist on the cooler portions of the structure aft of the ablative section; and, in some cases, may involve the ablative heat shield directly.

Dynamic stability and control considerations will be extremely critical due to non-linear aerodynamics, marginal static stability, and large inclinations of the body axes relative to the flight path. The limited lifting capacity will be used to the maximum to control the re-entry trajectory; and, accordingly, maneuvering at high angle of attack with the attendant inertia coupling problems is a serious consideration. Control of the vehicle will normally be through reaction jets, but it may be necessary to use aerodynamic surfaces for trim. These surfaces would be subjected to high heat rates which, in turn, dictate the structural character and the type of control required to actuate them. As in the high L/D vehicle, automatic control and trajectory equipment will be required and careful attention must be paid to closed loop dynamic stability problems.

By virtue of the low L/D configuration, this craft will not be suited for landing in the conventional mode. Consequently, auxiliary devices, such as inflatable wings, will be employed, thereby giving rise to associated problems of flutter, dynamic stability and control. Also, in the case of parachute landing in the vertical mode, touch down technique must be studied to minimize landing loads and careful attention paid to shock absorbing devices.

It is worth noting that for both the high and low L/D vehicles gas cap radiation will be an additional factor to consider in heat transfer calculations. It should also be noted that the early phases of a re-entry trajectory occur in the free molecule and transition flow regimes with the flow being highly ionized and dissociated. This requires careful attention to the aerodynamic and heat transfer characteristics of the flow.

Manned Spacecraft

This class of vehicles includes those primarily utilized for space missions for which there are no re-entry requirements. Accordingly, the principal vehicle design considerations stem from the necessity to provide a habitable enclosure incorporating life support provisions, environmental control, power, and crew protection equipment. A major component of any such system will be a pressure-tight enclosure wherein a "shirt-sleeve" environment may be maintained. Mission duration will be the primary determinant of overall size, meteoroid and radiation shielding weight,and subsystem equipment weight.

The temperature environment will be quite varied according to the nature of the mission. Principal inputs will result from solar radiation and internal heat sources. It should be noted that low-earth-orbit craft are exposed to a light-dark cycle of approximately 100 minutes. The net temperatures resulting will be a function of the absorbtion and radiation characteristics of the vehicle. In the case of a vehicle resting on the lunar surface external temperatures may range from +250° to -250° F during a lunar day - night cycle (i.e. 28 earth days). These considerations typically appear in the design of the basic structure, and the duty cycle, load, life, and power requirements of the environmental control system.

The major dynamic problems will be associated with structural response to forced excitation. Excitations will include the ignition of propulsion systems, meteoroid collisions, impact during docking operations, booster loads, and landing shocks on non-atmospheric planets. An additional dynamics problem stems from the cross coupling of structural modes due to angular rates about the body axes. In order to provide an artificial gravity environment for long-time space missions, these configurations take the shape of a wheel with the living quarters distributed around the periphery. The wheel is spun about its hub to create the required acceleration field. In view of the relatively large size, the stiffness levels are quite low and complex modal coupling problems exist. The coupling agent results from the angular rate of the wheel about the spin axis. The modes are excited easily through the movement of crew or the operation of the attitude control system. In the latter case, complex coupling exists between the control

system, flexible structure, and rigid body degrees of freedom. The consequences of these coupling phenomena are structural fatigue and possibly basic dynamic instability of the entire system.

For all manned vehicles boosted from the surface of the earth, a critical design condition is related to abort and escape in the event of a failure of the booster. Separation loads must be accounted for; and, in the event of a pad explosion, the vehicle must be capable of withstanding the overpressures of the outgoing shock waves, or else it must be capable of longitudinal accelerations sufficient to permit it to "outrun" the shock wave.

Unmanned Spacecraft

In many respects, unmanned spacecraft have essentially the same operating environment as their manned counterparts. Several differences are, however, significant. Without question, unmanned vehicles will always be used in scientific or exploratory endeavors in space prior to manned participation. Accordingly, the environmental conditions may frequently be difficult to predict, and thus the design of the necessary onboard equipment becomes a process subject to an elevated level of uncertainty. This fact is particularly aggravating in view of the total dependency of the mission on the successful operation of automatic equipment. It should be noted that since the spacecraft is unmanned, the amount of equipment is often increased beyond that necessary for a manned mission; and the reliability levels must be considerably increased for similar operational periods. Furthermore, since the missions will many times be of a scientific nature, it is not only equipment performance, but equipment accuracy that constitutes a major design consideration. It is apparent, therefore, that prediction of environment and the subsequent design of automatic equipment represents the basic theme in the design of an unmanned spacecraft.

The principal factors which require careful design analyses are the spacecraft heat balance, shock and vibration environments, meteoroid hazard and radiation levels. All of these items will serve as basic boundary conditions to the avionics engineer. Figure (17) illustrates a typical, but significant, interdependency between total spacecraft weight and reliability (expressed here as the

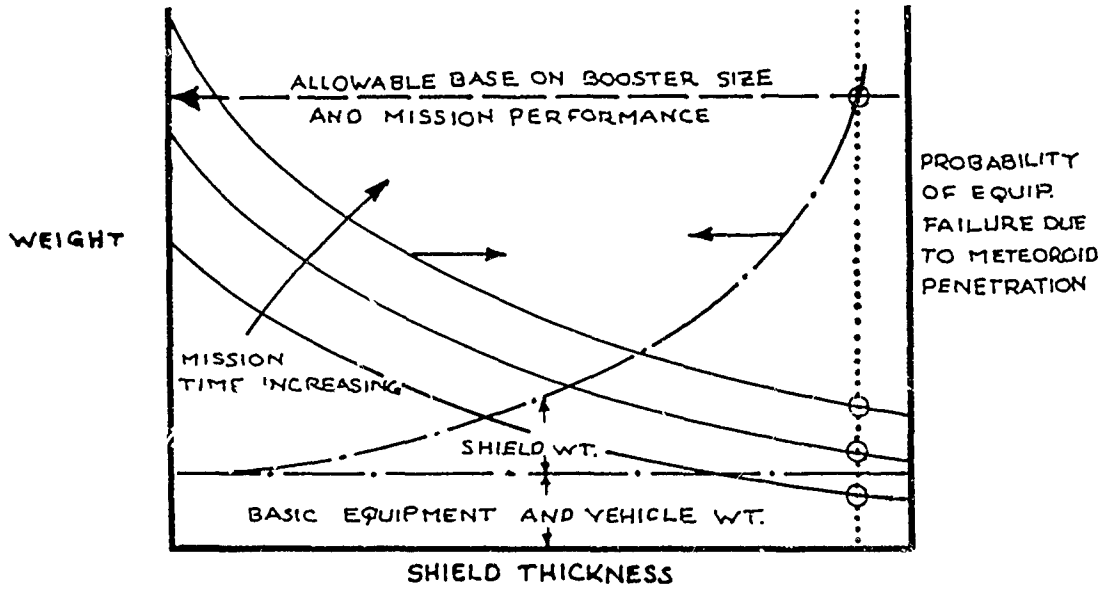


FIGURE 17 METEOROID SHIELD DESIGN

probability of a failure due to meteoroid collision). It will be noted that as the meteoroid shielding is increased in thickness, the probability of an equipment failure is reduced at the expense of total weight. This process is, of course, bounded by the payload capability of the launch vehicle and the required mission duration.

The structure will normally be of a simple truss or unpressurized monocoque design except insofar as pressurization is required by the dictates of special equipment or structural stability. The principal structural loads will result from the boost operation, stage separation, meteoroid collision, docking operations, reaction control or vernier propulsion operation, and landings on extraterrestrial bodies. It should be noted that unmanned spacecraft are frequently designed within more stringent weight limits than their manned counterparts. This results from the fact that they usually precede the manned mission by several years and thus must contend with a lower level of booster technology and performance.

Space Launch Vehicles

This type of vehicle will normally operate on an earth-to-space ballistic trajectory on a one-way trip basis. Since it is basically designed around a propulsion system, and invariably requires a high mass ratio, major elements of the propulsion system (i.e., fuel tanks, rocket cases, etc.) must double as basic airframe structure. In the case

of solid rockets, major load criteria will develop from the consideration of propellant cracking characteristics.

The principal problems relate to the stabilization of the system in its structural and rigid body modes. The significant servo-elastic problems involve body bending, inertial sensors, and reaction or vectored thrust controls. It should be noted that when gimbaled engines are used, they are major coupling agents. If liquid propulsion systems are utilized, fuel slosh along with variable mass characteristics due to fuel consumption must be accounted for in the dynamic analyses.

Vibration and noise due to engine exhaust, aerodynamic sources, and uneven burning will be a major determinant of structural characteristics and serve as a basic requirement against which onboard systems are designed. In determining the vibration characteristics, it is significant to note the principal differences which exist between the structure of a launch vehicle and that of an aircraft. Generally, the stiffness in cross sectional planes will be considerably lower with a heavy reliance placed upon internal pressure to maintain the structural integrity. In view of this, one must consider the possiblity of "breathing" or hoop modes. This problem may frequently be offset through the use of fuel or oxidizer tank "clusters". This latter arrangement, however, demands an equally stringent vibration and stiffness analysis of the cross sectional plane degrees of freedom. It also should be noted that many space launch vehicles may be regarded as non-holonomic articulated systems as evidenced by a large number of interconnections between stages and propulsion system components. The friction characteristics of these joints play a significant role in the determination of the basic vibration and damping characteristics. Figure (18) demonstrates the effect of vibration amplitude on the natural frequency of a typical mode.

Aerodynamic loads must be considered from the point of view of gusts and "on-the-pad" excitation. Furthermore, certain configurations require the addition of fins or vanes to provide inherent stability. In these cases, normal aerodynamic and flutter considerations apply: modified only by the predominance of high chordwise inertia loadings and rapid changes of flight conditions due to longitudinal acceleration.

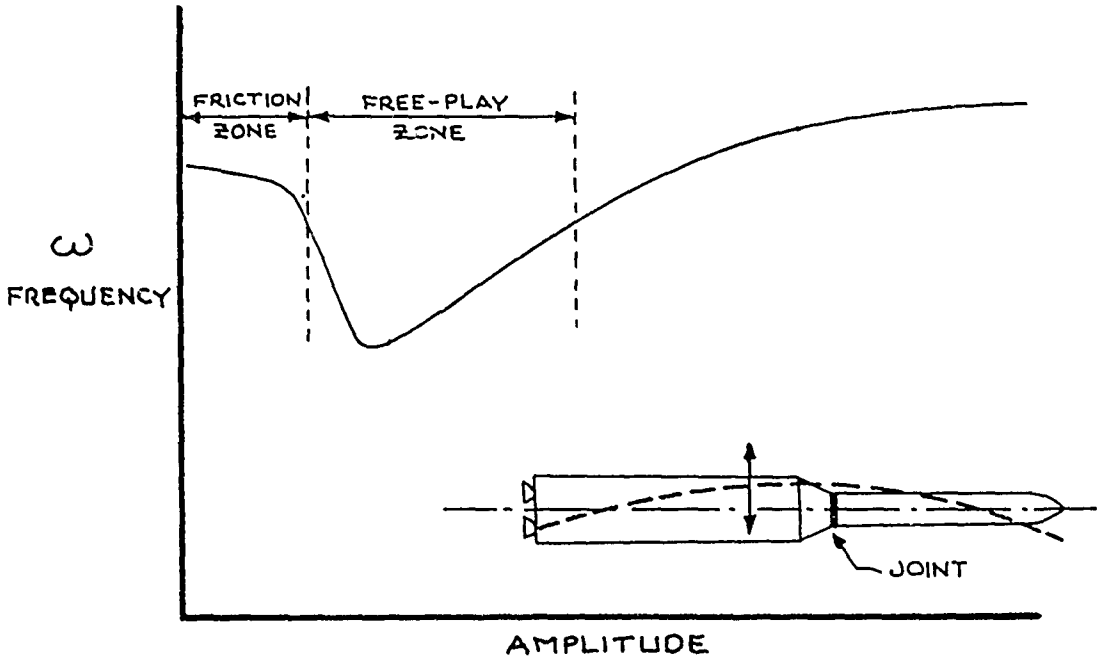


FIGURE 18 EFFECT OF JOINTS ON VIBRATION FREQUENCY

6. SUMMARY AND CONCLUSIONS

In the foregoing sections an attempt has been made to highlight some of the more critical influences of Aerothermoelasticity as it affects the design of several basic classes of aerospace vehicle. It is apparent that the viewpoint has been that of the designer who must continually attempt to weigh the relative emphasis of individual problems as they affect the particular system under consideration. In the following summarizing statements, an attempt is made to identify those particular problems of the aerothermoelastic family which appear to have primary influences in the design processes of the several basic aerospacecraft types. It should not be construed, however, that failure to mention individual problems in any way implies their lack of significance: since, in the final analysis, each design problem must be judged on its own merits.

The design of supersonic aircraft requires heavy emphasis on the problems of lifting surface flutter, fuselage and control system dynamics, panel flutter, and static aeroelasticity.

The hypersonic aircraft derives its principal aerothermoelastic considerations from its extended atmospheric flight range and the necessity of using cryogenic fuels. Accordingly, the thermodynamics of the cryogenic fuel tank-primary structure and heat shield arrangement must receive critical attention. Body bending - rigid body - control system dynamics will be inseparable; and panel flutter will be elevated still further in importance.

The high L/D spacecraft will be designed with the structural heat balance-thermal stress problem area as the major consideration. Concessions made to weight and size will lead to serious considerations relating to rigid body stability and control; and, again, panel flutter will enter as a critical item.

The low L/D re-entry spacecraft will be exposed to extremely critical combinations of high temperature and load. Therefore, the heat protection system becomes the primary design requirement. This, in turn, serves as a basis for

important materials, weight, and fabrication requirements. Again, rigid body stability and control problems will enter as critical dynamic considerations.

The manned spacecraft relies for its mission success upon its ability to meet life support requirements over extended space missions. The overall heat balance problem is extremely critical. In addition, the response of the structure to several types of basic excitation provides the basis for the design stress analysis. Full allowance must be made for the effects of non-linear inertia coupling between the several rigid and flexible degrees of freedom.

The unmanned spacecraft is designed to stringent reliability requirements. The environments under which the equipment must operate are often extreme in magnitude and include vibration, shock, radiation, and meteoroid hazards. Structures must be light weight and reliable, and this frequently dictates the use of unusual configurations or materials.

The space launch vehicle is characterized by the extremely light weight, flexible, and non-linear nature of its structure. It must be designed to withstand severe acoustic and inertia loadings; and its dynamic analysis must fully incorporate considerations of servo-elastic coupling.

In conclusion, it may be stated that Aerothermoelasticity, in many forms, enters in to the aerospace vehicle design process in a critical manner. It is apparent that an inadequate consideration of these problems will, in all classes of aerospace vehicles discussed, spell failure for the system. Accordingly, the importance of a full consideration of Aerothermoelasticity in all phases of the preliminary design process cannot be emphasized too strongly. This can only be accomplished by continued research into the fundamentals of the field accompanied by the development of simplified methods which will lend themselves readily to the time and monetary limitations of most typical preliminary design efforts.

THEORETICAL HYPERVELOCITY UNSTEADY AERODYNAMICS

Holt Ashley

and

Garabed Zartarian

Massachusetts Institute of Technology

ABSTRACT

Principal design information required of unsteady aerodynamic theory at hypersonic speeds is reviewed in the light of probable configurations and the nature of their time-dependent motions. Emphasis is placed on quasi-steadiness and on the reduction to equivalent steady flows. Concentrating on the airloads problem, approximate methods for preliminary estimation are discussed relative to pointed and blunted shapes over various ranges of the hypersonic parameter. There follow comments about more exact theories, research needed to assure their usefulness, and the role of the high-speed computer. The influences of viscosity and finite reaction rates must often be considered, and their relationship to unsteady phenomena is described.

LIST OF SYMBOLS

a	Speed of sound
c	Wing chord
C_p	Pressure coefficient (Eq. 3)
$C_{p_{02}}$	Coefficient of stagnation pressure behind shock
d	Height of blunt nose or diameter of blunted region in a section normal to body axis
F_z	Aerodynamic force in z-direction
$\vec{i}$	Unit vector in x-direction
k	Reduced frequency
ℓ	Body length
$M_\infty (= \frac{U_\infty}{a_\infty})$	Flight Mach number
$\vec{n}$	Unit inward normal vector to body surface
p	Static pressure
p_α	Static pressure due to incidence, camber, motion, etc. on surface of blunt-nosed configuration
p_β	Induced pressure on surface of blunt-nosed configuration
p_3	Pressure just behind shoulder
$\Delta p (= p_L - p_U)$	Lifting pressure difference on wing
$\vec{q}_b$	Velocity vector of body surface
$R_B(x,\varphi)$	Radius of cross section of slender body
R_N	Radius of curvature of blunt nose or leading edge
Re_x	Reynolds number based on free-stream conditions and streamwise distance behind leading edge
t	Time
T; T_w	Absolute temperature; wall temperature
U_∞	Flight speed

w	Fluid velocity in z-direction
x, y, z	Rectangular Cartesian coordinates (Fig. 1)
$\bar{x}, \bar{y}, \bar{z}$	Coordinates associated with large angle of attack (Fig. 2)
α	Angle of attack
γ	Ambient ratio of specific heats
γ_2	Specific-heat ratio in disturbed flow behind shock
δ	A general quantity denoting the largest of angle of attack, thickness ratio, fractional camber, or amplitude ratio of unsteady motion
$\varepsilon (= \frac{\rho_\infty}{\rho_2})$	Density ratio across strong shock
θ_N	Inclination of surface tangent, on two- or three-dimensional body, to the flight direction
$\theta_{EFF.}$	Value of θ_N on blunt nose adjusted for unsteady effect.
Λ	Sweep angle of leading edge
$\Lambda' (= \frac{\pi}{2} - \Lambda)$	Planform semi-vertex angle on low-aspect ratio wing
ρ	Density of gas
φ	Polar angle in body cross section (Figure 5)
ω	Circular frequency of simple harmonic motion
Ω	Sweep-angle-of-attack parameter (Eq. 22)

Subscripts, operators, etc.

$(\,)_\ell$	Leading edge of wing planform
$(\,)_L$	At lower surface of wing
$(\,)_N$	Property of nose surface or quantity just behind shock attached to pointed leading edge or vertex
$(\,)_U$	At upper surface of wing
$(\vec{\ })$	Vector
$O(\cdots)$	Identifies a quantity of the same order of magnitude as, or smaller than, $(\ldots)$

THEORETICAL HYPERVELOCITY UNSTEADY AERODYNAMICS

INTRODUCTION

Routine aerodynamic analyses of hypersonic flight vehicles are beginning to be required under circumstances where elastic deformations occur and where previous experience at lower Mach numbers would suggest that unsteady-flow effects must be taken into account. Despite extensive recent research efforts on hypersonic aerodynamics (cf. Refs. 1-4 as good summaries), few attempts have been made to assemble the necessary results in practically useful form. Faced with a difficult, nonlinear physical situation, the applied mathematicians have tended to focus on such simple problems as axisymmetric steady flow. Discouraging gaps remain, and promising techniques like three-dimensional characteristics are far from the degree of systematization desirable for engineering computations. Competent experimentalists are unable to agree when examining the validity of even such simple approximations as the blast-wave concept.

Some order is beginning to emerge, however, from the welter of ten years' intensive research, and there are configurations like thin, pointed wings for which the theory appears quite reliable. Ample progress is evident since the authors attempted a similar survey (Ref. 5) three years ago. The present paper is therefore being written, from the standpoint of the aeroelastician, with the double object of reviewing analytical methods for determining unsteady hypersonic airloads and pointing out some promising directions for future work. Since several parametric ranges must be covered, an immediate restriction is adopted to thin lifting surfaces and slender bodies. Both effectively pointed and blunt leading edges are considered. Approximate procedures are first summarized that are believed to be suitable for preliminary estimates of surface pressure distributions and generalized forces. Because certain of these may prove unreliable in the light of further experience, an effort is then made to identify the best available method for analyzing each case. Some of the latter presuppose considerable additional development, albeit clear guidelines can be laid down at the present time.

Invaluable advantage may be taken of two features peculiar to the hypersonic regime. The first is the well-known fact that surface static pressures can be predicted with acceptable accuracy by elementary theories which are less successful when it comes to other thermodynamic properties and flow-field details away from the body. The second is the tendency for time-dependent motions to be describable in "quasi-steady" terms, i.e., loads can be estimated by properly applying the instantaneous flow-tangency boundary condition but neglecting unsteady terms in the field differential equations. Other cases will be discussed where "equivalent steady flows" can be constructed.

The importance of unsteadiness is usually measured by the size of the reduced frequency*

$$k = \frac{\omega R_N}{U_\infty} \quad \text{or} \quad \frac{\omega l}{U_\infty} \quad \text{or} \quad \frac{\omega c}{U_\infty} \qquad (1)$$

based on nose radius R_N, body length l, wing chord c, or other dimension parallel to the flight direction. Using representative overall structural frequencies ω, one can put an upper limit of about 3000 rad.-ft./sec. on the product ωl even for elongated missiles and boosters. Thus one is led to a maximum $k = 0.3$ at $U_\infty = 10{,}000$ ft./sec. Much lower values will be typically encountered except in special problems like hypersonic panel flutter. A similar estimate of k can be made in connection with atmospheric turbulence and wind shears, and again $k = 0.5$ seems extraordinarily high. When accepting the assumption of small k, one should point out that certain theories mentioned below have the appearance of quasi-steadiness but actually apply up to $k = O(1)$.

The basic definition of hypersonic flow (Ref. 1) is, of course, that the Mach number M_∞ be large compared with unity; in most cases $M_\infty >> 1$ is an adequate assumption. On pointed configurations M_∞ occurs in the form of the hypersonic parameter $M_\infty \delta$, where for practical purposes δ is the largest of the quantities thickness ratio, angle of attack, nose inclination and maximum amplitude ratio of unsteady lateral motion.

---

* Important symbols are defined at the end of the paper.

When $M_\infty \delta << 1$, ordinary linearized aerodynamic theory is valid (supersonic flow). Above this regime the magnitude of $M_\infty \delta$ is useful for identifying ranges of validity of various methods.

Since the working fluid is generally air or a similar mixture of ignoble gases, the familiar approximate model of a perfect gas with constant specific heats is frequently inacceptable. Except near blunt noses, in fact, $M_\infty \delta$ serves to measure when real-gas effects begin to influence surface pressures (Refs. 5-6). Taking δ as semi-vertex angle on a wedge, Ref. 6 concludes that specific-heat variations must be accounted for when $M_\infty \delta \gtrsim 0.6\text{-}1.6$, the lower number being associated with the higher altitudes in the earth's atmosphere. For $M_\infty \delta \gtrsim 5.3\text{-}8.5$, oxygen molecules begin to dissociate, and deviations from the perfect gas law must also be considered. For slender, pointed vehicles one seems safe in using the perfect-gas hypothesis up to orbital speed. But this is distinctly not true either in a blunted region or in the sheath of hot gas which a blunt nose causes to envelop the afterbody.

Another limitation on the present survey is the neglect of any strong-interaction effects of viscosity. This puts a rough lower limit of unity on the value of

$$\sqrt{Re_x}/M_\infty^3$$

over nearly all the body surface, Re_x being free-stream Reynolds number based on distance x along a streamline from the nose stagnation point. Because the most severe aerothermoelastic phenomena will be encountered at relatively low altitudes and high dynamic pressures, this restriction is not severe. A later section goes into somewhat more detail on both viscous influences and finite reaction rates in the gas, but for a truly comprehensive treatment of transport phenomena one should turn to the last three chapters of Hayes and Probstein (Ref. 1).

In the process of the review which follows, numerous references are made to individual contributions. Nearly all of these turn out to be theoretical, because the experimental literature on unsteady hypersonic flow is almost nonexistent. Where reliance may be put on steady-state measurements to underwrite a quasi-steady theory, some confidence can naturally be deduced for its application to time-dependent situations.

Inasmuch as the majority of citations are made to literature in English, a word is in order about the extensive work done in Russia (see Probstein, Ref. 2, for a timely survey). Much of it has been devoted to unsteady-flow situations, and the word "unsteady" actually appears in the title of an important book by Stanyukovich (Ref. 4). However, the bulk of the Russian solutions concerns self-similar and symmetric problems, which have practical utility mainly for analogous two-dimensional and axisymmetric steady flows, so their value for aerothermoelastic design is limited. This comment is not intended to detract from the major significance of two areas of contribution: the piston analogies which have been derived for slender, pointed bodies, especially a recent extension to high angles of attack by Sychev (Ref. 7); and the numerical methods for thin shock layers due to Dorodnitsyn, Belotserkovskii and their collaborators (Refs. 8, 9).

It should finally be observed that the present paper draws much of its background from a study recently completed for North American Aviation, Inc., by one of the authors (Ref. 10). He is appreciative of permission granted to draw on that work, and acknowledges many helpful conversations with engineers at North American and information obtained from internal company reports.

SECTION I: THIN, POINTED WINGS

Four general limitations, which hold throughout all that follows, are first set down:

$$\left.\begin{aligned} & M_\infty^2 \gg 1 \\ & k < 0.5 \\ & \frac{1}{\chi} \equiv \frac{\sqrt{Re_x}}{M_\infty^3} > 1-10 \\ & \varepsilon \equiv \frac{\rho_\infty}{\rho_2} \ll 1 \end{aligned}\right\} \qquad (2)$$

(For blunt-nose regions)

These have been mentioned in the introduction, save for the requirement of small density ratio ε between the free stream and attached shock layer, which will be taken up in Section III.

Figure 1 shows a representative streamwise cross section of the almost-plane wing to be considered. Except at high mean incidence α or when the leading-edge sweep angle Λ approaches 90°, the elementary hypersonic theories for such thin lifting surfaces permit pressures to be calculated on an individual strip basis. Streamwise strips are chosen, but it can be shown for swept wings at $\alpha << 1$ that the hypersonic parameter has the same value whether sections are taken parallel to the flight direction or normal to the leading edge, so this choice is normally immaterial.

Approximate methods are listed below for several parametric ranges. Where convenient, formulas are reproduced from the cited references for the pressure coefficient at the wing surface,

$$C_p = \frac{p - p_\infty}{\frac{1}{2}\rho_\infty U_\infty^2}$$

$$= \frac{2}{\gamma M_\infty^2}\left[\frac{p}{p_\infty} - 1\right] \qquad (3)$$

It is not always easy to delimit the various parameters exactly because of the incomplete state of experimental research. Where limits appear only in order-of-magnitude form, the boundary has not been fixed with any better precision to the authors' knowledge. A typical question of this sort, which provides an opportunity for a valuable program of measurements, concerns the possible existence of an overlapping range of α wherein shock-expansion results can be faired into modified Newtonian on the compression side of a thin wing.

1.1 Low Values of the Hypersonic Parameter

Let the following conditions be added to the inequalities (2):

$$M_\infty \delta \leq 0.8\text{-}1.0 \qquad (4)$$

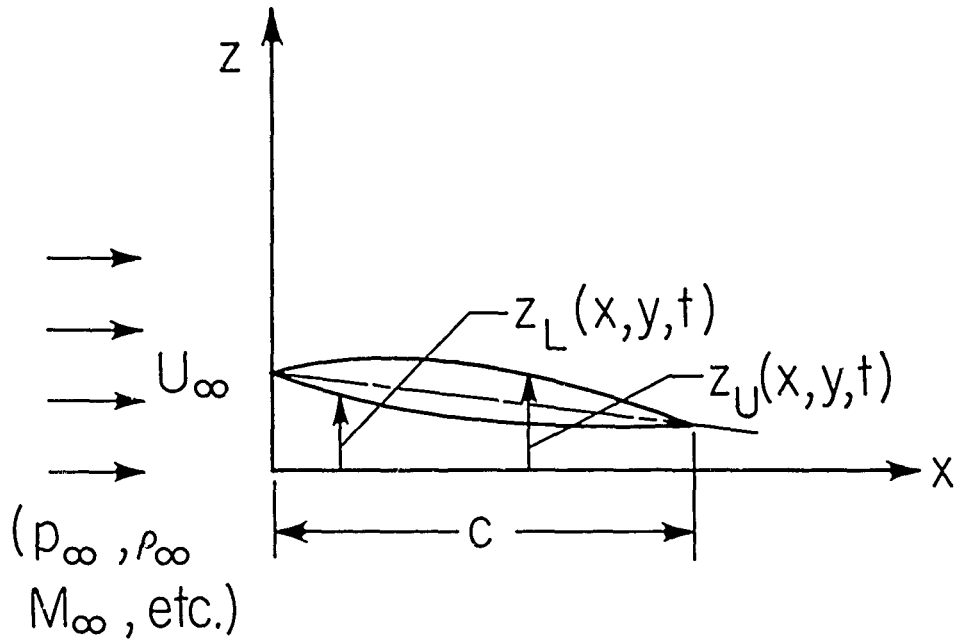


Figure 1. Cross section of thin, pointed wing performing small unsteady motion normal to a hypersonic airstream.

$$\delta \gg \frac{1}{M_\infty^3}$$

$$M_\infty \cos\Lambda \gtrsim 2\text{-}2.5 \qquad (4)$$

Although the flow is not strictly isentropic under these circumstances, Lighthill has pointed out (Ref. 11) that an excellent estimate of surface pressures can be obtained from the third-order expansion of the formula for isentropic pressure at the face of a one-dimensional piston moving into a perfect gas. For instance, the local C_p on the upper wing surface is related to the instantaneous normal velocity component w_U induced there by the combined surface slope and normal motion thus:

$$C_{P_U} = \frac{2}{M_\infty}\left[\frac{w_U}{U_\infty} + \frac{\gamma+1}{4}M_\infty\left(\frac{w_U}{U_\infty}\right)^2 + \frac{\gamma+1}{12}M_\infty^2\left(\frac{w_U}{U_\infty}\right)^3\right] \qquad (5)$$

Because of the implicit requirement $\delta << 1$, w_U can be found from the following linear operation on the surface position coordinate $z_U(x, y, t)$:

$$w_U = U_\infty \frac{\partial z_U}{\partial x} + \frac{\partial z_U}{\partial t} \qquad (6)$$

Overpressure is produced where the outward normal velocity is positive. Therefore, the lower-surface expression corresponding to Eq. (4) reads

$$C_{P_L} = \frac{2}{M_\infty}\left[-\frac{w_L}{U_\infty} + \frac{\gamma+1}{4}M_\infty\left(\frac{w_L}{U_\infty}\right)^2 - \frac{\gamma+1}{12}M_\infty^2\left(\frac{w_L}{U_\infty}\right)^3\right], \qquad (7)$$

where w_L is connected to z_L (Fig. 1) as in Eq. (6). For small oscillations and elastic deformations, it may prove convenient to separate z_U and z_L into a time-independent part due to thickness plus an unsteady increment from camber, α, etc. One can then sometimes justify linearizing the resulting relations between the generalized aerodynamic forces and the motion coordinates. When $M_\infty \delta < 0.4$, roughly, the $(w/U_\infty)^3$ -terms can be dropped from Eqs. (5) and (7). The force-motion relations are then linear without further approximation.

If the thickness ratio is extremely small, the condition $\delta >> M_\infty^{-3}$ may break down at lower hypersonic speeds. Landahl (Ref. 12) has shown how to remedy this inconsistency by an expansion in powers of δ and M_∞^{-2}. It is of interest that a formal identity exists between the results of second-order piston and tangent-wedge theories (cf. Eq. 7.3.2 of Ref. 1). The physical assumptions are indeed the same for steady flow, but piston theory must be regarded as an unsteady extension of the tangent-wedge approximation up to $k = O(1)$.

1.2 Larger Values of the Hypersonic Parameter

Consider next the parametric range

$$\left.\begin{aligned} M_\infty \delta &> 1.0 \\ M_\infty \cos\Lambda &\geq 2 \\ \cos\alpha &\cong 1 \end{aligned}\right\} \qquad (8)$$

Here one can employ the small-disturbance hypersonic similitude of Hayes and Van Dyke (Ref. 13 and Chap. 2 of Ref. 1), reduce unsteadiness to equivalent steady flows, and find pressures by the well known shock-expansion method. There is, incidentally, reason to place a lower limit on $M_\infty \delta$ when applying this procedure to wings at high Mach number. For $M_\infty \delta < 1.0$, however, the results are numerically very close to piston theory while the latter is computationally simpler.

Van Dyke and many others have demonstrated that the flow takes place in a series of slabs, each of which moves independently of the others with speed U_∞ in the x-direction.

For instance, on the upper surface

$$z = z_U(x, y, t) \tag{9}$$

the slab which passes the leading edge $x_\ell(y)$ at time t_o is located at

$$x = x_\ell + U_\infty [t - t_o] \tag{10}$$

at a later time t. Hence this slab experiences the same disturbances and equal pressures as if it pa sed, in steady flow, over a warped surface

$$z = z_U\left(x, y, t_o + \frac{x - x_\ell(y)}{U_\infty}\right) \tag{11}$$

On the equivalent wing, the chordwise distribution of surface slope may be written

$$\frac{dz_U}{dx} \equiv \frac{w_U}{U_\infty}(x, y, t_o)$$

$$= \left[\frac{\partial z_U}{\partial x}(x, y, t) + \frac{1}{U_\infty}\frac{\partial z_U}{\partial t}(x, y, t)\right]\Bigg|_{\substack{x=x \\ y=y \\ t=t_o+\frac{x-x_\ell(y)}{U_\infty}}} \tag{12}$$

(The development for the lower surface is sufficiently similar to be omitted here.)

As described in Ref. 6, the pressures at a particular t are calculated by picking several slabs, each associated with a different leading-edge passage time t_o. The pressure history experienced by each of these is transferred to the actual wing,

the desired t and x being inserted into Eq. (10) to fix t_o for that slab which passed the station at time t. The pressures are found from the known equivalent-wing slopes by the hypersonic shock-expansion method, which comes in different degrees of complexity depending upon whether a real or perfect gas must be assumed. The former approximation with $\gamma = 1.4$ is valid, at most, up to $M_\infty \delta = 1.6$ in air.

One first tests to see whether the nose slope

$$\theta_{NU}(y, t_o) = \frac{w_U}{U_\infty}(x_\ell, y, t_o) \tag{13}$$

is positive or negative. If positive, an oblique shock inclined to the flow direction at an angle β is attached to the upper leading edge. β and the surface pressure p_{NU} and Mach number M_{NU} just behind the shock are given in terms of θ_{NU} by simple formulas (Ref. 6). Provided no significant compressive turning occurs behind the leading edge, the pressures farther aft can be determined from the hypersonic Prandtl-Meyer expansion formula

$$\frac{p}{p_{NU}} = \left\{1 + \left(\frac{\gamma-1}{2}\right) M_{NU}\left[\frac{w_U}{U_\infty}(x, y, t_o) - \theta_{NU}(y, t_o)\right]\right\}^{\frac{2\gamma}{\gamma-1}} \tag{14}$$

If positive values of $\left[\frac{w_U}{U_\infty} - \theta_{NU}\right]$ are encountered, or if a positive discontinuity in chordwise slope occurs as at a control surface hingeline, a second shock may have to be inserted. On the other hand, if θ_{NU} itself is negative, an immediate expansion takes place at the nose to

$$\frac{p_{NU}}{p_\infty} = \left\{1 + \left(\frac{\gamma-1}{2}\right) M_\infty \theta_{NU}\right\}^{\frac{2\gamma}{\gamma-1}} \tag{15}$$

Pressures farther aft are then computed from Eq. (15) with θ_{NU} replaced by $w_U(x, y, t_o)/U_\infty$.

Whenever $M_\infty |\theta_{NU}| > 1.5$ or so, real-gas effects should be included both for the leading-edge shock and the subsequent expansion. These procedures will probably have to be incorporated into high-speed digital computer programs along lines that are now quite familiar to aerodynamicists. For instance, a convenient trial-and-error oblique shock program can be based on the Hansen and Heims formulation of the thermodynamics of air (Ref. 14). Alternatively, an averaged value γ_2 is often adopted for the specific-heat ratio in the disturbed part of the flow. Eggers et al. (Ref. 15) have demonstrated this to be an acceptable approximation if $\gamma \geq 1.3$, which will usually be the case for pointed surfaces.

1.3 High Angle of Attack

When α is no longer small enough that $\cos\alpha \cong 1$, the parameter $M_\infty \delta$ must be replaced by $M_\infty \sin\alpha$, which is evidently a large number. The windward surfaces of thin wings experience very high pressures, whereas the near vacuum in the lee has little influence on resultant airloads.

Figure 2 illustrates the cross section, in a plane containing U_∞, of such a wing which is performing small unsteady motions about the large mean α. Sychev (Ref. 7) has analyzed this situation for both two- and three-dimensional shapes, providing an important extension of the Hayes-Van Dyke hypersonic similitude. Near the wing surface the flow occurs in a series of $\bar{y}$-$\bar{z}$-slabs, each of which moves independently of the others with speed $U_\infty \cos\alpha$ in the $\bar{x}$-direction. A large crossflow component $U_\infty \sin\alpha$ exists parallel to $\bar{z}$ and must be superimposed on the smaller disturbance velocities due to $\partial \bar{z} v / \partial \bar{x}$, etc. As in Section 1.2, the possibility arises of replacing the unsteady problem by a sequence of equivalent steady flows. Thus the slab which passes the leading edge $\bar{x}_\ell$ $(\bar{y})$ at time t_o finds itself at

$$\bar{x} = \bar{x}_\ell + U_\infty \cos\alpha \left[t - t_o \right] \tag{16}$$

at later instant t. The chordwise distribution of surface slope on the warped wing associated with the t_o-slab is

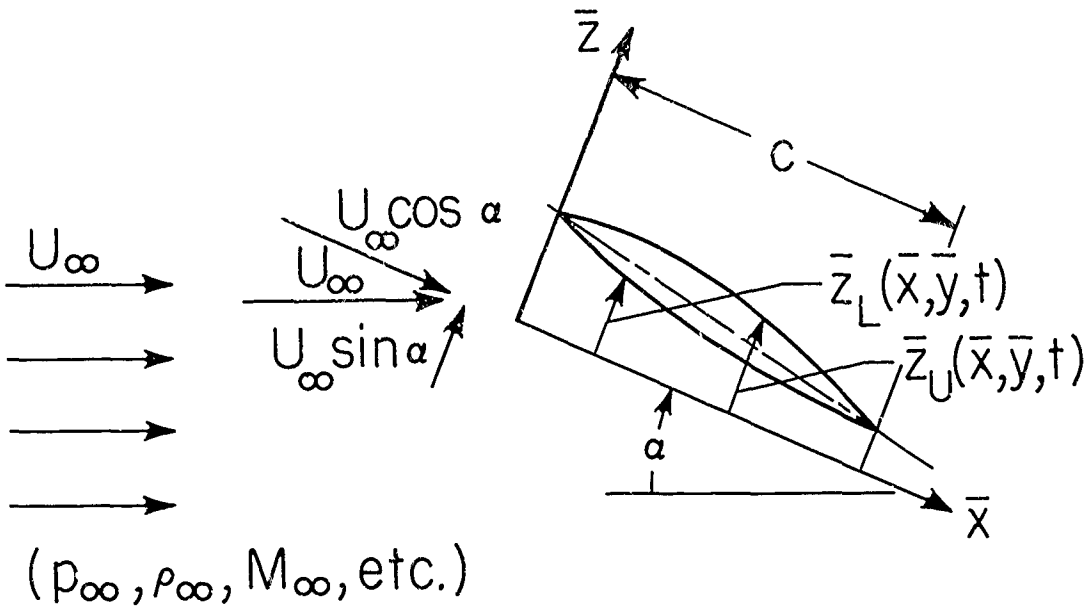


Figure 2. Alternate notation for wing section of Fig. 1 at high angle of attack α.

$$\frac{d\bar{z}_u}{d\bar{x}} \equiv \frac{\bar{w}_u(\bar{x},\bar{y},t_0)}{U_\infty \cos\alpha}$$

$$= \left[\frac{\partial \bar{z}_u}{\partial \bar{x}}(\bar{x},\bar{y},t) + \frac{1}{U_\infty \cos\alpha} \frac{\partial \bar{z}_u}{\partial t}(\bar{x},\bar{y},t) \right] \Bigg|_{\substack{\bar{x}=\bar{x} \\ \bar{y}=\bar{y} \\ t=t_0+\frac{\bar{x}-\bar{x}_\ell}{U_\infty \cos\alpha}}} ,$$

(17)

with a similar formula for $d\bar{z}_L/d\bar{x}$. Recalling that $d\bar{z}_u/d\bar{x}$ and $d\bar{z}_L/d\bar{x}$ are small numbers, one can say that the angles between the surface tangents and the stream direction are $\left(\frac{d\bar{z}_u}{d\bar{x}} - \alpha\right)$ and $\left(\alpha - \frac{d\bar{z}_L}{d\bar{x}}\right)$. Each of these quantities would give rise to compression if it were positive. Hence a positive α causes large upper-surface expansion and lower-surface compression, as indicated above.

Different methods of loading calculation are available, depending on whether the leading-edge shock on the compression side is attached or detached. In the former case, the real-gas shock-expansion procedure of Section 1.2 can be adapted to the high incidence. Looking at the lower, compression surface for positive α , the flow at the nose undergoes a turning

$$\theta_{NL}(\bar{y},t_0) = \alpha - \frac{\bar{w}_L(\bar{x},\bar{y},t_0)}{U_\infty \cos\alpha}$$

(18)

If $\Lambda \cong 0$, this angle determines directly the leading-edge shock and flow properties just behind it. For an appreciably swept edge, one uses the simple-sweep concept to compute the shock strength in crossflow planes (cf. Trimpi and Jones, Ref.

16), superimposing the velocity component $U_\infty \cos\alpha \sin\Lambda$ parallel to the leading edge afterward to get the full three-dimensional field. The emergent flow is then no longer quite parallel to the $\bar{x}$-$\bar{z}$-plane but slanted outward; any error introduced by subsequently assuming streamlines to lie in such planes is not regarded as serious.

The starting Mach number M_N and pressure p_N yielded by the shock calculation serve to initiate real-gas Prandtl-Meyer expansions downstream of the nose. The expansive turning angle at any point $\bar{x}$, $\bar{y}$ is found from the difference between $d\bar{z}_L/d\bar{x}$ there and $d\bar{z}_L/d\bar{x}$ at the leading edge $\bar{x}_\ell(y)$ for the same reference time t_o. The very low pressures on the upper surface are computed by a direct real-gas expansion in $\bar{x}$-$\bar{z}$-planes from free-stream conditions M_∞ and p_∞.

If α is so large that the shock detaches from the leading edge on the compression side, the pressures are probably best calculated by the modified Newtonian method (e.g., Ref. 3). The quasi-steady approximation seems well justified. One finds the inward unit normal vector $\vec{n}$ to the surface and the surface velocity vector $\vec{q}_b$ as seen in a coordinate system having the mean velocity of the wing. Provided the given point is on the windward side and not shadowed by any forward portion of the vehicle, the pressure coefficient (cf. Chap. 3, Ref. 1) is

$$C_p = C_{p_{02}} \frac{\left[(U_\infty \vec{i} - \vec{q}_b)\cdot\vec{n}\right]^2}{U_\infty^2} \tag{19}$$

In Eq. (19) $\vec{i}$ is a unit vector in the free-stream direction, and $C_{p_{02}}$ is stagnation pressure coefficient behind a normal shock at M_∞, a number somewhat less than 2.

The suggested form of Newtonian theory does not include shock-layer centrifugal effects either here or in the subsequent discussion of blunt leading edges. For thin wings the surface curvatures are very small. Moreover, steady-state data do not confirm the predicted centrifugal pressure drop even on appreciably curved shapes. Further research is obviously needed, and, in view of the probably quasi-steady character of the flow, this can be conducted along the lines of integral methods for thin shock layers discussed below. Another effect that could easily be included in the present formulation is the unsteady inertia load caused by the layer of dense fluid carried along with the vibrating surface. This topic is also taken up again in Section III.

On the leeward and shadowed wing surfaces, one will generally find pressures between p_∞ and pure vacuum. That is,

$$0 \geq C_p \geq -\frac{2}{\gamma M_\infty^2} \quad , \tag{20}$$

a very small range from the engineering standpoint.

1.4 The Problem of Large Sweep Angle

On low-aspect-ratio, highly-swept wings, many of the foregoing ideas fail for obvious physical reasons. Thus as one proceeds to smaller values of the leading-edge semivertex angle $\Lambda' \ (= \frac{\pi}{2} - \Lambda)$, one finds lower and lower angles of attack above which the shock is detached. Even though the Van Dyke and Sychev results are still correct, the utility of shock-expansion theory becomes progressively more limited. When taking up this problem of $\Lambda' \leq 20^\circ$ or so, three ranges of the hypersonic parameter are considered:

1) $M_\infty \delta \leq 0.5$,

2) $M_\infty \delta > 0.5$, and

3) α moderate to large (i.e., $M_\infty \delta$ or $M_\infty \sin\alpha >> 1$).

For the intermediate range the only available methods for loading estimation are along the lines of the variational scheme discussed in Ref. 6. In view of its complexity, further research is called for.

When $M_\infty \delta \leq 0.5$ it is justifiable to assume isentropic flow. For the lower M_∞'s Munk-Jones slender-body theory becomes a possibility,* although available experimental evidence on damping in pitch renders it questionable. Therefore, a more rigorous version of supersonic linearized theory (summarized by Miles, Ref. 17) is suggested. The subject and its literature are familiar to aeroelasitians and need not be elaborated here, except to point out that the approximation can be empirically refined to account for the wing thickness

---

* Provided the surface is slender enough in the sense that $M_\infty \tan\Lambda' \leq 0.3$, say.

distribution $[z_U - z_L]$. According to second-order piston theory the corrected load per unit area would be

$$\Delta p_t(x,y,t) = \Delta p(x,y,t)\left\{1+\left(\frac{\gamma+1}{4}\right)M_\infty \frac{\partial}{\partial x}[z_U - z_L]\right\} , \tag{21}$$

Δp being the linearized result.

The low-aspect-ratio wing at high incidence is susceptible to thin-shock-layer analysis on its windward side, but the raw Newtonian estimates of Eq. (19) are considered less acceptable than for wider planforms. Fortunately, recent work by J. D. Cole (briefly described by Messiter, Ref. 18) furnishes a higher-order description of the shock-layer structure on a plane, triangular wing at steady incidence α . It is believed an acceptable approximation simply to adapt their results, on a local flow basis, to more general motion of the configuration in Fig. 3. Cole expands the flat-delta solution in terms of density ratio ε across a shock at the normal Mach number $M_\infty \sin\alpha$. Suitably non-dimensionalized dependent variables turn out to be governed by the single parameter

$$\Omega = \frac{\tan\Lambda'}{\sqrt{\varepsilon}\tan\alpha} \tag{22}$$

When $\Omega \gg 2$ the windward shock is attached to the leading edge. The pressure coefficient, averaged across the span at any chordwise station $\bar{x}$, is then

$$C_{p_{AVE.}} = 2\sin^2\alpha + 2\varepsilon\sin^2\alpha\left[1+\frac{1}{\Omega^2}\right] \tag{23}$$

For $\Omega > 5$ it seems acceptable to set the local C_p equal to its average value.

In the extremely slender range when $\Omega < 0.25$, Cole finds

$$C_{p_{AVE.}} = 2\sin^2\alpha + 2\varepsilon\sin^2\alpha\, F(\Omega) , \tag{24}$$

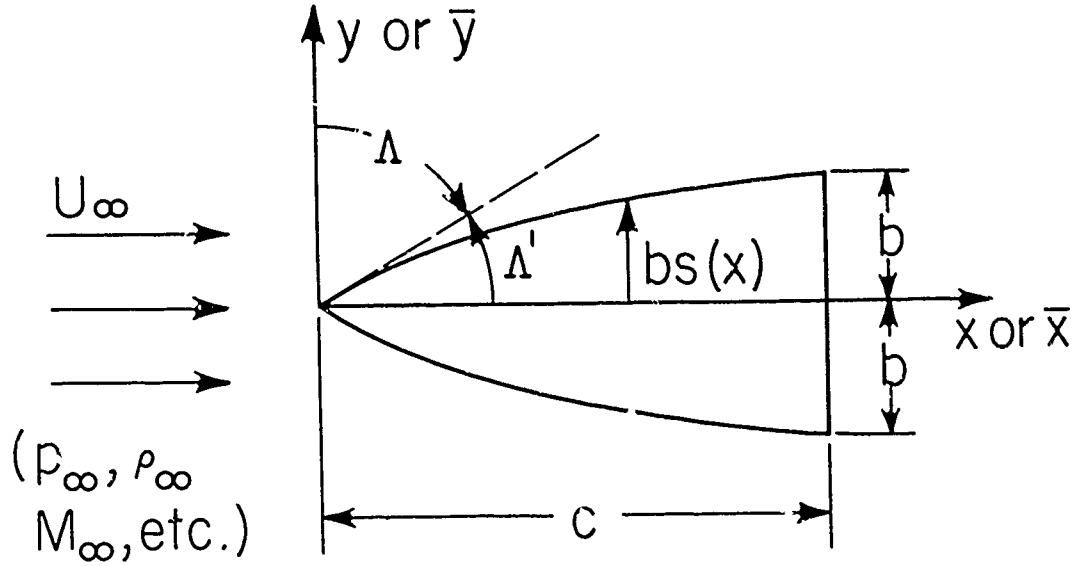


Figure 3. Plan view of a low-aspect-ratio, slender wing in hypersonic flight.

where

$$F(\Omega) = -1.225 - 2\Omega - 8\Omega \ln \Omega \tag{25}$$

A reasonable estimate for $C_{P_{AVE.}}$ over the entire Ω-scale can be constructed by fairing a smooth curve from Eq. (25) near $\Omega = 0$ up to the asymptotic value $F(\Omega) \sim 1 + \Omega^{-2}$ above $\Omega = 5$. The details of the spanwise C_p-variation can be computed, but they will be rather unimportant for such wings, which deform primarily in bending about chordwise axes.

Equations (23) through (25) imply a correction to Newtonian theory in the neighborhood of ± 10%. To extend the result to aeroelastic situations, one first replaces $2\sin^2\alpha$ by the "modified" $C_{P_0} \sin^2\alpha$. For vibrating triangular planforms, one proceeds as in 1.3, replacing α with $(\alpha - d\bar{z}_L/d\bar{x})$. When the planform has the more general shape of Fig. 3, Ω can be supplanted by an effective sweep parameter

$$\Omega_{EFF.} = \frac{b s(\bar{x})}{\bar{x}\sqrt{\varepsilon}\sin\alpha} \tag{26}$$

For $\Omega_{EFF} > 4$ or 5, the loading proves quite insensitive to any error in estimating this quantity.

1.5 Indirect Experimental Verification for Thin Wings

In the absence of any direct pressure or load measurements on oscillating thin wings at hypersonic speeds, one can turn to the substantially less attractive alternative of comparing experimental and theoretical flutter eigenvalues. The insoluble problem of untangling errors due to inadequate structural, dynamic and aerodynamic parts of the total representation of the system has often been discussed in the past. Nevertheless, successful flutter predictions certainly furnish greater confidence in a theory, and this has been the experience with primary lifting-surface instabilities, at least in the lower range of M_∞ 6.

Figure 4, adapted from Ref. 19 in the open literature, illustrates this point with respect to bending-torsion flutter of rectangular wings. The flutter speed U_f and frequency ω_f have been made dimensionless in standard fashion, using the semichord b, mass ratio μ and artificially uncoupled torsional frequency ω_{α_e}. (Note that the ordinate scales have suppressed zeros.) Predicted speeds above $M_\infty = 3$ clearly fall within the experimental error, and the same can be reasoned to be true of the frequencies. Thus the piston type of airload estimation, discussed under 1.1 above, receives some degree of confirmation. Less success has been achieved in predicting the results of some other flutter tests above $M_\infty = 5$, but the discrepancies can be attributed, at least in part, to the influence of boundary layer displacement thickness on the airloads.

SECTION II: SLENDER POINTED BODIES

Figure 5 depicts the sort of configuration considered in this section. The case of symmetrical motion with a vertical plane of symmetry is emphasized, wherein the mean line deforms according to some $z_B(x, t)$. Lateral motion can be treated by fairly obvious analogy. Thus a purely lateral $y_B(x, t)$ with a horizontal plane of symmetry is completely equivalent. When z_B and y_B occur in combination, direct superposition is possible for those theories which yield a linear relationship between loads and displacements.

Although cross-sectional shapes may be arbitrary, the quantitative illustrations below involve mainly the circular case where

$$R_B(x, \varphi) = R_B(x)$$

for reasons of limited space. With structural deformations in the elastic range, it is safe to assume that cross sections remain undistorted.

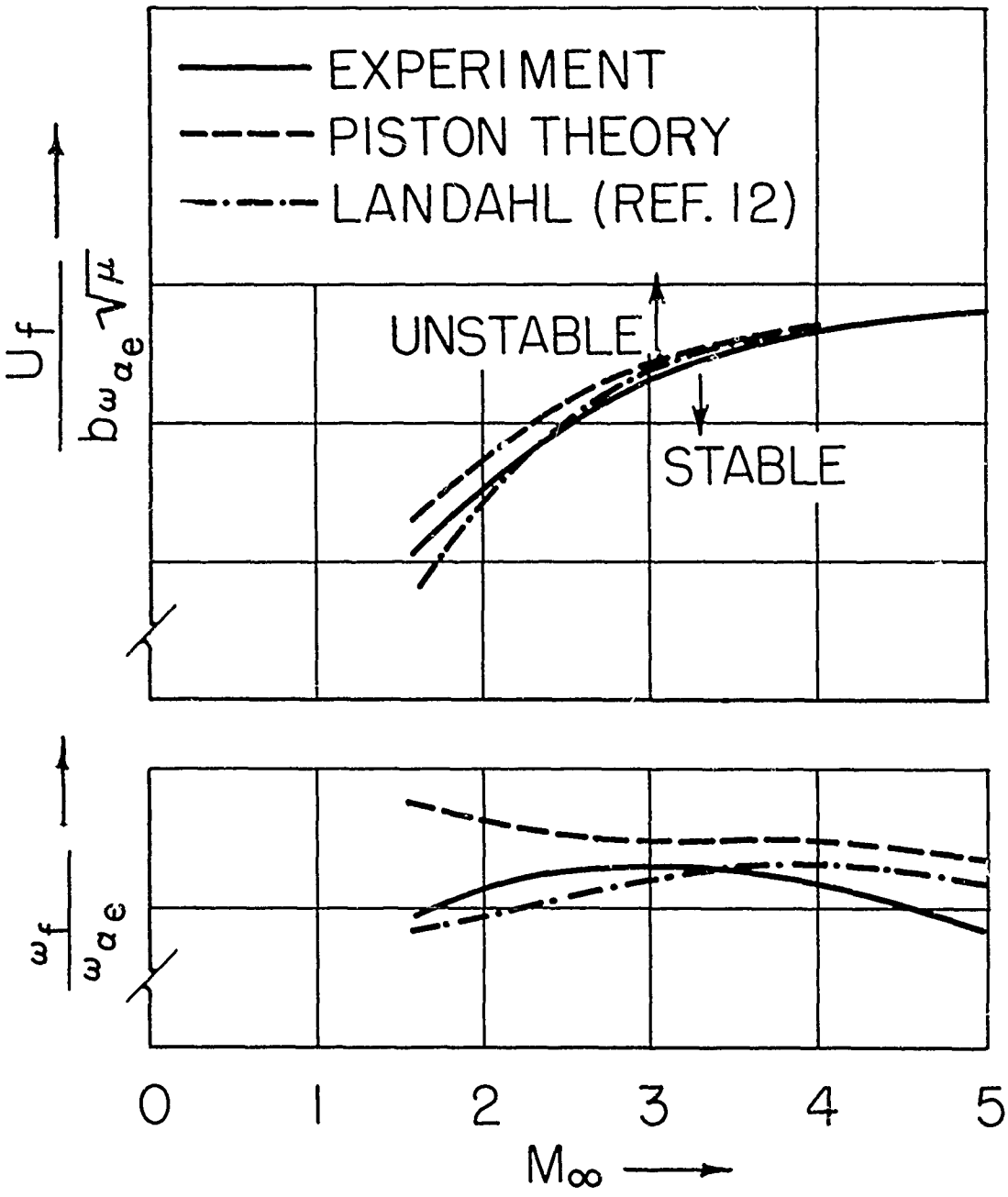


Figure 4. Dimensionless flutter speed and frequency for rectangular, cantilever wings in supersonic flow.

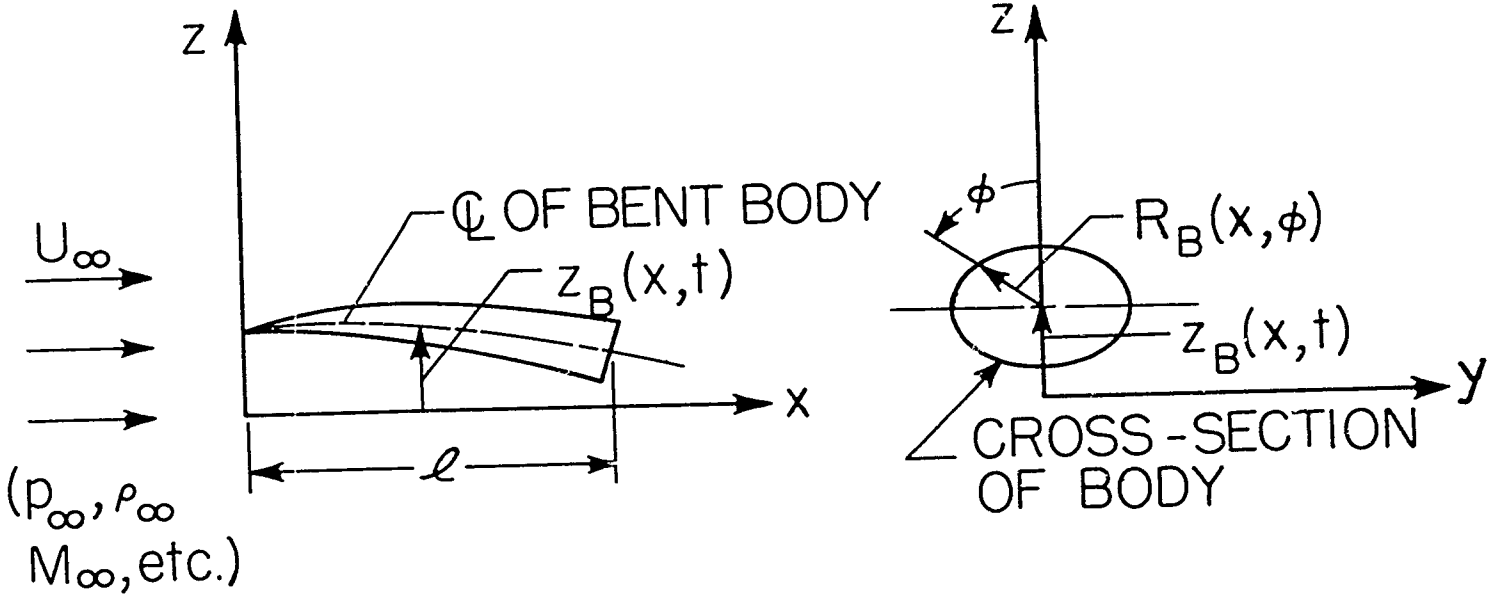


Figure 5. Slender, pointed body performing small unsteady motion in a hypersonic stream.

2.1 Low Values of the Hypersonic Parameter

The restrictions here are as follows:

$$\left.\begin{aligned} M_\infty \delta &\leq 0.5 \\ k^2 = \left(\frac{\omega l}{U_\infty}\right)^2 &\ll 1 \end{aligned}\right\} \qquad (27)$$

In these circumstances Munk-Jones slender-body theory is a safer approximation than in connection with low-aspect-ratio wings. Doubt has been cast on this method, however, by supersonic measurements of steady-state airloads due to angle of attack. Accordingly, experiments or more rigorous theory should be employed for the mean loadings, relying on slender-body formulas only for the incremental effects of vibration and deformation.

The most useful information on slender bodies is generally the normal force per unit axial length (e.g., Ref. 17 or Section 7-4 of Ref. 20)

$$\frac{\partial F_z}{\partial x}(x,t) = -\left(\frac{\partial}{\partial t} + U_\infty \frac{\partial}{\partial x}\right)\left[\rho_\infty S(x)\left(\frac{\partial z_B}{\partial t} + U_\infty \frac{\partial z_B}{\partial x}\right)\right] \qquad (28)$$

Here $\rho_\infty S'(x)$ is the cross-sectional virtual mass, which has been evaluated for a great many practically interesting shapes. Thus, for the circle, $S'(x)$ is just the actual area $\pi R_B^2(x)$; also the pressure distribution giving rise to the loading is readily found to be

$$\frac{p}{p_\infty} = \frac{-\cos\varphi}{\pi R_B(x)\, p_\infty} \frac{\partial F_z}{\partial x} \qquad (29)$$

Equation (29) yields only that part of C_p that is anti-symmetrical with respect to the x-y-plane, and one should consult a paper like Sears (Ref. 21) for information on the symmetrical portion.

Reference 22 shows how slender-body theory can be improved to include higher-order effects of Mach number and thickness ratio. Although the results to date are applicable only for rigid-body motions and oscillatory deformations of the form

$$z_B(x,t) \sim \left(\frac{x}{\ell}\right)^n e^{i\omega t}, \tag{30}$$

serious consideration should be given to exploiting this potential increase of accuracy for low hypersonic speeds. The work of Yates and Zeijdel (Ref. 23) should be mentioned.

2.2 Moderate Values of the Hypersonic Parameter

Next consider the range

$$0.5 < M_\infty \delta \leq 2 \tag{31}$$

The generalized shock-expansion schemes of Refs. 24, 6 and 25 hold the greatest promise in this regime. Unfortunately, their accuracy remains in question below $M_\infty \delta = 1$ for most body shapes, the precise minimum depending on the body curvatures in x-z and y-z-planes. For the $M_\infty \delta$ gap between roughly 0.5 and 1, Ref. 6 suggests a Rayleigh-Ritz solution of Bateman's variational principle. The object is to calculate the unsteady flow in each y-z slab which Ref. 13 has shown to be equivalent to the actual three-dimensional problem (see 1.2 above). There are no general lift or surface pressure formulas that can be reproduced here, and much developmental effort will be needed before the variational approach becomes routine for other than circular cross sections.

The upper limit $M_\infty \delta = 2$ is arbitrarily selected for the perfect-gas approximation, which is obviously acceptable at higher thickness ratios on a body than a two-dimensional wing profile. Strictly speaking, this limit should be examined more carefully for each configuration in the light of what is regarded as acceptable accuracy.

Van Dyke's hypersonic similitude (Ref. 13) yields equivalent steady flows just as in the case of wings. For example,

an oscillating body of revolution might be described by the equation

$$y^2 + \left[z - z_B(x,t) \right]^2 = R_B^2(x) \qquad (32)^*$$

The x-z-slab which passes the vertex x = 0 at time t_o would then "see" the following body:

$$y^2 + \left[z - z_B\left(x, t_o + \frac{x}{U_\infty}\right) \right]^2 = R_B^2(x) \qquad (33)$$

When $M_\infty \delta > 1$, the steady-state pressures are calculated by the shock-expansion scheme of Eggers, Savin et al. (Ref. 24, among others). After the fluid has passed through a yawed conical shock attached to the nose, the streamlines proceed along geodesic curves of the body surface. On each streamline, the pressure varies in accordance with the two-dimensional Prandtl-Meyer formula. For the slightly deformed body of revolution, the geodesics through the vertex are meridian lines φ = const. This case has been worked through in detail with many examples in Ref. 6; under hypersonic conditions the resulting load formulas are purely algebraic and quite easy to handle.

Noncircular cross sections present greater difficulties (Ref. 25), both in the determination of the nose shock and the complicated differential geometry of the geodesics. Nevertheless, Ref. 25 is successful in analyzing fairly general configurations with two planes of symmetry (prior to deformation). To avoid unwieldy manipulations, the expansion is conducted only along the streamlines at $\varphi = 0$, $\pi/2$, π and $(3/2)\pi$; the tangent-cone approximation is invoked to estimate the φ-variation of pressure around the periphery at any station x = const.

By way of experimental confirmation, some pressure measurements at M_∞ = 6 and 8 are reproduced from Ref. 25. The models, which are sketched in Fig. 6, had approximately elliptical cross sections, one with a straight axis and the other cambered so as to give a difference of 4° between the mean-line

---

* Provided the oscillatory motion $z_B(x,t)$ is sufficiently small, in the sense that

$$\frac{dz_B}{dx}(x,t) << \left(\frac{dR_B}{dx}\right)_N .$$

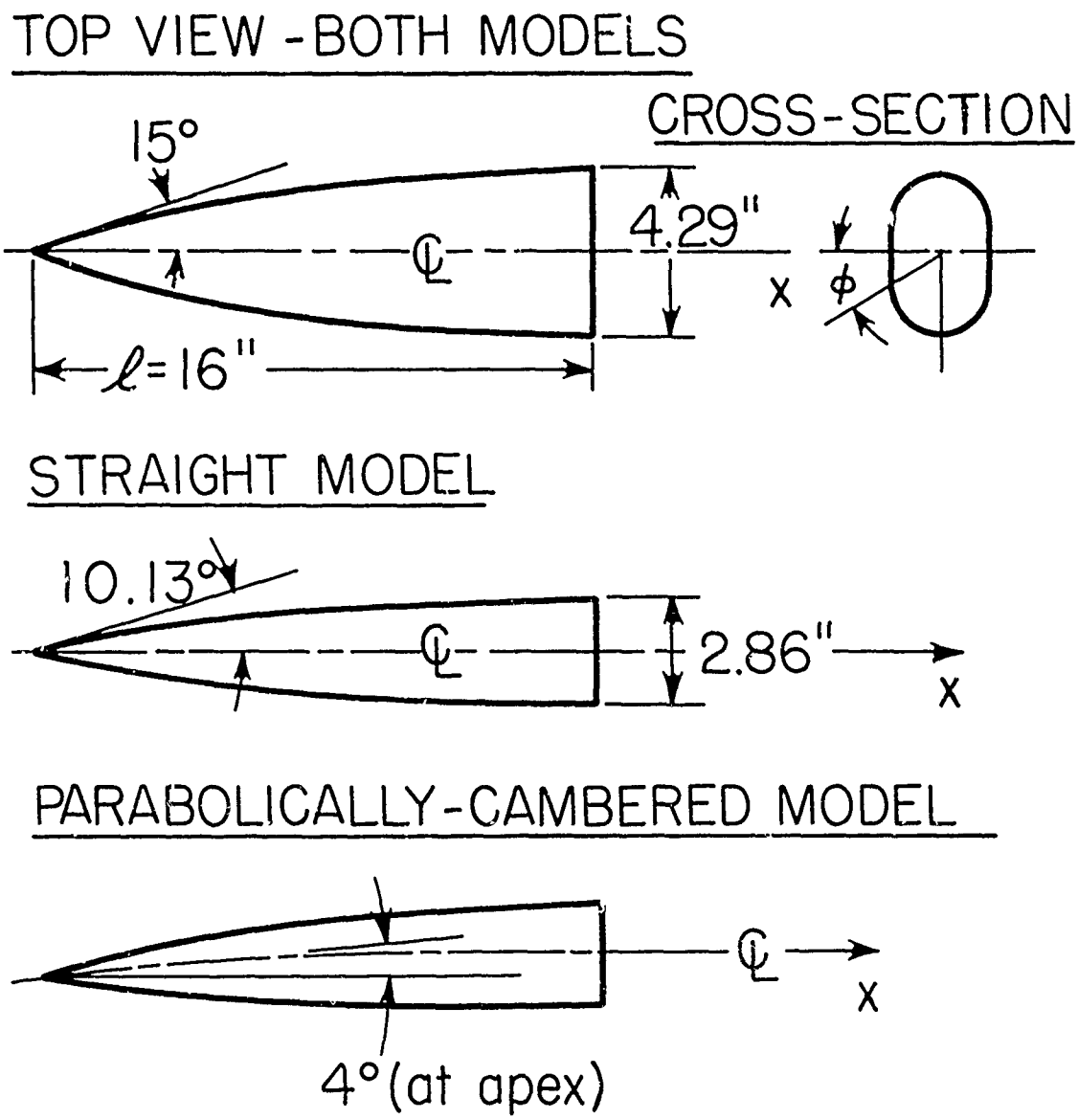


Figure 6. Geometry of two models used for pressure distribution measurements in hypersonic flow.

slopes at the vertex and the base. The second model might be regarded as the equivalent body for an uncambered configuration oscillating in pitch.

Figure 7 compares the axisymmetric lengthwise pressure distribution at $M_\infty = 8$, $(M_\infty \delta)_{AVE.} = 1.75$, on the first model with shock-expansion theory. The agreement is considerably improved by an adjustment for the effect of boundary-layer displacement thickness as shown by the dashed curve. It is significant that the incremental pressure due to incidence, shown in Fig. 8 as a function of φ for three lengthwise stations at $M_\infty = 6$, is less affected by viscosity, at least in the absence of separation, and apparently better susceptible of theoretical prediction. This increment is, of course, the quantity responsible for aeroelastic loading. Figure 9 presents total static pressure measured on the cambered model at $M_\infty = 8$ with the nose angle of attack held at zero. Here the boundary-layer correction explains most of the discrepancy from inviscid theory, but there is evidence of crossflow separation on the leeward side.

2.3 Large Values of the Hypersonic Parameter

In the range

$$\left.\begin{aligned} M_\infty \delta &> 2 \\ \cos\alpha &\cong 1 \end{aligned}\right\} \qquad (34)$$

the analysis of the preceding subsection must be refined to account for real-gas effects and possibly for nonlinearity in incidence at the vertex. Since the nose shock and flow properties just behind it can always be treated as quasi-steady, the extensive research which has been done on circular cones at yaw may be adapted to the case of the body of revolution. Other cross-sectional shapes in imperfect gas flow would seem to provide a topic for future work.

Given the pressure p_N and Mach number M_N as functions of the angle φ on streamlines emerging from the vertex, a real-gas expansion is done along each meridian $\varphi = \text{const.}$ (or in the manner outlined in Ref. 25 when the section is noncircular). The aforementioned constant-γ_2 scheme is probably adequate in most practical situations. If so, the procedure follows very closely that described by Refs. 6 and

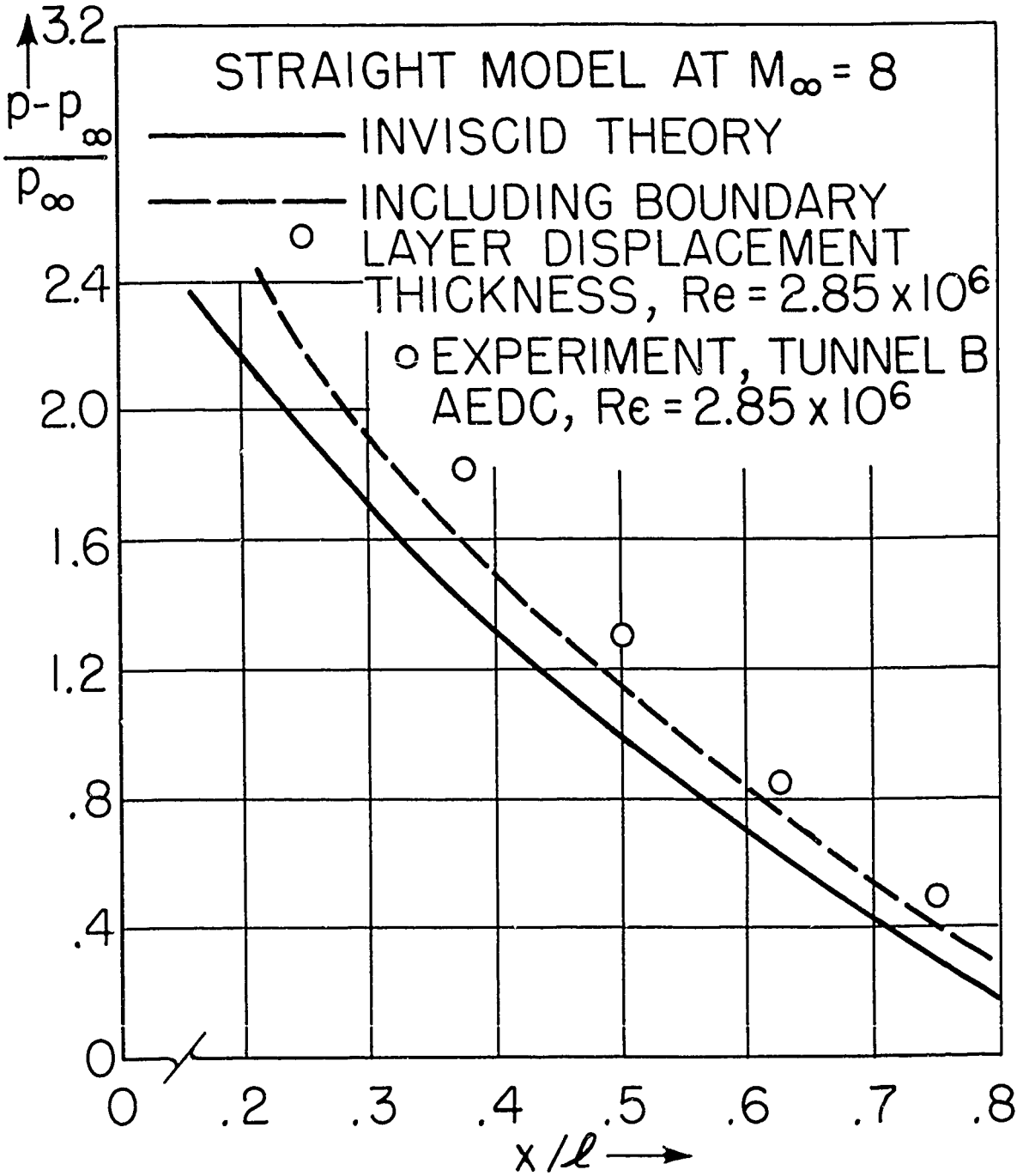


Figure 7. Pressure distribution along meridian $\varphi = 0$ of straight model at $\alpha = 0$ and $M_\infty = 8$.

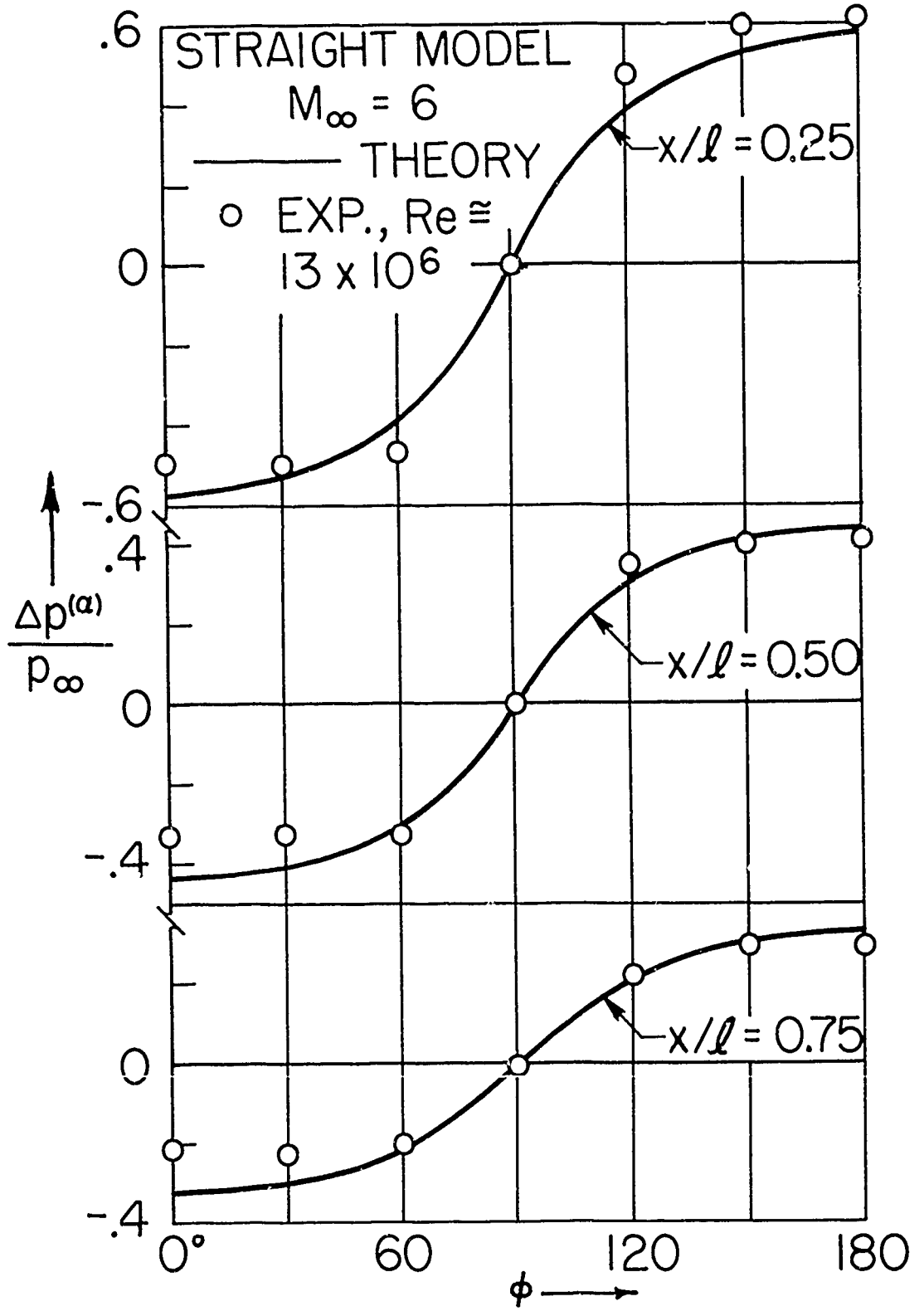


Figure 8. Circumferential distributions of incremental pressure due to angle of attack at three axial stations on straight model at $\alpha = 2^\circ$ and $M_\infty = 6$.

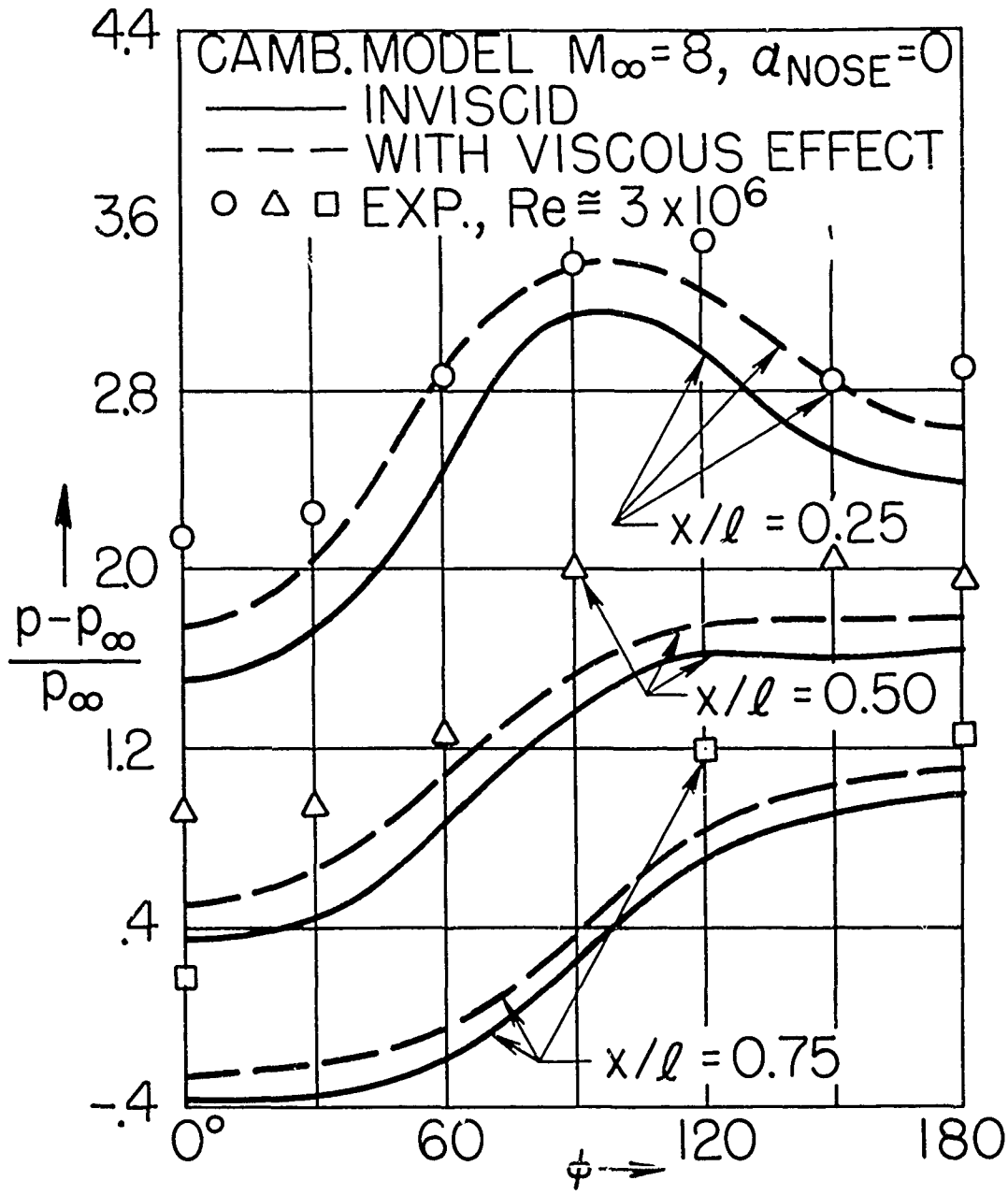


Figure 9. Circumferential distributions of pressure at three axial stations on cambered model at $\alpha_N = 0^\circ$ and $M_\infty = 8$.

25, except that γ_2 is substituted for γ in all appropriate formulas. If the flight conditions are so extreme that $\gamma_2 < 1.3$, numerical integration of the generalized expansion for real gas in thermodynamic equilibrium is indicated, pursuant to the discussion in Section 7.1 of Ref. 1 and the references given there.

2.4 High Angle of Attack

When α is no longer small enough that $\cos\alpha \cong 1$, only rough approximate methods are available for slender bodies. Consider the configuration of Fig. 5 reoriented to a set of $\bar{x}$-$\bar{y}$-$\bar{z}$-coordinates resembling Fig. 2. The results of Sychev (Ref. 7) once more show how to reduce unsteady problems to steady-state equivalents. For instance, the body of revolution "seen" by the $\bar{y}$-$\bar{z}$-slab which meets the vertex at t_o would have the equation

$$\bar{y}^2 + \left[\bar{z} - \bar{z}_B\left(\bar{x}, t_o + \frac{\bar{x}}{U_\infty \cos\alpha}\right)\right]^2 = R_B^2(\bar{x}) \tag{35}$$

Along any body meridian, the surface slope distribution works out to be

$$\frac{dR_B}{d\bar{x}} + \frac{d\bar{z}_B}{d\bar{x}}\cos\varphi = \frac{dR_B}{d\bar{x}} + \cos\varphi \left[\frac{\partial \bar{z}_B}{\partial \bar{x}}(\bar{x}, t) + \frac{1}{U_\infty \cos\alpha}\frac{\partial \bar{z}_B}{\partial t}(\bar{x}, t)\right] \Bigg|_{\substack{\bar{x} = \bar{x} \\ t = t_o + \frac{\bar{x}}{U_\infty \cos\alpha}}} \tag{36}$$

The sense of the angle in Eq. (36) is positive to produce compression. The quantity $\alpha\cos\varphi$ should be subtracted from

$$\frac{dR_B}{d\bar{x}} + \frac{d\bar{z}_B}{d\bar{x}}\cos\varphi$$

to give the total compressive turning from the stream direction. Although the equivalent body shape is easily determined, there is no way analogous to the theory of Cole and Messiter for predicting loads more accurately than the

Newtonian approximation. Equation (19) is therefore to be used for the windward surface, its application being mainly an exercise in trigonometry. Thus it is not difficult to prove for the axisymmetric body vibrating in the $\bar{x}$-$\bar{z}$-plane that

$$C_p \cong C_{P_{02}} \left\{ \cos^2\varphi \sin^2\alpha - 2\cos\varphi\sin\alpha \left[\frac{dR_B}{d\bar{x}} \cos\alpha + \frac{d\bar{z}_B}{d\bar{x}} \cos\varphi\cos\alpha \right] + \left[\frac{dR_B}{d\bar{x}} \cos\alpha + \frac{d\bar{z}_B}{d\bar{x}} \cos\varphi\cos\alpha \right]^2 \right\} \tag{37}$$

The last term in braces is probably negligible. When $\alpha > 0$, Eq. (37) should be employed for

$$\pi/2 < \varphi < 3\pi/2$$

with inequality (20) taking over on the low-pressure leeward side.

SECTION III: SLENDER WINGS AND BODIES WITH BLUNTED NOSES

Since sharply pointed noses are not a practical possibility for hypersonic designs, it is necessary to establish when a configuration is so appreciably blunted that the methods of Sections I and II fail. Such a wide variety of shapes is encountered that generalizations are impossible. But some assistance can be derived from the available steady-state research on blunted axisymmetric models and simple wings and bodies at incidence. It seems safe to conclude that where significant nose-induced loading occurs in steady flow it will also be present in unsteady, and conversely.

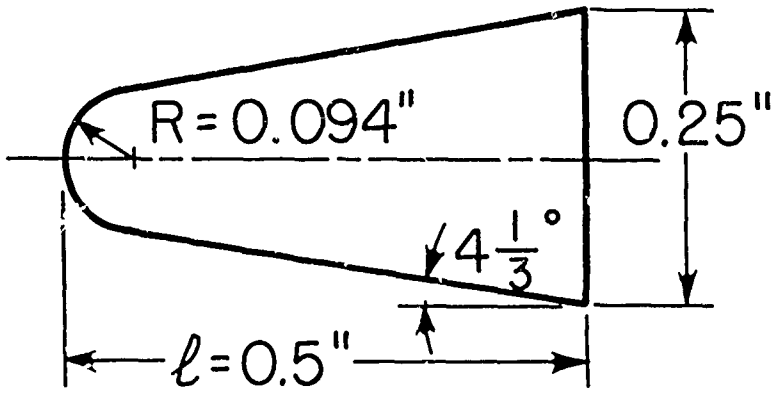
Postponing the discussion of viscosity to Section IV, a few general observations are first made. The pressures on the steeply inclined forward surface are obviously very high and

are predictable independently of what takes place farther aft. Regardless of whether Newtonian or more refined techniques are used to find the loads, however, the quasi-steady hypothesis seems strongly justified. One of the few experiments on an oscillating body under hypersonic conditions, conducted at Army Ballistic Missile Agency and briefly reported by Kennet (Ref. 31), reinforces this point. The model depicted in Fig. 10a was oscillated normal to an $M_\infty = 4.37$ airstream at 112.5 cycles/sec., and high-speed Schlieren films were made of the flow. The extreme positions of the bow shock relative to the model are sketched in Fig. 10b. The shock is seen to follow the instantaneous displacement very closely except several nose radii back along the afterbody. This quasi-steady behavior is explainable in terms of the reduced frequency based on nose radius, which had a typical value $k = 2.5 \times 10^{-3}$ despite the rather high frequency and low hypersonic speed.

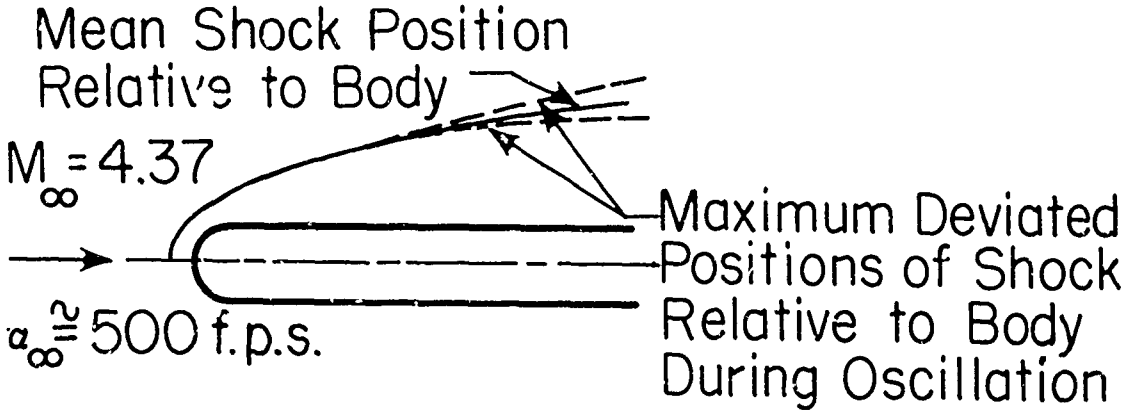
On the other hand, if one proceeds far enough aft on the streamlined portion of a lifting configuration, a region is usually found where loads depend on the local incidence and are insensitive to conditions at the nose. The methods of Sections I and II are adaptable here by arbitrarily replacing the actual fore-shape with a pointed nose or leading edge. This is true despite the presence of a hot entropy layer covering the surface, because evidence suggests that pressure is often transmitted through this layer as through a boundary layer (cf. Capiaux and Karchmar, Ref. 26, and the review of Sychev's work on pp. 73-74 of Ref. 2).

The size of the zone of induced pressures between the shoulder and the aforementioned aft region is the best measure of the importance of bluntness. Following Creager (Ref. 27) and others, the simplified theories suggested in 3.1 below merely add these induced pressures to those that would be felt in the absence of bluntness. Conclusions regarding the extent of the induction zone can be drawn from the data and analysis in such papers as Refs. 26 through 29.

As a typical example, Bertram and Henderson (Ref. 28) demonstrate that the normal force and pitching moment on a fully-blunted flat plate at $M_\infty = 20$ in perfect air can be predicted without reference to induced pressures at $\alpha = 20^\circ$ when the thickness ratio is 0.05 or less and at $\alpha = 5^\circ$ when the thickness ratio is 0.02 or less. More generally, it seems that leading-edge diameters in excess of c/M_∞^3 on wings and ℓ/M_∞^3 on bodies at $\alpha = 0^\circ$ call for consideration of induction. But as α is increased these limits become less stringent, and at $\alpha = 20^\circ$ values of $100\, c/M_\infty^3$ or $100\, \ell/M_\infty^3$ do not appear unreasonable, unless local pressures near the shoulder are required accurately.



(a) Geometry of Nose Section



$\alpha_p = 1.126°$; $\omega = 112.5$ c.p.s.

$k_R = \frac{\omega R}{U_\infty} = 0.002,5 \quad k_\ell = \frac{\omega \ell}{U_\infty} = 0.013,3$

(b) Shock Positions During Oscillation

Figure 10. Data on blunt model oscillated in an airstream at $M_\infty = 4.37$.

3.1 Approximate Theories

No effort is made, in this review of approximate schemes for load estimation, to distinguish parametric ranges in detail or separate wing-like and body-like configurations. The parameter $M_\infty \delta$ is large over the nose region in all cases. Unfortunately, these rough techniques are essentially the only ones available today for dealing with unsteady phenomena. Therefore, they are covered rather sketchily here, and in 3.2 the more important objective is pursued of recommending what research is needed to bring blunt-body theories up to the same satisfactory level of development that characterizes those for the pointed shapes.

A blunted lifting-surface profile at low incidence is illustrated in Fig. 11. Looking first at the region of large inclinations θ_N, shown in the inset, the loading there can be estimated on a two-dimensional crossflow basis by the Modified-Newtonian-Prandtl-Meyer theory of Wagner (Ref. 30). The same approach is equally valid near the nose of a body, if the stagnation point is assumed to be aligned with the instantaneous relative-wind direction and streamlines are taken to fan out radially from this point. In the case of the negligibly-swept wing, for example, the unsteady motion alters the instantaneous θ_N to

$$\theta_{EFF.} = \theta_N + \frac{\partial z_a}{\partial x}(x_\ell, y, t), \tag{38}$$

$z_a(x, y, t)$ being a coordinate describing the motion of the mean line. Starting from Eq. (38), one can construct the normal vector $\vec{n}$ and velocity vector $\vec{q}_b$ for the portion of the surface where the Newtonian Eq. (19) is used. Following Ref. 30, Eq. (19) is applied around to the value of $\theta_{EFF.}$ (θ_N if the motion is small enough) where both the pressure and pressure slope can be faired smoothly into the Prandtl-Meyer formulation. The latter then carries the calculation, again on a quasi-steady basis, around to just behind the shoulder or line of attachment of the nose to the afterbody. The shoulder pressure p_s thus computed will be a function of spanwise distance y and t on the upper or lower surface of the wing, and of polar angle φ and t on the body.

When the leading edge is a circular cylinder or the nose is a hemisphere, results like Eqs. (4.3.17) and (4.4.11) of Ref. 1, which constitute improvements to higher order in the

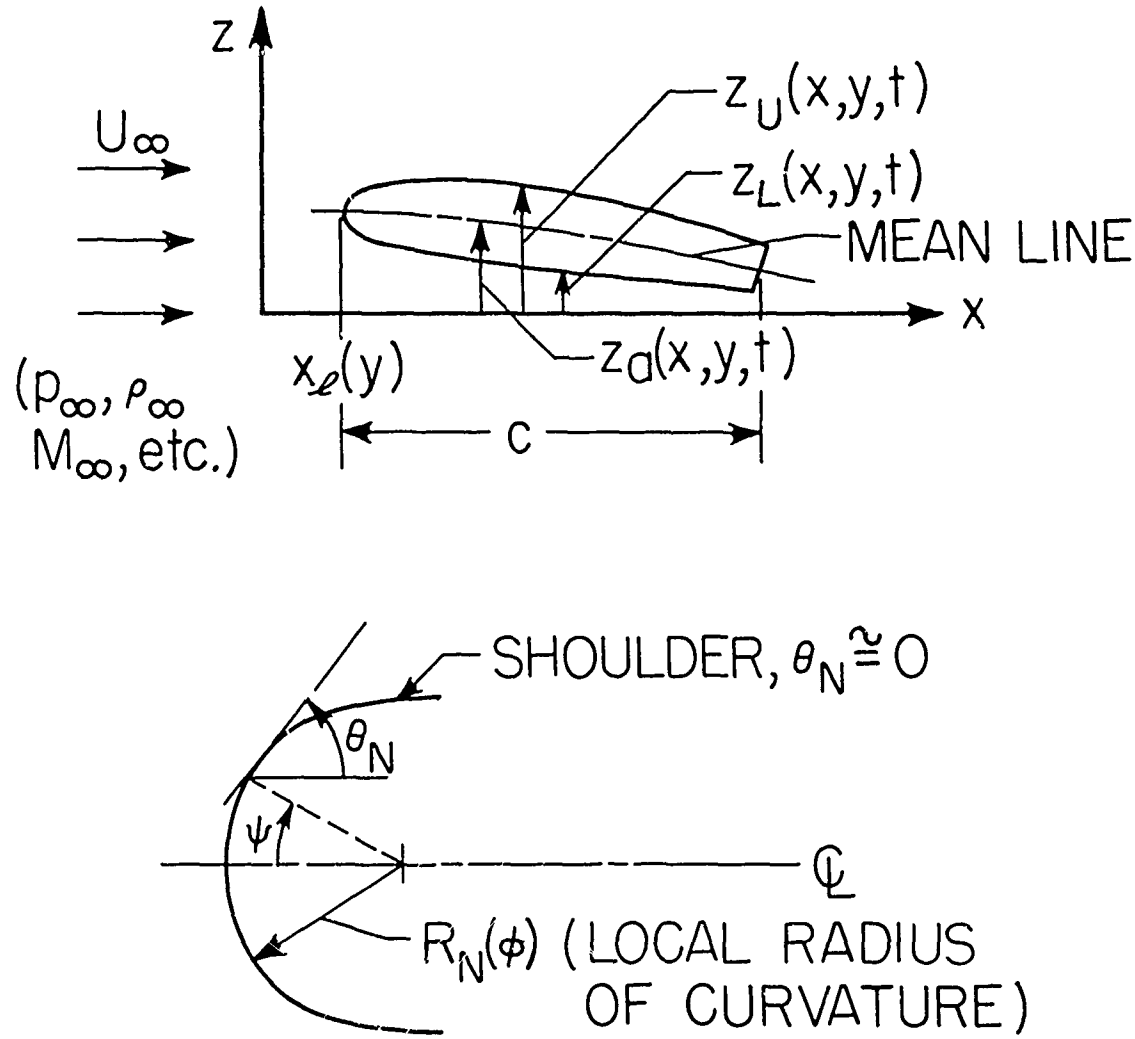


Figure 11. Typical cross section of a blunted, thin configuration performing unsteady motion $z_a(x, y, t)$ normal to a hypersonic airstream.

density ratio ϵ , may perhaps be employed to adjust Eq.(19). Moreover, if the nose has a large normal acceleration

$\partial^2 z_a / \partial t^2$ or $\partial^2 z_B / \partial t^2$, the mass of dense gas carried in the shock layer may give rise to an appreciable inertia force. The corresponding pressure increments turn out to be, approximately,

$$\delta C_p \cong \frac{\partial^2 z_a}{\partial t^2} \frac{R_N}{U_\infty^2} 4\cos\theta_N \tag{39}$$

on an unswept leading edge and

$$\delta C_p \cong \left[\frac{\partial^2 z_B}{\partial t^2}(0,t)\right] \frac{R_N}{U_\infty^2} 2\cos\theta_N \cos\varphi \tag{40}$$

on a hemisphere. These results have been developed from Section 3.7 of Ref. 1.

Beyond the shoulder over both the compression and expansion surfaces at low α , the pressures can be determined following streamwise strips on the wing, meridians on the body of revolution, and geodesics through an equivalent pointed nose on noncircular bodies. It is assumed that

$$\frac{p}{p_\infty} = \frac{p_\alpha + p_\beta}{p_\infty} - 1 \tag{41}$$

at any point, where the first part p_α is due to incidence, camber, and/or unsteady motion. p_α is to be found as discussed in Sections I or II, including real-gas effects but assuming that the particular surface is part of a thin, pointed airfoil or body. The former would have its leading edge at the upper or lower shoulder, as appropriate, whereas the latter must be arbitrarily provided with an equivalent pointed vertex, whose conical shape can usually be drawn by common sense.

The second contribution in Eq. (40), an induced pressure p_β, can be treated as independent of anything but nose shape and thickness when the motion is small. Many alternative schemes are available for estimating p_β, each distinct from the others and supported by suitably chosen experimental data. Until the conflicts are resolved, one is well-advised to choose the simplest. This appears to be Love's technique (Ref. 32, which is supported by the data of Ref. 33). His empirical formula reads

$$\frac{p_\beta}{p_\infty} = \frac{p_s}{p_\infty}\left[\frac{1}{1+\frac{x_s}{d}}\right] + \left[\frac{1}{1+\frac{d}{x_s}}\right]^{\frac{p_s}{p_\infty}} \qquad (42)$$

Here d is the thickness or nose diameter, and x_s is axial distance measured from the shoulder. p_β will naturally depend on x, y, t over the wing and x, φ, t over the body. Since Eq. (41) was developed for axisymmetric flows in Helium, an improved version will quite likely emerge. Nevertheless, it has the advantage of starting from the correct pressure p_s at $x_s = 0$ and approaching p_∞ in a reasonable asymptotic fashion at large distances. Incidentally, the term -1 which appears in Eq. (41) for the complete pressure corrects for the fact that both p_β and p_α approach the free-stream p_∞ when $x_s \to \infty$ and the incidence is zero.

The cases of large angle of attack α and high wing sweep Λ require special treatment, as discussed in Sections III and IV of Ref. 10. The basic philosophy is unchanged from the approximate procedure just described. The main modifications are that the p_α computation follows 1.3, 1.4 and 2.4, while the induced pressure p_β depends on distance $\bar{x}_s$ along a mean line which may be steeply inclined to the stream direction. The blunt wing of very low aspect ratio is perhaps best analyzed as a slender body, since it constitutes a limiting form of the latter with severely flattened cross sections.

3.2 More Refined Theories

Table 1 summarizes the theoretical methods which, in the authors' opinion, will ultimately provide the most rigorous, accurate means of determining unsteady hypersonic airloads. It has been prepared without regard to the current state of

TABLE 1

ULTIMATE BEST METHODS FOR
UNSTEADY HYPERSONIC AIRLOADS CALCULATION
Pointed Configurations

Parameter Range	Thin Wings	Slender Bodies
$M_\infty \delta \leq 1$ (Low to moderate L.E. sweep)	Attached L.E. shock, followed by shock-expansion or characteristics for the equivalent warp-wing problem (perfect gas)	Variational-Ritz solution of two-dimensional piston problem
$1 < M_\infty \delta < 1.5\text{-}2$ (Low to moderate L.E. sweep)		Conical nose shock, followed by three-dimensional characteristics (perfect gas)
$1.5\text{-}2 \leq M_\infty \delta$; $\cos\alpha \cong 1$ (Low to moderate L.E. sweep)	Attached shock, followed by real-gas shock-expansion or characteristics	Conical nose shock, followed by three-dimensional characteristics (real gas)
α Large (Low to moderate L.E. sweep)	Method of integral relations on windward side	Unsteady characteristics solution of Sychev's slab problem (real gas)
Λ Large $M_\infty \delta \leq 0.5\text{-}1$	Two-dimensional piston solution	(Not Applicable)
Λ Large $\cos\alpha \cong 1$	Unsteady characteristics solution of two-dimensional piston problem	
Λ Large α Large	Second-order Newtonian or method of integral relations on windward side	

continued next page...

TABLE 1
(concluded)

Blunted Configurations

Parameter Range	Blunted Wings	Slender, Blunted Bodies
α Small (Low to moderate L.E. sweep)	Method of integral relations on L.E., followed by real-gas characteristics	Method of integral relations on nose, followed by real-gas characteristics
α Large (Low to moderate L.E. sweep)	Method of integral relations on L.E. and windward surface; characteristics on leeward surface	Method of integral relations on nose and windward surface (?)
α Small Λ Large	Method of integral relations on forward portion, followed by real-gas three-dimensional characteristics	(Not applicable)
α Large Λ Large	Method of integral relations on L.E. and windward surface, followed by real-gas three-dimensional characteristics	(Not applicable)

development or to the amount of computational labor that will be involved, except for the proviso that computers of the size of the IBM 7090 are believed adequate for any practical job that will arise.

Both pointed and blunt configurations are included in the table, but for the former it will be noticed that several of the items correspond to methods already discussed in Sections I and II. That is, available and proved ways already exist to handle these problems well enough even for final-design purposes. Moreover, the improvements to be gained on pointed shapes generally by proceeding from current theories to such refinements as three-dimensional characteristics are not considered nearly as dramatic as what is possible when there is appreciable blunting. At least this is true when the ultimate purpose is a loading or aerothermoelastic investigation.

The remainder of this section is devoted to describing, with definitive references, those topics occurring in Table 1 which have not been taken up previously. The reader will be able to deduce several recommendations regarding the need for intensified research in potentially fruitful areas.

On nearly pointed wings of limited sweep the method of characteristics for two-dimensional, rotational supersonic flow is capable of carrying the calculation as far back as needed along any streamwise section, provided shocks are suitably inserted at the leading edge and other places with compressive turning. Characteristics are a classical theoretical procedure, discussed by Ferri (Ref. 34), in Section 7.1 of Ref. 1, and in many excellent papers cited there.

When the angle of attack of the thin wing becomes too large, or when a blunt leading edge is present, the shock detaches. The compression surface at high incidence and the blunted region are covered by a fairly thin shock layer containing highly rotational, often dissociated three-dimensional flow. In the long run the authors are confident that the integral-relations method of von Karman-Dorodnitsyn-Belotserkovskii (Refs. 8, 9, 35) offers the most promising general way of dealing with such problems. Equilibrium real-gas thermodynamics must be included (Ref. 31). To date the Belotserkovskii scheme has been used only for flows with two independent variables — two-dimensional, axisymmetric, conical and the like. The authors have examined the formulation for a fully three-dimensional situation,* however,

* The Sychev or Van Dyke similarities will reduce unsteady to steady flows for pointed configurations, while on blunt noses the quasi-steady hypothesis eliminates time.

and see no reason why a double integration and polynomial approximation cannot be made to yield ordinary differential equations in the most important coordinate. If no more than two strips in each of the directions of integration are employed, an IBM 7090 solution seems entirely feasible.

It is not believed that three strips will ever be required in practice with the integral-relations method. Figure 12 is reproduced from Ref. 35 to justify this observation and to illustrate the truly remarkable convergence that is typically achieved. In this figure the two-strip estimate of sonic-line location on a sphere at $M_\infty = 1.85$ is compared with measured data and seen to fall within the experimental scatter. The reader is reminded that the sonic line represents a much more difficult flow property to predict than surface pressure; moreover, the shock layer is much thicker and harder to analyze, by an integral procedure, at this low supersonic Mach number than in the hypersonic regime. Figure 13 presents a typical one-strip estimate of surface pressure at $M_\infty = 8.08$. Here the agreement is more than satisfactory. In most cases a single strip will probably prove adequate for engineering purposes. On page 216 of Ref. 1, Hayes and Probstein point out that this technique can be extended to arbitrary shapes "utilizing the hydrodynamic equations in general orthogonal coordinates." This advice has not always been taken in the past, but it is urged that the simplifications thereby achievable warrant the use of body-oriented axes whenever feasible.

Turning to other items in Table 1, it will be noticed that unsteady and three-dimensional characteristics are repeatedly referred to. For instance, on low-aspect-ratio wings the two-dimensional isentropic piston solution of Ref. 6 can no longer be used when α and/or M_∞ attain large values. Then one recommends characteristics as adapted to the independent variables y, z and t. Moreover, steady three-dimensional characteristics are the natural way of computing the supersonic-hypersonic flow regions over blunted bodies and low-aspect-ratio lifting surfaces, relying for initial values and forward shock shape on a Belotserkovskii analysis of the subsonic and slightly supersonic portions of the shock layer. This technique has been anticipated for many years and is now just on the threshold of application (see Fowell, Ref. 37, and Thornhill, Ref. 38, which contain comprehensive literature citations). It is believed to have a rich future in the era of the digital computer, however, and the versatility of a properly planned three-dimensional routine with steady and unsteady options is hard to overestimate. Real-gas, frozen-flow or other such refinements can be incorporated with considerable labor but no great conceptual difficulty.

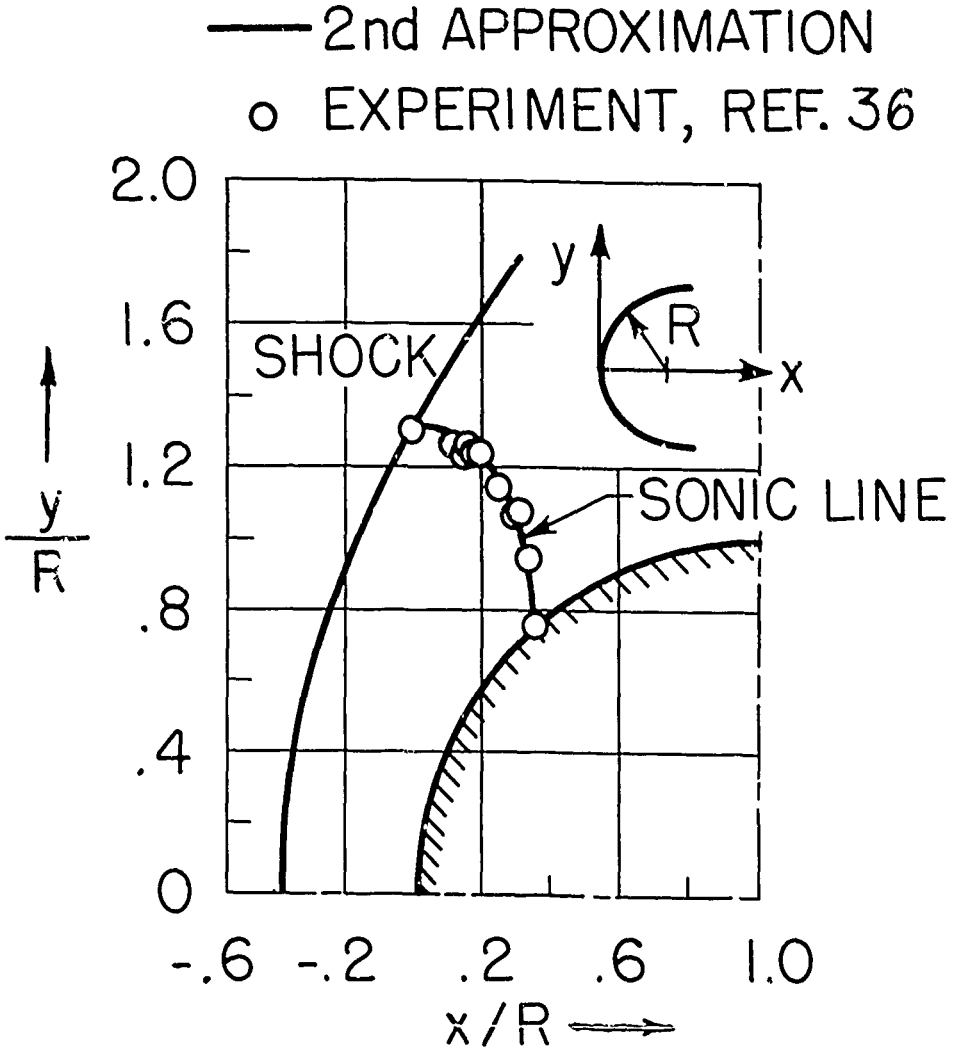


Figure 12. Two-strip Belotserkovskii prediction compared with measured sonic line location on a hemisphere at $M_\infty = 1.85$ in air.

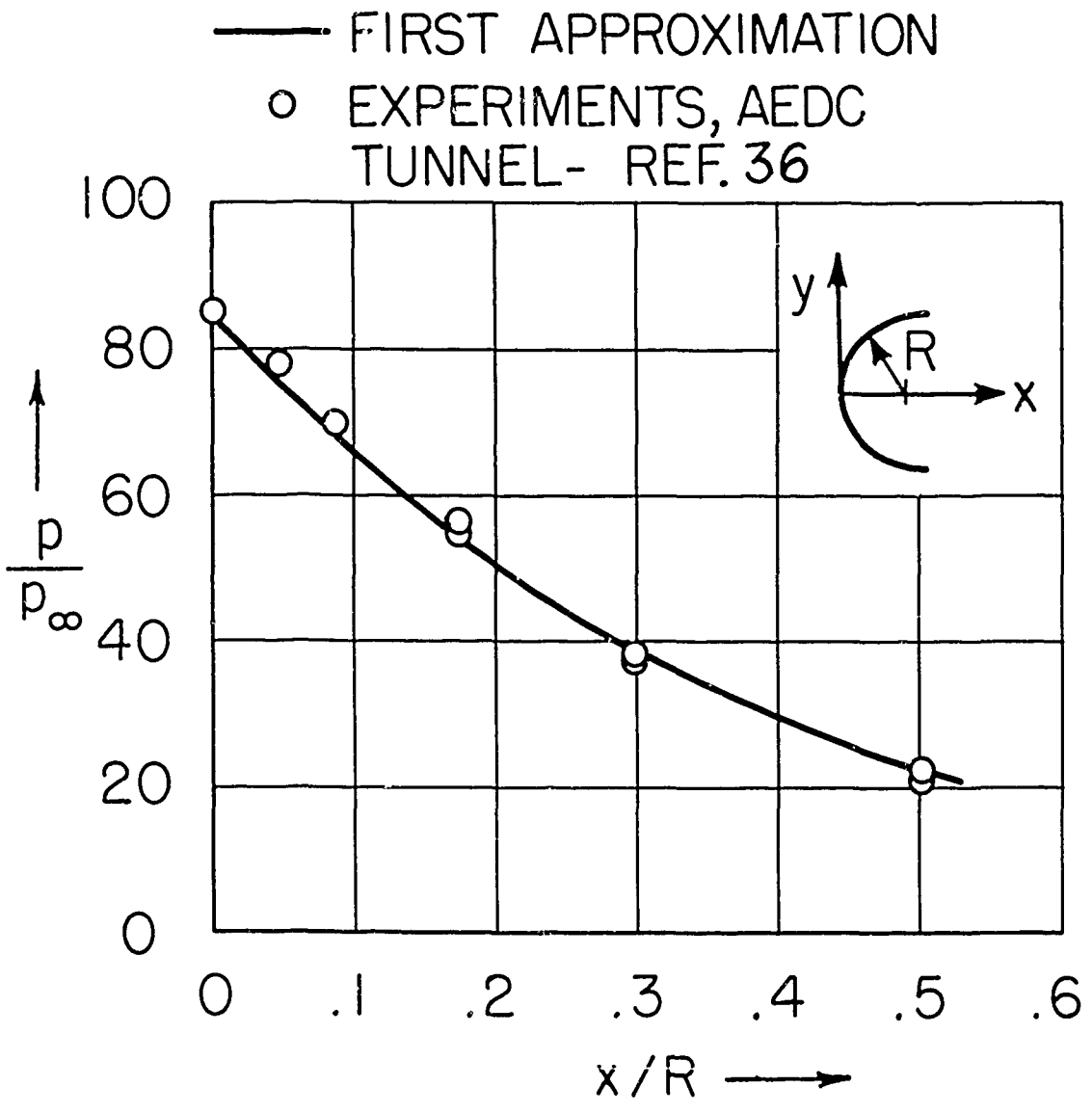


Figure 13. One-strip Belotserkovskii prediction compared with measured pressure distribution on a hemisphere at $M_\infty = 8.08$.

A few miscellaneous remarks are necessary to clarify some of the numerous implications of Table 1 that can only be treated very inadequately in a brief survey. For example, more effort is needed on circular and noncircular cones at yaw before pointed bodies can be analyzed over the full range of α and $M_\infty \delta$. The extension to higher orders in the incidence α_N and to ascertain how the shock detaches from the vertex constitutes a significant research topic. Only when these problems are solved will the necessary initial data be available for shock-expansion or characteristics computations of the flow aft over the configuration.

There presently exists a firm limitation of $k^2 \ll 1$, with k based on wing chord or body length, upon the theories proposed for blunt low-aspect-ratio wings and blunt bodies. This is because the Van Dyke and Sychev similarities are not strictly valid in the presence of bluntness, so that the equivalent-steady-flow concept may fail. It is possible that further examination of results of Chernyi (Ref. 29) and other studies reviewed in Ref. 2 will reveal circumstances when the similarity is preserved. The resolution of this question is important in connection with unsteady loadings that will be met in practice.

Finally, some problems can be anticipated when treating noses and rounded leading edges at incidence. Very few situations will occur where the sonic line is forced as far around as the shoulder*, so there is little reason to be concerned about upstream influences from the afterbody. Nevertheless, the forward shock-layer calculation will become more difficult when the nose does not have constant curvature, for then the stagnation point or line no longer faces directly into the instantaneous relative wind. Uncertainty about the location of stagnation will add another unknown when the method of integral relations is applied. To the authors' knowledge, problems like inclined elliptical leading edges and nonspherical noses have not been studied extensively except within the Newtonian framework.

---

* One exception is the low-aspect-ratio wing at high α, where the leading edge becomes a trailing edge; but then the shock layer is thin on the whole windward surface.

SECTION IV: THE EFFECTS OF VISCOSITY AND FINITE REACTION RATE

Two phenomena which may often have a significant influence on hypersonic pressure distributions have been left out of the foregoing. Both viscous stresses in the flow and deviations from thermodynamic equilibrium have consequences that are qualitatively and quantitatively different than at lower flight speeds, but their detailed analysis requires considering the physics of the gas far more deeply than is possible within the present survey. This section calls attention to when certain of their effects are expected to be important and gives clues as to where thorough treatments can be found in the literature.

Chapters 8 and 9 of Ref. 1 contain by far the best review of hypersonic viscous flow and should be carefully read by anyone concerned with the problem. When one is calculating loads on slender wings and bodies, the concept of the attached boundary layer as a thin, superficial region, through whose depth the pressure is transmitted unchanged from its "inviscid" value outside, retains validity. But two things happen to make its relative role greater: the region of disturbed flow external to the boundary layer is much reduced in extent, and the layer itself is thickened by the very high temperatures and associated low densities. The latter effect is much less pronounced when the body surface is fairly cool during a thermal transient than for a wall at equilibrium temperature, so the value of T_w must be accounted for.

From experience at lower speeds one will recall that the boundary layer's influence on pressures, if any, comes about through an apparent increase in body dimensions by the "displacement thickness" δ^*. For instance, in Fig. 1, the upper and lower surfaces would appear to have the coordinates (in steady flow)

$$\left[z_U(x,y) + \delta_U^*(x,y) \right] \qquad \text{and} \qquad \left[z_L(x,y) - \delta_L^*(x,y) \right].$$

In equations like (6) the surface slope is altered by an additive increment $\partial \delta^* / \delta x$, which can be computed from the standard theory of the compressible boundary layer. Unsteadiness in the external flow naturally causes changes in δ^*, as discussed by Moore (Ref. 39) among others, but at reduced frequencies below about 0.3 it is believed that the boundary layer can be treated on a quasi-steady basis (Ref. 40).

On appreciably blunted configurations, a displacement-thickness shape correction appears to constitute the only adjustment needed for analyzing aeroelastic problems. This conclusion stems from the observation that the maximum loads on nearly any flight trajectory occur at comparatively low altitudes in the atmosphere, where Reynolds numbers are relatively high. A revision will be needed when estimating loads on low-wing-loading, high-altitude devices like inflatable entry gliders and hypersonic sails.

Sharp-pointed configurations, however, require special handling. Near the leading edge or vertex there will always exist a small zone where $\partial\delta^*/\partial x$ is very large, so that the surface pressure is very much higher than it would be in the absence of viscosity. This is the region of "strong pressure interaction," which is discussed in Chapter 9 of Ref. 1, in Ref. 41, and in the many other papers cited by these authors. At any given distance x behind the leading edge, the magnitude of this effect is measured by the "viscous interaction parameter"

$$\bar{\chi} = \frac{M_\infty^3 \sqrt{C}}{\sqrt{Re_x}} \tag{43}$$

In Eq. (43), Re_x is the Reynolds number based on free-stream gas properties and on the length x :

$$Re_x = \frac{\rho_\infty U_\infty x}{\mu_\infty} , \tag{44}$$

μ_∞ being the dynamic viscosity coefficient. C is a dimensionless constant in a secant approximation to the relationship between viscosity and temperature; a suitable definition is given by the equation

$$\frac{\mu_w}{\mu_\infty} = C \frac{T_w}{T_\infty} \tag{45}$$

Values of $\bar{\chi}$ less than unity are identified with weak interaction, when (Ref. 41) "the self-induced pressure gradient is

assumed not to affect the boundary layer growth." Strong interaction occurs when

$$\bar{\chi} >> 1 \qquad (46)$$

Now $\bar{\chi} \sim 1/\sqrt{\chi}$ goes to infinity right at the leading edge or vertex. Hence there is always some region of strong interaction. The point with respect to hypersonic airloads estimation, however, is that the region where $\bar{\chi} > 1$ will nearly always be so small that the high pressure in this region can be neglected. This observation is at the root of the last general restriction listed in the Introduction.

Having dismissed strong interaction, one has the convenient result that, in the weak interaction zone, δ^* may be calculated for the inviscid surface pressure distribution, the incremental induced pressure $\delta p / p_\infty$ can then be determined from the resulting $\partial \delta^* / \delta x$, and the process is stopped at this point. There is no further coupling between the boundary layer and the external field.

Formulas for $\delta p / p_\infty$ are available from Ref. 41 and elsewhere in the literature. This increment is simply added to the inviscid pressure obtained as described in preceding sections. When the pointed leading edge is at positive incidence, the induced effect will be smaller relative to other sources of overpressure. It is also easy to deduce that where $\bar{\chi} < 0.1$ δp will only be a few percent of p_∞ and can probably be dismissed.

Incidentally, an illuminating discussion of the combined interplay of bluntness and viscosity, which has been overlooked here while considering the loads problem, will be found in Ref. 42.

The influence of nonequilibrium thermodynamics on hypersonic flow is taken up, among other places, in Chap. 7 of Ref. 1 and in Refs. 14, 43 and 44. For a first-glance indication of what is involved, one should look at Figs. 17, 18, 19 and 21 of Ref. 14 and at Fig. 1 of Ref. 44. The key question to be asked is whether the distance traveled by a fluid particle during the time required for a given effect (accommodation of molecular-vibration degrees of freedom, dissociation reaction, recombination reaction, etc.) to adjust essentially into equilibrium is appreciable by comparison with body dimensions. This can be answered by examining a parameter like

$$G = \frac{x}{U_\infty} \frac{\omega_i}{\rho}, \qquad (47)$$

where ω_i is the rate of production of accommodated molecules, new chemical species, etc. per unit volume.

In Refs. 14 and 43, this matter is studied primarily from the standpoint of the fluid properties in the attached shock layer ahead of a hypersonic blunt configuration. A first conclusion is that molecular vibrations in air can probably be assumed in equilibrium with the instantaneous temperature for practical purposes; they adjust in relatively few mean free paths, and their influence on pressures is quite small in any event. The oxygen dissociation, however, can produce large deviations of T and ρ at the higher altitudes on small-radius noses.

From the standpoint of surface pressure estimation, some general observations regarding the dissociation-recombination reaction are in order. Computed pressures in the attached shock layer adjacent to a blunt nose are quite insensitive to whether deviations from equilibrium are accounted for or not. Figure 17 of Ref. 14 and Figs. 7 and 12 of Ref. 43 are cited in confirmation. The farther the flow expands back around toward the streamlined portion of a blunted configuration, however, the more the pressure is influenced by the degree of recombination. Accordingly, there will exist flight conditions of practical interest where recombination rates must be introduced when calculating loads. Until the methods for doing this are systematized to a point of routine utility, the following suggestion is made: the computation should be repeated for the two extremes of 1) equilibrium flow ($G \gg 1$) and 2) flow frozen ($G \ll 1$) at the state occurring just behind the bow shock. (This procedure will, of course, be necessary only in connection with the refined methods of Table 1; the approximate methods outlined in 3.1 more or less bypass the whole problem.) The two resulting pressure distributions then provide limits between which the desired result lies. Consideration of the recombination values of G(Ref. 44) may then be used for an estimated interpolation. It is of interest that frozen flow takes place at a fixed, effective value of γ_2 (Ref. 1) and is consequently easier to analyze than the equilibrium case.

SECTION V: CONCLUSIONS

It should be clear that a principal conclusion of this survey is that methods of unsteady hypersonic airload estimation for slender, pointed wings and bodies are in a relatively satisfactory state of development, whereas a great deal remains to be done when appreciable effects of bluntness are present. The same statement is generally true of wing-body combinations and other more complicated configurations, about which it has not been possible to say much here. The work of authors like Savin (Ref. 45) and Scheuing et al. (Ref. 46) on such "interference" problems certainly deserves mention. A particularly interesting flow situation is the one which occurs near the concave intersection between the body and planar wing on the windward side of a lifting vehicle. This has been studied on a conical-flow basis in Ref. 46 and elsewhere, and it appears possible to predict quite accurately the high pressures which are carried over from one element to the other of the combination. On the other hand, typical fin and control-surface installations on blunted hypersonic gliders will require considerable further investigation; when separation, re-entrant wakes, etc. are involved, recourse to experiment will always be necessary.

A few additional conclusions and recommendations for continued research will now be singled out of the foregoing sections for special emphasis:

1. The use of the quasi-steady hypothesis for nose or leading edge regions, and the idea of steady flows equivalent to a given time-dependent motion of an elongated configuration, render the results of steady-state aerodynamic theory more broadly valuable for hypersonic aeroelastic calculations than has been the case in subsonic or supersonic flight. Further study is required on the equivalent wing and body concepts with bluntness and strong entropy layers.

2. Because of its extraordinary potential for the rigorous analysis of both steady and unsteady thin shock-layer regions, the method of integral relations should be made the subject of an intensive development program. Three-dimensional flow fields with real-gas effects, possibly nonequilibrium thermodynamics and boundary-layer interaction constitute the ultimate goal.

3. Systematic organization of the three-dimensional method of characteristics, both for steady and two-dimensional time-dependent situations, represents another very desirable and attainable objective. Real-gas phenomena should once more be included. Existing digital computing machines have the capacity for handling both three-dimensional integral relations and characteristics, if they are efficiently programmed. Maximum versatility should be sought after in these routines, and they will become progressively easier of practical application with the appearance of computers with greater storage and higher speed.

4. The influence of boundary-layer displacement thickness on unsteady hypersonic pressures will often have to be accounted for, especially over the forward portions of pointed surfaces. For aerothermoelastic purposes, however, both unsteadiness within the boundary layer and zones of strong interaction can nearly always be overlooked. Another viscous phenomenon which merits further experimental and theoretical investigation is crossflow separation on the leeward side of bodies at incidence; this will frequently make itself felt, even at small angles, in a forward shift of the center of pressure and other airload modifications.

5. With regard to nonequilibrium effects in hypersonic airflow, the single one which may often be expected to influence both steady and unsteady surface pressures is the recombination reaction of diatomic Oxygen. The aft portions of elongated shapes will often be exposed to a flow regime which falls partway between the extremes of frozen composition and thermodynamic equilibrium.

6. Most aeroelastic loading research to date has concentrated on small deviations from a steady trimmed flight condition. Especially in connection with dynamic stability, more attention is recommended to the very difficult question of large-amplitude unsteady motions.

REFERENCES

1. Hayes, W. D., and Probstein, R. F., Hypersonic Flow Theory, Academic Press, New York and London, 1959.

2. Probstein, R. F., Recent Soviet Advances in Inviscid Hypersonic Aerodynamics, Aerospace Engineering, Vol. 20, No. 7, July 1961, pp. 10-11, 68-81.

3. Lees, L., and Kubota, T., Inviscid Hypersonic Flow Over Blunt-Nosed Slender Bodies, Journal of the Aeronautical Sciences, Vol. 24, No. 3, March 1957, pp. 195-202.

4. Stanyukovich, K. P., Unsteady Motion of Continuous Media, English Translation edited by M. Holt, Pergamon Press, New York, 1961 (originally Gostekhizdat, Moscow, 1955).

5. Ashley, H., and Zartarian, G., Unsteady Flow and Instability of Lifting Surfaces, (paper CONFIDENTIAL) Proceedings of the Third Symposium on High-Speed Aerodynamics and Structures, San Diego, California, March 1958.

6. Zartarian, G., Unsteady Airloads on Pointed Airfoils and Slender Bodies at High Mach Numbers, WADC Technical Rept. 59-583, May 1959.

7. Sychev, V. V., Thin Bodies in Hypersonic Flow at High Angles of Attack, Doklady-USSR Academy of Sciences, Vol. 131, No. 4, 1960, pp. 776-779.

8. Dorodnitsyn, A. A., On a Method of Numerical Solution of Some Nonlinear Problems of Aero-Hydrodynamics, Proceedings of the Ninth International Congress of Applied Mechanics, Vol. I, Brussels, 1957.

9. Belotserkovskii, O. M., Flow Past a Circular Cylinder with a Detached Shock, Doklady Akad., Nauk SSSR, Vol. 113, 1957, pp. 509-512.

10. Ashley, H., Methods for Estimating Airloads on Wings and Bodies in Hypersonic Flight, North American Aviation, Inc., Report No. NA-61-757, July 1961.

11. Lighthill, M. J., Oscillating Airfoils at High Mach Number, Journal of the Aeronautical Sciences, Vol. 20, No. 6, June 1953, pp. 402-406.

12. Landahl, M. T., Unsteady Flow Around Thin Wings at High Mach Numbers, Journal of the Aeronautical Sciences, Vol. 24, No. 1, January 1957, pp. 33-38.

13. Van Dyke, M. D., A Study of Hypersonic Small Disturbance Theory, NACA Report 1194, 1954.

14. Hansen, C. F., and Heims, S. P., A Review of the Thermodynamic, Transport, and Chemical Properties of High-Temperature Air, NACA Technical Note 4359, July 1958.

15. Eggers, A. J., Jr., Syvertson, C. A., and Kraus, S., A Study of Inviscid Flow About Airfoils at High Supersonic Speed, NACA Report 1123, 1953.

16. Trimpi, R. L., and Jones, R. A., A Method of Solution with Tabulated Results for the Attached Oblique Shock-Wave System for Surfaces at Various Angles of Attack, Sweep, and Dihedral in an Equilibrium Real Gas Including the Atmosphere, NASA Technical Report R-63, 1960.

17. Miles, J. W., The Potential Theory of Unsteady Supersonic Flow, Cambridge Monographs on Mechanics and Applied Mathematics, Cambridge University Press, 1959.

18. Messiter, A. F., A Similarity Law for the Normal Force on a Delta Wing at Hypersonic Speeds, Readers' Forum, Journal of the Aero/Space Sciences, Vol. 26, No. 2, February 1959.

19. Ashley, H., Mykytow, W. J., and Martuccelli, J. R., Prediction of Lifting Surface Flutter at Supersonic Speeds, presented at the Second International Congress, International Council of the Aeronautical Sciences, Zurich, Switzerland, September 12-16, 1960, preprint by Pergamon Press, Ltd., London.

20. Bisplinghoff, R. L., Ashley, H., and Halfman, R. L., Aeroelasticity, Addison-Wesley Press, Cambridge, Mass., 1955.

21. Sears, W. R., Small Perturbation Theory, Section C, Vol. VI of High Speed Aerodynamics and Jet Propulsion, Princeton University Press, Princeton, New Jersey, 1954.

22. Zartarian, G., Ashley, H., et al., Forces and Moments on Oscillating Slender Wing-Body Combinations at Supersonic Speed, Parts I and II, AFOSR Technical Notes Nos. 57-386, April 1957, and 58-114, December 1957.

23. Yates, J. E., and Zeijdel, E. F. E., Unsteady Aerodynamic Forces on Slender Supersonic Aircraft with Flexible Wings and Bodies, paper No. 61-31, presented at the 29th Annual Meeting, Institute of the Aerospace Sciences, New York, January 1961.

24. Eggers, A. J., and Savin, R. C., A Unified Two-Dimensional Approach to the Calculation of Three-Dimensional Hypersonic Flow, with Application to Bodies of Revolution, NACA Report 1249, 1955.

25. Zartarian, G., and Hsu, P. T., Theoretical and Experimental Studies on Airloads Related to Hypersonic Aeroelastic Problems of General Slender Pointed Configurations, USAF Aeronautical Systems Division, Technical Report 61-7, April 1961.

26. Capiaux, R., and Karchmar, L., Flow Past Slender Blunt Bodies - A Review and Extension, Paper No. 61-210-1904, Institute of the Aerospace Sciences-American Rocket Society National Joint Meeting, June 1961.

27. Creager, M. O., An Approximate Method for Calculating Surface Pressures on Curved Profile Blunt Plates in Hypersonic Flow, NASA Technical Note D-71, September 1959.

28. Bertram, M. H., Recent Hypersonic Studies of Wings and Bodies, American Rocket Society Paper 1131-60, May 1960.

29. Chernyi, G. G., Effect of Slight Blunting of Leading Edge of an Immersed Body on the Flow Around It at Hypersonic Speeds, NASA Technical Translation F-35, June 1960.

30. Wagner, R. D., Some Aspects of the Modified Newtonian and Prandtl-Meyer-Expansion Method for Axisymmetric Blunt Bodies at Zero Angle of Attack, Readers' Forum, Journal of the Aero/Space Sciences, Vol. 26, No. 12, December 1959, pp. 851-852.

31. Kennet, H., Some Steady and Unsteady Hypersonic Flows Past Bluff Bodies, Sc.D. Thesis, Department of Aeronautics and Astronautics, Massachusetts Institute of Technology, June 1961 (to appear as AFOSR 1031).

32. Love, E. S., Prediction of Inviscid Induced Pressures from Round Leading Edge Blunting at Hypersonic Speeds, Journal of the American Rocket Society, Vol. 29, No. 10, part 1, October 1959, pp. 792-794.

33. Mueller, J. N., Close, W. H., and Henderson, A. H., An Investigation of Induced Pressure Phenomena on Axially Symmetric, Flow - Aligned, Cylindrical Models Equipped with Different Nose Shapes at Free-Stream Mach Numbers from 15.6 to 21 in Helium, NASA Technical Note D-373, May 1960.

34. Ferri, A., The Method of Characteristics, Section G, Vol VI of High Speed Aerodynamics and Jet Propulsion, Princeton University Press, Princeton, New Jersey, 1954.

35. Holt, M., and Hoffman, G. H., Calculation of Hypersonic Flow Past Spheres and Ellipsoids, Paper No. 61-209-1903, Institute of the Aerospace Sciences-American Rocket Society National Joint Meeting, June 1961.

36. Kendall, J. M., Jr., Experiments on Supersonic Blunt Body Flows, Progress Report 20-372, Jet Propulsion Laboratory, California Institute of Technology, February 1959.

37. Fowell, L. R., Flow Field Analysis for Lifting Re-Entry Configurations by the Method of Characteristics, Paper No. 61-208-1902, Institute of the Aerospace Sciences-American Rocket Society National Joint Meeting, June 1961.

38. Thornhill, C. K., The Numerical Method of Characteristics for Hyperbolic Problems in Three Independent Variables, British Armament Research Establishment, Report No. N29/48.

39. Moore, F. K., Aerodynamic Effects of Boundary Layer Unsteadiness, Proceedings of the Sixth Anglo-American Aeronautical Conference, Folkestone, September 1957.

40. Ashley, H., and Zartarian, G., Thickness and Boundary Layer Effects, Chapter 8, Vol. II of AGARD Manual of Aeroelasticity, W. P. Jones, Editor, Pergamon Press, London, 1961.

41. Bertram, M. H., Boundary Layer Displacement Effects in Air at Mach Numbers of 6.8 and 9.6, NASA Technical Report R-22, 1959.

42. Cheng, H. K., Hall, J. G., Golian, T. C., and Hertzberg, A., Boundary-Layer Displacement and Leading-Edge Bluntness Effects in High-Temperature Hypersonic Flow, Journal of the Aero/Space Sciences, Vol. 28, No. 5, May 1961, pp. 353-381.

43. Lick, W., Inviscid Flow of a Reacting Mixture of Gases Around a Blunt Body, Journal of Fluid Mechanics, Vol. 7, Part I, January 1960, pp. 128-144.

44. Whalen, R. J., Viscous and Inviscid Non-Equilibrium Gas Flows, Institute of the Aerospace Sciences Paper No. 61-23, presented at the 29th Annual Meeting, New York, January 1961.

45. Savin, R. C., Comparison of Shock-Expansion Theory with Experiment for the Lift, Drag, and Pitching-Moment Characteristics of Two Wing-Body Combinations at M = 5.0, NACA Technical Note 4385, September 1958.

46. Scheuing, R. A., et al., Theoretical Prediction of Pressures in Hypersonic Flow-Configurations with Attached Leading Edge Shock, Grumman Aircraft Engineering Corp., Research Report No. RE-134, April 1960.

PREDICTION OF STIFFNESS AND VIBRATION CHARACTERISTICS OF TRUSSES, MULTI-STAGE CYLINDERS, AND CLUSTERED CYLINDERS

Dr. Francis C. S. Hung
Donald J. Stone

North American Aviation, Inc.
Space & Information Systems Division

ABSTRACT

A review has been made of past work in stiffness and vibration prediction methods for trusses, cylinders, conical shells, multi-stage cylinders, and clustered cylinders. A method of stiffness and vibration analysis of trusses with temperature gradients is presented. Several approaches for the solution of problems relating to clustered cylinders are also discussed. Since adequate knowledge of the behavior of boosters is necessary for successful space flight, recommendations are made for future research in analytical predictions and tests to substantiate these analyses.

PREDICTION OF STIFFNESS AND VIBRATION CHARACTERISTICS OF TRUSSES, MULTI-STAGE CYLINDERS, AND CLUSTERED CYLINDERS

INTRODUCTION

With the increased emphasis on missiles and spacecraft, the interest in shells and clustered cylinders has grown very rapidly. In the early days of ballistic missiles, the diameters were small and they were easily idealized as simple shells. As the diameter of boosters becomes larger and larger, the use of beam theory is far from being accurate, since, in addition to the bending modes, the breathing modes enter into the picture. The presence of adapters and bulkheads renders the analytical process even more difficult.

In order to analyze the stiffness and vibration characteristics of cylinders, various shell theories have been used. Most of the approaches have been mathematical in nature, ignoring the effects of thickness variation and material degradation due to temperature. Since the development of the Saturn and Nova concepts, wide interest has been developed in methods of analysis of the stiffness and vibration characteristics of clustered boosters. Since these clustered cylinders involve a mounting problem to take care of the temperature expansion in the cryogenic regime, one end of the cylinders is usually fixed, while the other end is free to expand. This, of course, complicates the methods of analysis. To analyze these clusters even with a simple beam theory is in itself very complicated. So far, no attempt has been made to refine the analysis to include the shell breathing modes of clustered cylinders.

To alleviate the thermal stresses in re-entry vehicles, truss spars are usually used in wing structures. The advantage of a determinate truss is that the members are free to expand and contract according to their geometry. The thermal stress can be greatly reduced if ideal pin connection joints can be achieved. Unfortunately, three-dimensional pin connection is hard to achieve in practice. Secondary thermal stresses are bound to be induced in the connections. To analyze and evaluate the vibration characteristics of a simple determinate truss is no great task; but to evaluate the characteristics of trusses with joint restraint is a difficult one. So far, no elaborate or rapid process has been released. Since the present paper is only exploratory in nature, it will leave this investigation for future presentation. In the area of clustered cylinders, various methods and investigations have been conducted by Y. C. Fung, Federhofer, Hermann and Mirsky, and Yechiel Shulman. Using the power series expansion method, trigonometric mode shapes

method, Rayleigh-Ritz methods, shallow shell, and Flugge's shell theory, some of them found good correlation between theoretical and experimental results. Some of the authors established a comparison of the vibration frequencies with the variation of length to diameter, but none of them so far have conducted an engineering approach which would take care of cutouts and variation in thickness and material properties from point to point.

It is the intention of the authors to introduce an engineering method for finding the stiffness and vibration characteristics of cylinders, conic shells, and multiple staging through the use of the extension of the force and displacement method of Argyris. The equations for the symmetrical and anti-symmetrical loadings are presented; the equation for cantilevered shells and the free shells is tabulated. Because of the shortage of available manpower in programming, no complete mathematical data are available for comparison with test results. It is hoped that this paper serves as an elementary effort in the area of engineering methods of vibrations. Later results will be published when the program is further down the line. Also included in this paper will be a section tabulating the methods of clustered cylinders for the Flight Test Missile. It is sincerely hoped that these paragraphs will stimulate interest and research in the areas of trusses, cylinders, and clustered cylinders.

SECTION I: STATE OF THE ART

TRUSSES

In past years the truss has probably been the most studied of all redundant structures. However, it is only recently that methods have appeared which permit a ready solution to this type of structure. The previous methods required the formation and solution of a set of simultaneous equations. The inconvenience of solving these equations for a large structure usually resulted in the selection of configurations with a low degree of redundancy, thereby minimizing this tedious numerical task. A significant advance was made with the introduction of the moment distribution method developed by H. Cross. This well known method decreased the number of relationships required, but necessitated a large amount of arithmetical manipulation.

The advent of the electronic computer has stimulated the development of several new matrix methods of redundant structural analyses. The methods fall into two broad classifications: the method of forces, and the method of displacements. It has been shown by several authors that these two theories are completely analogous; however, the ease of applying them to different structures varies greatly. A complete treatise

on the application of the force method to various redundant structures was given by Professor Argyris in 1954 (ref. 1). In this paper, a simple, highly systematic method for the analysis of a redundant pin connected truss including the effects of temperature, initial strain, and non-linear stress-strain relationships is presented. This method is based upon the formulation of self-equilibrating load systems which relates the member loads to some unknown redundant force. The structure is made statically determinate by cutting the redundant members and a static load system is formed. The self-equilibrating load system and the static load system are combined, together with the flexibility matrices of the unassembled elements, to produce the true load distribution and flexibility matrix of the redundant structure. A tacit assumption is made that the correct value of the modulus of elasticity is known in the treatment of the effects of the non-linear stress-strain relationship. This implies that the correct stress level must also be known, thus indicating an iterative solution is required to find the converged value of stress.

A method for computing the stiffness influence coefficients of a simple pin-jointed truss was published by Turner, Clough, Martin and Topp in 1956 (ref. 2). This method falls under the broad category of displacement methods. The stiffness of the complete structure is obtained by summing the stiffnesses of the individual members, each formed for a common displacement. This analysis was later extended (ref. 3) to include the effect of geometric change as the structure deflects under load and temperature. The method of treating the large deflections as presented was essentially an iterative procedure. It should be noted that the method of Argyris, if extended to account for the changes in geometry between successive solutions, can also be effectively used for the analysis of structures possessing large deflections.

A variation of the force method for analyzing indeterminate trusses was presented by Wong in 1959 (ref. 4). The basic self-equilibrating stress systems used by Wong are essentially the same as those used by Argyris. The matrices are partitioned in a different manner, which leads to a slightly different form, but analogous to those of Argyris.

In the aforementioned analyses, the usual assumptions for a truss structure have been made, that is, frictionless pin joints and straight axial members. None of these analyses can be conveniently adapted to include the effects of rigidly connected joints. To rigorously analyze these effects would greatly increase the number of redundants and needlessly complicate the procedures for determining the stress distribution or structural influence coefficients.

In the preceeding discussion no distinction had been made as to whether the end results desired were to be the stress distribution or

the structural influence coefficients. For a truss with rigid joints, if this distinction is made, and a simplifying assumption as suggested in ref. 5 is made, then this type of structure can be treated with little more effort than the pinned truss. It is a principle of elementary geometry that the distortion of a truss structure is a function of the changes in length of the structural elements. If it can be assumed that the bending deflections of a member do not change their axial length, then such bending cannot influence the overall truss deflections. Thus, the influence coefficients of a rigid joint truss can be computed approximately if all the joints are assumed to be pinned. With the joint deflections being known, all the angles of the members can be computed. The end moments in any member can now be determined by one of several methods and a stress distribution reflecting both the axial loads and end moments can be made.

CYLINDERS

In the work of Y. C. Fung, E. E. Sechler and Kaplan (ref. 9), the frequency spectra and vibration modes of thin walled circular cylinders subjected to internal pressures are considered. It is shown that for very thin cylinders the internal pressure has a significant effect on the natural vibration characteristics. For these cylinders, particularly those having smaller length to diameter ratios, the mode associated with the lowest frequency is in general not the simplest mode. The exact number of circumferential modes, n, which occur in the mode associated with the lowest frequency, depend on the internal pressure, p. The experiments and the theory are in reasonable agreement. For cylinders with freely supported ends, Reissner's approximate frequency expression is adequate for prediction at high internal pressures for all values of n, and at lower internal pressures for $n \geqq 3$ (fig. 1).

The work of Federhofer (ref. 23) who used a power series expansion for the assumed mode shapes, probably provides a good first approximation for cones of wide vertex angles which approach a concentric circular plate in the limit. Due to the employment of these mode shapes, however, the accuracy of these results, when the other limiting case of circular cylinders is approached, cannot be expected to be good unless a large number of mode shapes are used, since the cylindrical mode shapes are trigonometric in nature.

Hermann and Mirsky (ref. 21) investigated the effect of taper on the vibrations of cylindrical shells using the cylinder's trigonometric mode shapes. Their results showed that the frequencies of the tapered shells are invariably higher than those of the corresponding untapered ones, for length-to-radius ratios greater than 3.

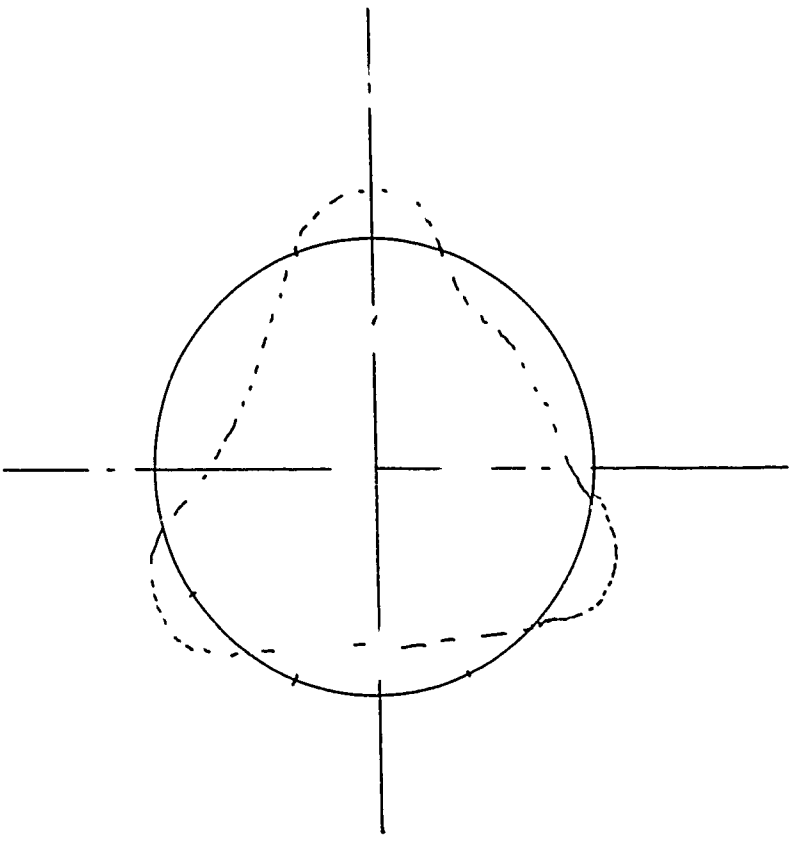


Figure 1. Breathing Modes

Yechiel Shulman (ref. 20) studied the flexual vibration characteristics of conical shells with small vertex angles (tapered, cylindrical shells) for the purpose of obtaining more reliable results than the ones obtained so far. This is done by using shell theories of differing complexity, by using various methods of solution, and by employing different assumed displacement and stress functions. The various shell theories used include shallow shell theory and Flugge's shell theory. In general, the effect of taper on a circular cylinder is to increase its membrane frequencies and to decrease its bending frequencies. The general case contains a combination of these two effects and therefore the frequencies may be higher, lower, or the same, depending on the shell's geometry and the particular vibration mode of interest.

Herbert Sanders used a Rayleigh-Ritz procedure to determine the natural frequencies for a certain class of mode shapes of a thin, conical shell built in on the edge with the smaller radius, and either simply supported or free on the outer edge. The comparison showed that the first six computed frequencies were within 5% of the measured values.

CLUSTERED CYLINDERS

Clustered cylinder engines have long been used. Usually they are held in place by a heavy spider web connection at one end and are free to expand at the other end. Since they are small in size, their neutral axes coincide with that of the shell. Common practice is to idealize them as a simple beam. With the introduction of the Saturn booster, the problem becomes much more complicated. To allow the differential contraction from cryogenics, four of the eight external tanks are free to move at the top spider web connection. In some of the bending modes the external tanks might move quite drastically from the nodal line of the neutral axes. In order to understand the dynamic loads and fuel sloshing effects on the outer tank walls, it may be necessary to idealize the eight external tanks apart from the central tank. Among the methods used are the strain energy method, method of least work, and Myklestad method.

STATICALLY DETERMINATE TRUSSES

Shown in fig. 2 is a cantilevered truss supported at 7 by horizontal force and at 8 by vertical and horizontal reactions.

$$b_o = \begin{bmatrix} 0 & 0 & 0 & 0 & 0 & 0 & 0 \\ +a/h & +a/h & 0 & 0 & 0 & 0 & 0 \\ +2a/h & +2a/h & +a/h & +a/h & 0 & 0 & 0 \\ -a/h & -a/h & 0 & 0 & 0 & 0 & 0 \\ -2a/h & -2a/h & -a/h & -a/h & 0 & 0 & 0 \\ -3a/h & -3a/h & -2a/h & -2a/h & -a/h & -a/h & 0 \\ -1 & 0 & 0 & 0 & 0 & 0 & 0 \\ -1 & -1 & -1 & 0 & 0 & 0 & 0 \\ -1 & -1 & -1 & -1 & -1 & 0 & 0 \\ -1 & -1 & -1 & -1 & -1 & -1 & -1 \\ +d/h & +d/h & 0 & 0 & 0 & 0 & 0 \\ +d/h & +d/h & +d/h & +d/h & 0 & 0 & 0 \\ +d/h & +d/h & +d/h & +d/h & +d/h & +d/h & 0 \end{bmatrix} \begin{matrix} 13 \\ 35 \\ 57 \\ 24 \\ 46 \\ 68 \\ 12 \\ 34 \\ 56 \\ 78 \\ 23 \\ 45 \\ 67 \end{matrix} \quad \text{Members}$$

$$R = \begin{bmatrix} M_1 \\ M_2 \\ M_3 \\ M_4 \\ M_5 \\ M_6 \\ M_7 \end{bmatrix}$$

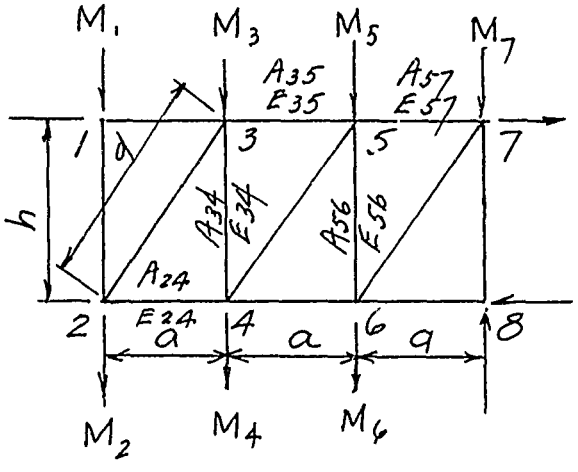


Figure 2. Statically Determinate Trusses

$$f = \begin{array}{c} \text{Members} \\ \left[\begin{array}{cccccccccccccc} \frac{a}{A_{13}E_{13}} & 0 & 0 & 0 & 0 & 0 & 0 & 0 & 0 & 0 & 0 & 0 & 0 & 13 \\ 0 & \frac{a}{A_{35}E_{35}} & 0 & 0 & 0 & 0 & 0 & 0 & 0 & 0 & 0 & 0 & 0 & 35 \\ 0 & 0 & \frac{a}{A_{57}E_{57}} & 0 & 0 & 0 & 0 & 0 & 0 & 0 & 0 & 0 & 0 & 57 \\ 0 & 0 & 0 & \frac{a}{A_{24}E_{24}} & 0 & 0 & 0 & 0 & 0 & 0 & 0 & 0 & 0 & 24 \\ 0 & 0 & 0 & 0 & \frac{a}{A_{46}E_{46}} & 0 & 0 & 0 & 0 & 0 & 0 & 0 & 0 & 46 \\ 0 & 0 & 0 & 0 & 0 & \frac{a}{A_{68}E_{68}} & 0 & 0 & 0 & 0 & 0 & 0 & 0 & 68 \\ 0 & 0 & 0 & 0 & 0 & 0 & \frac{h}{A_{12}E_{12}} & 0 & 0 & 0 & 0 & 0 & 0 & 12 \\ 0 & 0 & 0 & 0 & 0 & 0 & 0 & \frac{h}{A_{34}E_{34}} & 0 & 0 & 0 & 0 & 0 & 34 \\ 0 & 0 & 0 & 0 & 0 & 0 & 0 & 0 & \frac{h}{A_{56}E_{56}} & 0 & 0 & 0 & 0 & 56 \\ 0 & 0 & 0 & 0 & 0 & 0 & 0 & 0 & 0 & \frac{h}{A_{78}E_{78}} & 0 & 0 & 0 & 78 \\ 0 & 0 & 0 & 0 & 0 & 0 & 0 & 0 & 0 & 0 & \frac{d}{A_{23}E_{23}} & 0 & 0 & 23 \\ 0 & 0 & 0 & 0 & 0 & 0 & 0 & 0 & 0 & 0 & 0 & \frac{d}{A_{45}E_{45}} & 0 & 45 \\ 0 & 0 & 0 & 0 & 0 & 0 & 0 & 0 & 0 & 0 & 0 & 0 & \frac{d}{A_{67}E_{67}} & 67 \end{array}\right] \end{array}$$

$S = bR$

Generalized displacement $v = fS = fb_oR$ (1)

Vert. displacement $r = \bar{b}'v = \bar{b}'fb_oR$ (2)

Flexibility matrix, $F = \bar{b}'fb_o$ (3)

From the flexibility matrix, the vibration frequencies and mode shapes can be obtained.

For trusses with thermal gradient, the generalized displacement v

$v = fS + H$ (4)

where H is the column matrix of thermal distortions in members 13 to member 67

Vertic. displacement $v = \bar{b}'v = \bar{b}'f(b_oR+H)$ (5)

Flexibility matrix, $F = \bar{b}'f\ b_o$

If the vibration modes are initiated from thermally deflected position, H matrix can be neglected and the frequencies and mode shapes can be derived as usual.

$$\begin{bmatrix} r_1 \\ r_2 \\ r_3 \\ r_4 \\ r_5 \\ r_6 \\ r_7 \end{bmatrix} = -\omega^2 \begin{bmatrix} -0 & +a/h & 2a/h & -a/h & -2a/h & -3a/h & -1 & -1 & -1 & -1 & +d/h & +d/h & +d/h \\ 0 & +a/h & +2a/h & -a/h & -2a/h & -3a/h & 0 & -1 & -1 & -1 & +d/h & +d/h & +d/h \\ 0 & 0 & +a/h & 0 & -a/h & -2a/h & 0 & -1 & -1 & -1 & 0 & +d/h & +d/h \\ 0 & 0 & +a/h & 0 & -a/h & -2a/h & 0 & 0 & -1 & -1 & 0 & +d/h & +d/h \\ 0 & 0 & 0 & 0 & 0 & -a/h & 0 & 0 & -1 & -1 & 0 & 0 & +d/h \\ 0 & 0 & 0 & 0 & 0 & -a/h & 0 & 0 & 0 & -1 & 0 & 0 & +d/h \\ 0 & 0 & 0 & 0 & 0 & 0 & 0 & 0 & 0 & -1 & 0 & 0 & 0 \end{bmatrix} \times$$

$$\begin{bmatrix} \frac{a}{A_{13}E_{13}} & 0 & 0 & 0 & 0 & 0 & 0 & 0 & 0 & 0 & 0 & 0 & 0 \\ 0 & \frac{a}{A_{35}E_{35}} & 0 & 0 & 0 & 0 & 0 & 0 & 0 & 0 & 0 & 0 & 0 \\ 0 & 0 & \frac{a}{A_{57}E_{57}} & 0 & 0 & 0 & 0 & 0 & 0 & 0 & 0 & 0 & 0 \\ 0 & 0 & 0 & \frac{a}{A_{24}E_{24}} & 0 & 0 & 0 & 0 & 0 & 0 & 0 & 0 & 0 \\ 0 & 0 & 0 & 0 & \frac{a}{A_{46}E_{46}} & 0 & 0 & 0 & 0 & 0 & 0 & 0 & 0 \\ 0 & 0 & 0 & 0 & 0 & \frac{a}{A_{68}E_{68}} & 0 & 0 & 0 & 0 & 0 & 0 & 0 \\ 0 & 0 & 0 & 0 & 0 & 0 & \frac{h}{A_{12}E_{12}} & 0 & 0 & 0 & 0 & 0 & 0 \\ 0 & 0 & 0 & 0 & 0 & 0 & 0 & \frac{h}{A_{34}E_{34}} & 0 & 0 & 0 & 0 & 0 \\ 0 & 0 & 0 & 0 & 0 & 0 & 0 & 0 & \frac{h}{A_{56}E_{56}} & 0 & 0 & 0 & 0 \\ 0 & 0 & 0 & 0 & 0 & 0 & 0 & 0 & 0 & \frac{h}{A_{78}E_{78}} & 0 & 0 & 0 \\ 0 & 0 & 0 & 0 & 0 & 0 & 0 & 0 & 0 & 0 & \frac{d}{A_{23}E_{23}} & 0 & 0 \\ 0 & 0 & 0 & 0 & 0 & 0 & 0 & 0 & 0 & 0 & 0 & \frac{d}{A_{45}E_{45}} & 0 \\ 0 & 0 & 0 & 0 & 0 & 0 & 0 & 0 & 0 & 0 & 0 & 0 & \frac{d}{A_{67}E_{67}} \end{bmatrix}$$

Other matrices continued on next page.

$$
\begin{bmatrix}
0 & 0 & 0 & 0 & 0 & 0 & 0 \\
+a/h & +a/h & 0 & 0 & 0 & 0 & 0 \\
+2a/h & +2a/h & +a/h & +a/h & +a/h & +a/h & 0 \\
-a/h & -a/h & 0 & 0 & 0 & 0 & 0 \\
-2a/h & -2a/h & -a/h & -a/h & 0 & 0 & 0 \\
-3a/h & -3a/h & -2a/h & -2a/h & -a/h & -a/h & 0 \\
-1 & 0 & 0 & 0 & 0 & 0 & 0 \\
-1 & -1 & -1 & 0 & 0 & 0 & 0 \\
-1 & -1 & -1 & -1 & -1 & 0 & 0 \\
-1 & -1 & -1 & -1 & -1 & -1 & -1 \\
+d/h & +d/h & 0 & 0 & 0 & 0 & 0 \\
+d/h & +d/h & +d/h & +d/h & 0 & 0 & 0 \\
+d/h & +d/h & +d/h & +d/h & +d/h & +d/h & 0
\end{bmatrix}
\begin{bmatrix}
M_1 & 0 & 0 & 0 & 0 & 0 & 0 \\
0 & M_2 & 0 & 0 & 0 & 0 & 0 \\
0 & 0 & M_3 & 0 & 0 & 0 & 0 \\
0 & 0 & 0 & M_4 & 0 & 0 & 0 \\
0 & 0 & 0 & 0 & M_5 & 0 & 0 \\
0 & 0 & 0 & 0 & 0 & M_6 & 0 \\
0 & 0 & 0 & 0 & 0 & 0 & M_7
\end{bmatrix}
\begin{bmatrix}
r_1 \\ r_2 \\ r_3 \\ r_4 \\ r_5 \\ r_6 \\ r_7
\end{bmatrix}
$$

Where mass at any joint is derived by summing the mass of adjacent members midway to the next joint. Any additional weight at the joint is treated in a similar manner.

STATICALLY INDETERMINATE TRUSSES

For statically indeterminate trusses, the members 14, 36, and 58 are cut and indeterminate values of X_1, X_2 and X_3 are assigned to form the b_1 matrix. (fig. 3)

$$b_1 = \begin{array}{c} \begin{matrix} X_1 & X_2 & X_3 \end{matrix} \\ \left[\begin{array}{ccc|c} -a/d & 0 & 0 & 13 \\ 0 & -a/d & 0 & 35 \\ 0 & 0 & -a/d & 57 \\ -a/d & 0 & 0 & 24 \\ 0 & -a/d & 0 & 46 \\ 0 & 0 & -a/d & 18 \\ -h/d & 0 & 0 & 12 \\ -h/d & -h/d & 0 & 34 \\ 0 & -h/d & -h/d & 56 \\ 0 & 0 & -h/d & 78 \\ +1 & 0 & 0 & 23 \\ 0 & +1 & 0 & 45 \\ 0 & 0 & +1 & 67 \\ +1 & 0 & 0 & 14 \\ 0 & +1 & 0 & 36 \\ 0 & 0 & +1 & 58 \end{array}\right] \end{array} \qquad b_o = \begin{array}{c} \left[\begin{array}{ccccccc} 1 & 2 & 3 & 4 & 5 & 6 & 7 \\ 0 & 0 & 0 & 0 & 0 & 0 & 0 \\ +a/h & +a/h & 0 & 0 & 0 & 0 & 0 \\ +2a/h & +2a/h & +a/h & +a/h & 0 & 0 & 0 \\ -a/h & -a/h & 0 & 0 & 0 & 0 & 0 \\ -2a/h & -2a/h & -a/h & -a/h & 0 & 0 & 0 \\ -3a/h & -3a/h & -2a/h & -2a/h & -a/h & -a/h & 0 \\ -1 & 0 & 0 & 0 & 0 & 0 & 0 \\ -1 & -1 & -1 & 0 & 0 & 0 & 0 \\ -1 & -1 & -1 & -1 & -1 & 0 & 0 \\ -1 & -1 & -1 & -1 & -1 & -1 & -1 \\ +d/h & +d/h & 0 & 0 & 0 & 0 & 0 \\ +d/h & +d/h & +d/h & +d/h & 0 & 0 & 0 \\ +d/h & +d/h & +d/h & +d/h & +d/h & +d/h & 0 \\ 0 & 0 & 0 & 0 & 0 & 0 & 0 \\ 0 & 0 & 0 & 0 & 0 & 0 & 0 \\ 0 & 0 & 0 & 0 & 0 & 0 & 0 \end{array}\right] \end{array}$$

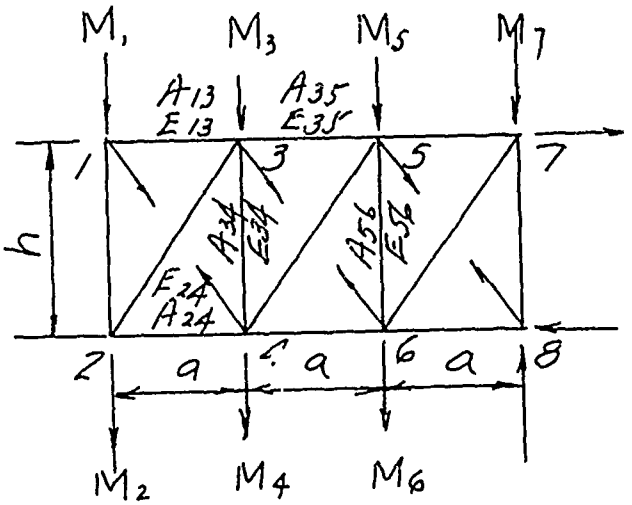


Figure 3. Statically Indeterminate Trusses

$$
f = \begin{bmatrix}
\frac{a}{A_{13}E_{13}} & 0 & 0 & 0 & 0 & 0 & 0 & 0 & 0 & 0 & 0 & 0 & 0 & 0 & 0 \\
0 & \frac{a}{A_{35}E_{35}} & 0 & 0 & 0 & 0 & 0 & 0 & 0 & 0 & 0 & 0 & 0 & 0 & 0 \\
0 & 0 & \frac{a}{A_{57}E_{57}} & 0 & 0 & 0 & 0 & 0 & 0 & 0 & 0 & 0 & 0 & 0 & 0 \\
0 & 0 & 0 & \frac{a}{A_{24}E_{24}} & 0 & 0 & 0 & 0 & 0 & 0 & 0 & 0 & 0 & 0 & 0 \\
0 & 0 & 0 & 0 & \frac{a}{A_{46}E_{46}} & 0 & 0 & 0 & 0 & 0 & 0 & 0 & 0 & 0 & 0 \\
0 & 0 & 0 & 0 & 0 & \frac{a}{A_{68}E_{68}} & 0 & 0 & 0 & 0 & 0 & 0 & 0 & 0 & 0 \\
0 & 0 & 0 & 0 & 0 & 0 & \frac{h}{A_{12}E_{12}} & 0 & 0 & 0 & 0 & 0 & 0 & 0 & 0 \\
0 & 0 & 0 & 0 & 0 & 0 & 0 & \frac{h}{A_{34}E_{34}} & 0 & 0 & 0 & 0 & 0 & 0 & 0 \\
0 & 0 & 0 & 0 & 0 & 0 & 0 & 0 & \frac{h}{A_{56}E_{56}} & 0 & 0 & 0 & 0 & 0 & 0 \\
0 & 0 & 0 & 0 & 0 & 0 & 0 & 0 & 0 & \frac{h}{A_{78}E_{78}} & 0 & 0 & 0 & 0 & 0 \\
0 & 0 & 0 & 0 & 0 & 0 & 0 & 0 & 0 & 0 & \frac{d}{A_{45}E_{45}} & 0 & 0 & 0 & 0 \\
0 & 0 & 0 & 0 & 0 & 0 & 0 & 0 & 0 & 0 & 0 & \frac{d}{A_{67}E_{67}} & 0 & 0 & 0 \\
0 & 0 & 0 & 0 & 0 & 0 & 0 & 0 & 0 & 0 & 0 & 0 & \frac{d}{A_{14}E_{14}} & 0 & 0 \\
0 & 0 & 0 & 0 & 0 & 0 & 0 & 0 & 0 & 0 & 0 & 0 & 0 & \frac{d}{A_{36}E_{36}} & 0 \\
0 & 0 & 0 & 0 & 0 & 0 & 0 & 0 & 0 & 0 & 0 & 0 & 0 & 0 & \frac{d}{A_{58}E_{58}}
\end{bmatrix}
$$

Stress in any member, $S = b_o R + b_1 X$ (6)

Virtual work, $b'_1 v = b'_1 f (b_o R + b_1 X) = 0$

$$X = -\left[b'_1 f b_1\right]^{-1} b'_1 f b_o R \quad (7)$$

The flexibility matrix $F = b'_o f(b_o - b_1 (b'_1 f b_1)^{-1} b'_1 f b_o$ (8)

The vibration equation can be set up as in the previous case.

SECTION III: STIFFNESS AND VIBRATION PREDICTION OF CONICAL SHELLS, CYLINDERS, AND MULTIPLE STAGE CYLINDERS

The matrix force method as presented first by Argyris (ref. 1) was extended to shell structures by Przemieniecki (ref. 25) and later by Argyris (ref. 29). These methods treat cylindrical shells of arbitrary cross section stiffened by flexible frames. The method presented in this paper is an extension to these works. The following analysis includes the effects of variable stringer, skin and frame cross sections, and can be applied to tapered conical shells. The present method also permits a more arbitrary external loading condition than that of Przemieniecki's. As the method contained herein closely follows that of(ref. 25), only a brief outline of the method will be given with special emphasis on the basic differences. A complete description of the force method is beyond the scope of this paper and therefore it is assumed that the reader is familiar with the basic method.

BASIC STRESS SYSTEM

The basic stress system, the b_o matrix, is derived from considering the shell structure a tube with four longerons (ref. 29) subjected to the loading shown in fig. 4.

Assuming a structure symmetrical about its vertical and horizontal centerlines, for simplicity the stringer forces at frames i and i+1 for the structures shown in fig. 4 are given by:

$$P_1^i = -\frac{1}{h_y^i} M_x^i \frac{\ell_1^{i,i+1}}{\ell^{i,i+1}} \qquad P_1^{i+1} = -\frac{1}{h_y^{i+1}} \left[M_x^i + S_y^i \ell^{i,i+1} + \sum_{j=1,8} V_j^i \ell_{i,i+1} \right] \frac{\ell_1^{i,i+1}}{\ell_{i,i+1}}$$

$$P_2^i = 0 \qquad P_2^{i+1} = 0$$

$$P_3^i = +\frac{1}{h_x^i} M_y^i \frac{\ell_3^{i,i+1}}{\ell^{i,i+1}} \qquad P_3^{i+1} = +\frac{1}{h^{i+1}} \left[M_y^i + S_x^i \ell^{i,i+1} + \sum_{j=1,8} H_j^i \ell^{i,i+1} \right] \frac{\ell_3^{i,i+1}}{\ell_{i,i+1}}$$

$$P_4^i = 0 \qquad P_4^{i+1} = 0$$

$$P_5^i = -P_1^i \qquad P_5^{i+1} = -P_1^{i+1}$$

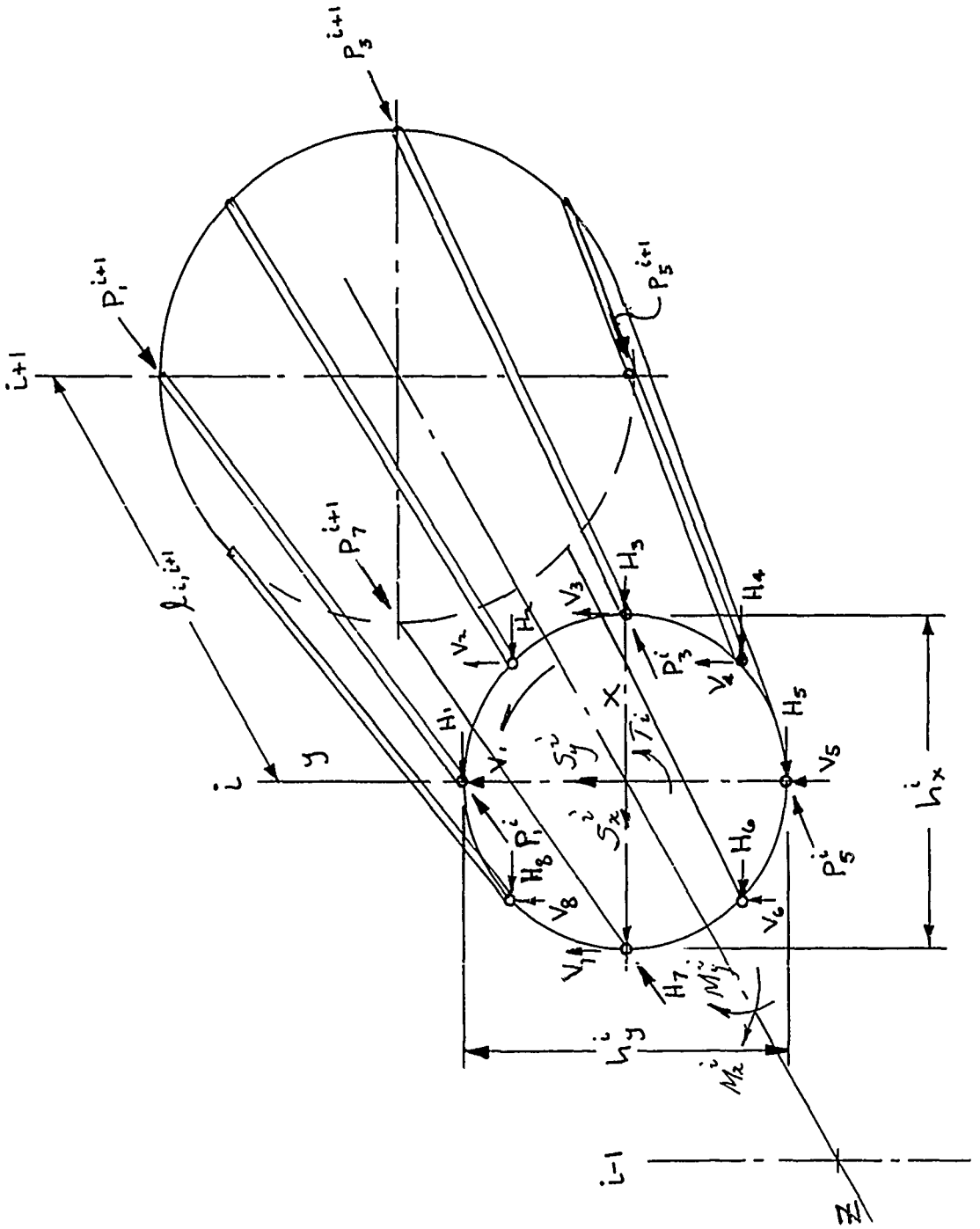


Figure 4. Basic Stress System

$$P_6^i = 0 \qquad P_6^{i+1} = 0$$

$$P_7^i = -P_3^i \qquad P_7^{i+1} = -P_3^{i+1}$$

$$P_8^i = 0 \qquad P_8^{i+1} = 0 \tag{9}$$

The shear flows due to the vertical and horizontal forces for the same structure are given by:

$$q_1^i = q_2^i = \frac{T^i}{2A_i} + \frac{\sum_{j=1,8} V_j^i x_j^i}{2A_i} + \frac{\sum_{j=1,8} H_j^i y_j^i}{2A_i} + \frac{S_y^i + \sum_{j=1,8} V_j^i}{2h_y^i}$$
$$+ \frac{S_x^i + \sum_{j=1,8} H_j^i}{2h_x^i} - \frac{M_x^i}{2(h_y^i)^2}\left(\frac{h_y^{i+1} - h_y^i}{\ell_{i,i+1}}\right) - \frac{M_y^i}{2(h_x^i)^2}\left(\frac{h_x^{i+1} - h_x^i}{\ell_{i,i+1}}\right)$$

$$q_3^i = q_4^i = \frac{T^i}{2A_i} + \frac{\sum_{j=1,8} V_j^i x_j^i}{2A_i} + \frac{\sum_{j=1,8} H_j^i y_j^i}{2A_i} + \frac{S_y^i + \sum_{j=1,8} V_j^i}{2h_y^i}$$
$$- \frac{S_x^i + \sum_{j=1,8} H_j^i}{2h_x^i} - \frac{M_x^i}{2(h_y^i)^2}\left(\frac{h_y^{i+1} - h_y^i}{\ell_{i,i+1}}\right) + \frac{M_y^i}{2(h_x^i)^2}\left(\frac{h_x^{i+1} - h_x^i}{\ell_{i,i+1}}\right)$$

$$q_5^i = q_6^i = \frac{T^i}{2A_i} + \frac{\sum_{j=1,8} V_j^i x_j^i}{2A_i} + \frac{\sum_{j=1,8} H_j^i y_j^i}{2A_i} - \frac{S_y^i + \sum_{j=1,8} V_j^i}{2h_y^i}$$
$$- \frac{S_x^i + \sum_{j=1,8} H_j^i}{2h_x^i} + \frac{M_x^i}{2(h_y^i)^2}\left(\frac{h_y^{i+1} - h_y^i}{\ell_{i,i+1}}\right) + \frac{M_y^i}{2(h_x^i)^2}\left(\frac{h_x^{i+1} - h_x^i}{\ell_{i,i+1}}\right)$$

$$q_7^i = q_8^i = \frac{T^i}{2A^i} + \frac{\sum_{j=1,8} V_j^i x_j^i}{2A_i} + \frac{\sum_{j=1,8} H_j^i y_j^i}{2A_i} - \frac{S_y^i + \sum_{j=1,8} V_j^i}{2h_y^i}$$
$$+ \frac{S_x^i + \sum_{j=1,8} H_j^i}{2h_x^i} + \frac{M_x^i}{2(h_y^i)^2}\left(\frac{h_y^{i+1} - h_y^i}{l_{i,i+1}}\right) - \frac{M_y^i}{2(h_x^i)^2}\left(\frac{h_x^{i+1} - h_x^i}{l_{i,i+1}}\right)$$

$$q_1^{i+1} = q_2^{i+1} = \frac{T^i}{2A_{i+1}} + \frac{\sum_{j=1,8} V_j^i x_j^i}{2A_{i+1}} + \frac{\sum_{j=1,8} H_j^i y_j^i}{2A_{i+1}} + \frac{(S_y^i + \sum_{j=1,8} V_j^i) h_y^i}{2(h_y^{i+1})^2} + \frac{(S_x^i + \sum_{j=1,8} H_j^i) h_x^i}{2(h_x^{i+1})^2}$$
$$- \frac{M_x^i + S_y^i l_{i,i+1}}{2(h_y^{i+1})^2}\left(\frac{h_y^{i+1} - h_y^i}{l_{i,i+1}}\right) - \frac{M_y^i + S_x^i l_{i,i+1}}{2(h_x^{i+1})^2}\left(\frac{h_x^{i+1} - h_x^i}{l_{i,i+1}}\right)$$

$$q_3^{i+1} = q_4^{i+1} = \frac{T^i}{2A_{i+1}} + \frac{\sum_{j=1,8} V_j^i x_j^i}{2A_{i+1}} + \frac{\sum_{j=1,8} H_j^i y_j^i}{2A_{i+1}} + \frac{(S_y^i + \sum_{j=1,8} V_j^i) h_y^i}{2(h_y^{i+1})^2} - \frac{(S_x^i + \sum_{j=1,8} H_j^i) h_x^i}{2(h_x^{i+1})^2}$$
$$- \frac{M_x^i + S_y^i l_{i,i+1}}{2(h_y^{i+1})^2}\left(\frac{h_y^{i+1} - h_y^i}{l_{i,i+1}}\right) + \frac{M_y^i + S_x^i l_{i,i+1}}{2(h_x^{i+1})^2}\left(\frac{h_x^{i+1} - h_x^i}{l_{i,i+1}}\right)$$

$$q_5^{i+1} = q_6^{i+1} = \frac{T^i}{2A_{i+1}} + \frac{\sum_{j=1,8} V_j^i x_j^i}{2A_{i+1}} + \frac{\sum_{j=1,8} H_j^i y_j^i}{2A_{i+1}} - \frac{(S_y^i + \sum_{j=1,8} V_j^i) h_y^i}{2(h_y^{i+1})^2} - \frac{(S_x^i + \sum_{j=1,8} H_j^i) h_x^i}{2(h_x^{i+1})^2}$$
$$+ \frac{M_x^i + S_y l_{i,i+1}}{2(h_y^{i+1})^2}\left(\frac{h_y^{i+1} - h_y^i}{l_{i,i+1}}\right) + \frac{M_y^i + S_x^i l_{i,i+1}}{2(h_x^{i+1})^2}\left(\frac{h_x^{i+1} - h_x^i}{l_{i,i+1}}\right)$$

$$q_7^{i+1} = q_8^{i+1} = \frac{T^i}{2A_{i+1}} + \frac{\sum_{j=1,8} V_j^i x_j^i}{2A_{i+1}} + \frac{\sum_{j=1,8} H_j^i y_j^i}{2A_{i+1}} - \frac{(S_y^i + \sum_{j=1,8} V_j^i) h_y^i}{2(h_y^{i+1})^2} + \frac{(S_x^i + \sum_{j=1,8} H_j^i) h_x^i}{2(h_x^{i+1})^2}$$
$$+ \frac{M_x^i + S_y^i l_{i,i+1}}{2(h_y^{i+1})^2}\left(\frac{h_y^{i+1} - h_y^i}{l_{i,i+1}}\right) - \frac{M_y^i + S_x^i l_{i,i+1}}{2(h_x^{i+1})^2}\left(\frac{h_x^{i+1} - h_x^i}{l_{i,i+1}}\right) \qquad (10)$$

The b_o matrix is formulated denoting the stringer loads as bo_{st} and the shear flows as bo_{sk}.

The basic stress system for the frames is identical to that given in ref. 25 except for the inclusion of a term to account for the stringer kick loads at frames where the stringers change direction. This additional term is given by

$$\left\{\begin{matrix} H \\ \cdots \\ V \end{matrix}\right\}^{i}_{\substack{\text{STRINGER} \\ \text{COMPONENT}}} = \begin{bmatrix} \frac{x_1^{i+1}-x_1^{i}}{\ell_1^{i,i+1}} & & 0 \\ & \ddots & \\ & & \frac{x_n^{i+1}-x_n^{i}}{\ell_n^{i,i+1}} \\ \hdashline \frac{y_1^{i+1}-y_1^{i}}{\ell_1^{i,i+1}} & & 0 \\ & \ddots & \\ 0 & & \frac{y_n^{i+1}-y_n^{i}}{\ell_n^{i,i+1}} \end{bmatrix} \left\{b_{o_{ST}}\right\}^{i,i+1} - \begin{bmatrix} \frac{x_1^{i}-x_1^{i-1}}{\ell_1^{i-1,i}} & & 0 \\ & \ddots & \\ & & \frac{x_n^{i}-x_n^{i-1}}{\ell_n^{i-1,i}} \\ \hdashline \frac{y_1^{i}-y_1^{i-1}}{\ell_1^{i-1,i}} & & 0 \\ & \ddots & \\ 0 & & \frac{y_n^{i}-y_n^{i-1}}{\ell_n^{i-1,i}} \end{bmatrix} \left\{b_{o_{ST}}\right\}^{i,i-1} \tag{11}$$

The bo_{frame} for one frame is then equal to

$$bo_f = \bar{b}o_f \, Ro_f \tag{12}$$

where $\bar{b}o_f$ is a transformation matrix which converts the loads on the frame into internal moments and forces and Ro_f is given by:

$$\left\{Ro_f\right\} = \underbrace{\left\{\begin{matrix} H \\ V \\ T \end{matrix}\right\}}_{\text{external}} + \underbrace{\left\{\begin{matrix} H \\ V \\ 0 \end{matrix}\right\}}_{\substack{\text{shear} \\ \text{flow}}} + \underbrace{\left\{\begin{matrix} H \\ V \\ 0 \end{matrix}\right\}}_{\substack{\text{stringer} \\ \text{component}}} \tag{13}$$

From these simple equations relating only to geometry of the shell, the complete bo matrix may be written as:

$$bo = \begin{bmatrix} bo_{st} \\ bo_{sk} \\ bo_{f} \end{bmatrix} \tag{14}$$

SELF-EQUILIBRATING SYSTEM

The minimum number of stringers necessary to form a self-equilibrating load system in a tapered shell circular or non-circular is seven in an unconnected open circuit. A general self-equilibrating load system must satisfy the condition of static equilibrium; therefore, in any seven stringer systems the following relationships must be satisfied. For simplicity in notation, let P_1 be the stringer load at frame i in bay i to i+1 for stringer 1, ℓ_1 be the length of stringer 1 in bay i to i-1, ℓ be the distance between frame i and the frame i-1 and also C^i_{12} and A^i_{12} be the chord distance and swept area between stringers 1 and 2 at frame i, respectively (see fig. 5).

$$P_1\frac{\ell}{\ell_1}+P_2\frac{\ell}{\ell_2}+P_3\frac{\ell}{\ell_3}+P_4\frac{\ell}{\ell_4}+P_5\frac{\ell}{\ell_5}+P_6\frac{\ell}{\ell_6}+P_7\frac{\ell}{\ell_7}=0$$

$$P_1\frac{y_1^i-y_1^{i+1}}{\ell_1}+P_2\frac{y_2^i-y_2^{i+1}}{\ell_2}+P_3\frac{y_3^i-y_3^{i+1}}{\ell_3}+P_4\frac{y_4^i-y_4^{i+1}}{\ell_4}+P_5\frac{y_5^i-y_5^{i+1}}{\ell_5}$$
$$+P_6\frac{y_6^i-y_6^{i+1}}{\ell_6}+P_7\frac{y_7^i-y_7^{i+1}}{\ell_7}=0$$

$$P_1\frac{x_1^i-x_1^{i+1}}{\ell_1}+P_2\frac{x_2^i-x_2^{i+1}}{\ell_2}+P_3\frac{x_3^i-x_3^{i+1}}{\ell_3}+P_4\frac{x_4^i-x_4^{i+1}}{\ell_4}+P_5\frac{x_5^i-x_5^{i+1}}{\ell_5}$$
$$+P_6\frac{x_6^i-x_6^{i+1}}{\ell_6}+P_7\frac{x_7^i-x_7^{i+1}}{\ell_7}=0$$

$$P_1\frac{\ell}{\ell_1}y_1^i+P_2\frac{\ell}{\ell_2}y_2^i+P_3\frac{\ell}{\ell_3}y_3^i+P_4\frac{\ell}{\ell_4}y_4^i+P_5\frac{\ell}{\ell_5}y_5^i+P_6\frac{\ell}{\ell_6}y_6^i+P_7\frac{\ell}{\ell_7}y_7^i=0$$

$$P_1\frac{\ell}{\ell_1}x_1^i+P_2\frac{\ell}{\ell_2}x_2^i+P_3\frac{\ell}{\ell_3}x_3^i+P_4\frac{\ell}{\ell_4}x_4^i+P_5\frac{\ell}{\ell_5}x_5^i+P_6\frac{\ell}{\ell_6}x_6^i+P_7\frac{\ell}{\ell_7}x_7^i=0$$

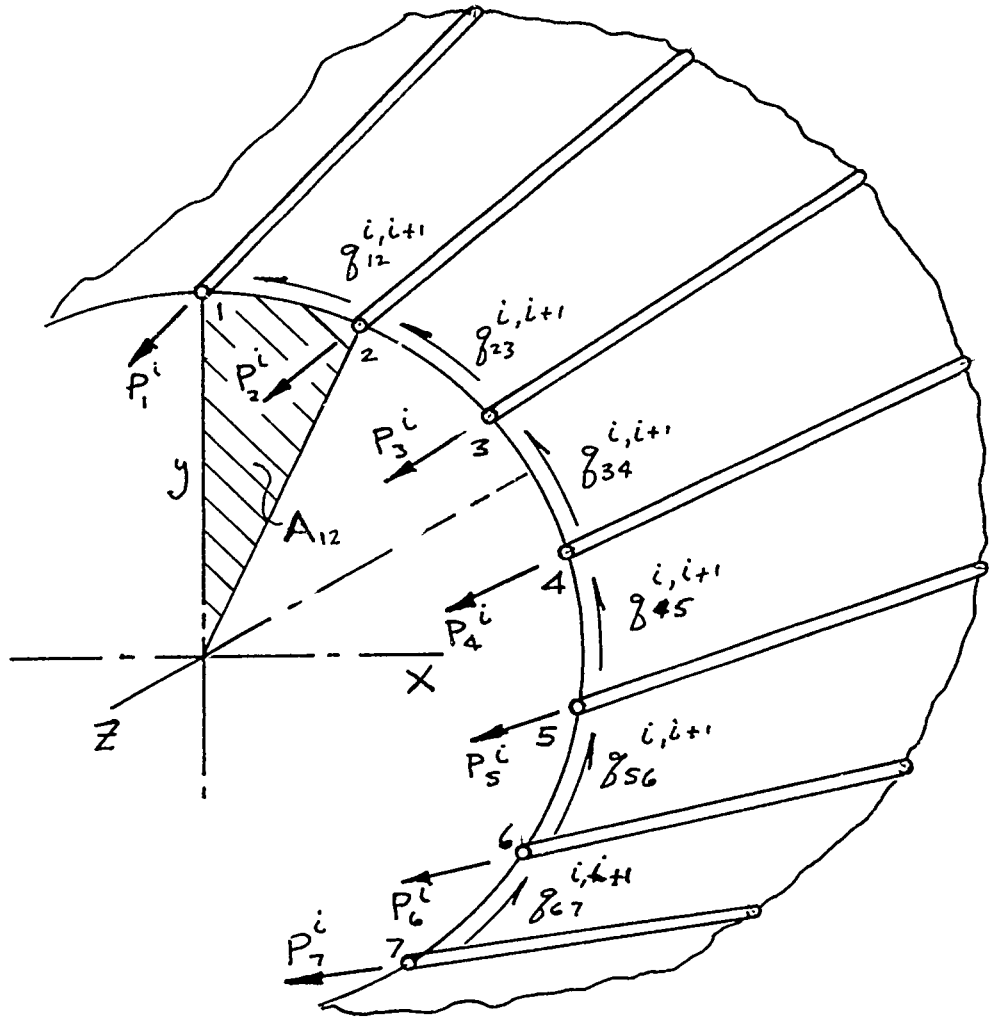


Figure 5. Self-Equilibrating Stress System - General Case

$$\frac{P_1}{\ell_1}\Big(\Big[x_1^i - x_1^{i+1}\Big]y_1^i - \Big[y_1^i - y_1^{i+1}\Big]x_1^i + \frac{C_{12}^{i+1}}{C_{12}^i}\frac{A_{12}^i}{2} + \frac{C_{23}^{i+1}}{C_{23}^i}\frac{A_{23}^i}{2} + \frac{C_{34}^{i+1}}{C_{34}^i}\frac{A_{34}^i}{2}$$

$$\frac{C_{45}^{i+1}}{C_{45}^i}\frac{A_{45}^i}{2} + \frac{C_{56}^{i+1}}{C_{56}^i}\frac{A_{56}^i}{2} + \frac{C_{67}^{i+1}}{C_{67}^i}\frac{A_{67}^i}{2}\Big) +$$

$$\frac{P_2}{\ell_2}\Big(\Big[x_2^i - x_2^{i+1}\Big]y_2^i - \Big[y_2^i - y_2^{i+1}\Big]x_2^i + \frac{C_{23}^{i+1}}{C_{23}^i}\frac{A_{23}^i}{2} + \frac{C_{34}^{i+1}}{C_{34}^i}\frac{A_{34}^i}{2} + \frac{C_{45}^{i+1}}{C_{45}^i}\frac{A_{45}^i}{2}$$

$$\frac{C_{56}^{i+1}}{C_{56}^i}\frac{A_{56}^i}{2} + \frac{C_{67}^{i+1}}{C_{67}^i}\frac{A_{67}^i}{2}\Big) +$$

$$\frac{P_3}{\ell_3}\Big(\Big[x_3^i - x_3^{i+1}\Big]y_3^i - \Big[y_3^i - y_3^{i+1}\Big]x_3^i + \frac{C_{34}^{i+1}}{C_{34}^i}\frac{A_{34}^i}{2} + \frac{C_{45}^{i+1}}{C_{45}^i}\frac{A_{45}^i}{2} + \frac{C_{56}^{i+1}}{C_{56}^i}\frac{A_{56}^i}{2} + \frac{C_{67}^{i+1}}{C_{67}^i}\frac{A_{67}^i}{2}\Big) +$$

$$\frac{P_4}{\ell_4}\Big(\Big[x_4^i - x_4^{i+1}\Big]y_4^i - \Big[y_4^i - y_4^{i+1}\Big]x_4^i + \frac{C_{45}^{i+1}}{C_{45}^i}\frac{A_{45}^i}{2} + \frac{C_{56}^{i+1}}{C_{56}^i}\frac{A_{56}^i}{2} + \frac{C_{67}^{i+1}}{C_{67}^i}\frac{A_{67}^i}{2}\Big) +$$

$$\frac{P_5}{\ell_5}\Big(\Big[x_5^i - x_5^{i+1}\Big]y_5^i - \Big[y_5^i - y_5^{i+1}\Big]x_5^i + \frac{C_{56}^{i+1}}{C_{56}^i}\frac{A_{56}^i}{2} + \frac{C_{67}^{i+1}}{C_{67}^i}\frac{A_{67}^i}{2}\Big) +$$

$$\frac{P_6}{\ell_6}\Big(\Big[x_6^i - x_6^{i+1}\Big]y_6^i - \Big[y_6^i - y_6^{i+1}\Big]x_6^i + \frac{C_{67}^{i+1}}{C_{67}^i}\frac{A_{67}^i}{2}\Big) +$$

$$\frac{P_7}{\ell_7}\Big(\Big[x_7^i - x_7^{i+1}\Big]y_7^i - \Big[y_7^i - y_7^{i+1}\Big]x_7^i\Big) = 0 \qquad (15)$$

In addition to the previous equations, some convenient relationship between the stringer loads must be introduced in order to assign values to the b_1 matrix. The equation suggested in ref. 25 is:

$$P_1\frac{\ell}{\ell_1} + P_2\frac{\ell}{\ell_2} + P_3\frac{\ell}{\ell_3} + P_4\frac{\ell}{\ell_4} + P_5\frac{\ell}{\ell_5} + P_6\frac{\ell}{\ell_6} + P_7\frac{\ell}{\ell_7} = X \qquad (15a)$$

These equations may be assembled into matrix form and the matrix inverted to give the stringer loads as a function of a generalized redundant force X. One column of the bl_{st} may be represented as:

$$\{P\} = \{bl_{st}\} \quad X \tag{16}$$

From equations 15 and 15a the special symmetrical and asymmetrical loadings may be deduced by the elimination of the unneeded equilibrium conditions. The shear flows in the skin panels at frame i in bay i to i+1 are given by:

$$q_{12} = -\frac{P_1}{l_1}\frac{C_{12}^{i+1}}{C_{12}^{i}}$$

$$q_{23} = -\left(\frac{P_1}{l_1}+\frac{P_2}{l_2}\right)\frac{C_{23}^{i+1}}{C_{23}^{i}}$$

$$q_{34} = -\left(\frac{P_1}{l_1}+\frac{P_2}{l_2}+\frac{P_3}{l_3}\right)\frac{C_{34}^{i+1}}{C_{34}^{i}}$$

$$q_{45} = -\left(\frac{P_1}{l_1}+\frac{P_2}{l_2}+\frac{P_3}{l_3}+\frac{P_4}{l_4}\right)\frac{C_{45}^{i+1}}{C_{45}^{i}}$$

$$q_{56} = -\left(\frac{P_1}{l_1}+\frac{P_2}{l_2}+\frac{P_3}{l_3}+\frac{P_4}{l_4}+\frac{P_5}{l_5}\right)\frac{C_{56}^{i+1}}{C_{56}^{i}}$$

$$q_{67} = -\left(\frac{P_1}{l_1}+\frac{P_2}{l_2}+\frac{P_3}{l_3}+\frac{P_4}{l_4}+\frac{P_5}{l_5}+\frac{P_6}{l_6}\right)\frac{C_{67}^{i+1}}{C_{67}^{i}} \tag{17}$$

The self-equilibrating shear flows may now be related to the generalized redundant force X. One typical column may be represented by:

$$\{q\} = \{bl_{sk}\} \quad X \tag{18}$$

The self-equilibrating shear flows and stringer loads may be transformed into concentrated frame loads in a manner similar to that employed for the basic stress system. This can be seen for the stringer component if in equation 11 the $\{bo_{st}\}$ matrices are replaced by the appropriate $\{bl_{st}\}$ matrices. The frame self-equilibrating stress system

may be calculated by:

$$b_{1_f} = \bar{b}_{1_f} R_{1_f} \tag{19}$$

where $\bar{b}_{1_f}$ is the same as the $\bar{b}_{o_f}$ matrix except for the exclusion of the external moment terms.

In addition to R_{1_f} frames loads, there are in general three redundancies on each frame leading to a b_{1_f} matrix. The method of treating these redundants for tapered shells is the same as that presented in ref. 25.

Combining the b_1 matrices for the stringers, skins, and frames, the complete b_1 matrix becomes:

$$b_1 = \begin{bmatrix} b_{1_{st}} & 0 \\ b_{1_{sk}} & 0 \\ b_{1_f} & b_{1_F} \end{bmatrix} \tag{20}$$

FLEXIBILITY MATRIX

The flexibility matrices presented herein have been developed to include the effects of members with tapered cross sections in order to make this method more compatible with actual hardware shells. For simplicity, the following assumptions have been made. For the skin panels; the shear flow varies linearly and the reciprocal of the chord distance, panel thickness and modulus of rigidity vary linearly. For the stringers; the shear flow varies linearly and the reciprocal of the area and modulus of elasticity varies linearly. For the frames; the moment varies linearly and the reciprocal of the modulus of elasticity and moment of inertia varies linearly. The individual flexibility matrices for a single element of the skin, stringer and frame, as shown in fig. 6, become:

$$f_{sk} = \left(C^i_{12}\right)^2 \ell_{i,i+1} \left\{ \frac{1}{C_i G_i t_i} + \frac{1}{2}\left[\left(\frac{1}{C_i G_i} \frac{t_i - t_{i+1}}{t_i t_{i+1}}\right) + \frac{1}{G_i t_i}\left(\frac{C_i - C_{i+1}}{C_i C_{i+1}}\right)\right.\right.$$

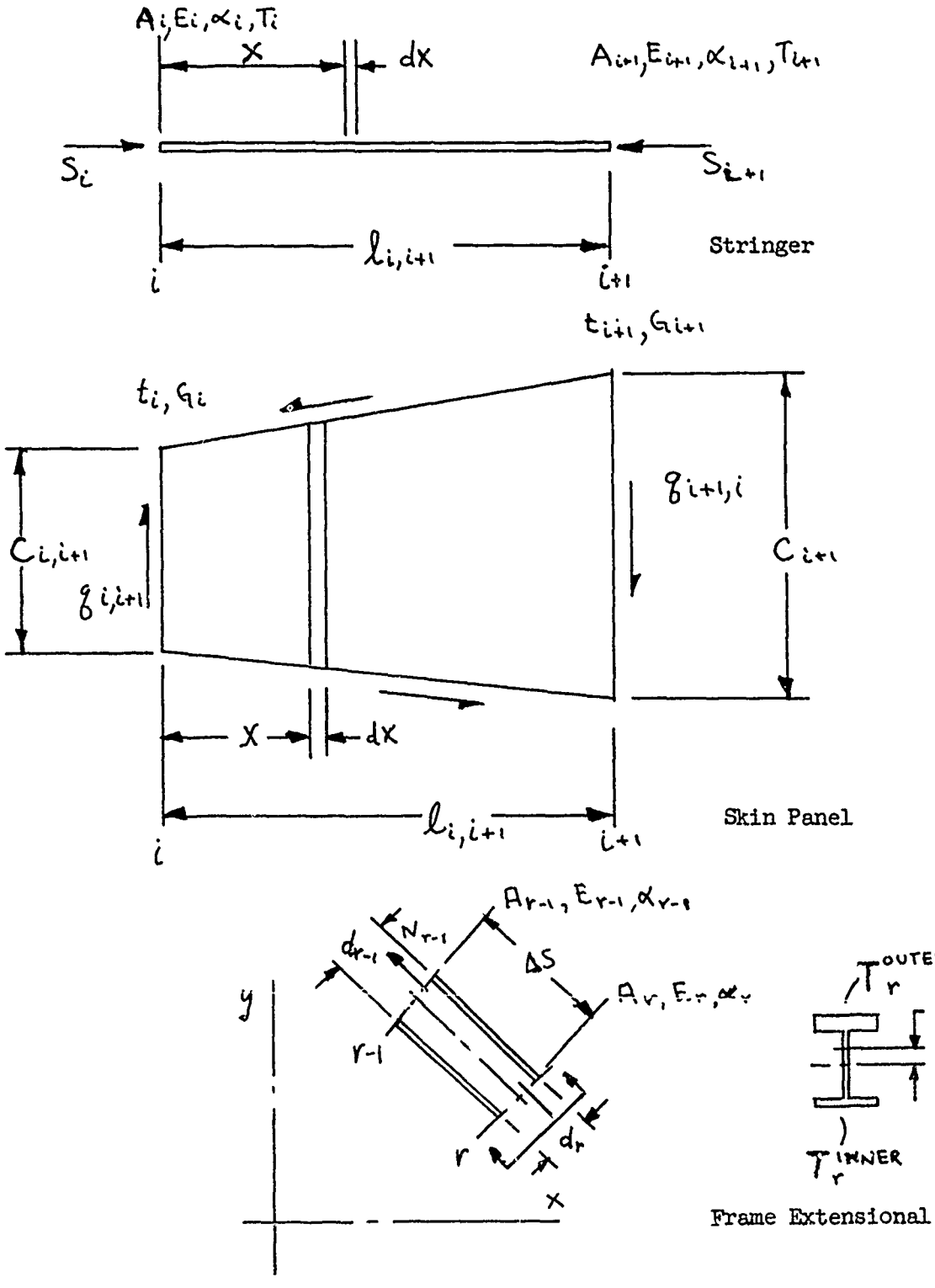


Figure 6. Flexibility Matrix and Thermal Strain Notation

$$+\frac{1}{C_i t_i}\left(\frac{G_i - G_{i+1}}{G_i G_{i+1}}\right)\Bigg] + \frac{1}{3}\left[\left(\frac{C_i - C_{i+1}}{C_i C_{i+1}}\right)\left(\frac{G_i - G_{i+1}}{G_i G_{i+1}}\right)\frac{1}{t_i}\right.$$

$$\left.+\left(\frac{C_i - C_{i+1}}{C_i C_{i+1}}\right)\left(\frac{t_i - t_{i+1}}{t_i t_{i+1}}\right)\frac{1}{G_i} + \left(\frac{G_i - G_{i+1}}{G_i G_{i+1}}\right)\left(\frac{t_i - t_{i+1}}{t_i t_{i+1}}\right)\frac{1}{C_i}\right]$$

$$+\frac{1}{4}\left[\left(\frac{G_i - G_{i+1}}{G_i G_{i+1}}\right)\left(\frac{C_i - C_{i+1}}{C_i C_{i+1}}\right)\left(\frac{t_i - t_{i+1}}{t_i t_{i+1}}\right)\right]$$

$$f_{ST} = \ell_{i,i+1}\begin{bmatrix} \frac{1}{5A_iE_i} + \frac{1}{20}\left(\frac{1}{A_iE_{i+1}} + \frac{1}{A_{i+1}E_i}\right) & \frac{1}{20A_iE_i} + \frac{1}{30}\left(\frac{1}{A_iE_{i+1}} + \frac{1}{A_{i+1}E_i}\right) \\ + \frac{1}{30A_{i+1}E_{i+1}} & + \frac{1}{20A_{i+1}E_{i+1}} \\ \frac{1}{20A_iE_i} + \frac{1}{30}\left(\frac{1}{A_iE_{i+1}} + \frac{1}{A_{i+1}E_i}\right) & \frac{1}{30A_iE_i} + \frac{1}{20}\left(\frac{1}{A_iE_{i+1}} + \frac{1}{A_{i+1}E_i}\right) \\ \frac{1}{20A_{i+1}E_{i+1}} & + \frac{1}{5A_{i+1}E_{i+1}} \end{bmatrix} \quad (21)$$

The frame moment flexibility matrix is identical to the stringer flexibility except that the stringer area term is replaced by the frame moment of inertia and ℓ_i, i+1 now represents the frame segment being considered. The frame extensional flexibility matrix may be computed from the following equation:

$$f_e = \Delta S \left[\frac{1}{3A_{r-1}E_{r-1}} + \frac{1}{6}\left(\frac{1}{A_{r-1}E_r} + \frac{1}{A_r E_{r-1}} \right) + \frac{1}{3A_r E_r} \right] \qquad (22)$$

where A is the frame cross sectional area and ΔS is the frame segment length.

From these equations the composite flexibility matrix can be constructed for the unassembled elements as

$$f = \begin{bmatrix} f_{st} & & \\ & f_{sk} & \\ & & f_f \end{bmatrix} \qquad (23)$$

THERMAL STRAINS

The effects of cutouts, initial strains and thermal gradients can easily be treated by use of the matrix force method. The technique by which cutouts and initial strains are treated is adequately presented in ref. 25 and will not be repeated here.

The thermal strains are computed in a manner similar to the flexibility matrices in that they are formed for independent, unassembled stringer and frame elements. The shear deformations in the skins due to the thermal gradients, in this case, have been neglected.

The equation for the thermal strains in a stringer segment is given by:

$$\{H_{st}\} = \ell \begin{bmatrix} \frac{\alpha_i}{4} + \frac{\alpha_{i+1}}{12} & \frac{\alpha_i + \alpha_{i+1}}{12} \\ \frac{\alpha_i + \alpha_{i+1}}{12} & \frac{\alpha_i}{12} + \frac{\alpha_{i+1}}{4} \end{bmatrix} \begin{Bmatrix} T_i \\ T_{i+1} \end{Bmatrix} \qquad (24)$$

where ℓ is the stringer length, α the coefficient of thermal expansion, and T the temperature as shown in fig. 6.

The curvature induced in a frame segment due to the effect of depthwise thermal gradients may be expressed by:

$$\left\{H_M\right\} = \Delta S \begin{bmatrix} \frac{\alpha_{r-1}}{5d_{r-1}} + \frac{\alpha_r}{20d_{r-1}} & \frac{\alpha_{r-1}}{20d_{r-1}} + \frac{\alpha_r}{30d_{r-1}} \\ + \frac{\alpha_{r-1}}{20d_r} + \frac{\alpha_r}{30d_r} & + \frac{\alpha_{r-1}}{30d_r} + \frac{\alpha_r}{20d_r} \\ \frac{\alpha_{r-1}}{20d_{r-1}} + \frac{\alpha_r}{30d_{r-1}} & \frac{\alpha_{r-1}}{30d_{r-1}} + \frac{\alpha_r}{20d_{r-1}} \\ + \frac{\alpha_{r-1}}{30d_r} + \frac{\alpha_r}{20d_r} & + \frac{\alpha_{r-1}}{20d_r} + \frac{\alpha_r}{5d_r} \end{bmatrix} \begin{Bmatrix} \Delta T_{r-1} \\ \Delta T_r \end{Bmatrix} \quad (25)$$

where ΔS is the length of frame segment, d is the frame depth, and ΔT is the depthwise thermal gradient as shown in fig. 6.

The extensional thermal strains induced in a frame segment may be computed by:

$$H_N = \Delta S \left\{ \alpha_{r-1} \left[\left(\frac{T^i_{r-1} - T^o_{r-1}}{6} \right) + e_{r-1} \left(\frac{T^i_{r-1} - T^o_{r-1}}{3} \right) \right.\right.$$
$$\left. + \left(\frac{T^i_r + T^o_r}{12} \right) + e_r \left(\frac{T^o_r - T^i_r}{6} \right) \right] + \alpha_r \left[\left(\frac{T^i_{r-1} - T^o_{r-1}}{12} \right) \right.$$
$$\left.\left. + e_{r-1} \left(\frac{T^o_{r-1} - T^i_{r-1}}{6} \right) + \left(\frac{T^i_r - T^o_r}{6} \right) + e_r \left(\frac{T^o_r - T^i_r}{3} \right) \right] \right\} \quad (26)$$

where T^{o}_{r-1} is the outer cap temperature at r-1 and e is the distance between the frame midplane and the neutral axis as shown in fig. 6.

COMPOSITE FLEXIBILITY MATRIX

The unknown self-equilibrating stress systems and the frame redundancies are calculated from the generalized compatibility equations obtained from the unit load method. The derivation of these equations is thoroughly discussed in ref. 25 and only the results will be shown here.

The unknown redundant forces may be computed from the following equation:

$$X = -(b'_1 fb_1)^{-1} \; b'_1 fb_o \; R \tag{27}$$

The true load distribution is given by:

$$S = b_o R - b_1 \; (b'_1 fb_1)^{-1} \; b'_1 fb_o \; R \tag{28}$$

where S is the partition column of stringer loads, skin shear flows and frame bending moments and axial loads, and R is the external loads H and V. The shell flexibility matrix for the loads R if no cutouts are present is given by:

$$F = b'_o \; fb_o - b'_o \; Fb_1 \; (b'_1 \; fb_1)^{-1} \; b'_1 \; fb_o \tag{29}$$

The displacements u and v in the x and y planes, respectively, can then be calculated from the following expression:

$$\begin{Bmatrix} u \\ v \end{Bmatrix} = \begin{bmatrix} F \end{bmatrix} \begin{Bmatrix} H \\ V \end{Bmatrix} \tag{30}$$

For the case where there are thermal strains H present, the unknown redundancies may be determined by:

$$X = -(b'_1 \; fb_1)^{-1} \; \left(b'_1 \; fb_o \; R + b'_1 \; H \right) \tag{31}$$

The true load distribution for this condition is:

$$S = \; b_o R - b_1 \; (b'_1 \; fb_1)^{-1} \; \; (b'_1 \; fb_o \; R + H) \tag{32}$$

EXAMPLE

In order to test the validity of any analytical approach, it is necessary to compare the results generated by that method with some generally accepted method or with test data. Przemieniecke, in ref. 25, presents a numerical example which considers a uniform cantilevered circular cylinder with a uniform edge frame loaded by a concentrated radial load. This particular case was chosen in order to make a direct comparison with results published in ref. 26. The shear flow and frame bending moment agree closely with the values obtained in ref. 26.

A structure similar to that described above was tested by the NACA (ref. 27) and the test data reported on in ref. 28. This structure, shown in fig. 7, consists of a radially loaded frame supported by a four-bay cantilevered shell. The shell had no stringers so that the longitudinal load carrying members were idealized by considering the skin area to be concentrated at symmetrically distributed locations.

The methods of analysis employed in ref. 28 were a least-work method and also a distributed stringer analysis. Good agreement was obtained between these analyses and the test results. The force method was applied to this same structure. A comparison between the analytically produced results and the test data where given, or the methods of ref. 28, are shown in figs. 8, 9, and 10. These figures show comparisons of the frame bending moment, the longitudinal stresses at frame 3 and the shear flow distribution in bay 1. As can be seen from these curves, an excellent agreement was obtained. The number of idealized longitudinal members were varied to determine their effect on the accuracy of the force method. It was found that for analyses with as few as eight stringers, little variation was obtained between this and the more detailed analyses. It is felt, therefore, that for all but very complicated structures, the number of idealized members may be kept small, thus minimizing the overall computational requirements. The author of ref. 28 had come to this same conclusion.

Unfortunately, no data of a similar nature have been found for a conical shell or a shell with thermal gradient imposed upon it, so that no test verification can be presented for the extensions made to the force method at this time.

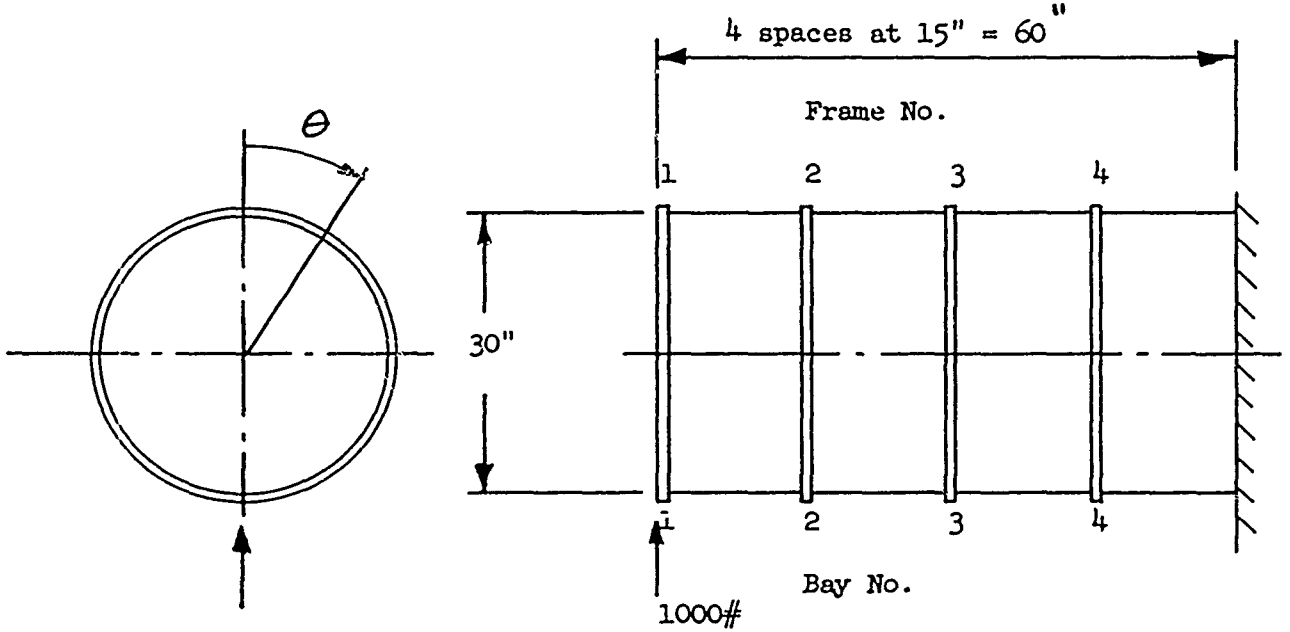


Figure 7. NACA Test Cylinder

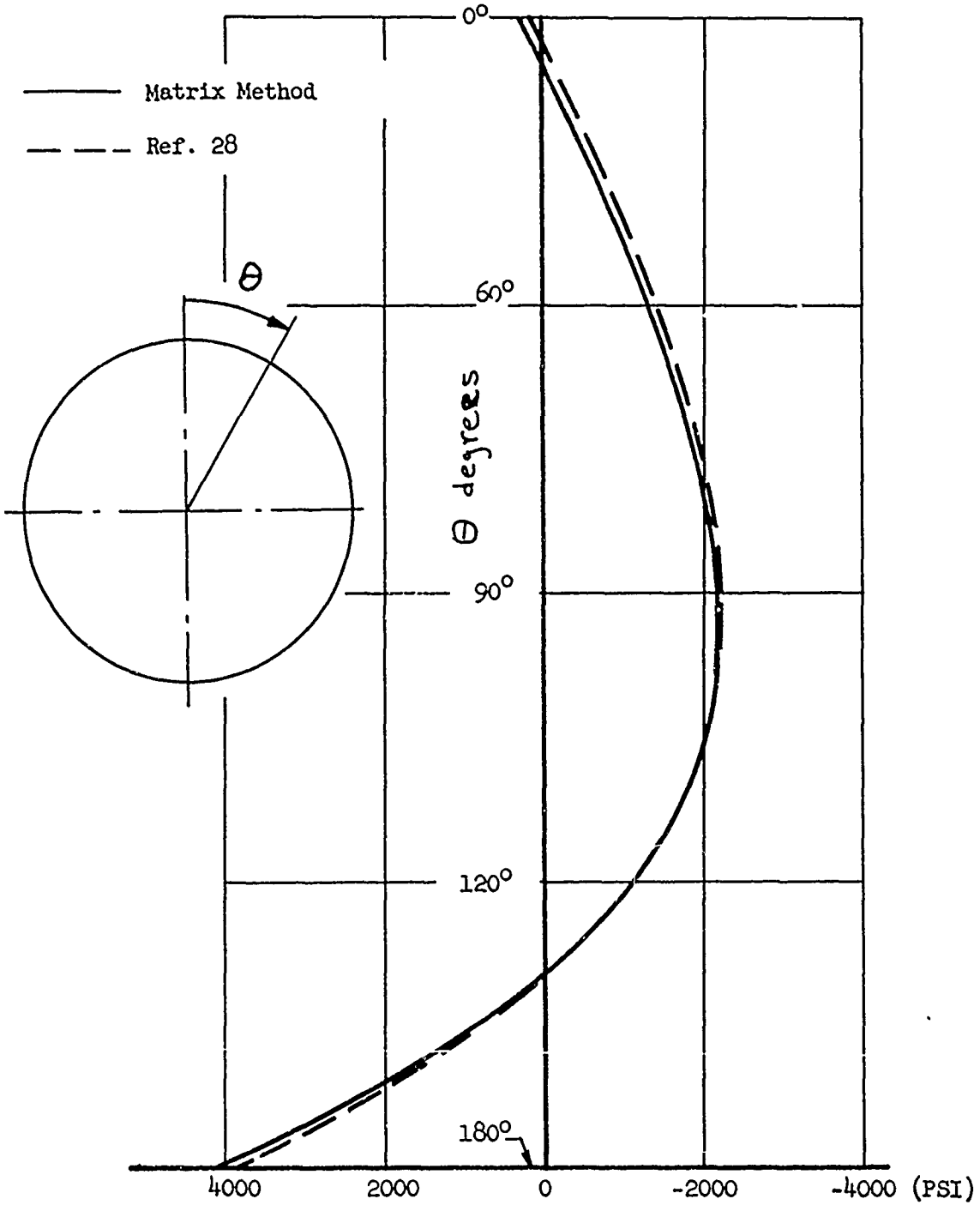


Figure 8. Shell Longitudinal Bending Stress, Frame 3

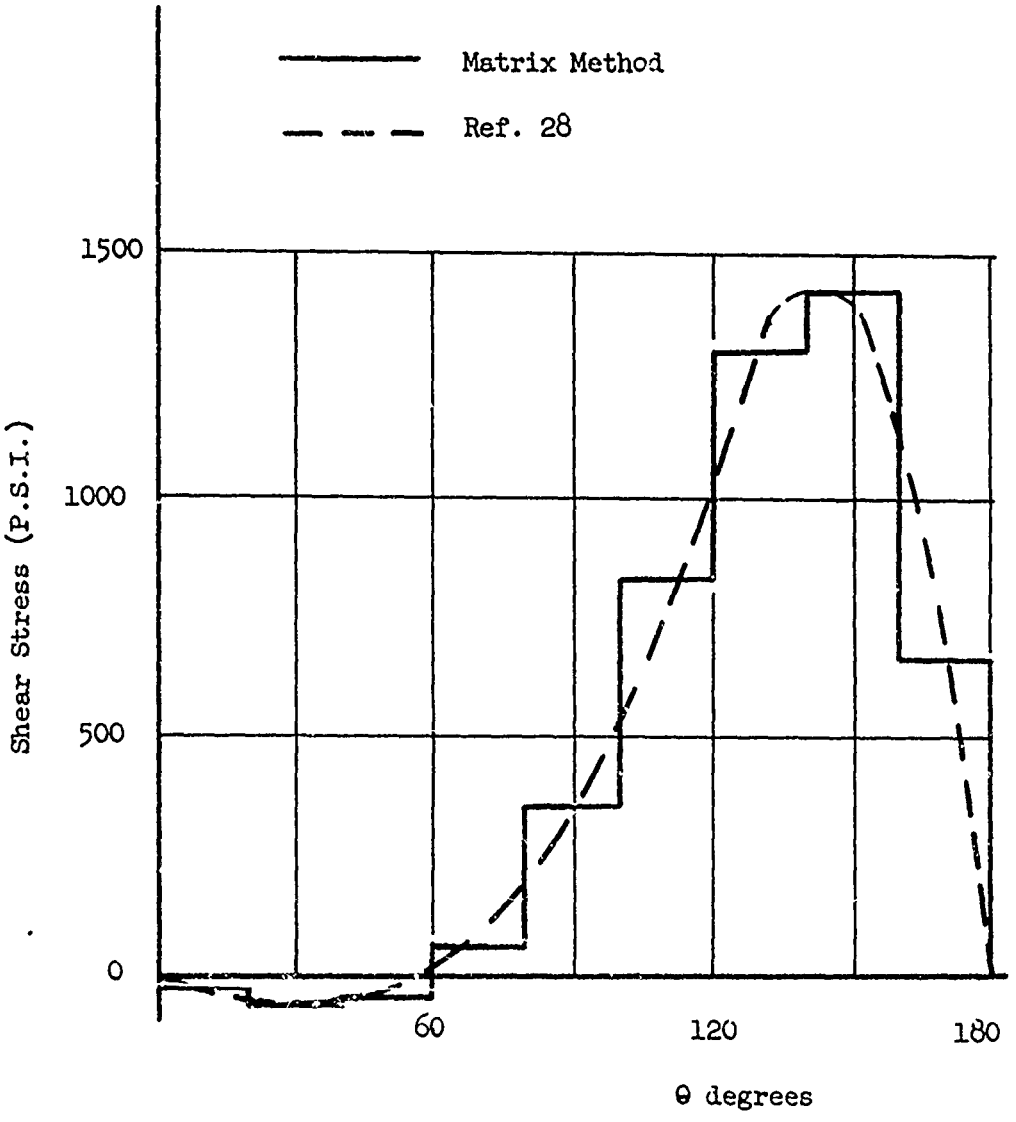


Figure 9. Shear Stress in Shell, Bay 1

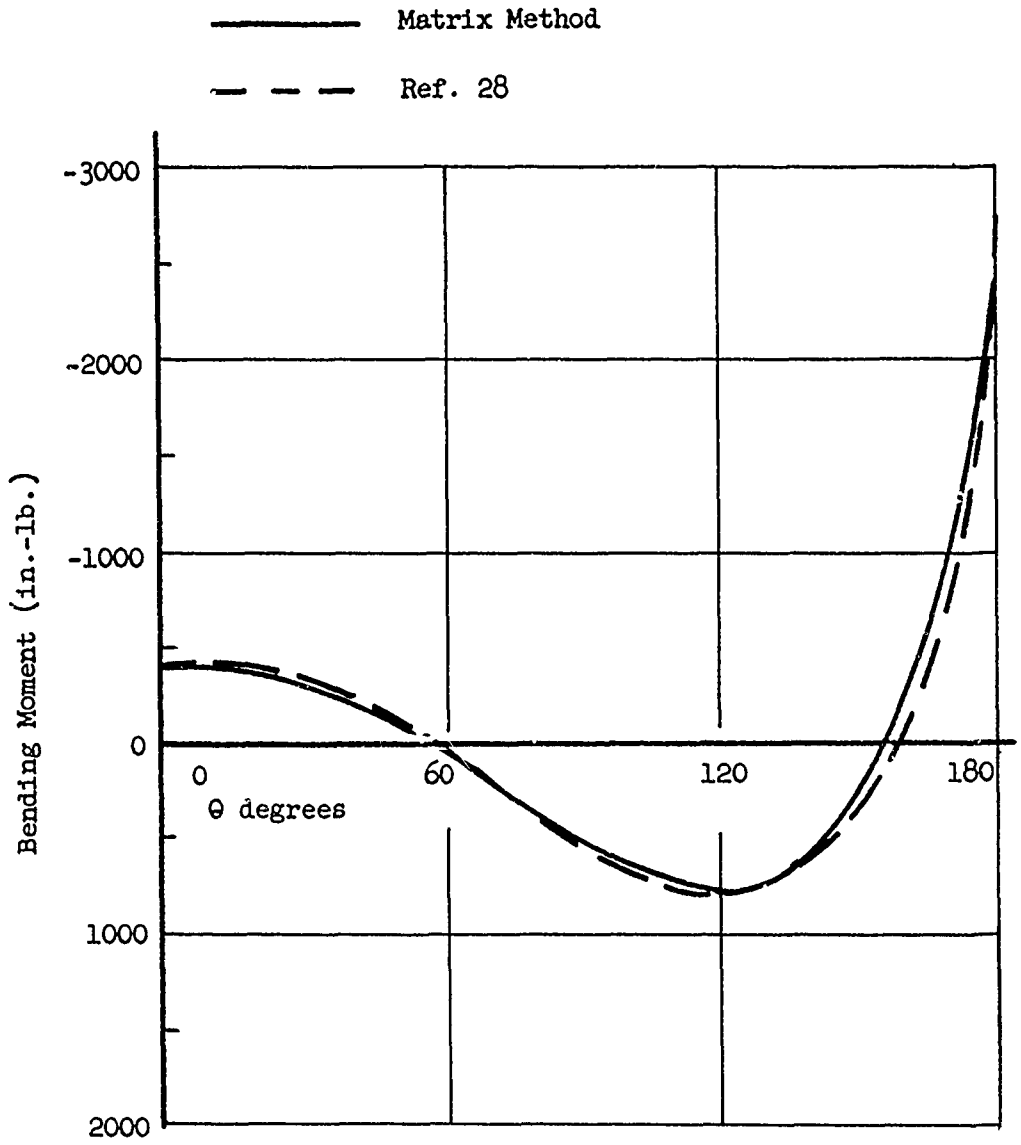


Figure 10. Frame Bending Moment, Frame 1

VIBRATION EQUATIONS

In general, a mass vibrating in a complex shell structure undergoes combined accelerations in all three planes. For the types of structures described previously, if it can be assumed that the Z component, i.e., the end shortening of the cylinders, can be ignored, then the problem of solving for the vibration frequencies and mode shapes can be greatly simplified. If sinusoidal motion can be assumed, a generalized acceleration $\ddot{q}$ can be expressed as a function of its maximum amplitude by

$$\ddot{q} = -\omega^2 q \tag{33}$$

where q may be either a translational or rotational displacement.

A mass vibrating in two planes may, therefore, be divided into its two components u and v and each treated separately if the cross coupling terms of the flexibility matrix are known.

The equations of motion of a point mass m_i vibrating in the x and y axes with amplitudes u and v, can then be calculated from:

$$\begin{aligned} H^i &= -\omega^2 m_i u^i \\ V^i &= -\omega^2 m_i v^i \end{aligned} \tag{34}$$

It has been previously shown that the forces H and V can be expressed as a function of the shell stiffness matrix $[\Delta]$ and the displacements u and v by:

$$\begin{Bmatrix} H \\ V \end{Bmatrix} = [\Delta] \begin{Bmatrix} u \\ v \end{Bmatrix} \tag{35}$$

where $[\Delta] = [F]^{-1}$

Equating the two equations for the forces H and V gives the following equation:

$$[\Delta] \begin{Bmatrix} u \\ v \end{Bmatrix} = -\omega^2 \left[\begin{array}{c:c} m & 0 \\ \hdashline 0 & m \end{array}\right] \begin{Bmatrix} u \\ v \end{Bmatrix} \tag{36}$$

The complete expression for the equation of motion becomes:

$$\begin{Bmatrix} u \\ v \end{Bmatrix} = -\omega^2 \begin{bmatrix} F \end{bmatrix} \left[\begin{array}{c|c} m & 0 \\ \hline 0 & m \end{array}\right] \begin{Bmatrix} u \\ v \end{Bmatrix} \tag{37}$$

This equation can be solved for its characteristic roots by any one of several methods developed for the solution of implicit matrix equations.

MULTIPLE STAGE CYLINDERS

The previous analysis was developed for a tapered shell with a single bay. An untapered shell can be treated by the expressions previously given by eliminating the second and third relationships of equation 15 and reducing the remaining equations to account for only a five stringer system.

The method of treating a cylinder with multiple bays is a simple extension to methods given earlier. Using these equations as basic building blocks, a cylinder of any size, limited only by existing computing equipment, may be analyzed.

The effect on the basic stress system, the bo matrix, at frame i due to the presence of adjacent bays, bay 1 through bay i-1 is given by the following equations:

$$S_y^i = \sum_{k=1,} \sum_{j=1,n} V_{j,k}$$

$$S_x^i = \sum_{k=1,i-1}^{-} \sum_{j=1,n} H_{j,k}$$

$$M_y^i = \sum_{k=1,i-1} \sum_{j=1,n} V_{j,k}\, l_{i,k}$$

$$M_x^i = \sum_{k=1,i-1} \sum_{j=1,n} H_{j,k}\, l_{i,k}$$

$$T^i = \sum_{k=1,i-1} \sum_{j=1,n} \left(V_{j,k} x_{j,k} + H_{j,k}\, y_{j,k} \right) \qquad (38)$$

where $H_{j,k}$, $V_{j,k}$, $y_{j,k}$, and $x_{j,k}$ are the horizontal and vertical forces and their torsional moment arms, respectively at stringer locations j at frame k, and n is the number of stringers. These equations merely sum the loads and moments applied to these adjacent bays. The equation used in conjunction with equations 9 and 10 lead to the complete b_r matrix of a multiple stage cylinder.

When treating a self-equilibrating stress system at frame i the shear flows on the adjacent sides of the frame in general affect not only frame i, but also frame i-1 and frame i+1. The stringer self-equilibrating loads at frame i in bay i-1, i may be computed by equating the horizontal components of the stringers in bay i, i+1 for which the relationships have been given previously in equations 15 and 15a.

SECTION IV: STIFFNESS AND VIBRATION PREDICTION OF CLUSTERED CYLINDERS

Presented in this section is a brief description of the methods used for analyzing the vibration methods of a proposed Flight Test Missile. The Flight Test Missile with a solid propellant rocket motor is designed to convey a nose capsule to high altitudes along various design trajectories. The propulsion system is comprised of a cluster of four solid propellant rocket motors. The flight article was aerodynamically stable and contained no guidance or control system although some thought was given to later adding a flight control system in the Flight Test Missile with a pressure tank in the middle. In order to know the basic frequencies and module shapes of the pressure tank which is supposed to contain a sensing element for the guidance system, it is necessary to idealize the shell, the pressure tank, and the four solid motors as three coupled beams. The solid engines are considered to be fixed to the shell at the rear end and simply supported at the front end. The pressure tank was idealized to be simply supported at both ends.

EQUATIONS FOR TRI-COUPLE BEAM MODAL CALCULATION

This section presents a method by which the natural frequencies of a tri-couple beam can be approximately determined.

The general matrix will first be developed for a simple free-free beam, and then the equations for the tri-couple beam will be developed with the use of this basic matrix. This method is basically Myklestad Method except that it considers the effects of rotary inertia, shear stiffness, and the initial boundary conditions of the additional beams being considered that produce the coupling effect.

The actual beam is represented by a beam consisting of lumped masses and lumped mass moment of inertias connected by constant EI and constant KAG beams (beam bending and beam shear stiffness, respectively). These beams are considered massless (see fig. 11).

The coordinate system is shown in fig. 11 where the "z" axis is perpendicular to the plane of the paper. The sign for moments, shears, slopes, and deflections are shown in fig. 11. The usual assumptions of thin bar theory are made. Loads other than inertial loads are neglected, and the elements of the sections are assumed to be in harmonic motion.

The units for the equations that are being developed are as follows:

m_i = lumped mass = $\frac{\#\ \text{sec.}^2}{\text{in.}}$

y = deflection, inches

M = moment, inch-pounds

S = shear, pounds

B^{θ} = slope due to bending, radians

s^{θ} = slope due to shear, radians

T^{θ} = total slope, radians

EI = bending beam stiffness, $\#\ (\text{in})^2$

KAG = shear beam stiffness, $\#$

I_{zz_i} = mass moment of inertia about c.g. of lumped mass, $\#$ in $(\text{sec})^2$

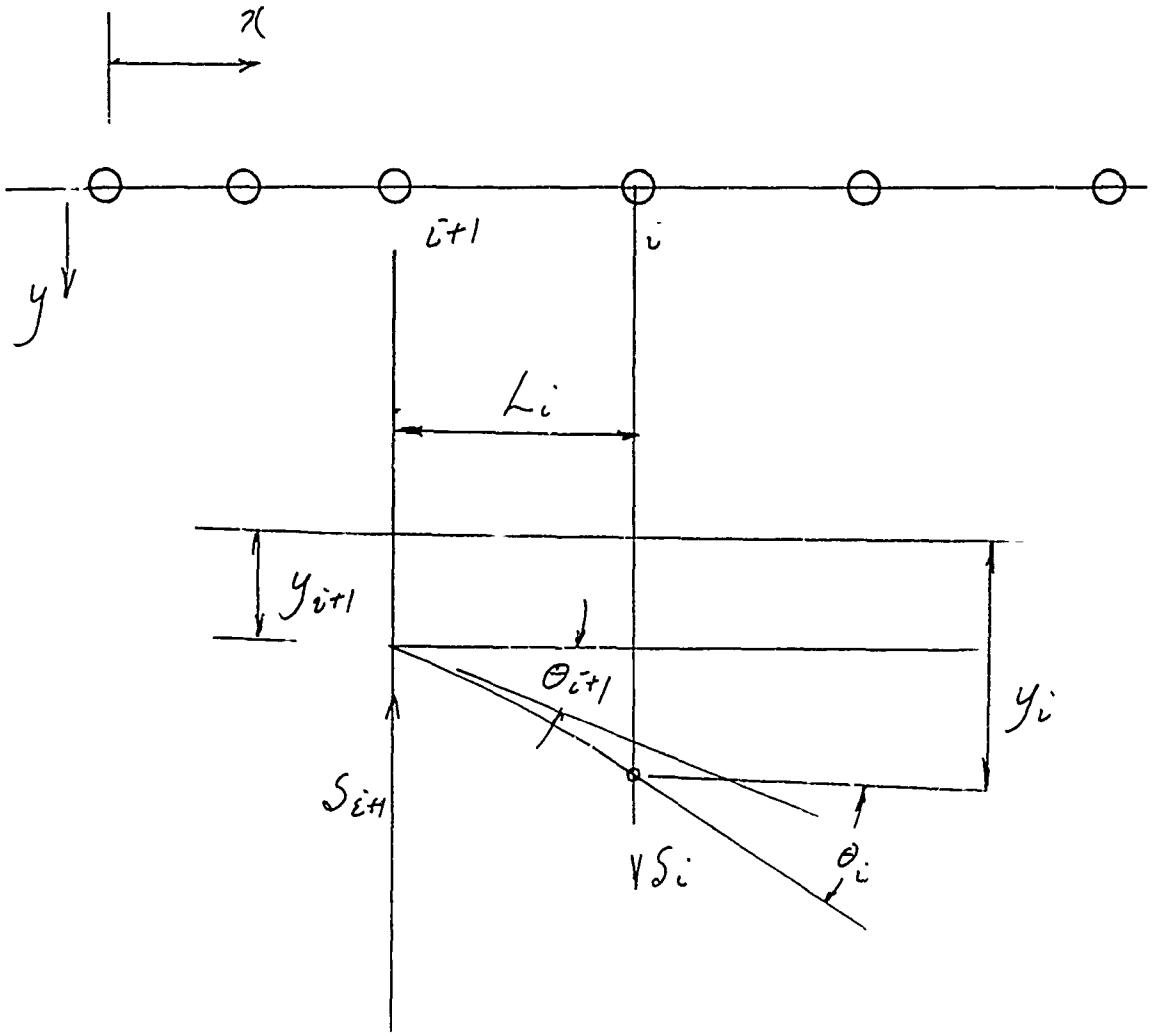


Figure 11. Lump Masses

(units for equations - continued)

L = length of beam, inches

= frequency, rad/sec.

The elastic coefficients for the i^{th} section of the uniform beam with unit load and moment are defined as follows:



$$B^{\theta} = \frac{L_i^2}{2EI_i} \qquad B^{y} = \frac{L_i^3}{3EI_i}$$

Bending Effect

$$B^{\theta} = \frac{L_i}{EI_i} \qquad B^{y} = \frac{L_i^2}{2EI_i}$$

$$s^{\theta} = \frac{1}{KAG_i} \qquad s^{y} = \frac{L_i}{KAG_i}$$

Shear Effect

(39)

Since the beam was assumed to be oscillating with simple harmonic motion, then y may be replaced by $- y\omega^2$, and θ with $- \theta\omega^2$, this will produce the inertia loading on the beam.

$$-m_i y = \omega^2 m_i y_i$$

$$-I_{zz_i} \theta = \omega^2 B^{\theta} I_{zz_i} \qquad (40)$$

The i^{th} section is taken to the right of mass i where S_i and M_i exist. From fig. 11 it is seen:

$$S_{i+1} = S_i + m_i \omega^2 y_i$$

$$M_{i+1} = M_i + S_i L_i + m_i \omega^2 y_i L_i + I_{zz_i} \omega^2 B^{\Theta}i \tag{40a}$$

To determine $B^{\Theta}i+1$ it is simpler to solve the angle $B^{\Theta}i$ working from left to right (see fig.11). The slope due to bending will be calculated and then the slope due to shear will be added to obtain the total slope.

$$B^{\Theta}i = B^{\Theta}i+1 + \frac{L_i^2}{2EI_i} (S_i + m_i \omega^2 y_i) + \frac{L_i}{EI_i} (M_i + I_{zz_i} \omega^2 B^{\Theta}i) \tag{41}$$

$$B^{\Theta}i+1 = -S_i \frac{L_i^2}{2EI_i} - M_i \frac{L_i}{EI_i} + B^{\Theta}i \left| 1 - I_{zz_i} \frac{2L_i}{EI_i} \right| - y_i \frac{M_i \omega^2 L_i^2}{2EI_i} \tag{42}$$

$$T^{O}i+1 = B^{\Theta}i+1 + \left[S_i + m_i \omega^2 y_i \right] \frac{1}{KAG_i} \tag{43}$$

$$y_i = y_{i+1} + B^{\Theta}i+1 L_i + \left(S_i + m_i \omega^2 y_i \right) \frac{L_i^3}{3EI_i} + \left(S_i + m_i \omega^2 y_i \right) \frac{L_i}{KAG_i} + \left(M_i + I_{zz_i} \omega^2 B^{\Theta}i \right) \frac{L_i^2}{2EI_i} \tag{44}$$

Substituting eq. (42) for $B^{\Theta}i+1$

$$y_{i+1} = S_i \left[\frac{L_i^3}{6EI_i} - \frac{L_i}{KAG_i} \right] + M_i \left[\frac{L_i^2}{2EI_i} \right] + B^{\Theta}i \left[-L_i + I_{zz_i} \frac{\omega^2 L_i^2}{2EI_i} \right] + y_i \left[1 + \frac{m_i \omega^2 L^3_i}{6EI_i} - \frac{L_i m_i \omega^2}{KAG_i} \right] \tag{45}$$

Using equations (40a), (41), (42), (43), and (45) a matrix can be formed as follows:

$$
\begin{array}{c}
\\
S_{i+1} \\
M_{i+1} \\
B^{\Theta}{}_{i+1} \\
T^{\Theta}{}_{i+1} \\
y_{i+1}
\end{array}
\left[\begin{array}{c|c|c|c|c}
1 & 0 & 0 & 0 & m_i \omega^2 \\
\hline
L_i & 1 & I_{zz_i}\omega^2 & 0 & m_i \omega^2 L_i \\
\hline
\dfrac{-L_i^2}{2EI_i} & \dfrac{-L_i}{EI_i} & 1-\dfrac{I_{zz_i}\omega^2 L_i}{EI_i} & 0 & \dfrac{-m_i \omega^2 L_i^2}{2EI_i} \\
\hline
\dfrac{-L_i^2}{2EI_i} + \dfrac{1}{KAG_i} & \dfrac{-L_i}{EI_i} & 1-\dfrac{I_{zz_i}\omega^2 L_i}{EI_i} & 0 & \dfrac{-m_i\omega^2 L_i^2}{2EI_i} + \dfrac{m_i^2}{KAG_i} \\
\hline
\dfrac{L_i^3}{6EI_i} - \dfrac{L_i}{KAG_i} & \dfrac{L_i^2}{2EI_i} & -L_i + \dfrac{I_{zz_i}\omega^2 L_i^2}{2EI_i} & 0 & 1 + \dfrac{m_i\omega^2 L^3{}_i}{6EI_i} - \dfrac{L_i m_i \omega^2}{KAG_i}
\end{array}\right]
\times
\left[\begin{array}{c} S_i \\ M_i \\ B^{\Theta}{}_i \\ T^{\Theta}{}_i \\ y_i \end{array}\right]
$$

This matrix is denoted by D_i. A trail frequency is then substituted into each of the section matrices, and by seccessive matrix multiplication a single matrix for the entire beam is determined.

$$D_T \quad D_n \quad D_{n-1} \ldots\ldots\ldots\ldots\ldots D_i \ldots\ldots\ldots D_1 \tag{45a}$$

The matrix D_T will look as follows:

$$
\begin{bmatrix}
N_{11} & N_{12} & N_{13} & N_{14} & N_{15} \\
N_{21} & N_{22} & N_{23} & N_{24} & N_{25} \\
N_{31} & N_{32} & N_{33} & N_{34} & N_{35} \\
N_{41} & N_{42} & N_{43} & N_{44} & N_{45} \\
N_{51} & N_{52} & N_{53} & N_{54} & N_{55}
\end{bmatrix}
$$

$$N_{14} = N_{24} = N_{34} = N_{44} = N_{54} = 0 \tag{46}$$

If the solution for a free-free beam is desired, the boundary condition is applied to the column matrix, shear (S_1) = 0 and moment (M_1) = 0, $T^{\theta}1 = B^{\theta}1$ is unknown, while $y_1 = 1$ (normalizing this end to 1.).

The D_T matrix is multiplied by the column matrix

$$\begin{vmatrix} S_n \\ M_n \\ B^{\theta}n \\ T^{\theta}n \\ y_n \end{vmatrix} = \begin{bmatrix} \quad \end{bmatrix} \begin{vmatrix} S_1 = 0 \\ M_1 = 0 \\ B^{\theta}1 = B^{\theta}1 \\ T^{\theta}1 = B^{\theta}1 \\ y_1 = 1 \end{vmatrix} \tag{47}$$

The shear and moment at the opposite end is equal to zero for a free-free beam.

$$N_{13}\ B^{\theta}1 + N_{15} = S_n = 0 \tag{48}$$

$$N_{23}\ B^{\theta}1 + N_{25} = M_n = 0 \tag{48a}$$

If the trial frequency (ω) chosen is a natural frequency, the boundary conditions will be satisfied and the determinant of equations (48) and (48a) must equal zero

$$N_{13}\ N_{25} - N_{15}\ N_{23} = 0 \tag{49}$$

If the boundary conditions are not satisfied, additional trail frequencies must be tried.

When a natural frequency has been determined, then $B^{\theta}1$ can be determined from eq. (48). The shear, moment, bending slope, total slope and deflections may now be determined at all stations.

$$\begin{vmatrix} S \\ M \\ B^{\theta} \\ T^{\theta} \\ y \end{vmatrix}_2 = \begin{bmatrix} D_1 \end{bmatrix} \begin{vmatrix} S \\ M \\ B^{\theta} \\ T^{\theta} \\ y \end{vmatrix}_1 \tag{50}$$

This is continued until the last station.

The equation will now be developed for the tri-couple structure. The outer shell of the Flight Test Missile is formed by beams "A", "C" and "D", the engine by beam "B" and the pressure tank by beam "E". This is shown in the diagram below.

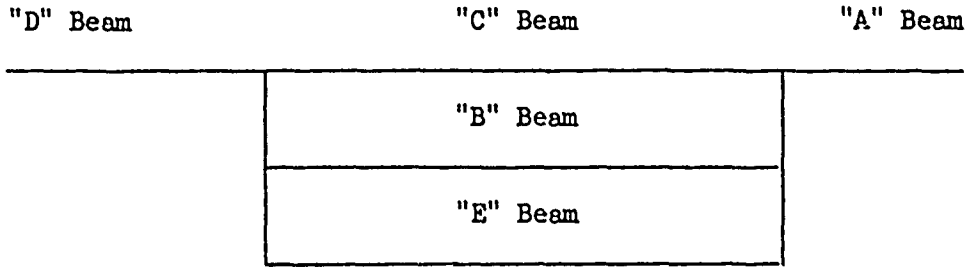


Figure 12. Beam Idealization

The product of the matrices of each beam will be noted as follows:

$A^{E}T$, $C^{D}T$, $D^{D}T$, $B^{D}T$, and $E^{D}T$ (note this is the same as eq. (45a). The elements of these matrices will be the same as shown in eq. (46), except that an additional subscript will be added for the particular beam.

"A" Beam

$$\begin{vmatrix} S_{An} \\ M_{An} \\ B^{\Theta}_{An} \\ T^{\Theta}_{An} \\ y_{An} \end{vmatrix} = \left| A^{D}T \right| \begin{vmatrix} S_{A1} = 0 \\ M_{A1} = 0 \\ B^{\Theta}_{A1} = B^{\Theta}_{A1} \\ T^{\Theta}_{A1} = B^{\Theta}_{A1} \\ y_{A1} = 1 \end{vmatrix} \tag{51}$$

The shear $(S_{A1}) = 0$ and the moment $(M_{A1}) = 0$ at the end, B^{Θ}_{A1} is the unknown slope, and y_{A1} is set equal to one in the normalizing process.

$$S_{An} = A^{N}_{13}\ B^{\Theta}_{A1} + A^{N}_{15} \tag{52}$$

$$M_{An} = A^{N}_{23}\ B^{\Theta}_{A1} + A^{N}_{25} \tag{53}$$

$$B^{\Theta}An = A^{N}_{33}\ B^{\Theta}_{A1} + A^{N}_{35} \tag{54}$$

$$T^{\Theta}An = A^{N}_{43}\ B^{\Theta}_{A1} + A^{N}_{45} \tag{55}$$

$$y_{An} = A^{N}_{53}\ B^{\Theta}_{A1} + A^{N}_{55} \tag{56}$$

All equations will be solved in terms of $B^{\theta}A1$.

"B" Beam

$$\begin{vmatrix} S_{Bn} \\ M_{Bn} \\ B^{\theta}_{Bn} \\ T^{\theta}_{Bn} \\ y_{Bn} \end{vmatrix} = \begin{bmatrix} B^{D}T \end{bmatrix} \begin{vmatrix} -S_{B1} \\ M_{B1} = 0 \\ B^{\theta}_{B1} \\ T^{\theta}_{B1} \\ y_{B1} = y_{An} \end{vmatrix} \tag{57}$$

The moment $(M_{B1}) = 0$ since the beam "B" is pin ended at this end, and the deflection at the beginning of beam "B" (y_{B1}) has to equal the deflection at the end of the "A" beam (y_{An}) since the beams are joined together at this station.

$$S_{Bn} = -B^{N}11\ S_{B1} + B^{N}13\ B^{\theta}_{B1} + B^{N}15\ y_{An} \tag{58}$$

$$M_{Bn} = -B^{N}21\ S_{B1} + B^{N}23\ B^{\theta}_{B1} + B^{N}25\ y_{An} \tag{59}$$

$$B^{\theta}_{Bn} = -B^{N}31\ S_{B1} + B^{N}33\ B^{\theta}_{B1} + B^{N}35\ y_{An} \tag{60}$$

$$T^{\theta}_{Bn} = -B^{N}41\ S_{B1} + B^{N}43\ B^{\theta}_{B1} + B^{N}45\ y_{An} \tag{61}$$

$$y_{Bn} = -B^{N}51\ S_{B1} + B^{N}53\ B^{\theta}_{B1} + B^{N}55\ y_{An} \tag{62}$$

"C" Beam

$$\begin{vmatrix} S_{Cn} \\ M_{Cn} \\ B^{\theta}_{Cn} \\ T^{\theta}_{Cn} \\ y_{Cn} \end{vmatrix} = \begin{bmatrix} C^{D}T \end{bmatrix} \begin{vmatrix} S_{C1} = S_{An} + S_{B1} + S_{E1} \\ M_{C1} = M_{An} \\ B^{\theta}_{C1} = B^{\theta}_{An} \\ T^{\theta}_{C1} = T^{\theta}_{An} \\ y_{C1} = y_{An} \end{vmatrix} \tag{63}$$

$$S_{Cn} = C^{N}11 \quad S_{An} + S_{B1} + S_{E1} + C^{N}12\ M_{An} + C^{N}13\ B^{\Theta}An + C^{N}15\ y_{An} \tag{64}$$

$$M_{Cn} = C^{N}21 \quad S_{An} + S_{B1} + S_{E1} + C^{N}22\ M_{An} + C^{N}23\ B^{\Theta}_{An} + C^{N}25\ y_{An} \tag{65}$$

$$B^{\Theta}_{Cn} = C^{N}31 \quad S_{An} + S_{B1} + S_{E1} + C^{N}32\ M_{An} + C^{N}33\ B^{\Theta}_{An} + C^{N}35\ y_{An} \tag{66}$$

$$T^{\Theta}_{Cn} = C^{N}41 \quad S_{An} + S_{B1} + S_{E1} + C^{N}42\ M_{An} + C^{N}43\ B^{\Theta}_{An} + C^{N}45\ y_{An} \tag{67}$$

$$y_{Cn} = C^{N}51 \quad S_{An} + S_{B1} + S_{E1} + C^{N}52\ M_{An} + C^{N}53\ B^{\Theta}_{An} + C^{N}55\ y_{An} \tag{68}$$

"D" Beam

$$\left| \begin{array}{l} S_{Dn} = 0 \\ M_{Dn} = 0 \\ B^{\Theta}_{Dn} \\ T^{\Theta}_{Dn} \\ y_{Dn} \end{array} \right| \quad \left[D^{D}T \right] \quad \left| \begin{array}{l} S_{D1} = S_{Bn} + S_{Cn} + S_{En} \\ M_{D1} = M_{Bn} + M_{Cn} \\ B^{\Theta}_{D1} = B^{\Theta}_{Cn} \\ T^{\Theta}_{D1} = T^{\Theta}_{Cn} \\ y_{D1} = y_{En} = y_{Cn} \end{array} \right| \tag{69}$$

Note: S_{Dn} and M_{Dn} are equal to zero since the shear and moment at this end are equal to zero.

$$S_{Dn} = D^{N}11 \left[S_{Bn} + S_{Cn} + S_{En} \right] + D^{N}12 \left[M_{Bn} + M_{Cn} \right] + D^{N}13\ B^{\Theta}_{Cn} + D^{N}15 \tag{70}$$
$$y_{En} = 0$$

$$M_{Dn} = D^{N}21 \left[S_{Bn} + S_{Cn} + S_{En} \right] + D^{N}22 \left[M_{Bn} + M_{Cn} \right] + D^{N}23\ B^{\Theta}_{Cn} + D^{N}25 \tag{71}$$
$$y_{En} = 0$$

"E" Beam

$$\begin{vmatrix} S_{En} \\ M_{En} = 0 \\ B^{\theta}_{En} \\ T^{\theta}_{En} \\ y_{En} \end{vmatrix} = \begin{bmatrix} \\ E^{D}T \\ \\ \end{bmatrix} \begin{vmatrix} -S_{El} \\ M_{El} = 0 \\ B^{\theta}_{El} \\ T^{\theta}_{El} \\ y_{El} = y_{An} \end{vmatrix} \tag{72}$$

M_{El} and M_{En} are both equal to zero since the "E" beam is hinged at each end.

$$S_{En} = -E^{N}11\ S_{El} + E^{N}13\ B^{\theta}_{El} + E^{N}15\ y_{An} \tag{73}$$

$$M_{En} = -E^{N}21\ S_{El} + E^{N}23\ B^{\theta}_{El} + E^{N}25\ y_{An} = 0 \tag{74}$$

$$B^{\theta}_{En} = -E^{N}31\ S_{El} + E^{N}33\ B^{\theta}_{El} + E^{N}35\ y_{An} \tag{75}$$

$$T^{\theta}_{En} = -E^{N}41\ S_{El} + E^{N}43\ B^{\theta}_{El} + E^{N}45\ y_{An} \tag{76}$$

$$y_{En} = -E^{N}51\ S_{El} + E^{N}53\ B^{\theta}_{El} + E^{N}55\ y_{An} \tag{77}$$

From eq. (74)

$$S_{El} = \frac{E^{N}23\ B^{\theta}_{El} + E^{N}25\ y_{An}}{E^{N}21} \tag{78}$$

$y_{En} = y_{Cn}$ (deflection of pressure tank and outer shell are equal at aft end)

Equating (77) to (68) and substituting (78)

$$C3\ B^{\theta}_{El} - C^{N}51\ S_{Bl} = C4\ B^{\epsilon}_{Al} + C5 \tag{79}$$

where $$C1 = E^{N}53 - \frac{E^{N}51\ E^{N}23}{E^{N}21} \tag{80}$$

$$C2 = E^{N}55 - \frac{E^{N}51\ E^{N}25}{E^{N}21} \tag{81}$$

$$C3 = C1 - \frac{C^{N}_{51}\, E^{N}_{23}}{E^{N}_{21}} \tag{82}$$

$$C4 = A^{N}_{13}\, C^{N}_{51} + A^{N}_{23}\, C^{N}_{52} + A^{N}_{33}\, C^{N}_{53} + A^{N}_{53}\left[C^{N}_{55} + \frac{C^{N}_{51}\, E^{N}_{25}}{E^{N}_{21}} - E^{N}_{55} + \frac{E^{N}_{51}\, E^{N}_{25}}{E^{N}_{21}} \right] \tag{83}$$

$$C5 = A^{N}_{15}\, C^{N}_{51} + A^{N}_{25}\, C^{N}_{52} + A^{N}_{35}\, C^{N}_{53} + A^{N}_{55}\left[C^{N}_{55} + \frac{C^{N}_{51}\, E^{N}_{25}}{E^{N}_{21}} - E^{N}_{55} + \frac{E^{N}_{51} E^{N}_{25}}{E^{N}_{21}} \right] \tag{84}$$

$B^{\Theta}_{Bn} = B^{\Theta}_{Cn}$ (slope of engine and outer shell are equal at aft end)

Equating (60) to (66) and substituting (78)

$$C6_{B^{\Theta}E1} + C7\, S_{B1} - B^{N}_{33}\, B^{\Theta}_{B1} - C8_{B\Theta A1} + C9 \tag{85}$$

$$C6 = \frac{C^{N}_{31}\, E^{N}_{23}}{E^{N}_{21}} \tag{86}$$

$$C7 = C^{N}_{31} + B^{N}_{31} \tag{87}$$

$$C8 = -A^{N}_{33}\, C^{N}_{31} - A^{N}_{23}\, C^{N}_{32} - A^{N}_{33}\, C^{N}_{33} + A^{N}_{53}\left[B^{N}_{35} - C^{N}_{35} - \frac{C^{N}_{31}\, E^{N}_{25}}{E^{N}_{21}} \right] \tag{88}$$

$$C9 = -A^{N}_{15}\, C^{N}_{31} - A^{N}_{25}\, C^{N}_{32} - A^{N}_{35}\, C^{N}_{33} + A^{N}_{55}\left[B^{N}_{35} - C^{N}_{35} - \frac{C^{N}_{31}\, E^{N}_{25}}{E^{N}_{21}} \right] \tag{89}$$

$y_{EN} = y_{Bn}$ (deflection of engine and pressure tank are equal at aft end)

$$C1 \quad B^{\Theta}E1 + B^{N}51\ S_{B1} - B^{N}53\ B^{\Theta}B1 = y_{An}\left[B^{N}55 - C2\right] \tag{90}$$

From eq. (79)

$$B^{\Theta}E1 = \frac{C4\ B^{\Theta}A1 + C25}{C3} + \frac{C^{N}51\ S_{B1}}{C3} \tag{91}$$

Putting eq. (91) into (90) and (85)

$$D8\ S_{B1} - B^{N}53\ B^{\Theta}B1 = C12\ B^{\Theta}A1 + C13 = K_2 \tag{92}$$

$$D1 = A^{N}53\left[B^{N}55 - C2\right] \tag{93}$$

$$D2 = A^{N}53\left[B^{N}55 - C2\right] \tag{94}$$

$$D8 = \frac{C1}{C3}\ C^{N}51 + B^{N}51 \tag{95}$$

$$C12 = D1 - \frac{C1}{C3}\ C4 \tag{96}$$

$$C13 = D2 - \frac{C1\ C5}{C3} \tag{97}$$

Eq. (91) in (85)

$$D7\ S_{B1} - B^{N}33\ B^{\Theta}B1 = C10\ B^{\Theta}A1 + C11 = K_1 \tag{98}$$

$$D7 = \frac{C6}{C3}\ C^{N}51 + C7 \tag{99}$$

$$C10 = C8 - \frac{C6\ C4}{C3} \tag{100}$$

$$C11 = C9 - \frac{C6\ C5}{C3} \tag{101}$$

Solving (98) and (92) simultaneously

$$S_{B1} = \frac{K_1 B^N_{53} - K_2 B^N_{33}}{RP} \tag{102}$$

$$B^\Theta_{B1} = \frac{K_1 D8 - K_2 D7}{RP} \tag{103}$$

$$RP = D7\ B^N_{53} - B^N_{33}\ D8 \tag{104}$$

$$S_{B1} = C14\ \Theta_{A1} + C15 \tag{105}$$

$$C14 = \frac{B^N_{53}\ C10 - B^N_{33}\ C12}{RP} \tag{106}$$

$$C15 = \frac{B^N_{53}\ C11 - B^N_{33}\ C13}{RP} \tag{107}$$

$$B^\Theta_{B1} = C16\ B^\Theta_{A1} + C17 \tag{108}$$

$$C16 = \frac{D8\ C10 - D7\ C12}{RP} \tag{109}$$

$$C17 = \frac{D8\ C11 - D7\ C13}{RP} \tag{110}$$

$$B^\Theta_{E1} = C18\ B^\Theta_{A1} + C19 \quad \text{From eq. (91)} \tag{111}$$

$$C18 = \frac{C4}{C3} + \frac{C^N_{51}}{C3}\ C14 \tag{112}$$

$$C19 = \frac{C5}{C3} + \frac{C^N_{51}}{C3}\ C15 \tag{113}$$

$$S_{E1} = C20\ B^\Theta_{A1} + C21 \quad \text{From eq. (78)} \tag{114}$$

$$C20 = \frac{E^N_{23}\ C18}{E^N_{21}} + \frac{E^N_{25}\ A^N_{53}}{E^N_{21}} \tag{115}$$

$$C21 = \frac{E^N_{23}\ C19}{E^N_{21}} + \frac{E^N_{25}\ A\ 55}{E^N_{21}} \tag{116}$$

$$S_{Bn} = C24\ B^\Theta_{A1} + C25 \quad \text{From eq. (58)}$$

$$C24 = -B^{N}11\ C14 + B^{N}13\ C16 + B^{N}15\ A^{N}53 \tag{117}$$

$$C25 = -B^{N}11\ C15 + B^{N}13\ C17 + B^{N}15\ A^{N}55 \tag{118}$$

$$S_{En} = C22\ B^{\Theta}A1 + C23 \qquad \text{From eq. (73)} \tag{119}$$

$$C22 = -E^{N}11\ C20 + E^{N}13\ C18 + E^{N}15\ A^{N}53 \tag{120}$$

$$C23 = -E^{N}11\ C21 + E^{N}13\ C19 + E^{N}15\ A^{N}55 \tag{121}$$

$$S_{Cn} = C26\ B^{\Theta}A1 + C27 \qquad \text{From eq. (64)} \tag{122}$$

$$C26 = C^{N}11\left[A^{N}13 + C14 + C20\right] + C^{N}12\ A^{N}23 + C^{N}13\ A^{N}33 + C^{N}15\ A^{N}53 \tag{123}$$

$$C27 = C^{N}11\left[A^{N}15 + C15 + C21\right] + C^{N}12\ A^{N}25 + C^{N}13\ A^{N}35 + C^{N}15\ A^{N}55 \tag{124}$$

$$M_{Cn} = C28\ B^{\Theta}A1 + C29 \qquad \text{From eq. (65)} \tag{125}$$

$$C28 = C^{N}21\left[A^{N}13 + C14 + C20\right] + C^{N}22\ A^{N}23 + C^{N}23\ A^{N}33 + C^{N}25\ A^{N}53 \tag{126}$$

$$C29 = C^{N}21\left[A^{N}15 + C15 + C21\right] + C^{N}22\ A^{N}25 + C^{N}23\ A^{N}35 + C^{N}25\ A^{N}55 \tag{127}$$

$$M_{Bn} = C30\ B^{\Theta}A1 + C31 \qquad \text{From eq. (59)} \tag{128}$$

$$C30 = -B^{N}21\ C14 + B^{N}23\ C16 + B^{N}25\ A^{N}53 \tag{129}$$

$$C31 = -B^{N}21\ C15 + B^{N}23\ C17 + B^{N}25\ A^{N}55 \tag{130}$$

$$S_{C1} = C32\ B^{\Theta}A1 + C33 \qquad \text{From eq. (63)} \tag{131}$$

$$C32 = A^{N}13 + C14 + C20 \tag{132}$$

$$C33 = A^{N}15 + C15 + C20 \tag{133}$$

$$S_{D1} = C34\ B^{\Theta}A1 + C35 \qquad \text{From eq. (69)} \tag{134}$$

$$C34 = C22 + C24 + C26 \tag{135}$$

$$C35 = C23 + C25 + C27 \tag{136}$$

$$M_{D1} = C36\ B^{\Theta}A1 + C37 \qquad \text{From eq. (69)} \tag{137}$$

$$C36 = C30 + C28 \tag{138}$$

$$C37 = C31 + C29 \tag{139}$$

$$B^{\hat{\Theta}}Cn = C38\ B^{\Theta}A1 + C39 \qquad \text{From eq. (66)} \tag{140}$$

$$C38 = C^{N}31\left[A^{N}13 + C14 + C20\right] + C^{N}32\ A^{N}23 + C^{N}33\ A^{N}33 + C^{N}35\ A^{N}53 \tag{141}$$

$$C39 = C^{N}31\left[A^{N}15 + C15 + C21\right] + C^{N}32\ A^{N}25 + C^{N}33\ A^{N}35 + C^{N}35\ A^{N}55 \tag{142}$$

$$y_{En} = C40\ B^{\Theta}A1 + C41 \qquad \text{From eq. (73)} \tag{143}$$

$$C40 = -E^{N}51\ C20 + E^{N}53\ C18 + E^{N}55\ A^{N}53 \tag{144}$$

$$C41 = -E^{N}51\ C21 + E^{N}53\ C19 + E^{N}55\ A^{N}55 \tag{145}$$

$$S_{Dn} = C70\ B^{\Theta}A1 + C71 = 0 \qquad \text{From eq. (70)} \tag{146}$$

$$C70 = D^{N}11\ C34 + D^{N}12\ C36 + D^{N}13\ C38 + D^{N}15\ C40 \tag{147}$$

$$C71 = D^{N}11\ C35 + D^{N}12\ C37 + D^{N}13\ C39 + D^{N}15\ C41 \tag{148}$$

$$M_{Dn} = C72\ B^{\Theta}A1 + C73 = 0 \qquad \text{From eq. (71)} \tag{149}$$

$$C72 = D^{N}21\ C34 + D^{N}22\ C36 + D^{N}23\ C38 + D^{N}25\ C40 \tag{150}$$

$$C73 = D^{N}21\ C35 + D^{N}22\ C37 + D^{N}23\ C39 + D^{N}25\ C41 \tag{151}$$

The determinant of equations (146) and (149) must equal zero for a natural frequency.

$$C70\ B^{\Theta}A1 + C71 = 0$$

$$C72\ B^{\Theta}A1 + C73 = 0$$

$$C70\ C73 - C71\ C72 = 0 \tag{152}$$

$$B^{\Theta}A1 = - \frac{C71}{C70} \tag{153}$$

$$B^{\Theta}A1 = - \frac{C73}{C72} \tag{154}$$

A trial frequency is chosen and when equation (152) is satisfied, then a natural frequency has been determined. The next problem is to determine the shear, moment, bending slope, total slope, and deflection for each of the beams. If the first column matrix is determined for each of the beams, then the data for each station can be determined as explained by eq. (50).

The first column matrix for each beam is:

Beam "A"

$$\begin{vmatrix} S_{A1} = 0 \\ M_{A1} = 0 \\ B^{\Theta}A1 = - \frac{C71}{C70} \\ T^{\Theta}A1 = B^{\Theta}A1 \\ y_{A1} = 1 \end{vmatrix}$$

Beam "B"

$$\begin{vmatrix} -S_{B1} = -C14\ B^{\Theta}A1 - C15 \\ M_{B1} = 0 \\ B^{\Theta}B1 = C16\ B^{\Theta}A1 + C17 \\ T^{\Theta}B1 = C16\ B^{\Theta}A1 + C17 \\ y_{B1} = A^{N}53\ B^{\Theta}A1 + A^{N}55 \end{vmatrix}$$

Beam "C"

$$\begin{vmatrix} S_{C1} = C32\ B^{\Theta}A1 + C33 \\ M_{C1} = A^{N}23\ B^{\Theta}A1 + A^{N}25 \end{vmatrix}$$

$$B^{\Theta}C1 = A^{N}33\ B^{\Theta}A1 + A^{N}35$$
$$T^{\Theta}C1 = B^{\Theta}C1$$
$$y_{C1} = A^{N}53\ B^{\Theta}A1 + A^{N}55$$

Beam "D"

$$S_{D1} = C34\ B^{\Theta}A1 + C35$$
$$M_{D1} = C36\ B^{\Theta}A1 + C37$$
$$B^{\Theta}D1 = C38\ B^{\Theta}A1 + C39$$
$$T^{\Theta}D1 = C38\ B^{\Theta}A1 + C39$$
$$y_{D1} = C40\ B^{\Theta}A1 + C41$$

Beam "E"

$$-S_{E1} = -C20\ B^{\Theta}A1 - C21$$
$$M_{E1} = 0$$
$$B^{\Theta}E1 = C18\ B^{\Theta}A1 + C19$$
$$T^{\Theta}E1 = B^{\Theta}E1$$
$$y_{E1} = A^{N}53\ B^{\Theta}A1 + A^{N}55$$

MODAL CALCULATIONS FOR

DYNAMICALLY IDEALIZED FLIGHT TEST MISSILE

Figs. 13, 14, and 15 show brief sketches of the Flight Test Missile composed of an outer shell (A), the engines (B), and the pressure tank (C). The idealized structure is snown in fig. 16. Beam "A" is the outer shell which is free at each end; Beam "B" the engine, is fixed at the right end and pinned at the left, and Beam "C" is the pressure tank that is pinned at each end. Each beam has a varying mass distribution (M).

The first two normal bending modes were calculated as 486 cps and 27.8 cps, respectively, representing the launch condition. These modes could also be interpreted as lateral modes because of general symmetry about the longitudinal axis. Fig. 17 shows the 1st mode shape, slope and frequency, while fig. 18 shows the mode shape and slope on a larger scale in the vicinity of the engine. The second mode similarly is presented in figs. 19 and 20.

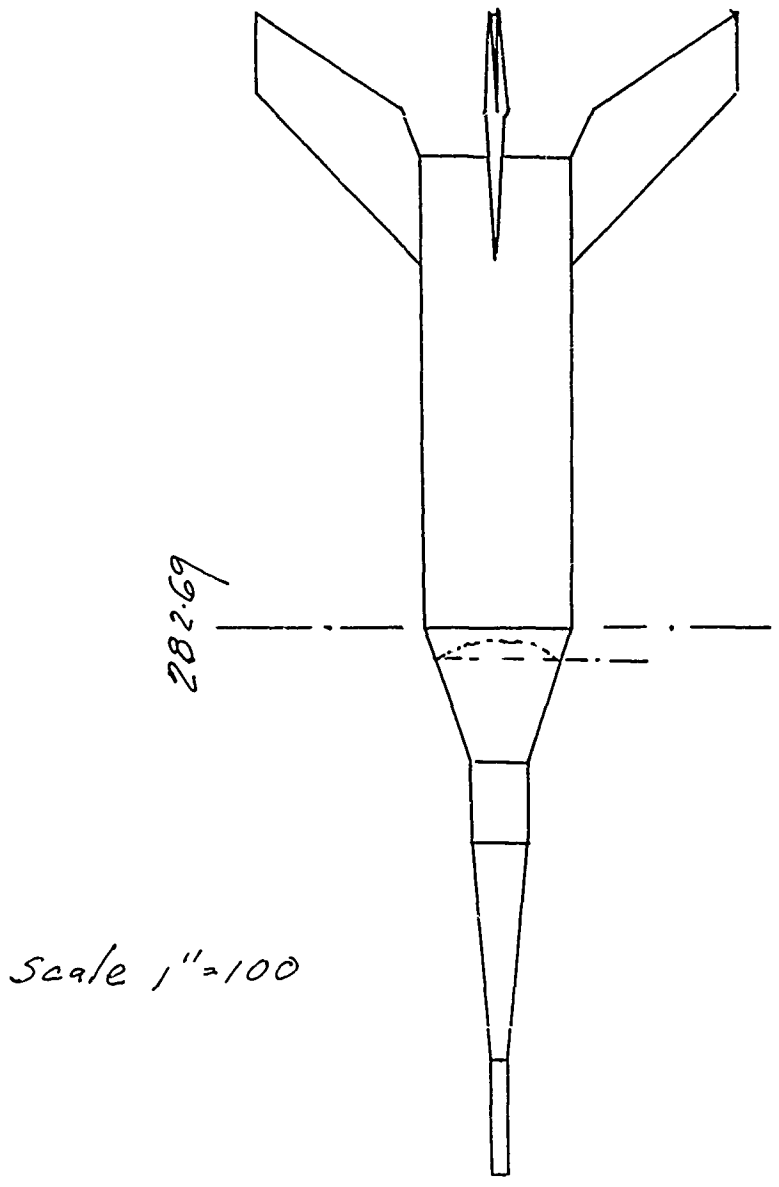


Figure 13. Flight Test Missile

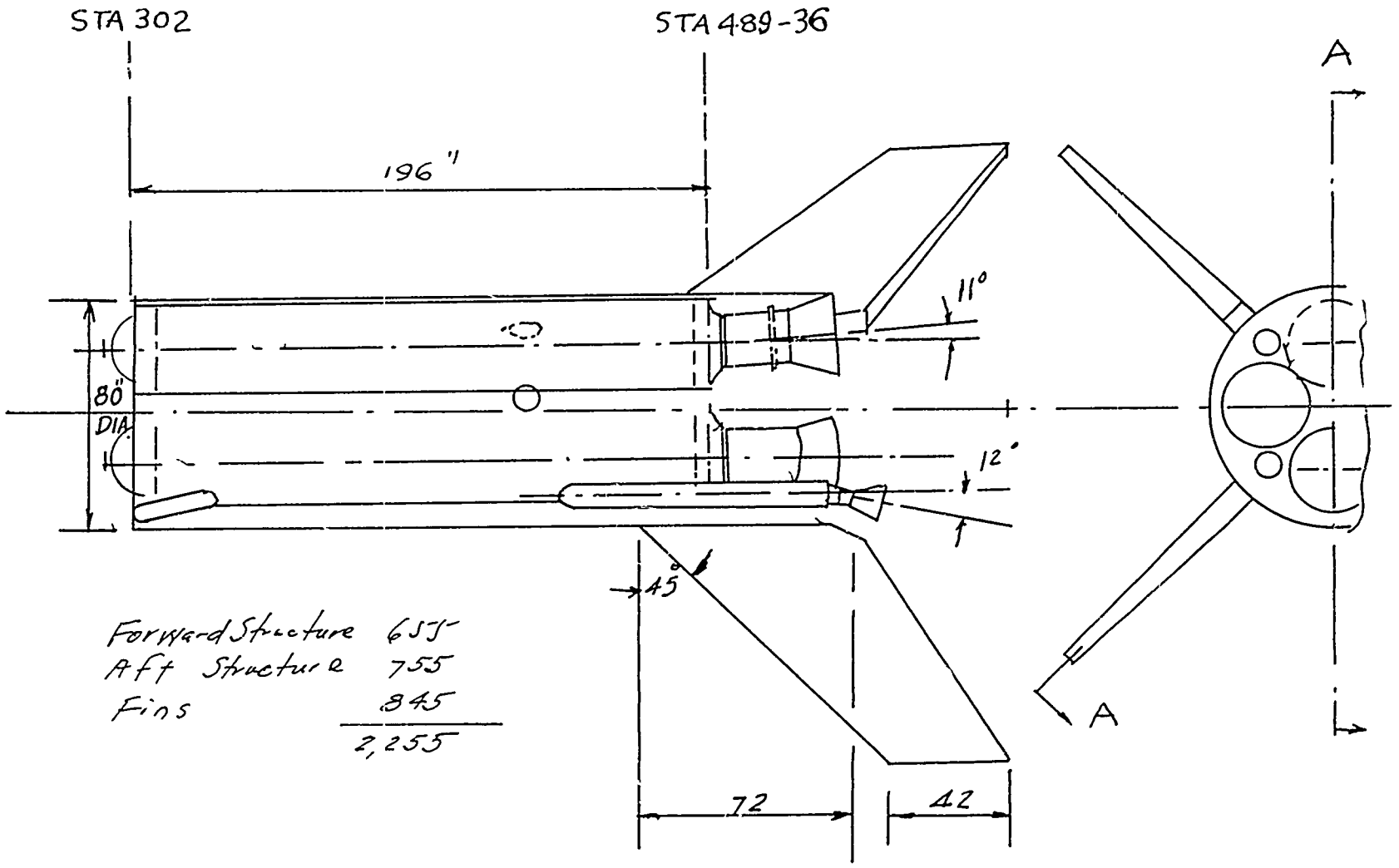


Figure 14. Solid Boosters of Flight Test Missile

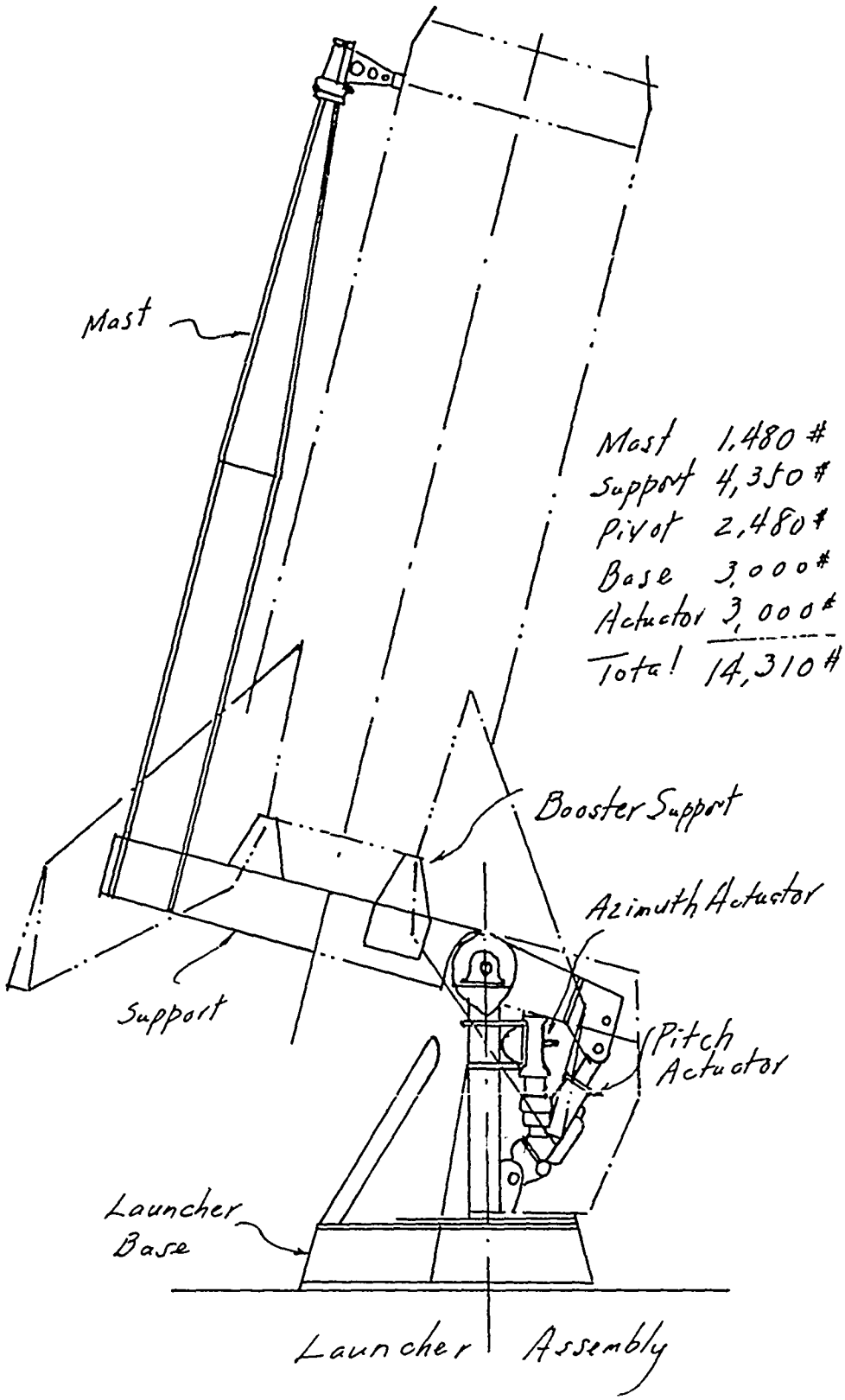


Figure 15. Launcher

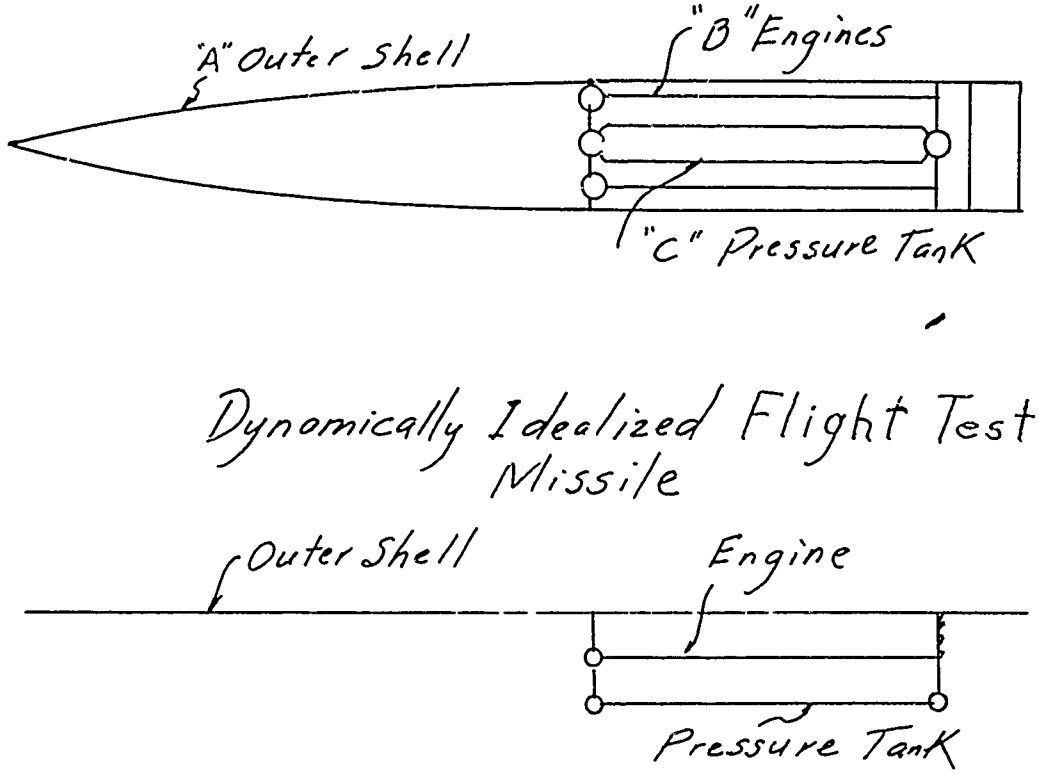


Figure 16. Dynamically Idealized Structure

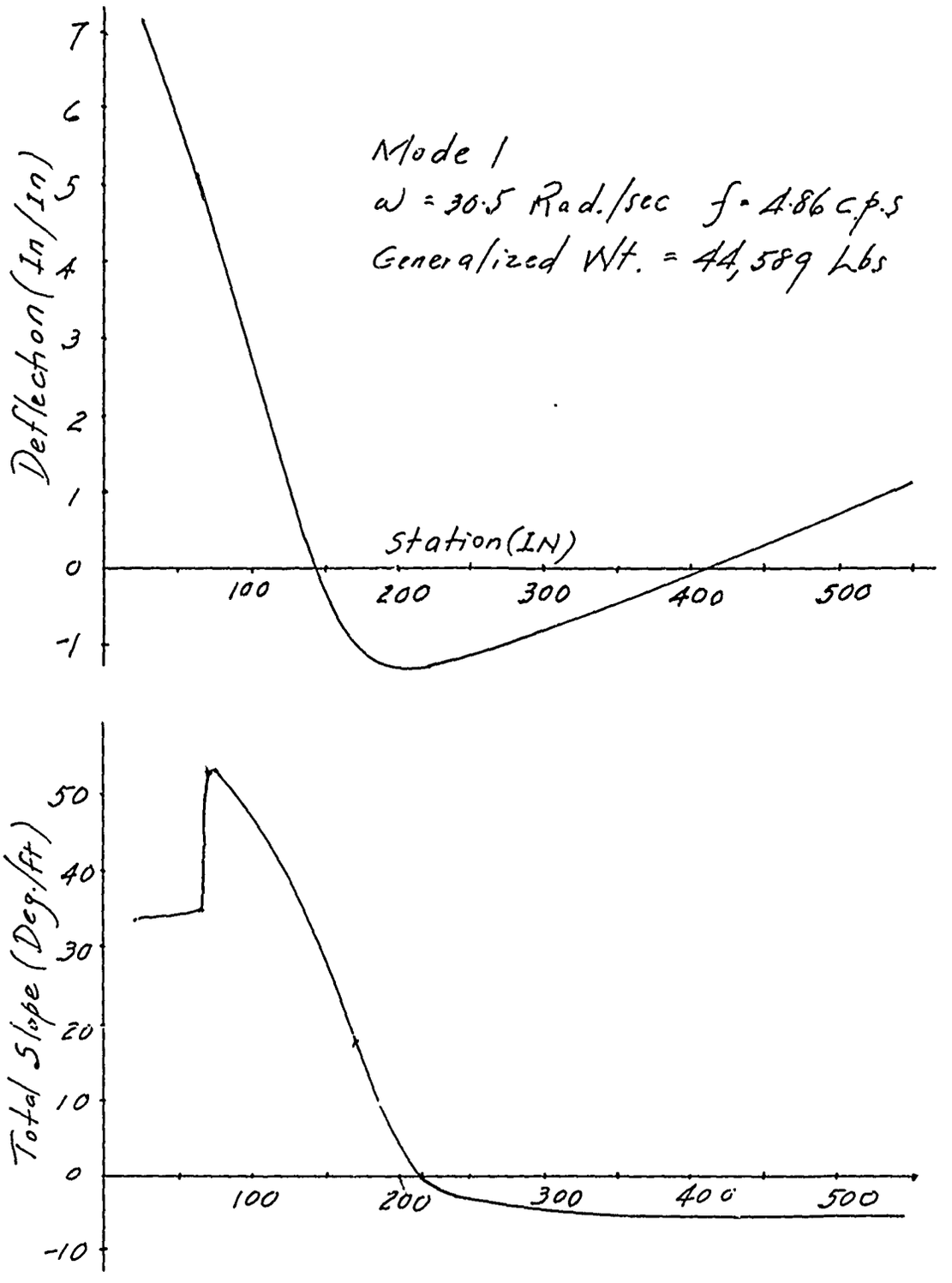


Figure 17. Missile, Mode 1

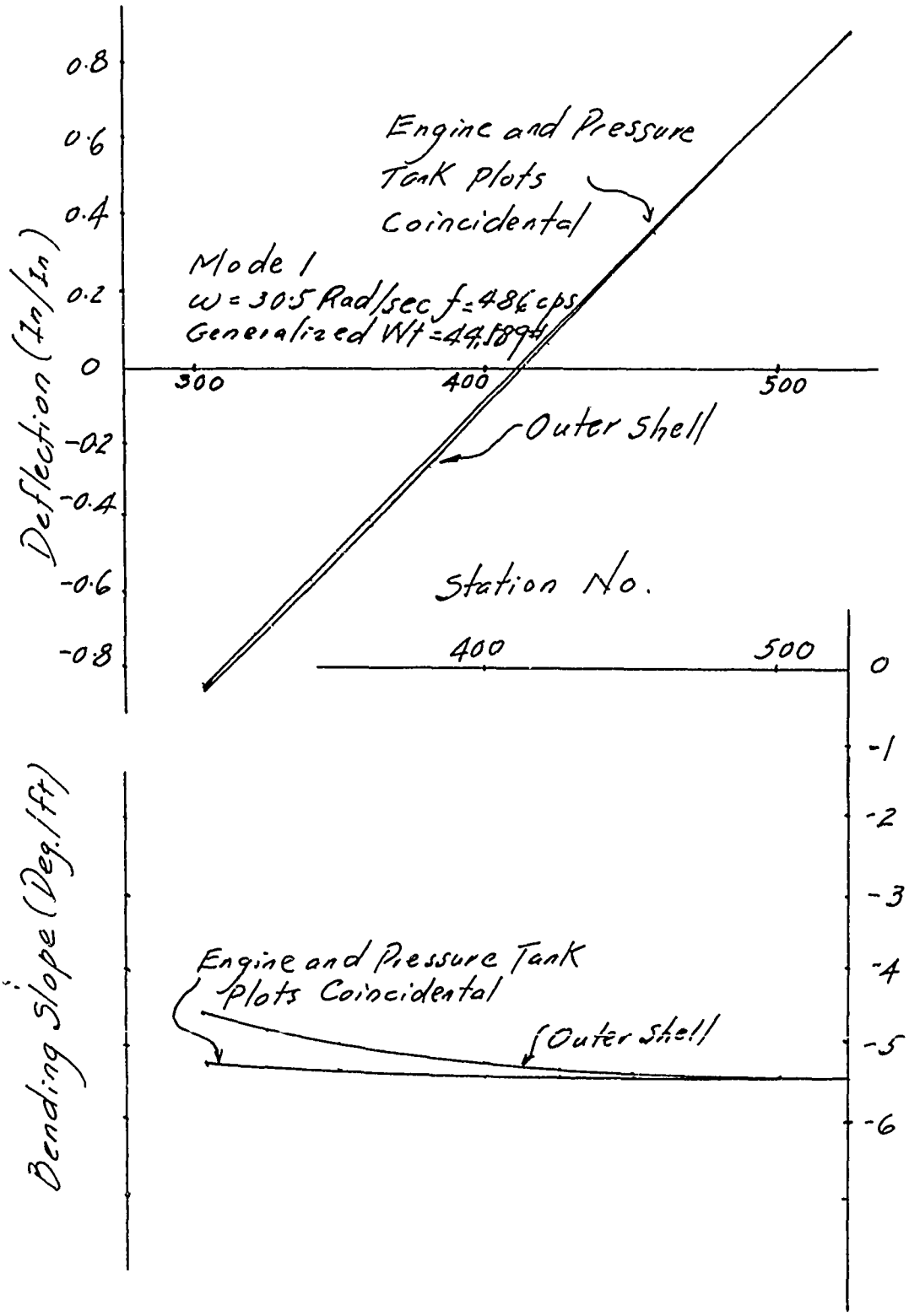


Figure 18. Enlarged Section of Missile Tankages, Mode 1

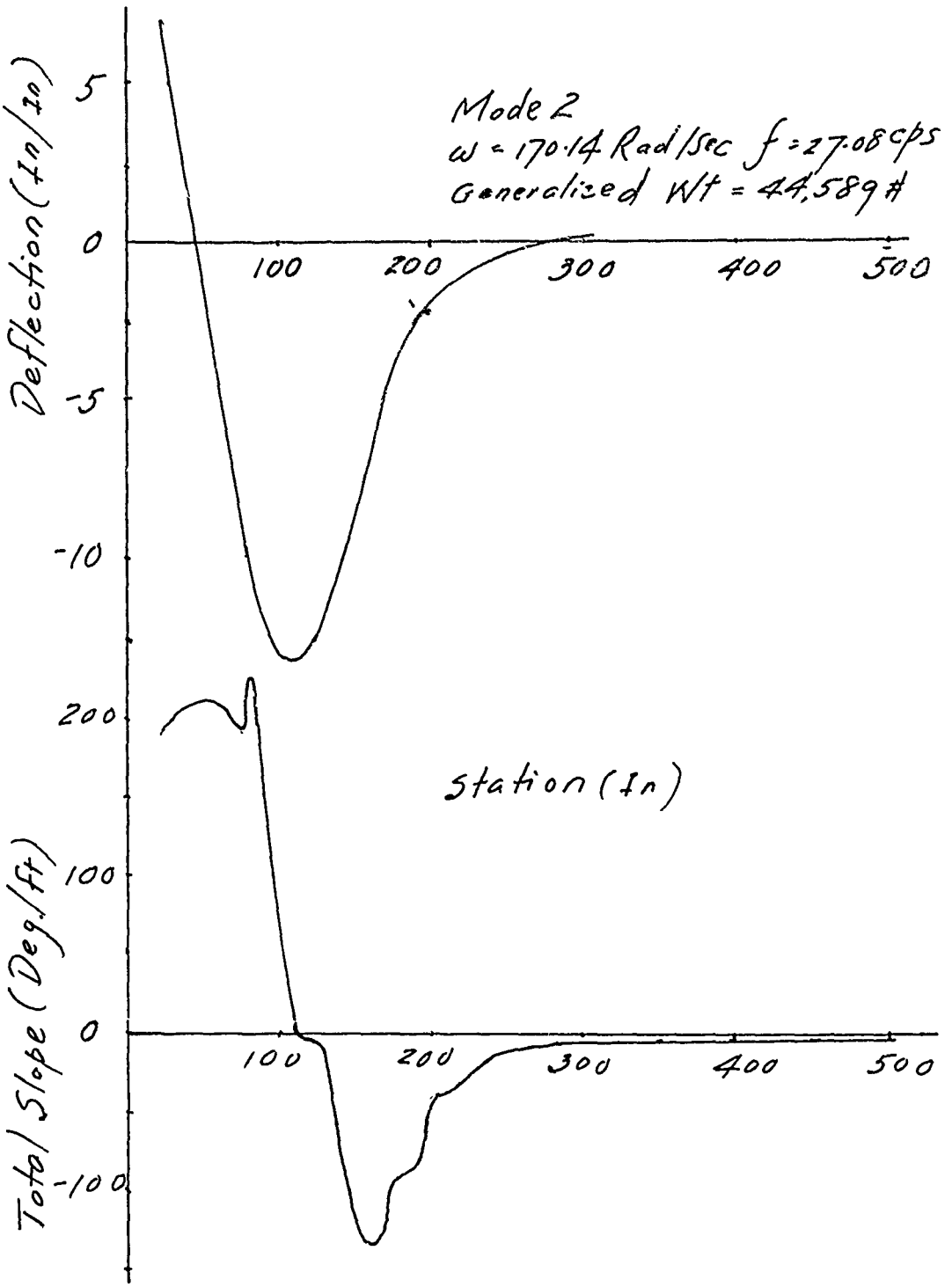


Figure 19. Missile, Mode 2

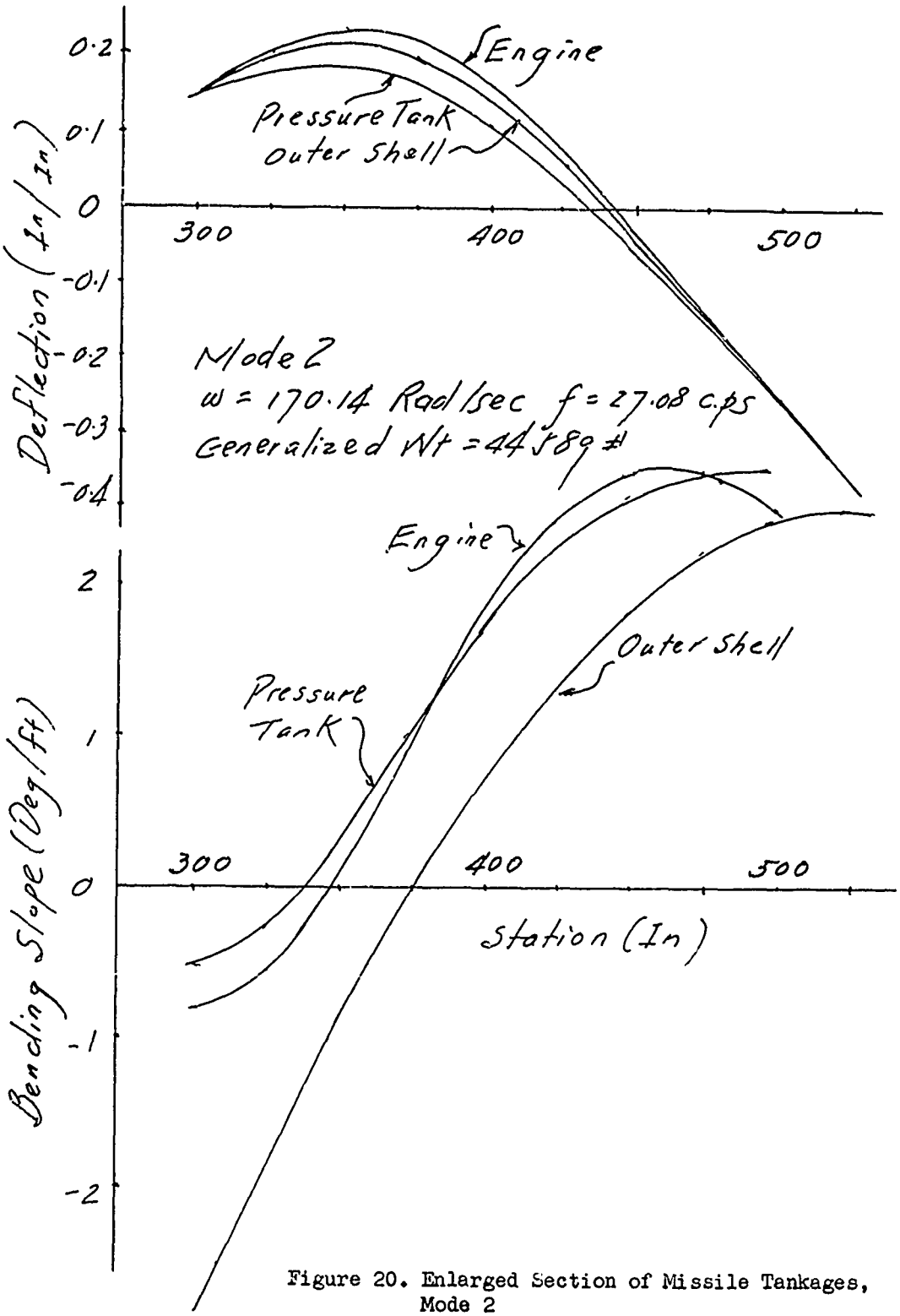


Figure 20. Enlarged Section of Missile Tankages, Mode 2

SECTION V RECOMMENDATIONS FOR FUTURE RESEARCH AND TEST PROGRAMS

Since the vibration characteristics of trusses, cylinders, and clustered cylinders have an important bearing on fuel sloshing, dynamic buckling and dynamic loads, acoustic fatigue and control systems, well planned efforts for the research and test program are warranted. The cost of such a research program may be large, but if the efforts are well coordinated between the various government agencies, universities and private industries, the objectives can be achieved at a much earlier date and with much less expense by cutting out the duplications and redundancies that may be initiated in various organizations.

TRUSSES

Simple statically determinate trusses with hinged joints which have been presented involve no great task, but in reality and in fabrication methods, no true three-dimensional hinged joint can be made. The various members coming into a joint may be connected together with gusset plates in various directions. In light aircraft structures a secondary stress introduced in these rigid joints can exceed the primary stress in light weight members. Especially under large thermal gradients, the joints would be twisted in various directions and stresses thereby introduced can be as large as the primary stresses. So actually, most of the statically determinant members are under a combined loading of moment and axial stress and this beam column action may cause additional weight to be added to the structural design. Trusses have been widely used in the Dyna-Soar program. Even though nothing has been published to date, we are sure that at the conclusion of the Dyna-Soar program many important analytical results and test data on trusses will be made known.

Besides the simple truss illustrated in the previous section, the support conditions of trusses presents a difficult problem. In many cases, trusses form an integral part of a combined shell and truss structure. In lifting body re-entry vehicles, it is especially hard to separate the body and truss structure because the trusses are connected and supported by frames of different shapes. It is highly desirable to study the vibration and stiffness characteristics of three-dimensional truss shell structures and initiate a test program to check out the analytical results with and without the presence of thermal gradients.

CYLINDERS

Thus far we have seen a mathematical approach and an engineering approach for simple shells cantilevered at one end. In actual practice, none of the flight vehicles are cantilevered or in a simple cylindrical form. Many of them will have bulkheads, diaphragms, domes and hemispherical ends, and some of them may be pressurized. Also, many of them may have hatches, air locks and cutouts, various space radiators, and auxiliary equipment. Analytical methods for these kinds of configurations will be much more involved and in certain instances cannot be completely solved. Since the mode shapes of such complicated cylinders are hard to interpret without having first an analytical solution, it is desirable that we conduct more mathematical and engineering analyses before we undertake scale model tests.

CONICAL SHELLS

In many large boosters the staging adapters are mostly in conical shapes. It will be hard to understand the overall behavior of the booster staging without knowing the individual behavior of the conical shells. In adapters, sections which, for example, house an engine compartment, the stabilizing pressures which are found in many of the booster tankages are not available to resist the vibration, motion and acoustic excitation imposed upon them. As the diameters of the boosters become larger, and engine thrust becomes bigger, it will be quite important to understand the characteristics of the conical shells to avoid failure from vibrational and acoustical environment.

MULTIPLE STAGE CYLINDERS

Thus far we have tried to understand the vibration and stiffness of individual cylinders and adapters. Since most of the booster stagings are made of many individual cylinders and adapters, a complete understanding of their multiple staging is even a greater task. If the individual stages are well analyzed and known, the multiple stages can be solved accurately if the matrices are partitioned properly and good precision is retained. For small cylinders, experimental methods and techniques present no great problem if frequencies and mode shapes are known beforehand, since the shakers and recorders can be programmed accurately to the analytical modes. These tests can be made either in a laboratory or in an open test stand. As boosters become large, full scale test is almost impossible, and methods for simulating joint fixity and staging connection are extremely difficult even in scalemodel testing.

CLUSTERED CYLINDERS

The biggest problem in the analysis of clustered cylinders lies in the computing capacity and mathematical precision. The difficulties encountered in the complete dynamic analysis of clustered cylinders do not lie solely in the modal analysis. In many solids and liquids the thrust variation and asymmetrical burning and viscoelastic characteristics of solid fuel make the complete understanding of the booster dynamics fairly difficult. Since large clustered liquid and solid boosters are being programmed, it is highly desirable that both governmental and private industries put additional emphasis on vibration and stiffness prediction methods and their accompanying tests.

CONCLUSION

The above presentation is a simple and brief summary of the mathematical and engineering approaches and prediction of the vibration and stiffness characteristics of trusses, shells and clustered cylinders. It is by no means complete and exhaustive; it only serves to excite, extract, and develop interest among governmental and private industries so that additional attention can be centered on analytical and experimental research. Since the task is gigantic and the cost is high, we sincerely hope that a strong cooperative effort between different agencies will solve the problems at an earlier date.

The effects of end shortening have no great influence on vibration frequencies when the length to diameter ratio is small. In multiple stage cylinders, the picture may change and its effects are being investigated.

ACKNOWLEDGMENT

The authors are very thankful to Mr. L. Nogawski for his contribution of the Flight Test Missile modal analysis and to Mrs. Louise Holmes for her contribution of typing.

REFERENCES

1. Argyris, J. H., Energy Theorems and Structural Analysis, Part I General Theory, Aircraft Engineering, Vol. XXVI, October, November, 1954. Vol. XXVII, February, March, April, May 1955.

2. Turner, M. J., Clough, R. W., Martin, H. C., Topp, L. J., Stiffness and Deflection Analysis of Complex Structures, Journal of Aeronautical Science, Vol. 23, No. 9, September 1956. pp. 805.

3. Turner, M. J., Dill, E. H., Martin, H. C., Melosh, R. J., Large Deflections of Structures Subjected to Heating and External Loads, Journal of the Aeronautical Science, Vol. 27, No. 2, February 1960. pp. 97.

4. Wong, C. K., Matrix Analysis of Statically Indeterminate Trusses, Proc. American Soc. C. E., Vol. 85, No. ST 3, Part 2, March 1959. pp. 23.

5. Parcel, J. J., and Maney, G. A., An Elementary Treatise on Statically Indeterminate Stresses, John Wiley & Sons, 1944.

6. Kalnins, A., and Naghdi, P. M., Axisymmetric Vibrations of Shallow Elastic Spherical Shells, Journal of the Acoustic Society of America, Vol. 32, No. 3, March 1960.

7. Greenspan, J. E., Vibrations of a Thick Walled Cylindrical Shell Journal of the Acoustic Society of America, Vol. 32, No. 5, May 1960.

8. Saunders, H., and Poolay, P. R., Inextensional Vibrations of a Sphere-Cone Shell Combination, Journal of the Acoustical Society of America, Vol. 31, No. 5, May 1959.

9. Fung, Y. C., Sechler, E. E., and Kaplan, H., On the Vibration of Thin Cylindrical Shells Under Internal Pressure, September 1957.

10. Arnold, R. N., and Warburton, G. B., Flexural Vibrations of the Walls of Thin Cylindrical Shells Having Freely Supported Ends, Proceedings of the Royal Society (London) Series A, Vol. 197, 1949. pp. 238.

11. Arnold, R. N., and Warburton, G. B., The Flexural Vibrations of Thin Cylinders, Journal and Proceedings of the Institution of Mechanical Engineers (London), Vol. 167, 1953. pp. 62-74.

12. Baron, M. S., and Bleich, H. H., Tables for Frequencies and Modes of Free Vibration of Infinitely Long Thin Cylindrical Shells, Trans. ASME, Vol. 21, No. 2, Journal of Applied Mechanics, June 1954. pp. 178-184.

13. Steven, M., Breathing Vibrations of a Cylindrical Membrane Under Internal Pressure, Convair Memo DC-7-057, Convair, San Diego, 1954.

14. Serbin, H., Breathing Vibrations of a Pressurized Cylindrical Shell, Report No. A-Atlas-152, Convair, San Diego, January 1955.

15. Reissner, E., Non-Linear Effects in Vibrations of Cylindrical Shells, Aeromechanics Report No. AM5-6, Ramo-Wooldridge Corp., August 1955.

16. Reissner, E., On Transverse Vibration of Thin Shallow Elastic Shells, Quarterly of Appl. Math., Vol. 13, No. 2, July 1955. pp. 169-176.

17. Fung, Y. C., On the Vibration of Thin Cylindrical Shells Under Internal Pressure, Aeromechanics Report No. AM5-8, Ramo-Wooldridge Corp., October 1955.

18. Tobias, S. A., A Theory of Imperfection for the Vibration of Elastic Bodies of Revolution, Eng. Vol., 172, 1951. pp. 409.

19. Grogolyuk, E. E., Small Oscillations of Thin Resilient Conical Shells, NASA TT F-25, May 1960.

20. Shulman, Yechiel, Vibration and Flutter of Cylindrical and Conical Shells, OSR Tech. Report No. 59-776.

21. Herrmann, G., and Mirsky, I., On Vibrations of Conical Shells, JAS 25.7 1958. pp. 451-458.

22. Partridge, G. R., Modes of Vibrations of a Loudspeaker Cone, Ph. D. Thesis, Yale 1950.

23. Federhofer, K., Eigenschwingungen der Kegelschale, Ingenieur-Archiv, 9, 1938. pp. 288-304.

25. Przemieniecki, J. S., Matrix Analysis of Shell Structures With Flexible Frames, The Aeronautical Quarterly, Vol. IX, November 1958. pp. 361.

26. Hoff, N. J., Salerno, V. L., and Beley, B. A., Shear Stress Concentration and Moment Reduction Factors for Reinforced Monocoque Cylinders Subjected to Concentrated Radial Loads, Journal of the Aeronautical Sciences, Vol. 16, May 1949.

27. Kuhn, P., Duberg, J. F., Griffith, G. E., The Effect of Concentrated Loads on Flexible Rings in Circular Shells, NACA AAR No. L5H23, 1945.

28. Jensen, W. R., On Simplified Fuselage-Structure Stress Distributions, Journal of the Aeronautical Sciences, Vol. 25, No. 10, October 1958. pp. 656.

29. Argyris, J. H., and Kelsey, S., The Analysis of Fuselages of Arbitrary Cross Section and Taper, Aircraft Engineering, March 1959.

A CONSIDERATION OF THE SIMILARITY REQUIREMENTS FOR AEROTHERMOELASTIC TESTS ON REDUCED SCALE MODELS

W. G. Molyneux

Royal Aircraft Establishment

ABSTRACT

The similarity requirements for model tests are established and different possibilities with regard to relaxations of these requirements are examined with the aim of devising an acceptable experimental technique for representative tests on models of reduced scale.

It appears that the representation of heating effects must of necessity be rather crude, but may nevertheless be adequate for aerothermoelastic research. Test techniques that provide a reasonably close representation of flight conditions require tunnels with heated flow and with subsidiary radiant heat in the working section. Failing this, models can be constructed with an effective stiffness representative of heated conditions for tests in conventional facilities.

This paper has been prepared for the A.S.D. symposium on Aerothermoelasticity at Dayton, Ohio, U.S.A. - Oct. 1961.

LIST OF SYMBOLS

a,b,c	displacements
B	suffix relating to body properties
c_B, c_P	specific heat
d_x	insulation thickness
E	Young's modulus
F	suffix denoting full scale
g	acceleration due to gravity
h	heat transfer coefficient
k, k_B	thermal conductivity
L	length
M	Mach number; suffix denoting model scale
p	pressure
Pr	Prandtl number
r	exponent of Reynold's number in heat transfer formulation
R_x	radiant heating rate
s	exponent of temperature ratio in heat transfer formulation
s_ϕ	exponent of temperature for temperature dependent property ϕ
t	time
T	temperature

LIST OF SYMBOLS (Cont'd.)

(T_o-T)	temperature difference; temperature change
T_{aw}	adiabatic wall temperature
T_a	free stream temperature
T_w	skin temperature
u,v,w	velocities
V	flow velocity
x,y,z	rectangular co-ordinates
α	coefficient of thermal expansion
γ	ratio of specific heats for gases
δ	skin thickness : typical length
ε	emissivity
λ	ratio aircraft property : model property
μ	viscosity
ρ , ρ_B	density
σ , σ_x , σ_y , σ_z	stress components
$\bar{\sigma}$	Stefan-Boltzmann radiation constant
τ_{xy}, τ_{xz}, τ_{yz}	shearing stress components
ν	Poisson's ratio

A CONSIDERATION OF THE SIMILARITY REQUIREMENTS FOR AEROTHERMOELASTIC TESTS ON REDUCED SCALE MODELS

INTRODUCTION

The problem of the simulation of aerodynamic and structural parameters between an aircraft and a scale model for an adequate representation of aeroelastic effects is one with which the aeroelastic engineer is well familiar. In the absence of kinetic heating effects, a degree of representation that is adequate for engineering purposes can generally be achieved without too much difficulty, and this, coupled with the inherent advantages of model tests in providing data in flow regimes where there are analytical difficulties, has led to an extensive use of scale representative models for aeroelastic work, particularly for flutter investigations. It is probably true to say that wind tunnel aeroelastic model tests are now accepted as an essential part of flutter clearance procedures for all aircraft with a supersonic capability. However, the effects of kinetic heating are not generally simulated using current techniques, and although this has imposed no serious limitation as yet it is apparent that some account must be taken of heating effects for future generations of high speed aircraft (Ref. 1).

Kinetic heating will have its influence on aeroelastic properties primarily by modifying the structural stiffnesses and the effect on stiffness will be in two forms; namely, a stiffness loss due to a degradation of material properties with temperature, and a loss resulting from an unfavourable stress distribution due to thermal expansion. The effect of thermal stress may far exceed the effect of material degradation, it may be at its worst during the transient heating stage of the structure, and it generally results in a structural stiffness that is non-linear with displacement (Refs. 2 and 3).

The aeroelastic engineer inevitably strives for the ideal in which these thermal effects, together with the aerodynamic and structural properties of the full scale aircraft are represented to model scale, since in this circumstance model test results and supporting calculations provide the best grounds for confidence in

full scale behaviour. A number of investigations have been made of the similarity parameters that need to be satisfied for this ideal to be realised (Refs.4, 5 and 6), but the outcome is far from encouraging. It appears that complete similarity can only be realised for a scale ratio of 1 : 1, and attempts to circumvent this difficulty by relaxations in some of the similarity requirements have not, as yet, led to a generally acceptable approach for aerothermoelastic model tests.

Accordingly, in what follows the similarity requirements are re-considered with a view to establishing generally acceptable (though possibly fairly crude) techniques for aerothermoelastic model tests. This consideration shows that techniques are practicable in which either models in the same materials as the aircraft are tested in a gas other than air to the same scale of temperature as the aircraft, or models in different materials than the aircraft are tested in air to a different scale of temperature. In both cases an approximation to overall similarity can best be obtained by providing controlled radiant heat in the tunnel working section to supplement the heating provided by the gas flow.

In the absence of heated flow tunnels, the best that can be done is to design models with reduced stiffness representative of heating effect for tests in 'cold' flow. However, a simple "effective" stiffness concept may not be adequate for all types of structure and work is required to establish the limitations of this approach.

SECTION 1: DETERMINATION OF THE SIMILARITY RELATIONSHIPS

The similarity parameters that need to be satisfied for aerothermoelastic work can conveniently be established from a consideration of the general equations for stress, displacement and temperature distribution of a body immersed in a hot, flowing gas.

The boundary layer flow of a viscous compressible perfect gas is described by the equations of motion, energy, continuity and state (Ref.7).

A typical equation from the three equations of motion is

$$\rho\left(\frac{\partial u}{\partial t}+u\frac{\partial u}{\partial x}+v\frac{\partial u}{\partial y}+w\frac{\partial u}{\partial z}\right)=-\frac{\partial p}{\partial x}+\mu\left(\frac{\partial^2 u}{\partial x^2}+\frac{\partial^2 u}{\partial y^2}+\frac{\partial^2 u}{\partial z^2}\right)$$

$$+\frac{\mu}{3}\frac{\partial}{\partial x}\left(\frac{\partial u}{\partial x}+\frac{\partial v}{\partial y}+\frac{\partial w}{\partial z}\right)$$

$$-\frac{2}{3}\frac{\partial \mu}{\partial x}\left(\frac{\partial u}{\partial x}+\frac{\partial v}{\partial y}+\frac{\partial w}{\partial z}\right)$$

$$+2\frac{\partial \mu}{\partial x}\frac{\partial u}{\partial x}+\frac{\partial \mu}{\partial y}\left(\frac{\partial u}{\partial y}+\frac{\partial v}{\partial x}\right)+\frac{\partial \mu}{\partial z}\left(\frac{\partial u}{\partial z}+\frac{\partial w}{\partial x}\right)$$

$$-\rho g_x\left(\frac{T-T_o}{T_o}\right). \qquad (1)$$

The equation of energy is

$$\rho\left(\frac{\partial(c_pT)}{\partial t}+u\frac{\partial(c_pT)}{\partial x}+v\frac{\partial(c_pT)}{\partial y}+w\frac{\partial(c_pT)}{\partial z}\right)=\frac{\partial p}{\partial t}+u\frac{\partial p}{\partial x}+v\frac{\partial p}{\partial y}+w\frac{\partial p}{\partial z}$$

$$+k\left(\frac{\partial^2 T}{\partial x^2}+\frac{\partial^2 T}{\partial y^2}+\frac{\partial^2 T}{\partial z^2}\right)$$

$$+\frac{\partial k}{\partial x}\frac{\partial T}{\partial x}+\frac{\partial k}{\partial y}\frac{\partial T}{\partial y}+\frac{\partial k}{\partial z}\frac{\partial T}{\partial z}$$

$$+\mu\left\{-\frac{2}{3}\left(\frac{\partial u}{\partial x}+\frac{\partial v}{\partial y}+\frac{\partial w}{\partial z}\right)^2\right.$$

$$+2\left(\frac{\partial u}{\partial x}\right)^2+2\left(\frac{\partial v}{\partial y}\right)^2$$

$$+2\left(\frac{\partial w}{\partial z}\right)^2+\left(\frac{\partial w}{\partial y}+\frac{\partial v}{\partial z}\right)^2$$

$$\left.+\left(\frac{\partial u}{\partial z}+\frac{\partial w}{\partial x}\right)^2+\left(\frac{\partial v}{\partial x}+\frac{\partial u}{\partial y}\right)^2\right\}. \qquad (2)$$

The equation of continuity is

$$\frac{\partial \rho}{\partial t} + u \frac{\partial \rho}{\partial x} + v \frac{\partial \rho}{\partial y} + w \frac{\partial \rho}{\partial z} + \rho \left(\frac{\partial u}{\partial x} + \frac{\partial v}{\partial y} + \frac{\partial w}{\partial z} \right) = 0 \qquad (3)$$

and the equation of state may be written

$$p = \rho c_p T \left(\frac{1-\gamma}{\gamma} \right) . \qquad (4)$$

The temperature distribution in a body is determined by the heat input at the surface and the flow of heat internally by conduction (Ref.8).

The heat transfer at the surface is determined by the equation (neglecting solar radiation)

$$k_B \frac{\partial T}{\partial n} = k \frac{\partial T}{\partial n} - \varepsilon \bar{\sigma} T^4 . \qquad (5)$$

Heat flow by conduction is determined by the equation

$$\frac{\partial}{\partial x} k_B \frac{\partial T}{\partial x} + \frac{\partial}{\partial y} k_B \frac{\partial T}{\partial y} + \frac{\partial}{\partial z} k_B \frac{\partial T}{\partial z} = c \rho_B \frac{\partial T}{\partial t} . \qquad (6)$$

The stress and deflection of an elastic body are determined by the stress-strain relationships, the equilibrium equations and the surface forces (Ref.9).

A typical equation from the six stress-strain equations is

$$\frac{\partial b}{\partial x} = \frac{1}{E}\left[\sigma_x - \nu(\sigma_y + \sigma_z)\right] + \alpha(T-T_o). \qquad (7)$$

A typical equation from the three equilibrium equations is

$$\partial \frac{\sigma x}{\partial x} + \partial \frac{\tau_{yx}}{\partial y} + \partial \frac{\tau_{zx}}{\partial z} + \rho_B g_x - \rho_B \frac{\partial^2 b}{\partial t^2} = 0. \qquad (8)$$

At the surface the normal stress is equal to the applied pressure, i.e.

$$\sigma_n = p_n. \qquad (9)$$

The above equations are adequate to describe the aeroelastic behaviour of a body in a hot flowing gas.

Now consider a second body in a similar gas flow, such that at all points in the field there is a constant ratio of corresponding properties, i.e. $E_2 = E_1\ \lambda_E$, $\sigma_2 = \sigma_1\ \lambda_\sigma$, $T_2 = T_1\ \sigma_T$ etc. In particular $\lambda_x = \lambda_y = \lambda_z = \lambda_b = \lambda_L$ i.e. there is complete geometrical similarity between the two bodies, including aerothermoelastic deflections. For this second body equations 1-9 above may be re-written

$$\frac{\lambda_\rho \lambda_V^2}{\lambda_L}\rho\left\{\frac{\lambda_L}{\lambda_V \lambda_{t_1}}\frac{\partial u}{\partial t} + u\frac{\partial u}{\partial x} + v\frac{\partial u}{\partial y} + w\frac{\partial u}{\partial z}\right\} = -\frac{\lambda_p}{\lambda_L}\frac{\partial p}{\partial x} + \frac{\lambda_\mu \lambda_V}{\lambda_L^2}\left\{\mu\left(\frac{\partial^2 u}{\partial x^2} + \frac{\partial^2 u}{\partial y^2} + \frac{\partial^2 u}{\partial z^2}\right)\right.$$

$$+ \frac{\mu}{3}\frac{\partial}{\partial x}\left(\frac{\partial u}{\partial x} + \frac{\partial v}{\partial y} + \frac{\partial w}{\partial z}\right)$$

$$- \frac{2}{3}\frac{\partial u}{\partial x}\left(\frac{\partial u}{\partial x} + \frac{\partial v}{\partial y} + \frac{\partial w}{\partial z}\right)$$

$$+ 2\frac{\partial \mu}{\partial x}\frac{\partial u}{\partial x} + \frac{\partial \mu}{\partial y}\left(\frac{\partial u}{\partial y} + \frac{\partial v}{\partial x}\right)$$

$$\left. + \frac{\partial \mu}{\partial z}\left(\frac{\partial u}{\partial z} + \frac{\partial w}{\partial x}\right)\right\}$$

$$- \lambda_\rho \lambda_g \rho g_x \frac{(T - T_o)}{T_o} \qquad (10)$$

$$\frac{\lambda_\rho \lambda_{c_p} \lambda_T \lambda_V}{\lambda_L} \rho \left\{ \frac{\lambda_L}{\lambda_V \lambda_{t_1}} \frac{\partial (c_p T)}{\partial t} + u \frac{\partial (c_p T)}{\partial x} + v \frac{\partial (c_p T)}{\partial y} + w \frac{\partial (c_p T)}{\partial z} \right\} =$$

$$= \frac{\lambda_p \lambda_V}{\lambda_L} \left\{ \frac{\lambda_L}{\lambda_V \lambda_{t_1}} \frac{\partial p}{\partial t} + u \frac{\partial p}{\partial x} + v \frac{\partial p}{\partial y} + w \frac{\partial p}{\partial z} \right\}$$

$$+ \frac{\lambda_k \lambda_T}{\lambda_L^2} \left\{ k \left(\frac{\partial^2 t}{\partial x^2} + \frac{\partial^2 T}{\partial y^2} + \frac{\partial^2 T}{\partial z^2} \right) + \frac{\partial k}{\partial x} \frac{\partial T}{\partial x} + \frac{\partial k}{\partial y} \frac{\partial T}{\partial y} + \frac{\partial k}{\partial z} \frac{\partial T}{\partial z} \right\}$$

$$+ \frac{\lambda_\mu \lambda_V^2}{\lambda_L^2} \mu \left\{ - \frac{2}{3} \left(\frac{\partial u}{\partial x} + \frac{\partial v}{\partial y} + \frac{\partial w}{\partial z} \right) + 2 \left(\frac{\partial u}{\partial x} \right)^2 + 2 \left(\frac{\partial v}{\partial y} \right)^2 \right.$$

$$+ 2 \left(\frac{\partial w}{\partial z} \right)^2 + \left(\frac{\partial w}{\partial y} + \frac{\partial v}{\partial z} \right)^2 + \left(\frac{\partial u}{\partial z} + \frac{\partial w}{\partial x} \right)^2$$

$$\left. + \left(\frac{\partial v}{\partial x} + \frac{\partial u}{\partial y} \right)^2 \right\} \qquad (11)$$

$$\frac{\lambda_\rho \lambda_V}{\lambda_L} \left\{ \frac{\lambda_L}{\lambda_V \lambda_{t_1}} \frac{\partial \rho}{\partial t} + u \frac{\partial \rho}{\partial x} + v \frac{\partial \rho}{\partial y} + w \frac{\partial \rho}{\partial z} + \rho \left(\frac{\partial u}{\partial x} + \frac{\partial v}{\partial y} + \frac{\partial w}{\partial z} \right) \right\} = 0 \qquad (12)$$

$$\frac{\lambda_p}{\lambda_\rho \lambda_{c_p} \lambda_T} p = \rho c_p T \frac{(1-\lambda_\gamma \gamma)}{\lambda_\gamma \gamma} \qquad (13)$$

$$\frac{\lambda_{k_B}\lambda_T}{\lambda_L} k_B \frac{\partial T}{\partial n} = \frac{\lambda_k \lambda_T}{\lambda_L} k \frac{\partial T}{\partial n} - \lambda_\varepsilon \lambda_T^4 \varepsilon \bar{\sigma} T^4 \qquad (14)$$

$$\frac{\lambda_k \lambda_T}{\lambda_L^2}\left(\frac{\partial}{\partial x} k_B \frac{\partial T}{\partial x} + \frac{\partial}{\partial y} k_B \frac{\partial T}{\partial y} + \frac{\partial}{\partial z} k_B \frac{\partial T}{\partial z}\right) = \frac{\lambda_c \lambda_{\rho_B} \lambda_T}{\lambda_{t_2}} c_{\rho_B} \frac{\partial T}{\partial t}$$

..... (15)

$$\frac{\lambda_b}{\lambda_L} \frac{\partial b}{\partial x} = \frac{\lambda_\sigma}{\lambda_E} \frac{1}{E}\left[\sigma_x - \lambda_\nu \nu (\sigma_y + \sigma_z)\right] + \lambda_\alpha \lambda_T \alpha (T - T_o) \qquad (16)$$

$$\frac{\lambda_\sigma}{\lambda_L}\left(\frac{\partial \sigma_x}{\partial x} + \frac{\partial \tau_{yx}}{\partial y} + \frac{\partial \tau_{zx}}{\partial z}\right) + \lambda_{\rho_B} \lambda_g \rho_B g_x - \lambda_{\rho_B} \frac{\lambda_b}{\lambda_{t_1}^2} \rho_B \frac{\partial^2 b}{\partial t^2} = 0$$

..... (17)

$$\lambda_\sigma \sigma_n = \lambda_p p_n . \qquad (18)$$

SECTION 1.1: SIMILARITY LAWS

For complete similitude in aerothermoelastic behaviour of the two bodies, corresponding equations in equations 1-9 and 10-18 must be identical. Recognising that $\frac{\mu V}{\rho c_p T L} = \left(\frac{\mu}{V\rho L}\right)\left(\frac{p}{\rho c_p T}\right)\left(\frac{V^2\rho}{p}\right)$ the following equations must be satisfied:

$$\frac{\lambda_L}{\lambda_V \lambda_{t_1}} = 1 \tag{19}$$

$$\frac{\lambda_p}{\lambda_\rho \lambda_V^2} = 1 \tag{20}$$

$$\frac{\lambda_\mu}{\lambda_V \lambda_\rho \lambda_L} = 1 \tag{21}$$

$$\frac{\lambda_g \lambda_L}{\lambda_V^2} = 1 \tag{22}$$

$$\frac{\lambda_p}{\lambda_\rho \lambda_{c_p} \lambda_T} = 1 \tag{23}$$

$$\frac{\lambda_k}{\lambda_V \lambda_\rho \lambda_{c_p} \lambda_L} = 1 \tag{24}$$

$$\lambda_\gamma = 1 \tag{25}$$

$$\frac{\lambda_k}{\lambda_{k_B}} = 1 \tag{26}$$

$$\frac{\lambda_\varepsilon \lambda_T^3 \lambda_L}{\lambda_{k_B}} = 1 \tag{27}$$

$$\frac{\lambda_{k_B} \lambda_{t_2}}{\lambda_c \lambda_{\rho_B} \lambda_L^2} = 1 \tag{28}$$

$$\lambda_\nu = 1 \tag{29}$$

$$\frac{\lambda_\sigma \lambda_b}{\lambda_E \lambda_L} = 1 \tag{30}$$

$$\frac{\lambda_\alpha \lambda_T \lambda_L}{\lambda_b} = 1 \tag{31}$$

$$\frac{\lambda_{\rho_B} \lambda_g \lambda_L}{\lambda_\sigma} = 1 \tag{32}$$

$$\frac{\lambda_{\rho_B} \lambda_b \lambda_L}{\lambda_\sigma \lambda_{t_1}^2} = 1 \tag{33}$$

$$\frac{\lambda_p}{\lambda_\sigma} = 1 \qquad (34)$$

$$\frac{\lambda_b}{\lambda_L} = 1 \; . \qquad (35)$$

The times scales λ_{t_1} and λ_{t_2} are distinguished, t_1 relating to the time for oscillatory or accelerated motions and t_2 to heat flow times. It may be legitimate to regard these two times as independent on the assumption that heat flow is independent of factors such as the characteristic frequency spectrum of the boundary layer or the vibrational environment of the body itself. This assumption is apparently of limited validity since it appears that boundary layer heat transfer can be influenced to some extent by certain frequency dependent effects such as the external noise environment.

The practice with regard to aeroelastic model tests in the absence of heating effects is to ignore Reynolds number simulation on the grounds that it is relatively unimportant, at least as regards the behaviour of main surfaces. This assumption cannot be supported when heating effects of the flow are included. The Reynolds number equations are equations 21 and 23 which may be written

$$\frac{\lambda_\mu}{\lambda_V \lambda_\rho \lambda_L} = \frac{1}{\lambda_{Re}} = 1$$

$$\frac{\lambda_k}{\lambda_V \lambda_\rho \lambda_{c_p} \lambda_L} = \frac{1}{\lambda_{Pr} \lambda_{Re}} = 1$$

SECTION 2 : COMPATIBILITY OF THE SIMILARITY EQUATIONS

In the main, little control can be exercised over the properties of structural materials, in the sense that once a particular material for model construction has been decided upon the properties E, ρ_B, c and ν take up a fixed relationship. The same is true for the properties α and k_B, for although significant variations in these properties can sometimes be achieved by slight changes in the constituent alloys of the material this is not a controllable variation. The relationship between the properties ρ, k, μ, c_p and γ for gases is similarly fixed, and a continuum in the relationship between material and gas properties is established by the need to satisfy equation 26. It follows that if the satisfaction of the similarity relationships depends upon a constant relationship between several of the properties of the structural material or the gas then compatibility is only likely to be achieved using the same materials or gas for both bodies, since to find a different material or gas with corresponding ratios of properties would be largely fortuitous.

A further feature to be borne in mind is that the same gravity field necessarily applies to both bodies so that λ_g is normally unity*.

For wind tunnel work a measure of independent control can be exercised over the quantities T, p and V, and these are termed the "disposable quantities".

Re-writing the similarity equations we obtain

---

*Gravity ratios other than unity might be feasible in some circumstances; for example a manoeuvre case for an aircraft provides a gravity field greater than unity, as do model tests on a whirling arm.

$$\lambda_T = \lambda_\alpha^{-1} \tag{36}$$

$$\lambda_V = \lambda_{c_P}^{\frac{1}{2}} \lambda_\alpha^{-\frac{1}{2}} \tag{37}$$

$$\lambda_p = \lambda_E \tag{38}$$

$$\lambda_\sigma = \lambda_E \tag{39}$$

$$\lambda_b = \lambda_L \tag{40}$$

$$\lambda_{t_1} = \lambda_{c_P}^{-\frac{1}{2}} \lambda_\alpha^{\frac{1}{2}} \lambda_L \tag{41}$$

$$\lambda_{t_2} = \lambda_c \lambda_{\rho_B} \lambda_{k_B}^{-1} \lambda_L^2 \tag{42}$$

$$\lambda_g = \lambda_{c_P} \lambda_\alpha^{-1} \lambda_L^{-1} \tag{43}$$

$$\lambda_\varepsilon = \lambda_{k_B} \lambda_\alpha^3 \lambda_L^{-1} \tag{44}$$

$$\lambda_\rho = \lambda_E \lambda_{c_P}^{-1} \lambda_\alpha \tag{45}$$

$$\lambda_\gamma = 1 \tag{46}$$

$$\lambda_\nu = 1 \tag{47}$$

$$\lambda_{\rho_B} = \lambda_E \lambda_{c_p}^{-1} \lambda_\alpha \tag{48}$$

$$\lambda_\mu = \lambda_E \lambda_{c_p}^{-\frac{1}{2}} \lambda_\alpha^{\frac{1}{2}} \lambda_L \tag{49}$$

$$\lambda_k = \lambda_E \lambda_{c_p}^{\frac{1}{2}} \lambda_\alpha^{\frac{1}{2}} \lambda_L \tag{50a}$$

$$\lambda_k = \lambda_{k_B} . \tag{50b}$$

If the requirements defined by equations 43-50 can be satisfied for the two bodies, then the disposable quantities λ_T, λ_V and λ_p can be adjusted to satisfy equations 36-38 and the stress, deflection and time scales are then defined by equations 39-42. However, since equations 45-50 all depend on achieving a constant relationship between different ratios of material and gas properties, they are unlikely to be satisfied except by using the same materials and gases for both bodies.

It then follows from equation 36 that the temperature scale must be the same for both bodies. Equations 36-50 now reduce to

$$\lambda_T = 1 \tag{51}$$

$$\lambda_V = 1 \tag{52}$$

$$\lambda_p = 1 \tag{53}$$

$$\lambda_\sigma = 1 \tag{54}$$

$$\lambda_b = \lambda_L \tag{55}$$

$$\lambda_{t_1} = \lambda_L \tag{56}$$

$$\lambda_{t_2} = \lambda_L^2 \tag{57}$$

$$\lambda_g = \lambda_L^{-1} \tag{58}$$

$$\lambda_\varepsilon = \lambda_L^{-1} \tag{59}$$

$$\lambda_\rho = 1 \tag{60}$$

$$\lambda_\gamma = 1 \tag{61}$$

$$\lambda_\nu = 1 \tag{62}$$

$$\lambda_\mu = \lambda_L \tag{63}$$

$$\lambda_k = \lambda_L \tag{64a}$$

$$\lambda_k = 1 \tag{64b}$$

The expressions for λ_μ and λ_k are incompatible with the initial assumptions except when λ_L is unity, i.e. complete similarity obtains only when the two bodies are the same in all respects, including size. This conclusion has been arrived at by many earlier investigators (e.g. Refs. 4, 5 and 6).

SECTION 3: APPROXIMATIONS TO SIMILARITY

Although tests on full scale components have their merits, the nature of existing facilities limits such tests to relatively small components.

For aerothermoelastic model work to be of anything like the value of the purely aeroelastic model work, and to make the best use of available experience and facilities, the ability to make representative tests on small scale models of full scale components is essential. It is apparent that this cannot be achieved if a complete representation is attempted, and accordingly some possible approaches are examined that involve a relaxation of the similarity conditions. It is worth bearing in mind that relaxations of similarity requirements, both with regard to structural and aerodynamic parameters, have been necessary for all the purely aeroelastic models tested in the past but this has not prevented their making an indispensible contribution to aircraft flutter clearance programmes.

SECTION 3.1: RELAXATION OF THE REYNOLDS NUMBER REQUIREMENT

The Reynolds number equation can be identified as the equation that is most difficult to satisfy for a reduced scale model. For tests in unheated flow the assumption is generally made that Reynolds number effects can be neglected entirely provided the Reynolds number for the model is greater than about 10^6 (based on the mean chord of the surface) and this has generally proved acceptable, at least for main surface flutter investigations. However, for heated

flow the Reynolds number is of first order importance in relation to heat transfer, which in turn influences structural stiffness and hence aeroelastic properties. The Reynolds number must therefore be taken into account for aerothermoelastic work, insofar as it is associated with heat transfer properties.

Now, as an approximation equation 5 can be replaced by the equation

$$k_B \frac{\partial T}{\partial n} = h(T_{aw}-T_w) - \varepsilon \bar{\sigma} T^4 . \qquad (65)$$

Strictly speaking this formulation applies for an isothermal surface, but in practice it appears to provide a fair approximation for non-isothermal surfaces.

At the same time the heat transfer coefficient h in the above equation is given approximately by (Ref.10)

$$h = A \frac{k}{x} \left(\frac{x \rho V}{\mu}\right)^r \left(\frac{\mu c_p}{k}\right)^{1/3} \left(\frac{T_a}{T_w}\right)^s \qquad (66)$$

where A, r and s are constants having different values for the laminar flow region than for the turbulent region, and x is measured from the leading edge in the laminar case, and from the transition point in the turbulent case*. In particular r = 0.5 for laminar flow and r = 0.8 for turbulent flow.

With these limitations in mind, on substituting for h in equation 65 the equation for the second body (replacing equation 14) is:-

---

*This formulation strictly applies only for incompressible flow, but there seems some justification for extending it to the compressible flow régime (Ref.11).

$$\frac{\lambda_{k_B}\lambda_T}{\lambda_L} k_B \frac{\partial T}{\partial n} = \frac{\lambda_k \lambda_T}{\lambda_L}\left(\frac{\lambda_L\lambda_\rho\lambda_V}{\lambda_\mu}\right)^r \left(\frac{\lambda_\mu\lambda_{c_P}}{\lambda_k}\right)^{1/3} A\frac{k}{x}\left(\frac{x\rho V}{\mu}\right)^r \left(\frac{\mu c_P}{k}\right)^{1/3}\left(\frac{T_a}{T_w}\right)^s (T_{aw}-T)$$

$$- \lambda_\varepsilon \lambda_T^4 \varepsilon \bar{\sigma} T^4$$

..... (67)

Hence, the similarity equation 26 is replaced by

$$\frac{\lambda_k}{\lambda_{k_B}}\left(\frac{\lambda_L\lambda_\rho\lambda_V}{\lambda_\mu}\right)^r \left(\frac{\lambda_\mu\lambda_{c_P}}{\lambda_k}\right)^{1/3} = 1 . \qquad (68)$$

If this equation is satisfied then heating rates for the two bodies will be to scale. Assuming other effects of Reynolds number can be neglected, it is then no longer necessary to satisfy the Reynolds number equations 21 and 24 independently. Accordingly, referring to equations 36-50, equations 49 and 50 are replaced by the single equation

$$\lambda_{k_B} = \lambda_k \left(\frac{\lambda_L\lambda_E\lambda_{c_P}^{-\frac{1}{2}}\lambda_\alpha^{\frac{1}{2}}}{\lambda_\mu}\right)^r \left(\frac{\lambda_\mu\lambda_{c_P}}{\lambda_k}\right)^{1/3}$$

and hence

$$\lambda_L = \lambda_{k_B}^{\frac{1}{r}} \lambda_E^{-1} \lambda_{c_P}^{-\frac{1}{2}} \lambda_\alpha^{-\frac{1}{2}} \lambda_k^{\left(\frac{r-1}{r}\right)} \lambda_{Pr}^{\left(\frac{3r-1}{3r}\right)} . \qquad (69)$$

It is apparent that if the same gas and materials are used for both bodies we again arrive at the conclusion that compatibility of the similarity equations obtains only when $\lambda_L = 1$. However, the

number of property dependent relationships is reduced by the above procedure and the possibility of using different gases and materials for the two bodies merits further consideration. In the main, properties of both structural materials and gases are affected by temperature, and in some cases significant anomalies in thermal properties as functions of temperature are obtained. A completely general treatment is impracticable in these circumstances, and some simplifying assumptions defining variation of material properties with temperature must be made.

For the present purposes it is assumed that within a limited range of temperature all temperature dependent material properties can be assumed to vary according to the law:-

$$\phi = \phi_o T^{s_\phi} \tag{70}$$

where ϕ = value of temperature dependent property at temperature T

ϕ_o = property value at reference temperature

s_ϕ = temperature exponent related to property ϕ.

Furthermore, we assume that the possible gases that could be used are such that

$$\begin{aligned} \mu &= \mu_o T^{0.7} \\ k &= k_o T^{0.9} \\ c_P &= c_{P_o} T^{0.2} \\ \gamma &= \gamma_o . \end{aligned} \tag{71}$$

In this circumstance Prandtl's number remains constant independent of temperature, which is in reasonable accordance with experimental data for most gases.

From equations 36 and 70 we obtain

$$\lambda_T = \lambda_{\alpha_o}^{-\left(\frac{1}{1+s_\alpha}\right)} \qquad (72)$$

and from equation 69 we then have

$$\lambda_L = \lambda_{c_{P_o}}^{-\frac{1}{2}} \lambda_{k_o}^{\left(\frac{r-1}{r}\right)} \lambda_{Pr}^{\left(\frac{3r-1}{3r}\right)} \lambda_{k_{B_o}}^{-\frac{1}{r}} \lambda_{E_o}^{-1} \lambda_{\alpha_o}^{-\{s_k - s_{k_B} + r(s_k - s_E - s_{c_P} + 0.5)\}/r(1+s_\alpha)} \qquad \ldots\ldots (73)$$

The main aim is to further the use of small scale models, i.e. we require $\lambda_L > 1$, where λ is the ratio full scale property : model scale property.

SECTION 3.1.1: WIND TUNNEL TESTS IN A GAS OTHER THAN AIR

In considering the possible use of a gas other than air for wind tunnel tests, the basic gas properties required are

$$\lambda_\rho = \lambda_E \lambda_\alpha \lambda_{c_p}^{-1} \tag{45}$$

$$\lambda_\gamma = 1 \tag{46}$$

$$\lambda_{c_{p_o}}^{-\frac{1}{2}} \lambda_{k_o}^{\left(\frac{r-1}{r}\right)} \lambda_{Pr}^{\left(\frac{3r-1}{3r}\right)} > 1 . \tag{74}$$

The inequality 74 follows from equation 73 if we assume that the gas is to further the aim $\lambda_L > 1$.

The properties of a number of gases are given in Table 1 and the air : gas property ratios are given in Table 2. It can be seen that inequality 74 is satisfied by all the gases considered whose density is significantly less than that of air. For hydrogen in particular quite large values are obtained.

If it is now assumed that the model is constructed in the same materials as the aircraft, equations 45, 46 and 73 reduce to

$$\lambda_\rho \lambda_{c_p} = 1$$

$$\lambda_\gamma = 1$$

$$\lambda_{c_p}^{-\frac{1}{2}} \lambda_k^{\left(\frac{r-1}{r}\right)} \lambda_{Pr}^{\left(\frac{3r-1}{3r}\right)} = \lambda_L . \tag{75}$$

Table 1

Average gas properties at $32^{\circ}F$ and atmospheric pressure

Gas	Density ρ Lb/Ft^3	Specific Heat c_p BTU/Lb $^{\circ}F$	Specific Heat Ratio γ	Dynamic Viscosity $\times 10^7$ μ Slugs/Ft Sec	Conductivity k BTU/Hr Ft $^{\circ}F$	Speed of Sound Ft/Sec	Boiling Point $^{\circ}K$
Hydrogen	0.0054	3.41	1.41	1.73	0.0950	4500	20
Helium	0.0108	1.26	1.67	3.80	0.0800	3200	4
Methane	0.0435	0.59	1.32	2.17	0.0175	1410	109
Ammonia	0.048	0.51	1.31	1.95	0.0123	1360	
Neon	0.0534	0.25	1.67	6.2	0.0270	1460	27
Nitrogen	0.076	0.245	1.40	3.5	0.014	1095	79
Air	0.078	0.24	1.40	3.6	0.014	1090	90
Argon	0.107	0.13	1.67	4.41	0.0094	1050	87
Carbon Dioxide	0.120	0.20	1.30	2.90	0.0082	850	195

Table 2

Property ratios λ; (Air : Gas)

Gas	λ_{ρ_o}	$\lambda_{c_{P_o}}$	λ_γ	λ_{μ_o}	λ_{k_o}	$\lambda_{Pr} = \frac{\lambda_{c_{P_o}} \lambda_{\mu_o}}{\lambda_{k_o}}$	$\lambda_{\rho_o} \lambda_{c_{P_o}}$	$\lambda_L = \frac{\left(\frac{r-1}{r}\right)\left(\frac{3r-1}{3r}\right) \lambda_{k_o} \lambda_{Pr}}{\lambda_{c_{P_o}}^{\frac{1}{2}}}$	
								r=0.5 Lam.	r=0.8 Turb.
Hydrogen	14.5	0.07	0.99	2.07	0.15	0.97	1.01	24.9	5.94
Helium	7.2	0.19	0.84	0.95	0.18	1.0	1.36	12.1	3.54
Methane	1.79	0.41	1.06	1.66	0.80	0.85	0.73	1.85	1.50
Ammonia	1.63	0.47	1.07	1.85	1.14	0.76	0.77	1.18	1.21
Neon	1.47	0.93	0.84	0.58	0.52	1.07	1.36	1.96	1.22
Nitrogen	1.03	0.98	1.00	1.03	1.00	1.00	1.01	1.00	1.00
Air	1.00	1.00	1.00	1.00	1.00	1.00	1.00	1.00	1.00
Argon	0.73	1.86	0.84	0.82	1.49	1.02	1.36	0.49	0.67
Carbon Dioxide	0.65	1.20	1.08	1.24	1.69	0.88	0.78	0.51	0.74
Methane + 5.19 (Helium)	4.83	0.207	0.87	0.94	0.206	0.95	1.00	10.5	3.14

It is apparent from Table 2 that for tests in hydrogen not only are the first two of these equations closely satisfied but the values of λ_L are adequate for a wide range of model tests. For tests in pure hydrogen the aircraft : model scale is fixed at 24.9 : 1 for a laminar flow model and 5.94 : 1 for a turbulent flow model. However, the model designer will generally want to work with the maximum scale of model that is practicable for a given facility, as this generally eases fabrication and handling problems, and hence some control over the model scale parameter is desirable. A possible way in which this might be achieved (though less ideally than for tests in hydrogen) is to use mixtures of gases. For example if it is assumed that the properties of gases vary linearly with mixture ratio* and suppose that we require the relationship $\lambda_\rho \lambda_{c_P} = 1$ to be satisfied for a binary mixture, then for two gases mixed in the ratio 1 : f we require

$$\frac{(\rho_1 + f\,\rho_2)\,(c_{P_1} + f\,c_{P_2})}{(1+f)^2} = \rho\, c_{P\,(air)}$$

i.e.

$$(\lambda_{\rho_1}^{-1} + f\lambda_{\rho_2}^{-1})(\lambda_{c_{P_1}}^{-1} + f\lambda_{c_{P_2}}^{-1})(1+f)^{-2} = 1 . \qquad (76)$$

This equation has been solved for a mixture of methane and helium, for which f = 5.19, and the values of the various property ratios are given in Table 2. Unfortunately, although this mixture enables tests on quite small models, and satisfies the requirement $\lambda_\rho \lambda_{c_P} = 1$, it does not satisfy the requirement $\lambda_\gamma = 1$. On the

---

*Investigations by Chapman (Ref. 12) show that this assumption is unjustified for some gas mixtures. For example helium-argon mixtures have lower values of Pr than for either gas in the pure state.

other hand it may not be necessary to satisfy $\lambda_\gamma = 1$ identically. Aeroelastic tests at transonic speeds in Freon 12 ($\lambda_\gamma = 1.21$) show quite good correlation with tests in air, so that the effect of γ is not too significant at these speeds. At high supersonic speeds ($M > 2$) there is evidence that the pressure distribution is often provided fairly accurately by piston theory (Ref. 13) and in this theory γ occurs only in the form $(1+\gamma)$ and in association with the thickness term. Hence, it may be permissible to neglect small errors in γ for thin surfaces (without excessive leading edge blunting) and for panels, and the majority of surfaces for aeroelastic investigations fall into this category.

Referring to the similarity equations 36-48, it is now apparent that the similarity equations that cannot be satisfied by laminar or turbulent flow models in the same materials as the aircraft and tested in hydrogen are:-

$$\lambda_g = \lambda_{c_p} \lambda_L^{-1}$$

$$\lambda_\varepsilon = \lambda_L^{-1}$$

$$\lambda_{\rho_B} = \lambda_{c_p}^{-1} .$$

These imply that for tests in hydrogen a model of reduced density is required in an increased gravitational field and with emissivity increasing as the reciprocal of model size. Since the aircraft surfaces will be designed for maximum emissivity, significantly higher emissivities for the model are unlikely to be achieved; since λ_g is unity, model deflections under gravitational load and free convective heat transfer will not be to scale; and since λ_{ρ_B} is unity for model and aircraft in the same materials, the frequency parameter for structural oscillations in the gas will not be to scale. However, the effects of frequency parameter on flutter characteristics are generally small so that failure to satisfy

$\lambda_{\rho_B} = \lambda_{c_p}^{-1}$ may not be important - it can of course be ignored completely for static aerothermoelastic tests.

Effects of deflection under gravitational load are generally negligible but the effects of free convective heat transfer and of emissivity may be of some significance. They must be ignored for present purposes.

Within these limitations, models can be constructed in the same materials as the aircraft to provide representative aerothermoelastic effects in laminar flow or in turbulent flow regions, but one single model does not provide for representative investigations in both régimes of flow simultaneously. A model constructed to a laminar flow scale will have less than true scale rate of heating in turbulent flow regions*, and vice-versa. Some possible ways of overcoming this difficulty are considered in section 3.2.

SECTION 3.1.2: WIND TUNNEL TESTS IN AIR

The similarity requirements for wind tunnel tests in air cannot possibly be satisfied unless the model is constructed in different materials than the aircraft, the temperature scale then being defined by equation 72, namely

$$\lambda_T = \lambda_{\alpha_o}^{-1/(1+s_\alpha)} . \qquad (72)$$

---

*Since Reynolds number for the model will be lower than full scale, natural transition from laminar to turbulent flow may not occur in the correct location. Leading edge roughness or some other device will be necessary to "trigger" the flow so that it changes from laminar to turbulent in the correct region for transition on the full scale aircraft.

For tests in air equation 73 becomes

$$\lambda_L = \lambda_{k_{B_o}}^{1/r} \lambda_{E_o}^{-1} \lambda_{\alpha_o}^{-\{s_k - s_{k_B} + r(s_k - s_E - s_{c_P} + 0.5)\}/r(1+s_\alpha)} . \qquad (77)$$

As an approximation it is assumed that

$$-s_E = s_\alpha = 0.2$$

$$s_{k_B} = 0$$

therefore

$$\lambda_L = \lambda_{k_{B_o}}^{\frac{1}{r}} \lambda_{E_o}^{-1} \lambda_{\alpha_o}^{-(0.8+1.3r)/1.2r} \qquad (78)$$

Property values for a number of materials are given in Table 3 and ratios of property values for full scale aircraft in duralumin and in stainless steel are given in Tables 4 and 5. It can be seen that to obtain values of λ_L greater than unity the model material must have a conductivity and expansion coefficient less than that of the aircraft material. The conductivity of duralumin is very high and hence most of the materials considered in Table 4 provide values of $\lambda_L > 1$ for a duralumin aircraft. The reverse is true for a nickel steel aircraft, and for the particular steel considered in Table 5 only glass and a low conductivity copper alloy provide values of $\lambda_L > 1$.

However, it appears that heating requirements in laminar or turbulent flow regions can be satisfied using models constructed in different materials than the aircraft and tested in a hot air tunnel at a temperature scale different from that for the aircraft.

Table 3

Average material properties at $68^{o}F$

Material	Temp. Coeff. of Expansion $\times 10^{6}$ $^{o}F^{-1}$ α	Young's Modulus $\times 10^{-6}$ Lb/In^2 E	Modulus Ratio ν	Conducty. $\frac{BTU}{Hr\ Ft\ ^{o}F}$ k_B	Specific Heat BTU/Lb ^{o}F c_B	Density Lb/Ft^3 ρ_B	Melt. Point ^{o}F
Duralumin	12.5	10.0	0.38	95	0.21	174	1250
Nickel Steel	5.5	29.5	0.39	15	0.11	490	2500
Carbon Steel	7	29.5	0.39	30	0.11	490	2500
Titanium	5	16	0.38	15	0.13	280	3270
Magnesium Alloy	16	6.5	0.37	40-87	0.24	112	1200
Copper Alloy	9.3	15.0	0.37	15-200	0.095	540	1940
Glass	4.7	8.0	0.40	0.44	0.20	169	2000
Cadmium	16.5	5.0	0.38	53	0.055	536	610
Nickel	7.1	28.5	0.38	52	0.11	550	2600
Silver	10.6	11.1	0.37	242	0.056	650	1760
Tin	11.7	7.7	0.375	37	0.054	453	446
Zinc	16.5	8.7	0.436	65	0.092	440	785

Table 4

Property ratios for a duralumin aircraft

Model Material	λ_{ρ_B}	λ_{α_o}	λ_{E_o}	$\lambda_{k_{B_o}}$	$\lambda_{c_{B_o}}$	λ_ν	$\lambda_L = \lambda_{k_{B_o}}^{1/r} \lambda_{E_o}^{-1} \lambda_{\alpha_o}^{\frac{-(0.8+1.3r)}{1.2r}}$		$\lambda_\varepsilon = \lambda_{k_{B_o}} \lambda_{\alpha_o}^{2.5} \lambda_L^{-1}$	
							r=0.5 Lam.	r=0.8 Turb.	r=0.5 Lam.	r=0.8 Turb.
Magnesium	1.55	0.78	1.55	2.4 1.09	0.88	1.03	6.75 1.39	3.06 1.07	< 1 < 1	< 1 < 1
Glass	1.04	2.70	1.35	216	1.05	0.95	3120	88	0.84	29.9
Titanium	0.62	2.5	0.62	6.3	1.61	1.0	6.96	2.79	8.95	22.3
Zinc	0.40	0.76	1.15	1.46	2.3	0.87	3.58	2.39	< 1	< 1
Tin	0.38	1.07	1.30	2.57	3.89	0.99	4.31	2.20	3.24	6.35
Nickel Steel	0.35	4.20	0.32	6.30	1.91	0.98	3.84	1.88	23.4	47.2
Carbon Steel	0.35	1.8	0.32	6.30	1.61	0.98	30.0	9.90	0.91	2.76
Cadmium	0.33	0.76	2.00	1.79	3.82	0.98	2.94	1.78	< 1	< 1
Copper	0.32	1.35	0.68	6.30 0.48	2.33	1.03	28.3 < 1	8.16 < 1	0.47 -	1.66 -
Nickel	0.32	1.76	0.35	1.83	1.91	0.98	2.44	2.01	3.07	3.73
Silver	0.27	1.18	0.90	0.39	3.86	1.03	< 1	< 1	-	-

Table 5

Property ratios for a nickel steel aircraft

Model Material	λ_{ρ_B}	λ_{α_o}	λ_{E_o}	$\lambda_{k_{B_o}}$	$\lambda_{c_{B_o}}$	λ_ν	$\lambda_L = \lambda_{k_{B_o}}^{1/r} \lambda_{E_o}^{-1} \lambda_{\alpha_o}^{\frac{-(0.8+1.3r)}{1.2r}}$	
							r = 0.5 Lam.	r = 0.8 Turb.
Magnesium	4.40	0.34	4.45	0.38 0.17	0.46	1.05	< 1 < 1	< 1 < 1
Duralumin	2.82	0.44	2.95	0.16	0.53	1.03	< 1	< 1
Glass	2.90	1.17	3.7	34.0	0.55	0.98	456	165
Titanium	1.75	1.10	1.85	1.0	0.85	1.03	< 1	< 1
Zinc	1.11	0.33	3.4	0.23	1.20	0.90	< 1	< 1
Tin	1.08	0.47	3.84	0.41	2.04	1.04	< 1	< 1
Carbon Steel	1.00	0.79	1.00	0.50	1.00	1.00	< 1	< 1
Cadmium	0.92	0.33	5.9	0.28	2.00	1.03	< 1	< 1
Copper	0.91	0.55	1.97	1.0 0.075	1.22	1.05	2.15 < 1	1.62 < 1
Nickel	0.89	0.77	1.03	0.29	1.00	1.03	< 1	< 1
Silver	0.75	0.52	2.66	0.06	1.97	1.05	< 1	< 1

Similarity parameters from equations 36-48 that are not satisfied identically are

$$\lambda_\nu = 1$$

$$\lambda_{\rho_B} = \lambda_{E_o} \lambda_{\alpha_o}^{0.1667}$$

$$\lambda_g = \lambda_{\alpha_o}^{-1} \lambda_L^{-1}$$

$$\lambda_\varepsilon = \lambda_{k_{B_o}} \lambda_{\alpha_o}^{2.5} \lambda_L^{-1} .$$

λ_ν is close to unity for nearly all the materials considered, and the requirement can therefore be regarded as satisfied. The values of $\lambda_{\alpha_o}^{0.1667}$ are also close to unity, and hence we require $\lambda_{\rho_B} \lambda_{E_o}^{-1} \doteq 1$, i.e. the model material must be equally as efficient as the aircraft material in terms of stiffness : weight ratio. Magnesium, duralumin, glass, titanium, carbon steel and nickel all satisfy this requirement approximately, and for models in these materials the density requirement may be regarded as satisfied. For the remaining materials the requirement cannot be satisfied and hence errors in frequency parameter will arise in oscillatory tests (see section 3.1.1). The λ_g requirement is fortuitously satisfied quite closely by a low conductivity copper alloy model of a steel aircraft, but the requirement is not satisfied in most cases and must be ignored. On the other hand for a duralumin aircraft, the emissivity requirement is such that model emissivity must generally be of the same order or lower than that for the aircraft, and this requirement can probably be satisfied. For example if carbon steel is used for a model of a duralumin aircraft, then the emissivity is 1.1 times that of the aircraft for a laminar flow model and 0.36 times that of the aircraft for a turbulent flow model.

A further feature to be noted is that models constructed in materials for which $\lambda_{\alpha_o} < 1$ require testing under a reduced temperature as compared with the aircraft. This is generally an attractive feature, since it reduces the demand on the absolute operating temperature of the tunnel heat exchanger. On the other hand refrigeration of the model may be required to provide correct starting conditions. Model materials for which $\lambda_{\alpha_o} > 1$ are less attractive by the same token; for some of these, representative high speed flight conditions are unattainable because of degradation in model material properties due to a too close approach to the melting point.

SECTION 3.2: APPROXIMATIONS TO OVERALL SIMILARITY

It appears from sections 3.1.1 and 3.1.2 that provided the heat transfer coefficient satisfies equation 66 models can be constructed in the same materials as the aircraft for tests in a gas other than air at unity temperature scale, or in different materials for tests in air at a different temperature scale. The models will provide complete representation in laminar or turbulent regions, but heating effects are not represented in both régimes of flow simultaneously. Such models are of value for investigations of local effects (e.g. panel flutter) or for investigations where the major load carrying structure lies wholly in the laminar or turbulent flow régime.

Since a laminar flow model has less than true scale heating rate in the turbulent regions (and vice-versa for a turbulent flow model), it follows that if some method of providing a local increase or decrease in heating rate can be devised, one single model will provide representative conditions in both flow régimes. The possibilities in this direction merit consideration.

SECTION 3.2.1: TURBULENT SCALE MODEL WITH INSULATION IN THE LAMINAR FLOW REGIONS

A possible method of reducing the heating rate in local areas is to cover the surface with a thin film of high conductivity, whose heat capacity relative to the wing structure, stiffness, and mass contributions can be neglected.

For a film of thickness d_x at x from the leading edge and of conductivity k_i, the effective heat transfer h_{e_M} at the wing surface at x is

$$h_{e_M}^{-1} = h_M^{-1} + \frac{d_x}{k_i}$$

where h_M is the heat transfer coefficient for the film surface at x and M refers to the model.

We require

$$\left(\frac{h_F}{h_{e_M}}\right)_{\text{laminar}} = \left(\frac{h_F}{h_M}\right)_{\text{turbulent}}$$

i.e.
$$\left(\lambda_h + h_F \frac{d_x}{k_i}\right)_{\text{laminar}} = \lambda_{h_{\text{turbulent}}} \qquad (79)$$

where F refers to full scale.

Now from equation 66

$$\lambda_h = \lambda_{c_p}^{\frac{r}{2}} \lambda_k^{(1-r)} \lambda_{Pr}^{\left(\frac{1-3r}{3}\right)} \lambda_L^r \qquad (80)$$

For a model built in aircraft materials and tested in a different gas

$$\lambda_L = \lambda_{c_p}^{-\frac{1}{2}} \lambda_k^{\left(\frac{r_1-1}{r_1}\right)} \lambda_{Pr}^{\left(\frac{3r_1-1}{3r_1}\right)} \qquad (75)$$

and hence for a model built to turbulent flow scale where $r = r_1 = 0.8$

$$\lambda_{h_{turbulent}} = 1 .$$

In the laminar flow region of the model $r = 0.5$, $r_1 = 0.8$, therefore

$$\lambda_{h_{laminar}} = \lambda_k^{0.375} \lambda_{Pr}^{0.125}$$

therefore

$$d_x = \frac{k_i}{h_{F\ laminar}} (1 - \lambda_k^{0.375} \lambda_{Pr}^{0.125}) . \qquad (81)$$

For a model built of different materials from the aircraft and tested in air

$$\lambda_L = \lambda_{k_B}^{\frac{1}{r_1}} \lambda_E^{-1} \lambda_\alpha^{-\frac{1}{2}} \lambda_{c_p}^{-\frac{1}{2}} \lambda_k^{\left(\frac{r_1-1}{r_1}\right)} \lambda_{Pr}^{\left(\frac{3r_1-1}{3r_1}\right)} \qquad (69)$$

and hence for a model built to turbulent flow scale where $r = r_1 = 0.8$

$$\lambda_{h_{turbulent}} = \lambda_{k_B} \lambda_E^{-0.8} \lambda_\alpha^{-0.4} = \lambda_{k_{B_o}} \lambda_{E_o}^{-0.8} \lambda_{\alpha_o}^{-0.467}$$

In the laminar flow region of the model $r = 0.5$, $r_1 = 0.8$, therefore

$$\lambda_{h_{laminar}} = \lambda_{k_B}^{0.625} \lambda_E^{-0.5} \lambda_\alpha^{-0.25} \lambda_k^{0.375} \lambda_{Pr}^{0.125} = \lambda_{k_{B_o}}^{0.625} \lambda_{E_o}^{-0.5} \lambda_{\alpha_o}^{-0.542}$$

therefore

$$d_x = \frac{k_i}{h_{F\ laminar}} \lambda_{k_{Bo}} \lambda_{E_o}^{-0.8} \lambda_{\alpha_o}^{-0.467} \left(1 - \lambda_{k_{B_o}}^{-0.375} \lambda_{E_o}^{0.3} \lambda_{\alpha_o}^{-0.075}\right). \quad \ldots\ldots (82)$$

It follows from equations 81 and 82 that d_x should increase in thickness from zero at the leading edge and inversely proportional to full scale heat transfer coefficient.

Equation 66 for the laminar flow heat transfer coefficient may be written (Ref. 10)

$$h_{F_{laminar}} = 0.332\, k_F\, x_F^{-0.5} (Re')^{0.5} (Pr)^{1/3} \qquad (83)$$

where Re' is Reynolds number/ft. For a high speed aircraft assuming $Re' = 10^7$, $Pr = 0.7$ the laminar heat transfer is

$$h_{F_{laminar}} \doteq 10^3\, k_F\, x^{-0.5}.$$

The insulant is unlikely to have a lower conductivity than air, and hence it follows that the required values of d_x are excessive, except for values of λ_L not greatly different from unity.

SECTION 3.2.2: LAMINAR SCALE MODEL WITH RADIANT HEATING IN THE TURBULENT FLOW REGION

A possible way of providing an increased heating rate in the turbulent flow regions of a model built to a laminar flow scale is to provide radiant heating lamps in the walls of the wind tunnel working section. In this circumstance the effective heat transfer in the turbulent flow region at a point distance x aft of the transition point is:-

$$h_{e_M} = h_M + \frac{R_x}{(T_{aw}-T_w)}$$

where R_x is the contribution to heating rate at x due to absorbtion of radiant heat.

We require

$$\left(\frac{h_F}{h_M}\right)_{\text{laminar}} = \left(\frac{h_F}{h_{e_M}}\right)_{\text{turbulent}}$$

therefore

$$\lambda_{h_{\text{laminar}}} = \left\{\lambda_h^{-1} + \frac{R_x}{(T_{aw}-T_w)\,h_F}\right\}^{-1}_{\text{turbulent}} . \qquad (84)$$

Following the procedure of section 3.2.1 we obtain; for a model built in aircraft materials and tested in a different gas

$$\frac{R_x}{(T_{aw}-T_w)} = \left(1-\lambda_k^{0.6}\ \lambda_{Pr}^{0.2}\right) h_{F_{turbulent}} \qquad (85)$$

and for a model built of different materials from the aircraft and tested in air

$$\frac{R_x}{(T_{aw}-T_w)} = \lambda_{k_{B_o}}^{-1}\ \lambda_{E_o}^{0.5}\ \lambda_{\alpha_o}^{0.292}\left(1-\lambda_{k_{B_o}}^{-0.6}\ \lambda_{E_o}^{0.3}\ \lambda_{\alpha_o}^{-0.225}\right) h_{F_{turbulent}} \qquad \ldots\ldots (86)$$

Equation 66 for the full scale turbulent flow heat transfer may be written (Ref. 10)

$$h_{F_{turbulent}} = 0.0296\ k_F\ x_F^{-0.2}(Re')^{0.8}(Pr)^{1/3}\left(\frac{T_a}{T_w}\right)^{0.44} \qquad \ldots\ldots (87)$$

where T_a is the free stream temperature of the air and T_w is the temperature at the surface. For a maximum heat transfer it is assumed that $T_a = T_w$. Following the same reasoning as in section 3.2.1 it follows that

$$h_{F_{turbulent}} \simeq 10^4\ k_F\ x_F^{-0.2}.$$

A consideration of Tables 2, 4 and 5 in relation to equations 85 and 86 indicates that the maximum rate of heating is

$$\frac{R_{x_{max}}}{(T_{aw}-T_w)} \triangleq h_{F_{turbulent}},$$

i.e. the radiant heater must be capable of providing heating rates equivalent to full scale turbulent flow values (approximately 40 Kw/ft^2 for $(T_{aw}-T_w) = 1000^oF$). It appears from Ref.14 that there is some prospect of providing heating rates of the required order using banks of quartz-tube lamps lining the walls of the working section, and it would also seem feasible to use a uniform heating system and to control the absorbtion in the different areas of the model by varying the surface finish. The heating rate provided by the lamps must tend to zero as $T_{aw} \rightarrow T_w$, and this requires control of the lamp supply voltage in relation to a measurement of temperature on the model, so as to follow a pre-calculated temperature-time history. Very rapid control is implied since the time scale for heating varies as the square of the length scale, and this may prove the limiting factor in relation to model scale.

However, the method appears to have attractive possibilities as a means of providing overall similarity for an aerothermoelastic model and merits further investigation.

SECTION 3.3: MODELS OF REDUCED EFFECTIVE STIFFNESS TESTED IN 'COLD' FLOW

Although the previous sections have indicated that an acceptable approach to aerothermoelastic similarity might be achieved using models tested in a hot gas stream, the unfortunate feature is that suitable heated flow tunnels of the type envisaged (see section 4) are conspicuous by their absence. In these circumstances some attempt must be made to design models with a reduced effective stiffness representative of thermal effects, which can

be tested in existing facilities (which generally provide little more than atmospheric stagnation temperatures).

This approach can never be wholly satisfactory, for it presupposes that an "effective" reduced stiffness, corresponding to heated conditions for the aircraft, can be calculated. In fact the effects of transient heating lead to thermal stress distributions producing effects on stiffness that are highly non-linear with displacement of the structure. Hence the effective stiffness for a 1g loading condition for the aircraft may be quite different from the zero 'g' load condition. Furthermore, certain effects of heating cannot be represented by a simple "effective" stiffness concept. For example Broadbent (Ref.15) considers an effect of thermal stress which leads to an anticlastic curvature (camber) of the wing chord causing a loss in flexural stiffness. Flutter then arises from the aerodynamic coupling due to change of wing camber, and not from the loss of stiffness.

However, assuming that an effective stiffness approach is acceptable, the approach to be followed is then the conventional one for 'cold' model tests. The similarity equations to be satisfied (neglecting gravitational effects) are equations 19, 20, 23, 25, 29, 30, 33, 34 and 35. From these we obtain, for tests in air,

$$\lambda_V = \lambda_T^{0.6}$$

$$\lambda_p = \lambda_\sigma = \lambda_{E_o} \lambda_T^{-0.2}$$

$$\lambda_\rho = \lambda_{\rho_B} = \lambda_{E_o} \lambda_T^{-1.4} .$$

If these relationships are satisfied, then the Mach number for the model will be the same as for the aircraft. Unfortunately existing wind tunnels are such that to satisfy these relationships generally presents some difficulty. The problem has been discussed in detail by Lambourne and Scruton (Ref.16), and it is apparent that the main difficulty results from the limited stagnation pressure

generally available in existing tunnels. For a model in the same materials as the aircraft, with skin thickness to the same scale as the geometric scale, this implies that the pressure relationship cannot be satisfied. This is generally overcome by assuming that the whole of the aircraft stiffness lies in the skin, and by varying the skin thickness scale relative to geometric scale the effective E for the model becomes $E\lambda_\delta^{-1}$ where λ_δ is the ratio of skin thickness scale to length scale. By using a model skin thickness less than the geometric scale, models can then be tested in tunnels with lower than full scale stagnation pressure. The requirement $\lambda_{\rho_B} = \lambda_\delta^{-1} \lambda_{E_o} \lambda_T^{-1.4}$ cannot generally be satisfied, but this affects only the frequency parameter and it is assumed that this can be ignored.

The limitations of aeroelastic model tests in 'cold' flow are well known (Ref.16), and little further need be said about them. Obviously, in the absence of heated flow tunnels, the best use must be made of existing facilities, and this necessitates the use of the effective stiffness concept so far as heating effects are concerned. However, more work is required to determine the types of structure for which an effective stiffness concept is likely to provide an adequate representation

SECTION 4: WIND TUNNEL FACILITIES

There are very few existing tunnels that provide for heating the flow. Those that do exist are generally of the intermittent type running from compressed air storage through a pre-heated exchanger into a fixed Mach number working section, but even these rarely provide stagnation conditions representative of high speed flight at low altitude. Neither do they have provision for radiant heater installations in the tunnel sidewalls.

The stagnation pressure and temperature appropriate to free flight conditions are shown in Figures 1 and 2. Free flight conditions are appropriate for the conditions of section 3.1.1, but for the conditions of sections 3.1.2 temperatures and

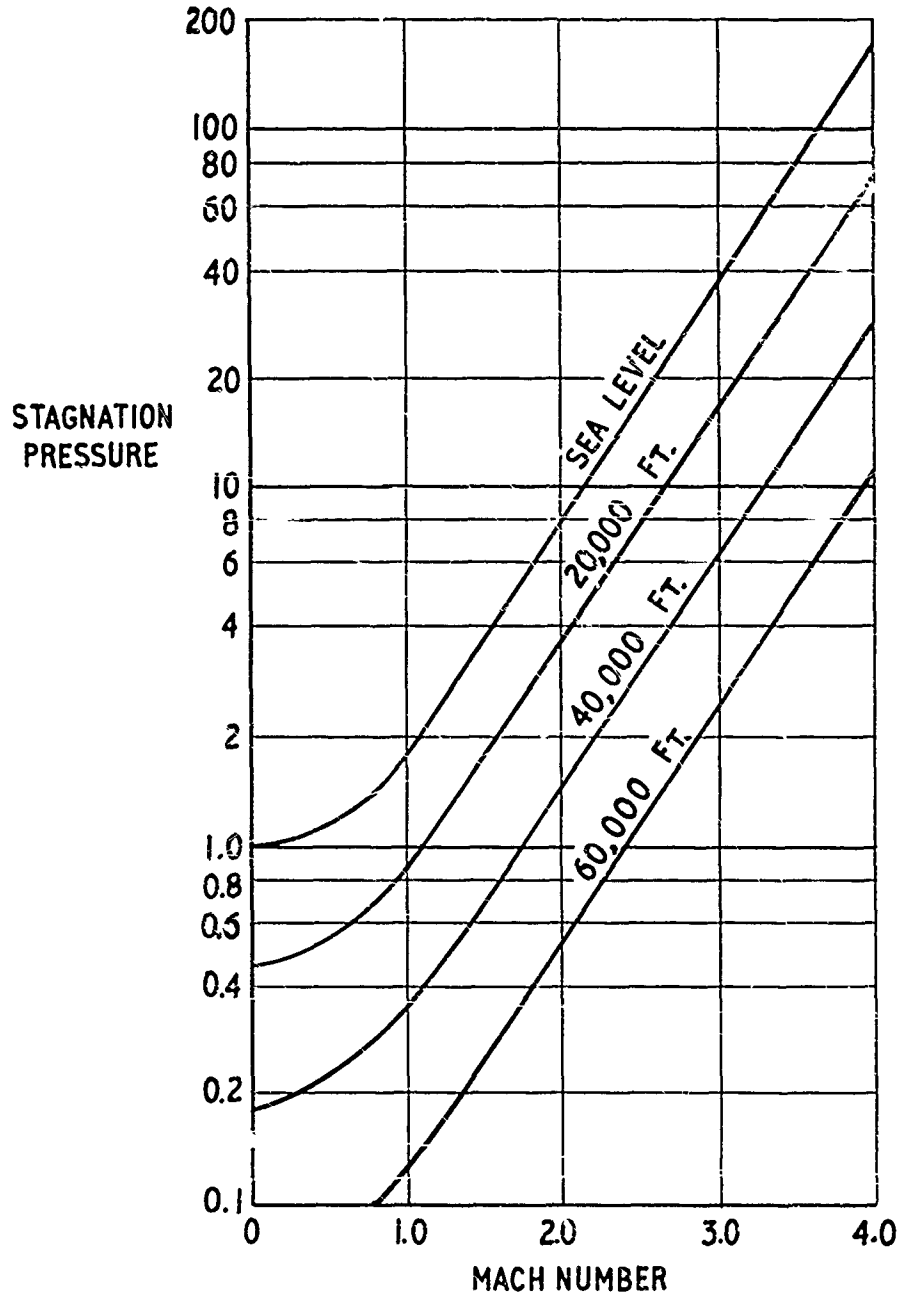


FIGURE 1

STAGNATION PRESSURE REQUIREMENTS FOR FREE FLIGHT SIMULATION

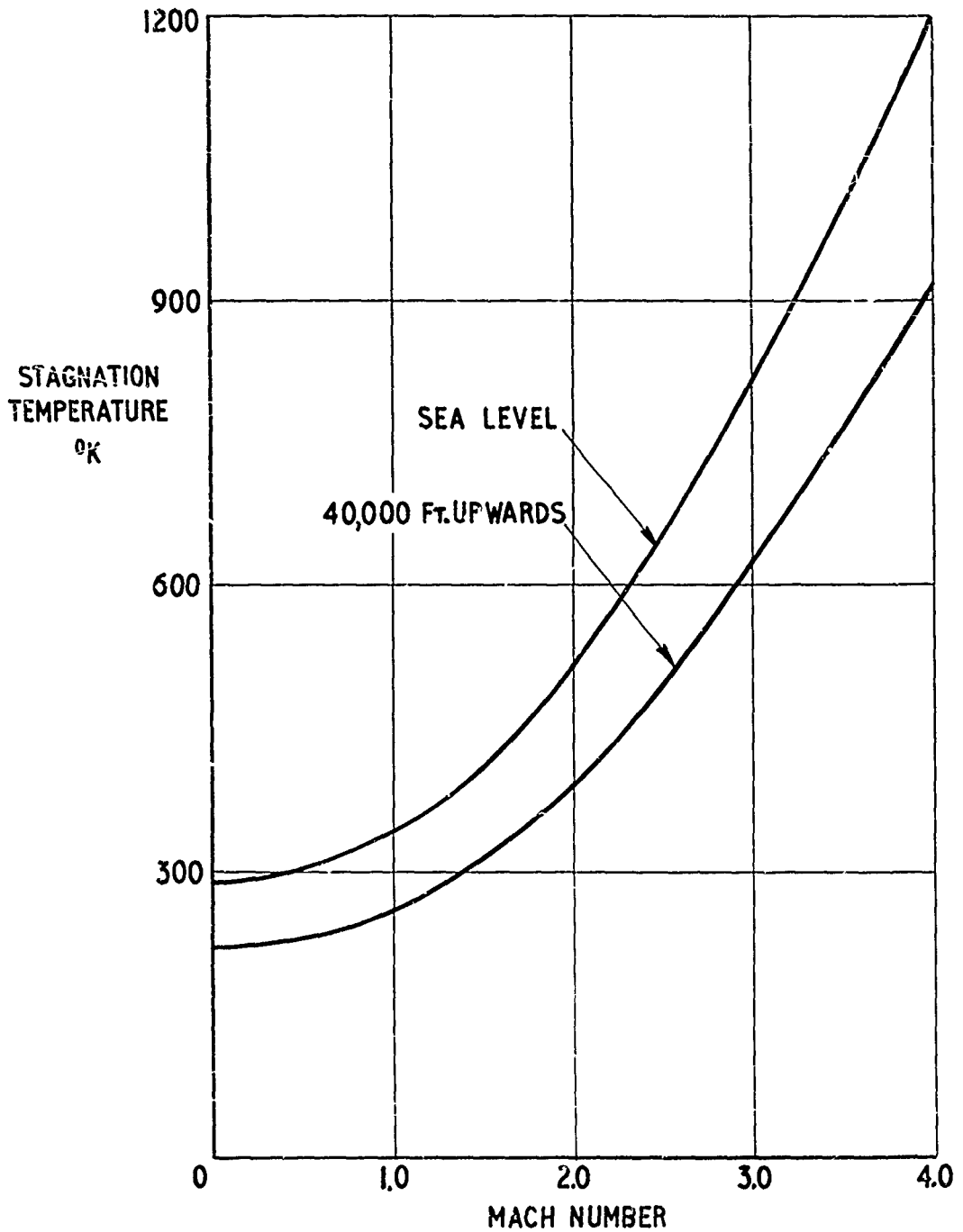


FIGURE 2

STAGNATION TEMPERATURE REQUIREMENTS FOR FREE FLIGHT SIMULATION

pressures greater than free flight may be required*. Quite obviously, in these circumstances, formidable engineering problems are involved simply in providing a wind tunnel of reasonable dimensions (say 2' x 2') that will withstand the temperatures and pressures involved.

Ideally of course, the tunnel conditions should be capable of controlled variation during a run so as to simulate the aircraft flight plan, and this requires control of stagnation pressure, stagnation temperature, Mach number and radiant heat. At the same time these quantities may need to be varied rapidly, since the time scale for model heating varies as the square of the length scale. For such a tunnel to be operated effectively, complete automation of tunnel control would probably be required. A block layout of a tunnel of this kind is shown in Figure 3.

Returning to reality, there may be some possibility of covering parts of the aircraft flight plan using models in existing tunnels, with the added provision of radiant heat in the working section. The problem of generally low stagnation pressure conditions in existing tunnels might be met to some extent by reducing model skin thickness scale relative to linear scale (as in 'cold' model work) though this will invalidate panel flutter results and results in an increased size of model being required**.

---

*Wind tunnel requirements are alleviated if a model material can be used having a higher coefficient of expansion, a lower elastic modulus and a lower conductivity than the aircraft material (e.g. magnesium in relation to an aircraft in dural). A search through the metal alloys and plastics may be rewarding in this respect.

**The quantities λ_{k_B}, λ_E, λ_{ρ_B} and λ_{c_B} are replaced by $\lambda_{k_B}\lambda_\delta^{-1}$, $\lambda_E\lambda_\delta$, $\lambda_{\rho_B}\lambda_\delta$ and $\lambda_{c_B}\lambda_\delta^{-1}$ respectively and only conduction in the skin plane is considered. Values of λ_L in Tables 2, 4 and 5 then require multiplying by a factor $\lambda_\delta^{\frac{-(1+r)}{r}}$.

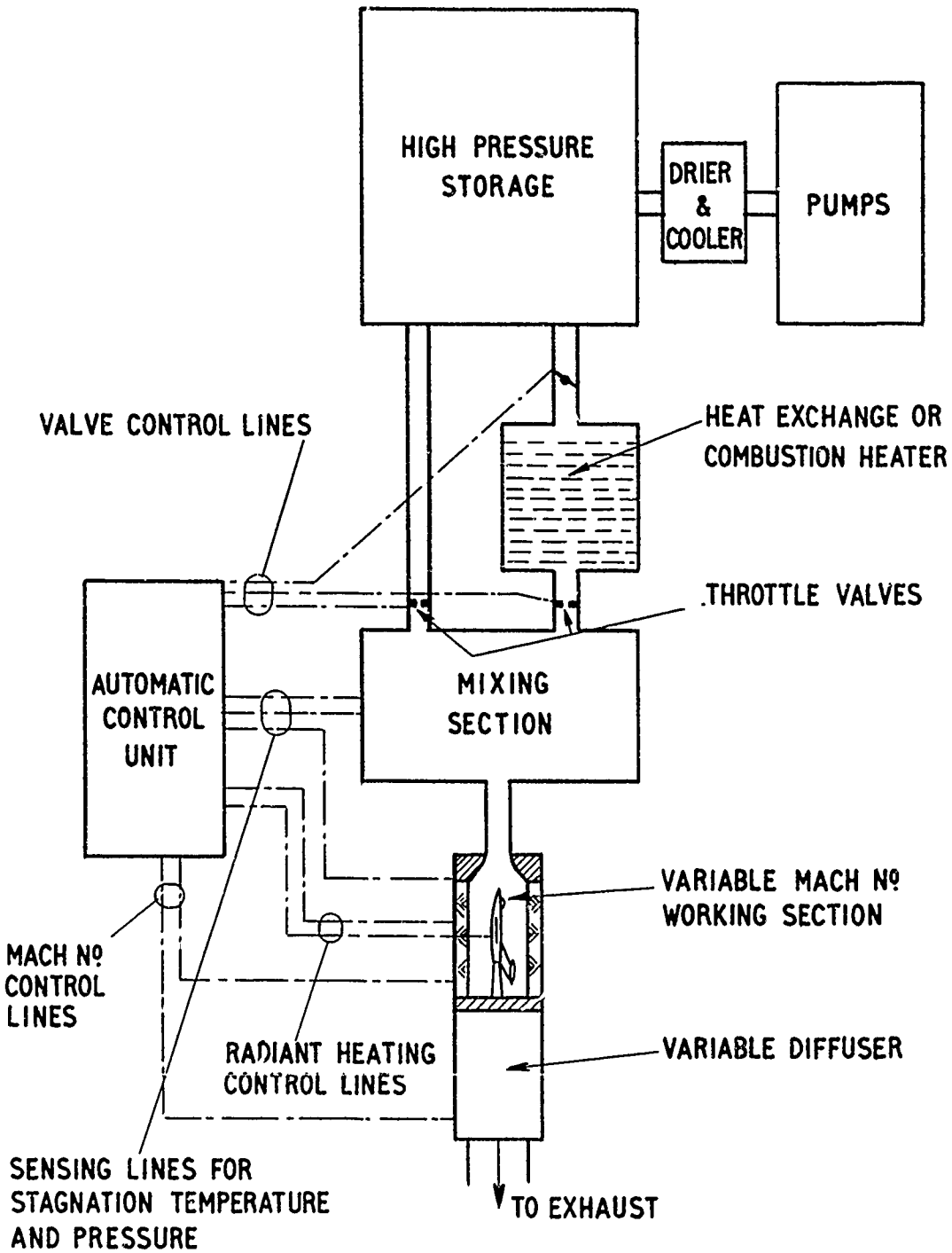


FIGURE 3
POSSIBLE TUNNEL LAYOUT

SECTION 5: MODEL CONSTRUCTION

There is, of course, little point in demonstrating that an approximation to aerothermoelastic similarity can be achieved for small scale models if it should then prove that the difficulties of model construction are insurmountable. If the tunnel size is large enough for models to be constructed using conventional riveting, welding and shaping procedures the problem is simplified, but this will rarely be the case.

The construction must be a closer replica of that for the aircraft than is usually the case for purely aeroelastic models, and the construction of the latter is formidable enough. Furthermore, few of the established techniques for the construction of small scale aeroelastic models are likely to be applicable in the thermal case.

Investigations of alternative methods of model construction are required, and in this respect a technique at present being developed at R.A.E. may ultimately be of value. This technique takes cognisance of the fact that several of the materials suitable for small scale aerothermoelastic models can be deposited electrolytically (e.g. nickel, cadmium, tin and zinc).

Nickel model wings of a duralumin aircraft ha- been made successfully by this process, a nickel skin of the required thickness being deposited directly onto a prepared former.

SECTION 6: CONCLUDING REMARKS

The foregoing considerations indicate that an approach to complete aerothermoelastic similarity can be achieved for small scale models, but models in the same materials as the aircraft must be tested in a different gas, while models in different materials can be tested in air. In both cases the wind tunnels required must have provision for heating the stream to full scale stagnation conditions (or higher), and controlled radiant heat in the working section is also necessary.

Areas where experimental investigations and development work are required are in the effectiveness of radiant heat in a supersonic tunnel and its control in relation to aerothermoelastic models, and in techniques of construction for these models. A survey of existing hot tunnels would also be of value in indicating their limitations with regard to the representation of full scale flight conditions, thus providing a datum for model similarity requirements.

REFERENCES

1. Bisplinghoff, R. L., Some Structural and Aeroelastic Considerations of High-Speed Flight, Nineteenth Wright Brothers Lecture, J.Ae.S., Vol. 23, No. 4, April 1956.

2. Budiansky, B. and Mayers, J., Influence of Aerodynamic Heating on the Effective Torsional Stiffness of Thin Wings, J.Ae.S., Vol. 23, No. 12, December 1956.

3. Mansfield, E. H., The Influence of Aerodynamic Heating on the Flexural Rigidity of a Thin Wing, ARC R & M 3115, September 1957.

4. Ting, L., Similarity Conditions for Testing High Speed Aircraft Models, Polytechnic Institute of Brooklyn, Dept. of Aero. Engineering and Applied Mechanics, PIBAL Rep. No. 308, AFOSR No. TN-56-548, November 1956.

5. O'Sullivan, W. J., Theory of Aircraft Structural Models Subjected to Aerodynamic Heating and External Loads, NACA TN 4115, September 1957.

6. Dugundji, J., Aerothermoelastic Modeling. Notes for a Special Summer Program in Aeroelasticity, Vol. 3, Chap. 14, Dept. of Aero. Engineering, MIT, 1958.

7. Howarth, L., Modern Developments in Fluid Dynamics, Vol. 1, Chap. X, Clarendon Press.

REFERENCES (Cont'd.)

8. Eckert, E. R. G., Introduction to the Transfer of Heat and Mass, McGraw Hill Book Co.

9. Timoshenko, S., Theory of Elasticity, McGraw Hill Book Co.

10. Houbolt, J. C., A Study of Several Aerothermoelastic Problems of Aircraft Structures in High-Speed Flight, Mitteilungen aus dem Institut für Flugzeugstatik und Liechtbau, No. 5, Verlag Leemann Zürich.

11. Young, G. B. W. and Janssen, F., The Compressible Boundary Layer, J.Ae.S., Vol. 19, No. 4, April 1952.

12. Chapman, D. R., Some Possibilities of Using Gas Mixtures Other Than Air in Aerodynamic Research, NACA Rep. 1259, 1956.

13. Ashley, H. and Zartarian, G., Piston Theory - A New Aerodynamic Tool for the Aeroelastician, J.Ae.S., Vol. 23, No. 12, December 1956.

14. Trussell, D. H. and Weidman, D. J., A Radiant Heater ± Simulate Aerodynamic Heating in a Wind Tunnel, NASA Tech. Note D-530, November 1960.

15. Broadbent, E. G., Flutter of an Untapered Wing Allowing for Thermal Effects, ARC Current Paper 442, 1959.

16. Lambourne, N. C. and Scruton, C., On Flutter Testing in High-Speed Wind Tunnels, ARC R & M 3054, 1958.

SESSION II

FLIGHT CONTROL

Chairman: Professor Bernard Etkin
University of Toronto

PREVIOUS PAGE
IS BLANK

FLIGHT CONTROL OF AEROTHERMOELASTICALLY AFFECTED VEHICLES

by

MELVIN B. ZISFEIN

Astromechanics Research Division

Giannini Controls Corporation

ABSTRACT

This paper begins with a brief description of the aeroelastic interactions which can influence the stability and control of a flight vehicle. Next, some highlights of the past decade's flight control aerothermoelasticity research are presented, leading to a description of present capabilities. The paper concludes with a discussion of some future problem areas and suggestions for some of the research which will be required for future flight vehicle design.

FLIGHT CONTROL OF AEROTHERMOELASTICALLY AFFECTED VEHICLES

INTRODUCTION

I will start by quoting a poem:

"Icarus, dicarus, dock
The vehicle flew at high Mach
The airframe got heated
The customer, cheated.
And the company went into hock."

This pearl was composed in 1953 by one of my associates at that time. It commemorates an occasion far more serious than the tone in which it was written and I present it here as a memento of an early aerothermoelastic ulcer (fortunately, not mine), and because it is consistent with the purpose of this paper. This purpose is, stated simply, to lay the foundations for the more technical dissertations to follow. For the benefit of the non-aeroelasticians in the audience, I will first describe some of the common aeroelastic interactions important to flight control. I warn the audience that brevity forces upon me the grossest of oversimplifications, but I hope to retain the essence of the story. I will next discuss some facets of the history of flight control aeroelasticity research over the past decade so that I might delineate particular problem areas and their solutions. I will conclude this paper with some thoughts for the future.

SECTION I FLIGHT CONTROL AEROELASTICITY

Let me begin by describing briefly the areas and problems normally considered by the flight control aeroelastician. Briefly, his task is to account for the effects of airframe flexibility on all of the parameters of vehicle static and dynamic stability and response, and to ensure that all flight control requirements are met by the flexible vehicle.

Let us consider several illustrations of these effects of flexibility on the various parameters of stability and control. In our first slide* we see what used to be regarded as a conventional airplane. If the wing

---

* In this paper, slides refer to Figures 1 through 7.

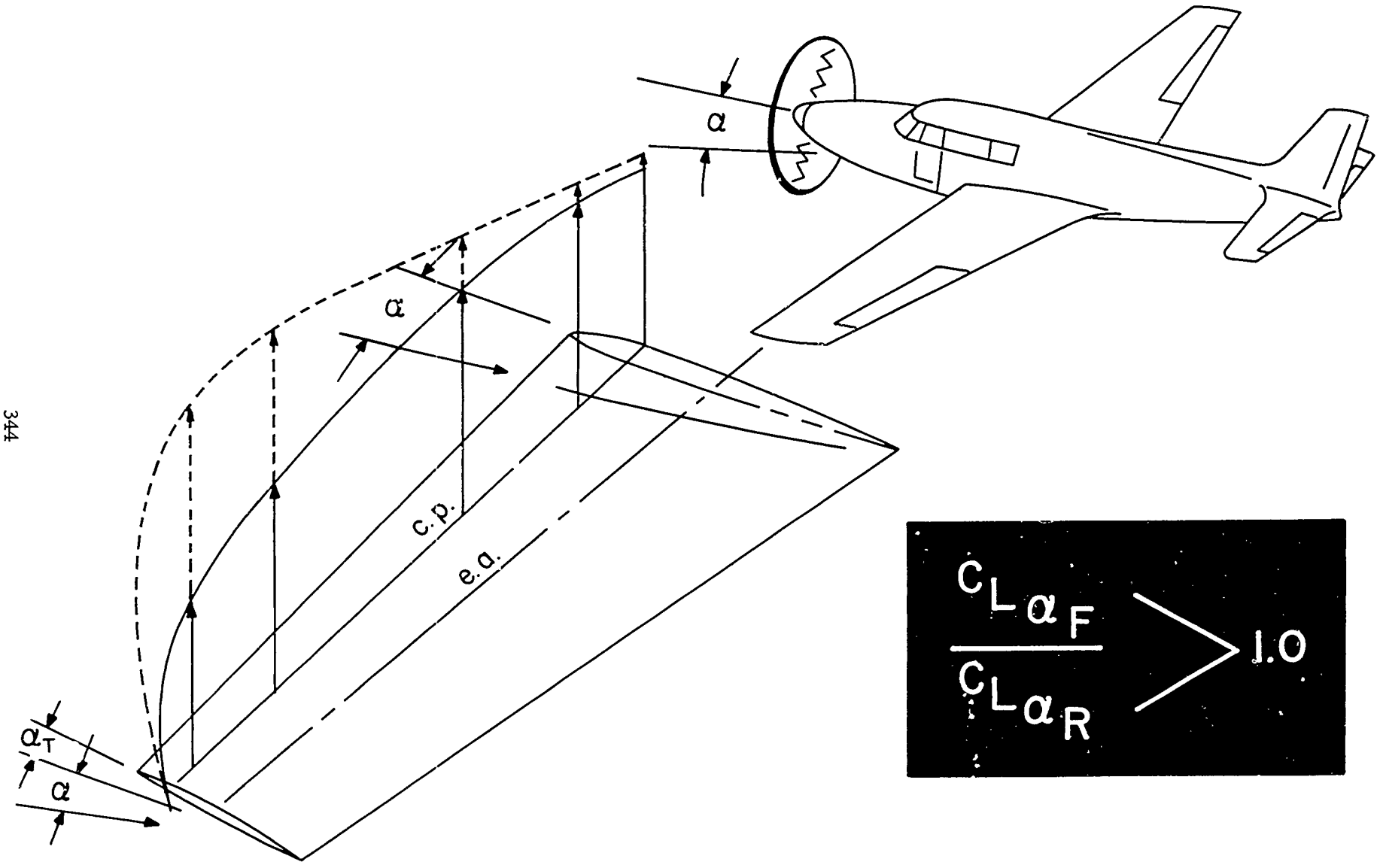


Figure 1. Convential Wing

(shown enlarged in the insert) were entirely rigid it would carry the spanwise load distribution shown in black. However, this wing is flexible and has a line of centers of pressure not coincident with its own zero twist axis. Therefore, the wing twists under its own airload. In the case shown here this twist brings on more airload which brings on some more twist which brings on some more airload until some equilibrium airload condition (shown dashed) is reached. Note that for the same wing root angle of attack the flexible wing will be carrying more lift than its rigid counterpart. This situation will exist for any wing root angle of attack below that associated with stall somewhere on the wing. Hence, the flexible wing shown here has a greater C_{L_α} than its rigid counterpart. The discrepancy between $C_{L_\alpha\ (Flexible)}$ and $C_{L_\alpha\ (Rigid)}$ for the wing shown will increase with dynamic pressure or wing flexibility until we encounter the familiar aeroelastic divergence; at which point the C_{L_α} of the flexible wing tends to increase without bound and the wing may be destroyed. Obviously, the C_{L_α} required for all stability and control work on the vehicle shown on the slide will be the flexible C_{L_α} as this will be the true lift behavior of the vehicle in flight. Hence, we might say that an obvious function of the stability and control aeroelastician is to transform the aerodynamicists' $C_{L_\alpha\ (Rigid)}$ to the more appropriate $C_{L_\alpha\ (Flexible)}$

What other stability and control derivatives of the example vehicle can be affected by vehicle flexibility? All of the derivatives can be! Are they all affected in the same way? No, they are not. Consider the effect of wing bending on the C_{L_α} ratio just considered. Being an unswept wing, a reasonable amount of bending will change no streamwise angles and hence will have no effect on the C_{L_α} ratio. However, bending will certainly produce meaningful changes the distribution of dihedral angle along the wingspan. Hence, two vehicles having identical wings like those shown in Slide 1, except that one is relatively rigid and the other is relatively flexible, could be expected to have vastly different values on the rolling derivative due to yaw, C_{l_β}. If these vehicles were traveling at speeds such that the centers of pressure of their lift distributions were coincident with their elastic axes, then their C_{L_α}'s would be identical and equal to the C_{L_α} of their rigid counterpart while at the same time their rolling derivatives, C_{l_β} would be quite different.

In Slide 2 we see a wing similar to the one that we just considered except that this wing is a swept wing. In essentially the same way as the wing in the previous figure, the airload is twisting

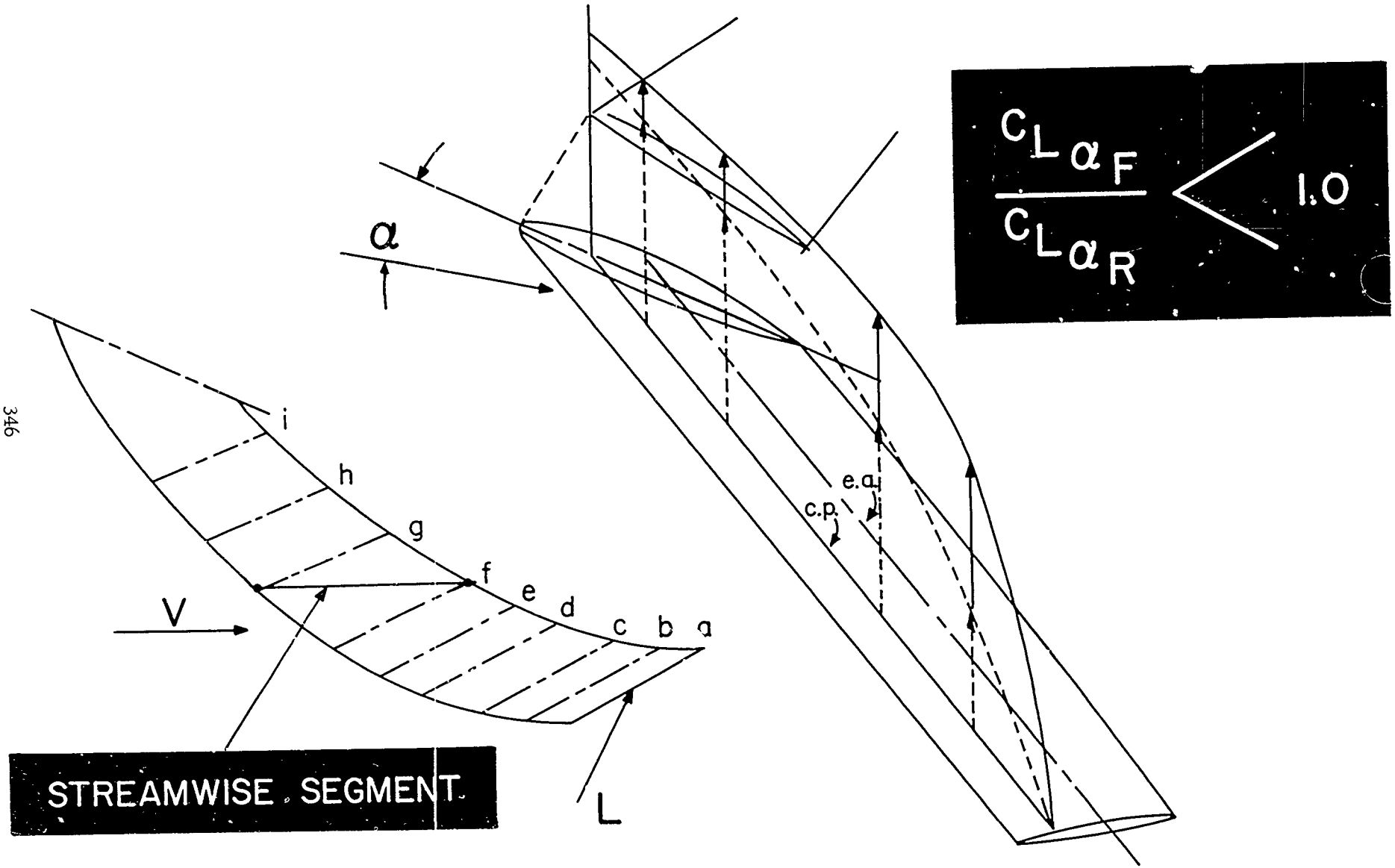


Figure 2. Swept Wing

this swept wing. However, here a component of the dihedral angle due to bending is felt by the airstream as a twist angle. For the swept back wing shown here this twist angle acts in such a way as to decrease the lift on the wing section. This effect is best shown by looking at the wing in the insert sketch which is shown greatly distorted. This wing is being bent up by the load L - lines of equal height are shown on the wing as dotted lines; the highest being line a, the next highest being line b, the next highest line c, and so on. From the sketch we see that the typical streamwise segment shown running between dotted lines f and g appears twisted to the air stream since its leading edge, g, is at a lower elevation than its trailing edge f. In the wing shown in this slide , this washout twist due to bending overcomes the wash-in twist due to torsion; the net effect being less lift on the flexible wing at the same angle of attack. Here we see a case where C_{L_α} of the flexible wing is lower than C_{L_α} of the rigid wing.

Now turning to a vehicle of more modern configuration in Slide 3 we find that there is so much opportunity for chordwise deformation and so little chance of having a really meaningful elastic axis that the concepts of bending and twist lose most of their meaning in describing the aeroelastic deformations of this wing. However, putting this vehicle at an angle of attack will result in a distribution of deformation along the span and chord which can be predicted and which acts in much the same manner as the previous deformations to redistribute the lifting load over the wing. Here again, for the same wing root angle of attack, the lifting pressure on the flexible wing is shown as dashed lines. In this case the mechanisms producing the distortion are considerably more subtle than the simple mechanisms discussed previously, but they are now well understood and they combine to produce the same net effect as before, namely that $C_{L_{\alpha\ (\text{Flexible})}}$ is different from $C_{L_{\alpha\ (\text{Rigid})}}$. Similarly, in analogous fashion, we can demonstrate that, in general, all of the remaining stability derivatives will be different on the flexible vehicle from those of its rigid counterpart. These differences must first be calculated and then used appropriately in the flight control design and analysis of the flexible vehicle.

The various stability derivatives corrected in this static or quasi-static fashion do describe, to an extent, even the dynamic properties of the flexible vehicle when the elastic modes of the vehicle are reasonably remote from the so-called rigid body modes of the vehicle. Under these circumstances the dynamic stability or dynamic response equations derived for the rigid vehicle may be used to describe the flexible vehicle merely by substituting the stability derivatives corrected for the quasi-static effects of flexibility for the various rigid body stability deriva-

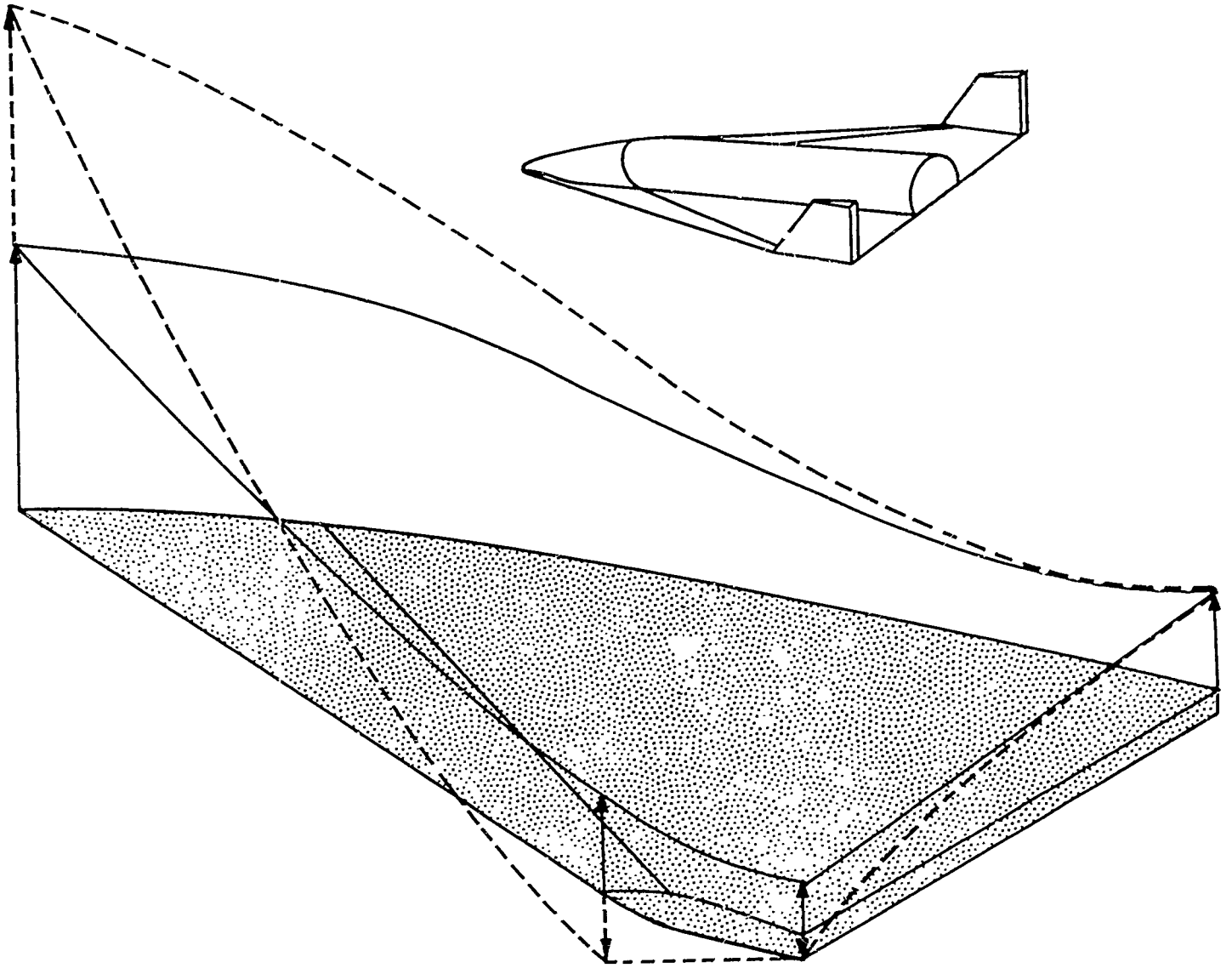


Figure 3. Modern Configuration

tives. This artifice has been used successfully in many instances. However, when automatic control or stability augmentation feedback loops are employed, considerable care must be taken to ensure that a mathematical fiction is not the end result. For instance, consider the typical reentry glider configuration shown in Slide 4. We assume a simple, single sensor feedback loop. Let us consider the longitudinal short period degrees of freedom combined with one flexible body degree of freedom. Considering first only the pitch and the vertical translation degrees of freedom, for a severe reentry condition we might encounter a root-locus diagram like that on the extreme lefthand side of the next slide, Slide 5. Here as we increase gain, the short period frequencies are seen to increase. However, no dynamic instabiltiy is shown. Next we modify our calculations substituting possible but severe quasi-static changes in C_{L_α} and C_{m_α} giving us the root-locus diagram second from the left on our slide. Dynamic behavior prediction is somewhat modified but the roots-loci are similar in that no instability is shown. Next we rewrite our equations of motion to admit the single additional degree of freedom of body bending. The root-locus diagram second from the right describes the dynamics of this case and shows marked decreases in stability with increasing gain and a definite region of instability involving the airplane short period and flexible body modes. If we assume that our hypothetical vehicle has a structure which is not thermally protected and we take into account the stiffness loss caused by aerodynamic heating, we bring together the short period and body bending frequencies to produce even more drastic changes in the vehicle stability as shown in the root-locus diagram at the extreme right of the slide.

To continue this basic description of possible aeroelasticity effects on flight control, I should mention also that class of quasi-static phenomena known popularly as aeroelastic control reversals. These effects are possibly the most familiar of all the various aeroelastic effects on flight control. These so-called reversal phenomena occur when a control force or moment applied to the vehicle so distorts the airframe that an aerodynamic force arises which usually tends to decrease the applied control force, but which in some cases may actually amplify it. The name "reversal" has been popularly applied to this variety of aeroelastic interaction because under severe circumstances the aeroelastically induced control force or moment can exceed the applied control force or moment making the vehicle behave as if a control force of opposite sense had been applied. Aileron reversal is the most common of these effects and this phenomenon has in the past been responsible for severe flight restrictions on a number of vehicles.

To conclude this review I should mention also the flexibilities within the hardware of a flight control system can have an important effect upon the flight control of the vehicle. This is a subject most frequently overlooked by all but the flight control aeroelastician and the flutter analyst, both of whom have long been aware of the importance of this area.

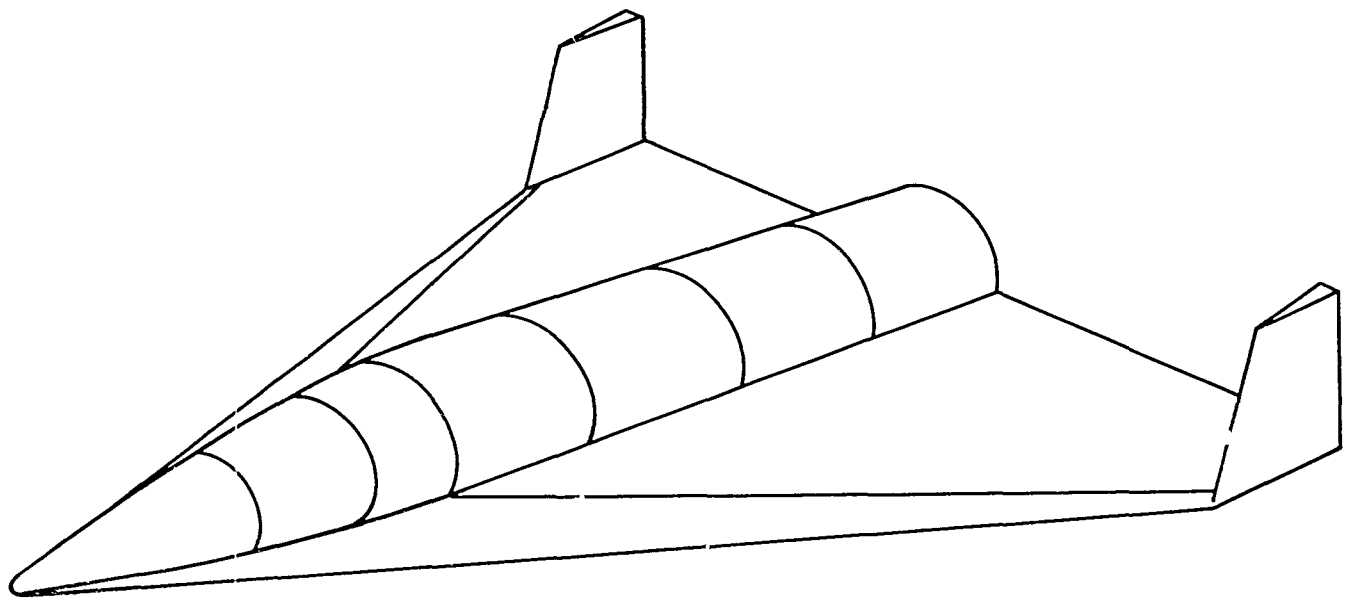


Figure 4. Typical Re-entry Glider Configuration

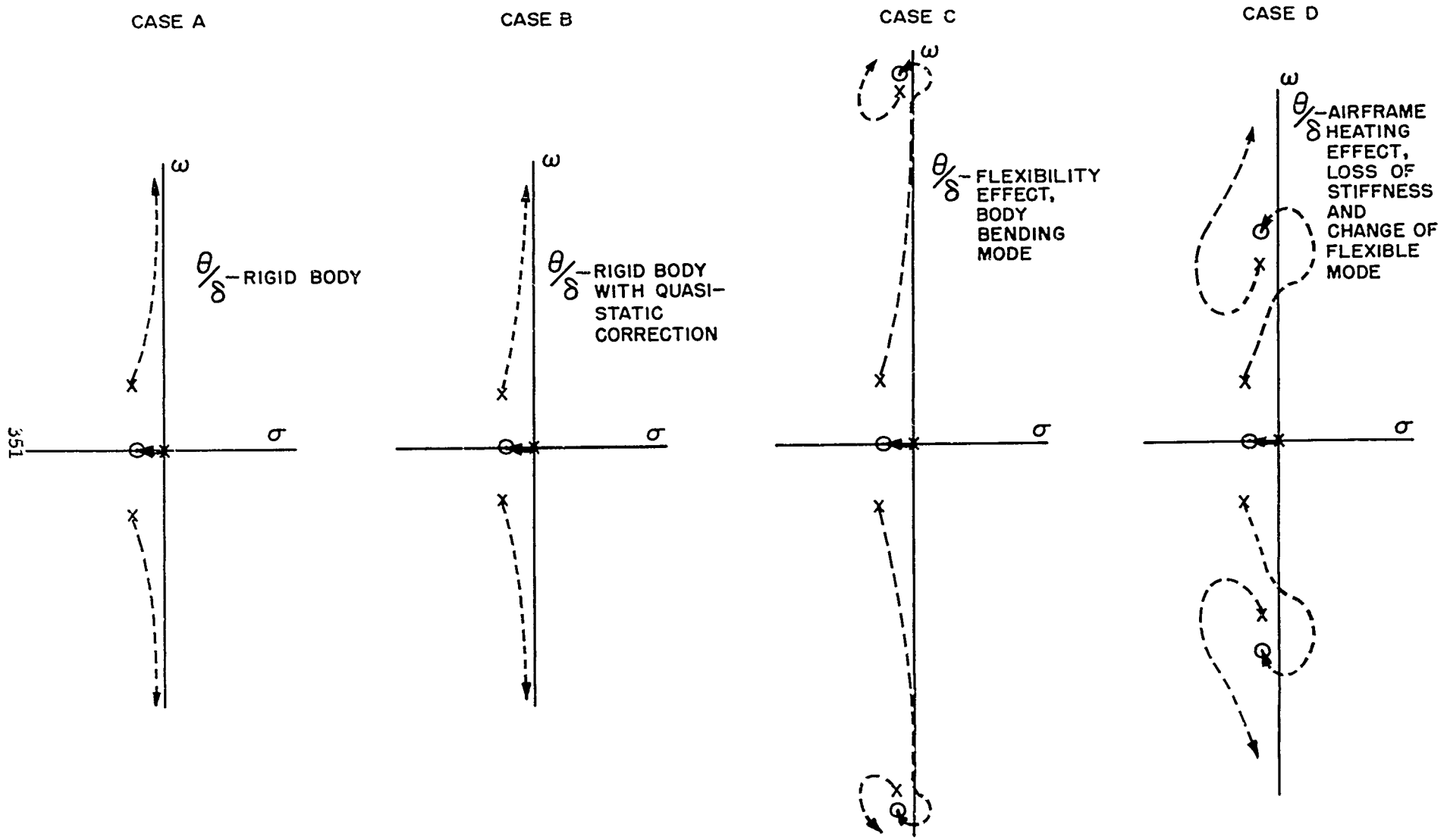


Figure 5. Root-Locus Diagram

SECTION II CURRENT STATUS OF AEROTHERMOELASTICITY

I would now like to highlight the current status of aeroelasticity technology as applied to flight control work and to suggest some areas where future research appears to be potentially profitable. That I might better do this let me summarize the status of aerothermoelasticity as we of the aircraft industry saw it in the early fifties.

Supersonic flow was, in gross, well understood and lift and drag estimates for low-aspect-ratio air vehicles were being made with some degree of confidence. Flight test results were being obtained with increasing frequency to increase this level of confidence. However, as soon as one left the area germane to the simple parameters of vehicle performance, the available fund of proven aerodynamic technology was indeed small and was certainly inadequate for the aeroelastic design jobs which lay ahead. The importance of aerodynamic heating was not appreciated in many quarters and the technology which the industry required to cope with aerothermal problems was, at that time, in various early stages of development. Much of this development was marked by heated but usually healthy controversy.

The structural side of the aerothermoelastic picture was, in these early days, even less well illuminated. "Simple beamology" was the common structural representation and the fact that a large number of the wing and tail structures then under consideration did not have any line, or group of nearby lines, which could be called an elastic axis was not appreciated until a much later date. This state of affairs caused the publication of very large errors in many design studies and analyses.

Aerodynamic load inputs were correspondingly crude. The distribution of lifting pressure over an arbitrarily deformed lifting surface at high air speeds could be calculated only at the expense of truly great computational labor, and, as a matter of fact, subsequent tests have proved that even these calculations were frequently seriously in error.

The combination of all of these aforementioned inputs into solutions for aerothermoelastic effects on stability and control was, strangely, in much better shape than the calculation of the inputs themselves. Certain basic and straightforward solution forms had been evolved for these problems during the thirties and forties and these forms proved (with not many exceptions) to be easily adapted to the design of aerothermoelastically affected vehicles as they were to their slower counterparts. However, the limitations of the analog and digital computing machinery

available at that time did engender some severe computational hardships.

This situation, wherein the method of solution is better known and much more straightforward than good aerodynamic and structural inputs to the solution, has been characteristic of both static and dynamic flight control aeroelasticity during the past decade. During the early fifties there was available no method of proven accuracy for the calculation of static or dynamic aerodynamic influence coefficients. During the same period there were available a number of methods for the calculation of the deformation influence coefficients of low-aspect-ratio built-up structures. Through these and standard vibration solutions, the modes and frequencies could also be calculated. However, no one really knew the absolute or relative accuracy of any of these methods since only one or two wing-like built-up structures had ever been tested to determine experimentally their deformation influence coefficients. (As a matter of fact, when we finally got around to testing, some of the published methods turned out to be very poor.)

Hence, to those of us deeply involved with the aeroelasticity of flight control it was vital that we concern ourselves with a series of topics not obviously related to flight control.

I list some:

1. The development of methods for the experimental determination of structural deformation influence coefficients for both unheated structures and for structures under steady state and transient aerodynamic heating.

2. The derivation of aerodynamic influence operators for subsonic, transonic, supersonic and hypersonic speed ranges.

3. Theoretical derivations of structural influence coefficients for built-up structures, both unheated and under conditions of aerodynamic heating.

From time to time I have seen various engineers express surprise that a topic such as the rib and spar orientation of a wing or its thermal stress pattern should be of any concern at all to the aerodynamic stability and control analyst. I can only reply that it would be impossible to evaluate the flight control system of the flexible vehicle without these and many other similar items of information.

Today's and tomorrow's programs contain papers presenting some of the latest outputs of these examinations of aeroelastic inputs. Dr. Covert will present a dissertation on aerodynamic operators and influence coefficients and Messrs. Donato, Batt, and Padlog will

extend some of this thinking into the hypersonic regime where nonlinear aerodynamics of lift has become the rule. Mr. Gallagher will also present some of his advanced work in structural operators.

Thus even today, we cannot say that the basic input problems confronting the flight control aeroelastician ten years ago are all solved. We can say, however, that these are largely solved and this is, in itself, a fine state of affairs. Surveying the situation in detail we find that most of the aerodynamic, thermodynamic and structural input data, so obviously lacking a decade ago, have been published. Much of this effort was performed under research contracts sponsored by the ASD Flight Control Laboratory and a large part of this is published in the various volumes of WADD Technical Reports 58-95 and 58-378. These reports constitute a readily useable text and manual permitting a sophisticated attack by even a relatively junior analyst.

SECTION III FUTURE AEROTHERMOELASTICITY

Now to the future, there are several areas where more of such information is needed. Hypersonic aeroelasticity has recently been studied and this topic will be covered in the paper by Messrs. Donato, Batt, and Padlog. I am sure that they will agree that basic and applied research in this area is far from complete. This is particularly true concerning analytical approaches to the problems of hypersonic aerodynamic operators and the prediction of structural stiffnesses of severely heated and thermally stressed structures. Two other areas where work is needed are those connected with good aerodynamic inputs due to nacelles and stores and a simple closed form technique for making low cost aeroelastic models from a known set of structural influence coefficients.

Another area where more knowledge might prove to be important concerns the development of simple comparators whereby an appreciation of aerothermoelastic implications in the basic postulation of a mission or vehicle requirement may be obtained at an early stage in the development of the vehicle. As a result of a recent consultative study for the ASD Flight Control Laboratory, it has become apparent that many decisions which are made during the conceptual stage of a weapon system's evolution can be responsible for severe aerothermoelastic problems which become evident at a much later date. My next two slides are presented to show the kind of information which a good aeroelastic comparator for early design might reveal. I must apologize here for a deliberate vagueness regarding these figures. Their ordinates are two trial comparators which we called the Nose (or Chordwise) Divergence Comparator and the Wing Divergence Comparator. Time does not allow me to derive the algebraic expressions here and security restrictions do not allow me to present any numbers. It will have to suf-

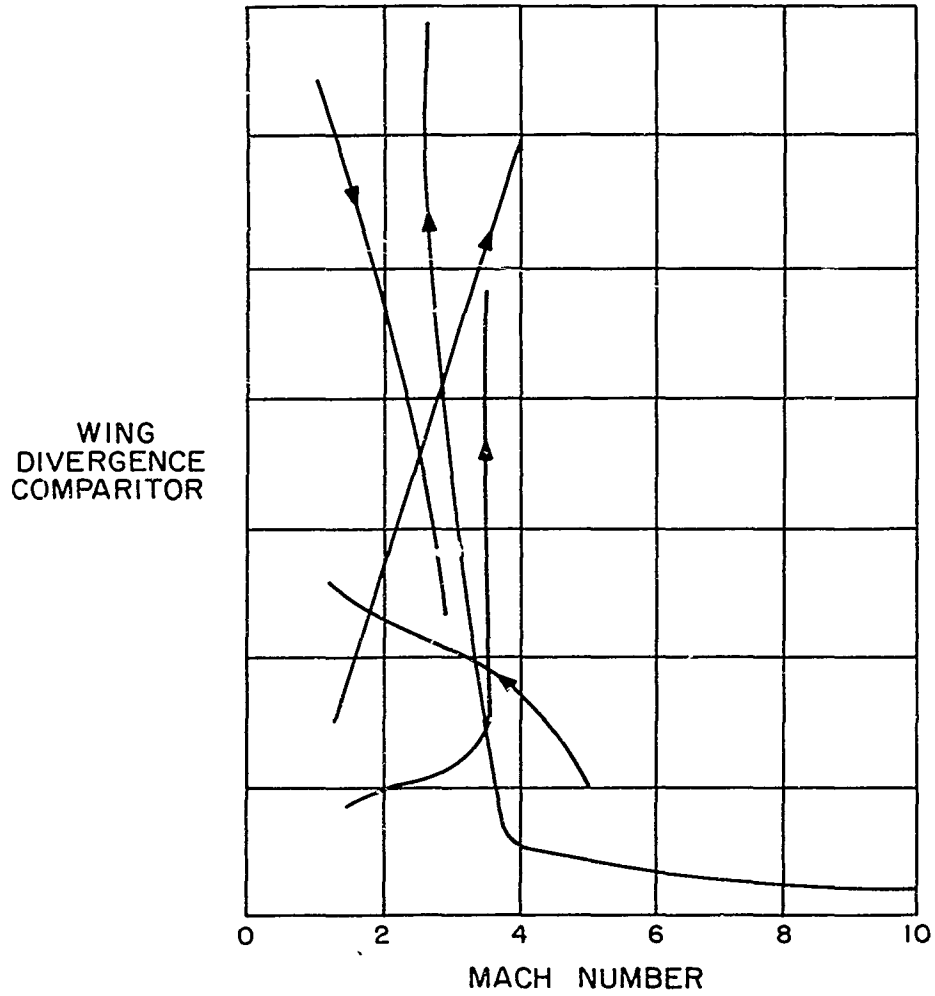


Figure 6. Wing Divergence Comparison

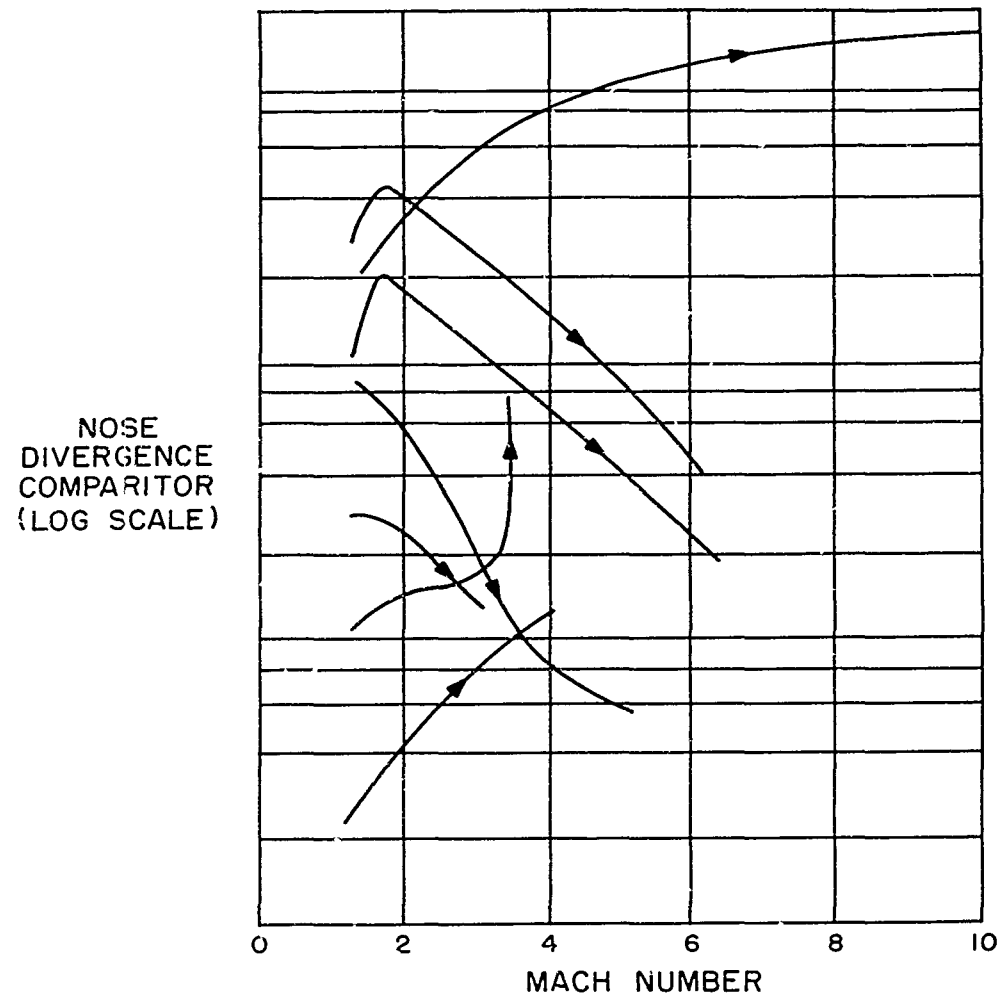


Figure 7. Nose Divergence Comparisor.

fice to say that the higher the value of the comparator the greater the chance of encountering the design problems implied by the name of the comparator of a problem related to this. For instance, high values of the Wing Divergence Comparator mean a relatively high probability of encountering those problems associated with divergence such as divergence itself, large aeroelastically induced C_{L_α} changes, large center of pressure shifts, etc. Now to the slides. The first of these slides, Slide 6, shows a Wing Divergence Comparator plotted vs. Mach number for a number of well known future vehicle systems. Proprietary restrictions prevent me from identifying the contractors, hence the vehicles themselves. However even under these restrictions we can learn a number of things from these comparisons. We observe that future missions will tend to be aerothermoelastically severe from Mach 1 to about Mach 4 and there appears to be ample justification for advanced aerothermoelastic test facilities in this range. Slide 6 shows an apparent marked absence of problem areas at Mach numbers higher than 4. This apparent drop-off in severity after Mach 4 may be caused by the limited amount of detailed data available to the Flight Control Laboratory on advanced systems similar to those shown here. We were able to find more data for the comparison of nose or chordwise divergence. This comparator is shown plotted logarithmically vs. Mach number in Slide 7. Here we see that some vehicle systems do tend to less severe comparator values with increasing Mach numbers as indicated on the previous slide, while others tend to more severe values. It is interesting to note that these two trends are generally indicative of two very different classes of mission. The curves which increase with increasing Mach number are typical of the class of usually unmanned flight vehicles which we have come to call "interceptors", while the curves which decrease with increasing Mach number are typical of what we have come to call "flyers". We have barely scratched the surface in this area of aerothermoelastic comparators for the earliest stages of design and a great deal of creative thought is required here.

Because of the security and proprietary restrictions which I mentioned earlier, this slide and the previous slide were presented more to illustrate the kind of work which might be done than to convey specific information.

What else does the flight control aeroelastician need for future vehicles? I feel that the most pressing need is for real understanding or feel for the interplay of vehicle flexibility and conventional dynamic stability and response. There is no absolute lack of analytical tools here, since given enough computational time and manpower we have the technology to design and analyze any reasonable configuration. What appears to be lacking is a feel for trends. If I consider, say a Mach

3 transport, is my automatic control system likely to be more satisfactory if my wing torsion is below fundamental bending or vice versa; what is the effect on the dynamic flight control picture of the stiffness loss due to aerodynamic heating, etc.? Some recent exploratory efforts by Computer Engineering Associates, Systems Technology, Inc. and our organization (all sponsored by the ASD Flight Control Laboratory) have been very illuminating. There is much more to be learned along these lines.

I have said that there is no absolute lack of analytical tools for the flexible vehicle closed loop control problem. What is lacking, however, is formalization. There is nowhere documented in text form the systematic approach that is to be used in the aeroservoelastic design of a flexible flight vehicle. Designs are currently handled on a catch as catch can basis. The successful manipulation of aeroelastically caused and unwanted bulges in a Nyquist locus is today an art, not a science. The successful aeroservoelastic design of, say, a multiloop, very flexible, long slender boosted vehicle frequently contains lessons which are new and highly instructive to even the most experienced analyst. What is clearly required is a formalization of aeroservoelastic design techniques so that these problems may be handled, perhaps not by recent graduates, but nevertheless at a far lower academic level than is required to cope with them today. I cite as an example of the feasibility of such a formalization the published formalization of static and quasi-static aeroelasticity found in WADD TR's 58-95 and 58-378.

The foregoing is not meant to imply that the design of a flexible flight vehicle is a closed subject which merely needs documentation. On the contrary, even though the need for formalization of existing technology is evident, this is, perhaps, one of our most fertile fields for ingenuity and the inventive approach. Messrs. Gregory and Davis will explore this area in their paper later today.

Another productive area for applied dynamic aeroelasticity research lies in creating an experimental technology whereby a flexible model of a vehicle can be flown in a wind tunnel so that a flight-test-like evaluation of its dynamic stability and load characteristics can be obtained at an early stage of design. The model- mounting, similitude, and data handling problems are difficult but these appear to be surmountable. Late last year the Flight Dynamics and Flight Control Laboratories of ASD solicited proposals on this effort and my associates and I were selected to perform the study. We are busily engaged in this work at present and I am happy to report that our early technical results are most encouraging.

SECTION IV SUMMARY

To summarize, I have described in vastly oversimplified form the static and dynamic aeroelasticity of flight control. I have discussed the progress in this field during the past decade and I have very briefly indicated a few of the problems which remain to be solved. There are others. I think it significant that whereas the bulk of flight control aeroelasticity research of the past decade lay in static and quasi-static aeroelasticity the bulk of the coming decade's effort appears to lie in the area of dynamic aeroelasticity as it affects flight control. I sincerely hope that these efforts are at least as successful as our work of the past decade.

APPENDIX A

SYSTEM AEROELASTIC COMPARATORS

The notion of a comparator has been discussed in the text. The derivations and comparators presented here are new and their use in system and mission study is somewhat experimental. Interpretation should be made with caution because it is believed that there is room for further development of the concept. It is offered here as a promising tool for system study during the earliest stages of design.

I. Comparators for Static Aeroelastic Phenomena

The comparators for the static aeroelastic phenomena of (a) wing divergence and (b) chordwise or nose divergence are developed from closed-form formulations by manipulation of the relevant parameters to yield simple but physically descriptive expressions which will be high in magnitude for severe conditions and low for mild conditions. The intent is to develop a comprehensive parameter made up of vehicle and flight path quantities, said parameter having high values for high probability of a serious problem and low values for low probability of a serious problem.

a. Wing Divergence Comparator

A comparator for wing torsional divergence may be obtained from the direct collocation matrix expression for the divergence of a finite wing,

$$\{\alpha_s\} = q^*[A]\{\alpha_s\}$$

$$\text{where } q^* = \frac{C_{L_\alpha} e_{1_{Ref}} \bar{c}^2 b^2 \cos\Lambda_L q}{GJ_{Ref}} \qquad (1)$$

The matrix $[A]$, although usually found from a long matrix equation, is made up of only normalized distributed quantities such as $\left[\frac{GJ_{Ref}}{GJ}\right]$, $\left[\frac{e_1}{e_{1_{Ref}}} \quad \frac{c}{\bar{c}}\right]$, etc.** The divergence eigen-value, q^*, is made up of the dynamic pressure q, a sweep angle function, and all of the dimensional "Reference" quantities used to normalize the components of the matrix $[A]$. Some experience with static aeroelasticity makes it clear that when going from one wing to another most of the change in divergence dynamic pressure comes from the changes in magnitude of the components of q^*. The distributive type changes in the components of $[A]$, while not negligible, are almost always secondary in importance. Therefore, for preliminary comparisons of divergence "proneness" of a vehicle and its flight path, the variations in $[A]$ are ignored and a wing divergence comparator is developed from the much more sensitive (and more easily obtained) q^*. Since we wish to operate further on q^* to get the simplest meaningful comparator let us call our wing divergence comparator $D^* = q^*$. Thus, from Equation (1), (replacing $\cos\Lambda$ by $g(\Lambda)$ for generality)

$$D^* = \frac{C_{L_\alpha} \; q \; \bar{c}^{-2} \; b^2 e_{1_{Ref}} g(\Lambda)}{GJ_{Ref}} \qquad (2)$$

Examining D^* for simplifications, the sweep angle function $g(\Lambda)$ may be crudely approximated by $\left(1 - \frac{\Lambda_{ea}}{\Lambda_{iso}}\right)$ for $\Lambda_{ea} < \Lambda_{iso}$, and its range is from 1 at $\Lambda_{ea} = 0$ to 0 at $\Lambda_{ea} \geq \Lambda_{iso}$. However, from the

---

**This is strictly true only for pure torsional divergence as any bending terms in $[A]$ will be multiplied by a factor of $b/\bar{c}$. However, going thru essentially the same type of reasoning and manipulations that we perform here, the bending expressions reduce to a comparator identical to the one we will get here.

preliminary-preliminary designers viewpoint sweep angle can be varied over a wide range. It would not be fair to penalize (perhaps severely) an evaluation of a mission because the sweep angle of one of the early study configurations had been selected by a designer without full consideration of the aeroelastic consequences. This angle would certainly be changed in a somewhat later phase of the design of the system.

It is consistent, then, to eliminate sweep angle from our comparator. (Note that in comparing formal contractor proposals which were to lead to a contract to build a vehicle, sweep angle would most certainly be retained in a comparator.)

Although GJ_{Ref} might be known to some of the submitting contractors, experience has shown that to this date it is seldom obtainable from their System Requirement study reports. Moreover, stiffness being related to strength, and strength being dictated by mission load factor requirement, this latter is a basic parameter. The relationship of GJ_{Ref} to load factor is determined by the following reasoning. The configuration performing its maneuver of maximum design g's will have a semispan lift of $n_z \frac{W_t}{2}$, that is, half the inertial loading, the resultant of which may be considered to act at approximately 1/3 semispan. The wing root moment is then $M_{Root} = \frac{n_z W_t b}{12}$. Stress is related to bending moment by $f = \frac{My}{I}$ so that

$$I_{Root} = \frac{M_{Root} y}{f_{Root}} = \frac{n_z W_t b \; t/2}{12 \; f_{Root}}$$

Now substituting the above in the identity $GJ_{Ref} = GJ_{Ref}$

$$GJ_{Ref} = \left(\frac{GJ}{EI}\right)_{Ref} \left(\frac{EI_{Ref}}{EI_{Root}}\right) \frac{En_z W_t bt}{24 \; f_{Root}} \quad \frac{c_{Root}}{c_{Root}}$$

Inspecting the elements of this, $\left(\frac{GJ}{EI}\right)_{Ref}$ should not vary by magnitudes

sure of the nose (c.p.) with respect to the bending deformation angle at a point y_o along the body axis (c.g. as the origin of y coordinates) is given by

$$\alpha_s = \int_{y = y_o}^{e_N} \frac{M}{EI(y)}\, dy$$

where M is the applied aerodynamic moment and e_N is the distance from the nose c.p. to the c.g. Replacing M by an equivalent force and moment arm, α_s becomes

$$\alpha_s = \int_{y_o}^{e_N} \frac{F(e_N - y)dy}{EI(y)} = F \int_{y_o}^{e_N} \frac{(e_N - y)dy}{EI(y)}$$

But the applied force is $F = (C_{L_\alpha}\ q\ S)_{Nose}\alpha$. Thus, forming $\frac{\alpha_s}{\alpha}$ which is our nose divergence parameter,

$$\frac{\alpha_s}{\alpha} = (C_{L_\alpha}\ q\ S)_{Nose} \int_{y_o}^{e_N} \frac{(e_N - y)dy}{EI(y)}$$

As a comparator, high values will give the indication of a high probability of a nose or chordwise divergence problem or a high probability of an aeroelastic effect related to nose or chordwise divergence, such as an excessive, aeroelastically-induced canard-surface C_{L_α} . The integral, for comparator purposes, should be evaluated at a consistent y_o, the c.g. being the most logical choice. Also, for most configurations EI(y) does not change drastically with y thereby enabling the choice of a typical or reference value. With these assumptions, the integral may be evaluated, and the comparator becomes

from one configuration to the next. The same can be said for the ratio $\frac{E(t/c)Root}{f_{Root}}$. This also applies to $\left(\frac{EI_{Ref}}{EI_{Root}}\right)$, the reference choice being consistent from one configuration to another. Constants like 24 are unnecessary in the comparator. Therefore, GJ_{Ref} should be replaced by $GJ_{Ref} = n_z W_t bc_{Root}$.

Assembly of all the previous comparator logic yields

$$D^* = \frac{C_{L_\alpha} \; q \; \bar{c}^2 b^2}{n_z W_t bc_{Root}} \qquad (3)$$

Since the product of span and chord is proportional to wing area S, Equation (3) finally becomes

$$D^* = \frac{C_{L_\alpha} \; qS}{n_z W_t} \qquad (4)$$

The reader is directed to the many approximations and deliberate cancellations which have occurred on the previous pages. These are the "stuff" of which comparators are made. A feeling for the "ball-park" magnitudes of the effects in question is sought, not specific values of these effects which, at so early a design stage, are impossible even to approximate with any reasonable degree of accuracy. Regarding this "ball-park" feel, note the physical interpretation of our comparator (Equation (4)). The numerator is total lift per unit angle of attack; in other words, a measure of the deforming forces available to act on the system. The denominator, before it was transformed thru strength to weight, was stiffness; in other words, a measure of the deformation resisting power of the ariframe. This is certainly a logical result.

b. Nose Divergence Comparator

A nose divergence comparator may be obtained by comparing the angle of bending deformation of a vehicle with respect to an input pitch angle. The angle of bending deformation at the center of pres-

$$\frac{\alpha_s}{\alpha} = \frac{(C_{L\alpha}\, q\, S)_{Nose}\, e_N^2}{2\, EI_{Typ}} = \frac{1}{2}\left(\frac{EI_{c.g.}}{EI_{Typ}}\right)\frac{(C_{L\alpha}\, q\, S)_{Nose}\, e_N^2}{EI_{c.g.}}$$

Comparatively, $\frac{EI_{c.g.}}{EI_{Typ}}$ should not vary by magnitudes from one configuration to the next, and may be eliminated. This yields the final form of the comparator,

$$\frac{\alpha_s}{\alpha} = N^* = \frac{(C_{L\alpha}\, q\, S)_{Nose}\, e_N^2}{EI_{c.g.}}$$

Although approached by a very different reasoning process, note the similarity to the wing divergence comparator, D .

II. Comparators for Dynamic Aeroelastic Phenomena

a. Flutter Comparator

From many excellent investigations performed by NASA and ASD, the so called Regier number $\sqrt{\mu}\,\frac{b_R \omega_\alpha}{a}$, and its reciprocal have proven to be good flutter parameters. However, the complexity of the flutter problem has, so far, inhibited the development of a simple but meaningful comparator, involving other parameters in addition to those of the Regier number. Time does not permit a complete investigation of the flutter equations to yield the desired comparator; therefore, until such parameter is developed, it is suggested that the Regier number be used as the flutter comparator, or

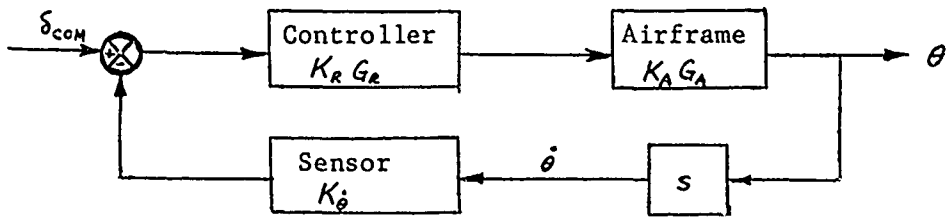
$$F^* = \sqrt{\mu}\,\frac{b_R \omega_\alpha}{a}$$

b. Aeroservoelastic Comparator

From the equations of motion of a booster type configuration controlled by gimballed thrust, the transfer function of pitch angle to control thrust angle was derived by us in a recent report as:

$$\frac{\theta_E}{\delta} = - \frac{\left\{ \left[\frac{x_T M_\xi}{I_\theta} + f_\xi(x_T) \frac{df_\xi(x_s)}{dx} \right] s^2 + \frac{x_T M_\xi}{I_\theta} \omega_\xi^2 \right\}}{s^2 \left\{ \frac{M_\xi}{T} s^2 + \frac{M_\xi}{T} \omega_\xi^2 + f_\xi(x_T) \frac{df_\xi(x_T)}{dx} \right\}}$$

neglecting aerodynamics. Now consider a rate loop such as



For $G_R \approx 1/s$ (crudely typical for a control actuator), then the around-the-loop transfer function becomes

$$\left(\frac{\dot\theta_E}{\delta}\right)_{AL} = - \frac{K_R K_{\dot\theta} \left[\frac{x_T M_\xi}{I_\theta} + f_\xi(x_T) \frac{df_\xi(x_s)}{dx} \right] \left\{ \frac{s^2}{\omega_\xi^2} + \frac{1}{1 + \frac{I_\theta}{M_\xi x_T} f_\xi(x_T) \frac{df_\xi(x_s)}{dx}} \right\}}{\frac{s^2}{\omega_\xi^2} \frac{\omega_\xi^2 M_\xi}{T} \left\{ \frac{s^2}{\omega_\xi^2} + 1 + \frac{T f_\xi(x_T)}{M_\xi \omega_\xi^2} \frac{df_\xi(x_T)}{dx} \right\}}$$

From this expression it may be seen that the relationship of $\frac{1}{1 + \frac{I_\theta f_\xi(x_T)}{x_T M_\xi} \frac{df_\xi(x_s)}{dx}}$ to $1 + \frac{T f_\xi(x_T)}{M_\xi \omega_\xi^2} \frac{df_\xi(x_T)}{dx}$ determines the stability whereas the gain $\frac{K_R K_{\dot\theta}}{\omega_\xi^2} \left(\frac{T x_T}{I_\theta} + \frac{T f_\xi(x_T)}{M_\xi} \frac{df_\xi(x_s)}{dx} \right)$ determines the degree of stability.

Therefore, since the configurations we will consider should be designed for stability, but will probably, in their critical conditions, not be excessively stable, it is the degree of stability which becomes our comparator. Thus

$$A^* = \frac{K_R K_{\dot\theta}}{\omega_\xi^2} \frac{T x_T}{I_\theta} \left(1 + \frac{I_\theta f_\xi(x_T)}{x_T M_\xi} \frac{df_\xi(x_s)}{dx} \right)$$

Since the sensor slope affects stability and degree of stability oppositely for comparative purposes and consistent with our ccomparator philosophy $\frac{df_{\xi}(x_s)}{dx}$ will be eliminated and the final form of the comparator is

$$A^* = \frac{K_R K_{\dot{\theta}}}{\omega_{\xi}^2} \frac{Tx_t}{I_{\theta}}$$

This comparator is proposed for cautious further exploration. To ascertain whether it is a meaningful comparator or "false prophet" will require considerable further investigation. However, it does have one very satisfying property. Namely, if we were to list those variables the increase of which have seemed to aggravate our booster aeroservoelastic design problems and form them into a numerator, and then list those variables the increase of which have seemed to alleviate our aeroservoelastic design problems and form them into a denominator, the result would be our comparator A^*.

REQUIRED PARAMETERS

In order to assess the probable degree of aeroelastic severity of past, present and future configurations and missions, a first attempt at the development of suitable comparators has been presented. This is a summary of the input information necessary for numerical comparisons.

a. Static Aeroelastic Comparators

$(C_{L_\alpha} q S)_{Wing}$ - the total lift of the wing per angle of attack

n_z - maximum maneuver g's used to design structure

W_t - total weight of configuration

S - wing area

$(C_{L_\alpha} q S)_{Nose}$ - total lift on nose per angle of attack

e_N - distance between nose c.p. and configuration c.g.

$EI(y_{c.g.})_{Body}$ - body bending stiffness at the c.g.

b. Dynamic Aeroelastic Comparators-

$\mu = \frac{m}{\pi \rho b_R^2}$ mass ratio of wing - cross-sectional for high aspect ratio wing generalized mass for low AR wing.

ω_α wing torsion resonant frequency

$K_R K_{\dot{\theta}}$ autopilot-sensor gain (rate loop)

I_θ pitch moment of inertia of configuration

T/W_t thrust to weight ratio

ω_ξ resonant frequency of airframe fundamental elastic mode

x_t distance from c.g. to point of control force

THE AERODYNAMICS OF DISTORTED SURFACES

Eugene E. Covert

Massachusetts Institute of Technology
Aerophysics Laboratory

ABSTRACT

The problem of computing the pressures on an aerodynamic surface subject to a smooth distortion is discussed in terms of linear and second order theories and an empirical approach. It is shown that the linear theory is valid only for very slight distortions. The empirical procedure is generally accurate to within 5 percent although it is hard to determine the limits of application. The second order procedures are generally more accurate and appear valid over a wide range of Mach numbers.

THE AERODYNAMICS OF DISTORTED SURFACES

INTRODUCTION

Before discussing the aerodynamics of distorted surfaces, it will be worth while to be more specific about the material to be covered. The intention is to consider the distortion of the basic surface shape as a result of finite loading on an elastic surface, or as a result of non-uniform heating, or as a result of loss of strength due to high temperature. In particular, the problem of calculating the aerodynamic influence of these distortions will be discussed. The origin of this problem can best be illustrated by elementary considerations. The local angle of attack at any point on the surface can be made up of the rigid body part α_R and the increment due to distortion $\Delta\alpha_D$. Thus, the total local angle of attack can be written as

$$\alpha_\ell = \alpha_R + \Delta\alpha_D \tag{1}$$

The load on an elemental surface can be written as

$$\delta L = \int q\, C_p(\alpha_\ell)\, dS \tag{2}$$

where the integration is over the region infinitesimal R, of interest. Here C_p can be regarded as an operator that converts the angle of attack into a distributed force. Finally, the existence of a structural operator will be assumed, and will be denoted by A. This operator converts the load into a local increment of angle of attack, thus,

$$\Delta\alpha_D = A(\delta L) \tag{3}$$

By substitution from Eq. (2),

$$\Delta\alpha_D = A\left\{q\int dS\; C_p(\alpha_\ell)\right\} \tag{4}$$

or

$$\Delta\alpha_D = A\left\{q\int dS\; C_p(\alpha_R + \Delta\alpha_D)\right\} \tag{5}$$

As long as C_p is a smoothly varying function of the angle, the operator can be expanded as a MacLauren series

$$A\left\{q\int dS\, C_p(\alpha_R+\Delta\alpha_D)\right\} = A\left\{q\int dS\, C_p(\alpha_R)\right\} + A\left\{q\int dS\, \frac{\partial C_p}{\partial\alpha}_{\alpha=\alpha_R}\right\}\Delta\alpha_D + \ldots \tag{6}$$

in which it is assumed that the higher order terms are smaller than the first order terms. As long as the deflections are small, the elastic operator is linear, so

$$\Delta\alpha_D = A\left\{q\int dS\, C_p(\alpha_R)\right\} + A\left\{q\int dS\, \frac{\partial C_p}{\partial\alpha}\right)_{\alpha=\alpha_R}\Delta\alpha_D + \ldots \tag{7}$$

Note that we have assumed the area is unchanged by this process. Equation (7) can be solved to give an approximation to $\Delta\alpha_D$,

$$\Delta\alpha_D = \frac{Aq\int dS\, C_p(\alpha_R)}{1 - Aq\int dS\, \frac{\partial C_p}{\partial\alpha}\Big)_{\alpha=\alpha_R}} \tag{8}$$

This equation shows that the assumption of small angles may not be valid at all times. When the denominator vanishes $\Delta\alpha_D$ is not even defined. This corresponds to elastic divergence. If the expansion (Eq. 6) included second order terms, the equation for $\Delta\alpha_D$ would be

$$\Delta\alpha_D \cong \frac{1 - qA\int dS\, C_{p_\alpha}}{qA\int dS\, C_{p_{\alpha\alpha}}}\left[1 - \sqrt{1 - \frac{2A\left(q\int dS\, C_p(\alpha_R)\right)\left(qA\int dS\, C_{p_{\alpha\alpha}}\right)}{\left(1 - qA\int dS\, C_{p_\alpha}\right)^2}}\right] \tag{9}$$

and up to but not including terms of third order would be

$$\Delta\alpha_D = \frac{qA\int dS\, C_p(\alpha_R)}{1-q\int dS \left.\frac{\partial C_p}{\partial \alpha}\right)_{\alpha=\alpha_R}} \left\{ 1 + \frac{1}{2}(Aq\int dS\, C_{p_{\alpha\alpha}})(Aq\int dS\, C_p(\alpha_R)) \frac{qA\int dS\, C_{p_{\alpha\alpha}}}{(1-qA\int dS\, C_{p_{\alpha\alpha}})^2} + \cdots \right.$$

(10)

Note that the divergence is the same or at least it has one root the same as before. In principle, Eq. (5) can always be solved for $\Delta\alpha_D$ - no matter what the functional dependence of C_p ; but at divergence the Eq. (5) is valid for any $\Delta\alpha_D$. Assuming that the $\Delta\alpha_D$ is known, somehow, then the value for the change in pressure coefficient can be found

$$\Delta C_p = C_p(\alpha_R + \Delta\alpha_D) - C_p(\alpha_R) \tag{11}$$

To a first order Eq. (6) gives

$$\Delta C_p = \frac{\partial C_p}{\partial \alpha}\Delta\alpha_D \tag{12}$$

and to a second order

$$\Delta C_p = \left(\frac{\partial C_p}{\partial \alpha} + \frac{1}{2}\frac{\partial^2 C_p}{\partial \alpha^2}\Delta\alpha_D\right)\Delta\alpha_D \tag{13}$$

If desirable, the change in lift and pitching moment, or any other aerodynamic parameter, can be calculated from ΔC_p. When the first order form of Eq. (6) is valid and $C_p(\alpha_R) = C_{p_\alpha}\alpha_R$ then

$$C_L = C_{L_R} + \frac{1}{S}\oint \frac{C_{p_\alpha}\alpha_R\, qA\int dS\, C_{p_\alpha}}{1 - qA\int dS\, C_{p_\alpha}} dS \tag{14}$$

and

$$C_{L_\alpha} = C_{L_{\alpha_R}} \left[1 + \frac{1}{C_{L_{\alpha_R}} S} \oint \frac{C_{p_\alpha} \, qA \int dS \; C_{p_\alpha}}{1 - qA \int dS \; C_{p_\alpha}} \, dS \right] \tag{15}$$

This linear form is a consequence of the pressure coefficient assumptions. More generally

$$C_{L_\alpha} = C_{L_{\alpha_R}} \left[1 + \frac{\frac{\partial}{\partial \alpha}}{C_{L_{\alpha_R}} S} \oint C_{p_\alpha} \frac{qA \int dS C_p(\alpha_R)}{-qA \int dS C_{p_\alpha}} \, dS \right] \tag{16}$$

which is not independent of angle of attack, even if the first order expansion of $C_p(\alpha)$ is valid. During the remaining discussion the problem of calculating δL will be considered. The discussion will include the application of linear theory, second order theory and a semi-empirical method of calculation. The basic outline of the method and a comparison with data will be presented. Finally, the sever ... techniques will be shown to be related by use of a more general perturbation technique.

ANALYSIS

1. Classical Linear Theory

The pressure coefficient on an arbitrary surface immersed in a supersonic stream cannot be computed exactly except under restricted conditions; and then only by a numerical process called the method of characteristics. When the surface is smooth, relatively plane and not inclined at too large an angle to the relative wind, it is possible to simplify the basic equations and reduce the problem to that of evaluating a surface integral. This procedure is now available in several references.* On the upper surface (z=0), the velocity potential for the perturbation velocity

$$\vec{v}_1 = - \nabla \phi$$

---

* Sears, Vol. 6, Princeton Series
Ferri, A., Elements of Supersonic Aerodynamics
Liepmann and Roshko, Elements of Gas Dynamics

is given by the integral, $z = 0^+$,

$$\phi_+ = -\frac{1}{\pi}\int_{R_w} \frac{w(\xi, \eta)\, d\xi, d\eta}{\sqrt{(x-\xi)^2 - \beta^2 (y-\eta)^2}} \tag{17}$$

where

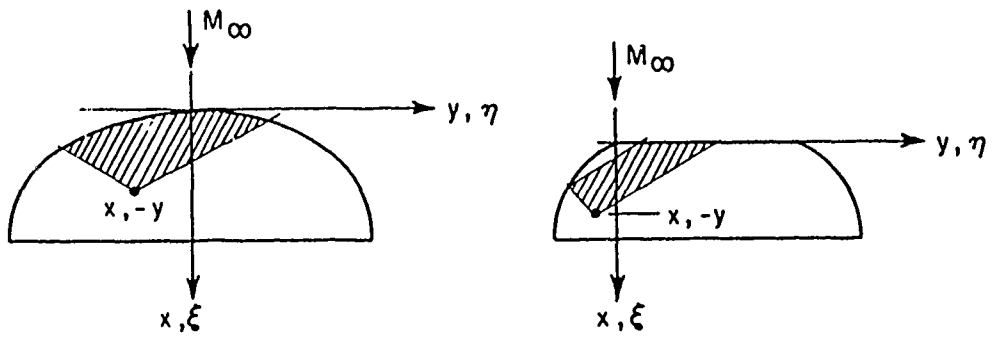
$\beta = \sqrt{M_\infty^2 - 1}$

M_∞ = Mach number at ∞

w = normal velocity at the surface

$w = U \frac{\partial f}{\partial z}$

if $f(x, y, z) = 0$ describes the shape of the surface. The region of integration R_w is shown below for the cases of subsonic and supersonic edges as the shaded region. This region is bounded by Mach lines



(a) SUPERSONIC (b) SUBSONIC

and the leading edge.

The difference in pressure from ambient

$$p_\ell - p_\infty = -\rho_\infty U_\infty \phi_x \tag{18a}$$

so that

$$C_p = -2\frac{\phi_x}{U_\infty} \tag{18b}$$

The load on an elemental area is δL, (positive upwards)

$$\delta L = \frac{-1}{2}\rho_\infty U_\infty^2 \int_R C_p \, dx \, dy = \rho_\infty U_\infty \int_R \phi_x \, dx \, dy \tag{19}$$

This equation can be integrated with respect to x to give, for a surface of width δy,

$$\delta L = \rho_\infty U_\infty \int_{\delta y} \left[\phi(x_\ell, y) - \phi(x_T, y) \right] dy \tag{20}$$

where x_ℓ is the coordinate of the leading edge of the element, x_T is the coordinate of the trailing edge. The load carried at element B due to an angle of attack distribution at A is called the aerodynamic influence coefficient and is denoted

$$K_{AB} = \frac{\delta L_B}{\alpha_A} \tag{21}$$

Note that K_{AB} can be identically zero if A lies outside the forward Mach cone of B. Finally,

$$K_{AB} = \frac{1}{\alpha_A} \rho_\infty U_\infty \int_{\delta y} \left[\phi(x_\ell, y) - \phi(x_T, y) \right] dy \tag{22}$$

Consequently, K_{AB} is easy to compute from δL_B.

The evaluation of Eq. (20) or (22) is not difficult, though tedius, once the value of the potential is known. However, the evaluation of Eq. (17) is somewhat more difficult for the general case. This is particularly true for the class of problems of interest here. The δL_B is strongly dependent upon the surface slope in the forward Mach cone from B but, since the problem is linear, it can be

resolved by superposition[1]. Hence, this discussion will be limited to the relative effectiveness of the techniques of determining ϕ. Unfortunately, the analytic evaluation of Eq. (17) is only available for a few cases. Consequently, the numerical procedures must be worked out. One such procedure has been given by Etkin (Ref. 1). This method provides a rigorous procedure, based upon linear theory, for computing the pressure distribution and influence coefficients. The potential is calculated by means of an integration matrix which is based upon the assumption that the angle of attack is constant over the integration element. Etkin compares the results obtained with his procedure with such exact solutions as were available. In particular, for a delta wing ($M_0 = 2, \Lambda = 30°$) with supersonic leading edges the maximum difference between his results and the results from conical flow theory were less than one percent.

Figure 1 shows a delta wing with $M_0 = \sqrt{2}$. The pressure coefficient is shown for two positions in this figure and is compared with exact solutions of the same camber in the case of linear theory. Again, the agreement is good, being better than two percent. It may be concluded that the integration procedure proposed by Etkin is valid representation of the linear theory. See Figure 2.

2. Classical Linear Theory and Higher Order Theories*

A practical method of calculating the linear theory pressure distribution on an arbitrary wing was discussed above. Since this method depends

---

[1] If w is a Dirac function inside the forward cone and zero outside the cone from B

$$\phi_{+_B} = \frac{-1}{\pi} \quad \frac{1}{\sqrt{(x-\xi_A)^2 - \beta^2 \ (y-\eta_A)^2}} \quad \text{per radian}$$

so

$$\delta L = \frac{\rho_\infty U_\infty}{\pi} \int_{\delta y} dy \left[\frac{1}{\sqrt{(x_L(y)-\xi_A)^2 - \beta^2 (y-\eta_A)^2}} - \frac{1}{\sqrt{(x_T(y)-\xi_A)^2 - \beta^2 (y-\eta_A)^2}} \right]$$

$$\text{if } (x-\xi)^2 > \beta^2 (y-\eta)^2$$

$$= 0 \qquad \text{if } (x-\xi)^2 < \beta^2 (y-\eta)^2$$

This expression can be substituted in Eq. (22).

* The material in this section is based upon the Princeton University Press Aeronautical Paperback, Higher Approximations in Aerodynamic Theory, M.J. Lighthill (Vol. VI, Div. E of the series High Speed Aerodynamics and Jet Propulsion, 1957).

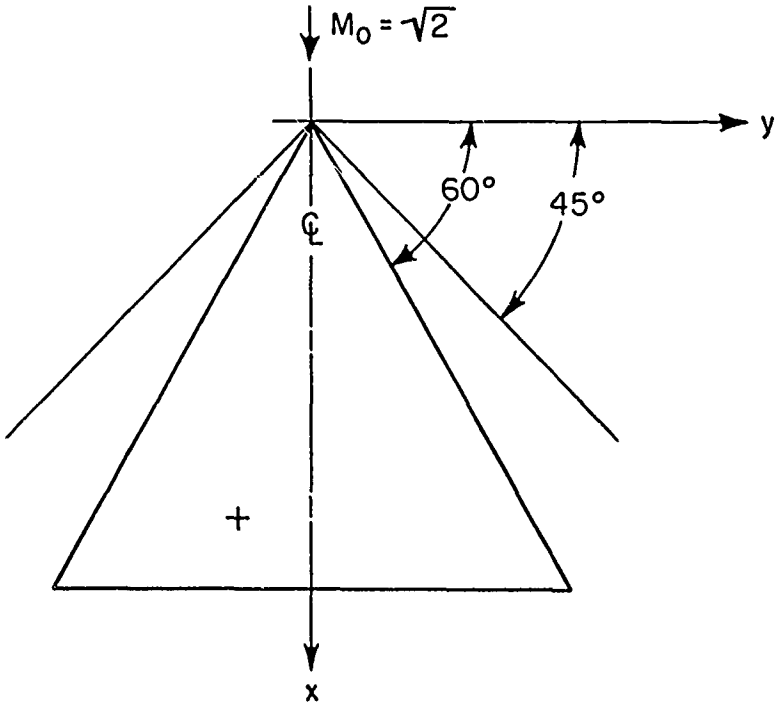


Figure 1. Geometry of delta wing

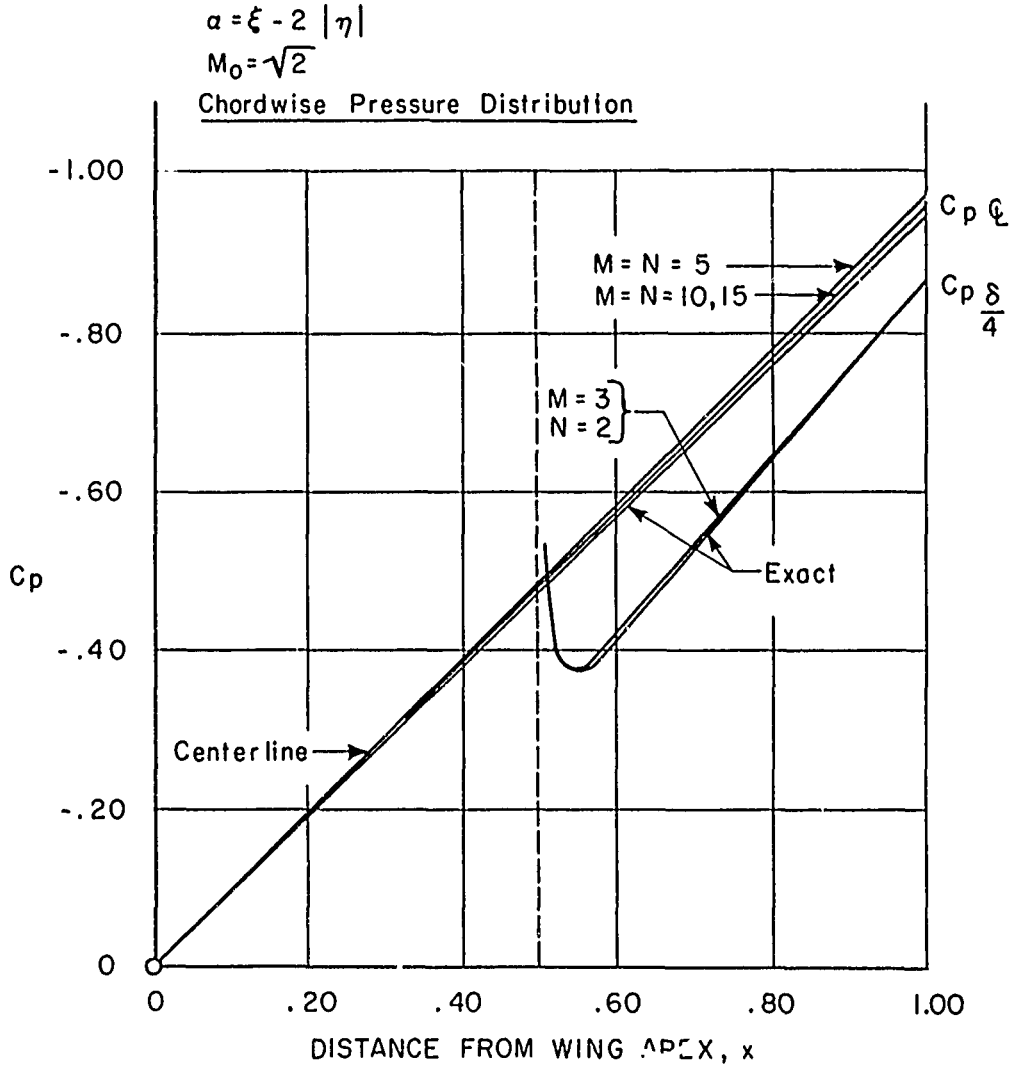


Figure 2. Comparison of Etkin's procedure with exact results

upon an approximate set of equations, it is reasonable to seek more exact solutions and attempt to prescribe the acceptable error. The linearized set of equations neglect three effects: the variable speed of sound, the variation in convection and the influence of shock waves. By a study of the supersonic flow past wedges and around sharp two-dimensional corners, it is found that the effects of the shock waves can be neglected. Part of the reason for this can be shown in terms of the specific entropy rise across a shock just strong enough to turn the flow through an angle θ. This entropy rise is approximately

$$S \sim C_p \frac{\gamma^2 - 1}{12} \frac{M_\infty^6}{(M_\infty^2 - 1)^{3/2}} \theta^3 \qquad (23)$$

(θ in radians)

Secondly, it can be shown that the pressure and angle relation involves the product of change in pressure (or angle) and S, while the changes in density, velocity and Mach number are proportional to S. Finally, the shock wave is an effective absorber of weak sound waves so that any propagation out to the shock is hardly reflected. The last effect has the consequence of allowing the flow to be approximated by simple wave or Prandtl-Meyer Theory. Figure 3(Fig.E., 3f from Lighthill) shows a comparison of simple wave theory, linear theory (Ackeret) and second order theory, Busemann, with the exact oblique shock results. Note that linear theory ($C_p = \frac{2\theta}{\beta}$) is generally 10 percent in error at the value of $\theta = 4°$. Second order theory is equally accurate up to $\theta = 12°$. Figure 4 (Fig. E 3g from Lighthill) shows a similar plot for the expansion side and the limits are about the same. Note that the linear theory under estimates the pressure on the compression side and over estimates on the suction side by about the same amount. This fortuitous circumstance accounts for the success that linear theory has achieved in predicting lift and drag and indicates why the moment is not predicted correctly.

The Busemann second order theory is a result from an expansion in the form

$$C_p = \frac{2\theta}{\beta} + \frac{(M_\infty^2 - 2)^2 + \gamma M_\infty^4}{2\beta^2} \theta^2 + 0(\theta^3) \qquad (24)$$

If these two terms are a good approximation, then it may be assumed that the effects of the variable sound speed and convection are included in the analysis to some extent. A comparison with the exact results given in Figs. 3 and 4 indicate this to be the case. It can be shown

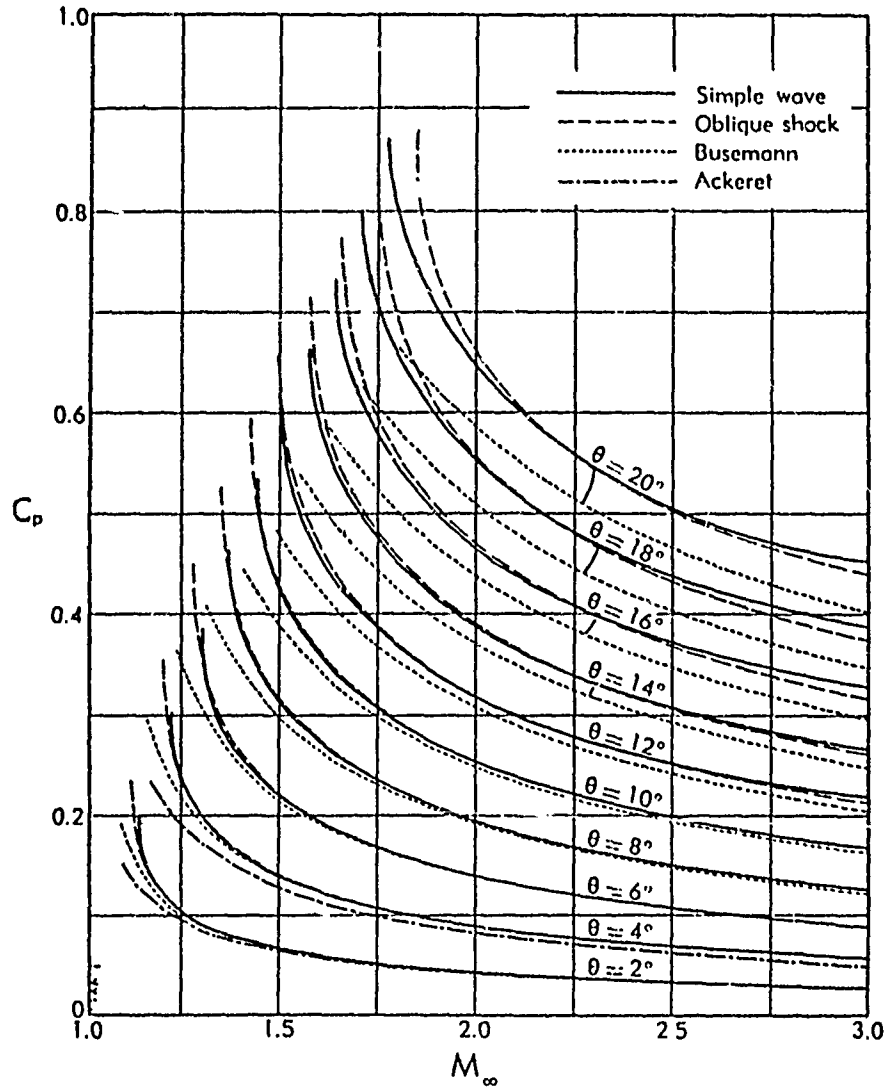


Figure 3. Comparison of exact and approximate calculations on compression side.
(Figure E 3f of Higher Approximations in Aerodynamic Theory by M. J. Lighthill - Vol. VI, Div. E of the series High Speed Aerodynamics and Jet Propulsion, 1957)

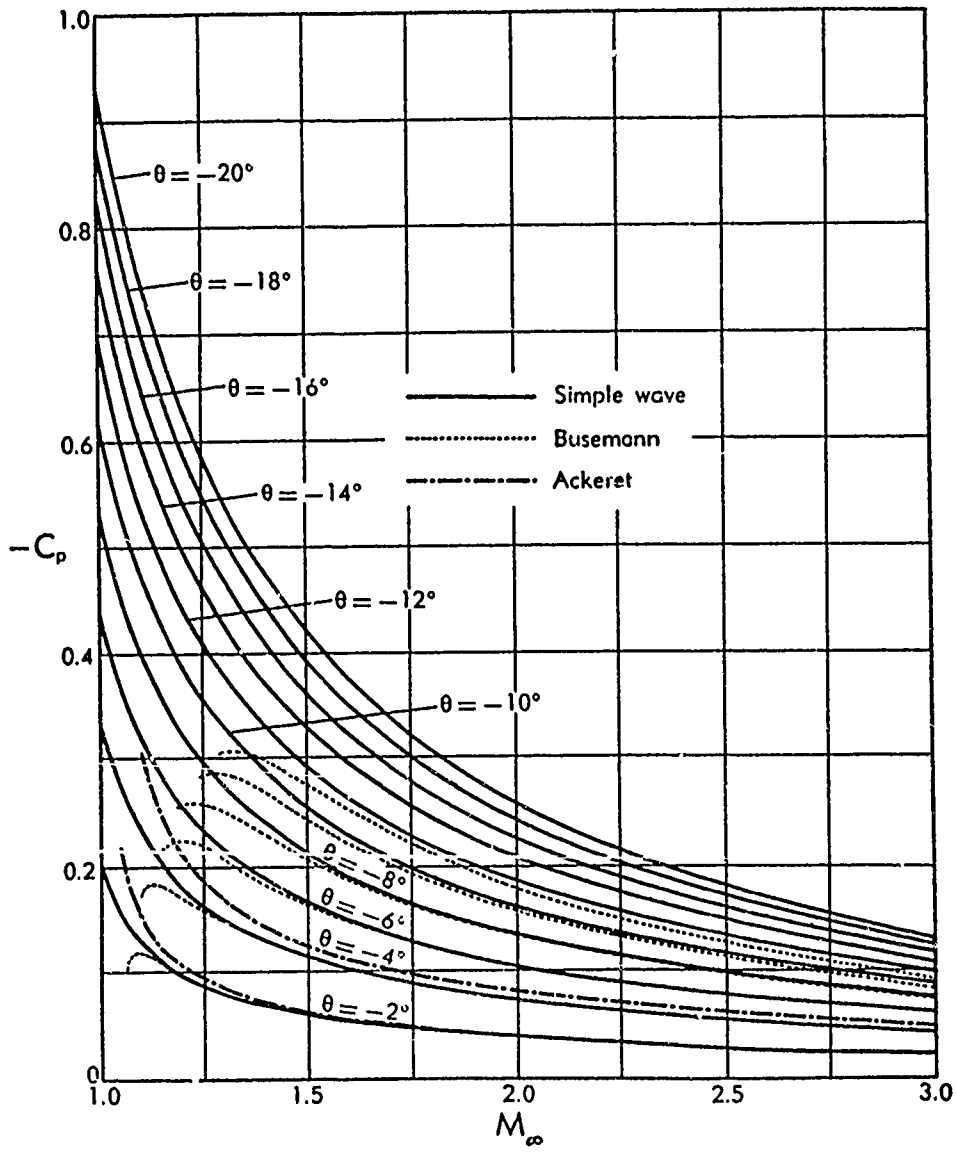


Figure 4. Comparison of exact and approximate calculations on expansion side

(Figure E 3g of Higher Approximations in Aerodynamic Theory by M. J. Lighthill - Vol. VI, Div. E of the series High Speed Aerodynamics and Jet Propulsion, 1957)

(cf Lighthill, p. 19) that if the first perturbation (ϕ) is governed by

$$\nabla^2 \phi_1 - M_\infty^2 \phi_{1xx} = 0 \tag{25}$$

the second approximation for the potential (ϕ_2) is the solution of

$$\nabla^2 \phi_2 - M_\infty^2 \phi_2 = (\gamma-1) M_\infty^2 \phi_{1x} \nabla^2 \phi_1 + 2M_\infty^2 \nabla \phi_1 \cdot \nabla \phi_{1x} \tag{26}$$

The ϕ_1 corresponds to Busemann's first term and ϕ_2 corresponds to Busemann's second term. The first term on the right-hand side of Eq. (26) allows for the variation in sound speed and the second term allows for the convection. Note in passing that a similar second order theory has been worked out for bodies of revolution by M.D. Van Dyke (Ref. 2).

As long as the flow is two-dimensional, as it is in many cases, the fact that the shock nearly absorbs the outgoing waves allows the use of "Shock-Expansion Theory" of Eggers and Syvertson (Ref. 3). In this theory (which presents the proof of the extension of Epstein's original Shock-Expansion Theory) it is possible to go to somewhat higher Mach numbers than is the case of the second order theories.

The primary reason for the success of the second order and shock-expansion theories seems to be that the first two types of non-linearities are included: the variable speed of sound and the variable convection process. Hence, it is of interest to consider the possibilities for second order theories of planar surfaces that will preclude the restriction to small angles that is necessitated by the use of linear theories. Beane (Ref. 4) has used a result of Landahl (Ref. 5) to compute a second order correction, valid for moderately high Mach number, in a similar application (Ref 6). In this calculation, the distortions are represented by classical linear theory and an interference potential is calculated for the distorted potential and the pressure distribution on the undistorted surface. Hence, this theory requires a knowledge of the exact pressure distribution on the undistorted wing from either experimental or theoretical results. This theory reduces to just integration and while it has not been reduced to the form of calculating influence coefficients, there is no theoretical restriction. Further, since this method is based upon the exact pressure distribution at zero distortion through the pressure coefficient, it would seem applicable to airfoils having blunt leading edges.

A final possibility would be that of linearizing the basic equations about the undistorted flow. This process is easy to carry out and contains all the elements that would seem to be necessary; the variable sound speed and variable convection are included in terms of the basic flow. This equation has variable coefficients and cannot generally be solved. However, to a first approximation, when wavelengths of the distortions are much shorter than the characteristic length of the basic flow, the form of the solution is identical with that given in Eq. (17) and (20). In this use of Eq. (17) and (20), it should be recalled that (a) β is now based upon local Mach number and integration is bounded by the variable

Mach lines and (b) the C_p is based on a local q and must therefore be multiplied by (q/q_∞).

The details for this approximation are given in the appendix.

3. Comparison with Experiment

Up to present the discussion has centered upon the development of a numerical procedure that is applicable to arbitrary wings. The limitations of linear theory were discussed in light of higher order theory and Beane's second order method was outlined. Since this method requires the use of linear theory, it follows that Etkin's numerical procedure can be used here also. In this section, the linear and second order theories will be compared with experimental data. First, the comparison with linear theory and experiment will be discussed briefly, then the distorted wings will be compared with the data.

Frick (Ref. 7) has presented a detailed comparison of the linear theory with experimental data. He finds, generally, that the linear theory is in best agreement when the leading edge is sharp enough for the shock to be attached. Further, the agreement is generally improved as the airfoil is thinner. As a rule, the calculated value for C_L and C_D are within five percent of the measured value for reasonable airfoils. The pitching moment is not this well represented. The distribution of the theoretical C_p is in qualitative agreement with the measured C_p except at places where the characteristic line (i.e., at wing-tip or wing-body junction) differs markedly from the free-stream characteristic. This point is mentioned in Appendix A in connection with the use of the more exact characteristics.

Generally, the use of the second order theory on thin wings and bodies improves the agreement with the experiment to the point where it can be argued that the data is more likely to be in error than the calculation. The use of shock-expansion theory also gives good results up to high Mach numbers, as is well known (Ref. 8).

The data on distorted surfaces is quite limited, the most recent tabulation by Mr. F.S. Thomas of ASD was made available by Mr. H. Max Davis. This data is given in Table 1.

Peterson (Ref. 9) has compared the data from a rectangular wing having a hexagonal cross section with calculations based on shock-expansion technique and finds better agreement both in level and in trend than with calculations based on linear theory (Figs. 5 and 6). He used the local linearization to estimate the effects at the tip and, in complete agreement with Frick's assertion, finds the local characteristic or Mach line to be more effective in predicting the location of the jump in pressure at the tip Mach line.

Etkin's procedure has been used by North American Aviation to estimate the effect of conical camber. This is the classical linear theory and, as was indicated above, is generally within five percent of the experimental results (in agreement with Etkin's original conjecture). In this application the wings were tested at a high enough Mach number that the leading edges were not transonic.

TABLE 1

DATA ON DISTORTED SURFACES

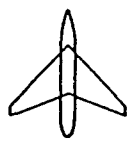
CONFIGURATION	MACH	P_0 & R_n	α	REMARKS	TWIST	CAMBER	REFERENCE
 $\Lambda c/4 = 45°$ AR = 4.0 $\lambda = 0.15$ S = 1.108 ft²	0.80—1.20	P_0 = 0.5 ATM $R_n = 1.4 \times 10^6$	$-4° \leq \alpha \leq 20°$	Wing Section Root = NACA65A206,A=0 $\frac{b}{2}$ —b= NACA65A203,A=8	None	None	NASA MEMO 10-20-58L
					Linear	"	NASA MEMO 12-28-58L
		P_0 = 1.0 ATM $R_n = 2.8 \times 10^6$	$-4° \leq \alpha \leq 12°$	0° Twist at 10% Semispan and 6° Washout at Tip	Quadratic	"	NASA MEMO 2-21-59L
					Cubic	"	NASA MEMO 2-12-59L
Same As Above	1.43	Same As Above	Same As Above	Same As Above	Same As Above	Same As Above	NASA TN D-528
 $\Lambda c/4 = 50°$ AR = 3.1 $\lambda = 0.20$ b = 15.75 in.	1.61	P_0 = 8 & 15 PSIA $R_n \times 10^6$ = 1.7—3.6	$-20° \leq \alpha \leq 20°$	Wing Section NACA 65A005 Twisted Wings Had 6° Washout at Tip	None	None	NACA RM L58D23
	2.01				Linear	"	
					Quadratic	"	Comparison With Theory in WADD TR 58-95 - Part I 58-378 - Part II
					Cubic	"	
					None	Λ = 0 Mean Line 4% High at Each Spanwise Station	
 Λ_{LE}=70°	0.4—3.0		$-4° \leq \alpha \leq 4°$		None	None	Data and Comparison with Theory in NAA Inc. Rpt. NA-61-175(S)
					"	0.03 Sin $\frac{\pi x}{c}$	
					"	0.015 Sin $\frac{2\pi x}{c}$	
					"	0.01 Sin $\frac{3\pi x}{c}$	

TABLE 1 (Cont'd)

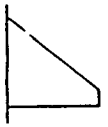
CONFIGURATION	MACH	P_0 & R_n	α	REMARKS	TWIST	CAMBER	REFERENCE
 $\Lambda_{LE} = 40°$ $AR = 3.5$ $\lambda = 0.15$ $b = 12.78^{in}$	1.51 1.99 3.01 3.55	$R_n = 3.26 \times 10^6$	$-8° \leq \alpha \leq 14°$	Wing Section NACA 65A-6% modified	None "	None Cubic $Z_c = .02 \times (3-4x^2)$	Boeing Airplane Co. Document No. D2-1030 Vol. I
						Reflex 1% Camber at $\frac{1}{4}$C 1% Camber at $\frac{3}{4}$C Anti-symmetric C rcular Arcs About $\frac{1}{2}$ C	Comparison With Theory in WADD Unpublished Notes

TABLE 1 (Cont'd)

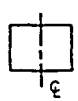
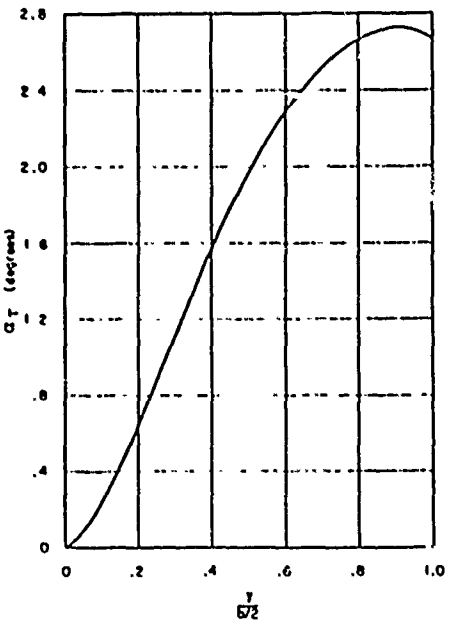
CONFIGURATION	MACH	α	REMARKS	TWIST	CAMBER	
 $\Lambda_{c/4} = 50°$ $\lambda = 0.2$ $AR = 3.5$			Wing Section NACA 65A005	None	Reflex Camber	To Be Tested by Mid '61
				Linear $\Delta\alpha = 6°$	NACA $\alpha = 0$ 4% mgn at each span station	
 $\Lambda_{LE} = 70°$ $AR = 1.456$			Wing Section NACA 65A003	None	None	To Be Tested by Mid '61
				None	$\alpha_{local} = KX$	
				Combination $\alpha_{local} = KXY$		
 $\Lambda_{TE} = 0°$ $\lambda = 0.72$ $AR = 1.3$			Sharp Leading Edge, 3% Airfoil	None	None	To Be Tested by Mid '61
				Combination $\alpha_{local} = -K \sin(\frac{Y}{b/2}\frac{3\pi}{2})\sin\frac{\pi x}{c}$		
 $\Lambda_{LE} = 70°$	6, 10, 18	-5°, 0°, 5°, 10°, 20°	Wedge Angle Normal to LE = 25° - 20 Pressure Taps on the Lower Surface	None	None	Report Available Nov. '61
				None	Circular Arc	
				None	Sine-Wave	
 $o = 0"$ $C = +5"$	Same As Above	Same As Above	Same As Above Maximum Distortion = 5°	None	None	Report Available Nov. '61
				None	Circular Arc	
				Linear Symmetrical Twist	None	

TABLE 1 (Cont'd)

CONFIGURATION	MACH	α	REMARKS	TWIST	CAMBER	
 AR = 2.0 Λ = 0°	2.5, 3.0, 4.0, 7.6	-5°, 0°, 5°, 10°		None	None	Report Available 30 July '61
				1st Bending Mode Velocity Mode Shape		
				1st Torsional Mode Velocity Mode Shape		
				1st. Bending Mode Deflection Mode Shape		
 Λ_{LL} = 70°	Same As Above	Same As Above		None	None	Report Available 30 July '61
				1st. Bending Mode		
				2nd. Bending Mode		
	2.0, 3.0, 4.0, 7.6	-3°, 0°, 3°, 6°, 10° 8 = 0° ± 20°	Total Circular Arc Body Angle = 6°	Undistorted Body		Report Available 30 July '61
				Circular Cambered Body		
				Reflex Cambered Body		



Twist Distribution

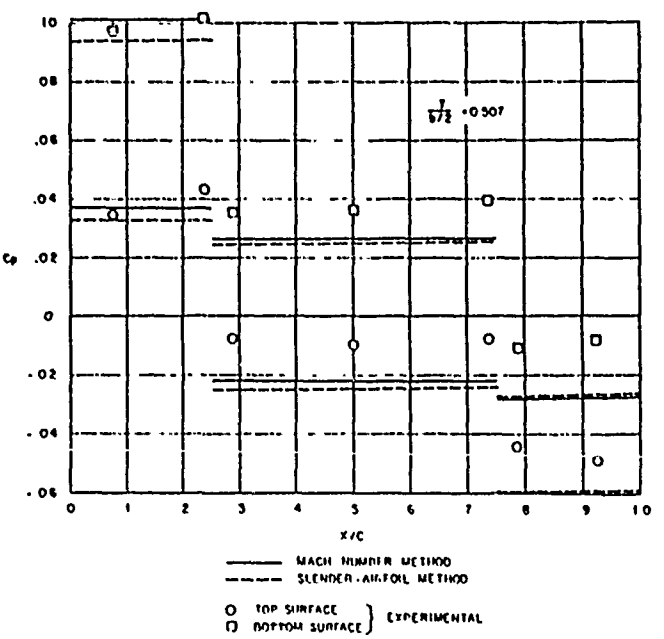
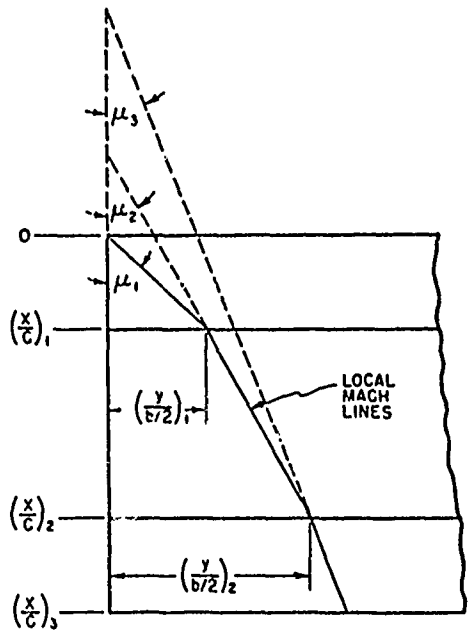


Figure 5. Comparison of approximate results with experimental results - hexagonal profile mid-span



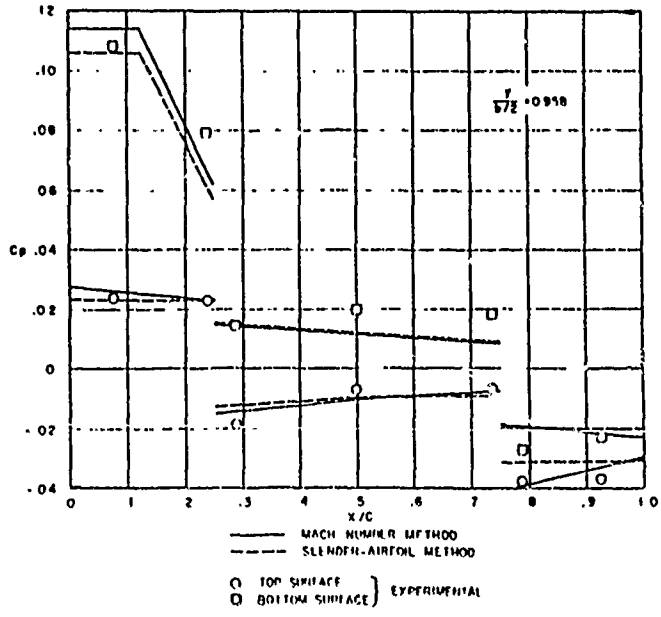


Figure 6. Comparison of approximate results with experimental results - hexagonal profile tip region

An empirical method was worked by Zisfein (Ref.10). This procedure is based upon linear theory and a set of correction elements. These correction elements are based upon the ratio of the experimental load distribution to the theoretical load distribution for the case of no twist. This ratio is assumed to be a universal function. C. Bartlett of the Aerophysics Lab., M.I.T. has used the data given in NASA TN-D-528 to test this particular assumption. The results are shown in Fig. 7 for three kinds of twist. Further, Zisfein's correction is based upon a five percent airfoil. Consequently, it may be expected that the use of his simple approximation might be limited to wings having only a few percent difference in thickness. Zisfein was able to overcome this difficulty by using the data for the untwisted wing, and comparing it with linear theory. This results in a correction matrix denoted by $\lfloor f \rceil$. It is assumed that the distorted surface can be represented by a fifth order polynomial.

Each term of the polynomial is substituted into the classical linear theory, the integrations are carried out and the resultant matrix is multiplied by $\lfloor f \rceil$ to construct the load influence matrix. There is here, at least, a superficial resemblance to Beane's method. However, the $\lfloor f \rceil$ matrix does not include the interference potential and its use is consequently restricted. Figure 8 shows a comparison of the spanwise load distribution computed by Zisfein's method with the data taken by Durgin. While the general trend is predicted, the absolute values differ by about five percent. The Zisfein procedure may be used when shock-expansion is not valid. On the other hand, the application of Beane's method tends to give an improvement over classical linear theory as shown in Figs. 9 and 10.

4. Extension to Higher Mach Numbers

In the usual derivation of the classical linear theory, it is assumed that the product of the local Mach number and the slope is small, i.e., $M\theta << 1$. However, as the Mach number increases, this requirement becomes increasingly severe. Referring again to Figs.3 and 4, it is seen that to keep the linear theory error less than five percent that $M\theta \leq .1$. At higher Mach numbers, the second order theory begins to diverge. However, the use of shock-expansion theory is still valid in the two-dimensional regions. The use of a basic flow field, a linear disturbance and the interference as proposed by Landal, Drougge and Beane can be shown to be valid up to Mach numbers of at least five.

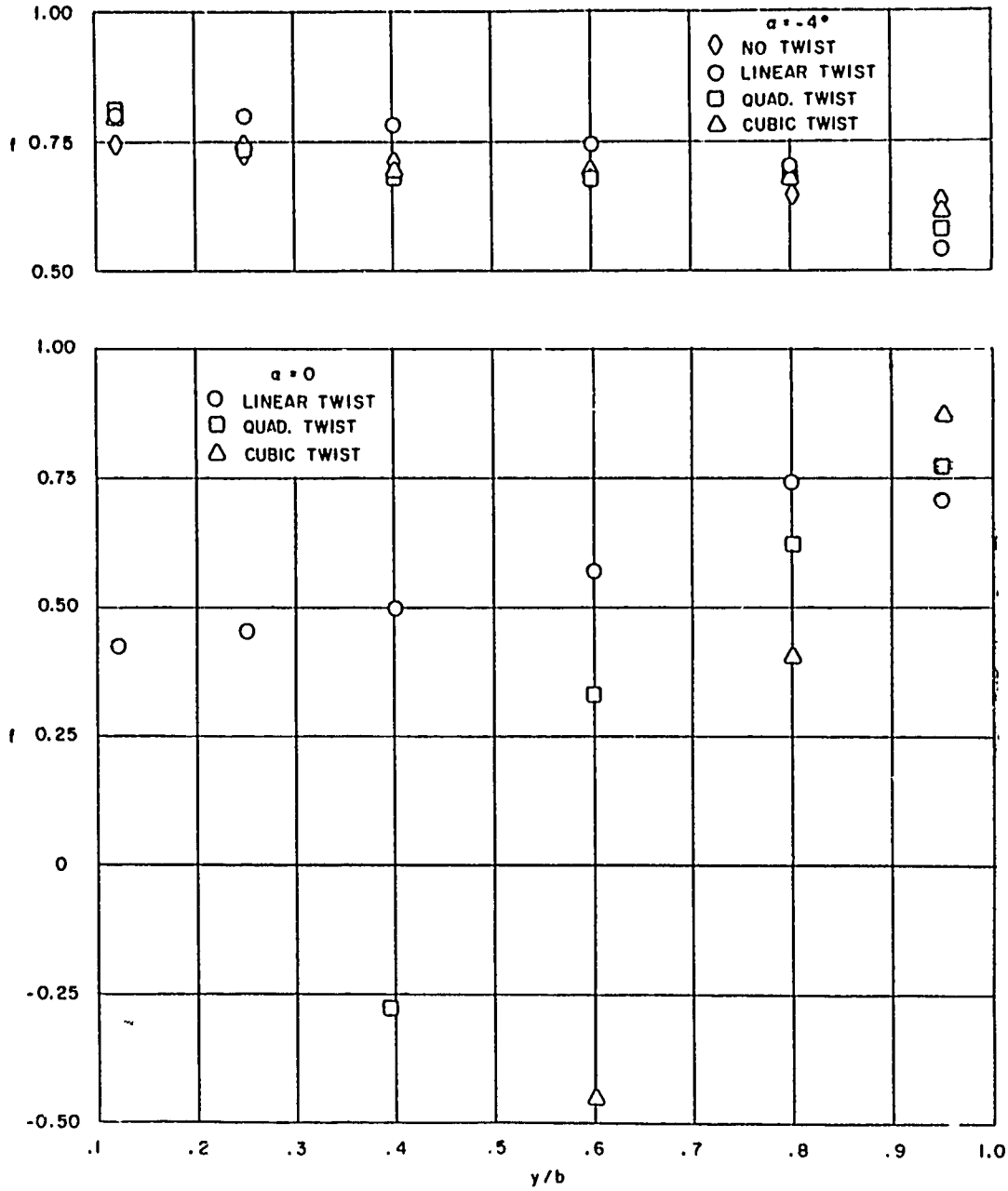


Figure 7a. Ratio of experimental spanwise load distribution to linear theory spanwise load distribution; $\alpha = -4, 0$

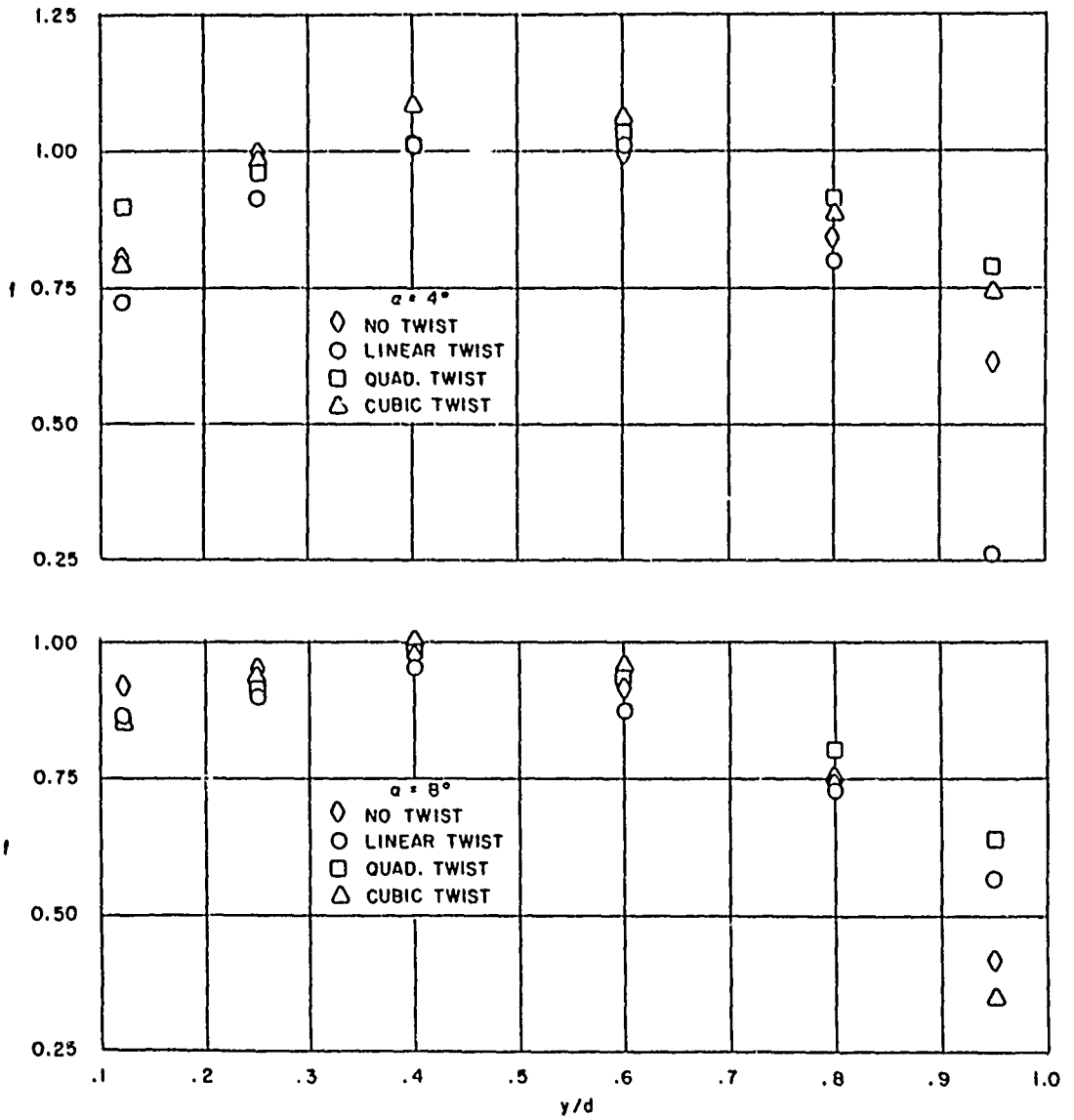


Figure 7b. Ratio of experimental spanwise load distribution to linear theory spanwise load distribution; α = 4, 8

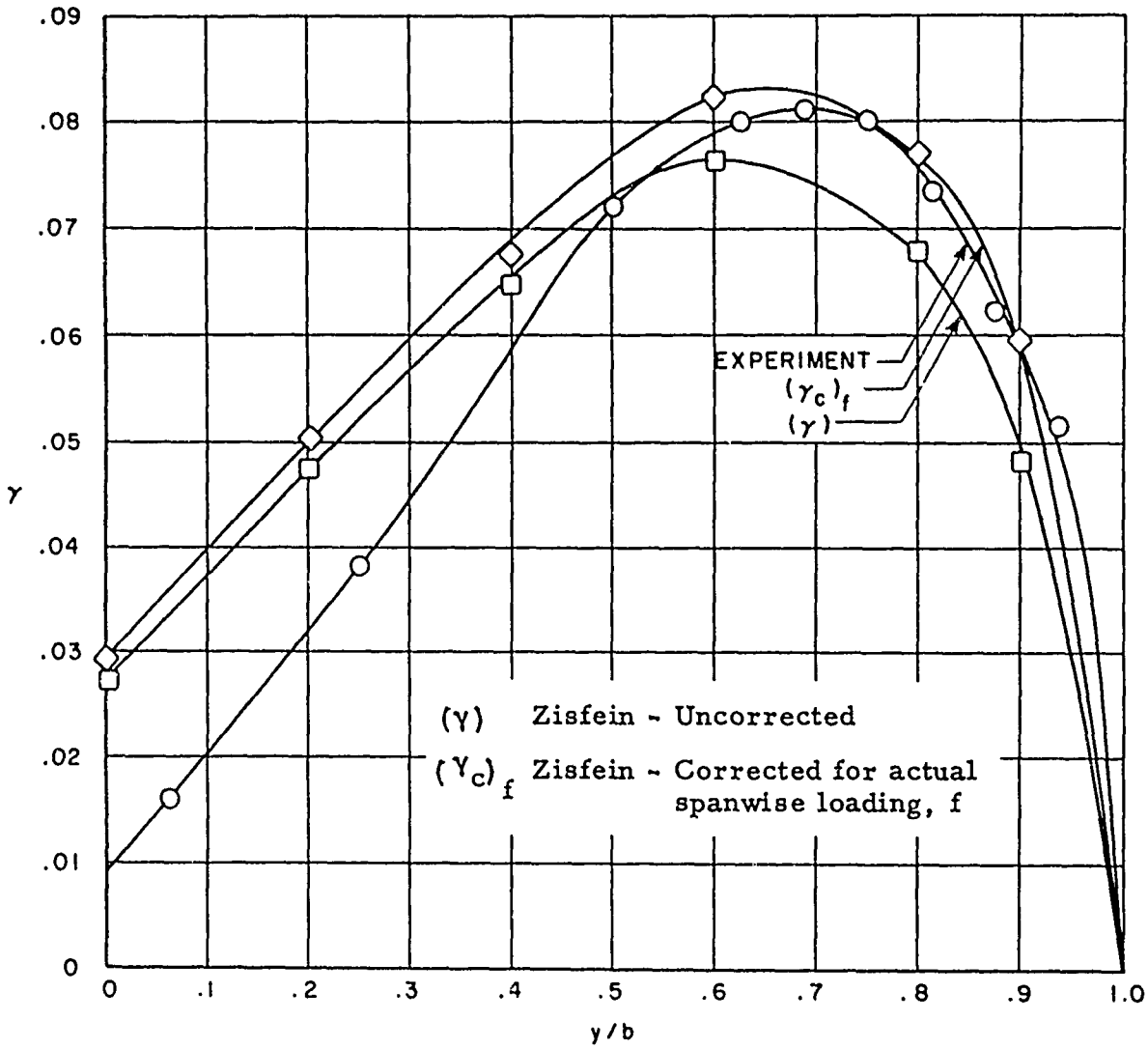


Figure 8. Comparison of measured spanwise loading and that calculated by a semi- empirical procedure

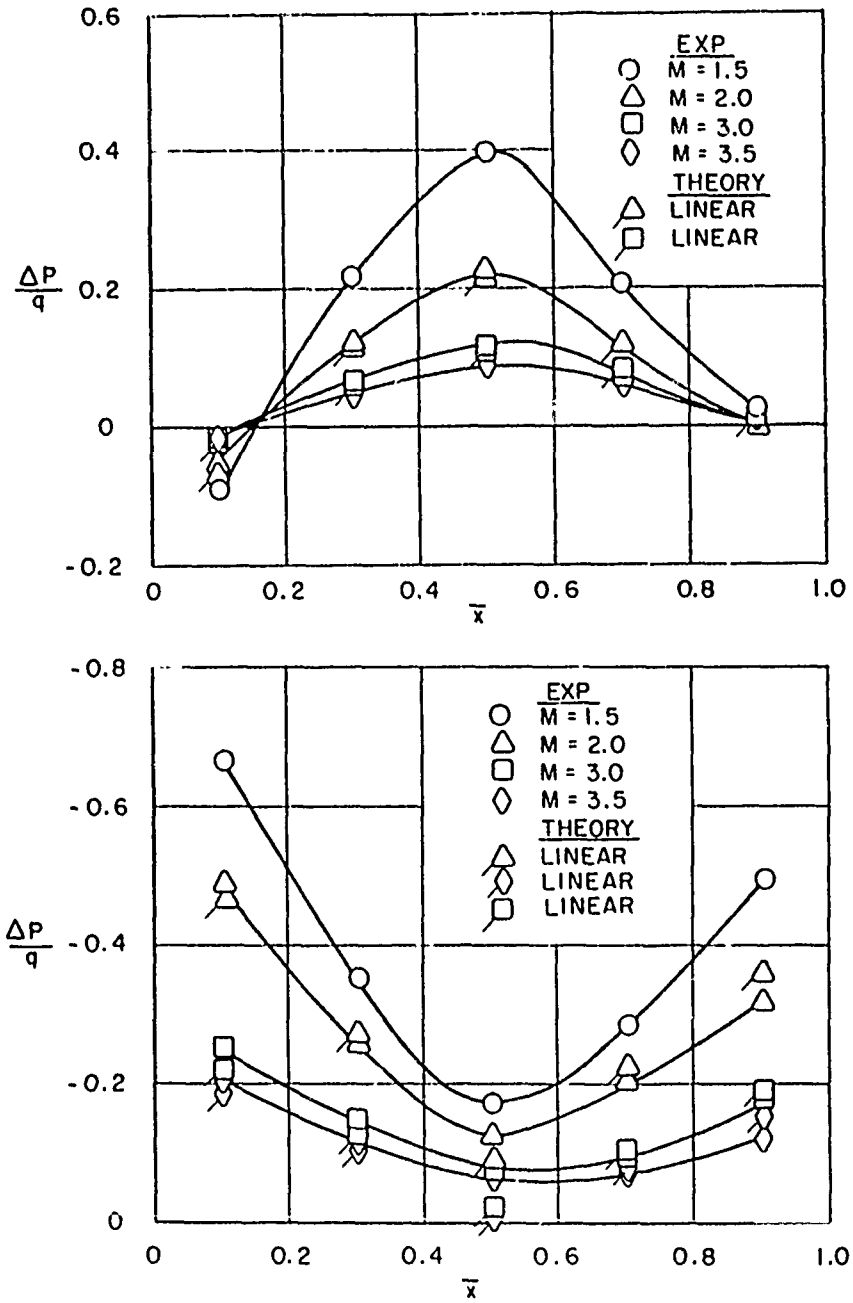


Figure 9. Comparison of measured chordwise loading with that calculated by perturbation about zero lift

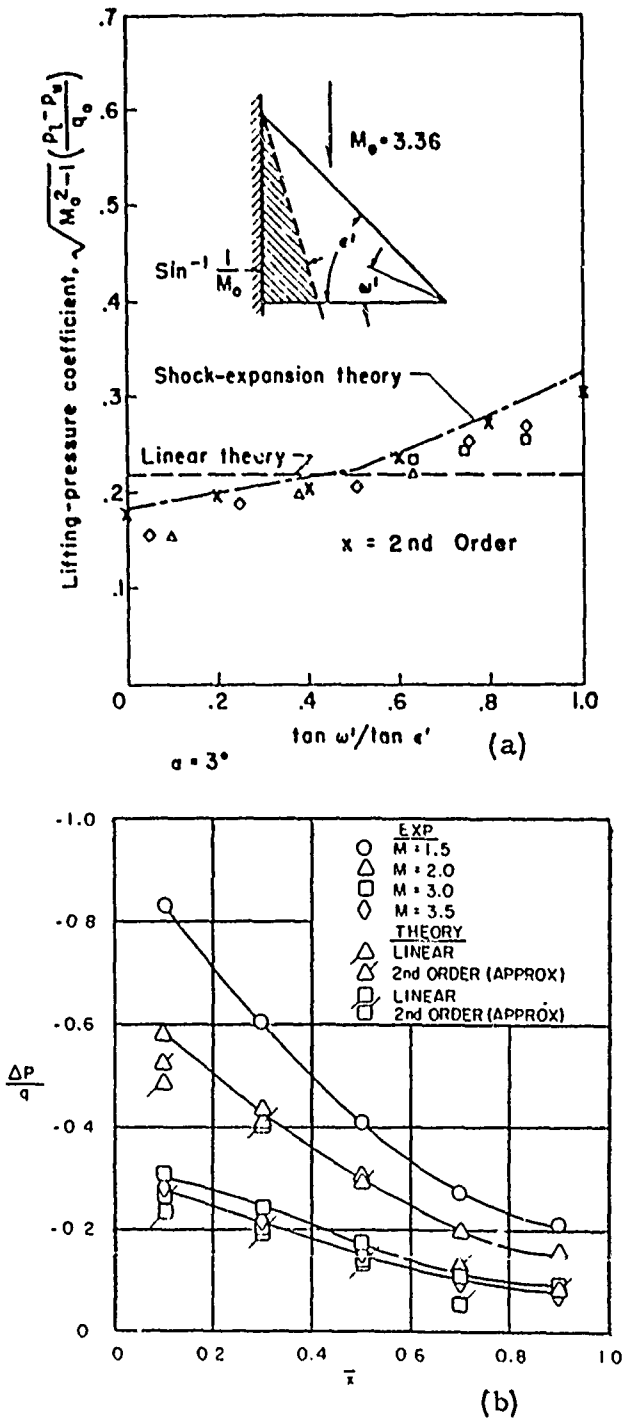


Figure 10. Comparison of measured loading and that calculated by second order theory (curve (a) from Elliott D. Katzen, "Limitations of Linear Theory in Predicting the Pressure Distribution on Triangular Wings," JAS, July 1955, p 515)

CONCLUSION

The distributed loads on distorted aerodynamic surfaces can generally be calculated to within five percent when the value of the product of the slope and the Mach number is less than 0.1. The error is less than ten percent when this product is less than about 0.25. This holds for a rapidly varying small camber or more slowly varying sharper camber as would be expected.

If a higher degree of accuracy is required, then one of two more accurate procedures is recommended. The first is that due to Beane, and the second involves the use of shock-expansion theory along the proper streamline.

Any other procedure, to provide a higher degree of accuracy, must account for the variation in the speed of sound and the non-uniform convection. The development of empirical procedures such as Zisfein's should account for these effects.

In a summary, it is concluded that:

1. As long as the wing is essentially two-dimensional and if the thickness ratio is less than three percent and the angle of attack is less than five degrees, then linear theory agrees well with experiment at $M_\infty > \sqrt{2}$.

2. For thicker wings at moderate Mach number and angles of attack, if the perturbation velocity due to angle of attack (or camber) is added to the basic velocity and then the local pressure is computed, the agreement between theory and experiment is good as long as the flow does not separate and the leading edge is not sonic or blunted.

3. At higher Mach numbers, the second order interference velocity must be included in the pressure.

4. Whenever the streamlines can be estimated, shock expansion theory provides results that agree well with measurement.

5. Since the second order theory and shock-expansion procedures both include the non-linear effects of
   a) variable convection and
   b) variable sound speeds,
   it is concluded that any procedure can be expected to give good agreement with calculation and measurements if it includes these two effects.

6. Since one consequence of the non-linearities is the change in shape of the Mach lines, it seems that the suggestions in paragraph 5 represent adoption of Whitham's hypothesis.

The results presented based on the use of local Mach number tend to agree with results based on the use of shock-expansion, which lend credence to this assertion.

7. Consequently, Zisfein's empirical procedure would produce satisfactory results as long as the correction matrix is based upon a wing with a thickness distribution that is similar to the wing under consideration.

8. For detailed application at moderate Mach number, either the procedure given in paragraph 2 or paragraph 7 seems adequate. Since a sound numerical procedure is now available for the use with linear theory, either method can be done with automatic computing. The method of paragraph 7 does not seem to be excluded from the upper transonic range.

The most serious limitations on the less empirical procedures are:

1. Limitations in strongly three dimensional regions.
2. Limitations in the upper transonic speed range.
3. Limitations caused by premature boundary layer separation and rolling up of vorticity.
4. Limitations due to secondary boundary potential flow interaction, this interaction is expected in variable pressure gradients, for example.

REFERENCES

1. Etkin, B., Numerical Integration Methods for Supersonic Wings in Steady and Oscillatory Motions, University of Toronto, Institute of Aerophysics, Report 36, November, 1955.

2. Van Dyke, Milton, D., "First and Second Order Theory of Supersonic Flow Past Bodies of Revolution," JAS, 1951.

3. Eggers, A.J. and Syvertson, C.A., Inviscid Flow About Airfoils at High Supersonic Speeds, NACA TN 2646, 1952

4. Beane, B.J., The Effects of Camber and Twist on Wing Pressure Distributions for Mach Numbers from 2.0 to 7.6: Part II: Comparison with Theory, Massachusetts Institute of Technology, Aerophysics Laboratory, TR 5, September 1961.

5. Landahl, Martin, "Unsteady Flow Around Thin Wings at High Mach Numbers," JAS, Jan. 1957, pp 33-38.

6. Landahl, Martin, Drougge, George and Beane, Beverly, "Theoretical and Experimental Investigation of Second Order Supersonic Wing-Body Interference," JAS, Vol. 27, No. 9, pp. 694-702, September 1960.

7. Frick, C.W., "The Experimental Aerodynamics of Wings at Transonic and Supersonic Speed," Aerodynamic Components of Aircraft at High Speeds, Vol. 7, Princeton Series, 1957, pp. 814-816.

8. Eggers, A.J.Jr., Syvertson, Clarence A., and Kraus, Samuel, A Study of Inviscid Flow About Airfoils at High Supersonic Speeds, NACA Report 1123, 1953.

9. Peterson, Robert L., Pressure Distribution on Warped Wings at Supersonic Velocities, Massachusetts Institute of Technology, Naval Supersonic Laboratory, TR 389, August 1960.

10. Zisfein, M., WADD TR 58-378, Part II, 58-95 Part I.

11. Johnson, William S. Jr., and Martin, George W., "An Aerodynamic - Influence - Coefficient Procedure for Wings Having Supersonic Trailing Edges and Streamwise Tips", Aerospace Engineering Review, p. 22, September 1961.

APPENDIX A

The basic laws that govern the motion of a perfect inviscid, non-conducting gas can be written in terms of conservation of mass, momentum and energy. These equations involve the six unknowns; velocity, $\vec{v}$, pressure, p, density, ρ and entropy, S. The latter three variables are called thermodynamic variables and are related by a state equation. For a perfect gas this may be written as

$$p = R \rho^{\gamma} e^{S/C_v} \tag{A-1}$$

Corresponding with the more common expression

$$p = \rho R T \tag{A-1a}$$

These two equations can be used to compute the local speed of sound from its definition

$$a^2 = \frac{\partial p}{\partial \rho}\Big)_S = \gamma (p/\rho) = \gamma R T \tag{A-2}$$

The local speed of sound can also be related to the conditions at infinity on the same streamline, by the formula

$$a_\infty^2 + \frac{\gamma - 1}{2} v_\infty^2 = a^2 + \frac{\gamma - 1}{2} v^2 \tag{A-3}$$

where the left hand side of this equation may vary from streamline to streamline.

Further, it is easy to eliminate variables and reduce the three conservation laws to the form

$$\text{div } \vec{v} - \frac{\vec{v} \cdot (\vec{v} \cdot \nabla) \vec{v}}{a^2} = 0 \tag{A-4}$$

The basic conservation laws that are assumed to apply in the

field of fluid mechanics are:

1. Conservation of mass

$$\text{div } \rho \vec{v} = 0$$

2. Conservation of momentum

$$\rho \left[(\vec{v} \cdot \nabla) \vec{v} \right] = -\nabla p$$

3. Conservation of energy

$$\rho \vec{v} \cdot \nabla S = 0$$

in an inviscid, non-conducting fluid.
Equation (1) can be written

$$\vec{v} \cdot (\nabla \chi) + \text{div } \vec{v} = 0$$

if $\chi = \ln\rho$

The existence of a thermodynamic state equation allows the pressure gradient (∇p) to be computed as

$$\nabla p = \left(\frac{\partial p}{\partial \rho}\right)_S \nabla \rho + \left(\frac{\partial p}{\partial S}\right)_\rho \nabla S$$

Thus, the law of conservation of momentum becomes

$$(\vec{v} \cdot \nabla) \vec{v} = -\left(\frac{\partial p}{\partial \rho}\right)_S \nabla \chi + \frac{1}{\rho} \left(\frac{\partial p}{\partial S}\right)_\rho \nabla S$$

Multiplying by $(\vec{v}\cdot)$

$$\vec{v} \cdot \left[(\vec{v} \cdot \nabla) \vec{v} \right] = -\left(\frac{\partial p}{\partial \rho}\right)_S \vec{v} \cdot \nabla \chi$$

and substituting

$$\operatorname{div} \vec{v} - \frac{\vec{v} \cdot \left[(\vec{v} \cdot \nabla) \vec{v} \right]}{\left(\frac{\partial p}{\partial \rho} \right)_S} = 0$$

This equation is valid throughout the flow field except at shock waves where the proper jump conditions must be accounted for.

Suppose, now, that the basic surface gives rise to a velocity field $\vec{v}_b$ which satisfies the equation

$$\operatorname{div} \vec{v}_b - \frac{\vec{v}_b \cdot (\vec{v}_b \cdot \nabla) \vec{v}_b}{a_b^2} = 0 \qquad \text{(A-5)}$$

The positive x axis is in the downstream direction, y is in the spanwise direction and z is positive upwards, forming a rectangular, right handed coordinate system whose origin is at the leading edge, hence, for a wing-like or planar surface the velocity vector

$$\vec{v}_b = u_b \hat{i} + v_b \hat{j} + w_b \hat{k} \qquad \text{(A-6)}$$

has a much larger longitudinal part (u_b) than transverse part.

The perturbed surface will give rise to the velocity $\vec{v}_1$, which is a solution to the equation,

$$\operatorname{div} \vec{v}_1 - \frac{\vec{v}_b \cdot (v_b \cdot \nabla) \vec{v}_1}{a_b^2} - \frac{2 \vec{v}_1 \cdot (\vec{v}_b \cdot \nabla) \vec{v}_b}{a_b^2} + \frac{2a_1}{ab} \operatorname{div} v_b \hat{i} = 0 \qquad \text{(A-7)}$$

The energy equation gives $a_1 \sim (\gamma - 1) M_b \vec{v} \cdot \hat{i}$ hence, the perturbation term for the speed of sound adds

$$-(\gamma - 1) M_b \frac{(\operatorname{div} \vec{v}_b) \vec{v}_1 \hat{i}}{a_b}$$

If it is assumed that the perturbation velocity is irrotational, then

$$\vec{v}_1 = -\nabla \phi \tag{A-8}$$

and, after using the magnitude arguments for a planar surface the equation for the perturbation becomes

$$(1-M_b^2)\ \phi_{xx} + \phi_{yy} + \phi_{zz} - \frac{M_b}{a_b}\left[2\ \frac{\partial \vec{v}_b}{\partial x} + (\gamma-1)\ (\nabla \cdot v_b)\ i \right] \cdot \nabla\ \phi = 0 \tag{A-9}$$

The basic surface is described by the equations

$$f_b\ (x, y, z) = 0 \tag{A-10}$$

and the perturbation from the total surface is assumed to have the form $\epsilon\ f_1\ (x, y, z)$ so the total perturbed body is described by

$$f(x, y, z) = f_b\ (x, y, z) + \epsilon f_1\ (x, y, z) = 0$$

The function f_1 is chosen to be of the order of f_b, hence, ϵ represents the fractional change coordinate.

The boundary conditions require that the perturbations vanish at the leading edge shock and the normal velocity components vanish at the surface; for the approximation the surface conditions will be satisfied at zero,

$$\phi_y = u_b \epsilon\ \frac{n_{1y}\ n_{bx}}{n_{by}^2} = v_b \epsilon \frac{n_{1y}}{n_{by}} \tag{A-11}$$

$$\phi_z = u_0 \epsilon\ \frac{n_{1z}\ n_{bx}}{n_{bz}^2} = w_b \epsilon \frac{n_{1z}}{n_{bz}} \tag{A-12}$$

where $\vec{n}_b$ is the basic normal vector and $\vec{n}_1$ is the perturbation normal. These conditions are satisfied in the mean plane. The definitions of n_b and n_1 are given in Appendix B. Note in passing that

$$v_b = u_b \frac{n_x}{n_y} , \quad w_b = u_b \frac{n_x}{n_z} \tag{A-13}$$

Note also that if v_b is the uniform external stream, then Eq. (9) reduces to the usual perturbation equation. The extra term on the left hand side of Eq. (9) is related to the usual second order terms (of Lighthill, M.J.; Higher Approximations in Aerodynamic Theory; Princeton Aeronautical Paperbacks; Princeton University Press, 1960, Eq. 2-14; p.19)

In this connection, the more common second order equation generally has the straight characteristics associated with M_∞ rather than the local Mach number. If one takes the value of $\vec{v}_b$ in (A-9) to be the first order value and the Mach number is taken as the free stream value then this equation reduces to that used by Landahl (Ref. 5).

The solution to Eq. (9), subject to the boundary conditions (11) and (12) is, generally, difficult to obtain. However, certain approximations can be made which will allow solutions under restricted circumstances. First assume that the primary variations in M_b and $((\vec{v}_b \cdot \nabla)\vec{v}_b/a_b^2)$ are in the x direction and secondly assume these variations are much more gradual than the variations in ϕ.
Let

$$\beta = \sqrt{M_b^2 - 1}$$

and

$$\lambda = \frac{u_b}{a_b^2} \frac{\partial u_b}{\partial x} \frac{(\gamma + 1)}{2}$$

then Eq. (9) becomes

$$-\beta^2 \phi_{xx} + \phi_{yy} + \phi_{zz} - \lambda \phi_x = 0 \tag{A-14}$$

It can be shown by direct substitution that if

$$\phi = e^{-(\lambda x / 2\beta^2)} \psi \tag{A-15}$$

the approximate equation becomes (if $\frac{d\lambda}{dx} \sim 0$)

$$\psi_{yy} + \psi_{zz} - \beta^2 \psi_{xx} + \frac{1}{2}\left(\frac{\lambda}{\beta}\right)^2 \psi = 0 \qquad \text{(A-16)}$$

This equation is the two-dimensional form of the Klein-Gordon Equation which has the singular outgoing solution

$$g = \frac{\beta}{\sqrt{(x-\xi)^2 - \beta\left[(y-\eta)^2 + (z-\phi)^2\right]}} - \frac{\lambda}{\sqrt{2}\beta} \int_{-\infty}^{\infty} \frac{1(\xi_1-\rho)\, J_1(k\sqrt{\xi_1-\rho^2})\, dt}{\sqrt{\xi_1^2-\rho^2}}$$

$$\rho^2 = t^2 + \left[(y-\eta)^2 + (z-\phi)^2\right] \; ; \; \xi_1 = \frac{(x-\xi)}{\beta} \qquad \text{(A-17)}$$

and approximately

$$g \sim \frac{\beta}{\sqrt{(x-\xi)^2 - \beta^2\left((y-\eta)^2 + (z-\phi)^2\right)}} - \frac{\lambda^2}{\sqrt{2}\beta^3} \sqrt{(x-\xi)^2 - \rho^2\left[(y-\eta)^2 + (z-\phi)^2\right]}$$

(A-18)

So the rapidly varying perturbation approximate singular solution ϕ_S is

$$\phi_S \cong \frac{\beta e^{-\frac{\lambda(x-\xi)}{2\beta^2}}}{R} - \frac{\lambda^2 e^{-\frac{\lambda(x-\xi)}{2\beta^2}}}{\sqrt{2}\,\beta^3} R \qquad \text{(A-19)}$$

where $R = \sqrt{(x-\xi)^2 - \beta^2\left[(y-\eta)^2 + (z-\xi)^2\right]}$ (A-20)

Hence the potential is

$$\phi(x, y, 0) = \frac{1}{2M_0\pi}\int_w w\,\phi_S\,(x, y, 0)\,dS \qquad (A\text{-}21)$$

where w denotes the velocity at the wing surface. Note that $\lambda \to 0$ this reduces to the usual solution. When χ is very small, the primary contribution is from the part of ϕ_S nearest to the equal sign. Since

$$\lambda \sim -2\gamma \nabla \ln\rho \cong -\frac{2\gamma}{\rho}\,\frac{\partial\rho}{\partial x} \qquad (A\text{-}22)$$

λ is generally quite small. The real effect then is that of changing the characteristics to a curvilinear system. This is an approximation to Whitham's conjecture (cf Lighthill loc cit p. 85) that states that "... The small perturbation theory gives a correct first approximation throughout the flow, provided that the value which it predicts for any physical quantity... is interpreted as the value, at that radial distance from the axis, on the exact Mach line which points downstream from the same point."

A similar point has been presented by Frick in discussing the effects of the body-root junction. He pointed out that the jump in the slope of the pressure distribution fell on the local Mach line, not the linearized line. He also shows evidence that linear theory agrees with experiment better when the wings are thinner. It is inferred that as the wing is thinner the characteristics approach the linear characteristics.

APPENDIX B

The normal to a surface described by the equation $f_0(x, y, z) = 0$ is

$$\vec{n} = \frac{f_{0_x}\hat{i} + f_{0_y}\hat{j} + f_{0_z}\hat{k}}{\sqrt{f_{0_x}^2 + f_{0_y}^2 + f_{0_z}^2}}$$

When

$$f = f_0 + \epsilon f_1 + \ldots$$

the first order correction to the normal, $\vec{n}_1$, i.e., let

$$\vec{n} = \vec{n}_0 + \epsilon \vec{n}_1 + 0(\epsilon^2)$$

is

$$\vec{n}_1 = \frac{f_{1_x}(1-n_{0_x}^2)\,i + f_{1_y}(1-n_{0_y}^2)\,j + f_{1_z}(1-n_{0_z}^2)\,k}{\sqrt{f_{0_x}^2 + f_{0_y}^2 + f_{0_z}^2}}$$

NONLINEAR HYPERSONIC THERMOELASTIC STABILITY AND CONTROL DERIVATIVES

Vincent W. Donato
Joseph Padlog
James R. Batt

Bell Aerosystems Company
Division of Bell Aerospace Corporation

ABSTRACT

The effect of hypersonic aerodynamic nonlinearities on static aeroelastic equilibrium solutions and the concomitant stability and control derivatives are presented. The classical two-dimensional aeroelastic model is initially studied and the results extended to more complex three-dimensional aeroelastic phenomena. Methods for the solution of the nonlinear static aeroelastic interaction equations are derived, and expressions for the flexible to rigid ratio of lifting pressure, span loading, and three-dimensional lift curve slope are developed. Results of a sample problem are presented to illustrate use of the numerical methods derived and to display the effects of aerodynamic nonlinearities.

LIST OF SYMBOLS

a	aerodynamic coefficient
$\bar{a}_{0_i}$	the value of $\Delta p_i/q$ at $\alpha_i = 0$
$\bar{a}_{1_i}$	tangent line slope
b	wing span, aerodynamic coefficient
c	wing chord
$\bar{c}$	wing average chord
c_ℓ	two dimensional lift coefficient
$c_{\ell_{F_n}}$	two dimensional nonlinear flexible lift coefficient
$c_{\ell_{R_n}}$	two dimensional nonlinear rigid lift coefficient
c_{ℓ_n}	two dimensional nonlinear lift coefficient
$c_{\ell_{F_\ell}}$	two dimensional linear flexible lift coefficient
$c_{\ell_{R_\ell}}$	two dimensional linear rigid lift coefficient
c_{ℓ_α}	two dimensional lift-curve slope
$c_{\ell_{\alpha_{F_n}}}$	two dimensional nonlinear flexible lift-curve slope
$c_{\ell_{\alpha_{R_n}}}$	two dimensional nonlinear rigid lift-curve slope
e	distance of the aerodynamic center from the wing elastic axis divided by the chord

SYMBOLS (CONT)

ℓ	two dimensional lift load per unit span
ℓ_n	two dimensional nonlinear lift load
ℓ_{F_n}	two dimensional nonlinear flexible lift load
ℓ_{R_n}	two dimensional nonlinear rigid lift load
$q = \frac{1}{2}\rho V^2$	dynamic pressure
$q_{D_\ell} = \frac{K}{ac^2e}$	linear divergence dynamic pressure
q_{D_n}	nonlinear divergence dynamic pressure
q_{n_i}	aerodynamic influence coefficient associated with n-th power of angle of attack at the i-th reference point
x^*, y^*	nondimensional coordinate system
C_{L_F}	three dimensional flexible lift coefficient
C_{L_R}	three dimensional rigid lift coefficient
C_{L_α}	three dimensional lift-curve slope
$C_{L_{\alpha_{F_n}}}$	three dimensional nonlinear flexible lift curve slope
$C_{L_{\alpha_{R_n}}}$	three dimensional nonlinear rigid lift curve slope
$F_i(\alpha_i)$	arbitrary function of angle of attack
K	torsional spring constant
M_e	elastic internal restoring moment

SYMBOLS (CONT)

M_a	aerodynamic moment
M_∞	free stream Mach number
Q_0, Q_1	aerodynamic influence coefficients
α	equilibrium angle of attack
α_g	geometric or rigid angle of attack in Equation (41)
α_s	elastic (structural) angle of twist
α_{REF}	aircraft reference angle
α_{b_i}	built in twist angle
α_{b_c}	built in camber angle
$\mu = \frac{b}{a}\alpha_g$	aerodynamic parameter
$\frac{\Delta p}{q}$	Plower surface - Pupper surface/q, lifting pressure
$\frac{\Delta p_n}{q}$	nonlinear lifting pressure component
τ	thickness ratio, maximum thickness of airfoil/ chord length
$\xi = \frac{x}{c}$	nondimensional chordwise coordinate
$\gamma = \frac{cc_\ell}{\bar{c}}$	nondimensional span loading

SUBSCRIPTS

i	i-th reference point
j	denotes solution after j-th iteration
$j+1$	denotes solution after j + 1st iteration
$j-1$	denotes solution after j - 1st iteration
ℓ	linear
n	nonlinear
$n = 0, 1, 2$	denotes power of angle of attack
D	divergence
F	flexible
R	rigid
N	N-th or last reference point

MATRICES

$\{\ \}$	column matrix
$\lfloor\ \rfloor$	row matrix
$[\ ]$	square or rectangular matrix
$\lfloor\ \rceil$	diagonal matrix
$\{1\}$	unit column matrix
$\{\bar{\alpha}\, g\}$	rigid angle of attack distribution defined by Equation (44)

$\{\alpha\}$ equilibrium angle of attack distribution

$\{\alpha_s\}$ structural twist distribution

$\{\alpha_g\}$ rigid or geometric angle of attack distribution

$\left\{\frac{\Delta p}{q}\right\}$ lifting pressure distribution

$\{R\}$ distribution of remainder terms in Equation (72)

$[Q_n]$ aerodynamic influence coefficient matrix

$[I]$ unit diagonal matrix

$[R_{w-a}]$ area resolving matrix

$[S]$ structural slope influence coefficient matrix

$$[M] = [[I] - q[S][Q_1]]^{-1}$$

$$[\Delta] = q[M][\Delta p_n / q_\alpha]$$

$[\Delta p_n / q_\alpha]$ diagonal matrix of nonlinear lifting pressure component

$[I]$ row integrating matrix performing integration given by $\int_0^1 f(x)\,dx$

$[I]$ integrating matrix performing integration given by $\int_x^1 f(x)\,dx$

NONLINEAR HYPERSONIC THERMOELASTIC STABILITY AND CONTROL DERIVATIVES*

INTRODUCTION

The objective of the investigation described in this paper was to develop methods for determining the aerothermoelastic effects on hypersonic stability and control. Work done in this investigation will be reported on and published in full in Reference 1. The accurate prediction of stability and control derivatives for flexible vehicles is predominantly concerned with the determination of static aeroelastic effects on the lifting surfaces of such configurations. Since the field of static aeroelasticity is concerned with the interaction of steady aerodynamic loads and structural deformations, it is necessary to have accurate and practical methods for:

a. Obtaining aerodynamic inputs to the aeroelastic equations.

b. Obtaining structural inputs to the aeroelastic equations.

c. Formulating the aeroelastic equations so that they are compatible with the inputs from Items a and b, and the solution of these equations to obtain the pertinent stability and control parameters.

The aerodynamic input to the aeroelastic matrix equations is usually in the form of an operator called an aerodynamic influence coefficient matrix. This matrix, when operating on an arbitrary angle of attack distribution, produces the resulting air load distribution. Use of

---

*The work described here was part of a study performed under Contract AF33(616)-6653 for the Aero Space Mechanics Branch, Flight Control Laboratory, Aeronautical Systems Division.

rigid subsonic and supersonic theoretical lifting pressures resulted in linear relationships between arbitrary angle of attack distributions and the resultant distributed loads. This linear relationship can be expressed mathematically as

$$\left\{\frac{\Delta p}{q}\right\} = \left[Q\right] \left\{\alpha\right\} \tag{1}$$

where $\left\{\frac{\Delta p}{q}\right\}$ is a column matrix of lifting pressures, $\left[Q\right]$ is an aerodynamic influence coefficient matrix, and $\left\{\alpha\right\}$ is an arbitrary angle of attack distribution. Previous static aeroelasticity studies conducted at Bell Aerosystems Company have resulted in methods for obtaining supersonic $\left[Q\right]$ matrices. These methods are discussed in detail in References 2 and 3*. Methods for obtaining subsonic line aerodynamic influence coefficients may be found in the literature (References 4 and 5). The technique described in Reference 2 may be used to expand these line matrices to field matrices.

In the hypersonic speed regime use of the "rigid" theories of aerodynamic load prediction result in nonlinear relationships between distributed loads and arbitrary angle of attack distributions. Furthermore it has been found that the nonlinear hypersonic lifting pressure relationships are point functions. That is, the lifting pressure relationship at a reference point, i, is a function of the angle of attack at only reference point i. This is in direct contrast to the subsonic and supersonic cases and leads, in the hypersonic case, to diagonal aerodynamic influence coefficient matrices.

---

*Both line and field type aerodynamic influence coefficient matrices were developed. A line aerodynamic influence coefficient is defined as "that quantity which relates the aerodynamic span load at a particular spanwise station to the angle of attack at another (or the same) spanwise station". A field aerodynamic influence coefficient is defined as "that quantity which relates the local aerodynamic lifting pressure at a particular reference point to the local angle of attack at another (or the same) reference point".

The hypersonic load-angle of attack relationship can be expressed mathematically as

$$\left(\frac{\Delta p}{q}\right)_i = F_i\,(\alpha_i) \tag{2}$$

where $(\Delta p/q)_i$ is the lifting pressure at reference point i. The function $F_i(\alpha_i)$ can take on several forms depending on the aerodynamic configuration and theory being used. Typical mathematical forms are

$$F_i(\alpha_i) = q_{0_i} + q_{1_i}\alpha_i + q_{2_i}\alpha_i^2 \tag{3}$$

$$F_i(\alpha_i) = q_{0_i} + q_{3_i}\alpha_i^3 \tag{4}$$

$$F_i(\alpha_i) = q_{0_i}\,\text{SIN}\,\alpha_i\,\text{COS}\,\alpha_i \tag{5}$$

As an illustration, Equation (4) can be expressed in matrix form as

$$\left\{\frac{\Delta p}{q}\right\} = \left[Q_0\right]\left\{1\right\} + \left[Q_3\right]\left\{\alpha^3\right\} \tag{6}$$

The matrices $\left[Q_0\right]$ and $\left[Q_3\right]$ are defined as hypersonic aerodynamic influence coefficient matrices. The formulation of these matrices is discussed in more detail in the Appendix. A complete discussion of methods to determine hypersonic aerodynamic influence coefficient matrices is presented in Reference 6.

Structural deformation influence coefficients constitute the structural inputs to the aeroelastic equations. For the linear case, the defining equation is given by

$$\left\{\alpha_S\right\} = q\left[S\right]\left\{\frac{\Delta p}{q}\right\} \tag{7}$$

where the elements of $\left\{\alpha_S\right\}$ are the local streamwise slopes at the reference points. $\left[S\right]$ is the structural, slope deformation influence coefficient matrix and relates the streamwise slopes at the reference points to the lifting pressures at these same points. For the linear case shown here $\left[S\right]$ is independent of α_S and $\frac{\Delta p}{q}$. In the case of large deflections $\left[S\right]$ becomes a nonlinear function of α_S, i.e., $\left[S\right] = \left[S\,(\alpha_S)\right]$.

The high temperatures and heating rates likely to be associated with configurations in the expected hypersonic environments may very well dictate, in the interests of structural efficiency, some form of protected structure such as one which is ablatively or non-ablatively insulated, cooled or some combination of these. However, these protective measures are not likely to preclude having a "hot" primary structure. Under these circumstances, the effects of modulus deterioration and thermal stress on the structural inputs must be considered. Very few practical analytical methods for predicting deflection influence coefficients for a thermally affected structure currently exist. As part of the work on the present study, practical analytical thermal deformation influence coefficient methods were developed and are reported in References 7 and 8. Additional work done at Bell Aerosystems Company in the field of structural influence coefficients is described in References 9 and 10. Deformation testing of a body and a wing-body combination was accomplished during the present study, under both ambient and thermal environmental conditions, in order to obtain influence coefficients. This experimental work was required in order to develop the necessary testing techniques and to have available test data to collaborate the validity of any available and any forthcoming theoretical methods. Results of the experimental program are detailed in Reference 11.

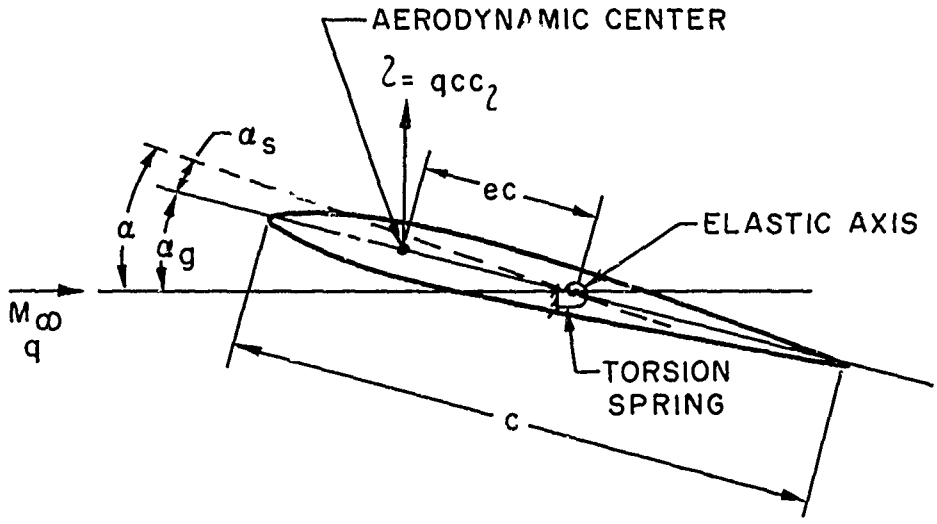
In attempting to set up the aeroelastic equations for the hypersonic speed range, difficulties arise because the aerodynamic relations between lifting load and angle of attack are no longer linear, as they were for the subsonic and lower supersonic ranges, and because the structural relations between load and deformation (when considering large deflections) are also nonlinear. Technical efforts in this study were restricted to using nonlinear aerodynamic inputs, along with linear structural inputs, to generate a nonlinear formulation of the aeroelastic problem and to employ various numerical techniques to effect an aeroelastic solution. In essence, the present study extends those methods previously developed for supersonic aeroelasticity discussed in Reference 12.

A brief resume of the contents of this paper follows. First, the various aspects of static aeroelastic phenomena that are affected by the

Reference to Section II of this paper or Reference 6 will reveal numerous other types of aerodynamic nonlinear forms. Also, in the interest of simplicity, the two-dimensional aeroelastic model is considered to have no control surface.

A. EFFECT OF AERODYNAMIC NONLINEARITIES ON TWO-DIMENSIONAL STATIC AEROELASTICITY MODEL

In an effort to determine the effects of aerodynamic nonlinearities on static equilibrium solutions, consideration is given to the classical two-dimensional airfoil shown in the following sketch. (See References 12, 13 and 14.)



For this mathematical model a linear solution is well known and therefore will serve as a basis of comparison with the nonlinear solution. The classical aeroelastic solution for this two-dimensional problem is based on the assumption that the aerodynamic lift coefficient, c_ℓ , is linearly related to the angle of attack, α . This linear relationship is given by the expression

$$c_\ell = a\alpha. \tag{8}$$

introduction of nonlinear aerodynamic relationships arising at hypersonic speeds are examined. Then hypersonic aeroelasticity is introduced through the consideration of the classical two-dimensional aeroelastic model. This derivation is extended and a numerical method, capable of predicting the three-dimensional static aeroelastic response of an aircraft, is developed. Use is made of these results to derive expressions for the flexible to rigid ratios of lifting pressure, span loading, and three-dimensional lift curve slope. Finally, results of a sample problem are presented to illustrate use of the numerical methods developed and to indicate the effects of aerodynamic nonlinearities on hypersonic stability and control.

SECTION I: DISCUSSION OF HYPERSONIC NONLINEAR STATIC AEROELASTIC PHENOMENA

The various aspects of static aeroelastic phenomena that are affected by the introduction of nonlinear aerodynamic relationships arising at hypersonic speeds are examined in this section. The significance and effects of aerodynamic nonlinearities are revealed in their simplest form by the analysis of the classical two-dimensional aeroelastic airfoil model. The results of this analysis are then used in Section II as a guide in the development of solution procedures for the analysis of nonlinear aeroelastic behavior associated with a three-dimensional lifting surface. Emphasis is placed on the effects of hypersonic aerodynamic nonlinearities upon the equilibrium angles of of attack and the ratios of flexible to rigid lift coefficients and lift-curve slopes.

Although not all static aeroelastic parameters are discussed in this section, it is felt that the solutions presented will give an insight into the effects of aerodynamic nonlinearities on static aeroelastic solutions. It is noted, for the sake of simplicity, that only one type or mathematical form of aerodynamic nonlinearity is discussed here.

In order to obtain a simple exact solution which will reveal the characteristics of nonlinear static aeroelastic phenomenon, the relationship between the lift coefficient and the equilibrium angle of attack is assumed to be of the following nonlinear form

$$c_{\ell} = a\alpha + b\alpha^2 . \qquad \alpha \geq 0 \tag{9}$$

The second term, $b\alpha^2$, on the right hand side of Equation (9) represents the nonlinear contribution to the lift coefficient. It should be realized that for this two-dimensional problem, Equation (9) is the counterpart of the nonlinear lifting pressure — angle of attack relationships discussed in Section II and in Reference 6.

The equation of static equilibrium for the aeroelastic model will now be formulated. The aerodynamic moment per unit span or applied moment per unit span about the elastic axis is given by

$$M_a = \ell ec = qec^2 c_{\ell} \tag{10}$$

where ℓ = lift load per unit span

c = chord of the wing section

e = distance of the aerodynamic center from the wing elastic axis divided by the chord

In order to simplify the presentation, the zero lift aerodynamic pitching moment about the aerodynamic center has been neglected. Eliminating the lift coefficient, c_{ℓ} , from Equation (10) by use of Equation (9), results in

$$M_a = qec^2 (a\alpha + b\alpha^2) \tag{11}$$

If K is defined as the torsional spring constant of the model, then the relationship for the elastic internal resisting moment per unit span is given by

$$M_e = K\alpha_s \tag{12}$$

where α_s is the elastic (structural) angle of twist as shown in the foregoing sketch.

In order to satisfy static equilibrium conditions, the externally applied aerodynamic moment, M_a , must equal the elastic internal resisting moment, M_e . This condition together with Equations (11) and (12) yields the following equilibrium equation

$$K\alpha_s = qc^2e(a\alpha + b\alpha^2). \tag{13}$$

By definition, the equilibrium angle of attack, α , is equal to the sum of the structural angle of twist, α_s , and the geometric angle of attack, α_g , i.e.,

$$\alpha = \alpha_s + \alpha_g. \tag{14}$$

Eliminating α_s from Equations (13) and (14) results in the following quadratic expression in the unknown, α .

$$\alpha^2 + \left(\frac{a}{b} - \frac{K}{qc^2eb}\right)\alpha + \frac{K}{qc^2eb}\alpha_g = 0 \tag{15}$$

or in nondimensional form

$$\left(\frac{\alpha}{\alpha_g}\right)^2 + \left(\frac{a}{b\alpha_g} - \frac{a q_{D_\ell}}{qb\alpha_g}\right)\left(\frac{\alpha}{\alpha_g}\right) + \frac{q_{D_\ell}}{q}\,\frac{a}{b\alpha_g} = 0 \tag{16}$$

where $q_{D_\ell} = \frac{K}{ac^2e}$. The symbol q_{D_ℓ} represents the divergence dynamic pressure for the corresponding linear case, i.e. when the coefficient b in Equation (9) equals zero.

1. Solution for Equilibrium Angles of Attack

The exact solution of Equation (16) is given by

$$\frac{\alpha}{\alpha_g} = \frac{-\left(1-\frac{q}{q_{D_\ell}}\right) \pm \sqrt{\left(1-\frac{q}{q_{D_\ell}}\right)^2 - 4\mu\,\frac{q}{q_{D_\ell}}}}{-2\left(\mu\,\frac{q}{q_{D_\ell}}\right)} \tag{17}$$

where $\mu = \frac{b}{a}\alpha_g$

It should be noted that if the coefficient b (and hence μ) is set equal to zero, the classical solution for the corresponding linear problem is obtained; i.e.

$$\frac{\alpha}{\alpha_g} = \frac{1}{1 - \frac{q}{q_{D_\ell}}} \quad . \tag{18}$$

The relationship between the dynamic pressure ratio and the equilibrium angle as given by Equation (17) is depicted graphically in Figure 1 for various values of the parameter μ. The static stability ranges deduced from Equation (17) are also shown in Figure 1. The circular symbol indicates the point of neutral stability, the dashed curve indicates the condition of unstable equilibrium and the solid curve refers to the condition of stable equilibrium. Hence, the divergence of the two-dimensional model is indicated by the circular symbols. At these points $\frac{\partial \alpha}{\partial q} = \infty$, which is the criterion for divergence.

The curves in Figure 1 clearly indicate the effect of the aerodynamic parameter, b, on the equilibrium angle of attack for the case where the aerodynamic center is forward of the elastic axis. For constant values of α_g and a, it is evident that increasing b, positively, increases the magnitude of the equilibrium angle of attack for a given value of q.

Equation (17) has also been replotted in Figure 2 to show the variation of the equilibrium angle of attack with α_g. As shown in this figure, $\frac{b}{a}$ is positive and is held constant, increasing the magnitude of α_g increases the equilibrium angle of attack more than a proportional amount.

2. Solutions for Ratios of Flexible to Rigid Lift Coefficients and Lift Curve Slopes

For purposes of determining the performance and stability and control of a flexible aircraft, it is desirable to know the effects of structural flexibility and aerodynamic nonlinearities on the lift coefficient and lift curve slope. These results are usually presented in the

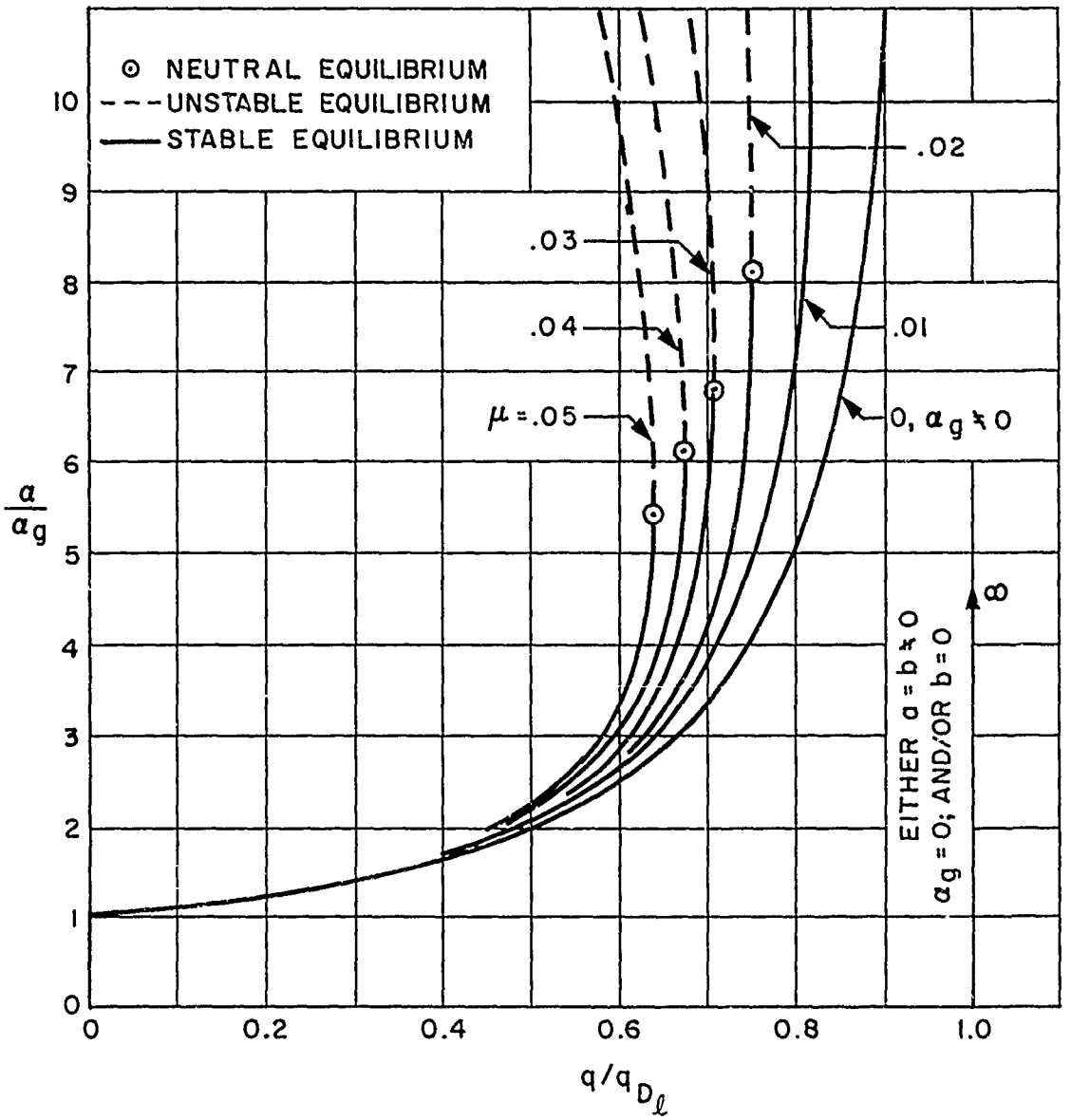


Figure 1. Variation of α/α_g with Dynamic Pressure and Parameter μ

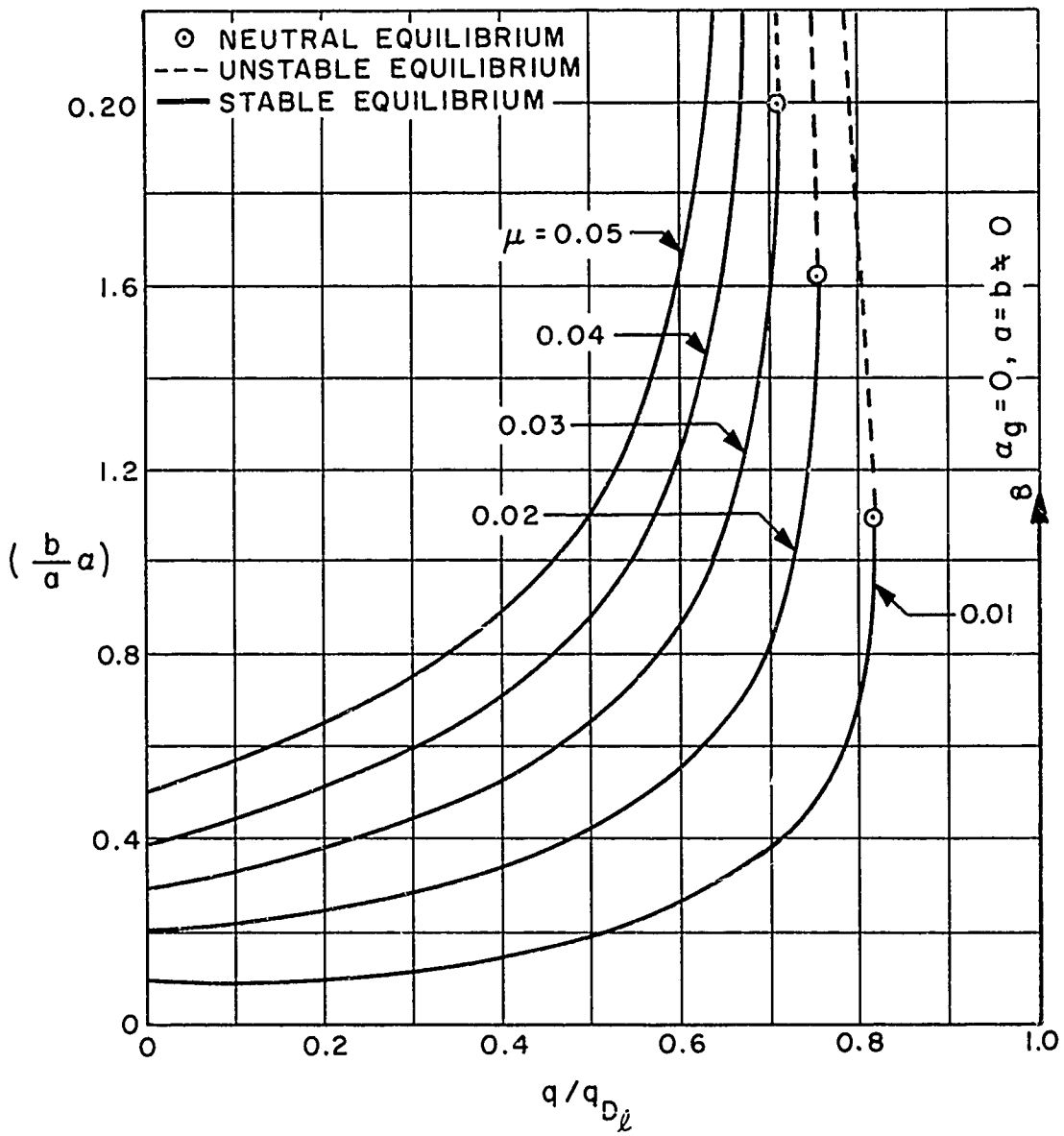


Figure 2. Variation of $(\frac{b}{a})a$ with Dynamic Pressure and Parameter μ

form of ratios of flexible to rigid lift coefficients and lift curve slopes.

The first parameter to be discussed is the ratio of the nonlinear flexible lift coefficient, $c_{\ell_{F_n}}$, to the nonlinear rigid lift coefficient, $c_{\ell_{R_n}}$. The nonlinear lifting load for the two-dimensional model is given by

$$\ell_n = qcc_{\ell_n} \tag{19}$$

For the flexible case Equation (19) can be written as

$$\ell_{F_n} = qcc_{\ell_{F_n}} \tag{20}$$

and for the rigid case as

$$\ell_{R_n} = qcc_{\ell_{R_n}} \cdot \tag{21}$$

Using Equation (9), the nonlinear lift coefficient for the flexible case can be written as

$$c_{\ell_{F_n}} = a\alpha + b\alpha^2 \tag{22}$$

and for the rigid case as

$$c_{\ell_{R_n}} = a\alpha_g + b\alpha_g^2 \cdot \tag{23}$$

Use of Equations (22) and (23) in Equations (20) and (21) yields the expression

$$\frac{\ell_{F_n}}{\ell_{R_n}} = \frac{c_{\ell_{F_n}}}{c_{\ell_{R_n}}} = \frac{a\alpha + b\alpha^2}{a\alpha_g + b\alpha_g^2} \tag{24}$$

or

$$\frac{c_{\ell_{F_n}}}{c_{\ell_{R_n}}} = \left[\frac{1+\mu\left(\frac{\alpha}{\alpha_g}\right)}{1+\mu}\right]\left(\frac{\alpha}{\alpha_g}\right) \tag{25}$$

where, again $\mu = \frac{b}{a}\alpha_g$.

The ratio of lift coefficients given by Equation (25) is shown in Figure 3 as a function of q/q_{D_ℓ} and μ . As before the circle symbols denote points of neutral stability. The curve for $\mu = 0$ yields the ratio $c_{\ell_{F_\ell}}/c_{\ell_{R_\ell}}$ i.e. the linear case, $b = 0$. The increase in this ratio over the linear case as μ increases for constant values of q/q_{D_ℓ} should be noted.

An additional parameter of interest is $\left(\frac{c_{\ell_{F_n}}}{c_{\ell_{R_n}}}\right)/\left(\frac{c_{\ell_{F_\ell}}}{c_{\ell_{R_\ell}}}\right)$ which will indicate the nonlinear aerodynamic effect upon the lift coefficients. The desired ratio can be expressed as

$$\frac{\left(\frac{c_{\ell_{F_n}}}{c_{\ell_{R_n}}}\right)}{\left(\frac{c_{\ell_{F_\ell}}}{c_{\ell_{R_\ell}}}\right)} = \frac{1+\mu\left(\frac{\alpha}{\alpha_g}\right)}{1+\mu} \quad . \tag{26}$$

Equation (26) is shown graphically in Figure 4 as a function of q/q_{D_ℓ} and μ . Increasing α_g or b increases the ratio for a constant value of q/q_{D_ℓ} .

A pertinent parameter to consider in aeroelastic analyses is $c_{\ell_{\alpha_{F_n}}}/c_{\ell_{\alpha_{R_n}}}$, the ratio of the nonlinear flexible lift curve slope to the nonlinear rigid lift curve slope. The lift curve slope is defined by the expression

$$c_{\ell_\alpha} = \frac{d c_\ell}{d\alpha_{REF.}} \tag{27}$$

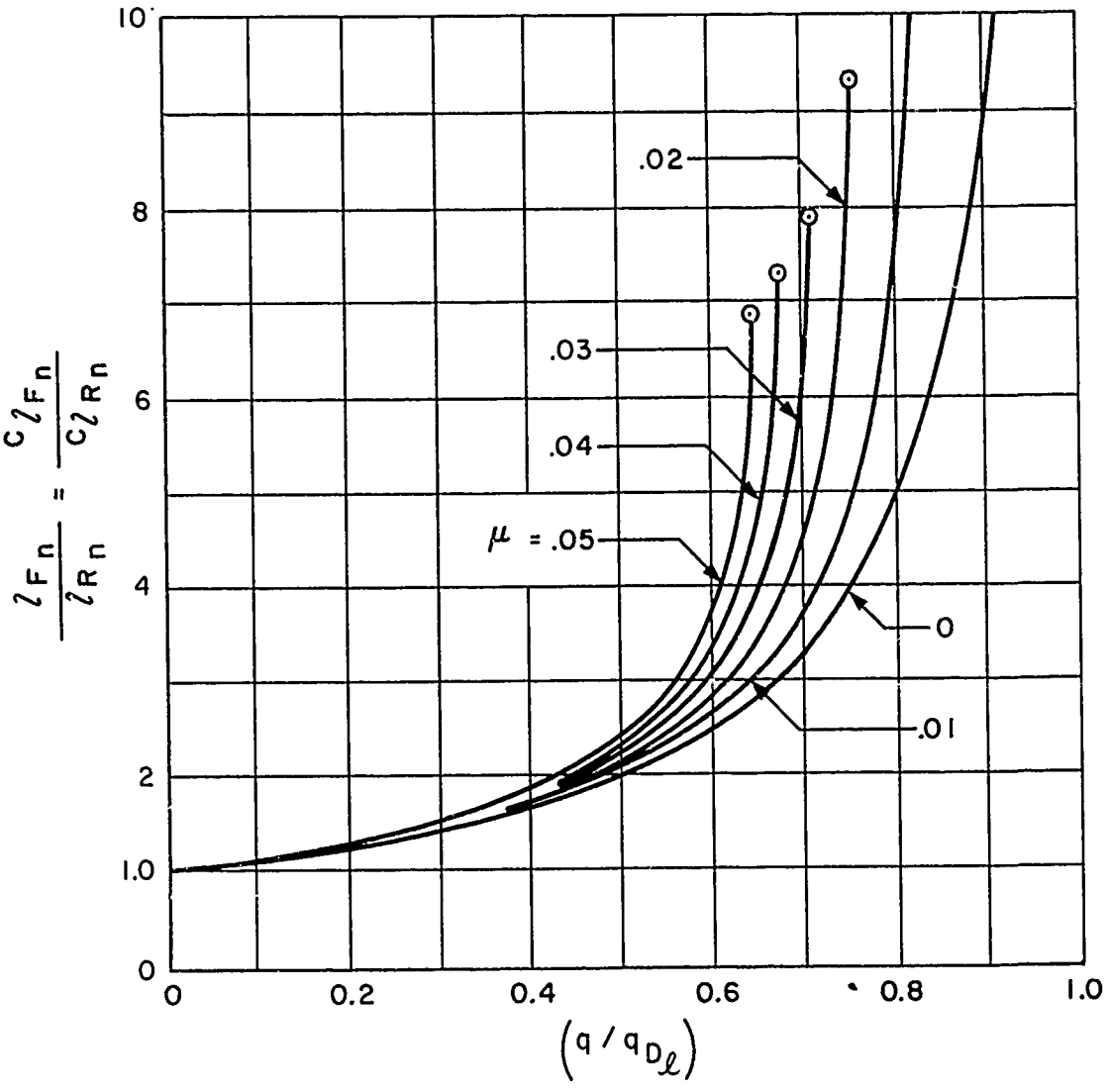


Figure 3. Variation of $c_{l_{Fn}}/c_{l_{Rn}}$ with q/q_{D_l} and μ

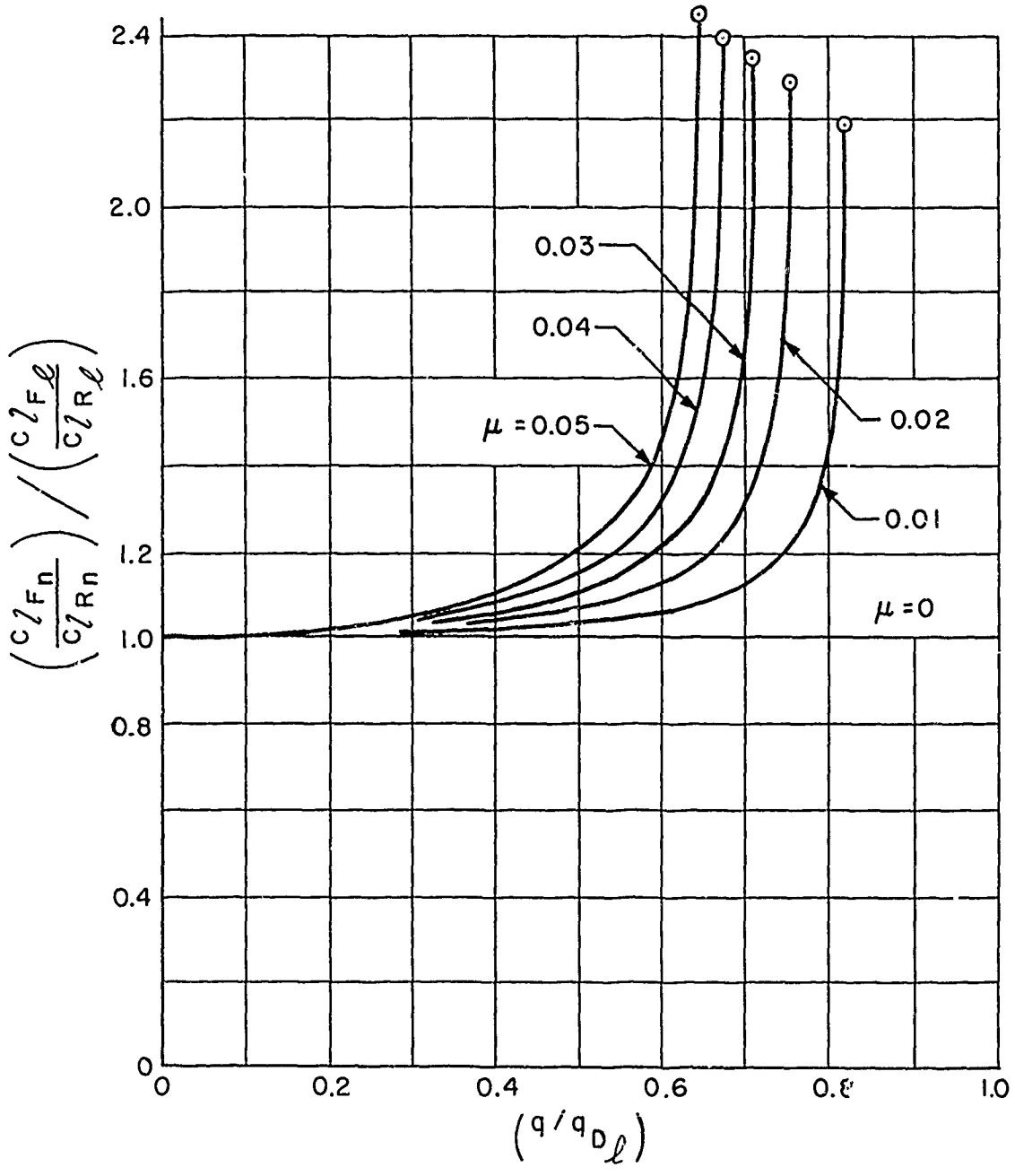


Figure 4. Variation of $\frac{c l_{F_n}}{c l_{R_n}} / \frac{c l_{F_\ell}}{c l_{R_\ell}}$ with q/q_D and μ

or, since in this case $\alpha_g = \alpha_{REF}$

$$c_{\ell_\alpha} = \frac{dc_\ell}{d\alpha_g} \quad . \tag{28}$$

Use of Equation (9) permits c_{ℓ_α} to be written, for the nonlinear flexible case, as

$$c_{\ell_{\alpha_{F_n}}} = (a + 2b\alpha)\frac{d\alpha}{d\alpha_g} \quad . \tag{29}$$

Likewise, for the nonlinear rigid case

$$c_{\ell_{\alpha_{R_n}}} = a + 2b\alpha_g \tag{30}$$

since in the rigid case $\alpha = \alpha_g$. Use of Equations (29) and (30) give the desired result as

$$\frac{c_{\ell_{\alpha_{F_n}}}}{c_{\ell_{\alpha_{R_n}}}} = \left[\frac{1 + 2\mu\left(\frac{\alpha}{\alpha_g}\right)}{1+2\mu}\right]\left(\frac{d\alpha}{d\alpha_g}\right) \quad . \tag{31}$$

The ratio $\left(\frac{\alpha}{\alpha_g}\right)$ can be obtained by use of Equations (14) and (17). The derivative $\left(\frac{d\alpha}{d\alpha_g}\right)$ is obtained by the use of the same equations and is given by the following expression

$$\frac{d\alpha}{d\alpha_g} = 1 + \frac{4\mu+2}{\left(\frac{q_{D_\ell}}{q} - 2\mu - 1\right) + R^{1/2}} + \frac{4\mu\,(\mu+1)}{\left[\left(\frac{q_{D_\ell}}{q} - 2\mu - 1\right) + R^{1/2}\right]^2} + \frac{4\mu\,(\mu+1)}{R^{1/2}\left[\left(\frac{q_{D_\ell}}{q} - 2\mu - 1\right) + R^{1/2}\right]^2}\left(\frac{q_{D_\ell}}{q}\right) \tag{32}$$

where

$$R^{1/2} = \sqrt{\left(\frac{q_{D_\ell}}{q} - 2\mu - 1 \right)^2 - 4\mu\ (\mu + 1)} \quad . \tag{33}$$

The ratio $c_{l_{\alpha_{F_n}}} / c_{l_{\alpha_{R_n}}}$, as defined by Equations (31) and (32), is shown in Figure 5 as a function of q/q_{D_ℓ} and μ.

SECTION II: METHODS FOR OBTAINING THREE-DIMENSIONAL NONLINEAR STATIC AEROELASTIC SOLUTIONS

Several methods capable of predicting the static aerothermoelastic response of lifting surfaces have been developed. Emphasis has been placed on the formulation of methods which take into account the nonlinear aerodynamic characteristics discussed briefly in the Introduction and in more detail in Reference 6. The discussion in this section is consistent with the assumption that the surface being analyzed is a diverging type surface, i.e., for a given rigid angle of attack distribution the flexible loading on the surface is greater than the rigid loading. Another way of describing a diverging type surface is to say that it possesses a finite divergence dynamic pressure. The methods presented are also directly applicable to nondiverging type surfaces; however, the differentiation between the types of surfaces is necessary in the presentation of the figures.

All of the methods developed are somewhat similar in that they all make use of an iterative process to effect a solution. However, they differ with regard to the particular mathematical representation of the nonlinear lifting pressure-angle of attack relationship that is employed. Of these methods, detailed consideration is given only to the more general method referred to as the "Nonlinear Lifting Pressure Component Method".

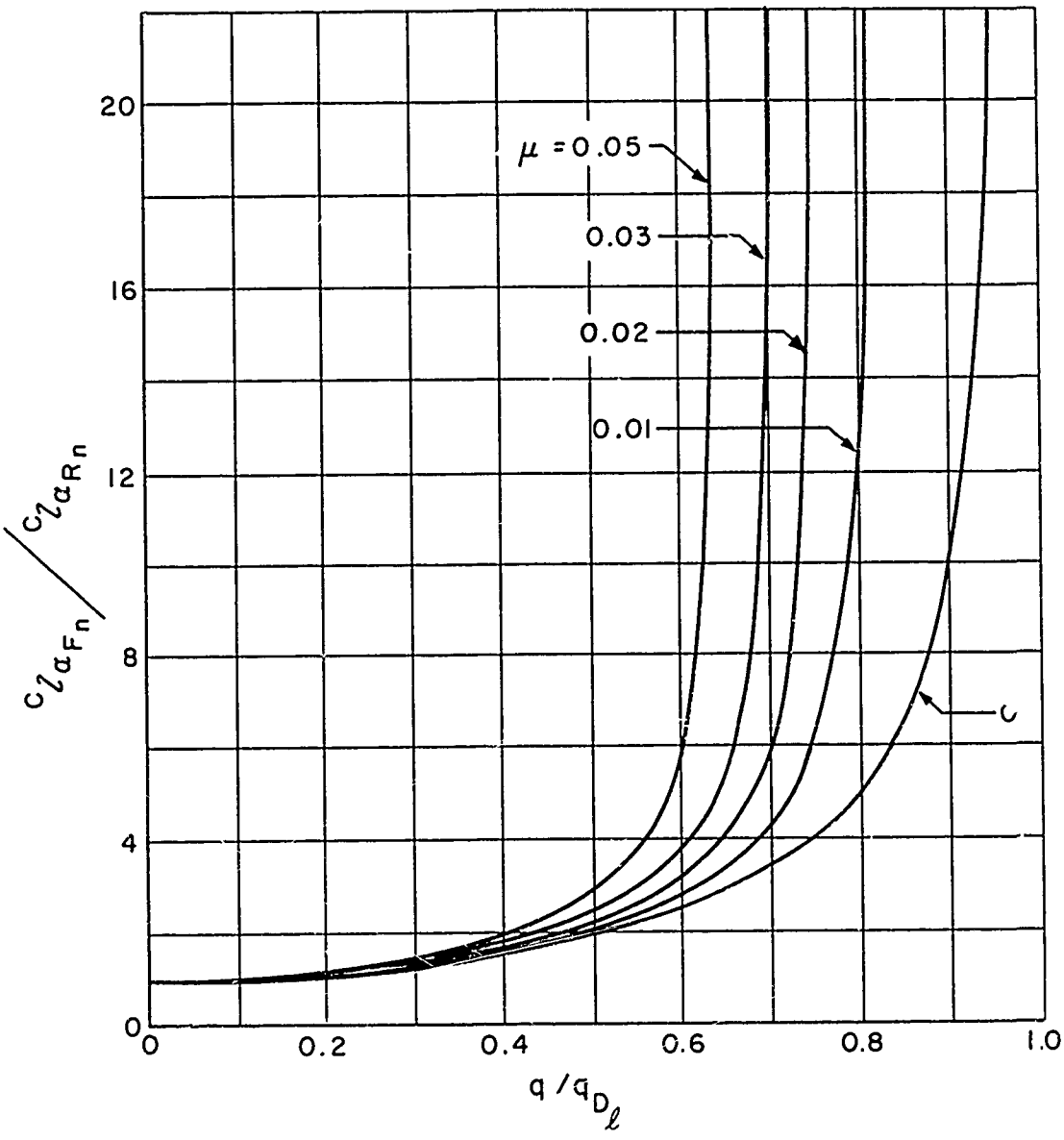


Figure 5. Variation of $\frac{c_{l_{\alpha_{F_n}}}}{c_{l_{\alpha_{R_n}}}}$ with q/q_{D_l} and μ

In this report the comparable hypersonic equations are given as:

Aerodynamic Equation

$$\left\{\frac{\Delta p}{q}\right\} = \left[Q_o\right]\left\{1\right\} + \left[Q_1\right]\left\{\alpha\right\} \tag{38}$$

Structural Deformation Equation

$$\left\{\alpha_s\right\} = q\left[S\right]\left\{\frac{\Delta p}{q}\right\} \tag{39}$$

Angular Equilibrium Equations

$$\left\{\alpha\right\} = \left\{\alpha_s\right\} + \left\{\alpha_g\right\} \tag{40}$$

$$\left\{\alpha_g\right\} = \alpha_{REF}\left\{1\right\} + \alpha_{b_i}\left\{1\right\} + \left\{\alpha_{b_t}\right\} \tag{41}$$

The nomenclature of Equations (38) through (40) will be used in the remainder of this paper since it is more convenient for the formulation and solution of the nonlinear static aeroelastic problem.

In the first linear method, which results in an exact solution and is referred to as the closed form solution, the equilibrium angles of attack are obtained directly by the elimination of $\left\{\alpha_s\right\}$ and $\left\{\frac{\Delta p}{q}\right\}$ from Equations (38) through (40) and solving for $\left\{\alpha\right\}$. The equilibrium angles of attack are, consequently, given by:

$$\left\{\alpha\right\} = \left[\left|1\right| - q\left[S\right]\left[Q_1\right]\right]^{-1}\left\{\left\{\alpha_g\right\} + q\left[S\right]\left[Q_o\right]\left\{1\right\}\right\}. \tag{42}$$

It will be noticed that the determination of $\left\{\alpha\right\}$ from Equation (42) involves the computation of the inverse matrix $\left[1 - q\left[S\right]\left[Q_1\right]\right]^{-1}$. The evaluation of the inverse matrix may be avoided by use of a second method.

A. DISCUSSION OF METHODS OF SOLUTION

1. Linear Methods

Before discussing the Nonlinear Lifting Pressure Component Method for obtaining solutions to the nonlinear static aeroelastic problem, two commonly employed methods (Reference 12) for solving the linear static aeroelastic problem are briefly reviewed.

Considering the case of the wing and control surface being nonindependently flexible and neglecting control surface deflections, the equations which are used in the solution of the linear static aeroelastic problem are given by (in the notation of Reference 12):

Aerodynamic Equation

$$\left\{\left(\frac{\Delta p}{q}\right)_{\alpha}\right\} = \left[Q_{\alpha}\right]\left\{\alpha\right\} \tag{34}$$

Structural Deformation Equation

$$\left\{\alpha_s\right\} = q\left[S_s\right]\left[R_{w-\alpha}\right]\left\{\left(\frac{\Delta p}{q}\right)_{\alpha}\right\} \tag{35}$$

Angular Equilibrium Equations

$$\left\{\alpha\right\} = \left\{\alpha_s\right\} + \left\{\alpha_g\right\} \tag{36}$$

$$\left\{\alpha_g\right\} = \alpha_{REF}\left\{1\right\} + \left\{\alpha_b\right\} \tag{37}$$

In Reference 12, $\left\{\alpha_b\right\}$ is the built-in angle of attack distribution of the rigid lifting surface. As such, it is made up of three parts:

(1) $\left\{\alpha_{b_c}\right\}$ - due to built-in camber

(2) $\left\{\alpha_{b_t}\right\}$ - due to built-in twist

(3) $\alpha_{b_i}\left\{1\right\}$ - due to incidence of the wing reference axis with respect to the aircraft reference axis

The second method gives an approximate solution to Equations (38) through (40) in the form of an infinite matrix power series and is referred to as the series solution (Reference 12). A series solution can be obtained by either expanding the inverse matrix of Equation (42) into a binomial matrix power series or from an iterative (relaxation) process performed using Equations (38) through (40). The latter means of determining the series solution will be demonstrated because it does provide some physical insight into the problem and because it is used in the static nonlinear aeroelastic development to follow. To simplify the derivation, $\{\alpha_s\}$ is first eliminated from Equations (39) and (40) to give the equilibrium angle of attack as a function of the local lifting pressures, thus,

$$\{\alpha\} = q\,[S]\,\left\{\frac{\Delta p}{q}\right\} + \{\alpha_g\} \quad . \tag{43}$$

As an aid in the development and understanding of the series solution and other methods to be discussed later, use will be made of the general graphical representation of Equations (38) and (43), shown in Figure 6, for a single reference point.

The series solution is developed by first considering the lifting surface as being perfectly rigid. From Equation (38) it can be seen that on the rigid surface the lifting pressure is made of two parts: 1) a starting lifting pressure, $[Q_o]\,\{1\}$, 2) a pressure obtained from an operation on the rigid angle of attack, $[Q_1]\,\{\alpha_g\}$. Any iterative or relaxation process should be started with the total initial value of one of the variables. In this case, this could be the total value of the rigid angle of attack distribution, i.e., $\{\alpha_g\}$ plus the angular distribution that causes $[Q_o]\,\{1\}$. Since the angular distribution that produces $[Q_o]\,\{1\}$ is not specified in this formulation of the problem, it becomes necessary to do a first relaxation on $[Q_o]\{1\}$ before arriving at a starting value of $\{\alpha\}$. In the present case, this results in having as a first approximation for $\{\alpha\}$ the following representation:

$$\{\alpha\}_o = \{\bar{\alpha}_g\} = \{\alpha_g\} + q\,[S]\,[Q_o]\,\{1\} \,. \tag{44}$$

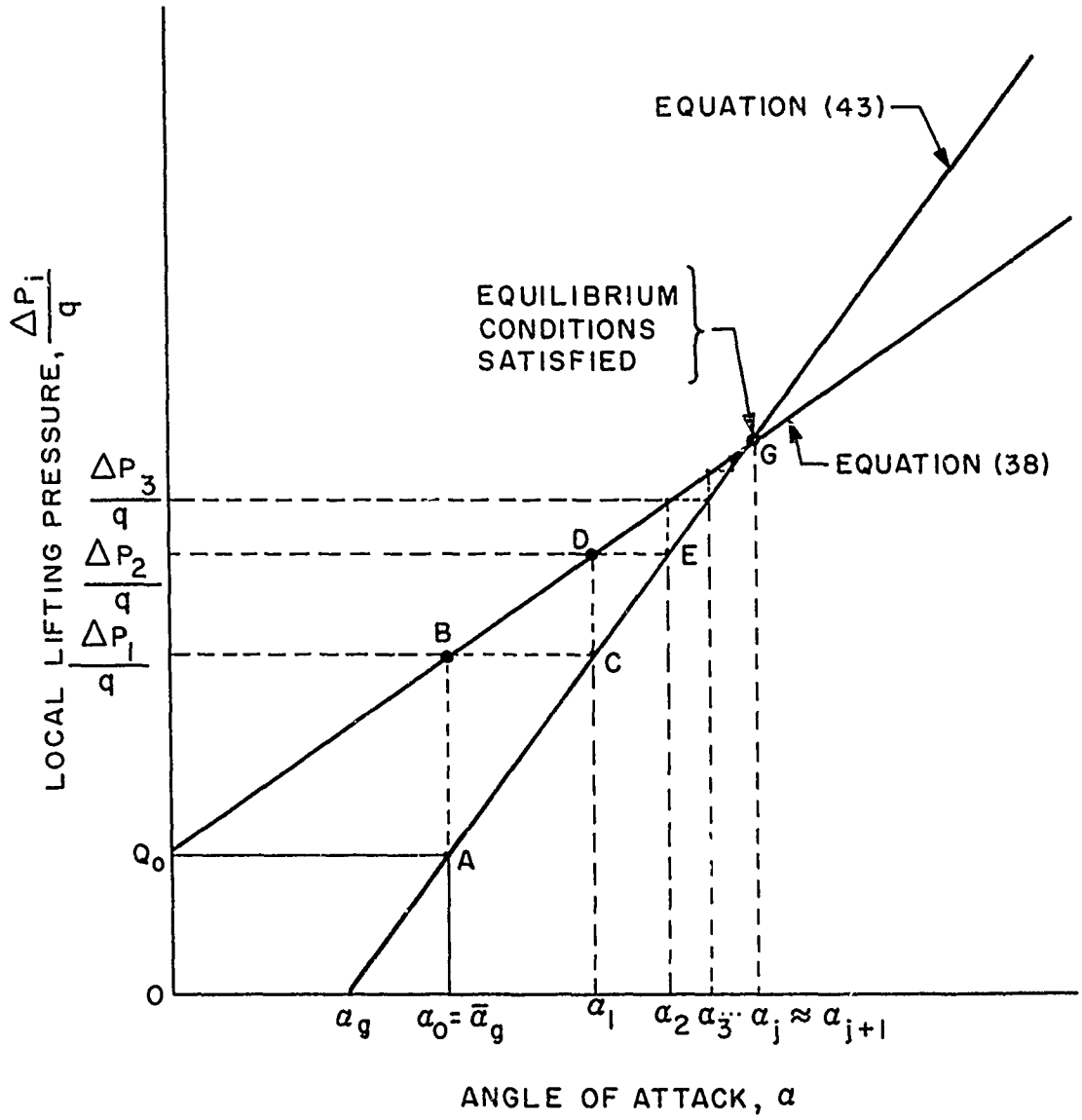


Figure 6. Illustration of Linear Series Solution

Next the first approximation to the lifting pressure indicated by point B in Figure 6 is computed using Equation (38) with $\{\alpha\} = \{\bar{\alpha}_g\}$.

Thus,

$$\left\{\frac{\Delta p}{q}\right\}_1 = \left[Q_0\right]\{1\} + \left[Q_1\right]\left\{\bar{\alpha}_g\right\} \tag{45}$$

Since the structure is actually flexible, the pressures $\left\{\frac{\Delta p}{q}\right\}_1$ will cause the structure to deform (or relax). The new deformed angle of attack $\{\alpha\}_1$ can be computed using Equation (43) with $\left\{\frac{\Delta p}{q}\right\} = \left\{\frac{\Delta p}{q}\right\}_1$. That is

$$\{\alpha\}_1 = q[S]\left\{\left[Q_0\right]\{1\} + \left[Q_1\right]\left\{\bar{\alpha}_g\right\}\right\} + \{\alpha_g\} \tag{46}$$

or

$$\{\alpha\}_1 = \left[[1] + q[S]\left[Q_1\right]\right]\left\{\bar{\alpha}_g\right\} \tag{47}$$

where

$$\left\{\bar{\alpha}_g\right\} = q[S]\left[Q_0\right]\{1\} + \{\alpha_g\}. \tag{48}$$

In the computation of $\{\alpha\}_1$, which is indicated by point C in Figure 6, it was assumed that the pressure $\left\{\frac{\Delta p}{q}\right\}_1$ was constant. However, for a flexible structure an increase in $\{\alpha\}$ will cause an increase in $\left\{\frac{\Delta p}{q}\right\}$, which in turn increases $\{\alpha\}$, etc., until the equilibrium condition is reached. Hence, the next approximation to $\{\alpha\}$ is obtained by repeating the above iterative process as illustrated in Figure 6 by the path ABCDE to point G where the values of $\left\{\frac{\Delta p}{q}\right\}$ and $\{\alpha\}$ satisfy the equilibrium conditions of the problem. The solution obtained after the j th approximation is expressed as

$$\left\{\alpha\right\}_j = \left[\left[1\right] + q\left[S\right]\left[Q_1\right] + q^2\left[\left[S\right]\left[Q_1\right]\right]^2 + \cdots + q^j\left[\left[S\right]\left[Q_1\right]^j\right]\right]\left\{\bar{\alpha}_g\right\}. \quad (49)$$

It should be noted that the binomial series expansion of Equation (42) also yields

$$\left\{\alpha\right\} = \left[\left[1\right] + q\left[S\right]\left[Q_1\right] + q^2\left[\left[S\right]\left[Q_1\right]\right]^2 + q^3\left[\left[S\right]\left[Q_1\right]\right]^3 + \cdots\right]\left\{\bar{\alpha}_g\right\}. \quad (50)$$

2. Application of Linear Series Method of Approach to the Nonlinear Case

The iterative procedure used to obtain a linear series solution can be readily applied to the situation where the aerodynamic lifting pressure angle of attack relationship is nonlinear. The procedure for the determination of a solution to the aerodynamically nonlinear aeroelasticity problem will be indicated with the aid of Figure 7.

As explained in the Introduction, at hypersonic speeds the local lifting pressure at a reference point can be expressed explicitly in terms of the local angle of attack at the same reference point by the relationship

$$\left\{\frac{\Delta p}{q}\right\}_i = F_i\left(\alpha_i\right) \quad (51)$$

where $F_i(\alpha_i)$ represents any function of the local angle of attack. A typical form of Equation (51) is graphically illustrated in Figure 7. In general, $F_i(\alpha_i)$ may be different for each selected reference point. All relationships of the form of Equation (51) can be assembled and written in matrix notation as

$$\left\{\frac{\Delta p}{q}\right\} = \left[F(\alpha)\right]\left\{1\right\} \quad (52)$$

The problem is to solve Equations (43) and (52) for the equilibrium values of $\left\{\alpha\right\}$ and $\left\{\frac{\Delta p}{q}\right\}$. Eliminating $\left\{\frac{\Delta p}{q}\right\}$ from these equations yields

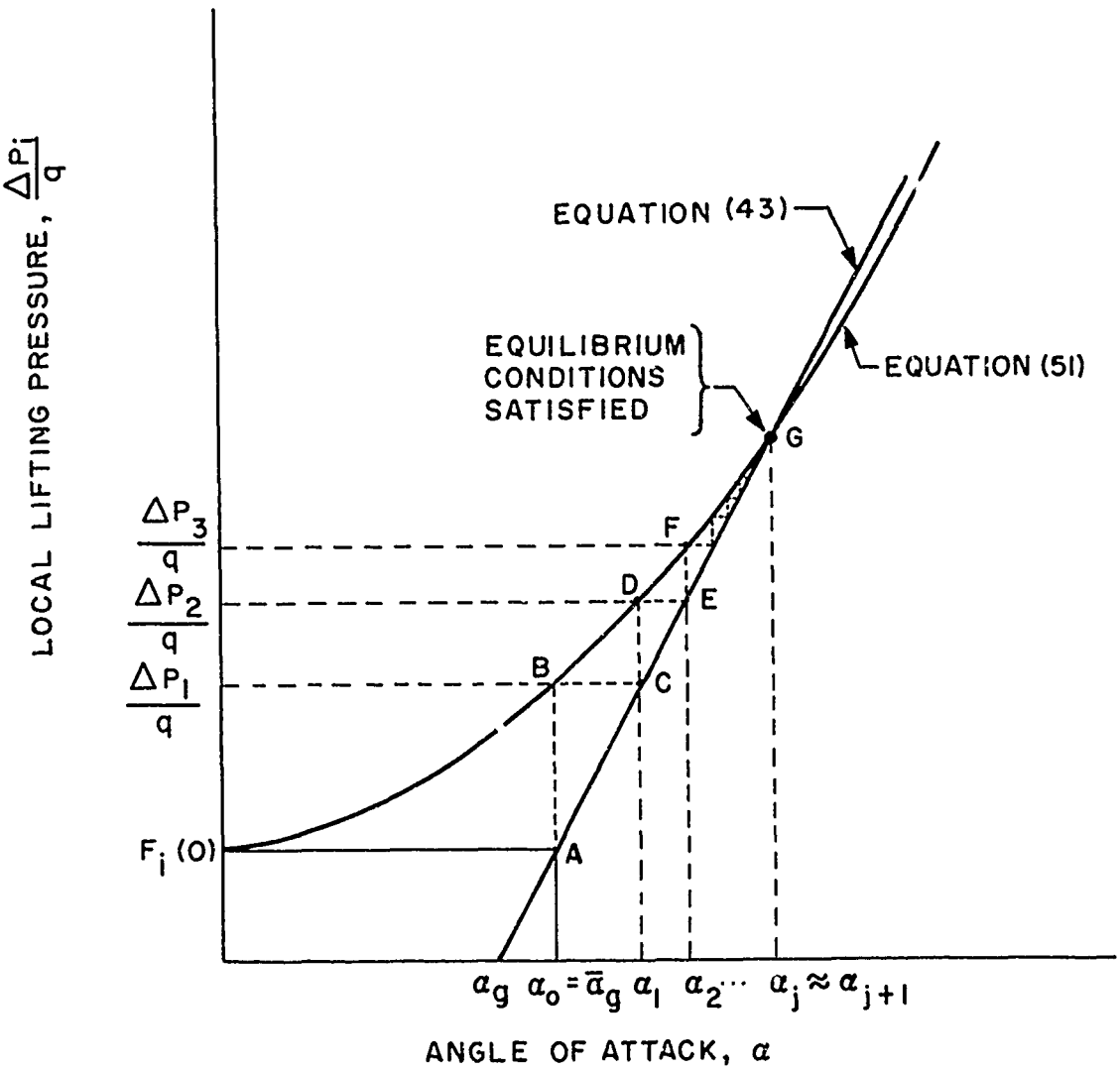


Figure 7. Illustration of Nonlinear Series Solution

$$\left\{\alpha\right\} = q\left[S\right]\left[F(\alpha)\right]\left\{1\right\} + \left\{\alpha_g\right\} \tag{53}$$

Due to the presence of the nonlinear functions of α_i in the aerodynamic matrix $\left[F(\alpha)\right]$, Equation (53) cannot be solved directly by matrix inversion as was done for the linear case (see Equation (42)) to obtain a closed form solution. However, the alternate iterative or series solution method of approach can be used to obtain a solution from Equations (43) and (52) in an identical manner as was done for the linear situation in Section II,A,1. As indicated in Figure 7 by the point G, the correct solution occurs at the point of intersection of the linear structural deformation lifting pressure-angle of attack curve and the nonlinear aerodynamic angle of attack-lifting pressure curve, i.e., when Equations (52) or (51) and (43) are simultaneously satisfied.

In accordance with this iterative method, the following computational steps are performed.

(1) The iterative process is initiated by assuming $\left\{\alpha\right\} = \left\{\alpha\right\}_0 = \left\{\bar{\alpha}_g\right\}$ and computing, using Equation (52), a first approximation to the pressures, i.e.,

$$\left\{\frac{\Delta p}{q}\right\}_1 = \left[F(\alpha_0)\right]_0 \left\{1\right\} \tag{54}$$

This approximation is shown in Figure 7 by point B.

(2) Let $\left\{\frac{\Delta p}{q}\right\} = \left\{\frac{\Delta p}{q}\right\}_1$, and compute, from Equation (43), the next approximation to the angles of attack, i.e.,

$$\left\{\alpha\right\}_1 = q\left[S\right]\left[F(\alpha_0)\right]_0 \left\{1\right\} + \left\{\alpha_g\right\} \tag{55}$$

This approximation is shown in Figure 7 by point C. Physically, this assumption is essentially equivalent

to assuming that the pressures $\left\{\frac{\Delta p}{q}\right\}_1$ are constant and allowing the structure to deform or relax to a new pseudo equilibrium state.

(3) Let $\{\alpha\} = \{\alpha\}_1$, and compute, using Equation (52), the pressures $\left\{\frac{\Delta p}{q}\right\}_2$ which are indicated by point D in Figure 7 thus,

$$\left\{\frac{\Delta p}{q}\right\}_2 = \left[F(\alpha_1)\right]_1 \{1\} \tag{56}$$

This equation is used to compute the next approximation to the angles of attack. If this iterative process is continued until $\{\alpha\}_j = \{\alpha\}_{j+1}$, it is evident that the path DEF to point G will be followed. The successive approximations to the equilibrium angles of attack obtained from this iterative procedure can be summarized as follows

$$\begin{aligned}
\{\alpha\}_0 &= \{\bar{\alpha}_g\} \\
\{\alpha\}_1 &= q[S]\left[F(\alpha_0)\right]_0 \{1\} + \{\alpha_g\} \\
\{\alpha\}_2 &= q[S]\left[F(\alpha_1)\right]_1 \{1\} + \{\alpha_g\} \\
&\vdots \\
\{\alpha\}_j &= q[S]\left[F(\alpha_{j-1})\right]_{j-1} \{1\} + \{\alpha_g\}
\end{aligned} \tag{57}$$

For illustrative purposes let the nonlinear lifting pressure-angle of attack relationship, Equation (52), be of the form

$$\left\{\frac{\Delta p}{q}\right\} = \left[F(\alpha)\right]\left\{1\right\} = \left[Q_0\right]\left\{1\right\} + \left[Q_1\right]\left\{\alpha\right\} + \left[Q_2\right]\left\{\alpha^2\right\}. \quad (58)$$

Then, in accordance with Equation (57), the first three successive approximations to the equilibrium angle of attack are

$$\begin{aligned}
\left\{\alpha\right\}_0 &= \left\{\bar{\alpha}_g\right\} \\
\left\{\alpha\right\}_1 &= \left\{\bar{\alpha}_g\right\} + q\left[S\right]\left[Q_1\right]\left\{\bar{\alpha}_g\right\} + q\left[S\right]\left[Q_2\right]\left\{\bar{\alpha}_g{}^2\right\} \qquad (59) \\
\left\{\alpha\right\}_2 &= \left\{\bar{\alpha}_g\right\} + q\left[S\right]\left[Q_1\right]\left\{\left\{\bar{\alpha}_g\right\} + q\left[S\right]\left[Q_1\right]\left\{\bar{\alpha}_g\right\} + q\left[S\right]\left[Q_2\right]\left[\bar{\alpha}_g\right]\left\{\bar{\alpha}_g\right\}\right\} \\
&\quad + q\left[S\right]\left[Q_2\right]\left[\left[\bar{\alpha}_g\right] + q\left[S\right]\left[Q_1\right]\left[\bar{\alpha}_g\right] + \left[S\right]\left[Q_2\right]\left[\bar{\alpha}_g{}^2\right]\right]\left\{\left\{\bar{\alpha}_g\right\}\right. \\
&\quad \left. + q\left[S\right]\left[Q_1\right]\left\{\bar{\alpha}_g\right\} + q\left[S\right]\left[Q_2\right]\left[\bar{\alpha}_g\right]\left\{\bar{\alpha}_g\right\}\right\}
\end{aligned}$$

It will be noted that for the corresponding linear case, i.e., for $\left[Q_2\right] = \left[0\right]$, the above expressions will reduce to the linear series solution given by Equation (49).

Various additional approaches involving different degrees of complexity can be used to formulate methods capable of obtaining a solution to the aerodynamically nonlinear aeroelasticity problem. However, only one of these methods, which is considered to be sufficiently general and of practical applicability is presented in the following section.

B. DEVELOPMENT OF GENERAL PURPOSE NONLINEAR LIFTING PRESSURE COMPONENT METHOD

1. Representation of Nonlinear Lifting Pressure-Angle of Attack Relationships

The method of solution presented in this section is based on a versatile representation of the nonlinear lifting pressure-angle of attack relationships. The Nonlinear Lifting Pressure Component Method uses the following mathematical representation of the lifting pressure-angle of attack relationship.

$$\frac{\Delta p_i}{q} = F_i(\alpha_i) = \bar{a}_{0_i} + \bar{a}_{1_i}\alpha_i + \frac{\Delta p_{n_i}}{q} \tag{60}$$

where, by definition, the term $\frac{\Delta p_{n_i}}{q}$ is given by

$$\frac{\Delta p_{n_i}}{q} \equiv F_i(\alpha_i) - \bar{a}_{0_i} - \bar{a}_{1_i}\alpha_i \quad . \tag{61}$$

If an α_i is factored from the last two terms on the right hand side of Equation (60), the lifting pressure-angle of attack relationship at a reference point, i, is represented by the following form

$$\frac{\Delta p_i}{q} = \bar{a}_{0_i} + \left(\bar{a}_{1_i} + \frac{\Delta p_{n_i}}{q\alpha_i}\right)\alpha_i \quad . \tag{62}$$

If the expression $\frac{\Delta p_{n_i}}{q\alpha_i}$ is considered to be independent of α_i, then the slope of the lifting pressure-angle of attack relationship given by Equation (62) can be considered as composed of the sum of two parts,one of which is a linear slope, $\bar{a}_{1_i}$, and the other a nonlinear secant slope, $\frac{\Delta p_{n_i}}{q\alpha_i}$.

For a lifting surface containing N reference points, the set of lifting pressure-angle of attack relationships can be represented in matrix form as

$$\left\{ \frac{\Delta p}{q} \right\} = \left[\bar{Q}_o\right]\{1\} + \left[\left[\bar{Q}_1\right] + \left[\frac{\Delta p_n}{q\alpha}\right]\right]\{\alpha\} \tag{63}$$

Equation (63) will now be combined with Equation (43) in order to obtain a solution for the equilibrium angle of attack. Eliminating $\left\{\frac{\Delta p}{q}\right\}$ from Equations (43) and (63) results in the expression

$$\{\alpha\} = q[S]\left[\left[\bar{Q}_1\right] + \left[\frac{\Delta p_n}{q\alpha}\right]\right]\{\alpha\} + q[S]\left[\bar{Q}_o\right]\{1\} + \{\alpha_g\} \cdot \tag{64}$$

Rearranging Equation (64) into the following form

$$\left[\left[1\right] - q[S]\left[\bar{Q}_1\right] - q[S]\left[\frac{\Delta p_n}{q\alpha}\right]\right]\{\alpha\} = \{\alpha_g\} + q[S]\left[\bar{Q}_o\right]\{1\} \tag{65}$$

and factoring out the matrix expression $\left[\left[1\right] - q[S]\left[\bar{Q}_1\right]\right] = [M]^{-1}$ from the left hand side of Equation (65) results in

$$[M]^{-1}\left[\left[1\right] - [M]\, q\,[S]\left[\frac{\Delta p_n}{q\alpha}\right]\right]\{\alpha\} = \{\bar{\alpha}_g\} \tag{66}$$

or

$$\left[\left[1\right] - [M]\; q[S]\left[\frac{\Delta p_n}{q\alpha}\right]\right]\{\alpha\} = [M]\{\bar{\alpha}_g\} \tag{67}$$

For convenience, let the expression which contains the nonlinear secant slope term be defined as

$$[\Delta] = q[M][S]\left[\frac{\Delta p_n}{q\alpha}\right] \tag{68}$$

and also let

$$\{\alpha_o\} = [M]\{\bar{\alpha}_g\} \tag{69}$$

Equation (67) can now be written as

$$\left[\left[1\right] - [\Delta]\right]\{\alpha\} = [M]\{\bar{\alpha}_g\} \tag{70}$$

Solving Equation (70) for $\{\alpha\}$, while considering $[\Delta]$ to be independent of $\{\alpha\}$, results in

$$\{\alpha\} = \left[[I] - [\Delta]\right]^{-1} [M] \{\bar{\alpha}_g\} \tag{71}$$

A solution for $\{\alpha\}$ can be obtained from Equation (71) by an iterative process. However, each iteration requires computing the inverse $\left[[I] - [\Delta]\right]^{-1}$. This can be avoided by expanding the inverse matrix $\left[[I] - [\Delta]\right]^{-1}$ into a matrix power series. Doing this, Equation (71) reduces to

$$\{\alpha\} = \left[[I] + [\Delta] + [\Delta]^2 + [\Delta]^3 + \cdots\right] [M] \{\bar{\alpha}_g\} + \{R\} \tag{72}$$

where the matrix $\{R\}$ is a remainder term. It should be noted that a solution can be obtained from Equation (72) by assuming $\{R\} = \{0\}$ and iterating the remaining expression.* However, the remaining truncated expression will be an approximate representation of equilibrium conditions and hence better convergence characteristics and more accurate results would be obtained if the remainder term were included. The remainder term will now be determined.

Equation (70) can be rearranged into the following form

$$\{\alpha\} = [M] \{\bar{\alpha}_g\} + [\Delta] \{\alpha\} \tag{73}$$

---

*It should be noted that for the matrix power series given by Equation (72) to converge, the absolute value of the largest eigenvalue of $[\Delta]$ must be less than one. (See Reference 12, p 317.)

A comparison of Equations (72) and (73) reveals that the term $[M]\{\bar{\alpha}_g\}$ in Equation (73) represents the first term in the series expansion of Equation (75) and the term $[\Delta]\{\alpha\}$ equals the remainder term $\{R\}$ after the first term in the series. The expression for the remainder term $\{R\}$ after the first two terms in the series can be obtained as follows: Premultiply Equation (70) by $[[I] + [\Delta]]$, thus

$$[[I] + [\Delta]][[I] - [\Delta]]\{\alpha\} = [[I] + [\Delta]][M]\{\bar{\alpha}_g\} = [[I] + [\Delta]]\{\alpha_o\} \quad (74)$$

or

$$[[I] - [\Delta]^2]\{\alpha\} = [[I] + [\Delta]]\{\alpha_o\} \quad (75)$$

and, upon rearranging Equation (75),

$$\{\alpha\} = [[I] + [\Delta]]\{\alpha_o\} + [\Delta]^2\{\alpha\} \quad (76)$$

where the term $[\Delta]^2\{\alpha\}$ equals the remainder term $\{R\}$ in Equation (72) if the first two terms in the series were only used.

If Equation (70) is premultiplied by $[[I] + [\Delta] + [\Delta]^2]$, the following equation is obtained

$$[[I] + [\Delta] + [\Delta]^2][[I] - [\Delta]]\{\alpha\} = [[I] + [\Delta] + [\Delta]^2]\{\alpha_o\} \quad (77)$$

or

$$[[I] - [\Delta]^3]\{\alpha\} = [[I] + [\Delta] + [\Delta]^2]\{\alpha_o\} \quad (78)$$

and, finally

$$\{\alpha\} = [[I] + [\Delta] + [\Delta]^2]\{\alpha_o\} + [\Delta]^3\{\alpha\} \quad (79)$$

where the term $[\Delta]^{\cdot} \{\alpha\}$ equals the remainder after the first three terms in the series. The continuation of the above process will produce equilibrium relations which include additional terms in the series given by Equation (72). All the equilibrium relationships are now summarized starting with Equation (73).

$$\{\alpha\}^{(1)} = \{\alpha_0\} + [\Delta]\{\alpha\}$$

$$\{\alpha\}^{(2)} = \left[[1] + [\Delta]\right]\{\alpha_0\} + [\Delta]^2\{\alpha\}$$

$$\{\alpha\}^{(3)} = \left[[1] + [\Delta] + [\Delta]^2\right]\{\alpha_0\} + [\Delta]^3\{\alpha\} \qquad (80)$$

$$\vdots \qquad \vdots \qquad \vdots$$

$$\{\alpha\}^{(k)} = \left[[1] + [\Delta] + [\Delta]^2 + \cdots + [\Delta]^{k-1}\right]\{\alpha_0\} + [\Delta]^k\{\alpha\}$$

$$\text{or} \quad \{\alpha\}^{(k)} = \left[\sum_{r=0}^{k-1} [\Delta]^r\right]\{\alpha_0\} + [\Delta]^k\{\alpha\} \quad . \qquad (81)$$

where the superscript (k) denotes a specific equilibrium relationship.

It should be emphasized that each relation of the form of Equation (81) is an exact representation of equilibrium conditions as defined by Equations (39), (40) and (63). Consequently, a solution may be obtained using any one of Equations (81) in accordance with an iterative process. With regard to Equations (81), the iterative process is initiated by setting $[\Delta] = [0]$, which essentially linearizes Equations (81) (i.e. $\left[\frac{\Delta p_n}{q}\right] = [0]$).

As an illustration of the manner in which any one of Equations (81) effect a solution, the computational step by step results obtained by use of Equation (76), for which $k = 2$, will be explained with the aid of Figure 8.

(1) The initial approximation is obtained, as stated above, by setting $[\Delta] = [0]$ in Equation (76). This results in

$$\{\alpha\}_0 = [M]\{\bar{\alpha}_g\} \tag{82}$$

The linearized approximation is shown by point A in Figure 8.

(2) The next approximation is obtained by first evaluating $[\Delta(\alpha_0)]$ by setting $\{\alpha\} = \{\alpha\}_0$ in Equation (68). Then the next approximation is obtained from Equation (76) and results in

$$\{\alpha\}_1 = \left[[I] + [\Delta(\alpha_0)]_1\right]\{\alpha\}_0 + [\Delta(\alpha_0)]_1^2\{\alpha\}_0 \tag{83}$$

and is shown as point E in Figure 8. It will be noticed that the path followed in this single computation is BCDE.

(3) By setting $\{\alpha\} = \{\alpha\}_1$, determining $[\Delta(\alpha_1)]_2$ from Equation (68) and letting $[\Delta] = [\Delta(\alpha_1)]_2$ in Equation (76) the next approximation is obtained as

$$\{\alpha\}_2 = \left[[I] + [\Delta(\alpha_1)]_2\right]\{\alpha\}_0 + [\Delta(\alpha_1)]_2^2\{\alpha\}_1 \tag{84}$$

This approximation is illustrated by point G in Figure 8.

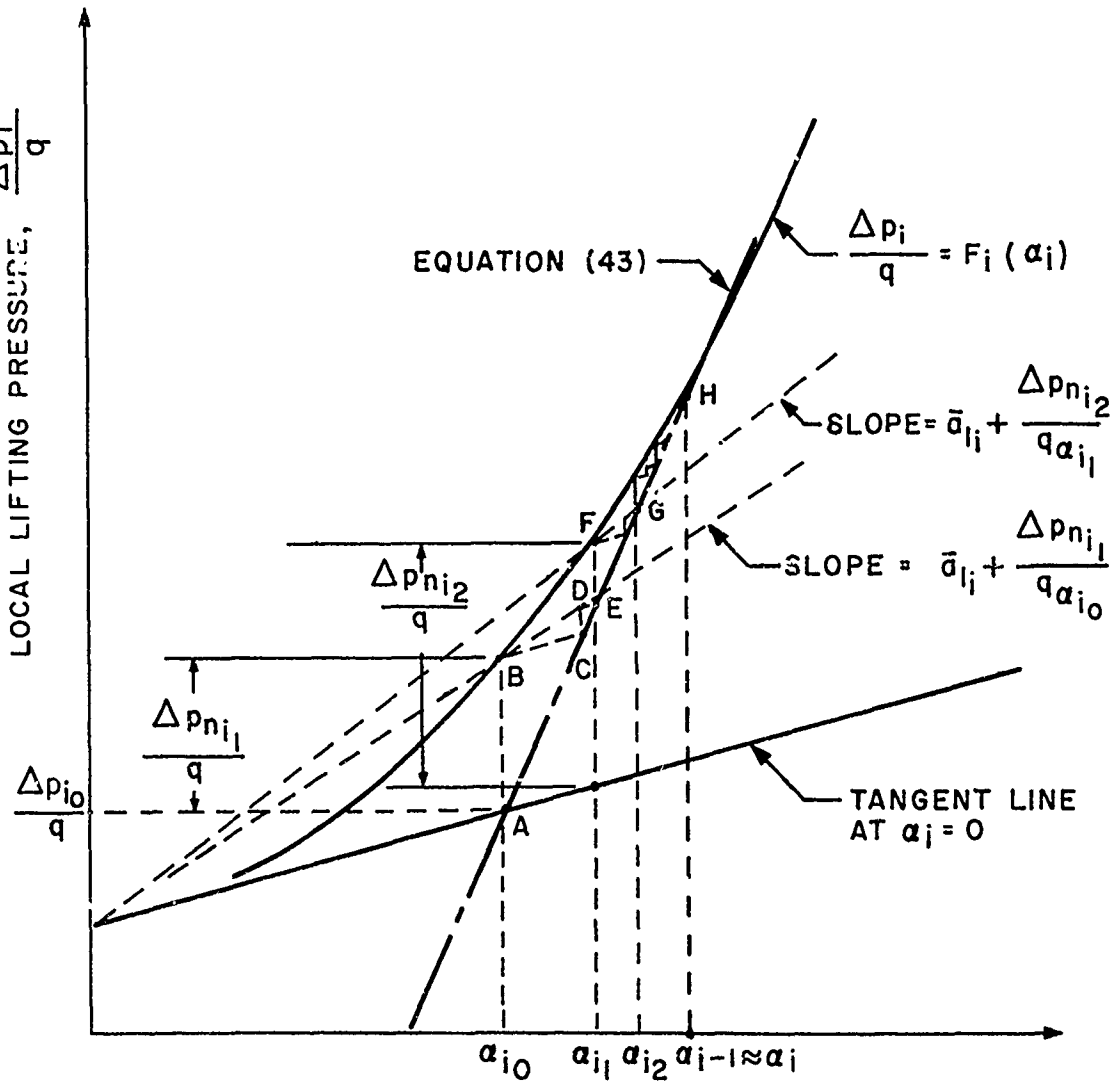


Figure 8. Illustration of Extended Nonlinear Lifting Pressure Component Solution, k = 2

Continuation of these computational steps will result in an approximate solution as indicated, in Figure 8, by point H, which satisfies the condition $\{\alpha\}_{j-1} = \{\alpha\}_j$. The computational steps performed in accordance with this method can be summarized, for the general case, as follows:

$$\{\alpha\}_0 = [M]\{\bar{\alpha}_g\}$$

$$\{\alpha\}_1 = \left[\sum_{r=0}^{k-1} [\Delta(\alpha_0)]_1^r\right]\{\alpha\}_0 + [\Delta(\alpha_0)]_1^k \{\alpha\}_0 \qquad (85)$$

$$\{\alpha\}_2 = \left[\sum_{r=0}^{k-1} [\Delta(\alpha_1)]_2^r\right]\{\alpha\}_0 + [\Delta(\alpha_1)]_2^k \{\alpha\}_1$$

$$\vdots \qquad \vdots \qquad \vdots$$

$$\{\alpha\}_j = \left[\sum_{r=0}^{k-1} [\Delta(\alpha_{j-1})]_j^r\right]\{\alpha\}_0 + [\Delta(\alpha_{j-1})]_j^k \{\alpha\}_{j-1}$$

SECTION III: THE EFFECT OF AERODYNAMIC NONLINEARITIES ON FLEXIBLE HYPERSONIC STABILITY AND CONTROL DERIVATIVES

Methods for determining the effects of flexibility on stability and control derivatives for the case of both linear aerodynamic and structural inputs have been presented in detail in Reference 12. This section of the present paper deals with the effects of nonlinear aerodynamic inputs (while still retaining the linear structural inputs) on the flexible derivatives. As was done in Reference 12, expressions for the

flexible to rigid ratios of the derivatives of interest have been developed. The reader is referred to References 15, 16 and 17 for comprehensive discussions of such derivatives as associated with the rigid aircraft.

It should be recognized that the derivatives are obtained basically in the same manner as was done for the linear case in Reference 12. That is, for a given set of rigid input angles, the flexible and rigid nondimensional lifting pressures are obtained, these $\left(\frac{\Delta p}{q}\right)$ distributions are integrated to give nondimensional span loadings, and these γ distributions in turn are integrated to give either lift or moment coefficients; finally, these coefficients are then differentiated with respect to the variables of interest to yield expressions for the desired stability derivatives.

In the discussion that follows only the case of a diverging type surface is considered, i.e., where $C_{L_F} \geq C_{L_R}$. It will be obvious to the reader that the developed techniques and procedures can also be readily used for a nondiverging type surface. In addition, only the expression for the flexible to rigid ratio of C_{L_α} for the main lifting surface (wing) of a flight vehicle is derived. The necessary approach to determine other pertinent stability and control derivative ratios should be obvious from the C_{L_α} development.

A. C_{L_α} (WING)

C_{L_α} is defined as the slope of the wing C_L vs α_{REF} curve. The lift coefficient, resulting from lift on the wing due to angle of attack, is, of course, given by

$$C_L = \int_0^{1.0} \gamma \, d y^* \tag{86}$$

where

$$y^* = \frac{y}{(b/2)} \tag{87}$$

or, in matrix form, as

$$C_L = \lfloor I \rfloor \{\gamma\} \tag{88}$$

where $\gamma = \frac{cc_l}{\bar{c}}$ is the nondimensional span loading on the surface. Thus, the equations for the flexible and rigid C_L's are given respectively by

$$C_{L_F} = \lfloor I \rfloor \{\gamma\}_F \tag{89}$$

$$C_{L_R} = \lfloor I \rfloor \{\gamma\}_R \tag{90}$$

The span loadings are obtained by integrating the lifting pressure distributions in the chordwise direction, i.e., for a given spanwise station,

$$\gamma = \frac{c}{\bar{c}} \int_0^{1.0} \left(\frac{\Delta p}{q}\right) dx^* \tag{91}$$

where

$$x^* = \frac{x_{t.e.} - x_{\ell.e.}}{c} \tag{92}$$

or for all the stations, in matrix form, as

$$\{\gamma\} = \left\lfloor \frac{c}{\bar{c}} \right\rceil [I] \left\{\frac{\Delta p}{q}\right\}^* \tag{93}$$

For the flexible and rigid cases, Equation (93) becomes

$$\{\gamma\}_F = \left\lfloor \frac{c}{\bar{c}} \right\rceil [I] \left\{\frac{\Delta p}{q}\right\}_F \tag{94}$$

---

*The reader is referred to Reference 12 for discussions of integrating matrices such as $\lfloor I \rfloor$ and $[I]$ and their use in integrating pressures and span loadings.

$$\{\gamma\}_R = \left[\frac{c}{\bar{c}}\right] [I] \left\{\frac{\Delta p}{q}\right\}_R . \tag{95}$$

In order to make the development of the expressions for C_{L_α} more definitized, a specified mathematical type of relationship between $\frac{\Delta p}{q}$ and α will be assumed in the discussion that follows. This does not detract at all from the generality of the approach to be shown, but does help to clarify the steps of the procedure. The relationship used is

$$\left\{\frac{\Delta p}{q}\right\}_F = [Q_0] \{1\} + [Q_1] \{\alpha\} + [Q_2] \{\alpha^2\} \tag{96}$$

$$\left\{\frac{\Delta p}{q}\right\}_R = [Q_0] \{1\} + [Q_1] \{\alpha_g\} + [Q_2] \{\alpha_g^2\} \ * \tag{97}$$

Combining Equations (89), (94), (96) and (90), (95), (97) results in

$$C_{L_F} = [I] \left[\frac{c}{\bar{c}}\right] [I] \left\{[Q_0] \{1\} + [Q_1] \{\alpha\} + [Q_2] \{\alpha^2\}\right\} \tag{98}$$

$$C_{L_R} = [I] \left[\frac{c}{\bar{c}}\right] [I] \left\{[Q_0] \{1\} + [Q_1] \{\alpha_g\} + [Q_2] \{\alpha_g^2\}\right\} \tag{99}$$

$\{\alpha_g\}$ is defined as

$$[\alpha_g] = \alpha_{REF} [1] + \alpha_{b_i} [1] + [\alpha_{b_f}] \tag{100}$$

---

*It should be realized that for the particular nonlinear case being considered here, as well as for the general nonlinear case, the lifting pressures (and C_{L_α}) are a function of other angles besides $\{\alpha_g\}$, e.g., control surface deflection angle, damping in roll angle, sideslip angle, etc. However, in the development for C_{L_α} being presented, only the case of $\{\alpha_g\}$ as input will be considered.

or

$$\{\alpha_g\} = \alpha_{REF}\{1\} + \alpha_{b_i}\{1\} + \{\alpha_{b_t}\} \tag{101}$$

It should be noted, since α_{b_i} and $\{\alpha_{b_t}\}$ are not functions of α_{REF}, that

$$\left\lfloor \frac{\partial \alpha_g}{\partial \alpha_{REF}} \right\rfloor = \lfloor 1 \rfloor \quad \text{OR} \quad \left\{ \frac{\partial \alpha}{\partial \alpha_{REF}} \right\} = \{1\}. \tag{102}$$

Referring to Equations (98) and (99), and realizing that

$$C_{L_\alpha} = \frac{\partial C_L}{\partial \alpha_{REF}} \tag{103}$$

the flexible and rigid expressions for C_{L_α} may be obtained by differentiating these equations with respect to α_{REF}, i.e.,

$$C_{L_{\alpha_F}} = \lfloor I \rfloor \left\lfloor \frac{c}{\bar{c}} \right\rfloor [I] \left\{ \lfloor Q_1 \rfloor \left\{ \frac{\partial \alpha}{\partial \alpha_{REF}} \right\} + 2 \lfloor Q_2 \rfloor \lfloor \alpha \rfloor \left\{ \frac{\partial \alpha}{\partial \alpha_{REF}} \right\} \right\} \tag{104}$$

$$C_{L_{\alpha_R}} = \lfloor I \rfloor \left\lfloor \frac{c}{\bar{c}} \right\rfloor [I] \left\{ \lfloor Q_1 \rfloor \{1\} + 2 \lfloor Q_2 \rfloor \{\alpha_g\} \right\}. \tag{105}$$

It should be recognized that in writing the expression for $C_{L_{\alpha_R}}$, advantage has been taken of the relation given by Equation (102) to eliminate $\left\{ \frac{\partial \alpha_g}{\partial \alpha_{REF}} \right\}$ from the equation. The flexible to rigid ratio of the lift curve slopes is then, of course, given by

$$\left(\frac{C_{L_{\alpha_F}}}{C_{L_{\alpha_R}}} \right)_n = \frac{\lfloor I \rfloor \left\lfloor \frac{c}{\bar{c}} \right\rfloor [I] \left[\lfloor Q_1 \rfloor + 2 \lfloor Q_2 \rfloor \lfloor \alpha \rfloor \right] \left\{ \frac{\partial \alpha}{\partial \alpha_{REF}} \right\}}{\lfloor I \rfloor \left\lfloor \frac{c}{\bar{c}} \right\rfloor [I] \left\{ \lfloor Q_1 \rfloor \{1\} + 2 \lfloor Q_2 \rfloor \{\alpha_g\} \right\}} \tag{106}$$

where the subscript, n , has been added to designate "nonlinear". Methods for obtaining the solutions for the equilibrium angle of attack distribution $\{\alpha\}$ have, of course, been presented in Section II. The distributions of $\left\{\frac{\partial \alpha}{\partial \alpha_{REF}}\right\}$ are obtained simply by graphically or numerically differentiating $\{\alpha\}$ with respect to α_{REF} , i.e., for the given Mach number and q of interest, this just involves running a number of solutions for $\{\alpha\}$ with different values of α_{REF} as inputs, and then using such data to obtain $\frac{\partial \alpha}{\partial \alpha_{REF}}$ for all the reference points at the desired values of α_{REF} .

As might be expected, the expressions for both the flexible and rigid C_{L_α}'s , as well as their ratio, are functions of $\{\alpha_g\}$; $C_{L_{\alpha_R}}$ is an explicit function of $\{\alpha_g\}$ while $C_{L_{\alpha_F}}$ is an implicit function of $\{\alpha_g\}$ since $[\alpha]$ and $\left\{\frac{\partial \alpha}{\partial \alpha_{REF}}\right\}$ are both functions of $\{\alpha_g\}$. It is of interest to obtain the corresponding expressions for the flexible to rigid ratio of C_{L_α} for the linear case (by setting $[Q_2] = [0]$ in Equation (106))

$$\left(\frac{C_{L_{\alpha_F}}}{C_{L_{\alpha_R}}}\right)_{\ell} = \frac{[I]\left[\frac{c}{\bar{c}}\right][I][Q_1]\left\{\frac{\partial \alpha}{\partial \alpha_{REF}}\right\}}{[I]\left[\frac{c}{\bar{c}}\right][I][Q_1]\{1\}} . \tag{107}$$

Using the notation of Section II, the linear expression for $\{\alpha\}$ is given by

$$\{\alpha\} = \left[[1] - q[S][Q_1]\right]^{-1}\{\alpha_g\} \tag{108}$$

and, since $\left\{\frac{\partial \alpha_g}{\partial \alpha_{REF}}\right\} = \{1\}$,

$$\left\{\frac{\partial \alpha}{\partial \alpha_{REF}}\right\} = \left[[1] - q[S][Q_1]\right]^{-1}\{1\} . \tag{109}$$

Hence, Equation (107) may be rewritten as

$$\left(\frac{C_{L_{\alpha_F}}}{C_{L_{\alpha_R}}}\right)_{\ell} = \frac{\left[I\right]\left[\frac{c}{\bar{c}}\right]\left[I\right]\left[Q_I\right]\left[\left[I\right]-q\left[S\right]\left[Q_I\right]\right]^{-1}\left\{I\right\}}{\left[I\right]\left[\frac{c}{\bar{c}}\right]\left[I\right]\left[Q_I\right]\left\{I\right\}} \quad * \qquad (110)$$

While it is not obvious from examination of Equation (107) that the linear expression for the C_{L_α} ratio is independent of $\{\alpha_g\}$, this fact becomes quite evident from inspection of the alternate linear formulation as given by Equation (110).

It is of some interest to consider the special case of $\alpha_{b_i}\{1\} = \{\alpha_{b_f}\} = \{0\}$, i.e., $\{\alpha_g\} = \alpha_{REF}\{1\}$. For this case it can be shown for $\alpha_{REF} = 0$, that $\{\alpha\} = \{0\}$ but $\left\{\frac{\partial \alpha}{\partial \alpha_{REF}}\right\} = \left[\left[I\right]-q\left[S\right]\left[Q_I\right]\right]^{-1}\{1\}$. Hence, the expression for the nonlinear flexible to rigid ratio of the lift curve slope, as given by Equation (106), reduces to

$$\left(\frac{C_{L_{\alpha_F}}}{C_{L_{\alpha_R}}}\right)_n = \frac{\left[I\right]\left[\frac{c}{\bar{c}}\right]\left[I\right]\left[Q_I\right]\left[\left[I\right]-q\left[S\right]\left[Q_I\right]\right]^{-1}\left\{I\right\}}{\left[I\right]\left[\frac{c}{\bar{c}}\right]\left[I\right]\left[Q_I\right]\left\{I\right\}}, \{\alpha_g\} = \{0\}$$

which, when compared with Equation (110), is seen to be identical to the expression for the linear flexible to rigid ratio of C_{L_α}. A typical plot of $\left(\frac{C_{L_{\alpha_F}}}{C_{L_{\alpha_R}}}\right)$ vs α_{REF} (with $\{\alpha_g\} = \alpha_{REF}\{1\}$) for constant Mach number and altitude is presented in Figure 9; both the linear and nonlinear curves are shown.

---

*This is also the form of the C_{L_α} ratio for the linear case as given on Page 289 of Reference 12.

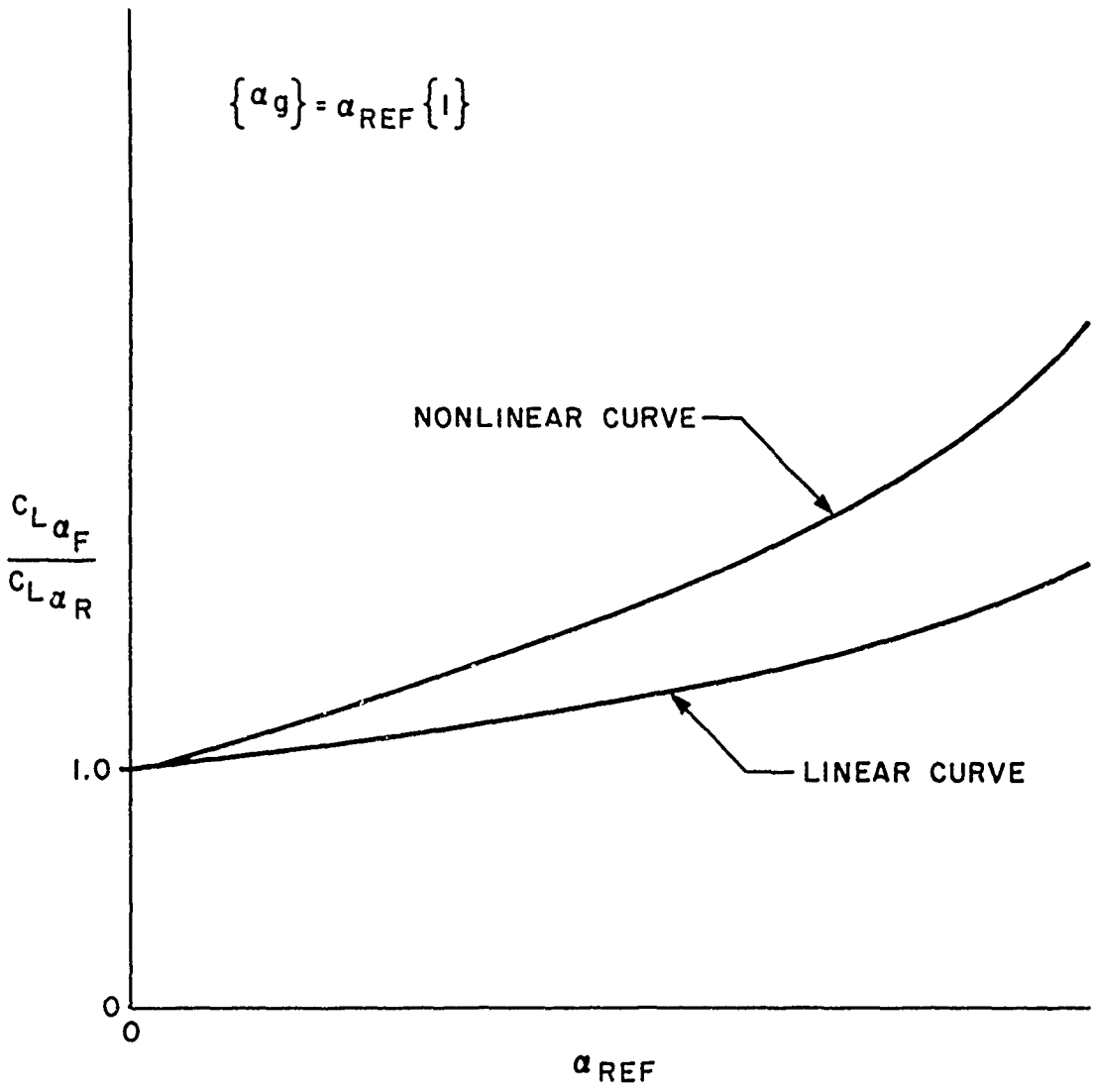


Figure 9. Typical Graph of Flexible to Rigid Ratio of Lift Curve Slopes vs α_{REF} for a Diverging Type Surface (Constant Mach Number and Altitude)

For the general nonlinear case $\left(\frac{C_{L_{\alpha_F}}}{C_{L_{\alpha_R}}}\right)$ is a function, not only of Mach number and altitude (through q), as was true of the linear case, but also α_{REF}. Having three sets of variables rather than two to contend with, it is almost mandatory that carpet graphs be used to present the aeroelastic results applicable to a flexible flight vehicle. Perhaps the best method of presentation of such results is to plot a separate carpet graph for each Mach number considered, and on each graph use α_{REF} and altitude (h) as the two variables. A typical graph of this type is shown in Figure 10 for a clipped delta wing having a 45-degree swept leading edge at a free stream Mach number of 8. This carpet indicates the increased severity of the nonlinear effects on the wing lift curve slope as the rigid angle of attack is increased and the altitude is decreased.

Now that adequate numerical methods have been developed to handle the introduction of nonlinear aerodynamics in the aerothermoelastic stability and control picture, future required work in this field entails the inclusion of nonlinear structural inputs due to large deflections, along with the nonlinear aerodynamic inputs, in the formulation of the static aeroelastic problem, and the development of methods for the solution of the increasingly complex resultant equations for the flexible stability derivatives of interest.

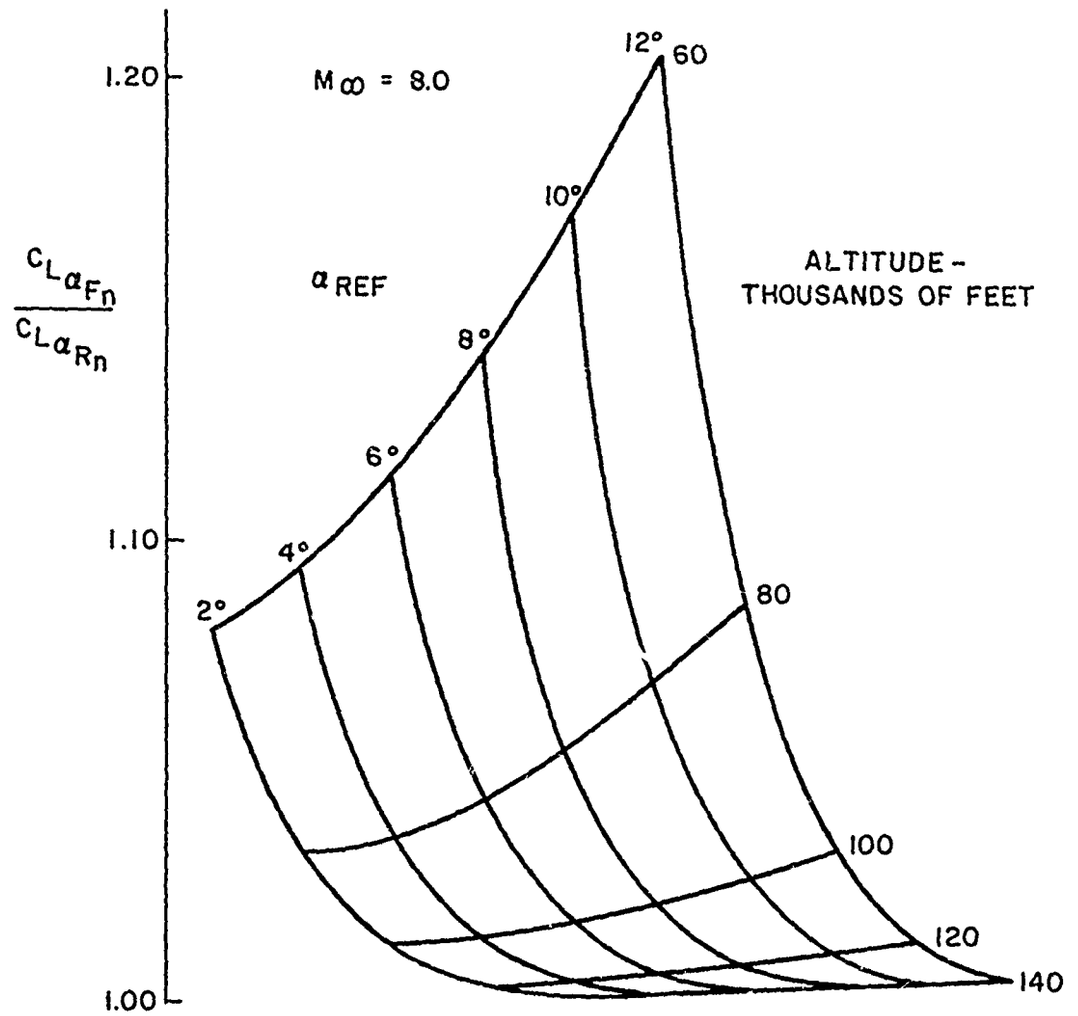


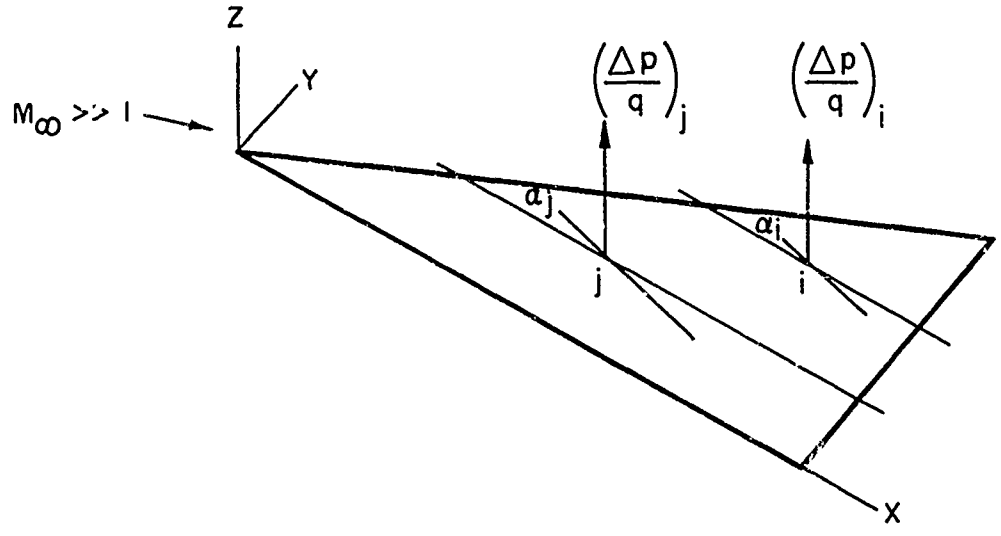
Figure 10. Results of Sample Problem Carpet Graph of $\left(\frac{C_{L\alpha_F}}{C_{L\alpha_R}}\right)_n$ vs α_{REF} and Altitude, $M\infty$ = 8.0

APPENDIX

HYPERSONIC AERODYNAMIC INFLUENCE COEFFICIENT MATRICES

The concept of an aerodynamic influence coefficient, or an array of such coefficients, which is called an aerodynamic influence coefficient matrix, has been previously discussed in Reference 2. In that reference an aerodynamic influence coefficient was defined, for a swept wing in supersonic flow, as "that quantity which relates the aerodynamic span load at a particular spanwise station to the angle of attack at another, or the same, spanwise station". This definition is based on a physical model in which each chord of the wing is at a constant angle of attack, that is, there are no local variations of angle of attack in the chordwise direction. This concept was labeled the line approach. Consideration of local variations of angle of attack in the chordwise direction leads to the field approach. In this approach a field aerodynamic influence coefficient is defined as "that quantity which relates the local aerodynamic lifting pressure at a particular reference point to the local angle of attack at another, or the same, reference point." Methods for generating aerodynamic influence coefficient matrices for these two approaches were developed in References 2 and 3. The concept of an aerodynamic influence coefficient in hypersonic flow will now be introduced.

Consider the half-span swept wing shown in the sketch below with the hypersonic "pressure loadings" $\left(\frac{\Delta p}{q}\right)_i$ and $\left(\frac{\Delta p}{q}\right)_j$ at points i and j, respectively. It has been demonstrated in Reference 6 that the lifting pressure at point i is a function of the angle of attack at point i only and not at j as well. Likewise, $\left(\frac{\Delta p}{q}\right)_j$ is a function of α_j only. In this manner the "influence" of α_j upon the $\left(\frac{\Delta p}{q}\right)_i$ does not exist. Also, α_i does not affect $\left(\frac{\Delta p}{q}\right)_j$. Therefore, one only needs to consider the basic relationship between $\left(\frac{\Delta p}{q}\right)_i$ and α_i in order to determine the desired aerodynamic influence coefficients. Aerodynamic



influence coefficients in the hypersonic case are defined as, "those quantities which relate the aerodynamic load (or pressure) at a particular point to the angle of attack at the same point and only that point". This definition will yield diagonal influence coefficient matrices since the off-diagonal elements are zero. The off-diagonal elements relate the aerodynamic load to angles of attack at other points than the one in question and this relation or influence does not exist in the hypersonic case. The above definition can best be shown mathematically. In general, it may be written that

$$\left(\frac{\Delta p}{q}\right)_i = F_i(\alpha_i). \tag{A-1}$$

Typical forms of $F_i(\alpha_i)$ are

$$F_i(\alpha_i) = q_{2_i}\,\alpha_i^{\,2} \tag{A-2}$$

$$F_i(\alpha_i) = q_{1_i}\,\alpha_i + q_{3_i}\,\alpha_i^{\,3} \tag{A-3}$$

$$F_i(\alpha_i) = q_{o_i} + q_{1_i}\,\alpha_i + q_{2_i}\,\alpha_i^2 \qquad \text{(A-4)}$$

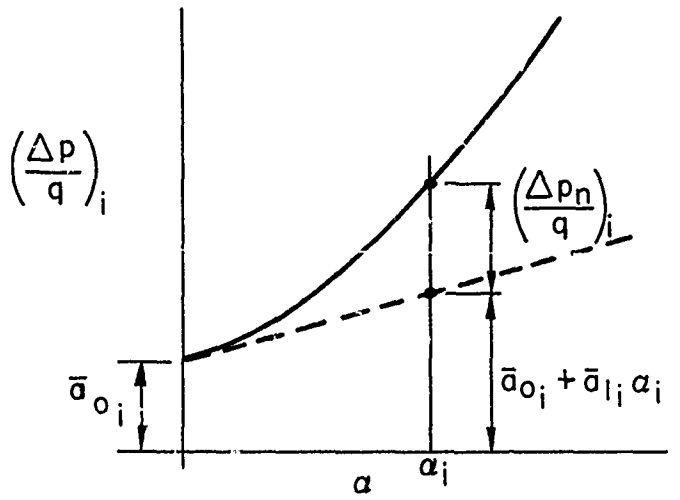
$$F_i(\alpha_i) = q_{1_i} \sin \alpha_i \cos \alpha_i \qquad \text{(A-5)}$$

The quantities q_{o_i} , q_{1_i} , q_{2_i} , etc. are hypersonic aerodynamic influence coefficients as previously defined. The subscripts o , 1 , ..., n on the influence coefficients are equal to the powers of α_i which they premultiply. The influence coefficients are functions of numerous aerodynamic parameters such as chordwise position, airfoil thickness ratio and Mach number. The numerical value and mathematical form of the coefficients vary with airfoil shape and the hypersonic flow phenomena under consideration.

The aeroelastic interaction solution developed in Section II assumes that the lifting pressure at a point is of the general form

$$\left(\frac{\Delta p}{q}\right)_i = \bar{a}_{o_i} + \bar{a}_{1_i}\,\alpha_i + \left(\frac{\Delta p_n}{q}\right)_i \qquad \text{(A-6)}$$

where the term $\left(\frac{\Delta p_n}{q}\right)_i$ is the non-linear component of the lifting pressure as shown in the sketch below. This term is usually a quadratic or cubic equation in α_i or a trignometric function of α_i .



The aerodynamic influence coefficients $\bar{a}_{0_i}$ and $\bar{a}_{1_i}$ can be determined from the basic lifting pressure expressions or can be chosen in an arbitrary fashion in order to expedite the method of solution described in Section II. In some instances, Equation (A-6) will consist of only the nonlinear portion of the lifting pressure $\left(\frac{\Delta p_n}{q}\right)_i$. In these cases the aerodynamic influence coefficients $\bar{a}_{0_i}$ and $\bar{a}_{1_i}$ need to be specified before an aeroelastic solution can be obtained. Equation (A-5) is a sample case of this. However, in the majority of cases $\left(\frac{\Delta p_n}{q}\right)_i$ can be easily determined by inspection of the basic lifting pressure relationship.

Equations (A-1) to (A-6) can very readily be put in matrix form. This is highly desirable since it preserves existing static aeroelastic notation and matrix techniques previously developed in supersonic aeroelasticity studies. For example, Equation (A-3) can be written in matrix form, for N reference points, as

$$\left\{\frac{\Delta p}{q}\right\} = \left[Q_1\right]\left\{\alpha\right\} + \left\{\frac{\Delta p_n}{q}\right\}; \quad \left\{\frac{\Delta p_n}{q}\right\} = \left[Q_3\right]\left\{\alpha^3\right\} \qquad \text{(A-7)}$$

where

$$\left[Q_1\right] = \begin{bmatrix} q_{1_1} & q_{1_2} & q_{1_3} \cdots & & & 0 \\ & & & & q_{1_i} \cdots & q_{1_N} \\ 0 & & & & & \end{bmatrix}$$

$$\left[Q_3\right] = \begin{bmatrix} q_{3_1} & q_{3_2} & q_{3_3} \cdots & & & 0 \\ & & & & q_{3_i} \cdots & q_{3_N} \\ 0 & & & & & \end{bmatrix}$$

The diagonal matrices, $[Q]$, are denoted as aerodynamic influence coefficient matrices. In order to generate aerodynamic influence coefficient matrices, it is necessary to use the results of theoretical investigations such as those discussed in Reference 6 to calculate the elements in the $[Q]$ matrices. It is noted here that if an Aeroelastician had experimental lifting pressure data, it could be mathematically described such that $[Q]$ matrices of the above form could be obtained.

The theoretical investigations of Reference 6 have used existing hypersonic pressure prediction methods to generate inputs to the $[Q]$ matrices. The theoretical work of Messrs. Dorrance, (Reference 18); Ivey, Klunker and Bowen (Reference 19); Grimminger, Williams and Young (Reference 20); Cheng (Reference 21); Lees and Probstein (Reference 22); and Creager (Reference 23) were used extensively to formulate the basic lifting pressure functions and the resultant aerodynamic influence coefficients. Graphical presentations of the influence coefficients were devised in order to aid the Aeroelastician to easily obtain $[Q]$ matrices. The graphs were designed so that only the pertinent parameters upon which the aerodynamic influence coefficients depend are shown. Therefore in practice the Aeroelastician need not have knowledge of hypersonic aerodynamics as such but only a working knowledge of the basic parameters upon which the influence coefficients depend. Once the influence coefficients are determined they are just arranged in the proper diagonal position in the $[Q]$ matrix of interest. Figure 11 presents a sample graph of the aerodynamic influence coefficient q_{2_i} obtained for a slender sharp nose airfoil with a half-diamond cross-sectional shape using Dorrance's method (Reference 18). Inspection of Figure 11 reveals that q_{2_i} is a function of streamwise position (reference point location) ξ_i, Mach number M_∞ and thickness ratio τ (τ = maximum thickness of airfoil/chord length).

Use of Dorrance's work has led to the following general form for the lifting pressure

$$\left(\frac{\Delta p}{q}\right)_i = q_{0_i} + q_{1_i}\,\alpha_i + q_{2_i}\,\alpha_i^2 + q_{3_i}\,\alpha_i^3 \qquad \text{(A-8)}$$

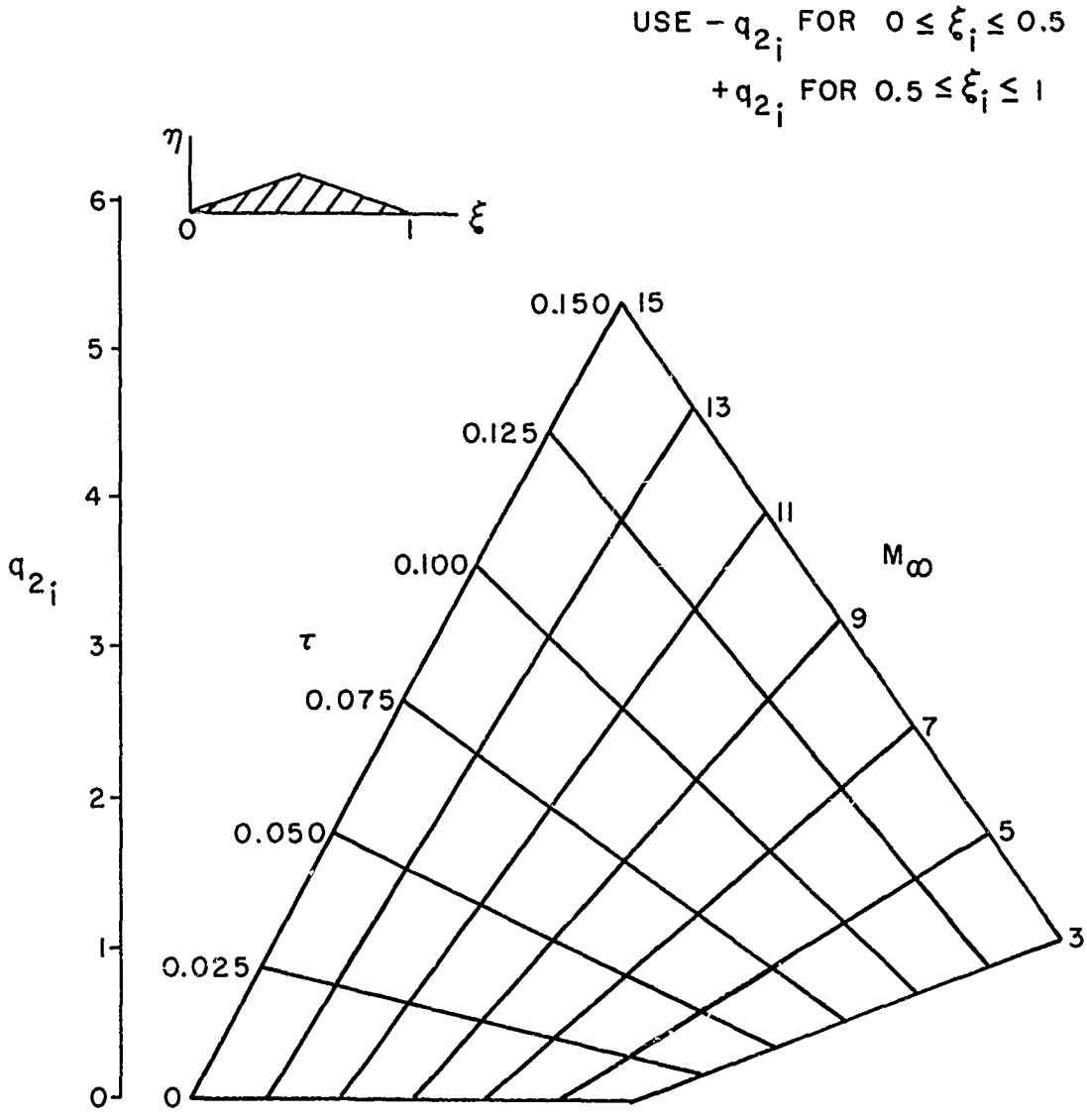


Figure 11. Sample Carpet Graph of Aerodynamic Influence Coefficient q_{2_i} – Half Diamond Airfoil Section, Dorrance's Method

or in matrix form, for N reference points

$$\left\{\frac{\Delta p}{q}\right\} = \left[Q_0\right] + \left[Q_1\right]\left\{\alpha\right\} + \left\{\frac{\Delta p_n}{q}\right\}, \qquad \text{(A-9)}$$

$$\left\{\frac{\Delta p_n}{q}\right\} = \left[Q_2\right]\left\{\alpha^2\right\} + \left[Q_3\right]\left\{\alpha^3\right\}. \qquad \text{(A-10)}$$

Equations similar to Equation (A-9) have been obtained using the methods proposed by the aforementioned investigators. Numerous carpet graphs such as that shown in Figure 11 have been obtained using Dorrance's work, as well as others, and are to be presented in Reference 6.

REFERENCES

1. Padlog, J., Donato, V. W. and Batt, J. R., Thermoelastic Effects on Hypersonic Stability and Control. Part III - Hypersonic Aeroelasticity. ASD TR 61-287. (To be published.)

2. Zisfein, M. B., Donato, V. W. and Farrell, R. F., (Unclassified Title) Supersonic Aeroelastic Effects on Static Stability and Control, Part I - Aerodynamics, Volumes I and II. WADC TR 58-95, December 1958 (Confidential).

3. Batt, J. R. and Farrell, R. F., (Unclassified Title) Thermal Effects on Static Aeroelastic Stability and Control - Part II - Aerodynamics, Volumes I and II. WADC TR 58-378, December 1959 (Confidential).

4. Diederich, F. W., A Simple Approximate Method for Calculating Spanwise Lift Distributions and Aerodynamic Influence Coefficients at Subsonic Speeds. NACA TN 2751, August 1952.

5. Gray, W. and Schenk, K., A Method for Calculating the Subsonic Steady-State Loading on An Airplane with a Wing of Arbitrary Planform and Stiffness. NACA TN 3030. December 1953.

6. Batt, J. R., Thermoelastic Effects on Hypersonic Stability and Control. Part I - Hypersonic Aerodynamics. ASD TR 61-287. (To be published.)

7. Gallagher, R. H. and Huff, R. D., Thermoelastic Effects on Hypersonic Stability and Control. Part II - Volume 1, Elastic Response Determinations for Severely Heated Wings. ASD TR 61-287. (To be published.)

8. Gallagher, R. H. and Huff, R. D., Thermoelastic Effects on Hypersonic Stability and Control, Part II, Volume 3, Elastic Response Analysis of Fuselage and Combined Wing Fuselage Structures. ASD TR 61-287. (To be published.)

9. Rattinger, I. and Gallagher, R. H., Supersonic Aeroelastic Effects on Static Stability and Control, Part II - Structures. WADC TR 58-95, April 1960.

10. Gallagher, R. H., Quinn, J. F. and Turrentine, D., Thermal Effects on Static Aeroelastic Stability and Control, Part III - Experimental and Analytical Methods for the Determination of Thermally-Affected Wing Deflectional Behavior. WADC TR 58-378, January 1960.

11. Quinn, J. F., Thermoelastic Effects on Hypersonic Stability and Control. Part II, Volume 2 - Elevated Temperature Deflection Influence Coefficient Tests. ASD TR 61-287. (To be published.)

12. Donato, V. W., Supersonic Aeroelastic Effects on Static Stability and Control. Part III, Aeroelastic Interaction. WADC TR 58-95. July 1960.

13. Bisplinghoff, R. L., Ashley, H. and Halfman, R. L., Aeroelasticity. Addison-Wesley Publishing Company, Inc. 1955.

14. Fung, Y. C., An Introduction to the Theory of Aeroelasticity. John Wiley and Sons, Inc. 1955.

15. Etkin, B., Dynamics of Flight, Stability and Control. John Wiley and Sons, Inc. 1959.

16. Perkins, C. D. and Hage, R. E., Airplane Performance, Stability and Control. John Wiley and Sons, Inc. September 1954.

17. McRuer, D. T., Bates, C. L. and Ashkenas, I. L., Dynamics of the Airframe. Bureau of Aeronautics Report AE-61-4 II. September 1952.

18. Dorrance, W. H., Two Dimensional Airfoils at Moderate Hypersonic Speeds. Journal of the Aeronautical Sciences. Volume 19. September 1952.

19. Ivey, H., Klunker, E. and Bowen, E., A Method for Determining the Aerodynamic Characteristics of Two- and Three-Dimensional Shapes at Hypersonic Speeds. NACA TN 1613. July 1948.

20. Grimminger, G., Williams, E. and Young, G., Lift on Inclined Bodies of Revolution. Journal of Aeronautical Sciences. Volume 17. pp. 675-690. November 1950.

21. Cheng, H. K., Hall, J. G., Golian, T. C. and Hertzberg, A., Boundary Layer Displacement and Leading Edge Bluntness Effects in High Temperature Hypersonic Flow. AFSOR TN 59-1193. CAL Report No. AD-1052-A-9. January 1960.

22. Lees, L. and Probstein, R., Hypersonic Viscous Flow Over a Flat Plate. Princeton University Report No. 195. April 1952.

23. Creager, M. O., The Effect of Leading Edge Sweep and Surface Inclination on the Hypersonic Flow Field Over a Blunt Flat Plate. NASA M12-26-58A. January 1959. (See also NACA TN 4142, NASA M5-12-59A, IAS Paper No. 59-113, NASA TN D-71 and NASA TN D-313.)

FLIGHT CONTROL OF HYPERSONIC VEHICLES WITH A TEMPERATURE SENSING LOOP

Daniel O. Dommasch

DODCO, INC.

ABSTRACT

The concepts of optimum control theory are applied to the general problem of controlling the descent of a hypersonic re-entry system in an incompletely defined environment. It is shown that the effects of thermoaeroelastic deformations and other variables which alter the vehicles characteristics as well as the uncertainties arising from undefined environmental conditions can readily be handled by an optimum adaptive macro-micro controller. Because of the magnitude of the changes to be expected in atmospheric characteristics from point to point about the earth and from day to day in a time sense, it is concluded that preprogrammed descents whose success is predicated on the assumption that a statistical standard atmosphere will be encountered are likely to cause destruction of a re-entry vehicle or failure to perform an assigned mission.

LIST OF SYMBOLS

ρ	air density, slugs/ft.^{3}
T, T_s	skin temperature at sensor location, ^oR
t	time, seconds
Δt	time increment, seconds
e	error signal
J	integral, mass moment of inertia
λ	Lagrange multiplier
α_x	generalized angular acceleration command
δJ	first variation of J
$\delta^2 J$	second variation of J
θ	pitch angle, radians
r_e	response factor
k_g	gain factor
r_t	$(\Delta t/2)(\dot{T}_n - \dot{T}_{n-1})/(\theta_n - \theta_{n-1})$
T_D	desired temperature, ^oR
e_{av}	average error
a_p	present flight path acceleration, ft/sec.^{2}
V_p	present flight path velocity, ft/sec.
V_f	final velocity, ft/sec.
s_d	desired distance to go, ft.
α	angle of attack, radians

LIST OF SYMBOLS (CONT'D)

φ_p	bank angle of principal axis, radians
φ_r	bank angle of lift vector, radians
m	vehicle mass, slugs
V_r	relative velocity, ft/sec.
V_a	absolute velocity, ft/sec.
ϕ	inclination of navigational great circle course to north polar axis, radians
γ_r	inclination of V_r to local horizontal, radians
Λ_r	angular range in instantaneous navigational great circle from equatorial plane, radians
τ	response factor, seconds
L	lift, lbs.
R	reaction rocket thrust, lbs.
$L+R\cos\alpha$	increment normal load
Δn_n	incremental normal load factor = $(L + R\cos\alpha)/mg$
β	side slip angle, radians
h_g	geometric height above earth, ft.
c	wing chord, ft.
S	wing area, $ft.^2$

FLIGHT CONTROL OF HYPERSONIC VEHICLES WITH A TEMPERATURE SENSING LOOP

INTRODUCTION

It is appropriate, I think, to begin any discussion of a control problem with an analysis of the system to be controlled, its mission in life and the nature of the environment in which the system is to function. The control problem we need to consider here is somewhat complicated by the dual restrictions that neither the nature of the environment in which we are going to operate nor the specific characteristics of the system to be controlled can be established ahead of time with any degree of precision. Moreover it is entirely probable that the characteristics of the system will change with time and as a function of the nature of the flight path followed in the atmosphere. In the light of these statements it would be rather careless of us to presume at the outset that we have a linear problem to deal with, and accordingly our lack of information becomes even greater since we cannot make use of the great simplifications provided by the use of linearized control theory.

In spite of the opening statements, our position is by no means hopeless, and as a matter of fact it is hardly novel, on the contrary it is possible to achieve a control solution without undue complication provided only that we do not try to oversimplify the problem too early in the game. The problem we face is no different in principle than the problem faced by a pilot flying an airplane which is unfamiliar to him. To fly the airplane, he has no need to know the precise value of $C_{L_{max}}$ nor the control effectiveness parameters nor does he need to know any numbers spelling out the stability parameters associated with the airplane. What he does need to know is that a given control motion results in a given rotation about one of the airplane axes, he requires warning of an inpending stall, and a rough knowledge that there are some limitations he ought to observe so as to avoid destruction of the airplane. If the airplane is flyable in the first place, the pilot can quickly adapt himself to its characteristics even if the airplane is completely marginal. Thus the Wright brothers never had flying lessions, but somehow managed to fly their first airplane which would be considered totally unacceptable and possibly unflyable, under current military specifications.

I think then that it is clear that we do not need to have a great deal of precise information on hand to effect control, but it is essential that we do have information on the direction of response to a given control action and as to the limitations which we need to observe to avoid destruction of the vehicle we want to control. In the absence of this information control is indeed impossible. It is essential also, that, at least at sensor locations there shall exist the same trend of response for short term actions as for long term action, otherwise sensed data becomes useless for the particular control problem at hand. In other words we require consistent short and long term response characteristics of the system.

In the absence of preconceived data concerning the nature of our vehicle and its environment, one needs to make measurements along the way, however this involves new problems based on sensor location, response and accuracy limitations, and it is possible to have too much data to handle just as it is possible to have too little. It is evident, I think, that we want to optimize data acquisition and handling requirements from the standpoint of achieving the simplest, least expensive and most reliable system.

When we deal with re-entry systems which because of their basic nature cannot avoid operation at elevated temperatures, structural deformation can occur even in the absence of large applied loads, and in the event that we have both high loadings and high temperatures, then we may expect to encounter rather severe temporary warping as well as permanent structural deformation, even though destructive failure does not occur. At hypersonic velocities even relatively minor deformations alter the pressure distribution over the vehicle with the result that both heating and aerodynamic coefficients become a function of aerothermoelastic effects, and conversely.

Evidently these interactions can be minimized by keeping both the temperature and aerodynamic loadings as small as possible, and any flight control system for an advanced flight vehicle should be capable of accomplishing both these purposes. To summarize our problem we have that:

(a) Our environment of operation is incompletely defined.
(b) Our vehicular characteristics are unknown.
(c) We must limit sensor requirements to a minimum.
(d) Our vehicle must be controllable in that it exhibits consistent short and long term response characteristics at least at critical sensor locations.
(e) The control system must seek to minimize both temperature and structural loadings while still accomplishing the mission of the entire system.

If we presume that our mission is to go from some point (conceivably outside of the atmosphere) to a given geographical location on the surface of the earth, then we shall show that in spite of the aforementioned restrictions, a control system can be constructed to do the job while maintaining the integrity of our vehicle and its contents. To this end our mission requirements are:

1. Our vehicle must be flown safely.
2. It must achieve a desired longitudinal range.
3. It must achieve a desired lateral range.

We shall now consider environmental and vehicular characteristic uncertainties in more detail.

ENVIRONMENTAL AND VEHICULAR CHARACTERISTIC UNCERTAINTIES

The operating environment of any high speed vehicle is the earth's atmosphere whose characteristics vary considerably with time, place and altitude. At sea level the temperature may reach a peak of perhaps 160° F and achieve a minimum value of about -100° F, although these two extremes are not likely to occur at the same geographic location. On the cold day the barometric pressure is likely to be high, whereas under high temperature conditions it is generally low. Barometric pressures at sea level vary from about 27" Hg to 32" Hg. Considering these extremes, the ratio of maximum to minimum densities which might be encountered at sea level is obtained from the equation of state as

$$\frac{\rho_{max.}}{\rho_{min.}} = \frac{459.6 + 160}{459.6 - 100} \times \frac{32}{27} = 2.04$$

This is an extreme-value ratio and such a change in air density is not likely to be encountered at sea level unless we travel from an extreme desert region to some point above the arctic circle.

At re-entry altitudes the observed density variations are considerably greater than at sea level showing a ratio

$$\frac{\rho_{max.}}{\rho_{min.}} = 6$$

on the basis of data contained in reference 1. The causes for this scatter are far from well defined; part may be due to computational

procedures, part to instrumentation problems and so on, but there is little reason to believe that the atmospheric density does not, in fact, display at least the density variation exhibited by the test data. If we are somewhat optimistic and assume that we must cope only with a fourfold density variation at any given altitude in the re-entry region, then we find that working from a nominal standard or model atmosphere, we may first encounter a sufficiently dense atmosphere to produce tangible aerodynamic effects over a spread of altitudes of $\pm$ 30,000 ft. from the assumed standard. What this means is that the exact geometric altitude at which re-entry is initiated is not a defined quantity. Moreover the heat transfer coefficient is roughly proportional to $\sqrt{\rho}V^3$, so that a factor of four on density involves a change in heat transfer coefficient of about 2.

The fact that the characteristics of the atmosphere vary with time and geographic location is seen to militate strongly against the use of a preprogramming control system designed on the assumption that standard or averaged atmospheric characteristics are going to be encountered during re-entry and descent. But our problem is more involved than this since even were the atmosphere completely defined for us we would still have to know quite a bit about our aircraft's characteristics if we hoped to standardize our flight path to any degree, and we have no guaranteed theories or substantial fund of test data which establish aerodynamic characteristics or actual heat transfer coefficients for re-entry velocities.

Some astonishingly comprehensive work has been accomplished by various investigators in the area of heat transfer in hypersonic flow fields and reference 4, presents a seemingly all inclusive relation for heat transfer in the vicinity of a stagnation point which we understand has stood up well under experimental investigation, however there is a marked difference between computing heat transfer with a known pressure distribution and attempting to estimate structural temperatures in a flow field which is not completely defined. Unfortunately it is this type of flow field which exists around a hypersonic winged airplane, so that even were there no structural deformations to contend with, there exists considerable question concerning the exact values of heat transfer coefficients, for instance, at a wing fuselage junction of a vehicle at an arbitrary angle of attack and an arbitrary angle of side slip. Lest this uncertainity be viewed too lightly, let us remember that even today we have no theories adequate to predict, analytically, the pressure distribution on and in the vicinity of an airplane such as a Piper Cub, so that for airplanes such as these we still need to use empirical techniques to properly locate a source of static pressure for air speed measuring purposes.

When we now add the influences of structural deformations resulting from aerothermoelastic effects, we must face the fact

that neither our heating characteristics nor our aerodynamic parameters can be assumed defined to the degree that we can depend (for control purposes), on the assumption that they are known quantities. We must therefore divorce our control system synthesis completely from any dependence on precisely defined environmental or vehicular aerodynamic and heating characteristics. This brings us, heuristically at least, to the thought that we should employ some type of adaptive logic to design the over-all control system for advanced flight vehicles, and this thought is explored further in the following section.

THE NEED FOR ADAPTIVE LOGIC

To originate our discussion of adaptive logic we first introduce the terms "macro" and "micro" control to differentiate between those functions which determine the degree of closure on a given temperature or given space location and those required to maintain the airplane's orientation with respect to a given axes system in such a way that the desired end conditions are ultimately achieved. Thus macro-control inolves the making of certain decisions which were formerly the prerogative of a human pilot as well as some decisions he would normally be incapable of making, while micro-control includes, what can broadly be described as, auto-pilot functions. The macro and micro-control functions can most expediently be combined into a single non-linear logic system with the macro-commands being directly translated into micro-functions.

Speaking strictly from a conceptual standpoint, it is recognized that adaptive control is the antithesis or preprogramming since the need for adaptation arises only in the event that we are uncertain of our ability to attain in practice, an a-priori group of assumed operating conditions which could otherwise be utilized as a basis for preprogramming. It is believed that control of trajectories in space as well as in the upper reaches of the atmosphere can only practically be accomplished on an adaptive basis if we deal with winged, controlled and manned systems. It is conceded at the outset that if we had certain knowledge of the conditions we could expect to encounter during re-entry, that preprogramming would probably lead to better control, at least as far as the stipulation of the path or paths to be followed is concerned. However, we do not now have this knowledge.

The variability of atmospheric characteristics produces major problems in the control of range and skipping tendencies which must be considered in the design of a generalized flight control system for a successful re-entry vehicle.

The actual speed and flight path inclination at the time of re-entry are not precisely defined ahead of time so that the use of pre-programming as a means of range and temperature control is not likely to produce either a desired range or a desired temperature. Similarly the fact that the earth is rotating and carries the atmosphere with it means that a given absolute re-entry velocity (absolute velocity is the inertial space speed of our object referenced to the earth's center, and therefore, differs from the relative speed by the amount of the atmospheric absolute speed due to rotation of the earth) will produce different relative re-entry velocities dependent on our latitude and compass heading. Since the absolute atmospheric velocity at the equator is close to 1500 ft/sec., an absolute re-entry velocity of 25,000 ft/sec., in the East to West direction at the equator would produce a relative velocity of 26,500 ft/sec., whereas if our direction were West to East, our relative velocity would be 23,500 ft/sec. This is the extreme case, however, at 45° latitude the earth still produces about 1,000 ft/sec., of absolute velocity so that the contributions of this velocity component are by no means trivial even at the central latitudes. The variations of relative re-entry velocity due to latitude and azimuth, and the variations in this velocity as well as the variations in the angle of the flight path at re-entry due to indeterminate re-entry altitude all combine to produce a substantial spread of conditions to which any re-entry system must adapt if it is to fulfill its purpose. Lack of ability to compensate for these varying initial conditions can lead to destruction of the vehicle or failure to achieve desired terminal conditions.

The fact that local heating rates may show anomalous behavior as regards angle of attack changes introduces difficulties both in establishing proper temperature sensing locations and the synthesis of control logic which in turn influence the basic airplane and control system designs.

It is evident that before we can achieve a proper descent control system, we must impose the following requirements upon the airframe:

1. The design must be physically capable of accomplishing a safe re-entry, and there must exist a range of temperatures at which flight is possible and which do not destroy the airframe.
2. The re-entry speed and attitude must be sufficiently controllable through retro-fire to make it physically possible to re-enter safely (very few meteors can safely enter the atmosphere because of either excessive speed or excessive inclination angle).
3. Sufficient control must be available to change angle of attack and curve the flight path as required by thermal or range maneuvers.

4. There must exist a logical correlation between angle of attack change and heating rate at critical sensing points on our re-entry body. If this correlation does not exist for all angles of attack, then we must limit operation to those angles where it does exist.

5. Interaction of aerothermoelastic effects with the control system response must be minimized.

The importance of the proper heating rate response cannot be overemphasized. Control of range and temperature either individually or collectively, is possible only if there exist both positive and logical airplane range and temperature responses to changes in vehicular angle of attack (which is the only fundamental parameter we can control on a relatively short time basis). At orbital speeds, and at speeds close to orbital, a slight increase in angle of attack may cause a sufficient increase in lift (in spite of very low dynamic pressures) to cause an exit from the atmosphere with the result that aerodynamic path control is lost and the vehicle seeks a new orbital apogee approximately 180° of angular range from the point at which the attempted re-entry occurred. This situation is untenable from the point of view of establishing proper range control and is the result of attempting to re-enter at too great an angle of attack or at too shallow a flight path inclination; severe skipping can also occur in the event that too low a commanded temperature is specified which rapidly forces an increase in angle of attack at near orbital speed. Thus there exist limitations both on re-entry angle of attack and on specified temperature which if ignored can lead to unpredictable range performance. Re-entries will normally occur at velocities greater than the circular orbital speed required at the re-entry altitude unless multiple retro-fire periods are employed, and this fact intensifies the skipping problem. As we shall see later, a properly designed lateral range control system has the ability to eliminate a primary skip, and therefore when properly used can provide for predictable in-atmospheric range. If simultaneous control of range and temperature is desired, the range and temperature responses must be compatible. For properly placed sensors and proper aerodynamic design there will exist an angle of attack range over which an increase in angle of attack produces (at the sensor) a decrease in boundary layer heat transfer and vice-versa.* Normally one cannot expect that this will hold true

*The zero angle of attack stagnation points of various components of the re-entry vehicle are theoretically satisfactory locations provided the minimum angle of attack is set at perhaps 5° to 10° so as to insure that stagnation conditions are never encountered at the sensor itself.

for all angles of attack, however, there must exist a working range of angles wherein proper response occurs: If this does not hold true, direct temperature control is not possible. Indeed we face an impossible control problem unless we can postulate logical response in the anticipated flight areas, as explained below.

The boundary layer heating rate depends on density and velocity, increasing with an increase in either of these quantities. A decrease in angle of attack, on a long term basis will tend to increase speed and increase density, i.e., will tend to increase temperature, while an increase in angle of attack on a long term basis will invert this characteristics. Accordingly, we have compatible short term and long term characteristics only in the event that the boundary layer heating rate decreases (at the sensor) with increase in angle of attack (other factors held constant) on an immediate or short term basis, and there exists an impossible control problem in the event that the heating rate, shows an increase with angle of attack, because in this event corrections made on an immediate basis must ultimately produce just the reverse of the response desired. It follows that a fundamental requirement for a successful re-entry configuration is that at the critical sensor(s) location(s) there must exist an increase in heating rate corresponding to a decreased angle of attack in the operating angle of attack region.

Range control is essentially an energy management proposition in those regions wherein slant range does not enter the picture. Thus to increase range we decrease drag and to decrease range we increase drag. Accordingly in the absence of devices capable of producing drag without altering the lift, an increase in range accompanies a decrease in angle of attack and a decrease in range accompanies an increase in angle of attack within the domain permitted by temperature response considerations. It follows that an increased range demand implies higher operating temperatures and that range potential is limited by the maximum permissible operating temperature.

For the configurations considered for numerical examples of control system functions, no cases were encountered where an increase in sinking speed (due to increased drag) counteracted the basic trends mentioned above, (i.e., the flight path angle never becomes so negative as to cause an excessive heating rate, due to encountering high density atmospheric regions before the velocity had been sufficiently reduced).

On the basis of this discussion, it would appear that a great deal can be accomplished with proper control techniques, and extended simulation studies of a proposed unified optimum adaptive control system reveal that basic missions can be carried out without the necessity of encountering excessive structural loadings or excessive temperatures. We therefore find that by proper control

logic design it is possible to provide mission trajectories which do not tend to violate limitations imposed by the presence of aerothermoelastic effects, and further, the fact that we may directly control skin temperature means that thermal weakening of the structure can be minimized simply by establishing the maximum temperature at a low enough value to insure maintenance of structural integrity. There are, however, limits to this process since if we desire to control range then we are forced to accept finite variations in temperature during the flight.

A UNIFIED APPROACH

Before presenting a brief description of the analysis technique applicable to the synthesis of the unified temperature, longitudinal and lateral range control system designed to meet the requirements set forth in the previous section of this paper, we shall present a brief physical description of how the system functions.

The system is designed to maintain zero side slip, and to accomplish this requires either an aerodynamic or inertial side slip sensing system. Inertial platforms are available which provide the desired input information based on lateral axis acceleration measurement, and development work on aerodynamic sensors which can function at hypervelocities is well underway. The control of longitudinal and lateral range requires navigational inputs which establish present location with respect to the target and with respect to the instantaneous inclination of the earth great circle course followed by the controlled vehicle. These data can be derived from platform measurements, or through the use of data-link procedures.

Control of lateral attitude (bank) requires sensing of bank angle, rate of bank and banking acceleration and these are required inputs to be obtained by gyro instrument measurements. Similarly pitch control requires sensing of pitch attitude, pitch rate and pitch acceleration, which quantities are again obtained from gyro instruments. If a stable platform is available this single unit provides all necessary inertial data inputs.

The control and monitoring of skin temperature requires that temperature, T, and its time rate of change, $\dot{T}$, be measured directly using buried sensors. The location of these sensors is critical since they must be located at a point (or points) where an increase in angle of attack provides for a decrease in temperature. The selection of the sensor locations must be determined by actual tests.

The proposed system can become divergent from a temperature control standpoint if negative angles of attack are achieved, and therefore angle of attack measurement is required, based either on

platform data or air data sensing. There is also a requirements for limiting maximum angles of attack to those values at which satisfactory control can be achieved.

The proposed unified central control system may, for convenience be viewed as consisting of three interacting loops. In the case of longitudinal range and temperature control, the interaction is direct while the lateral or cross range system interacts only indirectly with the other two and conversely.

The fundamental error signals are derived on a macro basis, however, micro-control logic is required to stabilize short term dynamic response of the entire vehicle as well as to null the basic commands. Thus all control logic functions have been combined without attempt at artificial separation which could lead, in this case, to excessive complication.

For longitudinal control, all major functions are conducted through the pitch attitude-temperature stabilization logic slaved to the demands of the range control loop which functions so as to alter the commanded temperature. Numerical analyses reveal that within the operating range investigated, interaction between the range and temperature systems is stable. The temperature loop will override the range loop only in the event that the vehicle integrity is threatened. Cross range control is obtained through lateral and directional commands imposed on the basis of lateral range error translated to terms defining the instantaneous tilt of the earth great circle course required to cause the vehicle to pass directly over the target at its time of arrival; again stable interaction is encountered.

Because macro-control involves control of motion of the vehicle's c.g in relative space (earth reference space) while micro-control is based on orientation of the vehicle axes both in absolute (solar) space as well as with reference to the rotating earth, the dynamics of the problem involve several axes systems and cross coupling effects.

The unified control system is of the non-linear, sample data type and because there are no stability criteria which may be used to determine that the performance of such a system will be satisfactory on an a-priori basis, an extensive amount of simulation of the system, considering a wide variety of operating conditions, was conducted using the two LGP-30 computers and an IBM 1620 installed at DODCO and the Datatron 220 unit at the Signal Corps Engineering Laboratories, Fort Monmouth, New Jersey. The basic runs were conducted using three different sets of angle of attack boundary layer heating rate characteristics and three different atmospheres which represented the density extremes indicated by data collected by the Cambridge Research Center. No operating difficulties or instability problems were encountered throughout the range of operating conditions investigated

and in all cases successful descents were obtained. For the cases considered, the total load factor never exceeded a value of one and fuel consumption requirements for the control system, which was for these studies presumed to be of the reaction type, were found to be entirely nominal.

In this connection it is important to note that the fuel use requirements depend primarly on the static stability characteristics of the controlled vehicle. For all of the numerical studies, a neutrally stable airframe was utilized, however, increased fuel consumption will result in the event that the actual system is either statically stable or unstable. The deleterous effects of stability on the energy input requirements of the control system can, of course, be eliminated by providing some means of achieving aerodynamic trim so that continued control action will not be required to overcome the tendency of the airplane to seek its own neutral location. Thus there exists a requirement for a trim system on all re-entry vehicles. This trim system should preferably operate on an aerodynamic basis to avoid the requirement for additional fuel utilization for its functioning.

It is emphasized that the system proposed here has the dual functions of achieving control in the first place starting with rather sizable errors and, subsequent to this it must function effectively on a regulatory basis. The numerical analyses conducted reveal that the proposed system meets both the control and regulation requirements. In this connection, we note that no control is exercised other than over attitude, until a given skin temperature is exceeded, at which time the system is triggered into operation. This sequence is required since, unless propulsive rockets are used, there is no way to control the trajectory in space until a sufficiently dense atmosphere is reached to provide for the production of normal lifting forces, and the skin temperature achieved is used as a means of detecting that the air density is sufficient to permit control.

Numerical analyses have shown that provided the bank angle is restricted to a maximum value of 60°, and provided that this angle is maintained for the duration of the primary skip, this skip is sufficiently inhibited at absolute speeds of about 26,000 ft/sec., or less to avoid loss of control due to exit from the atmosphere.

The problem of skip control therefore appears to be solved by the proposed system, at least for the case of re-entry from satellite orbits, and it is possible to insure predictable in-atmospheric range performance (which is the first requirement for the design of a retro-fire point selection system). In this connection (the density was varied at any given altitude by a factor of four), it was found

that a properly specified range was obtainable in all atmospheres with typical lifting re-entry configurations.

DEVELOPMENT OF CONTROL LOGIC

The complete development of the equations defining the unified control system is contained in reference 3, and no attempt will be made here to duplicate the effort of that report; rather we will summarize as briefly as possible, the concepts used to system synthesis.

To begin with we make note of the fact that regardless of how hard we may try, there is nothing which we can do instantaneously to correct a detected error. What we can do is take corrective action which we hope will reduce this error in the near future, with the term "near future" referring to the time $t + \Delta t$ where t is our present time. If sub "n" represents present conditions and n + 1, the conditions at $t + \Delta t$ then we want to make the error at (n+1) as small as possible, i.e., we want to minimize e_{n+1}. We are restrained from making e_{n+1} identically equal to zero because our control actions are limited by the authority of the controller and by the inertial and response characteristics of the controlled vehicle. These limitations are introduced using an arbitrary Lagrange multiplier λ, and on applying the sufficient conditions for the existence of a solution to a varied integral (i.e., $\delta^2 J \neq 0$), we obtain the criterion that we wish to maximize the integral

$$J = \int_{t}^{t + \Delta t} \left(\frac{1}{e_{n+1}} + \frac{\lambda}{\alpha_x}\right) dt \qquad \text{.....(1)}$$

where α_x is the commanded angular acceleration.

In this equation (which applies to any control problem) e_{n+1} is generated by a Taylor series expansion about the point "n" in terms of sensed data at the point n, with the effects of the unknown α_x included in the expansion. The excitation signal is generated by imposing the necessary condition for rendering J a maximum, i.e.,

$$\delta J = 0 \qquad \text{.....(2)}$$

where δ signifies the first variation of J. The existence of a solution is guaranteed by the fact that the form of (1) is such that the second variation of J (i.e., $\delta^2 J$) does not vanish.

In general the imposition of the condition $\delta J = 0$, in equation (1) leads to a single Euler - Lagrange equation which has two or more solutions, and the proper solution is selected using the principle of least action.

The above discussion does not constitute a proof of validity of the procedure described, however this proof is contained in references 3 and 5 which should be consulted if further details are desired. Skipping all derivation steps, application of the foregoing principles leads to the following control equations.

PITCH CONTROL AND TEMPERATURE CONTROL LOOP

$$\ddot{\theta}_x = \frac{-K(e_{n+1})_{nc}}{\pm\sqrt{1/m} - 1} \qquad \text{.....(3)}$$

where

$\ddot{\theta}_x$ = pitching acceleration command

$k = 2/k_g r_t r_a \overline{\Delta t}^2$

k_g - gain factor

$m = -\lambda r_t r_a \overline{\Delta t}^2/2$, where λ is a positive number

Δt = prediction time increment (normally 0.2 seconds)

r_t = temperature response factor = $(\Delta t/2)(\dot{T}_n - \dot{T}_{n-1})/(\theta_n - \theta_{n-1})$, normally negative

r_a = airplane response factor (normally unity)

$(e_{n+1})_{nc} = e_n - r_t\dot{\theta}_n\Delta t - \dot{T}_n\Delta t$

$e_n = T_{D_n} - T_{s_n}$ ....(4)

T_{D_n} desired temperature at "n" (establishing by the range controller)

T_{s_n} = sensed temperature at "n"

$\dot{T}_n = (dT/dt)_n$ = sensed rate of change of temperature at sensor

Notes:

(1) The temperature response factor r_+ cannot be measured without lag and to avoid control system malfunction its determination is limited as follows

if $/\Delta\theta/ < 0.10^o$ use last value of r_+

if $r_+ > -20$ use $r_+ = -20$

λ has a value of between +10 and +30.

(2) To select the proper value of $\ddot{\theta}_x$ from equation (3), determine $(\dot{e}_n/e_n)\Delta t$, if, $-1 < (\dot{e}_n/e_n)\Delta t < m-2$, use the plus sign on the radical, otherwise use the minus sign on the radical.

(3) A value of m = 9 gives a 2 to 1 gain switch.

COMBINED PITCH, RANGE AND TEMPERATURE CONTROL

For this case equation (3) still holds, however the desired temperature in (4) is computed from

$$T_D = T_n - \frac{dT}{da}\left(a_p + \frac{V_p^2 - V_f^2}{2s_d}\right) \qquad \text{.....(5)}$$

where, dT/da is the temperature-acceleration response factor (set at a constant value of 10)

a = acceleration along flight path

a_p = present acceleration

V_p = present velocity

V_f = desired final velocity

s_d = distance to go from one present location to the target.

In the above, T_D is bounded by

$$T_{D_{max.}} > T_D > T_{D_{min.}} \quad \text{(to be set by the airframe (limits))}$$

$$\alpha_{max.} > \alpha > \alpha_{min.} \quad \text{(to be set by control requirements)}$$

where α = angle of attack.

Notes:

(1) Control of range is relinquished if $T_D > T_{D_{max.}}$, at which time the temperature control loop holds T_D at $T_{D_{max.}}$ until parallel computation indicates that T_D has fallen below $T_{D_{max.}}$. When control is relinquished, V_f is automatically reduced by 10% of its existing value to force a greater deceleration and lowered temperature of operation. This occurs each time the temperature loop takes over, but V_f is not reduced below 1,000 ft/sec. in the event that the lower limit on V_f is reached, the range command was too great for the environmental pattern, and target attainment is questionable, but not necessarily impossible.

(2) The terminal conditions, V_f and desired location, must be set into the system using navigational data.

THE CROSS RANGE CONTROL LOOP

$$\ddot{\varphi}_x = \frac{-k_\varphi (e_{n+1})_{nc\varphi_p}}{\pm\sqrt{1/m_\varphi} - 1} = \text{roll acceleration command about the principal roll axis} \quad \text{.....(6)}$$

$$(e_{n+1})_{nc\dot{\varphi}_p} = \Delta\varphi_p - \dot{\varphi}_{n_p}\Delta t \quad (\varphi_p \text{ is the roll angle about the principal axis in inertial space})$$

$$\Delta\varphi_p = e_{\varphi_r}(\cos\alpha) = e_{\varphi_p} = \varphi_{e_p} - \varphi_{n_p}$$

k_φ = roll gain setting factor

where:

$m_\varphi = 9$

$\ddot{\varphi}_x$ is the commanded banking acceleration

$\dot{\varphi}_n$ is the sensed rate of roll

$e_{\varphi_r} = \Delta\varphi_r = \varphi_{r_d} - \varphi_r$ (where φ_r is the roll angle of the lift vector)

$$\sin\varphi_r = \frac{mV_r\,[\dot{\phi}_d\cos\gamma_r/\cos\Lambda_r - 2\Omega\cos\phi\sin(\Lambda_r-\gamma_r)]}{L + R\cos\alpha}$$

m = vehicle mass

V_r = relative velocity (may be taken equal to absolute velocity for control computation)

$\dot{\phi}_d$ = desired rate of tilt of navigational great circle

$L + R\cos\alpha$ = total external force normal to flight path along fuselage symmetry axis (measured inertially as a function of normal axis load factor) = Note $\Delta n_n = (L + R\cos\alpha)/mg$

γ_r = inclination of flight path to local horizontal (measured inertially)

Λ_r = angular location from equator of vehicle in its instantaneous great circle course

Ω = absolute angular rotation of earth in solar space

$\dot{\phi}_d = (\phi_d - \phi_n)/\tau$

ϕ_d = desired tilt of plane of navigational great circle

ϕ_n = actual tilt of instantaneous plane of motion

τ = response factor (normally 100 seconds)

Notes:

(1) ϕ_d and ϕ_n are obtained from the navigational and guidance system.

(2) The proper value of $\ddot{\varphi}_x$ is selected by computing $(e_{n\varphi}/e_{n\varphi_p})\Delta t$

if $-1 < (\dot{e}_{n\varphi_p}/e_{n\varphi_p})\Delta t < m-2$

use the plus sign on the radical, otherwise use the minus sign.

Using these control equations and a rather elaborate simulation program, the unified control logic was subjected to a wide variety of operating conditions and in general satisfactory performance was obtained. We shall forego discussion of the details of the simulation equations with the thought that those interested in these will refer to reference 3. A summary of the control system logic is presented in Figure 1, which illustrates both the initiation of control action and the continued operation of the system on a sample data basis. To speed simulation one and two second sample times were utilized and satisfactory results were obtained in spite of the "noise" introduced by these excessive intervals. For control system operation a sample-compute time interval of from 0.1 to 0.2 second should prove more than adequate, providing a safety factor of 10 over the simulation study. In the flow diagram of Figure 1, alternate sources of α, V_r and β are illustrated, since either air data or platform data may be used to obtained these quantities.

SIMULATION RESULTS

The operation of the unified control system was examined over a wide range of operating conditions involving an arbitrary tenfold variation of a heat transfer coefficient multiplying factor, various

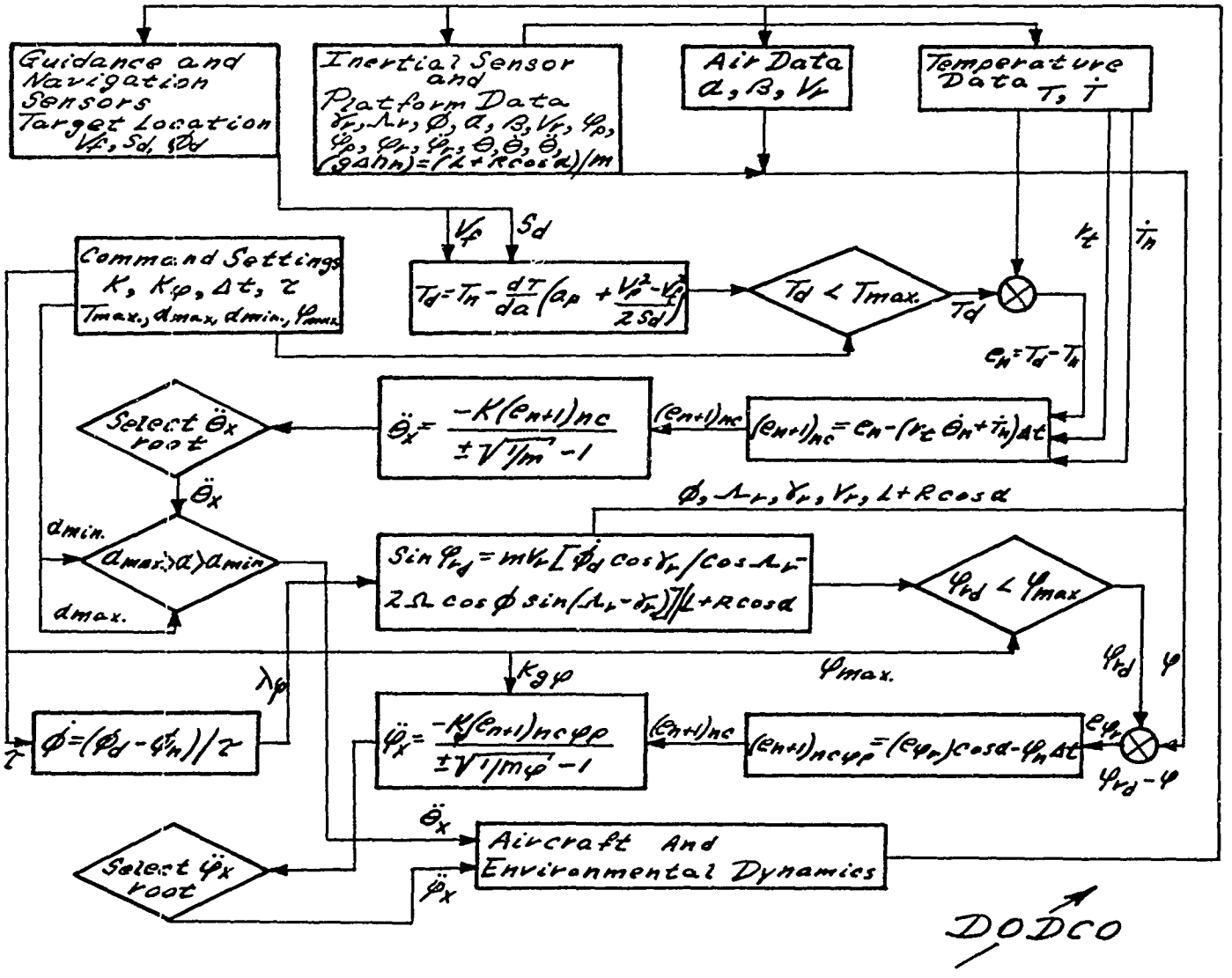


Figure 1. Summary of the Control System Logic

non linear heat transfer coefficient-angle of attack relationships, varying emissivity, wing loadings ranging from 10 to 40 psf., varying stability characteristics, various lift drag equations and considering atmospheres having twice the density and 1/2 the density of the 1959 ARDC Model as well as the density of the model. For the details of the complete study, reference 3 should be consulted. For our present purposes, it will suffice to examine the results obtained from examination of a single configuration, using a single set of initial conditions representing those obtained following a relatively low altitude retro-fire. The conditions used were

Initial skin temperature 1300°R

$\phi = 45^{\circ}$

$\zeta = 30^{\circ}$ (N. latitude) $\xi = 0$ (relative longitude)

V_a = absolute velocity = 25497.5 fps.

$V_r = 24409.2$ fps.

$\gamma_a = -1^{\circ}$ at hg = 275,000 ft. ($\gamma_r = -1.03461^{\circ}$)

$\alpha_i = 15^{\circ}$ (re-entry attitude)

The test vehicle had the following characteristics

W = gross weight = 10,000 lbs. (310 slugs)

S = wing area = 500 sq. ft.

C_{D_e} = parasite drag coefficient = 0.005

$K = \partial C_D / \partial C_l^{\,2} = 2.66$

a = lift slope = 0.6 per radian

$\partial C_M / \partial \dot{\theta}$ = damping in pitch factor = 0.02 per radian per second

c = mean wing chord = 30.00 ft.

J_y = pitching moment of inertia = 100,000 slugs - ft.^{2}

x = moment arm of pitch control rocket = 30 ft.

Maximum reaction thrust = $\pm$ 600.00 lbs.

$\alpha_{max.} = +60^\circ$, $\alpha_{min.} = +5^\circ$

$\lambda = +10$

$k_g = 333.33$

All runs sought and achieved the same terminal conditions

V_f = 10,000 fps., $\zeta = 26^\circ$, $\xi = 103.5^\circ$

The normal load factor history showed no values of n (total load factor) greater than 1, so that aeroelastic effects are minimized. For the series of runs considered, to achieve comparative results, a basic run was made using the 1959 ARDC atmosphere model, and then atmospheres were considered which, at all altitudes had densities of $\rho_s/2$, $2\rho_s/3$, $3\rho_s/2$ and $2\rho_s$, wher ρ_s = standard density.

The result of this particular simulation study are shown in Figures 2, 3, 4 and 5, which present, as a function of atmospheric density and time

Geometric Altitude, h_g (Figure 2)

Sensed Temperature, T_s (Figure 3)

Angle of Attack, α (Figure 4)

Flight Path Inclination, γ (Figure 5)

For all runs, very modest amounts of reaction thrust were required once the initial transients were damped.

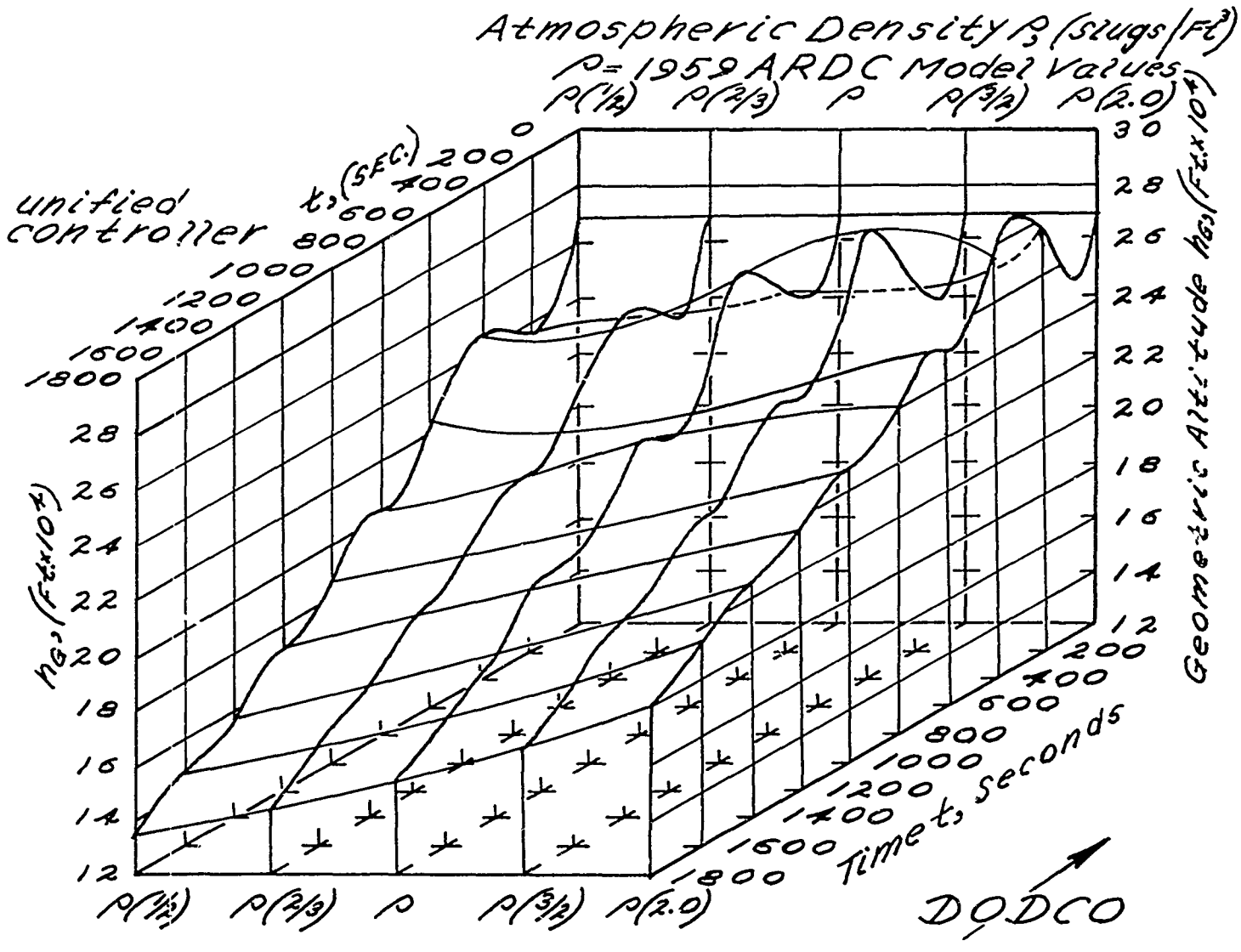


Figure 2. Altitude Vs Density and Time

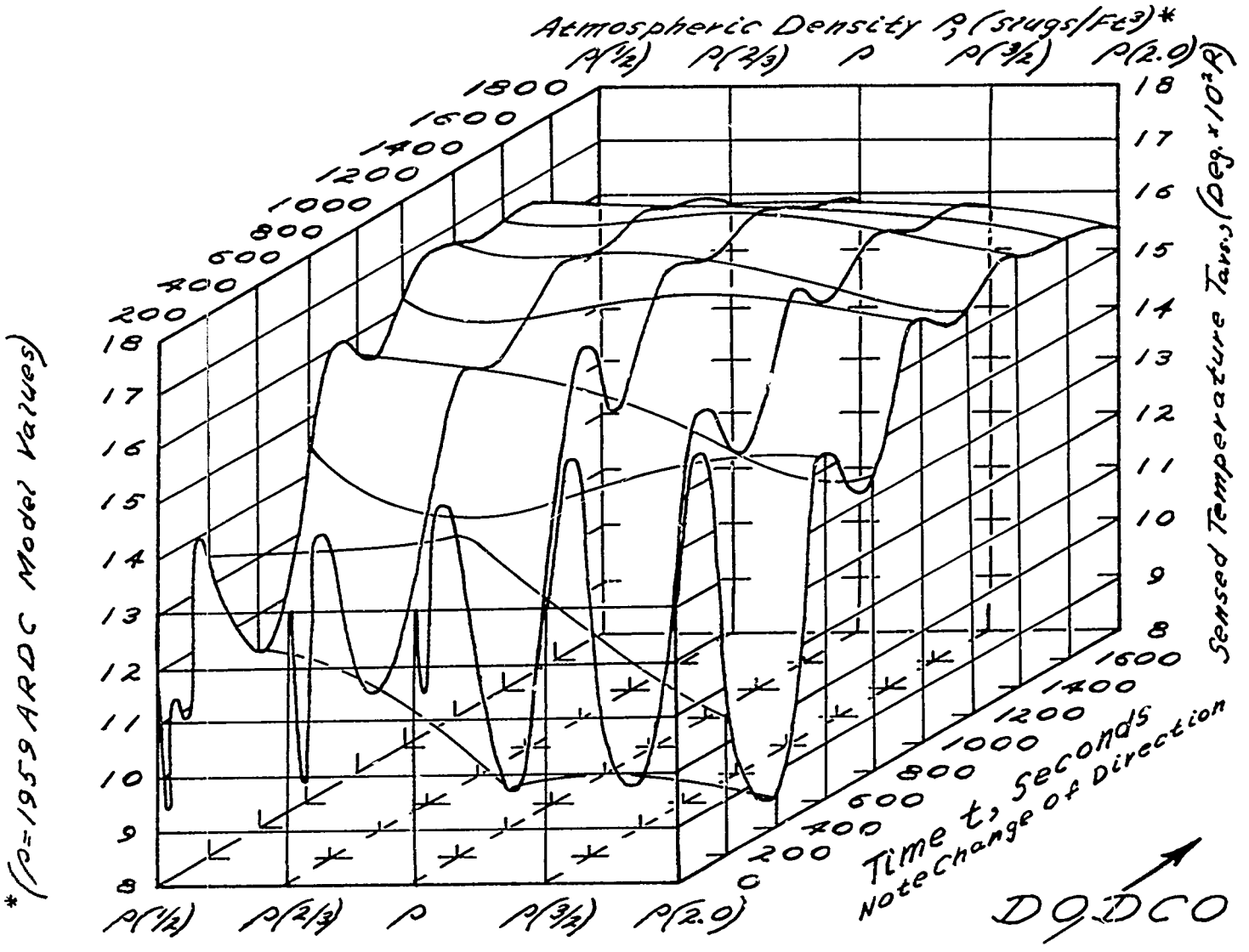


Figure 3. Sensed Temperature Vs Density and Time

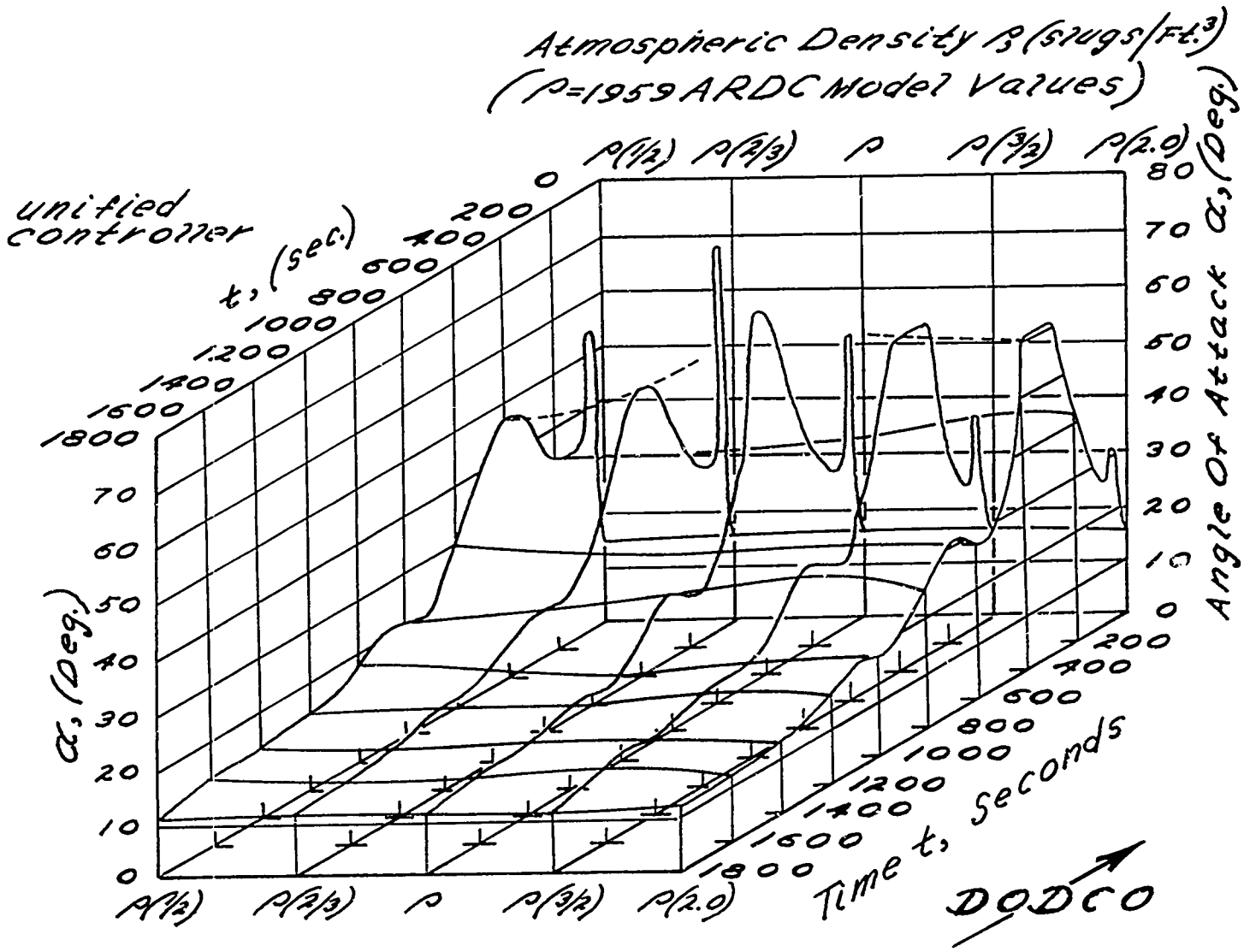


Figure 4. Angle of Attack Vs Density and Time

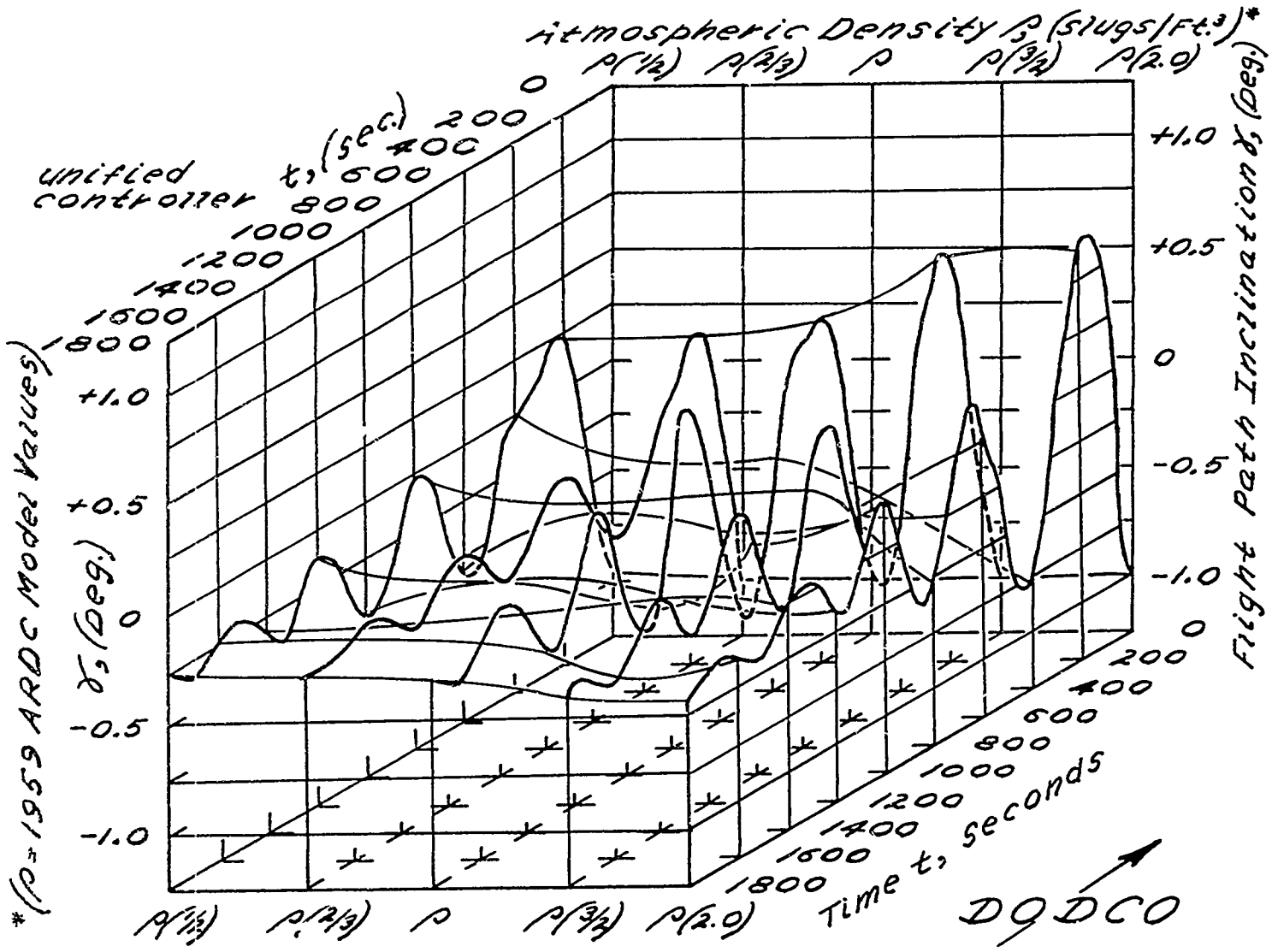


Figure 5. Flight Path Inclination Vs Density and Time

Time does not permit a more detailed discussion of the numerical data nor a presentation of auxiliary results, and we must again suggest examination of reference 3 to those interested in details.

The important item to note from examination of Figures 2 through 5 is that the trajectories obtained in the various atmospheres are not in phase with one another, and that it is quite evident that pre-programming techniques based on a preconceived notion of the environment would not have provided safe or predictable descents.

CONCLUDING REMARKS

Control of advanced flight vehicles is complicated by many factors the most important of which are the lack of really precise knowledge concerning the pressure distribution about the vehicle, its aerodynamic heating characteristics, its stability and performance parameters and the interaction of aerothermoelastic effects with the purely aerodynamic influences.

If we consider a re-entry system, we may start out with the fact that the initial attainable range is essentially infinite, and the most critical factors in determining ability to achieve a given target destination are (1) the existence of predictable in-atmospheric range regardless of atmospheric characteristics and (2) the selection of the proper point for retro-fire. The descent of the vehicle is governed by the consideration that we must dissipate a given amount of energy before achieving the target in such a way as to avoid destroying the vehicle because of overheating, excessive structural loading or by the combined aerothermoelastic influences. In addition we must utilize the minimum possible amount of control energy since the amount of fuel or accumulated energy available for control is limited by weight considerations. It is, of course, possible to convert some of the heat energy generated during the descent to provide for powering of the control system, and high efficienty semi-oxide convertors have been developed in the laboratory which might function in this fashion, however even in this case, one pays a weight penalty if large amounts of energy are to be handled.

On the basis of the analytical effort reported on herein, it appears that a unified central control system can be manufactured using existing components and relatively simple logic for the computer functions which has the capability of insuring successful descents in a poorly defined environment for vehicles whose characteristics are only incompletely specified. The system not only restrains temperature of the vehicle skin, but as well has the capacity to seek a specified target on the earth's surface. The system is conservative of control energy and minimizes structural loadings so that it has the inherent capacity to minimize aeroelastic effects. Finally the system performs no miracles, it will not, for instance, maximize range and was not designed to do this since there seems little point in striving for maximum range when one starts out with a range potential which is essentially infinite. On the other hand it does provide predictable range regardless of the atmospheric characteristics provided only that the vehicle itself meets the requirement that it has a consistent and logical response to control action.

REFERENCES

1. Minzner, R. A., Champion, K. S. W., and Pond, H. L., The ARDC Model Atmosphere, 1959, AFCRC-TR-59-267, Geophysics Research Directorate, ARCRC-ARDC-USAF, Bedford, Massachusetts.

2. Minzner, R. A., and Ripley, W. S., The ARDC Model Atmosphere, 1956, AFCRC-TM-56-204, Ibid Ref. 1.

3. Dommasch, D. O., Macro and Micro Control of the Descent of Advanced Flight Vehicles Capable of Superorbital Speeds, DODCO TR #87, November 30, 1960, prepared under Air Force Contract AF 33(616)-6117.

4. Fay, J. A., and Riddell, F. R., Theory of Stagnation Point Heat Transfer in Dissociated Air, JAS, Volume 25 No. 2, February 1958.

5. Dommasch, D. O., and Barron, R. L., The Theory and Application of Optimum Limited Information Adaptive Flight Control Techniques, WADC TR 59-468, October 1959.

FUTURE CONTROL SYSTEMS FOR VEHICLES WITH LARGE AEROTHERMOELASTIC EFFECTS

P. C. Gregory and H. M. Davis

Flight Control Laboratory
Aeronautical Systems Division

ABSTRACT

The fundamental concept of adaptive control system design practice is described and illustrated. A discussion shows how such systems function to provide constant dynamic performance in spite of changes in control gain and vehicle dynamics caused by such things as aerothermoelasticity. Applications are projected for using advanced techniques to stabilize and control the vehicle and its structural modes with a reliable increase of system performance. A summary of adaptive control techniques is presented.

FUTURE CONTROL SYSTEMS FOR VEHICLES WITH LARGE AEROTHERMOELASTIC EFFECTS

INTRODUCTION

A new philosophy of control system design has evolved in response to changing mission requirements and the increasingly greater variations in the dynamics of new aircraft and aerospace vehicles. The class of systems which results from the application of this design philosophy is called self adaptive control systems. A self adaptive flight control system is defined as one which has the capability of changing its parameters through an internal process of measurement, evaluation, and adjustment to adapt to a changing environment, either external or internal to the vehicle under control.

Before discussing the application of adaptive control systems to aerothermoelastic flight control problems, a short summary of the concepts and characteristics of self adaptation will be presented. Benefits derived from adaptive control systems can usually be placed into two categories, performance and reliability. A self adaptive technique will improve the performance of a flight control system by furnishing invariant response, or optimum handling qualities, throughout the flight regime, by automatically blending aerodynamic and reaction controls where required, by simplifying the design of outer loop functions such as angle of attack hold, automatic approach and landing, attitude hold, energy management, and by furnishing a system which can be depended upon to operate successfully on the initial vehicle flight without the requirement for adjustments based on flight testing. The last is vitally important for future space type missions. Increases in reliability are less concrete and more argumentative but are generally listed as being caused by the system simplification possible in the outer loop if the stability loop is invariant, the possibility for combining redundant systems with full operating capability in each parallel channel, and the lack of a requirement for air data in the stability loop. This last should in no

way be interpreted to mean that there is no requirement for air data on a manned vehicle since the outer loops as well as the display systems for the pilot will require it.

Frequent criticism of these systems centers around the fact that most of them require a chatter or a lightly damped excitation of the servo valve or the main power actuator. However investigations to date have indicated that the magnitude of this chatter will be no more than, and perhaps less than, that existing because of air turbulence and system noise. In addition, such disturbances are not detectable by the pilot and have had no detrimental effect in flight tests conducted to date.

Analysis of these systems is at best difficult and at the present time is carried out chiefly by a point by point linearized treatment via root locus techniques. This has proved to be very effective and several self adaptive systems designed in this manner have been operated successfully.

In all of the previous discussion the single most important feature of self adaptive systems insofar as this conference is concerned has not been mentioned but only implied. In saying that the function of a self adaptive system is to compensate for varying dynamics, it is implied that it will also compensate to some extent for unknown or unexpected variations in system parameters. The self adaptive techniques in use at the present will do this. The question is then, how unknown can the system parameters be and over what range of variation can they be compensated? To answer these questions, it is necessary to take a more detailed look at the present class of self adaptive systems.

SECTION I: HIGH GAIN SELF-ADAPTIVE SYSTEMS

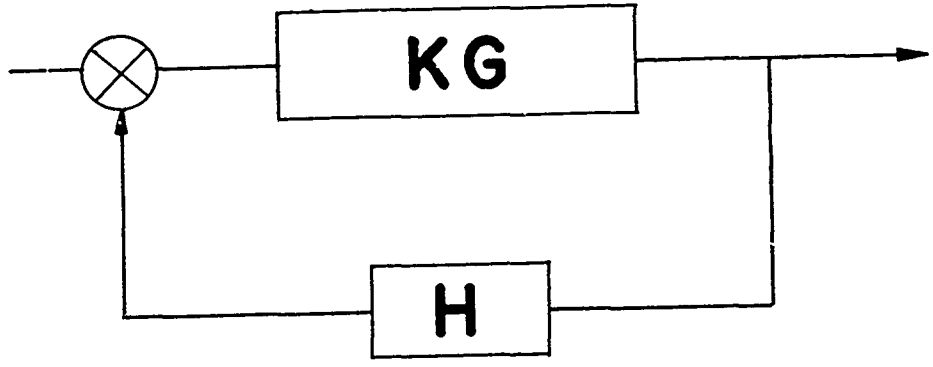
During the original self adaptive investigations sponsored by the Aeronautical Systems Division, USAF, a wide gamut of approaches was pursued to insure the success of the program. Of these approaches, the simplest and easiest to mechanize were the "high gain" systems. Therefore, these techniques have pushed to the fore and are the type that are presently being applied to weapon systems. It has long been

known via linear control theory that if the forward loop gain of a system can be made very high as shown in Figure 1, then the response of the system is dependent only upon the dynamics of the feedback.

In practice, however, because of the system non-linearities and bandwidth limitations, as the gain of the system is raised it will go unstable. Therefore the standard design practice for automatic flight control systems has been to design the system with the lowest possible value of gain consistent with the desired performance. Variations from desired performance at different flight conditions are minimized by open loop programming of inner and outer loop gains as functions of measured flight conditions (altitude, Mach, or dynamic pressure). The new design approach of the "high gain" systems is to monitor the controlled element's dynamic performance as the gain is raised until a dynamic parameter which has a priori been determined to be the first to go unstable, approaches instability. If the system has been properly designed, keeping the gain at this high value will insure acceptable and invariant dynamic response. The acceptable response is defined by an electronic model representing the desired handling qualities (e.g., those determined by Cornell Aeronautical Laboratory and published in references 1, 2, and 3) or the desired dynamic control performance of a missile. This model can be a range of values of coefficients in a second order equation which describes the relationship between stick force and normal acceleration about the axis under consideration. Typical acceptable values for the pitch axis are a natural frequency of three radians per second and a damping ratio of 0.7. The roll and yaw axes are usually represented by first order models.

This model is placed either in the feedback or as a pre-filter and then as system gain is raised the response will be forced to be almost identical to the dynamics of the model. Systems which operate in this manner have been developed by General Electric, Minneapolis-Honeywell, and Autonetics.

The system developed by the General Electric Company was flight tested in an F-106 under Navy sponsorship and subsequently tested on the X-15 simulator under Air Force



$$\frac{\dot{\theta}_o}{\dot{\theta}_i} = \frac{KG}{1+KGH}$$

if $K >> 0$

$$\frac{\dot{\theta}_o}{\dot{\theta}_i} = \frac{1}{H}$$

Figure 1. High Gain System

sponsorship. It performed very satisfactorily in both applications. A block diagram of the technique is shown in Figure 2. It should be emphasized that this figure and the following ones only illustrate the techniques conceptually; the exact details of the systems are contained in the references.

The system gain is determined by a frequency sensor which monitors the response at a particular frequency and raises or lowers the gain to maintain a pole at this frequency. This is Region A on Figure 3 which is a root locus plot of the variables. When the gain is raised the dominant aircraft pole is moved from Region C to Region B. The aircraft pole can move through a wide range in Region C but it will still be forced into Region B when the gain is raised. This represents the ability of the system to compensate for varying aircraft conditions. Handling qualities are produced by an inverse model in the feedback. For more details of these efforts and a detailed explanation of the complete system and its mechanization, see references 4, 5, and 6.

The Autonetics technique has been developed under company funds and has received some breadboard investigation on the B-70 simulator. This system (the block diagram is shown in Figure 4) is excited by a dither input and the gain is adjusted to maintain the response of the system constant at the dither frequency. Optimum response is furnished by an inverse model of handling qualities in the feedback. A root locus plot of the system would be similar to Figure 3, however, it should be emphasized that it is the amplitude of the response at the frequency ω_0 which is being measured and controlled and not the frequency itself. The details of this system are in reference 7.

The Minneapolis-Honeywell system was developed under both company and Air Force sponsorship and was flight tested in an F-101, operated on the X-15 simulator, and is presently being mechanized for flight test in the X-15, the flights starting in October 1961. Honeywell uses a saturating type non-linearity in the feed forward loop, Figure 5, which causes the system to limit cycle at a given frequency when the gain is raised. By monitoring this frequency it is possible to maintain a low amplitude limit cycle which indicates the system gain is at the optimum value. Handling qualities

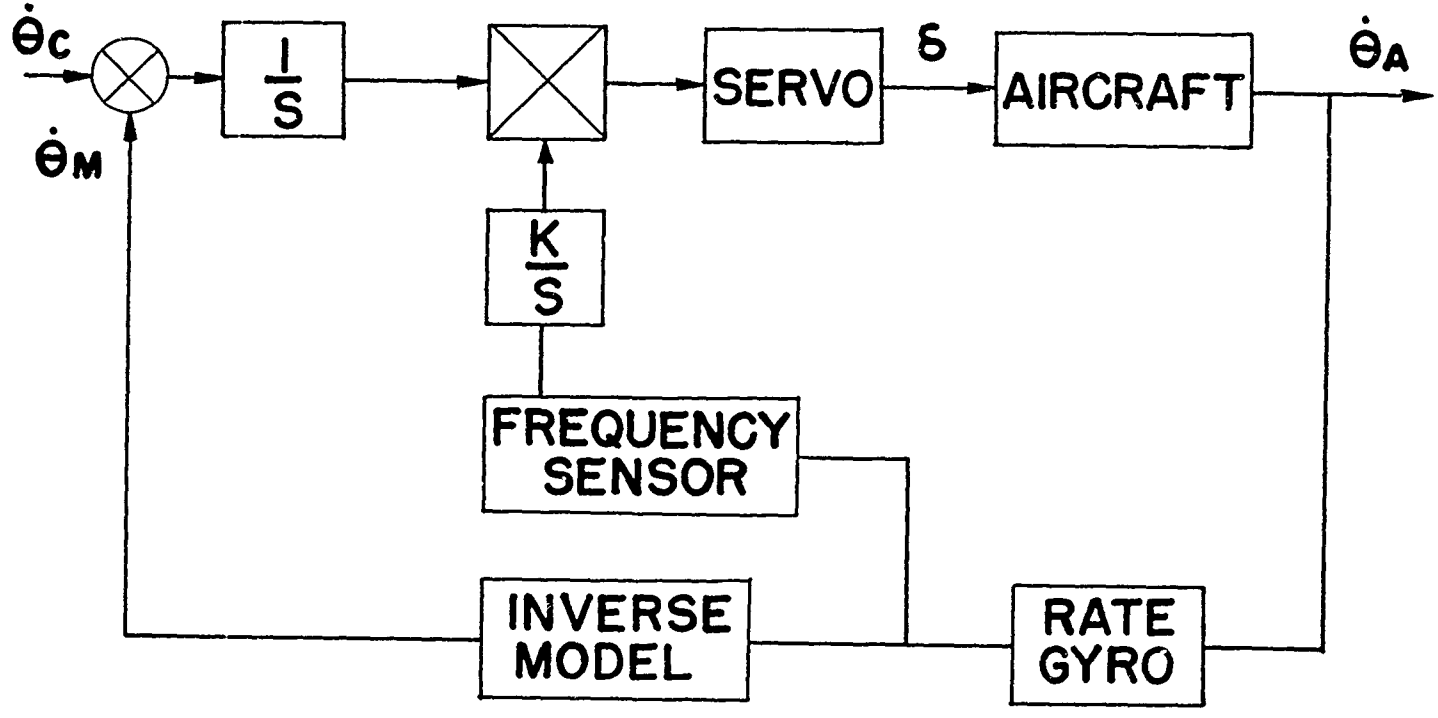


Figure 2. G, E. Technique

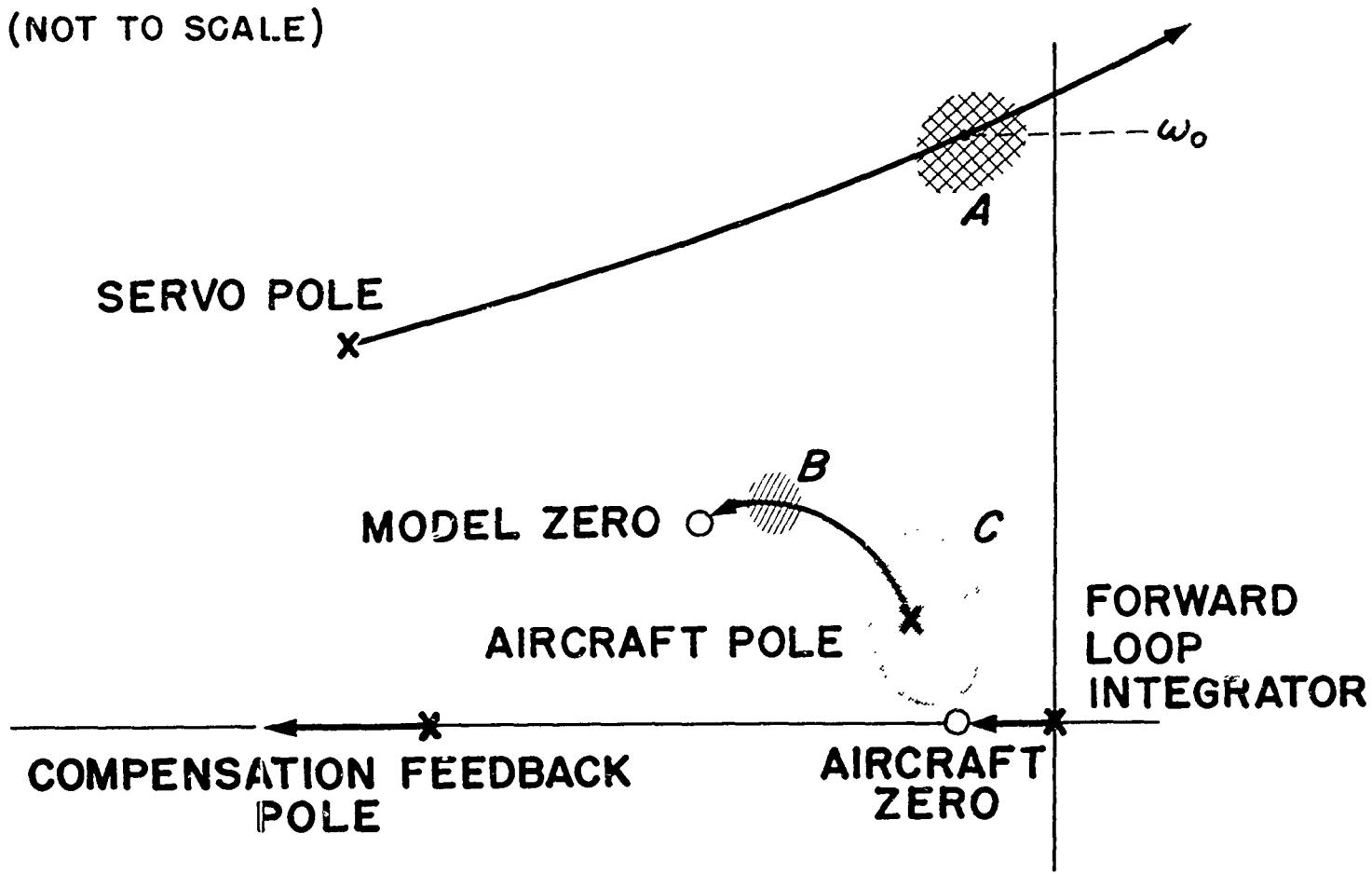


Figure 3. Root-Locus Diagram of G.E. Technique

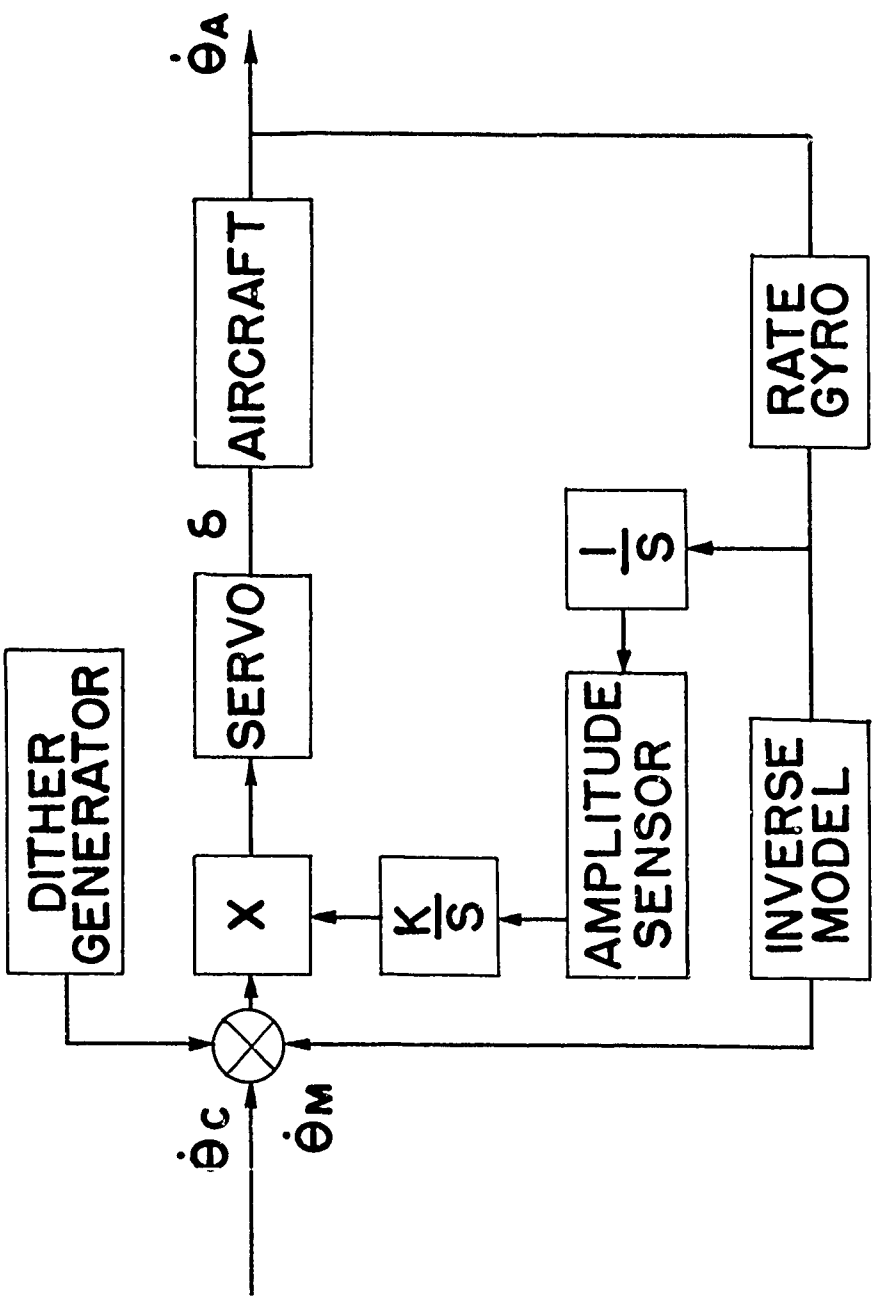


Figure 4. , :tonetics Technique

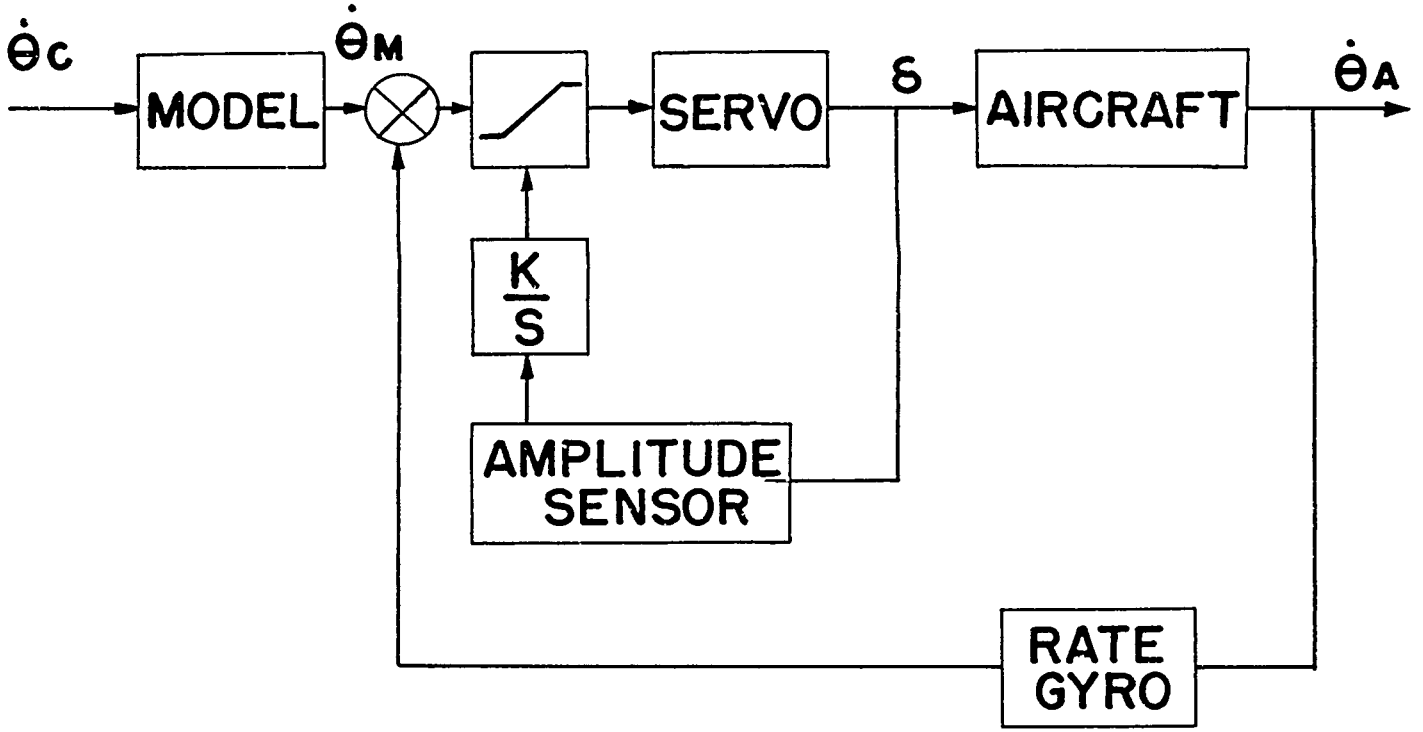


Figure 5. Honeywell Technique

are furnished by a pre-filter type of model. A root locus plot of this technique, Figure 6, appears similar to the earlier ones, however, it should be noted that the aircraft is driven into compensation zeros on the real axis rather than model zeros and that the model poles remain fixed since the model is outside the control loop. Again it is the amplitude of the oscillation at ω_o which is being monitored. The system being tested in the X-15 is a complete automatic flight control system with hold modes for angle of attack and attitude, and provisions for accepting commands from energy management or automatic approach and landing computers. For a description of this system the reader is referred to references 8 and 9.

The above techniques permit the design of an automatic control system without exact knowledge of the vehicle parameters but still require a knowledge of the form of the equations of motion and a good knowledge of the numerical values of the system dynamics associated with the sensing and actuation elements. These systems have a varying noise sensitivity and their application to control situations where structural flexibility occurs at control frequencies is greatly complicated. Nevertheless the techniques are simple and in their way quite powerful. They are established control approaches and it is our opinion that their capability to provide good control in the face of new problems such as aerothermoelasticity should be established before an attempt is made to utilize or develop a more powerful approach. At this point an examination of the application of adaptive control system techniques to aerothermoelastically effected vehicles is in order.

SECTION II: AEROTHERMOELASTIC EFFECTS

A well known example is the forward loop transfer function for pitch due to elevator input. The underlined terms in Figure 7 are normally expected to show the greatest changes in the rigid body modes due to aerothermoelasticity. The velocity dependent terms of the phugoid will certainly be effected, but for this example, these terms will be assumed sufficiently separated in frequency to be of minor importance to the stability of the pitch loop.

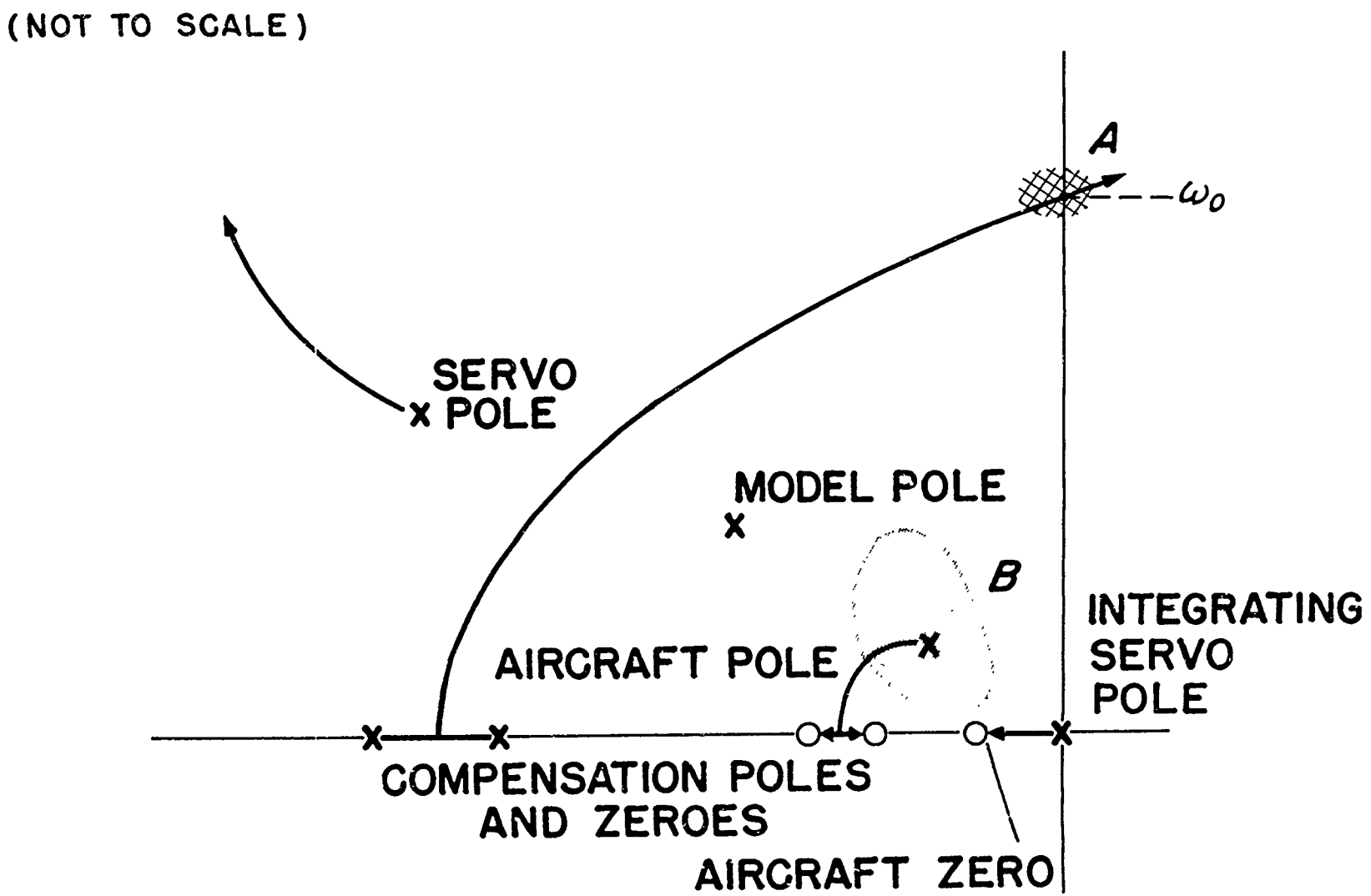


Figure 6. Root-Locus Diagram of Honeywell Technique

$$\frac{\theta(S)}{\delta_e(S)} = \frac{\underline{A_\theta}\left(S + \frac{1}{T_{\theta_1}}\right)\left(S + \underline{\frac{1}{T_{\theta_2}}}\right)}{\left(S^2 + 2\zeta_p\omega_p S + \omega_p^2\right)\left(S^2 + \underline{2\zeta_{sp}\omega_{sp}}S + \underline{\omega_{sp}^2}\right)}$$

$$A_\theta \doteq \frac{1}{2}\frac{\rho U^2 c}{I_y} C_{m_\delta}$$

$$\omega_{sp}^2 \doteq -\frac{\rho U^2 S}{2I_y} C_{L_\alpha}\left(\frac{C_m}{C_L} + \frac{\rho S c}{4m} C_{mq}\right)$$

$$2\zeta_{sp}\omega_{sp} \doteq \frac{\rho U S}{2m}\left[C_{L_\alpha} + C_D - \frac{mc^2}{2I_y}\left(C_{mq} + C_{m_{\dot\alpha}}\right)\right]$$

$$\frac{1}{T_{\theta_2}} \doteq \frac{\rho U S}{2m} C_{L_\alpha}$$

Figure 7. Forward Loop Transfer Function for Pitch Due to Elevator Input

The gain term, A_θ , forms part of the gain for the closed loop. As previously discussed control loop gain is perhaps the most important single parameter to the adaptive control system. Quite frequently there is a loss of hypersonic control effectiveness due to aerothermoelastic effects. Often the loss is nonlinear. Change in the total forward loop gain can be compensated for by the present class of high gain adjusting techniques. Variations of up to 70 to 1 in gain can be compensated for if the system dynamics and the actuator dynamics are separated by a factor of 5 or 6 and good quality sensors are used.

Existing self adaptive systems are also capable of integrating aerodynamic and reaction controls for re-entry type vehicles. They do so by turning on the reaction jets when the control system gain, for aerodynamic controls, reaches its highest value.

These systems will compensate for loss of gain or elevator effectiveness due to any cause including, for example, dynamic pressure and velocity changes, losses due to aerothermoelasticity, servo degradation, or electrical or mechanical component degradation until the moments available are below those required to stabilize the vehicle. If the above systems have large-enough reaction jets, then these systems will use them to control the vehicle after the control surfaces become ineffective due to any reason. Beyond this point there is nothing further that any flight control system can do. No automatic flight control system can operate without the ability to produce moments.

A type of system could be postulated that would recognize the source of the loss of control effectiveness as aerothermoelastic rather than loss of dynamic pressure due to leaving the earth's atmosphere (in fact a direct measure of dynamic pressure should serve for this) and cause a change in the control surfaces, such as a structural servo tab which would improve control effectiveness. This would enable the high gain type of system to compensate for greater variations in the vehicle. Of course in addition to loss of control effectiveness, divergence and reversal of controls exist. Unfortunately, the present systems do not recognize the possibility of control reversal. Possibly a way could be found

to incorporate this ability into the techniques but after all of these changes the systems would bear little resemblance to their present form.

Several problems must be carefully considered when applying the first generation of adaptive control systems. For instance, as the gain of the actuator is increased to compensate for a loss of control surface effectiveness or a change in vehicle dynamics the frequency of the control loop must stay well below that of the structural modes. In this respect the early adaptive control systems are limited by some of the same phenomena as conventional systems. This point will be re-examined in a later section.

Aerothermoelastic effects on the forward loop are also manifested by changes in pole locations as can be inferred by the approximations shown for the frequency and damping. Trends for changes in pole location are strongly dependent on configuration but typically the short period frequency is decreased by a reduction of the static margin and the lift curve slope and the damping in pitch may also be slightly less than for the rigid configuration. The aircraft zero will also be effected. An adaptive control system can accommodate a limited amount of pole wander due to any cause provided that the essential nature of the problem is not drastically altered. For example, consider a typical root locus plot for the pitch loop, such as Figure 8.

As has been previously pointed out, the servo pole must be well separated from the aircraft dynamics. If the servo root were to be reduced along a line of constant damping, as shown in Figure 8, a point will be reached where the root locus will change to that represented by the dashed lines. If the servo is reduced further the configuration will change to that of the dashed and dotted lines. It is of interest to note that regardless of which pole forms the locus which goes unstable, the cross-over point tends to be at the same frequency. This means that the techriques as described previously will continue to work but their ability to compensate for changing surface effectiveness by gain changes is sharply reduced.

This high gain type of system is also very sensitive to the location of the compensation pole at C on Figure 9. As

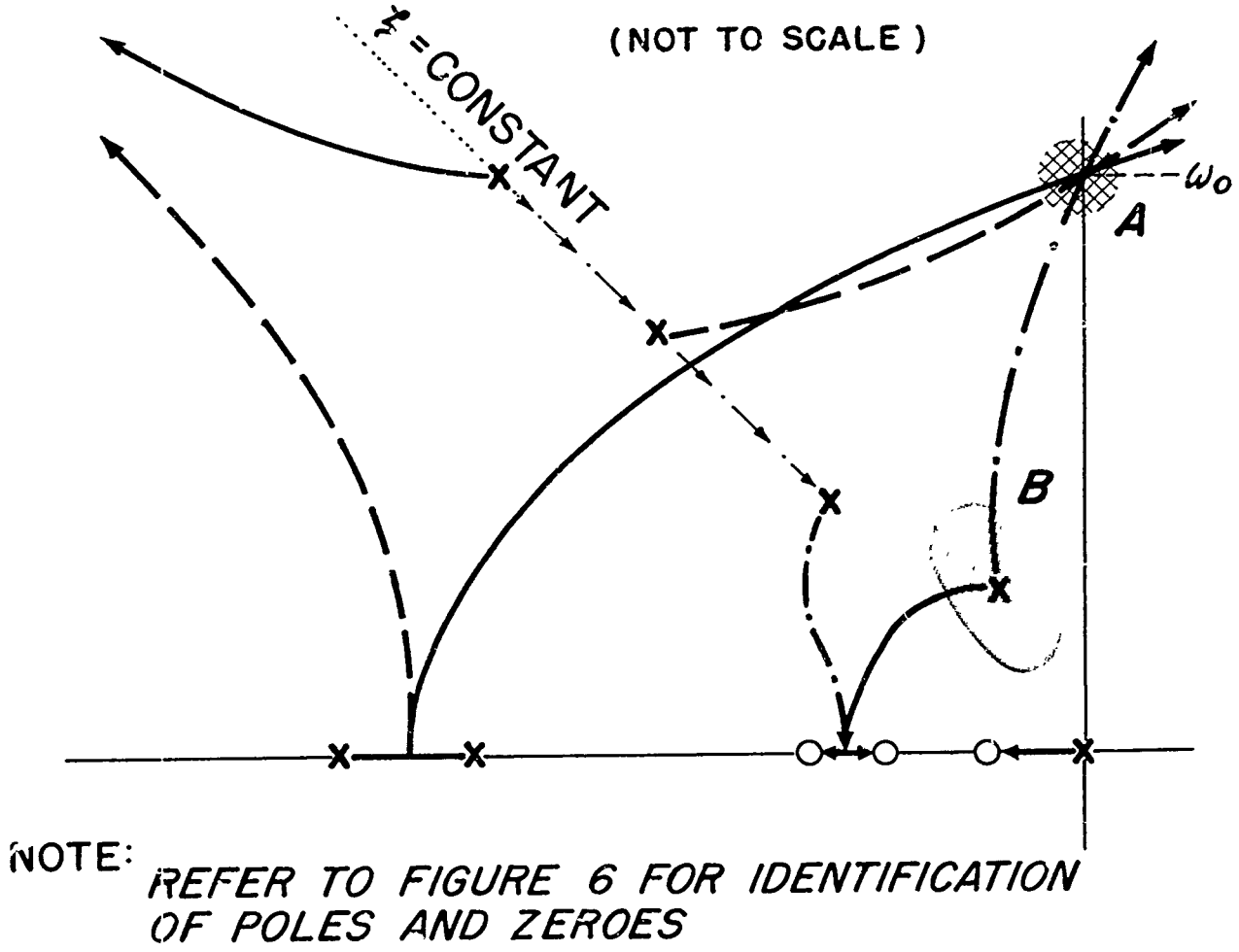


Figure 8. Root-Locus Plot for Pitch Loop Showing Effects of Reducing Servo Root Along Line of Constant Damping

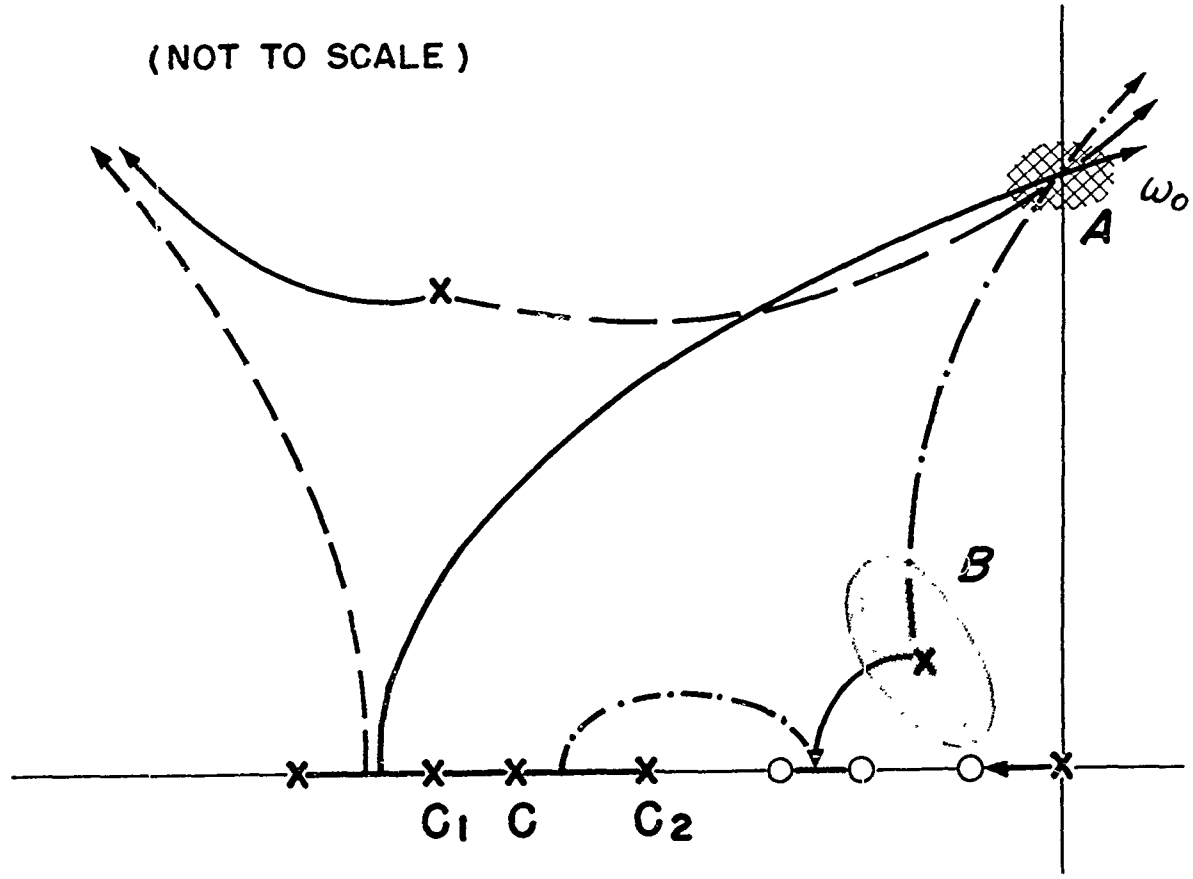


Figure 9. Root-Locus Plot for Pitch Loop Showing Effects of Location of Compensation Pole

the pole is moved to the left the result is shown by the dashed line. This results in the servo mode rather than the compensation mode being the first to go unstable. If the pole at C is moved to the right, the compensation is attracted to the zeros on the real axis and the aircraft poles form the unstable locus. This has the same effect as before, that is, a sharp reduction in the capability of the system to compensate for gain changes. However it also suggests that if intelligence were provided to the system to properly adjust the compensation pole C, then the system's capability could be extended. No known work is being done at the present to convert this from a mere postulation to an acceptable operating technique, but it is planned to investigate the possibilities of this in more detail in the near future.

It is also possible for this type of system to compensate for unstable dynamics. Regardless of whether the poles are real or complex, the general shape of the root locus is shown in Figure 10. The vehicle pole will be attracted from the right half plane to the left or stable plane while the gain is being raised. The design of this type of system must be very carefully accomplished to insure that raising the gain will stabilize the vehicle poles without driving the higher frequency structural poles unstable. This type of system has been designed for ICBM type vehicles and has been operated on simulators with considerable success. It should again be emphasized that the rigid body and structural modes must be well separated to insure the success of the high gain techniques.

With this short discussion as a background of the problems and capabilities of the present self adaptive techniques, it is now possible to consider methods which may result in a greater system capability.

SECTION III: ADDITIONAL SELF ADAPTIVE TECHNIQUES

There are several other self adaptive flight control systems in existence that have received little or no flight test or simulator mechanization but are or have been designed for flight control purposes. The techniques are listed below:

DODCO: This technique, mentioned in the previous paper, was developed through the application of variational

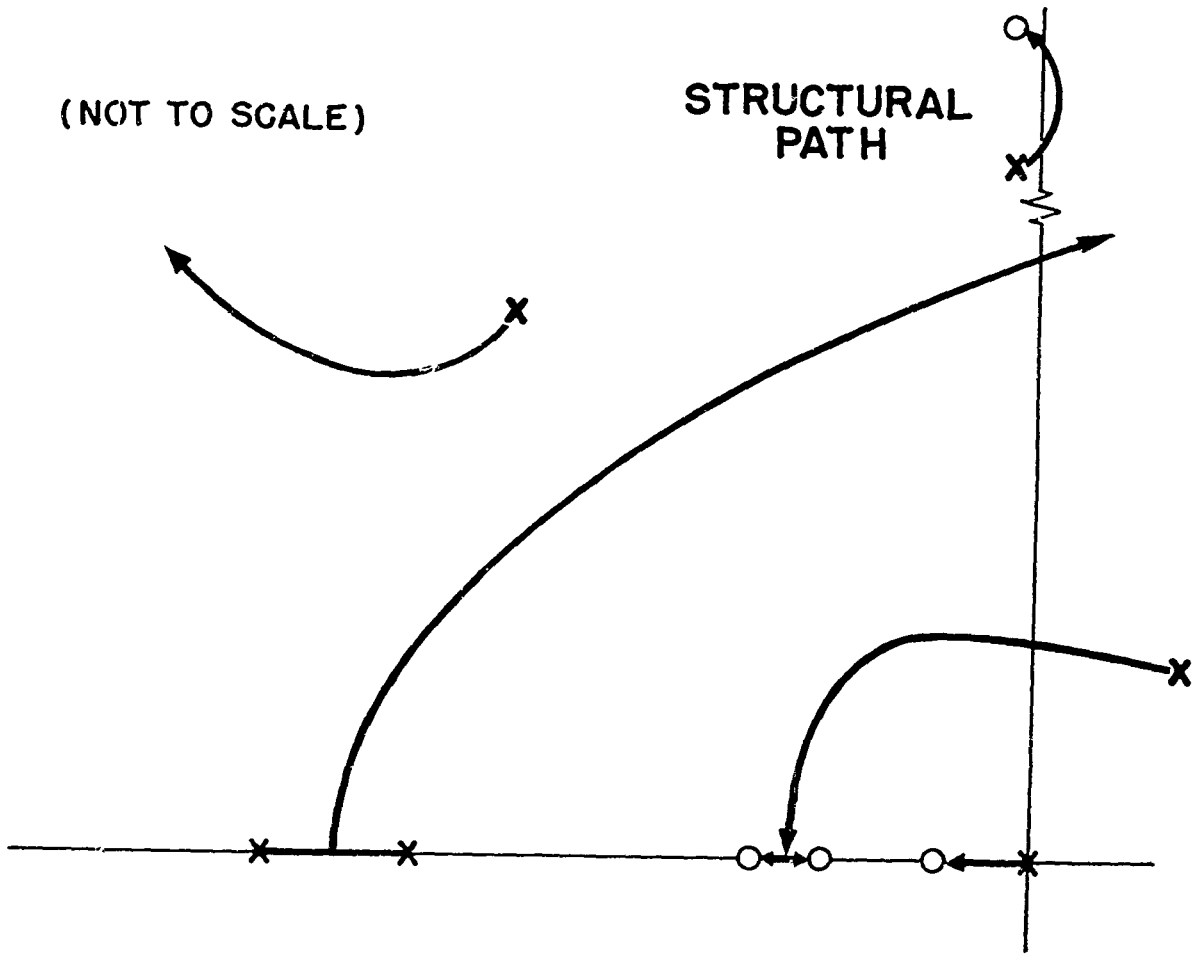


Figure 10. General Shape of Root Locus

calculus to a limited information flight control problem. A description of the application and an evaluation of the use of this technique is contained in reference 11. The system uses an error and error rate criteria to switch between two gains, one of which is greater than that required to drive the system unstable and the other is a stable value. For most applications these gains will differ from each other by approximately two. A block diagram of the system is shown in Figure 11. To properly use this system the servo must be of the rate or velocity type and the sensor associated with the highest level of information used must have a bandwidth approximately 10 times greater than the control range. This means, for example, that to operate a good pitch rate stability loop an angular accelerometer with a natural frequency of approximately 25 to 30 cps is required. This type of high gain switching system uses a pre-filter model to provide optimum handling qualities. Simulations to date indicate that if a good quality angular accelerometer is used the performance of the system will be comparable to the previous high gain techniques. The technique has not been flight tested but is being applied with good results to outer loop control.

Bendix: The Bendix system has been operated on a B-58 simulator and is presently being mechanized for flight test in an F-102. It is a digital sampled data system which operates by controlling the gain to affect error minimization at sampling instants. The system uses a pre-filter type of model. The exact details of the system are classified confidential and can be obtained from references 12 and 13.

MIT: The latest modifications to the MIT rate integrating system are described in reference 14. This system has two adjusting loops. Both the gain and damping factors are adjusted. The error adjusting scheme has been changed from a direct minimization loop to a null seeking loop which has significantly improved the performance of the system. Details of the previous system are available in references 15 and 16. The earlier system was flight tested in an F-94 and F-101 some time ago. It uses a reference model in parallelwith the system to furnish an optimization criteria.

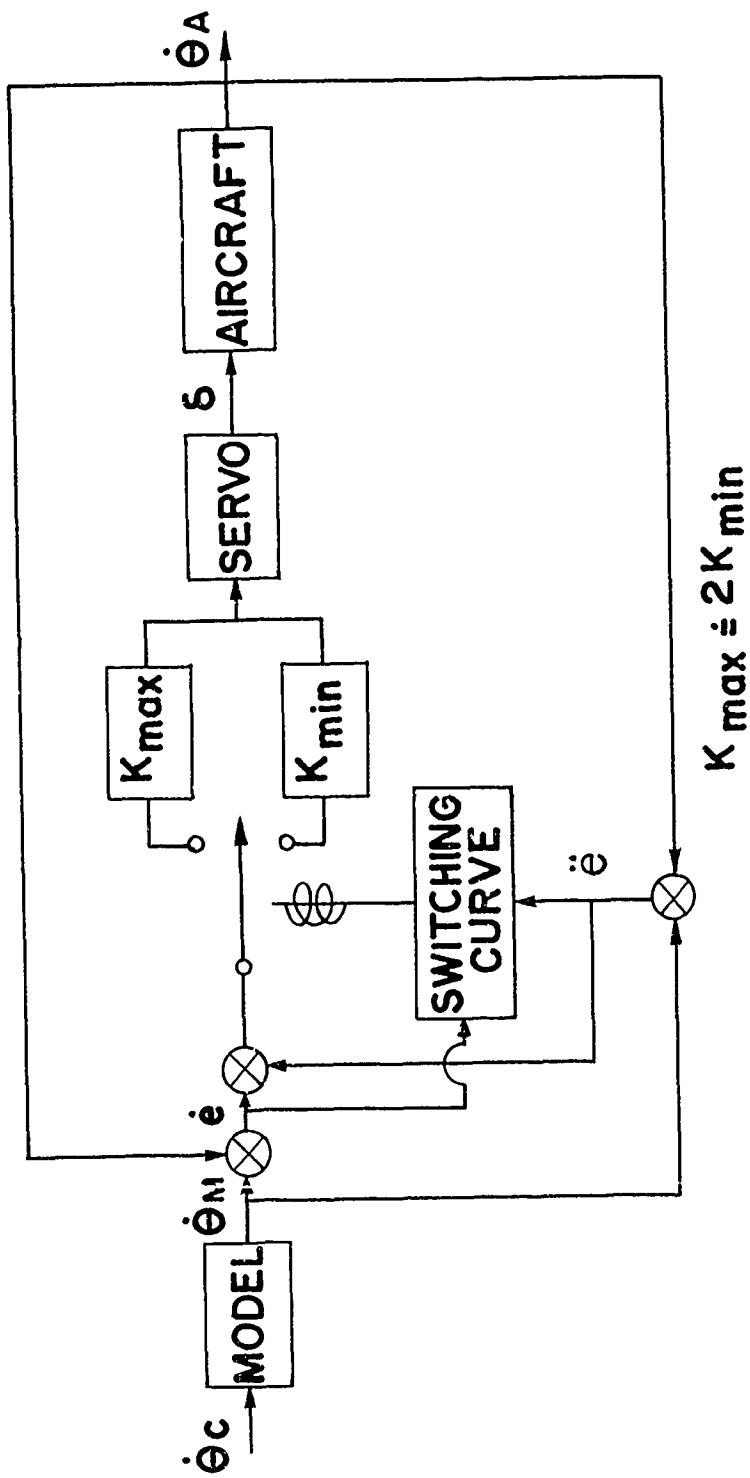


Figure 11. DODCO System

Aeronutronics: This system uses cross correlation techniques to determine the impulse response. The measuring part of the technique was flight tested in an F-100C with very good results. If the system were completed, the optimization criteria would be built into an adjusting mechanism which acts on the measured impulse response. Application of this technique has not been continued by the Air Force because of the time required to measure the response and the hardware complexity of getting the data and operating on it. A more detailed description of this system is contained in references 15 and 17.

It should be emphasized that the techniques described do not encompass all of the adaptive techniques conceived but represent the principal ones applied to the flight control area. The capabilities of the last techniques listed are largely unknown or in the process of being determined. They are listed here because, for some applications, they may have more capability to compensate for varying or unknown vehicle parameters than the high gain techniques. Later reports will more explicitly detail their capabilities.

The key to building a better or second generation self adaptive flight control system rests in the ability of the system to identify directly the value of the parameters it is attempting to vary. Present systems identify and control a parameter (gain) which is a priori related to the control system performance. A better technique must identify the value of a parameter directly connected with system performance, such as the coefficients of the equations of motion or of a higher order transfer function that reflects an approximation to the closed loop plant dynamics.

A program to devise such a system was started with Sperry, Phoenix in 1960 using correlation techniques and a recursion relationship to determine the Z-transform of the system. From this transform the system synthesizes a control program which will compensate for the identified dynamics. This type of system has the capability to identify control reversal. The capability of this type of system has not been fully established but the first report from this program should be published in December 1961. Present plans are to continue this type of investigation and expand it as methods of

identification and synthesis that are more accurate and that obtain information faster become available.

The major limitations of any parameter identification scheme are the time required to actually measure the required data and the equipment required to make the calculations. Of these two limitations, the first is considered to be the most basic and the most significant. Reference 18 states that the identification time of a sampling or cross correlator type identifier is independent of the impulse response being estimated if the system is linear and the received signal energy is large compared to the noise power density spectrum, but that it is of the order of 10 to 100 times the significant duration of the impulse response. Thus it may never be possible, due to the rapid change of significant system parameters, to use a parameter identification scheme as the sole means of control. A sudden violent instability as sometimes exhibited by flutter modes could fail a structure before the control system could act effectively. A better plan may prove to be a combination of the present fast acting high gain systems with a slower identification scheme which changes some system bias. The high gain system then acts as a vernier to insure stability.

Future efforts will look into this in more detail as more specific information regarding mission requirements becomes available.

SECTION IV: DYNAMIC INTERACTIONS

In all of the previous discussion it has been assumed that the sole effect of aerothermoelasticity is a static one and it has been carefully pointed out that structural modes must be well separated from the rigid body modes. The well recognized fact that it is sometimes impossible to clearly distinguish between aeroelastic modes and those oscillations associated with dynamic stability has led to the general acceptance of the principle, if not the actual implementation, that the complete dynamic analysis of very flexible systems should be carried out on a unified, cooperative basis. (See, for example, pg 554, reference 19) These experiences have started many control system engineers on various approaches to increase the systems tolerance for or even to utilize the effect of elasticity. Servo systems for control of flutter

have been demonstrated. Designs for optimum flight control systems involving aeroelastically tailored surfaces have been prepared. Control system designs for reducing structural loads due to aircraft and missile gust response exist now. Progress is being made in unifying the analytic approaches of the aeroelastician and the control system analyst so that mutual benefit can be more readily derived from the two different methods. It would seem possible to foresee applications of new control system developments to aerothermoelastic systems where the overall result is optimized with respect to flight path control, structural plus control system weight, power, costs, reliability, etc. Admittedly much basic work must be accomplished before this postulation can be a design reality.

Both control systems and structural engineers have been reluctant to advocate the use of an automatic system to provide artificial structural stiffness or damping. The primary reason has been the relatively low reliability of the electronic systems which have the speed of response required to make the plan feasible. Recent developments, reported on in reference 20, indicate that the reliability of electronic systems, when properly designed, can approach or exceed that of present mechanical flight control systems. This is accomplished through the use of code redundancy consisting of the transmission of more digital bits of information than are required for system operation. The additional bits are used to check and correct the required information bits and since they are not directly required to achieve desired dynamic performance, they are called redundant. The simplest example of this might be representation of a digital word by repetition of each bit of information. Thus the information 101 would be transmitted as 111000111. Then the equipment through majority logic would recognize the information as long as no more than one of the redundant bits in each information block fails. Thus 101010101 would be recognized by the system as 101, the original transmission. Note that three bits in the total word have failed. For a 100 hour mission an electronic system designed in this manner could be expected to have an equivalent reliability of 0.9998 or better. This would be an equivalent MTBF of approximately 5×10^5 hours. A present program with the General Electric Company is mechanizing such a system for verification and demonstration of these concepts.

As the "state of the art" of reliable design progresses consideration should be given to design trade offs of weight and system complexity. On some future weapon systems, for instance a Mach 3 nuclear bomber, system feasibility may depend upon automatic stabilization of the structure of a long thin vehicle. If reliability and fail-safety were assured it may be possible to avoid the weight penalties associated with reactor shielding or strengthening a structure of high fineness ratio.

In an attempt to establish a capability to avoid coupling problems, present ASD programs are working on the development of adaptive techniques which will permit separation of rigid and structural responses even at the same frequencies. A report, reference 21, describing the operation of a digital adaptive system which will decouple the rigid and elastic modes has been prepared by McDonnell Aircraft. The ability of a high gain system to control a flexible ballistic missile has been demonstrated by Minneapolis Honeywell, reference 22, and evaluated by Space Technology Laboratories on an ICBM simulator. In this case it was necessary to use multiple sensors (2), with the outputs blended to aid the system but increases in frequency tolerance and mode shape tolerance were significant. The details of the system and the evaluation are in a classified report, reference 23.

A considerable amount of work is being started by the NASA at the Marshall Space Flight Center aimed at solving the problems of flexible Saturn type boosters. Future Air Force programs can be expected to place increased emphasis on the development of these types of techniques; however, it should be emphasized that the objective of these programs at the present is not to provide damping to a structural mode but to refrain from exciting or forcing such a mode. Additional efforts will be required to develop a technique for positive control of elasticity.

The extension of self adaptive control techniques to the control of dynamic structural problems for the reduction of loads and stiffness requirements and thus weight is a natural and planned next step and a significant one for future large aerospace configurations.

SECTION V: ENERGY MANAGEMENT

The optimum path from one point to another has seldom been a simple geometric relationship. Cruise control for increasing range illustrates this point and is a form of energy management. For re-entry configurations we are faced with optimumly managing kinetic and potential energy to control dispersion, optimize range, control heating rates and total heat input, control loads, etc. The constraints on the problem are at least partially caused by the aerothermoelastic capacity of the airframe.

The proper management of the vehicle's energy within this multitude of constraints represents one of the greatest flight control problems of the future. If manned vehicles are ever to achieve even a limited maneuvering capability during re-entry, the control system must utilize a prediction capability to operate within vehicle constraints. The system must predict the future effects of a present control action before that action can be safely initiated. The previous paper has discussed many of the variables and unknowns regarding re-entry conditions and has postulated one solution using an adaptive approach. This work was accomplished under the sponsorship of the ASD Flight Control Laboratory. Several other programs are underway and more are planned for the future. Additional applications of adaptive techniques and advanced mathematical techniques such as Pontriagin's maximum principle and Bellman's dynamic programming principles will be made in an attempt to develop optimum solutions.

Previous efforts have outlined the control requirements, reference 24. Current programs with General Electric, Bendix, and Bell are attempting to develop solutions from a systems standpoint for re-entry of winged vehicles from near earth, near circular orbits with longitudinal and lateral maneuvering. Reports from these programs should be available in the near future.

SECTION VI: SUMMARY

The problems encountered during the design of flight control systems for future aerospace vehicles will be as diverse as the missions and configurations. However, a

significant improvement in performance for structurally flexible vehicles could be realized if techniques are developed for identifying the best locations for introducing control forces into structural modes and for placing redundant or multiple sensors.

Higher performance requirements have stimulated the development of self adaptive systems for the classic flight control problem. Their inherent capability for compensating for uncertainties now makes possible the development of flight control systems that will operate successfully on the first flight for research type vehicles. Increased mission requirements are lowering allowances for structural weight and thus reducing stiffness and heat capacity. Smaller design margins are inevitable. Structural dynamic response control will become an acute requirement. Adaptive techniques represent, at present, the only type of design technique which will permit compensation for changing conditions and uncertainties while meeting the dynamic performance requirements in future missions.

In general, future effort will attempt to provide methods of design and techniques of control which will permit the designer to build a better system with less knowledge of the numerical value or form of the parameters of the system. This is not to say that the designer will not use all information available as it would be foolish not to do so, but it is an attempt to permit design of a system whose successful operation is less dependent upon a priori knowledge.

REFERENCES

1. Harper, R. P., "Flight Evaluation of Various Longitudinal Handling Qualities in a Variable-Stability Jet Fighter", WADC TR 55-299, July 1955.

2. Chalk, C. R., "Additional Flight Evaluations of Various Longitudinal Handling Qualities in a Variable Stability Jet Fighter", WADC TR 57-719, Part I, March 1958, Part II, July 1958.

3. Bull, G., "Minimum Flyable Longitudinal Handling Qualities of Airplanes". Cornell Aeronautical Laboratory Report No. TB-1313-F-1, December 1959.

4. General Electric Company, Armament and Control Section, LMED, "Navy Self Adaptive Control Flight Test Evaluation", Final Report, 31 December 1960.

5. General Electric Company, Armament and Control Section, LMED, "Self Adaptive Control System Evaluation on X-15 Simulator", LMEJ 4465, 6 April 1961.

6. Farr, J. E., Hoffman, D. P., Cooper, N. R., "Evaluation of the G. E. Self Adaptive Control System on the X-15 Flight Control Simulator", WADD TR 61-81, April 1961.

7. Schuler, J. M., Chalk, C. R., Schlehorn, A. O., "Application and Evaluation of Certain Adaptive Control Techniques in Advanced Flight Vehicles", ASD TR 61-104, Volume I, 31 July 1961.

8. Smyth, R. K., "Self Adaptive System for Re-entry Glider Control", Proceedings of the 1961 NAECON Conference, May, 1961.

9. Boskovich, B., Cole, G. H., Mellen, D. L., "Advanced Flight Vehicle Self Adaptive Flight Control System", Part I Study, Part II Design, WADD TR 60-651, (CONFIDENTIAL)

10. Gregory, P. C., "Self Adaptive Flight Control Studies Applicable to Dyna-Soar", Proceedings of the USAF-NASA Joint Conference on Lifting Manned Hyper-Velocity and Re-entry Vehicles, April 1961 (SECRET)

11. Rynaski, E. G., Schuler, J. M., "Application and Evaluation of Certain Adaptive Control Techniques in Advanced Flight Vehicles", ASD TR 61-104, Volume II, 31 July 1961

12. McGough, J. G., "A Self Adaptive Flight Control System Using Sampled Data Techniques", Eclipse Pioneer Report No. A7211-136, 30 December 1959, (CONFIDENTIAL)

13. Unger, A., McGough, J., "Sampled Data Adaptive Flight Control System", Eclipse Pioneer Report SDAS-I 31 May 1961 (CONFIDENTIAL)

14. Osburn, P. V., Whitaker, H. P., Kezer, A., "New Developments in the Design of Model Reference Adaptive Control Systems", IAS Paper No. 61-39, January 1961.

15. Gregory, P. C., Editor, "Proceedings of the Self Adaptive Flight Control Systems Symposium", WADC TR 59-49, March 1959.

16. Whitaker, H. P., "An Adaptive System for Control of the Dynamic Performance of Aircraft and Spacecraft," IAS Paper No. 59-100, June 1959.

17. Aeronutronic, "A Study to Determine the Feasibility of a Self Optimizing Automatic Flight Control System", WADD TR 60-201, 30 April 1960.

18. Cooper, G. R., Lindenlaub, J. C., "Limits on the Identification Time for Linear Systems", Purdue University Report (to be published as an ASD TR), 1 February 1961.

19. Bisplinghoff, R. H., Ashley, H., Holfman, R. L., "Aeroelasticity", Addison-Wesley, Cambridge, Mass., 1955.

20. Fleck, J. J., Marx, M. F., et al, "Research and Feasibility Study to Achieve Reliability in Automatic Flight Control Systems", WADD TR 61-264, April 1961.

21. Zabarszky, John, Luedde, W. J., Wendl, M. J., "New Flight Control Techniques for a Highly Elastic Booster", ASD TR 61-231, May 1961.

22. Prince, L. T., "New Flight Control System Techniques for a Highly Elastic Booster", ASD TR 61-174, July 1961.

23. Blackburn, E. P., Nesbit, R. A., et al, "Technical Evaluation of Autopilot Proposed by Minneapolis-Honeywell for Titan II", STL/TR-60-0000-09230, 15 July 1960, (CONFIDENTIAL, LIMITED DISTRIBUTION)

24. General Electric Company, "Flight Control Study of a Manned Re-entry Vehicle", WADD TR 60-695, Volume I and II, July 1960.

SESSION III

AEROTHERMODYNAMICS

Chairman: Dr. Alfred J. Eggers, Jr.
Ames Research Center, NASA

PREVIOUS PAGE
IS BLANK

HEATING PROBLEMS OF ENTRY INTO PLANETARY ATMOSPHERES FROM SUPERCIRCULAR ORBITING VELOCITIES

Sinclaire M. Scala[1]
Space Sciences Laboratory
General Electric Company
Missile and Space Vehicle Department
King of Prussia, Pennsylvania

ABSTRACT

A brief review is given of the influence of trajectory parameters on the severity of the environmental conditions to which a vehicle in a planetary atmosphere traveling at supercircular velocities will be exposed. The governing equations for the determination of heat transfer in partially ionized gases are presented and discussed. Currently available theoretical techniques of estimating the transport and thermodynamic properties of partially ionized gases are reviewed, and inadequacies are summarized. Available theories for predicting the convective (aerothermochemical) and radiative heat transfer at superorbital flight speeds are discussed, new theoretical and experimental results are given, and suggestions for needed future work are outlined. Some estimates are given of the anticipated thermal stress levels which will be encountered during lifting re-entry from outer space. Finally, an integrated approach to the determination of the solution to the aerothermo-viscoelastic problem of supercircular flight is outlined.

---

[1]Manager, High Altitude Aerodynamics

HEATING PROBLEMS OF ENTRY INTO PLANETARY ATMOSPHERES FROM SUPERCIRCULAR ORBITING VELOCITIES

INTRODUCTION

It is well known that during hypersonic entry of a spacecraft into a planetary atmosphere, the surface of the vehicle is exposed to severe heating conditions.

In order to predict the aerothermodynamic and structural behavior of a material utilized as a thermal shield during hypersonic entry, it is necessary to examine in great detail the physicochemical processes that occur above and below the surface of the vehicle. In particular, one must be able to predict the chemical species which are formed at the surface and in the condensed phase (due to endothermic or exothermic decomposition processes), the conduction of heat into the interior, and the resulting thermal and mechanical stresses.

Initially, at the very highest altitudes, where the gas density is low, the mean free path of the ambient gas particles is considerably larger than a typical vehicle dimension and the vehicle is in the free molecular flow regime. Heat transfer to the surface then occurs by means of direct molecular collisions (thermal accommodation and surface catalysis) of the free stream particles at the surface of the vehicle. In this case, the local energy transfer at the surface depends on the vehicle speed, the local geometry, the chemical

species present in the atmosphere, the surface material and its temperature. It is noted that a complete theory for this type of interaction has been recently developed by Gilbert and Scala (Reference 1) for convex bodies during hypersonic entry into the earth's atmosphere including flight speeds up to 50,000 feet per second.

During flight at the lower altitudes, a shock wave forms, and the free stream gas is heated as it flows through the shock wave. That is, the directed kinetic energy of the particles is converted into thermal (internal) energy which is sufficient to cause dissociation and partial ionization of the gas. This hot chemically reacting gas flows around the vehicle and heat is transferred to the surface of the vehicle by means of aerodynamic and radiant heat transfer processes.

Analytical studies of this problem require a formulation of the governing equations for the conservation of mass, momentum, energy, and chemically reacting species, appropriate to the geometry of the vehicle. These conservation laws are a coupled system of nonlinear partial differential equations of high order and have split boundary conditions. This is, therefore, a formidable mathematical problem, and hence the solution to the system of differential equations must be generated by means of a high speed digital computer, such as the IBM 7090.

In addition to the complexity of the mathematics, there are additional complexities which reside in the determination of the transport and thermodynamic properties of the gases present in the viscous layer. Since, as is well known, there is a paucity of experimental data at temperatures above $5000^{\circ}R$, a theoretical treatment is also required here. Techniques for calculating these

gas properties at high temperature have been developed by a number of investigators including Scala and Baulknight (References 2 and 3), Gilmore (Reference 4), Hilsenrath and Beckett (Reference 5), Hansen (Reference 6) and Baulknight (References 7 to 9).

The determination of the hypersonic heat transfer then depends on the integration of a set of coupled nonlinear partial differential equations (Reference 10) which represent the conservation laws for the multicomponent gas mixture which flows over the surface. The problem is further complicated by the presence of heterogeneous chemical reactions such as surface catalysis, vaporization, pyrolysis, depolymerization, sublimation and surface combustion, which occur within the condensed phase and at the interface between the gas phase and the condensed phase. The effect of these physicochemical processes is to alter the local structure of the viscous layer, which in turn, produces a change in the heat transfer at the surface of the vehicle.

With regard to radiative transfer from the hot gas cap (shock layer), it has been found that four types of processes are of primary interest as radiators, and different quantum mechanical techniques are used (References 11, 12) for obtaining the absorption coefficients which are required in order to calculate the emissivity of the gas layer.

These processes include:

1. ultraviolet-visible molecular band spectra, (electronic-vibrational excitation)

2. infrared band spectra, (rotation-vibrational excitation)

3. free-free electronic continuum radiation (scattering of electrons)

4. free-bound electronic continuum radiation (electron capture)

Here again, as in the case of the gas dynamic heat transfer, the radiant heat transfer will depend critically on the density, temperature and chemical composition of the gas in the shock layer.

For entry into the earth's atmosphere, the gas consists initially of a mixture of oxygen and nitrogen molecules (except in the ionosphere) and, hence, effectively one must consider the contributions of O, O_2, N, N_2 NO, O^-, NO^+, N^+, NO_2, etc., to the aerodynamic and radiant heat transfer.

Examination of Table 1 shows that carbon dioxide is present in the atmospheres of Mars and Venus and, hence, the contributions of gaseous atomic carbon and molecular species containing carbon must also be considered in analyzing both the gas dynamic and radiant heat transfer, as well as the aerothermodynamic response of real materials (surface interaction phenomena).

Thus, for example, in the viscous boundary layer which forms over a vehicle entering the Martian atmosphere, one finds that the neutral species include O, O_2, N, N_2, C(g), CO and CO_2, whereas in the Venusian atmosphere, due to the larger free stream concentration of carbon dioxide, one expects that CN and C_2 will also be present in the shock layer. In addition, depending on the flight speed, charged particles such as C^+ will also be in the shock layer.

TABLE 1.

CHEMICAL COMPOSITIONS OF THE PLANETARY ATMOSPHERES OF EARTH, MARS AND VENUS

CHEMICAL SPECIES	MASS FRACTIONS		
	EARTH*	MARS**	VENUS***
N_2	75.4	96.30	10
O_2	23.2	-	-
CO_2	0.1	1.94	90
A	1.3	1.76	-

CHEMICAL SPECIES	ELEMENTAL MASS RATIOS		
	EARTH	MARS	VENUS
O/N	0.3086	0.0147	6.54
C/N	0.00036	0.0055	2.46
A/N	0.01725	0.0183	-

REFERENCES:

*J.A.Ratcliffe, "Physics of the Upper Atmosphere," Academic Press, 1960.

**D.J. Alderson, "Mars Atmosphere Model - II," J.P.L. Report, Dec. 1960.

***Carl Gazley, Jr., "Deceleration and Heating of a Body Entering a Planetary Atmosphere from Space," Rand Corporation Report P 955, Feb. 1957.

From the foregoing, it becomes clear that in order to predict the heat transfer rate during planetary entry, one first requires a knowledge of the undisturbed environmental conditions, including density, temperature and chemical composition as a function of altitude. One must also have a knowledge of relaxation times, reaction kinetics and thermodynamic properties in order to predict the new gas state in the plasma sheath which forms around the vehicle. Finally, one must have a detailed knowledge of the physicochemical properties of the molecules, atoms and ions in order to predict the combined radiative and convective heat transfer rate. It is noted that only after the heat transfer rate has been determined realistically, can one proceed to solve the transient heat conduction equation, determine the temperature distribution within the vehicle structure, and calculate the resulting thermal stress levels.

TRAJECTORY CONSIDERATIONS

A number of references have recently been published which treat the problem of determining the trajectories of space vehicles which enter a planetary atmosphere at supercircular speed. These include the work of Chapman (Reference 13), Lees et al (Reference 14), Grant (Reference 15), Wong and Slye (Reference 16), Hildebrand (Reference 17), Luidens (Reference 18) and Eggers and Wong (Reference 19). These analyses show that the dissipation of vehicle energy during the deceleration phases of a mission can be accomplished more efficiently by means of atmospheric braking than by use of propulsive (retro-rocket) braking.

It is noted, however, that guidance requirements become severe, since entry of the vehicle must take place in a very narrow region of the atmosphere. The extent of the region is established by defining acceptable decelerations and heating conditions. This region is called the "entry corridor" and its limits are termed the "overshoot" and "undershoot" bounds.

The "overshoot bound" is defined as that approach flight path having the least atmospheric penetration consistent with achieving sustained flight within the atmosphere. The "undershoot bound" is defined as that approach flight path that results in the deepest penetration of the atmosphere consistent with the imposed acceleration and heating limits of the vehicle and its payload. The actual depth of atmospheric penetration depends on the mode of vehicle operation during the atmospheric portion of its flight.

As pointed out in References 14 to 19, the use of lifting entry appears attractive in reducing accelerations and providing a wider entry corridor. Modulating the lift and drag can reduce the total heat load and provide an even wider entry corridor.

It is not usually possible to generalize, since the exact determination of an entry trajectory can come only from the numerical integration of the non-linear differential equations of motion. However, it is found that the aerodynamic corridor depth can be increased by increasing the maximum lift to drag ratio, increasing the loading limit, and by decreasing the entry velocity. Unfortunately, it is found that the entry corridor having favorable thermodynamic characteristics is generally smaller than the aerodynamically attainable corridors. That is, a higher lift to drag ratio acts to increase the flight time, while higher loading tends to give higher stagnation pressures, both of which result in a higher total heat transfer to the vehicle.

In passing, it is noted that the entry velocity of the planetary entry vehicle will, of course, depend critically on the flight time and the transfer orbit. The idealized minimum energy (Hohmann) trajectory to Mars would require approximately 259 days of travel time, whereas, that to Venus would require approximately 145 days. Upon making use of the vis viva integral:

$$V_{impact}^2 \approx V_h^2 + V_{escape}^2 \tag{1}$$

and utilizing the data of Table 2, Dugan (Reference 20), and Dugan and Simsic (Reference 21), one finds that the entry velocities for Mars and Venus are given by:

$$V_{impact}\,_{Mars} \approx 19,000 \text{ ft./sec.} \tag{2}$$

$$V_{impact}\,_{Venus} \approx 34,700 \text{ ft./sec.} \tag{3}$$

TABLE 2. SATELLITE AND ESCAPE VELOCITIES FOR THE NEAR PLANETS*

Planet	Satellite Velocity	Escape Velocity
Mercury	10,000 ft./ sec.	14,100 ft./ sec.
Venus	24,100 ft./sec.	34,100 ft./sec.
Earth	25,900 ft./sec.	36,700 ft./sec.
Mars	11,800 ft./sec.	16,700 ft./sec.
Jupiter	141,000 ft./sec.	200,000 ft./sec.
Saturn	85,000 ft./sec.	120,000 ft./sec.

*Reference: Handbook of Satellites and Space Travel, General Electric Co. M.S.V.D. Document No. 58SD131, April 1958.

If the flight times to Mars and Venus are reduced to 105 days and 58 days, respectively, for example, considerably more thrust is required at vehicle launch and the resulting entry velocities become:

$$V_{\text{impact}}{}_{\text{Mars}} \approx 40{,}500 \text{ ft./sec.} \quad (4)$$

$$V_{\text{impact}}{}_{\text{Venus}} \approx 55{,}200 \text{ ft./sec.} \quad (5)$$

It is clear that a shorter flight time results in a more severe entry condition.

MODEL ATMOSPHERE

Although fairly good data is available on the earth's atmosphere (References 22, 23), the situation is not as clear cut for our nearest heavenly neighbors.

Although a number of models of the Martian and Venusian atmospheres have already been proposed (References 24 to 29), the nature of these models requires a reappraisal from an important engineering viewpoint. By this is meant a critical evaluation of those physical quantities which relate to the study of planetary entry. These include the composition, temperature and density distribution.

The approach in the past has been to assume an isothermal model, or an adiabatic temperature lapse near the surface coupled with an isothermal model for the upper atmosphere. These approaches are adequate for many scientific investigations, but should be closely questioned when one considers the planetary entry of a space vehicle.

The information available on the atmosphere of Mars is probably greater than for any other planet except our own, and several monographs are available which discuss the planet in great detail as well as the nature of its atmosphere. Probably the most neglected regions of planetary atmospheres have been the outer regions. The reason is undoubtedly due to the difficulty of measurements of the regions from terrestrial observatories. The detail of information available for the surface is large enough that even surface weather charts have been constructed to demonstrate the similarity of the Martian atmosphere to the terrestrial atmosphere. It should therefore be obvious that mean atmospheric conditions at the lower altitudes are relatively well known. The composition of the atmosphere

is similarly fairly well known and general agreement can usually be found favoring a nitrogen rich atmosphere.

The situation for Venus is entirely different and the existing model atmospheres contain more speculation than observational evidence. The surface characteristics are unknown due to the ever present enveloping clouds. Recent observations would suggest a high temperature (some 600°C) in the lower atmosphere which conflicts with prior hypotheses. The surface pressure is expected to be equivalent to one or two earth atmospheres, again depending on the hypothesis selected.

The atmosphere is known to contain some CO_2 and some H_2O although the amount of the former ranges greatly with the various hypotheses. The main constituent of the Venusian atmosphere has been postulated as being either nitrogen, carbon dioxide, or argon. The effect on a planetary entry vehicle, of the possible conditions to be encountered, should certainly be investigated as it is not too likely that the present uncertainties can be resolved from terrestrial observations of the Venusian atmosphere. Such a study would enhance our ability to analyze more rapidly the results of Venusian probes. Without such a study the analysis of flight test data obtained by a Venusian probe, which has encountered conditions other than those contained in the design model, would prove laborious indeed.

In any event, the presently existing isothermal model atmospheres for Mars and Venus may prove inadequate for use in engineering design studies of the dynamical behavior of a planetary entry vehicle. The validity of this statement can be realized by a consideration of the earth's atmosphere. If one introduces an isothermal model for the earth's atmosphere, it is found that departures

from the ARDC-1959 model atmosphere are negligible below 75 kilometers. Above 75 kilometers the density values of the ARDC-1959 model are much higher than indicated by the isothermal model. That is, the isothermal model yields densities which are two orders of magnitude lower than the ARDC-1959 model at altitudes above 200 kilometers.

It is further noted that recent satellite measurements favor increasing the ARDC-1959 density values, which would further increase the discrepancy between the actual distribution and an isothermal model. The significance of these large departures from the isothermal model suggests the existence of a high temperature thermosphere above 75 kilometers. Of equal significance is the relatively small departure of the isothermal model from the ARDC-1959 model below 75 kilometers. These points therefore suggest that the isothermal models proposed for Mars nd Venus may indeed be a reasonable approximation of conditions at lower levels. However, the question now is whether or not one may expect to encounter a thermosphere in the atmospheres of Mars and Venus. Should one encounter such a condition, the effect would be to increase the density at high altitudes.

The cause of the earth's thermosphere is postulated as being due to conduction from the hot solar coronal gases, whose kinetic temperature is of the order of 100,000^{o}K at the earth's distance from the sun. If this hypothesis is correct, then it follows that the atmospheres of Mars and Venus would also contain a high temperature thermosphere.

That is, although an isothermal model atmosphere represents a reasonable approximation for the lower altitude range, at the higher altitudes the temperature probably rises (as is the case in the earth's atmosphere), and forms a high temperature thermosphere. The effect of such a high temperature thermosphere, on

any planet, is to cause an increase of density at the upper atmospheric levels which may be several orders of magnitude higher than that given by the isothermal model. Assuming that such a thermosphere exists, it follows that the isothermal model density values currently being used in calculating high altitude entry trajectories may be off by an order of magnitude or more.

GOVERNING EQUATIONS FOR CONVECTIVE HEAT TRANSFER IN A PARTIALLY IONIZED GAS

During hypersonic flight in a planetary atmosphere, the free stream gas is dissociated and partially ionized by the shock wave which precedes the vehicle. For known ambient conditions in the free stream gas (e.g., pressure, density, temperature and gas composition) one may readily determine the downstream conditions behind a detached shock wave after thermochemical equilibrium is attained. The resulting thermochemical state can be determined by solving a simultaneous set of algebraic equations known as the Rankine-Hugoniot relations.

These may be written:

$$\rho_1 V_1 = \rho_2 V_2 \tag{6}$$

$$P_1 + \rho_1 V_1^2 = P_2 + \rho_2 V_2^2 \tag{7}$$

$$h_1 + \frac{V_1^2}{2} = h_2 + \frac{V_2^2}{2} \tag{8}$$

and represent the conservation of mass, momentum and energy across a normal shock wave, respectively. Equations (6), (7) and (8) relate the density ρ, the gas velocity V, the pressure P and the enthalpy h at the upstream location 1 to the downstream location 2. In order to solve this system of algebraic equations, one must introduce the equation of state which can be written:

$$P = \rho \frac{R}{\overline{M}} T \tag{9}$$

where R is the universal gas constant and $\bar{M}$ is the mean molecular weight of the gas.

The chief difficulty in solving this set of equations resides in the fact that in a chemically reacting gas the enthalpy h and the mean molecular weight $\bar{M}$ depend on the gas composition. The latter depends on the pressure and temperature which are unknowns. Thus, in order to proceed, one requires a knowledge of the equilibria of the resulting gaseous system downstream of the shock wave, and hence an appropriate set of equilibrium constants must be introduced in order to form a closed system of equations. Since the various K_p functions are single-valued functions of the temperature, the major difficulty in this problem, which arises from the dependence of the gas properties on the gas composition, may be successfully treated by means of an iterative technique.

By way of illustration, if one considers partially ionized nitrogen, which consists of the four species N_2, N, N^+ and e^-, then the simultaneous use of Dalton's law, the equilibrium constants given in Figure 1, and the assumption of "no charge separation" yields the variation of equilibrium gas composition with temperature shown in Figure 2.

Once the planetary atmosphere has been established and the alteration in the ambient free stream conditions has been determined from solutions of the normal shock equations, attention may be focussed on the prediction of the heat transferred to the vehicle during entry. Although, under certain circumstances, there may be a coupling between the fluid dynamic and radiative heat transfer processes, the phenomena will be discussed in terms of the basic physicochemical constructs appropriate to each.

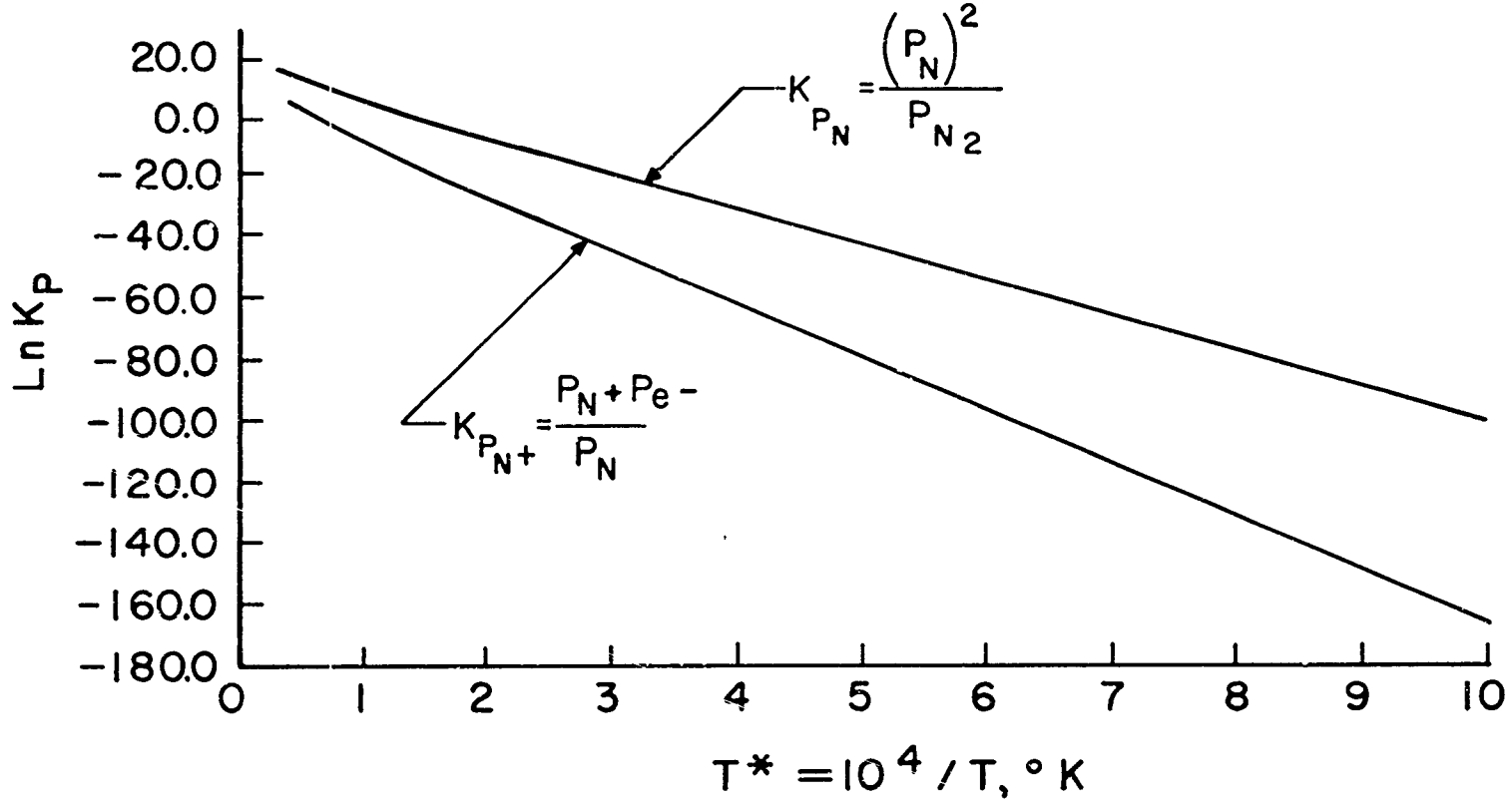


FIGURE 1

EQUILIBRIUM CONSTANTS FOR DISSOCIATION AND IONIZATION OF NITROGEN, $N_2 \rightleftharpoons 2N$; $N \rightleftharpoons N^+ + e^-$

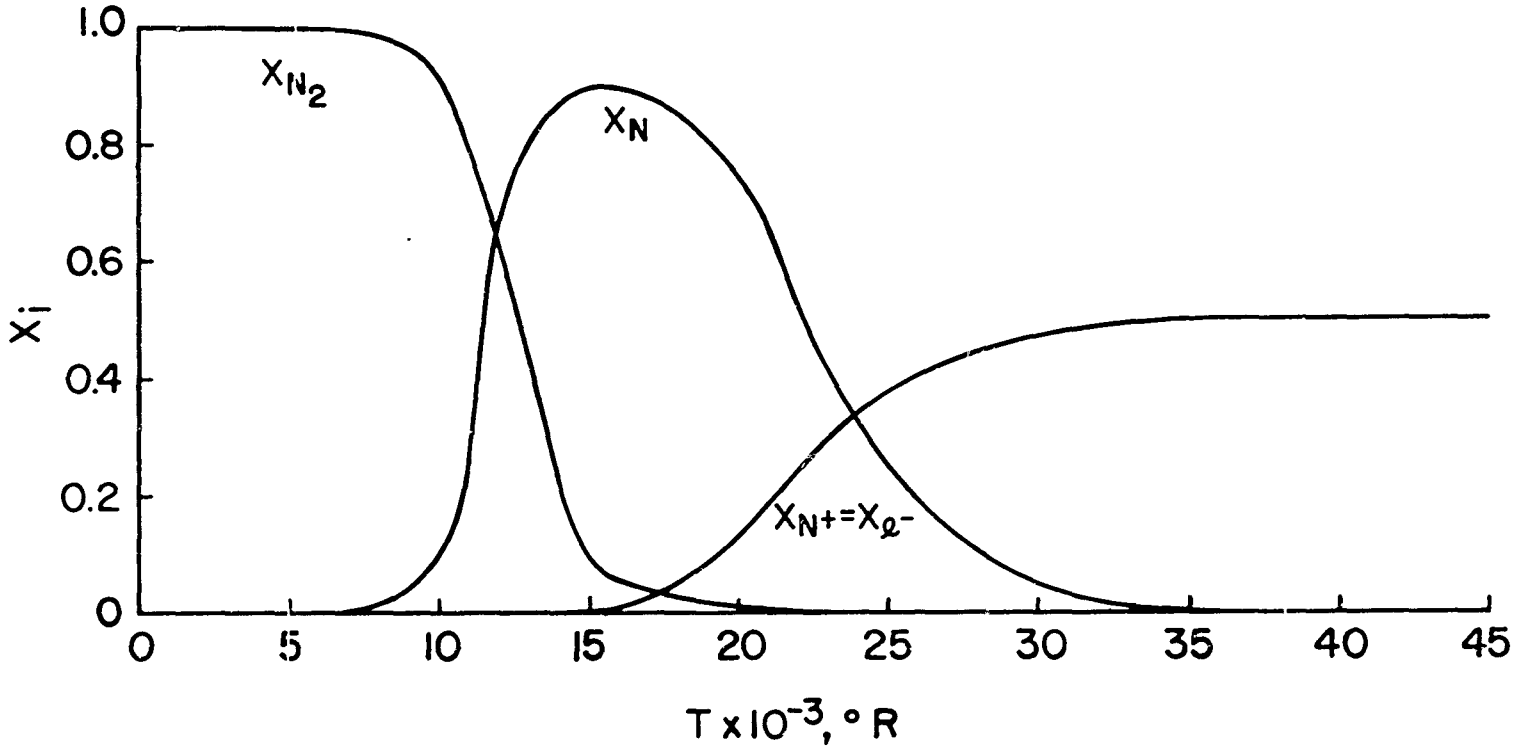


FIGURE 2

MOLE FRACTIONS vs TEMPERATURE
FOR 4-COMPONENT NITROGEN
(PRESSURE=1 ATM, NO CHARGE SEPARATION)

Let us first proceed to list the governing fluid dynamic equations, which may be written compactly in vector notation. Note that the following conservation equations are appropriate for the analysis of heat transfer in both the continuum and quasi-continuum (low Reynolds number) regimes.

Conservation of Mass

$$\frac{\partial \rho}{\partial t} + \nabla \cdot (\rho \vec{v}) = 0 \tag{10}$$

Conservation of Chemical Species i

$$\frac{\partial \rho_i}{\partial t} + \nabla \cdot (\rho_i \vec{v}_i) = \dot{w}_i \tag{11}$$

Conservation of Momentum

$$\rho \frac{d\vec{v}}{dt} = \nabla \cdot \underset{\sim}{\tau} + \sum_i \rho_i \vec{F}_i + \rho_e \vec{E} + \vec{j} \times \vec{B} \tag{12}$$

Conservation of Energy

$$\begin{aligned} \rho \bar{C}_P \frac{dT}{dt} &= \frac{dP}{dt} + \nabla \cdot (K \nabla T) + \Phi \\ &+ \frac{j^2}{\sigma} - \sum_i \rho_i C_{Pi} \vec{V}_i \cdot \nabla T - \nabla \cdot \vec{Q}_{Rad} \\ &+ \frac{RT}{n_t} \sum_i \sum_{j \neq i} \frac{n_j \bar{D}_i}{M_i D_{ij}} (\vec{V}_j - \vec{V}_i) \\ &+ \sum_i \rho_i \vec{V}_i \cdot \vec{F}_i - \sum_i \dot{w}_i h_i \end{aligned} \tag{13}$$

In addition, when the gas is ionized, one has the Maxwell equations,

$$\nabla \times \underrightarrow{B} = \frac{4\pi\mu}{C} \underrightarrow{j} \tag{14}$$

$$\nabla \times \underrightarrow{E} = -\frac{1}{C} \frac{\partial \underrightarrow{B}}{\partial t} \tag{15}$$

$$\nabla \cdot \underrightarrow{B} = 0 \tag{16}$$

$$\nabla \cdot \underrightarrow{E} = 4\pi e \tag{17}$$

and Ohm's Law:

$$\underrightarrow{j} = \sigma \left[\underrightarrow{E} + \frac{1}{C} (\underrightarrow{V} \times \underrightarrow{B}) \right] \tag{18}$$

It is noted that one must consider this complete system of equations because the gas may contain many chemical species including O, O_2, N, N_2, CO, CO_2, C(g), etc., and further, depending on the entry velocity, the gas may be not only dissociated, but also partially ionized. It is seen that apart from differences in the transport and thermodynamic properties (to be discussed in the following section), there are significant differences in the governing equations, when compared with those utilized by other investigators in the past, for studies of dissociated gases.

The major complication is due to the diffusion velocity. In a multicomponent gas, diffusion depends on interactions (collisions) between all species which are present, and hence Fick's law, which is an excellent representation in a binary mixture, no longer applies. Thus, in a gas consisting of N chemical species, one requires N-1 diffusion equations [of the form of Equation (11)]. Further,

although the binary diffusion coefficients are symmetric, the multicomponent diffusion coefficients are not, hence $N^2 - N$ diffusion coefficients are required.

It is noted that if charge separation occurs, then the divergence of the local electric field intensity $\underrightarrow{E}$ depends on the local net charge in the gas ϱ, (Equation 17). This phenomenon gives rise to the force $\varrho \underrightarrow{E}$ appearing in Equation (12). If no currents flow in the ionized gas, the only dissipative mechanism present will be the ordinary viscous dissipation term. In general, however, electrical dissipation known as ohmic heating should be included; this is given by the j^2/σ term appearing in the energy equation, [Equation (13)].

The effects of chemical reactions such as dissociation, ionization, recombination, deionization appear directly in the diffusion equations and energy equation through the chemical source term $\dot{w}_i$, where the enthalpy of species i is given by

$$h_i = \int_{T_{ref.}}^{T} C_{p_i} dT + \Delta h_{f_i}^{o} \qquad (19)$$

Here, C_{p_i} is the specific heat of the i^{th} species and $\nabla h_{f_i}^{o}$ is the chemical heat of formation. The effects of the chemical reactions appear indirectly in the altered transport and thermodynamic properties of the mixture, which is reflected in altered values of the Prandtl and Lewis numbers. Note further, that the coupled radiative effects appear directly in the energy equation in the term $\nabla \cdot \underrightarrow{Q}_{Rad}$.

TRANSPORT AND THERMODYNAMIC PROPERTIES OF PARTIALLY IONIZED GASES

As noted earlier, the transport and thermodynamic properties of the gaseous mixture must be known first, if meaningful theoretical calculations of the heat and mass transfer rates at the vehicle surface are to be performed in the continuum and quasi-continuum flight regimes. Since the properties of the gaseous mixture are not only temperature dependent but also composition dependent, they are not known a priori, and must be calculated during the solution of the viscous layer problem. Therefore, one must first calculate the properties of the pure species, and then store these data in the memory of the electronic computer which can then calculate the properties of the gas mixture in terms of the local gas composition and local gas temperature, in the viscous layer.

The required transport properties of the pure species include the viscosity coefficients, the self diffusion coefficients (required for the computation of the thermal conductivity), and the binary diffusion coefficients (required for the computation of the multicomponent diffusion coefficients and the viscosity of the mixture). The thermodynamic properties of the gaseous mixture are also composition and temperature dependent, hence, here also, one must first calculate the specific heats and enthalpies (including chemical heats of formation) of the pure species as a function of temperature.

Thus, for a gas consisting of N chemical species, one requires a total of $(N^2 + 3N)/2$ transport properties and 2N thermodynamic properties.

As the free stream gas is heated from its initial state to temperatures of the order of $10,000^{\circ}K$, the composition changes from a mixture of molecules, by means of a sequence of chemical reactions, to a mixture of molecules and

atoms, and then to a mixture of atoms, ions and electrons. At the moment, the first transition to atoms and molecules has been treated extensively, and it would appear that the high temperature transport and thermodynamic properties of neutral particle interactions are reasonably well understood. The higher temperature regime, or second transition, is somewhat less certain.

Actually, the transport and thermodynamic properties are each determined in a different manner, and hence the uncertainties in the calculated results for both are also different. The transport properties may be calculated utilizing kinetic theory, which requires the experimental determination of certain molecular properties (collision cross-sections). The thermodynamic properties may be calculated using statistical mechanical theory which requires certain spectroscopic observations. While molecular spectroscopy has been developed over the years and has become a basic research tool, and hence much useful experimental data is available, very little useful experimental work has yet been done on the development of crossed-beam techniques which can yield experimental data on cross-sections in the range of energies of interest, for the atoms and ions of interest.

Thus, although the predicted thermodynamic properties are reasonably correct (in agreement with experimental data) at high temperatures, it has been estimated that the transport properties of dissociated gases may be in error by as much as fifty percent at temperatures above 5500^{o}K, (Reference 30). This would result in uncertainties in the resulting heat transfer predictions of approximately twenty-five percent, (Reference 3).

In treating a system in which a second transition occurs, one must in some way analyze the problem in terms of interaction potentials which are realistic for atom-ion, atom-electron, ion-ion, ion-electron and electron-electron

encounters. Unfortunately, as already noted, there is a paucity of information, either experimental or theoretical, on these collision phenomena.

Some high velocity scattering work has been done on mixtures of helium and nitrogen, and argon and nitrogen, for the purpose of determining the potential of $N_2 - N_2$ interactions, (Reference 51). These data were obtained at high energies (of the order of 500-2100 ev) and certain correlation equations were used to relate the $H_e - N_2$ potential to the $N_2 - N_2$ potential. Throughout the literature, there are reports of charge transfer cross-sections, e.g., for reactions of H^+ in H_2, or ionization cross-sections measured for ions, (K^+). Most, if not all, of the cross-sections have been determined at energies corresponding to hundreds of electron-volts (i.e. beyond the range of interest).

Since experimental data are lacking, one is justified in utilizing theoretical techniques of estimating the necessary cross-sections and hence the collision integrals for atom-ion-electron interactions. The various transport coefficients can then be calculated in terms of such integrals, and the thermodynamic properties computed using the formulas of statistical mechanics including the effects of electronic excitation.

Ideally, all possible interactions in the computation of the transport and thermodynamic properties should be considered. This becomes quite involved theoretically and almost impossible experimentally. It will be assumed here that the system under investigation is sufficiently dilute so that all interactions of interest (both neutral and charged) involve encounters between like (self) or dissimilar (binary) pairs of particles. Hence, if we let the symbols A and M denote any atomic and any molecular species respectively, then we find that there are sixteen basic types of encounters. As shown in Table 3, there are

TABLE 3.

INTERMOLECULAR ENCOUNTERS RECOMMENDED FOR

DETERMINATION OF TRANSPORT PROPERTIES

IN HIGH TEMPERATURE GASES

CHARGE	SPECIES	TYPE	APPROPRIATE POTENTIAL FUNCTION ¢
Neutral	M	Self	Buckingham Exponential 6
	A	Self	"Squishy" Sphere
Charged	A^+, M^+	Self	Shielded Coulombic Repulsion
	e^-	Self	Shielded Coulombic Repulsion
Neutral	M+A	Binary	"Squishy" Sphere
	A+A	Binary	"Squishy" Sphere
Charged	$M+A^+$	Binary	Charge Induced Dipole
	$M+M^+$	Binary	Charge Induced Dipole
	$M+e^-$	Binary	Charge Induced Dipole
	$A+A^+$	Binary	Charge Induced Dipole
	$A+M^+$	Binary	Charge Induced Dipole
	$A+e^-$	Binary	Charge Induced Dipole
	A^++M^+	Binary	Shielded Coulombic Repulsion
	$A^+ e^-$	Binary	Shielded Coulombic Attraction
	M^++e^-	Binary	Shielded Coulombic Attraction

five different intermolecular potential functions which are suggested as being appropriate to the mathematical description of these interactions, including the Buckingham exponential 6, "squishy" sphere, shielded coulombic repulsion, charge-induced dipole and shielded coulombic attraction. It should be noted that for the potential function involving coulombic attraction the use of a rigid sphere "cut-off" may be introduced in order to prevent the physically untenable situation of the passage of one charged particle through another due to the short-range attractive forces. Note that although the Lennard-Jones 6:12 potential function had been used in earlier studies, it is being superseded by the Buckingham exponential six because the latter is believed to be somewhat more representative at higher gas temperatures.

The transport properties can be described by the distribution function $f_i^{(1)}(\underrightarrow{r}, \underrightarrow{P}, t)$ which is the solution to the well known Maxwell-Boltzmann integro-differential equation.

$$\frac{\partial f_i^{(1)}}{\partial t} + \frac{1}{m_i}\left(\underrightarrow{P_i}\frac{\partial f_i}{\partial \underrightarrow{r}} + \underrightarrow{X_i}\frac{\partial f_i}{\partial \underrightarrow{P_i}}\right) = \sum_j \left(\Gamma_{ij}^{(+)} - \Gamma_{ij}^{(-)}\right) \qquad (20)$$

The right hand side of Equation (20) accounts for the collision processes occurring between the components of the system. The Maxwell-Boltzmann equation may be solved by means of the Enskog (perturbation) technique which ultimately reduces the equations to linear integrals and finally to a set of linear algebraic equations. Chapman and Cowling (Reference 32) and Hirschfelder, Curtiss and Bird (Reference 33) have shown that the coefficients of these algebraic equations may be expressed as definite integrals, $\Omega^{(1,s)}$. Recently, Cohen, Spitzer and Routly (Reference 34), derived a modified equation which they considered more appropriate for inverse square forces, and treated the distant encounters by means of the Fokker-Planck equation.

Following the Hirschfelder, Curtiss and Bird technique (Reference 33) the omega integrals from which the various transport coefficients may be computed are expressed as:

$$\Omega_{ij} = \sqrt{\frac{2\pi kT}{\mu_{ij}}} \int_0^\infty \int_0^\infty e^{-V^2} V^{2S+3} (1-\cos^l X)\, db\, dV \tag{21}$$

or

$$\Omega^{(1,s)} = \sqrt{\frac{kT}{2\pi\mu}} \int_0^\infty e^{-V^2} V^{2S+3} Q_{(g)}\, dV \tag{22}$$

where the angle of deflection X is a function of the relative velocity (g) and the impact parameter (b) expressed as:

$$X(g,b) = \pi - 2b \int_{r_m}^\infty \frac{dr}{r^2 \sqrt{1-b^2/r^2 - 2\phi(r)/\mu g^2}} \tag{23}$$

and the cross-section is:

$$Q^{(1)}_{(g)} = 2\pi \int_0^\infty (1-\cos^l X)\, bdb \tag{24}$$

The important considerations involved in the computation of the transport properties using the $\Omega^{(1,s)}$ integrals center around the choice of the interaction potential $\phi(r)$, and the particular choice of Q values used. Interactions involving charged particles are characterized by long range coulombic forces, and hence it is found that the cross-sections computed utilizing Equation (24) diverge at the upper limit if taken to infinity. This is due to the dominant electrostatic forces which vary as $1/r^2$ and hence the potential diminishes with distance more slowly than do forces between neutrals. This, of course, would tend to make it difficult to define binary encounters unless a "cut-off" is introduced.

In the ensuing analysis, it will be assumed that in determining the effect of ionization on stagnation point heat transfer, one may treat the gas as a four component mixture of partially ionized nitrogen. Consequently, in Figure 3 are given the specific heats of the three species N, N_2 and N^+ as a function of temperature, (Reference 4). Note that the specific heat of the electron is a constant, i.e., 9,120 BTU/lb.$^{\circ}$R. The enthalpies follow directly by substitution into Equation (19), and integration. (See Figure 4).

In calculating the transport properties of the pure species, certain simplifications were introduced. Thus, for the moment, until the transport properties of the pure species corresponding to Table 3 become available, the rigid sphere and Lennard-Jones 6:12 model were utilized for the neutral interactions. Otherwise the potential functions given in Table 3 were utilized. (It is noted that for the moment the rigid sphere cut-off was not utilized with the shielded coulombic potential.) For the appropriate equations for the transport properties of the pure species, see for example Reference 33.

The results of the computations are shown in Figures 5 through 7. Note that those properties marked with an asterisk are composition dependent even for the pure species, (unlike neutral encounters). For other recent suggested theoretical approaches see Reference 35 and 36.

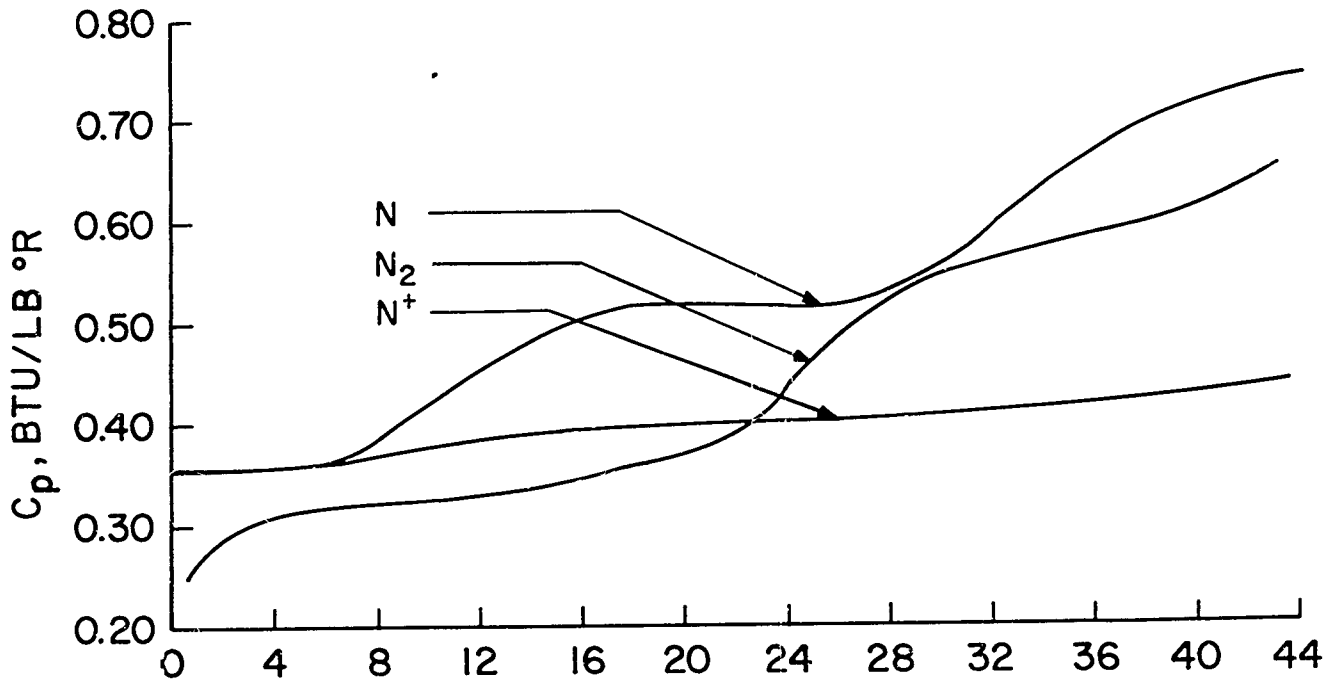


FIGURE 3

SPECIFIC HEAT VS TEMPERATURE

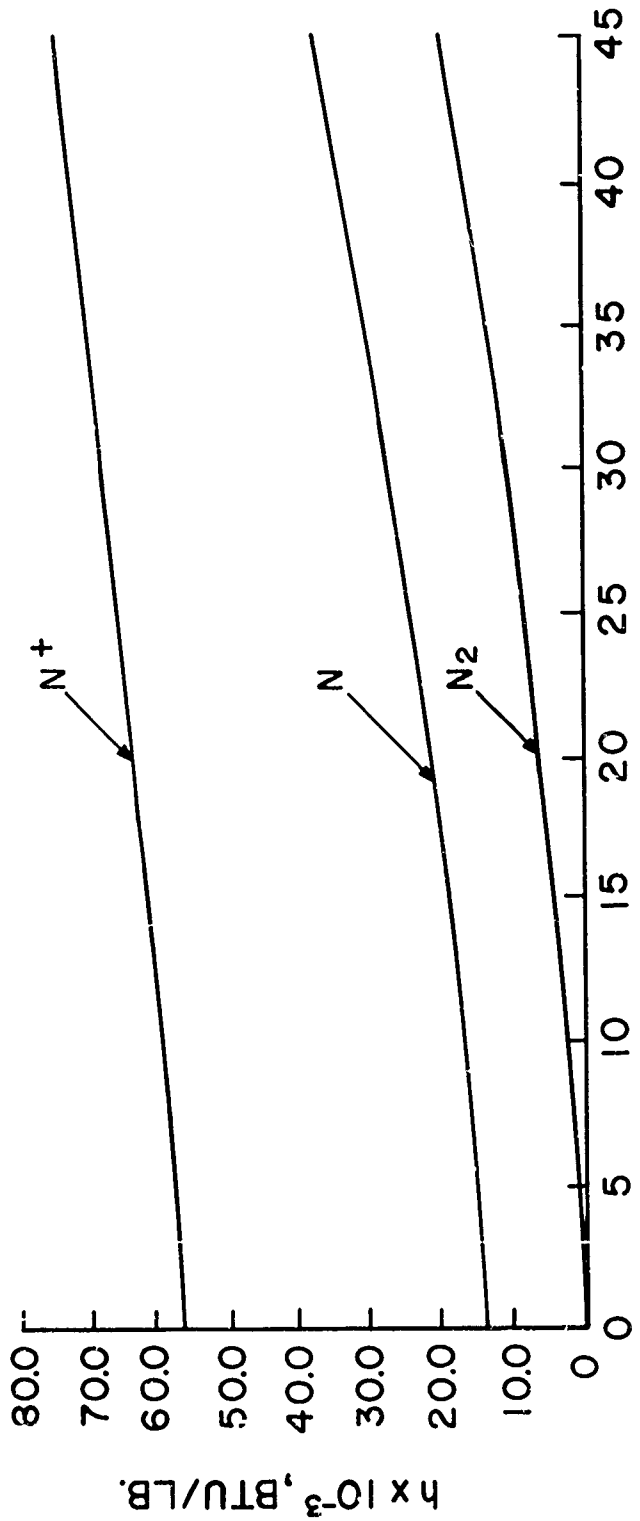


FIGURE 4

ENTHALPY VS. TEMPERATURE

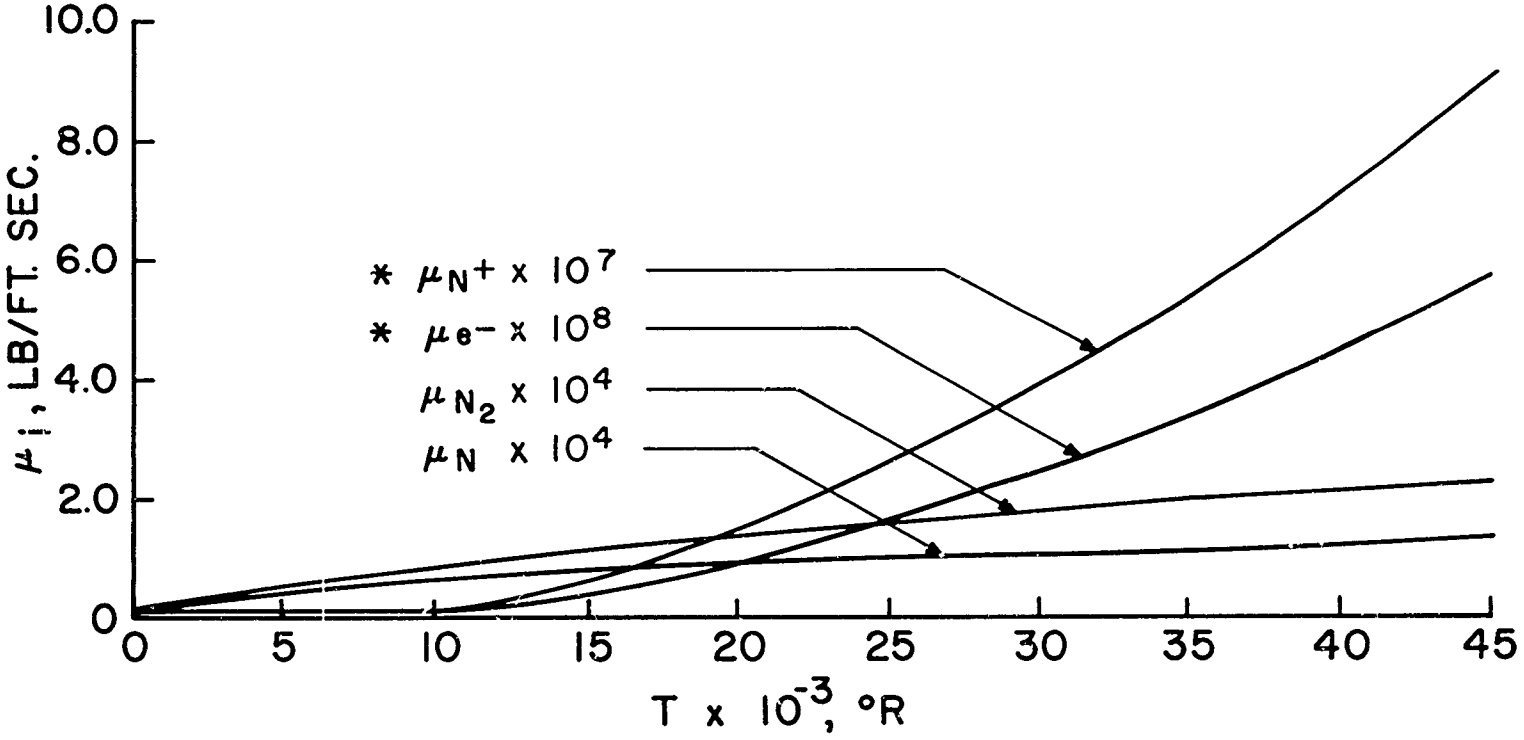


FIGURE 5

VISCOSITY vs TEMPERATURE

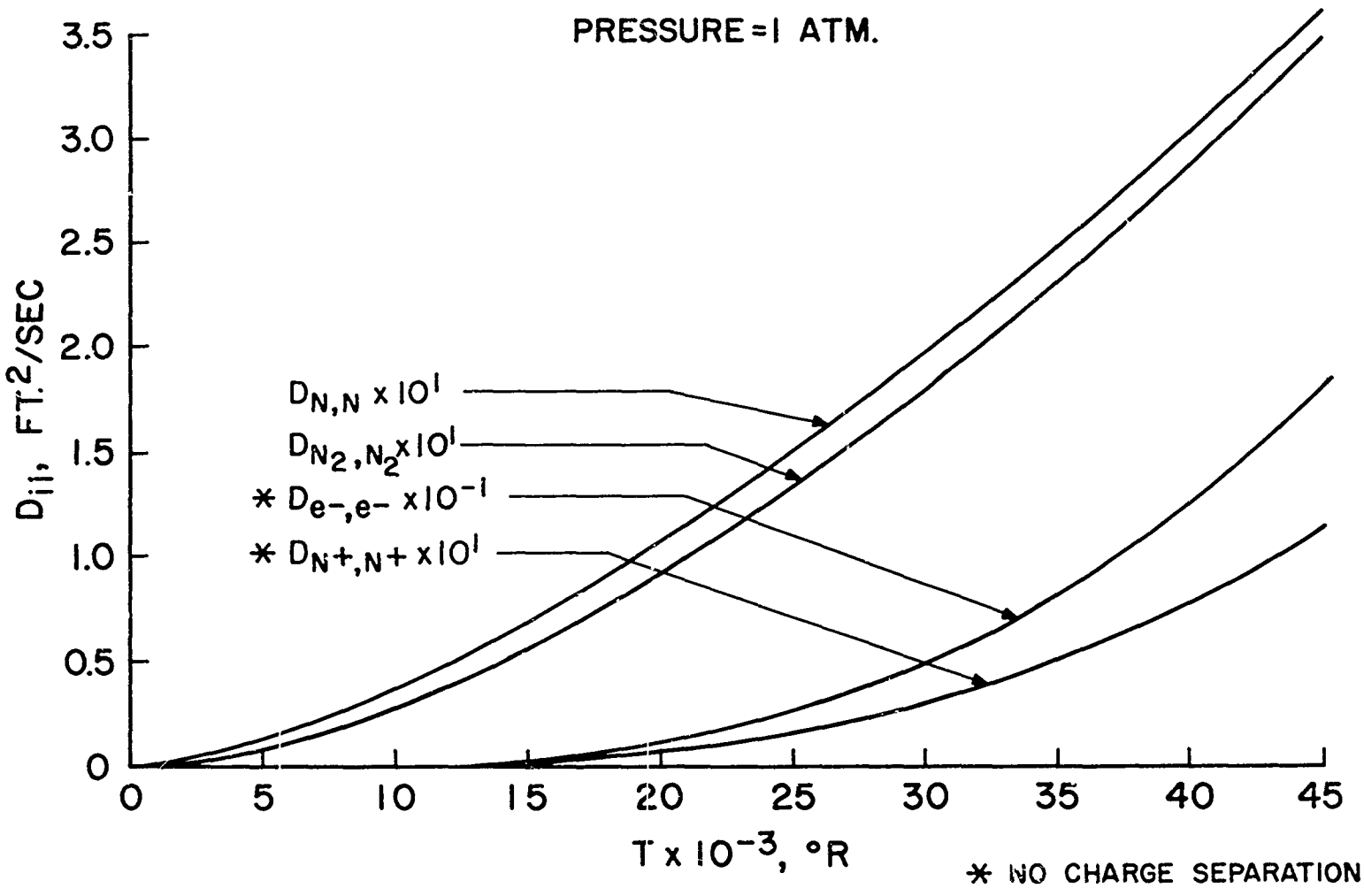


FIGURE 6

SELF DIFFUSION VS. TEMPERATURE

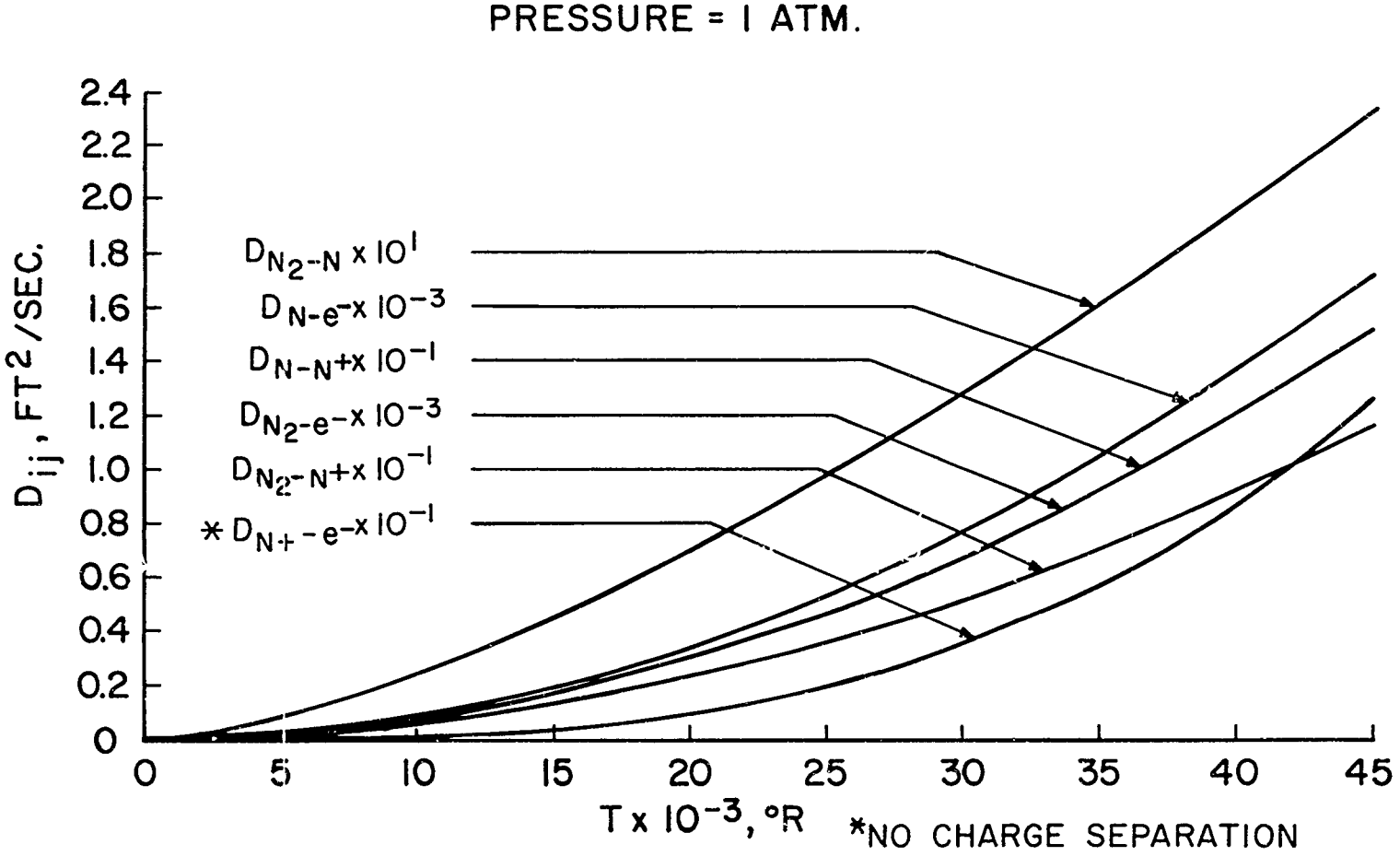


FIGURE 7

BINARY DIFFUSION VS. TEMPERATURE

IONIZATION EFFECTS ON CONVECTIVE HEAT TRANSFER

A number of recent studies have concerned themselves with the effects of ionization upon hypersonic stagnation point heat transfer, (Reference 37-42).

Rutowski (Reference 37) and Bershader and Rutowski (Reference 39) do not consider air, and hence do not obtain results which are particularly useful for planetary entry. Adams (Reference 38), Cohen (Reference 41) and Hoshizaki (Reference 42), in virtue of their particular assumptions, find that the effects of ionization are no more than thirty percent larger than would have been obtained by simple extrapolation of results obtained earlier for dissociated air.

However, when the transport and thermodynamic properties shown in Figures 3 to 7 are introduced into the multicomponent boundary layer equations with variable properties and the following assumptions are made:

1. Partially ionized air can be treated in first approximation as a four component gas including the species N_2, N, N^+ and e^-.
2. Thermal diffusion is neglected.
3. There is no charge separation.
4. There are no electric or magnetic fields.
5. The electrical dissipation term is negligible.
6. There are no external forces.
7. The gas is in "local thermochemical equilibrium".
8. There is no coupling between the flow and the radiative transport processes.
9. Low Reynolds number effects are neglected.

Then one obtains the representative boundary layer profiles shown in Figures 8 to 12. In these figures, η denotes the non-dimensional distance from the surface as given by the Dorodnitsyn transformation (Reference 3).

Figure 8 shows the velocity distribution through the boundary layer for three typical supercircular flight speeds. Figure 9 shows the corresponding temperature profiles. Figure 10 shows the variation of gas composition. Figure 11 shows the properties of the gaseous mixture, which were computed self-consistently with the temperature and gas composition. Figure 12 shows the variation of the chemical source terms $\dot{w}_i$ through the boundary layer.

It is interesting that when one calculates the resulting convective heat transfer to the surface, there is a remarkable increase above what had been predicted in the earlier theories. (See Figure 13). This may be attributed in part to the fact that the multicomponent Lewis numbers which were computed for this gas vary between order unity and order 10^5. This would indicate that the assumption of Lewis number equal to unity is poor.

Some experimental data recently obtained by Dr. Warren of the G. E. Space Sciences Laboratory in a new hyperthermal shock tube is also shown in Figure 13. In spite of the scatter in the experimental data, the agreement between the new theory and data is seen to be reasonable. This lends confidence to the assumptions and to the theoretical model utilized in this study.

The very interesting result is that at speeds near escape velocity, the contribution of ionization to stagnation point convective heat transfer results in a factor of 2.5 above a simple extrapolation of the dissociated air heat transfer results. It remains to be seen what results will be obtained with other theoretical models.

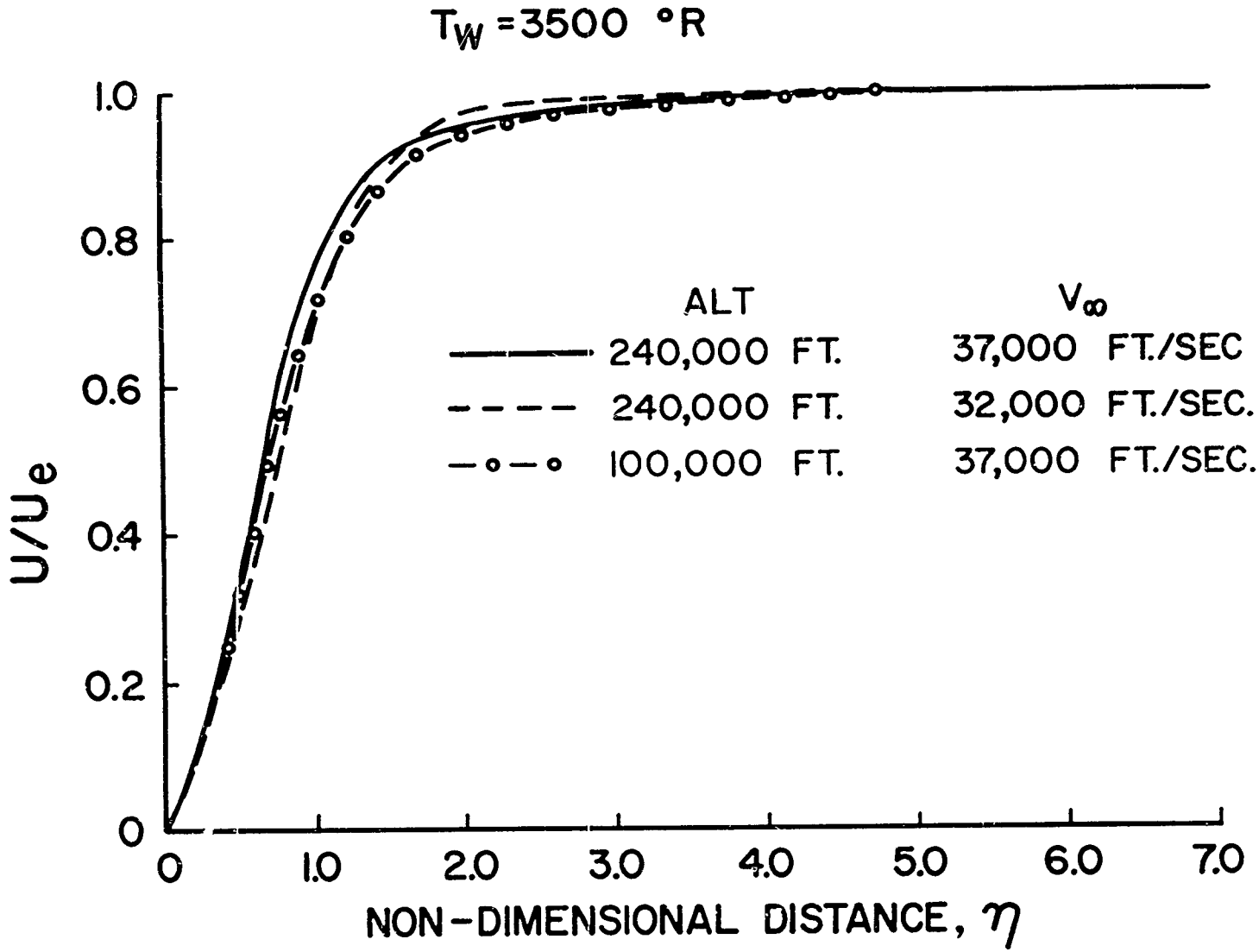


FIGURE 8

VELOCITY PROFILES

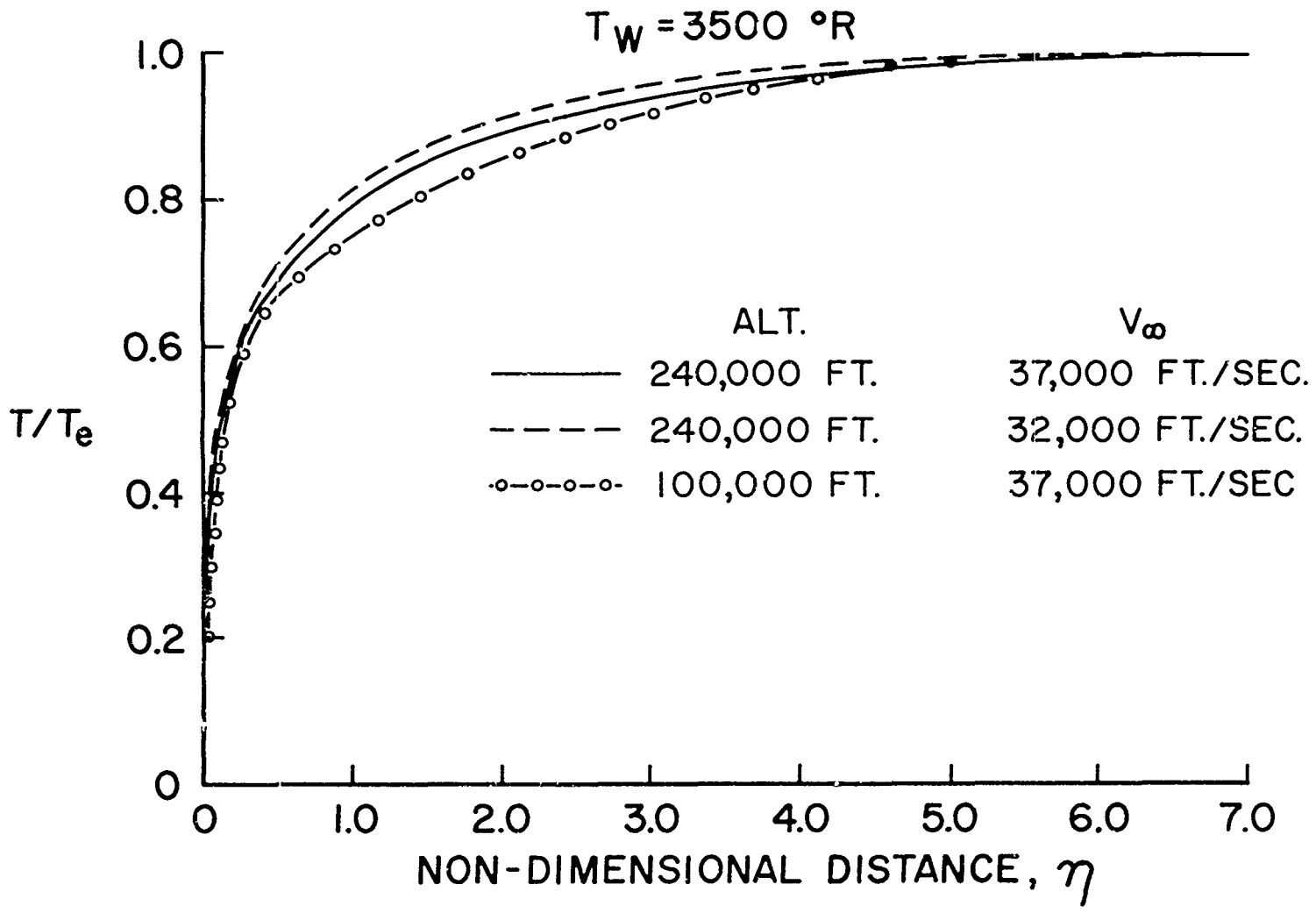


FIGURE 9

TEMPERATURE PROFILES

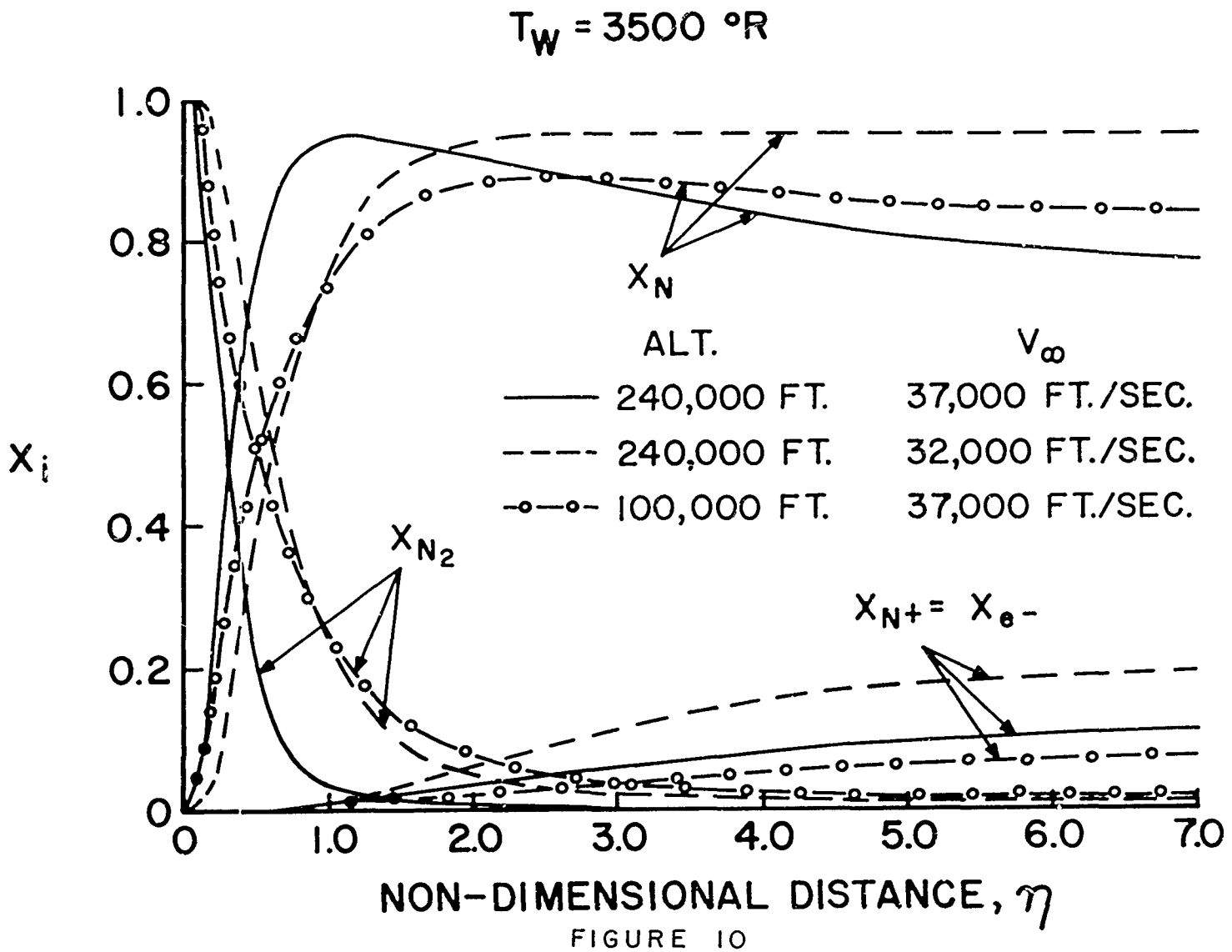


FIGURE 10

MOLE FRACTIONS OF CHEMICAL SPECIES

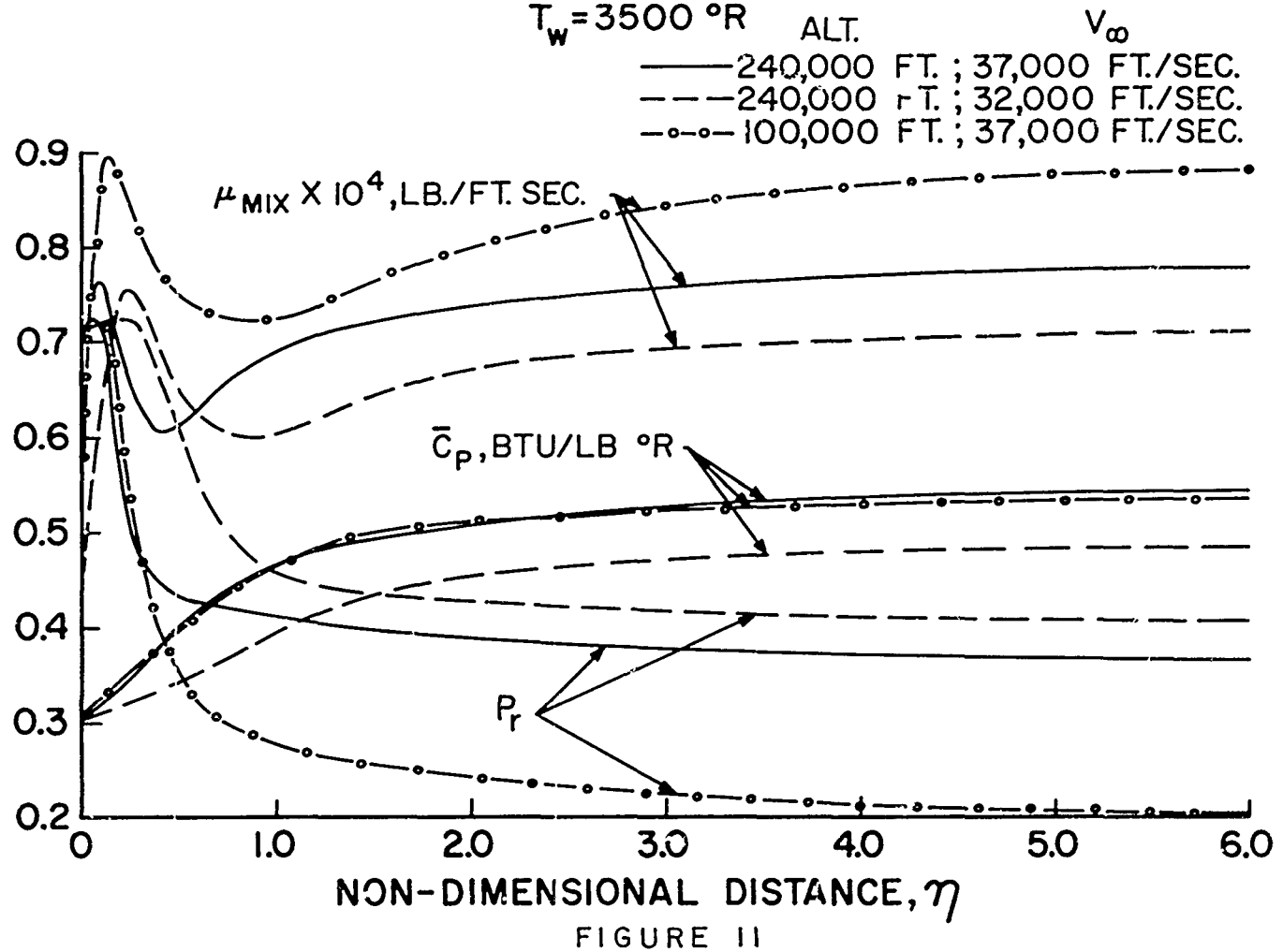


FIGURE 11

VISCOSITY, SPECIFIC HEAT, PRANDTL NUMBER

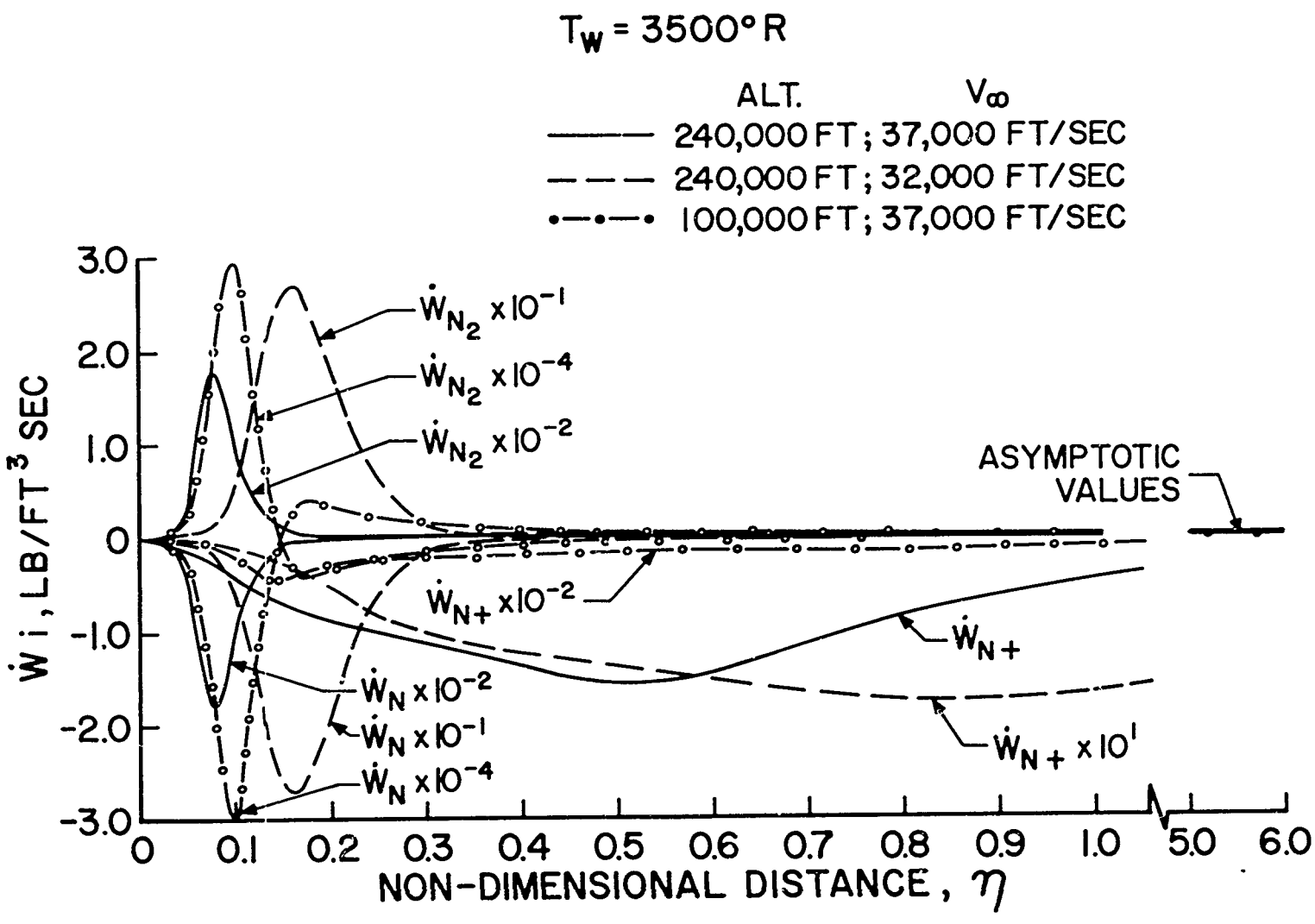


FIGURE 12

CHEMICAL SOURCE TERMS FOR IONIZATION REACTIONS

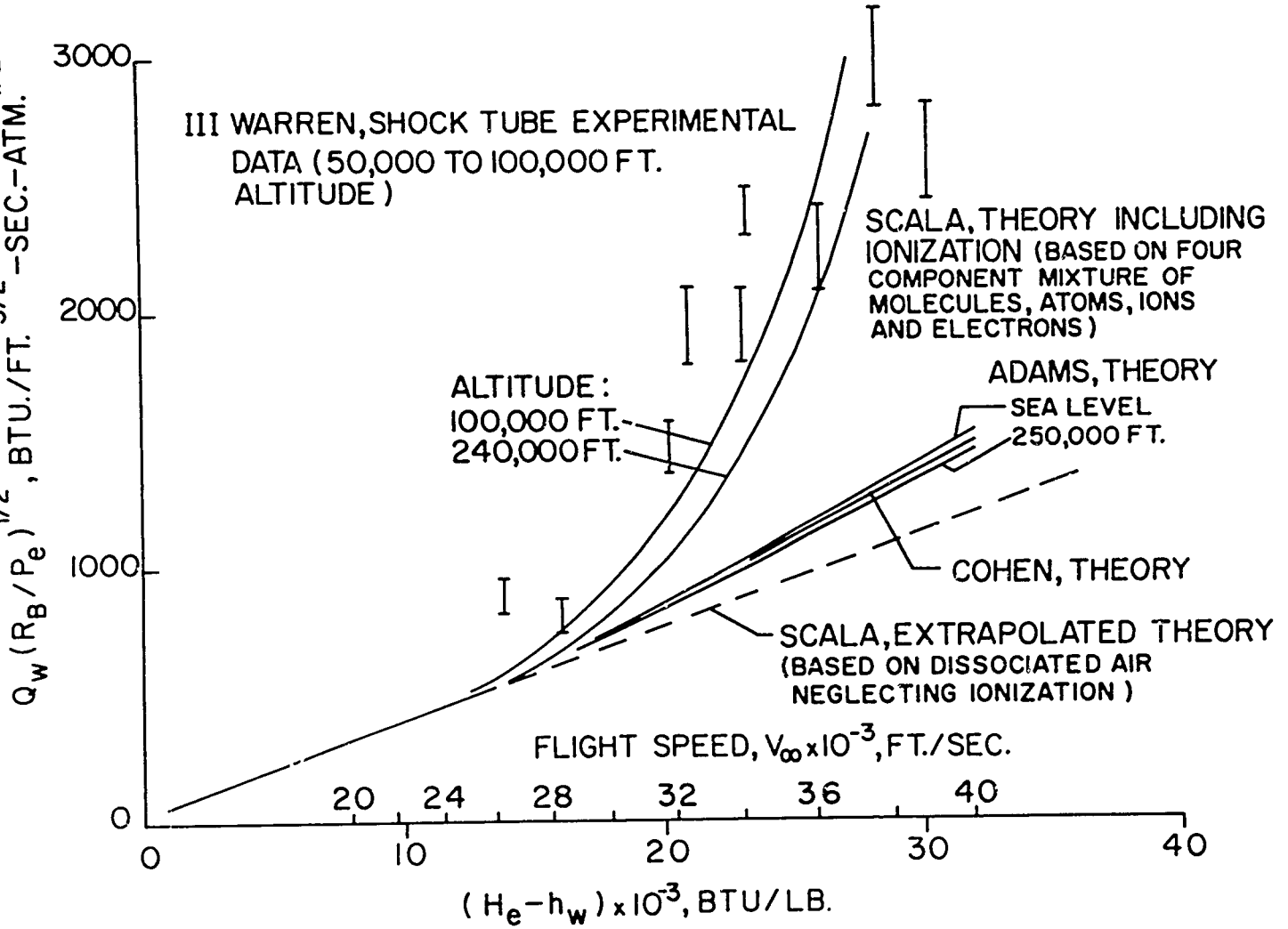


FIGURE 13

HYPERVELOCITY STAGNATION POINT HEAT TRANSFER

RADIANT HEAT TRANSFER

The problems associated with the determination of the radiative energy transfer from the hot gas cap (shock layer) to an entry vehicle are formidable, and as noted, different quantum mechanical techniques have been developed (References 11, 12, 43-46) in order to predict the contributions to the radiative flux.

In this section, we will review briefly the theoretical background for those calculations which lead to the "precise" determination of radiative heat transfer.

In any quantitative description of the radiation from a gas, one may choose to deal with the linear gaseous absorption coefficient k, the gaseous emissivity ϵ, or the actual intensity in units of energy per unit surface area emitted by some boundary of the gas. (All three will be discussed briefly here.) Following Breene and Nardone (Reference 46) we may recall Lambert's Law for the absorption of radiant energy as:

$$I = I_o e^{-kx} = I_o e^{-N\sigma x} \tag{25}$$

where I_o is the intensity of the incident beam, I is the intensity in the beam after it traverses x units of the gas, k is the linear absorption coefficient of the gas, σ is the cross section for this absorption and N is the density of absorbing particles. Insofar as this equation is concerned, we may consider it as applying:

1. at a particular radiant frequency
2. as a mean over a band of frequencies
3. as a mean over the entire spectrum.

It should be noted that N and σ must be individually considered for each of the types of radiation absorbing processes, and, if there are several for the frequency or frequency region of interest, they must be summed.

If it is assumed that local thermodynamic equilibrium prevails, or equivalently that Kirchoff's Law holds, then the gaseous emissivity may be written:

$$\epsilon = 1 - e^{-kx} \tag{26}$$

Then, also the emissivity expressions introduced in Equation (25) and (26) may be used to obtain the actual radiant intensity:

$$I_\nu = \epsilon_\nu B_\nu = B_\nu (1 - e^{-\sigma N x}) \tag{27}$$

where B_ν, the Planck black body curve, is given by:

$$B_\nu = \frac{8\pi h \nu^3}{C^3} \left[\exp\left(\frac{h\nu}{kT}\right) - 1 \right]^{-1} \tag{28}$$

Here, we refer to a given frequency ν, but if we desire the result over the entire spectrum, we may write:

$$I = \bar{\epsilon}\,\bar{\sigma}\,T^4 ; \bar{\sigma} = \frac{2k^4\pi^5}{15h^3C^2} \tag{29}$$

and, of course, the total black body intensity may be re-expressed in any desired units.

The general problem consists of obtaining the cross-section or absorption coefficient for whatever processes contribute to the radiation from a high tempera-

ture partially ionized CON gaseous system. Since the air system has already been treated extensively, we will first briefly list those processes which have already been found to be important for radiation from air at temperatures corresponding to sub-orbital flight speeds, and then we will add the additional contributions from the additional processes which occur at supercircular flight speeds or which are due to chemical species containing carbon. In the temperature range of interest one has (Reference 46):

1. Ultraviolet-visible Band Spectra
   The beta system of NO
   The gamma system of NO
   The Schuman-Runge system of oxygen
   The first positive system of nitrogen
   The second positive system of nitrogen
   The first negative system of the positive nitrogen ion

2. Infrared Band Spectra
   The infrared spectrum of NO

3. Bound Free Continua
   The bound free continuum of the negative oxygen ion

4. Free Free Continua
   The free free continuum of oxygen
   The free free continuum of nitrogen

To this list, it is postulated that for a CON gaseous mixture, at elevated temperature, one must add (Reference 47):

1. Ultraviolet-visible Band Spectra

   The CO_2 system

   The CN system

   The CO band system

   The C_2 band system

2. Infrared Band Spectra

   The infrared spectrum of CO_2

   The infrared spectrum of CN

   The infrared spectrum of CO

3. Bound Free Continua

   The bound free continuum of atomic carbon

4. Free Free Continua

   The free free continuum of the positive oxygen ion

   The free free continuum of the positive nitrogen ion

   The free free continuum of atomic carbon

5. Deionization Continua

   The deionization continuum of oxygen

   The deionization continuum of nitrogen

Two points must be made here. The first is that one does not necessarily know in advance of the actual computations which bands will yield significant contributions in a given frequency range. The second is that the calculated values of the radiant energy transfer coefficients depend on the concentrations of the species, and hence the contributions of chemical species containing only oxygen

and/or nitrogen given in the first list would not contribute in the same manner in a CON system as in an air system.

At still higher temperatures, other radiation processes become important, but those listed above will suffice for discussion purposes. In the following paragraphs, some of the methods of calculating the contributions will be discussed.

For the ultraviolet-visible frequency range, Breene has appealed to the Mayer-Goody Model (References 48, 49) for an electronic-vibrational band in developing digital computer programs for the ultraviolet-visible emissivity or absorption coefficient. Essentially, this consists of assuming a statistical distribution of spectral lines (broadened into a continuous distribution of radiation in the band), in a given spectral region for each electronic-vibrational band, and then one sums contributions from the various bands from each spectral interval.

Analytical expressions for the form of the absorption coefficient have readily been developed (including the assumption that the halfwidths of the spectral lines are very large). The resulting emissivity expression and the absorption coefficient expression, inferrable from it, have been programmed for the IBM 704 and, later for the IBM 7090. In carrying out the calculation for a particular frequency, the computing machine checks all bands in the system under consideration. When all contributions amounting to more than a certain minimum have been obtained for the summation at that frequency - the inclusion of twenty or thirty bands is quite normal - the computer then calculates the absorption coefficient (or the emissivity) and moves on to the next frequency. Different molecular band systems simply require different input coefficients.

Although the physical processes involved are, of course, quite distinct, the rotational constants are really what give rise to the obvious differences between

an electronic-vibrational band and a rotation-vibrational band. In the latter case, the rotational constants are practically the same in the upper and lower states. When one makes such an assumption, one obtains a symmetric distribution of intensity in the band which is typical of infrared spectra. Note that no electronic transition occurs here as in the case of the ultraviolet-visible spectra.

In general, the absorption cross-section has been determined by Breene by first calculating matrix elements using generalized IBM 7090 computer programs. (The resulting cross-section is both temperature and density independent.)

Bremsstrahlung radiation (free free continuua) may be considered as arising due to the deflection of the incident electron by an atom, the resultant acceleration from the deflected electron. From the quantum point of view, such radiation results from transitions on the part of the free electron between different states in the presence of the particular atom. Breene has also carried out the calculations leading to the cross-sections for these continua.

The procedure utilized has been to first obtain the wave functions for the free electron in the field of the neutral atom in question (References 50 to 52). These programs for the free electron wave functions are then applied to the computation of the matrix elements required for the cross-sections (Reference 53). Further details on all of these computations may be obtained from Reference 46.

Some remarks must be made concerning "non-equilibrium" radiation. First, we distinguish between non-equilibrium radiation due to the absence of thermal equilibrium, in which case there is a temperature overshoot due to the relaxation phenomena associated with equipartition of energy in a mixture of

polyatomic gases. An indication of the temperature overshoot can be obtained from the recent work of Talbot and Scala on shock wave structure (Reference 54).

The other type of non-equilibrium radiation, which arises as a consequence of the absence of chemical equilibrium in the gas is more readily evaluated by considering the chemical kinetics of the flow (References 55, 56). Thus for each possible chemical reaction, one writes:

$$\alpha A + \beta B + M \rightleftharpoons \gamma A_\delta B_\epsilon + M \tag{30}$$

and the chemical kinetic equation may be then written:

$$\frac{\partial n_{A_\delta B_\epsilon}}{\partial t} = \sum_N \left[K_{f_N} (n_A)^\alpha (n_B)^\beta - K_{b_N} (n_{A_\delta B_\epsilon})^\gamma \right] n_N \tag{31}$$

where n_i is the number of moles of species i per unit volume, and for stoichiometry $\delta = \alpha/\gamma$ and $\epsilon = \beta/\gamma$. In Equation (31) K_{f_N} is the forward rate and K_{b_N} is the backward rate of the same chemical reaction. It is noted that due to microscopic reversibility, the equilibrium constant K_N is simply the ratio of the forward rate to the backward rate, i.e.

$$K_N = \frac{K_{f_N}}{K_{b_N}} \tag{32}$$

where K_N is a function of temperature which may be readily determined from statistical mechanics. Since one may readily calculate all of the equilibrium constants for the gaseous system, it is clear then that one requires an independent knowledge of either the forward or backward rate of each reaction, since Equation (32) may be used to eliminate either K_{f_N} or K_{b_N}. It must be noted that K_f is

not a constant, but has a functional dependence on temperature which may be written in the Arrhenius form:

$$K_f = a \left(\frac{T}{T_o}\right)^b e^{-E/RT}$$

and may be estimated utilizing collision rate theory (Reference 57) or determined experimentally. Therefore, one may proceed to perform calculations for the case of finite reaction kinetics after having first established the magnitude of the constants a, b and E.

Once the composition of the nonequilibrium gas is known at a given point in the gas cap one proceeds to determine the gas emissivities and the radiation intensity as a function of density and temperature in a manner analogous to the equilibrium gas computation.

THERMAL STRESS

In order to determine the thermal stress distribution within a refractory solid, which is utilized as a thermal shield at the leading edges of a hypersonic lifting re-entry vehicle, one must first determine the internal temperature distribution. Thus, not only must one consider the convective and radiative heat transfer to the surface, one must also determine the extent of chemical interactions such as oxidation, and other forms of mass transfer, at the surface, (Reference 58). Accordingly, one must obtain the solution to the equation for the internal temperature distribution:

$$\rho C_p \frac{\partial T}{\partial t} = \frac{1}{r}\frac{\partial}{\partial r}\left(K_r\, r \frac{\partial T}{\partial r}\right) + \frac{1}{r^2}\frac{\partial}{\partial \Psi}\left(K_\Psi \frac{\partial T}{\partial \Psi}\right) + \frac{\partial}{\partial z}\left(K_z \frac{\partial T}{\partial z}\right) \qquad (33)$$

subject to the initial condition:

$$T(r, \Psi, Z, 0) = T_0 \qquad (34)$$

the surface boundary condition:

$$\frac{\partial T}{\partial r}\left[s(r, \Psi, z, t), t\right] = \frac{1}{K_r}\left[Q(s,t) + \sigma \epsilon_g T_g^4 - \sigma \epsilon_w T_w^4\right] \qquad (35)$$

and the inner boundary condition (insulated wall):

$$\frac{\partial T}{\partial r}(r_i, \Psi, z, t) = 0 \qquad (36)$$

In general, the governing equations for the radial and tangential components of the thermal stress may then be determined by integrating the following equations (Reference 59).

Radial Stress

$$r^2 \frac{d^2\sigma_r}{dr^2} + 3r \frac{d\sigma_r}{dr} + \psi\sigma_r = \phi T - \Omega r \frac{dT}{dr} \tag{37}$$

Tangential Stress

$$\sigma_\psi = \sigma_r + r\frac{d\sigma_r}{dr} \tag{38}$$

subject to the boundary conditions

$$\begin{aligned} r &= r_i, \quad \sigma_r = 0 \\ r &= R_B, \quad \sigma_r = 0 \end{aligned} \tag{39}$$

where ψ, ϕ amd Ω represent the structural properties of the material.

Upon calculating the radial stresses for two refractory materials such as commercial and pyrolytic graphite along a typical lifting re-entry trajectory, it is found that for commercial graphite the normalized stress is of the order of 150 degrees R in tension, whereas for pyrolytic graphite the normalized radial stress is of the order of 400 degrees R in compression (Reference 59).

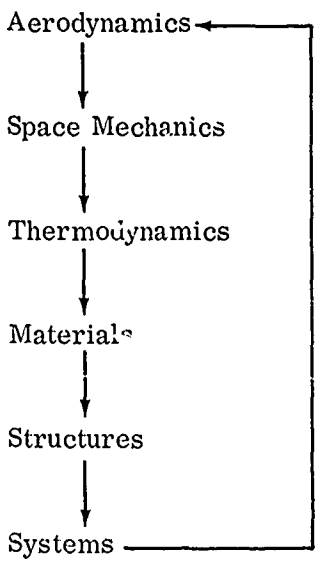
Clearly, additional work is required to tailor the degree of anisotropy of the material to the environmental conditions, as suggested in Reference 59, so that the thermal stresses are minimized.

SYSTEMS APPROACH TO MATERIALS RESEARCH

The aerothermodynamic heating problems of lifting entry vehicles traveling at supercircular velocities require a fundamentally different materials approach than did the ballistic re-entry problem. During ballistic re-entry, severe heating occurs over a time period of the order of several minutes, whereas hypersonic lifting vehicles are subjected to prolonged heating for times of the order of several hours.

Because of the long heating times and heat flux levels encountered, special materials problems exist at the leading edges of the aerodynamic control surfaces (i.e., nose, wings and fins), since it is readily found that radiation equilibrium temperatures can easily exceed 4000 degrees R (Reference 58).

The usual approach to the determination of suitable materials for flight applications consists of a vertical sequence of steps as follows:



In the past, fortunately, sufficient time was available so that information could be passed across these interfaces so that each group could perform its function relatively independently of all of the others, up until the time a pulse passed through the network.

Because of the severe aerothermodynamic and structural requirements which will be placed upon advanced materials, and because of shorter lead times, it becomes essential that an integrated approach be established at the outset. Today, it must be recognized that the aerothermodynamic properties (and hence the structural properties) of a given material are critically dependent on the environment in which the material must perform. Further, the aerodynamic performance may be critically dependent on the structural configuration selected.

Therefore, an integrated horizontal approach is required at the outset, to ensure that all necessary data will be generated simultaneously for each category of materials which qualifies for careful scrutiny.

Thus, it is the author's belief that if an integrated research and development program is carried out, according to the relationships and responsibilities shown in Table 4, it should be possible to carry out meaningful exploratory studies leading to the rapid development of new thermal protection techniques.

TABLE 4. SYSTEMS APPROACH TO MATERIALS RESEARCH

MATERIALS DEVELOPMENT	PHYSICAL CHEMISTRY	INTERACTIONS WITH SPACE ENVIRONMENT	STRUCTURES DEVELOPMENT
1. Define new materials.		1. Establish theoretically and utilizing test facilities the aero-thermochemical response of material in flight environment.	1. Evolve new structural concepts
2. Establish their thermal, chemical and structural properties.		2. Provide systems information on aerodynamic, geometric and trajectory considerations for a given mission.	2. Establish structural performance of materials for flight application including thermal and dynamic effects.

ACKNOWLEDGMENTS

The author wishes to acknowledge the helpful discussions held with Professor Charles Curtiss of the University of Wisconsin, as well as his colleagues at the Space Sciences Laboratory including Jacob Enoch, R. G. Breene, Charles Baulknight, Walter Warren, Peter deVries, Donald Vachon and Miss Maria Nardone.

The numerical solutions were obtained on an IBM 7090 digital computer by Mr. Frank Bosworth who programmed the governing equations. Many of the preliminary calculations as well as the preparation of the graphs were performed by Messers C. Cook, L. Gilbert, and J. Wilson.

The results presented herein were supported in part by NASA under contract NASr - 32.

REFERENCES

1. Gilbert, L. M. and Scala, S. M., Free Molecular Heat Transfer in the Ionosphere, AAS Preprint 61-72, March, 1961, to be published in the Proceedings of the AAS Symposium on "Interactions of Space Vehicles with an Ionized Atmosphere".

2. Scala, S. M. and Baulknight, C. W., 'Transport and Thermodynamic Properties in the Hypersonic Laminar Boundary Layer, Part I - Properties of the Pure Species", American Rocket Society Journal, Vol. 29, No. 1, pp. 39-45, January 1959.

3. Scala, S. M. and Baulknight, C. W., "Transport and Thermodynamic Properties in the Hypersonic Laminar Boundary Layer, Part 2 - Applications" American Rocket Society Journal, Vol, 30, No. 4, pp. 329-336, April 1960.

4. Gilmore, R. R., Equilibrium Composition and Thermodynamic Properties of Air to 24,000°K, Rand Corporation RM-1543, August 1955.

5. Hilsenrath, J. and Beckett C. W., Tables of Thermodynamic Properties of Argon-Free Air to 15,000°K, Arnold Engineering Development Center Report AEDC TN-56-12, September 1956.

6. Hansen, C. F., Approximations for the Thermodynamic and Transport Properties of High Temperature Air, NACA TN 4150, March 1958.

7. Baulknight, C. W., "The Calculation of Transport Properties at Elevated Temperature", Transport Properties in Gases, Northwestern University Press, pp. 89-91, January 1958.

8. Baulknight, C. W., "Transport Properties of Multicomponent Gas Mixtures at High Temperatures", Thermodynamic and Transport Properties of Gases, Liquids and Solids, McGraw Hill Book Co., pp. 92-99, February 1959.

9. Baulknight, C. W., "Transport Property Equations", Proceedings of the Fourth International Conference on Ionization Phenomena in Gases, North Holland Publishing Co., 1960.

10. Scala, S. M., The Equations of Motion in a Multicomponent Chemically Reacting Gas, General Electric Co., MSVD Report TIS R 58 SD 205, December 1957.

11. Breene, R. G., "Infrared Emissivity of High Temperature Air", J. Chem. Phys., Vol, 29, p. 512, 1958.

12. Breene, R. G. and Nardone, M. C., "Wave Functions for the Free Electron", Phys. Rev., Vol. 115, p. 93, 1959.

13. Chapman, D. R., An Analysis of the Corridor and Entrance Requirements for Supercircular Entry into Planetary Atmospheres, NASA TR R-55, 1959.

14. Lees, L., Hartwig, F. W., and Cohen, C. B., "Use of Aerodynamic Lift During Entry into the Earth's Atmosphere, Jet Propulsion, Vol. 29, No. 9, September 1959, p. 633.

15. Grant, F. C., Analysis of Low-Acceleration Lifting Entry from Escape Speed, NASA TN D-249, June 1960.

16. Wong, T. J. and Slyc, R. E., The Effect of Lift on Entry Corridor Depth and Guidance Requirements for the Return Lunar Flight, NASA TR R-80, 1960.

17. Hildebrand, R. B., Manned Return from Space, presented at the Second International Congress of the Aeronautical Sciences, Zurich, Switzerland, September 1960.

18. Luidens, R. W., Approximate Analysis of Atmospheric Entry Corridors and Angles, NASA TN D-590, January 1961.

19. Eggers, A. J. and Wong T. J., Motion and Heating During Atmospheric Entry, ARS Preprint 1675-61, April 1961.

20. Dugan, J. F., Fr., Analysis of Trajectory Parameters for Probe and Round-Trip Missions to Mars, NASA TN D-281, June 1960.

21. Dugan, J. F., Jr. and Simsic, C. R., Analysis of Trajectory Parameters for Probe and Round-Trip Missions to Venus, NASA TN D-470, November 1960.

22. Miller, L. E., "Molecular Weight of Air at High Altitudes", J. Geophysical Research, Vol. 62, No. 3, September 1957, pp. 351-365.

23. Air Force Cambridge Research Center, ARDC Model Atmosphere 1959, General Electric Co., MSVD, Document No. PIBA-2.

24. Gazley, C., Jr., Deceleration and Heating of a Body Entering a Planetary Atmosphere from Space, Rand Corporation Report P-955, February 1957.

25. Goody, R. M., "The Atmosphere of Mars", Journal of the British Interplanetary Society, Vol. 16, No. 2, April-June 1957.

26. Dole, S. H., The Atmosphere of Venus, Rand Corporation Report P 978, October 1956.

27. de Vaucouleurs, G., "The Physical Environment on Mars", Chapter 39, Physics and Medicine of the Atmosphere and Space, Wiley and Sons, 1960.

28. Hess, S. L., "Blue Haze and the Vertical Structure of the

Martian Atmosphere", Astro. Jour. Vol. 127, No. 3, May 1958.

29. King, J. I. F., The Dynamic Stability of the Upper Atmosphere of Venus, General Electric Co., MSVD TIS R60SD453, October 1960.

30. Curtiss, C., Private Communication.

31. Amdur, I., Mason, E. and Jordon, J., Scattering of High Velocity Neutral Particles, Technical Report No. 1, Department of Chemistry, M.I. T., May 1957.

32. Chapman, S. and Cowling, T. G., The Mathematical Theory of Non-uniform Gases, Cambridge University Press, 1939.

33. Hirschfelder, J. O., Curtiss, C. and Bird, R. B., Molecular Theory of Gases and Liquids, John Wiley and Sons, Inc. 1954.

34. Cohen, R., Spitzer, L. and Routly, R., "The Electrical Conductivity of an Ionized Gas", Phys. Rev., Vol. 80, p. 230, 1950.

35. Thomas Jr., M., Transport Properties of High Temperature Gases, ARS Preprint 1996-61, August 1961.

36. Peng, T. and Pindroh, A. L., An Improved Calculation of Gas Properties at High Temperatures: Air, ARS Preprint 1995-61, August 1961.

37. Rutowski, R. W., "Stagnation Point Heat Transfer in a Partially Ionized Gas", Proceedings of the 1959 Heat Transfer and Fluid Mechanics Institute, Los Angeles, California, p. 110.

38. Adams, M. C., A Look at the Heat Transfer Problem at Super Satellite Speeds, ARS Prepring 1556-60, December

1960.

39. Bershader, D. and Rutowski, R. W., Studies of an Argon Shock-Layer Plasma, ARS Preprint 1998-61, August 1961.

40. Fay, J. A., Plasma Boundary Layers, ARS Preprint 2010-61, August 1961.

41. Cohen, N. B., Boundary Layer Similar Solutions and Correlation Equations for Laminar Heat Transfer Distribution in Equilibrium Air at Velocities up to 41,100 Feet per Second, NASA TR R-118, 1961.

42. Hoshizaki, H., Heat Transfer in Planetary Atmospheres at Super-Satellite Speeds, ARS Preprint 2173-61, October 1961.

43. Keck, J., Kivel, B. and Wentink, T., "Emissivity of High Temperature Air", 1957, Heat Transfer and Fluid Mechanics Institute, Stanford, California, Stanford University Press, pp. 279-294, 1957.

44. Meyerott, R. E., "Radiation Heat Transfer to Hypersonic Vehicles", Combustion and Propulsion, Third A.G.A.R.D. Colloquium, Pergamon Press, pp. 431-450, March 1958.

45. Wurster, W. H., Glick, H. S. and Treanor, C. E., Radiative Properties of High Temperature Air, Cornell Aeronautical Laboratory, Report QM 997-A1, September 1957.

46. Breene, R. G. and Nardone, M. C., Radiant Emission from High Temperature Air, General Electric Co., MSVD TIS R61SD020, May 1961.

47. Breene, R. G., Private Communication.

48. Mayer, H., Methods of Opacity Calculations, Los Alamos Scientific Lab., Report LA 647, AECD-1870 (1947).

49. Goody, R. M., Quart. J. Roy. Met. Soc., Vol. 78, p. 165 (1952).

50. Breene, R. G., "Analytic Wave Functions I. Atoms with 1s, 2s and 2p Electrons", Phys. Rev. Vol. 111, p. 1111 (1958).

51. Breene, R. G., "Analytic Wave Functions II. Atoms with 1s, 2s, 2p, 3s and 3p Electrons", Phys. Rev., Vol. 113, p. 809 (1959).

52. Breene, R. G., "Analytic Wave Functions III. The Spin-Orbit, the Spin-Other, and Spin-Spin Interactions", Phys. Rev., Vol. 119, p. 1516 (1960).

53. Breene, R. G. and Nardone, M., "Free Free Continuum of Oxygen", J. Opt. Soc. Vol. 50, p. 1111 (1960).

54. Talbot, L. and Scala, S. M., "Shock Wave Structure in a Relaxing Diatomic Gas", Proceedings of the Second International Congress on Rarefied Gas Dynamics, Berkeley, California, August 1960.

55. Hammerling, P., Teare, J. D. and Kivel, B., "Non-Equilibrium Electrical and Radiative Properties of High Temperature Air, Nitrogen and Oxygen", 4th International Conference on Ionization Phenomena in Gases, Uppsala, Sweden, August 1959.

56. Camm, J. C., Kivel, B., Taylor, R. L. and Teare J. D., Absolute Intensity of Non-equilibrium Radiation in Air and Stagnation Heating at High Altitudes, AVCO Research Report 93, December 1959.

57. Friess, S. L. and Weissberger, A., Investigation of Rates and Mechanisms of Reactions, Interscience Publishers, Inc., 1953.

58. Nolan, E. J. and Scala, S. M., The Aerothermodynamic Behavior of Pyrolytic Graphite During Sustained Hypersonic Flight, ARS Preprint 1696-61, April 1961.

59. Scala, S. M., Nolan, E. J. and Garber, A. M., The Aerothermo-Viscoelastic Response of an Orthotropic Material During Hypersonic Flight, ARS Preprint 2150-61, October 1961.

HEAT TRANSFER DUE TO THE INTERACTION BETWEEN A SWEPT PLANAR SHOCK WAVE AND A LAMINAR BOUNDARY LAYER*

Anthony Martellucci and Paul A. Libby

General Applied Science Laboratories, Inc.

ABSTRACT

In this report, there is studied by theoretical means the interaction between a laminar boundary layer on a flat plate and a planar shock wave which is swept with respect to the flow external to the boundary layer but normal to the plate. A model for the inviscid flow is discussed first. It is shown that for a planar shock, the effect of sweep is easily included and thus that a model for two-dimensional flow is basic to the problem. The analysis is compared to available data for two-dimensional flows and shown to be in good agreement therewith. Application to the case of sweep and heat transfer will be presented in a subsequent report.

---

* This work was supported by the Flight Branch of the Flight Dynamics Laboratory, U.S.A.F., Aeronautical Systems Division, Air Force Systems Command, under Contract No. AF-33 (616)-7721. Mr. Richard D. Neumann was the Project Engineer.

LIST OF SYMBOLS

C_H	Chapman constant
F_1	quantity defined in Equation (13)
F_3	quantity defined in Equation (14)
g	H/H_e
H	stagnation enthalpy
h	static enthalpy
K_1, K_2, K_3	quantities defined in Equation (39)
M	μ_e/μ_{e_o}
M_e	Mach number
P	static pressure
R	gas constant
R	ρ_e/ρ_{e_o}
T	static temperature
t	$\int_o^y (\rho/\rho_e)dy$
U	u_e/u_{e_o}
V	total velocity = $u^2 + w^2$
W	H_w/H_e
$\tilde{W}$	w/w_e
Z	$-d\zeta/d(x/\delta_{t_o})$
$\tilde{z}$	quantity defined in Equation (21a)
u, v, w	orthogonal velocity components
x, y, z	cartesian coordinate system
γ	ratio of specific heats
δ	boundary layer thickness
δ_t	transformed boundary layer thickness $\int_o^\delta (\rho/\rho_e)\,dy$
δ^*	displacement thickness
Δ	δ_t/δ_{t_o}
Δ^*	δ^*/δ_{t_o}
ζ	u_e/u_{e_o}
θ	$\delta_t F_1$
μ	coefficient of viscosity

ρ	density
τ	t/δ_t

Subscripts

e	edge of boundary layer
o	upstream of interaction
t	stagnation conditions
w	wall
∞	downstream of interaction

HEAT TRANSFER DUE TO THE INTERACTION BETWEEN A SWEPT PLANAR SHOCK WAVE AND A LAMINAR BOUNDARY LAYER

INTRODUCTION

The problem of the interaction between a boundary layer and a shock wave, either incident upon the layer or generated by a concave corner, has been studied extensively. The early research was motivated by the experimental observations carried out, for example, by Fage and Sargent (Reference 1), Liepmann (Reference 2) and Ackeret, Feldmann, and Rott (Reference 3). These indicated that significant alterations of transonic and supersonic flow patterns occur when shock waves are incident upon or arise from surfaces with significant boundary layers. These alterations are characterized by an interaction between the essentially inviscid flow with shocks and the boundary layer.

Previous Research

Subsequent to these early experimental studies, further experimental and extensive theoretical studies have been carried out on this problem. Of particular interest to the present study will be those concerned with shock waves incident on plane surfaces involving laminar boundary layers, i.e., with Reynolds numbers sufficiently low so that the boundary layer throughout the interaction region will be laminar. The careful experimental studies of Hakkinen, Greber, Trilling, and Abarbanel (Reference 4) provide the most complete data for this case. The free stream Mach number in these tests was 2.0 and the overall static pressure ratio from far upstream to far downstream of interaction was varied up to 2.4. Velocity profiles, wall static pressure distributions and skin friction were measured throughout the interaction region. In addition, Chapman et al (Reference 5) provide inter alia one static pressure distribution on the wall with a pressure ratio of 2.15 and a free stream Mach number of 2.4.

The theoretical studies of the shock wave incident upon a planar wall involving a laminar boundary layer have been based on the boundary layer theory. Thus the interaction has been idealized so as to involve an essentially inviscid, external flow and a boundary layer with a relatively simple coupling, for example, one based on linearized supersonic flow, between the boundary layer behavior and the external flow. The most extensive calculations have been those based on the Crocco-Lees theory of mixing (References 6 to 11). This theory is a modification of the usual integral method of boundary layer analysis based on certain parameters characterizing the boundary layer profiles. Interrelationships among these parameters are obtained from similarity solutions of the boundary layer equations.

Physical Features and Theoretical Difficulties

Consider the main features of the interaction when separation occurs (cf. Figure 1); these are presently well understood as a result of past research. The boundary layer far upstream of the incident shock is assumed to be that associated with a flat plate; the influence of the incident shock results in a thickening of the layer with a resultant upstream compression zone as shown. This changes the inclination with respect to the wall of the incident shock without altering significantly the flow deflection therethrough*. If, as assumed here, the pressure rise is sufficient, the boundary layer will separate; after separation, little additional compression of the boundary layer can be tolerated until the incident shock is reached at the so-called shock impingement point. The shock is reflected from the separated region as from a constant pressure surface. This reflection forces the boundary layer to reattach and to turn so as to cause further compression until the overall pressure rise is achieved. Thus the

---

* The importance of this behavior of the incident shock was pointed out to the authors by Dr. Antonio Ferri; it appears not to have been employed in previous analyses. As will be seen below, it largely eliminates the need for iteration in the problem of the oblique incident shock provided the boundary layer characteristics upstream of interaction are known.

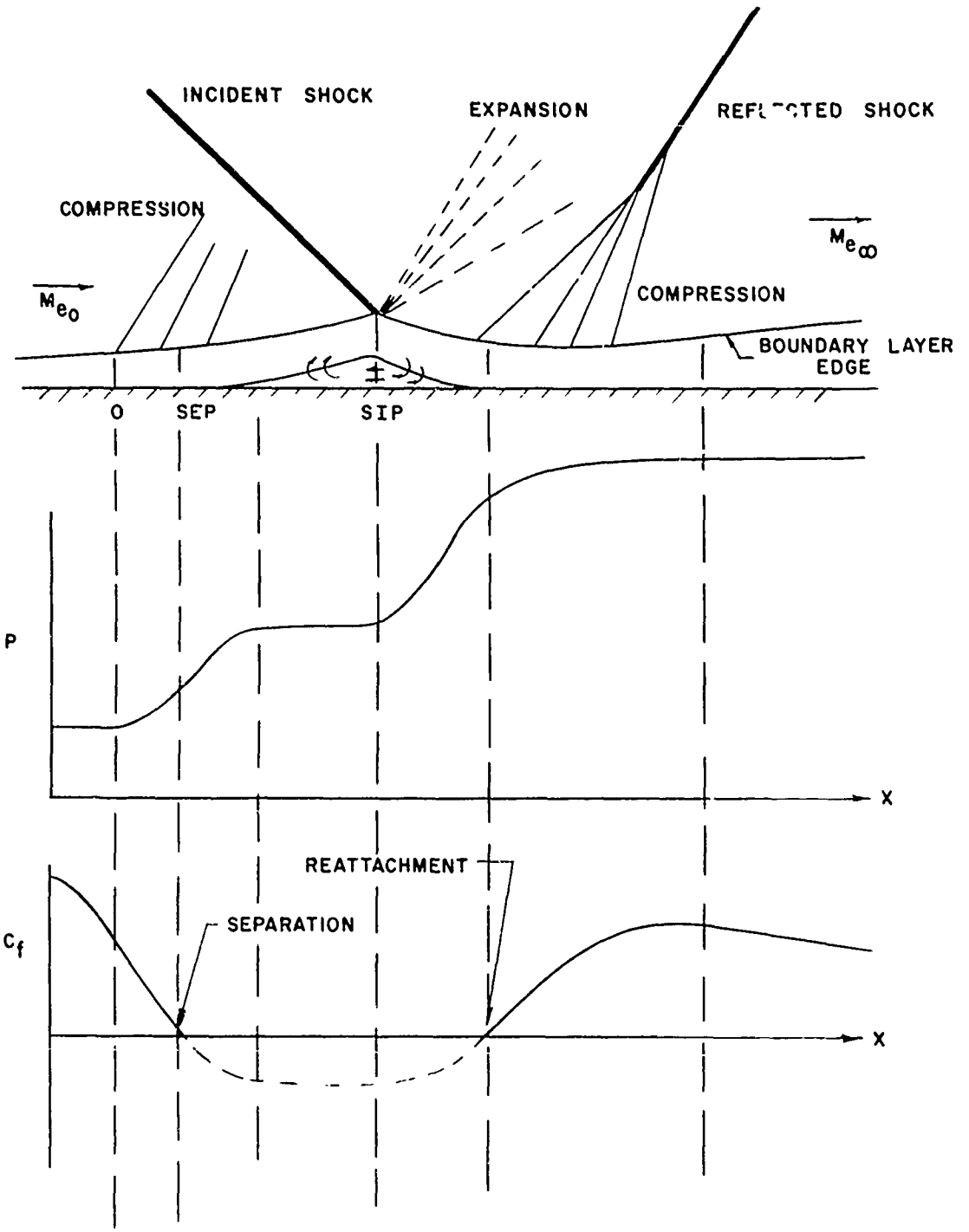


FIG. 1. SCHEMATIC REPRESENTATION OF OBLIQUE SHOCK INCIDENT ON A LAMINAR BOUNDARY LAYER

static pressure on the wall is characterized by an upstream compression, a "plateau" of constant pressure, and a final compression after the point of shock incidence.

In this problem, the difficulties in the analysis of the physical scheme discussed above are associated with the necessity (1) to assure boundary layer behavior of the flat plate type far upstream and downstream of interactions; (2) to describe the boundary layer profiles associated with separation and reattachment; and (3) to assure proper matching of the boundary layer upstream and downstream of the point of shock impingement. The most successful and advanced theories overcoming these difficulties and leading to reasonable agreement with experiment are those of Glick (Reference 10) and Bray et al (Reference 11); the former is limited to the adiabatic case while both have been applied to pressure ratios less than roughly three and to free stream Mach numbers less than 5.8.

The Problem Discussed

In the present report, there is considered a generalization of the studies described above to the interaction between a laminar boundary layer and a planar shock, which is normal to a plane surface but swept with respect to the flow far upstream. The flow and the coordinate system used in its treatment are shown schematically in Figure 2. Although this interaction can arise in supersonic flow, the main motivation for this study is provided by a problem which arises on hypersonic vehicles; thus the heat transfer in the interaction region will be of prime interest. Consider an unswept fin in the form of a wedge on a planar surface such as a wing. The shock wave caused by such a wedge can be idealized as shown in Figure 2; this is true even if the wedge is blunted provided the shock wave far from the leading edge is considered. It is noted that the analysis presented here can be readily modified for the case of a swept fin; the shock wave will still be normal as in Figure 2 but will have on its downstream side an accelerating, pressure gradient which must be superposed on that associated with the boundary layer behavior.

There are two features which complicate the presently considered problem; one is the sweep which results in three-dimensionality of the boundary layer and the second is the normality of the incident shock.

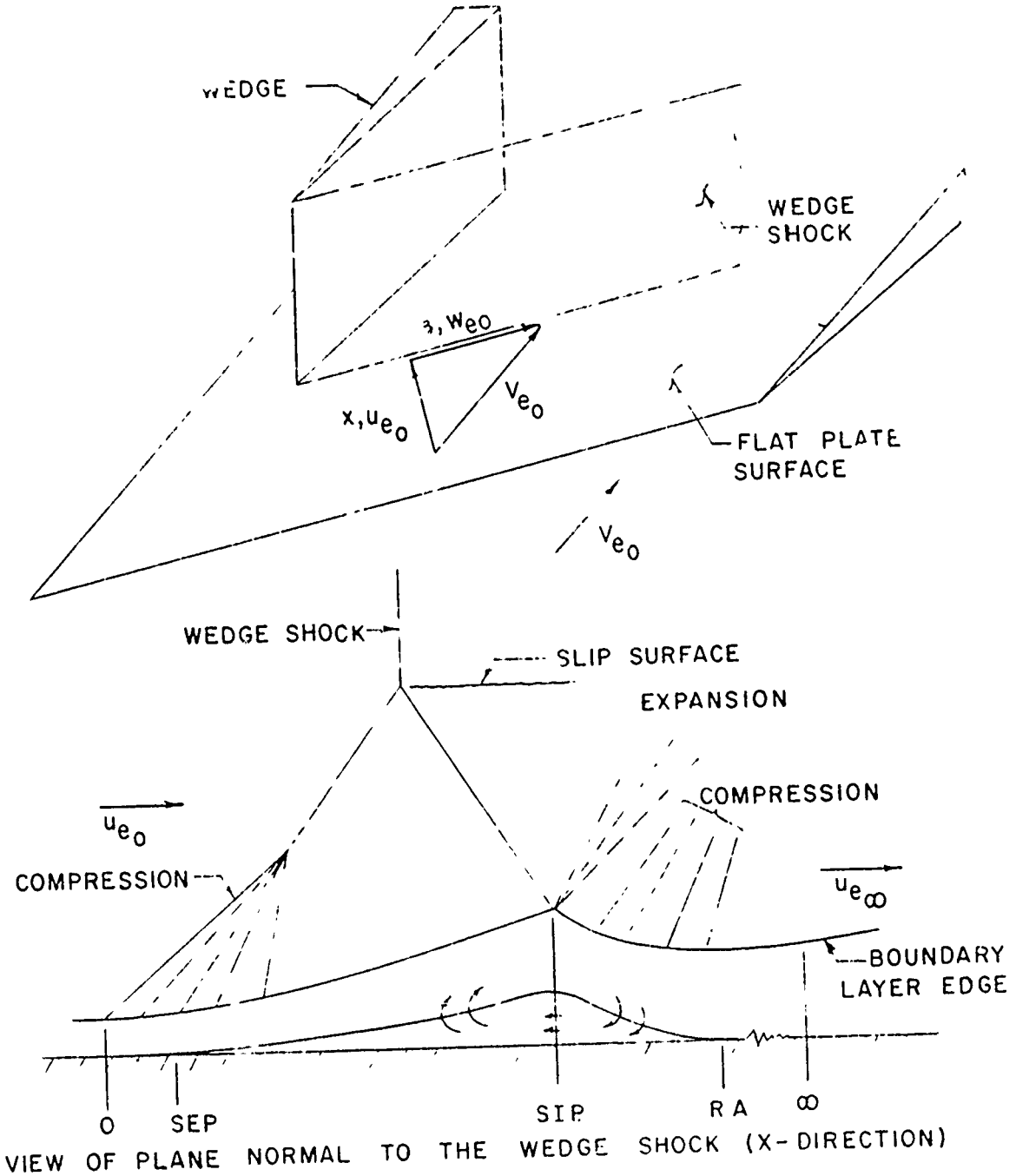


FIG. 2. SCHEMATIC REPRESENTATION OF THE THREE-DIMENSIONAL MODEL

In the analysis which follows, it will be shown that the first feature does not lead to essential difficulties provided $\partial/\partial z \simeq 0$; the velocity component in the z-direction can be considered separately and after the flow in the x-y plane, i.e., the two-dimensional problem, is determined. As a consequence the three-dimensionality enters in a simple and easily treated manner.

The second feature, the normality of the incident shock introduces difficulties with respect to the model for the external, inviscid flow. These are due to the existence of subsonic flow in the x-y plane $\left[(u^2 + v^2)/a^2 < 1\right]$ at large values of y. It will be seen from the analysis below that there appear to be two plausible models which can be assumed a priori and which can be verified as being consistent with the boundary layer behavior a posteriori. It may be that each model will arise depending on the static pressure ratio, the free stream Mach number and the Reynolds number characterizing the undisturbed boundary layer upstream of interaction.

Since the analysis reduces to the consideration of a two-dimensional interaction problem, it would have been possible to employ an adoption of the Crocco-Lees analysis. However, a more conventional integral method following Karman-Pohlhausen has been employed on the basis of the following considerations: Bray et al (Reference 11) concluded that "the results of the Crocco-Lees method, ..., are probably no better than those obtained much more readily by a Pohlhausen type of method". Moreover, Carlson (Reference 12) and Bloom (Reference 13) as well as Bray et al (Reference 11) have recently employed a conventional integral method for flows involving separation and reattachment and have indicated that such a method gives reasonable results.

Accordingly, a conventional integral method based on the profiles of Libby and Visich (Reference 14) was employed. However, several of the techniques used in solving the resulting equations were suggested by Glick (Reference 10) in connection with his study of the Crocco-Lees method.

The report is organized as follows: In the next section, the treatment of the boundary layer equations is discussed first. In Appendix B, the detailed development of the final equations employed

in the numerical integration is given while the main body of the report contains only the final forms of the equations. The treatment of the velocity component in the z-direction (cf. Figure 2) is presented so as to indicate the reduction of the problem to an almost two-dimensional one. Since the only available data correspond to the interaction with a two-dimensional oblique shock wave, the flow model therefor and the integration method minimizing iteration are discussed first. The problem of the inviscid flow model for an incident shock which is normal is presented next. Finally, there are described the integration and iteration techniques required for this latter case. In the next section, the predictions of theory and experiment for the case of an oblique incident shock are carried out; excellent agreement is demonstrated. The last section is devoted to concluding remarks.

The numerical results corresponding to heat transfer and to sweep will be presented in a separate report.

The authors are pleased to acknowledge the helpful and stimulating discussions with Dr. Antonio Ferri concerning the inviscid flow models. In addition, Dr. Lu Ting contributed to the early developments of the analysis of the two-dimensional problem.

ANALYSIS

Consider the flow over a flat surface with a pressure gradient such as that induced by a shock impinging on a boundary layer. Figure 2 schematically depicts the flow and the coordinate system under consideration. It is assumed that the changes in the direction parallel to the shock surface are approximately zero (i.e. $\partial/\partial z \simeq 0$) for both the boundary layer and the inviscid flow. This implies that the boundary layer characteristics upstream of the interaction region, i.e., a given x, are the same for all z and that the incident shock has a larger radius of curvature. In many problems of hypersonic flow this assumption will only yield a first approximation to the actual flow. In principal first order corrections for $\partial/\partial z \neq 0$ effects can be computed but the numerical complications would be considerable. It will be shown below that in view of the assumption $\partial/\partial z \simeq 0$, the velocity components in the w-direction can be considered separately and after the flow in the x-y plane is determined. Thus the problem is reduced to a two-dimensional one.

Basic Equations

The basic partial differential equations describing the laminar compressible boundary layer of a perfect gas with a constant Prandtl number of unity, a Chapman viscosity-temperature relation, and a constant coefficient of specific heat with $\partial/\partial z = 0$ are:

$$\rho u u_x + \rho v u_y = -p_x + (\mu u_y)_y \tag{1}$$

$$\rho u w_x + \rho v w_y = (\mu w_y)_y \tag{2}$$

$$(\rho u)_x + (\rho v)_y = 0 \tag{3}$$

$$\rho u H_x + \rho v H_y = (\mu H_y)_y \tag{4}$$

$$p = \rho RT \tag{5}$$

$$\mu = C_H \mu_w (T/T_w) \tag{6}$$

where $$H \equiv \left[(u^2 + w^2)/2 \right] + h \tag{6a}$$

Approximate solutions of Equations (1) - (6) can be obtained by the von Karman - Pohlhausen technique; moreover the Dorodnitzyn-Howarth transformation simplifies the analysis. There result the following equations:

$$\frac{d}{dx}\left[\delta_t \int_0^1 U(1-U)d\tau\right] + \theta\left(\frac{2}{u_e}\frac{du_e}{dx} + \frac{1}{\rho_e}\frac{d\rho_e}{dx}\right) + \frac{\delta^*}{u_e}\frac{du_e}{dx} =$$

$$\frac{(\mu u_y)_w}{\rho_e u_e^2} = \frac{C_H \mu_e (U_\tau)_w}{\rho_e u_e \delta_t} \tag{7}$$

$$\frac{d}{dx}\left[\delta_t \int_0^1 U(1-\tilde{W})\,d\tau\right] + \left[\delta_t \int_0^1 U(1-\tilde{W})\,d\tau\right]\frac{1}{\rho_e u_e}\frac{d(\rho_e u_e)}{dx} =$$

$$= \frac{C_H \mu_e}{\rho_e u_e \delta_t}(\tilde{W}_\tau)_w \tag{8}$$

$$\frac{d}{dx}\left[\delta_t \int_0^1 U(1-g)\,d\tau\right] + \left[\delta_t \int_0^1 U(1-g)\,d\tau\right]\frac{1}{\rho_e u_e}\frac{d(\rho_e u_e)}{dx} =$$

$$= \frac{(\mu H_y)_y}{\rho_e u_e H_e} = \frac{C_H \mu_e}{\rho_e u_e \delta_t} \left(g_\tau\right)_w \qquad (9)$$

where

$$U \equiv \frac{u}{u_e} , \qquad g \equiv \frac{H}{H_e} , \quad \text{and} \quad \tilde{W} \equiv \frac{w}{w_e}$$

Now examination of either Equations (2) and (4) or Equations (8) and (9) and consideration of the boundary conditions on w and H indicate that for the problem under discussion with a constant enthalpy at the wall $w \sim H$ so that

$$\tilde{W} \equiv w/w_e = (H-H_w)/(H_e-H_w) = (g-W)/(1-W) \qquad (10)$$

where

$W \equiv H_w/H_e$. Therefore, Equation (10) permits the influence of the w-velocity component to be eliminated in Equation (7) and thus a two-dimensional problem to be treated.*

The profiles which will be employed for U and g are those frequently used in boundary layer analyses and are given for example, in Reference 14.

$$U = (2\tau - 2\tau^3 + \tau^4) + \frac{\tilde{z}}{3} (\tau - 3\tau^2 + 3\tau^3 - \tau^4) \qquad (11)$$

$$g = 1 - (1-W)(1 - 10\tau^3 + 15\tau^4 - 6\tau^5) + \\ + b_1 (\tau - 6\tau^3 + 8\tau^4 - 3\tau^5) \qquad (12)$$

---

* Note that w is implicitly in δ^* in Equation (7)

where

$$\tilde{z} = \frac{\rho_e^2 \, \delta_t^2}{2C_H \rho_w \mu_e} \quad \frac{du_e}{dx} \tag{12a}$$

From Equation (11) it can be seen that separation is characterized by $\tilde{z} = -6$; moreover, reverse flow profiles correspond to $\tilde{z} < -6$.

With the profiles for U and g prescribed, the integrals in Equations (7) and (9) are as follows:

$$F_1 \equiv \int_o^1 U(1-U)\, d\tau = \frac{37}{315} - \frac{2}{945}\,\tilde{z} - \frac{1}{2268}\,\tilde{z}^2 \tag{13}$$

$$F_3 \equiv \int_o^1 U(1-g)\, d\tau = (1-W)\left(\frac{17}{70} + \frac{31}{2520}\,\tilde{z}\right) - \frac{79}{1260}\, b_1 - \frac{19}{7560}\, b_1 \tilde{z} \tag{14}$$

The final integral is

$$\delta^*/\delta_t = \int_o^1 \left[(\rho_e/\rho) - (u / u_e)\right] d\tau \tag{15}$$

and will contain the effect of sweep. Consider an approximate equation of state

$$h/h_e \approx \rho_e/\rho \tag{16}$$

Therefore

$$\frac{\rho_e}{\rho} = \frac{g - (w_e^2/2H_e)\,\tilde{W}^2 - (u_{e_o}^2/2H_e)\,\zeta^2 U^2}{(1 - w_e^2/2H_e) - (u_{e_o}^2/2H_e)\,\zeta^2} \tag{17}$$

where $\zeta \equiv u_e/u_{e_o}$

Substitution of Equation (10) for $\tilde{W}$ into Equation (17) and integration yields a relation for δ^*/δ_t as a function of $\tilde{z}$, b_1, and ζ (See Appendix A for details); namely,

$$\delta^*/\delta_t = F_1(b_1, \tilde{z})\, K_1(\zeta) - F_2(\tilde{z})\, K_1(\zeta)\, K_3(\zeta) - F_3(\tilde{z}) \quad (18)$$

It will now be convenient for future numerical analysis to treat ζ as the independent variable; this is possible if $\tilde{z}$, which is usually considered to be related through Equation (12a) with the properties of the external stream and δ_t, is treated as a dependent variable. The distribution of flow properties with respect to the space coordinate x will be obtained by a final integration of Equation (12a) after these properties have been determined as functions of ζ. To effect this transformation let

$$\left.\begin{aligned} \Delta &\equiv \delta_t/\delta_{t_o} \\ \Delta^* &\equiv \delta^*/\delta_{t_o} \\ Z &\equiv -d\zeta/d(x/\delta_{t_o}) \\ R &\equiv \rho_e/\rho_{e_o} \\ M &\equiv \mu_e/\mu_{e_o} \\ \text{and} \quad \theta &\equiv \delta_t F_1 \end{aligned}\right\} \quad (19)$$

Note that δ_{t_o} is the transformed boundary layer thickness upstream of the interaction region and that this is a parameter of the problem. The equations that result are

$$\frac{d}{d\zeta}(F_1 \Delta) + F_1 \Delta\left(\frac{2}{\zeta} + \frac{1}{R}\frac{dR}{d\zeta}\right) + \frac{\Delta^*}{\zeta} = -\frac{C_H M}{\zeta R \Delta}\left(\frac{\mu_e}{\rho_e u_e}\right)_o \frac{2+(\tilde{z}/3)}{\delta_{t_o} Z} \tag{20}$$

$$\frac{d}{d\zeta}(F_3 \Delta) + F_3 \Delta\left(\frac{1}{\zeta} + \frac{1}{R}\frac{dR}{d\zeta}\right) = -\frac{C_H M b_1}{\zeta R \Delta}\left(\frac{\mu_e}{\rho_e u_e}\right)_o \frac{1}{\delta_{t_o} Z} \tag{21}$$

where

$$\tilde{z} = \frac{R \Delta^2 Z}{2 C_H^2 M^2}\left(\frac{\rho_e u_e \delta_t}{\mu_e}\right)\left(\frac{\mu_w}{\mu_{e_o}}\right)$$

By suitable manipulation and combination of Equations (13), (14), (18), (20) and (21) the following nonlinear first-order differential equations result (cf. Appendix B for details):

$$\frac{d\Delta}{d\zeta} = G_1 \left(\Delta, \Delta^*, \tilde{z}, b_1, \zeta \right) \tag{22}$$

$$\frac{d\tilde{z}}{d\zeta} = G_2 \left(\Delta, \Delta^*, \tilde{z}, b_1 \zeta \right) \tag{23}$$

$$\frac{db_1}{d\zeta} = G_3 \left(\Delta, \Delta^*, \tilde{z}, b_1, \zeta \right) \tag{24}$$

These three equations involve four dependent variables (i.e., Δ, Δ^*, $\tilde{z}$, and b_1). The fourth equation is obtained from the coupling between the boundary layer behavior and the inviscid external flow.

In accordance with the usual idealization of the interaction discussed in the Introduction, the external flow will be treated as one isentropic flow upstream of the shock and a second such flow downstream thereof. Accordingly, the relation between change in speed and flow deflection in differential form for both flows will be

$$d\theta = - \sqrt{M_e^2 - 1} \quad (du_e/u_e) \tag{25}$$

Now assume that the velocity ratio external to the boundary layer immediately upstream of the shock is denoted as ζ_s, a quantity which is unknown a priori, and that the isentropic exponent γ in the external flow is constant. Then according to a second order theory

$$d\theta = \sqrt{M_{e_o}^2 - 1} \left\{ (\zeta - 1) + (\zeta - 1)^2 \left[1 + (\gamma - 1)(M_{e_o}^4/2) \right] / M_{e_o}^2 - 1) \right\} \tag{26}$$

for $\zeta_s \leq \zeta \leq 1$ and

$$d\theta = -\sqrt{M_{e_\infty}^2 - 1}\left\{\left[\zeta(u_{e_o}/u_{e_\infty}) - 1\right] + \left[\zeta(u_{e_o}/u_{e_\infty}) - 1\right]^2 \left[1 + \right.\right.$$

$$\left.\left. + (\gamma-1)(M_{e_\infty}^4/2)/(M_{e_\infty}^2 - 1)\right]\right\} \qquad (27)$$

for $\zeta_\infty \leq \zeta \leq \zeta_s$ where $\zeta_\infty \equiv (u_{e_\infty}/u_{e_o})$.

The rate of turning of the inviscid flow is related to the rate at which the boundary layer displaces the inviscid streamlines (i.e. to the displacement thickness). Therefore, for the upstream calculation,

$$d\theta = \frac{d\delta^*}{dx} - \left(\frac{d\delta^*}{dx}\right)_o = \left(-Z\frac{d\Delta^*}{d\zeta}\right) - \left(-Z\frac{d\Delta^*}{d\zeta}\right)_o \qquad (28)$$

while for the downstream calculation

$$d\theta = \frac{d\delta^*}{dx} - \left(\frac{d\delta^*}{dx}\right)_\infty = \left(-Z\frac{d\Delta^*}{d\zeta}\right) - \left(-Z\frac{d\Delta^*}{d\zeta}\right)_\infty \qquad (29)$$

The quantities $(d\delta^*/dx)_o$ and $(d\delta^*/dx)_\infty$ require some explanation; these quantities are the flow deflections far removed from the interaction region and are thus small compared to $d\delta^*/dx$ within the interaction region. However, they are given values which correspond to the local "flat plate" solutions, i.e. $(d\delta^*/dx)_o$ has the value given by $u_e = u_{e_o}$, $\delta_t = \delta_{t_o}$ while $(d\delta^*/dx)_\infty$ has the value given by $u_e = u_{e_\infty}$ and $\delta_t = \delta_{t_\infty}$. Now δ_{t_o}, u_{e_o} and u_{e_∞} are treated as known parameters of the problem; on the contrary, δ_{t_∞} is unknown a priori and must be determined from the solution along with the velocity ratio at the shock, ζ_s.

Equations (26) and (27) can be expressed symbolically as

$$\frac{d\Delta^*}{d\zeta} = \frac{1}{Z}\ G_4(\zeta) \qquad (30)$$

where

$$G_4(\zeta) = \left(Z\frac{d\Delta^*}{d\zeta}\right)_o - (1-\zeta)\sqrt{M_{e_o}^2 - 1} + (1-\zeta)^2\ \frac{1+\frac{\gamma-1}{2}M_{e_o}^4}{\sqrt{M_{e_o}^2 - 1}} \qquad (30a)$$

for the range $\zeta_s \le \zeta \le 1$

and

$$G_4(\zeta) = \left(Z\frac{d\Delta^*}{d\zeta}\right)_\infty - \left(1-\zeta\frac{u_{e_o}}{u_{e_\infty}}\right)\sqrt{M_{e_\infty}^2 - 1} + \left(1-\zeta\frac{u_{e_o}}{u_{e_\infty}}\right)^2\ \frac{1+\frac{\gamma-1}{2}M_{e_\infty}^4}{\sqrt{M_{e_\infty}^2 - 1}} \qquad (30b)$$

for the range $\zeta_\infty \le \zeta \le \zeta_s$.

The simultaneous solution of equations (22), (23), (24) and (30) in the four unknowns (i.e., Δ, Δ^*, $\tilde{z}$, b_1) yields the solution in the ζ plane. The extent of this region in the physical plane can be determined from the integration of equation (19) for Z; namely,

$$x = -\delta_{t_o}\int_{\zeta_\infty}^{\zeta} Z^{-1}\,d\zeta + \text{Constant.}$$

The constant of integration can be conveniently evaluated by setting $x = 0$ at $\zeta = \zeta_s$.

Thus

$$x = \delta_{t_o}\int_{\zeta}^{\zeta_s} Z^{-1}\,d\zeta \qquad (\zeta_\infty \le \zeta \le \zeta_s) \qquad (31)$$

and

$$x = -\delta_{t_o}\int_{\zeta_s}^{\zeta} Z^{-1}\,d\zeta \qquad (\zeta_s \le \zeta \le 1) \qquad (32)$$

Behavior of the Solution at $x \longrightarrow \pm \infty$

At the ends of the interval $\zeta_\infty \leq \zeta \leq 1$, the solution must correspond to "flat plate" solutions. However, at the end points $\tilde{z}$ does not approach zero but rather approaches a small, positive value corresponding to weak interaction between the boundary layer and the inviscid flow. These end point values on $\tilde{z}$ also correspond to the values of $(Zd\Delta^*/d\zeta)_0$ and $(Zd\Delta^*/d\zeta)_\infty$ in Equations (30a) and (30b). The boundary values of all the dependent variables will be discussed below in more detail; it is sufficient for the present purpose to recognize that in the interaction region $\tilde{z} < 0$ and that as $\tilde{z}$ changes sign, i.e. $\tilde{z} = 0$, $d/d\zeta \longrightarrow \infty$. These singularities are removed by treating Δ as the independent variable; thus Equations (23), (24) and (30) can be written formally as

$$d\Delta^* / d\Delta = Z(d\Delta^*/d\zeta) / \left[Z(d\Delta/d\zeta)\right] \tag{33}$$

$$d\tilde{z}/d\Delta = Z(d\tilde{z}/d\zeta) / \left[Z(d\Delta/d\zeta)\right] \tag{34}$$

and $$db_1/d\Delta = Z(db_1/d\zeta) / \left[Z(d\Delta/d\zeta)\right] \tag{35}$$

where all the derivatives on the left are finite. Thus at the end points of the range of ζ, Δ was employed as the independent variable while in the interior of the range either ζ or Δ was used.

COMPUTATIONAL PROCEDURE

The solution to the shock wave-boundary layer interaction problem entails the simultaneous solution of either Equations (22) to (24) and Equation (30) or Equations (22), (33), (34), and (35). These equations are nonlinear, first-order differential equations. Consider the initial value of these equations; there are, in general, two types of problems of interest. In both it is assumed that W, ζ_∞, and the characteristics of the inviscid flow upstream of the interaction region are known. In one type of problem the boundary layer properties "upstream" of interaction are specified; thus, for example δ_{t_o}, $b_{1\,o}$ are known. Now if $\tilde{z} \ll 1$, Δ^*_o can be computed from the known values of δ_{t_o}, $b_{1\,o}$, and W and a value of $\tilde{z}_o > 0$ estimated from Equation (18). In addition $(Z\, d\Delta^*/d\zeta)_o$ in Equation (30a) can be computed from the standard "flat plate" equations. Thus the integration can proceed from $\zeta = 1$ with Δ as the independent variable. From $\tilde{z} = \tilde{z}_o$ to $\tilde{z} = 0$, ζ increases while for $\tilde{z} < 0$, ζ decreases; when $\tilde{z} = -6$ separation occurs. The integration in the direction of ζ decreasing is continued until either ζ approaches a constant value ζ_n or on the basis of previous results a sufficiently small value of ζ is reached. It is interesting to note that for each set of initial values, i.e. those values of $\zeta = 1$, a minimum value of $\zeta = \zeta_n$ is obtained. At this value $\tilde{z}$ and b_1 approach constant values while Δ increases without limit; this solution corresponds to a boundary layer growing linearly with x with similar profiles and would appear to have applicability to the flow upstream of a step*.

The solution for the downstream region must, in general, be initiated by an integration from $\zeta = \zeta_\infty$. It is necessary to assume a value for Δ_∞; $b_{1\,\infty} = b_{1\,o}$ as is consistent with the assumption of flat plate behavior far downstream, then $\tilde{z}_\infty$ can be estimated in the same manner as $\tilde{z}_o$ and the value of $(Z\, d\Delta^*/d\zeta)_\infty$ in Equation (30b) computed. The integration can then be carried out first for decreasing ζ until $\tilde{z} = 0$ and then for increasing ζ as $\tilde{z} < 0$. At some value of ζ, the curve for one of the dependent variables, say Δ, given by this downstream solution will intersect the corresponding curve from upstream solution. However, at this same value of ζ the solution for Δ^* will not be continuous implying that the assumed

* The discussion in this section may be clarified by reference to Fig. 9.

value for Δ_∞ was incorrect. A systematic correction procedure can be employed to determine the proper value for Δ_∞. The value of ζ at the intersection point of the upstream and downstream solutions is denoted ζ_s. Note that it is assumed that continuity of Δ^* at ζ_s assures continuity in b_1 and $\tilde{z}$. For $b_1 \equiv 0$, i.e. for the adiabatic case, continuity in $\tilde{z}$ is assured. There are cases for which the value $\zeta = \zeta_s$ can be estimated a priori so that the downstream solution can be started at $\zeta = \zeta_s$, with Δ^*, b_1, and $\tilde{z}$ continuous, and continued to $\zeta = \zeta_\infty$. One such case is that of the oblique incident shock sufficiently weak so that it may be considered isentropic; in this case the flow deflection through the shock is essentially unaltered by the upstream compression. Moreover, the deflection through the expansion far downstream of shock impingement is equal to that through the shock. These considerations employed in connection with Equations (27) and (28) permit ζ_s to be determined. A second case is that of a normal shock in which it can be assumed that the pressure downstream of the shock corresponding to the second leg is equal to that behind the normal shock and the flow deflection is zero. In this case, ζ_s is readily computed from the shock conditions.

In both of these cases it is necessary to estimate the value of $(Z\, d\Delta^*/d\zeta)_\infty$ in Equation (30b) since this depends on Δ_∞ a priori. However, this quantity is small and is unknown, in general, and a correction procedure should be rapidly convergent. It should be noted that if ζ_s is known, Δ_∞ is obtained from the calculation as $\zeta \longrightarrow \zeta_\infty$.

These considerations must be altered somewhat in a second type of problem in which the shock position with respect to a leading edge, for example, is specified. In this case, the extent of the upstream region of influence is unknown a priori. As a consequence it is necessary to assume values for $R_{\delta t_o}$, determine the proper solution as described above and carry out the integration to obtain the distribution of boundary layer characteristics in the physical plane. In general, the distribution of δ_t will not be constant with the location of the leading edge of interaction so that $R_{\delta t_o}$ must be altered*.

* It was found from the numerical analysis leading to Figure 9 ($b_1 \equiv 0$) that the value of Δ_∞ corresponding to solutions for a range of $R_{\delta t_o}$ was essentially independent thereof.

COMPARISON OF THEORY WITH EXPERIMENT

The method outlined in this report was used to compute the properties in the region of interaction where a shock impinges on a laminar boundary layer. Since the only available data correspond to the interaction with a two-dimensional oblique shock wave, for the adiabatic wall case, numerical examples were computed for this comparison and the validity of the method was demonstrated. The present report considers only the two-dimensional adiabatic wall comparison. Numerical examples for both the two-dimensional and the three-dimensional heat transfer cases will be presented in a subsequent report.

A. Comparison with the Experiments of Hakkinen, Greber, Trilling and Abarbanel (Ref. 4)

Two discrete problems have been computed and, in both cases, the free stream Mach number was 2.0. The experimental data presented consisted of measured pressure and shear distribution and velocity profiles in the region of interaction. The difficulties in achieving a proper comparison with the experimental data presented arose because of the incomplete presentation of the conditions for the experiments. In both cases presented, the authors had to approximate certain test conditions. However, the presentation of velocity profiles upstream of the interaction region minimized the iteration necessary to achieve the correct $R_{\delta_{t_o}}$.

The first case corresponds to an interaction where the pressure rise across the shock system corresponds to $P_{e_\infty}/P_{e_o} = 1.40$. The Reynolds number based on the x distance to the shock impingement point is 2.96×10^5. A summary of the input parameters for the numerical computation are listed in Table I. The comparison of the theory with experiment for the pressure and shear distributions are shown in Figure 3. The velocity profile comparison is shown in Figure 4. The agreement shown therein is good, however, as was mentioned above, better knowledge of the test conditions (e.g. T_w, T_o) would result in a closer agreement between the experimental C_f and the computed C_f upstream and downstream of interaction. The solution generated for Δ, Δ^*, and $\tilde{z}$ in the ζ plane are shown in Figure 5.

TABLE 1

SUMMARY OF INPUT PARAMETERS

	Case I (Ref. 4)	Case II (Ref. 4)	Case III (Ref. 5)
M_{e_o}	2.00	2.00	2.40
M_{e_∞}	1.781	1.856	1.905
u_{e_o}, fps	1734.3	1734.3	1846.1
w_{e_o}, fps	0	0	0
ζ_∞	0.9346	0.9579	0.8864
$b_{1_o} = b_{1_\infty}$	0	0	0
P_{e_∞}/P_{e_o}	1.40	1.25	2.15
$R_{\delta t_o}$	2680	3800	1500
C_H	0.92	0.92	0.90
$\left(Z \frac{d\Delta^*}{d\zeta}\right)_o$	-0.003573	-0.003374	-0.004760
$\left(Z \frac{d\Delta^*}{d\zeta}\right)_\infty$	-0.001367	-0.002672	-0.001539
Δ_∞	2.19	1.716	3.10
R_{x_s}	2.96×10^5	2.87×10^5	0.54×10^5

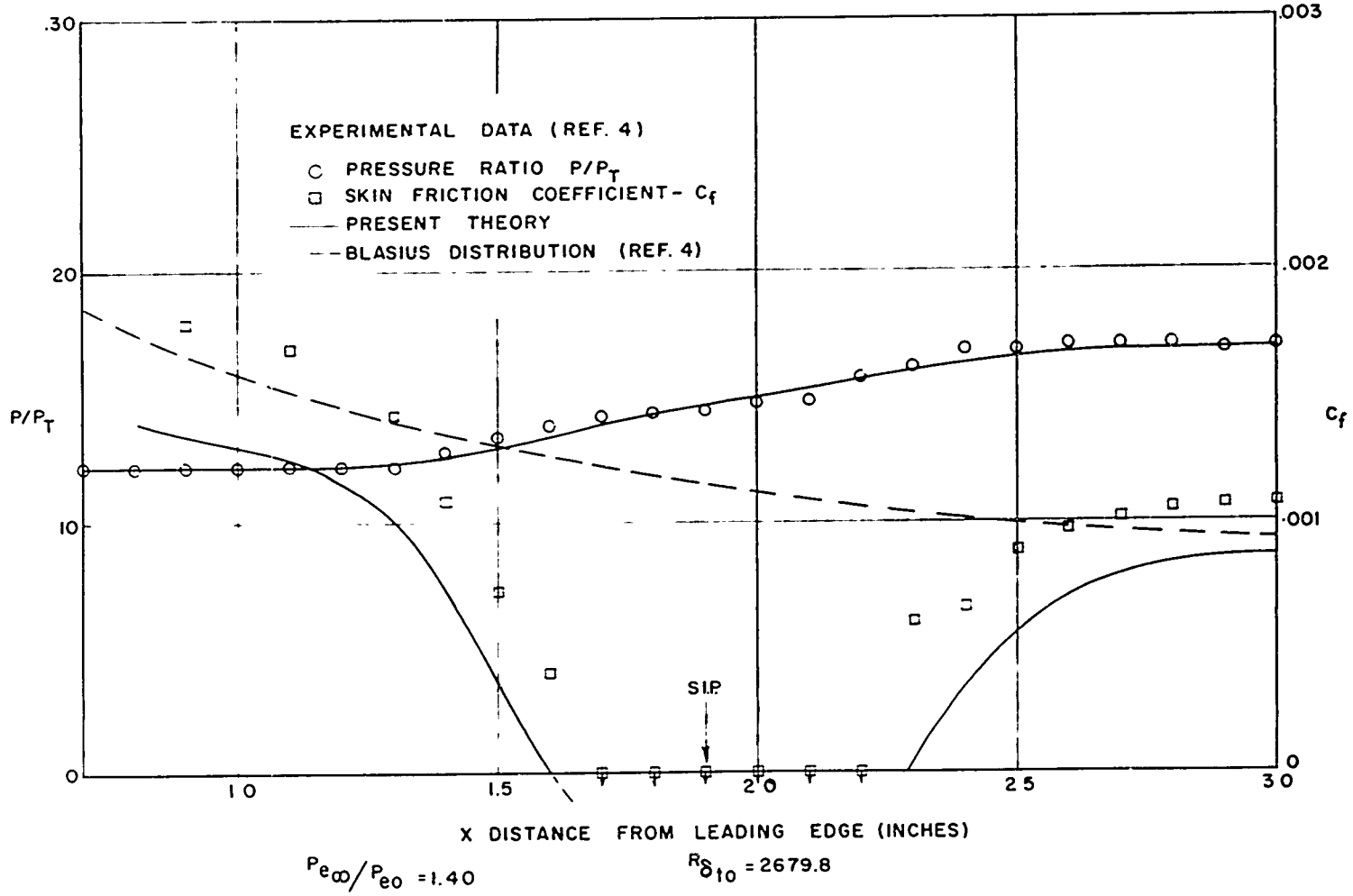


FIG. 3. COMPARISON OF PRESENT THEORY AND EXPERIMENT FOR PRESSURE AND WALL SHEAR DISTRIBUTIONS INDUCED BY AN INCIDENT SHOCK, $M_{e_o} = 2.0$ (CASE I)

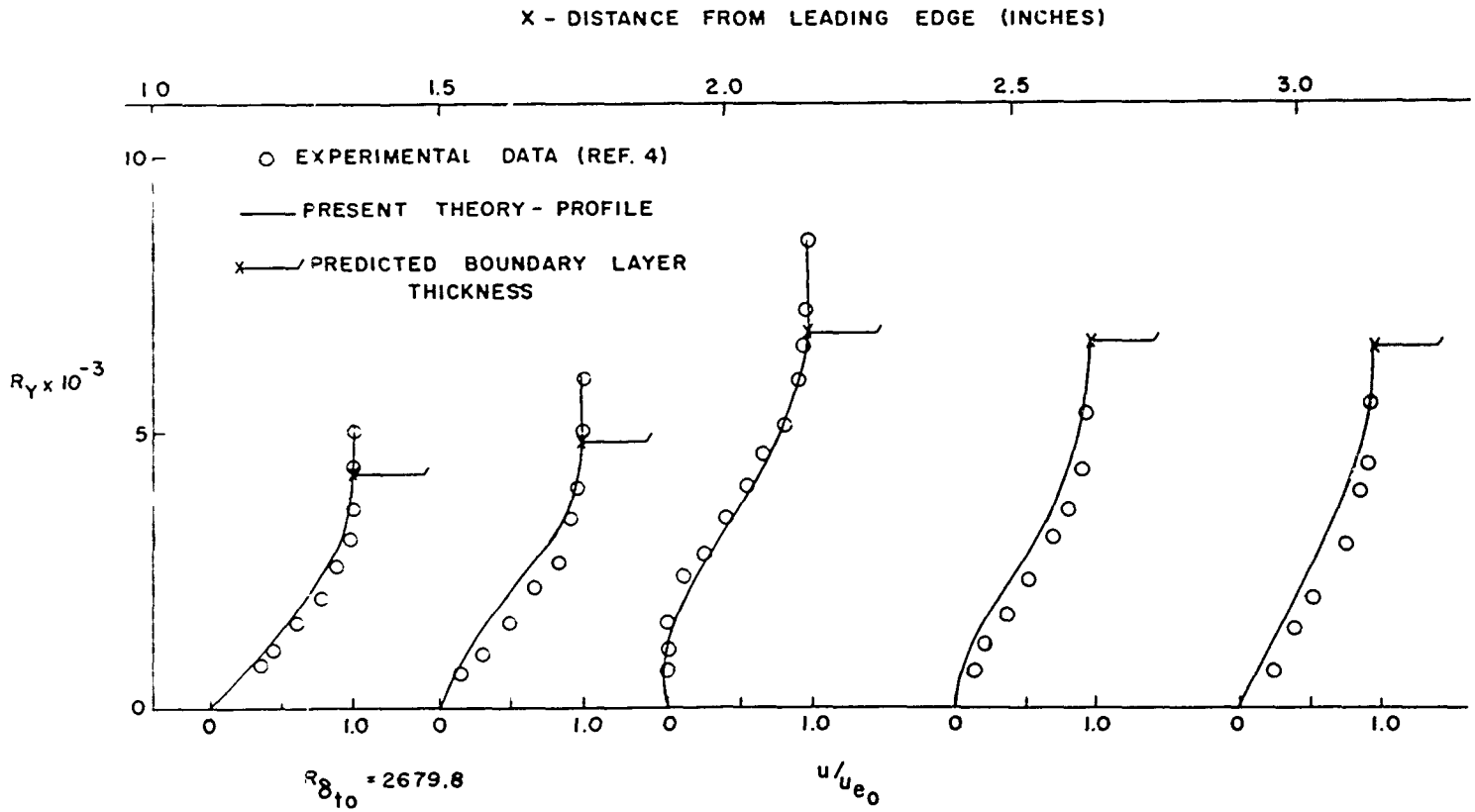


FIG. 4. COMPARISON OF PRESENT THEORY AND EXPERIMENT FOR VELOCITY PROFILES IN THE INTERACTION REGION (CASE I)

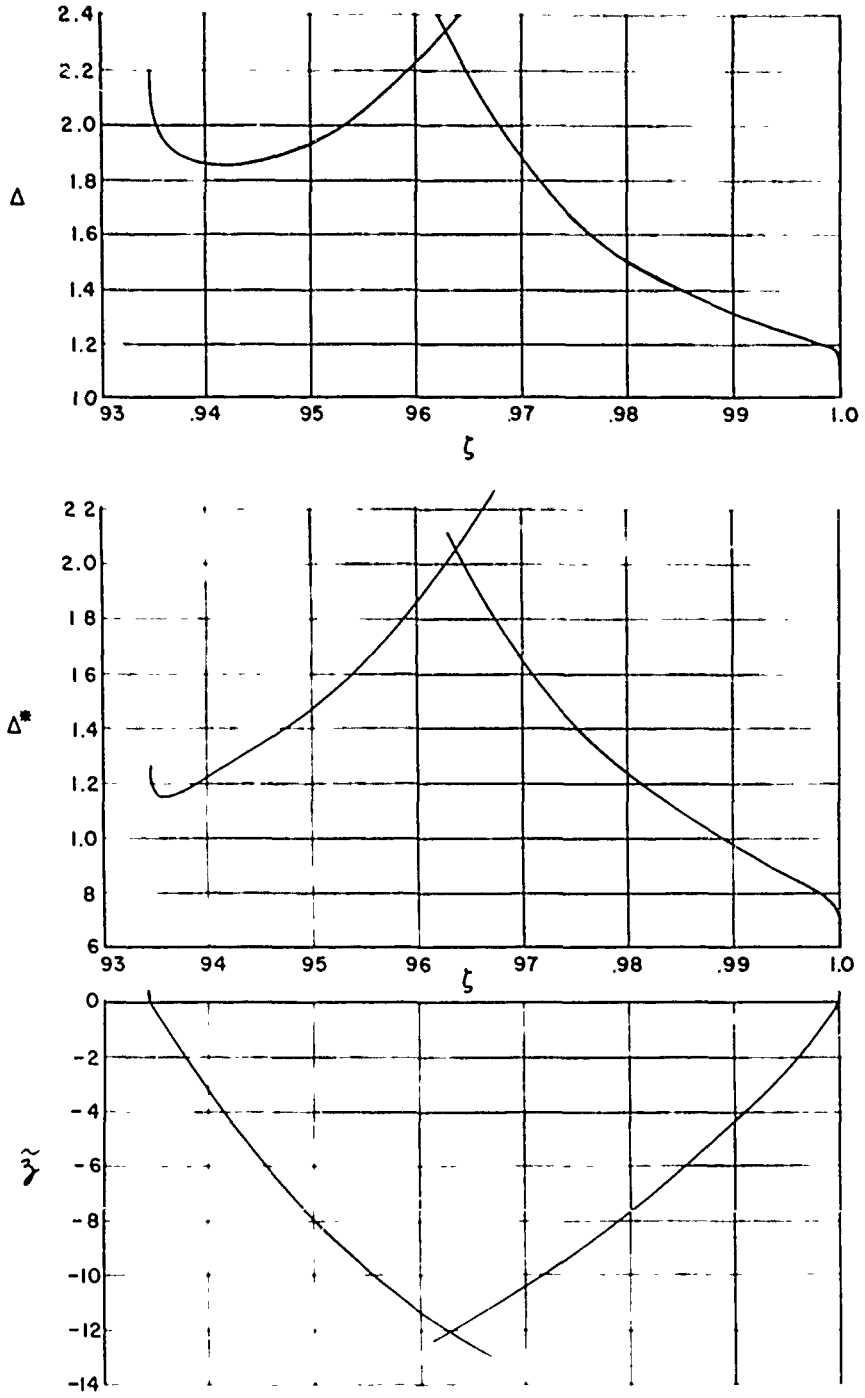


FIG. 5. GRAPHIC REPRESENTATION OF THE SOLUTION GENERATED FOR THE BOUNDARY LAYER THICKNESS, DISPLACEMENT THICKNESS, AND SHEAR PARAMETER AT WALL (CASE I)

The second numerical example corresponds to a pressure rise across the shock system of 1.25 with a Reynolds number based on x to the shock impingement point of 2.87×10^5. A summary of the input parameters for the numerical computation are listed in Table I. The comparison of the theory and experiment for the pressure and shear distributions are shown in Figure 6, while the velocity profile comparison is shown in Figure 7; good agreement is also shown therewith. The solution as generated in the ζ plane is shown in Figure 8.

B. Comparison with the Experimental Data of Chapman, Kuehn and Larson (Ref. 5)

The pressure distribution for the interaction of a two-dimensional oblique shock with a laminar boundary layer in a flat plate is presented in Ref. 5. The experiments were conducted at a nominal Mach number of 2.40 with the Reynolds number based on the x distance to the shock impingement point of 0.54×10^5. A summary of the input parameters for the numerical computation are listed in Table I. The associated pressure rise across the shock system was 2.15. Calculations were performed for several values of $R_{\delta_{t_o}}$ and the effect of this parameter on the Δ solution in the ζ plane are shown in Figure 9. The pressure distribution dependency on $R_{\delta_{t_o}}$ is shown in Figure 10, whereas the comparison of the solution obtained for an $R_{\delta_{t_o}} = 1500$, with the experimental data, is presented in Figure 11. The results of the analysis are shown to be in good agreement with experiment.

From Figure 9, one will note that the value of ζ_s and Δ_∞ are essentially independent of $R_{\delta_{t_o}}$. Thus where the comparison of the theory with experiment is desired, two iterations are necessary. However, the second iteration for $R_{\delta_{t_o}}$ was performed only after the value of Δ_∞ had been determined. For a system with a given overall pressure rise, for small values of $R_{\delta_{t_o}}$ the pressure will rise nonatonically from P_{e_o} to P_{e_∞} without a plateau (Fig. 10). As the value of $R_{\delta_{t_o}}$ is increased, the presence of a plateau begins becoming imminent; for larger values of $R_{\delta_{t_o}}$ the length of the plateau becomes more pronounced. Thus the existence of a pressure plateau depends on the value of $R_{\delta_{t_o}}$.

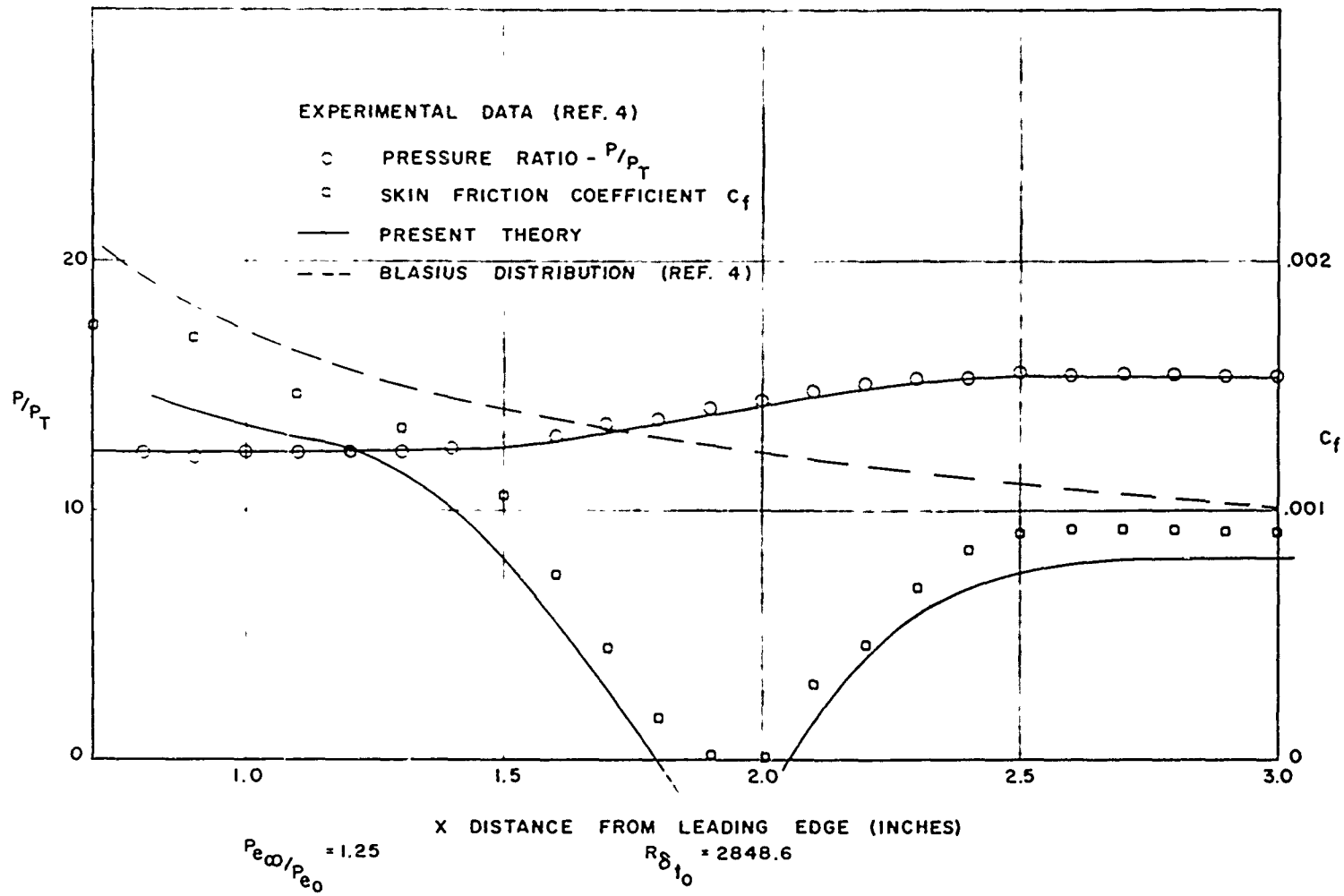


FIG. 6. COMPARISON OF PRESENT THEORY AND EXPERIMENT FOR PRESSURE AND WALL SHEAR DISTRIBUTIONS INDUCED BY AN INCIDENT SHOCK, $M_{e_0} = 2.0$ (CASE II)

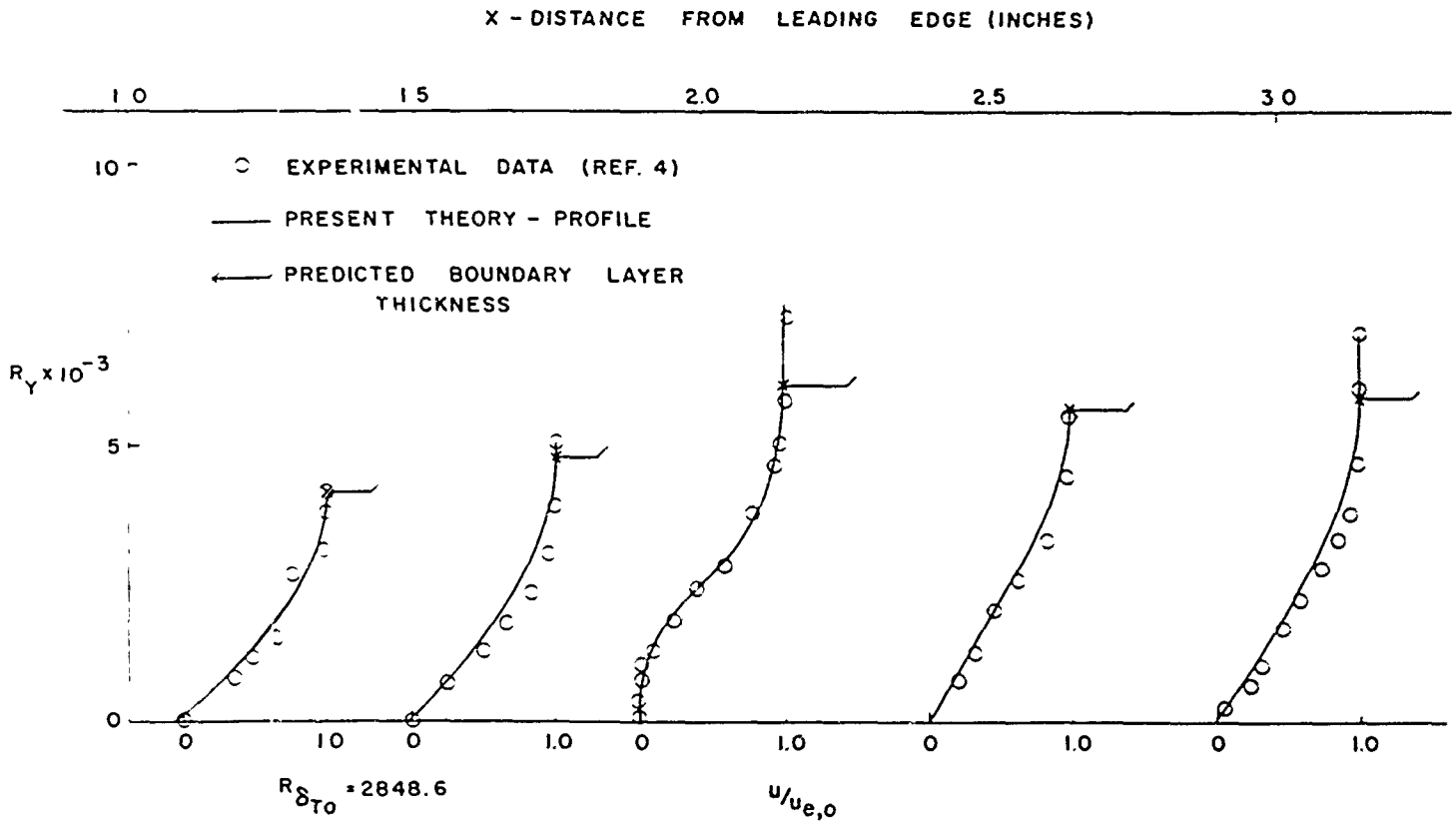


FIG. 7. COMPARISON OF PRESENT THEORY AND EXPERIMENT FOR VELOCITY PROFILES IN THE INTERACTION REGION (CASE II)

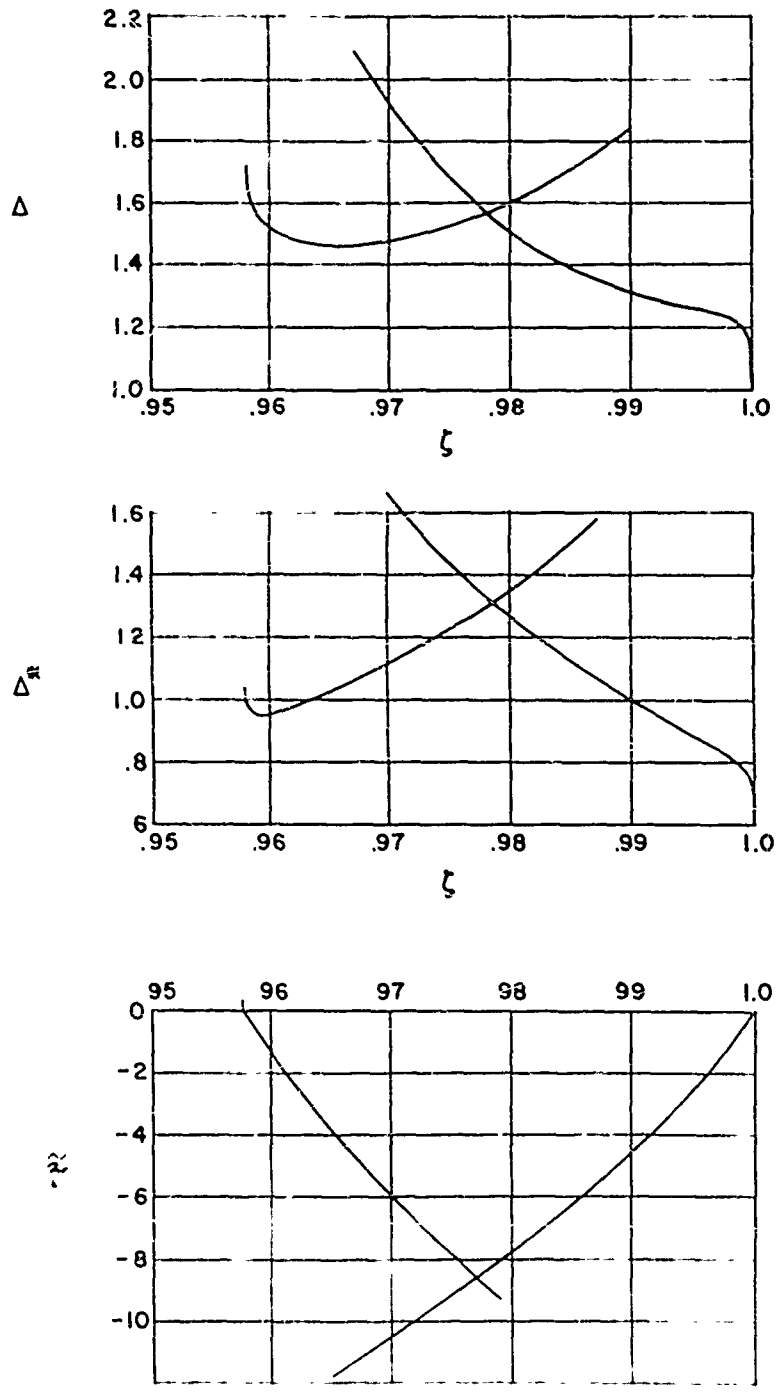


FIG. 8. GRAPHIC REPRESENTATION OF THE SOLUTION GENERATED FOR THE BOUNDARY LAYER THICKNESS, DISPLACEMENT THICKNESS, AND SHEAR PARAMETER AT WALL (CASE II)

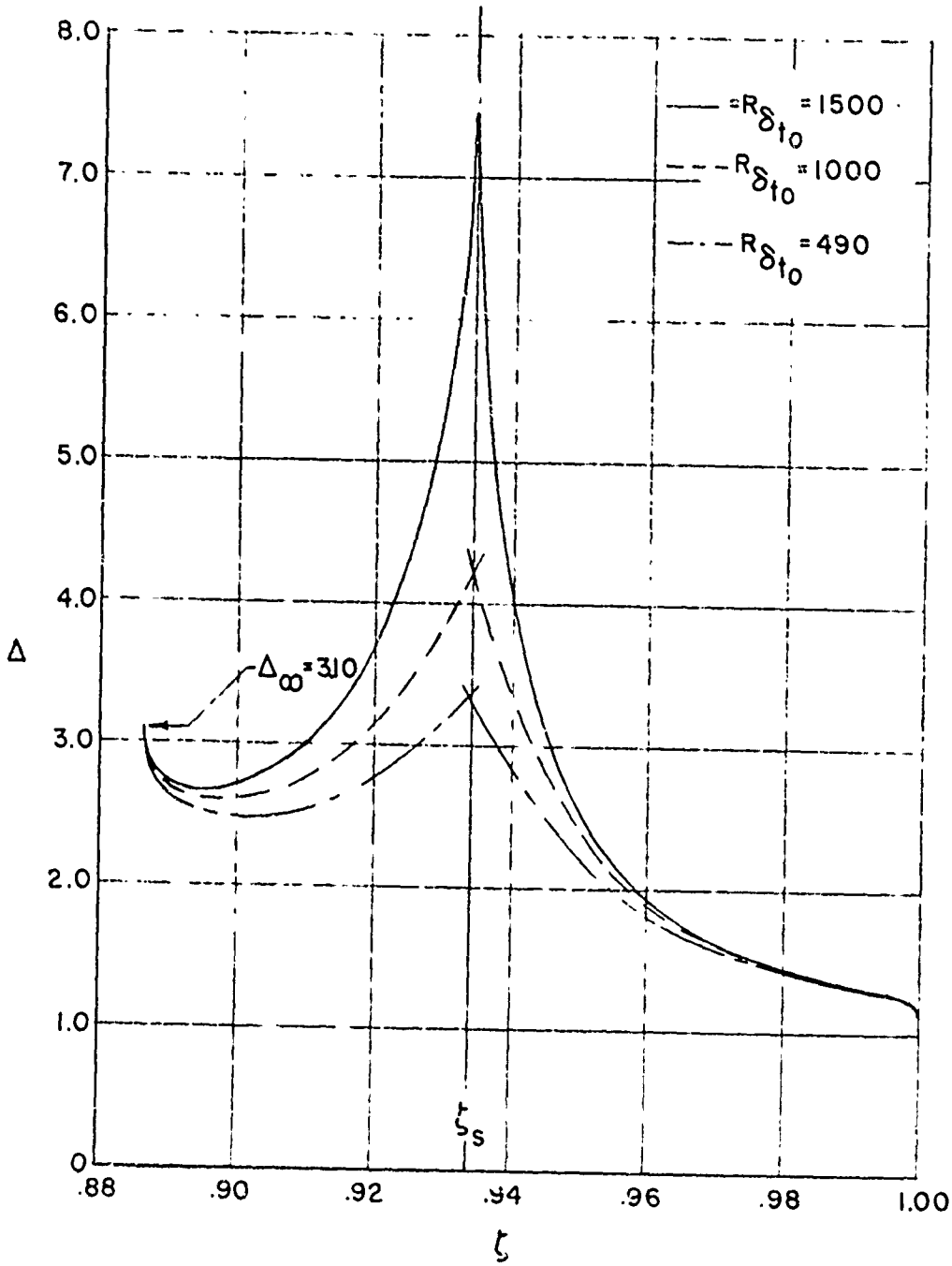


FIG. 9. EFFECT OF $R_{\delta_{t_0}}$ ON THE SOLUTION FOR Δ

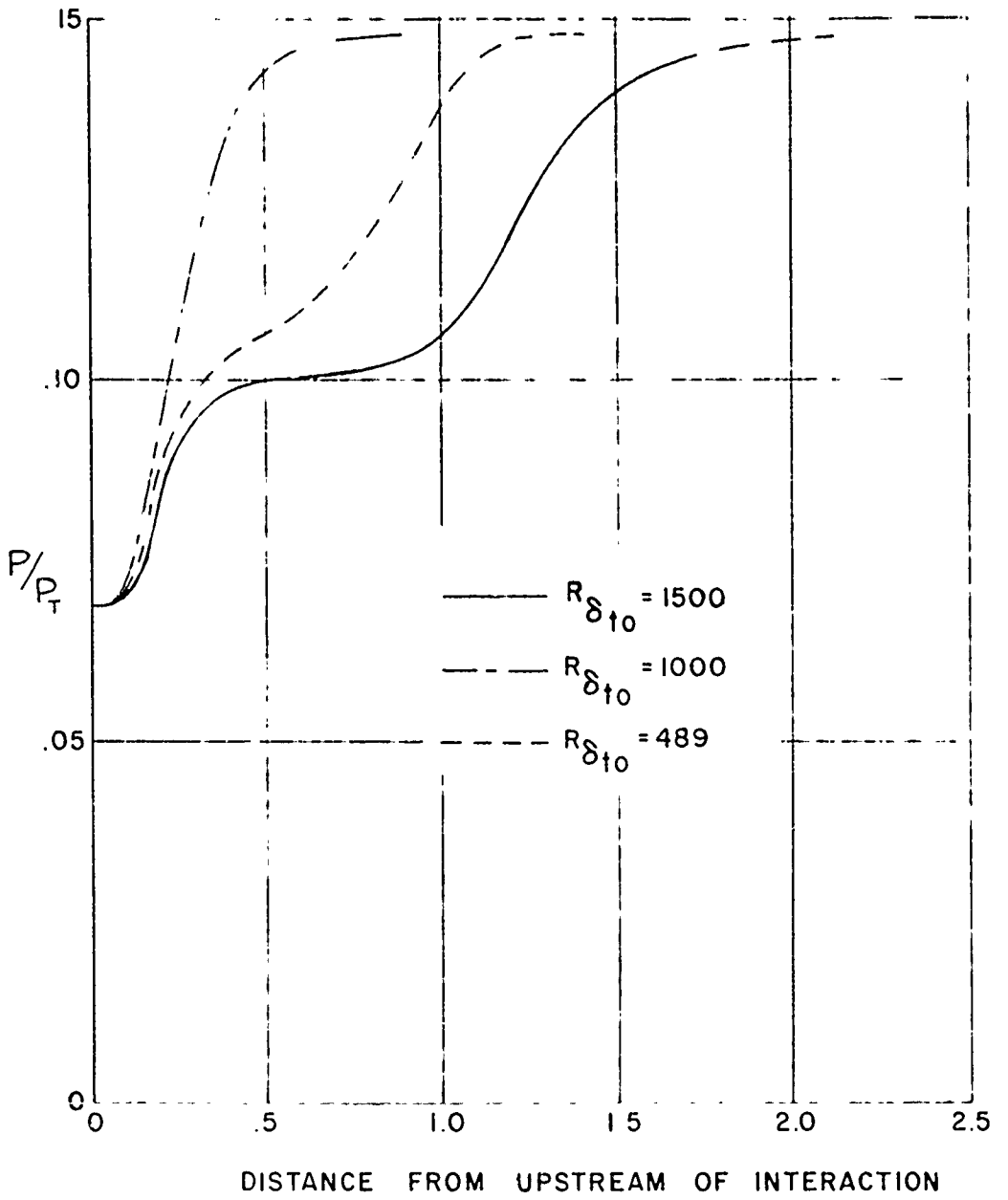


FIG. 10. EFFECT OF $R_{\delta_{to}}$ ON THE PRESSURE DISTRIBUTION IN THE INTERACTION REGION

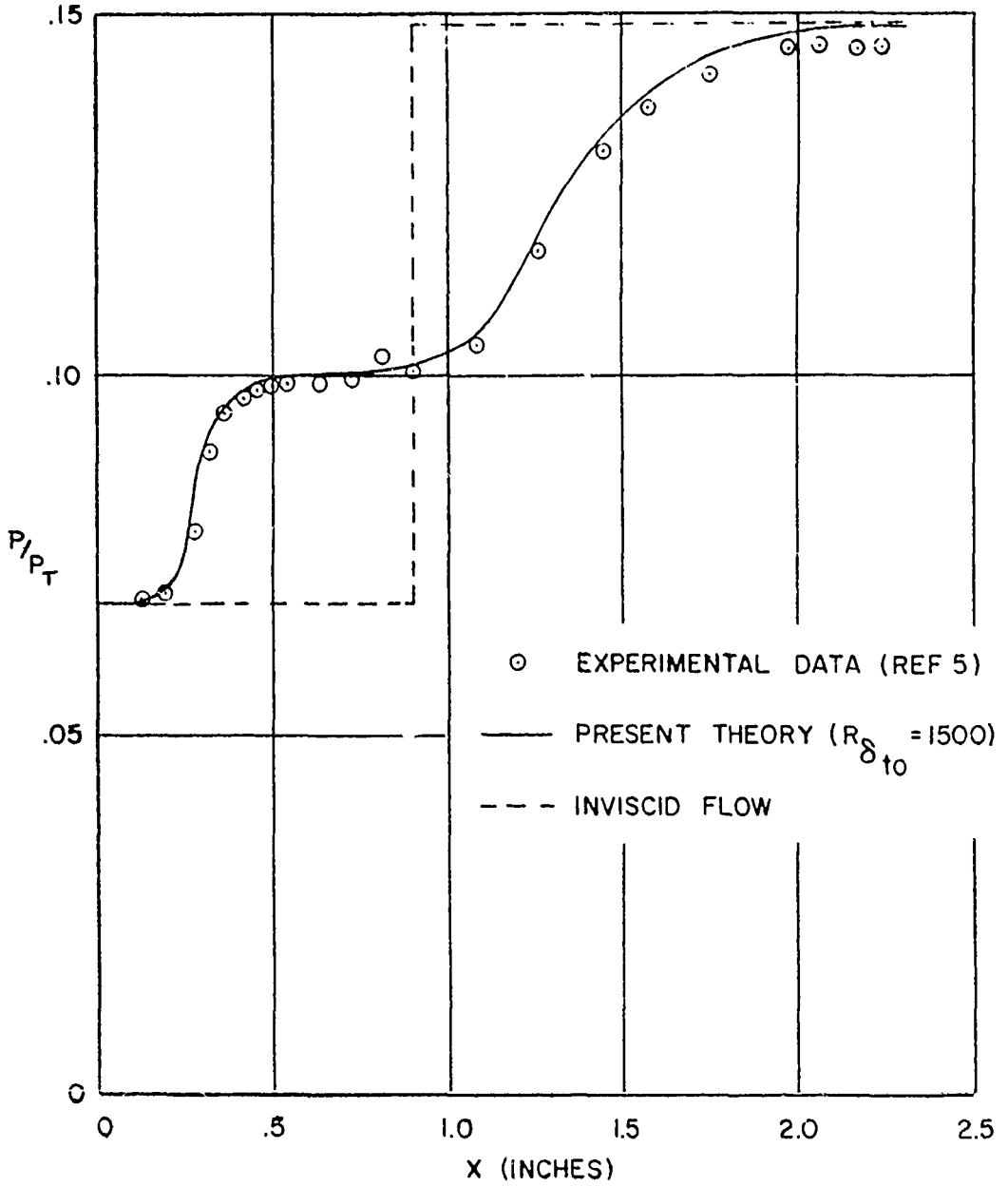


FIG. 11. COMPARISON OF PRESENT THEORY AND EXPERIMENT FOR THE PRESSURE DISTRIBUTION INDUCED BY AN INCIDENT SHOCK, $M_{e_o} = 2.40$ (CASE III).

The numerical computations were performed on a Bendix G-15 Digital Computer. A typical calculation for both the upstream and downstream legs of the solution requires approximately five hours of computing time on the Bendix which is comparable to roughly one minute on an IBM 7090.

CONCLUDING REMARKS

The interaction between a laminar boundary layer on a flat plate and a planar shock wave which is swept with respect to the flow external to the boundary layer but normal to the plate has been formulated. For a planar shock, the effect of sweep is easily included and thus a model for two-dimensional flow is basic to the problem. With the acceptance of the "lambda" shock as the inviscid model, it was shown that the interaction involves two pressure-flow deflection relations, one applicable upstream of the second leg of the "lambda" and one downstream thereof. A constant pressure reflection of this second leg from the boundary layer was assumed. Many of the features used in the past for the two-dimensional interaction between an incident oblique shock and a laminar boundary layer were incorporated in the present model.

The boundary layer equations corresponding to the swept case were postulated and the relation between the tangential velocity component and the stagnation enthalpy were used to eliminate this component in the momentum equation corresponding to the direction normal to the shock. Thus the two-dimensional boundary layer interaction in planes normal to the shock could be considered first; the spanwise boundary layer and secondary flow effects could then be considered.

The technique of solution for the boundary layer properties is based on an integral method for the momentum and energy equations with the pressure distribution unknown. As in previous investigations the velocity external to the boundary layer was considered to be the independent variable. As a result, the range of integration was defined by the flow conditions far from the region of interaction which

is known a priori from inviscid flow considerations. The end points of this range are singular since they transform upon final integration into $x \longrightarrow \pm \infty$. In general, the numerical integration is carried out separately from the end points of the interval with iteration employed to yield matching at the intersection point of the upstream and downstream solutions.

To verify the validity of the inviscid flow model and the accuracy of the treatment of the boundary layer, there was considered first the two-dimensional adiabatic wall case, for which accurate and carefully obtained experimental data and the results of previous analyses are available. In a subsequent report, the method will be applied to the two-dimensional and the sweep case with heat transfer.

Several numerical examples are presented for the two-dimensional interaction case, and the results are compared to the available experimental data. The analysis is shown to be in good agreement therewith.

For a problem, in which the boundary layer thickness upstream of interaction is known, the unknown parameter to the problem is the boundary layer thickness at the downstream edge of the interaction region, Δ_∞. Under some circumstances, the value of Δ_∞ can be found with essentially no iteration. When verification of experimental data involving a fixed shock location is desired, two parameters must be determined; namely, Δ_∞ and the value of the Reynolds number based on the transformed boundary layer thickness upstream of interaction.

APPENDIX A

Consider the nondimensional integral for displacement thickness

$$\frac{\Delta^*}{\Delta} = \frac{\delta^*}{\delta_t} = \int_o^1 \left(\frac{\rho_e}{\rho} - \frac{u}{u_e} \right) \, d\tau \tag{15}$$

With the assumption that $\frac{\partial P}{\partial y} = 0$ across the boundary layer, and for a gas with a constant specific heat

$$\frac{\rho_e}{\rho} \approx \frac{h}{h_e} \tag{16}$$

but

$$\frac{h}{h_e} = \frac{H - \frac{u^2 + w^2}{2}}{H_e - \frac{u_e^2 + w_e^2}{2}} = \frac{\frac{H}{H_e} - \frac{u^2}{2H_e} - \frac{w^2}{2H_e}}{1 - \frac{u_e^2}{2H_e} - \frac{w_e^2}{2H_e}} \tag{36}$$

Therefore

$$\frac{\rho_e}{\rho} = \frac{g - \left(\frac{w_e^2}{2H_e} \right) \tilde{W}^2 - \left(\frac{u_{e_o}^2}{2H_e} \right) \left(\frac{u_e}{u_{e_o}} \right)^2 U^2}{\left(1 - \frac{w_e^2}{2H_e} \right) - \left(\frac{u_{e_o}^2}{2H_e} \right) \left(\frac{u_e}{u_{e_o}} \right)^2} \tag{37}$$

The profiles used for u/u_e, and H/H_e are taken from Libby and Visich (Reference 14).

$$\text{i.e. } U \equiv \frac{u}{u_e} = 2\tau - 2\tau^3 + \tau^4 + \frac{\tilde{z}}{3} (\tau - 3\tau^2 + 3\tau^3 - \tau^4) \tag{11}$$

(12)

$$g \equiv \frac{H}{H_e} = 1 - (1-W)(1-10\tau^3 + 15\tau^4 - 6\tau^5) + b_1 (\tau - 6\tau^3 + 8\tau^4 - 3\tau^5)$$

From the Crocco relation

$$\tilde{W} \equiv \frac{w}{w_e} = \frac{H-H_w}{H_e-H_w} = \frac{H/H_e - H_w/H_e}{1 - H_w/H_e} = \frac{g - W}{1 - W} \qquad (10)$$

Therefore Equation (37) becomes

$$\frac{\rho_e}{\rho} = K_1 \left\{ (1+2WK_2)\, g - K_2\, g^2 - W^2 K_2 - K_3 U^2 \right\} \qquad (38)$$

where

$$\left.\begin{aligned} K_1 &= \frac{1}{1 - \frac{w_e^2}{2H_e} - K_3} \\ K_2 &= \frac{w_e^2}{2H_e (1 - W)^2} \\ K_3 &= \frac{u_{e_o}^2}{2H_e}\, \zeta^2 \end{aligned}\right\} \qquad (39)$$

Substituting Equations (11), (12), and (38) into (15) and integrating yields

$$\frac{\Delta^*}{\Delta} = AK_1 - BK_1 K_3 - C \qquad (18)$$

where

$$A + K_2 \left\{ \frac{1}{2K_2} (1+W) - \frac{181}{462} (1-W)^2 + \left[\frac{1+2WK_2}{10K_2} + \frac{311}{2310} (1-W) - \frac{1}{5} \right] b_1 - \frac{52}{3465} b_1^2 \right\} \quad \begin{pmatrix} w_e \neq 0 \\ W \neq 1.0 \end{pmatrix}$$

$$B = \frac{367}{630} + \frac{213}{11340}\ \tilde{z} + \frac{1}{2268}\ \tilde{z}^2$$

and

$$C = \frac{7}{10} + \frac{\tilde{z}}{60}$$

when $w_e = 0$ but $W \neq 1$

$$A = \frac{1}{2}(1 + W) + \frac{1}{10}\ b_1$$

and when $W = 1$ and $b_1 = 0$

$$A = 1 - \frac{w_e^2}{2H_e}$$

For a flat plate, a simple relationship exists between W and b_1, which can be readily determined by means of Equations (2), (4) and the Crocco relation.

That is

$$H = A + Bu = H_w + (1-W)\ H_e \frac{u}{u_e} \qquad (40)$$

differentiating

$$\frac{1}{H_e}\left(\frac{\partial H}{\partial \tau}\right)_w = (1-W)\left[\frac{\partial}{\partial \tau}\left(\frac{u}{u_e}\right)\right]_w \qquad (41)$$

but

$$\left(\frac{\partial g}{\partial \tau}\right)_w \equiv \frac{1}{H_e}\left(\frac{\partial H}{\partial \tau}\right)_w = b_1 \qquad (42)$$

and $$\left[\frac{\partial}{\partial t}\left(\frac{u}{u_e}\right)\right]_w = 2 + \frac{\tilde{z}}{3} \tag{43}$$

For a flat plate solution $\tilde{z} = 0$; therefore

$$b_1 = 2\,(1 - W) \tag{44}$$

APPENDIX B

DEVELOPMENT OF THE BOUNDARY LAYER EQUATIONS

The basic partial differential equations describing the laminar compressible boundary layer of a perfect gas with a constant Prandtl number of unity, a Chapman viscosity-temperature relation, and a constant coefficient of specific heat are:

Momentum in the x-Direction

$$\rho u u_x + \rho v u_y = -p_x + (\mu u_y)_y \qquad (1)$$

Momentum in the z-Direction

$$\rho u w_x + \rho v w_y = (\mu w_y)_y \qquad (2)$$

Energy Equation

$$\rho u H_x + \rho v H_y = (\mu H_y)_y \qquad (4)$$

Continuity

$$(\rho u)_x + (\rho v)_y = 0 \qquad (3)$$

Equations (1) to (4) can be formulated for approximate solution by an extension of the von Karman integral technique. That is, Equations (1), (2), and (4) are multiplied by dy and are integrated from the wall to the edge of the boundary layer.

By applying the continuity equation (Equation (3)) and the Dorodnitzyn transformation which involves the definition of the normal coordinate t such that for a given x

$$dt = \frac{\rho}{\rho_e}\, dy \qquad (45)$$

and with the introduction of the boundary layer thickness

$$\delta_t = \int_o^{\delta} \left(\frac{\rho}{\rho_e}\right) dy \qquad (46)$$

Equations (1), (2), & (4) become

$$\frac{d}{dx}\left[\delta_t \int_o^1 U(1-U)d\tau\right] + \theta\left(\frac{2}{u_e}\frac{du_e}{dx} + \frac{1}{\rho_e}\frac{d\rho_e}{dx}\right) + \frac{\delta^*}{u_e}\frac{du_e}{dx} =$$

$$= \frac{C_H \mu_e (U_\tau)_w}{\rho_e u_e \delta_t} \qquad (7)$$

$$\frac{d}{dx}\left[\delta_t \int_o^1 U(1-\tilde{W})d\tau\right] + \left[\delta_t \int_o^1 U(1-\tilde{W})d\tau\right]\frac{1}{\rho_e u_e}\frac{d}{dx}(\rho_e u_e) =$$

$$= \frac{C_H \mu_e (\tilde{W}_\tau)_w}{\rho_e u_e \delta_t} \qquad (8)$$

$$\frac{d}{dx}\left[\delta_t \int_o^1 U(1-g)d\tau\right] + \left[\delta_t \int_o^1 U(1-g)d\tau\right]\frac{1}{\rho_e u_e}\frac{d}{dx}(\rho_e u_e) =$$

$$= \frac{C_H \mu_e}{\rho_e u_e \delta_t}(g_\tau)_w \qquad (9)$$

Equations (8) and (9) are identical in $\tilde{W}$ and g , hence only the equation for g need be considered and $\tilde{W}$ can be determined from the Crocco relation

$$\tilde{W} = \frac{w}{w_e} = \frac{H - H_w}{H_\epsilon - H_w} = \frac{g-W}{1-W} \qquad (10)$$

With the introduction of the parameter

$$Z = -\frac{d\zeta}{d(x/\delta_{t_o})} \qquad (47)$$

Equations (7) and (8) can be rewritten with ζ as the independent variable. Let

$$\Delta \equiv \frac{\delta_t}{\delta_{t_o}} \quad , \quad \Delta^* = \frac{\delta^*}{\delta_{t_o}}$$

$$R = \frac{\rho_e}{\rho_{e_o}} \quad \text{and} \quad M = \frac{\mu_e}{\mu_{e_o}}$$

Therefore Equation (7) becomes

$$\frac{d}{d\zeta}(F_1 \Delta) = -F_1 \Delta \left(\frac{2}{\zeta} + \frac{1}{R}\frac{dR}{d\zeta}\right) - \frac{\Delta^*}{\zeta} - \frac{C_H M}{\zeta \Delta R Z}\left(\frac{\mu_e}{\rho_e u_e \delta_t}\right)_o \left(2+\frac{\tilde{z}}{3}\right) \qquad (20)$$

and Equation (8) becomes

$$\frac{d}{d\zeta}(F_3 \Delta) = -F_3 \Delta \left(\frac{1}{\zeta} + \frac{1}{R}\frac{dR}{d\zeta}\right) - \frac{C_H M b_1}{\zeta \Delta R Z}\left(\frac{\mu_e}{\rho_e u_e \delta_t}\right)_o \qquad (21)$$

and

$$\tilde{z} = \frac{\rho_e^2 \delta_t^2}{2 C_H \rho_w \mu_e}\frac{du_e}{dx} = \frac{R \Delta^2}{2 C_H^2 M^2}\left(\frac{\rho_e u_e \delta_t}{\mu_e}\right)\left(\frac{\mu_w}{\mu_{e_o}}\right) Z \qquad (21a)$$

Using the profiles of Reference 14 for U and g, the integrals, F_1, and F_3 can be evaluated, i.e.

$$F_1 = \int_o^1 U(1-U)\, d\tau = \frac{37}{315} - \frac{2\tilde{z}}{945} - \frac{\tilde{z}^2}{2268} \qquad (13)$$

$$F_3 = \int_o^1 U(1-g)\, d\tau = (1-W)\left(\frac{17}{70} \quad \frac{31\tilde{z}}{2520}\right) - b_1\left(\frac{79}{1260} + \frac{19\tilde{z}}{7560}\right) \qquad (14)$$

Equations (20) and (21) are not in a convenient form for numerical

solution. However, with utilization of Equation (18) from Appendix A and Equations (20) and (21), three nonlinear differential equations result in four dependent variables, namely Δ, Δ^*, $\tilde{z}$, and b_1. Now

$$\frac{\Delta^*}{\Delta} \equiv F_4 = A(b_1)\, K_1(\zeta) - B(\tilde{z})\, K_1(\zeta) K_3(\zeta) - C(\tilde{z}) \qquad (18)$$

differentiating

$$\frac{d\Delta^*}{d\zeta} \equiv H_1 = F_4 \frac{d\Delta}{d\zeta} + \Delta \frac{\partial F_4}{\partial \tilde{z}} \frac{d\tilde{z}}{d\zeta} + \Delta \frac{\partial F_4}{\partial b_1} \frac{db_1}{d\zeta} + \Delta \frac{\partial F_4}{\partial \zeta} \qquad (48)$$

Expanding the L. H. S. of (20) and (21)

$$\frac{d}{d\zeta}(F_1 \Delta) \equiv H_2 = F_1 \frac{d\Delta}{d\zeta} + \Delta \frac{\partial F_1}{\partial \tilde{z}} \frac{d\tilde{z}}{d\zeta} + 0 \qquad (49)$$

$$\frac{d}{d\zeta}(F_3 \Delta) \equiv H_3 = F_3 \frac{d\Delta}{d\zeta} + \Delta \frac{\partial F_3}{\partial \tilde{z}} \frac{d\tilde{z}}{d\zeta} + \Delta \frac{\partial F_3}{\partial b_1} \frac{db_1}{d\zeta} \qquad (50)$$

Setting up Equations (48) - (50) in matrix form

$$\begin{vmatrix} H_1 - \Delta \dfrac{\partial F_4}{\partial \zeta} \\ H_2 \\ H_3 \end{vmatrix} = \begin{vmatrix} \dfrac{d\Delta}{d\zeta} \\ \dfrac{d\tilde{z}}{d\zeta} \\ \dfrac{db_1}{d\zeta} \end{vmatrix} \begin{vmatrix} F_4 & \Delta \dfrac{\partial F_4}{\partial \tilde{z}} & \Delta \dfrac{\partial F_4}{\partial b_1} \\ F_1 & \Delta \dfrac{\partial F_1}{\partial \tilde{z}} & 0 \\ F_3 & \Delta \dfrac{\partial F_3}{\partial \tilde{z}} & \Delta \dfrac{\partial F_3}{\partial b_1} \end{vmatrix} \qquad (51)$$

Thus

$$\frac{d\Delta}{d\zeta} = G_1 (\Delta, \Delta^*, \tilde{z}, b_1, \zeta) \qquad (22)$$

$$\frac{d\tilde{z}}{d\zeta} = G_2 (\Delta, \Delta^*, \tilde{z}, b_1, \zeta) \qquad (23)$$

$$\frac{db_1}{d\zeta} = G_3 (\Delta, \Delta^*, \tilde{z}, b_1, \zeta) \qquad (24)$$

where

$$G_1 = \frac{1}{L}\left\{H_2 \left[\frac{\partial F_4}{\partial \tilde{z}} \frac{\partial F_3}{\partial b_1} - \frac{\partial F_4}{\partial b_1} \frac{\partial F_3}{\partial \tilde{z}}\right] - \frac{\partial F_1}{\partial \tilde{z}}\left[\left(H_1 - \Delta \frac{\partial F_4}{\partial \zeta}\right) \frac{\partial F_3}{\partial b_1} - H_3 \frac{\partial F_4}{\partial b_1}\right]\right\}$$

$$G_2 = \frac{1}{L}\left\{\left(H_1 - \Delta \frac{\partial F_4}{\partial \zeta}\right) \frac{F_1}{\Delta} \frac{\partial F_3}{\partial b_1} + \frac{1}{\Delta} \frac{\partial F_4}{\partial b_1} (F_3 H_2 - F_1 H_3) - \frac{F_4}{\Delta} H_2 \frac{\partial F_3}{\partial b_1}\right\}$$

$$G_3 = \frac{1}{L}\left\{\frac{F_3}{\Delta}\left[\frac{\partial F_1}{\partial \tilde{z}}\left(H_1 - \Delta \frac{\partial F_4}{\partial \zeta}\right) - H_2 \frac{\partial F_4}{\partial \tilde{z}}\right] - \frac{1}{\Delta} \frac{\partial F_3}{\partial \tilde{z}}\left[F_1\left(H_1 - \Delta \frac{\partial F_4}{\partial \zeta}\right) - H_2 F_4\right] + \right.$$

$$\left. + \frac{H_3}{\Delta}\left[F_1 \frac{\partial F_4}{\partial \tilde{z}} - F_4 \frac{\partial F_1}{\partial \tilde{z}}\right]\right\}$$

$$\text{Denominator} = L = F_1\left[\frac{\partial F_4}{\partial \tilde{z}} \frac{\partial F_3}{\partial b_1} - \frac{\partial F_4}{\partial b_1} \frac{\partial F_3}{\partial \tilde{z}}\right] - \frac{\partial F_1}{\partial \tilde{z}}\left[F_4 \frac{\partial F_3}{\partial b_1} - F_3 \frac{\partial F_4}{\partial b_1}\right]$$

and

$$\frac{\partial F_1}{\partial \tilde{z}} = -\left(\frac{2}{945} + \frac{\tilde{z}}{1134}\right)$$

$$\frac{\partial F_3}{\partial \tilde{z}} = \frac{31(1-W)}{2520} - \frac{19b_1}{7560}$$

$$\frac{\partial F_4}{\partial \tilde{z}} = -\frac{1}{60} - K_1 K_3\left(\frac{213}{11340} + \frac{\tilde{z}}{1134}\right)$$

$$\frac{\partial F_3}{\partial b_1} = -\left(\frac{79}{1260} + \frac{19\tilde{z}}{7560}\right)$$

$$\frac{\partial F_4}{\partial b_1} = K_2\left[\frac{1 + 2WK_2}{10K_2} + \frac{311}{2310}(1-W) - \frac{1}{5}\right] - \frac{104K_2}{3465} b_1$$

$$\frac{\partial F_4}{\partial \zeta} = \left[\frac{2}{\zeta}\left(\frac{\Delta^*}{\Delta} + C\right)\left(1 + K_1 K_3\right) - AK_1\right]$$

REFERENCES

1. Fage, A. and Sargent, R. F., Shock Wave and Boundary Layer Phenomena Near a Flat Surface, Proceedings of the Royal Society of London, Series A, Vol. 190, No. 1020, pp. 1-20, June 1947.

2. Liepmann, H. W., The Interaction Between Boundary Layer and Shock Waves in Transonic Flow, Journal of the Aeronautical Sciences, Vol. 13, No. 12, pp. 623-637, December 1946.

3. Ackeret, J., Feldmann, F., and Rott, N., Investigation of Compression Shocks and Boundary Layers in Gases Moving at High Speed, NACA TM 1113, 1947.

4. Hakkinen, R. J., Greber, I., Trilling, L., and Abarbanel, S. S., The Interaction of an Oblique Shock Wave with a Laminar Boundary Layer, NASA Memorandum 2-18-59W, March 1959.

5. Chapman, D. R., Kuehn, D. M., and Larson, H. K., Investigation of Separated Flows in Supersonic and Subsonic Streams with Emphasis on the Effect of Transition, NACA TR 1356, 1958.

6. Crocco, L. and Lees, L., A Mixing Theory for the Interaction Between Dissipative Flows and Nearly Isentropic Streams, Journal of the Aeronautical Sciences, Vol. 19, No. 10, pp. 649-676, October 1952.

7. Crocco, L., Considerations on the Shock-Boundary Layer Interaction, Proceedings of the Conference on High-Speed Aeronautics, Polytechnic Institute of Brooklyn, January 20-22, 1955.

8. Cheng, S. I. and Bray, K. N. C., On the Mixing Theory of Crocco and Lees and Its Application of the Interaction of Shock Wave and Laminar Boundary Layer, Part I, Generals and Formulation, Princeton University, Department of Aeronautical Engineering, Report 376, AFOSR TN 57-283, May 1957.

9. Cheng, S. I., and Chang, I. D., On the Mixing Theory of Crocco and Lees and Its Application to the Interaction of Shock Wave and Laminar Boundary Layer, Part II, Results and Discussion, Princeton University, Department of Aeronautical Engineering, Report 376, AFOSR TN 58-3, November 1957.

10. Glick, H. S., Modified Crocco-Lees Mixing Theory for Supersonic Separated and Reattaching Flows, GALCIT, Hypersonic Research Project Memorandum No. 53, May 2, 1960.

11. Bray, K. N. C., Gadd, G. E., and Woodger, M., Some Calculations by the Crocco-Lees and Other Methods of Interaction Between Shock Waves and Laminar Boundary Layers, Including Effects of Heat Transfer and Suction, Aeronautical Research Council A.R.C. 21,834, F.M. 2937, 5 April 1960, (ASTIA No. AD 241490).

12. Carlson, W. O., Heat Transfer in Laminar Separated and Wake Flow Regions, Heat Transfer and Fluid Mechanics Institute, Stanford University Press, June 1959.

13. Bloom, M. H., On Moderately Separated Viscous Flows, Journal of the Aerospace Sciences, Vol. 28, No. 4, pp. 339-340, April 1961.

14. Libby, P. A. and Visich, M., Jr., Laminar Heat Transfer in Two-Dimensional Subsonic Effusors, Journal of the Aeronautical Sciences, Vol. 22, No. 6, pp. 425-431, June 1955.

DETERMINATION OF HYPERSONIC AERODYNAMIC LOADS AND DERIVATIVES ON RE-ENTRY GLIDE VEHICLES

Frank S. Malvestuto, Jr.

Lockheed-California Company
A Division of Lockheed Aircraft Corporation

ABSTRACT

This paper presents a number of physical concepts pertaining to the reaction of inviscid flows to bodies moving at high speeds. A physical interpretation is given to the hypersonic similarity parameter. The total aerodynamic force on a body is delineated on the basis of this interpretation and upon a synthesis of the total force in terms of primary forces that control the reaction of the fluid. Within the framework of these concepts, formulas are presented for the calculation of the inviscid hypersonic pressures for vehicles composed of planar surfaces.

DETERMINATION OF HYPERSONIC AERODYNAMIC LOADS AND DERIVATIVES ON RE-ENTRY GLIDE VEHICLES

INTRODUCTION

The prediction of the gas dynamic force and moment reactions on a vehicle as it traverses the atmosphere depends essentially on a proper solution of the system of partial differential equations that governs the disturbance flow produced by the moving vehicle and that satisfies the appropriate kinematical conditions prescribed along the boundaries of the region of disturbance. Very few solutions are available for the aerodynamic forces and moments acting on arbitrary bodies moving in known flows. The primary reasons are:

1. Theoretical models of the dynamics of gas motions are not always available.

2. Solutions to the differential equations governing the body disturbance flow are difficult to determine.

3. The surfaces and lines along which initial conditions and boundary conditions must be satisfied are not prescribed a priori or are too complex, geometrically, within the framework of existing theoretical techniques.

As a result of these basic difficulties, various investigators have devised theoretical techniques that allow the evaluation of the aerodynamics of bodies of simple geometry such as cone bodies, two-dimensional flat plates, etc.. These theoretical approaches are valid provided the similarity parameters such as Mach number and Reynolds number and the surface attitude of the body relative to the free stream meet certain prescribed requirements. Other available approaches are more or less engineering schemes to extrapolate the available theoretical techniques so that rough evaluations of the aerodynamics of a vehicle can be made for conditions of vehicle geometry and attitudes that are beyond the theoretical limits of these quantities stipulated in the theoretical techniques.

In reference (1) a unified approach for the reliable prediction of vehicle aerodynamics is proposed and discussed in detail. The proposed approach is essentially an engineering procedure for the prediction of vehicle aerodynamics that is based upon a rational interpretation of the vehicle net force and moment in terms of the behavior and magnitude of the components of these quantities. The unified approach is composed of four operations. These operations for vehicles moving at constant speed along flat trajectories are as follows:

1. Tearing - a geometric operation in which the complete configuration is decomposed into the most complex element for which aerodynamic knowledge is available.

2. Aerodynamic Synthesis - an algebraic operation in which the net aerodynamic force or moment of each element is evaluated by first calculating a sub-set of the aerodynamic quantity and secondly summing these sub-forces or sub-moments into the net aerodynamics of the element.

3. Aerodynamic Interference - an algebraic operation in which the contribution to an element of the aerodynamic influence or interference of neighboring elements is determined.

4. Configuration Synthesis - a geometric operation in which the evaluation of the vehicle net force or net moment is a synthesis of the aerodynamic quantities of the elements and of the incremental forces or moments produced by aerodynamic interference.

The successive application of these four operations will result in a rational evaluation of the vehicle aerodynamics. The application of this approach to vehicles performing time dependent maneuvers and/or maneuvers along non-flat trajectories involves primarily an appreciable extension of the tearing operation defined previously

so as to include the tearing of "motion-geometry" spaces. A detailed expose of this generalized operation is currently under preparation by the author.

The primary purpose of the present paper is to present a few of the physical concepts of INVISCID flow action and reaction that provided a basis for the analytical development of the unified approach described in reference 1. We will discuss briefly the following items:

1. A Physical Interpretation of the Hypersonic Similarity Parameter.

2. Symmetric and Anti-symmetric Inviscid Disturbance Forces.

3. Relations for the Approximate Evaluation of Hypersonic Forces.

SECTION I: A PHYSICAL INTERPRETATION OF THE HYPERSONIC SIMILARITY PARAMETER

We will start the present discussion with a description of the physical process that defines the role of the well known similarity parameter, $M\alpha$, as a parameter controlling the variation of aerodynamic quantities with Mach number and with angle of attack or with the local slope of a surface, δ, with respect to the free-stream direction. If we express Mach number as the ratio of the velocity of a moving point disturbance to the speed of propagation of the disturbance wave caused by the point, then it is clear that the parameter $M\alpha$ becomes

$$\left(\frac{V}{a_0}\right)\alpha \qquad (1)$$

For our purposes, the moving point is simply an infinitesimal area of a surface that is moving in some specified direction. For example, a plate at some angle of attack, α, and with forward velocity, V_∞, will have its lower surface moving at a speed, V_N, equal to $V_\infty \sin\alpha_0$ in a direction normal to the lower surface of the plate. An infinitesimal area of this lower surface will act as a

disturbance point and transmit a disturbance wave of velocity a_1 into the surrounding fluid. For small angles of attack for which the $\text{Sin}\,\alpha_o \approx \alpha_o$ the velocity of the disturbance point is $V_N = V_\infty \alpha$ and the ratio of this quantity to the speed of wave propagation is:

$$\frac{V_N}{a_1} = \left(\frac{V_\infty}{a_1}\right)\alpha = M_\infty \alpha \left(\frac{a_\infty}{a_1}\right)$$

or

$$M_\infty \alpha = \frac{V_N}{a_\infty} \tag{2}$$

The similarity parameter $K = M_\infty \alpha$ can therefore be interpreted, under the restriction $\sin\alpha \approx \alpha$, as the ratio of the normal velocity of a surface point to the speed of sound or speed of wave propagation in the free stream flow. A parameter that can be simply related to K is the ratio $\left(\frac{V_\infty}{a_1}\right)\alpha$, which can be considered as the "local" similarity parameter and denoted by K_1. This parameter is obviously related to K in the following way.

$$K_1 = K\,\frac{a_\infty}{a_1} = \frac{V_N}{a_1} \tag{3}$$

When K_1 is less than one the magnitude of the normal velocity of a surface point is less than the local speed of sound or the local speed of wave propagation. When K_1 is greater than one the magnitude of the normal velocity of a surface point is greater than the local speed of sound. We now propose to show that the mode of disturbance pressure reaction on the moving surface depends upon the relative magnitude of K_1, that is if K_1 is less than one or greater than one. First, we resolve the resultant velocity V_∞ of a segment of the surface into its normal velocity component V_N and into its tangential velocity component V_T and inspect the propagation of fluid disturbances produced by the segment when moving only in the direction of V_N. Figure 1 is an illustration of these items. When the surface segment, assumed flat for simplicity, moves normal to its plane, each point of the segment acts as a source of disturbance and the segment transmits disturbances into the flow that propagate at the local velocity of sound. The disturbed fluid suffers a change in momentum

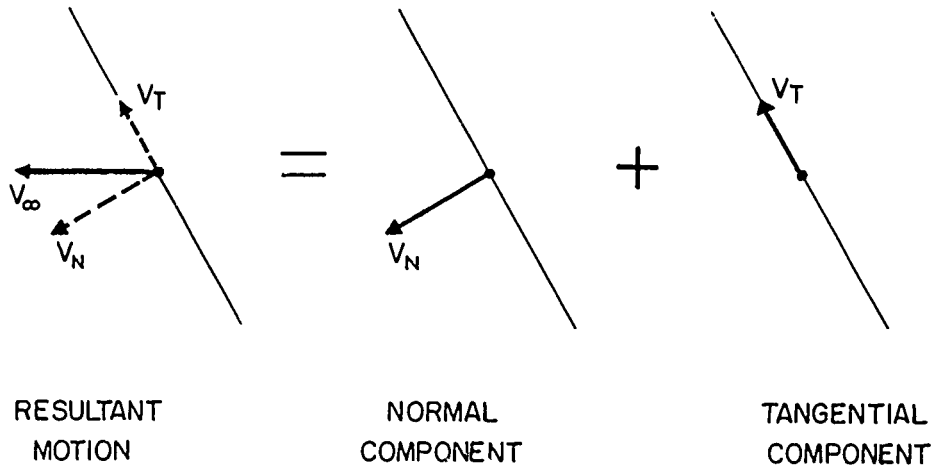


FIGURE I.— COMPONENT MOTIONS OF A FLAT PLATE MOVING WITH VELOCITY V_∞

which in an infinitesimal time results in a fluid pressure reaction along the segment surface. If V_N is less than the local speed of sound, a_1, the elemental pressure of each disturbance wave will be transmitted to all points of the segment. Stated differently, each disturbance produces a variable distribution of reaction pressure along the plane of the segment. Now if the segment in addition to its normal velocity has a velocity V_T then the magnitude of the pressure and the distribution of pressure on the segment will vary according to the magnitudes of the velocities V_N and V_T. If the resultant velocity, V_∞, of V_N and V_T becomes supersonic, then the disturbance field may be bounded by the shock attached to the leading edge of the segment and by the surface of the segment. The elemental pressure, however, transmitted to the segment as a result of a disturbance from a point of the segment will still "wipe" the region of the segment aft of the location of the disturbance source. We can describe this condition by labelling the segment subsonic for $K_1 < 1$.

Assume now that $K_1 > 1$, the segment moves normal to its plane ($V_T = o$) at a speed greater than the local speed of propagation of disturbances. Now the elemental disturbances produced by each point of the segment cannot transmit pressures to all points of the segment (neglecting edge effects) because the disturbance points or sources are moving at a velocity V_N relative to the undisturbed flow that is greater in magnitude than the speed of propagation of the disturbance produced by the segment. For this case then the elemental pressure reaction on the segment occurs only in the local neighborhood of the disturbance source and there is no significant influence of this elemental pressure external to the disturbance point. It is appropriate to label the disturbance flow associated with this mode of pressure reaction, "impact flow"; and the pressure reaction on the segment, "impact surface pressure". Now if we superimpose a tangential velocity V_T on the segment, the mode of pressure reaction on the surface will not change as long as $K_1 > 1$. The magnitude of the pressure reaction to a principal order is also independent of the axial velocity. Thus the axial velocity has an insignificant effect on the surface pressure when $K_1 > 1$ or when the segment is "supersonic" and an important effect on the surface pressure when the segment is subsonic ($K_1 < 1$). For this later case as indicated previously the

disturbance produced by the plate can propagate away from the plate, and the pressure reactions along the plate from these disturbances depend upon the relative location of the plate and the elemental disturbance fields at any instant of time.

For supersonic speeds the relation between K_1 and K_∞ can be obtained from the shock flow relations. It turns out that when $K_1 = 1$, the free-stream parameter K_∞ is approximately 5/3. Figure 2 has been prepared in order to illustrate the salient features of the preceding remarks. This figure is an illustration of the variation of the ratio of shock angle to angle of attack, θ/α, with the local hypersonic similarily parameter, $K_1 = \frac{V_N}{a_1}$. For values of $K_1 << 1$ it is noted that for a given angle of attack the disturbance field is large, that is $\theta/\alpha >> 1$. This extent of the disturbance field in this case is primarily a function of the speed of wave propagation a_1. Now as we increase V_N relative to a_1 the disturbance field becomes less dependent on a_1 and for values of $V_N > a_1$, that is $K_1 > 1$, the extent of the disturbance field depends primarily on the normal velocity of the plate, that is $\frac{\theta}{\alpha}$ is approximately constant for $K_1 > 1$. In figure 3 we show the relation that must exist between the shock angle and the angle of attack for $K_1 = \frac{V_N}{a_1}$ to be equal to one. It is also clearly evident from this figure that the relation $K = M_\infty \alpha = 5/3$ is an excellent approximation to this relation as we stated previously. We also show in figure 3 an approximate explicit relation between θ and α that satisfies the condition $K_1 = 1$. This relation is $\theta = 5/3\ \alpha$. Figure 4 is an attempt to illustrate for a flat plate two-dimensional wing the statements made previously regarding the strong dependence of the compression surface pressure P_1 on V_N, the normal velocity of the plate. It is noted from this figure that for values of $K_1 > 1$ the surface pressure P_1 for any specified free-stream Mach number, M_∞, varies directly as V_N^2. This quadratic relationship between the surface pressure and V_N is a necessary relationship for the generation of impact pressures and forces as we shall show subsequently.

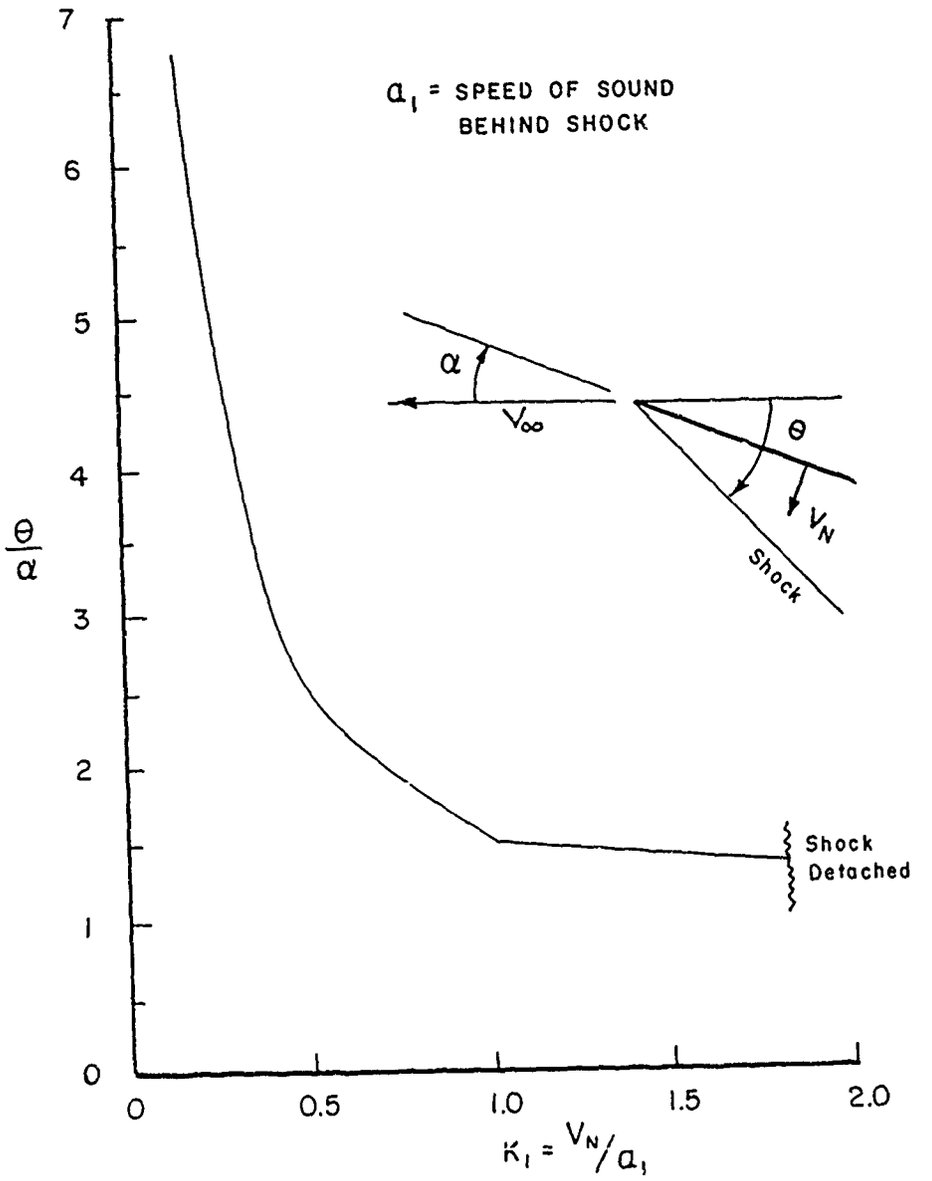


FIGURE 2.—VARIATION OF RATIO θ/α WITH $K_1 = \frac{V_N}{a_1}$ FOR A TWO-DIMENSION FLAT PLATE

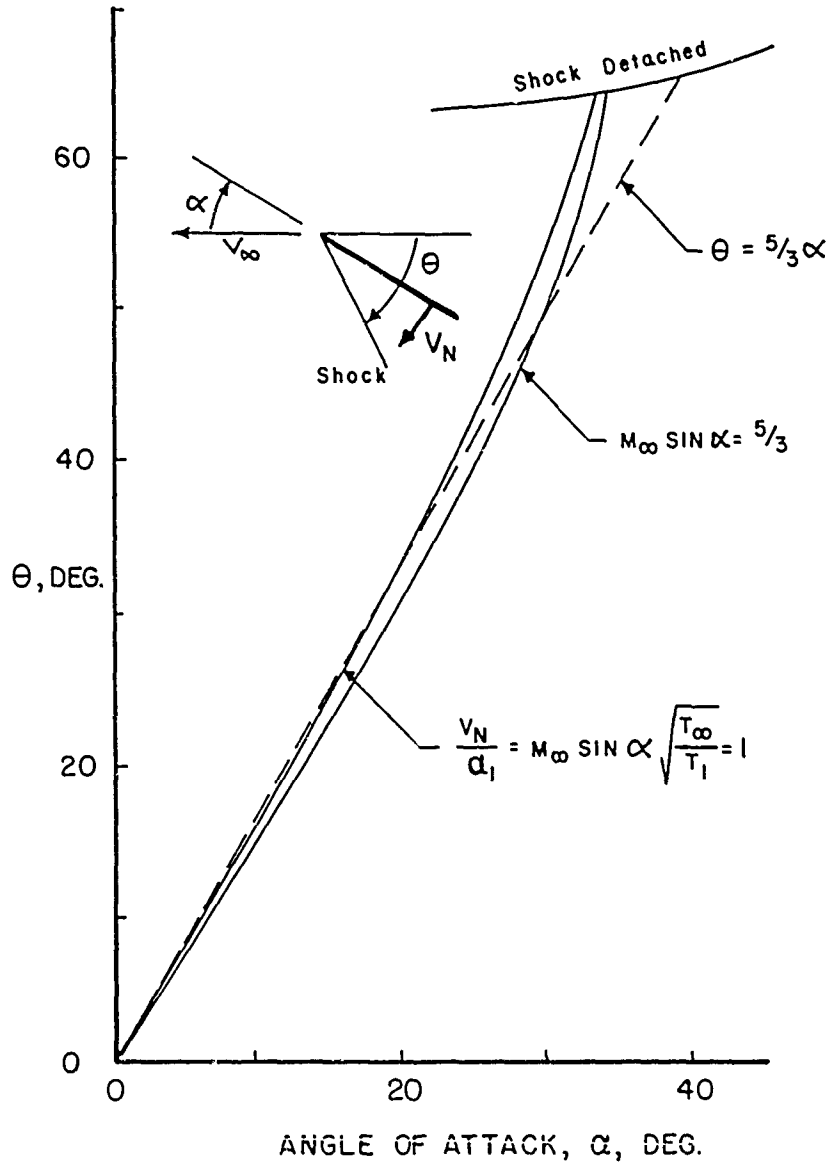


FIGURE 3.— THE RELATION BETWEEN θ AND α THAT SATISFIES THE CONDITION $K_1=1$

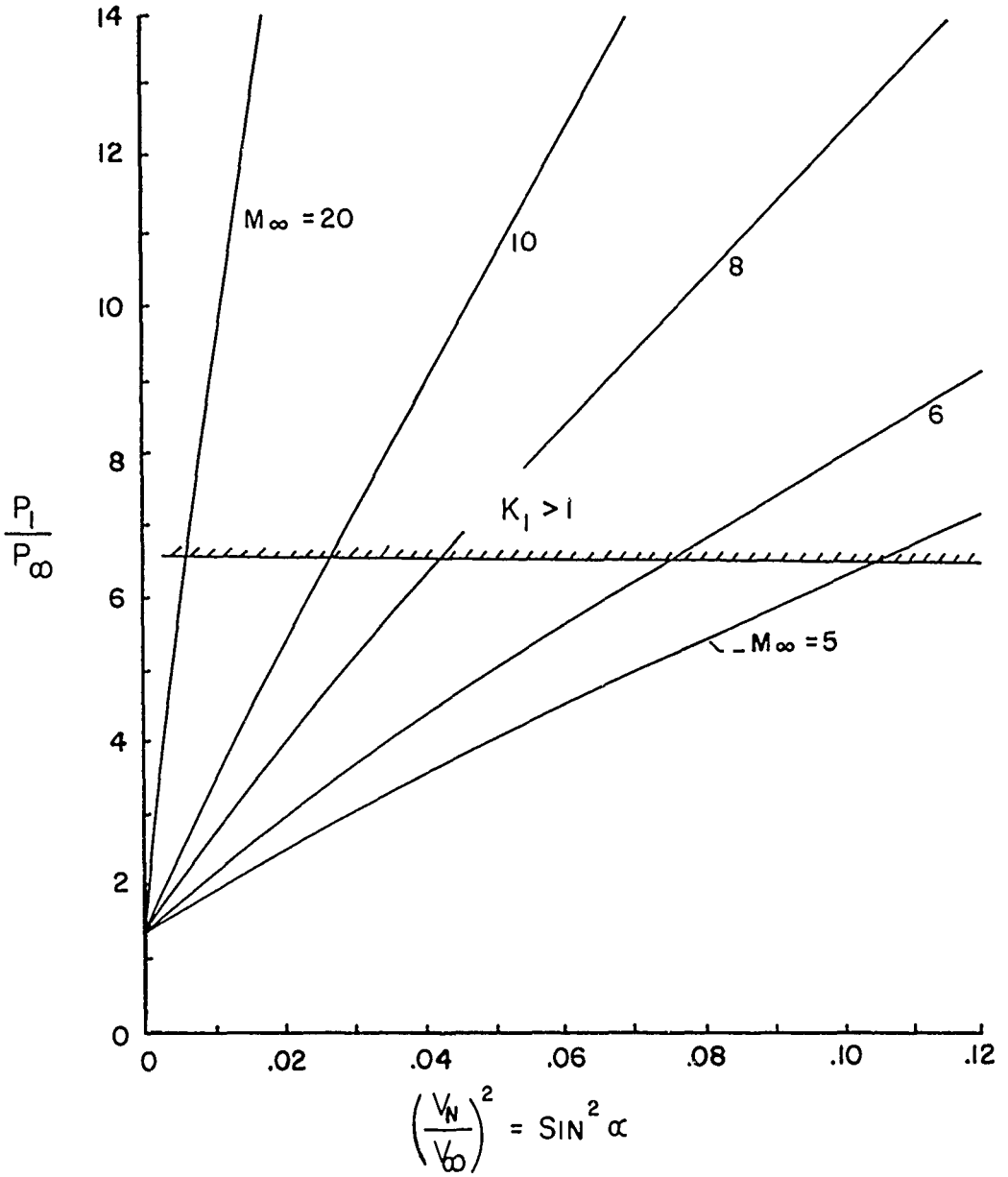


FIGURE 4.—VARIATION OF PRESSURE RATIO $\left(\frac{P_1}{P_\infty}\right)$ WITH VELOCITY RATIO $\left(\frac{V_N}{V_\infty}\right)^2$

SECTION II: SYMMETRIC AND ANTI-SYMMETRIC INVISCID DISTURBANCE FORCES

The purpose of this section is to present a few thoughts involving symmetric and non-symmetric flows and forces that will reflect the significance of the interpretations of the hypersonic similarity parameter described in Section I. In the ensuing discussion we shall consider only elements with three orthogonal planes of symmetry. Figure 5 is an illustration of such an element and the orthogonal planes of symmetry. In the subsequent discussion we will call the plane of symmetry AON the "vertical" plane. In a similar way the planes of symmetry NOY and AOY will be called the "cross-flow" plane and "chord" plane respectively. We make the further assumption that the velocity of motion of the element, V_∞, is in the vertical plane of symmetry and the vector in this plane that defines the velocity makes an angle α with the A axis (see figure 5). The components of V_∞ along the A-axis and N-axis will be denoted by V_A and V_N respectively. For convenience in what follows the direction of the A-axis will be called the axial direction and the velocities and forces in this direction the axial velocity and axial force respectively. In the same way for the N-axis we will use the connotations normal direction, normal velocity and normal force.

With the acceptance of the aforestated definitions we define a symmetrical force as:

> The force in a plane of symmetry of the element as it moves in the direction of the axis of symmetry of that plane.

It is clear that in this case, the element produces a disturbance flow that is symmetrical with respect to the direction of motion. Figure 6 is an illustration of two symmetrical flows corresponding to movements in the axial direction and in the normal direction. We postulate that symmetrical forces are proportional to the square of the velocity of motion of the element, that is,

$$F_i^s = F_o V_i^2 , \quad i = A, N \tag{4}$$

where

F_o is a function of Mach number, Reynolds number and element geometry.

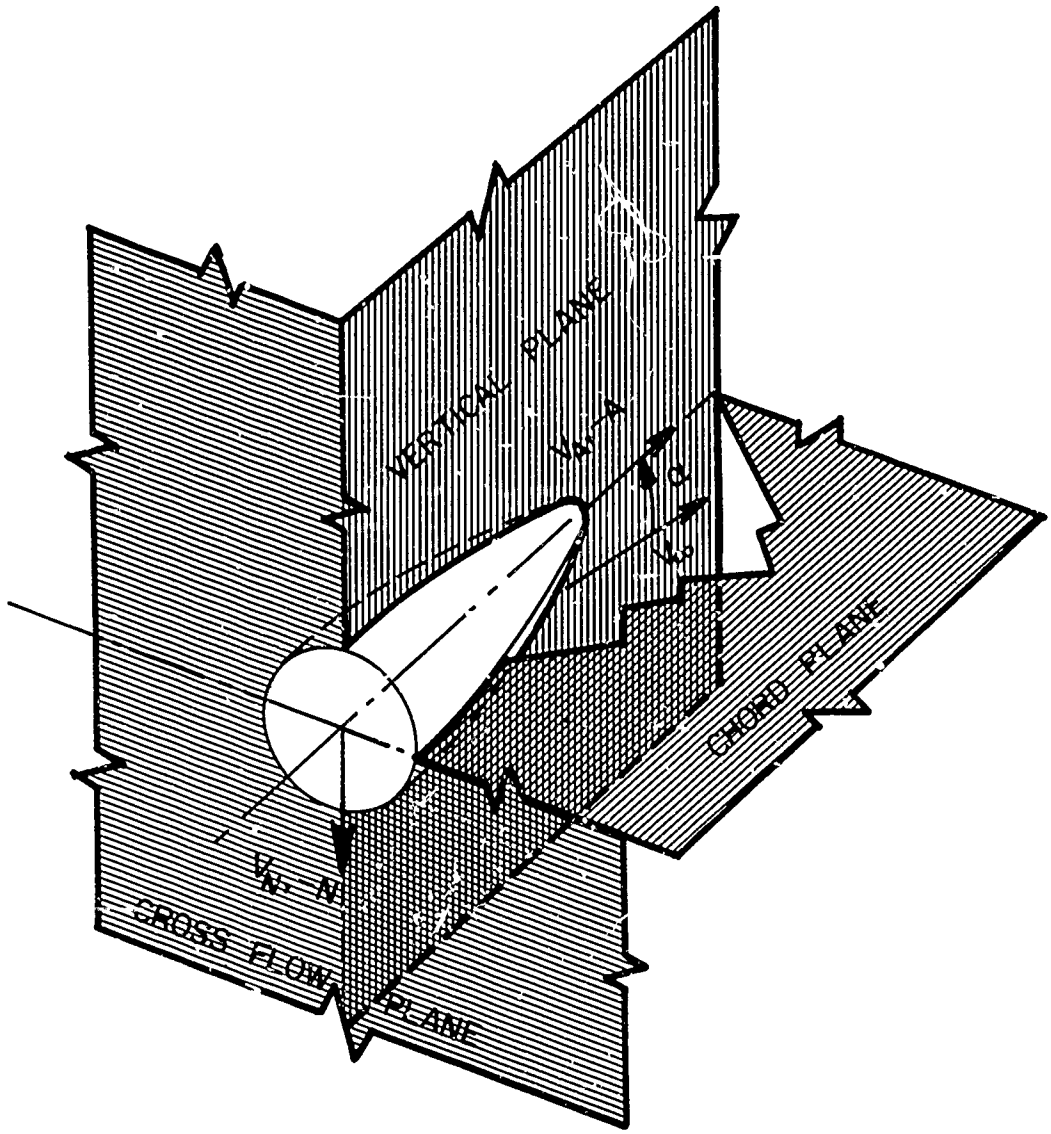


FIGURE 5.— REFERENCE AXES SYSTEM

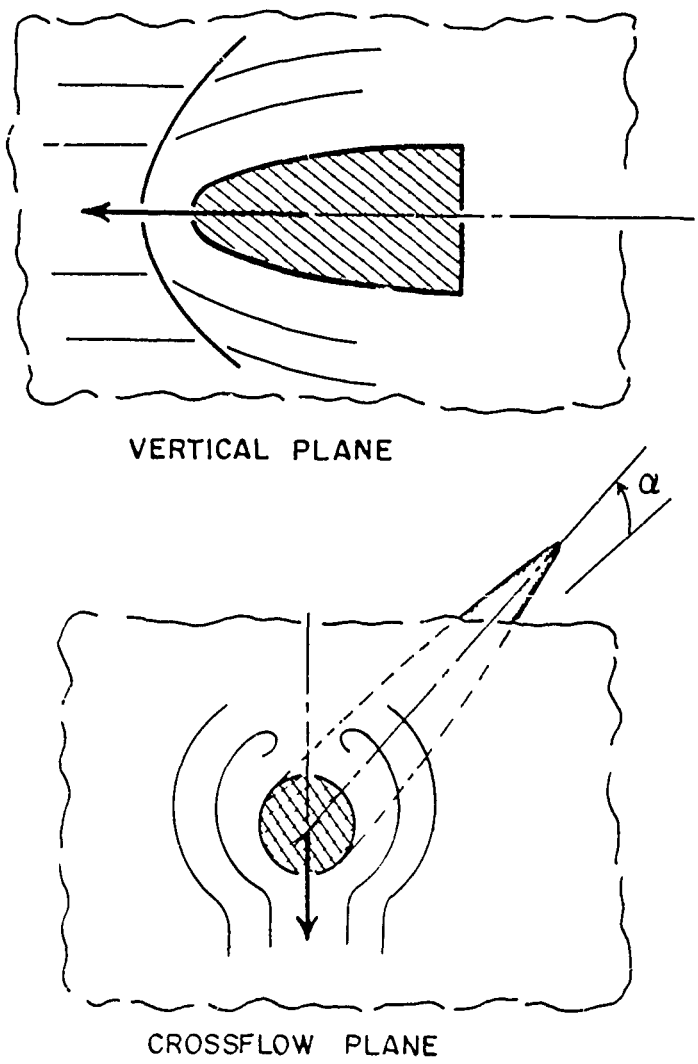


FIGURE 6 — ILLUSTRATIONS OF SYMMETRICAL FLOWS

Superscript "s" denotes symmetrical force. For zero angle of attack of the element the appropriate symmetrical force is an axial force. For the element at 90 degrees angle of attack, the symmetrical force is the normal force. If we accept the possibility of the existence of symmetrical forces when the element is at some non-zero angle of attack, then these forces can be expressed in terms of α as follows:

$$A^s = A^s_o V_A^2 = A^s_o V_\infty^2 \cos^2\alpha \qquad (5)$$

$$N^s = N^s_o V_N^2 = N^s_o V_\infty^2 \sin^2\alpha \qquad (6)$$

The series expansion of these expressions in terms of α in the neighborhood of $\alpha = 0$ yields

$$A^s = A^s_o V_\infty^2 \left[1 - \alpha^2 + 1/3\,\alpha^4 - 2/45\,\alpha^6 + \cdots\right] \qquad (7)$$

and

$$N^s = N^s_o V_\infty^2 \left[\alpha^2 - 1/3\,\alpha^4 + 2/45\,\alpha^6 - \cdots\right] \qquad (8)$$

Substituting V_N/V_∞ in these expressions for α, as a valid approximation, in the neighborhood of $\alpha = 0$ and multiplying the terms in the brackets by V_∞^2 we obtain

$$A^s = A^s_o \left[1 - (1 - 1/3\,\alpha^2 + 2/45\,\alpha^4 - \cdots) V_N^2\right] \qquad (9)$$

$$N^s = N^s_o \left[V_N^2 - (1/3\,\alpha^2 - 2/45\,\alpha^4 + \cdots) V_N^2\right] \qquad (10)$$

The collection of terms of the right hand side of equations (9) and (10) respectively may be considered as sets of sub-forces that represent the contributions of the axial and symmetrical forces to the total aerodynamic force on the element when it is moving at some non-zero angle of attack. If any of the axial or normal sub-forces have the same functional form in the velocities V_A or V_N as the primary axial or primary normal force then the contribution of that symmetrical sub-force is invariant with angle of attack. To illustrate this latter point more clearly we write equations (9) and (10) in the following form:

$$A^s = A_o^s - A_o^s \alpha^2 f_s(\alpha) V_N^2 \tag{11}$$

$$N^s = N_o^s V_N^2 - N_o^s \alpha^2 g_s(\alpha) V_N^2 \tag{12}$$

where

$$F_s(\alpha) = \left({}^1/_2 \alpha^2 - {}^1/_3 + {}^2/_{45} \alpha^2 - \cdots \right)$$

$$g_s(\alpha^2) = \left({}^1/_3 - {}^2/_{45} \alpha^2 + \cdots \right)$$

It is clear from equation (12) that the normal sub-force, $N_o^s V_N^2$, that exists when $0° < \alpha < 90°$ is the same function of V_N^2 as the primary normal force that exists at $\alpha = 90°$. Stated more descriptively, the above results imply that pure symmetrical forces such as $N_o^s V_N^2$ can exist when the velocity of motion of the element is not parallel to an axis of symmetry of the element. Before proceeding with a discussion of the sub-forces of equations (11) and (12) that depend on angle of attack, α, in addition to the normal velocity, we must discuss the concept of anti-symmetric forces.

For motion in the axial direction the symmetrical force is a function of V_A^2. If the thickness of the element is assumed to be zero, that is, the element is contained in the chord plane of symmetry then, of course, the axial force is zero. If however, in addition to the axial velocity, V_A, a small normal velocity, V_N $(\frac{V_N}{V_A} \to 0)$, is given to the planar element a force is experienced by the element in a direction that is normal to its chord plane if we exclude possible edge forces. This force is a function of the product of the axial velocity and normal velocity, $V_A V_N$ (or $V_\infty V_N$) and is appropriately named an anti-symmetric force because of the change only in the direction of the force with a change in the direction of the normal velocity, V_N.

An excellent example of an aerodynamic antisymmetric force is the inviscid "aerodynamic lift" on thin surfaces based upon the Circulation theory of lift (reference 2). All linear theories for the prediction of an anti-symmetric force such as a normal force acting

on a thin plate are based upon the assumption that the aerodynamic force on the plate is directly proportional to the first order product of the velocities $V_A V_N$ or $V_\infty V_N$. For example the theoretical normal force acting on a two-dimensional wing of zero thickness that is moving at supersonic speeds is given by the following expression (reference 3) provided the angle of attack of the wing is small

$$N = \frac{2\rho_\infty c}{\sqrt{M_\infty^2 - 1}} V_\infty^2 \alpha \tag{13}$$

The angle of attack α is properly approximated by $\frac{V_N}{V_\infty}$ for values of α in the neighborhood of zero and we, therefore, can express the normal force as

$$N = \frac{2\rho_\infty c}{\sqrt{M_\infty^2 - 1}} V_\infty V_N \tag{14}$$

For planar elements a general anti-symmetric relationship between the normal force and the angle of attack is provided by the sine relation, that is

$$N^S = N_c^S V_\infty^2 \sin\alpha \tag{15}$$

where $\sin\alpha = \frac{V_N}{V_\infty}$ and N_o is a parameter independent of α. A proper set of sub-forces of this primary force is given by the terms of the series expansion of $\sin\alpha$

$$N^A = N_o^A V_\infty^2 \left[\alpha - 1/3! \alpha^3 + 1/5! \alpha^5 - \cdots \right]$$

or

$$N^A = N_o^A \left[V_N V_\infty - 1/6 \alpha V_N^2 + 1/120 \alpha^3 V_N^2 - \cdots \right] \tag{16}$$

$$N_A = N_o^A V_N V_\infty - \alpha g_A(\alpha) V_N^2 \tag{17}$$

where

$$g_A(\alpha^2) = \left(1/6 - 1/120 \alpha^2 + \cdots \right) \tag{18}$$

Equation (18) reveals two types of sub-forces associated with the prescribed $\mathrm{Sin}\alpha$ variation of the primary normal force with angle of attack. The sub-force $N_o^A V_N V_\infty$ which retains the functional form of the primary force and the set of sub-forces composed of the terms of the expression $\alpha g_A(\alpha^2)\, V_N^2$. These latter sub-forces are proportional to V_N^2 as are the symmetrical normal sub-force (see equation (12)); however, they are anti-symmetrical because of the linear dependence of these forces on angle of attack (see equation (18)).

It was stated in our discussion of symmetrical normal forces that it was necessary to discuss anti-symmetric forces before we could adequately discuss the symmetrical normal sub-forces that depend on angle of attack. We will now discuss these forces as well as the α-dependent anti-symmetrical sub-forces. First it is necessary to emphasize that the underlying assumption of the previous and subsequent discussion is that the aerodynamic forces acting on bodies or elements moving through an inviscid fluid or gas are of two basic types: forces that depend on the square of the velocity of motion when it is parallel to an axis of symmetry of the body, and forces that depend upon the product of the components of the velocity of motion when the velocity is not parallel to an axis of symmetry of the body. The former force has been labelled a symmetric force and the latter an anti-symmetric force. In an attempt to establish the relative invariance of each of these force fields when acting simultaneously and in order to also establish the degree of dependence of these forces during their simultaneous action, sets of sub-forces of the primary forces were established and these sub-forces were examined in order to assess the degree of dependency between the primary types of forces. It turns out that both the symmetrical normal force, N^S, and the anti-symmetric normal force, N^A, have sub-forces that are invariant with angle of attack and in addition each of these primary forces have sub-forces whose analytical form varies with angle of attack. For the symmetrical normal force these α-coupled sub-forces are from equation (12) characterized by

$$\alpha^2 g_S(\alpha^2)\, V_N^2 \tag{19}$$

The corresponding anti-symmetrical sub-forces obtained from equation (18) are given by expressions of the type

$$\alpha\, g_A(\alpha^2)\, V_N^2 \tag{20}$$

The g-functions of these expressions are always positive. The total set of these sub-forces represents the contribution of interaction effects between the symmetric and anti-symmetric forces to the net force acting on a body. The similar dependence of these sub-forces on V_N^2 reflects the strong influence of the cross-flow velocity V_N on these interaction forces.

We are now in a position to express the net primary forces on an element in terms of symmetric and anti-symmetric sub-forces. We shall illustrate this operation for the normal force only. The net normal force is expressed as follows:

$$N = N^A + N^S$$

or

$$N = \dot{N}_0^A V_N V_\infty + N_0^S V_N^2 + N_\alpha^S \alpha^2 g_S(\alpha^2) V_N^2 + N_\alpha^A \alpha\, g_A(\alpha^2) V_N^2 \qquad (21)$$

where

N_α^S , N_α^A are parameters independent of α and are not necessarily equal to N_0^S or N_0^A.

The first two terms of the right hand side of equation (21) represent the contributions of the sub-forces that are invariant with angle of attack. The last two terms are the α-coupled sub-forces discussed above. The full significance of this equation can be described more clearly by an illustrative application of this result to a two-dimensional flat plate moving at a hypersonic Mach number such that $\sqrt{M_\infty^2 - 1} \approx M_\infty$. The lower surface of the plate will be denoted by the subscript "ℓ" and the upper surface by the subscript "u". In terms of the lower and upper surface sub-forces, the normal aerodynamic force acting on the plate can be expressed as

$$N = (\Delta N)_0^S V_N V_\infty + (\Delta N)_0^A V_N^2 + (\Delta N)_\alpha^S \alpha^2 g_S(\alpha^2) V_N^2 + (\Delta N)_\alpha^A \alpha\, g_A(\alpha^2) V_N^2 \qquad (22)$$

where

$$(\Delta N)_0^S = (N_0^S)_\ell - (N_0^S)_u \ , \ (\Delta N)_0^A = (N_0^A)_\ell - (N_0^A)_u \ , \ \cdots$$

Within the limitations of hypersonic small disturbance theory (reference 4) the lower and upper surface forces can be accurately approximated by the following series expansions presented in Table I.

TABLE I

$\frac{N_\ell}{\frac{1}{2}\rho_\infty c} = \bar{N}_\ell = \frac{p_{LOWER} - p_\infty}{\frac{1}{2}\rho_\infty} = C_{p_\ell} V_\infty^2$	$\frac{N_u}{\frac{1}{2}\rho_\infty c} = \bar{N}_u = \frac{p_{UPPER} - p_\infty}{\frac{1}{2}\rho_\infty} = C_{p_u} V_N^2$
$K = M_\infty \alpha < 5/3$	$K = M_\infty \alpha < 5$
$\bar{N}_\ell = \frac{2}{M_\infty} V_N V_\infty + \alpha\, g_\ell^A(\alpha^2) V_N^2 + 1.20\, V_N^2$	$\bar{N}_u = -\frac{2}{M_\infty} V_N V_\infty - \alpha\, g_u^A(\alpha^2) V_N^2 + 1.20\, V_N^2 + \alpha^2\, g_u^S(\alpha^2) V_N^2$
$K > 5/3$	$K \geq 5$
$\bar{N}_\ell = 2.4\, V_N^2 + \frac{1}{\alpha^{*2}}\, g_\ell(\alpha^{*2}) V_N^2$	$\bar{N}_u = 0$

WHERE:

$$\alpha^* = \frac{V_N}{a_\infty} = K, \quad c = \text{chord of plate}, \quad \gamma = 1.4$$

$$g_\ell^A(\alpha^2) = 0.36\, M_\infty - 0.032\, M_\infty^3 \alpha^2 + 0.006\, M_\infty^5 \alpha^4 - \cdots$$

$$g_u^A(\alpha^2) = 0.40\, M_\infty + 0.0096\, M_\infty^3 \alpha^2 + 0.000018\, M_\infty^5 \alpha^4 + \cdots$$

$$g_u^S(\alpha^2) = 0.08\, M_\infty^2 + 0.00064\, M_\infty^4 \alpha^2 + \cdots$$

$$g_\ell^S(\alpha^{*2}) = 5/3 - 1.158\, \frac{1}{\alpha^{*2}} + 1.608\, \frac{1}{\alpha^{*4}} - \cdots$$

The functional forms of the normal sub-forces (or sub-pressures) exhibited in Table I are in complete agreement with the corresponding sub-forces of equations (21) and (22) derived from the general considerations of symmetric and anti-symmetric forces discussed previously. The pure anti-symmetric and symmetric sub-forces, that is the $N_o^S V_N V_\infty$ and $N_o^A V_N^2$ terms are clearly in evidence. The terms representing the α-coupled sub-forces with their direct dependence on the square of V_N, the cross-flow velocity are in accord with our general results. Note also from the tabulated sub-forces of Table I that the algebraic sum of the lower and upper surface coefficients of the pure anti-symmetric force is finite and equal to $\frac{4}{M_\infty}$; whereas, the sum of the lower and upper surface coefficients for the pure symmetric sub-force is zero. The relations are easily established from the well known properties of the behaviors of symmetric and anti-symmetric functions plus the requirement that the resultant normal force acting on the plate must change sign with V_N as V_N approaches zero through a positive and negative range of values. The implications of this result on the development of approximate formulas for the calculation of hypersonic "pressure" forces will be discussed in a later section.

There are a number of significant facts pertaining to the mechanism of aerodynamic force reaction on bodies moving at high speeds that can be learned from the preceding table. First it is clear from the tabulated expressions for the upper surface or "expansion surface" sub-forces that the total normal force of the upper surface can become zero when the symmetrical sub-forces are equal in magnitude to the anti-symmetrical sub-forces. That is when

$$\frac{2}{M_\infty} V_N V_\infty + \alpha\, g_U^A(\alpha^2) V_N^2 = 1.20\, V_N^2 + \alpha^2\, g_U^S(\alpha^2) V_N^2 \qquad (23)$$

The onset of this null expansion force occurs when $K = M_\infty \alpha = 5$ for $\gamma = 1.4$. The second point to be made deals with the magnitude of the sub-forces acting on the lower surface of the two-dimensional wing. For values of K less than 5/3 the compression sub-forces are predominantly anti-symmetrical. For values of $K > 5/3$, the compression sub-forces are of the symmetric type. The transition from anti-symmetric forces to symmetrical forces at $K = 5/3$ is important to note. This value of K is to an excellent approximation the ratio of the normal velocity of the wing to the velocity of sound behind

the shock equal to one ($K_1 = 1$) as we stated in Section I. It is clear therefore that transition from anti-symmetric forces to symmetric forces occurs when the Mach number normal to the compression surface changes from a subsonic value ($K_1 < 1$) to a supersonic value ($K_1 > 1$). Note also from Table I that the expression for the compression sub-force for $K > 5/3$ is a function of an angle $\alpha^* = \frac{V_N}{a_\infty}$ and not a function of the angle of attack of the plate. This result is further evidence of the validity of the statement made in Section I concerning the independency of compression force and angle of attack when $K > 5/3$.

For values of K greater than 5 it is noted from the expressions for the compression sub-forces that the α^*-coupled symmetrical sub-force is approximately zero and the pure symmetrical sub-force remains finite and equal to $2.4\ V_N^2$. This value of K therefore represents a good approximation to the onset of discontinuous flow over the plate since for $K > 5$ the upper surface normal force is zero. For $\gamma = 1$ instead of 1.4 the compression force for values of $K > 5$ is approximately $2V_N^2$ the well known classical Newtonian relation for normal force. Figure 7 is an attempt to illustrate the mechanism of the sub-force actions discussed above as the angle of attack is increased from a small value ($M_\infty \alpha < 5/3$) to a large value ($M_\infty \alpha > 5$).

There is one additional point we wish to make concerning the increased magnitude of the compression surface symmetrical sub-force when the value of K increases and becomes greater than 5/3. From Table I we note that this sub-force is $1.2V_N^2$ for $K < 5/3$ and $2.4V_N^2$ for $K > 5/3$. If we approximate the lower surface flow by the flow of a distribution of sources that aerodynamically simulates the lower surface of the plate then the doubling of the magnitude of the symmetrical force can be considered as the result of doubling the strength of the source distribution in order to eliminate the flux through the forward cones of these disturbances when the Mach number normal to the plate is greater than one.

We conclude this section by referring the reader to a graphical representation of the "$M_\infty \alpha$" domains that is presented in figure 8. The relationship and relative extent of the domain within which a particular sub-force or sub-pressure is predominant is clearly evident from this figure.

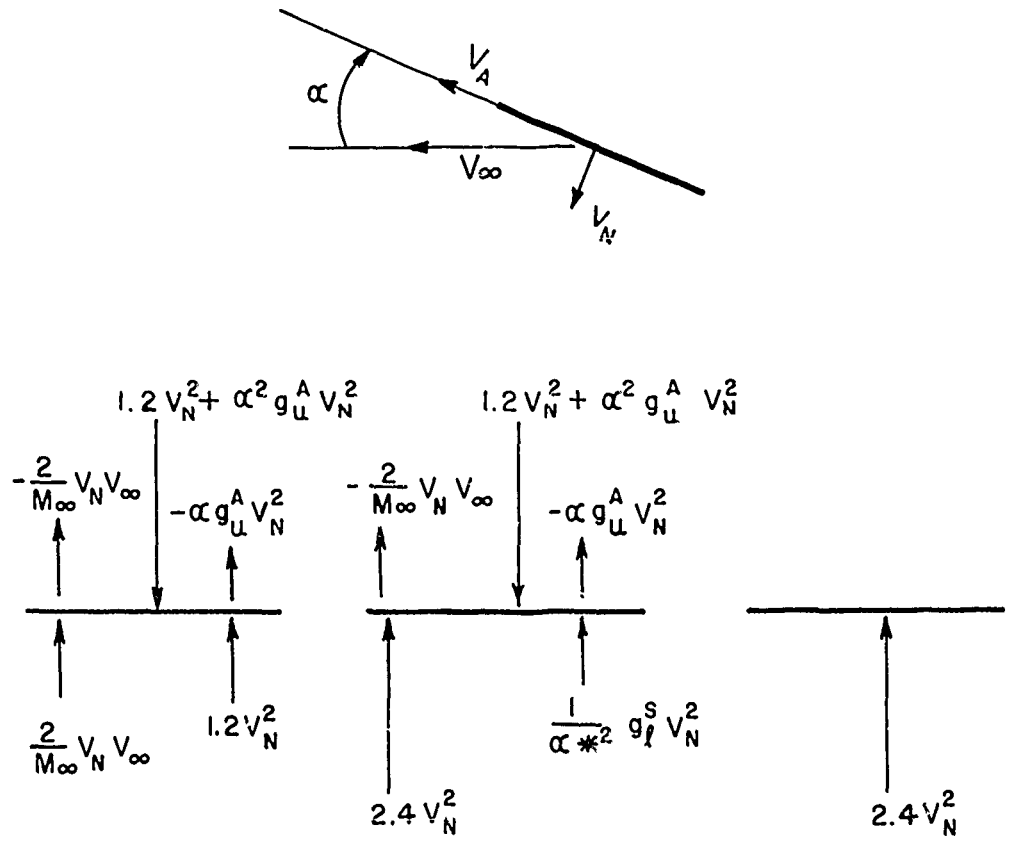


FIGURE 7. - VARIATION OF THE DISTRIBUTION OF SUB-FORCES WITH THE PARAMETER $M_\infty \alpha$

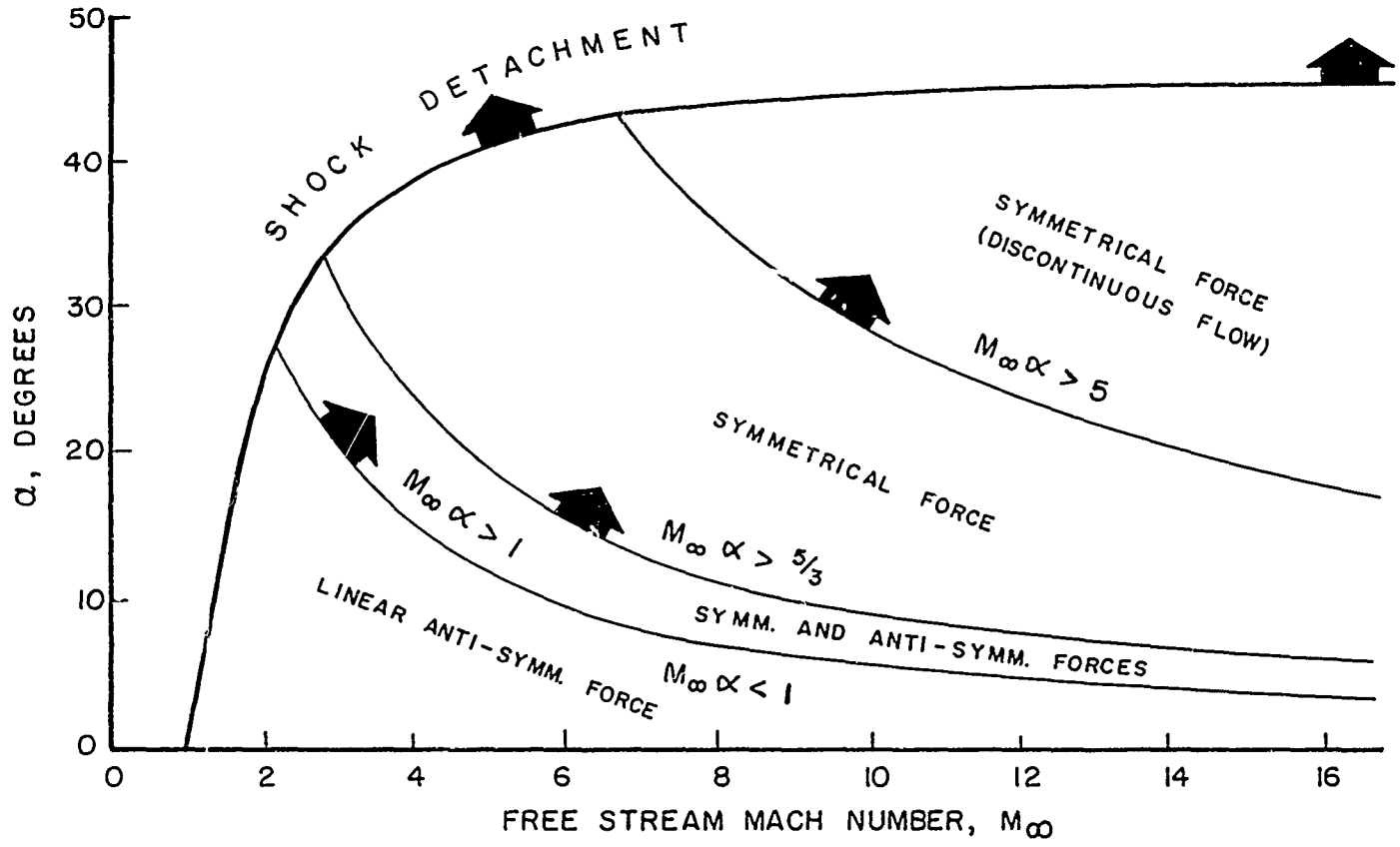


FIGURE 8.— $M_\infty \alpha$ DOMAINS FOR THE COMPRESSION SUB-FORCES OF TWO-DIMENSIONAL PLATES

SECTION III: RELATIONS FOR THE APPROXIMATE EVALUATION OF HYPERSONIC FORCES

The foregoing concepts will now be used as a basis for the development of approximate analytical expressions for the calculation of the aerodynamics of component elements. The following discussion is a description of the development of these expressions. In a later section these expressions are used to evaluate the aerodynamic characteristics of a number of re-entry configurations.

The starting point of the analytical development is the expressions for the pressure coefficients tabulated in Table 1. It is clear that although the tabulated expressions have been derived for the upper (expansion) and lower (compression) surfaces of a sharp edge two dimensional plate, they are also equally applicable to the expansion surface and compression surface of sharp leading edge planar elements, provided there is no communication of flow between the expansion and compression surfaces of the element. For convenience the expressions for pressure coefficients listed in Table 1 are repeated here and recast in a form more suitable for analytical interpretation.

$K_\ell = M_\infty \delta_\ell < 5/3$ AND $K_u = M_\infty \delta_u < 5$

$$\frac{C_p^\ell}{\delta_\ell^2} = \frac{2}{K_\ell} + 1.20 + 0.36\, K_\ell - 0.0323\, K_\ell^3 + 0.0006\, K_\ell^5 \qquad (24)$$

$$\frac{C_p^u}{\delta_u^2} = -\frac{2}{K_u} + 1.20 - 0.40\, K_u + 0.08\, K_u^2 - 0.0096\, K_u^3 + 0.00064\, K_u^4 - 0.0000\, K_u^5 \qquad (25)$$

$5/3 < K_\ell < 5$ AND $K_u < 5$

$$\frac{C_p^\ell}{\delta_\ell^2} = 2.4 + \frac{5}{3K_\ell^2} - \frac{1.158}{K_\ell^4} + \frac{1.608}{K_\ell^6} + \cdots \qquad (26)$$

$$\frac{C_p^u}{\delta_u^2} = \text{RIGHT HAND SIDE OF EQUATION (25)}$$

$K_l > 5$ AND $K_u > 5$

$$\frac{C_p^\ell}{\delta_\ell^2} = \text{RIGHT HAND SIDE OF EQUATION (26)}$$

$$\frac{C_p^u}{\delta_u^2} = 0 \qquad (27)$$

where:

Subscripts "ℓ" and "u" denote the lower surface and upper surface of planar element respectively.

K is the hypersonic similarity parameter.

δ is the angle of attack of a differential element of the planar surface.

Equations (24) to (27) exhibit the strong functional dependence of C_p/δ^2 on the similarity parameter $K = M_\infty \delta$. Note also the algebraic equivalence of the δ^2 sub-forces of the upper and lower surface for $K_\ell < 5/3$ that is for a Mach number normal to the compression surface that is less than one and the increase in the magnitude of

the coefficient of δ^2 , from 1.2 to 2.4, when $K_\ell > 5/3$ that is when the Mach number normal to the compression surface is greater than one. It is clear therefore that any proposed modification of the expressions (24) to (27) for the pressure coefficients of planar elements must incorporate the change in the magnitude of the compression δ^2 sub-force as we proceed from $K_\ell < 5/3$ to $K_\ell > 5/3$ and must accept the full equivalence of the coefficients of the expansion and of the compression δ^2 sub-pressures for $K_\ell < 5/3$. Of course any changes to the coefficients of the δ^2 sub-pressures must reflect in appropriate changes to the other terms of the preceding expressions that represent the subset of higher order sub-pressures. There is one additional important point we wish to make. The partitioning of the compression and expansion sub-pressures into domains of K discussed previously allows direct understandable approximations to be made to the preceding expressions for the pressure coefficients since the predominant sub-pressure terms in each domain of K are clearly evident.

We are now in a position to present analytical approximations to the pressure coefficients for the compression surface and expansion surface of planar surfaces. The following assumptions will be made based upon the preceding discussion.

For $K_\ell < 5/3$, terms of order K and higher will be approximated by a constant, h_o^ℓ, in the expression (24) for compression pressures.

For $K_\ell > 5/3$, terms of negative powers greater than 2 will be neglected in the expression (25) for compression pressure. This corresponds to a second order variation in angle of attack.

In the expression (26) for the expansion pressures terms of order K_u and higher will be approximated by a constant, h_o^u.

The coefficient of a_2 of the δ^2 sub-pressure terms of the compression pressure coefficient and expansion pressure coefficient will be replaced by an arbitrary parameter, ξ_o.

The constants h_o^ℓ and h_o^u that replace the K term and higher order terms in the expressions for the compression and for expansion pressure coefficients are determined by the value assigned to ξ_o and the physical boundary conditions of the aerodynamic field of the planar surface.

Based upon these assumptions the following approximate expressions for the pressure coefficients of equations (24) to (27) are readily obtained.

$K_\ell < 5/3$, $K_u < 5$

$$\frac{C_p^\ell}{\delta_\ell} \approx \frac{2}{K_\ell} + \xi_o + h_o^\ell \tag{28}$$

$$\frac{C_p^u}{\delta_u^2} \approx -\frac{2}{K_u} + \xi_o + h_o^u \tag{29}$$

$5/3 < K_\ell$, $K_u < 5$

$$\frac{C_p^\ell}{\delta_\ell^2} \approx 2\,\xi_o + \frac{5}{3K_\ell^2} \tag{30}$$

$$\frac{C_p^u}{\delta_u^2} \approx \text{RIGHT HAND SIDE OF EQUATION (29)}$$

$5/3 < K_\ell$, $K_u > 5$

$$\frac{C_p^\ell}{\delta_\ell^2} = \text{RIGHT HAND SIDE OF EQUATION (30)}$$

$$\frac{C_p^u}{\delta_u^2} = 0 \tag{31}$$

The specific applicability of equations (28) to (31) depends upon a knowledge of ξ_o and of course the evaluation of the constants h_o^ℓ and h_o^u.

First let us determine h_o^l as a function of ξ_o by considering the behavior of C_p^l / δ^2 in the neighborhood of $K_l = 5/3$. From equation (28) we have

$$\frac{C_p^l}{\delta_l^2} \longrightarrow \frac{6}{5} + \xi_o + h_o^l, \quad K_l \longrightarrow 5/3 \tag{32}$$

From equation (30) the expression for $\frac{C_p^l}{\delta_l^2}$ for $K_l > 5/3$ is $2\xi_o + \frac{5}{3K_l^2}$. As $K_l \longrightarrow 5/3$ this expression yields

$$\frac{C_p^l}{\delta_l^2} \longrightarrow 2\xi_o + 3/5 \tag{33}$$

If we accept the requirement that the limiting values of $\frac{C_p^l}{\delta_l^2}$ expressed in (32) and (33) are equal as $K_l \longrightarrow 5/3$, then the constant h_o^l is equal to

$$h_o^l = (\xi_o - 3/5) \tag{34}$$

In a similar manner the value of h_o^u in terms of ξ_o is determined by the condition that $C_p^u / \delta_u^2 = 0$ for $K_u \geq 5$ (see equation (31)).

$$\frac{C_p^u}{\delta_u^2} = -2/5 + \xi_o + 5 = 0, \quad K_u = 5$$

Solving this equation for h_o^u yields:

$$h_o^u = -(\xi_o - 2/5) \tag{35}$$

The parameter ξ_o must now be determined. A glance at equation (30) reveals that $2\xi_o$ is approximately the compression pressure coefficient for large values of K_l (say $K_l > 5$). In the present study we will accept the relation

$$2\xi_o \approx C_{p_{STAG.}} \tag{36}$$

which is in accord with the proposal of Lees that for $K_\ell \rightarrow \infty$ the surface pressure coefficient is approximated to a satisfactory degree by the stagnation pressure coefficient at a particular Mach number. A reasonable engineering approximation to the actual values of $C_{p_{stag.}}$ for Mach numbers greater than 2.0 is

$$C_{p_{STAG.}} \approx 1.80 , \quad M_\infty \geq 2.0$$

We will use this value of $C_{p_{stag.}}$ as a good approximation to $2\xi_o$, that is, $\xi_o = 0.90$. We wish to emphasize, however, that the preceding formulation of expressions for the evaluation of pressure coefficients provides for a reasonable degree of flexibility in the choice of values for ξ_o within practical limits. The fact that the value of ξ_o contributes to the magnitude of the coefficients of the important compression and expansion δ^2 sub-pressures at small as well as at large angles of attack assures the proper distribution of the effect of ξ_o on the total surface pressures for a large range of the similarity parameter $K = M_\infty \alpha$. With the assumption that $2\xi_o = 1.80$, the following numerical values of h_o^ℓ and h_o^u are established.

$$h_o^\ell = \left(\frac{9}{10} - \frac{3}{5}\right) = 0.30 \tag{37}$$

and

$$h_o^u = -\left(\frac{9}{10} - \frac{2}{5}\right) = -0.50 \tag{38}$$

Note that the coefficient h_o^ℓ properly reflects the entropy change through the attached shock by having a value that is less in magnitude than h_o^u, the coefficient that approximates the effects of the higher order terms on the isentropic expansion pressure coefficient.

Now if in the equations (28) to (30) for the pressure coefficients we set $\xi_o = 0.90$ and substitute the numerical values for h_o^ℓ and h_o^u from equations (37) and (38) we obtain the following approximate expressions for the pressure coefficients for the compression and expansion surfaces of a planar element.

$K_\ell \leq 5/3,\ K_u \leq 5$

$$\frac{C_P^\ell}{\delta_\ell^2} \approx \frac{2}{K_\ell} + 0.90 + 0.30 \tag{39}$$

$$\frac{C_P^u}{\delta_u^2} \approx -\frac{2}{K_u} + 0.90 - 0.50 \tag{40}$$

$5/3 \leq K_\ell,\ K_u \leq 5$

$$\frac{C_P^\ell}{\delta_\ell^2} \approx 1.80 + \frac{5}{3K_\ell^2} \tag{41}$$

$$\frac{C_P^u}{\delta_u^2} = \text{RIGHT HAND SIDE OF EQUATION (40)}$$

$5/3 < K_\ell,\ K_u \geq 5$

$$\frac{C_P^\ell}{\delta_\ell^2} = \text{RIGHT HAND SIDE OF EQUATION (41)}$$

$$\frac{C_P^u}{\delta_u^2} = 0 \tag{42}$$

The expressions (39) to (42) are the approximate relations for the calculation of the compression and expansion pressure coefficients that are applied in a subsequent section to the calculation of the aerodynamics of a number of re-entry vehicles. We wish to emphasize that although equations (39) and (40) retain only terms to the second order in δ, the second order terms $0.30\ \delta_\ell^{\,2}$ and $-0.50\ \delta_u^{\,2}$ do <u>reflect</u> the approximate contributions of δ^3 terms and higher

order terms to the pressure coefficients. To illustrate this point, consider again equations (39) and (40) for the lower and upper surface pressure coefficients for the conditions $K_\ell < 5/3$ and $K_u < 5$. In these equations the numerical coefficient 0.90 represents the value chosen for ξ_0, the parametric coefficient of δ^2 sub-pressures. It is clear that these sub-pressures do not contribute to the normal force for the range of K under consideration in accordance with our previous remarks regarding the required null contribution of these sub-pressures to the "lifting" pressure. Now consider the numerical coefficients 0.30 and -0.50. These coefficients are the values of h_0^ℓ and h_0^u respectively. Now the second order terms formed from these constants (that is $0.30\ \delta_\ell^2$ and $-0.50\ \delta_u^2$) are approximations of the contributions of the δ^3 terms to the pressure coefficients and do contribute to the "lifting" pressure as required.

For example, if equations (39) and (40) are applied to a flat plate ($\delta_\ell = \delta_u = \alpha$, $K_\ell = K_u = K$) the following result for lifting pressure is obtained.

$$M_\infty \alpha < 5/3$$

$$C_{P_{LIFTING}} = C_P^\ell - C_P^u = 4/\sqrt{M_\infty^2 - 1}\ \alpha + 0.8\alpha^2$$

The term $0.8\alpha^2$ is the quadratic approximation to the contribution of the δ^3 terms + higher order terms to the lifting pressure. It is not the contribution of the symmetrical α^2 sub-pressure to the lifting pressure. This contribution is zero as previously stated for $K_\ell < 5/3$.

It is possible to extend the order of approximation of the preceding equations (39) to (40) so as to include δ^3 terms. If this extension is made the following expressions are obtained, expressed in terms of ξ_0, h_0^ℓ and h_0^u.

$$K_\ell \le 5/3,\ K_u \le 5$$

$$\frac{C_P^\ell}{\delta_\ell^2} = \frac{2}{K_\ell} + \xi_0 + \frac{3}{5}\left(\xi_0 - \frac{3}{5}\right) K_\ell \qquad (43)$$

$$\frac{C_p^u}{\delta_u^2} = -\frac{2}{K_u} + \xi_0 - \frac{1}{5}\left(\xi_0 - \frac{2}{5}\right)K_u \qquad (44)$$

A simple analysis reveals that the maximum value of ξ_0 permissible in these equations, that is compatible with the assumptions and approximations made in the development of equations (28) to (31) is the value $\xi_0 = 0.80$. Larger values of ξ_0 such as $\xi_0 = 0.90$ results in the introduction of an artificial positive pressure along the "expansion" surface for values of K_u between 4.0 and 5.0. This pressure however is extremely small, $O(\delta_u^3)$, and is a negligible contribution to the net pressures acting on the surface. There is one additional point we wish to make concerning the third order approximations of equations (43) and (44). If we accept the previously stated assumption that forces of the magnitude of C_p^u to approach zero as $K_u \rightarrow 5$; as it should from the exact variation of isentropic C_p^u with K_u, then the magnitude of the coefficient of K_u (that is h_o^u) in the approximate expression (44) for C_p^u is smaller than the magnitude of the corresponding coefficient h_o^ℓ of K_ℓ in expression (43) for C_p^ℓ. This result, that is $h_o^u < h_o^\ell$, implies that the entropy change across the attached leading edge shock increases the magnitude of the contribution of the δ^3 term to C_p^ℓ relative to the corresponding isentropic contribution of the δ_u^3 to C_p^u. This result is contrary to the result of precise shock-expansion analysis which reveals that the entropy change through the shock produces a reduction in magnitude of the coefficient of the δ_ℓ^3 - term relative to the magnitude of the corresponding coefficient of δ_u^3 in the expansion pressure expression. It is clear from our previous discussion that retaining only terms to the second order in δ completely removes the afore stated restriction on ξ_0 and the incompatibility of the magnitudes of the h_o^ℓ and h_o^u constants.

We will complete the present discussion by an illustration of the applicability of the preceding pressure expressions to the calculation of normal force coefficients for two configurations. These configurations are a delta configuration and a conoid configuration.

Comparisons of the variations of the calculated and experimentally determined normal force coefficients with angle of attack are shown in figures (9) and (10) for each of these configurations. The calculated variations are based upon Newtonian theory ($C_p = K \sin^2 \alpha$) and upon the present theory. It is evident from these comparisons that the present theory yields a satisfactory analytical approximation to the experimental variations.

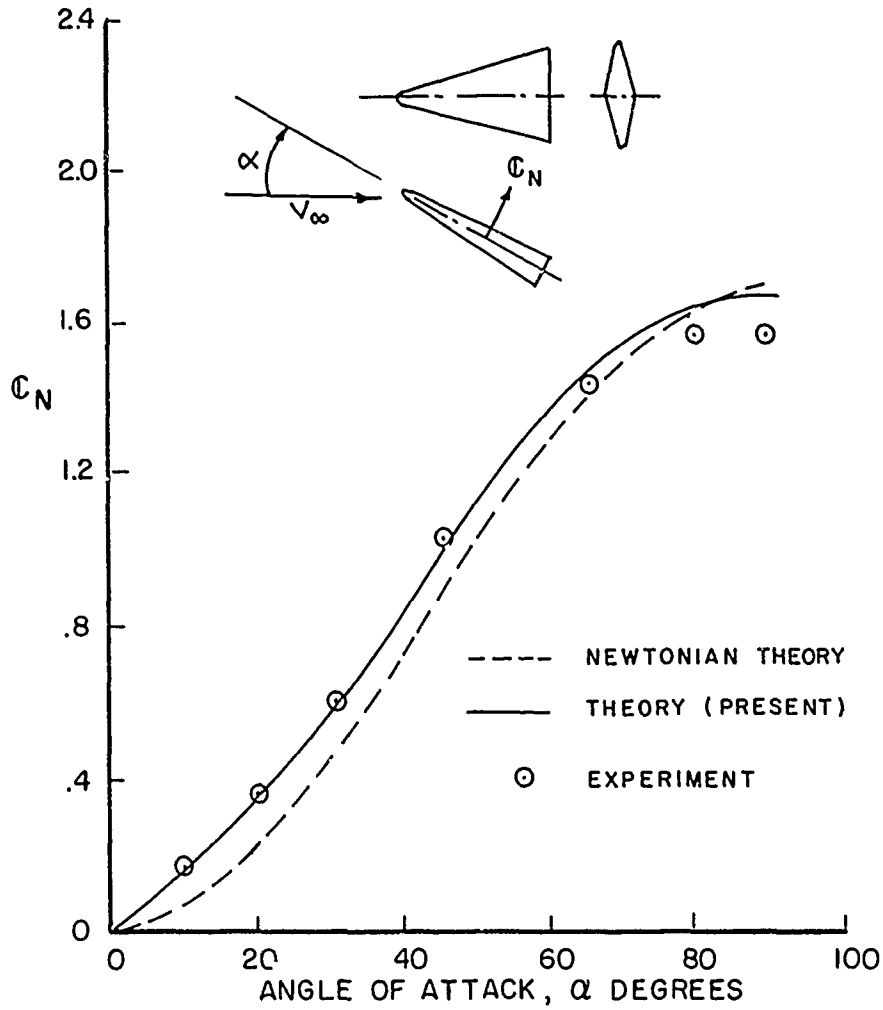


FIGURE 9.— COMPARISON OF CALCULATED AND EXPERIMENTAL NORMAL FORCE COEFFICIENTS FOR A DELTA WING

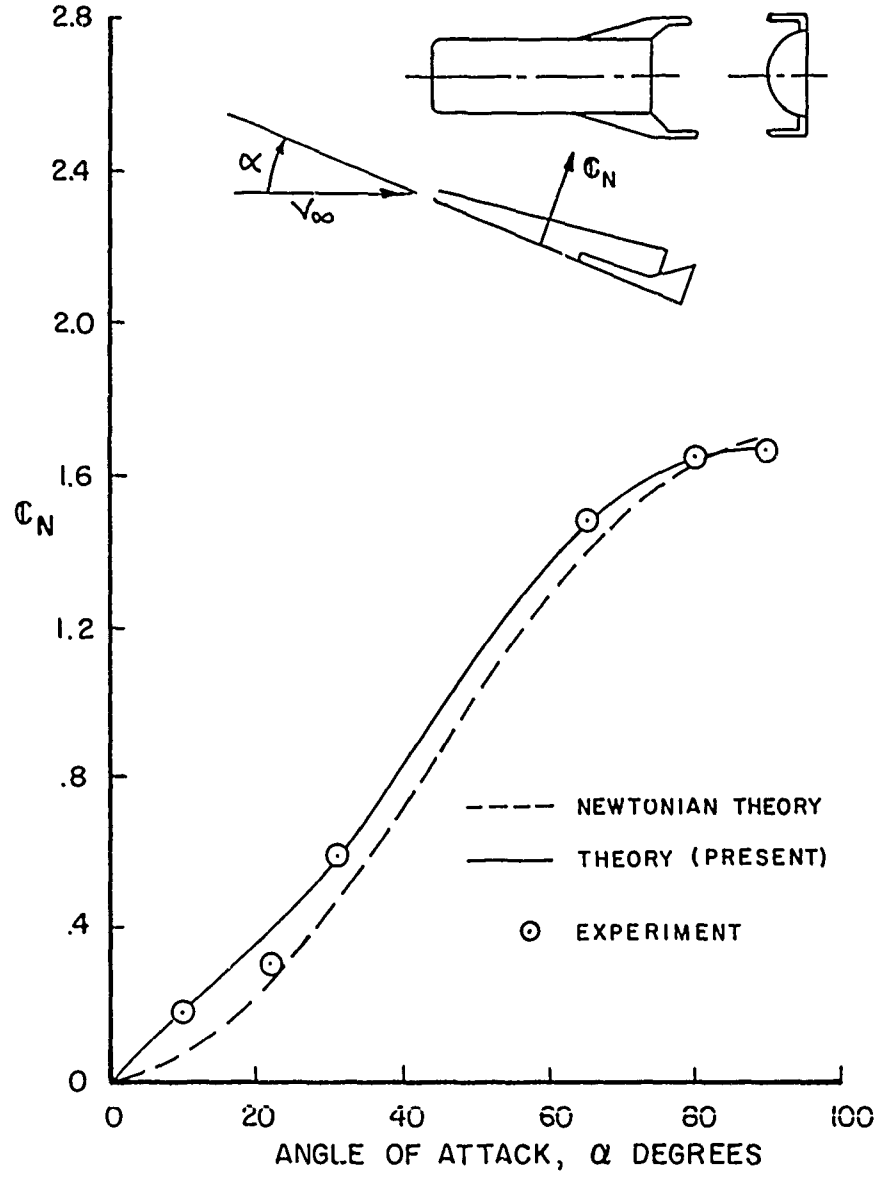


FIGURE 10.- COMPARISON OF CALCULATED AND EXPERIMENTAL NORMAL FORCE COEFFICIENTS FOR A CONOID BODY

REFERENCES

1. Malvestuto, F. S., Sullivan, P. J., Mortzschky, H. A., Marcy, W. L. and Larrivee, J., (Title UNCLASSIFIED) Study to Determine Aerodynamic Characteristics on Hypersonic Re-Entry Configurations Part II, Theoretical and Empirical Analysis, Vol. 1, Analysis, WADD TR 61-56, May, 1961. CONFIDENTIAL report.

2. Robinson, A. and Laurmann, J. A., Wing Theory, Cambridge University, 1956.

3. Ackeret, J., Uber Luftkrafte auf Flugel, die mit grosserer als Schallgeschwindigkeit bewegt werden, Z. Flugtech. Vol. 16 (1925) pp. 72-4. Translated as Tech. Memor. Nat. Adv. Comm. Aero., Wash., no. 317.

4. Van Dyke, M. D., A Study of Hypersonic Small-Disturbance Theory, NACA TN 3173, 1954.

A CRITICAL REVIEW OF PREDICTION TECHNIQUES APPLICABLE TO RE-ENTRY VEHICLES

Richard D. Neumann
Edward T. Meleason, 2nd Lt., USAF
Flight Dynamics Laboratory
Aeronautical Systems Division

ABSTRACT

The state of the art with regard to aerothermodynamics has progressed from the development of a rational theory for determination of stagnation point heating rates to the development of a practical lifting re-entry device in less than five years time. Due to this phenomenal rate of advance, borne of necessity, the field of aerothermodynamics is today as much art as science - lacking is the ordered development of procedures necessary for the analysis of new and varied weapon systems as well as timely and meaningful tests. At the same time, new vehicles are posing problems of an increasingly diverse nature encompassing new flow regimes, new aerodynamic heating mechanisms and new vehicle design concepts. Despite these difficulties, much has been done both theoretically and experimentally to advance the fund of knowledge concerning aerothermodynamics. This paper will attempt to outline that progress and underscore some of the problems connected with an engineering evaluation of the aerodynamic heating on arbitrary lifting re-entry devices.

LIST OF SYMBOLS

n	heating parameter (Equation A-4)
$\dot{q}$	heat transfer rate, btu/ft^2 sec
R	radius, ft
V	velocity, ft/sec
Z	altitude, ft
C_D	drag coefficient
C_L	lift coefficient
L_D	ratio of lift to drag
α	angle of attack
δ	angular position of the leading edge stagnation line, measured from the zero angle of attack position
ϵ	density ratio across the shock
Λ	sweep angle
$\bar{\chi}$	viscous interaction parameter

Subscripts

B	body
CONV	convection
eff	effective
HGR	hot gas radiation
MAX	maximum
n	normal
OPT	optimum
STAG	stagnation
Λ	sweep
∞	free stream
2D	two dimensional

A CRITICAL REVIEW OF PREDICTION TECHNIQUES APPLICABLE TO RE-ENTRY VEHICLES

INTRODUCTION

The use of more sophisticated lifting re-entry systems for return from both orbit and space has posed to the engineer serious problems of thermal protection. Unlike their ballistic predecessors, these vehicles are composed of complex geometries and traverse regions where they encounter many diverse induced environments. This paper will consider the aerodynamic heating of such configurations and the development of design procedures for their analysis.

Although complete generality is the goal of the paper, it is obvious that some reasonable compromise between generality, volume, and utility must be reached. Accordingly, it was concluded to enumerate many of the phenomena connected with aerodynamic heating of these vehicles, referring to a large extent to published papers on the subject. In addition, in an attempt to present an up-to-date resumé of the state of the art, new work of an unclassified nature will be outlined. Classified literature of course cannot be presented.

References 1 through 3 present a cross section of the basic procedures involved in the evaluation of aerodynamic heating of lifting entry systems. For the most part these methods will not be included in this paper; however, the reader is invited to review these works for a more complete understanding of the field.

In the review of this subject two areas were seen to play important parts. These areas are the evaluation of flow regimes encountered by the re-entrant vehicle and the evaluation of the magnitude and variation of aerodynamic heating over the vehicle surface in these regimes. This paper will therefore be subdivided into sections to cover each of these areas, with a concluding section for the analysis of the combined vehicle and conclusions of the paper.

FLOW REGIMES

First analysis of the aerodynamic heating assumed a simple equilibrium flow model wherein the boundary layer was considered thin in comparison with the shock layer. This model was expedient in that it decoupled the boundary layer-shock layer influence and allowed simplified solutions to the aerodynamic heating. It was also quite acceptable for the ballistic missile case which preceeded lifting vehicles for re-entry. Unfortunately, as glide entry systems developed, a trend to lighter and lower wing loading vehicles also developed. These vehicles may decelerate in a region where the foregoing model is not appropriate and corrections to the model must be made. Coincidently, the effects of real gas flows and chemical non-equilibrium appeared so that these several effects must be considered. In addition to these formidable problems of orbital re-entry, the implications of near space entry are now becoming important and here not only are we interested in the low density chemically reacting gas but also with new mechanisms of heat transfer brought about by the presence of appreciable ionization in the shock layer and the transference of energy to the body by radiation. This section will therefore discuss the various flow phenomena encountered and point out qualitatively where they occur. The following sections will then describe the implications of the flow phenomena on the re-entrant system.

Flow regimes can conveniently be grouped into three general areas based on predominant flow phenomena as shown in Table 1. These include (1) classical hypersonic flow where the thin boundary layer assumption holds and the flow is in chemical equilibrium; (2) low density chemically reactive flows where molecular dissociated non-equilibrium flow exists in addition to low density shock layer-boundary layer interaction; and (3) ionized gas flow found in the superorbital flight regime. General characteristics of these regions are found in the aforementioned table. Definition of these flow regimes in terms of energy and density considerations has been treated by various authors. Figure 1 presents the approximate boundaries recognized by current technology on an altitude - velocity plot. The region of validity of classical hypersonic flow has been defined by Probstein (4) who predicts the emergence of significant low density interaction effects at an altitude of approximately 200,000 feet. Probstein's analysis is concerned primarily with the appearance of density dependent phenomena. The establishment of a boundary between chemical equilibrium and frozen flow has been attempted by Ferri (5), Kivel (6), Hankey (1), and others. The general consensus is that chemical non-equilibrium also exists in the inviscid flow field at about 200,000 feet.

The boundaries presented in Figure 1 assume a vehicle nose dimension of one foot radius due to the popularity of this particular simplification

TABLE 1

GENERAL CHARACTERISTICS OF AEROTHERMODYNAMIC FLOW REGIMES

	Region of Classical Hypersonic Flow Analysis	Region of Significant Low Density Effects	Region of Appreciable Ionization
Major Flow Characteristics	Continuum Flow Chemical Equilibrium Thin Boundary Layer	Variations in Shock Wave Structure Chemical Non-equilibrium	Ionized Gases
Significant Heating Effects	Convection	Convection Viscous Effects Vorticity	Convection Hot Gas Radiation
General Description	$Z < 200,000$ $V < 30,000$	$Z > 200,000$	$V > 30,000$

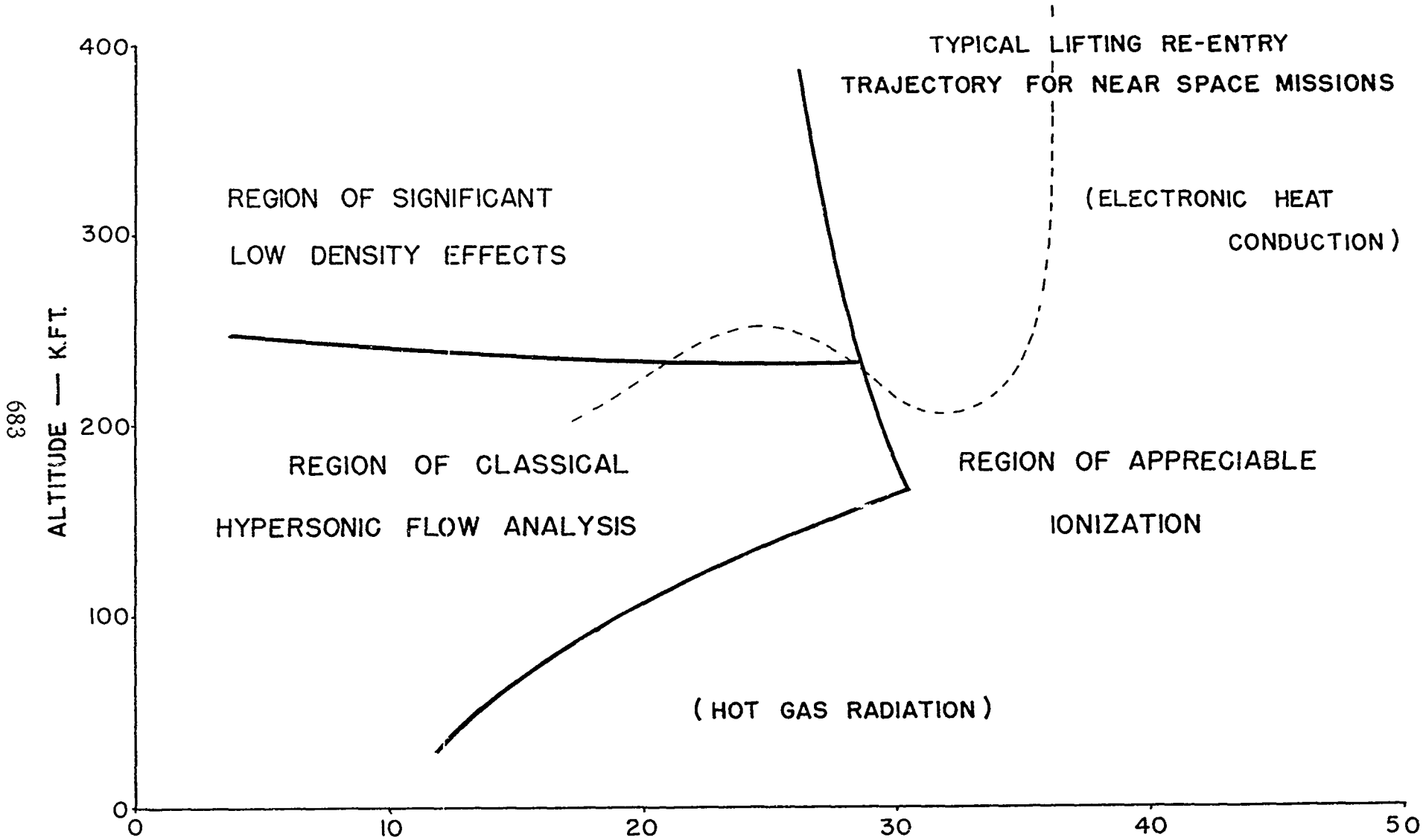


FIGURE I FLOW REGIMES

in analytical treatments. It should however be remembered that all these phenomena are dependent on the body radius which may, in certain cases, be significantly different from one foot, shifting the boundaries of the various regions and even bringing into consideration new phenomena.

The regions of appreciable ionization and radiation heating can be inferred by choosing a certain equilibrium electron density. This analysis has chosen one percent free electrons. First effects of this ionization are seen in the electronic heat conduction to the surface of the body. In addition to this, increasing the velocity or alternately decreasing the altitude at a given velocity will introduce the new mechanism of hot gas radiation heating. Mac Adams (7) has considered these phenomena and has outlined their influence. At this conference Dr. Scala has presented a paper on some recent work being performed in this area at General Electric.

DESIGN ANALYSIS

Now that the flow regimes have been delineated and their general features described, the very formidable problem of the design analysis of generalized three dimensional configurations presents itself. For a field as new as atmospheric entry of lifting configurations no preset notions of reverenced configurations should be present. Two classes of configurations are however emerging as desirable design choices. These are the highly swept delta planform of the Dyna-Soar type and the lifting body configuration such as pioneered by NASA Ames and critically investigated at the Aeronautical Systems Division. Both types embody the same geometrical contours - i.e., blunt spherical noses, highly swept cylindrical segments and flat or curved lower surfaces. This section will therefore investigate these basic elements of lifting configurations throughout the three flow regimes previously outlined. Further, the following section will synthesize the final configuration from these design procedures.

Even more unconventional than the planform of these vehicles is their entry attitude. As few as ten years ago high angles of attack denoted some twenty or thirty degrees. At the start of the Dyna-Soar program it appeared that the angle of attack during re-entry could be limited to the range between L/D_{max} (about 10 to 15 degrees) and $C_{L_{max}}$ (about 55 degrees). Figure 2 illustrates these attitude regimes for a typical lifting configuration. Today we are faced with many design concepts and some analysis of vehicles which fly, in the broadest sense of the word, at almost 90 degrees to the local horizontal for a sizeable portion of their entry trajectory. In order to approach our goal of

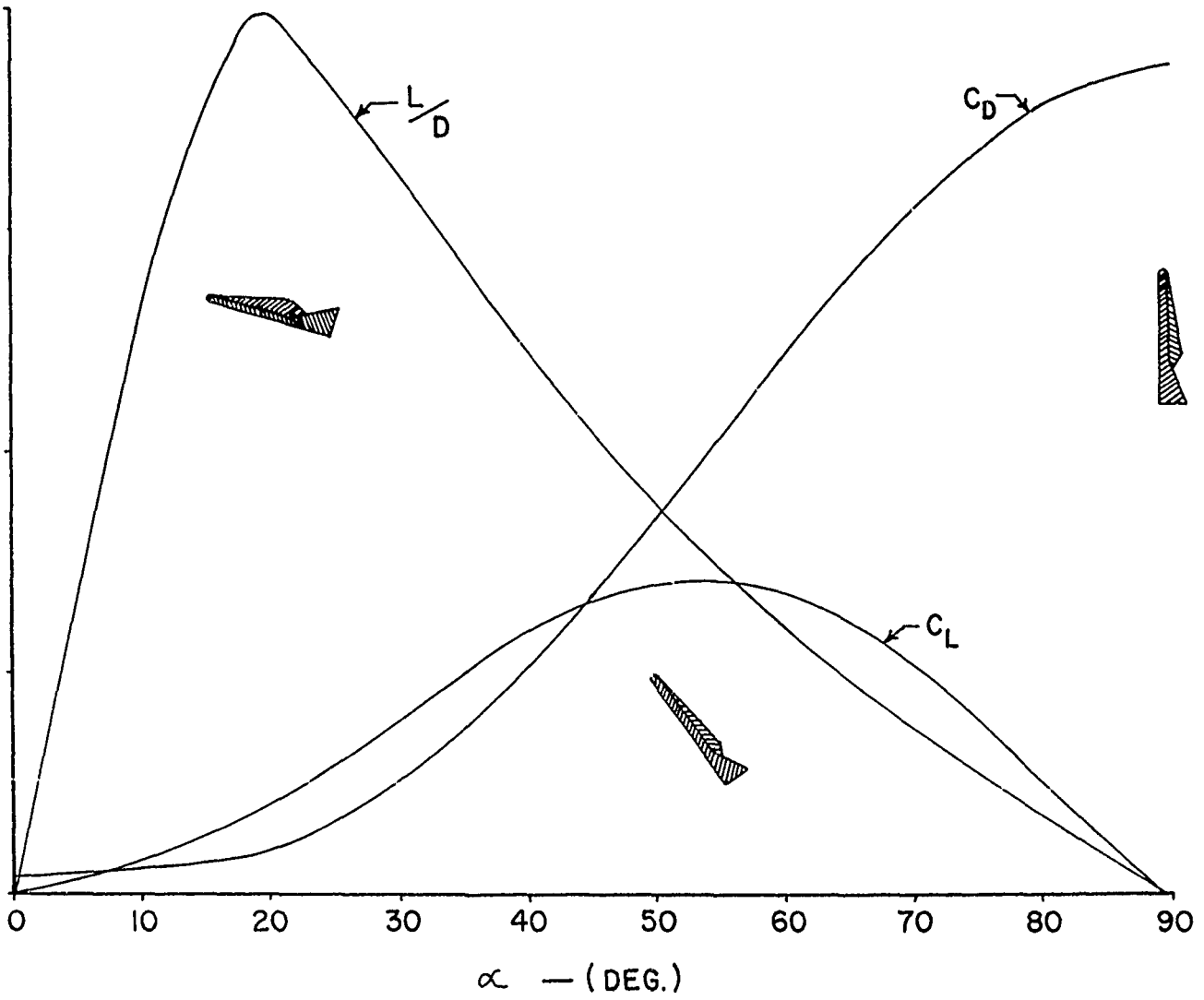


FIGURE 2 ATTITUDE REGIMES FOR TYPICAL LIFTING RE-ENTRY VEHICLES

completeness, the analysis will be extended whenever possible to include these vehicular concepts.

Stagnation Point Flows

The stagnation region of a blunt spherical body is one of the most thoroughly treated items in the study of hypersonic aerothermodynamics. A classical piece of literature on this problem is the paper of Fay and Riddell (8) who treated the cases of air in chemical equilibrium and frozen non-equilibrium. As a result of their study, as well as others, it has become commonplace to use the rule of thumb that the stagnation heating rate can be reduced according to the inverse square root of the body radius. This is however not a universal truth. As the entry velocity increases to that of lunar return and space entry speeds, this rule of thumb loses its significance entirely as radiation from the hot gas layer becomes an important or even dominant mechanism. One interesting by-product of the combined hot gas radiation and convective heating environment is that one may define an optimum sphere nose radius*, which is given by the equation:

$$R_{OPT} = \left(\frac{\epsilon^{1/2}}{2n}\right)^{2/3} \qquad (1)$$

Figure 3 shows the relative heating parameter plotted vs the body radius for various values of the parameter "n". Unfortunately, this parameter can only be bounded in the region of interest for re-entering glide systems due to the onset of non-equilibrium hot gas radiation. Its equilibrium value, however, for moderate entry angles ($\gamma \approx 7°$) is of the order of 1/10 and its non-equilibrium value can be expected to be higher, perhaps by an order of magnitude (c.f. ref. (7)). In addition to the region where superorbital effects are important, several effects arise due exclusively to the low Reynolds number flows. Hoshizaki (9), Probstein (10), Van Dyke (11) and others have shown that these low densities produce a shock generated vorticity as well as other lesser second order effects that may increase the stagnation point heating by a factor of two or more. This problem will be fully discussed in a paper by Mr. Hoshizaki later in this conference. These two problems, then, - entry at super-orbital speeds and the analysis of low Reynolds number flows - bound the region of applicability of the Fay and Riddell solution and in fact form the frontier to our present detailed understanding of stagnation region flows.

---

*A full development of this equation is given in Appendix A of this paper.

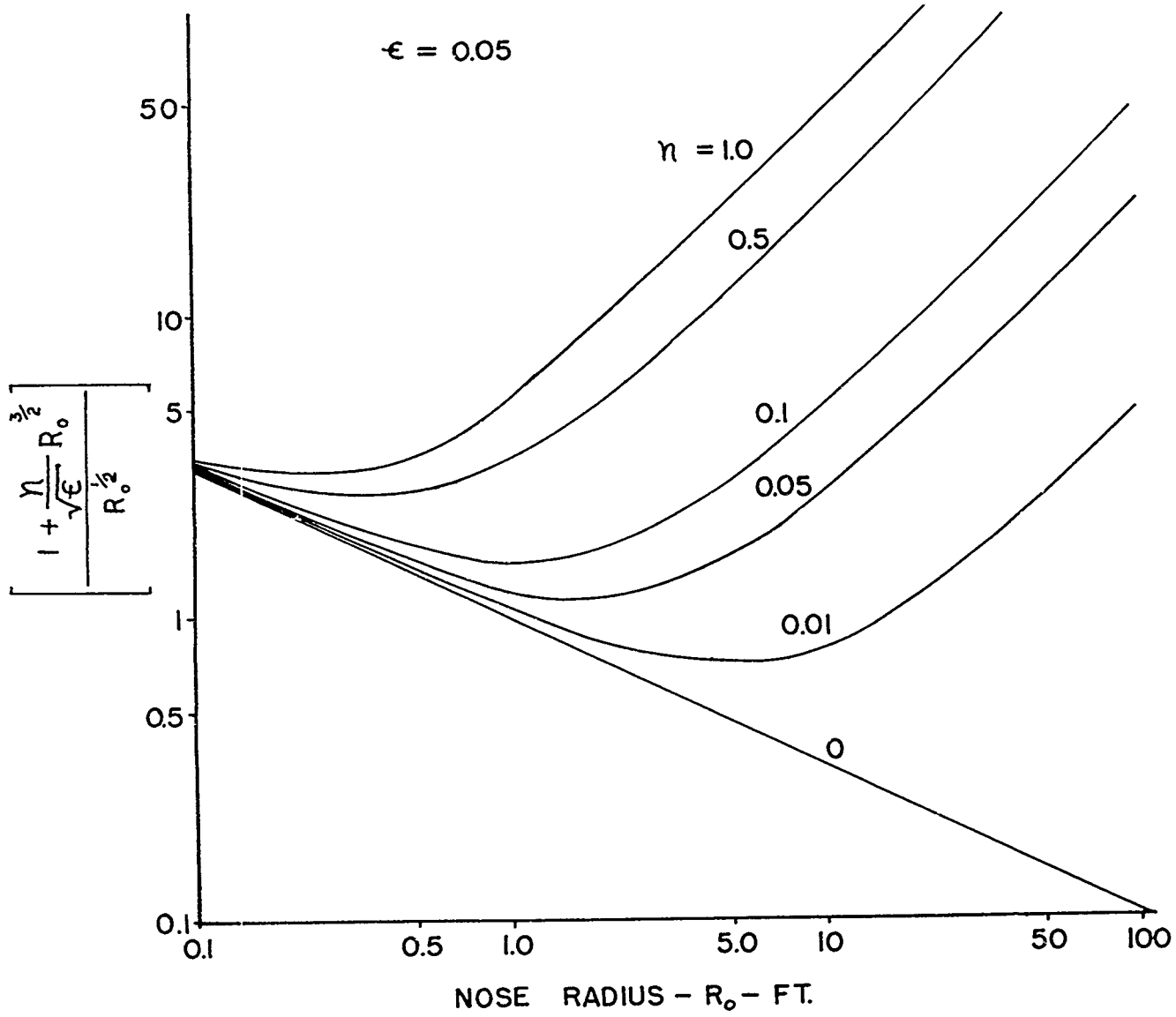


FIGURE 3 RELATIVE HEATING PARAMETER VS BODY RADIUS FOR VARIOUS VALUES OF THE PARAMETER "η"

Swept Cylinder Flows

By the conventional Mangler boundary layer transformation, the stagnation point solution may be transformed into a two dimensional cylinder solution where the cylinder is oriented normal to the free stream flow. Lees (12) has obtained a simplified expression for the two dimensional cylinder heating rate, as have others in the field. An interesting problem is describing what occurs when the cylinder is swept to high angles with respect to the free stream and further what happens when this highly swept cylinder (which can be thought of now as a leading edge) is brought to an angle of attack. Taking these problems in order, the following is observed. As the cylinder is swept to higher angles, the heating rate varies as the "n"th power of the cosine of the swept angle - i.e., $\dot{q}_\Lambda / \dot{q}_{\Lambda 0} = \cos^n \Lambda$ where "n" is some constant between generally accepted values of 1.0 and 1.5. One problem that has been noticed here is that all the data which verify this constant are low Mach number data ($M_\infty \leq 10$). At high sweep angles, these low free stream Mach numbers yield transonic Mach numbers normal to the leading edge ($M_n \approx 2.0$ to 3.0). In this region it has been shown (13) that the spanwise velocity gradient is a strong function of the Mach number. It appears further that if higher Mach number data is used, the "n" does in fact approach a value of 3/2 as contrasted with 1.0 for the lower Mach number data.

As the swept cylinder is pitched to an angle of attack the "effective sweep" of the cylinder is decreased according to the geometric relationship $\Lambda_{eff} = \sin^{-1}(\sin\Lambda \cos\alpha)$. In this situation the angle to the stagnation line, " δ ", measured from the zero angle of attack position becomes: $\delta = \tan^{-1}\left(\frac{\tan\alpha}{\cos\Lambda}\right)$. This geometric model appears to predict the stagnation line movement quite satisfactorily at low angles of attack; however, it loses its validity rapidly for angles of attack greater than 15 degrees. In an attempt to obtain at least a conservative if not an exact estimate of the variation of δ with the angle of attack, the slope of the geometric expression for δ was obtained at zero angle of attack and linearly extended to $\delta = 90°$. The resultant expression ($\delta/\alpha = \cos^{-1}\Lambda$) seems to match the data remarkably well in the limited range of Mach and Reynolds numbers available in the literature (Figure 4). Further, this linearized scheme will predict the angle of attack where the stagnation line intersects the lower surface (see Figure 5) for conservative design of the leading edge heat protection system.

In addition to the prediction of the stagnation line movement with angle of attack, the magnitude of the resultant leading edge heating with

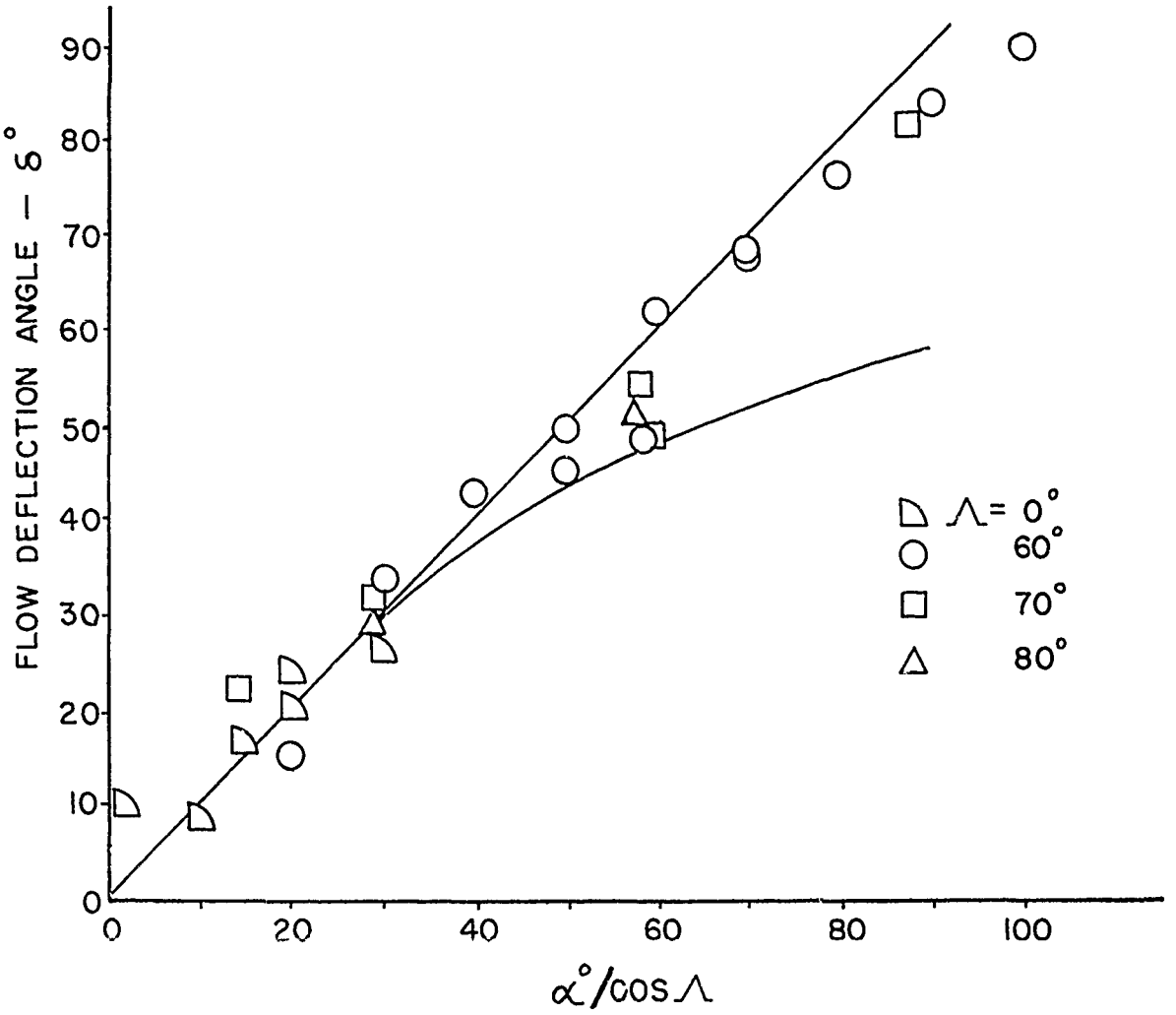


FIGURE 4 LEADING EDGE STAGNATION LINE LOCATION AS A FUNCTION OF ANGLE OF ATTACK AND SWEEP ANGLE

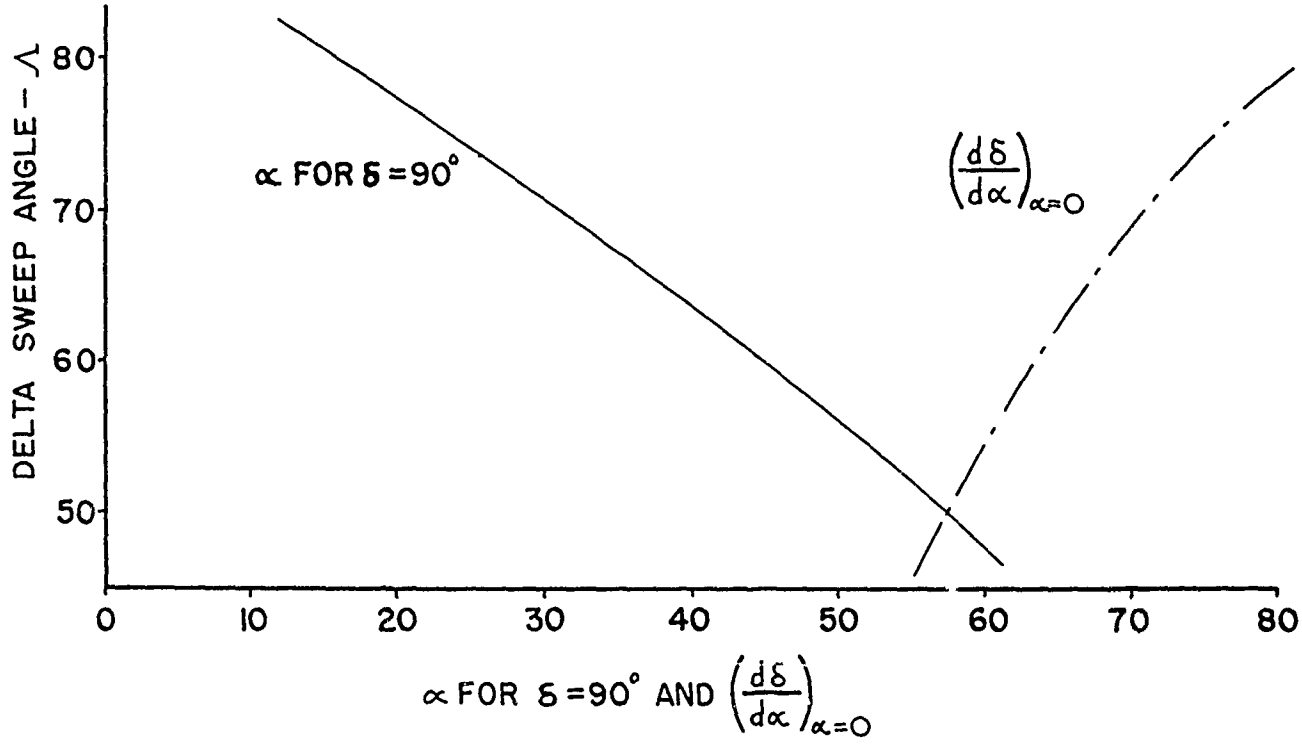


FIGURE 5 ANGLE OF ATTACK PRODUCING STAGNATION CONDITIONS ON THE LOWER SURFACE AS A FUNCTION OF SWEEP ANGLE

both sweep and angle of attack is calculable with the aforementioned uncertainty on the "n"th power of the cosine of the sweep angle. The resultant equation, which is ratioed to the stagnation point heating rate, is given as:

$$\frac{\dot{q}_\Lambda}{\dot{q}_{STAG}} = \frac{\left[1-\sin^2\Lambda\cos^2\alpha\right]^{n/2}}{\sqrt{2}} \qquad (2)$$

which reverts back to the familiar cosine "n"th power of the sweep for zero angles of attack.

The low density effects obtained on the spherical nose do not appear on swept cylinders until a much lower shock Reynolds numbers so that these effects need not be considered in the preliminary design of lifting re-entry systems. Analogous to this, the radiation heating of leading edges is not considered a problem because of the high sweep and hence lower effective stagnation temperature of the leading edge coupled with the small radius of the leading edge necessary to attain aerodynamic glide efficiency.

Above the angle of attack where the flow deflection angle, δ, reaches the lower surface, the leading edge is no longer a critical problem. At this vehicle attitude the lower surface flow is of prime importance and, as will be pointed out in the next section, the leading edge becomes the effective trailing edge for severe angles of attack ($\alpha \geq 55$ degrees).

Flat Plate Flows

The analysis of the lower surface of a delta or lifting body configuration has been made assuming, by strip theory, that the lower surface is a flat plate. As we will see later in this paper, this is not a valid assumption; however, this analysis will give some valuable insight into the centerline heating of the vehicle. In addition, the use of this model simplifies the theoretical analysis considerably and allows at least some estimates to be made theoretically.

The calculation of flat plate heating on the surface in the classical hypersonic regime has reached a state of engineering completion. The work of Dr. Eckert (14) on the reference temperature and enthalpy methods as well as many so-called simplified methods (c.f. Hankey, Neumann and Flinn (1)) will give the degree of accuracy required for design analysis. Basically, however, these methods suffer from several shortcomings. They do not consider viscous interaction effects and they are limited in angle of attack by the oblique shock assumptions.

In the region of appreciable shock interaction and nose bluntness, the approaches of Cheng et al (15) and Kaplan (16) will give first order design accuracy. Unfortunately, very little data is available in this region with which to correlate these studies. As the viscous interaction parameter is increased still further ($\bar{\chi}$ in the order of hundreds), the only known experimental work is that of Nagamatsu and Sheer (17) for pressure distribution on a sharp flat plate in the viscous interaction region from 2.5 to 756. The Aeronautical Systems Division also has an experimental program in this area which will measure both heat transfer and pressure in the viscous interaction range from 5.0 to 300. Elements of this program have been completed in the Arnold Engineering Development Center's Hot Shot facility and are reported in reference 18.

Blunt Body Flows

As the angle of attack is increased to 90 degrees, the spanwise component of the flow becomes dominant and we may think of the delta wing as a series of spanwise lamina (normal to the centerline). This approach has been taken by Cole and Brainerd (19). The region of applicability of this approach for a flat surface appears to be between an angle of attack of 70 degrees and 90 degrees and the procedure is particularly amenable to highly swept delta surfaces ($\Lambda \approx 70$ degrees). Analogous to this, GASL (20) has shown that the heat transfer on a cone at even moderate angles of attack can be predicted by a yawed cylinder approximation.

The exclusion of chemical non-equilibrium effects from the foregoing comments is a result of the present uncertainty concerning the surface catalysticity of structural materials and the resultant degree of conservatism afforded by the assumption of molecular equilibrium in the flow. In all fairness it must be said, however, that current theoretical analyses as well as laboratory scale experiments have shown a sizeable reduction in the aerodynamic heating due to the onset of chemically frozen flows where the surface does not recombine the flow and, if presently planned free flight tests show the same trend, an increase in aerodynamic efficiency due to lower surface temperatures and lower nose radii may be affected.

This section has dealt with some aspects of the determination of the aerodynamic heating over simple geometrical shapes approximating a lifting entry configuration. Although design procedures do in fact exist for these vehicles they are confined to regions of geometric symmetry where the three dimensional flow may be approximated by a two dimensional

model. In addition, the complex shock-boundary layer interaction effects have been treated very lightly and an appalling lack of data exists in the low density regime for realistic three dimensional configurations.

THE VEHICLE

Following a discussion of the flow regimes encountered by a re-entrant vehicle as well as the geometric components making up such a vehicle, the discussion here will center about the synthesis of the entire vehicle based on the previous sections. Unfortunately, the two dimensional models and the use of symmetrical sections do not apply here since we are faced with a distinctly three dimensional surface such as a delta wing or a lifting body. Bertram (2), as well as others, has made it clear that the flow on such configurations is neither planar nor conical in nature but varies from a viscous inflow at low angles of attack to an outflow at high attack angles. See for instance Figure 6 of this paper. This deviation of the viscous flow from strip theory manifests itself in the piling up of the boundary layer on the centerline at low angles of attack ($\alpha \approx 0^\circ$) and a thinning of the centerline boundary layer at high angles of attack ($\alpha \approx 55^\circ$). The resultant change in the boundary layer thickness and the invariance of the inviscid flow phenomena cause a decrease or increase in the aerodynamic heating to the centerline. The procedures previously given will certainly aid in the preliminary analysis of these vehicles; however, three dimensional methods or many hours of wind tunnel investigations are necessary for their detailed design. Some glimmer of hope has been shown in the recent interest in the three dimensional characteristics approach both in ths country and abroad (c.f. Fowell (21), Moretti (22), and Probstein (23)). One of these authors at least, Dr. Moretti, has developed an operating program which is presently in the final check out phase at the Aeronautical Systems Division. This program will treat arbitrary geometries without the restriction of axial symmetry at variable angles of attack. Reference 22 gives a full account of its theoretical development and Figures 7 and 8 show samples of the output for a delta wing at ten degrees angle of attack. A combination of this computer program to obtain inviscid streamlines and the work of Dr. Vaglio-Laurin to compute heat transfer (24) will greatly improve the accuracy of methods in the classical hypersonic regime and possibly even allow correction of the two dimensional methods for more accurate design analysis. Certainly it is yielding a greater insight into the flow about arbitrary shapes at hypersonic speeds than previously afforded the engineer.

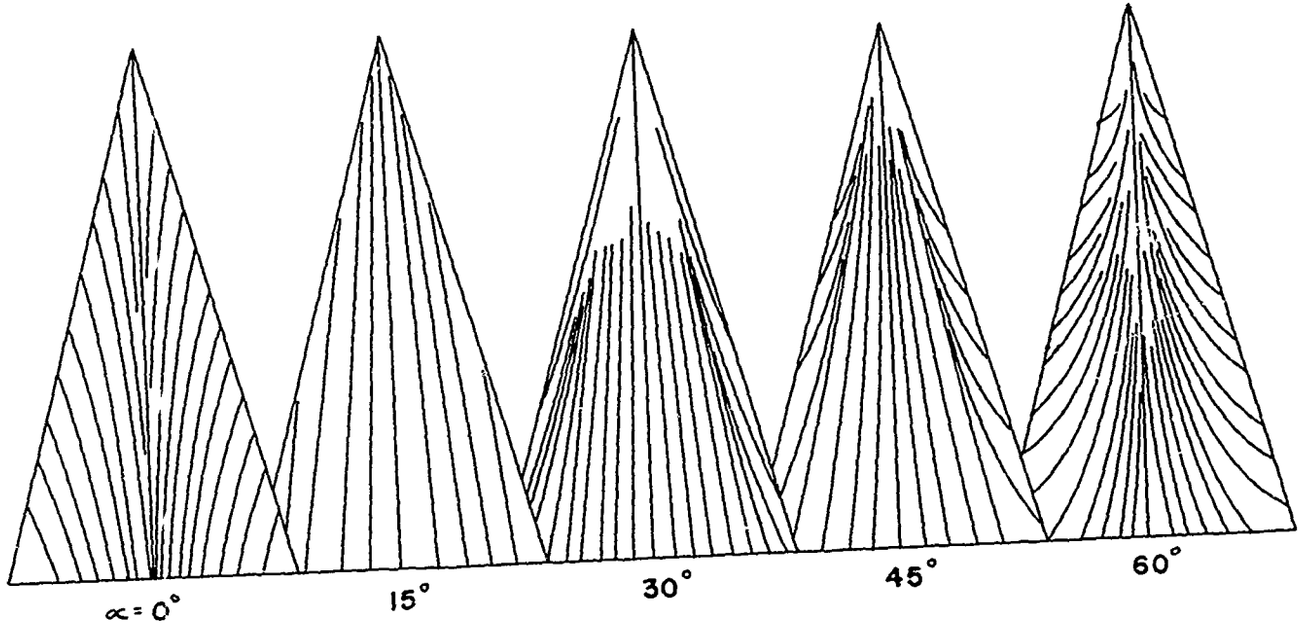


FIGURE 6 LOWER SURFACE FLOW PATTERNS ON FLAT DELTA WINGS

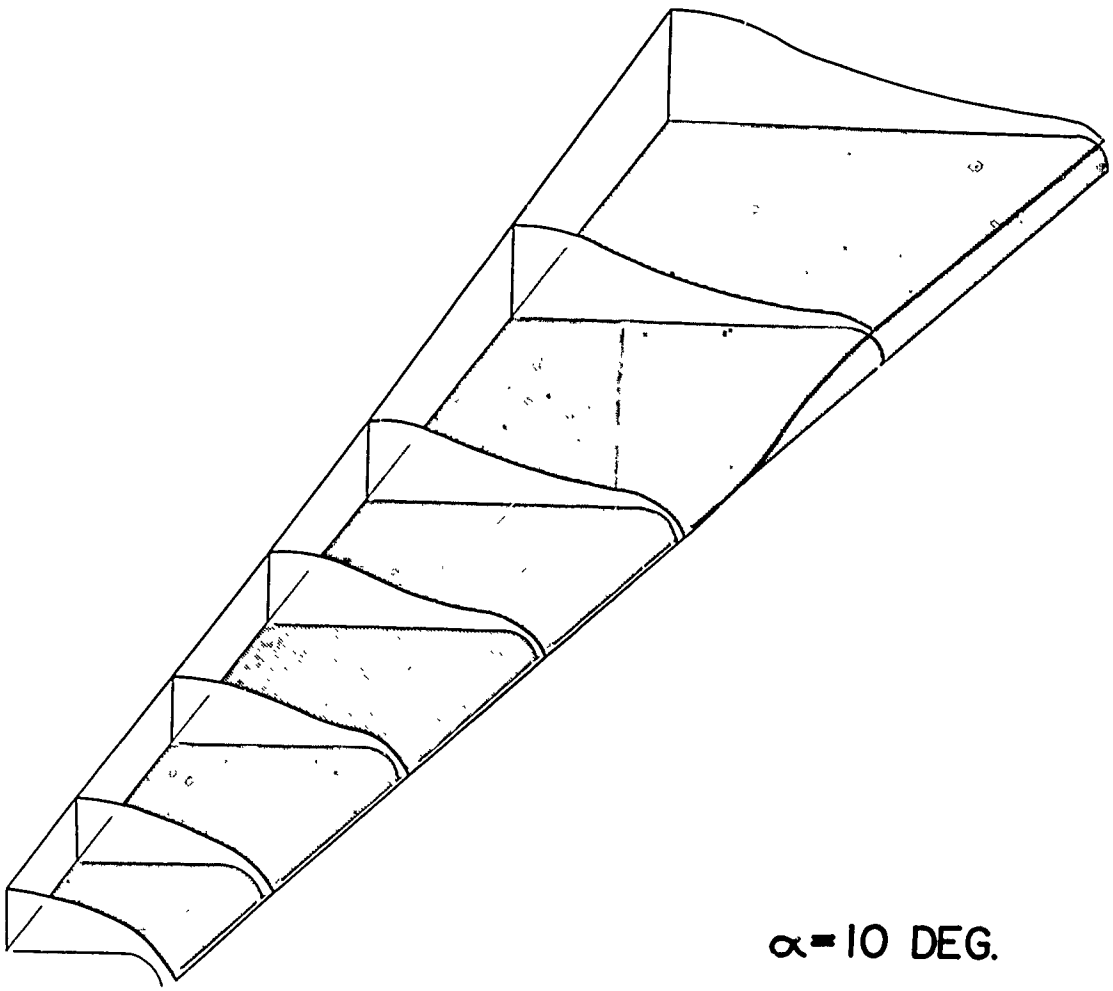


FIGURE 7

COMPUTED SHOCK WAVE SHAPE ABOUT THE COMPRESSION SURFACE OF A DELTA WING

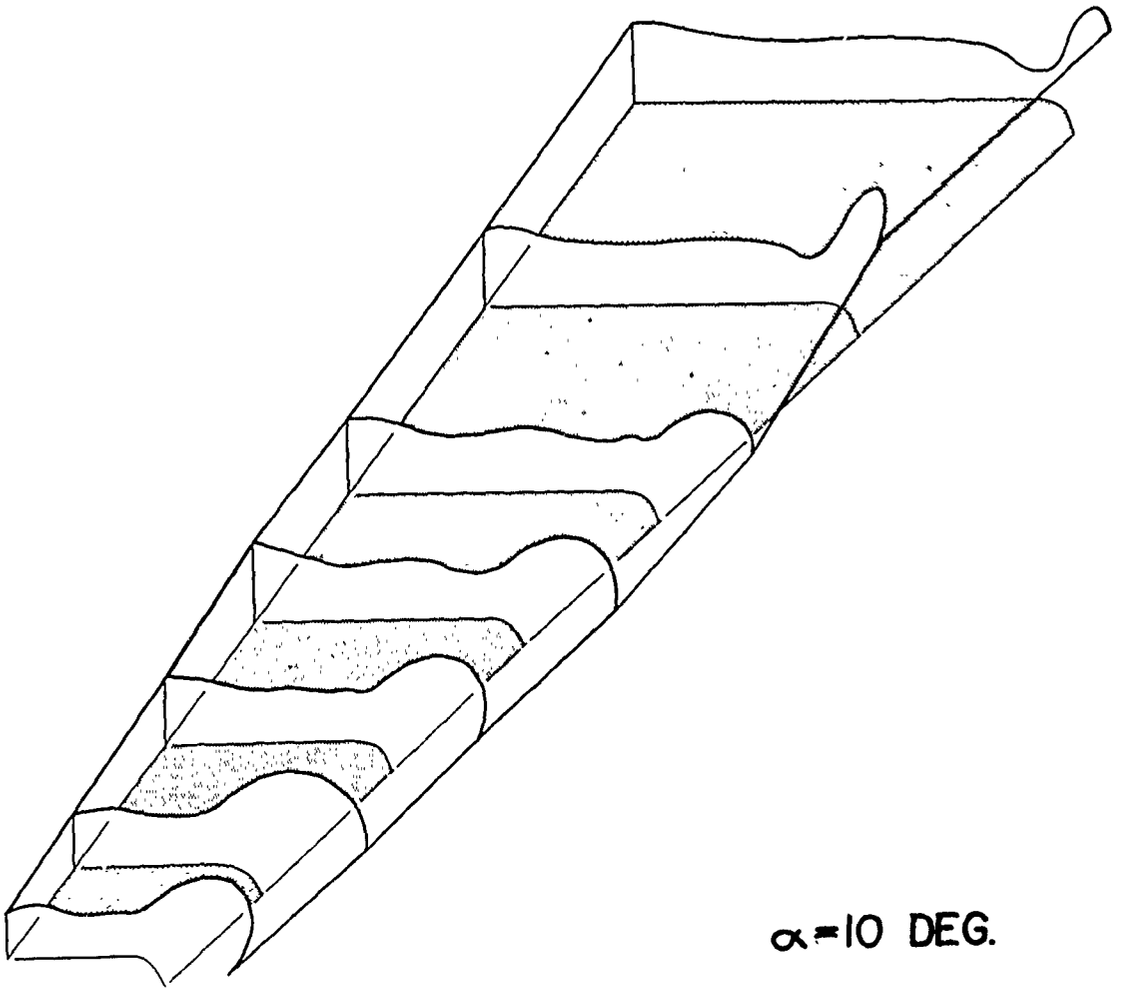


FIGURE 8

COMPUTED PRESSURE DISTRIBUTION OVER
THE COMPRESSION SURFACE OF A DELTA WING

CONCLUSIONS

As can be surmised from the previous discussions, there remain many detailed problems in the area of hypersonic aerothermodynamics which require attention. The analytical work of Moretti and Vaglio-Laurin and the experimental efforts of Bertram and Henderson, as well as others, represent the current level of sophistication in hypersonic flow description and heat transfer analysis. These techniques are, however, limited to the classical hypersonic flow regime and are restricted geometrically to simple body shapes without surface perturbations. The extension of this type of analysis to include low density effects and superorbital phenomena is seriously handicapped at present by the analytical complexity of the problem as well as the state of development of advanced hypervelocity facilities and their instrumentation.

Flow descriptions and heat transfer analysis of truly complex configurations, considering problems of shock wave impingement and shock wave-boundary layer interactions, are only beginning to be investigated. Chemical non-equilibrium effects, particularly in the superorbital regime, are known only within an order of magnitude at selected points on the surface of the vehicle and distributions of the quantities are completely unknown.

It must be concluded that while the basic technology of hypersonic aerothermodynamics has developed significantly in the past few years, the development of rational design procedures for the analysis of new vehicular concepts - and the reporting of these techniques - has not. As a result, there exists a need for considerable refinement of techniques on virtually all fronts before a truly knowledgeable preliminary design of a generalized glide re-entry vehicle becomes a reality.

APPENDIX A

DEVELOPMENT OF THE OPTIMUM SPHERE NOSE RADIUS EQUATION FOR SUPERORBITAL ENTRY OF A LIFTING VEHICLE

In the entry of lifting configurations from space, the processes of both convective heating and hot gas radiation must be considered. If both these processes are included in the total heating rate equation and the resultant equation is differentiated with respect to the body radius, an optimum sphere nose radius will be evident. This development of the equation assumes that the two modes of aerodynamic heating may be linearly combined to give the total heating. We write the total heating rate equation as the following:

$$\dot{q}_{total} = \dot{q}_{HGR} + \dot{q}_{CONV.} \qquad \text{A-1}$$

Further, we see from the form of the equations for hot gas radiation and convective heating that:

$$\dot{q}_{CONV} \propto R^{-\frac{1}{2}}$$

$$\dot{q}_{HGR} \propto R\epsilon^{-\frac{1}{2}} \quad \text{so;} \quad \dot{q}_{HGR} = n\epsilon^{-\frac{1}{2}} R^{\frac{3}{2}} \dot{q}_{CONV} \qquad \text{A-2}$$

So that we can finally write:

$$\dot{q}_{total} \propto \frac{1 + n\epsilon^{-\frac{1}{2}} R^{\frac{3}{2}}}{R^{\frac{1}{2}}} \qquad \text{A-3}$$

where "n" is defined in our equations as

$$n \triangleq 1.4865 \times 10^{-41} \left(\frac{\rho_\infty}{\rho_0}\right) V_\infty^{9.5} \qquad \text{A-4}$$

This definition is based on Lees' simplified expressions for convective heat transfer and hot gas radiation as presented in reference 12. It is evident that the equation for $\dot{q}_{total}$ (A-3) has the proper form since the limiting cases of "n" going to zero and "n" going to a very large number give us the extremes of pure convective heating and overpowering hot gas radiation heating.

If we now differentiate equation A-3 with respect to the body radius and solve for the minimum, the following equation is obtained:

$$R_{OPT} = \left[\frac{\epsilon^{\frac{1}{2}}}{2n}\right]^{\frac{2}{3}} \qquad \text{A-5}$$

Figure A-1 shows the quantity "n" plotted on an altitude - velocity plot. This calculation is based on an equilibrium model of hot gas radiation and must be modified for the inclusion of radiation non-equilibrium.

The linear addition of the convective and hot gas radiation heating is indeed a first approximation to the actual case; however, at the altitudes which we are considering the assumption is thought to be reasonably accurate. In addition to this approximation, the assumption of an optically thin gas was made and again in this region this assumption was found to be quite good for realistic radii (i.e., R_B = 20 feet or less).

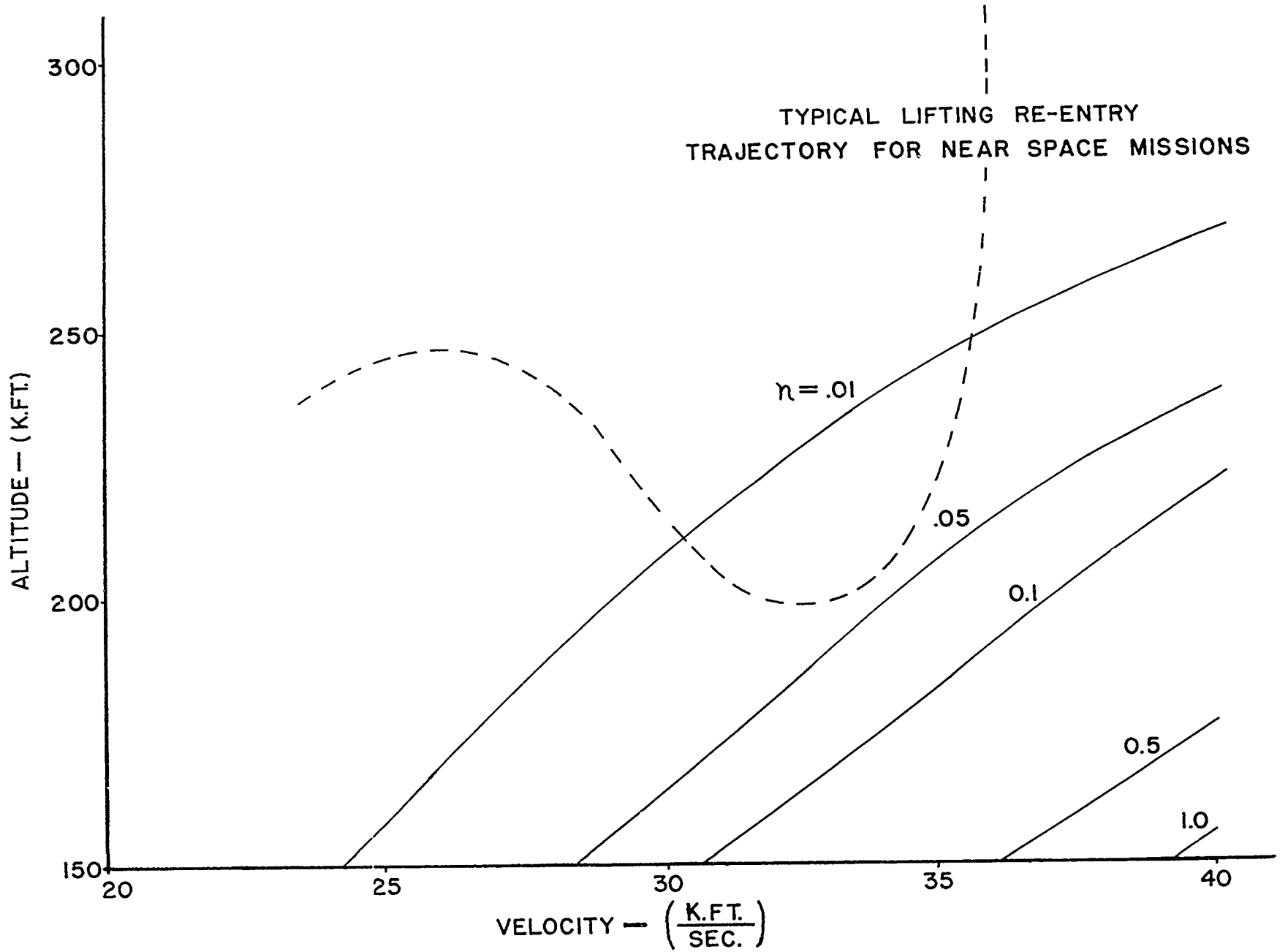


FIGURE A-I HEATING PARAMETER "η" AS A FUNCTION OF ALTITUDE AND VELOCITY

REFERENCES

1. Hankey, W. L., Neumann, R. D., and Flinn, E. H., Design Procedures For Computing Aerodynamic Heating at Hypersonic Speeds, WADC TR 59-610, June 1960, (ASTIA Document No. 239943)

2. Bertram, M. H., and Henderson, A. Jr., "Recent Hypersonic Studies of Wings and Bodies", American Rocket Society Journal, Vol. 31, No. 8, 1961, pp 1129-1139.

3. Brunner, M. J., "Analysis of Aerodynamic Heating for a Re-entrant Space Vehicle", Transactions of the ASME, Vol. 81, No. 3 Ser. C. 1959.

4. Probstein, R. F., "Shock Wave and Flow Field Development in Hypersonic Re-entry", American Rocket Society Journal, Vol. 31, No. 2, 1961.

5. Ferri, A., A Review of Some Recent Developments in Hypersonic Flow, WADC TN 58-230, Sept 1958 (ASTIA Document No. 155822)

6. Kivel, B., "Radiation From Hot Air and Stagnation Heating", Journal of the Aerospace Sciences, Vol. 28, No. 2, 1961, pp 96-102.

7. Adams, Mac C., A Look at the Heat Transfer Problem at Super - Satellite Speeds, Avco - Everett Research Laboratories AMP No. 53, December 1960 (Also released as American Rocket Society Preprint 1556-60).

8. Fay, J. A., and Riddell, F. R., "Theory of Stagnation Point Heat Transfer in Dissociated Air", Journal of the Aeronautical Sciences, Vol. 25, No. 2, 1958.

9. Hoshizaki, H., Niece, S., and Chan, K. K., Stagnation Point Heat Transfer Rates at Low Reynolds' Numbers, Institute of the Aeronautical Sciences Paper 60-68, 1960.

10. Probstein, R. F., and Nelson, H. K., Viscous Aerodynamic Characteristics in Hypersonic Rarified Gas Flow, AVCO Research Report 48, March 1959.

11. Van Dyke, M., Effect of External Vorticity on Stagnation Point Viscous Flows, American Rocket Society Preprint No. 1966-61, 1961.

12. Lees, L., "Recovery Dynamics - Heat Transfer at Hypersonic Speeds in a Planetary Atmosphere", Space Technology, ed. by H. Siefert, John Wiley and Sons, Inc., New York, 1960.

13. Wisniewski, R. J., Methods of Predicting Laminar Heating Rates on Hypersonic Vehicles, NASA TN D-201, Dec. 1959.

14. Eckert, E. R. G., Survey of Heat Transfer at High Speeds, WADC TR 54-70, April 1954.

15. Cheng, H. H., Hall, J. G., Golian, T. C., and Hertzberg, A., Boundary Layer Displacement and Leading - Edge Bluntness Effects in High Temperature Hypersonic Flow, IAS Paper 60-38, 1960. (also Journal of the Aerospace Sciences, Vol. 28, No. 5, 1961, pp. 353-381.)

16. Kaplan, M., Low Density Effects on Heat Transfer in Hypersonic Flight, General Electric TIS 61 AS 45, March 1961.

17. Nagamatsu, H. T., Sheer, R. E., and Schmid, J. R., "High Temperature Rarified Hypersonic Flow Over a Flat Plate", American Rocket Society Journal, Vol. 31. No. 7, July 1961, pp. 902-910.

18. Wallace, A. R., and Swain, W. N., Pressure Distribution Tests on Blunted Plate and Cone at Mach Numbers 20 to 23, AEDC TN 60-236, Jan. 1961 (Confidential).

19. Cole, J. D., and Brainerd, J. J., Variational Procedure for Minimizing Heating Effects During the Re-entry of a Lifting Vehicle, Vol. II - Heat Transfer to Slender Hypersonic Delta Wings Near 90 Incidence, WADD TR 60-369 - Vol. II, 1960.

20. Anon - Aerodynamics Department, Laminar Heat Transfer to the Most Windward Ray of A 15 Degree Spherically Blunted Cone at Angle of Attack, GASL TR No. 157, April 1960 (ASTIA Document No. 256177).

21. Fowell, L. R., Flow Field Analysis for Lifting Re-entry Configurations by the Method of Characteristics, Institute of the Aeronautical Sciences Paper 61, 208-1902, 1961.

22. Moretti, G., "Three-Dimensional Flow Field Analysis in Re-entry Problems", Transactions of the Sixth Symposium on Ballistic Missile and Aerospace Technology, 1961.

23. Probstein, R. F., "Recent Advances in Inviscid Hypersonic Aerodynamics", Aerospace Engineering, Vol. 20, No. 7, 1961, pp. 10-12 and ff.

24. Vaglio-Laurin, R., "Laminar Heat Transfer on Three-Dimensional Blunt Nosed Bodies in Hypersonic Flow", American Rocket Society Journal, Vol. 29, No. 2, Feb. 1959, pp. 123-129.

TURBULENT BOUNDARY LAYERS ON HIGHLY COOLED SURFACES AT HIGH MACH NUMBERS

Andrew F. Burke

Cornell Aeronautical Laboratory, Inc.

ABSTRACT

The structure and integrated properties of turbulent boundary layers on highly cooled surfaces at Mach numbers up to 16 are deduced from pitot pressure surveys taken at the exit of a conical nozzle in the Cornell Aeronautical Laboratory 48" Hypersonic Shock Tunnel. It is shown that predictions of boundary layer displacement thickness determined by using the equivalent flat-plate method and the reference temperature concept for relating compressible to incompressible skin-friction coefficients are in good agreement with the experimental data. The existence of a thick laminar sublayer at high Mach numbers and low Reynolds numbers is confirmed experimentally.

TURBULENT BOUNDARY LAYERS ON HIGHLY COOLED SURFACES AT HIGH MACH NUMBERS

INTRODUCTION

The computation of compressible turbulent boundary-layer development[1-3] and the resultant heat transfer and skin friction is not on nearly as sound a theoretical foundation as the corresponding calculations for the case of a compressible laminar boundary layer.[4] The primary reason for this is the difficulty of determining and expressing in analytical form those terms in the turbulent boundary-layer equations related to momentum and energy transport. As a result, most, if not all, of the analyses of turbulent flow are semi-empirical in nature. In many cases, the data used as a partial basis for the analysis and as experimental confirmation of the validity of the resultant method were obtained at flow conditions far from those at which application is desired. This is true particularly when hypersonic flow conditions are being considered. Thus, the need for experimental data pertaining to turbulent boundary layers at hypersonic flow conditions is clear.

The one condition that characterizes the boundary layer on any body in hypersonic flight is the large heat transfer across the layer into the body (i.e., a small wall-to-total enthalpy ratio). However, the Mach number at the edge of the boundary layer can be as low as subsonic or as high as the flight value, and in the case of a slightly blunted, slender body, varies along the body itself from subsonic in the nose region to hypersonic far back on the slender afterbody. Hence, two extreme cases of boundary layer flow resulting from hypersonic flight are evident. First, there is the case where bluntness dominates (the local entropy is nearly that behind the normal shock at the nose) and the Mach number at the edge of the boundary layer is subsonic or moderately supersonic. This case is considered in Refs. 5 and 6. The second case is that of the flow over a sharp, slender body or far back on a slightly blunted, slender body where the Mach number external to the boundary layer is hypersonic (the entropy is nearly that behind the oblique shock generated by the slender body). The latter case, which is considered in this paper, is related to the flow in a hypersonic shock tunnel nozzle. In both the slightly blunted slender body and nozzle flows, boundary layer transition can occur near a sonic region and the flow expands downstream at increasing Mach number and decreasing Reynolds number. The nozzle is a convenient place in which to conduct boundary layer studies because of the high effective flow-stagnation pressure and long effective boundary-layer growth lengths there. This similarity between

the flows permits one to make general conclusions about the turbulent flow over slender bodies from experimental data taken in nozzles.

A careful experimental investigation of turbulent boundary layers on moderately cooled ($H_w/H_T \approx .5$) surfaces at external Mach numbers up to 7.7 is reported in Ref. 7. The experimental programs* presented here extend the range of available data to more highly cooled wall conditions ($H_w/H_T \approx .1$) and higher Mach numbers.

LIST OF SYMBOLS

a, b, λ	Constants
A	Nozzle area
A_m	Constant in the general skin friction law (Eq. 8)
C_o	Constant in the form factor equation (Eq. 6)
C_f	Skin friction coefficient
C_p	Specific heat at constant pressure
d_*	Nozzle throat diameter
h	Static enthalpy
H	Total enthalpy
H_i	Incompressible boundary layer form factor
K	Constant relating the reference and total temperatures
ℓ ($=r_*/\theta_c$)	Reference length for the nozzle
ℓ_t	Distance from the end of shock tube to the nozzle throat exit
M	Mach number
m	Reynolds number exponent in the general skin friction law (Eq. 8)
n	Exponent in the outer turbulent flow velocity profile expression $[u/u_e = (y/\delta)^{1/n}]$

*Part of the Wave Superheater Tunnel project supported by the Advanced Research Projects Agency under Contract AF 40(600)-804

p	Pressure
p_o'	Pitot pressure
$\dot{q}$	Heat transfer rate
r	Cylindrical radius
$Re_L (=\rho uL/\mu)$	Reynolds number based on length L
T	Temperature
u	Velocity
x	Axial distance
y	Distance normal to the wall
β	Pressure gradient parameter
γ	Ratio of specific heats
θ	Boundary layer momentum thickness (Eq. 21b)
θ_c	Conical nozzle half-angle
μ	Viscosity
ω	Exponent in the viscosity law
δ	Boundary layer thickness
δ_*	Boundary layer displacement thickness (Eq. 21a)
ρ	Density
$\Lambda (= 158/Re_\delta)$	Variable in equation determining the laminar sublayer
τ	Skin friction

Subscripts

b. l.	within the boundary layer
e	at the edge of the boundary layer
L	at the edge of the laminar sublayer
o, T	stagnation or supply conditions
r	evaluated at the reference temperature
w	at the wall
*	nozzle throat or sonic conditions

SECTION I: EXPERIMENTAL STUDIES

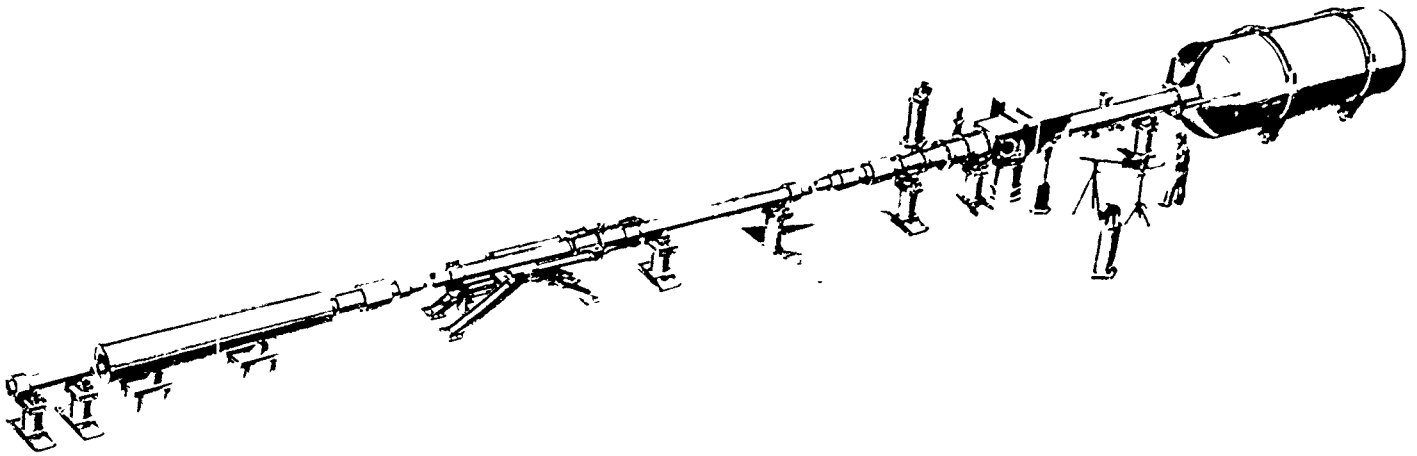
Two experimental studies[8] which yielded data pertaining to turbulent boundary-layer characteristics on highly cooled surfaces have recently been conducted in the CAL 48" Hypersonic Shock Tunnel. In the first of these investigations, pitot pressure surveys were made of the boundary layer at the exit of a 10.5° half-angle conical nozzle at Mach numbers between 8 and 16 and Reynolds numbers per foot of 3×10^4 to 1.9×10^6. Secondly, heat transfer measurements were made on the inside surface of a co'lector-expansion nozzle model. Details of these programs, the shock tunnel, and associated instrumentation are discussed in the following sections.

A. The 48" Hypersonic Shock Tunnel and Associated Instrumentation

The basic components of the shock tunnel are shown in Fig. 1. Helium and helium-air mixtures are used as the driver gas at pressures to 6000 psi and at temperatures varying from room temperature to 1400°R. Corresponding maximum tunnel reservoir conditions using air as the driven gas are 4000 psi and 5600°R for "tailored interface" operation.[9] A test time (defined as the time over which the reservoir pressure is constant - Fig. 2) of approximately 6 milliseconds is thus achieved. Three axisymmetric nozzles are used to expand the shock-compressed gas to the test section; namely, (1) a contoured nozzle having a 24" exit diameter and a design Mach number of 8, (2) a conical (10.5° half angle) nozzle having a 24" exit diameter and a Mach number range of 6 to 18, (3) a contoured nozzle having a 48" exit diameter and a design Mach number of 16.

Pressure transducers[10] have been developed at CAL which meet the particular requirements of shock tunnel testing. The piezo-electric elements are extremely sensitive, allowing pressures as low as .002 psi to be measured. Compensation and isolation techniques have been employed to minimize the sensitivity of the transducers to acceleration and thermal effects. The pitot pressure rake shown in Fig. 3 was used to make the boundary layer surveys. The outputs of the transducers are recorded on film using cameras in conjunction with oscilloscopes.

Thin-film resistance thermometers[11] were used for heat transfer measurements. They are strips of platinum about 5 mm. x .5 mm. and .1 micron thick which have been deposited on and fused to pyrex glass buttons. The resistance of the gage is a linear function of temperature. Since the heat capacity of the gage itself is negligible, the film temperature is the instantaneous surface temperature of the glass and may be related to the heat transfer rate. The thin-film



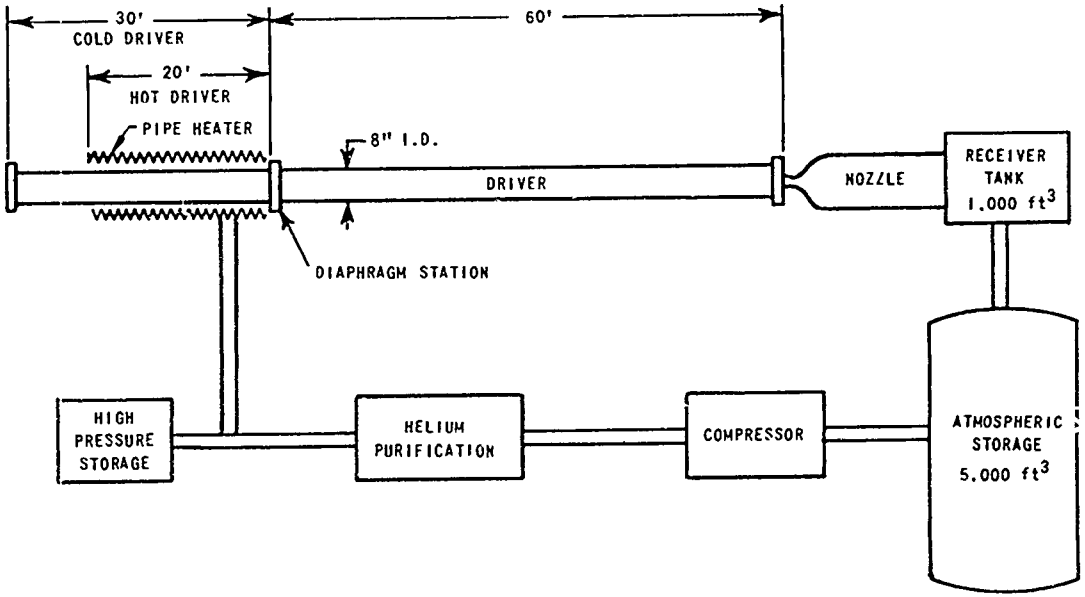
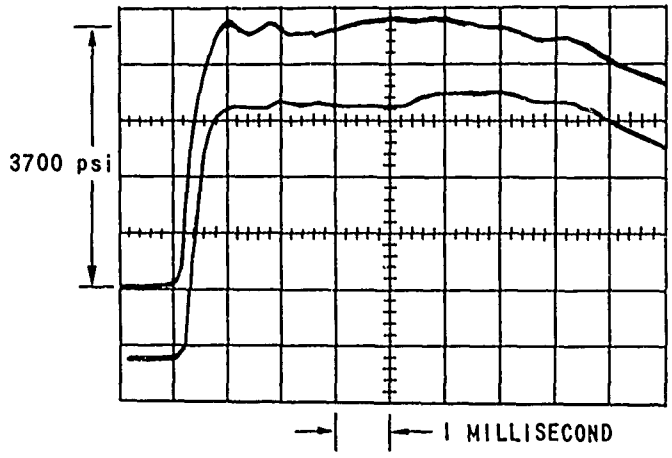
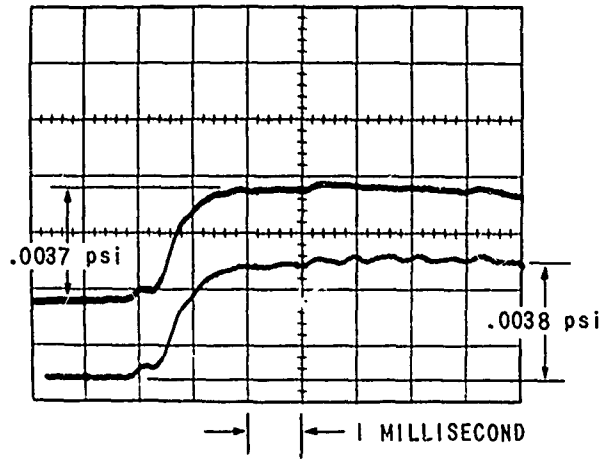


Figure 1 BASIC COMPONENTS OF THE CORNELL AERONAUTICAL LABORATORY 48" HYPERSONIC SHOCK TUNNEL



TYPICAL SHOCK TUNNEL SUPPLY PRESSURE TRACE



TYPICAL STATIC PRESSURE TRACE USING CAL PIEZO-ELETRIC PRESSURE TRANDUCERS

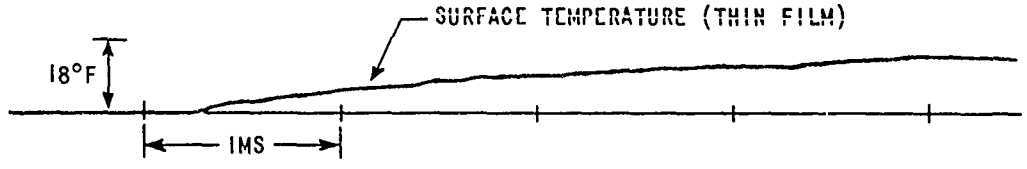
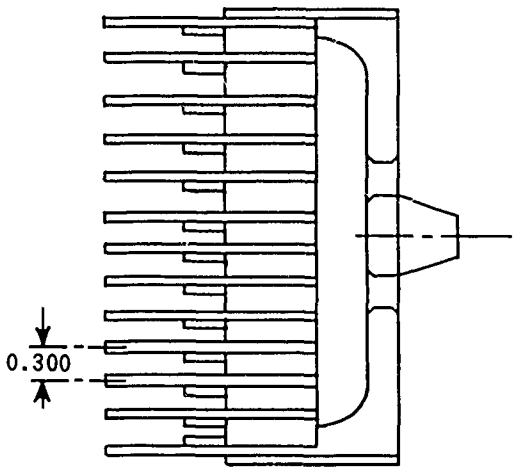
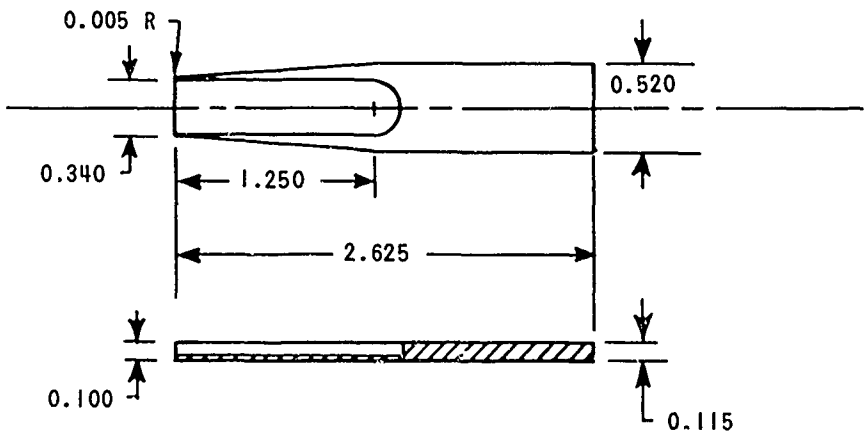


Figure 2 TEMPERATURE TRACE USING THIN FILM HEAT TRANSFER GAGE



RAKE ASSEMBLY



INDIVIDUAL PROBE DETAILS

Figure 3 BOUNDARY LAYER SURVEY RAKE

gages have been used to measure heating rates as low as .3 Btu/ft^2 sec. and as high as 2000 Btu/ft^2 sec. When, as in one of the present programs, the glass temperature changes significantly during the run, the change of the thermal properties of the glass must be taken into account in the data reduction.

For both the determination of pressure and heat transfer, the maximum instrumentation and recording errors are believed to be about 10%.

B. Nozzle Boundary Layer Studies

Pitot pressure surveys were taken through the boundary layer at the exit (the rake was positioned within .5" of the exit) of the 10.5° half-angle cone nozzle for a series of Mach numbers (8, 12, 14, 16) at several nominally constant Reynolds numbers. For most runs, the total temperature was about 4300°R which produces a wall-to-total-stagnation enthalpy ratio of .12. Several runs were made at other enthalpy levels. Table I lists the pertinent test conditions for each run.

Typical pitot pressure profiles ($p_{o'_{b.l.}}/p_o$ vs. y) are given in Fig. 4. The corresponding Mach number profile obtained from $p_{o'_{b.l.}}/p_e$ is shown in Fig. 5. The usual assumption of negligible static-pressure change across the boundary layer was made. The effect of free-stream Mach number and Reynolds number on the profiles is clear from the figures. The local probe Reynolds number based on its minimum inlet dimension becomes quite small (the order of 1) near the wall for low pressure runs. The pitot pressure data taken at the very low probe Reynolds numbers were consistent with those taken at the higher values and the integrated boundary-layer characteristics also remained self-consistent. The results of Ref. 12 indicate that large errors occur for Re_d less than about 15; but little, if any, evidence of this was apparent in the data here.

The assertion that the boundary layers surveyed were turbulent and that the effective length for the layers is the distance from the nozzle throat to its exit implies that transition from laminar to turbulent flow occurred near the throat. It was not possible to confirm this directly from measurements, but its reasonableness can be seen from throat Reynolds number considerations. The throat Reynolds numbers based on throat diameter and boundary layer growth length from the end of the shock tube to the exit of the throat are listed in Table I. In fully developed pipe flow, transition[13] usually occurs when the flow Reynolds number based on pipe diameter is greater than 10^4, even for smooth surfaces and low free-stream turbulence. Using

TABLE I

BOUNDARY LAYER SURVEY TEST CONDITIONS

RUN	MACH NO.	Re/ft x 0^{-5}	$Re_{*_{d_*}}$ x 10^{-5}	$Re_{*\ell_t}$ x 10^{-5}	Re_δ x 10^{-5}	T_o °R	T_w °R	$T\infty$ °R	P_o psi	THROAT DIAM. INCHES	NOZZLE LENGTH
1	13.05	.54	3.3	16.8	.173	3530	530	112	309	.40	10.5° CONE
2	13.45	51	4.87	29.3	.183	5120	↓	170	854	.30	65" LONG
3	10.95	61	3.78	15.0	.172	3350	↓	148	215	.625	↓
4	8.0	1 1	6.14	19.0	.242	3350	↓	280	160	1.363	↓
5	8.2	5.9	3.45	107.0	↓	↓	↓	↓	945	1.363	↓
6	8.25	13 6	8.03	249.0	1.82	3530	↓	275	2235	1.363	↓
7	16.3	2.2	1.55	127.0	.788	4500	↓	95	3660	.20	↓
8	15.8	.29	2.0	16.5	.131	4330	↓	99	461	.20	↓
9	14.0	2.15	16.2	97.2	.698	4480	↓	130	2530	.30	↓
10	13.75	.42	2.98	17.9	.164	4390	↓	130	463	.30	↓
11	12.65	2.18	1.67	8.55	.655	4530	↓	163	1980	.40	↓
12	10.65	2.03	13.9	55.0	.575	4300	↓	220	1015	.625	↓
13	7.8	.78	4.38	13.6	.165	4350	↓	390	148	1.363	↓
14	8.95	1.25	8.68	29.0	.302	4350	↓	300	415	.963	↓
15	7.75	3.75	14.5	45.0	1.11	2820	↓	240	316	1.363	CONTOURED 120" LONG
16	7.75	18.8	82.7	256.0	4.22	3080	↓	260	1975	1.363	↓

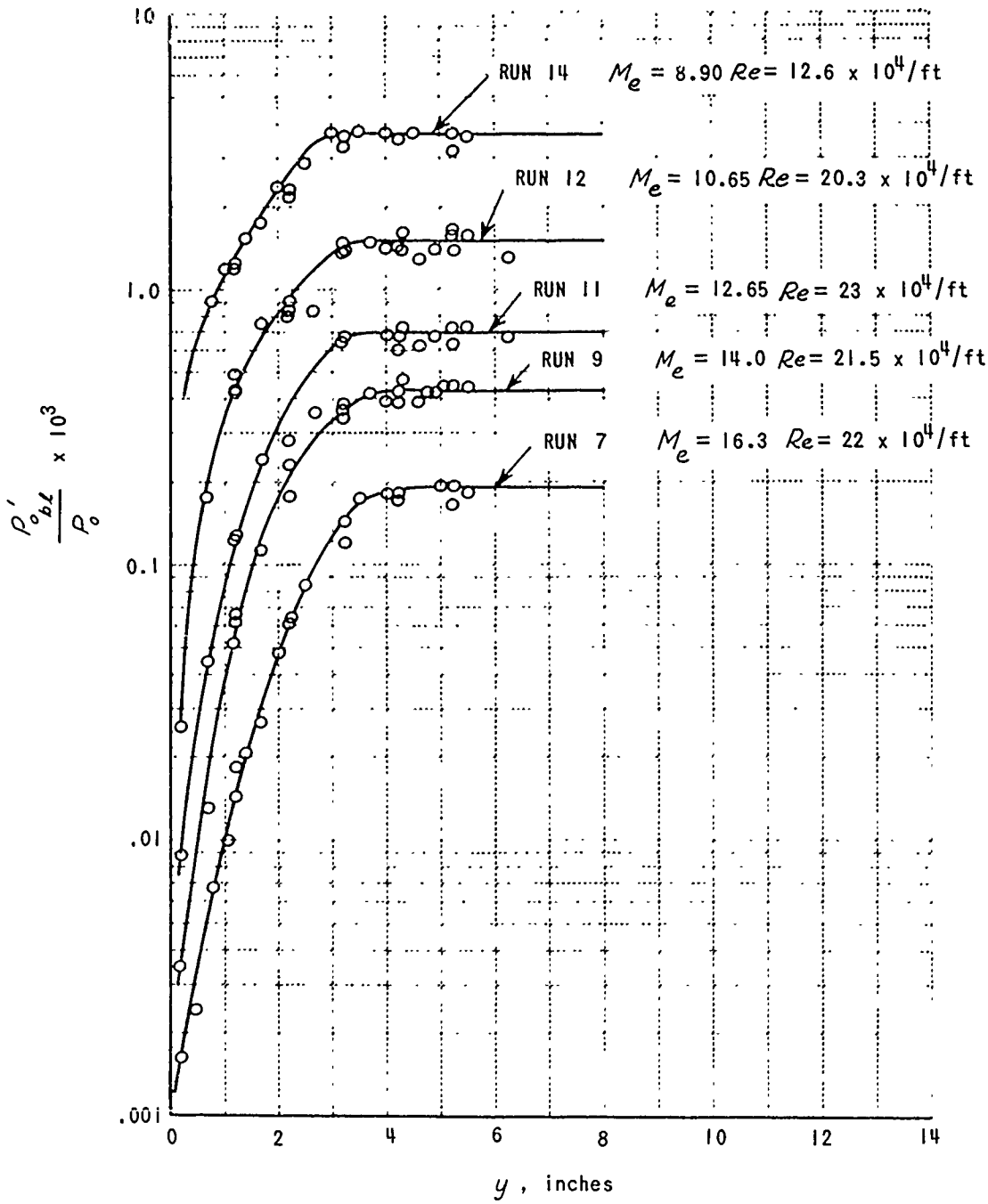


Figure 4a EFFECT OF MACH NUMBER ON THE BOUNDARY LAYER PROFILE AT CONSTANT REYNOLD'S NUMBER

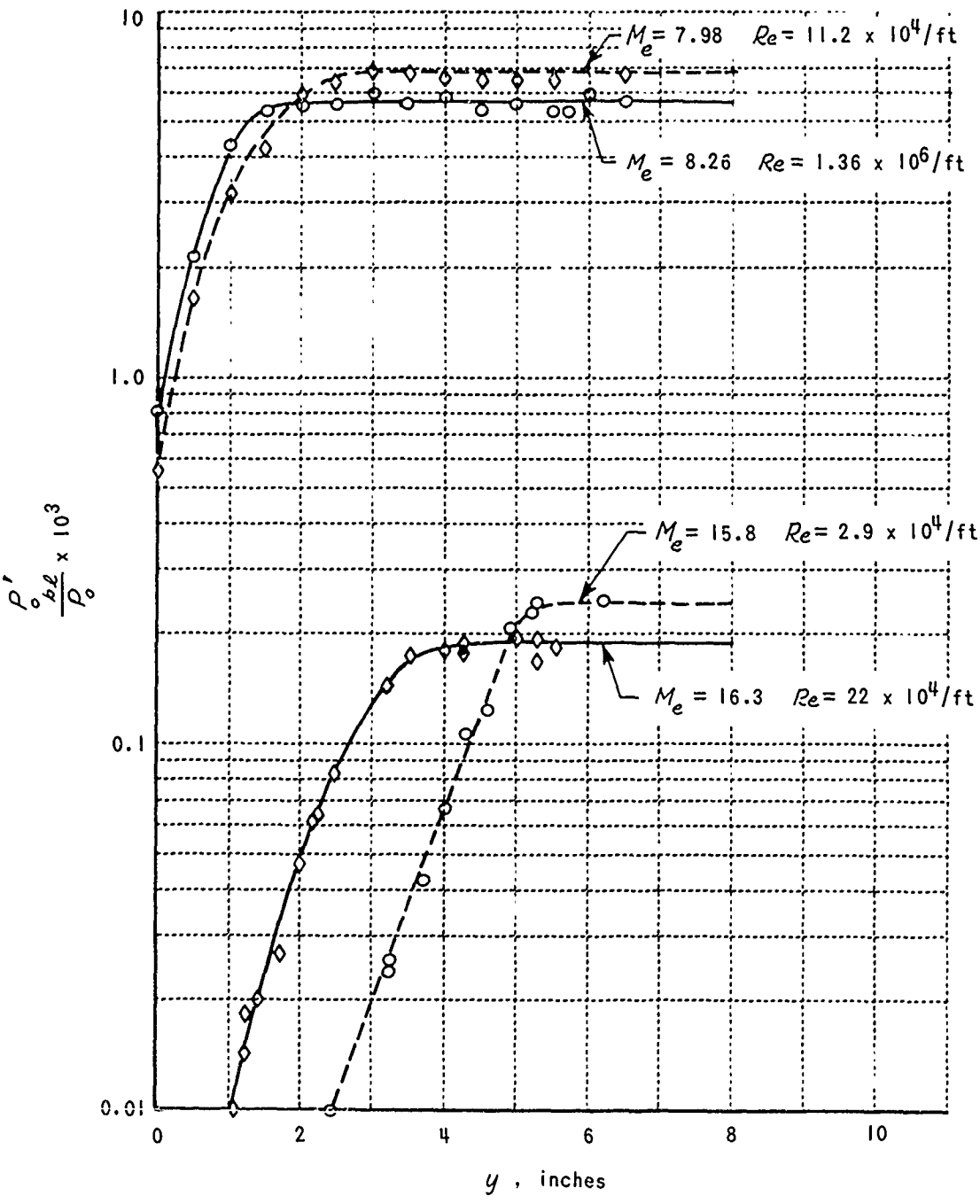


Figure 4b EFFECT OF REYNOLDS NUMBER ON THE BOUNDARY LAYER PROFILE AT TWO MACH NUMBERS

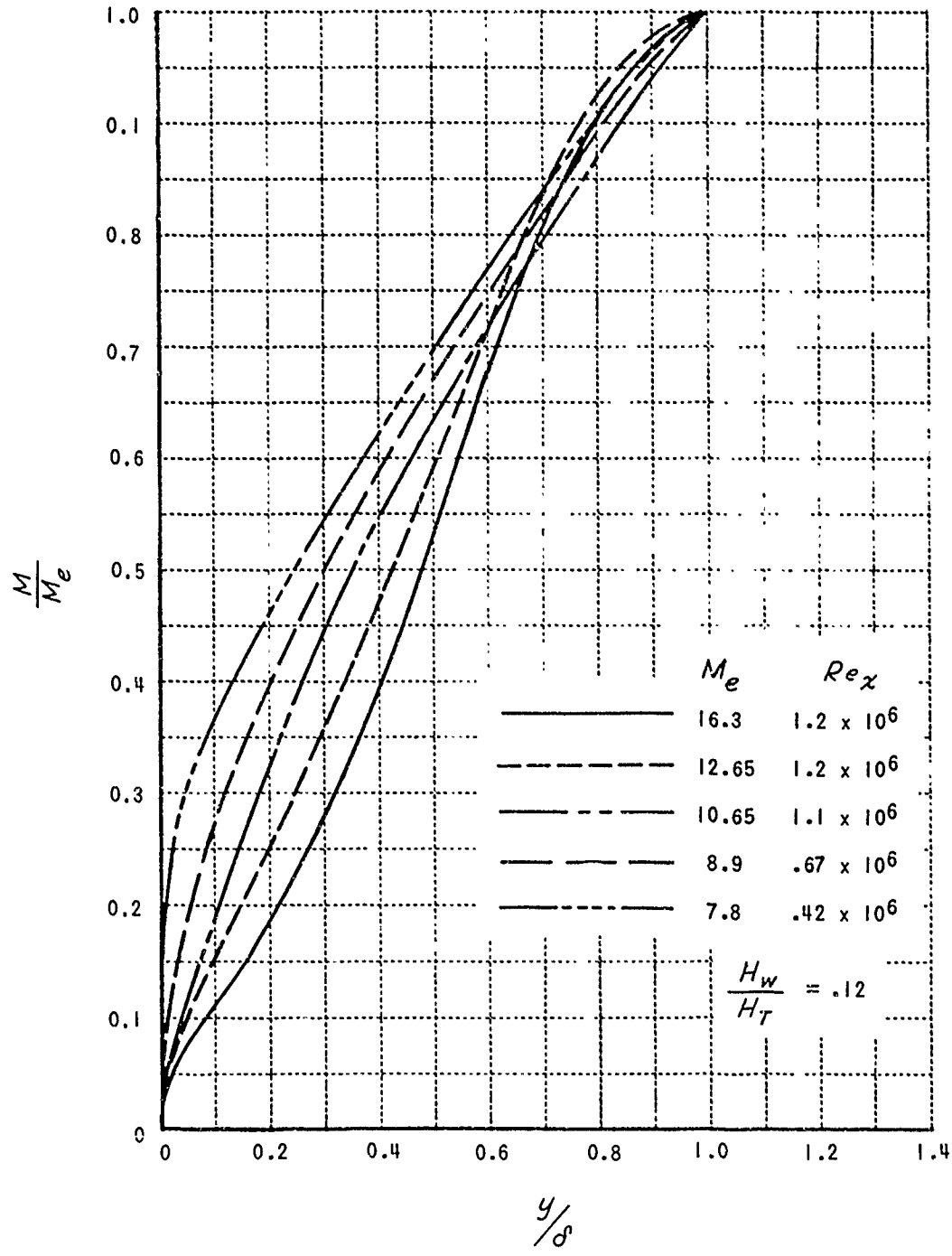


Figure 5 BOUNDARY LAYER MACH NUMBER DISTRIBUTIONS

this criterion, transition would occur upstream of the throat for all the runs. Considering a Reynolds number based on the boundary layer growth length, transition[13] usually occurs in the range 10^5--10^6. From this point of view, the nozzle boundary layer also became fully turbulent near the throat.

C. Collector-Expansion Nozzle Studies

The shock tunnel was used to supply the high temperature and high pressure gas for the test of a collector-expansion nozzle. The model was located downstream of the sonic throat in the tunnel as shown in Fig. 6. The inlet Mach number to the model was maintained at 2.2 while the inlet Reynolds number per foot was varied between 3.5×10^6 and 28×10^6. The total enthalpy of the gas was 44×10^6 ft-lb/slug, corresponding to a stagnation temperature of 5400°R. The interior wall of the nozzle model was instrumented with thin-film heat-transfer gages at various axial locations (Fig. 7).

Summary curves of the data are given in Fig. 8, plotted as a function of distance along the nozzle. The data are presented in terms of $\dot{q}/p_o^{.8}$ because classical turbulent flow, flat-plate theory predicts that this parameter is independent of inlet flow stagnation pressure in the range of total enthalpy of this program. Hence, when $\dot{q}/p_o^{.8}$ is used, the data for different supply pressures, p_o, should correlate on a single curve.

SECTION II: ANALYTICAL BASIS FOR THE DATA CORRELATION

The boundary-layer development on the surface of wind tunnel nozzles has been analyzed in detail by several authors.[14, 15] In this section, a simplified method of approach to the problem applicable to hypersonic flow is given. It is assumed that over much of the nozzle length

$$\text{(a)}\ \frac{\gamma-1}{2} M_e^2 \gg 1$$

$$\text{(b)}\ A/A_* \gg 1 \qquad (1)$$

$$\text{(c)}\ T_w \sim T_e \ll T_o$$

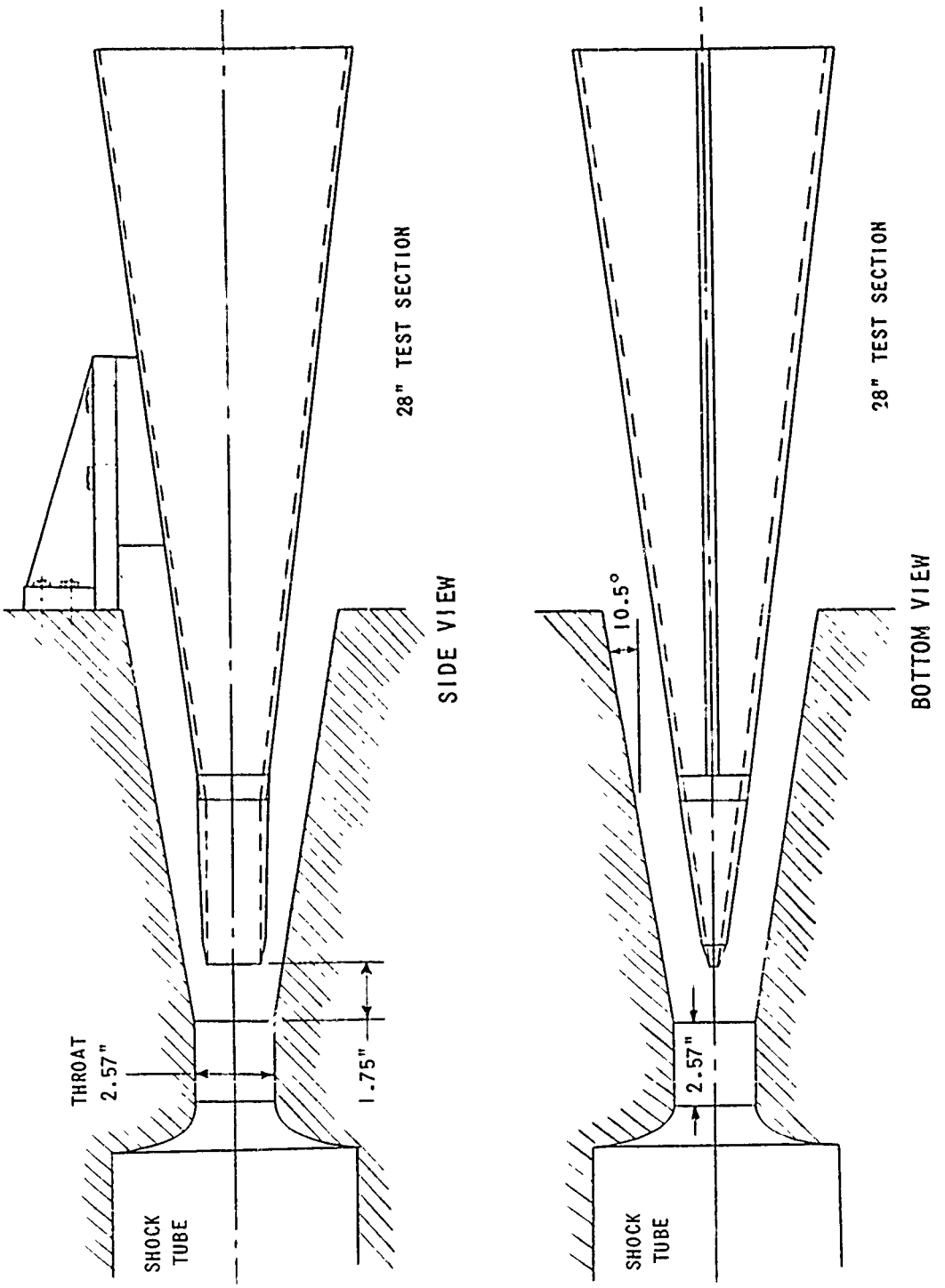


Figure 6 NOZZLE-MODEL INSTALLATION

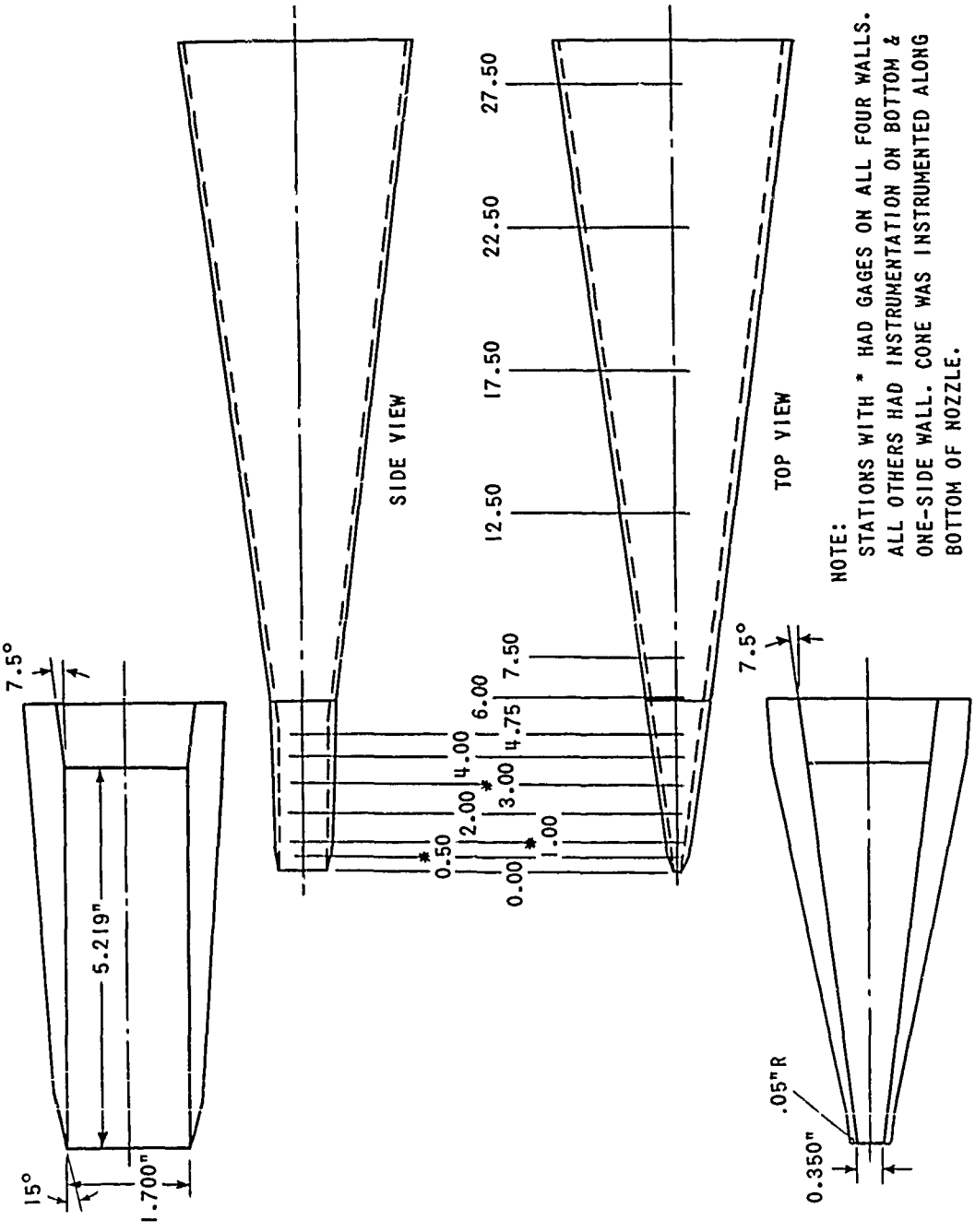


Figure 7 COLLECTOR-EXPANSION NOZZLE MODEL

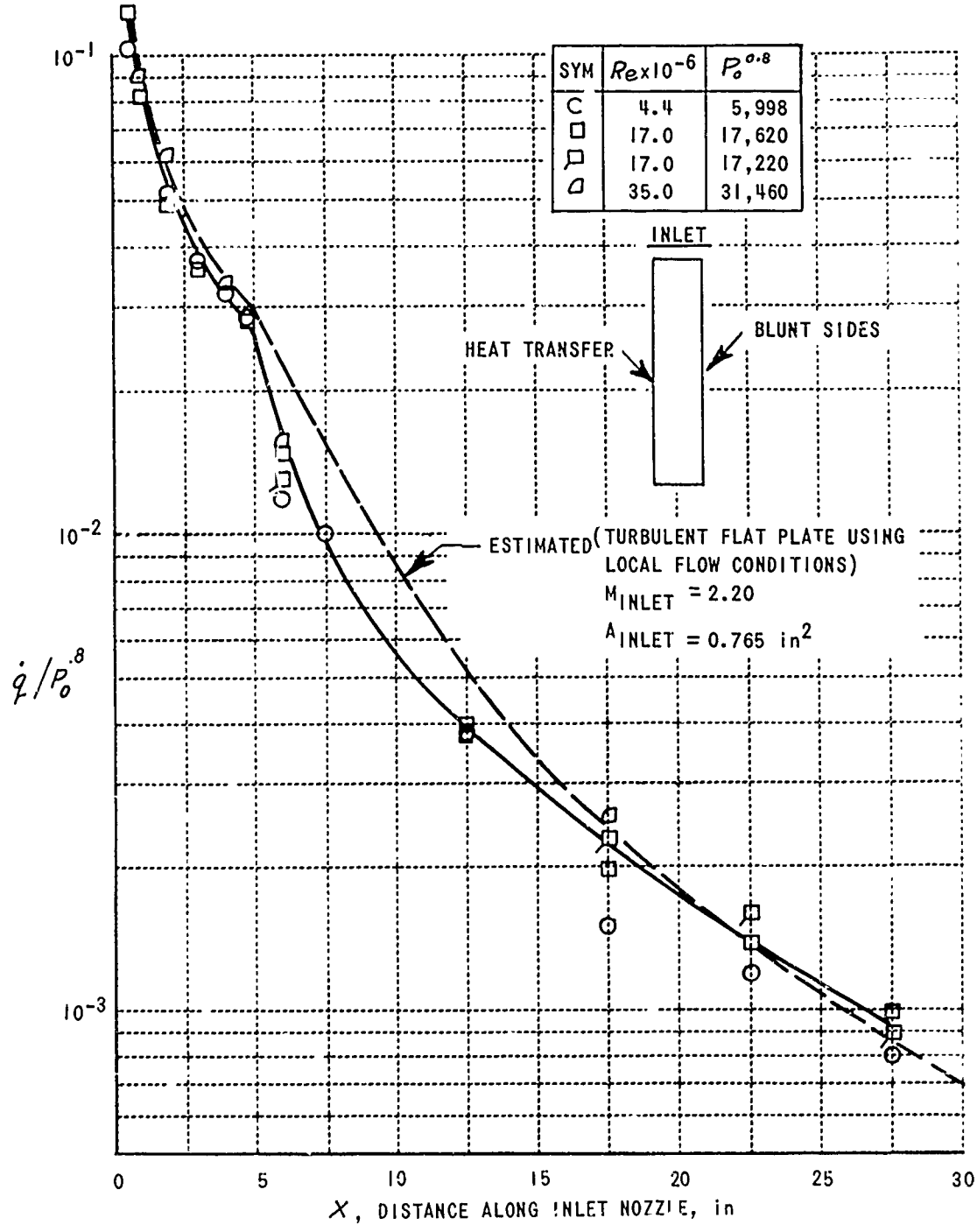


Figure 8 COLLECTOR - EXPANSION NOZZLE HEAT TRANSFER RATES

In general, the integrated boundary-layer momentum equation[5] can be written as

$$\frac{d\theta}{dx} + \theta\left[\left(2+\frac{\delta_1}{\theta}\right)\frac{1}{u_e}\frac{du_e}{dx} + \frac{1}{\rho_e}\frac{d\rho_e}{dx} + \frac{1}{r}\frac{dr}{dx}\right] = \frac{C_f}{2} \tag{2}$$

The factor multiplying θ in Eq. (2) can be simplified using assumptions (1).

The one-dimensional continuity equation states that

$$\rho_e A u_e = \dot{m} = \text{constant}$$

Using (1a-b)

$$r = \theta_c x, \quad A = \pi r^2, \quad u_e = \text{const.}$$

hence

$$\rho_e x^2 = \frac{\dot{m}}{\pi \theta_c^2 u_e}$$

Then

$$\frac{1}{\rho_e}\frac{d\rho_e}{dx} + \frac{1}{r}\frac{dr}{dx} = -\frac{1}{x}$$

Assuming ideal gas relations are valid and making an expansion in terms of $\left(\frac{\gamma-1}{2}M_e^2\right)^{-1}$, which is a small quantity, it can be shown that

$$\frac{1}{u_e}\frac{du_e}{dx} = \frac{2}{M_e}\frac{dM_e}{dx}\Big/(\gamma-1)M_e^2 \tag{3}$$

Next, a relation between M_e and x is needed. The nozzle area ratio at a given x station is given by

$$\frac{A_*}{A} = \frac{r_*^2/\theta_c^2}{x^2}$$

where r_* is the nozzle throat radius. Define a reference length ℓ as $\ell = r_*/\theta_c$. Thus

$$\frac{A_*}{A} = \bar{x}^{-2}, \quad \bar{x} = \frac{x}{\ell} \tag{4}$$

Again, using ideal gas relations between area ratio and Mach number,

$$M = \left(\frac{\gamma+1}{\gamma-1}\right)^{\frac{\gamma+1}{4}} \bar{x}^{(\gamma-1)} \tag{5}$$

A simple relationship between δ_* and θ is derived in Ref. 14, assuming a Stewartson type coordinate transformation is valid for turbulent flow.

$$\frac{\delta_*}{\theta} = \frac{T_o}{T_e}\left(1 + H_i \frac{T_w}{T_o}\right) = C_o M_e^2 \tag{6}$$

where $C_o = \frac{\gamma - 1}{2}\left(1 + H_i\, T_w/T_o\right)$

H_i, which is the boundary-layer form factor in the transformed "incompressible" plane, varies over a small range with 1.5 a reasonable mean value. Now using Eqs. (3--6) in Eq. (2) one obtains

$$\frac{d\theta}{dx} + (2C_o - 1)\frac{\theta}{x} = \frac{c_f}{2} \tag{7}$$

where all length variables (θ, x) are non-dimensionalized using ℓ.

A skin-friction law of the form

$$\frac{\tau}{\rho_r u_e^2} = A_m \left(\frac{\rho_r u_e x}{\mu_r}\right)^{-1/m} \tag{8}$$

is assumed, where "r" refers to the reference temperature (T_r) defined[5] as

$$T_r = .22\,(T_o - T_e) + .5\,(T_w + T_e)$$

For the cool wall case, T_r can be taken as

$$T_r = K\,T_o\,, \quad K = 1/4$$

In terms of free-stream quantities, Eq. (8) becomes

$$\frac{c_f}{2} = A_m \left(\frac{\rho_r}{\rho_e}\right)^{1-1/m} \left(\frac{\mu_r}{\mu_e}\right)^{1/m} \left(\frac{\rho_e u_e x}{\mu_e}\right)^{-1/m}$$

For classical laminar and turbulent flow the constants (Am, m) are

	m	Am
Laminar	2	.334
Turbulent	5	.029

Using the simple form of Reynolds analogy, the corresponding heat transfer is given by

$$\frac{\dot{q}}{\rho_e u_e (H_T - H_w)} = \frac{C_f}{2} \tag{9}$$

The solution to Eq. (7) can be determined in closed form for two cases of interest. The first case corresponds to a local similarity-type solution in which changes in flow properties along the nozzle are taken into account. The second case is simply the equivalent flat-plate approach, whose only justification is that it has in many situations in the past yielded results in reasonable agreement with experiment.

Consider first the local similarity-type solution. In this case, the skin-friction term becomes

$$C_f \sim K^{1-\frac{1+\omega}{m}} (M_e^2)^{\frac{1-m}{m} + \frac{1}{m(\gamma-1)}} \left(\frac{\rho_0 \sqrt{2H_0}\, \ell}{\mu_0}\right)^{-1/m} \bar{x}^{-1/m}$$

where subscript "o" refers to nozzle stagnation conditions and $\mu \sim T^{\omega}$

Using Eq. (5) and substituting for M_e in terms of $\bar{x}$,

$$C_f \sim K^{1-\frac{1+\omega}{m}} \bar{x}^{n} \left(\frac{\rho_0 \sqrt{2H_0}\, \ell}{\mu_0}\right)^{-1/m} \tag{10}$$

$$n = 2\,\frac{[1 + (1-m)(\gamma-1)]}{m}$$

Now Eq. (7) becomes

$$\frac{d\theta}{d\bar{x}} + \theta\left(\frac{2C_0 - 1}{\bar{x}}\right) = \lambda\, \bar{x}^{n}$$

which is a linear ordinary differential equation whose solution can be written by inspection.

$$\frac{\theta}{\bar{x}} = \frac{\lambda\, \bar{x}^{n}}{n + 2C_0} \tag{11}$$

It was assumed that $\theta = 0$ at $x = 0$. After considerable algebraic manipulation, Eq. (11) can be expressed in terms of quantities appropriate for nozzle flows. Hence,

$$\frac{\theta}{\bar{x}} = A_m \left[\frac{m}{(2\gamma - 1) - 2m(\gamma - 1 - C_0)}\right] \frac{\left(\frac{\gamma-1}{2} M_e^2\right)^{\frac{1+\omega-m}{m}}}{\left(\frac{\rho_e u_e x}{\mu_e}\right)^{1/m}} \tag{12}$$

Using Eq. (6),

$$\frac{\delta^*}{x} = A_m C_0 \left[\frac{m}{(2\gamma-1) - 2m(\gamma-1-C_0)}\right] \left(\frac{\gamma-1}{8}\right)^{\frac{1+\omega-m}{m}} \frac{(M_e)^{\frac{2(1+\omega)}{m}}}{\left(\frac{\rho_e u_e x}{\mu_e}\right)^{1/m}} \tag{13}$$

Next, consider the simple equivalent flat-plate case. In this case, variation of flow quantities along the nozzle are ignored, so Eq. (7) becomes

$$\frac{d\theta}{dx} = \frac{C_f}{2} \sim x^{-1/m} \tag{14}$$

and the integration is simple.

$$\frac{\theta}{x} = \frac{A_m}{1-1/m} \frac{\left(\frac{\gamma-1}{8} M_e^2\right)^{\frac{1+\omega-m}{m}}}{\left(\frac{\rho_e u_e x}{\mu_e}\right)^{1/m}} \tag{15}$$

and

$$\frac{\delta^*}{x} = \frac{C_0 A_m}{1-1/m} \left(\frac{\gamma-1}{8}\right)^{\frac{1+\omega-m}{m}} \frac{(M_e^2)^{\frac{1+\omega}{m}}}{\left(\frac{\rho_e u_e x}{\mu_e}\right)^{1/m}}$$

It is interesting to note that the functional dependence of Eqs. (14) and (15) on M_e and Re_x are identical.

Return briefly to Eq. (14) which can be written as

$$\frac{d\theta}{dx} = A_m \frac{\rho_r}{\rho_e} \left(\frac{\rho_r u_e x}{\mu_r}\right)^{-1/m}$$

Using Eq. (6)

$$\frac{d[\delta^* C_0^{-1} M_e^{-2}]}{dx} = \frac{A_m}{K} \frac{T_e}{T_0} \left(\frac{\rho_r u_e x}{\mu_r}\right)^{-1/m} \tag{16}$$

Consistent with the equivalent flat-plate assumption, Eq. (16) becomes

$$\frac{d\delta^*}{dx} = \frac{2 C_0 A_m}{(\gamma-1) K} \left(\frac{\rho_r u_e x}{\mu_r}\right)^{-1/m}$$

or

$$\frac{\delta^*}{x} = \frac{2 C_0 A_m}{(\gamma-1) K (1-1/m)} \left(\frac{\rho_r u_e x}{\mu_r}\right)^{-1/m} \tag{17}$$

Eq. (17) suggests that nozzle-displacement thickness data can be correlated in terms of a Reynolds number based on reference density and viscosity independent of M_e.

SECTION III: BOUNDARY LAYER DATA ANALYSES AND CORRELATION

The boundary layer data were analyzed and correlated to determine to what extent the assumptions and empirical results customarily used in turbulent boundary-layer analyses were valid at hypersonic flow conditions.

The basic assumption made in the analysis was that the Crocco energy relation

$$H = a + b\,u$$

$$\frac{H - H_w}{H_e - H_w} = u/u_e \tag{18}$$

was valid. Eq. (18) is rigorously valid for a flow with zero pressure gradient and Prandtl number equal to one. In the case of laminar flow where solutions to the boundary layer equations can be obtained the Crocco relation is in reasonable agreement (Fig. 9) with the numerical solutions[16] for a very favorable pressure gradient ($\beta = 2$) and a highly cooled wall ($H_w/H_T \approx 0$). It is probable that Eq. (18) becomes a better approximation in the turbulent case as it does in the laminar case when H_w/H_T approaches zero. The turbulent[7] and laminar cases are compared in Fig. 9 for $H_w/H_T = .5$. Since no measurement was made in the study reported here from which the local total enthalpy profile in the boundary layer could be determined directly, Eq. (18) was applied to relate the Mach number, velocity, and temperature profiles.

$$\frac{u}{u_e} = \frac{\frac{T_w - T_o}{T_e} - \sqrt{\left(\frac{T_w - T_o}{T_e}\right)^2 - 4\frac{T_w}{T_e}\left[\frac{T_e - T_o}{T_e} - \left(\frac{M_e}{M}\right)^2\right]}}{2\left[\frac{T_e - T_o}{T_e} - \left(\frac{M_e}{M}\right)^2\right]} \tag{19a}$$

$$\frac{T}{T_e} = \frac{\rho_e}{\rho} = \frac{T_w}{T_e} - \left(\frac{T_w - T_o}{T_e}\right)\frac{u}{u_e} - \left(\frac{T_o - T_e}{T_e}\right)\left(\frac{u}{u_e}\right)^2 \tag{19b}$$

Typical boundary-layer profiles calculated using Eq. (19) are shown in Figs. 10 and 11. Note that the shock tunnel results agree quite well with those from continuous flow[17] and Hot-shot tunnels.[18]

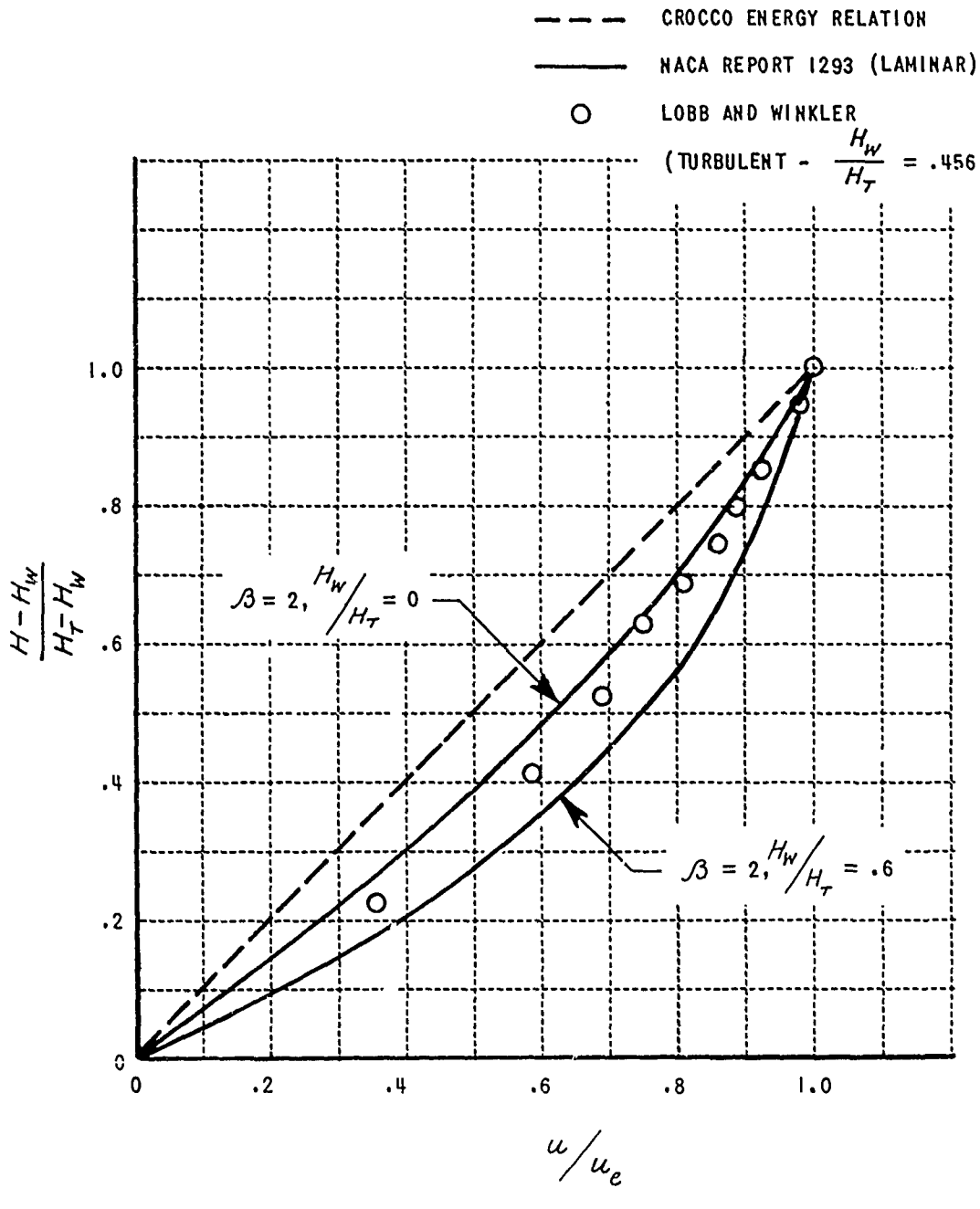


Figure 9 BOUNDARY LAYER TOTAL ENTHALPY DISTRIBUTION

SYM.	MACH NO.	Re_δ	FACILITY
○	8.25	1.8×10^5	CAL
◆	8.07	6.3×10^5	A.E.D.C.
□	15.8	1.3×10^4	CAL

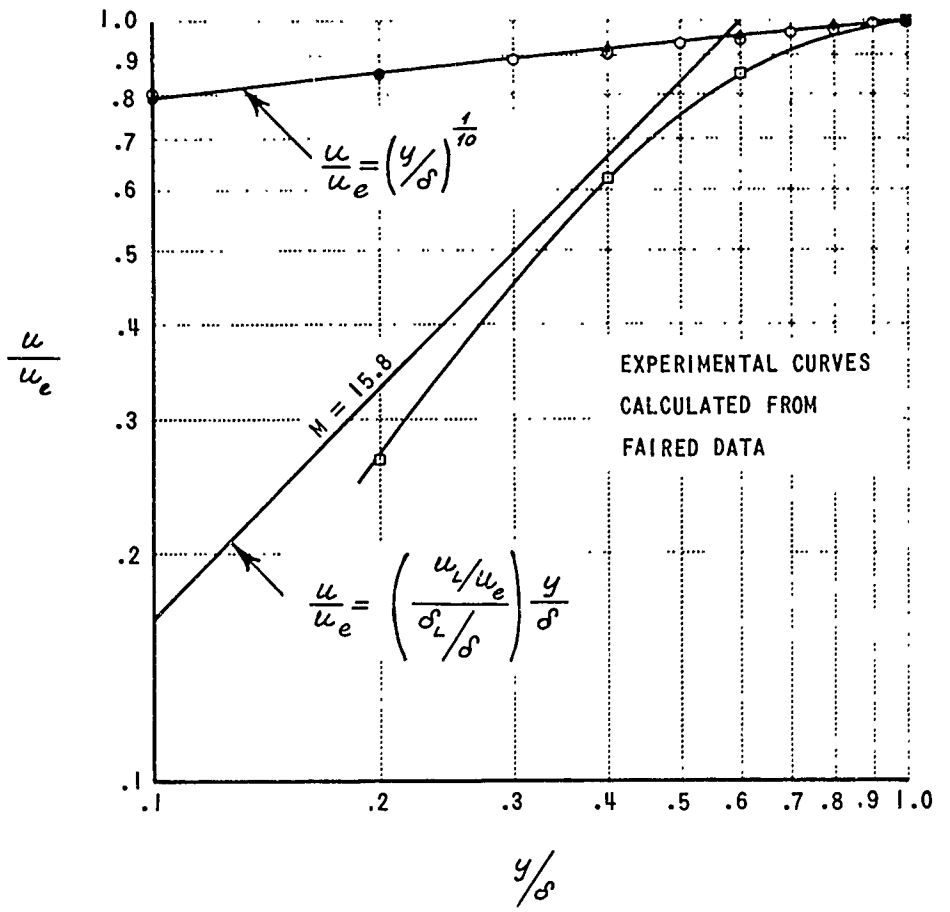


Figure 10a BOUNDARY LAYER VELOCITY PROFILES

SYM.	MACH NO.	Re_δ	FACILITY
○	16.3	7.9×10^4	CAL
□	14.0	7×10^4	CAL
◇	12.6	6.5×10^4	CAL

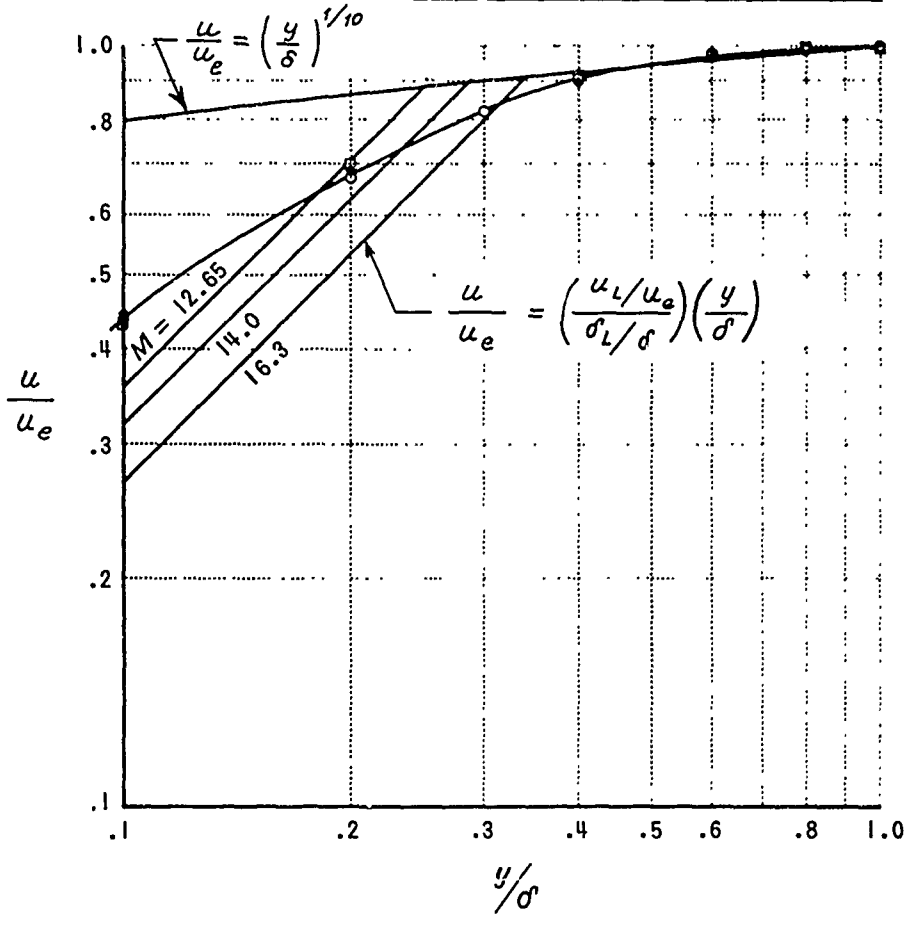


Figure 10b

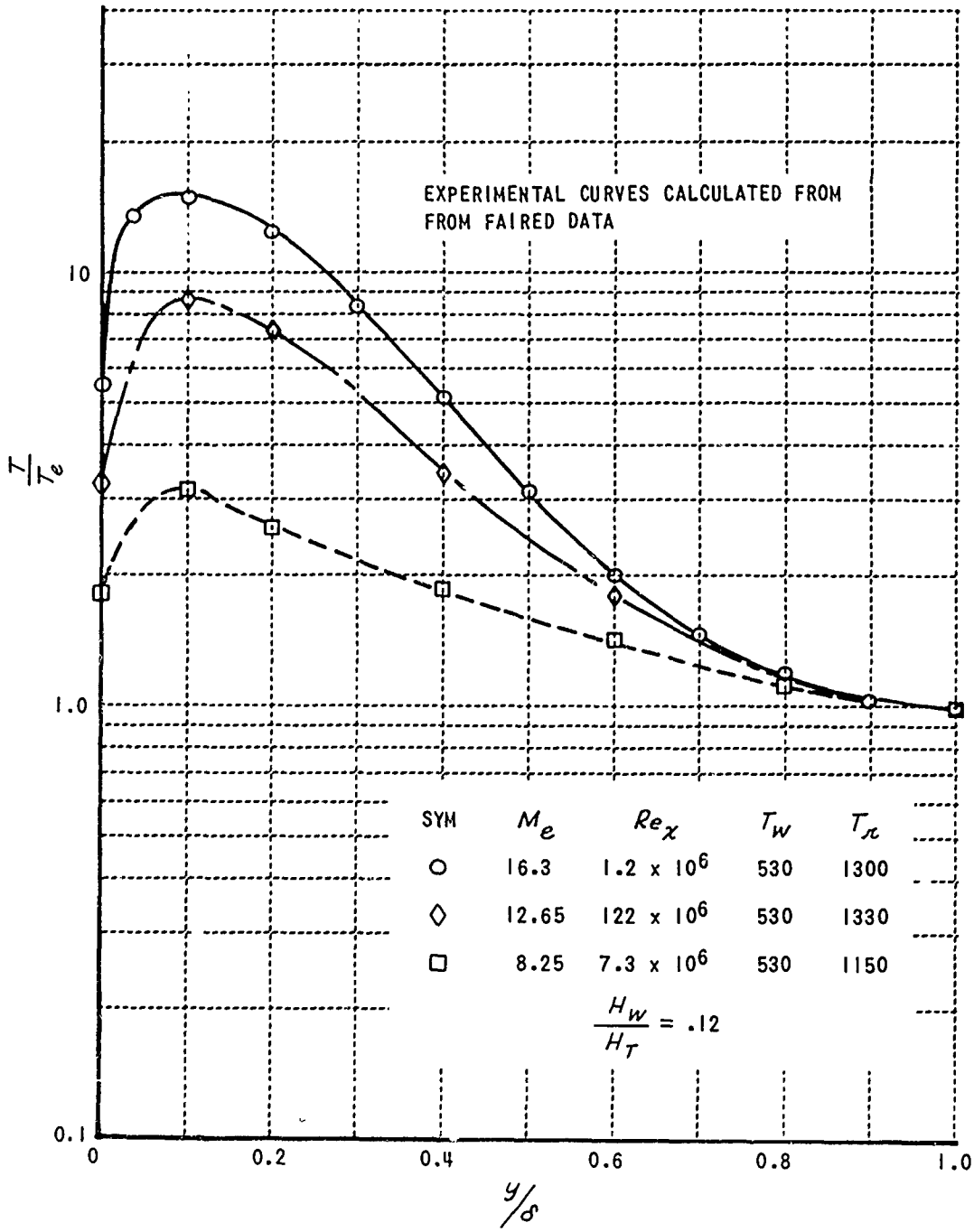


Figure 11 EFFECT OF MACH NUMBER ON BOUNDARY LAYER TEMPERATURE PROFILES

The boundary layer velocity profiles were analyzed assuming the structure to consist of an outer turbulent layer where $u/u_e = (y/\delta)^{1/n}$ and an inner laminar sublayer where $u/u_e \sim y/\delta$. The method given in Ref. 19 was applied to estimate the thickness (δ_L/δ) and the velocity (u_L/u_e) at the edge of the laminar sublayer.

$$\Lambda^{-(1+\omega)}\left(\frac{u_L}{u_e}\right)^{\frac{n+1}{\omega+1}} + \frac{\gamma-1}{2}M_e^2\left(\frac{u_L}{u_e}\right)^2 + \left(\frac{\gamma-1}{2}M_e^2 + \frac{T_w}{T_0}\right) = \left(1-\frac{T_w}{T_0}\right)\frac{u_L}{u_e} \quad (20a)$$

$$\frac{\delta_L}{\delta} = \left(\frac{u_L}{u_e}\right)^n \quad (20b)$$

where $\Lambda = 158/Re_\delta$, $\mu \sim T^\omega$. Calculations were carried out for $n = 9$, $\omega = 1$, and $T_w/T_0 = 0$ for $M_e = 8$, 12, 16 and Re_δ from 1×10^4 to 5×10^5. The results are given in Figs. 12 and 13. It is clear that at high Mach numbers and low Re_δ, the laminar sublayer becomes quite tnick. The estimates of the laminar sublayer corresponding to the measured profiles are indicated in Fig. 10. The agreement is good in some cases and only fair in others.

The integrated boundary-layer parameters, δ^* and θ, are related to the boundary-layer thickness, δ, by the following integral relations.

$$\frac{\delta^*}{\delta} = 1 - \int_0^1 \frac{\rho u}{\rho_e u_e}\, d(y/\delta) \quad (21a)$$

$$\frac{\theta}{\delta} = \int_0^1 \frac{\rho u}{\rho_e u_e}\left(1 - u/u_e\right) d(y/\delta) \quad (21b)$$

Eq. (21) was evaluated using the profiles given by Eq. (19). The results as a function of Mach number are shown in Fig. 14. Even though velocity profiles were found to be dependent on Reynolds number, the integrated parameters are primarily a function of Mach number since the strong dependence of the boundary-layer density profiles (Fig. 11) on Mach number dominates the weaker Reynolds number effect on the velocity profiles. The boundary-layer thickness was defined as that distance from wall where the pitot pressure was 99% of the free-stream value.

The ratio δ^*/δ was also calculated from nozzle-area ratio considerations. The effective nozzle area was determined from the known throat area and the measured Mach number at the edge of the boundary layer. Note from Fig. 14c that the agreement between δ^*/δ calculated in this manner and from the integrated boundary-layer

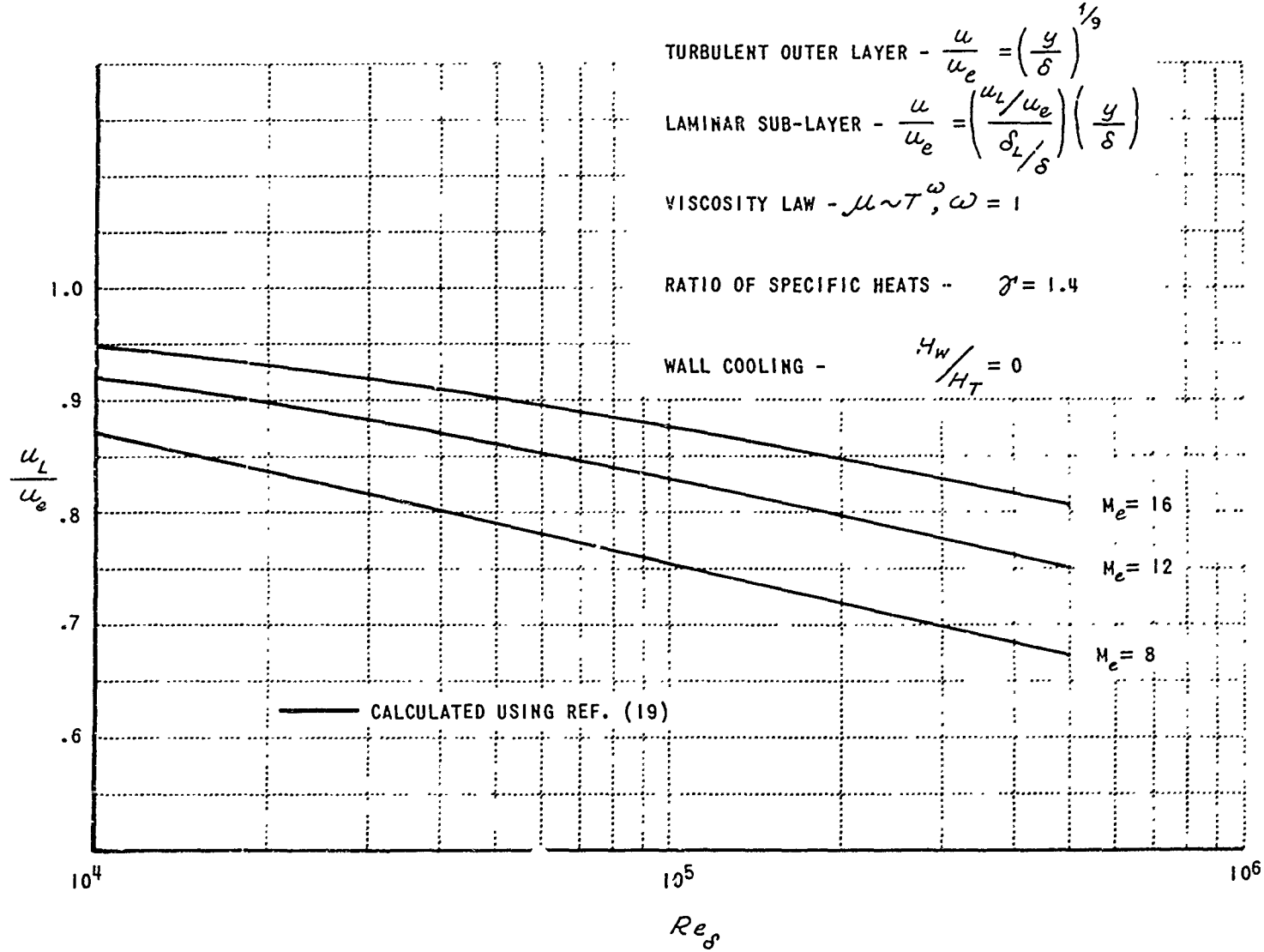


Figure 12 VELOCITY RATIO AT THE EDGE OF THE LAMINAR SUB-LAYER

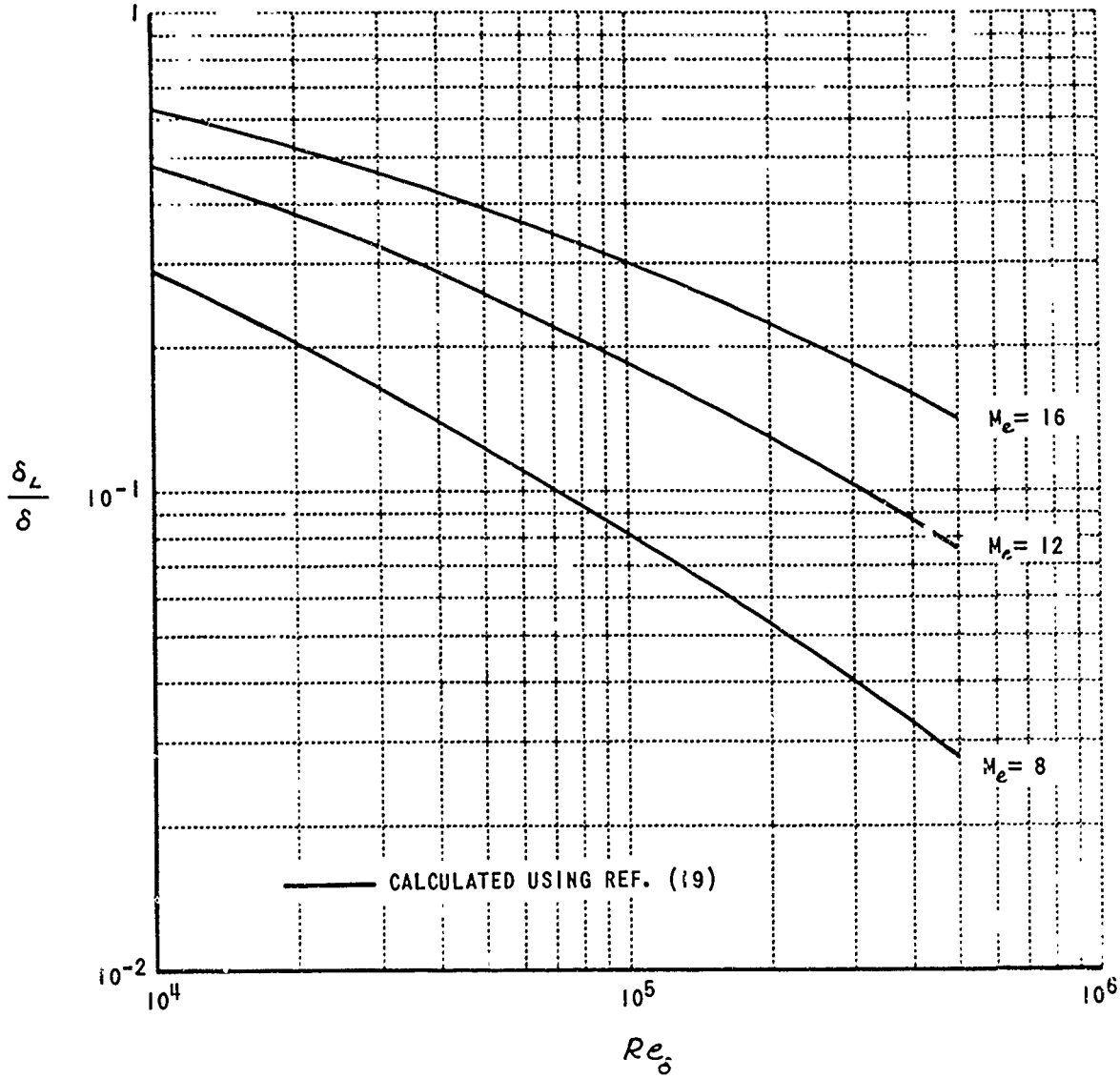


Figure 13 EXTENT OF THE LAMINAR SUB-LAYER

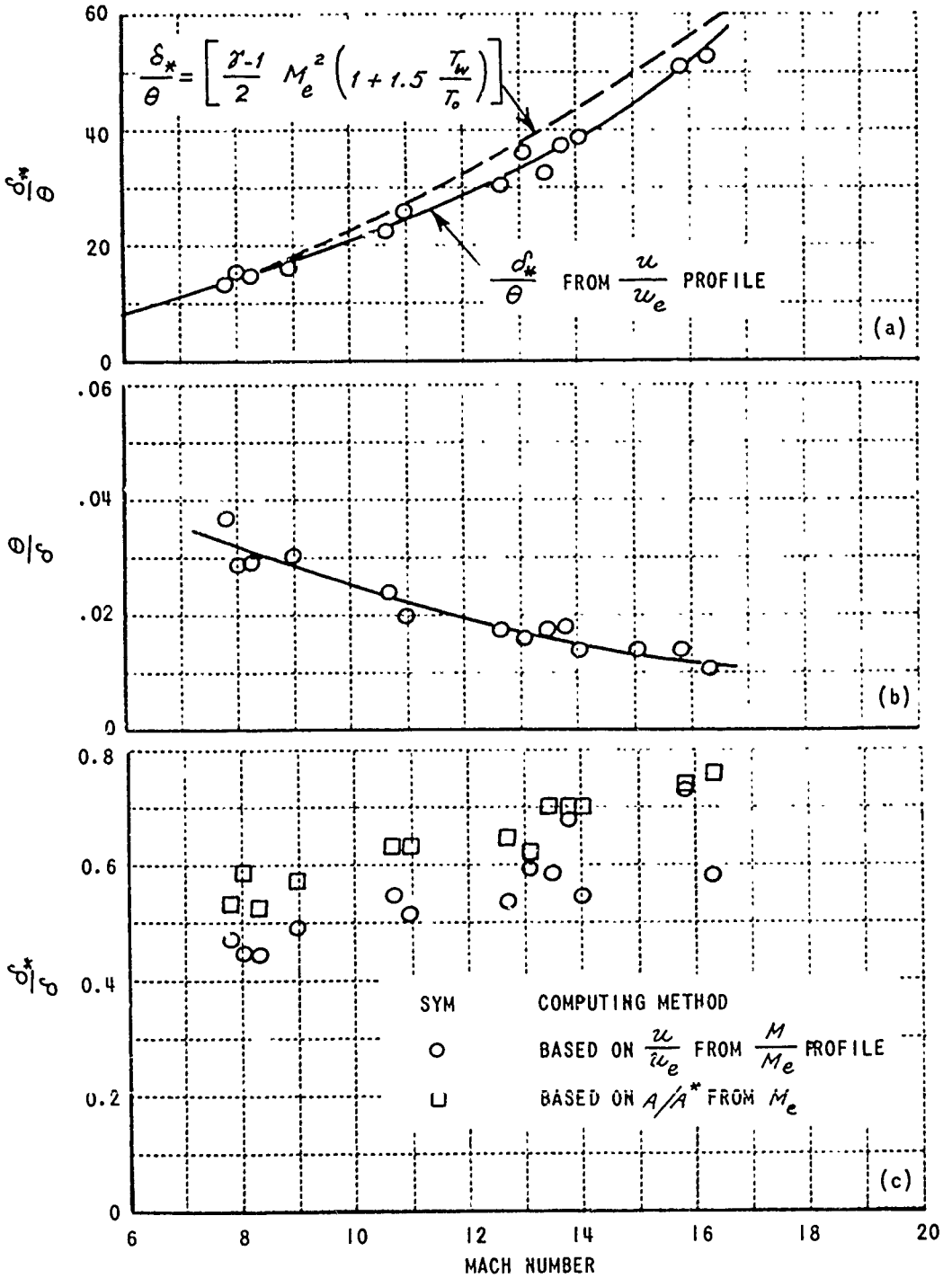


Figure 14 INTEGRATED BOUNDARY LAYER CHARACTERISTICS

profiles is usually quite good. However, it should be pointed out that this ratio when determined from area ratios is quite sensitive to the selection of M_e. This was especially true at $M_e < 10$ where the boundary layer effect was smaller than at higher Mach numbers. Integrating the profiles is a much more reliable way of getting $\delta*/\delta$ since it is not very sensitive to the small uncertainties of $\pm .2$ which exist in the determination of M_e. Nevertheless, the agreement between the two methods gives some experimental justification for the use of the Crocco energy relations in the determination of the profiles. A comparison between the form factor $\delta*/\theta$ calculated from the profiles and the analytical expression (Eq. 6) derived in Ref. 14 using a Stewartson type boundary-layer transformation is shown in Fig. 14a. The agreement is not surprising as it is primarily dependent on the assumption of the Crocco energy relation which was used in the calculation of both θ and $\delta*$.

Empirical relations for $\delta*/x$, δ/x and $\delta*/\delta$ which fit the data were developed.

$$\frac{\delta_*}{x} = .0463 \frac{M_e^{1.311}}{(Re_x)^{.276}} \tag{22a}$$

$$\frac{\delta}{x} = .066 \frac{M_e^{.824}}{(Re_x)^{.166}} \tag{22b}$$

$$\frac{\delta_*}{\delta} = .703 \frac{M_e^{.487}}{(Re_x)^{.11}} \tag{22c}$$

"x" is the distance between the nozzle exit and throat. The curves corresponding to the empirical relations above are given in Figs. 15 and 16. The CAL experimental data presented are for a wall-to-total enthalpy ratio of .11. It was not possible from a few runs made at slightly lower wall-to-total enthalpy ratios to determine the effect of further wall cooling on $\delta*$ and δ. Boundary-layer results obtained in contoured nozzles at CAL, in continuous flow tunnels (moderately cool wall) at Sandia[20] and Ohio State,[21] and in Hot-shot tunnels[18] are also shown in Figs. 15 and 16. The agreement of all the data with the empirical relation (Eq. 22) is good. An empirical relation[22] developed by J. Lee for the calculation of displacement thickness in hypersonic wind tunnel nozzles is also indicated in Fig. 15 for comparison. Note that in the Reynolds number (Re_x) range $10^6 - 10^7$ for which Lee developed his relation, the two expressions do not give a significantly different result.

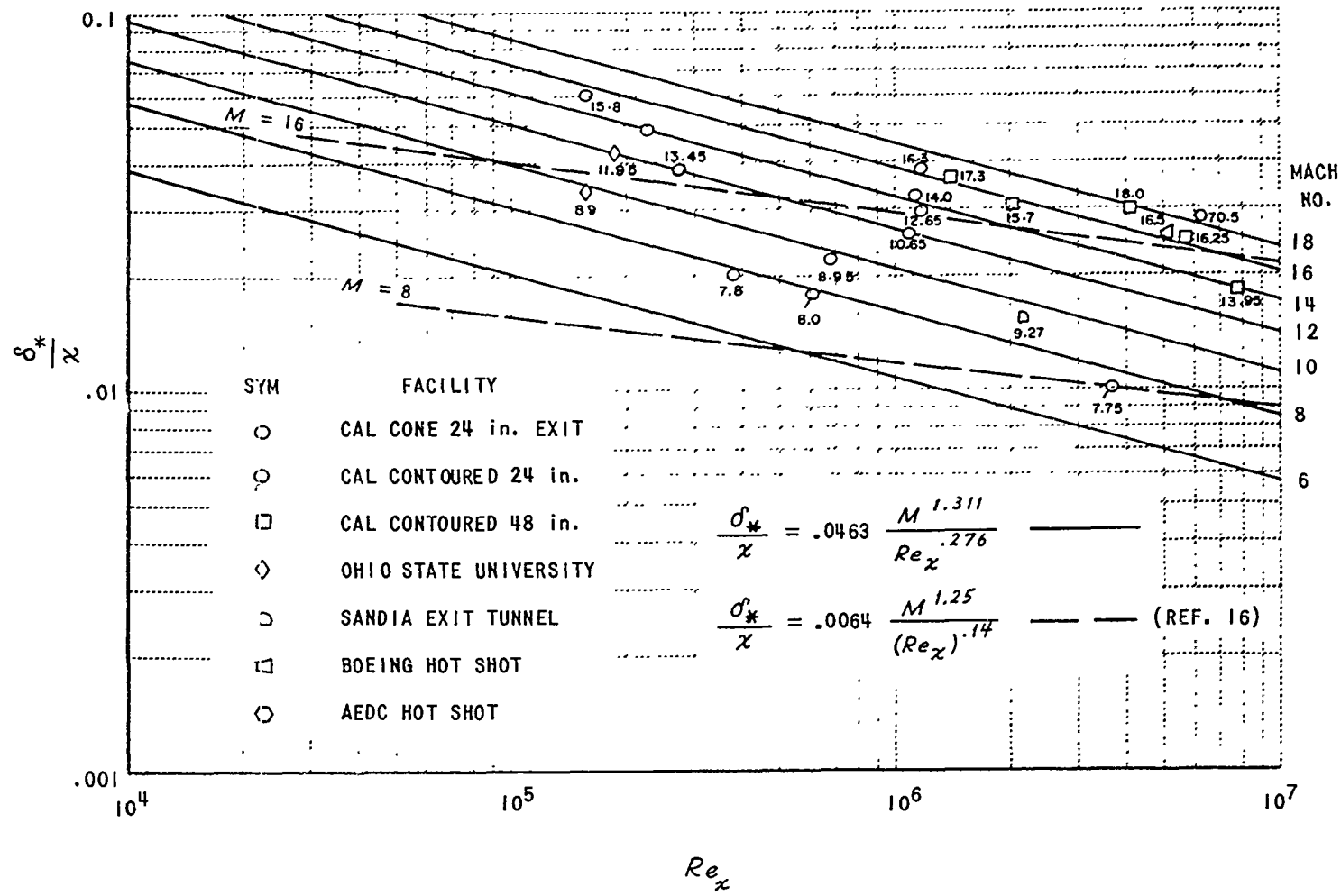


Figure 15 CORRELATED BOUNDARY LAYER DISPLACEMENT THICKNESS DATA

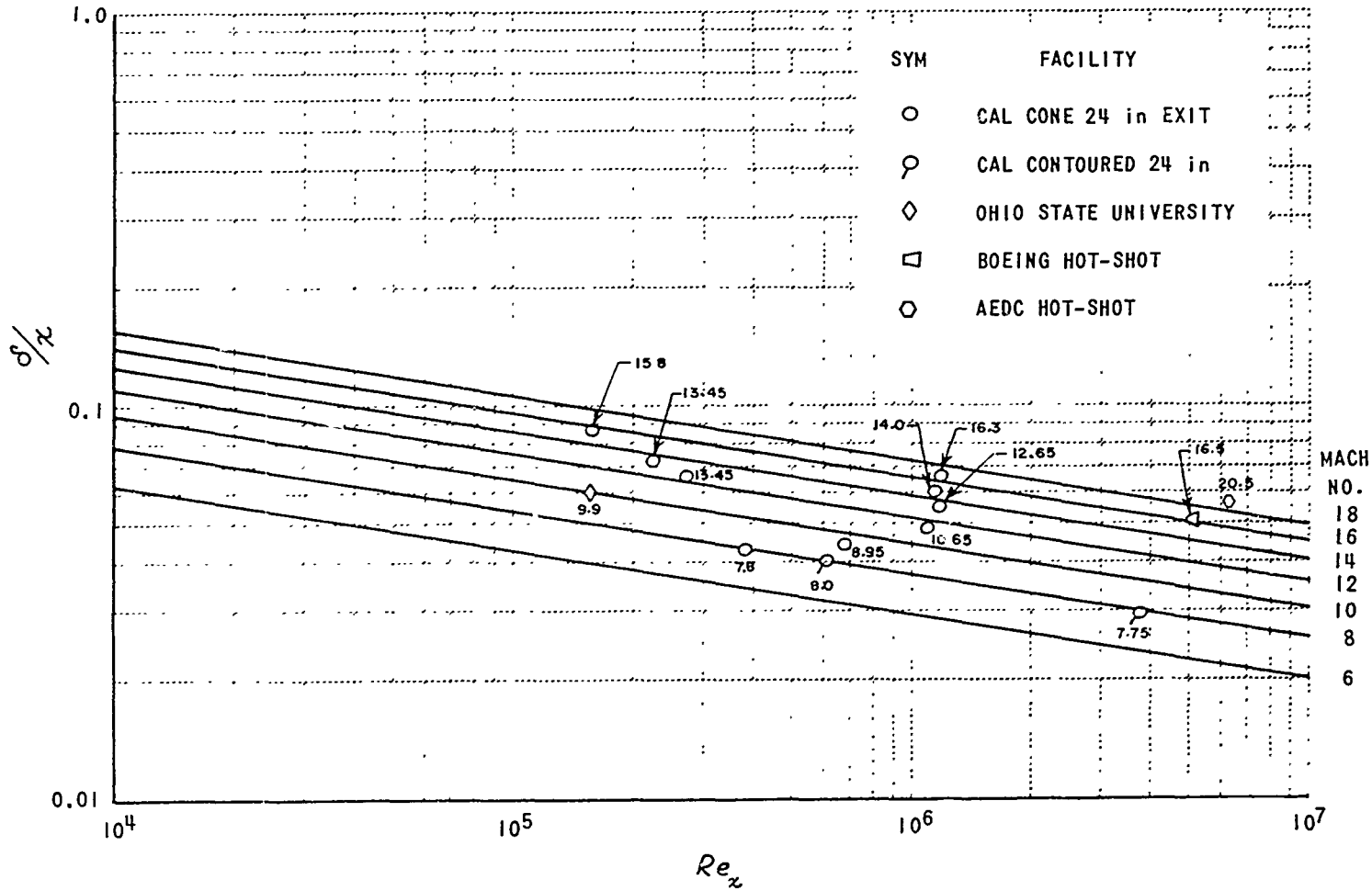


Figure 16 CORRELATED BOUNDARY LAYER THICKNESS DATA

It was shown analytically in Section II that the boundary-layer displacement thickness in a hypersonic nozzle can be written in the same form as the empirical relations (Eq. 22)

$$\frac{\delta_*}{x} \sim \frac{M_e^{\,a}}{Re_x^{\,b}}$$

The particular expression obtained using the equivalent flat-plate approach was

$$\frac{\delta_*}{x} = \frac{c_o A_m}{1-1/m}\left(\frac{\gamma-1}{2}\right)^{\frac{1+\omega}{m}-1}\frac{M_e^{\frac{2(1+\omega)}{m}}}{(Re_x)^{1/m}} \qquad (15)$$

where it was assumed that

$$\frac{\tau}{\rho_r u_e^2} = A_m\left(\frac{\rho_r u_e x}{\mu_r}\right)^{-1/m}$$

The expression corresponding to the equivalent flat plate is being used in preference to the one corresponding to the local similarity approach because the factor $m/(2\gamma - 1) - 2m(\gamma - 1 - c_o)$ in Eq. (13) is felt to be undesirably sensitive to m. Also the equivalent flat-plate method was found (Appendix I) to yield good results for the heat transfer distribution in an expanding flow. The constants Am and m which give a good fit to the experimental data were determined for $\omega = 1$, $\gamma = 1.4$, $T_w/T_o = .11$.

$$\frac{\delta_*}{x} = .08\frac{M_e^{\,1.21}}{Re_x^{\,.3}}, \quad A_m = .073, \quad m = 3.33 \qquad (23)$$

Eq. (8) fits the data (Fig. 15) almost as well as Eq. (22a) and, in addition, is consistent with general result, Eq. (15). The friction relation implied by Eq. (23)

$$\frac{\tau}{\rho_r u_e^2} = .073\left(\frac{\rho_r u_e x}{\mu_r}\right)^{-1/3.33}$$

is between the classical turbulent (m = 5) and laminar (m = 2) relations as might be expected from the velocity profiles (Fig. 10).

It was indicated by Eq. (17) that the Mach number dependence in the correlation of displacement thickness results could be removed by plotting δ_*/x as a function of $Re_{rx}\left(=\frac{\rho_r u_e x}{\mu_r}\right)$. Such a plot is given in Fig. 17. All the data are seen to correlate quite well and the

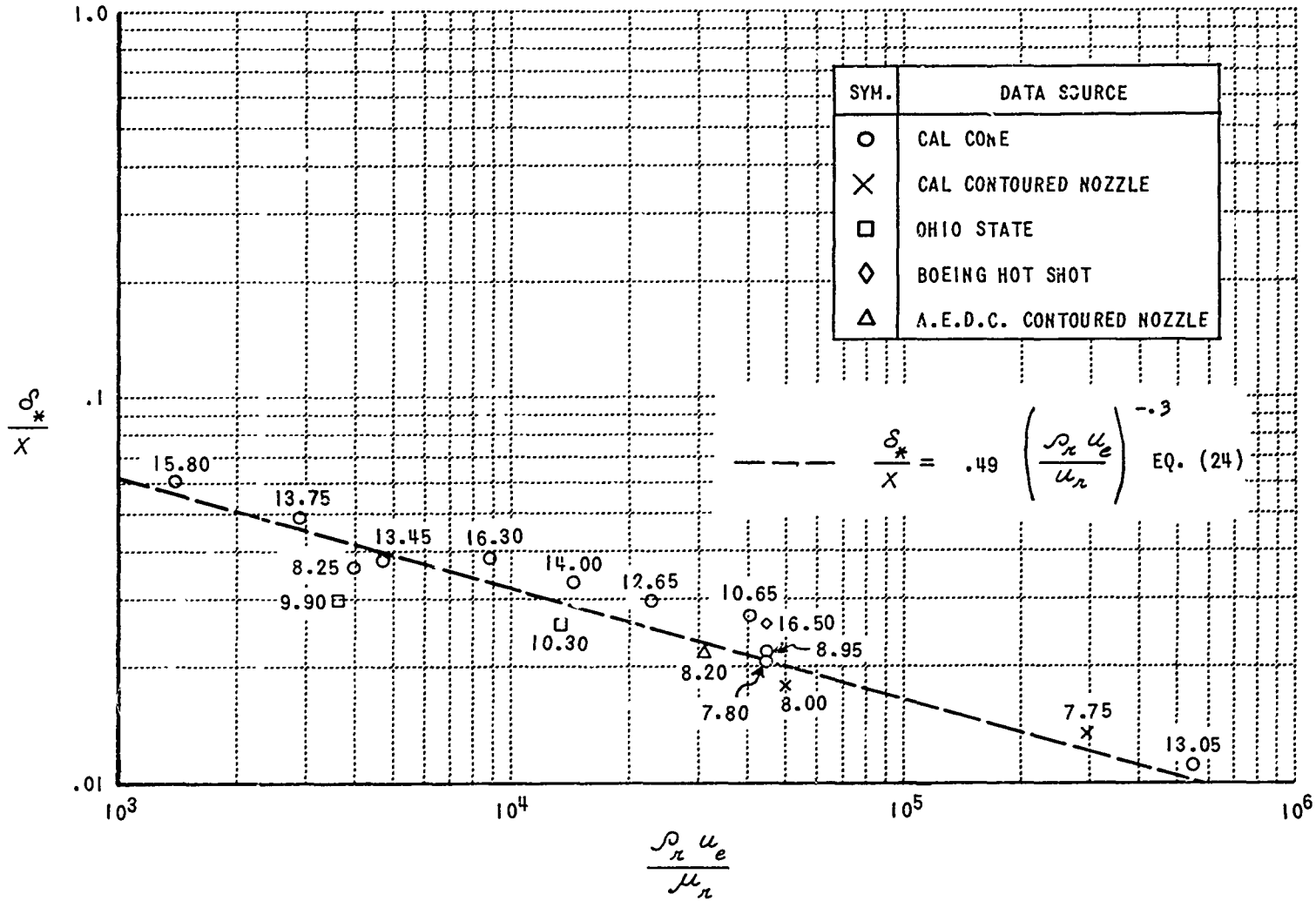


Figure 17 BOUNDARY LAYER DISPLACEMENT THICKNESS CORRELATED IN TERMS OF A REYNOLDS NUMBER BASED ON THE REFERENCE TEMPERATURE

prediction of Eq. (17) reasonably well confirmed. Hence, δ^*/x can also be written as

$$\frac{\delta_*}{x} = .49\left(\frac{\rho_r u_e x}{\mu_r}\right)^{-.3} \tag{24}$$

The correlated results discussed in the previous two paragraphs indicate that the equivalent flat-plate method and the reference temperature concept for the relating of incompressible and compressible skin-friction coefficients yield results in good agreement with experimental data for turbulent boundary layers on highly cooled surfaces at high Mach numbers.

APPENDIX I: CORRELATION OF THE COLLECTOR-EXPANSION NOZZLE HEAT TRANSFER DATA

As described in Section I-C, the heat transfer distribution in a collector-expansion nozzle model was determined. The data are given in Fig. 8. Calculations of the expected heat transfer were made using the equivalent flat-plate method discussed in Section II.

$$\dot{q} = \frac{.029}{P_r^{2/3}} \rho_e u_e (H_T - H_W)\left(\frac{\rho_r}{\rho_e}\right)^{.8}\left(\frac{\mu_r}{\mu_e}\right)^{.2} \frac{1}{\left(\frac{\rho_e u_e x}{\mu_e}\right)^{.2}} \tag{I. 1}$$

This corresponds to Eq. (9), with m = 5, Am = .029, and is the classical turbulent-flow heat-transfer equation. The local flow conditions (ρ_e, u_e, μ_e) were determined using the model inlet conditions (M_{in}, p_o, T_o) and the geometric area ratio in the model. The results of the calculations are shown on Fig. 8 with reasonable agreement between the predictions and the experimental data. As suggested by Eq. (I. 1) the dependence of the heat transfer on the stagnation density level may be accounted for by the use of the parameter $\dot{q}/p_o{}^{.8}$ rather than $\dot{q}$.

The agreement shown in Fig. 8 between the calculated and measured heat transfer distributions indicates that the simple equivalent flat-plate method is an acceptable calculation procedure in the case of expanding flow having large favorable pressure gradients as long as the pressure change is continuous and not abrupt. Note that in the neighborhood of the sudden change (x = 5 in Fig. 8), the difference between theory and experiment is larger. The results also indicate that the use of the reference enthalpy method as it relates to the skin friction law (Eq. 8) and the effective flow properties is valid for highly cooled walls and moderately high total temperatures.

REFERENCES

1. Mager, A.: "Transformation of the Compressible Turbulent Boundary Layer," J. A. S., 25, 5, 305, May 1958.

2. Cohen, N. B.: "A Method for Computing Turbulent Heat Transfer in the Presence of a Streamwise Pressure Gradient for Bodies in High-Speed Flow," NASA Memo 1-2-59L, March 1959.

3. Reshotko, E., and Tucker, M.: "Approximate Calculation of the Compressible Turbulent Boundary Layer with Heat Transfer and Arbitrary Pressure Gradient," NACA TN 4154, December 1957.

4. Hayes, W. D., and Probstein, R. F.: Hypersonic Flow Theory, Academic Press, 1959.

5. Rose, P. H.; Probstein, R. F.; and Adams, M. C.: "Turbulent Heat Transfer through a Highly Cooled Partially Dissociated Boundary Layer," J. A. S., 25, 12, 751, December 1958.

6. Offenhartz, E., and Weisblatt, H.: "Experimental Determination of the Turbulent Heat Transfer Rate Distribution along a Slender Blunt Nosed Body from Shock Tube Tests," AVCO RAD-TR-9-59-18, May 25, 1959.

7. Lobb, R. K.; Winkler, E. M.; and Persh, J.: "Experimental Investigation of Turbulent Boundary Layers in Hypersonic Flow," J. A. S., 22, 1, 1, January 1955.

8. Burke, A. F., and Carpenter, J. E.: "Wave Superheater Hypersonic Tunnel, Semi-Annual Report, July 1960--January 1961," (U), AEDC TN-61-44 (Confidential).

9. Wittliff, C. E.; Glick, H. S.; Wilson, M. R.; and Hertzberg, A.: "The Tailored-Interface Hypersonic Shock Tunnel," J. A. S., 26, 4, 219, April 1959.

10. MacArthur, R. C.: "The Eyes and Ears of a Shock Tunnel," Cornell Aeronautical Laboratory Research Trends, Vol. VIII, No. 3, Fall 1960.

11. Vidal, R. B.: "Model Instrumentation Techniques for Heat Transfer and Force Measurements in a Hypersonic Shock Tunnel," CAL Report AD-917-A-1, February 1956.

12. Sherman, F. S.: "New Experiments on Impact Pressure Interpretation in Supersonic and Subsonic Rarefied Air," NACA TN 2995, September 1953.

13. Schlichting, H.: Boundary Layer Theory, Fourth Edition, McGraw-Hill Book Co., 1960.

14. Sivells, J., and Payne, R.: "A Method of Calculating Turbulent Boundary Layer Growth at Hypersonic Mach Numbers," AEDC TR-59-3, 1959.

15. Johnson, A.: "A Method of Calculating Boundary Layer Thickness in Axisymmetric Nozzles with Laminar Hypersonic Flow," Sandia Report SC-4370(RR), 1959.

16. Cohen, C. B., and Reshotko, E.: "Similar Solutions for the Compressible Laminar Boundary Layer with Heat Transfer and Pressure Gradient," NACA Report 1293, 1956.

17. Private Communication from J. Sivells, Gas Dynamics Facility, ARO, Inc.

18. Lukasiewicz, J., et al.: "Development of Capacitance and Inductance Driven Hot Shot Tunnels," AEDC TN-60-222, January 1961.

19. Donaldson, C. duP.: "Heat Transfer and Skin Friction for Turbulent Boundary Layers on Heated or Cooled Surfaces at High Speeds," NACA RM L52H04, October 1952.

20. Randall, D.: "Operational Experience with the Sandia Pilot Hypersonic Wind Tunnel," Paper presented at the 14th Supersonic Tunnel Association Meeting, October 1960.

21. Private Communication from J. Lee, Aerodynamics Laboratory, Ohio State University.

22. Lee, J.: "Axisymmetric Nozzles for Hypersonic Flow," Ohio State Research Foundation Report 459-1, July 1959.

THE VISCOUS BLUNT-BODY PROBLEM

H. Hoshizaki

Lockheed Missiles & Space Company
Sunnyvale, California

ABSTRACT

A brief review of several papers dealing with the effect of shock-generated vorticity on stagnation-point heat transfer is presented. Shock detachment distances, velocity and enthalpy profiles, and heat-transfer rates are compared.

An analysis is then presented which attempts to describe the flow around a blunt body when the shock layer is completely viscous.

An integral method is employed to reduce the governing equations to a set of total differential equations which describe the shape of the shock wave. Insufficient boundary conditions exist at the stagnation point to solve the equations. The downstream boundary condition that the shock angle approach the inviscid value, or that all disturbances at large distances from the body vanish, is necessary. These boundary conditions preclude a simple solution to the viscous blunt-body problem. A method for determining an approximate solution is indicated.

LIST OF SYMBOLS

a	velocity profile coefficients
b	enthalpy profile coefficients
C_i	mass fraction of species
C_p	total specific heat at constant pressure
$\bar{C}_p$	frozen specific heat at constant pressure
D_{ij}	diffusion coefficient for a multicomponent system
$\mathcal{D}_{ij}$	diffusion coefficient for a binary system
F_1	defined by Eq. (20c)
F_2	defined by Eq. (20d)
f	velocity function, Eq. (18)
g	enthalpy function, Eq. (19)
h	static enthalpy
h_i	static enthalpy of i^{th} species, including enthalpy of formation
H	total enthalpy
k	total thermal conductivity
$\bar{k}$	frozen thermal conductivity
M_i	molecular weight of species i
n_i	moles of species i per unit volume
n_t	total number of moles per unit volume
P	static pressure

Pr	total Prandtl number, $Pr = C_p\mu/k$
$\dot{q}$	energy flux
r	body radius measured from body centerline
R_b	body radius
$\tilde{Re}$	Reynolds number, $\rho_\infty U_\infty R_b/\mu_\delta$
Re_δ	Reynolds number, $\rho_\delta U_\infty R/\mu_\delta$
S	distance along shock wave
T	temperature
u	velocity component parallel to body
U_∞	free-stream velocity
v	velocity component normal to surface
X_i	mole fraction of species i, $X_i = n_i/n_t$
x, y	body-oriented coordinate system
γ	isentropic index
δ	shock detachment distance
$\tilde{\delta}$	defined by Eq. (12d)
δ_v	boundary layer thickness
δ^*	momentum thickness Eq. (15)
δ^{**}	modified momentum thickness Eq. (16)
δ_E^*	enthalpy thickness Eq. (17)
ϵ	difference between body and shock angle
η	Dorodnitzyn variable Eq. (12a)
θ	body angle
κ	body curvature
$\tilde{\kappa}$	$1 + \kappa y$
μ	dynamic viscosity

ν	kinematic viscosity
ρ	density
$\bar{\rho}$	density ratio across shock, ρ_∞/ρ_δ
ϕ	shock angle
ω	vorticity

Subscripts

B.L.	boundary layer
FM	free molecule
o	stagnation point
S.L.	shock layer
i	i^{th} chemical species
w	wall quantities
δ	quantities immediately behind shock
∞	free stream condition

Primes denote differentiation.

THE VISCOUS BLUNT BODY PROBLEM

INTRODUCTION

When heat transfer and shear to a hypervelocity vehicle are computed by conventional methods, the shock layer is considered to be separable into an inviscid and viscous region. The viscous region is, of course, the boundary layer. One assumes that there is no interaction between the inviscid flow and the boundary layer. This assumption is valid as long as the boundary layer remains very thin with respect to the shock-layer thickness and the gradients in the inviscid flow are much smaller than the gradients which exist in the boundary layer. Ferri and Libby (Ref. 1) point out that when the bow shock is highly curved, the varying shock strength can produce large entropy gradients and vorticity which may interact with the vorticity generated by viscosity in the boundary layer. The degree of interaction depends on the relative magnitude of the two vorticities. When the two vorticities are of the same order of magnitude, there can be a considerable interaction between the inviscid flow and the boundary layer. This interaction can have a significant effect on the heat transfer and shear to the body.

The problem of determining the effect of external vorticity on heat transfer and shear has been considered by many authors (Refs. 2 – 12). Their work can be placed in two broad categories: (1) the vorticity interaction regime and (2) the viscous shock-layer regime. These papers are briefly reviewed and comparisons are made where possible.

In all of the above investigations, the bow shock shape is assumed to be a known quantity. In the present paper, the problem of determining the shock shape and the attendant flow field when the shock layer is completely viscous is considered. A direct solution is sought in which the shock shape and the shock-layer flow characteristics are determined for a given body shape.

SECTION I. THE VORTICITY INTERACTION REGIME

In the vorticity interaction regime, the boundary-layer equations are assumed to be applicable with the outer boundary conditions modified to account for the external vorticity. The surface boundary conditions are usually taken to be the zero slip and zero temperature jump conditions.

There is disagreement among several authors on how the outer boundary conditions should be modified. The particular point in question is whether or not the effect of the pressure gradient due to the boundary-layer displacement thickness is of the same order as the effect of external vorticity. Van Dyke (Ref. 4) gives a clear discussion of this point and the viewpoints of numerous authors for flow over a flat plate and around blunt bodies. He also shows by means of an inner and outer expansion technique that for flow over a blunt body, the induced pressure gradient must be taken into account. His results confirm the conclusion reached by Murray (Ref. 12) for flow over a flat plate.

The increase in heat transfer caused by the interaction of the external vorticity with the boundary-layer vorticity is significantly affected by the induced pressure gradient. Hayes and Probstein (Ref. 13), for example, neglect the induced pressure gradient and obtain for the effect of external vorticity on stagnation point heat transfer

$$\frac{\dot{q}_{vort.}}{\dot{q}_{B.L.}} = 1 + 0.19\Omega$$

where

$$\Omega = \frac{1 - \frac{8}{3}\bar{\rho}}{\sqrt{2\bar{\rho}}\left(\frac{8}{3}\bar{\rho}\right)^{3/4}} \left(\frac{\rho_w \mu_w}{\rho_\delta \mu_\delta}\right)^{1/2} \frac{(1 - \bar{\rho})^{1/2}}{\sqrt{\tilde{Re}}}$$

For $\bar{\rho} = 0.167$ and $\rho\mu = \text{const.}$,

$$\frac{\dot{q}_{vort.}}{\dot{q}_{B.L.}} = 1 + \frac{0.305}{\sqrt{\tilde{Re}}}$$

Van Dyke (Ref. 14), in an extension of his previous work to compressible flow, includes the induced pressure gradient and obtains for the same conditions

$$\frac{\dot{q}_{vort.}}{\dot{q}_{B.L.}} = 1 + \frac{0.8419}{\sqrt{\tilde{Re}}}$$

which predicts that the effect of external vorticity is almost three times as large as that predicted by Hayes and Probstein. For strong shocks ($\gamma \to 1$), Van Dyke

indicates that the vorticity effect, which is given by the second term in the above equation, varies as $(\bar{\rho})^{-5/4}$. For $\bar{\rho} = 0.10$, Van Dyke's prediction for the effect of vorticity on heat transfer is about twice that predicted by Hayes and Probstein. It should be noted that the above increase in heat transfer is due only to external vorticity and does not include the effects of body curvature and displacement thickness. The above results will be discussed further in a subsequent section.

SECTION II: THE VISCOUS SHOCK-LAYER REGIME

In the viscous shock-layer regime, as the name implies, the shock layer is completely viscous, and one cannot distinguish between a viscous layer near the wall and a nearly inviscid region away from the wall Ho and Probstein (Ref. 6), Herring (Ref. 9), and Cheng (Ref. 11) have considered the compressible flow near the stagnation point of a blunt body under the above conditions. Ferri, Zakkay and Ting (Ref. 10) have also considered this problem and their work will be classified, perhaps improperly, as a viscous shock-layer solution for the purposes of this discussion, since they apply their results in the same Reynolds number range as the previously mentioned authors.

The works of the above authors differ principally in the governing equations and the outer boundary conditions applied behind the shock wave. The zero slip and zero temperature jump boundary conditions are employed at the wall by all of the above authors. The main differences in their analysis are conveniently summarized in the following table:

Author	Governing Equations	Boundary Conditions Behind Shock Wave	Gas Properties
Ho and Probstein	Navier-Stokes	Inviscid Strong Shock Relations	$\mu \sim \sqrt{h}$, $\rho \sim \frac{1}{T}$
Herring	Boundary Layer	Inviscid Strong Shock Relations	$\rho\mu$ = const. $\rho \sim \frac{1}{T}$
Cheng	Boundary Layer plus Centrifugal-Force Term	Inviscid Strong Shock Relations Modified for Heat Conduction and Shear Behind Shock	$\rho\mu$ = const. $\rho \sim \frac{1}{T}$
Ferri, Zakkay and Ting	Boundary Layer	Inviscid Strong Shock Relations	$\rho\mu$ = const. $\rho \sim \frac{1}{T}$

In all of the analyses, the shock wave is assumed to be a thin discontinuity in the flow.

In Figure 1, the results for the shock detachment for a sphere obtained by Ho and Probstein, Herring, and Cheng are presented. These results are for a highly cooled wall which, because of the higher average density in the shock layer, causes the shock detachment distance to be less than the inviscid value. The inviscid values were obtained from Ref. 15. There is a significant difference in the results obtained by these authors, especially at the lower Reynolds numbers considered. Ho and Probstein's results show that the shock detachment distance begins to increase with decreasing Reynolds number at very low Reynolds numbers. The flow model on which their analysis is based is, admittedly, probably not valid at these low Reynolds numbers. Cheng's results, on the other hand, show a rapid decrease in shock detachment distance at very low Reynolds number.

Also shown in Figure 1 are the incompressible results of Probstein and Kemp (Ref. 5). In this case, the shock detachment distance is greater than the inviscid value due to the viscous retardation of the flow in the shock layer.

The corresponding velocity and enthalpy profiles are presented in Figures 2 and 3, respectively. These profiles are quite similar in appearance, but note that the normal distance has been normalized to the shock detachment distance. Since the results for the shock detachment distance vary significantly, the actual velocity and enthalpy at a given point from the body can also vary significantly. Also note the reduction in the value of the velocity and enthalpy immediately behind the shock in Cheng's results. This is due to the boundary conditions employed by Cheng behind the shock wave which take the heat conduction and shear into account.

The heat-transfer results obtained by these authors are compared in Figure 4. The results are normalized to the free-molecule heat-transfer rate which is given by

$$\dot{q}_{FM} = \frac{1}{2} \rho_\infty U_\infty^3$$

Also shown in Figure 4 for comparison purposes are the boundary-layer values as calculated by Fay and Riddell (Ref. 16) for a dissociated boundary layer and by Reshotko and Cohen (Ref. 17) for $\rho\mu$ = constant. The constant-density value for the stagnation point velocity gradient (Ref. 13) was used with the boundary layer theories.

$$\frac{R}{U_\infty} \left(\frac{du}{dx} \right)_o = (1 - \bar{\rho}) \sqrt{\frac{8}{3} \bar{\rho}}$$

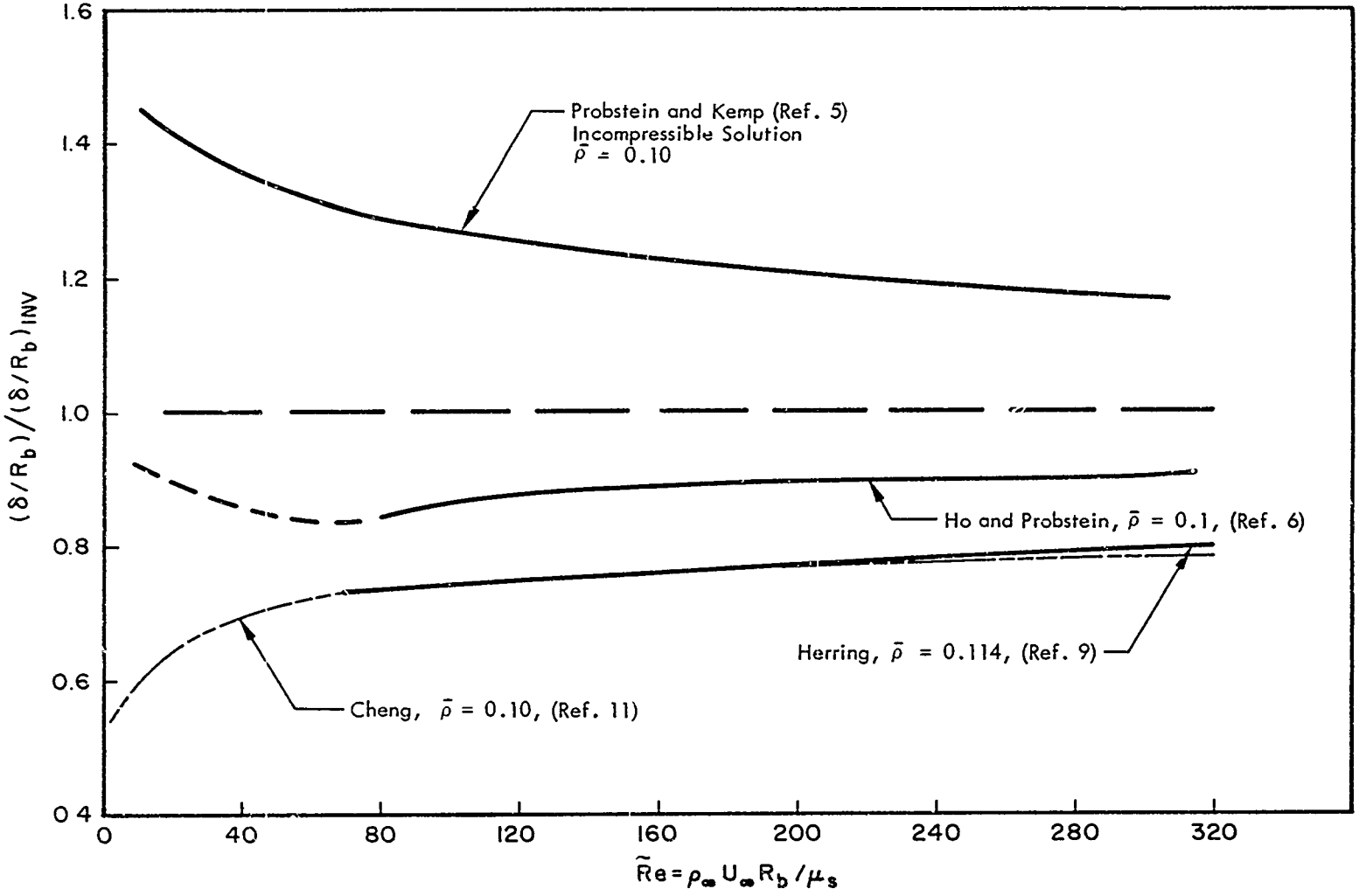


Figure 1 Shock Detachment Distance for a Sphere

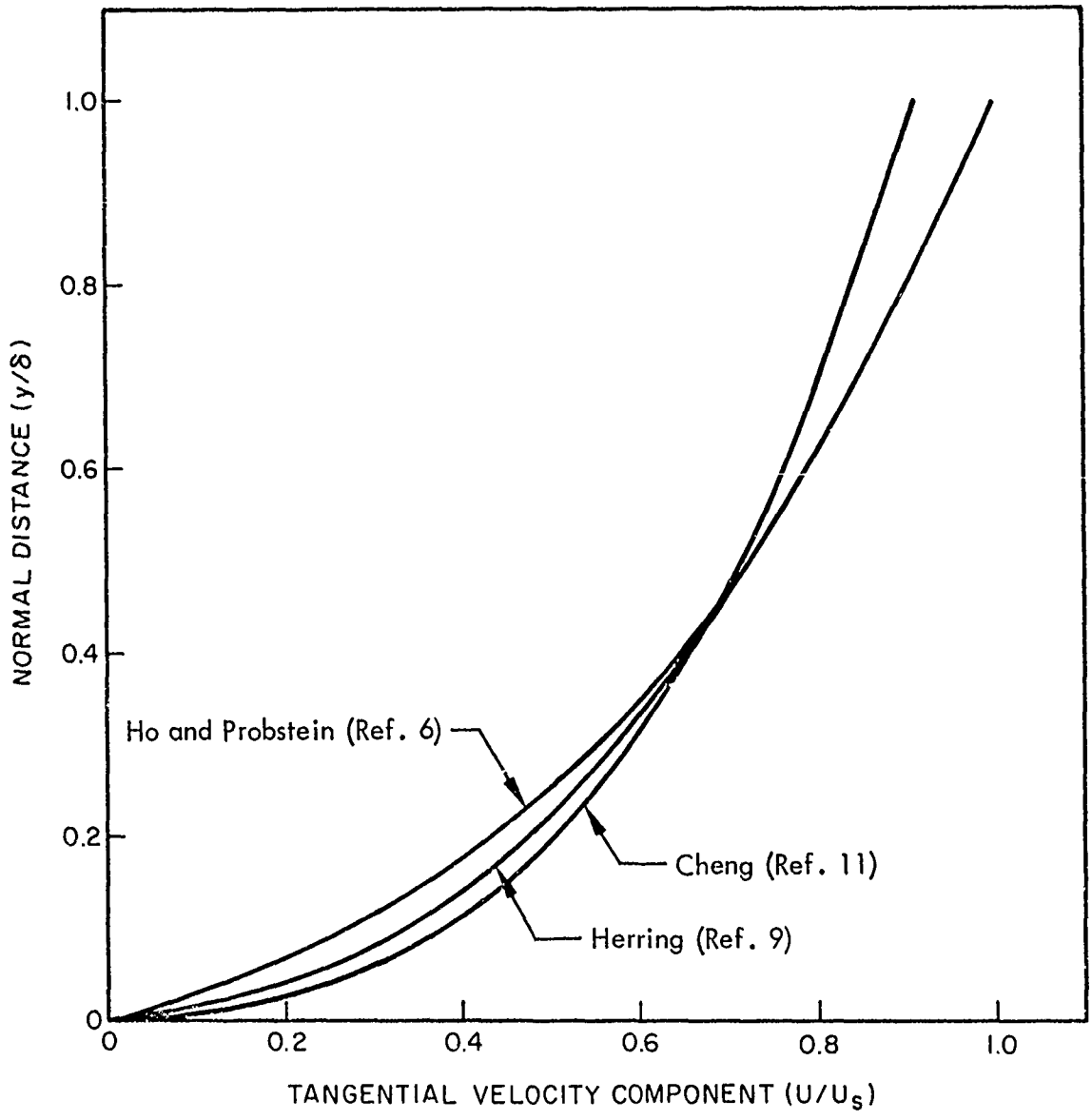


Figure 2 Velocity Profiles for $\tilde{\mathrm{Re}} \simeq 100$, $\bar{\rho} = 0.10$

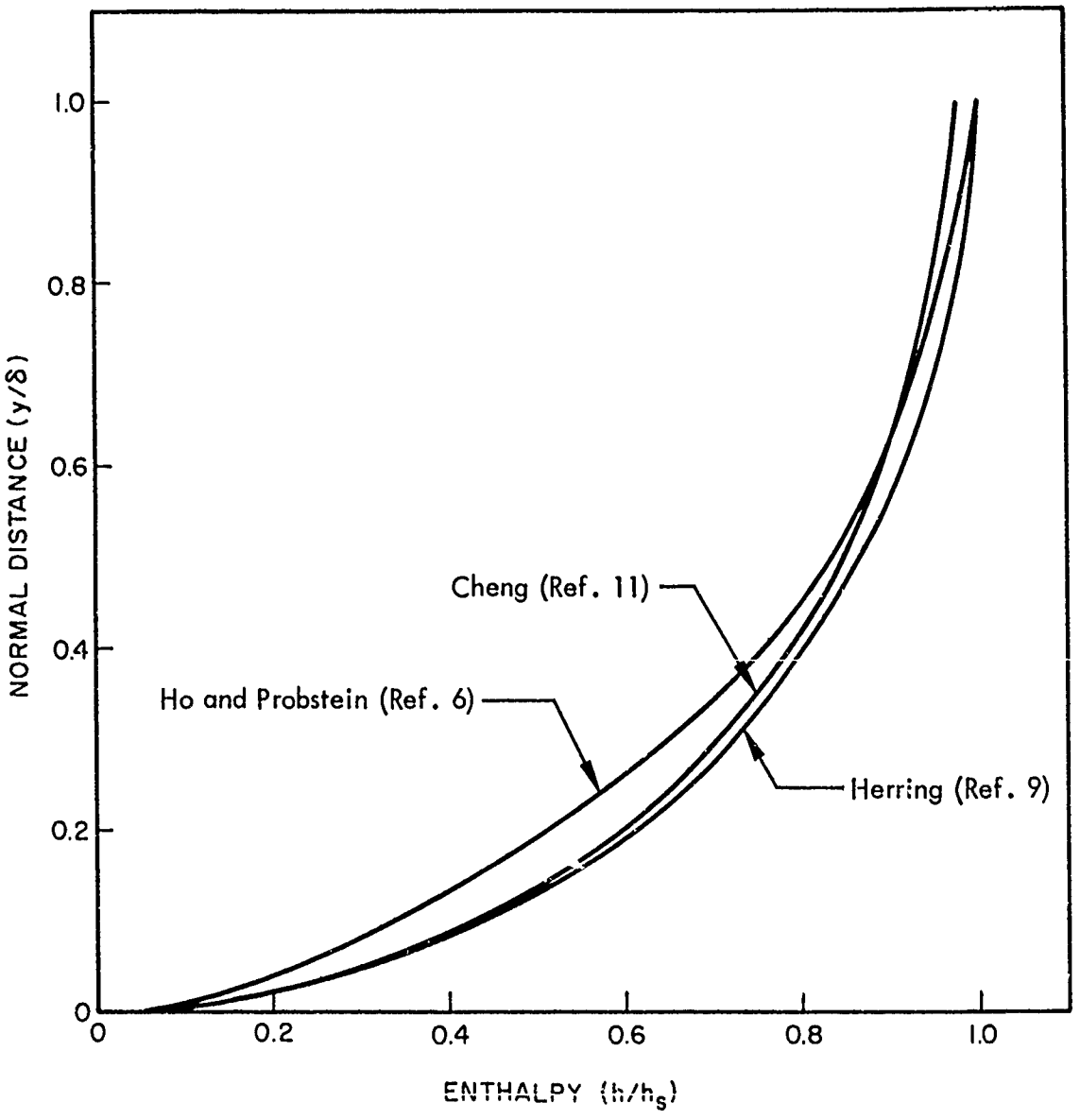


Figure 3 Enthalpy Profiles for $\tilde{\mathrm{Re}} \simeq 100$, $\bar{\rho} = 0.10$

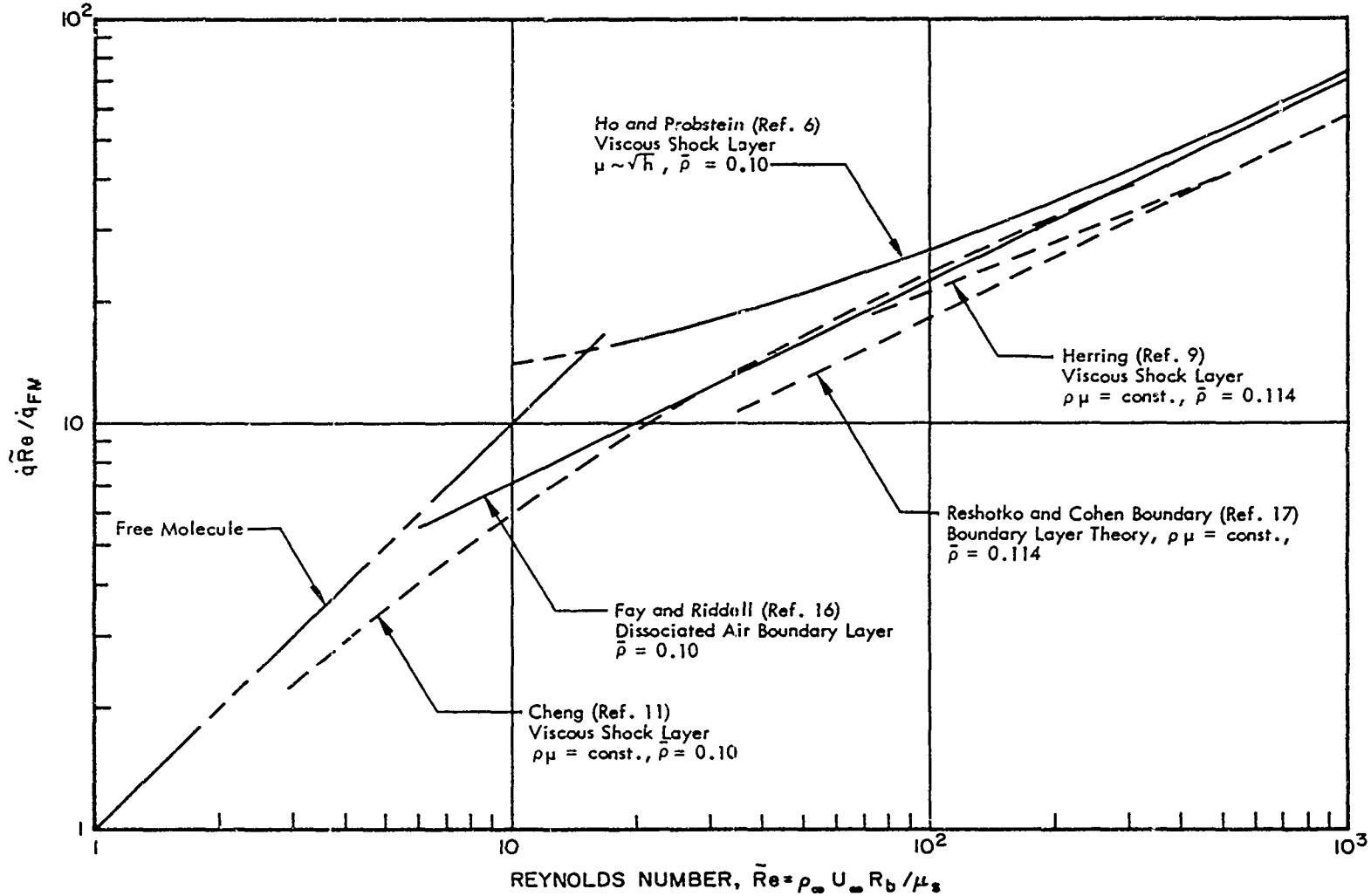


Figure 4 Comparison of Heat-Transfer Results

Ho and Probstein neglect dissociation but take the viscosity proportional to the square root of the enthalpy. Their results can probably be compared best to the Fay and Riddell boundary-layer theory. It is seen that the viscous shock layer results of Ho and Probstein fall above the Fay and Riddell values and approach them at high Reynolds number. This increase in heat transfer over the boundary-layer values at low Reynolds number is due mainly to the external vorticity.

Herring and Cheng assume $\rho\mu$ = constant so that their results should be properly compared to the boundary-layer values of Reshotko and Cohen. Herring's results lie above and approach the Reshotko and Cohen values at the higher Reynolds numbers. Cheng's results, on the other hand, are substantially higher than the Reshotko and Cohen values at the higher Reynolds numbers and then fall below the boundary-layer values at very low Reynolds numbers. This fall-off can probably be attributed to the decrease in enthalpy and velocity due to heat conduction and shear immediately behind the shock.

The effect of external vorticity on heat transfer can be more clearly seen by normalizing the viscous shock layer results to appropriate boundary-layer values. Some care must be exercised in selecting the boundary-layer reference value since there is a significant difference in the results of Fay and Riddell for a dissociated air-boundary layer and Reshotko and Cohen's results for a perfect gas boundary layer (see Figure 4).

In Figure 5, the various results obtained for the ratio of shock layer to boundary-layer heat transfer is presented. Ho and Probstein's results are referenced to Fay and Riddell, while Cheng and Herring's results are referenced to Reshotko and Cohen. Ferri et al., Hayes and Probstein, and Van Dyke all obtain the heat-transfer ratio directly. All of the results are for a density ratio of 0.10. Ho and Probstein, Herring, Hayes and Probstein, and Van Dyke are in general agreement and predict a much smaller effect of external vorticity than Ferri et al. and Cheng. Herring's results are in fair agreement with Ho and Probstein except that his results fall abruptly to one. Van Dyke's inner and outer expansion technique gives results, for the effect of external vorticity only, which are roughly twice those given by Hayes and Probstein's vorticity interaction theory.

The ratio of shock layer to boundary-layer heat transfer is not only a function of Reynolds number but is also a function of the density ratio across the shock, $\bar{\rho}$. In fact, the heat transfer ratio is dependent far more strongly on the density ratio than on the Reynolds number. This is illustrated in Figure 6. All of the theories considered, with the exception of Cheng's, indicate that the heat-transfer ratio is inversely proportional to the density ratio raised to some power greater than unity. Cheng's results show a very weak dependence on density ratio.

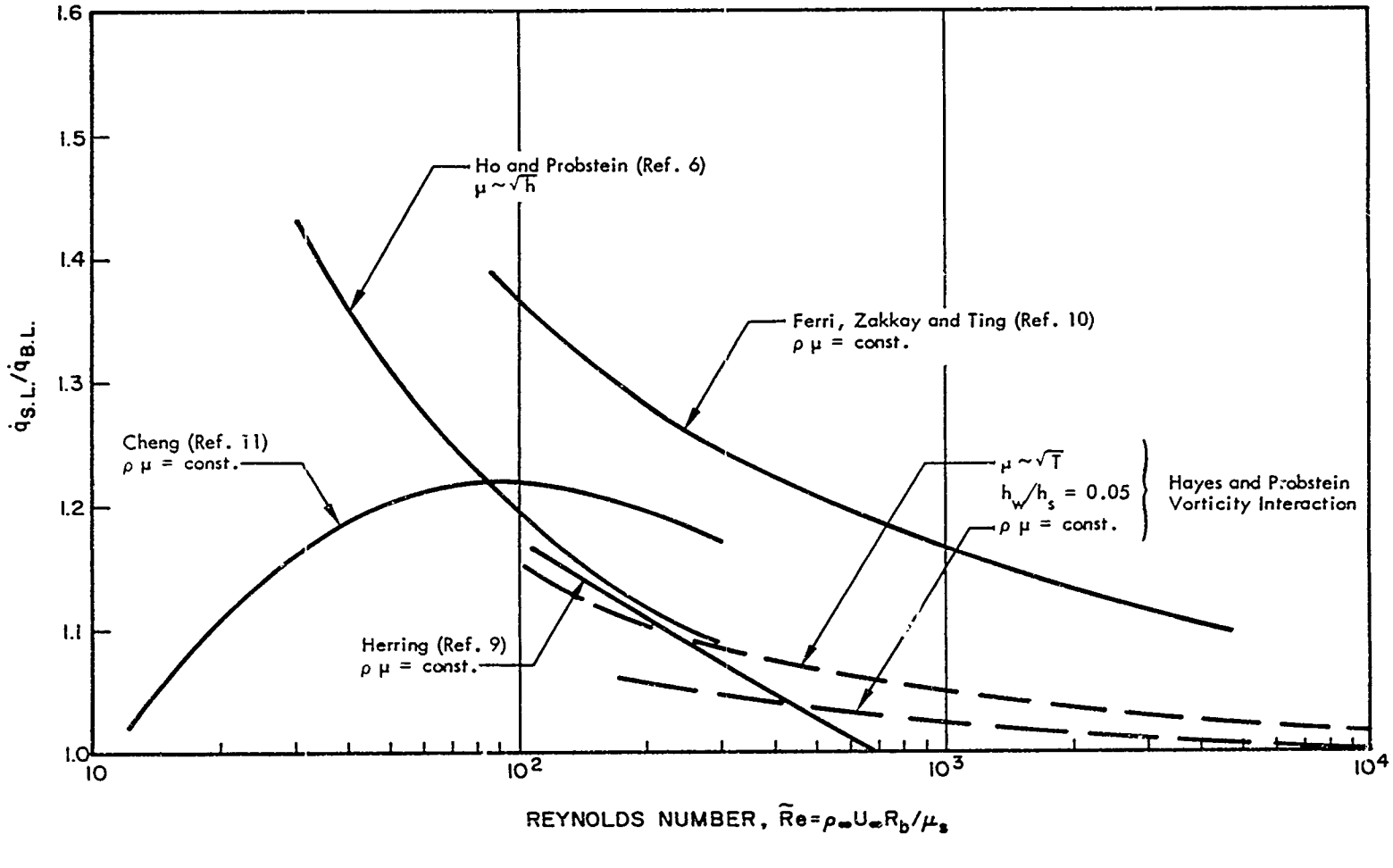


Figure 5 Comparison . Ratio of Shock Layer to Boundary Layer Heat-Transfer Results for $\bar{\rho}$ = 0.10

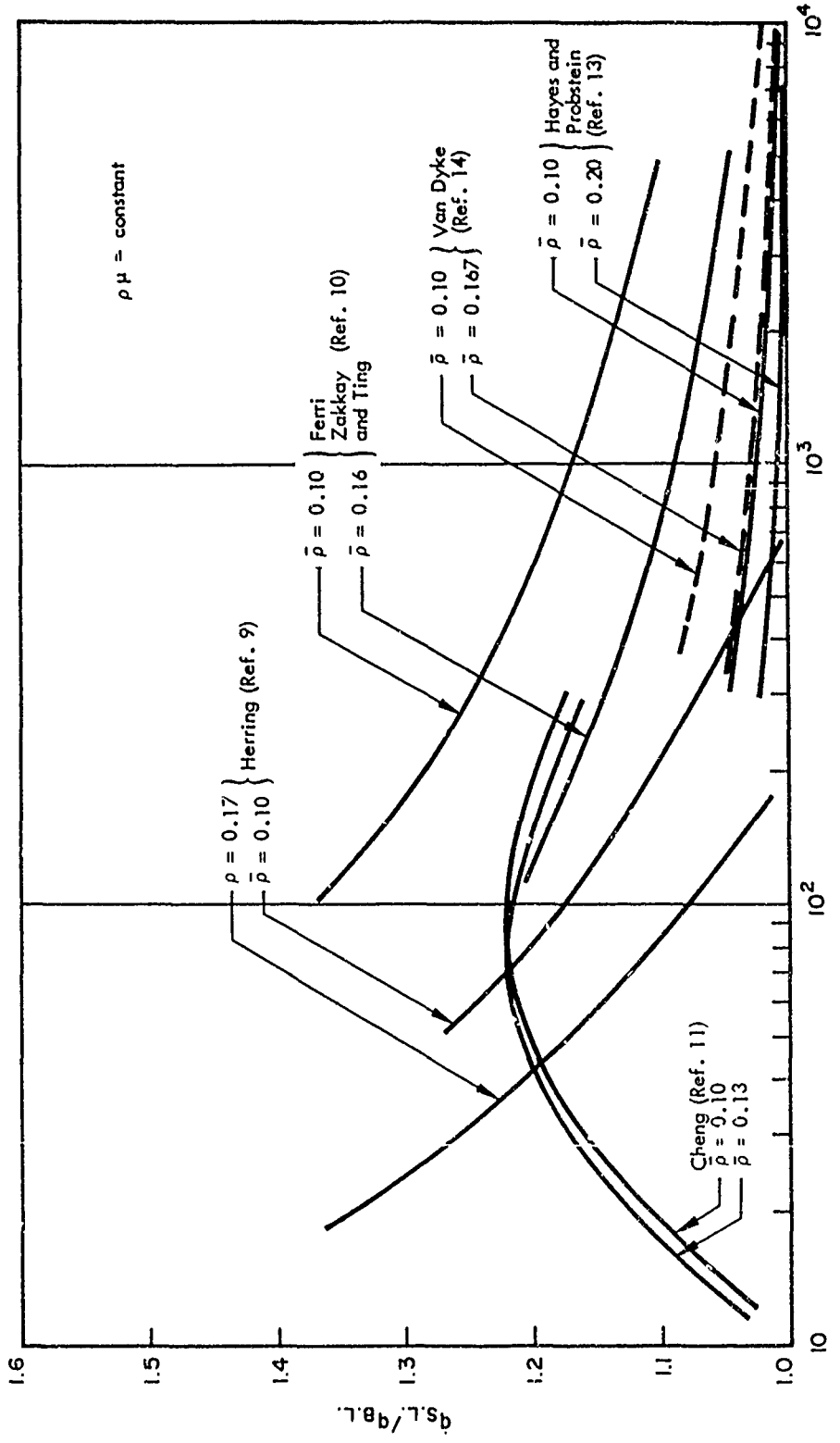


Figure 6 Effect of Density Ratio on Shock Layer to Boundary-Layer Heat-Transfer Ratio

In Figure 7, experimental data presented by Ferri and Zakkay (Ref. 18) are compared to the results of various theories. Cheng and Ferri et al. are in good agreement with the data, while Hayes and Probstein's and Van Dyke's predictions are somewhat low. Although the data were obtained for $0.153 \leq \bar{\rho} \leq 0.167$, Cheng's prediction for $\bar{\rho} = 0.13$ is used since his results are weakly dependent on $\bar{\rho}$.

SECTION III: DISCUSSION OF THE VISCOUS BLUNT-BODY PROBLEM

In all of the papers discussed above, with the exception of Van Dyke's work (Ref. 14), the bow shock shape is assumed known. Van Dyke starts with the inviscid flow obtained by neglecting the boundary layer as the first term of his outer expansion and then corrects the shock shape for the influence of the viscous layer (second term in outer expansion). This correction to the shock shape has been made to date, only at the stagnation point.

The problem presently considered is that of determining the shape of the bow shock when the shock layer is completely viscous. For a viscous shock layer, the shock shape and the shock-layer flow characteristics are closely related. This can be easily seen when one considers that cooling the shock layer reduces the shock detachment distance (Figure 1), and that small changes in the shock detachment distance can result in significant changes in the shock curvature. The reader is reminded that the pressure gradient and the vorticity behind the shock are dependent on the shock curvature. If there is a uniform reduction in the shock detachment distance, the shock curvature will not be affected. However, one would expect that the shock detachment distance will increase more rapidly than the viscous layer around a blunt body. In other words, the shock layer becomes less viscous around the body so that the reduction in shock detachment distance will be a maximum at the stagnation point and will decrease around the body. This means that the shock will be flatter than the inviscid shape with a consequent reduction in the pressure gradient and vorticity behind the shock. Hence, there is a compensating effect which will oppose the increase in heat transfer caused by the shock-generated vorticity.

In addition to the flattening of the shock near the stagnation point, the present analysis attempts to take into account the upstream influence of the flow, i.e., the stagnation point is not considered independently of the flow away from it. An integral method similar to that employed by Maslen and Moeckel (Ref. 19) in their solution of the inviscid blunt body problem is used to reduce the governing equations to a set of total differential equations. It is shown that the symmetry conditions at the stagnation point do not provide sufficient conditions to determine

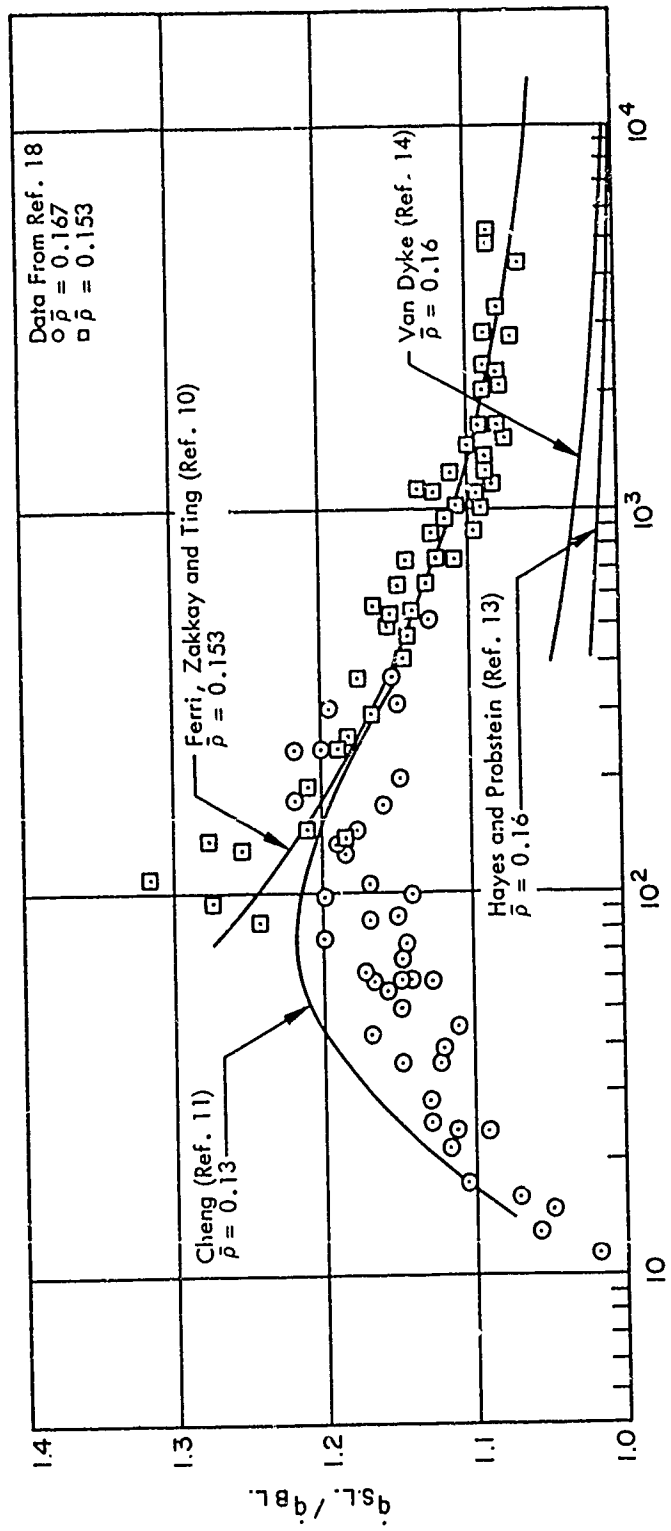


Figure 7 Comparison of Theory With Experimental Data

the shock shape. An additional boundary condition is necessary. This additional boundary condition can be considered to be the condition that all disturbances far from the body vanish or that the shock angle approach the inviscid value. In practice, these are difficult boundary conditions to satisfy. In the present analysis, a method for obtaining an approximate solution is indicated in which the downstream boundary conditions are not directly satisfied.

The air is assumed to be in equilibrium and real gas effects are taken into account. The total thermodynamic and transport property method discussed by Hirschfelder (Ref. 20) is used to include the effects of dissociation and ionization.

SECTION IV: GOVERNING EQUATIONS

In the present analysis, the gas is considered to be a continuum. The conditions under which this assumption is valid have been discussed by Hayes and Probstein (Ref. 13). According to their results, the gas behind the bow shock of a blunt hypervelocity vehicle is a continuum for free-stream Reynolds numbers greater than approximately 100 based on body radius. It is possible under certain conditions for the gas in the stagnation region to be a continuum, while away from the stagnation point, due to a flow expansion, the gas is not a continuum. This situation is not considered in this investigation.

The shock layer is assumed to be completely viscous and the Navier-Stokes equations are simplified accordingly. The shock-detachment distance from inviscid flow theory is approximately

$$\frac{\delta}{R_b} \simeq \bar{\rho}$$

and from boundary-layer theory

$$\frac{\delta_v}{R} \simeq \frac{3}{\sqrt{Re_\delta}}$$

The shock-detachment distance and viscous layer thickness are set equal to obtain

$$\bar{\rho}^2 Re_s \approx 9$$

If the upper limit in Reynolds number is arbitrarily defined by $\delta_v = 0.1\delta$ and by noting that $\rho^{-2} << 1$, the Reynolds number range in which the present analysis is valid is found to be $10^2 \leq Re_\delta \leq 10^4$.

If one neglects all terms of order $\bar{\rho}^2$ and higher, the Navier-Stokes equations in a body-oriented coordinate system (Fig. 8) can be simplified to:

x-mom

$$\left(\frac{r}{r_w}\right)^n \rho \tilde{\kappa}\left[u\frac{\partial u}{\partial x} + \tilde{\kappa}\, v\frac{\partial u}{\partial y} + \kappa\, uv\right] = -\frac{\partial P}{\partial x} + \frac{\partial}{\partial y}\left[\left\{\left(\frac{r}{r_w}\right)^n + 2\kappa y\right\}\mu\frac{\partial u}{\partial y} - \kappa\,\mu u\right] \quad (1)$$

y-mom

$$\rho\,\kappa\, u^2 = \frac{\partial P}{\partial y} \quad (2)$$

energy

$$\frac{\rho u}{\tilde{\kappa}}\frac{\partial h}{\partial x} + \rho v\frac{\partial h}{\partial y} = u\frac{\partial P}{\partial x} + v\frac{\partial P}{\partial y} + \frac{1}{r^{n}\tilde{\kappa}}\frac{\partial}{\partial y}\left(r^{n}\tilde{\kappa}\,\bar{k}\frac{\partial T}{\partial y}\right)$$

$$+ \frac{1}{r^{n}\tilde{\kappa}}\frac{\partial}{\partial y}\left[r^{n}\tilde{\kappa}\sum_i h_i\left(\frac{n_t^2}{\rho}\sum_{j\neq i} M_i M_j D_{ij}\frac{\partial X_j}{\partial y}\right)\right]$$

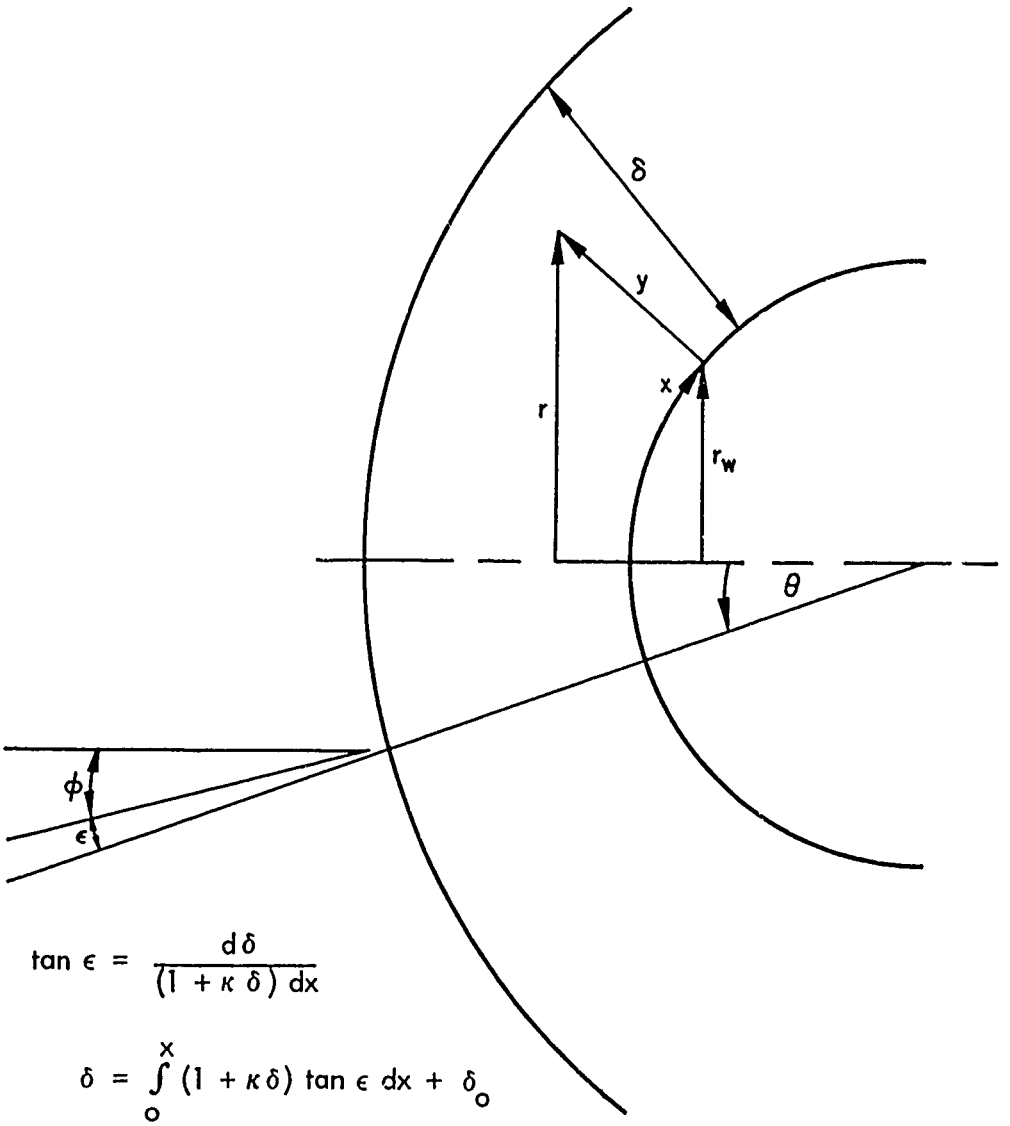
$$+ \mu\left[\tilde{\kappa}\frac{\partial}{\partial y}\left(\frac{u}{\tilde{\kappa}}\right)\right]^2 \quad (3)$$

cont.

$$\frac{\partial}{\partial x}(r^n \rho u) + \frac{\partial}{\partial y}(r^n \tilde{\kappa} f v) = 0 \quad (4)$$

where diffusion due to temperature and pressure gradients and external forces have been neglected and where $n = 1$ and $n = 0$ for axisymmetric and plane flow, respectively.

Note that the above equations are just the boundary-layer equations with the addition of the curvature terms. A body-oriented coordinate system is used, since a direct solution to the viscous blunt-body problem is sought, i.e., for a specified body shape, the shock shape and flow field are to be determined.



$$\tan \epsilon = \frac{d\delta}{(1 + \kappa \delta)\, dx}$$

$$\delta = \int_0^x (1 + \kappa\delta) \tan \epsilon \, dx + \delta_o$$

$$r = r_w + y \sin \theta$$

Figure 8 Body-Oriented Coordinate System

The above equations should be valid as long as the entire shock layer remains viscous. This implies that the shock layer must everywhere be thin. Such is the case for a blunt-nosed cone many nose-diameters downstream of the stagnation point. On a hemisphere-cylinder, the present analysis is valid only up to the shoulder. Downstream of the shoulder, the flow will be inviscid behind the shock with a boundary-layer-type flow beneath it. In the inviscid region, Eq. (2) is not valid.

The energy equation can be written in a simpler form by taking the effects of dissociation and ionization into account by means of the total thermodynamic and transport property concept. This concept is discussed by Hirschfelder (Ref. 20) and utilized by Hansen (Ref. 21) to compute the properties of air. In order to make use of this concept, the molar concentration must be a function of temperature only. This is approximately true in the shock layer, since the dependence of concentration on pressure is fairly weak and the pressure variation across the shock layer is expected to be small, according to the stagnation point results of Ho and Probstein (Ref. 6). With this approximation, a total thermal conductivity can be defined which is equal to the sum of the thermal conductivity due to molecular collisions and to chemical reactions.

It is also convenient to define a total specific heat as

$$C_P = \frac{\partial h}{\partial T}$$

The enthalpy in the shock layer can also be assumed to be a function of temperature only by the same arguments used for the molar concentration. In terms of the total properties, the energy equation is

$$\frac{\rho u}{\tilde{\kappa}} \frac{\partial h}{\partial x} + \rho v \frac{\partial h}{\partial y} = u \frac{\partial P}{\partial x} + v \frac{\partial P}{\partial y} + \frac{1}{r^{n_{\tilde{\kappa}}}} \frac{\partial}{\partial y} \left(r^{n_{\tilde{\kappa}}} \frac{\mu}{Pr} \frac{\partial h}{\partial y} \right) + \mu \left[\tilde{\kappa} \frac{\partial}{\partial y} \left(\frac{u}{\tilde{\kappa}} \right) \right]^2 \qquad (5)$$

where $Pr = C_P \mu / k$ is the total Prandtl number and

$$C_P = \sum_i h_i \frac{dC_i}{dT} + \sum_i C_i \, C_{P_i} \qquad (6)$$

$$k = \bar{k} - \sum_i h_i \left(\frac{n_t^2}{\rho} \sum_{j \neq i} M_i M_j D_{ij} \frac{dX_i}{dT} \right) \qquad (7)$$

The pressure gradient terms in the energy equation can be eliminated and the energy equation written in terms of the total enthalpy by means of the two momentum equations. After some manipulations and by consistently neglecting terms of order $\bar{\rho}^2$ and higher, one obtains

$$\rho\left(\frac{r}{r_w}\right)^n\left[u\frac{\partial H}{\partial x}+\bar{\kappa}\ v\frac{\partial H}{\partial y}\right]=\frac{\partial}{\partial y}\left[\frac{\mu}{\bar{\kappa}}\left\{\left(\frac{r}{r_w}\right)^n+2\kappa y\right\}\left\{\frac{\partial H}{\partial y}+\left(\frac{1}{Pr}-1\right)\frac{\partial h}{\partial y}\right\}\right]$$

$$-\kappa\frac{\partial}{\partial y}\left(\mu u^2\right) \tag{8}$$

In this form the energy equation can be easily integrated across the shock layer.

SECTION V: INTEGRAL FORM OF THE MOMENTUM AND ENERGY EQUATIONS

The momentum and energy equations are integrated across the shock layer to reduce the governing equations to a set of total differential equations. A solution to these equations will satisfy the momentum and energy equation in the large. Only the tangential momentum and energy equation are actually integrated. The continuity equation is used to eliminate the normal velocity component, while the normal momentum equation is used to manipulate the pressure gradient term into a form suitable for integration. The analysis at this point follows closely the work of Maslen and Moeckel (Ref. 19) for the inviscid flow about a blunt body. The addition of the viscous terms presents no difficulty. By means of the normal momentum and continuity equations, the tangential momentum equation can be written as

$$\frac{\partial}{\partial x}\left[\left(\frac{r}{r_w}\right)^n\rho u^2\right]-y\rho u^2\frac{d\kappa}{dx}+\frac{\partial}{\partial y}\left[\tilde{\kappa}^2\left(\frac{r}{r_w}\right)^n\rho v u\right]+\frac{n}{r_w}\tilde{\kappa}\left(\frac{r}{r_w}\right)^n\rho u^2\frac{dr_w}{dx}$$

$$=-\frac{\partial}{\partial y}\left(y\frac{\partial P}{\partial x}\right)+\frac{\partial}{\partial y}\left[\left\{\left(\frac{r}{r_w}\right)^n+2\kappa y\right\}\mu\frac{\partial u}{\partial y}-\kappa\mu u\right] \tag{9}$$

Equations (8) and (9) are now integrated across the shock layer to obtain

X - mom.

$$\frac{d}{dx}\int_o^\delta f(f-1)\frac{\rho}{\rho_{\delta,o}}\left(\frac{r}{r_w}\right)^n dy + \frac{n\tilde{\kappa}_\delta}{r_w}\frac{dr_w}{dx}\int_o^\delta f\left(\frac{\tilde{\kappa}}{\tilde{\kappa}_\delta} f - 1\right)\left(\frac{r}{r_w}\right)^n \frac{\rho}{\rho_{\delta,o}}\, dy$$

$$+ \frac{1}{u_\delta}\frac{du_\delta}{dx}\left[\int_o^\delta f(f-1)\frac{\rho}{\rho_{\delta,o}}\left(\frac{r}{r_w}\right)^n dy + \int_o^\delta f^2 \frac{\rho}{\rho_{\delta,o}}\left(\frac{r}{r_w}\right)^n dy\right.$$

$$\left. - \kappa\delta\int_o^\delta f\frac{\rho}{\rho_{\delta,o}}\left(\frac{r}{r_w}\right)^n dy\right] - \frac{d\kappa}{dx}\int_o^\delta y f^2 \frac{\rho}{\rho_{\delta,o}} dy - \kappa\delta\frac{d}{dx}\int_o^\delta f\frac{\rho}{\rho_{\delta,o}}\left(\frac{r}{r_w}\right)^n dy$$

$$= -\frac{\delta}{\rho_{\delta,o}u_\delta^2}\left(\frac{\partial P}{\partial x}\right)_\delta + \frac{1}{\rho_{\delta,o}u_\delta}\left[\left\{\left(\frac{r_\delta}{r_w}\right)^n + 2\kappa\delta\right\}\mu_\delta\left(\frac{\partial t}{\partial y}\right)_\delta - \mu_w\left(\frac{\partial f}{\partial y}\right)_w - \kappa\mu_\delta\right] \quad (10)$$

energy

$$\frac{d}{dx}\int_o f(g-1)\frac{\rho}{\rho_{\delta,o}}\left(\frac{r}{r_w}\right)^n dy + \left(\frac{1}{u_\delta}\frac{du_\delta}{dx} + \frac{n}{r_w}\frac{dr_w}{dx}\right.$$

$$\left. - \frac{1}{H_\delta - H_w}\frac{dH_w}{dx}\right)\int_o^\delta f(g-1)\frac{\rho}{\rho_{\delta,o}}\left(\frac{r}{r_w}\right)^n dy$$

$$= \frac{\mu}{\rho_{\delta,o}u_\delta}\left(\frac{r}{r_w}\right)^n\left[\frac{\tilde{\kappa}}{Pr}\frac{\partial g}{\partial y} + \left(1 - \frac{1}{Pr}\right)\frac{u_\delta^2}{2(H_\delta - H_w)}\frac{\partial(f^2)}{\partial y} - \frac{u_\delta^2}{H_\delta - H_w}\kappa f^2\right]\Bigg|_o^\delta \quad (11)$$

where

$$f = \frac{u}{u_\delta} \quad \text{and} \quad g = \frac{H - H_w}{H_\delta - H_w}$$

The compressibility effects can be reduced significantly by introducing the Dorodnitzyn variable defined by

$$\eta = \frac{\int_0^y \left(\frac{r}{r_w}\right)^n \frac{\rho}{\rho_{\delta,o}}\, dy}{\int_0^{\delta} \left(\frac{r}{r_w}\right)^n \frac{\rho}{\rho_{\delta,o}}\, dy} \tag{12a}$$

so that

$$y = \tilde{\delta} \int_0^{\eta} \left(\frac{r_w}{r}\right)^n \frac{\rho_{\delta,o}}{\rho}\, d\eta \tag{12b}$$

$$\delta = \tilde{\delta} \int_0^1 \frac{\rho_{\delta,o}}{\rho}\, d\eta - n\tilde{\delta}^2 \frac{\sin\theta}{2r_w} \left(\int_0^1 \frac{\rho_{\delta,o}}{\rho}\, d\eta\right)^2 \tag{12c}$$

where

$$\tilde{\delta} = \int_0^{\delta} \left(\frac{r}{r_w}\right)^{\eta} \frac{\rho}{\rho_{\delta,o}}\, dy \tag{12d}$$

In terms of the Dorodnitzyn variable η, the momentum and energy equations become mom.

$$\frac{d\delta^*}{dx} + n\frac{\tilde{\kappa}_\delta}{r_w}\frac{dr_w}{dx}\delta^{**} + \frac{1}{u_\delta}\frac{du_\delta}{dx}\left[\delta^* + \tilde{\delta}\int_0^1 f^2\, d\eta - \kappa\delta\tilde{\delta}\int_0^1 f\, d\eta\right] \tag{13}$$

$$-\frac{d\kappa}{dx}\tilde{\delta}^2 \int_0^1 f^2 \int_0^{\eta} \frac{\rho_{\delta,o}}{\rho}\, d\eta'\, d\eta - \kappa\delta\frac{d}{dx}\left(\tilde{\delta}\int_0^1 f\, d\eta\right) = -\frac{\delta}{\rho_{\delta,o}u_\delta^2}\left(\frac{\partial\rho}{\partial x}\right)_\delta$$

$$+\frac{\mu_\delta}{\rho_{\delta,o}u_\delta}\left[\left\{\left(\frac{r_\delta}{r_w}\right)^n + 2\kappa\delta\right\} f'(1)\frac{1}{\tilde{\delta}}\left(\frac{r_\delta}{r_w}\right)^n \frac{\rho_\delta}{\rho_{\delta,o}} - \frac{\mu_w}{\mu_\delta} f'(o)\frac{1}{\tilde{\delta}}\frac{\rho_w}{\rho_{\delta,o}} - \kappa\right]$$

energy

$$\frac{d\delta_E^*}{dx} + \left[\frac{1}{H_\delta - H_w}\frac{dH_w}{dx} + \frac{1}{u_\delta}\frac{du_\delta}{dx} + \frac{n}{r_w}\frac{dr_w}{dx}\right]\delta_E^*$$

$$= \frac{\mu_\delta}{u_\delta \rho_{\delta,o}}\left[\left(\frac{r_\delta}{r_w}\right)^n\left\{\left(\frac{r_\delta}{r_w}\right)^n + \kappa\delta\right\}\frac{1}{\tilde{\delta}}\frac{\rho_\delta}{\rho_{\delta,o}}\left\{\frac{g'(1)}{(Pr)_\delta} + \left(1 - \frac{1}{(Pr)_\delta}\right)\frac{u_\delta^2}{(H_\delta - H_w)}f'(1)\right\}\right.$$

$$\left. - \frac{\mu_w \rho_w}{\mu_\delta \rho_{\delta,o}}\frac{1}{\tilde{\delta}}\left\{\frac{g'(o)}{(Pr)_w}\right\} - \frac{\kappa\, u_\delta^2}{H_\delta - H_w}\right] \tag{14}$$

where the two momentum thicknesses are defined by

$$\delta^* = \tilde{\delta}\int_o^1 f(f - 1)\, d\eta \tag{15}$$

$$\delta^{**} = \tilde{\delta}\int_o^1 f\left(\frac{\tilde{\kappa}}{\tilde{\kappa}_\delta} f - 1\right) d\eta \tag{16}$$

and an enthalpy thickness by

$$\delta_E^* = \tilde{\delta}\int_o^1 f(g - 1)\, d\eta \tag{17}$$

The primes denote differentiation with respect to η.

In the present problem, there is only one unknown thickness, namely, the shock-layer thickness. The other unknown quantity to be determined from Eqs. (13) and (14) is the enthalpy gradient at the wall. All other quantities can be expressed in terms of the shock layer thickness and its derivatives and the wall enthalpy gradient.

SECTION VI: VELOCITY AND ENTHALPY PROFILES

Before Eqs. (13) and (14) can be solved, the integrals which appear there must first be evaluated. In order to accomplish this, the velocity and enthalpy profiles are assumed to be representable by fourth-order polynomials in η. The zero slip boundary conditions are used at the wall. Behind the shock wave, the Rankine-Hugoniot relations are employed. Cheng (Ref. 11) indicates that at the lower Reynolds number considered herein, the Rankine-Hugoniot relations should be modified to include tangential stress and heat conduction immediately behind the shock. These modifications should not affect the success or failure of the approximate solution attempted here, but may affect the magnitude of the numerical results.

The velocity and enthalpy profiles are assumed to be of the form

$$f = \frac{u}{u_\delta} = a_o(x) + a_1(x)\,\eta + a_2(x)\,\eta^2 + a_3(x)\,\eta^3 + a_4(x)\,\eta^4 \qquad (18)$$

$$g = \frac{H - H_w}{H_\delta - H_w} = b_o(x) + b_1(x)\,\eta + b_2(x)\,\eta^2 + b_3(x)\,\eta^3 + b_4(x)\,\eta^4 \qquad (19)$$

where a_1 and b_1 are functions of x only. Nine boundary conditions will be specified which will enable nine of the ten coefficients to be written in terms of the remaining coefficient. This one remaining coefficient, along with the shock-detachment distance, will be determined by solving the momentum and energy equations [Eqs. (13) and (14)].

Four boundary conditions are specified immediately behind the shock and five at the wall. The four boundary conditions used behind the shock in the body-oriented system (Fig. 8) are as follows:

(1) $u = u_\delta$ or $f(1) = 1$. (20a)

For later use note that

$$\frac{u_\delta}{u_\infty} = \sin\phi\,(\cos\theta\cos\phi + \sin\theta\sin\phi) \qquad (20b)$$

(2) $v = v_\delta$. By means of the continuity equation this boundary condition can be written as

$$\int_0^1 f\,d\eta = \frac{1}{n+1}\left(\frac{r_\delta}{r_w}\right)^{n+1} \frac{r_w}{\tilde{\delta}}\,\bar{\rho}_o\,\frac{u_\infty}{u_\delta} = F_1 \qquad (20c)$$

Equation (20c) is equivalent to an overall mass balance. The condition $v = 0$ at $y = 0$ was used to obtain Eq. (20c).

(3) $\omega = \omega_\delta$. This boundary condition is equivalent to satisfying the inviscid tangential momentum equation behind the shock. For strong shock waves

$$- \omega_\delta = \frac{1}{\bar{\rho}} (1 - \bar{\rho})^2 \, U_\infty \sin \phi \, \frac{d\phi}{ds}$$

$$\frac{d\phi}{ds} = \cos \phi \, \frac{d\phi}{dx} \, \frac{dx}{dr_\delta}$$

The vorticity can also be written as

$$- \omega_\delta = \left(\frac{\partial u}{\partial y} + \frac{u\kappa}{\tilde{\kappa}} \right)_\delta = f'(1) \, \frac{u_\delta}{\tilde{\delta}} \left(\frac{r_\delta}{r_w} \right)^n \frac{\rho_\delta}{\rho_{\delta,o}} + \frac{u_\delta \, \kappa}{\tilde{\kappa}_\delta}$$

Solving for $f'(1)$

$$f'(1) = \tilde{\delta} \left(\frac{r_w}{r_\delta} \right)^n \frac{\rho_{\delta,o}}{\rho_\delta} \left[\frac{1}{\bar{\rho}} (1 - 2\bar{\rho})(1 - \kappa\delta) \, \frac{d\phi}{dx} - \kappa \right] = F_2 \quad (20d)$$

(4) $H = H_\delta$ or $g(1) = 1$ (20e)

$$H_\delta = \frac{U_\infty^2}{2}$$

The following five boundary conditions at the wall are used:

(5) $u = 0$, or $f(0) = 0$ (20f)

(6) $f'''(0) = 0$ (20g)

This boundary condition is obtained by evaluating the momentum boundary-layer equation, without the curvature terms, at the wall. The curvature terms are unimportant near the wall. It was also assumed that near the wall, $\rho\mu = (\rho\mu)_w$.

(7) $H = H_w$ or $g(0) = 0$ (20h)

$$(8)\quad g''(0) = \left[1 - (Pr)_w\right] \frac{U_\infty^2}{H_\delta - H_w} \frac{u_\delta^2}{U_\infty^2} f'^2(0) \tag{20i}$$

$$(9)\quad g'''(0) = 3\left[1 - (Pr)_w\right] \frac{U_\infty^2}{H_\delta - H_w} \frac{u_\delta^2}{U_\infty^2} f'(0)\, f''(0) \tag{20j}$$

Boundary conditions (8) and (9) were obtained from the energy equation and the derivative of the energy equation, evaluated at the wall, under the same assumptions used to obtain boundary condition (6).

The above boundary conditions are all expressed in terms of known functions of body geometry, the shock-detachment distance, and the shock angle and its derivative.

The velocity and enthalpy profiles can now be written as

$$\frac{u}{u_\delta} = f = \left(10 F_1 + \frac{2}{3} F_2 - \frac{14}{3}\right)\left(\eta - \frac{9}{4}\eta^2 + \frac{7}{8}\eta^4\right) + 15 F_1\left(\frac{1}{2}\eta^2 - \frac{1}{4}\eta^4\right) + \frac{1}{4} F_2 \eta^4 - \frac{3}{2}\eta^2 + \frac{3}{4}\eta^4 \tag{21}$$

$$\frac{H - H_w}{H_\delta - H_w} = g = b_1(\eta - \eta^4) + \frac{U_\infty^2}{2(H_\delta - H_w)}\left[1 - (Pr)_w\right]\left(\frac{u_\delta}{U_\infty}\right)^2 \left(10 F_1 + \frac{2}{3} F_2 - \frac{14}{3}\right)^2 \times \left[(\eta^2 - \eta^4) + \frac{9}{2}(-\eta^3 + \eta^4)\right] + \frac{3}{2}\frac{U_\infty^2}{H_\delta - H_w}\left[1 - (Pr)_w\right]\left(\frac{u_\delta}{U_\infty}\right)^2 \left(10 F_1 + \frac{2}{3} F_2 - \frac{14}{3}\right)(5F_1 - 1)(\eta^3 - \eta^4) + \eta^4 \tag{22}$$

where F_1 and F_2 are defined by Eqs. (20c) and (20d).

The momentum and enthalpy thicknesses from Eqs. (15) and (17) become

$$\frac{\delta^*}{\delta} = 1.3492 F_1^2 + 0.0034 F_2^2 + 0.0450 F_1 F_2 - 1.5608 F_1 - 0.0570 F_2 + 0.3076 \tag{23}$$

$$\frac{\delta^* E}{\tilde{\delta}} = (0.3373\, b_1 - 0.9206)\, F_1 - (0.0033\, b_1 + 0.0106)\, F_2$$

$$+ 0.0013\, b_1 + 0.1376 + \left(\frac{u_\delta}{U_\infty}\right)^2 \frac{H}{H_\delta - H_w}\left[1 - (Pr)_w\right]\left[-0.6184\right.$$

$$+ 1.2582\, F_1 + 0.2820\, F_2 - 0.2824\, F_1 F_2 + 0.2309\, F_1^2$$

$$- 0.0430\, F_2^2 - 0.2771\, F_1^2 F_2 + 0.0153\, F_2^2 F_1 - 0.1928\, F_1^3$$

$$\left. + 0.0022\, F_2^3\right] \qquad (24)$$

In the remainder of this analysis, the two momentum thicknesses, δ^* and δ^{**}, are set equal.

SECTION VII: FLUID PROPERTIES

The present analysis is valid for a dissociated as well as for an ionized gas. The only restriction is in the availability of total thermodynamic and transport properties. Since the flow immediately behind the shock is assumed to be inviscid, the Rankine-Hugoniot relations are also necessary inputs for this analysis.

Hansen (Ref. 21) has calculated the properties of air for temperatures up to 15,000°K over a wide range of pressures. His results for the appropriate properties can be approximated by empirical relations. These approximations are valid for wall temperatures less than 1500°K, for flight velocities less than 45,000 fps, and for all stagnation pressures normally encountered in flight. The density-viscosity ratio is approximated by

$$(\rho\mu)_w/(\rho\mu)_\delta = 0.9(h_w/h_\delta)^{0.367} \qquad (25)$$

where the static enthalpy cooling ratio is approximated by

$$\frac{h_w}{h_\delta} = \frac{h_w}{H_\delta \cos^2\phi} \simeq \frac{h_w}{H_\delta \cos^2\theta} \qquad (26)$$

The density variation across the shock layer, ρ_δ/ρ, appears only in the integrand in Eqs. (13) and (14). Hence, a rough approximation for ρ_δ/ρ will suffice. The density is approximated by

$$\frac{\rho_\delta}{\rho} = 0.1 + 0.9\left[g - f^2\left(\frac{u_\delta}{U_\infty}\right)^2\right] \tag{27}$$

where the effect of the small pressure variations across the shock layer has been neglected.

In addition to the property variation across the shock layer, the variation along the shock wave is necessary. In particular, the variations of viscosity and density along and immediately behind the shock are required. The viscosity is approximated by

$$\frac{\mu_\delta}{\mu_{\delta,o}} = \left(\frac{h_\delta}{H_\delta}\right)^{0.36} \approx (\cos\phi)^{0.72} \tag{28}$$

The density variation, $\rho_\delta/\rho_{\delta,o}$, cannot be conveniently approximated by a simple function and is therefore used in tabular form.

SECTION VIII: APPROXIMATE METHOD OF SOLUTION

The momentum and energy equations, Eqs. (14) and (15), contain several auxiliary functions which are conveniently treated as additional dependent variables. There are a total of nine dependent variables so that the problem is now one of solving nine simultaneous first-order equations. The boundary conditions for these equations are obtained from symmetry conditions at the stagnation point and limiting forms of the differential equations valid only at the stagnation-point. It is thus found that all but one of the necessary boundary conditions are given at the stagnation point. An additional boundary condition downstream of the stagnation point is necessary. This situation is similar to that found in attempting to solve the direct inviscid blunt-body problem (Ref. 13). In the inviscid case, a singularity exists near the sonic point which serves as a downstream boundary condition. This singularity is attributed to the fact that the flow field changes from an elliptic to a hyperbolic one across the sonic line. Since no such change occurs within the entire shock layer for the viscous case, a downstream singularity should probably not be expected. In the viscous case, the requirement that far from the body the shock

angle should approach the inviscid value and that disturbances behind the shock vanish, do exist but these conditions are quite difficult to satisfy.

It should be noted that if the shock curvature at the stagnation point is assumed known, the need for an additional boundary condition is eliminated and the solution can be locally determined at the stagnation point. This is the important assumption made by the majority of the authors discussed in the previous sections. With the stagnation point solution in hand, the equations can be integrated around the body. A serious objection to this scheme is that it does not allow for any upstream influence.

In the present analysis, a guess is made for the stagnation-point detachment distance which will, in principle, enable the equations to be integrated around the body. The shape of the shock wave will then be monitored to see if another normal shock develops or if the shock turns into the body. The initial guess for the shock detachment distance will then be adjusted until a smooth shock wave develops. Current expectations are that the downstream shock shape will be sufficiently sensitive to the initial guess for the shock-detachment distance that, for practical purposes, the adjustments can be ignored. Furthermore, it is expected that the shock-shape variations will be minor during these adjustments until a downstream normal shock suddenly develops or the shock turns rapidly into the body.

No numerical solutions have yet been obtained. The equations are currently being programmed for solution on a high-speed digital computer.

SECTION IX: REFERENCES

1. Ferri, A. and Libby, P.A., "Note on an Interaction Between the Boundary Layer and the Inviscid Flor," J. Aeronaut. Sci., Vol. 21, No. 2. 1956. p. 130.

2. Mark, R. M., "Effect of Externally Generated Vorticity on Laminar Heat Transfer," J. Aeronaut. Sci., Vol. 24, No. 12. 1957. pp. 923–924.

3. Kemp, N. H., "Vorticity Interaction at an Axisymmetric Stagnation Point in a Viscous Incompressible Fluid," J. Aero/Space Sci., Vol. 26, No. 8. 1959. pp. 543–544.

4. Lockheed Missiles and Space Division, Higher Approximations in Boundary-Layer Theory, by M. Van Dyke, LMSD-703097, Sunnyvale, Calif., October 1960.

5. Probstein, R. F., and Kemp, N. H., "Viscous Aerodynamic Characteristics in Hypersonic Rarefied Gas Flow," J. Aero/Space Sci., Vol. 27. 1960. pp. 174–192.

6. Ho, H. T., and Probstein, R. F., The Compressible Viscous Layer in Rarefied Hypersonic Flow, Brown University, ARL TN 60-132, August 1960.

7. Oguchi, H., "Hypersonic Flow Near the Forward Stagnation Point of a Blunt Body of Revolution," J. Aero/Space Sci., Vol. 25, No. 12. December 1958. pp. 789–790.

8. Lockheed Missiles and Space Division, Shock-Generated Vorticity Effects at Low Reynolds Numbers, by H. Hoshizaki, LMSD-48381, Vol. 1. January 1959. pp. 9–43.

9. Herring, T. K., "The Boundary Layer near the Stagnation Point in Hypersonic Flow Past a Sphere," J. Fluid Mech., Vol. 7. 1960. pp. 257–272.

10. Ferri, A., Zakay, V., and Ting, L., Blunt Body Heat Transfer at Hypersonic Speeds and Low Reynolds Numbers, Polytechnic Institute of Brooklyn, ARL TN 60-140, June 1960.

11. Cheng, H. K., Hypersonic Shock-Layer Theory at the Stagnation Region at Low Reynolds Number, Cornell Aeronautical Laboratory, Inc., Report No. AF-1285-A-7, April 1961.

12. Murray, J. D., The Boundary Layer on a Flat Plate When the Main Stream has Uniform Shear, Harvard Univ. Div. Eng. Appl. Phys., June 1958.

13. Hayes, W. D., and Probstein, R. F., Hypersonic Flow Theory, New York, Academic Press, 1959, pp. 372, 388–394, and Chapters 5 and 6.

14. Van Dyke, M., Second-Order Boundary-Layer Theory For Blunt Bodies in Hypersonic Flow, Proceedings of the ARS International Hypersonic Conference at MIT, August 16–18, 1961.

15. Lockheed Missiles and Space Division, Supersonic Flow Around Blunt Bodies – An Extension of Van Dyke's Technique. by M. Vinokur and R. W. Sanders. LMSD-48381, Vol. I. January 1959. pp. 41–56; also private communications with authors.

16. Fay, J. A., and Riddell, F. R., "Theory of Stagnation Point Heat Transfer in Dissociated Air," J. Aero. Sci., Vol. 25. 1958. pp. 73–85.

17. Reshotko, E., and Cohen, C. B., Heat Transfer at the Forward Stagnation Point of Blunt Bodies, NACA TN 3513, July 1955.

18. Ferri, A., and Zakkay, V., Measurements of Stagnation Point Heat Transfer at Low Reynolds Numbers, Polytechnic Institute of Brooklyn, Aero. Eng. Appl. Mech., Report No. ARL 38, April 1961.

19. Maslen, S. H., and Moeckel, W. E., "Inviscid Hypersonic Flow Past Blunt Bodies," J. Aero. Sci., Vol. 24, No. 9. September 1957. pp. 683–693.

20. Hirschfelder, J. O., "Heat Transfer in Chemically Reacting Mixture, I," J. Chem. Phys., Vol. 26, No. 2. February 1957.

21. Hansen, C. F., Approximations for the Thermodynamic and Transport Properties of High-Temperature Air," NASA TR R-50, 1959.

SESSION IV

STRUCTURES

Chairman: Mr. Martin Goland
Southwest Research Institute

A SURVEY OF STRUCTURAL DESIGN PROBLEMS IN A COMBINED THERMAL AND LOAD ENVIRONMENT

Robert S. Levy, Harold Switzky, Marvin Forray,
Malcolm Newman, and Claus J. Meissner

REPUBLIC AVIATION CORPORATION
Applied Research and Development Department

ABSTRACT

A survey is presented outlining the structural design problems introduced by aerodynamic heating of flight vehicle structures. Thermoelastic problems in beams, plates, and shells are reviewed. Comments are made upon structural stability and the effects of nonlinear material behavior. An attempt is made to define those problem areas which have been adequately treated analytically and/or empirically and the areas requiring additional research. The application of digital and analog computers to these problems is also discussed.

A SURVEY OF STRUCTURAL DESIGN PROBLEMS IN A COMBINED THERMAL AND LOAD ENVIRONMENT

INTRODUCTION

Modern aerospace vehicles, and those which are currently being planned, present the structures engineer with a variety of new problems, many of which result from the effects of aerodynamic heating. The two main effects of elevated temperature are the introduction of thermal stresses and distortions into the structure and reduction of the strength and rigidity of structural materials. It is the purpose of this paper to survey and review the methods of analysis available for treating structural elements and assemblies subjected to thermal stress and mechanical load.

Since plates, shells, and beams are three main categories which include most strucutral elements of aerospace structures, the major portion of this discussion is devoted to methods for determining stresses and deflections of these components in the presence of thermal gradients and mechanical load. A brief discussion of the bending and slab problems of plates is followed by comments on the various cases which have been solved. Many solutions are available within the limiting assumptions of small deflection theory and uniform, isotropic material behavior. Some work has been done in applying large deflection theory to circular and rectangular plates.

Many thermo-mechanical shell analyses which have been adequately treated in the literature are described. It is found that these are largely limited to axisymmetric problems of thin shells assuming small deflection theory and uniform material properties. Some problems involving asymmetrical temperature and temperature-dependent material properties are discussed. A review is made of recent advances in buckling analysis of thin cylindrical and conical shells.

The problems of beams subjected to thermal and mechanical loads are discussed with reference to the differences between the engineering beam theory solutions and "exact" elasticity solutions. Simple engineering analysis methods are indicated which are considered valuable for many practical problems.

A brief general discussion of stability is included which points out the dependence of stability analysis upon the material deformation characteristics. Special mention is made of the nonlinear and time-dependent relationships which are so important in many structures designed to operate at elevated temperatures. Note is made of the fact that most of the work in this field has been for columns under relatively simple conditions and that much more extensive studies are required.

The last section discusses the valuable contributions made by various types of computers and the relative advantages of digital and analog types are considered. The methods of solution employed by the various computers in applications to thermal and mechanical load problems are briefly described.

A complete survey of structural design problems in a combined thermal and load environment would have to be much more extensive than the necessarily limited scope of the present paper. Among the important problem areas left to others are the effects of load-temperature history on structural materials. Short time and cumulative damage to the physical properties at room and elevated temperature are of major importance, including creep, fatigue, and the phenomena (thermal fatigue and creep fatigue) resulting from thermal cycling and thermally induced vibrations. Also omitted are discussions of design procedures for minimizing thermal stresses and the important problems of limit analysis associated with the fracture or collapse of a structure under "ultimate" combinations of heat and load. No mention is made of what may be one of the most difficult and sensitive problems of all, the definition of the design criteria by which the structural adequacy may be judged; general criteria must be established for each type of vehicle and specific criteria for each model.

SECTION I: THERMO-ELASTIC INVESTIGATIONS

A. THERMO-ELASTIC ANALYSIS OF PLATES

A plate is defined as a non-rigid three dimensional structure in which one dimension, the thickness, is much smaller than the remaining two dimensions.

The classical theory of plates is based upon the following assumptions:

(1) The material is assumed to be homogeneous, isotropic, and to obey Hooke's Law.

(2) The constant thickness of the plate is small compared to its other dimensions.

(3) The deflections of the plate are limited in magnitude and are of the order of the plate thickness. It can be shown that this restriction means that the effects of the normal deflections upon stretching of the middle plane of the plate are negligible. Therefore only negligible stresses are induced in the median plane of the plate when the plate is loaded normally.

(4) Plane sections which before bending are normal to the median plane of the plate remain, under the above conditions, plane and normal to the median plane after bending. (Figure 1).

(5) The normal stresses through the thickness of the plate are negligible because the surface loads are small compared to the bending stresses induced in the plate.

There are three kinds of thermal-mechanical problems.

- Bending Problems - occur when the temperature varies in the thickness direction and the mechanical loads are normal pressures.

- Slab Problems - occur when the plate is loaded by mechanical forces parallel to the middle plane of the plate which are uniform through the thickness and the temperature varies in the planform direction only. This is a plane-stress problem.

- Instability Problems - take place when there is edge restraint to expansion in the direction parallel to the middle plane of the plate.

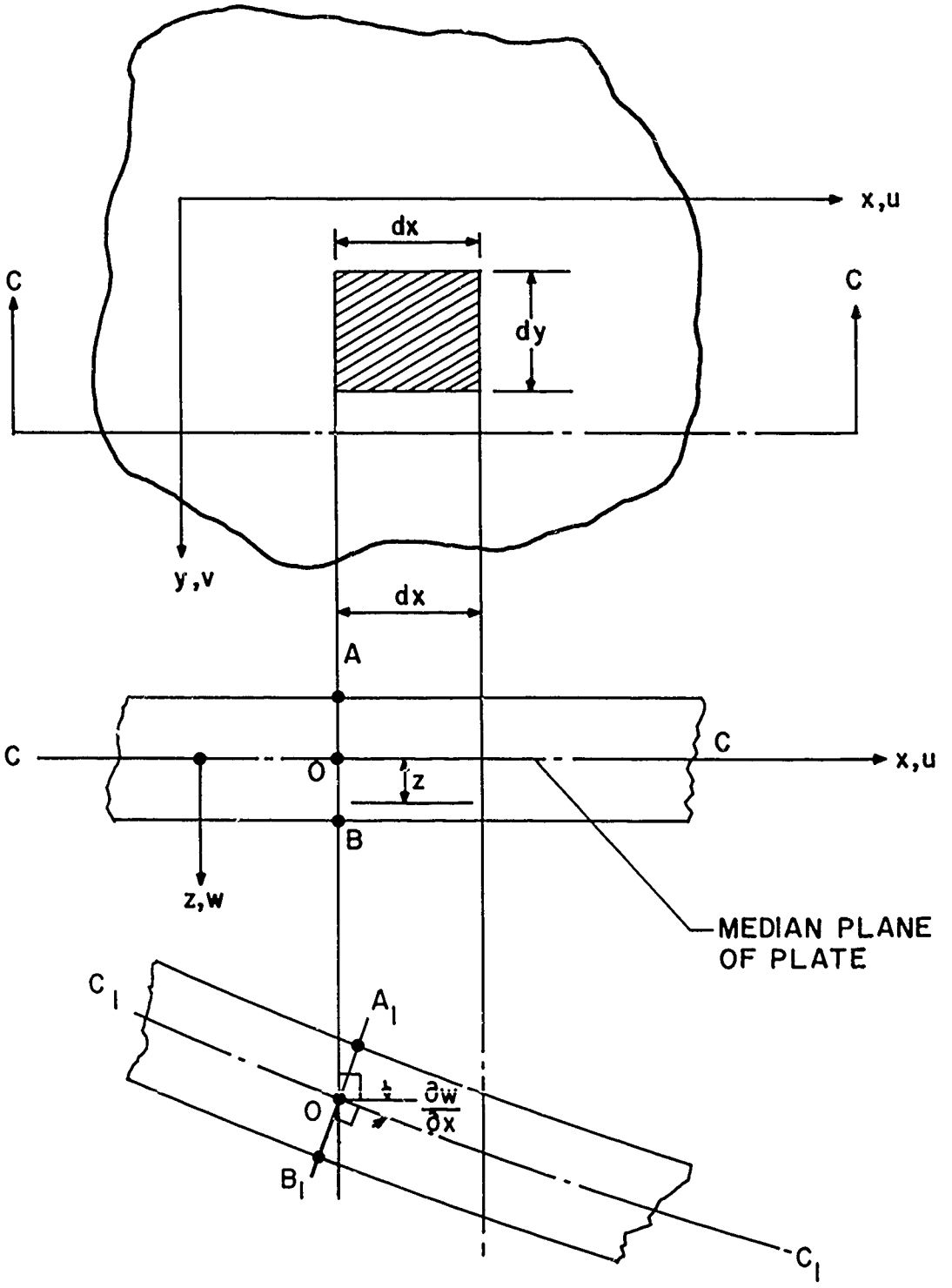


FIGURE I. CROSS SECTION OF PLATE BEFORE AND AFTER DEFORMATION

The direct approach to plate problems (as well as other thermo-elastic problems) is to derive the equations of equilibrium of forces and compatibility of displacements. These equations are in the form of differential equations which must be solved subject to prescribed boundary conditions.

1. Bending Problems - Small Deflections

The differential equation governing the bending problem (for plates of constant thickness and material properties in the absence of midplane forces or restraints) is

$$D\nabla^4 w = P - \frac{1}{1-\nu}\nabla^2 M_T \tag{1}$$

where P is the normal pressure, and where D and M_T are given, respectively, by

$$D = \frac{Eh^3}{12(1-\nu^2)} \qquad \text{(Plate flexural rigidity)}$$

$$M_T = \alpha E \int_h Tz\,dz\,. \qquad \text{(Thermal moment)}$$

Equation (1) must be solved subject to the appropriate boundary conditions.

a. Circular Plates

1) The axisymmetric bending problem

Explicit solutions (1)*are readily obtained for circular plates, with arbitrary boundary conditions under temperatures varying only in the radial (r) and thickness (z) directions. In such cases Eq. (1) becomes

$$\frac{1}{r}\frac{d}{dr}\left\{ r\frac{d}{dr}\left[\frac{1}{r}\frac{d}{dr}\left(r\frac{dw}{dr}\right)\right]\right\} = -\frac{\nabla^2 M_T}{1-\nu} \tag{2}$$

and the solution is obtained by successive integration. This solution applies equally well to solid circular plates as well as circular plates with concentric holes. Formulas and curves for the deflection, moments, and shears for solid and hollow circular plates subject to a linear thermal gradient through the thickness may be found in References 2-5 where several important boundary conditions are accommodated.

---

*Numbers in parentheses correspond to the references tabulated in Section IV.

2) The asymmetrical bending problem

Comparison of Eq. (1) with the mechanical loading problem reveals that this differential equation is identical with that which would result if the plate were acted upon by an equivalent pressure (P_e) given by

$$P_e = P - \frac{1}{1-\nu} \nabla^2 M_T . \tag{3}$$

The solution of the asymmetrical mechanical problem was originally developed by Reissner (6). The application of this theory to the asymmetrical thermal problem, restricted only to a linear gradient through the thickness with a general temperature distribution over the planform, may be found in Reference 7. Furthermore, the extension to a completely general three dimensional temperature distribution will be made by the same authors in a forthcoming article.

b. Rectangular Plates

A free rectangular plate subjected to a linear temperature distribution through the thickness and constant temperature over the planform is unstressed according to three dimensional - small deflection theory as well as classical plate theory. When the full expression for the curvatures are employed, the plate becomes curved and fits a sphere of a curvature directly proportional to the difference in surface temperature and inversely proportional to the thickness (8). For a rectangular plate with linear thermal gradient through the thickness and fully restrained against rotation normal to the edges, but free to expand in the midplane, the normal deflection is identically zero and the bending moments are given by

$$M_x = M_y = - \frac{E\alpha \Delta T h^2}{12(1-\nu)} \tag{4}$$

where x and y are orthogonal coordinates parallel to the edges of the plate and ΔT is the difference in surface temperature.

The corresponding problem of a rectangular plate with edges simply supported for bending may then be obtained by superposition of the fully clamped problem and the mechanical problem of a plate with uniform bending moments along the edges of magnitude $\frac{E\alpha \Delta T h^2}{12(1-\nu)}$. This problem was extended in two ways (9): the temperatures may be nonlinear through the thickness and the supports are simply supported beams offering linearly elastic restraint for translation and zero restraint for torsion.

2. Bending - Large Deflections

The post buckling behavior of rectangular plates due to a tent-like temperature distribution in one direction was investigated by Gossard, Seide, and Roberts (10). The plate was simply supported for bending but unrestrained in the plane. This was a sequel to the work done by Heldenfels and Roberts (11) where the plane stress solution corresponding to the unbuckled state was presented. Here, the critical temperature was determined, and then the post-buckling behavior is determined approximately by using a Galerkin procedure applied to differential equations which were set up by using the v. Karman large strain-displacement relations. A comparison of centerline deflections is made with experimental results for a plate of aspect ratio 1.57. The maximum deflection was approximately 0.6 of the thickness. The resulting comparison was satisfactory. However, this is approximately at the beginning of the so-called large deflection range.

The large deflection analysis for a plate strip subjected to normal pressure and heating was treated by Williams (12) Results are plotted for clamped and simply supported edge conditions in the case of uniform temperature and uniform pressures. The theory allows for the normal pressure and temperature to vary over the width but not through the thickness. In a second paper (13), Williams extended the analysis and design charts to the case where the temperature may have any distribution through the plate thickness. The assumption that plane sections remain plane is employed and the arbitrary temperature distribution is represented completely by the average temperature and the "first temperature moment" about the middle surface. The convenient nondimensional design charts cover equilibrium positions in the buckling and nonbuckling range and show maximum stress and central deflection as a function of pressure, average temperature, and thermal moment for cases of both clamped and simply supported edges.

The calculations cover the region between thick plates and membranes, namely $1 \leq \frac{\text{central deflection}}{\text{thickness}} \leq 4$.

The problem of the buckling and postbuckling behavior of a solid circular bulkhead (plate) subjected to elevated temperatures and mechanical loads was considered by Newman and Forray (14). An exact mathematical formulation within the framework of the v. Karman large strain-displacement relations is developed. The equilibrium equations and boundary conditions are derived by employing the calculus of variations for arbitrary axisymmetrical temperatures and normal distributed loading. These equations are nonlinear, ordinary differential equations which must be solved subject to prescribed boundary conditions. Numerical results and curves are presented for the special case of a simply supported circular plate with radially immovable boundaries, subject to a uniform pressure and an arbitrary temperature variation through the thickness (no planform variation).

3. Slab Problems

Slab problems are usually treated as plane stress problems, i.e., $\sigma_{zx} = \sigma_{zy} = \sigma_{zz} = 0$. The effects of the mechanical loads and temperature may be superposed.

The requirements of equilibrium and compatibility in the xy midplane are satisfied if an Airy stress function $\phi(x,y)$ can be obtained such that

$$\nabla^4 \phi = - E\alpha\nabla^2 T \tag{5}$$

where

$$\sigma_{xx} = \frac{\partial^2 \phi}{\partial y^2}, \quad \sigma_{xy} = -\frac{\partial^2 \phi}{\partial x \partial y}, \quad \sigma_{yy} = \frac{\partial^2 \phi}{\partial x^2}. \tag{6}$$

The similarity between Eqs. (5) and (1) of the bending problem is apparent where $\phi \sim w$, $E\alpha T \sim \frac{M_T}{1-\upsilon}$ so that the mathematical techniques are essentially the same for the two kinds of problems.

a. Circular Plates and Rings

The problem of a thin solid or hollow circular disk with temperature varying only with the radius (axisymmetric) case is found in Reference 15. The particular case of a circular disk with concentric hole subject to a power law temperature distribution in the radial direction was solved in Reference 16, with application to the problem of a disk mounted on a shaft. The circular plate with a central hot spot is developed in References 17 and 18.

The thermal stress problem in solid circular plates due to an asymmetrical temperature distribution over the planform and no variation through the thickness was solved by Horvay (19). This method was then applied to rings in References 20-22 where formulas and tables for the determination of stresses were presented.

b. Rectangular Plates

An approximate variational method for calculation of thermal stresses in free rectangular plates was developed by Heldenfels and Roberts (11) together with some experimental results for a tent-like variation in temperature in one direction (short direction). Singer, Anliker, and Lederman (23) used a procedure whereby the problem was reduced to that of determining the end effects of the self-equilibrating thermal stresses at the short sides of the plates. This problem

was then solved by applying the method of self-equilibrating polynomials developed by Horvay (24). This technique is applicable to plates with aspect ratio greater than two and with the temperature variation restricted to one direction. Mendelson and Hirschberg (25) employed a collocation procedure whereby the partial differential equation for the Airy stress function is satisfied everywhere in one direction but only at a finite number of points in the other direction. The problem is thereby reduced to the solution of a set of ordinary differential equations of the fourth order for some unknown functions. The main disadvantage of the collocation method is that there is an appreciable amount of computational work required in solving the simultaneous differential equations. Prezemieniecki (26) employed the characteristic functions (eigenfunctions) representing normal modes of vibration of a uniform clamped-clamped beam to determine an approximate solution for the thermal stress problem in rectangular isotropic plates. The temperatures $T = T(x,y)$ are assumed to be expressible in a double infinite series of the forementioned well-tabulated eigenfunctions (27) where the coefficients are obtained in a completely analogous manner to that of Fourier coefficients. An Airy stress function is assumed to be also expressed in a double infinite series of characteristic functions and the coefficients are obtained by satisfying differential Eq. (5). The solution of the infinite number of simultaneous linear algebraic equations is then approached by an iteration procedure. A numerical solution for a parabolic temperature variation in one direction is then obtained.

Recently, Gatewood (28) presented an interesting paper on thermal stresses in plates using a three dimensional approach rather than to make the conventional plane stress or plane strain solutions. It is assumed that the temperature is a polynomial in the thickness variable and that the normal stress "σ_z" is a polynomial in z. The temperature in the plane of the plate may be large although there is some restriction on the form. For the special case of $T = T(x,y)$ the stresses in the plane of the plate are presented as the plane stress solution plus correcting terms due to the plate thickness where the correcting terms involve the product of the temperature gradient and the ratio of the plate thickness to the plate length in the direction of the gradient. In many cases, the corrections are small even for moderately thick plates. The axisymmetric problem of a circular plate due to temperature which varies in the radial direction as a constant times a power of the radial coordinate is treated in detail.

Work is in progress for the determination of the deflections, in-plane and bending stresses of rectangular plates due to three dimensional temperature distributions $T = T(x,y,z)$. See Reference 29. The solution of this very general problem (plane stress and bending) will be done for various combinations of in-plane and bending restraints, such as no restraint for in-plane expansion and all edges simply supported for bending, etc.

4. Observations and Remarks

It should be clear that the bending and in-plane analyses of plates subject to elevated temperature has been progressing rapidly over the last ten years. There are many important problems that should be considered such as the large deflections of rectangular plates due to temperature, the thermal stresses in skew panels, and the determination of displacements and stresses in the neighborhood of discontinuities such as cutouts, local reinforcements, etc. Furthermore, the variation of the mechanical properties with temperature should be included in the analyses. Reference 30 includes this variation in the analysis of a rectangular plate with a concentric rectangular cutout subject to a two dimensional temperature distribution and uniform tensile force in each of the two directions.

B. THERMO-ELASTIC ANALYSIS OF SHELLS

Current design practices in aerospace vehicles rely heavily on the high structural rigidity typical of thin shell construction. In meeting aerodynamic, heat transfer and other functional requirements, these shells assume a variety of shapes and because of their many practical applications, shells of revolution in particular have received a considerable amount of attention in the literature. It appears that the first significant work on shells of revolution was performed by Reissner (31) who derived a convenient form of the basic differential equations for the axisymmetric deformations in spherical shells and reduced the analysis to the integration of a second order differential equation. Following this, Meissner (32, 33) generalized Reissner's work to encompass the axisymmetric deformations of shells of revolution of arbitrary shape and thickness. However, the large number of terms involved in the asymptotic integration techniques used made the solutions unwieldy for practical applications. Simplified solutions were later developed by neglecting terms of the order $\sqrt{\left(\frac{t}{R}\right)_{max}}$ compared with unity (where t is the shell thickness and R is the radius of curvature of the middle surface) and since, for most practical applications, the shell thicknesses lie in the range

$$\frac{1}{1000} \leq \frac{t}{R} \leq \frac{1}{50}$$

this assumption appears to be reasonable. The above, however, does not in itself differentiate thin shells from thick ones. Such a differentiation arises when one establishes the ratio of t/R which may be neglected as compared to unity. For most engineering purposes the criteria

$$\left[\frac{t}{R}\right]_{max} \leq \frac{1}{20}$$

may be used to distinguish thin shells from thick ones (34).

Following the pioneering work, many papers on shells appeared, most of the earlier ones being based on Love's equations (35). In recent years the literature on shells has grown at an extremely rapid pace, attracting many authors. These include for example, Reissner (36, 37) on shells of revolution, Synge, Chien and others on general tensor formulations for shells of arbitrary shape (38–40), and many more. Almost all of the literature was concerned with mechanically loaded, isothermal shells and it is only during the past ten years that a significant amount of work has appeared on the subject of thermal stresses and deformations in shells. Correspondingly, over this time period the need for practical analytical and design procedures in this area has become more acute because of the increasingly severe thermal environments being experienced by aerospace vehicles.

In analyzing thermo-elastic problems in shells, the basic shell equations for the isothermal case must be modified through the inclusion of thermal strains in Hooke's Law for the stress-strain relationships. It is pointed out by several authors (Goodier (41) for example) that, assuming constant material properties, this results in a formulation of the problem which is mathematically analogous to considering an equivalent isothermal problem with fictitious mechanical loads. To illustrate this principle, consider the general case of a thin shell in which the temperature T varies arbitrarily through the thickness t and over the surface of the shell. It can be shown that under the assumptions of thin shell theory, integrated terms $\int_t \alpha T dz$ (proportional to the local average αT through the thickness) produce thermal expansions of free elements of the shell which can be negated by the application of uniform normal stresses in the middle plane through the element thickness. However, because of curvature, additional forces normal to the shell middle surface must be applied in order to maintain equilibrium. Due to the variation of $\int_t \alpha T dz$ over the shell, tangential forces must also be applied at the middle surface to maintain equilibrium. Thus, in restoring the shell elements to their undeformed positions we have induced thermal stresses and are left with the problem of an isothermal shell loaded by normal and tangential forces. Similarly, due to integrated terms $\int_t \alpha T z dz$ (which are proportional to what is sometimes called the thermal moments), curvatures of free shell elements are produced. These are negated by moments which vary over the shell middle plane because of the variation of $\int_t \alpha T z dz$ over the shell surface. Transverse shearing forces and consequently normal forces are required for equilibrium. Again, the compatibility stresses caused by restoring the thermal deformations must be superposed upon the solution of an isothermally loaded shell.

In view of this mathematical analogy the question is raised as to what difficulties exist in practical thermo-elastic shell analysis, as distinguished from the isothermal case. One difficulty arises because the equivalent isothermal loads corresponding to a given temperature distribution are usually complex, while most isothermal solutions available in the literature consider simple surface loadings (usually uniform and normal pressure). Secondly, if the material

properties are significantly temperature-dependent and the temperature varies over the shell surface, the isothermal analogy corresponds to a shell with varying thickness. Almost all available isothermal solutions, however, consider shells of uniform thickness. Consequently, in order to obtain design information for most of the different thermo-elastic problems encountered in practice, it appears that direct formulations and solutions (either analytic or numerical) should be attempted.

1. Problem Areas Investigated

The literature contains many investigations on thermal stresses in shells. Almost all of the problems solved relate to shells of revolution (primarily cylindrical, spherical and conical configurations), both because of their importance from a practical standpoint and because of the mathematical simplification which results for this special case. It is found that the degree of complexity occurring in a given problem is intimately related to the type of temperature variation being considered. A brief survey of significant areas of investigation is presented below for the purpose of indicating, to some extent, the present state of the art. Only a small choice of the material on the subject is listed.

a. Cylindrical Shells

Problems concerning axisymmetric temperature distribution in thin cylindrical shells have received considerable attention. Timoshenko (42) shows that for a constant temperature gradient through the thickness the stresses at the inner and outer surfaces away from the shell edges are

$$\sigma_x = \sigma_\theta = \pm \frac{E\alpha \Delta T}{2(1-\nu)}$$

where σ_x and σ_θ are longitudinal and hoop stresses, respectively, ΔT is the difference between the inner and outer surface temperatures, and the positive sign refers to the outer surface. Near the edges of the cylinder, local stresses are obtained by solving the edge loading problem necessary to match the boundary conditions. Arbitrarily varying temperatures in the axial direction (but constant through the thickness) are also treated in Reference 42. In Reference 43 these results are extended to include interaction analyses between cylinders and bulkheads. Design methods for calculating wall thicknesses which result in specified radii of curvature or stress distribution are presented by Hammitt (44) for thin cylinders subjected to linear temperatures along the meridian. The edge stresses are caused by heavy edge flanges which enforce the requirement of zero edge slope and unrestrained radial deflection. Thin tubes with hot generating circles and generating lines such as can occur during seam welding, were analyzed by Den Hartog (45).

Unsymmetrical temperature distributions in thin cylinders with temperatures which vary around the circumference and through the thickness, but not along the length, are considered by Goodier (41) where other references are given. Bijlaard (46) presents the linear partial differential equations for the displacement components in thin cylindrical shells subjected to general temperature distributions (with the exception that the variation through the thickness is linear). For simply supported ends, the system of equations is solved by employing a double Fourier series for the temperature and displacements. For clamped shells, a solution is worked out using "normal functions" (47).

On the subject of thick cylindrical shells, almost all the analyses to be found in the literature are for the limiting cases of plane strain (long cylinders with no axial temperature variation) or plane stress (very short cylinders or disks). Timoshenko and Goodier (48) treat the plane strain problem for temperatures which vary arbitrarily in the radial direction. Jaeger (49) presents specific forms of this solution for the transient thermal stresses corresponding to the solutions of the following heat transfer problems:

(1) Cylinder $0 \leq r \leq a$ initially at a constant temperature T_o whose surface is kept at temperature T_1 for $t > 0$.

(2) Cylinder $0 \leq r \leq a$ initially at uniform temperature T_o with heat transfer between the cylinder and a medium at temperature T_1 for $t > 0$.

(3) The hollow cylinder with the outer surface kept at an elevated temperature T_1 and with no heat loss from the inner surface.

The plane strain solution for thermal stresses in a thick hollow cylinder subjected to a plane-harmonic (steady state) temperature distribution $T(r, \theta)$, expressed in the form of a Fourier series

$$\sum_{n=0}^{\infty} F_n(r) \cos n\theta + \sum_{n=1}^{\infty} G_n(r) \sin n\theta,$$

is given in (48) and also by Boley and Weiner (50) employing a different approach. It is shown that only the terms for which $n=0$ and $n=1$ cause stresses in the plane of the cross section. The equivalent plane stress problem for a hollow circular disk was solved for a general temperature $T(r, \theta)$ of the above form, not necessarily harmonic, by Forray (51). A Fourier series, plane strain solution (long cylinder) is also obtained by Kraus and Sonnemann (52) for the case in which the temperature decays exponentially in the radial direction and is arbitrary circumferentially. Chang and Chu (53) analyze the plane strain and plane stress problems of a metal tube with radial temperature distribution combined with internal and external pressure. The main point of departure here is that the

variation of Young's modulus with temperature is considered; E vs. T is assumed to be given graphically, and a particular example is studied. Hilton (54) likewise considered temperature dependent material properties in thick cylinders (for incompressible materials).

One of the more recent areas of investigation relating to thermal stresses in cylinders is concerned with the analysis of solid propellant grains. These are essentially thick cylinders bonded to cylindrical liners or motor casings. Analyses have been carried out in order to establish criteria which preclude bond separation or fracture due to thermal environment. Zwick (55) performed the plane strain analysis for an annular concentric rocket propellant casing case-bonded to an outer metallic cylinder. The stresses are determined for the casing when the temperature of the outer shell is suddenly changed while the inner surface is assumed to be thermally insulated. It is found that if the shell material is much stiffer than the grain material (higher elastic modulus) then, if the shell is not too thin, the maximum stress occurs either when the assembly is subjected to the new environmental temperature or else after a long exposure. Ungar and Shaffer (56) considered the same problem with the exception that both long (plane-strain) and very short (plane-stress) assemblies are studied under conditions of sudden environmental change. It is concluded that under otherwise identical conditions the bond stress in a very long assembly always exceeds that in a very short assembly. Further, for elastically stiff but thermally thin casings:

- All thermally induced stresses attain their maximum (absolute) values either immediately when the assembly is subjected to a new environmental temperature or else after a long exposure.

- The bond stresses in a given assembly, when the grain configuration and material cannot be changed, may be reduced by selecting a casing which:

  (1) is thinner and has a smaller elastic modulus.

  (2) has a smaller linear thermal expansion coefficient (to reduce the initial stress) and one more nearly equal to that of the propellant (to reduce the final stress).

- The bond stresses are virtually unaffected by changes in the Poisson's ratio of the casing material.

Parr (57) later presented the analysis for elastic stresses in a three-material composite, representing a hollow, case-bonded propellant grain, linear and motor casing. The environment consisted of internal pressure and radially varying temperature; more recently Wilson (58) employed conformal mapping and the complex variable procedure of Muskhelishvili (59) to analyze the stresses and displacements in a solid propellant grain perforated internally by a star-shaped configuration and bonded peripherally to an elastic motor casing.

Conditions of plane strain with internal pressure and uniform axial load were assumed.

b. Spherical, Conical and Other Shells

Axisymmetric analyses for solid and hollow spherical shells subject to general radial temperature distributions T(r) appear in (48) where the simplification due to spherical symmetry permits a theory of elasticity solution, valid for both thick and thin shells. Other axisymmetric analyses for spherical shells are presented by Trostel (60), McDowell and Sternberg (61) and Cowper (62) who considered a thin shell made up of several dissimilar layers, bonded together, subject to a steady temperature gradient through the thickness and uniform pressure. The problem of a conical shell under pressure and with temperature varying arbitrarily along the meridian and linearly through the thickness (axisymmetric) was treated by Huth (63) using linear theory and thin shell assumptions. The governing fourth order differential equation for the meridional shearing force was solved in terms of Thompson Functions and particular integrals, using methods developed by Meissner (32) and Meriam (64). The numerical example of a clamped cone with a temperature distribution typical of a laminar boundary layer is given. For this case there are high bending moments at the apex and boundary layer effects (sharp changes in stresses and moments) near the clamped edge. Sibiriakov (65) treats the case of a truncated cone located in a gas stream; the temperature varies exponentially along the meridian and trigonometrically around the periphery. Numerical results for the stresses are presented but an approximate semi-momentless theory (i.e., only hoop moments are considered) is used in the analysis, and further, it is assumed that hoop strains are zero. As a result, the validity of the solution appears to be questionable.

Thin ogival shells are analyzed by DeSilva (66) who determines the thermal stresses and displacement for an axisymmetric temperature distribution using Reissner's small deformation theory (37) modified to include thermoelastic effects. An asymptotic solution of the homogeneous differential equations is obtained by Langer's integration technique (67) and an approximate particular solution is given by extending Hildebrand's work (68). Numerical results for a specific example are given. Sutherland and Shook (69) derive the thermo-elasticity equations for thick shells of revolution in ogival coordinates. Tehcniques are presented for use at the boundaries and at the axis of revolution. No solutions are given and the equations are unwieldy, but numerical procedures may possibly be applicable

Langhaar and Boresi have conducted a general investigation on thermal stresses in shells (70) with the purpose of developing a theory which accommodates three-dimensional (unsymmetrical) temperature distributions. Small deflections, isotropy, linear elastic behavior, and thin shell assumptions are employed. The main results are in the form of relations between force resultants, bending moments and displacements. Special equations are found for

arbitrary cylindrical shells, circular conical shells and flat plates. The results were later applied (71) to cylindrical and shperical shells, comparing some of the results with three-dimensional elasticity solutions. Inconsistencies were found to occur because of the thin shell approximations. Radkowski et al (72) have developed a general numerical analysis for thin shells of revolution with rotationally symmetric pressure and temperature distribution. The technique permits specification of geometry by discrete data points and determines elastic stresses, strains and displacements for multi-layer, multi-sectional shells of revolution where surface loads, temperatures, thicknesses and material properties may vary arbitrarily in the meridional direction. Temperature and material properties may also vary through the thickness. The solution has been programmed and uses 2 X 2 coefficient matrices, thereby minimizing convergence problems. Comparisons are made with known exact and approximate solutions to demonstrate accuracy.

c. Thermal Buckling

Some recent investigations have been conducted on thermal buckling of cylindrical shells subjected to temperatures which vary in the circumferential direction only. Lu (73), employing Galerkin's method, performed an analysis based on an extension of Donnell's eighth order linear equation and performed tests on brass cylinders, showing good agreement with the theory for radius-thickness ratios in excess of 500. Abir and Nardo (74, 75) analyzed the same problem from a different point of view and obtained similar results. Fourier series deflection functions, satisfying the boundary conditions were substituted into Donnell's equations and by setting a determinant of the Fourier coefficients for the normal deflections equal to zero, eigenvalues for the peak buckling stresses were obtained. It was found that the peak buckling stress, that is, the maximum axial stress, is close to the critical stress of the cylinder when it is subjected to uniform axial compression if the variation of the intensity of this stress is not large within a half-wave length of the buckling pattern. To verify this conclusion, tests were run (75) on unreinforced and reinforced cylinders constructed of cold rolled steel. In general, the test results were higher than the predictions based on empirical results for uniform loading. Also presented in Reference 75 are empirical formulas and tests results for uniformly heated free-free reinforced conical shells and unreinforced conical shells heated axisymmetrically. It is concluded, on the basis of arguments presented by Hoff (76), that a free-free conical shell, with moderate taper, heated axisymmetrically with arbitrary temperature gradients, is not likely to buckle. This conclusion was supported by the experimental results.

Analytical results pertaining to buckling of axisymmetrically heated cylinders, supported elastically by an inner core (as for example, in case-bonded propellant grains), have been obtained by Zak and Bollard (77).

2. Observations and Remarks

The work that has been done up to the present time in the field of thermo-elastic and thermal buckling analysis of shells, appears to be far from adequate in meeting current design needs. Since variations in material properties with temperature can significantly affect results, a more realistic approach would be to consider such effects more fully in future investigations. Also, since analytical solutions are in many cases too complicated or unattainable, it is felt that more emphasis should be placed on the development of digital computer programs for numerical analysis (as in Reference 72). Other areas which appear to require more attention are:

(1) Thick shells of revolution.

(2) Analysis of shells subjected to arbitrary (asymmetrical) temperature distributions.

(3) Thermal buckling.

Finally, since large temperature gradients in thin shells produce large deflections, nonlinear large deflection analyses, considering large strain displacement relations, should be initiated.

C. THERMO-ELASTIC ANALYSIS OF BEAMS

The calculation of the behavior of beams under thermal and/or conventional loadings is usually performed under the Bernoulli-Euler assumption that sections which are plane and perpendicular to the axis before loading remain so after loading, and that the Poisson ratio effect may be neglected. The validity of this assumption is examined in detail in Reference 78. An extensive treatment of thermo-elastic beam analysis is presented in this excellent text, and a summary of this material is presented in Paragraphs C.1-C.4 of this section.

1. Thermal Stresses in Unrestrained Beams

The beam is referred to an orthogonal coordinate system (Figure 2) where x is the axis of centroids (if E is a variable, then the so-called centroidal elastic axis may be used). The axes y and z are orthogonal centroidal axes in the cross section. In accordance with the assumption that plane sections remain plane we write the axial displacement in the form

$$u = K_1 y + K_2 z + K_3, \tag{7}$$

where $K_1 = K_i$ (x) are to be determined from the requirement that

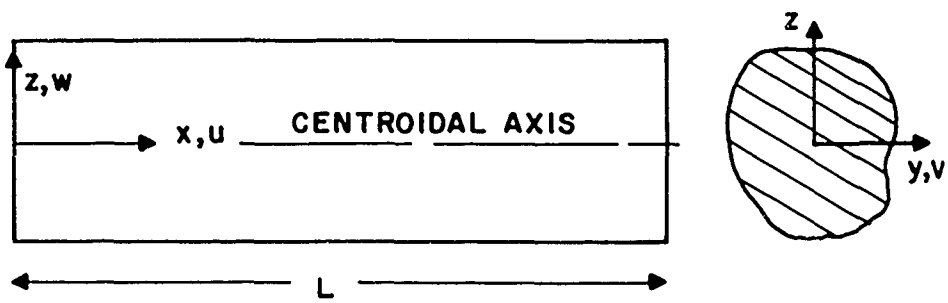


FIGURE 2. GEOMETRY AND DISPLACEMENT COMPONENTS

$$\int_A \sigma_{xx}\, dA = \int_A \sigma_{xx}\, y\, dA = \int_A \sigma_{xx}\, z\, dA = 0 \tag{8}$$

where $\sigma_{xx} = E\,(\epsilon_{xx} - \alpha T)$ and the integrations extend over the entire cross sectional area A. Equations (8) state that the resultant forces and bending moments are zero. A solution on the basis of Eqs. (8) will thus correspond in general not to zero tractions at all points of the end faces of the beams and therefore does not represent the correct solution of the problem. However, the required correction is the solution of the isothermal problem corresponding to the negative of these self-equilibrating tractions applied over the end faces. From Saint Venant's principle, the effect of this correction is small except in regions adjacent to the ends of the beam and extending over a length of the order of magnitude of the maximum cross sectional dimension.

Continuing with the solution,

$$\sigma_{xx} = E\left[K_1' y + K_2' z + K_3' - \alpha T\right] \tag{9}$$

where $(\ )' \equiv \frac{d(\ )}{dx}$. Substitution of Eq. 9 into 8 and solving for K_i' $(i = 1, 2, 3)$ yields (78)

$$\sigma_{xx} = -E\alpha T + \frac{P_T}{A} + \frac{(I_y M_{Tz} - I_{yz} M_{Ty})\, y + (I_z M_{Ty} - I_{yz} M_{Tz})\, z}{I_y I_z - I_{yz}^2} \tag{10}$$

where

$$A = \int_A dA,\quad I_z = \int_A y^2 dA,\quad I_y = \int_A z^2 dA,\quad I_{yz} = \int_A yz\, dA$$

$$P_T = \int_A E\alpha T\, da,\quad M_{Ty} = \int_A E\alpha T z\, dA,\quad M_{Tz} = \int_A E\alpha T y\, dA$$

and

$$\int_A y\, dA = \int_A z\, dA = 0$$

by definition of the term centroid. Note that if E is considered as a variable then the concept of elastic centroidal axis may be introduced where $\int Ey\, dA = \int Ez\, dA = 0$ by definition.

If, in addition, the y and z axes are chosen to be principal centroidal axes, then $I_{yz} = 0$ and

$$\sigma_{xx} = - E\alpha T + \frac{P_T}{A} + \frac{M_{Tz}y}{I_z} + \frac{M_{Ty}z}{I_y} . \tag{11}$$

The axial displacement u can be readily obtained by a simple integration. Relative to the beam end $x = 0$,

$$u(x,y,z) = \frac{1}{E}\int_0^x \left[\frac{P_T}{A} + y\,\frac{(I_y M_{Tz} - I_{yz} M_{Ty})}{I_y I_z - I_{yz}^2} + z\,\frac{(I_z M_{Ty} - I_{yz} M_{Tz})}{I_y I_z - I_{yz}^2} \right] dx. \tag{12}$$

The average axial displacement u (over the cross section) is given by

$$\bar{u} = \frac{1}{A}\int_A u(x,y,z)\,dA = \frac{1}{E}\int_0^x \frac{P_T}{A}\,dx \tag{13}$$

and in particular

$$\bar{u}\Big]_{x = L} = \frac{1}{E}\int_0^L \frac{P_T}{A}\,dx \tag{14}$$

The displacements v and w in the cross section are obtained by considering that the relative rotations of planes per unit of axial length yield the curvatures

$\frac{d^2v}{dx^2}$ and $\frac{d^2w}{dx^2}$ given by

$$\frac{d^2v}{dx^2} = - \frac{1}{E}\,\frac{(I_y M_{Tz} - I_{yz} M_{Ty})}{I_y I_z - I_{yz}^2}$$

$$\frac{d^2w}{dx^2} = - \frac{1}{E}\,\frac{(I_z M_{Ty} - I_{yz} M_{Tz})}{I_y I_z - I_{yz}^2} . \tag{15}$$

From these two differential equations, the displacements v and w in the y- and z-directions, respectively, can be obtained by integration for any given temperature distribution $T = T(x,y,z)$. In particular, for principal centroidal axis the displacement differential equations become

$$\frac{d^2v}{dx^2} = -\frac{M_{Tz}}{EI_z}$$

$$\frac{d^2w}{dx^2} = -\frac{M_{Ty}}{EI_y} \tag{16}$$

Equations (15) and (16) above constitute the small deflection equations for a free beam due to a three dimensional temperature. If the beam is loaded with transverse distributed and/or concentrated loads in addition to prescribed axial loads P, then for small deflections

$$\bar{u}]_{x=L} = \int_0^{L(P_T + P)} \frac{}{AE}\, dx \tag{17}$$

where $P > 0$ and $P < 0$ indicate tensile and compressive loads, respectively.

Similarly, if we denote the bending moments due to all these loads (and reactions) by M_z and M_y, when they cause rotation about the z and y axes, respectively, we have

$$\frac{d^2v}{dx^2} = -\frac{M_{Tz} + M_z}{EI_z}$$

$$\frac{d^2w}{dx^2} = -\frac{M_{Ty} + M_y}{EI_y} \,. \tag{18}$$

Similarly, additional axial stresses are due to the mechanical loads which must be superposed upon the stresses determined from Eqs. (10) or (11).

Several examples are shown in Reference 78, pages 314-317, where unloaded statistically indeterminate beams are solved for various boundary restraints. If, for example, a uniform beam is clamped for bending at both ends (but free for axial expansion) and subjected to a temperature $T = T(y,z)$ it is found that the deflection $w = v = 0$, while

$$\sigma_{xx} = -\alpha E T + \frac{P_T}{A} \,. \tag{19}$$

This illustrates that thermal stresses may result even when no deflections are present. Furthermore, the converse is also possible, that is, deflections may occur without there being any stresses. In fact, if

$$T = a(x) + b(x)y + c(x)z \tag{20}$$

which implies that T is linear in the cross sectional coordinates, then Eq. (10) (for unrestrained beams) yields $\sigma_{xx} = 0$. This fails to meet the requirement of general three dimensional theory (Reference 78, pp 95-97 or 83, pp 1.12-1.15) that T be linear in x as well. The comparison of the results from the elementary and more exact theories will be considered in Paragraph C.4 of this section.

2. Thermal Shear Stresses in Open Section Thin-Walled Beams

In many practical applications, the knowledge of the shear stress in beams is important. The calculation of these stress components cannot always be performed by elementary means when the beams are subjected to arbitrary thermal stimuli. However, in the case of thin-walled beams the determination of the average values of shearing stress may be accomplished by an elementary procedure.

Consider a beam of thin-walled open cross section as shown in Figure 3; the extension to closed and multicell beams may be carried out by methods analogous to those used in constant temperature problems. The thickness t may vary in general with arc length s measured from a free end, i.e., $t = t(s)$. Equilibrium of an element (Figure 4) yields the equation

$$\frac{\partial \sigma_{xx}}{\partial x} + \frac{1}{t}\frac{\partial q}{\partial s} = 0 \tag{21}$$

where $q = \sigma_{xx} t$ = shear flow. Integration yields

$$q = -\int_{s=0}^{s=s} \frac{\partial \sigma_{xx}}{\partial x}\, dA \tag{22}$$

where $dA = tds$ and the lower limit of integration has been chosen so as to satisfy the boundary condition that the shear flow be zero at the free edge $s = 0$. Substitution of Eq. (10) into Eq. (22) yields the shear flow

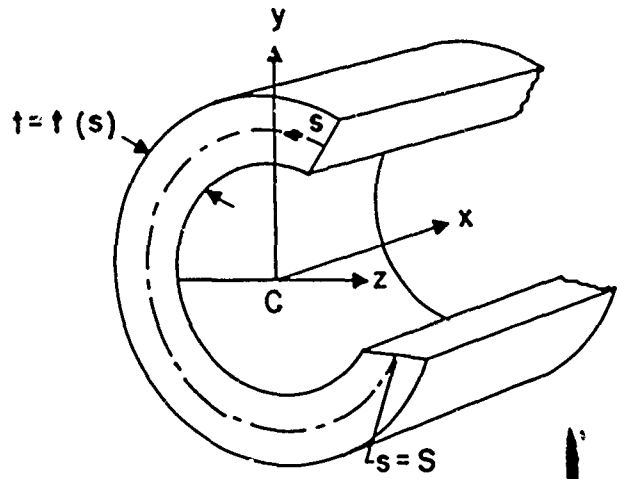


FIGURE 3. OPEN THIN-WALLED BEAM WITH POINT C AS CENTROID OF SECTION

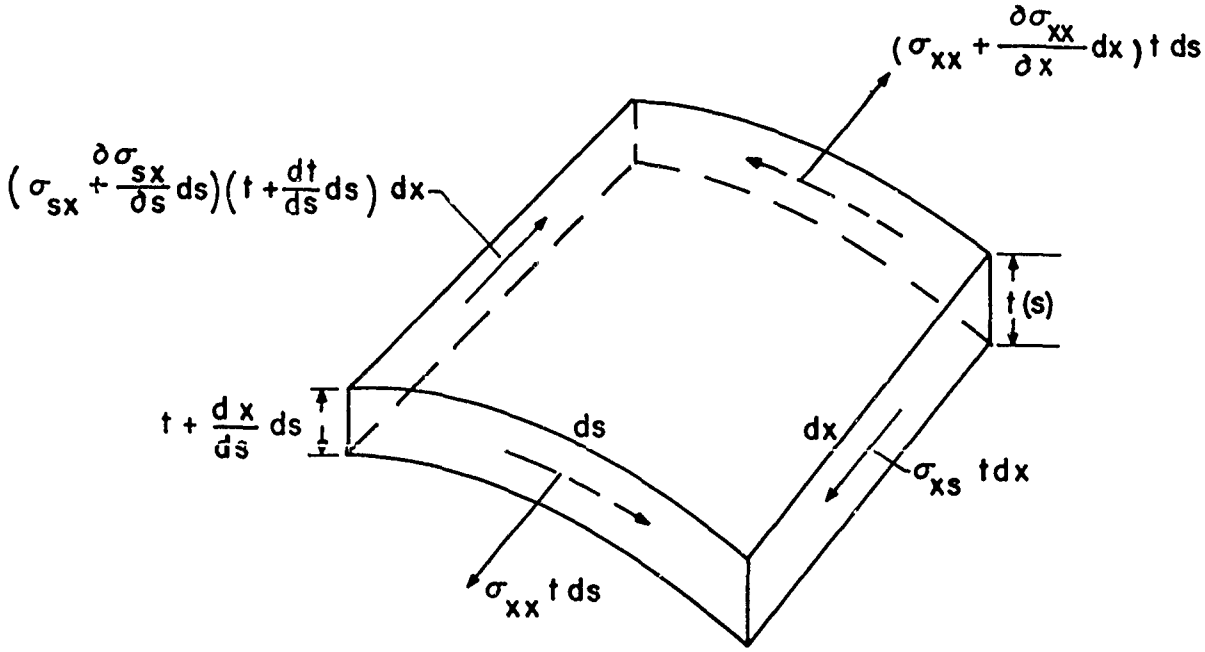


FIGURE 4. ELEMENT OF THIN-WALLED BEAM IN EQUILIBRIUM

$$q = \int_0^s \alpha E T' ds - \frac{P'_T}{A} \int_0^s t ds + Q_y \frac{I_{yz} M'_{Tz} - I_z M'_{Ty}}{I_y I_z - I_{yz}^2} + Q_z \frac{I_{yz} M'_{Ty} - I_y M'_{Tz}}{I_y I_z - I_{yz}^2} \tag{23}$$

where primes indicate differentiation with respect to x, and where

$$Q_y = Q_y(s) = \int_0^s z dA$$

$$Q_z = Q_z(s) = \int_0^s y dA \tag{24}$$

are the static moments of the portion of the cross section between $s = 0$ and $s = s$ with respect to the y and z centroidal axes. Note that $Q_y(S) = Q_z(S) = 0$ because of the choice of centroidal axes and that all the boundary conditions are satisfied. If the centroidal axes are also principal axes, then

$$q = \int_0^s \alpha E T' ds - \frac{P'_T}{A} \int_0^s t ds - \frac{M'_{Ty} Q_y}{I_y} - \frac{M'_{Tz} Q_z}{I_z} . \tag{25}$$

3. Elasticity Approach to Beam Problems

a. Rectangular Beam with Temperature Variation Through the Depth Only

This problem is solved by the semi-inverse method of elasticity. The form of the stress components are assumed as follows:

$$\sigma_{yy} = \sigma_{yx} = \sigma_{zy} = \sigma_{zx} = \sigma_{zz} = 0$$

and

$$\sigma_{xx} = \sigma_{xx}(z)$$

where z denotes the depth coordinate.

The three dimensional equations of equilibrium are satisfied identically while the compatibility equations in terms of the stress components are satisfied if, and only if,

$$\frac{d^2}{dz^2}(\sigma_{xx} + \alpha ET) = 0 \qquad \text{(constant } E\alpha \text{ is assumed).}$$

Therefore, integration yields

$$\sigma_{xx} = -\alpha ET + C_1 + C_2 z \tag{26}$$

where C_1 and C_2 are determined from the "average" boundary conditions

$$\int_h \sigma_{xx} dz = \int_h \sigma_{xx} z dz = 0 \qquad \text{(h is depth)} \tag{27}$$

which stipulates that there is no resultant force and moment on the beam. This yields finally

$$\sigma_{xx} = -\alpha ET + \frac{N_T}{h} + \frac{12zM_T}{h^3} = -\alpha ET + \frac{bN_T}{A} + \frac{z(bM_T)}{I} \tag{28}$$

where

$$N_T = \int_h E\alpha T dz \quad \text{and} \quad M_T = \int_h E\alpha T z dz$$

$$A = \text{cross sectional area} = bh$$

$$I = \frac{bh^3}{12} . \tag{29}$$

From the stress components, the strain and displacement components (outside of a rigid body displacement) are readily determined.

- Strain Components

$$\epsilon_{xx} = \frac{1}{E}\left[\frac{bN_T}{A} + \frac{z}{I} bM_T\right]$$

$$\epsilon_{zz} = -\frac{\upsilon}{E}\left(\frac{bN_T}{A} + \frac{zbM_T}{I}\right) + \frac{(1+\upsilon)\alpha T}{E} \tag{30}$$

$$\epsilon_{xz} = \epsilon_{xy} = \epsilon_{yy} = \epsilon_{yz} = 0$$

- Displacement Components (aside from rigid body displacements)

$$u = \frac{x}{E}\left[\frac{bN_T}{A} + \frac{z}{I}\,bM_T\right] \tag{31a}$$

$$w = \frac{-bM_T x^2}{2EI} - \frac{\upsilon}{E}\left[\frac{bN_T z}{A} + \frac{bM_T z^2}{2I}\right] + \alpha\frac{(1+\upsilon)}{E}\int_0^z T\,dz \tag{31b}$$

Remarks

(1) The form for the stress Eq. (28) could readily be obtained by the elementary process of restraining the elements of the beam by applying stresses equal to $-\alpha ET$ and then removing the resultant force and traction on the boundary.

(2) The solution Eq. (31a) for the axial displacement u shows that plane sections remain plane since u is linear in z.

(3) Neglecting $\left(\frac{\partial w}{\partial x}\right)^2$ in comparison to unity, we have

$$\frac{1}{R} \approx \frac{\partial^2 w}{\partial x^2} = -\frac{bM_T}{EI}$$

which means that the curvature is proportional to M_T.

(4) The preceding formulas are also simplified when the temperature distribution is either symmetrical ($T(z) = T(-z)$) or antisymmetrical ($T(z) = -T(-z)$) about the middle plane $z = 0$. For symmetrical distributions, $M_T = 0$ and the resulting curvature of the beam is zero. For antisymmetrical temperature distributions, $N_T = 0$ and the mean value of the displacement u is zero.

It is always possible to express the given temperature distribution as the sum of three components T_1, T_2, T_3 where $T_1 = a + bz$, $T_2(z) = T_2(-z)$, and $T_3(z) = -T_3(-z)$. The stresses, strains, or displacements due to T are the sum of those due to T_1, T_2, and T_3 acting separately. Since T_1 is linear, it causes strains and displacements but no stresses. The stress distribution due to T_2 above is symmetrical, while that due to T_3 is antisymmetrical.

b. Circular Beam of Rectangular Cross Section with Radial Temperature Variations

The problem is the determination of the stresses in a rectangular beam whose median line describes an arc of a circle of radius $\frac{a+b}{2}$ where b - a is the depth of section. All bounding surfaces are free of traction. The temperature variation is given by $T = T(r)$ and the stress function $\phi = \phi(r)$ is employed. The differential equation $\nabla^4\phi + E\alpha\nabla^2 T = 0$ is expressed in factored form by Boley and Weiner (78), pp 299-300, as

$$\frac{1}{r}\frac{d}{dr}\left(r\frac{d}{dr}\right)\left[\frac{1}{r}\frac{d}{dr}\left(r\frac{d\phi}{dr}\right) + \alpha ET\right] = 0 \tag{32}$$

Equation (32) is readily integrated to yield

$$\phi = A_1 \text{Log}\left(\frac{r}{a}\right) + A_2\left(\frac{r}{a}\right)^2 \text{Log}\left(\frac{r}{a}\right) + A_3\left(\frac{r}{a}\right)^2 + A_4 - E\alpha\int_a^r\left[\frac{1}{r_2}\int_a^{r_2} Tr_1 dr_1\right]dr_2 . \tag{33}$$

The boundary conditions are $\phi = \frac{d\phi}{dr} = 0$ on $r = a, b$ and the resulting force and moment on the end faces are then automatically zero. Use of Saint Venant's principle may then be employed. The stress components are readily determined by matching these boundary conditions.

Interesting checks of this solution may be made by comparing this solution with that of Timoshenko and Goodier (79), p 61, for a beam in pure bending, and for a curved beam according to the strength of materials approach (80).

4. Comparison of the Elementary Beam Solution with Two Dimensional Thermo-elastic Solution

The determination of the thermal stresses in beams has been developed from the strength of materials viewpoint (Paragraph C.1 of this section) and from an elasticity approach by applying a semi-inverse procedure (Paragraph C.3 of this section). A natural question is - how accurate is the strength of materials approach? One procedure is to solve a reasonably general problem by both procedures and to compare results. This was done by Boley in Reference 80a. The problem considered was a rectangular beam of small width b in the z direction,

and occupying the region $-c \leq y \leq c$, $0 \leq x \leq L$ where $b \ll 2c \ll L$. The plane stress solution was obtained for a temperature $T = T(x,y)$. The solution of this problem required the determination of a stress function $\phi = \phi(x,y)$ such that

$$\nabla^4 \phi + \alpha E \nabla^2 T = 0 \tag{34}$$

$$(\nabla^2 = \frac{\partial^2}{\partial x^2} + \frac{\partial^2}{\partial y^2}, \quad \nabla^4 = \nabla^2 \nabla^2)$$

with the boundary conditions

$$\phi = \frac{\partial \phi}{\partial y} = 0 \text{ at } y = \pm c. \tag{35}$$

It is further required to satisfy the average zero traction boundary conditions on $x = 0, L$ namely

$$\int_{-c}^{c} \sigma_{xx} dy = \int_{-c}^{c} \sigma_{xy} dy = \int_{-c}^{c} \sigma_{xx} y dy = 0. \tag{36}$$

This was solved by writing the stress function in the form

$$\phi = \phi_1 + \phi_2 + \phi_3 + \ldots \tag{37}$$

where the functions ϕ_i satisfy

$$\begin{aligned}
\frac{\partial^4 \phi_1}{\partial y^4} &= -\alpha E \frac{\partial^2 T}{\partial y^2} \\
\frac{\partial^4 \phi_2}{\partial y^4} &= -\alpha E \frac{\partial^2 T}{\partial x^2} - 2 \frac{\partial^4 \phi_1}{\partial x^4} \\
\frac{\partial^4 \phi_i}{\partial y^4} &= -2 \frac{\partial^4 \phi_{i-1}}{\partial x^2 \partial y^2} - \frac{\partial^4 \phi_{i-2}}{\partial x^4}, \quad \text{for } i = 3, 4, \ldots
\end{aligned} \tag{38}$$

and

$$\sigma_{xxi} = \frac{\partial^2 \phi_i}{\partial y^2}, \quad \sigma_{yyi} = \frac{\partial^2 \phi_i}{\partial x^2}, \quad \sigma_{xyi} = -\frac{\partial^2 \phi_i}{\partial x \partial y} \tag{39}$$

Each of the functions ϕ_i is to satisfy the boundary conditions of Eq. (35). Furthermore, substitution of Eq. (37) into Eq. (34) and applying Eq. (38) shows that the differential equation is satisfied. It is shown in Reference 80a that the solution for the stress component σ_{xx} may be written in terms of an infinite series, each successive term involving derivatives with respect to x of higher and higher order for the rectangular beam of width b and height 2c. Thus

$$\begin{aligned}\frac{\sigma_{xx}}{\alpha E} = &\left[-T + \frac{\int_{-c}^{c} T dA}{A} + \frac{y}{I}\int_{-c}^{c} Ty dA \right] + b\frac{\partial^2}{\partial x^2}\left\{ y\int_{-c}^{y} T dA \right. \\ &- \int_{-c}^{y} Ty dA - \frac{c}{12}\left(1 - \frac{6y}{c} + 6\left(\frac{y}{c}\right)^2\right)\int_{-c}^{c} T dA \\ &+ \frac{1}{20}\left[10 + 21\frac{y}{c} - 10\left(\frac{y}{c}\right)^2\right]\int_{-c}^{c} Ty dA - \frac{1}{4c}\int_{-c}^{c} Ty^2 dA \\ &\left. - \frac{y}{4c^3}\int_{-c}^{c} Ty^3 dA \right\} + (\text{terms containing only fourth and higher derivatives of } T \text{ with respect to } x).\end{aligned} \tag{40}$$

The term in the first bracket of the right hand side of this equation is identical with that given by the elementary solution. Therefore, it follows that this term represents the "exact" solution for temperatures which are either constant or that vary linearly along the span. However, if the temperature variation along the span is expressible as a polynomial of the second or third degree, then the term $b\frac{\partial^2}{\partial x^2}\{\quad\}$ will not be zero and there is a discrepancy between the two. Naturally, as the representation of the temperature requires more and more terms of the power series in the spanwise coordinate, additional corrections will be introduced. It is clear, however, that if the temperature distribution is smooth, i.e., if it is expressible in a rapidly convergent power series, then the contribution of the higher derivatives will be small and the strength of materials approach provides a good approximation. The same conclusion, namely that the

elementary formula for displacements is satisfactory for smooth temperature distributions, can be shown to be valid as well.

Similarly, the case of a free beam with arbitrary simply connected cross section and linear spanwise temperature distribution was considered by Boley and Tolins (81). It is shown that if the temperature T is such that

$$T = T_1 (y,z) + x\, T_2 (y,z) \tag{41}$$

then the elementary strength of materials approach gives the correct result if, and only if, $\nabla^2 T = \left(\frac{\partial^2}{\partial y^2} + \frac{\partial^2}{\partial z^2} \right) T = 0$. This means that the two results coincide when the temperature is a plane harmonic function of y and z. In particular, for a thin-walled open section, it was shown in Reference 81 that the correction required in the elementary formula is of the order of t/S where t is the thickness and S is the median line arc length in the cross section, provided that T is either constant or linear in the thickness coordinate. The solution for the general case of a beam of arbitrary cross section and arbitrary temperature has been considered by Barrekette (82) and, qualitatively, the previous discussion holds.

5. Numerical Solutions Accommodating Varying Material Properties

Methods of thermo-elastic beam analysis which account for temperature-dependent variations in Young's modulus (E) and coefficient of expansion (α) are presented by Switzky, Forray, and Newman in Reference 83, wherein the thermo-elastic equations of engineering beam theory previously discussed in Paragraph C.1 of this section (Eqs. 10-18) are solved numerically using various integration techniques. A discussion of some of these techniques follows:

a. Finite Sum Method

The beam cross section is subdivided into a finite number of small elemental areas (Figure 5), such that the variation of αT and E in each element is also small. The method is then based on solving the thermo-elastic equations for an approximate geometry consisting of a finite number of points of concentrated elastic area located at the centroids of elements. A general solution is outlined in tabular form and illustrated by a numerical example. The method is adaptable to all cross sectional shapes and the degree of accuracy increases with the decrease in the size of elements. Digital computing machines can be employed.

b. Power Series Method

The average αT profile in a direction normal to a principal bending axis is approximated by a power series of the form

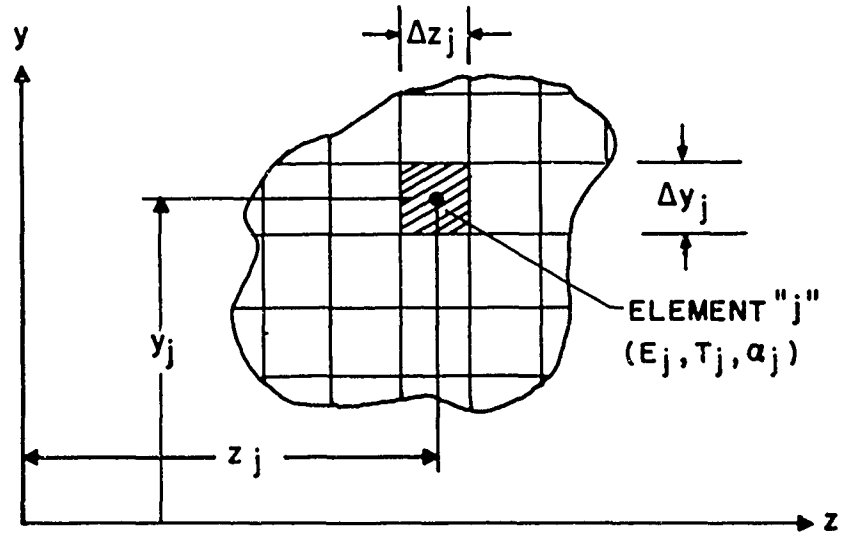


FIGURE 5. FINITE SUM METHOD - ELEMENT BREAKDOWN OF CROSS SECTION.

$$\alpha T = \sum_{L=0}^{n} a_L s^L$$

where the a_L are constant coefficients and s is the normal distance from the reference axis. A fitting technique is develcped in Reference 83, where a conversion matrix is used to determine the power series coefficients from specified αT values at discrete, equally spaced data points.

Having obtained the power series representation for the αT distribution, general solutions of the thermo-elastic beam equations are then developed for beams with two practical types of cross section geometry:

(1) Continuous elastic cross sections, where the elastic width (Eb) is monotonically continuous through the depth or on each side of a bending axis of symmetry (Figures 6(a) and (b)).

(2) Discontinuous elastic cross sections with elastic width variation of the multi-rectangular type as exemplified by tees, channels, I-Beams and built-up sections (Figure 6(c)).

c. Solution for Continuous Elastic Cross Sections

Approximate representations of continuous cross sectional geometries having monotonic elastic width variation are given by the following basic expression:

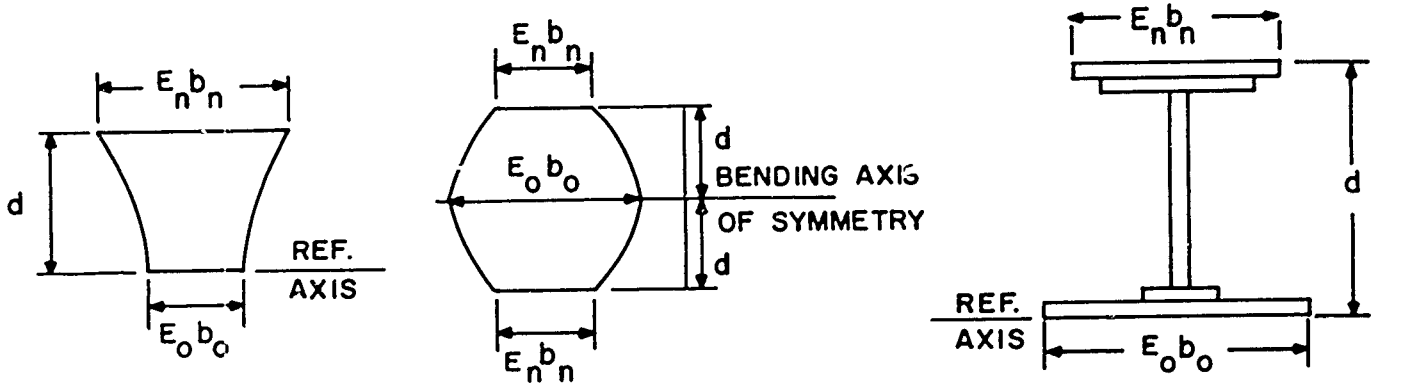
$$Eb = E_o b_o \left[1 + \beta s^K\right]; \quad \begin{matrix} \beta \geq -1 \\ K \geq 0 \end{matrix}$$

where the taper parameter (β) defines the ratio of width at the extreme fiber to the elastic width at the reference axis and the shape parameter (K) defines the type of elastic width variation. Figure 7 presents a summary of the geometric shapes represented through the complete range of the parameters.

The solution of the thermo-elastic beam equations is given in terms of these parameters and the coefficients of the power series for αT. Nondimensional design curves and an illustrative numerical example are presented.

d. Solution for Discontinuous Elastic Cross Sections

In order to systematize the solution, the geometry is expressed in terms of step parameters which define the elastic section properties. A general solution is then given in terms of these parameters and the coefficients of the power series for αT. Based on this solution, nondimensional design curves for



(a) Monotonically Continuous Elastic Width Variation

(b) Elastic Widths Monotonically Continuous and Symmetrical About the Bending Axis

(c) Multi-rectangular Discontinuous Elastic Width Variation

FIGURE 6. TYPICAL CONFIGURATIONS OF ELASTIC CROSS SECTION AREAS

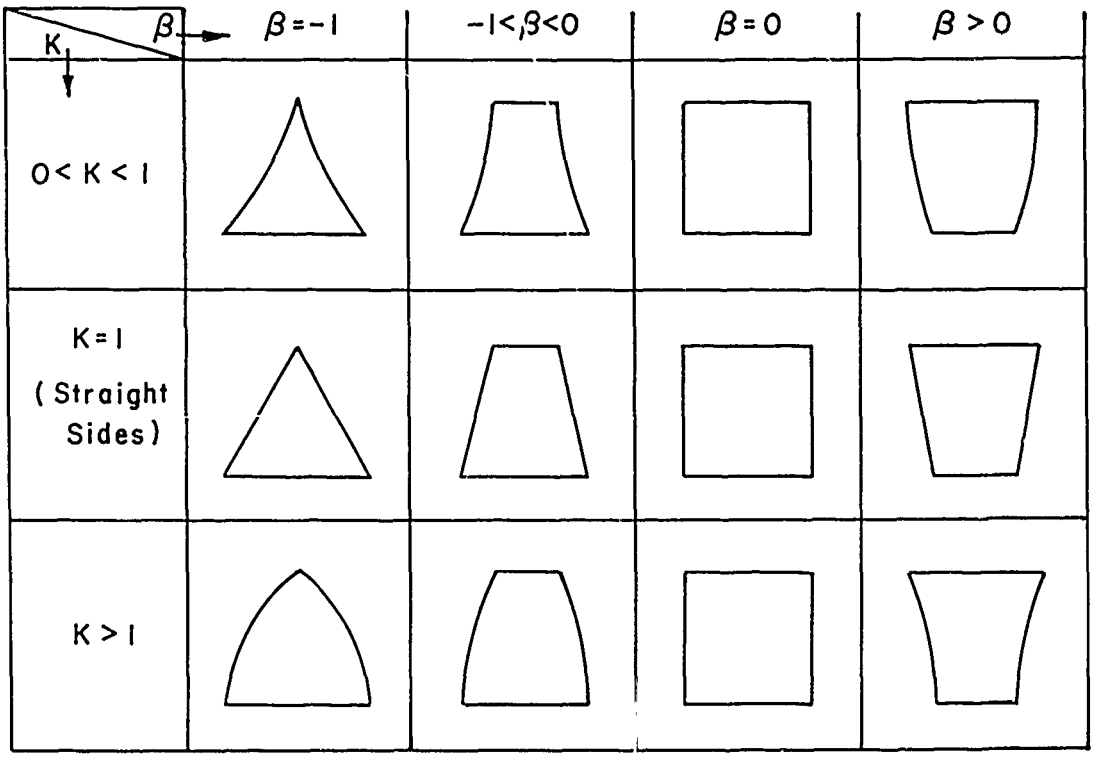


FIGURE 7. MONOTONIC GEOMETRIC SHAPES DEFINED BY PARAMETERS β AND K

I-Beams are presented and illustrative numerical examples are worked out, including the analysis for the stresses in a three-web, built-up box beam of dissimilar materials.

In general, the power series method is most applicable to problems in which the directions of the principal axes are known from symmetry and bending occurs about only one of these axes. Under such conditions, numerical computations are minimized and the power series method usually has a distinct advantage over the finite sum method.

SECTION II: STABILITY AND NONLINEAR MATERIAL BEHAVIOR

A. STABILITY

The stability of compression elements is of great importance in determining the strength and rigidity of a structure. If the applied load exceeds the load that produces general instability, the structure is obviously inadequate. However, in some cases the decrease in rigidity at loads less than the buckling load may also be critical.

As the element is loaded in compression, it becomes progressively more flexible (84) in proportion to the ratio $\frac{1}{1-\epsilon/\epsilon_{cr}}$ where ϵ is the strain and ϵ_{cr} is the strain at which the element buckles. This can produce overstressing of other regions and a reduction in the stiffness of the structure. This increases the overall deflections and lowers the natural frequency and may seriously affect the aero-elastic behavior of the vehicle.

Buckling or excessive deformations of structural elements exposed to the external airflow may cause serious consequences. Drag may be increased due to degrading the aerodynamic cleanliness. The airflow may be disturbed and may produce turbulence which increases aerodynamic heating and acoustic pressure fluctuations. The reduction in rigidity of buckled panels makes them much more vulnerable to panel flutter.

The stability of a structural element can be evaluated by observing the incremental load δF necessary to cause an instantaneous incremental deflection δw. The ratio $\delta F/\delta w$, which is a measure of the stiffness, becomes exceedingly small when the structure approaches instability. A structure of given geometry, boundary conditions, and material, can become unstable for various load-temperature time histories. In a column, for example, the external load increases the deformations of the structure and tends to reduce its stiffness because of increasing axial and bending stresses. Temperature reduces the stiffness of the material and may also introduce destabilizing thermal stresses and deflections. Time at load and temperature permits the structure to creep, increasing the axial strain, the lateral deflections, and the bending stresses, with a resultant reduction in the stiffness.

The quantitative analysis of the interaction of load, temperature, and time on the stability of a structure is quite complex. Solutions can only be obtained in a limited number of specific cases. Some other histories are amenable to approximate solution. In some cases, it is possible to estimate both upper and lower bounds to the correct solution. A general solution encompassing all types of histories cannot be expressed in a closed form (equation of state) since the structure is generally affected by its past history.

A few types of problems together with some of the proposed methods of analysis are discussed below. The problems can be roughly separated into time-independent and time-dependent categories. The time-dependent solutions avoid considering the loss in stiffness due to creep but consider in varying degrees the effects of nonlinear elastic behavior. The time-dependent solutions employ special mathematical models of the geometry and material behavior which make the problems tractable. Solutions are presented in terms of a critical time at which a structure subjected to a given load and temperature will become unstable. Most of the available solutions are for the time to failure of an idealized column subjected to constant load and temperature.

1. Time-Independent Solutions

a. Linear Material with No Thermal Stresses

The assumption of linearity of the material simplifies the problem by permitting the equations which solve the stability problem to remain linear. The geometry and temperature may combine to make the stiffness (e.g., EI) vary with position but linearity of the material implies that the stiffness does not change with load. The solution of these problems serve as a first approximation for more complex problems.

1) Solution of differential equations

Nontrivial eigenvalue solutions of the homogeneous differential equilibrium equation (e.g., $(EIw'')'' + (Fw')' = 0$ for a column) results in the determination of a critical load which depends upon the homogeneous boundary conditions and the distribution of stiffness within the structure. The technique is illustrated in many texts. Timoshenko (85), Bleich (86), etc., contain excellent discussions of the stability problems for columns, plates, and shells and illustrate many of the methods for solving the problem. Gerard and Becker (87) contains a compilation of the results which are of interest to the analyst of aircraft structures.

There are a number of structures (particularly shells) which exhibit instability due to the large deflections. The solutions are not obtained in terms of eigenvalue solutions of homogeneous equations. Since the large deflection equations are nonlinear and, in most cases, not amenable to direct analytical solutions, energy methods such as the Galerkin and Rayleigh-Ritz Techniques are usually employed to obtain approximate solutions.

2) Energy solutions

Employing the principle of stationary potential, which equates the change of work done by the external forces due to a virtual displacement to the corresponding change in strain energy, results in the solution for the critical

load provided that the correct deflection mode is employed. The energy principle can also be utilized to obtain approximate solutions when the deflection mode is not known exactly. The sense of the error in the solution can be determined by the method of approximating the deflection mode. Assuming deflection modes which satisfy the boundary conditions identically will result in always overestimating the buckling load (e.g., Rayleigh-Ritz and Galerkin methods). It is also possible to assume deflection modes that represent less restrained boundary conditions but that when properly combined, satisfy the actual boundary conditions (e.g., Treffetz method) to obtain an underestimate of the buckling load. The energy methods are illustrated in various texts such as Timoshenko (85), Bleich (86), etc. An illustration of the lower bound technique can be found in Budiansky and HuPai (88).

b. Linear Material with Thermal Stresses

Self-equilibrating thermal stresses are generated by nonlinear thermal expansion. A structure may have tensile and compressive stresses superimposed upon the stresses caused by the boundary loads and body forces. The boundary loads may be mechanically applied loads or the loads caused by restraint against thermal expansions of the structure. The compressive thermal stresses produce a destabilizing effect on the structure which can produce instability with lower applied loads. The problem requires the determination of the stress distribution due to the applied loads and temperatures and then an evaluation of the stability of the structure. Solutions can be separated roughly into two types, corresponding to small and large deflection theories. The small deflection theory assumes that the lateral deflections are small enough that they have a negligible effect upon the strains. Solutions of this type are summarized by Boley (89) and VanDerNeut (90) and are illustrated in various papers (91-95). Some aspects of the thermal buckling of shells was discussed previously. The large deflection theory considers the effect of lateral deflections. As an example, the lateral deflection of an axially restrained structure, with an initial eccentricity, would increase with temperature without approaching the condition of instability previously defined. A linear material structure would continue to deflect with increasing temperature until a failing stress or maximum permissible deflection is attained. Solution for the deformations and loads in eccentric structures (columns and plates) can be found in various texts (e.g., Gatewood (84), Boley (89), etc.) and papers (95-97).

c. Nonlinear Material With no Thermal Stresses

The nonlinearity of the material results in a variation of the stiffness with the applied load. This makes the governing equations nonlinear and the solution becomes more difficult. The nonlinearity is accentuated by temperature which reduces the proportional limit of the material.

Solutions are usually presented by introducing a plasticity factor into the linear solution (See Paragraph 4.1.a of this section). The plasticity

factor results in a reduced modulus (E_R) which when substituted for E in a linear solution for the buckling stress would result in the observed buckling stress. The value of E_R depends upon the stress-strain relationship of the material, the applied stresses, and the boundary conditions. Analytical work on various mathematical models has resulted in expressions for E_R. Stowell (98) presented formulations of E_R for columns and plates, by considering the relative amount of twisting and bending energies (without stress reversal) in the structure due to the boundary conditions and an octahedral stress-strain relationship. The results, with minor modifications, are employed by most of the aircraft industry. Experiments (99) have indicated that the stability of a structure at different uniform temperatures can be obtained by determining E_R from the stress-strain relationship at these temperatures.

Since the stability of a structure loaded beyond the proportional limit is a function of the shape of the stress-strain curve, it becomes advisable to approximate this curve by a mathematical formulation which simplifies the calculations required. Expressing the stress-strain relationship in nondimensional form (e.g., Ramberg-Osgood (100) or Switzky et al (101) permits presentation of many solutions on one graph (Figure 8) rather than requiring graphs for every material and every temperature. The introduction of inaccuracy by the nondimensional approach may be accepted, in some cases, to obtain the benefits of simplification in the design and analysis of the structure.

d. Additional Problems

Many problems remain in the fields of columns, plates, and shells, with special emphasis on the effect of thermal stresses. In addition, the effect of eccentricity upon stability must be more fully evaluated. The eccentricity (which may be more pronounced due to thermal gradients) decreases the stability of the structure by causing bending stresses which produce reductions in the stiffness of the structure. Some work has been done on the effect of eccentricity on columns. Timoshenko (85) and others considered a secant law for obtaining the load which produces an allowable maximum stress. Shanley (102) presented interaction curves for allowable moment and axial force. Costello et al (103) present the effect of eccentric loads in terms of an effective length which would produce buckling. In addition, interaction moment and force curves for constant depth of yielding are presented. Carlson (104) evaluated the effective length of an eccentric column by a cross-plot of the strain variation against the resulting moment and axial force for the given stress-strain relationship (this technique was also employed with isochronous stress-strain curves for time-dependent solutions). Switzky (105) approximates the reduction of stiffness in terms of the initial eccentricity and the average stress on the column. Experimental data (104, 106 and 107) would indicate that the trends are correct, however, more analytical and experimental work needs to be done in this field to obtain simple and reliable analysis methods.

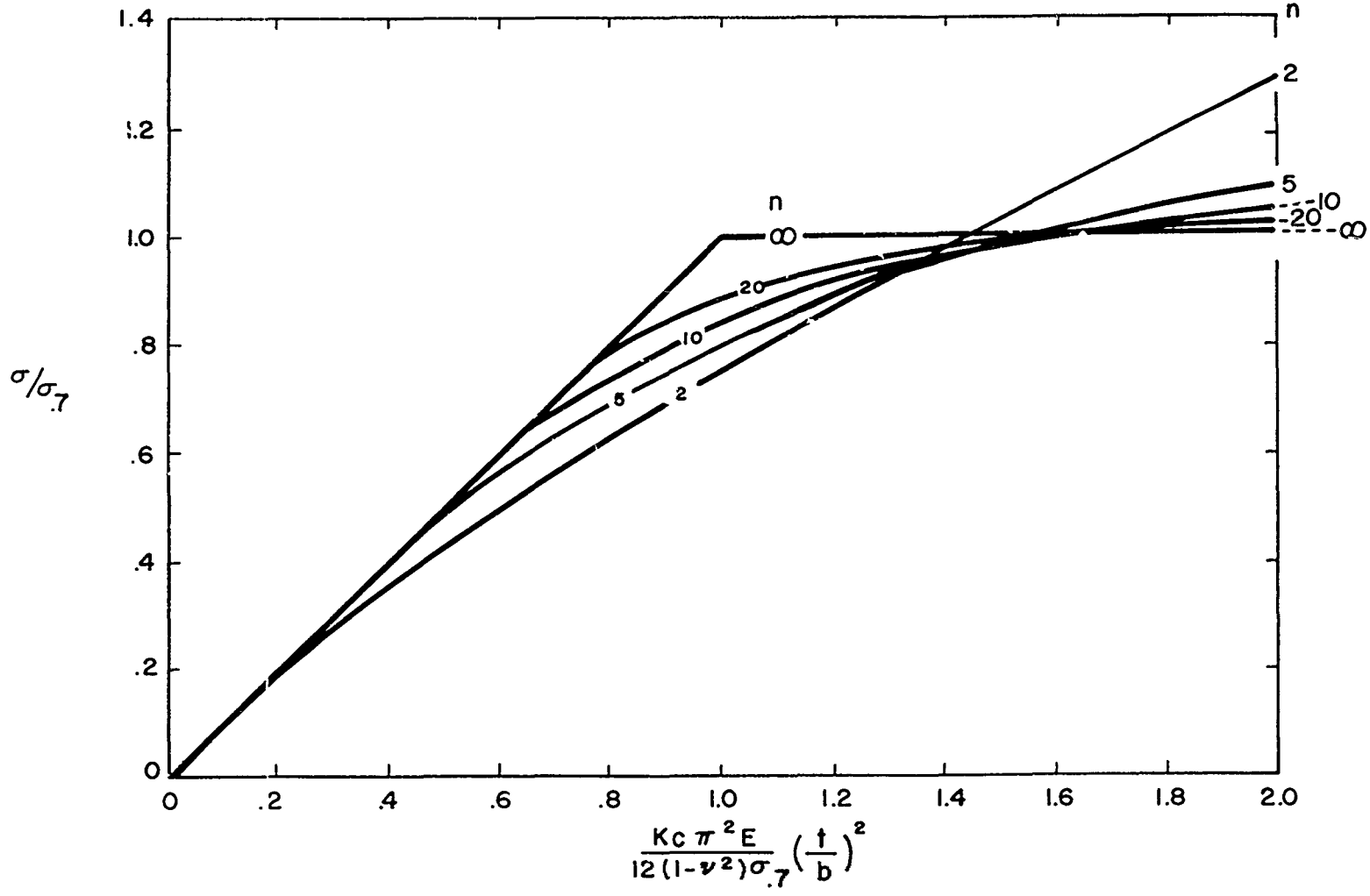


FIGURE 8. NONDIMENSIONAL COMPRESSIVE BUCKLING STRESS FOR SIMPLE SUPPORTED PLATE [REF.(87)]

2. Time-Dependent Solutions

All materials exhibit creep when subjected to stresses and high temperatures. It is unrealistic to require that a structure endure indefinitely since all loaded structures would fail in creep after a sufficiently long period of time. All that the engineer can demand of a structure is that it perform its duties reliably for its required lifetime. Thus, the analyses have been concerned with the "critical time" at which the structure becomes inadequate. The critical time, in addition to being a function of the stress-strain relationship, the geometry, and boundary conditions, is also dependent upon the stress-creep rate relationship of the material. Since the material exhibits disproportionate higher creep rates with higher stresses, the structure becomes unstable in a limited time, whereas Kempner (108) indicates that a linear relationship of creep rate and stress would produce instability only after exceedingly long times.

Most of the analytical work has been performed on columns with little work done on plates and shells. The case treated is usually a straight or initially eccentric column, composed of a material with mathematically simple stress-strain and stress-strain rate laws, and subjected to constant load and temperature. Results are then employed to approximate the creep buckling behavior of other types of structures with different load-temperature histories. Semi-empirical approaches such as "isochronous stress-strain curves" and "critical strain" have also been employed with some success. The assumptions made to simplify the solution of the problem should always be accompanied by test programs to evaluate the influence of these assumptions and to note the agreement between theory and tests.

a. Viscous Models (Columns)

Various approaches have been employed such as solving the differential equilibrium equation for a material that exhibits both linear elastic and viscous strains with stress. In this approach it is usually assumed that the column is perfectly straight. Typical solutions (109) are given in terms of the "critical time" necessary to satisfy equations of the form

$$P = P_E\left(\frac{E^*}{E + E^*}\right)$$

where P = the applied constant compressive load
P_E = the Euler buckling load
E = the initial (Young's) modulus
E^* = the tangent modulus of the stress strain curve for constant strain rates

The value of E^* decreases with time and can be obtained as a function of ϵ (Figure 9). The time necessary to reduce E^* to a value of $\frac{E}{\frac{P_E}{P} - 1}$ corresponds to the "critical time."

Another approach is to assume that the column exhibits an initial eccentricity in the fundamental deflection mode and this shape is maintained throughout the buckling process. The problem is usually solved for an H column, infinitely stiff in shear, with all the bending area concentrated at the centroids of the flanges. This results in critical times which are a function of the "Euler Strain", the strain rate, the cross sectional geometry, and the initial eccentricity. The above approach requires a mathematical formulation of the stress-strain rate relationship

(e.g., the power law $\dot{\epsilon} = \lambda\ (\sigma/E)^n$.

A typical result (110) for the critical time (t_{cr}) is

$$t_{cr} = 1/3 \left[(\epsilon_E - \epsilon_o)/\dot{\epsilon} \right] \log\ (2r/a_i) \qquad \text{For } n = 3$$

where ϵ_E = Euler strain = $\left(\frac{\pi r}{l}\right)^2$ for a simple supported column
ϵ_o = Elastic strain due to stress σ
$\dot{\epsilon}$ = Strain rate due to σ
r = Radius of gyration of column
a_i = amplitude of initial eccentricity of fundamental mode.

Summaries of various theories of creep buckling can be found in Hoff (110), Boley and Weiner (111), and DeVeubeke (112).

b. Isochronous Stress-Strain Curves

Another approach is to construct a time-dependent stress-strain relationship similar to the short-time relationship. Hypothetical stress-strain curves at constant times are constructed from the short-time stress versus strain curves and the creep strain at constant stress versus time data. These curves are employed in a manner similar to the time-independent nonlinear solution mentioned previously. The effective modulus to be employed with these hypothetical curves is questionable. The tangent modulus (E_T) is suggested by Shanley (113) and experimental data (104, 106) would seem to indicate that it usually results in conservative (shorter) estimates of the experimental critical time. Another modulus $2\ EE^*/(E + E^*)$ has been proposed by Gerard (114).

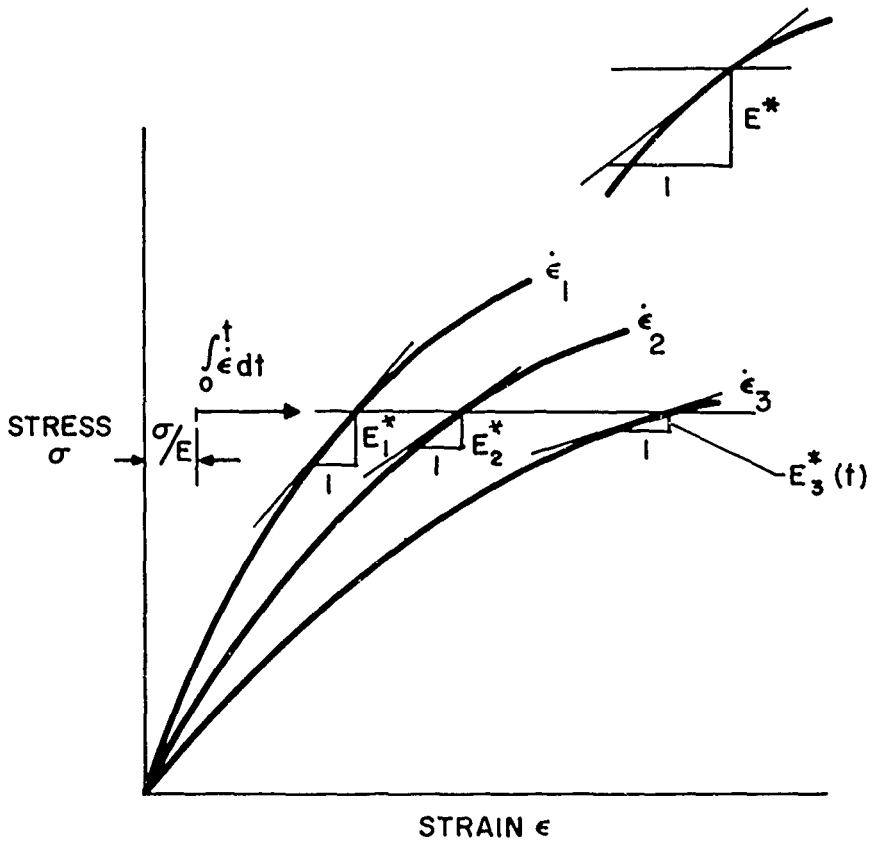


FIGURE 9. STRESS VS STRAIN FOR CONSTANT STRAIN RATES OF A VISCOUS MATERIAL, AND THE DETERMINATION OF $E^*(t)$.

Additional analytical and experimental investigations must be conducted to determine the reliability and applicability of the effective moduli under all probable circumstances.

If the stress-strain relationship can be formulated mathematically to include with sufficient accuracy, the effects of time, then the isochronous stress-strain approach coupled with a definition of an effective modulus can be employed to obtain nondimensional curves for the critical time for given loads, geometries, and boundary conditions. Such an approach (101) could reduce the labor of solution and the amount of test data required.

c. Critical Strain

There is an average axial strain (ϵ_{cr}) associated with the instability of a structure in a time-independent solution. For the linear material this is the "Euler Strain" (e.g., $\epsilon_E = \left(\frac{\pi r}{l}\right)^2$ for a column). With nonlinear materials this is decreased by the ratio (E_R/E_S). Gerard (115) conjectured that a structure would buckle when the average axial strain due to stress and time became equal to ϵ_{cr}. Some experimental data (116-118) has indicated creep buckling in the vicinity of a characteristic "critical strain." Analytical (97) and experimental (119) investigations would seem to indicate that the "Euler Strain" should be an upper bound on the buckling strain with reductions due to the nonlinearity and eccentricity of the structure which may result in a buckling strain below $\epsilon_E\left(\frac{E_R}{E_S}\right)$.

The critical strain approach to the buckling of structures simplifies the analytical techniques to investigate stability after a complex load-temperature-time history. A cumulative deformation theory (see Part B of this section) can be employed to determine the average axial strain history of the structure and to estimate its structural adequacy in stability.

d. Additional Areas of Work

More work remains to be done in evaluating the stability of a structure for the more complex histories, (cyclic, etc.) and in extending the problem to include eccentricities, thermal gradients and stresses, different geometries (e.g., plates, shells) and boundary conditions.

B. MATERIAL BEHAVIOR

In the foregoing part of this Section II, some of the mechanical properties of materials necessary for stability analysis were mentioned. It was shown how these properties are intimately associated with the analysis to predict buckling. Some of the other material information required for design analysis is mentioned below. Since aerospace vehicles will be subjected to a wide variety of stress-temperature histories, it becomes difficult to test all candidate materials for all conditions. Therefore, prediction methods to permit estimates to be made for design analysis are useful.

1. Short-Time Strength After Exposure

The strength at temperature after exposure (F_{TE}) can change from a value available in the virgin material (F_{TV}) to its minimum strength in the annealed condition (F_{TA}). A deterioration ratio, $D = \frac{F_{TE} - F_{TA}}{F_{TV} - F_{TA}}$, should give a good indication of the effect of exposure on the strength of the material (Figure 10). The form of the deterioration ratio was suggested by Brownfield and Badger (120) where F_{TA} was taken as the strength after a reference exposure. The deterioration ratio plot tends to reduce the scatter in experimental data plotted against an exposure parameter. In addition, the effect of exposure on the stress-strain relationship can be illustrated by plots of stress versus the exposure parameters for constant values of strain (Figure 11). Some of the exposure parameters employed are the Larson-Miller parameter (121), the Manson Haferd parameter (122), and the Dorn parameter (123).

2. Deformation History

The stress distribution, the deformations, the stability, and the failure of the structure are dependent upon the deformations of the material during the load-temperature-time history. The subsequent response of the material will depend upon the previous history. The analyst must be able to estimate the material deformations in a relatively simple manner without having to resort to tests which duplicate the exact history. Several methods are described below for estimating material deformations from constant load creep curves.

a. Strain Hardening Rule

The "Strain Hardening Rule" assumes that the creep deformation depends primarily upon the creep strain accumulated in the previous history. Thus the subsequent creep deformation behavior for a given stress will be identical to the behavior that follows the same deformation at that stress.

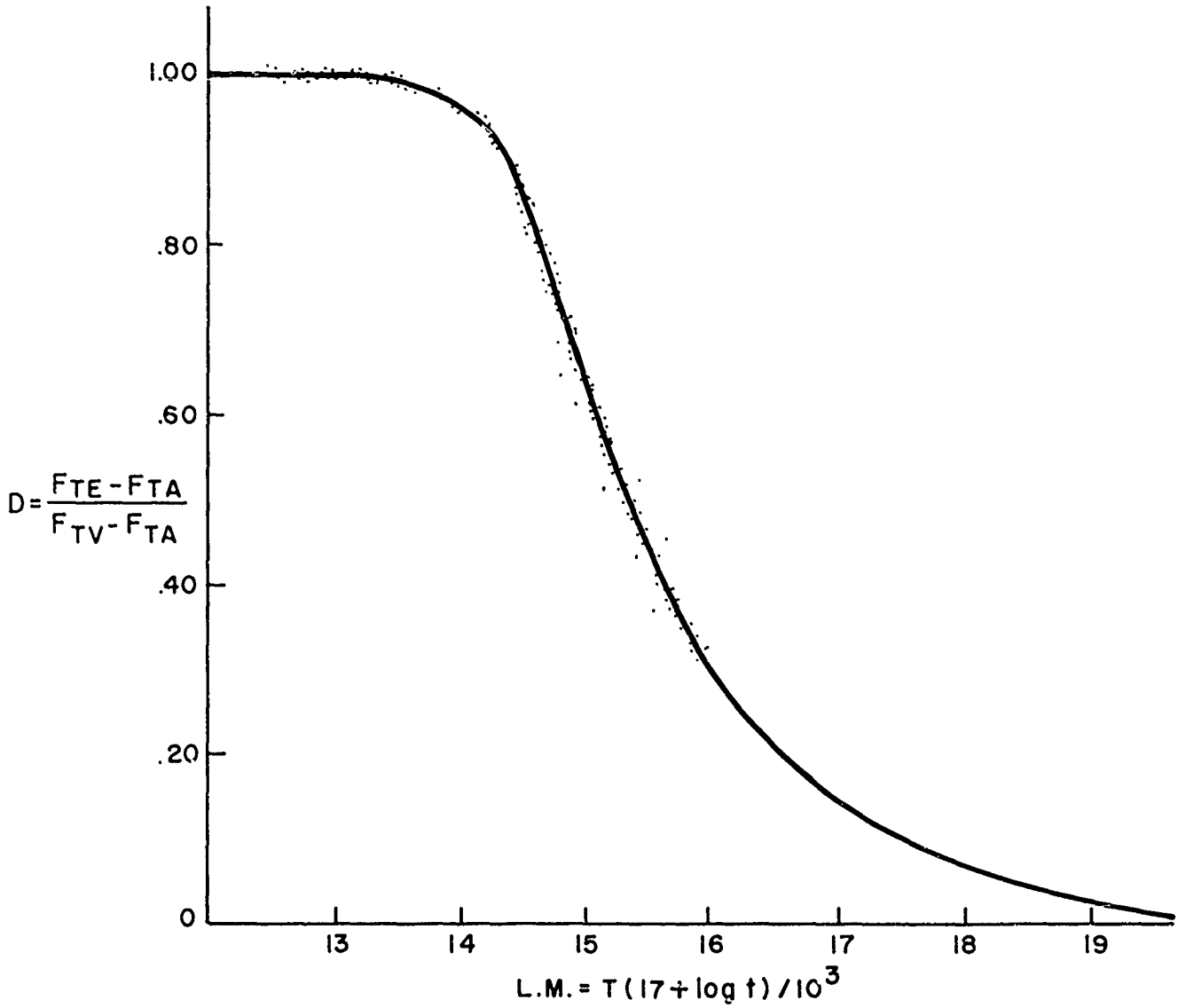


FIGURE 10. STRENGTH DETERIORATION AS A FUNCTION OF LARSEN-MILLER EXPOSURE PARAMETER. [REF. (120)]

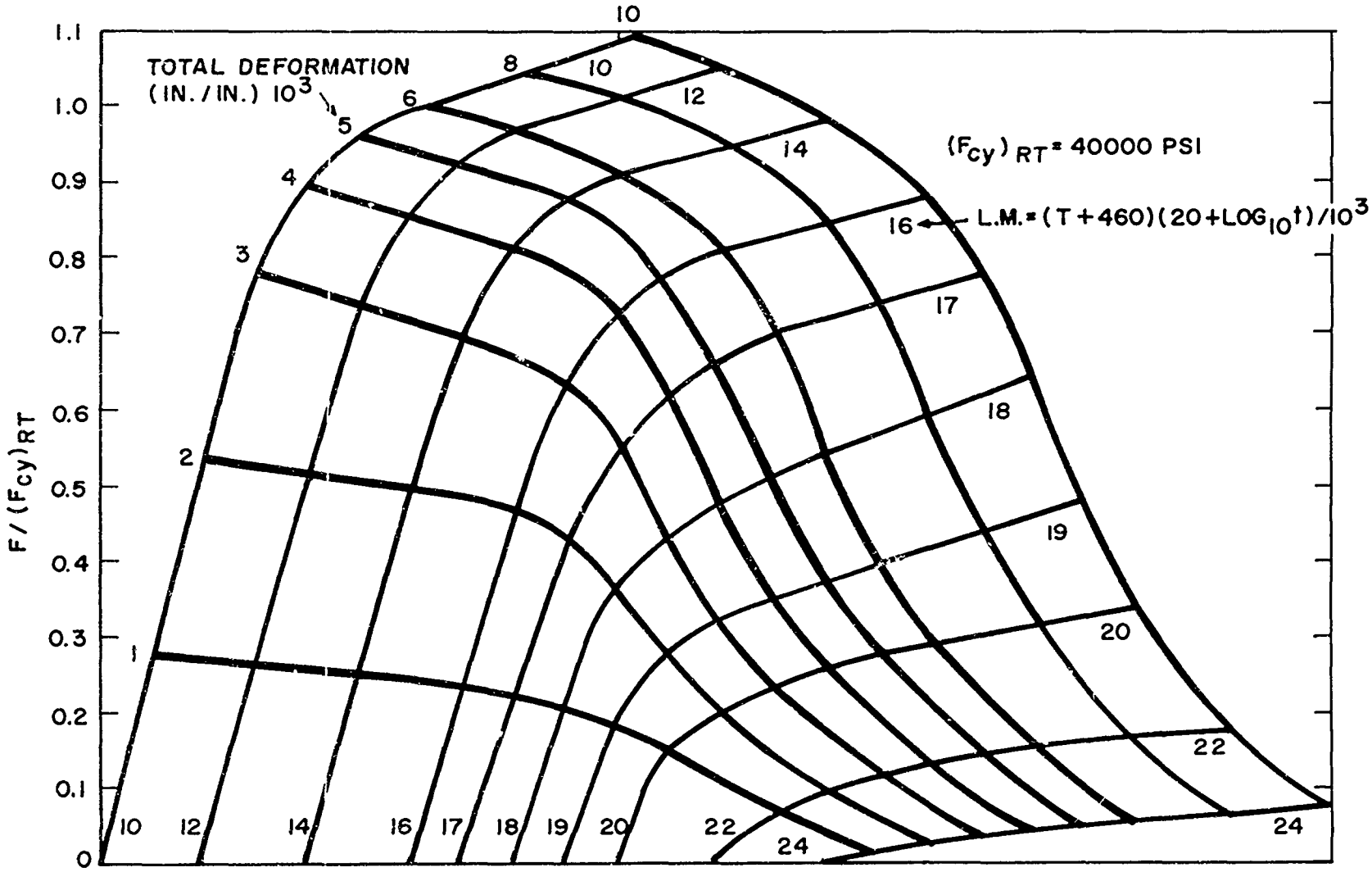


FIGURE 11. STRAIN CURVES FOR 2024-T3 CLAD ALUMINUM ALLOY SHEET [REF. (84)]

b. Time Hardening Rule

The "Time Hardening Rule" assumes that the creep deformation depends primarily upon the thermal aging of the material. Thus the subsequent creep deformation behavior depends upon the previous temperature time history. A previous exposure is converted to the reference temperature and equivalent time by means of an exposure parameter (as for example, the Larson-Miller parameter) and the material is assumed to subsequently behave as if it had been exposed to the given stress and temperature for the equivalent time.

c. Life Fraction Rule

The "Life Fraction Rule" assumes that subsequent deformation depends upon the ratios of the expended time (t_i) at a given stress and temperature to the allowable time (t_{if}) at that stress and temperature. Basically it assumes a linear damage theory where the previous sequence of loading does not affect its subsequent behavior. The previous exposure is converted to a sum of life fraction ratios whose sum is employed to obtain an equivalent time (t_r) at the reference stress and temperature which would result in the same life fraction ratio ($t_r/t_{rf} = \Sigma t_i/t_{if}$).

The above rules suffer from the same problems as the exposure parameters. The reliability depends upon the material and the history. If the material is insignificantly affected by factors which are not accounted for then the prediction method is quite reliable. However, if some neglected factors are significant and the history brings them into play, then the prediction method becomes unreliable.

3. Failure Theories

The structure could fail in a number of ways. It can fail in short-time mechanical and/or thermal loadings after the material properties have been degraded due to the previous exposure. It could also fail in time-dependent modes such as fatigue, excessive deformations, creep instability, rupture, etc. The deformation rules noted above can be employed to predict failure by exceeding allowable deformations, critical strains or by rupturing.

4. Additional Areas of Work

A great deal more work is necessary to develop and evaluate prediction methods which will be simple and reliable. More experimental work is required to obtain a clear picture of material behavior.

The effect of combined stresses, reversed stresses (Bauschinger effect, etc.), and the difference between compression and tension loadings should be investigated. The factors of strain hardening, thermal and stress aging, recovery, relaxation, oxidation, corrosion, ductility, crack formation and propagation, etc., must be assessed for each structure considering the material, the history, the required performance, and the criteria of structural adequacy.

SECTION III: UTILIZATION OF COMPUTERS FOR THERMO-MECHANICAL PROBLEMS

In recent years, three general types of computers have been developed which are useful in the solution of engineering and scientific problems. These are the digital computer, the direct analog computer, and the differential analyzer. There is no doubt that many problems would be unsolved today without their use. However, the choice of a particular computer to be applied to a problem is not always easy. Hopefully, the following text will establish some guide lines for this choice. A brief description of computers is given, followed by some recent applications of these computers to analysis, and finally, some of the mathematical techniques used for computer solutions are outlined.

A. COMPUTER DESCRIPTIONS

1. The Digital Computer

The electronic digital computer is the most versatile tool for numerical calculation yet devised. Any calculation which lends itself to numerical procedures can be programmed.

To appreciate its capabilities and limitations, it is desirable to consider the five functional units of a digital computer system.

(1) Input device (Punched cards, tape, manual)

(2) Output device (Punched cards, tape, printed paper)

(3) Memory Unit (Electrostatic or Electro-magnetic core, or drum, tape)

(4) Control Unit (Electronic Instruction Interpreter)

(5) Arithmetic Unit (Unit where actual operations on numbers proceed)

The last three are of greatest concern to a stress analyst. The memory must be sufficiently great to store all program instructions and intermediate results. It must also have fast accessibility. Usually a large modern computer uses a combination of electromagnetic core, drum, and tape. Their accessibility speed is listed in order, the core being the fastest, and they may be used to combine their most desirable features in the most efficient manner. Drums are useful when more storage capacity is required for the program; their access time is much faster than tape. Some machines which have large electromagnetic core units, such as the IBM 7090, have no drums at all, but do have tape units.

The Control and Arithmetic units, respectively, interpret the instructions and execute them. It is the ability of the control unit to operate on coded instructions that gives the digital computer the unique capability of selecting alternate courses of computation on the basis of intermediate results, i.e., to make logical decisions.

The instructions to perform a given sequence of operations, known as a program, have to be coded in special "machine language," usually requiring the use of a computer specialist as an intermediary between the problem originator and the machine. An example of a program that has been written is the solution to the problem of the complex structural assembly of a wing by Turner, et al (124). Each structural component has a force-deflection relationship representable in matric form. The elements of the matrices can be computed from basic geometric and cross section data, and the remainder of the solution steps, involving matrix manipulation, can all be programmed to proceed automatically. Also, because of the extensive memory and the ability to make logical decisions, the digital computer is uniquely suited for detailed iterative optimization analyses. Generalized digital computing schemes have been conceived for sequential computation of structural matrices from basic data, computation of thermal stresses due to the external loads and thermal gradients, and finally, computation of new element data for minimum weight subject to suitable practical minima and maxima (125). Cyclic operation of such a program would lead to automatic weight optimization of the structure.

This type computer has also been employed in the solution of ordinary and partial differential equations. A recent example of considerable interest is the numerical solution by Radowski et al (126) of the linear, ordinary differential equations which occur in the small deflection analysis of thin shells, including thermal effects.

2. The Direct Analog Computer

As reported by Basin et al (127) many useful results have been gained from application of the C. E. A. Direct Analogy Analog Computer, also known as the McCann Computer. The computer elements consist of resistors, capacitors, transformers, and constant current generators (feedback amplifiers). They are suitably arranged so that their interconnection can be established on a wiring patchboard, and when properly connected, form electrical circuits governed by the same algebraic equations as the structural components which they represent.

Ryder (128) describes the action of this type of direct analog computer by stating that it simulates electrically the behavior of the structure, so that:

> Forces and moments obey equilibrium relationships analogous to Kirchhoff's First Law of current flow continuity.

- Voltage differences are proportional to the deflection or slope differences between two points on a structure.

- Compatibility of slopes and deflections is assured in the simulator by the parallel voltage compatibility relations of Kirchhoff's Second Law.

Using appropriate networks of transformers and resistors, the response is the same, in terms of voltage and current, as is that of deformation and generalized force. Very high quality components are required so that the analogy is not destroyed by parasitic currents.

The computer is best applied to preliminary analysis of structural assemblies. The manual accessibility of potentiometers, permitting immediate changes in the circuit components representing internal or boundary restraint flexibilities, makes it possible for the stress analyst to study the effect of these variations on the internal load distribution while the problem is in the machine. Changes in geometry are not easy to make and should be avoided.

The computer elements, particularly the transformers, are precisely made so that electrical analogies can be accurately constructed. They are therefore quite expensive. Despite their high precision, some imperfections remain which place a limit on the practical size of the analog network. However, this size is adequate for many static problems in preliminary design work in which it may be permissible to make the assumptions necessary to fit a problem into the machine.

Ryder (128) suggests the use of the "Energy Analog" which substitutes the condition that the elastic energy (strain energy) is simulated by half the resistive power loss in the analog, in place of the force-deflection relationships employed by the McCann computer. When the internal forces in the structure are simulated by the currents, the analog can be constructed solely on the basis of strain energy expressed in terms of these forces and compliances, subject to equilibrium conditions. It is often possible to economize on circuit components by using this method. Unfortunately the deflections are then not explicitly available for measurement which is not a serious drawback if only the internal forces are needed. However one economic advantage is gained because circuit inaccuacies are relatively easily predicted and compensation by power injection at appropriate points would make it feasible to use components with less stringent accuracy requirements than that of the McCann computer.

3. Differential Analyzers

The type of analog computer known as a differential analyzer has also been applied to structural problems. Warfield (129) states that it is best suited for solving ordinary differential equations with a single independent variable, or sets of simultaneous equations of this type. Partial differential equations are solvable if they are first expressed as finite difference equations.

These computers consist of operational amplifiers, and high precision potentiometers. When combined with resistors and/or capacitors, the amplifiers operate as constant multipliers, integrators, summers, function multipliers or function generators. The implied operations enable the computer to solve the mathematical problems in an electrically analogous way. The number of available elements determines the scope of computations which can be undertaken. The results appear (usually) on graphs, each channel of information being recorded as a separate plot automatically.

The static structural problem of a plate is solved on the computer by expressing the problem as a set of finite difference equations and by representing them by the appropriate electronic network of adders and multipliers. Clymer (130) showed that this and all other types of structural elements which can be used for idealization in the analysis of structural assemblies are similarly representable using finite differences. The large amount of equipment required limits the application to fairly small problems. The computer can choose alternate courses of action only with human intervention or if coupled with a digital computer.

B. COMPUTER APPLICATIONS

Computers have been applied to many complex problems amenable to analytic treatment and numerical evaluation. Without them, the numerical methods of solution of certain classes of differential equations could not have proceeded.

The application of computers to the linearly elastic problem of complex structural assemblies has been well documented in the survey by Warren et al (131) in which many of the pertinent references in this area are reviewed. Lansing, et al (132) report successful large deflection calculations of a laterally loaded square plate, using a stepwise flexibility approach. Basin, et al (127) use an iterative technique for a similar problem with the direct analog computer. The equivalent mechanical kick loads (out of plane forces) caused by the deformations due to mechanical loads and thermal strains have to be recalculated for each step in the solution. Turner, et al (133) discuss some of the instability possibilities due to thermally induced stresses. They also give stiffness matrices of a stringer and a plane-stress plate which consist of the linear matrix and a matrix which is a function of the incremental deformation. Another approach given by Wilson (134) appears quite interesting. It suggests use of the Ramberg-Osgood, or similar, stress-strain relationships to define element flexibilities in terms of the incremental load values.

The approach to solution of monolithic nonlinear problems has been discussed elsewhere herein and will not be repeated here.

Another fruitful application of computers is that of weight optimization such as discussed by Meissner (125). This process is nonlinear even for a linearly elastic structure and requires iterative procedures. Cross section properties of

components of structural assemblies can be computed as a function of the applied loads and permissible stresses, subject to practical limits. If the structure is redundant, the internal forces will have to be recomputed on the basis of the new cross section properties and then the process repeated.

Practical numerical solutions of problems facing us even now will involve the processing of a tremendous amount of data which occurs as input or as intermediate results when iterative techniques of solution are used. The digital computer is well suited to this purpose. An example is the problem of large deflections in structures caused by thermal gradients as well as mechanical loads. Lansing, et al (132) show that the structural component stiffness matrices are functions of the displacements and forces.

The effects of cross section property changes due to changes in Young's modulus caused by temperature changes could be included in the analysis of structural assemblies as formulated by Switzky et al (135). Creep analysis and fatigue analysis of complex structural assemblies will require the handling of very large amounts of data. In the case of creep, as discussed by Huang (136), the data consists of the load-time-temperature histories combined with the variable material properties under the corresponding conditions. Fatigue analyses of structural assemblies will require, as one step, the calculation of stresses in each structural component for many loading conditions to establish a stress spectrum for each component.

C. TECHNIQUES AND DIFFICULTIES IN SOLVING PROBLEMS

1. Solution Techniques

In order to appreciate the work the computers have to do, some applicable mathematical solution techniques for structural problems with thermal and mechanical loadings are given below.

Consider a monolithic structure consisting of uniformly distributed material such as that of a rectangular plate in plane stress. This structural problem can be furmulated as a two dimensional isothermal problem in elasticity and requires the solution of the bi-Laplacian equation in two dimensions, that is, $\nabla^4 \phi = 0$, subject to the satisfaction of boundary displacement and/or traction conditions. The plane stress problems of a rectangular plate may, for example, be solved by assuming a polynomial or Fourier series expression for ϕ, suitably adjusting coefficients to obtain various realistic boundary deflection, slope and traction conditions. It is often necessary to be content with deflection functions which satisfy the kinematic boundary conditions at every point but which result in boundary equilibrium only in an integrated manner; that is to say, the over-all equilibrium with the boundary forces of moment shear and torsion may be satisfied, but the point to point satisfaction of traction equilibrium at the boundary may not.

It is well known that numerical solutions of partial differential equations can be obtained by using a finite difference formulation. This method can be applied to the solution of the small deflection plate bending problem defined by the equation $D\nabla^4 w = q$ and the specified boundary conditions. By the method of finite differences, the partial differential equation is replaced by a system of linear algebraic equations, where the unknowns are the deflections at designated grid points. For example, this technique has been applied to constant or varying thickness plate and shell problems. The non-uniformity of thickness is evident in the equation coefficient formulation, as given by Mills (137) and Conte et al (138) and does not cause any additional difficulty in the finite difference procedure.

Another way of solving non-uniform monolithic problems is that of assuming the structure to be composed of many small typical elements. The solution of each element problem is obtained using physically reasonable assumptions of compatible strain conditions and equilibrated stress conditions, resulting in corresponding equilibrium and compatibility equations. The joint action of such components in a structural assembly is then expressed as a set of simultaneous equations. Melosh (139) employed this technique for solving variable thickness plate bending problems. The stiffness matrix for a plate element was derived. The algebraic addition of the elements of plate matrices where compatibility is required, at least piecewise, results in the matrix of a plate with varying thickness. This is the coefficient matrix of a set of simultaneous plate deflection equations.

This approach is also taken for more complex structural assemblies which are not amenable to direct analytic treatment. Some of the structural elements, such as plates (see above) may require some careful analytic treatment; others that can be considered as beam or stringer elements have stiffness or flexibility matrices obtained from strength of materials considerations. Archer et al (140) and Samson et al (141) describe many structural idealizations and the corresponding matrices. By taking this approach, complete analytic freedom with respect to material location and joining methods is obtained. We are cautioned by Rattinger et al (142) that a primary source of error in this approach is the idealization of the components and the degree to which the analysis prescribes the enforcement of compatibility and equilibrium between them. A second source of error arises from possible oversimplification of the action of idealized components. For example, if direct stresses in a wing skin contribute significantly to the strain energy in the structure then the idealization of the action of the skin panels should result in matric expressions which imply this strain energy. Assumption of "pure shear" panel action of such skins could be a gross oversimplification for the problem.

All analyses based upon break-up of the structure into idealized elements result in the basic formulation

$$[a]\{X\} = \{b\}$$

which implies a number of linear algebraic operations.

These equations represent the inter-relationship of the force-deflection behavior of the structural elements and the externally applied forces. The simultaneous equations may have both deflections and forces as terms in the unknown vector $\{X\}$, as given by Samson and Bergmann (141) and Klein (143). The Force-Matrix or Flexibility Method as given by Argyris (144), shows the basic equations formulated as:

$$\left[\begin{array}{c|c} a_{11} & a_{12} \\ \hline a_{21} & a_{22} \end{array}\right] \times \left\{\begin{array}{c} F \\ \hline R \end{array}\right\} = \left\{\begin{array}{c} \Delta \\ \hline \delta \end{array}\right\}$$

The unknowns in these partitioned equations are the redundant forces $\{R\}$ and the deflections $\{\Delta\}$. $\{F\}$ are the external forces and $\{\delta\}$ are the relative deformations of the structure at the location of the redundant forces. Notice that all elements of the vector $\left\{\begin{array}{c} F \\ \hline R \end{array}\right\}$ are forces, whence the name of the method. The Stiffness Method as described by Turner et al (124) is formulated so that the deformations are the primary unknowns. The external known forces are the right hand sides.

In many important problems, the effects of temperature gradients in structures show up as "thermal loading" terms, which are self-equilibrated force systems that would have the same effect as the temperature variations in the structures. Furthermore, the changes in cross-section properties due to variations of Young's modulus with temperature may have to be considered.

A method for determining thermal effects on complex structural assemblies is given by Meissner (145). The approach is that of calculating equivalent mechanical loads which cause deformations of the structural elements in their unrestrained, cut-apart state, equal to those caused by the temperature terms. In the linearly elastic case, the thermal stresses in the unrestrained elements can be superposed upon the stresses due to the equivalent loads on the complex structural assembly.

2. Problem Solution Difficulties

Any problem involving the solution of a large system of simultaneous equations suffers from round off error and losses of significant decimal places due to subtraction, if an elimination type process is used. Iterative procedures, however, such as those given by Lehman (146) and Conte et al (138) have been very useful for this purpose permitting any desired degree of precision in the answers to problems with well conditioned coefficient matrices. One of the desirable characteristics in such problems is the predominance of the diagonal

terms. The matrices should of course be non-singular. The inversion of large matrices should be avoided, because the required iterative techniques are very time consuming.

Convergence problems are also encountered in the solution of monolithic structure where the unknown deflections are expressed as power, Fourier or other infinite series. Such difficulties have been encountered by Mills (137) in the problem of large deflections in variable thickness plates where a polynomial expression was used for the deflection function.

D. CONCLUSIONS

Development of computers is an area in which much progress is being made. Further improvements in problem solution techniques are also necessary. More work is required in the understanding and formulation of creep and fatigue analysis, the derivation of more realistic structural element stiffness or flexibility matrices, and in the iterative numerical techniques required for solution of nonlinear problems.

It appears therefore that the versatility and the ability to make logical decisions qualifies the digital computer as most universally applicable to scientific and detailed engineering problems. The feasibility of many solutions hinge on this combination of qualities. However, the detailed nature of the instructions makes rigorous program checkout before acceptance highly desirable. It has been observed that programming and checkout can be very time consuming. This detail must therefore be considered part of the job when a program is contemplated. Further development of operational components and machine "language" should ease this burden. The ability of the computer to process large amounts of data is sure to increase in any case.

The limitations in the types of structural problems which the analog computers can handle consist mainly in the fact that they must use either finite difference representations or direct strength of materials analogies of lumped structural elements, and that there are also limitations on the electrical precision of the networks. Furthermore, these computers cannot make logical decisions automatically. However, to be quite fair, a reasonable comparison of computer applications can be made, assuming a generalized structural problem has been programmed for a digital computer, and that the idealization methods of this problem for the differential analyzer and the direct analog computer are known. If the problem fits all three installations, it will probably be solved in about the same length of calendar time. Obviously, if a problem is so large that it cannot be put into a form which fits an analog computer or a differential analyzer, the use of a digital computer will be mandatory, with the attendant tedious programming. Some problems can be generalized so that the need for numerical solutions can be anticipated, and lead time difficulties can be avoided. If, however, the problem to be solved has not been programmed for a digital computer, the employment of the analog computer or differential analyzer may be able to yield a sufficiently accurate solution.

SECTION IV: REFERENCES

THERMO-ELASTIC ANALYSIS OF PLATES (Section I-A)

1. Boley, B.A. and Weiner, J.H., Theory of Thermal Stresses, John Wiley and Sons, Inc., 1960, pp. 397-399.

2. Forray, M. and Newman, M., "Axisymmetric Bending Stresses in Solid Circular Plates with Thermal Gradients", Journal of the AeroSpace Sciences, Vol. 27, No. 9, September 1960. pp. 717-718.

3. Newman, M. and Forray, M., "Bending Stresses Due to Temperature in Hollow Circular Plates, Part I", Journal of the AeroSpace Sciences, Vol. 27, No. 10, October 1960. pp. 792-793.

4. Forray, M. and Newman, M., "Bending Stresses Due to Temperature in Hollow Circular Plates, Part II", Journal of the AeroSpace Sciences, Vol. 27, No. 11, November 1960. pp. 870-871.

5. Newman, M. and Forray, M., "Bending Stresses Due to Temperature in Hollow Circular Plates, Part III", Journal of the AeroSpace Sciences, Vol. 27, No. 12, December 1960. pp. 951-952.

6. Reissner, E., "The Effect of Transverse Shear Deformation on the Bending of Elastic Plates", Journal of Applied Mechanics, Trans. ASME, Vol. 67, 1945. p. A-69.

7. Forray, M. and Newman, M., "Bending of Circular Plates Due to Asymmetric Temperature Distribution", Journal of AeroSpace Sciences (to be published October 1961 - approximate date).

8. Timoshenko, S., Theory of Plates and Shells, First Edition, McGraw-Hill Book Co., Inc., 1940.

9. Forray, M. and Newman, M., "The Analysis and Test of Rectangular Panels with Temperature Gradients Through the Thickness", Republic Aviation Corporation, 688-4 (This work will appear as a WADD Technical Report).

10. Gossard, H., Seide, P., and Roberts, W., Thermal Buckling of Plates, NACA TN 2771, August 1952.

11. Heldenfels, R., and Roberts, W., Experimental and Theoretical Determination of Thermal Stresses in a Flat Plate, NACA TN 2769, 1952.

12. Williams, M.L., "Large Deflection Analysis for a Plate Strip Subjected to Normal Pressure and Heating", Journal of Applied Mechanics, Trans. ASME, Vol. 77, 1955. pp. 458-464.

13. Williams, M.L., "Further Large Deflection Analysis for a Plate Strip Subjected to Normal Pressure and Heating", Journal of Applied Mechanics, Paper 57-A14.

14. Newman, M. and Forray, M., "Axisymmetric Large Deflections of Circular Plates Subjected to Thermal and Mechanical Loads", Republic Aviation Corporation RDSR-10 (To be published as a WADD Technical Report).

15. Timoshenko, S. and Goodier, J N., Theory of Elasticity, Second Edition, McGraw-Hill Book Co., Inc., New York, 1951. pp. 406-408.

16. Norbury, J.F., "Thermal Stresses in Disks of Constant Thickness", Aircraft Engineering, May, 1957. pp. 132-137.

17. Parkes, E.W., "The Stresses in a Plate Due to a Local Hot Spot", Aircraft Engineering, March, 1957. pp.67-69.

18. Forray, M. and Zaid, M., "Thermal Stresses in a Solid Circular Bulkhead", Journal of the Aeronautical Sciences, January 1958. pp. 63-64.

19. Horvay, G., "Transient Thermal Stresses in Circular Disks and Cylinders", Transactions of the ASME, January 1954. pp. 127-135.

20. Forray, M., "Thermal Stresses in Rings", Journal of the AeroSpace Sciences, Readers' Forum, Vol. 26, No. 5, May 1959. pp. 310-311.

21. Forray, M., "Formulas for the Determination of Thermal Stresses in Rings", Journal of the AeroSpace Sciences, Readers' Forum, Vol. 27, No. 3, March 1960. pp. 238-240.

22. Forray, M., "Table for Thermal Stresses in Rings", Journal of the AeroSpace Sciences, Readers' Forum, Vol. 27, No. 6, June 1960. pp. 478-479.

23. Singer, J., Anliker, M., and Lederman, S., "Thermal Stresses and Thermal Buckling", WADC Technical Report 57-69, Polytechnic Institute of Brooklyn, April 1957.

24. Horvay, G., "The End Problem of Rectangular Strips", Journal of Applied Mechanics, Vol. 20, March 1953, pp. 87-94 and December 1953, pp. 576-582.

25. Mendelson, A. and Hirschberg, M., Analysis of Elastic Thermal Stress in Thin Plate with Spanwise and Chordwise Variation of Temperature Thickness, NACA TN 3778, November 1956.

26. Przemieniecki, J.S., "Thermal Stresses in Rectangular Plates", The Aeronautical Quarterly, Vol. X, Part I, February 1959. pp. 65-78.

27. Young, D. and Felgar, R.P., Tables of Characteristic Functions Representing Normal Modes of Vibration of a Beam, Publication No. 4193, University of Texas, 1949.

28. Gatewood, B.E., "Thermal Stresses in Moderately Thick Elastic Plates", Journal of Applied Mechanics, Trans. ASME Series E, September 1959. pp. 432-436.

29. Newman, M., "Study Program for the Analysis and Test of Rectangular Panels with Temperature Gradients Through the Thickness", Republic Aviation Corporation, 688-3.

30. Huang, P.C. and Van Der Maas, C.J., "Theoretical and Experimental Studies of the Stresses and Strains Around Cutouts in Loaded, Unevenly Heated Plates", WADC Technical Report 59-2, Astia Document No. AD 212565, March 1959.

THERMO-ELASTIC ANALYSIS OF SHELLS (Section I-B)

31. Reissner, H., Spannungen in Kugelschalen (Kuppeln.), Müller-Breslau-Festchr., 1912.

32. Meissner, E., "Das Elastizitätsgesetz Für Dünne Schalen Von Ringflächen, Kugel-Und Kegelform", Phys. Zeitschr., Bd. 14, 1913.

33. Meissner, E., "Über Elastizität Und Festigkeit Dünner Schalen", Viertelschr. D. Natur. Ges., Bd. 60, Zürich, 1915.

34. Novozhilov, V.V., The Theory of Thin Shells, P. Noordhoff Ltd., - Groningen - The Netherlands, 1959. p. 2.

35. Love, A.E.H., Mathematical Theory of Elasticity, Fourth Edition, 1927.

36. Reissner, E., "A New Derivation of the Equations for the Deformation of Elastic Shells", American Journal of Mathematics, Vol. 63, 1941. pp. 177-184.

37. Reissner, E., "Rotationally Symmetric Problems in the Theory of Thin Elastic Shells", Proc. 3rd U.S. Nat'l. Congr. of Appl. Mech., Providence, R.I., 1958. pp. 51-69.

38. Synge, J.L. and Chien, W.Z., The Intrinsic Theory of Elastic Shells and Plates, Kármán Anniv. Vol., Pasadena, 1941. pp. 103-120.

39. Zerna, W., "Beitrag Zur Allgemeinen Schalenbiegetheorie", Ing. - Arch., Vol. 17, 1949. pp. 149-164.

40. Parkus, H., "Die Grundgleichungen Der Schalentheorie in Allgemeinen Koordinaten", Österr., Ing. - Arch., Vol. 4, 1950. pp. 160-174.

41. Goodier, J.N., "Thermal Stress and Deformation", Journal of Applied Mechanics, Vol. 24, No. 3, September 1957. p. 472.

42. Timoshenko, S. and Woinowsky-Krieger, S., Theory of Plates and Shells, Second Edition, McGraw-Hill Book Company, Inc., 1959. pp. 497-501.

43. Switzky, H., Forray, M., and Newman, M., Thermo-Structural Analysis Manual, Republic Aviation Corporation Report No. RAC 679-1(128), September 1960 (to be issued as WADD TR 60-517).

44. Hammitt, F.G., "Axial-Temperature-Gradient Bending Stresses in Tubes", Journal of Applied Mechanics, Vol. 25, No. 1, March 1958, pp. 109-114.

45. Den Hartog, J.P., "Temperature Stresses in Flat Rectangular Plates and in Thin Cylindrical Tubes", Journal of the Franklin Institute, August 1936.

46. Bijlaard, P.P., "Differential Equations for Cylindrical Shells with Arbitrary Temperature Distribution", Journal of the Aeronautical Sciences, September 1958. pp. 594-5.

47. Bijlaard, P.P., "Buckling Stress of Thin Cylindrical Clamped Shells Subjected to Hydrostatic Pressure", Journal of the Aeronautical Sciences, Vol. 21, No. 12, December 1954. pp. 852-3.

48. Timoshenko, S. and Goodier, J.N., Theory of Elasticity, McGraw-Hill Book Company, Inc., 1951.

49. Jaeger, J.C., "On Thermal Stresses in Circular Cylinders", Philosophic Magazine, Vol. 36, 1945. pp. 414-428.

50. Boley, B.A. and Weiner, J.H., Theory of Thermal Stresses, John Wiley and Sons, Inc., 1960. pp. 292-298.

51. Forray, M., "Thermal Stresses in Rings", Journal of the Aeronautical Sciences, Readers' Forum, Vol. 26, No. 5, May 1959. pp. 310-311.

52. Kraus, H., and Sonnemann, G., "Thermal Stresses in Hollow Cylinders Due to Asymmetrical Heat Generation", Transactions of the American Society of Mechanical Engineers, 81A (Journal of Engineering Power), Vol. 4, October 1959. pp. 449-454.

53. Chang, C.C., and Chu, W.H., "Stresses in a Metal Tube Under Both High Radial Temperature Variation and Internal Pressure", Journal of Applied Mechanics, Vol. 21, 1954. pp. 101-108.

54. Hilton, H.H., "Thermal Stresses in Bodies Exhibiting Temperature-Dependent Elastic Properties", Journal of Applied Mechanics, Vol. 19, 1952. pp. 350-354.

55. Zwick, S.A., "Thermal Stresses in an Infinite, Hollow Case-Bonded Cylinder", Jet Propulsion, Vol. 27, No. 8, August 1957. pp. 872-876.

56. Ungar, E.E., and Shaffer, B.W., "Thermally Induced Bond Stresses in Case-Bonded Propellant Grains", American Rocket Society Journal, April 1960. pp. 366-8.

57. Parr, C.H., "Stress-Strain Equations for Case-Bonded Solid Propellant Grains", American Rocket Society Journal, August 1960. p. 778.

58. Wilson, H.B. Jr., "Stresses Owing to Internal Pressure in Solid Propellant Rocket Grains", American Rocket Society Journal, March 1961. pp. 309-317.

59. Muskhelishvili, N.I., Some Basic Problems of the Mathematical Theory of Elasticity, P. Noordhoff Ltd., Groningen - Holland, 1953.

60. Trostel, R., "Transient Thermal Stresses in a Hollow Sphere", Ing. - Arch., 24, 6, 1956. pp. 373-391.

61. McDowell, E.L., and Sternberg, E., Axisymmetric Thermal Stresses in a Spherical Shell of Arbitrary Thickness, American Society of Mechanical Engineers, Summer Conference, Berkeley, California, Paper 57-APM-14, June 1957.

62. Cowper, G.R., Thermal Stresses in Multi-Layer Spherical Shells, National Research Council of Canada, NRC Aero. Rpt. LR-300, February 1961.

63. Huth, J.H., "Thermal Stresses in Conical Shells," Journal of the Aeronautical Sciences, Vol. 20, No. 9, September 1953. pp. 613-6.

64. Meriam, J.L., Stresses and Displacements in Rotating Conical Shells, Yale University School of Engineering, Publication No. 73, November 1942.

65. Sibiriakov, V.A.,"Determination of Temperature Induced Stresses in a Conical Shell", American Rocket Society Journal, Vol. 30, No. 11, November 1960. pp. 1041-1046.

66. DeSilva, C.N., Thermal Stresses in the Bending of Ogival Shells, Presented at the Institute of AeroSpace Sciences 29th Annual Meeting, New York, N.Y., IAS Paper No. 61-13, January 23-25, 1961.

67. Langer, R., "On the Asymptotic Solutions of Ordinary Differential Equations, with Reference to the Stokes' Phenomenon about a Singular Point", Trans, Am. Math. Soc., Vol. 37, No. 5, May 1935. pp. 397-416.

68. Hildebrand, F.B., On Asymptotic Integration in Shell Theory, Proc. 3rd Symposium in Applied Math., Vol. 3, McGraw-Hill Book Co., Inc., 1950. pp. 53-66.

69. Sutherland, R.D. and Shook, R.G., Thermo-Elastic Equations Applicable to Thick-Wall Pointed Shells of Revolution, AFOSR TN 59-1274 (Convair Division General Dynamics Corp. TM-349-14) November 1959.

70. Langhaar, H.L., and Boresi, A.P., A General Investigation of Thermal Stresses in Shells, University of Illinois T. & A.M. Report No. 124, October 1957.

71. Langhaar, H.L., and Boresi, A.P., Thermal Stress Problems of Shells, University of Illinois T. & A.M. Report 131, March 1958.

72. Radowski, P.P., Davis, R.M., and Bolduc, M.R., A Numerical Analysis of the Equations of Thin Shells of Revolution, presented at the American Rocket Society 15th Annual Meeting, Shoreham Hotel, Washington, D.C., Paper No. 1580-60, December 5-8, 1960.

73. Lu, S.Y., Thermal Stresses and Thermal Buckling of Cylindrical Shells, Carnegie Institute of Technology, Ph.D. Dissertation, 1959.

74. Abir, D. and Nardo, S.V., "Thermal Buckling of Circular Cylindrical Shells Under Circumferential Temperature Gradients", Journal of the Aeronautical Sciences, Vol. 26, No. 12, December 1959. pp. 803-808.

75. Abir, D. and others, Thermal Buckling of Circular Cylindrical and Conical Thin-Walled Shells, WADC TR 58-104 (ASTIA Document No. AD151068) April 1958.

76. Hoff, N.J., "Buckling of Thin Cylindrical Shell Under Hoop Stresses Varying in Axial Direction", Journal of Applied Mechanics, Vol.24, 1957. pp. 405-412.

77. Zak, A.R., and Bollard, R.J.H., Elastic Buckling of Cylindrical Thin Shells Under Axial and Thermal Loads, American Rocket Society Solid Propellant Rocket Conference, Paper 1591. February 1-3, 1961.

THERMO-ELASTIC ANALYSIS OF BEAMS (Section I-C)

78. Boley, B.A. and Weiner, J.H., Theory of Thermal Stress, John Wiley and Sons, Inc. 1960.

79. Timoshenko, S. and Goodier, J.N., Theory of Elasticity, Second Edition, McGraw-Hill Book Company, Inc. 1951.

80. Boley, B.A. and Barrekette, E.S., "Thermal Stresses in Curved Beams", Journal of the Aeronautical Sciences, Vol. 25, No. 10, October 1958. pp. 627-630, 643.

80a. Boley, B.A., "The Determination of Temperature, Stresses, and Deflections in Two Dimensional Thermo-Elastic Problems", Journal of the Aeronautical Sciences, Vol. 22, No. 1, January 1956. pp. 67-75.

81. Boley, B.A. and Tolins, I.S., Thermo-elastic Stresses and Deflections in Thin-Walled Beams, WADC Tech. Rep. 54-426 (ASTIA Document No. AD 97342). December 1954.

82. Barrekette, E.S., Thermo-elastic Stresses in Beams, WADC Tech. Rep. 59-178 (ASTIA Document No. AD 213475). February 1959.

83. Switzky, H., Forray, M. and Newman, M., Thermo-Structural Analysis Manual, Republic Aviation Corporation Report No. 679-1(128), September 1960 (to be issued as WADD TR 60-517).

STABILITY AND NONLINEAR MATERIAL BEHAVIOR (Section II)

84. Gatewood, B.E., Thermal Stresses, McGraw-Hill Book Company, Inc. 1957. Chapter 8.

85. Timoshenko, S., Theory of Elastic Stability, McGraw-Hill Book Company, Inc., New York. 1936

86. Bleich, F., Buckling Strength of Metal Structures, McGraw-Hill Book Company, Inc. 1952.

87. Gerard, G. and Becker, H., Handbook of Structural Stability,
Part I - "Buckling of Flat Plates" - NACA TN 3781, July 1957
Part III - "Buckling of Curved Plates and Shells" - NACA 3783, August 1957

88. Budiansky, B. and HuPai, C., Lagrangian Multiplier Method of Finding Upper and Lower Limits to Critical Stresses of Clamped Plate, NACA TR 848, 1946.

89. Boley, B.A. and Weiner, J.M., Thermo-elastic Stability and Related Problems, Chapter 13 of "Theory of Thermal Stresses" - John Wiley and Sons, Inc., New York. 1960.

90. Van Der Neut, A., Buckling Caused by Thermal Stresses, Chapter 11 of "High Temperature Effects in Aircraft Structures" - Agardograph No. 28, Edited by N.J. Hoff. Pergamon Press, Inc., New York. 1958.

91. Gossard, M.L., Seide, P. and Roberts, W.M., Thermal Buckling of Plates, NACA TN 2771, August 1952.

92. Singer, J., Anliker, J. and Lederman, S., Thermal Stresses and Thermal Buckling, WADC TR 57-9, December 1956.

93. Miura, K, Thermal Buckling of Rectangular Plates, Tokyo University, Aeronautical Research Institute Report 353, May 1960.

94. Klosner, J.M. and Forray, M.J., "Buckling of Simply Supported Rectangular Plates Under Arbitrary Symmetrical Temperature Distributions", Journal of the Aeronautical Sciences, March 1958.

95. Newman, M. and Forray, M.J., Axisymmetric Large Deflections of Circular Plates Subjected to Thermal and Mechanical Loads, Republic Aviation Corporation Report No. 411 (ARD-679-3), June 1961.

96. Forray, M.J. and Newman, M., Beam Columns Subjected to Elevated Temperature and Mechanical Loads, Republic Aviation Corporation RDSR-8, April 1961.

97 Switzky, H., Approximate Solution of An Axially Restrained Column Subjected to Elevated Temperature and Lateral Loads, Republic Aviation Corporation RDSR 9 (to be issued).

98. Stowell, E.Z., A Unified Theory of Plastic Buckling of Columns and Plates, NACA TR 898, 1948.

99. Heimerl, G.J. and Roberts, W.M., Determination of Plate Compressive Strengths at Elevated Temperatures, NACA TR 960, 1950.

100. Ramberg, W. and Osgood, W.R., Description of Stress-Strain Curves by Three Parameters, NACA TN 902, 1943.

101. Switzky, H., Forray, M.J. and Newman, M., Thermo-Structural Analysis Manual, Section 3, Republic Aviation Corporation Report No. RAC-679-1(128) September 1960. (To be issued as WADD TR 60-517.)

102. Shanley, F.R., Strength Analysis of Eccentrically Loaded Columns, Engineering Research Report 54-58, University of California at Los Angeles, 1954.

103. Costello, G.A., Sidebottom, O.M. and Pocs, E., Inelastic Design of Load Carrying Members, Part II - "The Effect of End Conditions on the Collapse Load of Columns", WADD TR 60-580, January 1961.

104. Carlson, R.L., "Time-Dependent Tangent Modulus Applied to Column Creep Buckling", Journal of Applied Mechanics, Vol. 23 No. 3, p. 390, September 1956.

105. Switzky, H., Eccentric Columns, Republic Aviation Corporation RDSR-11 (to be issued).

106. Carlson, R.L., Bodine, E.G. and Manning, G.K., Investigation of Compressive Creep Properties of Aluminum Columns at Elevated Temperatures, Part 4 - "Additional Studies", WADC TR 52-251, April 1956.

107. Winkler, J.E., Effect of Transverse Temperature Gradient on Column Strength, Society of Experimental Stress Analysis Paper 674, May 1961.

108. Kempner, J. and Pohle, F.V., "On The Nonexistence of a Finite Critical Time for Linear Viscoelastic Columns," Journal of the Aeronautical Sciences, Vol. 20, No. 8, August 1953. p. 572.

109. Rabotnov, G.N. and Shesterikov, S.A., "Creep Stability of Columns and Plates", Journal of the Mechanics and Physics of Solids, Vol. 6, 1957. p. 27.

110. Hoff, N.J., A Survey of the Theories of Creep Buckling, Stanford University SUDAER Report 80, June 1958.

111. Boley, B.A. and Weiner, J.H., Viscoelastic Stress Analysis, Chapter 15 of "Theory of Thermal Stresses", John Wiley and Sons, Inc., New York. 1960.

112. DeVeubeke, B.F., Creep Buckling, Chapter 14 of "High Temperature Effects in Aircraft Structures", Agardograph No. 28, Edited by N.J. Hoff, Pergamon Press, Inc., New York, 1958.

113. Shanley, F.R., Principles of Creep Buckling, Chapter 19 of "Weight-Strength Analysis of Aircraft Structures", Edited by Shanley, F.R., McGraw-Hill Book Co., Inc., New York, 1952.

114. Gerard, G., "Note on Creep Buckling of Columns", Journal of the Aeronautical Sciences, Vol. 19, No. 10, October 1952. p. 714.

115. Gerard, G., "A Creep Buckling Hypothesis", Journal of the Aeronautical Sciences, Vol. 23, No. 9, September 1956. p. 879.

116. Deveikis, W.D., Investigation of the Compressive Strength and Creep Lifetime of 7075-T6 Aluminum Alloy Plates at Elevated Temperatures, NACA TN-4111, November 1957.

117. Mathauser, F.E. and Deveikis, W.D., Investigation of the Compressive Strength and Creep Lifetime of 2024-T3 Aluminum Alloy Plates at Elevated Temperatures, NACA TN 3552, January 1956.

118. Garard, G. and Gilbert, A.C., "A Critical Strain Approach to Creep Buckling of Plates and Shells", Journal of the Aeronautical Sciences, Vol. 25, No. 7, July 1958. p. 429.

119. Rudnick, A., Carlson, R.L. and Manning, G.K., The Compressive Creep Buckling of Metal Columns, Part VI - "Effect of Initial Imperfection", WADC TR 52 251.

120. Brownfield, C.D. and Badger, D.M., Effects of Temperature-Time-Stress Histories on the Mechanical Properties of Aircraft Structural Metallic Materials, Part II - "Stressed Exposure of 7075-T6", WADC TR 56-585, September 1960.

121. Larson, F.R and Miller, S., "A Time-Temperature Relationship for Rupture and Creep Stresses", Transactions of the American Society of Mechanical Engineers, Vol. 74, No. 5, July 1952. p. 765.

122. Manson, S.S. and Haferd, A.M., A Linear Time-Temperature Relation for Extrapolation of Creep and Stress-Rupture Data", NACA TN 2890, March 1953.

123. Dorn, J.E., The Spectrum of Activation Energies for Creep, American Society of Metals Seminar on Creep and Recovery, 1957. p. 255.

124. Turner, Clough, Martin and Topp, "Stiffness and Deflection Analysis of Complex Structures", Journal of the Aeronautical Sciences, Vol. 23, No. 9, September 1956. p. 805.

125. Meissner, C.J., Some Considerations for the Preliminary Structural Design of Liquid Fueled Boosters, Fifth Symposium on Ballistic Missile and Space Technology, Los Angeles, August 1960.

126. Radowski, P.P., Davis, R.M. and Bolduc, M.R., A Numerical Solution of the Equations of Thin Shells of Revolution, Presented at American Rocket Society 15th Annual Meeting, Washington, D.C., December 5-8, 1960. Paper 1580-60.

127. Basin, M.A., McNeal, R.H. and Shields, J.H., "Direct Analog Method of Analysis of the Influence of Aero-Dynamic Heating on the Static Characteristics of Wings", Journal of the AeroSpace Sciences, Vol. 26, No. 3, March 1959. p. 145.

128. Ryder, F.L., "Energy vs. Compatibility Analogs in Electrical Simulators of Structures", Journal of the Aerospace Sciences, Vol. 26, No. 2, February 1959.

129. Warfield, J.N., Introduction to Electronic Analog Computers, Prentice-Hall, 1959.

130. Clymer, A.B., Handbook of Equations and Operational Analog Circuits for the Solution of Structural Problems, North American Aviation Engineering Department, Columbus, Ohio. 1960.

131. Warren, D.S., Castle, R.A. and Gloria, R.C., An Evaluation of the State-of-the-Art of Thermo-Mechanical Analysis of Structures, WADD TR 61-152, May 1961.

132. Lansing, W., Jones, I.W. and Ratner, P., A Matrix Force Method for Analyzing Heated Wings, Including Large Deflections, Symposium: "Structural Dynamics of High Speed Flight", Aerospace Industries Association and Office of Naval Research, Los Angeles, California, April 24-26, 1961.

133. Turner, Dill, Martin and Melosh, "Large Deflections of Structures Subjected to Heating and External Loads", Journal of the AeroSpace Sciences, Vol. 27, No. 2, February 1960 p. 97.

134. Wilson, E.L., Matrix Analysis of Nonlinear Structures, Proceedings of the Second Conference on Electronic Computation-ASCE, Pittsburgh, Pennsylvania, September 8-9, 1960. p. 415.

135. Switzky, H., Forray, M. and Newman, M., Thermo-Structural Analysis Manual, Republic Aviation Corporation Report No. 879-1(128), September 1960 (to be issued as WADD TR 60-517).

136. Huang, P.C., Time-Dependent, Elasto-Plastic Bending Analysis for Structures Under Arbitrary Load-Temperature Environments, WADD TR 60-541, Part I. April 1960.

137. Mills, W.R., An Equivalent Plate Method of Structural Analysis for Elevated Temperature Structures, Part I - Procedures for Including Temperature Effects in Structural Analyses of Elastic Wings, WADC TR 57-754, January 1958.

138. Conte, S.D., Miller, K.L. and Sensenig, C.B., The Numerical Solution of Axi-Symmetrical Problems in Elasticity, Space Technology Laboratories, Inc., Report STL TR 60-0000-00302.

139. Melosh, R.J., "A Stiffness Matrix for the Analysis of Thin Plates in Bending", Journal of the AeroSpace Sciences, Vol. 28, No. 1, January 1961. p. 34

140. Archer, J.S. and Samson, C.H., Structural Idealization for Digital Computer Analysis, Proceedings of the Second Conference on Electronic Computation-ASCE, Pittsburgh, Pennsylvania, September 8-9, 1960. p. 283.

141. Samson, C., Jr. and Bergman, H., "Analysis of Low Aspect Ratio Aircraft Structures", Journal of the AeroSpace Sciences, Vol. 27, No. 9, September 1960. p. 679.

142. Rattinger, I. and Gallagher, R.H., Supersonic Aeroelastic Effects on Static Stability and Control, Part II - Structures, WADC TR 58-95, April 1960.

143. Klein, B., "A Simple Method of Matric Structural Analysis", Journal of the Aeronautical Sciences:

Part I - Vol. 24, No. 1, January 1957. p. 40.
Part II - Effects of Taper and Consideration of Curvature, Vol. 24, No. 11, November 1957. p. 813.
Part III - Analysis of Flexible Frames and Stiffened Cylindrical Shells, Vol. 25, No. 6, June 1958. p. 385.
Part IV - Nonlinear Problems, Vol. 26, No. 6, June 1959. p. 351.
Part V - Structures Containing Plate Elements of Arbitrary Shape and Thickness, Vol. 27, No. 11, November 1960. p. 859.

144. Argyris, J.H. and Kelsey, S., The Matrix Force Method of Structural Analysis and Some New Applications, Aeronautical Research Council of Great Britain R & M 3034, 1957.

145. Meissner, C.J., Direct Beam Stiffness Matrix Calculations Including Shear Effects, Republic Aviation Corporation RDSB-9, June 20, 1961.

146. Lehman, F.G., Simultaneous Equations Solved by Over-Relaxation, Proceedings of the Second Conference on Electronic Computation-ASCE, Pittsburgh, Pennsylvania, September 8-9, 1960, p. 503.

MATERIALS AND CONSTRUCTION CONCEPTS FOR STRUCTURES SUBJECTED TO SEVERE KINETIC HEATING

Charles J. Cosenza

ASD Flight Dynamics Laboratory

Robert D. Guyton

Universal Technology Corporation

M/Sgt. Jesse C. Ingram, Jr.

ASD Flight Dynamics Laboratory

ABSTRACT

Technical advances during the past few years have established 2500°F structural concepts for application to aerospace vehicle design. Detailed structural evaluations of the refractory metal, insulative, thermostructural configurations have been conducted during the past few years; experimental test results have validated the static thermoelastic design analyses and construction techniques employed in the development of these concepts. Further efforts are being conducted to extend capabilities to 5000°F structural concepts that exhibit reliability and high integrity. Considerable research studies are being directed toward the composite and combined ablative-radiative structures to operate in this hyperthermantic environment. Programs in support of these technological areas are discussed in terms of objectives, scope, progress and problem areas.

MATERIALS AND CONSTRUCTION CONCEPTS FOR STRUCTURES SUBJECTED TO SEVERE KINETIC HEATING

INTRODUCTION

Structural requirements for higher performance flight vehicles during the past ten years have resulted in marked achievements being made in the application of higher strength, corrosion resistant steels. Probably the most notable advancement has been in sandwich construction of the brazed cellular honeycomb and resistance welded corrugation supported types. Today, however, the most advanced of these is not considered reliable for any structural utilization above 1600°F and this would be under very low loads or for short time periods except where temperatures are below 900°F.

The mission requirements of future flight vehicles dictate that certain structural elements sustain equilibrium temperatures as high as 4500°F during re-entry from super-orbital flights. Similar structural components may experience temperatures no greater than 3000°F during re-entry from sub-orbital flights.

The first efforts to meet structural requirements for hypersonic flight environments were begun by the Flight Dynamics Laboratory early in 1958 with the Bell Leading Edge Program which investigated molybdenum and graphite. Next was the McDonnell refractory metal component which was fabricated from columbium alloys. Along with the latter program was another effort with Bell and one with Boeing. The first two mentioned (of these four) demonstrated a capability approaching 2500°F and the latter two were limited to about 1800°F.

Since mission requirements have continually increased, thereby increasing the demands made on materials, it has become necessary to explore the potentials of more rare and unique materials. These include the more attractive refractory metal alloys, also super alloys of nickel and cobalt, the newer ceramics and graphites and combinations of the metallics and non-metallics. Various modes of insulation and cooling must also be investigated.

This paper briefly presents the recent past efforts of the Flight Dynamics Laboratory and, in more detail, the present efforts and future plans. Various combinations of materials in composite configurations are discussed and it will be shown that many trade-offs are available. Specific materials applications in given configurations will depend upon reasonably well calculated or predicted environments which are evolved from trajectory studies. Actual flight, however, must be accomplished to verify ground simulation and predictions.

I. BACKGROUND AND GENERAL DISCUSSION

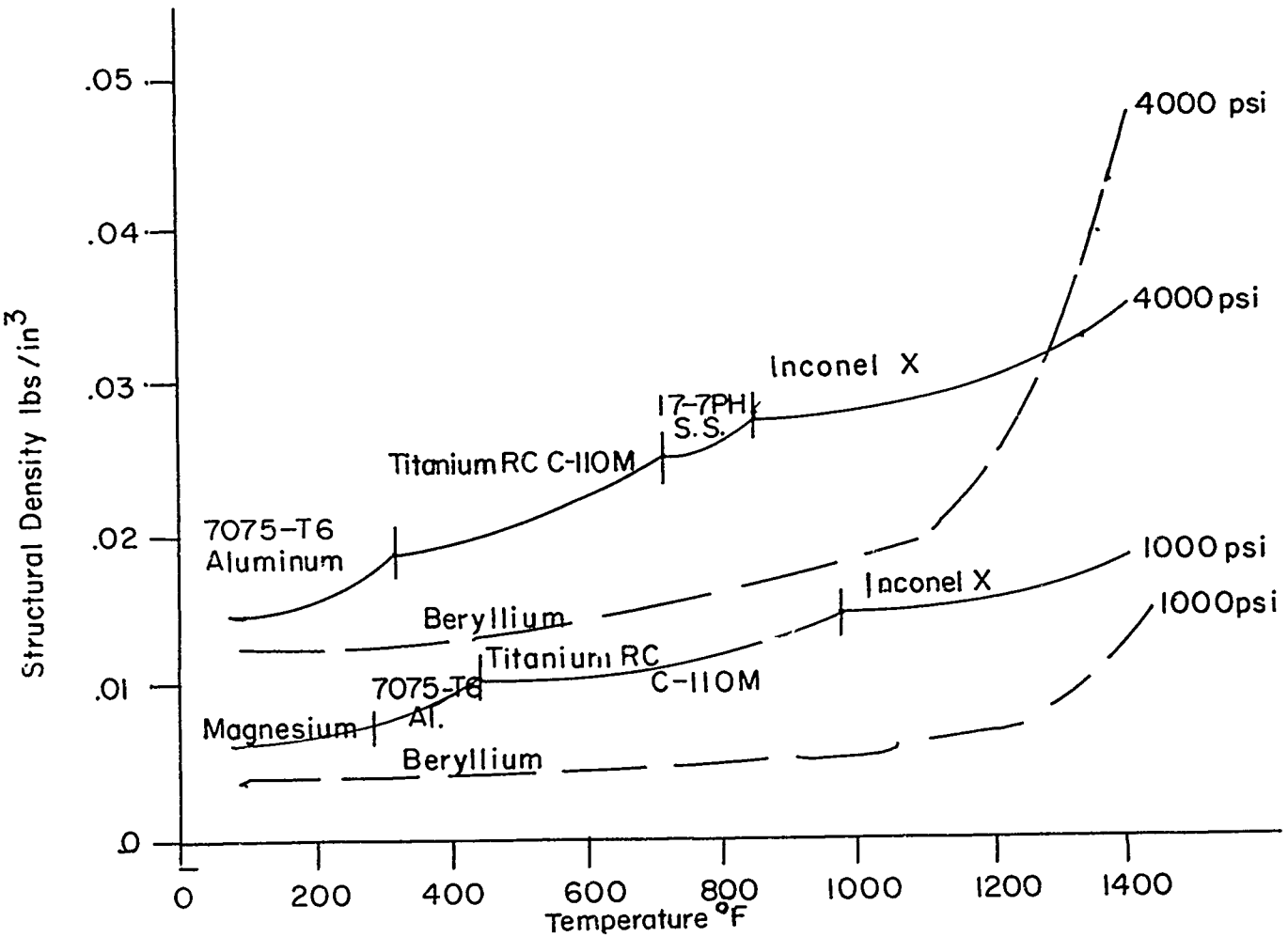
During the past ten years the design of efficient structural configurations has necessitated the exploitation of all new materials and material systems capable of withstanding aerothermal loads encountered during the operational life of advanced flight vehicles. In this total structural research effort, high temperature materials with high strength-to-weight efficiencies have not been developed at a rate commensurate with the rapid increase in vehicle performance requirements. Increased speed capabilities and the resulting heating conditions have advanced so rapidly that the maximum permissible temperatures of available airframe materials has been reached, and in many cases exceeded. It is becoming more pronounced that structural capability is seriously limiting hypervelocity vehicle performance in certain flight regimes.

To design around the materials shortcomings and availability status, several unique design approaches and construction concepts have been evaluated for their overall suitability to airframe design. Several large-scale research programs are presently being conducted to further define the potential for other advanced concepts. The first approach is the conventional one in which a heat-sustaining structure is developed, utilizing materials which have the required structural properties at elevated temperatures. Another approach limits the maximum operating temperatures of the load carrying structure by providing sufficient protection devices which can preclude this temperature either by absorbing most of the heat or by radiating it back to the atmosphere. Still, other approaches for cooling techniques and composite systems are being investigated for application in extremely high temperature regimes.

Since the early 1950's and continuing today, a concerted effort has been directed toward the heat resistant structural configurations optimized from standpoints of structural weight, producibility and integrity parameters. Figure 1 presents a plot of the temperature versus structural density representation of multiweb beams in bending at a M/h^2c of 1000 and 4000 psi. The temperature range considered is from 70°F to 1400°F, which is considered to be near the upper temperature limit for present-day heat resistant structures. In the structural loading index M/h^2c, M is the total applied bending moment, h is beam depth and c is the chordwise length. Identical beam proportions were used for all computations.

Aluminum, magnesium, titanium and steel alloys have been utilized extensively in airframe applications during the past years and fabrication processes, required to attain various structural shapes and forms have been developed and are being employed in present day weapon systems development programs. Beryllium structures have not reached this technological level, however, the outstanding potential for beryllium can be readily noted from the plot. Relating the aforementioned loading indices to a delta wing vehicle, the apparent savings in structural weight could be from 30% to 60% in the temperature range of 1000°F. Why there has not been more use of beryllium in structural applications can be understood, however, when beryllium fabrication and construction techniques are investigated. The brittleness problem, high cost, handling, joining and component assembly are critical, unresolved factors that contribute to the limited usage currently associated with beryllium structures technology. There is every intention to continue exploration of the outstanding potential for beryllium structures.

Recent tests at room and elevated temperatures have shown that beryllium compression panels can develop very high strengths, even in the post buckling regime at room temperature and with almost imperceptible post-buckling deflections normal to the sheet. Further tests have shown that the notch sensitivity of beryllium sheet at low temperature is not sufficiently great to preclude primary structural applications. Experiments have also confirmed that under biaxial tension states of stress (e.g., 2:1 or 1:1 stress ratios) cross-rolled beryllium sheet exhibits extraordinary amounts of increased strength as compared to its uniaxial strength (possibly 100% increase). Efforts are needed which will establish the amount of this apparent increase in strength and then, structural applications wherein the phenomenon is studied for possible areas of utilization rather than toward searching for methods for eliminating it. Pressure



TEMPERATURE vs STRUCTURAL DENSITY REPRESENTATION OF MULTIWEB BEAMS IN BENDING AT A M/h^2c OF 1000 AND 4000 psi

FIGURE 1

vessels and built-up panels could be used for this evaluation.

Another form of construction which has been used extensively during the past several years is sandwich construction. In structural applications, where the flexural rigidity requirements were great and weight was an important consideration, sandwich construction has been utilized. It can be stated that more sandwich composite structures will be utilized in future airframe applications designed on the basis of fairly low loads yet very rigid aerothermoelastic criteria.

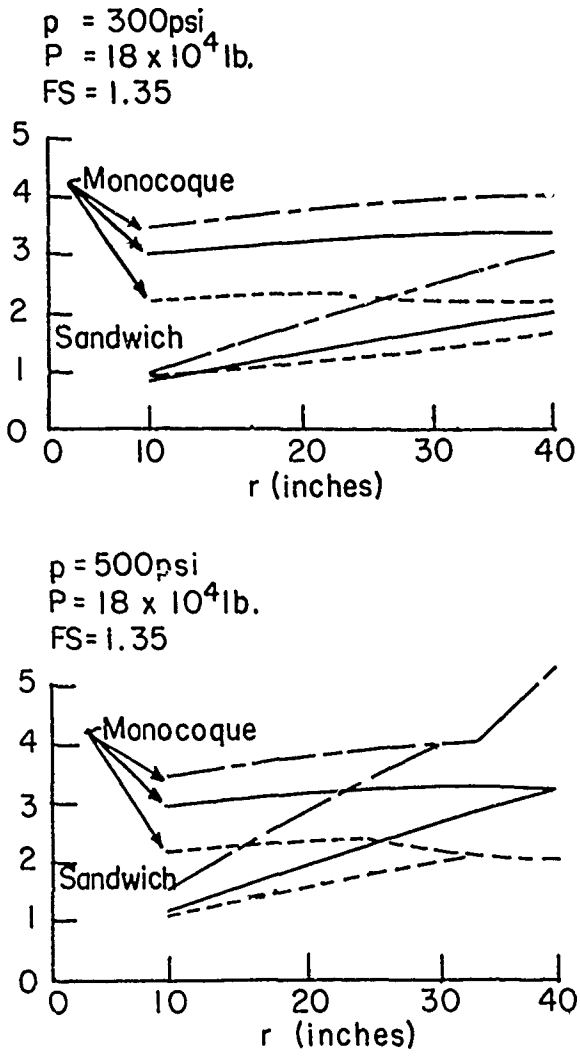
There are two basic criteria which should be adopted in the development of efficient sandwich structures. These criteria may be stated thusly:

a. The composite sandwich must act as an integral load carrying unit wherein the plate-material strength rather than instability governs the design.

b. Choice of core configuration, bonding materials and fabrication processes must be selected so that core weight and bonding weight is considered light (of the order of 15 to 25%), relative to the total structural weight.

The first item involves the choice of structural materials and material systems developed into optimum configurations. The second item, however, is more difficult to evaluate. Some of the problems encountered here are local instabilities such as crippling and dimpling. The detailed design of an optimum sandwich structure entails careful analyses of the structural loading parameters whereby the core (stabilizing element) weight is not excessively high relative to the load carrying members. A full depth sandwich beam in bending and at low loadings is an example of this situation. Obviously, the construction variables and volume considerations dictate, in certain cases, the ultimate choice of a sandwich structure.

One area of Air Force interest for sandwich construction is rocket motor cases and tankage structures. This form of construction has not been used extensively in the past because light weight materials have been available or because internal pressures have been depended upon to provide additional stability. Neither of these two solutions may be totally satisfactory for future applications. Figure 2 presents the weight per unit area for a cylindrical shell of a given radius and for a specific design case. Filament-wound



LEGEND–

——— Steel

——— Titanium

------- Filament-wound "fibergiass"

WEIGHT VERSUS RADIUS FOR CYLINDERS SUBJECTED TO AXIAL COMPRESSION

FIGURE 2

"fiberglass," titanium and steel have been considered as structural materials with both sandwich and monocoque construction being analyzed. It can be noted that the fiberglass sandwich offers a weight advantage, except for cases having extremely small radii. Economical aspects and producibility factors would be considered in certain instances where weight differences are not significant. Our programs are considering these total factors.

The discussion to this point has been concerned with the structural materials and configurations that may be considered for load carrying applications up to 1500°F but this capability is hardly satisfactory to meet future mission requirements of the Air Force. The following part of our discussion, therefore, will be concerned with the program activities that are currently being conducted to increase the total Air Force thermostructural capabilities.

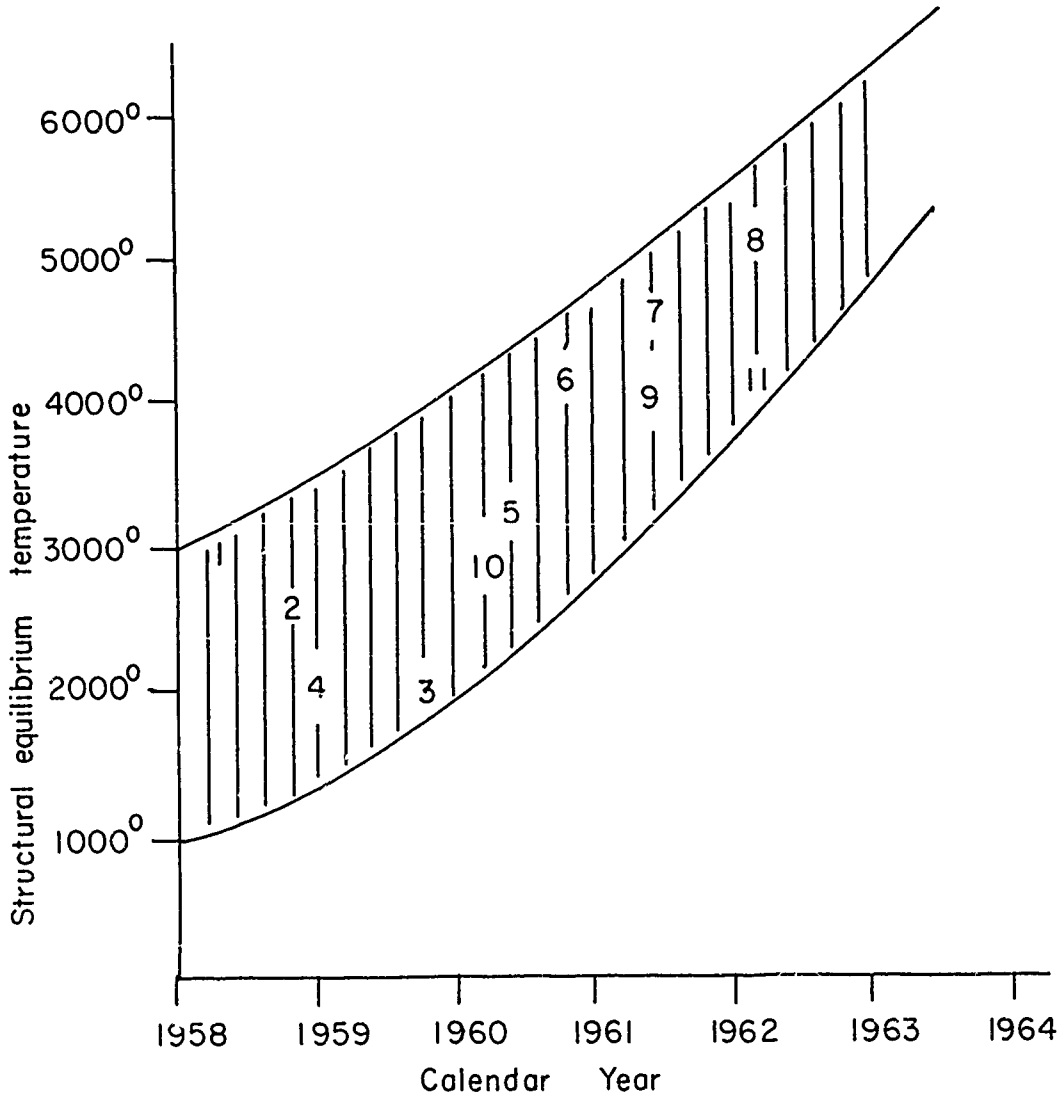
Figure 3 indicates the research cycle that has been established for re-entry structures technology. In 1958, programs were initiated for 3000°F structures. Radiative metallic configurations and their technologies were most advanced at that time. Response of ductile metallic assemblies to design loads could be predicted, unique thermal characteristics were fairly well known and construction processes had been investigated in some detail. Our efforts involved the determination of detailed design parameters, accurate experimental evaluation of coated built-up refractory material assemblies and confirmation of design theories. Materials investigated included the super alloys and alloys of molybdenum and columbium under various thermal loads and combinations of thermal/structural conditions of loading.

Beyond the 3000°F temperatures, composites are being evaluated to attain 5000°F capabilities. Combinations of absorptive, insulated, insulated and cooled, and radiative structures are being investigated for the 5000°F applications. Thermal capabilities, thermal shock characteristics and many physical and mechanical properties of the materials were virtually unknown; capabilities for a structural system utilizing these materials had not been determined. Efforts have been expedited to determine attractive design features for the composites, size limitations, optimization of the system and design techniques for these composites. Under this structural design area, foamed ceramics, high temperature insulators, active cooling schemes,

APPLICATION:

1. Leading edge
2. High temp. load carrying component
3. Light weight structures
4. Structural Sealing
5. Thermantic panels
6. Composite structures
7. Tungsten/tantalum leading surfaces
8. Cooled structures
9. Brittle structures technology
10. Structural fastening devices

11. ASSET



PROGRESS IN RE-ENTRY STRUCTURES RESEARCH

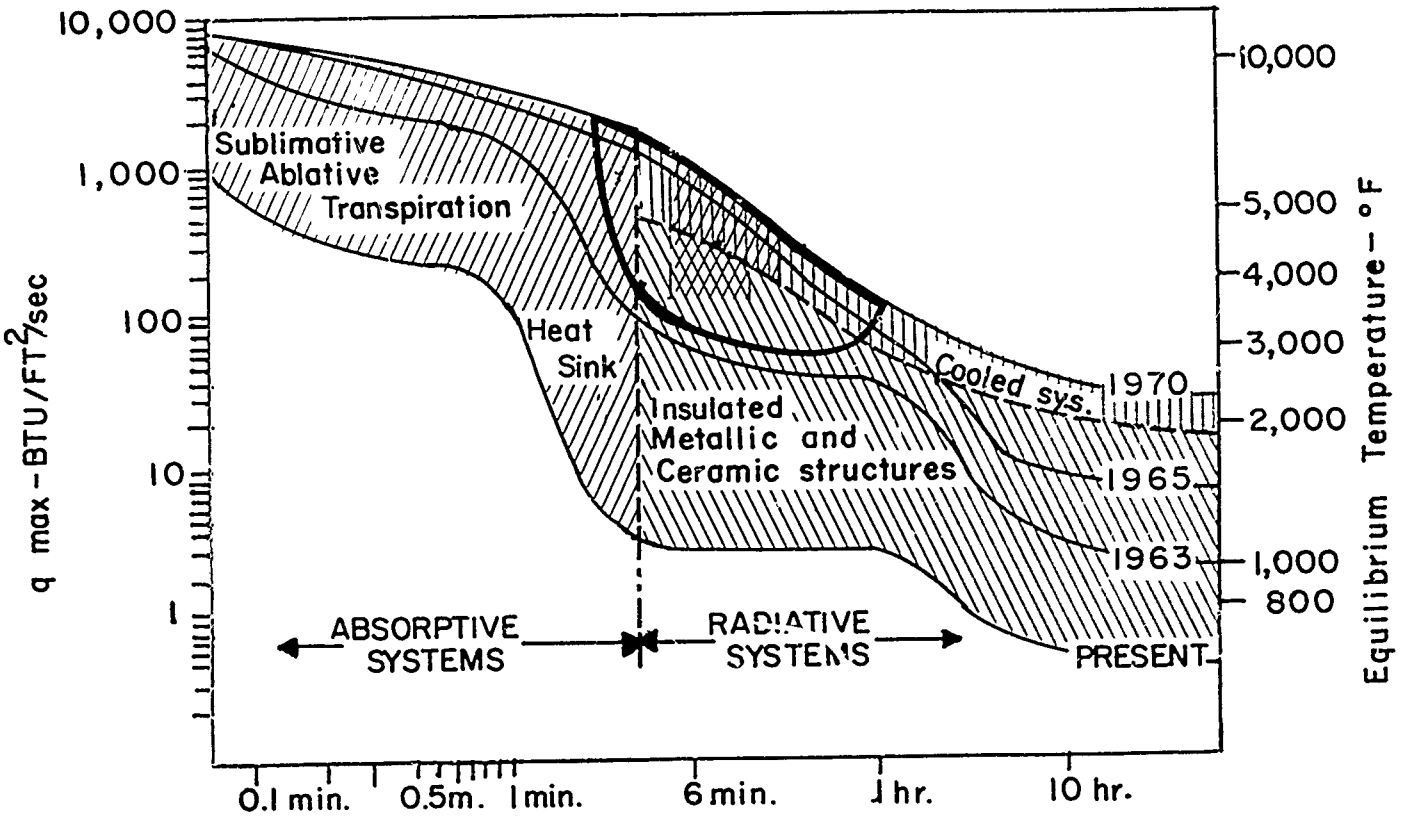
FIGURE 3

heat radiating components and other advanced concepts are being investigated.

Our programs are expected to fill gaps and extend technological areas of prime importance to future mission requirements. From these very broad outlines, basic criteria are formulated from which detailed programs are planned. Figure 4 shows the relationship between various structural systems as a function of temperature, heat flux and time at elevated temperatures. The region of primary concern is encircled. It will be noted that the encircled area includes the super-orbital vehicles, the low altitude orbit return and the hypervelocity glide vehicle operational regimes. The critical design problems appear to be concentrated in the super orbital return vehicle mis .on where the integration of several different concepts, including ablation materials, active cooling, ceramics and metallic load carrying members, be required to survive these environments. The other highly critical performance regime will be the hypersonic flight vehicles that operate for extended time periods. Economy, reuseability, and reliability parameters must be considered in the design of those vehicles.

The indicated progress trends represent significant advancements in structural technologies. Our present-day structural capabilities permit sustained flight in low aerodynamic heating areas of high dynamic pressures and aeroelastic influences. Structural design approaches for the short duration, one shot flight applications, exist in the moderate temperature environments. Within the near future, structural capabilities will be provided to achieve re-entry from low altitude orbits and to explore the atmospheric hypersonic flight regimes. The refractory metallic and non-metallic configurations offer the earliest solution for research vehicles that will investigate the flight performance corridors of interest. Further scientific advances in the design of thermantic or cooled structural configurations will significantly extend the ability to obtain increased payloads, greater maneuverability and overall performance benefits for extreme altitude orbit vehicles.

As a preliminary basis for field of interest orientation and advanced planning, a study of re-entry as related to future structural requirements has been completed. The most important aspect of this study presented practical ballistic and glide super-orbital



STRUCTURAL CONFIGURATIONS FOR ELEVATED TEMPERATURES

FIGURE 4

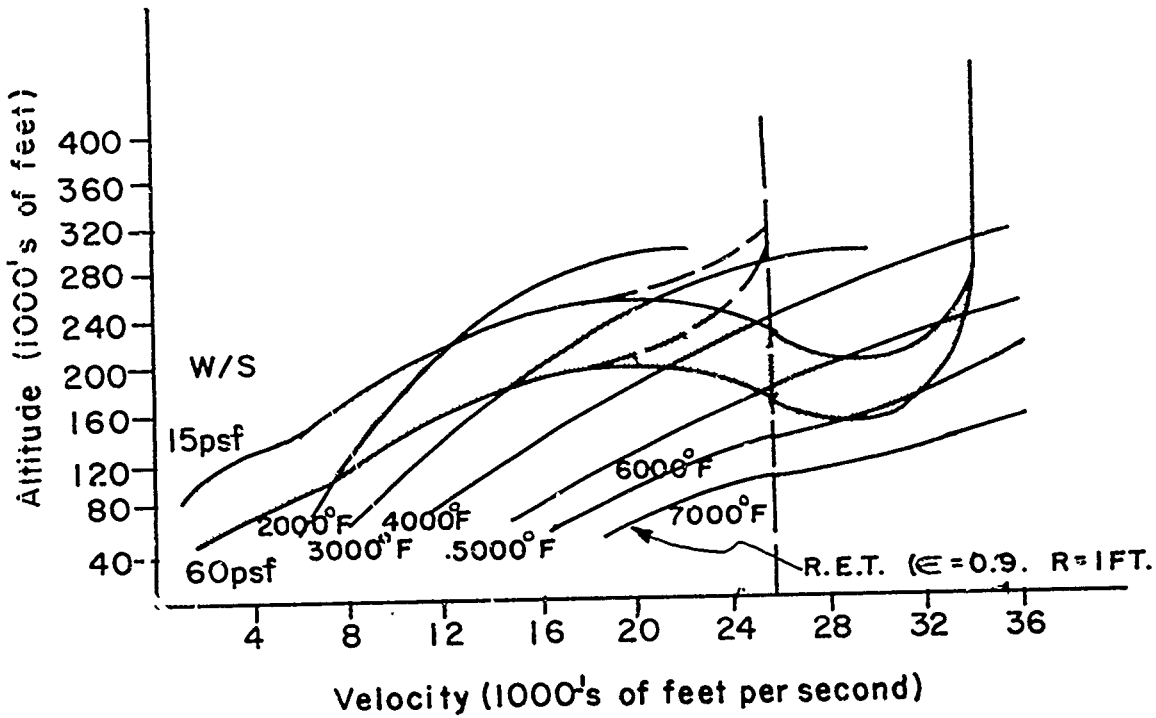
re-entry trajectories with accompanying loading and heat flux histories. This program has provided information from which preliminary vehicle design and mission trajectories can be derived, thus pointing out critical areas for investigation and also the outstanding problems. One type of re-entry mission is represented in Figure 5. It is typical of super-orbital re-entry (in this case 35,000 fps and initial re-entry of -10° at 400,000 ft. altitude) where a corridor is shown for controlled vehicles with a wing loading of 15 - 60 psf. The radiation equilibrium temperatures shown are for a one foot stagnation point radius assuming a material emmittance rating of 0.9. As can be seen by the temperature profile, active cooling must be used during part of the mission, whereas radiation cooling would be adequate and within the present structure's state-of-the-art during the portion of re-entry below 25,000 ft/sec. It is therefore necessary to develop means of active and passive cooling and to then combine them into an optimum thermal protection system for any given vehicle and mission. The present primary mission of advanced structural research is to concentrate on the conception and development of basic thermal protection systems. Total vehicle cooling systems will then be detailed and designed for integral operational efficiency when specific vehicles or classes of vehicles are under development.

A discussion is made of 1960-1970 material properties and the theory is proposed that with the stringent requirements which will be imposed on materials, the designer might gain by improving design concepts rather than rely on improved materials. A particular study is made of passive hot structures protected by ablation only during peak heating as opposed to cool structures protected by ablation throughout the re-entry. Conclusions drawn throughout the report are summarized and a program of needed research is outlined. The report, which is currently being published, is listed as WADD Technical Report 60-866.

II. DETAILED PROGRAM EFFORTS

REFRACTORY METAL STRUCTURES

Since 1958, our efforts have been directed toward the evaluation of those structural materials identified as being somewhat available on the commercial market. The molybdenum and columbium alloys have been investigated extensively in airframe applications



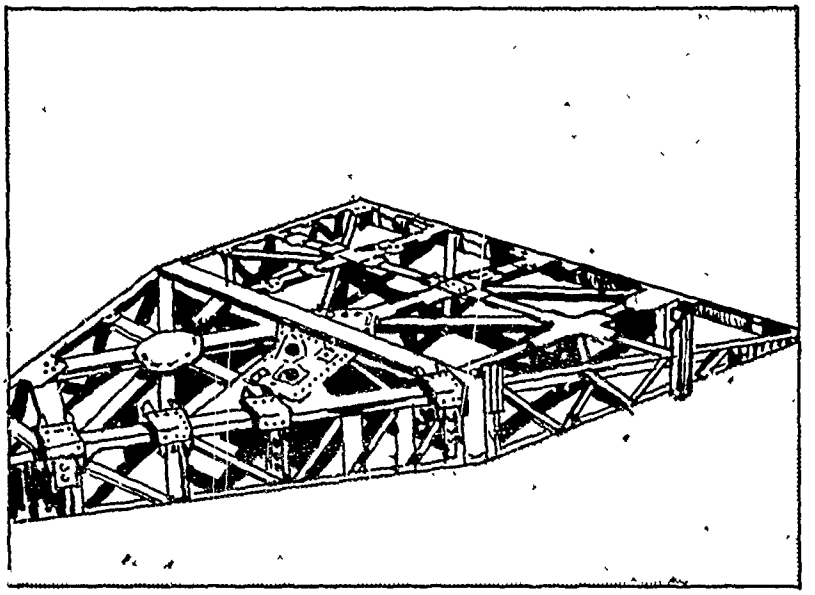
CONCEPTUAL RE-ENTRY CORRIDOR

FIGURE 5

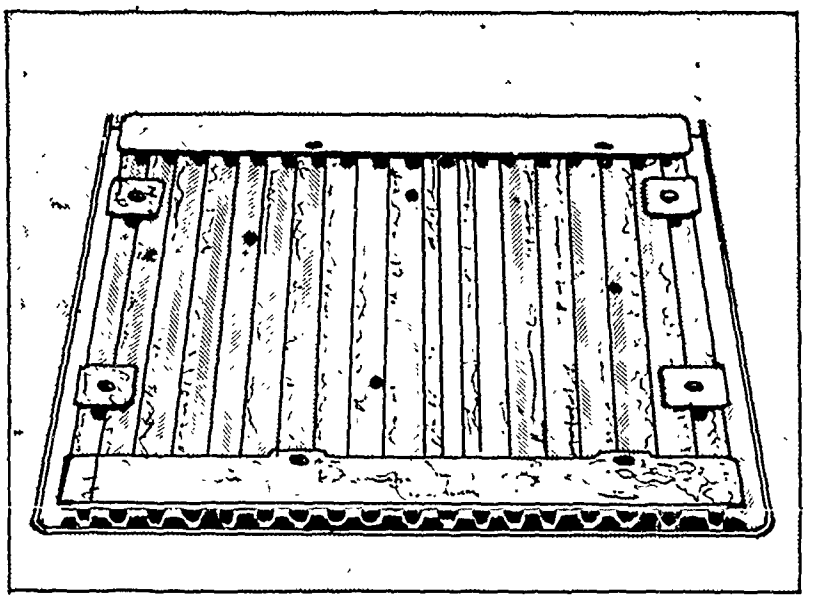
such as radiation shields and leading surfaces. Graphite materials have been considered for 3000°F structural applications. The leading edge program, wherein siliconized graphite and the molybdenum alloys were evaluated relative to coating integrity, thermal stresses, strain, material quality and fabrication techniques, was the initial effort in refractory metal and non-metal structures. Particular emphasis in this program was directed toward the performance of coated structural surfaces under thermal loads representative of re-entry conditions for the 20 to 30 psf load class of re-entry vehicles. While design values of 3000°F could not be duplicated in test facilities, results did confirm that the molybdenum and graphite materials could be utilized in leading edge applications in the 2500°F to 3000°F range. Extremely valuable information has been collected in this program and the application of this data in vehicle design is being effected today.

Research efforts were continued in the refractory metal structures with the initiation of the McDonnell refractory metal structural component program. Total scope of the two programs was very similar. In the structural component program it was determined that coated refractory metals fabricated into structural shapes would be evaluated under structural loads as well as 2500°F thermal loads. The expected payoff from this program would be the development of an approach leading to a hot monocoque or semi-monocoque structural configuration which could reduce structural weights by some 30 to 50% as compared to the use of refractory metal panels for thermal shielding. It is additionally important to determine the response of coated refractory metal structures to actual structural deformations and stresses. This program will provide factual information that can be used to realistically assess the structural potential for refractory metals.

Figure 6 shows the configuration finally chosen which was a fixed-fin, deflecting-rudder (hinged) having a planform of approximately 17 1/2 sq. ft. and the principal material chosen was the columbium base alloy F-48. Some FS-80 and FS-82B were used for fasteners and fittings. The coating finally chosen was an aluminum-silicon-chronium compound which was applied as a cold slurry and subsequently diffusion heat-treated in an argon atmosphere. Numerous problems plagued the program due to inexperienced personnel, overtaxing of equipment, lack of material uniformity, etc. Most of these have been resolved and such an effort now could be pursued much more expeditiously and with a much greater degree of reliability.



Fin - rudder combination



Panel

Figure 6. Refractory Fixed-Fin Reflecting Rudder and Panel

The program is essentially finished with tests having been completed in mid-July 1961. Tests included several thermal cycles, three of which reached an equilibrium temperature of 2425°F (surface), and several load cycles (at temperature) up to 150% of design ultimate. Not all test objectives were met due to limitations of test equipment, however, there was no evidence of imminent failure except for localized skin-wrinkling and panel corner-warping and these are considered to be only design problems. Reports on this subject are presently being published.

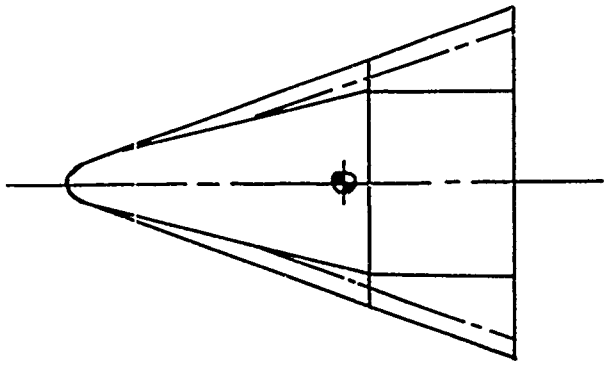
In view of the success of this program, including the ability to fabricate and protect a very attractive columbium base alloy structure which has good elevated temperature capabilities, any arbitrary decisions to use the refractory metals only in thermal-shield, no-load applications should be critically reviewed.

PROJECT ASSET

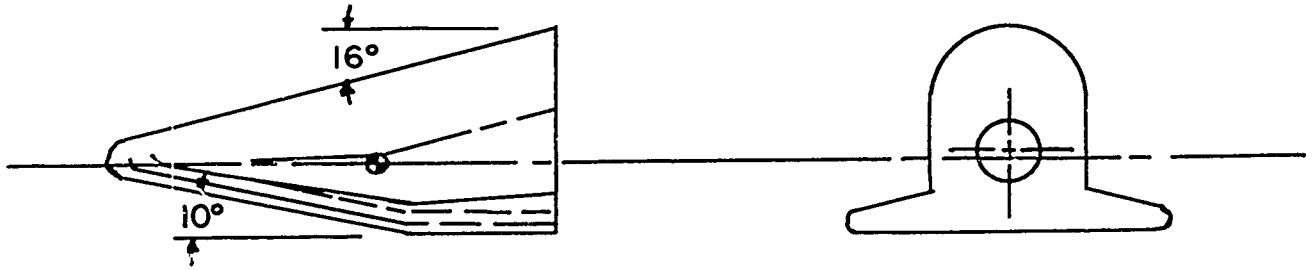
To further define the response of aerothermoelastic/structural systems under re-entry conditions, a flight test program has been considered to subject test vehicles to actual re-entry environments. This program is identified by the title of "Project ASSET".

The program has been planned to provide an economical and feasible means for evaluating aerothermodynamic, structural and aerothermoelastic theories and approaches. The purpose of the program would be to supplement and verify the validity of ground facility data by obtaining basic knowledge of the actual free flight environment in the critical heating regime surrounding hypersonic lifting re-entry vehicles. Furthermore, this program would substantiate the practicality of several advanced structural and material concepts, verify the validity of aerothermoelastic prediction methods, and obtain aeroelastic stability data in a real environment.

The vehicle configuration as shown in Figure 7 will be a flat bottomed 70 degree swept delta wing with a planform area of 14 square feet and cone cylinder body on the upper surface. The diameter of the nose is six inches and the diameter of the leading edge is four inches. These are the minimum sizes dictated by the thermodynamic environment and material limitations.



Length	69.0 inches
Span	54.88 inches
Wing sweep	70° (true)
Wing area	14 square feet
Nose tip radius	3 inches
Leading edge radius	2 inches
Weight	600-700 pounds

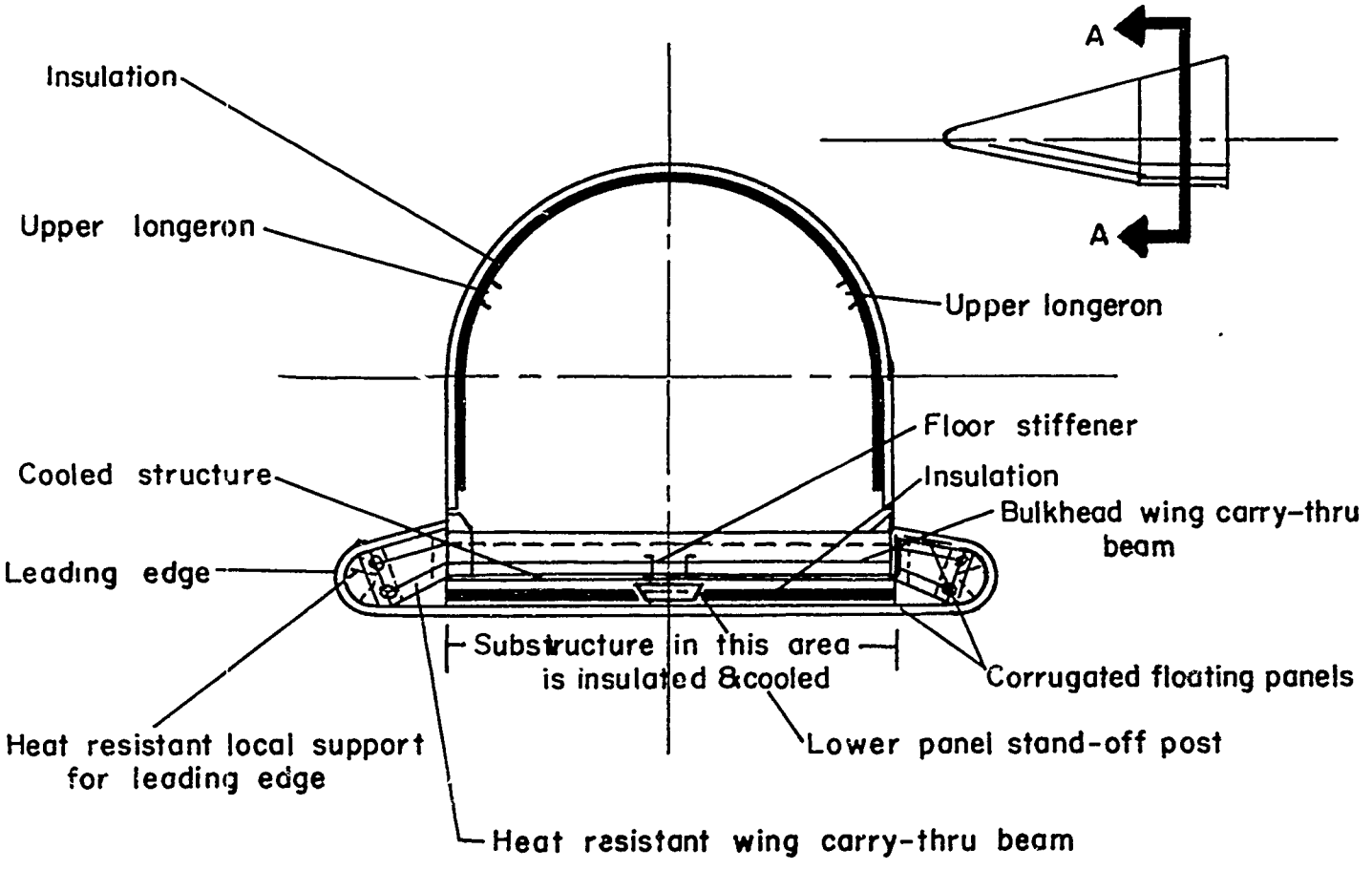


VEHICLE CONFIGURATION
FIGURE 7

The vehicles are designed to test full scale components of various structural concepts and materials. Hot gas infiltration, material oxidation rates, and other environmental effects will be investigated. The assessment of aerothermoelastic problems will include the accuracy of theoretical prediction methods for estimating thermal effects on structural dynamic characteristics and aeroelastic instabilities. These vehicles will be designed with both local and overall flexibilities to provide representative aerothermoelastic characteristics and to yield meaningful data on phenomena such as structural vibrations, hinge moments and unsteady aerodynamics. Aerothermodynamic data obtained can be used to verify and/or modify existing theoretical methods for predicting the pressures and temperatures on typical configurations and will correlate ground facility data. Data from all of the vehicle flights will be telemetered via X-Band and VHF, internally recorded for delayed playback, and the vehicle and data package subsequently recovered. X-Band telemetry will be employed in order to transmit the data through the ionized sheath surrounding the vehicle.

Figure 8 presents the major structural design features. The nose cone and leading surfaces of the vehicle will utilize graphite, ceramics and refractory metals. The lower fuselage area will utilize both insulated and cooled structures. The two types of systems currently considered acceptable for this application are the Bell double wall tube sheet and the Chance Vought wetted blanket (Thermosorb) concepts. The lower surface heat shields will be constructed of refractory metals, namely, TZM molybdenum, Cb 74 columbium and 5 Zr columbium. The upper fuselage area will be insulated and constructed of circumferential corrugations with shingled external skins of columbium and super alloy materials. The wing structure will be cooled by radiation only.

Structural materials will be used in relation to their temperature capabilities. The graphite and ceramic materials will be used in those areas where temperatures in excess of 2700°F are expected. Coated molybdenum radiation shields will be used where temperatures range between 2700°F and 3100°F while coated columbium will have application where temperatures are between 1800°F and 2700°F. Super alloy materials are utilized extensively below 1800°F. The cooled structure will probably be made of aluminum.



SECTION A-A

STRUCTURAL CONFIGURATION

FIGURE 8

Although several materials and structural approaches will be utilized, conservative design and construction practices will be used to assure the structural integrity of the vehicle. Current major efforts involve the evaluation of several columbium alloys, including the F - 48 and Cb - 74 materials, to define their favorable characteristics for this vehicle application. Emphasis will not be placed on obtaining an optimum design for the predicted flight environment, but rather on obtaining a reliable vehicle which provides maximum data on the selected materials and design concepts.

OBJECTIVE SUMMARY

The programs discussed so far have been oriented to support the low altitude orbit re-entry vehicles. Results from these programs are being applied toward the design of the Dyna Soar and medium wing loading class of re-entry vehicles. The prime intent of these programs has been to develop structural concepts that can operate efficiently in a 3000°F environment for a maximum period of time of two to five hours.

There is now an urgent requirement to move beyond the 3000°F range to much higher capabilities. Growing interest in deep space probes, super orbital vehicles and large payload carrying vehicles has dictated the necessity to attain advanced structural concepts that can survive much higher thermal loads. Initial efforts in these areas were begun in late 1959 on a very modest scale.

THERMANTIC PANEL STRUCTURES

This program began as a feasibility study to determine the characteristics of a ceramic thermal shield, foamed in place in a honeycomb core (or similar binders) that would be brazed or bonded to load carrying members. Alumina, silica, zirconia and various combinations of these materials were investigated for effects of density and processing variations. Stainless steel and Inconel core materials were utilized for the binder material. Several core sizes were evaluated and a corrugated cell wall of minimum thickness and 1/2 to 3/4" in cell size appears optimum. Stainless steel and beryllium were

utilized as the load carrying structure.

Several types of construction have evolved from recent efforts to achieve a high efficiency insulating system. Figure 9 shows the details of a representative thermantic panel. The load bearing and insulation requirements are divided, yet the entire construction is an integral panel. The load bearing structure consists of a lightweight steel, beryllium or super alloy, depending on temperature and load requirements. It is significant to note that under current efforts, 36 inch X 36 inch double curvature beryllium panels have been fabricated utilizing steel core materials and silver-lithium braze alloys. Structural cooling is optional, depending on design requirements. The corrugated double skin panels provide the volume capacity for a cooling system at small weight penalties.

The thermal shield uses a foam of low density ceramic type insulation for the heat shield surface. Densities of the order of 35 lb/ft^3 are being investigated with the specific purpose of attaining the best combinations of conductivity, emissivity and thermal shock properties. Through the introduction of certain additives, such as nickel oxide-chrome oxide, emissivity values have been increased significantly up to 3000°F. A value of 0.8 is our goal and this appears possible at this stage of development.

To lower the conductivity and reduce weight, a second layer of fibrous or particulate insulation is utilized under the ceramic layer.

The weight (and sometimes space) requirements for applications of the thermantic construction concept demand the highest efficiency possible from the secondary insulation. A quick survey shows that the felt type and particulate-fiber insulations are the most efficient but are not useful above 2200°F. Examples of some of the high efficiency insulations that are being considered for typical application are the "MIN-K" and Micro-Fiber Quartz", the "Fiberfrax" blankets and papers of the Carborundum Company, and the potassium titanate "Blocks" and "Loose fibers" of the DuPont Company.

Based on the presently available information, emphasis will be

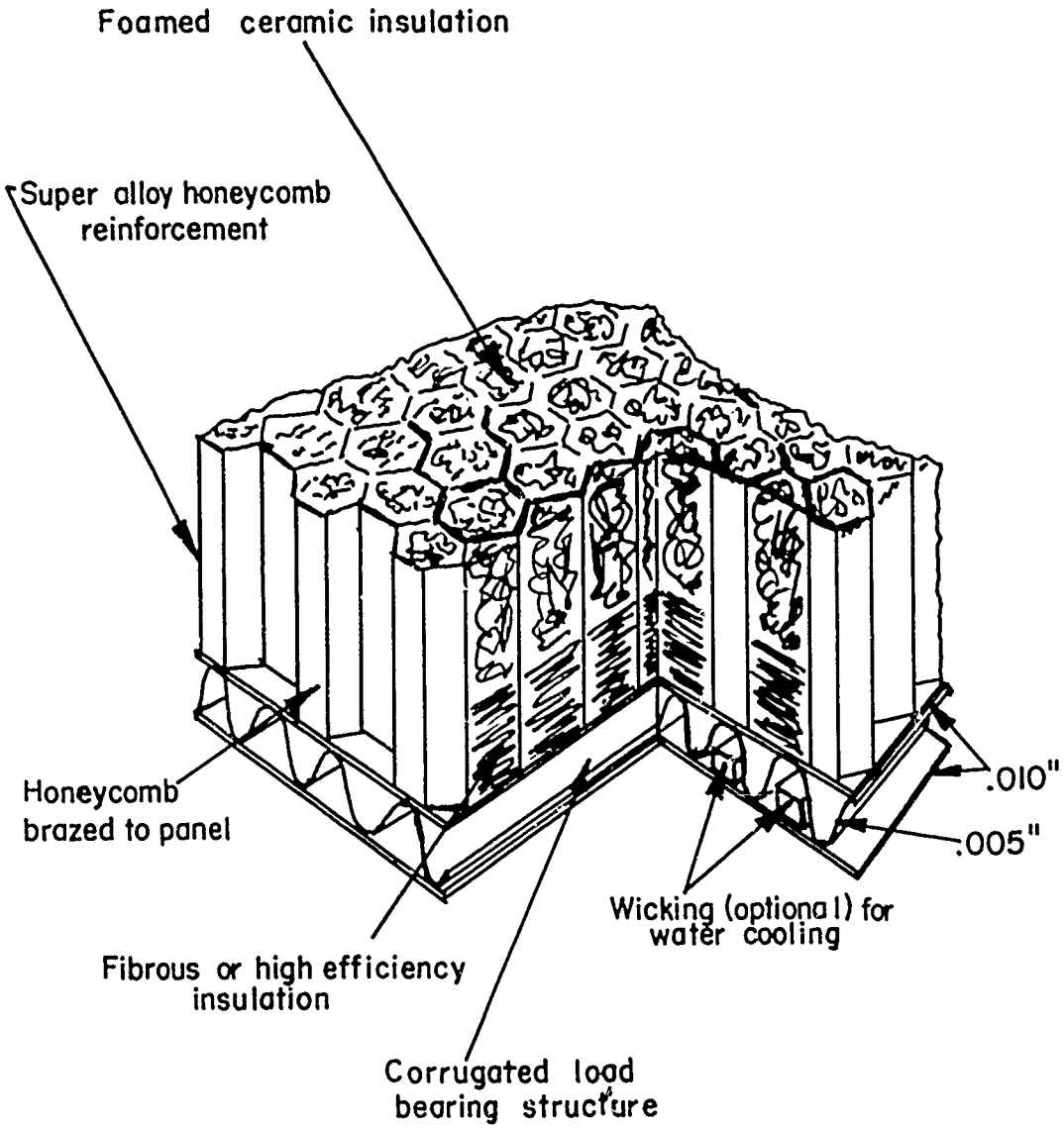


Figure 9. Thermanic Panel

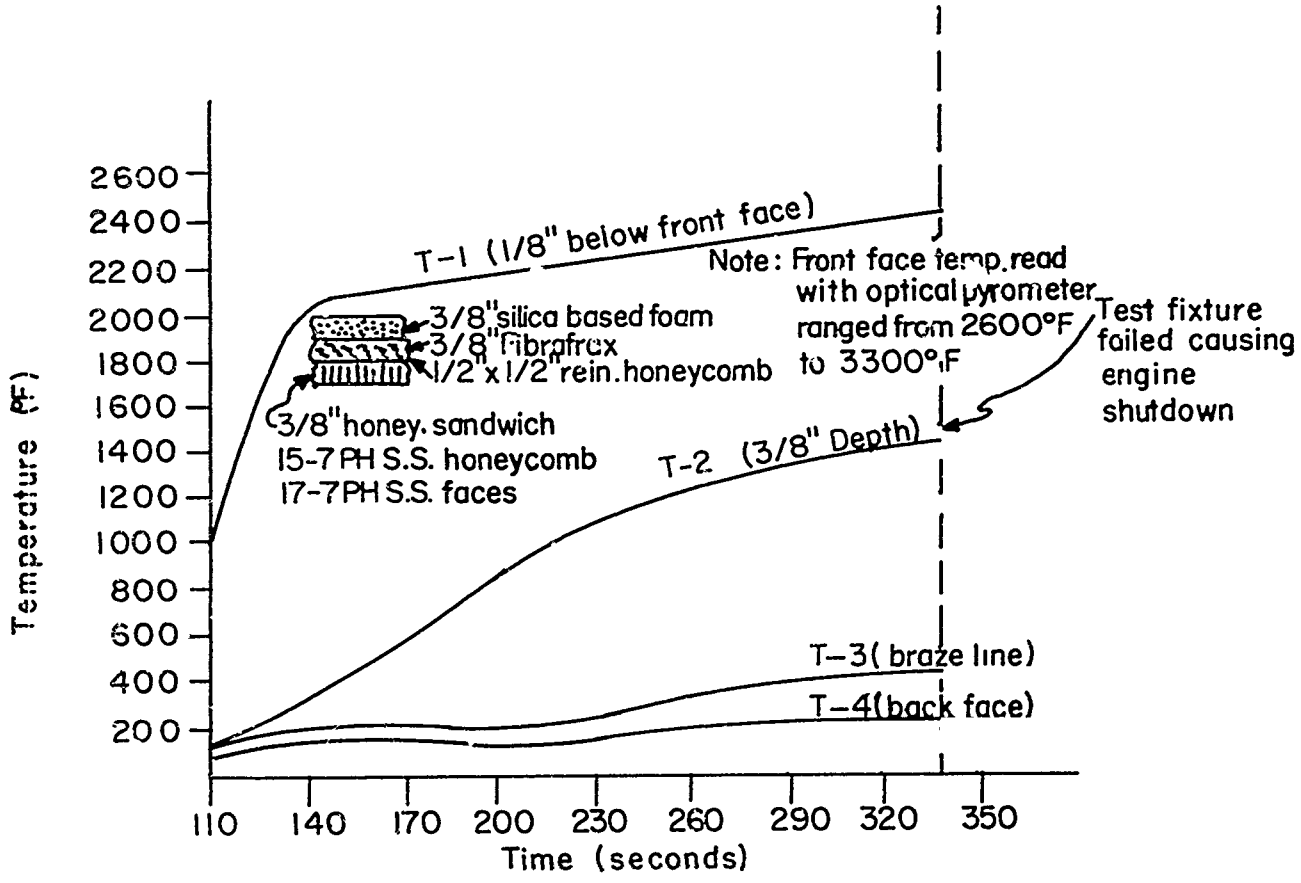
placed on the potassium titanate materials. They exhibit thermal conductivity values equal to, or lower than, the other materials with a correspondingly lighter density. They are also capable of reflecting 90% of infra-red radiation, which becomes an important consideration when these materials are utilized above 500°F. Other products, such as a zirconia fiber blanket now in the development stage, will also be evaluated as they become available.

The feasibility of foamed in place ceramic panel construction has been demonstrated through test programs that have been underway since early 1960. A series of test panels was tested in the afterburner exhaust of a J-75 engine, other samples were exposed for several hours to temperatures of 2000 - 2800°F under radiant heat lamps and tests have been conducted in the supersonic exhaust of an 8 inch ram jet burner.

The results were sufficiently satisfactory to establish the feasibility of this construction and to encourage further work. After several months of development work, a series of improved panels was constructed incorporating engineered ceramic foams and protective coatings on the reinforcement metal. Three ceramic formulations were developed for use in the improved panels; silica, zirconia, and alumina based porous ceramics. Temperature limits for the three designs are approximately as follows: silica - 3100°F, and zirconia - 3800°F. It is expected that the zirconia material is applicable in temperatures considerably in excess of 4000°F though the panel thickness would be greater than that used in the test units.

Figure 10 presents the temperature distribution through the panel. The panel which weighed 4.3 lb/ft^2 retained structural integrity during the entire test which had to be halted because the holding fixture melted. Because difficulties were experienced in controlling temperatures, the panel was subjected to cycling thermal exposures between 2500°F and possibly 3300°F. Also, the fixture failure resulted in water quenching of the panel at the time of maximum temperatures. Despite the severity of this exposure, no thermal stress failures occurred. Dynamic pressure produced a loading on the panel of about 3/4 ton, and the noise level was estimated at 150-170 db. Both of these conditions are considerably in excess of hypersonic re-entry design conditions.

Possibilities for extending the functions of this construction



RESULTS OF RAM JET EXPOSURE TESTS

FIGURE 10

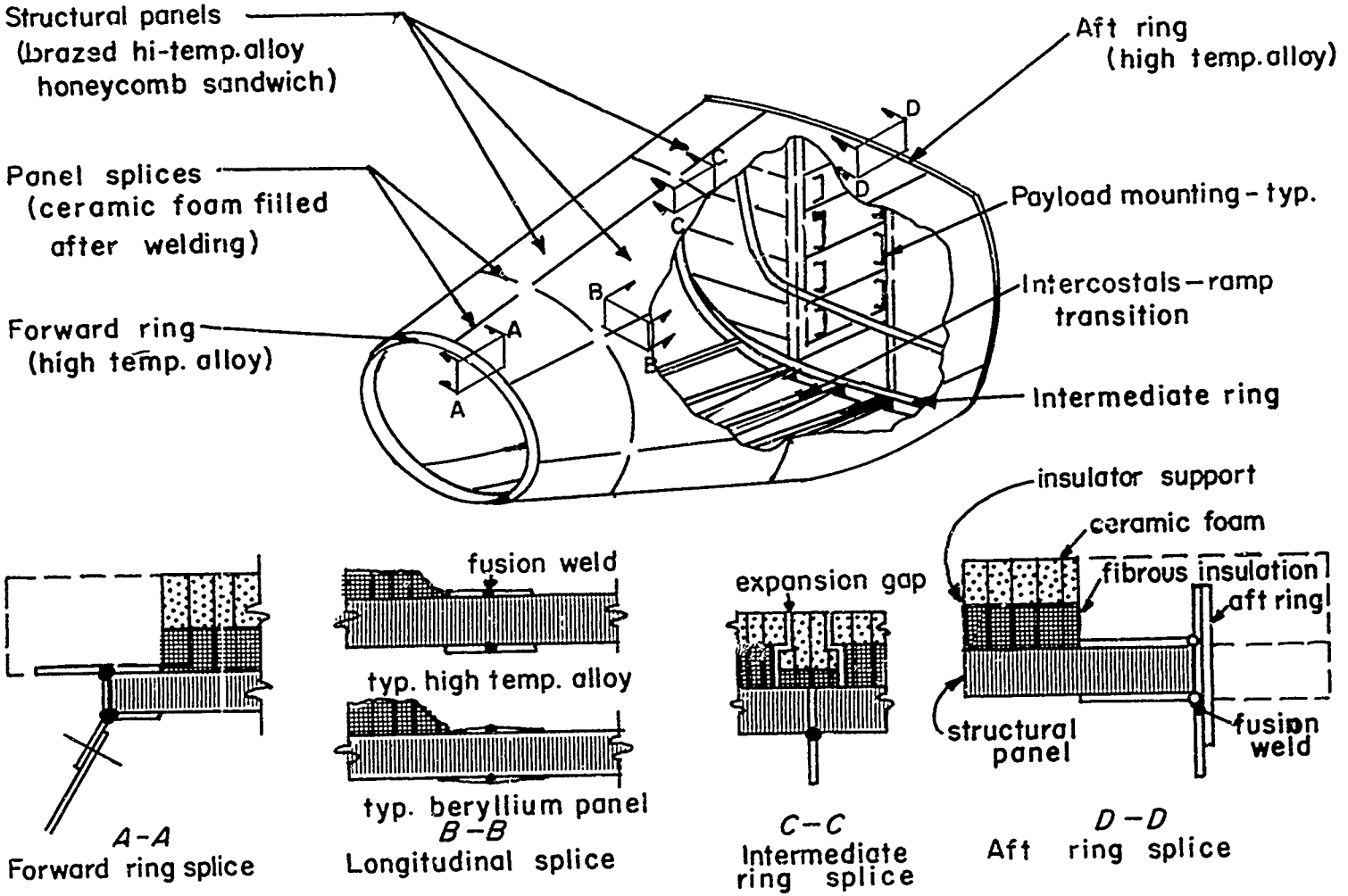
include the utilization of the ablative properties of ceramics or plastics. For example, for super-orbital re-entry a portion of a ceramic or plastic component may ablate, and when speeds are reduced, the remaining ceramic would act as a radiation cooled structure. Transpiration cooling during super-orbital velocities is also compatible with porous ceramic heat shields. In a transpiration system, the coolant fluid may be ejected through ports which are connected to an internal compartmental cooling system.

The thermantic structure is compatible with the requirements of all compact shape vehicles, such as the lifting body, where total structural deformations are minimal. Further, a total weight of less than 4.5 lb/sq ft of vehicle, wetted area appear realistic. Figure 11 shows a typical forward section of a re-entry lift body and represents our future efforts in the thermantic structures area. This program will involve the detailed design, construction and test of a section approximately 9 feet in length with a diameter tapering between 2 and 4 feet. The structure is basically a semi monocoque structure consisting of a thermally protected brazed sandwich shell stabilized by conventional inertia bulkheads.

This component will be tested at the Aeronautical Systems Division under combinations of loads, temperatures and vibrations typical of the lifting body re-entry trajectory. Plans call for thermal tests above 3000°F provided test capabilities can meet these stringent conditions within our program schedule. Tests are to be considered to be conducted in early 1963.

HIGH TEMPERATURE COMPOSITES

Other programs concerned with differences in types of construction are being conducted. The Martin Company began work in July 1960 on a program to design and test a nose structure, for use in 4000°F environments. After initial screening of available materials and composite construction techniques, it was decided to utilize foamed, sintered ceramics in this program. This was based on the inherent lightness and good insulating characteristics of foam, plus uniform properties of the sintered bond. This prevents sintering and eventual deformation of the ceramic at high temperatures. Three commercial foams were selected for detailed investigation in this program: silicon carbide, alumina and zirconia. Silicon carbide proved hard to obtain with a reasonable



STRUCTURAL ARRANGEMENT LIFTING BODY VEHICLE
FIGURE II

degree of uniformity, was excessively expensive, and failed at 3300°F due to oxidation. It was subsequently dropped from the program. The other two materials, alumina and zirconia, are produced by Ipsen Company, Rockford, Illinois, by one of the best ceramic foaming processes available. The high quality, non-burnout type brick can be mass produced with good uniformity and in a wide range of densities.

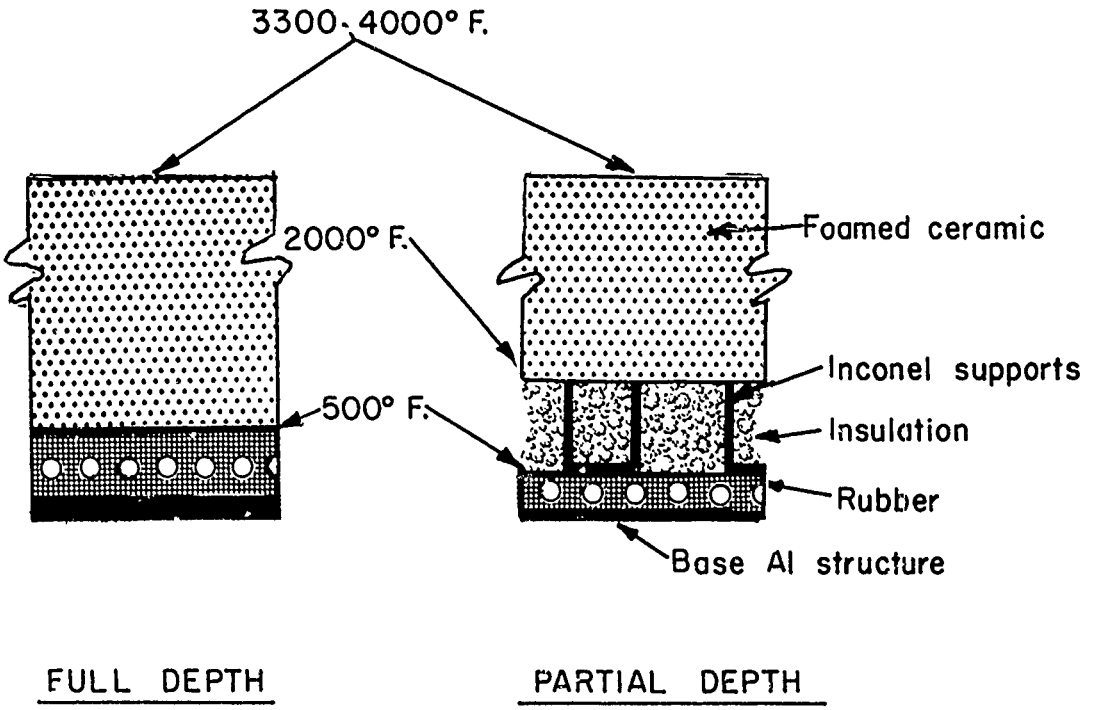
Alumina has shown satisfactory results to 3300°F, where cell wall softening begins to occur. Zirconia, being very thermal shock sensitive has poorly withstood realistic re-entry temperature pulses. It has, however, where temperature change rates are small, a maximum temperature potential of approximately 4000°F. Development of the foamed zirconia is continuing. One seemingly critical factor effecting thermal shock and thus the practical application of zirconia is the orientation of a meterial module relative to the direction of foaming during ceramic manufacture.

Figure 12 shows representative samples of two structural approaches for attaching ceramic modules to a basic vehicle structure. Surface temperatures will vary, depending upon ceramic capabilities. Attachment section will be at temperatures of 2000°F for partial depth and 500°F for full depth; making use of the foam's insulating qualities. The primary design for the section is to allow three degrees of freedom for ceramic expansion or contraction. The rubber attachments will have integral water cooling channels to keep the attachment section at design temperatures.

Total nose construction will place individual modules (as just shown) in concentric rings; where the size of a module will be determined by its thermal expansion characteristics. Thus, for an alumina construction module the maximum size is 4 inches in diameter or its equivalent. Zirconia, if its thermal shock resistance can be improved, will probably require segments of no larger than 2 inches maximum dimension. Module assembly techniques are now being given detailed design studies and tests; the results of which shall become available shortly.

STRUCTURAL COOLING TECHNIQUES

Preliminary program planning is currently underway at ASD for a high energy, active thermal protection system for glide vehicles.



CERAMIC MODULE SUPPORT

FIGURE 12

This includes ablative, transpirative, or boundary layer mass injection in general. No such effort is presently under contract. Work, however, is proceeding on means for connective, or internal cooling systems. These thermal protection systems involve the Chance Vought thermosorb concept and the Bell double wall approach. Both integrate cooling into basic vehicle structure. Both concepts are being studied for possible application in several of our programs where cooling provides weight savings for the total structural system.

TUNGSTEN/TANTALUM FRONTAL SECTIONS

A recent work effort calls for the design, fabrication, protection and testing of efficient structures for the frontal section of super-orbital, lifting re-entry vehicles. Tungsten and tantalum alloy materials are to be utilized in the design, calling for operation to surface temperatures of 4500°F or greater. This present task will require significant extensions to the present state-of-the-art in materials, design, fabrication and testing at elevated temperatures. The program is intended to provide a working capability in design and fabrication of a successful hypersonic structural section of the broadest possible application.

The components will consist of structural members supporting a refractory facing. The structural members will be of tungsten, tantalum, or their alloys. The refractory facing will be reinforced by tungsten or tantalum in the form of a spun cone, open face honeycomb, corrugated mesh or other reinforcing techniques. It is expected that the most efficient design will be evolved during the early phases of the program.

Several design approaches to the structure can be categorized as either ablative, cooled, heat-resistant or composite. The ablative structure is represented typically through the use of structural plastics, quartz or pyrolytic graphite, though the latter material is consumed through oxidation and erosion processes as well as sublimation. The cooled structure, typified by the use of transpiration of fluids at the stagnation region, has proved valuable in rocket nozzle applications, though the time of operation there is quite short. The use of lithium as a coolant is theoretically of great advantage because of its high total heat capacity and low density. The heat-resistant structure depends

on the use of refractory materials which have sufficient structural strength at temperature, and which either by themselves or in combination with coatings, can resist the design environments imposed along with high temperature. The use of tungsten, zirconia, thoria, or composites of this class of materials is required in such an approach.

Additional screening of materials and processes for integrated systems will be conducted during the early phases of the program. Capabilities of several alloys of tungsten and tantalum will be followed as they advance in their present state of research development. The properties and adaptability of several thermal protection systems will also be investigated if current research effort discloses desirable characteristics within acceptable time limits.

INFLATABLE STRUCTURES

The problem of providing a reliable structure for re-entry vehicles is primarily associated with the load-temperature-time history, as discussed earlier. The inflatable, light-weight structures approach attempts to avoid or minimize several thermostructural problems encountered in the more conventional rigid re-entry structural concepts. Use of this concept allows the design of a low wing loading glide vehicle of coated metal fabric that is capable of 1500°F to 2000°F surface temperatures. This light weight, pressure stabilized structure with large leading edge radii results in lower decelerations (being initiated at higher altitudes) thereby reducing heating problems and aeroelastic loads. Figure 13 presents a plot of the volumetric efficiency parameters versus increased weight for the rigid and non-rigid structural concepts. The outstanding potential for the expandable concept is readily apparent. A substantial volume could be placed in orbit at a very small weight increase in the vehicle weight. Because of the packaged configuration during boost, the increased weight for the total system is likewise very small.

There are many existing problem areas associated with inflatable structures. Materials investigations have been conducted; however, no detailed structural evaluation programs have been performed. Preliminary design studies indicate that the inflatable structural approach is feasible but further material and structural

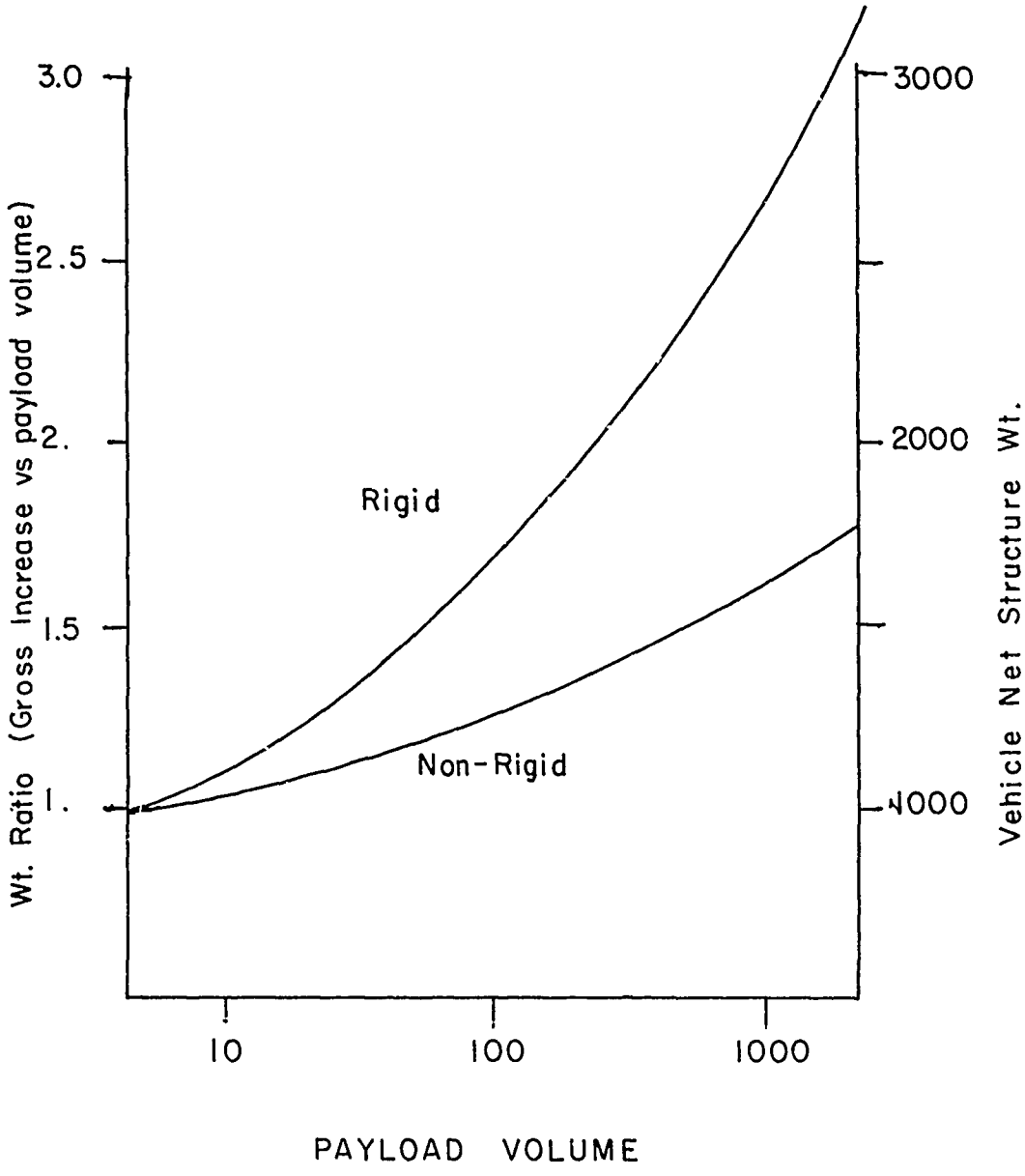


Figure 13. Plot of Volumetric Efficiency Versus Increased Weight for Rigid and Non-Rigid Structural Concepts

studies must be conducted to evaluate the concept. Actual flight test demonstrations are required to prove feasibility. Areas of investigation that would apply to a re-entry vehicle are: boost loads, packaging capability, inflating characteristics, environmental effects, structural strength and materials compatability. Correlation of theoretical analyses - experimental data appears to be the critical area that must be investigated.

MATRIX STRUCTURAL ANALYSIS OF HEATED AIRFRAMES

Richard H. Gallagher

Bell Aerosystems Company
Division of Bell Aerospace Corporation

ABSTRACT

This paper discusses the application of matrix structural analysis methods to the solution of the deformational response problems of heated airframes. Emphasis is placed on the analysis of built-up, low aspect ratio lifting surfaces. Both the force and displacement approaches are considered and, for each, the analysis process leading from basic data to the various facets of structural response is provided in outline. Based on a review of recorded applications, topics in need of further development, as well as new applications, are delineated.

MATRIX STRUCTURAL ANALYSIS OF HEATED AIRFRAMES

INTRODUCTION

All major airframe structures departments are today aware of the extremely powerful analysis tools available in techniques of matrix structural analysis. After a rapid period of development beginning in the early 1950's, coincident with the appearance of the high speed digital computer (the device necessary for success in their use), these techniques have progressed to a point where they now appear in most design offices in the form of automatic computational programs for the analysis of linear, unheated structural systems. The objective of the present paper is to review and establish the status of matrix structural analysis techniques with respect to the problems of heated structures, which are prone to experience nonlinear behavior, and to describe topics in need of further study as a direct result of elevated temperature conditions. Problems occasioned by future vehicle structural requirements, independent of the temperature environment, are also cited.

Methods of matrix structural analysis have developed predominantly along two lines. One of these is the "Method of Forces", or "Flexibility" approach. The former title derives from the fact that the governing equations are stated as a direct relationship between the applied loads and certain internal forces. The second approach is "Displacement" or "Stiffness" method, wherein relationships between the applied loads and the displacements of specified points are formed and solved. Both definitions, in the context of this paper, are further qualified by the proviso that the governing equations be based on an analytical model composed of discrete structural elements-plate segments, bars, etc. Thus, methods which result in a matrix statement of the problem but are based on assumptions of the unknown forces or displacements as continuous functions with undetermined coefficients are

not considered. To the extent possible, however, note will be taken of applications formulated specifically for analog as well as digital computers.

The force and displacement approaches have been presented by some authors (see References 1 and 2) as exact counterparts of each other. These authors demonstrated an analogy or "duality" extending from basic physical principles through the process of structural idealization to equivalent formulations of the matrix equations. This duality will be recognized, but not stressed, in subsequent sections.

To be sure, the force and displacement techniques are not the only possible forms for matrix structural analysis. "Mixed" methods, involving the direct solution for both forces and displacements, have been proposed (References 3 through 5). The only complete exposition of such concepts has been given by Klein (Reference 3) who has run the complete gamut of problems touched upon in this paper. The technique of Reference 3 can be contracted to a displacement formulation of the problem; the contraction to a force approach formulation would appear to be possible but has yet to be demonstrated.

Taking note, at this point, of the contribution of reference 3 to the subject topics, the attention of this paper will be limited to conventional formulations of the force and displacement approaches. The sections of this paper, with the exception of the concluding section, have subheadings which independently treat the direct solution for forces and displacements. To lend clarity to subsequent sections a brief review of a representative formulation of each is given in the first section. The practice at Bell Aerosystems, and at other airframe organizations as well, is to employ a given approach to matrix structural analysis as a means of obtaining the complete solution for the "response" of a structure, i.e., for stresses, displacements, stiffness, and flexibility. To emphasize this point the brief review of each approach encompasses a sequence of operations leading from basic data to the complete solution for structural response.

The review of formulations for linear, unheated structures is followed by a discussion of the problems introduced into structural

analysis by aerodynamic heating. With these in mind, the published applications of matrix structural analysis to such problems are described. Knowledge of recorded applications not only indicates where theory and practical experience is yet lacking, but also demonstrates the types of analytical idealizations required for an acceptable level of accuracy.

In assessing topics for future work it has been found more convenient to subdivide the headings into linear elastic, nonlinear elastic, and inelastic problems rather than into the categories of force and displacement approaches. This is because the state of the art in both approaches is generally deficient with respect to identical topics in heated structure analysis.

SECTION I: REVIEW OF BASIC CONCEPTS

A. FORCE METHODS

Matrix force analysis techniques have been presented in a remarkably large number of references. Argyris (Reference 6), in an excellent historical review of methods of matrix structural analysis, traced the development of the force approach from the beginnings of the concepts upon which it is based (attributed to Maxwell, Mohr and Mueller-Breslau) through to the initial development of the basic principles of the matrix force method and thence to the publication date of his paper (1958). A number of references were mentioned for the latter period. Many more have accumulated since the appearance of Argyris' survey. In aggregate, these papers represent a wide divergence of viewpoints on the treatment of special conditions, e.g., wing cutouts, means for the formation of input data, and the relationship between the technique and the idealization of the structure. Numerous questions related to these viewpoints are yet to be resolved.

Nevertheless, the majority of recent papers as well as a predominance of industry computational programs conform to the same approximate outline when the analysis of unheated structures for linear behavior is involved. A simple formulation, in conformity with this outline, can be obtained by analogy with the rudimentary analysis problem illustrated in Figure 1. The rigid frame shown is indeterminate to the first degree. The solution for the state of displacement and for the internal forces can be conveniently obtained by first cutting the structure so as to reduce one of the internal or reactive forces to zero, rendering the structure statically determinate.

Let this force, the "redundant" X, be the horizontal reaction at Point B. Then, the elementary application of any one of a number of procedures for displacement determinations (Castigliano's Theorem, Virtual Work) permits the calculation of the displacement at the Cut B due to the applied load P. Designating δ_{B_P} as the displacement at B due to a unit value of the applied load, the total displacement resulting from P is given by $\delta_{B_{P_n}} \times P$. Similarly, if δ_{B_1} is the displacement at B due to a unit value of X, the redundant causes a displacement $\delta_{B_1} X$. Since there is no displacement at B in the actual structure, one can write:

$$\delta_{B_P} \times P + \delta_{B_1} X = 0 \tag{1}$$

and, solving for X:

$$X = - \delta_{B_1}^{-1} \delta_{B_P} \times P \tag{2}$$

Furthermore, if a stress in the cut structure is expressed as $s_0 P$ and the stress at the same point in the cut structure is related to the redundant by the term s_X, then the stress s in the actual structure is given by:

$$s = \left(s_0 - s_X \delta_{B_1}^{-1} \delta_{B_P} \right) P \tag{3}$$

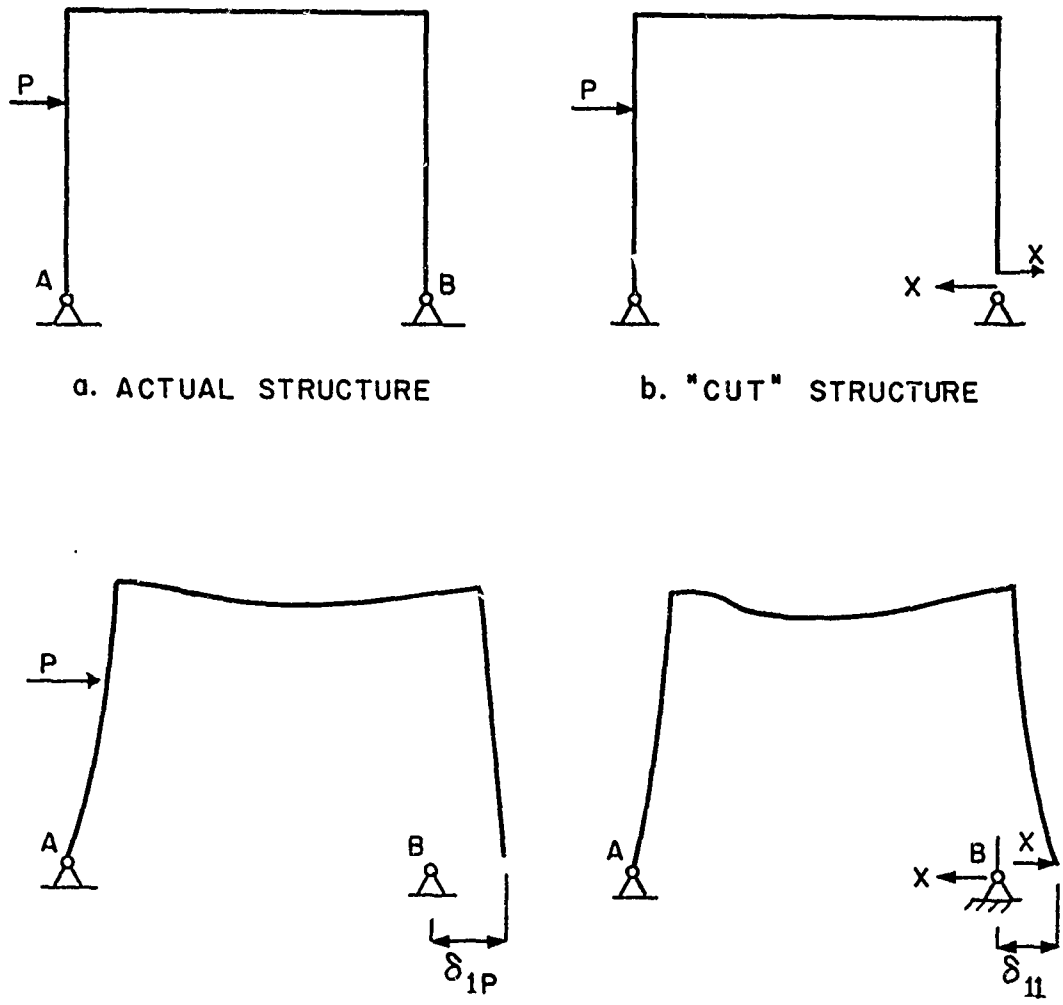


Figure 1. Indeterminate Frame

Corresponding formulas for a complex indeterminate structure can be constructed if the matrices $[\delta_{IP}]$ and $[\delta_{II}]$ are defined as sets of influence coefficients for relative displacements at the cuts due to the applied loads $\{P\}$ and the redundant forces $\{X\}$.

Then $$[\delta_{IP}]\{P\} + [\delta_{II}]\{X\} = 0 \tag{4}$$

and $$\{X\} = -[\delta_{II}]^{-1}[\delta_{IP}]\{P\} \tag{5}$$

In a system of reasonable complexity it is not possible to directly construct the matrices $[\delta_{IP}]$ and $[\delta_{II}]$ as easily as was done with the terms δ_{BP} and δ_{BI}. Hence, these matrices are further subdivided by constructing one matrix denoted here by $[\alpha_{ij}]$, and the two matrices $[g_{im}]$ and $[g_{ir}]$. $[\alpha_{ij}]$ is the matrix of "flexibilities" or displacement characteristics of the discrete elements of the system with respect to certain stresses (or generalized forces) acting upon them. The matrices $[g_{im}]$ and $[g_{ir}]$ relate the applied loads and redundants, respectively, to the stresses (or generalized forces) of the elements. It is then shown, in standard developments (Reference 7) of the matrix force method, that

$$[\delta_{IP}] = [g_{ir}]^T [\alpha_{ij}][g_{im}] \tag{6}$$

$$[\delta_{II}] = [g_{ir}]^T [\alpha_{ij}][g_{ir}] \tag{7}$$

(The superscript T designates the transpose of the indicated matrix.)

Relatively complete formulations can now be given. The solution for the redundancies becomes:

$$\{X\} = -\left[[g_{ir}]^T [\alpha_{ij}][g_{ir}]\right]^{-1}\left[[g_{ir}]^T [\alpha_{ij}][g_{im}]\right]\{P\} \tag{8}$$

The total state of internal stress, $\{S\}$, is basically given by:

$$\{S\} = [g_{im}]\{P\} + [g_{ir}]\{X\} \tag{9}$$

Thus, utilizing Equation (8), but with the definitions of Equations (6) and (7):

$$\{S\} = \left[[g_{im}] - [g_{ir}] [\delta_{11}]^{-1} [\delta_{1P}] \right] \{P\} \tag{10}$$

To establish the displacement influence coefficients for the actual structure, certain subsidiary sets of displacement influence coefficients must first be defined. Let $[\bar{\delta}_{PP}]$ denote the influence coefficients for the applied load points in the "cut" structure with respect to the applied loads. This matrix can be obtained as:

$$[\bar{\delta}_{PP}] = [g_{im}]^T [\alpha_{ij}] [g_{im}] \tag{11}$$

The matrix of displacement influence coefficients $[\delta_{P1}]$ for the applied load points with respect to the redundants proves to be the transpose of $[\delta_{1P}]$. It follows, from direct physical reasoning, that the displacement influence coefficients $[\delta_{PP}]$ for the actual structure are given by:

$$[\delta_{PP}] = [\bar{\delta}_{PP}] - [\delta_{1P}] [\delta_{11}]^{-1} [\delta_{1P}] \tag{12}$$

In summary, it is seen that the important solution quantities are represented by Equations (10) and (12), and stem from three basic input data matrices: $[\alpha_{ij}]$, $[g_{im}]$, and $[g_{ir}]$. It is useful to recognize, in practical applications, that the matrix $[g_{im}]$ may be based on any internal force system statically equivalent to the applied loads. It is also well established that the redundants can be more efficiently defined than a as pairs of forces at single "cuts".

The above treatment of matrix force method concepts, while superficial, is believed sufficient for the purposes of describing advances made in the direction of heated structure analysis. The most exhaustive treatment of the force approach may be found in the work of Argyris (Reference 1). Other, recent, expositions of the matrix force approach are given in References 8 and 9.

B. DISPLACEMENT METHODS

The first complete formulations of the matrix displacement approach were due to Turner, Clough, Martin and Topp (Reference 10), and to Argyris (Reference 1). The term "complete formulations" is intended to convey the meaning that the associated analysis procedure, starting with the definition of load, geometric, and material property data, consists entirely of a sequence of matrix operations. Earlier references (e.g. 11 and 12) had contributed to the fundamental theory of the discrete element analysis of complex systems with displacements as unknowns, but dealt with only one matrix - the stiffness matrix for the entire structure - in the solution process.

The differences between References 1 and 10, in terms of the sequence of operations leading to a solution, lie mainly in the technique for assembling the individual elements to form the complete structure. Differences of a more fundamental sort exist in the means employed to derive the force - displacement properties of the individual elements and in the deformational behavior represented by these properties. The following review is patterned after Reference 10; comments are appended concerning the technique of Reference 1.

The discrete elements in a displacement analysis are commonly defined by specified boundary points, sufficient in number to establish an assumed stress and deformational behavior. For such elements, it is first necessary to derive relationships between the displacements of the boundary or "node" points and forces acting at these points. The node point forces are either actual concentrated forces or are equivalent to stresses acting on the area subtended by the point. General expressions can be written, based on assumptions as to stress and/or deformational behavior, relating these forces ($\{F\}$) and displacements ($\{\Delta\}$). Expressed in matrix form, the relationships are

$$\{F\} = [k]\{\Delta\} \tag{13}$$

where $[k]$ is the "element stiffness matrix". An example of the development of the stiffness matrix for the simplest type of element, the

two-force member, is illustrated in Figure 2.

The elements are assembled to form the complete analytical model of the structure by joining all elements at their respective juncture points, applying in the process the requirements of juncture point equilibrium and compatibility. Thus, the components of internal loads $\{F\}$ and external loads $\{P\}$ at each point are related by equilibrium requirements, i.e., $\Sigma F_X = P_X$, etc. The respective coordinate displacements of the corner points of all elements meeting at a point are equal, a requirement that satisfies compatibility. If follows that the stiffness matrix($[K]$) for the complete structure can be assembled by merely adding element stiffness coefficients having identical subscripts. This results in a set of equations:

$$\{P\} = [K]\{\Delta\} \tag{14}$$

Force and displacement boundary conditions can be readily, imposed by assigning the pertinent P's and Δ's their known values. $[K]$ will be altered in the process, and taking note of this fact without a change in symbolism, the solution to the altered Equation (14) becomes:

$$\{\Delta\} = [K]^{-1}\{P\} = [\delta_{PP}]\{P\} \tag{15}$$

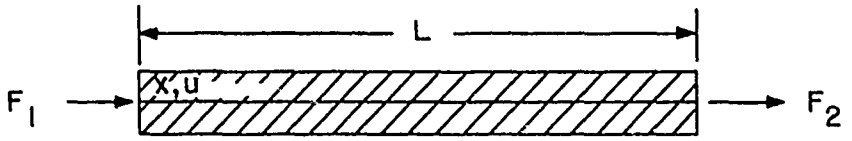
Where, as in the force approach, $[\delta_{PP}]$ represents the set of displacement influence coefficients.

The solution for element internal forces ($\{F\}$) can be effected by multiplying the element stiffness matrices by the now-known values of displacement ($\{\Delta\}$). For the sake of providing an expression for this operation let $\{F\}$ symbolize a column of all specified internal forces and $[\bar{k}]$ a properly constructed array of all the element stiffness coefficients. Then

$$\{\bar{F}\} = [\bar{k}]\{\Delta\} \tag{16}$$

$\{\bar{F}\}$ can be considered the counterpart of $\{S\}$ in Equation (10).

If the element stiffness matrices $[k]$ are basically expressed in some convenient local coordinate system it is necessary to transform



1. STIFFNESS EQUATIONS FOR UNHEATED CONDITIONS:

$$\epsilon = \frac{du}{dx} = \frac{u_2 - u_1}{L}$$

$$\sigma = E\epsilon$$

$$F_2 = A\sigma$$

$$F_2 = \frac{AE}{L}(u_2 - u_1)$$

$$F_1 = -F_2 = \frac{AE}{L}(u_1 - u_2)$$

2. IN MATRIX FORM:

$$\{F\} = [k]\{w\}$$

$$\{F\} = \begin{Bmatrix} F_1 \\ F_2 \end{Bmatrix}, [k] = \begin{bmatrix} \frac{AE}{L} & \frac{-AE}{L} \\ \frac{-AE}{L} & \frac{AE}{L} \end{bmatrix}, \{u\} \quad \begin{Bmatrix} u_1 \\ u_2 \end{Bmatrix}$$

3. FOR UNIFORM TEMPERATURE CHANGE T:

$$F_2^{\alpha} = -AE\alpha T$$

$$F_1^{\alpha} = -F_2^{\alpha} = AE\alpha T$$

Figure 2. Two-Force Member

the corner forces and displacements into components consistent with the coordinate directions of the structure as a whole prior to constructing Equation (14). The procedure described in Reference 1 replaces the application of transformations to the individual element stiffness matrices. Let $[a]$ signify a matrix relating the applied loads and the internal forces and $[k_e]$ an array of the element stiffnesses consistent with the arrangement of $[a]$. Then, analogous to Equation (7):

$$[K] = [a]^T [k_e] [a] \tag{17}$$

where $[K]$ is identical to the matrix defined in connection with Equation (14). Argyris (Reference 1), on the basis of the unit load and displacements theorems, has established a complete duality for the force and displacement formulations.

SECTION II: PROBLEM AREAS

There is ample evidence to show that matrix methods of structural analysis can be efficiently applied to yield accurate predictions of the linear stress and deflectional behavior of highly complicated configurations for unheated conditions. How, then, do conditions of aerodynamic heating and configuration trends affect this assessment?

Excluding, momentarily, questions of configuration, the principal effects of aerodynamic heating occur as a result of (a) influences on the material properties and (b) nonlinear temperature distributions. The elevated temperature effects on material properties not only reduce stiffness by elastic modulus deterioration but also intensify the likelihood of inelastic deformations being experienced by a reduction in the range of elastic behavior. A review of the effects of nonuniform temperature requires a knowledge of the configuration. Figure 3, which represents an outline of a wing and fuselage, has been drawn to

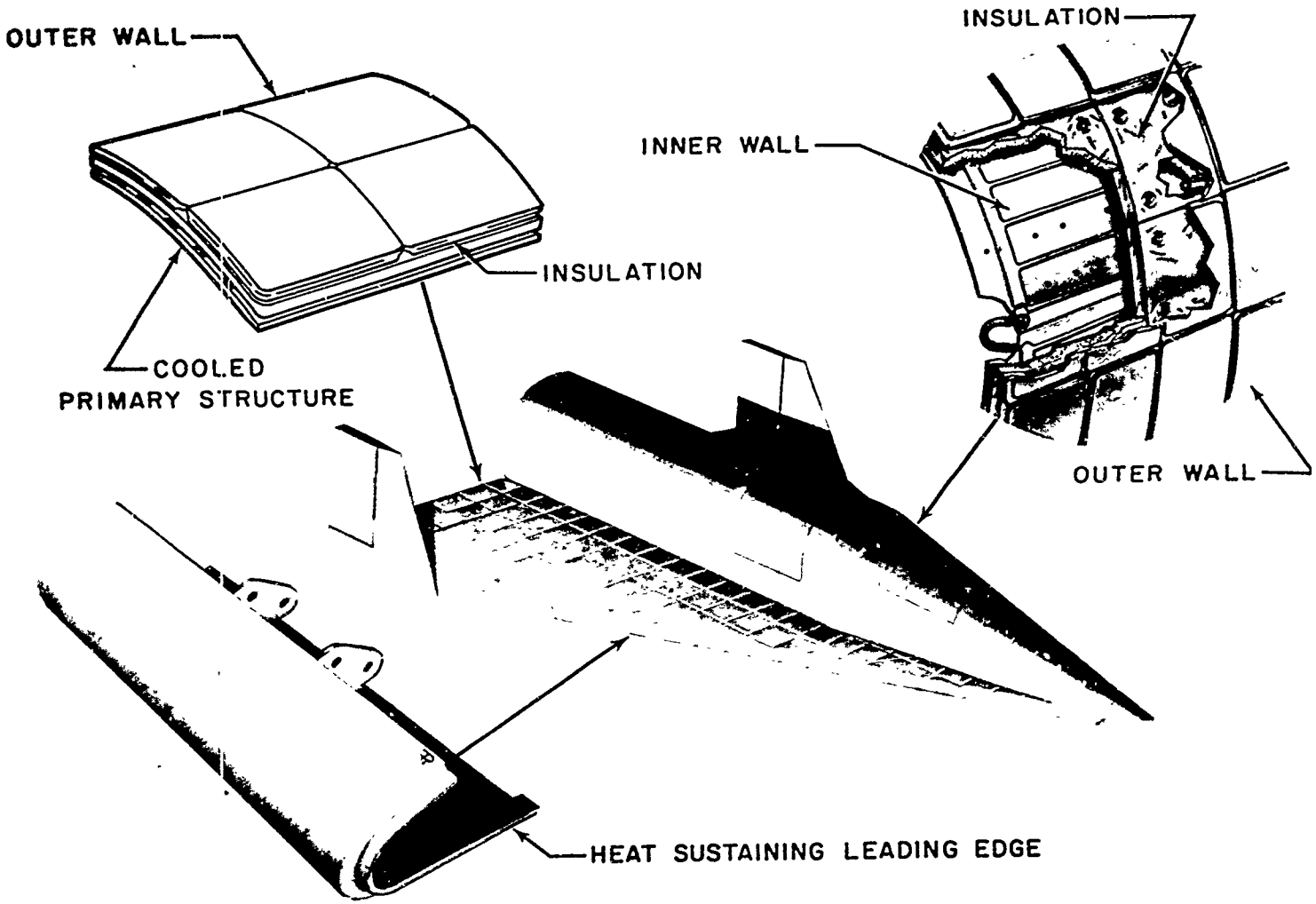


FIGURE 3 CONCEPTS IN HYPERSONIC VEHICLE STRUCTURAL DESIGN

illustrate some features of advanced configurations studied at Bell Aerosystems. Occasional reference will be made to these in the following discussion.

Consider first the lifting surface. It is clear that no single geometric form is representative of all advanced designs. The aspect ratio and leading edge sweep angle may be large or small. The wing cross-section may be nearly solid or built-up with thin skins. No new structural analysis problems are introduced by such factors, however. The related problems motivated the original development of matrix structural analysis techniques and have been successfully resolved.

The new problems arise in connection with severe elevated temperature environments. Leading edge temperatures will be relatively high but taper off rapidly in the direction normal to the edge line. This factor, together with temperature discontinuities at the fuselage juncture, produces the major nonuniformities in the chordwise and spanwise temperature profile. At finite angles of attack the upper and lower surface temperatures will differ, and this depthwise temperature profile will be implemented in the case of built-up constructions by the complexity of heat transfer conditions between the skins and internal members. The latter has the effect of producing localized irregularities in the skin temperature distribution and a significant difference in temperature between the skin and internal members.

Thus, in the least, the analyst must be prepared to assign a different "characteristic" temperature and the associated material properties to each discrete element of the idealization. Then, the computational program must be equipped to determine the displacements and stresses due to nonuniform temperature gradients. The most significant displacements are those which deform, or "warp", the wing out of its plane. The thermal stresses introduce loadings generally absent in unheated applications - net chordwise and spanwise compressive and tensile stresses. The effects on stiffness with respect to lateral loading will generally be adverse. For beamlike wings the effect has been simply described as a loss in torsional stiffness. In terms of complex structure analysis, it is analogous to a compressed plate action. These phenomena must be accounted for in the governing formulations.

Nonlinear behavior may also appear. One effect of the above-cited stiffness reductions can be deflections that are many times greater than the wing thickness. This results in a large deflection stress system in the wing midplane having the same type of effect on deflectional stiffness as a midplane thermal stress system. The large deflection stress system is nonlinearly related to the deflections, however, and the entire problem becomes nonlinear. Under such conditions, the initial shape of the wing has a bearing on stiffness. Here, not only must the governing formulations be modified, but provision must also be made for a greatly extended computational effort since iterative or step-by-step solution techniques are dictated.

Another form of nonlinear behavior may be present in the form of inelastic deformations. Inelastic deformations are commonly assumed to be the result of two mechanisms: time-independent plastic flow and creep. The resulting state of deformation is a function of the load and temperature history. Solutions therefore require the same order of computational complexity as for geometrically nonlinear problems plus an extremely detailed knowledge of material inelastic response.

The details of wing construction are subject to the same qualification as the wing configuration as a whole, i.e., no constructional form is representative of all advanced designs. Corrugated spar and rib webs have been proposed to improve skin compressive strength and alleviate thermal stress. The latter purpose may also be served by truss-type webs. It has not been demonstrated that the behavior of these unconventional elements can be accurately represented by relationships derived for flat plate and beamlike internal members.

"Isolated" components, for example the heat-sustaining leading edge and the outer-wall panel featured with insulated constructions, may now prove critical to the structural integrity of the entire lifting surface design. The two components cited represent entirely different stress analysis problems. The heat-sustaining leading edge will likely be composed of a brittle material and have the form of a short, open, shell (see Figure 3) or even a three-dimensional solid. Applied loadings will be light but the temperatures will vary radically in each direction. Due to geometric complexity and "end effects" the complete

thermal stress picture cannot be calculated to any degree of accuracy by use of existing, approximate, formulations. There is a need for rapid, accurate solutions.

The maximum stresses in outer-wall panels will not necessarily result from nonuniform temperatures gradients. If the panel is "thermally-thin" the temperature will be essentially uniform and the stresses will be due to normal airloadings. When temperature gradients do occur they will be across the thickness of the panel, producing a tendency to warp out-of-plane. The governing differential equations are well-known but hand-computed solutions for specific support conditions can only be achieved at the expense of considerable time and effort. Here again it would be advantageous to draw upon the capabilities of high-speed computing devices.

Consider next the fuselage. A typical fuselage, has, in the past, taken the form of a curved sheet cylinder stiffened at various intervals in the axial direction by rings and at intervals in the circumferential direction by stringers and longerons. Now, it may prove efficient in the interests of thermal stress alleviation to provide a statically determinate trusswork as the supporting frame for a surface composed of individual panels. Also, there is the possible desirability of employing pure shell forms: conics, cylinders, spheres. Singly and in combination these shells may serve the function of pressurized propellant containers as an integral part of the fuselage structures.

The built-up forms of fuselage construction present analysis problems that are, in some respects, different from those of built-up wing constructions. The fuselage is three-dimensional with a sharply curved cross-section. Hence, many more node points than for a wing analysis are generally required and it is not clear to what extent the curvature can be replaced in the idealization by a polygonized representation. On the other hand, it has not yet been demonstrated that critical stiffness loss and geometrically nonlinear behaviors are of significant concern.

The analysis of a three-dimensional trusswork should present no difficulty. The problems of shell constructions are almost limitless, however, and have engaged the interests of the most outstanding

theoreticians in applied mechanics. Formulas and solution techniques have been devised for many of the simple geometric forms and loading conditions, but, even for these, a number of phenomena remain analytically inpredictable. A notable example is cylindrical shell stability under axial compression. The need for versatile numerical analysis tools for shell structures is considerable.

The next question to be considered is, therefore: to what extent has the state-of-the-art of matrix structural analysis advanced over basic principles to provide a means for solving the problems and satisfying the needs described above? The following section is attempt to provide an answer to this question within the scope of the writer's knowledge of recent developments.

SECTION III: STATE-OF-THE-ART FOR HEATED AND NONLINEAR CONDITIONS

A. FORCE METHODS

Few contributions to the literature have been specifically concerned with the use of matrix structural analysis techniques in the prediction of the behavior of heated airframes. These have been almost entirely concerned with problems of planar configurations, i.e., lifting surfaces.

It cannot be said that the solution for elastic, linear thermal stresses in a nonuniformly heated structure represents an advance in basic theory. Although devoid of illustrative examples, early references(1 and 13) on the matrix force method provide sufficient detail for such determinations. A simple description of the concept is as follows. Let the "cut" structure deform in consequence of not only applied loads but also the thermal expansions. The relative displacements at the cuts due to thermal expansion can be denoted as $\{\Delta_T\}$. Then, the total

relative displacements are $[\delta_{1P}]\{P\} + \{\Delta T\}$ and by the same reasoning employed with Equations (4) and (5),

$$\{X\} = -[\delta_{11}]^{-1}\left\{[\delta_{1P}]\{P\} + \{\Delta_T\}\right\} \tag{18}$$

hence, from Equations (9) and (10)

$$\{S\} = \left[[g_{im}] - [g_{ir}][\delta_{11}]^{-1}[\delta_{1P}]\right]\{P\} - [\delta_{11}]^{-1}\{\Delta_T\} \tag{19}$$

the displacement influence coefficients $[\delta_{PP}]$ are not affected and are therefore calculable from Equation (12).

Grzedzielski (Reference 14) has taken a somewhat different approach to force method thermal stress analysis and illustrated its use by solving for the thermal stresses in a swept multiweb wing. The merits of alternative techniques in force method thermal stress analysis were debated by Grzedzielski (Reference 15),and Argyris and Kelsey (Reference 16) in a series of articles in theJournal of the Royal Aeronautical Society.

The most comprehensive treatment published to-date on the subject of force method analyses for the thermally-induced stiffness reductions and large deflectional behavior of lifting surfaces was presented by Lansing, Jones and Ratner (Reference 17). The governing equations were formulated so as to permit the straightforward extension of existing computational programs. It is therefore of general interest to briefly review this development.

Reference 17 makes a distinction between the equations to be solved for behavior symmetrical and antisymmetrical about the wing midplane. The latter behavior corresponds to the response of the wing to airloadings; the former relates to force systems whose values are constant across the depth of the wing. The symmetric, or "midplane" force systems stem from chordwise and spanwise temperature variations and from large displacements normal to the wing midplane. Accepting, momentarily, the contention that these forces are calculable, it can be seen from the idealization of Figure 4 that they contribute a net force normal to the midplane at each nodal point.

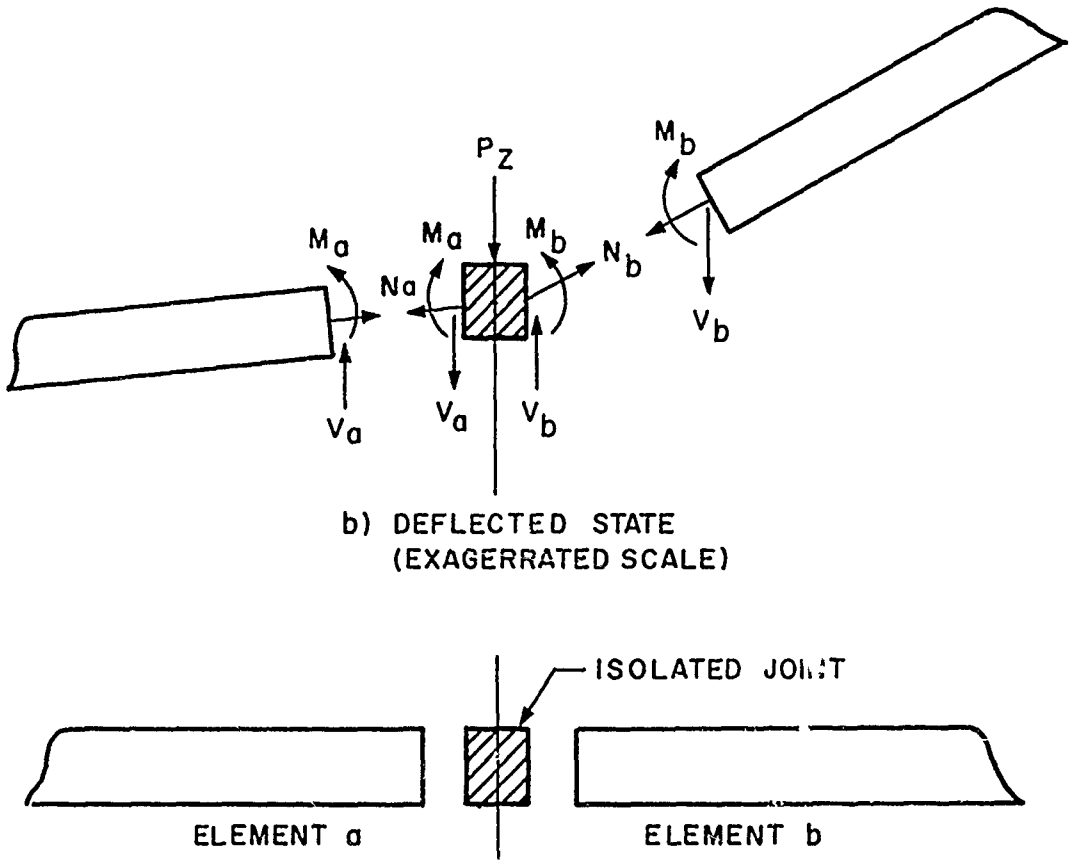


Figure 4. Midplane Force System

Let the column matrix of all such net normal forces be designated $\{\bar{P}_Z\}$. Since they result from the product of the midplane forces and the slopes of the elements upon which they act, and the slopes can be expressed in terms of the difference between nodal point displacements, the following set of equations can be formed:

$$\{\bar{P}_Z\} = [N]\{W\} \tag{20}$$

The nodal point displacements are listed in $\{W\}$, the terms of $[N]$ consist of the midplane force values and whatever geometric properties are necessary to transform the displacements into slopes. Now, excluding for simplicity in this review the displacements due to temperature gradients across the depth of the wing, the node point displacements $\{W\}$ can be expressed as functions of the applied loads $\{\bar{P}_Z\}$ and the net normal loads $\{\bar{P}_Z\} = [N]\{W\}$ with use of the usual displacement influence coefficients $[\delta_{PP}]$, i.e.

$$\{W\} = [\delta_{PP}]\{P_Z\} + [\delta_{PP}][N]\{W\} \tag{21}$$

solving for $\{W\}$:

$$\{W\} = \left[[I] - [\delta_{PP}][N]\right]^{-1}[\delta_{PP}]\{P\} = [\delta_{PP}]_R\{P\} \tag{22}$$

Hence, the usual set of displacement influence coefficients takes the revised form $[\delta_{PP}]_R$ where

$$[\delta_{PP}]_R = \left[[I] - [\delta_{PP}][N]\right]^{-1}[\delta_{PP}] \tag{23}$$

If the midplane stress system is due to temperature gradients alone all equations are linear. The determination of the midplane thermal stress system is achieved using the procedure indicated above by Equations (18) and (19); the procedure is demonstrated in Reference 17. Hence, a given midplane temperature distribution leads to a specific set of values $[N]$, which modify deflectional stiffness. The situation is illustrated in Figure 5. The solid line represents the relationship between a normal load applied at a specific poin and the displacement at a given point consistent with the appropriate term in the basic flexibility matrix $[\delta_{PP}]$. The dotted line shows the same relationship modified by the influence of the midplane force system, i.e. consistent with the

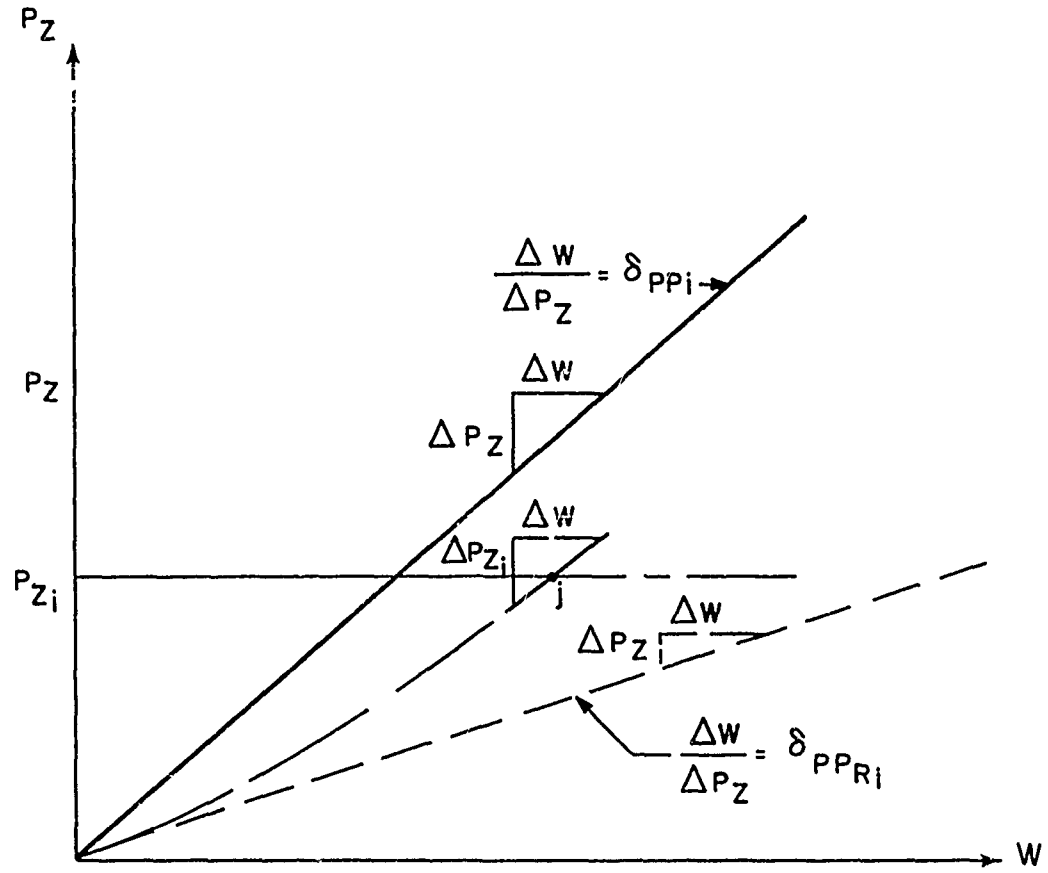


Figure 5. Determination of Midplane Thermo Stress System

appropriate term in the flexibility matrix $\left[\delta_{PP}\right]_R$. Although the modification is shown as a reduction in stiffness, certain individual stiffness coefficients many increase.

Reference 17 also demonstrates means for determining how severe the midplane stress system must be to cause buckling. Assume all midplane forces increase proportionally so that the matrix indicative of the effects of the midplane forces can now be expressed as $\lambda\left[N\right]$, where λ is the eigenvalue for buckling. For buckling conditions the applied loadings $\left\{P_Z\right\}$ are taken as zero and Equation (21) becomes:

$$\left\{w\right\} = \lambda\left[\delta_{PP}\right]\left[N\right]\left\{w\right\} \tag{24}$$

or,

$$\frac{1}{\lambda}\left\{w\right\} = \left[\delta_{PP}\right]\left[N\right]\left\{w\right\} \tag{25}$$

Standard iterative techniques can be applied to yield the eigenvalues and eigenvectors from Equation (25). Reference 17 shows that excellent agreement with standard plate buckling solutions can be obtained with use of the matrix force method.

If the deflections are large, the midplane forces are a function of the squares and products of the node point deflections, and the complete set of equations, including those associated with the midplane force determinations, are nonlinear. The dotted line of Figure 5 illustrates a nonlinear force-displacement behavior existing when deflectional stiffness is also modified by midplane thermal stresses. An objective of the solution will be to evaluate the stiffness $\left(\frac{\Delta P_{Z_i}}{\Delta w_i}\right)$ for incremental displacements about the load level of interest, P_{Z_i} . Reference 17 presents a procedure for accomplishing this objective. The techniques for nonlinear analysis are illustrated by a solution for an unheated, square, flat plate.

A development dealing with the above phenomena, but with emphasis on force method solutions for inelasticity, was set forth by Denke (Reference 18) in 1956. He provided modified statements of the governing force method equations and exemplified their use by solving for the inelastic stresses and displacements of a single cell, three-rib, swept wing. The solution was based on a Ramberg-Osgood Stress-Strain Law.

Application of the matrix force approach to problems in inelasticity has also been discussed in References 1, 8, 19, and 20. Argyris and Kelsey (Reference 1) described the formulation of inelastic complex structure problems for a monotonically increasing stress-strain law. Both creep and plastic flow were incorporated by Kron (Reference 19) in his tensorial approach known as the "Method of Tearing". This approach is unfamiliar to the writer, who is therefore unable to assess the scope of the work in Reference 19 with respect to the matrix force method as it is discussed herein. Reference 20 presented the analysis of an inplane-loaded axial force member-shear panel idealization for two approximate representations of material stress-strain response. Analyses were also performed to indicate the errors resulting from superposition of nonlinear solutions; for the conditions treated the errors proved to be less than ten percent. The concepts of these analyses stemmed from the work of Reference 18.

The ASD-sponsored study described in Reference 20 had for an overall objective the evaluation of the state-of-the-art of thermomechanical analysis of flight structures. While some further results will be mentioned in subsequent sections, the complete report was not available at the time this paper was prepared. Note should therefore be taken of the existence of Reference 20 as, among other things, a source of information on subject topics absent from this paper.

B. DISPLACEMENT METHODS

Probably the earliest application of discrete element concepts to the thermal stress analysis of a complex, built-up wing structure can be found in the NACA Report by Heldenfels (Reference 21). With use of an axial force member-shear panel idealization and the displacements of spar-rib intersection points as unknowns, a stiffness

matrix formulation was constructed. The problem required the solution of 24 simultaneous equations. This work predated the appearance of off-the-shelf, high speed, large capacity, computing equipment.

As in the case of the force approach, the solution to linear thermal stress problems requires no significant extension of elementary displacement analysis techniques. Consequently, although the aspects of the solution process under conditions of nonuniform temperature have been detailed (C.F., Reference 1) illustrative applications have been scarce. This situation has no doubt been influenced by a lack of both realistic problems and test data for comparison purposes.

Matrix displacement analyses for linear thermal stress conditions can be accomplished by use of the following concepts. General expressions are first derived for the node point forces ($\{F^{\alpha}\}$) required to fully restrain the heated discrete elements, resulting in the following form of the element force-displacement equations (see Equation (13)):

$$\{F\} = [k]\{\Delta\} + \{F^{\alpha}\} \tag{26}$$

Figure 2 includes the determination of the element thermal forces $\{F^{\alpha}\}$ for a uniformly heated two-force member.

The assembly of the element equations to form the set of equations for the complete structure yields:

$$\{P\} = [K]\{\Delta\} + \{P^{\alpha}\} \tag{27}$$

where the $\{P^{\alpha}\}$ terms are the net values of the pertinent $\{F^{\alpha}\}$ terms. Solving,

$$\{\Delta\} = [\delta_{PP}]\{P\} - [\delta_{PP}]\{P^{\alpha}\} \tag{28}$$

Again, the elastic characteristics of the structure embodied in $[\delta_{PP}]$, are affected only to the extent that the temperatures effect the elastic moduli.

Matrix displacement analyses for linear thermal stresses have recently appeared (References 22 to 24) as adjuncts to solutions for the stiffness loss of lifting surfaces due to midplane thermal stress systems. The usefulness of the matrix displacement approach was also recently demonstrated (Reference 25) for the linear thermoelastic analysis of structural components usually dealt with by means of conventional elasticity theory solution approaches. Stiffness equations were derived for a three-dimensional solid element (a tetrahedron) and an analysis was provided of a well-known plane stress problem for which both experimental and alternate theoretical results had been reported (Reference 26).

The thermally-induced wing stiffness loss problem was first given attention by complex structure analysis practitioners in Reference 22. There, the equivalent plate idealization was applied in a form suitable for analog computation. The formulations for inplane deformational analysis were solved to yield the inplane thermal stresses, which were then treated as knowns in the evaluations of the deflections of the equivalent plate. The authors illustrated their development with an analysis of a hypothetical multiweb wing. Similar work, including both analog and digital applications, has been reported by Harder, et. al. (Reference 23).

Another approach to the problem of wing stiffness loss analysis was taken in Reference 24, where element stiffness matrix concepts and a flexural element-torsion cell idealization for deflectional behavior were adopted. The idealization for midplane thermal force analysis was the axial force member-shear panel scheme. In applying the known values of the midplane thermal forces to the deflectional analysis their effect was represented as that of end axial forces on the flexural elements. Hence, the flexural elements were provided with beam-column stiffness matrices. No examples were given, but Reference 24 included heated multiweb wing test results. An extension of the analytical method and comparisons with the test results were contained in a subsequent report, discussed below.

Chronologically, the next contribution was made by Turner, Dill, Martin and Melosh (Reference 27). These authors provided an important theoretical development of stiffness analysis procedures into

the range of large displacements. Dealing primarily with questions of incremental stiffness, they derived extended force-displacement equations for the axial force member and triangular plate element in plane stress, and outlined promising solution processes. No numerical solutions were effected, however.

Work originating in Reference 24 was extended in Reference 29. Explicit relationships were derived for the stiffness analysis of high-solidity heated wings on the basis of the equivalent plate idealization. The flexural element-torsion cell approach of Reference 24 was simplified by representing the effects of midplane forces on deflectional stiffness in terms of components normal to the midplane at the node points. The relationships for both idealizations included midplane thermal stress, large deflection, and initial displacement effects.

The detailed developments of Reference 29 permitted the formulation of matrix displacement statements for the analysis of wings irrespective of the specific idealization. Thus, as in the case of the force-method formulations of Reference 17, straightforward extensions to existing computational programs were indicated. The work of Reference 29, summarized in Reference 30, can be reviewed with use of Figure 4 and the same assumptions outlined in the previous description of the corresponding extension to force methods. The stiffness equations for displacements normal to the plane take the form:

$$\{P_Z\} = [K]\{W\} - [N]\{W\} \tag{29}$$

The matrix $[N]$ has the identical physical meaning as in Equation (20). Although certain idealizations require deflectional analysis formulations involving angular or inplane loadings and displacements, they can, in general, be operated upon to yield the same form as Equation (29).

Assuming, for the present, that the midplane forces are known, the solution to Equation (29) is:

$$\{W\} = \left[[K] - [N]\right]^{-1}\{P_Z\} \tag{30}$$

The revised flexibility coefficients are therefore $[\delta_{PP}]_R = [[K] + [N]]$. The solution for buckling again requires the replacement of $[N]$ by $\lambda[N]$ and setting $\{P_Z\} = 0$. The resulting equation then takes the identical form as Equation (25), i.e.

$$\frac{1}{\lambda}\{W\} = [\delta_{PP}][N]\{W\} \qquad (25)$$

The stiffness formulations for inplane analysis, too extensive to describe here, may be found in References 29 and 30. These references also present analyses of the multiweb wing test results (Reference 24) and apply the equivalent plate idealization to the prediction of the heated plate test data of Reference 30. Excellent agreement was obtained with the latter; extreme difficulties were encountered, however, in attempting to effect convergent solutions.

Apart from References 25, 29, 31 and 32, the writer is not cognizant of contributions to the extension of matrix displacement methods to permit inelastic analysis. Reference 32 is of limited scope, being a treatment of plane-framework structures for monotonically increasing loads into the time-independent plastic flow range. Reference 31, on the other hand, presented techniques for all classes of structures and plasticity phenomena. Emphasis was placed on conditions of time-dependent loadings and temperatures, with inelastic deformations accruing from both time-independent plastic flow and creep. Stiffness matrices for the axial force member and the triangular plate element in plane stress were extended to include consideration of inelastic displacements.

The developments of Reference 31 were illustrated by the solution for the stresses and displacements of a plate with a centrally-located hole under cyclically-varying applied loads and temperatures. The results were employed in the prediction of the failure of a test specimen. Further applications of the concepts of Reference 31 are outlined in References 25 and 29. Reference 25 discusses the inelastic analysis of built-up wings, while Reference 29 provides inelastic terms for the tetrahedronal element force-displacement equations. Neither reference presents a numerical solution, however.

Section II directed attention to two areas in which the advantages of matrix structural analysis techniques, if brought to bear, could prove of immense value. These were in the solution of plate problems, e.g., outer wall panels, and problems relating to all classes of shell structures. Beginnings have been recorded in both areas. Reference 32 derived a possible stiffness matrix for a rectangular plate element in bending. The use of these elements in the analyses of structures of nonrectangular planform via the familiar device of forming a saw-toothed representation of the boundaries was suggested. Reference 33 contained illustrations of the application of triangular plate element stiffness matrices for plane stress behavior to the solution of some membrane shell problems possessing known closed-form solutions. An acceptable level of agreement was attained. A problem involving bending deformations was also solved and provided results in agreement with those obtained by other means. No explicit statement of stiffnesses for plate elements in bending was given. The plate element bending stiffnesses of Reference 32 would appear useful in shell analyses within the limitations of the rectangular form.

SECTION IV: FUTURE WORK

A. ELASTIC SYSTEMS-LINEAR

The theories of matrix structural analysis are complete enough for the solution of all types of linear elastic systems. Deficiencies are apparent, however, in (1) the detailed relationships for specific idealizations, (2) experience in application to practical problems, and (3) the area of computational efficiency.

Now that many questions connected with the procedural frameworks of the possible approaches to matrix structural analysis have been resolved, greater attention is being given to problems of forming realistic structural idealizations. These problems have a definite connection with computational efficiency. For example, discrete element force-displacement equations violate, in general, conditions of

equilibrium and/or compatibility either within the elements or along their juncture with the other elements in the assembled model. Since these shortcomings cannot be rectified, the practicing analyst must be made aware of techniques for minimizing the resulting errors in the most efficient manner.

The errors inherent in idealizations for multiweb wing analysis were investigated in Reference 34. The entire question of analysis error was attacked in an orderly manner in Reference 20. Both references concluded that much work remains in the direction of clarifying detailed questions in structural idealization. Those which existed at the start of the studies of References 20 and 34 could only be partially answered within the scope of these investigations; some new questions were posed by the results.

Comparing the specific new problems described in Section II and the state-of-the-art of matrix structural analysis recounted in the preceding section, it can be said that there is a need for the development and evaluation of simple element relationships for plate bending. As previously noted, one such set of relationships has been proposed (Reference 32) for the unheated rectangular plate element. There are other possible formulations for this geometric form as well as an indicated need for less regular geometries. Temperature gradients across the thickness of the element should also be accounted for. When plate bending stiffnesses and flexibilities are well-established, efficient solutions for the stresses and displacements of high-solidity wings, outer-wall panels, and shell-type heat sustaining leading edge components will follow directly.

The field of discrete element thin shell analysis is largely unexplored. Reference 33 has provided a valuable beginning. This work should be continued into the area of instability problems. Plate elements also play an important part here, being the necessary ingredient for solutions more accurate than those provided by membrane behavior idealizations.

Two future requirements in matrix structural analysis transcend the category of elastic, linear systems and have equal or greater significance in categories discussed in succeeding sections. These are the

needs for (1) extended computer capacity and (2) experimental data for comparison purposes. With respect to the present topic, the term "extended computer capacity" is intended to mean the capability of being able to solve extremely large systems efficiently and with confidence in the results. An ultimate objective of the structural analyst can be considered the discrete element solution for the elastic response of the complete airframe-wing, fuselage, tail, etc. - in free flight. This will require, in terms representing an order of magnitude, 1000 unknowns. Some investigators are known to have favored the use of a stiffness matrix of 1200th order in the analysis of a wing alone. The solution for a shell of no particular complexity may demand in excess of 1000 unknowns.

The development of experimental data, proceeding in cognizance of the nature of the analysis techniques, will necessarily be expensive. Single-valued results, e.g., failure loads, are no longer sufficient. In the least, displacement influence coefficients for numerous points constitute valid comparison parameters. Available test data is most inadequate in the case of elevated temperature conditions.

B. ELASTIC SYSTEMS - NONLINEAR

The matter of computational capacity can immediately be brought to mind in connection with the analysis of geometrically nonlinear conditions. Because of the iterative or step-by-step nature of the solution process, nonlinear problems may overtax existing facilities when concerned with structures that are solvable well within program capacity when their behavior is linear. Short of requiring a machine of greater capacity, the critical need is to determine which of the possible solution techniques is most efficient under a given set of conditions.

Unfamiliar difficulties have been encountered (References 28 and 29) in effecting a convergent solution to the large deflection problem of a heated plate. Few accounts of numerical solutions to large deflection problems are to be found in the literature and none parallel the experiences of References 28 and 29. It is felt that the difficulties of solution were characteristic of the displacement formulation for discrete element systems. Thus, if the discrete element approach is to hold the

promise for nonlinear solutions that it has had in the linear range, means for circumventing convergence problems must be well-defined and criteria for convergence must be established.

In addition to the difficulties of nonlinear analysis of the structure per se, there remain questions as to the integration of the resulting elastic response characteristics into aeroelastic equations and the eventual solution for either vibrational behavior or flexible stability and control derivatives. With respect to the latter, the aerodynamic and elastic characteristics may appear in any combination of linear and nonlinear behaviors. The nature of these situations introduces a demand for test data in the presence of aerodynamic phenomena.

C. INELASTIC PROBLEMS

The capabilities of matrix structural analysis techniques in handling inelastic problems are hampered by a striking lack of fundamental knowledge of material behavior under conditions of varying stress and temperature. Since inelastic analysis procedures in the framework of the subject techniques have been established (References 18 and 31) it is clear that these material properties and the associated "rules" represent a principal area for needed future work. As a result of studies at Bell Aerosystems, two specific recommendations for future work can be offered. These are:

(1) Existing time-independent plastic strain and creep laws should be evaluated and extended. Many basic tests for varying temperature and stress (including biaxial and triaxial stress) conditions are needed for comparison purposes.

(2) A general mathematical representation of the inelastic response of a strain hardenable material subjected to varying tension and compression triaxial stresses should be formulated.

Solutions to certain inelastic problems of practical importance have been solved with the use of available material property data. These solutions pertain to simple geometries and loadings. The new

procedures of matrix structural analysis should now be applied to the same classes of problems but for more complex, realistic conditions. A case in point is the creep buckling of stiffened panels, for which a valid analysis procedure has yet to be demonstrated although satisfactory predictions have been made for the same phenomena in prismatic members. Another potentially useful area is the analysis of crack propagation under fatigue loading; the geometric form of a fatigue crack is easily represented by discrete elements.

In a general sense, a great deal of practical experience in inelastic matrix structural analysis remains to be accumulated and reported upon. As with geometrically nonlinear problems there is an acute need to clarify matters of computational efficiency in consequence of the repetition of large-order numerical operations.

SECTION V: CONCLUDING REMARKS

This review of matrix structural analysis techniques and their relationship to the solution of elevated temperature problems has been heavily influenced by the belief that both force and displacement approaches will continue to be advanced with vigor by approximately equal numbers of practical analysts. This belief is fostered, if for no other reason, by the fact that programs in existence at various organizations have in each case emerged from a costly developmental process. Users are only now in the process of amortizing their investment.

By way of a capsule assessment of the relative status of the alternate approaches to matrix structural analysis in the domain of advanced structures problems, it appears to the writer that displacement techniques are at present further advanced in terms of the classes of structures for which solutions have been demonstrated. Stiffness matrices for tetrahedrons and similar geometric forms have been derived and applied to three-dimensional solids. Plate elements in

bending and plane stress have been used to effect stiffness solutions for shell structures. Elemental stiffness relationships have, in general, conformed more closely to theory of elasticity concepts. No fundamental theoretical disability precludes the derivation of corresponding flexibility matrices, however, and notable advances have recently been recorded (References 20 and 36)in promoting the force approach beyond the confines of the familiar axial force member - shear field idealization.

Displacement techniques would also appear to have reached a more advanced state of development with regard to automatic features in the computational process. The procedure described in Reference 10, for example, provides information sufficient to write a program that requires an input of only geometric load and material property data in forming a solution. On the other hand, the authors of the survey of matrix structural analysis reported in Reference 20 could not report a corresponding degree of automation in established force method programs. Here again, advances are being recorded (Reference 36) and the question ultimately should not represent any real advantage of one technique over the other. Indeed, with the continued growth of computational capacity, mixed force-displacement procedures may ultimately demonstrate advantages not apparent at the present time.

As a final comment a step is proposed which, in the belief of the writer, contains the maximum possibility for rapid advancement of matrix structural analysis techniques towards the solution of future problems. This is the organized exchange of information by industry groups. None exists at present. The primary objective would be to free the structures research engineer from a task that is unproductive of advances in theory, and to improve the tools he has available to effect progress. The same proposal has been discussed in detail elsewhere (Reference 37). Thoughtful objections to it have been raised; these include the proprietary status of most, if not all, worthwhile program information, a lack of program documentation, and difficulties in the interchangeability of coded instructions. Furthermore, numerous information exchange groups already exist in the technical community as a whole.

None of these objections or shortcomings represents an insurmountable difficulty. In particular, the relative uniformity of the type of computing machine in use, and the scale of the operations performed, dictates having a committee limited in scope to matrix structural analysis techniques. A study (Reference 38) of these matters has concluded that among such a conformity of interests is precisely where cooperative activity should be greatest. It is important to note, however, that benefits could be realized even without the intention of actually exchanging coded programs.

Necessarily, other adverse factors cited above can be resolved only after an attempt has been made to organize a group. It is clearly outside the province of a single industry member to undertake this arrangement. What is necessary is that the prospective members be brought together by an agency possessing only the broadest interests.

REFERENCES

1. Argyris, J. H. and Kelsey, S., Energy Theorems and Structural Analysis, Butterworths Scientific Publishers, London, England, 1960.

2. Langefors, B., "Theory of Aircraft Structural Analysis", Z. Flugwiss., June 1958, pp 281-291.

3. Klein, B., "A Simple Method of Matrix Structural Analysis", Journal of the Aero/Space Sciences, Part I, Vol. 24, January 1957, Part II, Vol. 24, November 1957, Part III, Vol. 25, June 1958, Part IV, Vol. 26, June 1959, Part V, Vol. 27, November 1960.

4. Borges, J. F., Computer Analysis of Structures Proc. 2nd Conference on Electronic Computation, Structural Div. ASCE, New York, 1960.

5. Asplund, S. O., On Identical Formulations of the Force, Deformation, and Matrix Methods in Linear Elastostatics, Unpublished Reference.

6. Argyris, J. H., "On the Analysis of Complex Elastic Structures", Applied Mechanics Reviews, Vol. 11, July 1958, p 331.

7. Wehle, L. B. and Lansing, W., "A Method for Reducing the Analysis of Complex Redundant Structures to a Routine Procedure", Journal of the Aeronautical Sciences, Vol. 19, November 1952. p 677.

8. Crichlow, W. J. and Haggenmacher, G. W., "The Analysis of Redundant Structures by the Use of High-Speed Digital Computers", Journal of the Aero/Space Sciences. Vol. 27. August 1960. p 545.

9. Morice, P. B., Linear Structural Analysis, Thames and Hudson Publishers, London, England, 1959.

10. Turner, M. J., Clough, R. W., Martin, H. C. and Topp, L. J., "Stiffness and Deflection Analysis of Complex Structures", Journal of the Aeronautical Sciences. Vol. 23.September 1956. p 805.

11. Levy, S., "Structural Analysis and Influence Coefficients for Delta Wings", Journal of the Aeronautical Sciences, Vol. 20.July 1953. p 449.

12. Thomann, G. E. A., "Aeroelastic Problems of Low Aspect Ratio Wings — Part I — Structural Analysis", Aircraft Engineering, Vol. 28. February 1956. p 36.

13. Denke, P. H., A Matric Method of Structural Analysis, Proc. of the 2nd U. S. Nat'l Congress of Applied Mechanics, ASME, New York, 1954.

14. Grzedzielski, A. L. M., Organization of a Large Computation in Aircraft Stress Analysis, Aeronautical Report LR-257, National Research Council of Canada, July 1959.

15. Grzedzielski, A. L. M., "Some Applications of the Matrix Force Method of Structural Analysis", Journal of the Royal Aeronautical Society, Vol. 64.June 1960, Discussion. Vol. 65.February 1961.

16. Argyris, J. H. and Kelsey, S., "Initial Strains in the Matrix Force Method of Structural Analysis", Journal of the Royal Aeronautical Society, Vol. 64.August 1960, Discussion. Vol. 65. February 1961.

17. Lansing, W., Jones, I. and Ratner, P., A Matrix Force Method for Analyzing Heated Wings, Including Large Deflections, Proc. of the AIA-ONR Symposium on the Structural Dynamics of High-Speed Flight, Los Angeles, Calif., April 1961.

18. Denke, P. H. "A Matric Solution of Certain Nonlinear Problems in Structural Analysis", Journal of the Aeronautical Sciences, Vol. 23. No. 3, pp 231-6.

19. Kron, G., "Solution of Complex Nonlinear Plastic Structures by the Method of Tearing", Journal of the Aeronautical Sciences, Vol. 23. June 1956, p 557.

20. Warren, D. S., Castle, R. D. and Gloria, R. C., An Evaluation of the State-of-the-Art of the Thermo-Mechanical Analysis of Structures, WADD TR 60-271, April 1960.

21. Heldenfels, R. R., A Numerical Method for the Stress Analysis of Stiffened-Shell Structures Under Nonuniform Temperature Distributions, NACA Report 1043, 1951.

22. Basin, M., MacNeal, R. and Shields, J. H., "Direct-Analog Method of Analysis of the Influence of Aerodynamic Heating on the Static Characteristics of Thin Wings", Journal of the Aero/Space Sciences. Vol. 26.March 1959. p 145.

23. Harder, R. L., Lock, K., McCann, D. G., Wilts, C. H. and Royce, W. W., Supersonic Flutter Analysis Including Aerodynamic Heating Effects, WADC TR 59-559, 1960.

24. Gallagher, R. H., Quinn, J. F. and Turrentine, D., Thermal Effects on Static Stability and Control, Part III. WADC TR 58-378, December 1959.

25. Gallagher, R. H., Padlog, J. and Bijlaard, P. P., Stress Analysis of Heated Complex Shapes ARS Paper No. 1693-61, April 1961.

26. Heldenfels, R. R. and Roberts, W., Experimental and Theoretical Determination of Thermal Stresses in a Flat Plate, NACA TN 2769, August 1952.

27. Turner, M. J., Dill, E. H., Martin, H. C. and Melosh, H. R. "Large Deflection of Structures Subjected to Heating and External Loads", Journal of the Aero/Space Sciences, Vol. 27.February 1960. p 97.

28. Gallagher, R. and Huff, R., Thermoelastic Effects on Hypersonic Stability and Control, Part II, Vol. I, Elastic Response Determinations for Severely Heated Wings, ASD TR 61-287, 1961.

29. Gallagher, R. H., Quinn, J. F. and Padlog, J., Deformational Response Determinations for Practical Heated Wing Structures, Proc. of the AIA-ONR Symposium on the Structural Dynamics of High-Speed Flight, Los Angeles, Calif., April 1961.

30. Vosteen, L. F. and Fuller, K., Behavior of a Cantilever Plate Under Rapid-Heating Conditions, NACA RM L55 E 20c, July 1955.

31. Padlog, J., Huff, R. and Holloway, G., Inelastic Behavior of Structures Subjected to Cyclic Thermal and Mechanical Stressing Conditions, WADD TR 60-271, April 1960.

32. Melosh, R. J., "A Stiffness Matrix for the Analysis of Thin Plates in Bending", Journal of the Aero/Space Sciences, Vol. 28. January 1961, p 34.

33. Greene, B. E., Strome, D. R. and Weikel, R. C., Application of the Stiffness Method to the Analysis of Shell Structures, ASME Preprint 61-AV-58, March 1961.

34. Rattinger, I. and Gallagher, R., Supersonic Aeroelastic Effects on Static Stability and Control, Part II - Structures, WADC TR 58-95, April 1960.

35. Langefors, B., Triangular Plates in Structural Analysis, SAAB Report LNC-140, 1961.

36. Denke, P. H., A General Digital Computer Analysis of Statically Indeterminate Structures, Report to the Agard Structures and Materials Panel, Aachen, Germany, September 1959.

37. Gallagher, R. H. and Rattinger, I., The Experimental and Theoretical Determination of the Elastic Characteristics of Modern Airframes, Report to the Agard Structures and Materials Panel, Athens, Greece, September 1960.

38. Chang, J. C. L., Computer Program Exchange: Myth and Reality, Proc. 2nd Conference on Electronic Computation, Structural Div., ASCE, New York 1960.

TRANSIENT STRUCTURAL PERFORMANCE UNDER AN INTERMITTENT LOAD-TEMPERATURE-TIME ENVIRONMENT

P. C. Huang

The Martin Company

ABSTRACT

This paper presents the analytical methods and computer solutions for various types of structural elements under the applications of load and temperature, which may vary intermittently with time.

The time-dependent structural parameters such as stress, the corresponding deformation components, etc., can be calculated with the inclusion of temperature-dependent nonlinear mechanical properties of the material.

Results of an extensive experimental correlation program are also shown for a long flat plate of aluminum subjected to intermittent axial and bending loads at continually varying elevated temperatures.

The correlation test was run at high temperatures for this material to yield approximately 1% strain with 34 hours.

The maximum difference between theoretical and experimental deflection data was found to be within 10%.

TRANSIENT STRUCTURAL PERFORMANCE UNDER AN INTERMITTENT LOAD-TEMPERATURE-TIME ENVIRONMENT

INTRODUCTION

In the presence of thermal stress, residual stress, creep and material deterioration, each aero-space vehicle responds differently in thermal flight. To design a vehicle which can withstand such varying load and temperature exposures, the time parameter must be considered in the analysis. The prime factor is the instability of material property at elevated temperature environments, a parameter which complicates the static design procedure. This procedure may be subdivided into the following three major phases:

(1) The environmental inputs (concerned with the establishment of input step functions).

(2) Methods of analysis (concerned with the selection of proper time-dependent analytical procedures for calculation of structural responses).

(3) Design allowables (concerned with the determination of allowable stresses, design criteria, etc.).

In addition, other significant areas, i.e., thermal fatigue, creep fatigue, theory of strengths, etc., must also be considered in the design (Ref. 1). In this paper, however, only item (2) will be concerned.

For any pair of input functions (load and temperature) time-dependent responses of stress and strain can be expected throughout the anticipated life span of the vehicle. These time-dependent structural responses are greatly influenced by the residual strains and stresses which may have values of the same order of magnitude as the structural responses (Refs. 2, 3, 4 and 5). These residuals, which not only directly affect the stress distribution but also may cause premature failure of the structure, can be traced to:

(1) Material plasticity. When an intermittent load is applied to the structure, permanent residual strains will be produced after the intermittent load is removed. A set of self-equilibrating permanent stresses may result from the

presence of the residual strain. It should be noted that residual stress may be continual fluctuation while the residual strains increase steadily.

(2) Material creep. When the fibers are creeping at different rates, even at elastic stress levels, residuals would also be produced due to negligible creep recovery.

These residuals would cause premature buckling of compression members, decrease structural rigidity (Refs. 4, 6 and 7) and affect the mechanical properties of the material. The latter should be incorporated into a structural analysis.

Incomplete technical knowledge prevents the incorporation of this change of mechanical properties into a solution at this time; however, this variance seems to be slight as compared to that of other high temperature factors. It can be seen in experimental work performed in Martin laboratories (Refs. 2 and 3) that satisfactory correlations were obtained for a time-dependent bending-axial analysis where the variation of mechanical property due to residuals was neglected in the solution.

Since creep constitutes an important part in a time-dependent analysis (Refs. 8, 9 and 10), many creep formulas can be found for constant load and temperature environments (Refs. 8, 11 and 12). For a varying load and temperature condition, these formulas must be supplemented by other rules, i.e., the time-hardening rule, the strain-hardening rule or the life-fraction rule, to account for the changing levels in stress and/or temperature (Refs. 2 and 8). These rules depend upon the total time or the total accumulated residual strain and the instantaneous stress; therefore, a time-interval procedure appears most feasible, using a high speed digital computer, since the proper creep properties can be inserted at time intervals based on the results from previous calculations.

The other major obstacles in a creep analysis are the prior creep effects on material properties and the creep flow conditions under multidimensional stress space. The permanent creep strain is known to reduce the ductility of the material, to decrease strain-hardening effects, to lower ultimate strengths and to raise slightly the modulus of elasticity (Ref. 13). However, the scope of influence and the method of handling such data are not yet available. At present, the creep flow conditions under multidimensional stress space are handled in a manner similar to their counterparts in plastic flow conditions (Ref. 8). The rules in the theory of plastic flow and the Hencky-Mises yield condition have been adapted for determining the creep flow. Although the basic flow characteristics may be quite

different, this adaptation seems to be justified due to their similarity in macroflow phenomena whereby the flow rules have been derived (Ref. 14). Further studies in these areas, especially under varying temperature conditions, will improve the time-dependent analyses.

When a column is subjected to a load less than its Euler load, at an elevated temperature a gradual bowing with time occurs due to creeping of the fibers until rupture suddenly occurs. This is generally known as creep buckling (Refs. 21, 22, 23, 24, 25 and 26). Owing to the continuous deformation of the column, the extreme fiber on the concave side of the column may be crushed before buckling occurs.

Therefore, in considering the creep buckling of columns, the following items should be noted:

(1) The time-dependent Euler load.

(2) The maximum stress in a column.

(3) The time taken to reach any specified deflection.

(4) The time taken to reach imminent failure.

The time-dependent Euler load fluctuates with the value of the flexural rigidity, EI, of the column which is affected continuously by the temperature and the inelastic strains in the structure. The deflections of a column are originated by applying load to the slightly imperfect column; then, additional deflections due to creep continue. This imperfection is the result of tolerance of workmanship. It must be carefully controlled since a column would creep faster with a large initial imperfection, and the subsequent maximum stress and creep life would likewise be affected. The tolerance of straightness of a compression member thus becomes a very important parameter in the time-dependent analysis.

Numerous papers have been written concerning structural analyses in the presence of creep. However, not one considers the important aspects of time-dependent loading and/or temperature conditions. The primary subjects for investigation, where cases of nonuniform stress occur, are beams and columns. The typical approach is the formulation of the problem in terms of a selected creep law, with the ensuing solution in terms of the material constants of the creep law. The works by Libove, Kempner and Patel on the creep buckling of columns (Refs. 22, 35, 36, 37 and 38) are of this type. Hu and Triner (Ref. 39) studied bending creep and its application to beam columns in this manner also. Time increment procedures using the concept of

creeping for an interval at constant stress followed by an instantaneous redistribution of stress have been used by Lin in studying columns (Ref. 21) and beam columns (Ref. 40), and also by Poritsky and Fend (Ref. 41) in studying the relief of thermal stresses through creeping.

A method of solution of creep problems known as the elastic analog was first proposed by Hoff (Ref. 9). It has been applied to the analysis of many types of problems by investigators associated with the Polytechnic Institute of Brooklyn (Refs. 10, 24, 42, 43, 44, 45 and 46). This procedure relates the state of stress in a body under creep to that of a nonlinear elastic body through similarity of strain rate and stress-strain relationships. Experimental investigations have been included in the work performed at the Battelle Memorial Institute on creep buckling of columns. A summary of this work by Carlson and Manning (Ref. 25) advocates an approximate method of solution based on the use of creep data in the form of isochronous stress-strain curves. This is an extension of the isotangent-modulus method presented by Shanley (Ref. 26). Further work by Carlson, Briendel and Manning (Ref. 32) validates the basic soundness of the formulation of Hoff and deVeubeke (Refs. 33 and 34) for the column creep-buckling problem.

Thermal stress will be produced when the thermal expansion of a fiber is prevented either by external constraints or by continuity of the medium. Since the compatibility equations of a continuous body are differential equations of second order, a nonlinear thermal expansion will produce thermal stresses in the body with unrestrained boundaries (Refs. 15, 16, 17 and 18). Due to the relaxation ability in the plastic flow, the existence of thermal stress does not affect the ultimate strength of a stabilized structure. However, compressive stress components in unfavorable locations would greatly reduce the stability criteria and stiffness of the element (Refs. 6 and 19). It can be shown that a tent-type temperature distribution causes premature buckling of a rectangular plate and a rise in lateral deflections after buckling. A recessed-type temperature distribution reduces the lateral deflections, but yields a much higher maximum compressive stress which is responsible for a sudden rupture failure. This indicates that the existence of temperature gradients and/or residual stresses in a plate element, regardless of their shapes, is always unfavorable to the structure in the postbuckling stage and the working load should be kept below the critical buckling value with a proper margin of safety at all times (Ref. 20).

Other details such as rivet and bolt joints, welds and bonds, etc., also are affected by the intermittent load and temperature functions. An exact analysis for a joint, in the present state of art, is very

complicated (Refs. 27, 28, 29 and 30). Even at room temperature environment, a design of the joint usually resorts to the more simplified and rational concept of limit design. Thermal stresses and residual stresses, as discussed above, do not affect the tensile ultimate load of a structure. The compression ultimate usually is governed by the structure itself which is less stiff than a joint. It is believed that the design of joints under such environments would be more elaborate than that for room temperature. However, the procedure is believed to be semiempirical in nature, and experimental work should be performed to determine the inherent problems in a joint under such environments before more rigorous theoretical work should be attempted.

A time-dependent stress analysis calculates the structural responses, i.e., stress, strain, etc., of a vehicle for a certain mission, which are significant parameters in determining the allowable stresses and the margins of safety for the vehicle. Since the material responses are dependent upon the prior history of input functions, the ultimate strengths (expressed in terms of applied loads) vary with the input step-functions and take fluctuating values along the life span. Further, they must be evaluated individually, owing to the dependence of the ultimate load on the configuration of the vehicle. Once the strength criteria, e.g., maximum stress theory, maximum strain theory, etc. (Ref. 14) are adopted, the ultimate can be obtained by finding the smallest failing load under all possible combinations of load-temperature inputs. For compression members, the lowest environmental critical buckling load under all conditions can be taken as the compressive ultimate. The deformation criteria also should be investigated in the design of heated structures since the time-dependent behavior of displacement, thermal distortion, etc., must be controlled for the performance of the vehicle.

I. DEVELOPMENT OF ANALYTICAL METHODS

A. MATERIAL BEHAVIOR AT ELEVATED TEMPERATURE

In order to predict the performance of a structural component subjected to elevated temperature, a time-dependent analytical method must be utilized. Such a method could be developed by replacing Hooke's law with time and temperature-dependent material properties

and formulating the field equations for a particular structure with the aid of equations of equilibrium and compatibility. However, the variation of material properties with time and temperature is very complicated and is difficult to express in applicable form. In addition, the solution of such a problem would be so difficult that it probably would be limited to simplified instances. A more flexible time-interval procedure is better suited for such an analysis. In this approach, analyses are made at various time intervals that constitute the complete life span. At each time interval, the corresponding material properties are employed in the analyses, thus eliminating the formulation of material behavior equations.

Material behavior under an elevated temperature environment has been described briefly. For the formulation of structural behavior, it is convenient to consider three significant phenomena independently although they occur simultaneously. They are:

(1) A change of material properties.

(2) Effects due to thermal expansion.

(3) Creep of the material.

Little practical work has been done on the evaluation of material behavior under complicated environments. Considering the status of current material research, any such complicated structural analysis must utilize some assumptions to account for the certain material behavior in addition to the available data. In these analyses, the following main features pertaining to material properties are employed:

(1) All elastic strain is recoverable.

(2) Inelastic strain associated with stress decreases linearly according to the inverse of the modulus of elasticity during unloading. Upon reapplication of load, stress increases linearly according to modulus until the stress reaches the magnitude of the original stress-strain curve. At this point, further plastic straining follows the original stress-strain curve.

(3) No loss of accumulated creep strain under decreasing load or due to a sudden drop of load is assumed.

(4) The material responds instantaneously to any sudden change of load and/or temperature.

(5) Creep recovery, i.e., recoverable creep strain after removal of applied loads, is not accounted for.

(6) The creep behavior of material is assumed to follow either the time-hardening or strain-hardening rule.

In a solution, all the creep, as well as plastic strain, is being accumulated continuously. This total inelastic strain at any instant represents the past history of loading and temperature prior to that point, and the residual stresses can be readily calculated by removing all the acting loads and temperature by virtue of the postulation of item (2).

B. TIME-DEPENDENT STRUCTURAL ANALYSIS

In developing a method of stress analysis for a structure under a varying elevated temperature environment, the requirements are not only to obtain stress and strain distributions at a particular time, but, more important, to yield a stress-strain history for the life of the structure. It is also important to be able to obtain total ultimate load data utilizing the relieving effect of plastic strain on highly stressed portions.

The effects of elevated temperature on material behavior in such a structural analysis can be conveniently included when the total strain is considered in three separate parts: (1) strain associated with stress, (2) free thermal expansion and (3) accumulated creep strain. Each of the three phenomena described previously then shows its effect independently. When the equations which describe the behavior of a particular structure are formulated in this manner, the solution is very adaptable to analysis by a time-increment procedure. This approach also fulfills the requirements for a useful time-dependent analysis and is especially adapted to varying environmental input. Under a time-increment procedure, the first solution is performed as a short time analysis so that no creep strain is present. The stress distribution is found using the applicable instantaneous stress-strain curves for the various temperatures occurring, such that conditions of equilibrium and compatibility of total strain are satisfied. The creep strain which occurs during the first increment is then found, assuming that the stress distribution remains steady. This creep strain distribution is then added to the existing total strain and a new stress distribution is found. This sequence is then repeated for each time step using a particular rule for determining creep rate under varying stress. Changes in load or temperature are made by considering time increments of zero length so that no additional creep strain increments

occur. Time effects on stress-strain relationships due to "soaking" can be accounted for by including a time-dependent correction to the stress-strain curves used.

Because of the laborious calculations involved in making a long series of analyses to cover the lifetime of a structural element, use of a high speed computer is essential.

C. EQUATIONS FOR ELEVATED-TEMPERATURE STRUCTURAL ANALYSIS

The derivations of equations and ensuing procedures for their solution are presented in Ref. 2 for tension and bending members, and in Ref. 31 for columns, plates and torsional members. The derivations are based on the principles set forth previously and result in the basic equations now presented.

1. Tension and Bending Members

When a member whose longitudinal axis is parallel to the Z-axis is subjected to an axial load P, and bending moments M_x about the X-axis and M_y about the Y-axis, a cross section rotates about some n-axis and remains plane. The strain at any point is given by

$$\epsilon_n - \phi y_n = \epsilon' + \alpha \Delta T + \epsilon^c$$

where

ϵ_n = the strain at the axis of rotation

ϕ = the angle of rotation

ϵ' = the strain associated with stress

$\alpha \Delta T$ = the free thermal expansion

ϵ^c = the accumulated creep strain.

The stress at any point is given by

$$\sigma = E_S \epsilon' = k E_R \epsilon'$$

where

E_S = the secant modulus

E_R = the modulus of elasticity at the base temperature

$k = E_S/E_R$, an effectivity factor.

The angle of rotation of the cross section, ϕ, is found by either

$$\phi = \frac{\bar{M}_y + E_R \bar{Q}'_{y_c}}{-E_R (I'_{x_c y_c} \cos \beta - I'_{y_c} \sin \beta)}$$

or

$$\phi = \frac{\bar{M}_x - E_R \bar{Q}'_{x_c}}{E_R (I'_{x_c} \cos \beta - I'_{x_c y_c} \sin \beta)}$$

where

$\bar{M}_x$ = the net moment about the X-centroidal axis

$\bar{M}_y$ = the net moment about the Y-centroidal axis

$\bar{Q}'_{x_c} = \int_A k (\alpha \Delta T + \epsilon^c) y_c \, dA$

$\bar{Q}'_{y_c} = \int_A k (\alpha \Delta T + \epsilon^c) x_c \, dA$

$I'_{x_c y_c}$ = the product of inertia of the effective area with respect to the X- and Y-centroidal axes

I'_{x_c} = the moment of inertia of the effective area about the X-axis

I'_{y_c} = the moment of inertia of the effective area about the Y-axis

β = the angle between the X-axis and the n-axis.

The strain ϵ_n is found by

$$\epsilon_n = \frac{P + E_R Q'}{E_R A'}$$

where

$$Q' = \int_A k\,(\alpha \Delta T + \epsilon^c)\, dA$$

A' = the effective area.

2. Columns

If a column has a small initial crookedness, lateral deflection will occur when the load is applied. For a column whose axis is parallel to the X-axis and which has an axis of symmetry along the Z-axis, each cross section will rotate about a centroidal axis parallel to the Y-axis when the loading is in the plane of symmetry. The strain at any point is given by

$$\epsilon_c - \phi z_c = \epsilon' + \alpha \Delta T + \epsilon^c$$

where

ϵ_c = the strain at the centroidal axis

ϕ = the angle of rotation

z_c = the distance from the centroidal axis

ϵ' = strain associated with stress

$\alpha \Delta T$ = the free thermal expansion

ϵ^c = the accumulated creep strain.

The stress, σ, is given by

$$\sigma = E_S \epsilon' = k E_R \epsilon'$$

where

E_S = the secant modulus

E_R = the modulus of elasticity at the base temperature

k = E_S/E_R, an effectivity factor.

For a compressive load P, the strain ϵ_c is given by

$$\epsilon_c = \frac{-P + E_R Q'}{E_R A'}$$

where

$$Q' = \int_A k\,(\alpha \Delta T + \epsilon^c)\, dA$$

$$A' = \int_A k\, d\, A, \text{ the effective area.}$$

If the initial crookedness can be represented by $\delta_0 \sin \frac{\pi x}{L}$ where δ_0 is the maximum crookedness measured at the midlength and L is the total length, the angle of rotation ϕ is given by

$$\phi = - \frac{P\,(\delta_0 \sin \frac{\pi x}{L} + w) + M_y + E_R \bar{Q}'_c}{E_R I'_{y_c}}$$

where

w = the deflection

M_y = the applied end moment about the centroidal axis

$\bar{Q}'_c = \int_A k\, z_c\, (\alpha \Delta T + \epsilon^c)\, dA$

I'_{y_c} = the moment of inertia of the effective area about the centroidal axis.

The deflection w is determined from the solution of the differential equation

$$\frac{d^2 w}{d x^2} + \frac{P w}{E_R I'_{y_c}} = - \frac{P \delta_0 \sin \frac{\pi x}{L} + M_y + \bar{Q}'_c E_R}{E_R I'_{y_c}} .$$

3. Plates

The behavior of a plate is given by two differential equations in terms of the deflection, w, and a stress function, ϕ. For a plate of

uniform thickness, h, with the X- and Y-axes lying in the middle plane of the plate, the stress function, ϕ, is defined by the in-plane forces, N_x, N_y and N_{xy}, by

$$\frac{\partial^2 \phi}{\partial y^2} = N_x \; ; \; \frac{\partial^2 \phi}{\partial x^2} = N_y \; ; \; \frac{\partial^2 \phi}{\partial x \, \partial y} = -N_{xy}$$

with body forces neglected, where

$$N_x = \int_{-h/2}^{h/2} \sigma_x \, dz \; ; \; N_y = \int_{-h/2}^{h/2} \sigma_y \, dz \; ; \; N_{xy} = \int_{-h/2}^{h/2} \tau_{xy} \, dz.$$

Considering a plate with no temperature gradient through the thickness, the two differential equations are

$$a \nabla^4 \phi + \left(\frac{\partial^2 a}{\partial y^2} - \nu \frac{\partial^2 a}{\partial x^2} \right) \frac{\partial^2 \phi}{\partial y^2} + \left(\frac{\partial^2 a}{\partial x^2} - \nu \frac{\partial^2 a}{\partial y^2} \right) \frac{\partial^2 \phi}{\partial x^2}$$

$$+ 2 \frac{\partial a}{\partial y} \left(\frac{\partial^3 \phi}{\partial y^3} + \frac{\partial^3 \phi}{\partial x^2 \partial y} \right) + 2 \frac{\partial a}{\partial x} \left(\frac{\partial^3 \phi}{\partial x^3} + \frac{\partial^3 \phi}{\partial x \partial y^2} \right) + 2 (1$$

$$+ \nu) \frac{\partial^2 a}{\partial x \partial y} \frac{\partial^2 \phi}{\partial x \partial y} + E_R \left[h \left(\nabla^2 \alpha \triangle T \right) + \frac{\partial^2 Q_y}{\partial x^2} - \frac{\partial^2 Q_{xy}}{\partial x \partial y} + \frac{\partial^2 Q_x}{\partial y^2} \right] = 0$$

$$k \nabla^4 w - \left[\frac{N_x}{D} - \left(\frac{\partial^2 k}{\partial x^2} + \nu \frac{\partial^2 k}{\partial y^2} \right) \right] \frac{\partial^2 w}{\partial x^2} - \left[\frac{N_y}{D} - \left(\frac{\partial^2 k}{\partial y^2} \right. \right.$$

$$\left. \left. + \nu \frac{\partial^2 k}{\partial x^2} \right) \right] \frac{\partial^2 w}{\partial y^2} - 2 \left[\frac{N_{xy}}{D} - (1 - \nu) \frac{\partial^2 k}{\partial x \partial y} \right] \frac{\partial^2 w}{\partial x \partial y} + 2 \frac{\partial k}{\partial x} \left(\frac{\partial^3 w}{\partial x^3} \right.$$

$$\left. + \frac{\partial^3 w}{\partial x \partial y^2} \right) + 2 \frac{\partial k}{\partial y} \left(\frac{\partial^3 w}{\partial x^2 \partial y} + \frac{\partial^3 w}{\partial y^3} \right) - \frac{1}{D} \left[p + N_x \frac{\partial^2 w_0}{\partial x^2} + 2 N_{xy} \frac{\partial^2 w_0}{\partial x \partial y} \right.$$

$$\left. + N_y \frac{\partial^2 w_0}{\partial y^2} - \frac{\partial^2 \bar{Q}_x'}{\partial x^2} - (1 - \nu) \frac{\partial^2 \bar{Q}_{xy}}{\partial x \partial y} - \frac{\partial^2 \bar{Q}_y'}{\partial y^2} \right] = 0$$

where

$a = \frac{E_R}{E_T}$, $k = \frac{E_T}{E_R}$

ν = Poisson's ratio

E_R = base temperature modulus of elasticity

$\alpha\Delta T$ = free thermal expansion

p = applied lateral load

$$Q_x = \int_{-\frac{h}{2}}^{\frac{h}{2}} \epsilon_x^c \, dz$$

$$Q_y = \int_{-\frac{h}{2}}^{\frac{h}{2}} \epsilon_y^c \, dz$$

$$Q_{xy} = \int_{-\frac{h}{2}}^{\frac{h}{2}} \gamma_{xy}^c \, dz$$

$$D = \frac{E_R h^3}{12(1 - \nu^2)}$$

$$\overline{Q}'_x = \frac{kE_R}{1 - \nu^2} \int_{-\frac{h}{2}}^{\frac{h}{2}} (\epsilon_x^c + \nu\epsilon_y^c) \, z dz .$$

$$\bar{Q}'_y = \frac{kE_R}{1-\nu^2}\int_{-\frac{h}{2}}^{\frac{h}{2}} (\epsilon_y^c + \nu\epsilon_x^c)\, z\,dz$$

$$\bar{Q}'_{xy} = \frac{kE_R}{1-\nu^2}\int_{-\frac{h}{2}}^{\frac{h}{2}} \gamma_{xy}^c\, z\,dz$$

$$\nabla^4 = \frac{\partial^4}{\partial x^4} + 2\,\frac{\partial^4}{\partial x^2\,\partial y^2} + \frac{\partial^4}{\partial y^4}$$

$$\nabla^2 = \frac{\partial^2}{\partial x^2} + \frac{\partial^2}{\partial y^2}$$

ϵ_x^c = creep strain in X-direction

ϵ_y^c = creep strain in Y-direction

γ_{xy}^c = shear creep strain.

These equations are solved in conjunction with proper boundary conditions for edge support and applied end load.

After solution of these equations, the stresses can be obtained from

$$\sigma_x = \frac{N_x}{h} + \frac{kE_R}{1-\nu^2}\left[\left(\frac{Q_x + \nu Q_y}{h}\right) - (\epsilon_x^c + \nu\epsilon_y^c) - z\left(\frac{\partial^2 w}{\partial x^2} + \nu\frac{\partial^2 w}{\partial y^2}\right)\right]$$

$$\sigma_y = \frac{N_y}{h} + \frac{kE_R}{1-\nu^2}\left[\left(\frac{Q_y + \nu Q_x}{h}\right) - (\epsilon_y^c + \nu\epsilon_x^c) - z\left(\frac{\partial^2 w}{\partial y^2} + \nu\frac{\partial^2 w}{\partial x^2}\right)\right]$$

$$\tau_{xy} = \frac{N_{xy}}{h} + \frac{kE_R}{2(1+\nu)}\left[\frac{Q_{xy}}{h} - \gamma_{xy}^c - 2z\,\frac{\partial^2 w}{\partial x\,\partial y}\right]$$

4. Circular Torsion Members

When a circular torsion member of uniform temperature whose axis is along the Z-axis is subjected to a torque, T, the strain associated with stress, $\gamma'_{z\theta}$ at a given radius, r, is given by

$$\gamma'_{z\theta} = r\psi - \gamma^c_{z\theta}$$

where

ψ = the angle of twist per unit length

$\gamma^c_{z\theta}$ = the accumulated shear creep strain.

The twist angle is found from equation

$$\psi = \frac{T + T_c}{G_E J_p}$$

where

$$T_c = 2\pi G_E \int_{r_i}^{r_o} kr^2 \gamma^c_{z\theta}\, dr$$

G_E = modulus of elasticity in shear

$$J_p = 2\pi \int_{r_i}^{r_o} kr^3\, dr$$

$$k = \frac{G_{sec}}{G_E}, \text{ effectivity factor.}$$

For a hollow shaft, r_i is the inner radius and r_o is the outer radius; for a solid shaft, r_i is taken as zero.

The stress at any point is given by

$$\tau_{z\theta} = kG_E \gamma'_{z\theta} .$$

D. DIGITAL COMPUTER PROGRAM

A great many calculations are involved in the use of time-increment procedures; however, the arrangement is suitable for automatic computation, and the problems described have been programmed for the IBM-7090 digital computer. Basically, the development of the program is as follows. On the first step, no creep is existent. Assuming elastic relationships, a strain distribution is obtained by use of the equations of structural behavior. The comparable stress distribution, based on the actual complete stress-strain curve for the material at that temperature, is found and the resultant internal loads are computed and compared to the external loads. If inelastic effects create an imbalance, the strain and then the stress distribution are corrected until the equilibrium conditions are satisfied. With the correct stress distribution thus obtained, it is assumed that this remains constant for a time increment, and the creep strain due to this stress is obtained. This creep is then added to the total strain which must again satisfy the structural equations, and the correct stress distribution is found by the iterative process. Assuming that this new stress distribution will remain constant for the next time increment, the creep strain is found, based on one of the creep rules. The analysis is continued in this manner for the life of the structure. Changes in load and temperature are handled by removal of the previous load in the manner described in the assumptions followed by application of the new environmental input. A numerical example will be given for each program as follows.

1. Beams

The first example is based on the verification program run for the tension and bending analysis, full details of which are reported in Martin Report RR-16, Part II. The specimen of 2024T-4 aluminum alloy was essentially a large tension coupon with a test section 66 inches long, 14 inches wide and 1/4 inch thick. Various axial loads, moments and transverse temperature gradients were continuously applied in a random order and strain data were recorded. Figure 1 shows the environmental input, divided into block functions of load, and temperature gradient as designated by edge temperature and center-line temperature. Changes in load or temperature were accomplished in a short time which should be incidental in the overall long-time analysis. The total time of testing is slightly over 34 hours, with two intermediate shutdown periods provided. Figure 2 shows the experimental total strain as read by a pair of back-to-back strain

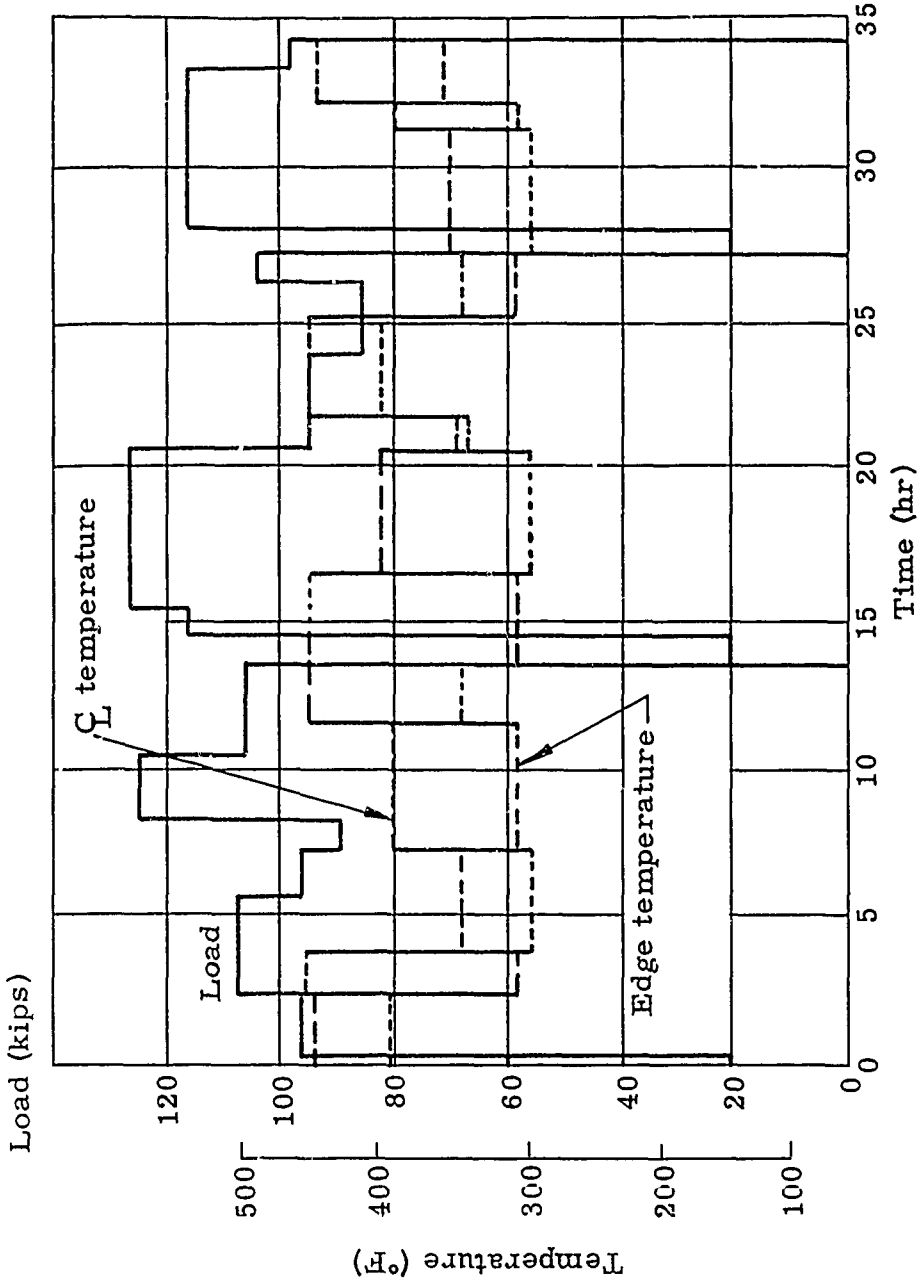


Fig. 1. Environmental Input

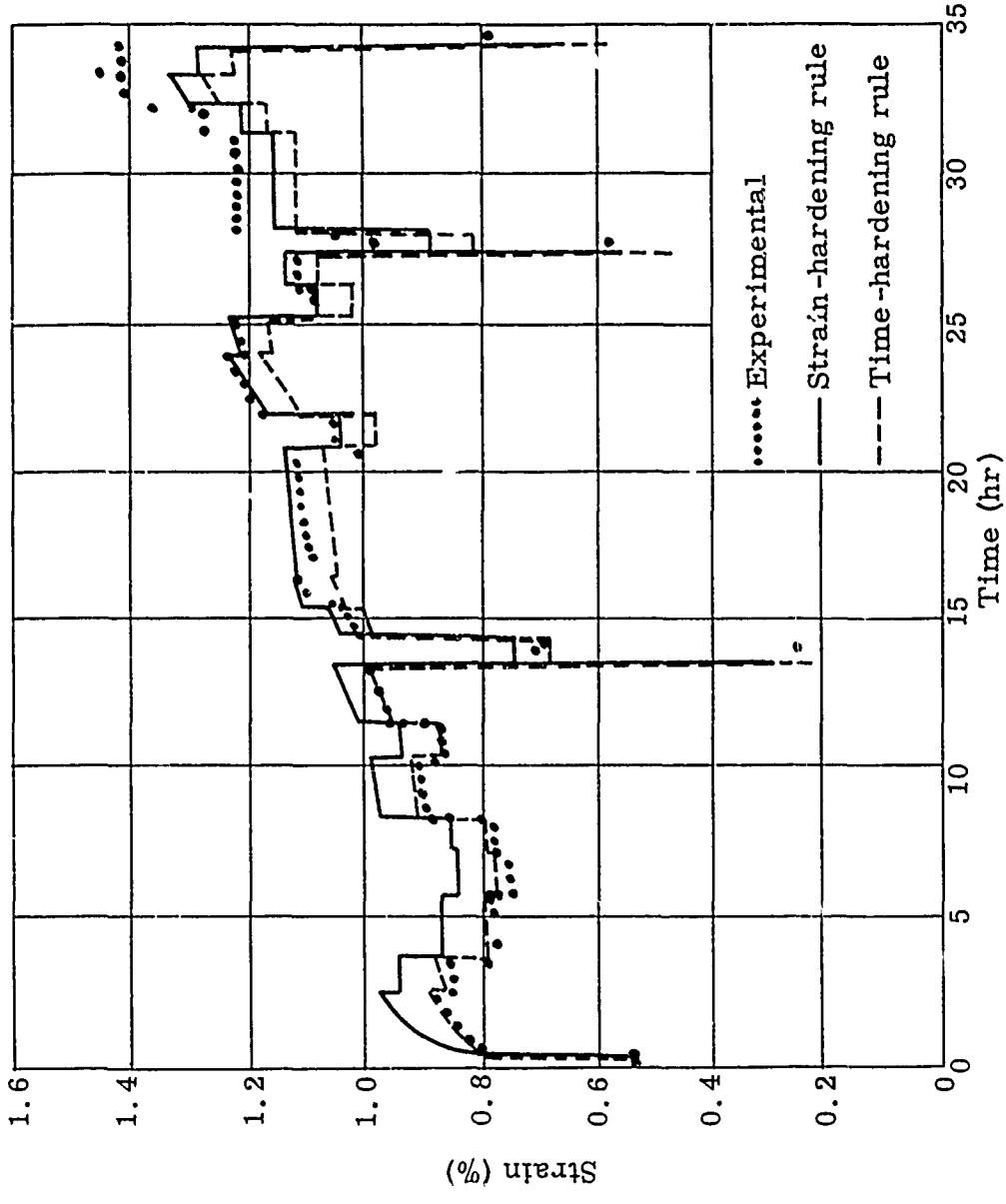


Fig. 2. Comparison of Results

gages located 2.5 inches from the longitudinal center line, compared with the theoretical strain at that point as computed by the strain-hardening rule and the time-hardening rule. The changes in load and temperature are recorded as vertical lines, with the residual strains for shutdown periods also indicated. Primary creep is noticed in the early portions (evidenced by a decreasing rate) and various creep rates appear after that, with various combinations of load and temperature. While the data are generally in good agreement, the overall experimental data tend to increase at a greater rate than the theoretical, a development which could be caused by an accumulation of errors. It is interesting to note that the correlation is quite close for the time-hardening rule for the first portion and close to the strain-hardening rule for the second portion. Although it is not advisable to draw conclusions from an isolated piece of experimentation such as this, perhaps this does indicate that initially the time of applied load shows a greater effect than the accumulated strain, whereas when more strain is accumulated, this has a more pronounced effect. Needless to say, other conjectures can be made; however, the main conclusion remains that the theoretical analysis does a reasonable job of predicting the time-dependent behavior of this structure.

2. Columns

The column has a cross section 1 inch by 1-1/2 inches and a length of 16 inches with an initial crookedness of 1/20 inch. The cross section is divided into eight elements, 1-1/2 inches by 1/8 inch. The time-dependent load and temperature distribution, which varies in the Z-direction, applied to column is shown in Fig. 3.

Results are summarized in Fig. 4 (showing the deflection of the midlength of the column with time) and Fig. 5 (showing the maximum and minimum stresses which occur as a function of time).

3. Plates

The plate is 10 inches by 15 inches with a thickness of 0.2 inch and initial deflection of 0.002 inch at the center. The time-dependent load and temperature distribution, which varies in the Y-direction, applied to the plate is shown in Fig. 6.

Results are summarized in Fig. 7 (showing the deflection of the center with time) and Fig. 8 (showing the maximum and minimum principal stresses which occur in the plate as a function of time).

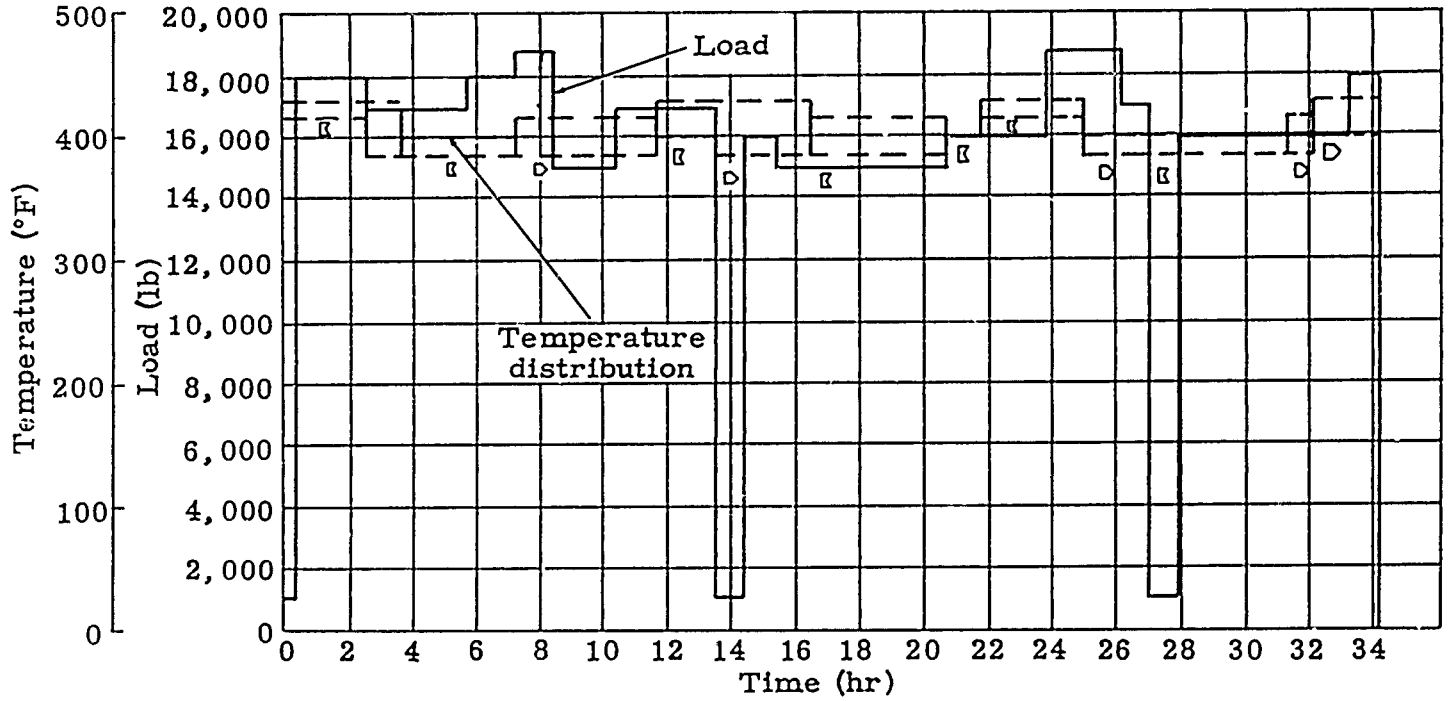


Fig. 3. Sample Column Creep Analysis Problem, Applied Load and Temperature

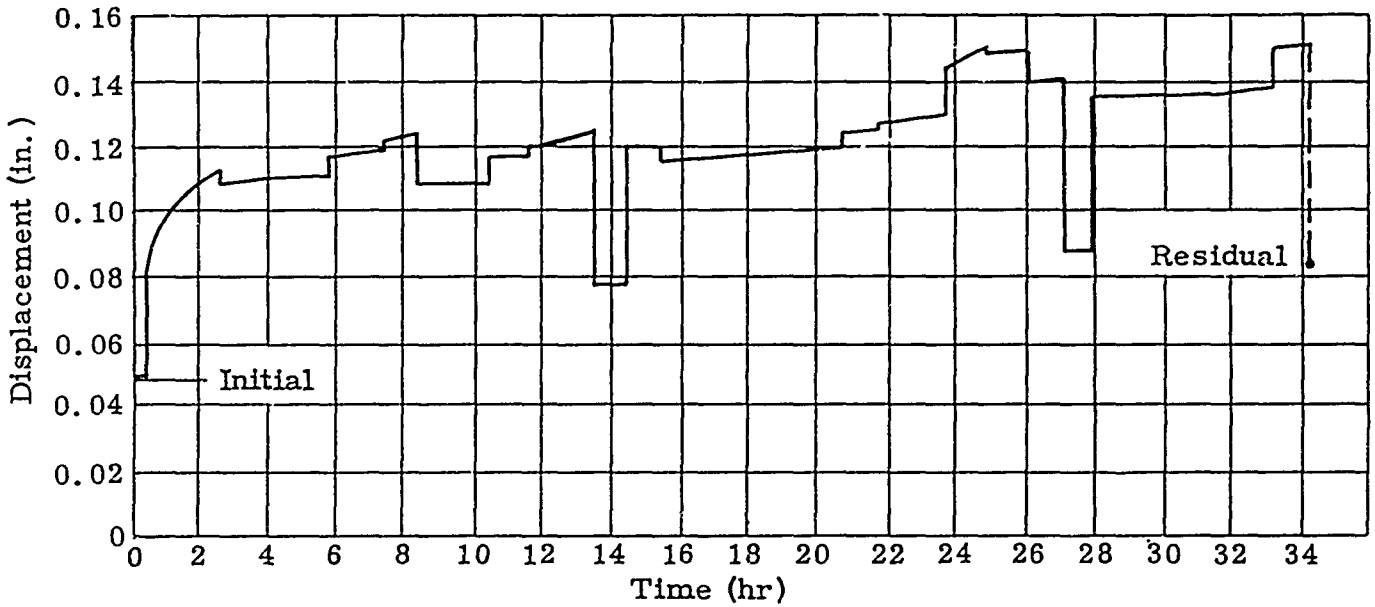


Fig. 4. Sample Column Creep Analysis Problem, Displacement of Center Versus Time

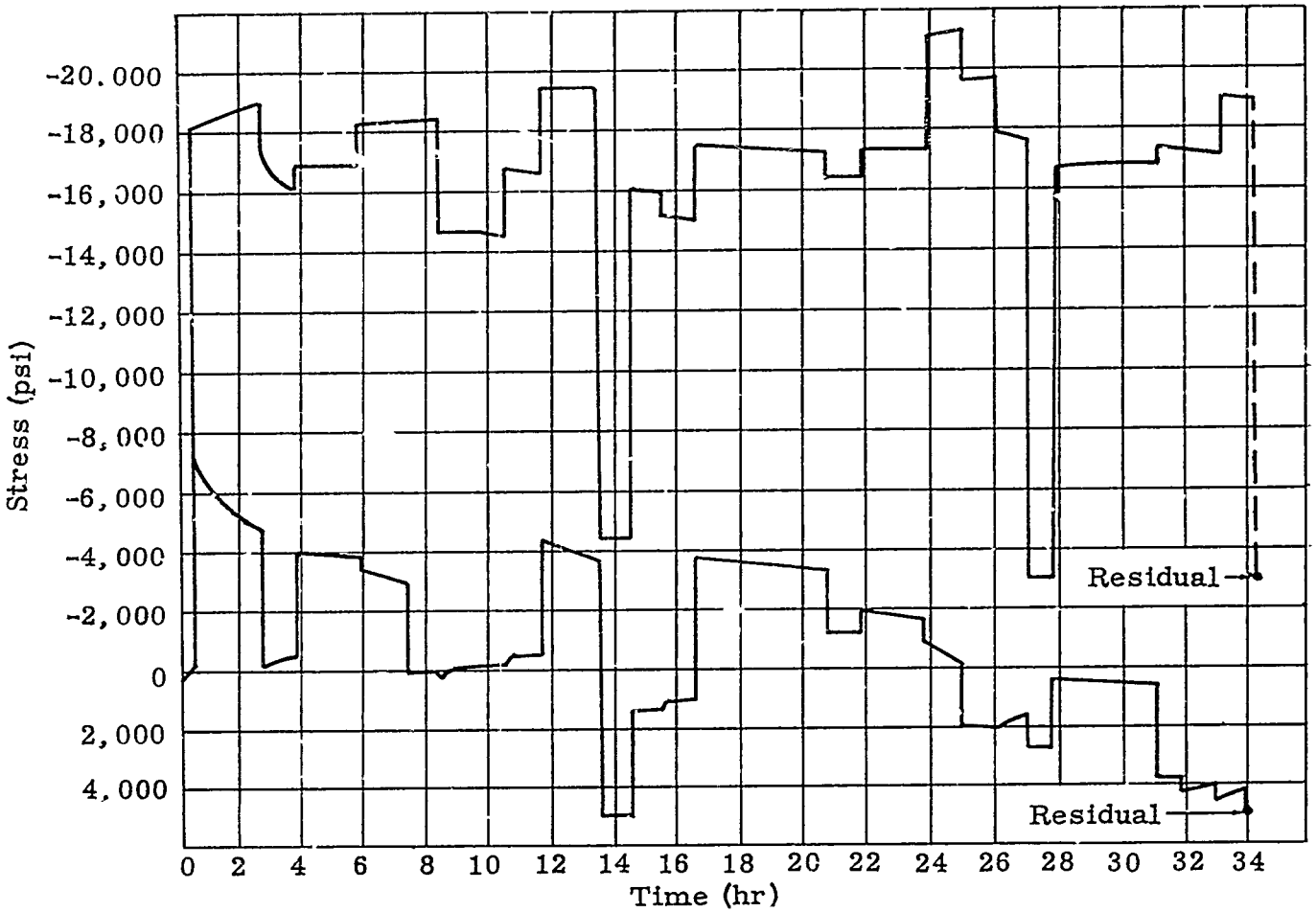


Fig. 5. Sample Column Creep Analysis Problem, Maximum and Minimum Stresses at Midlength Versus Time

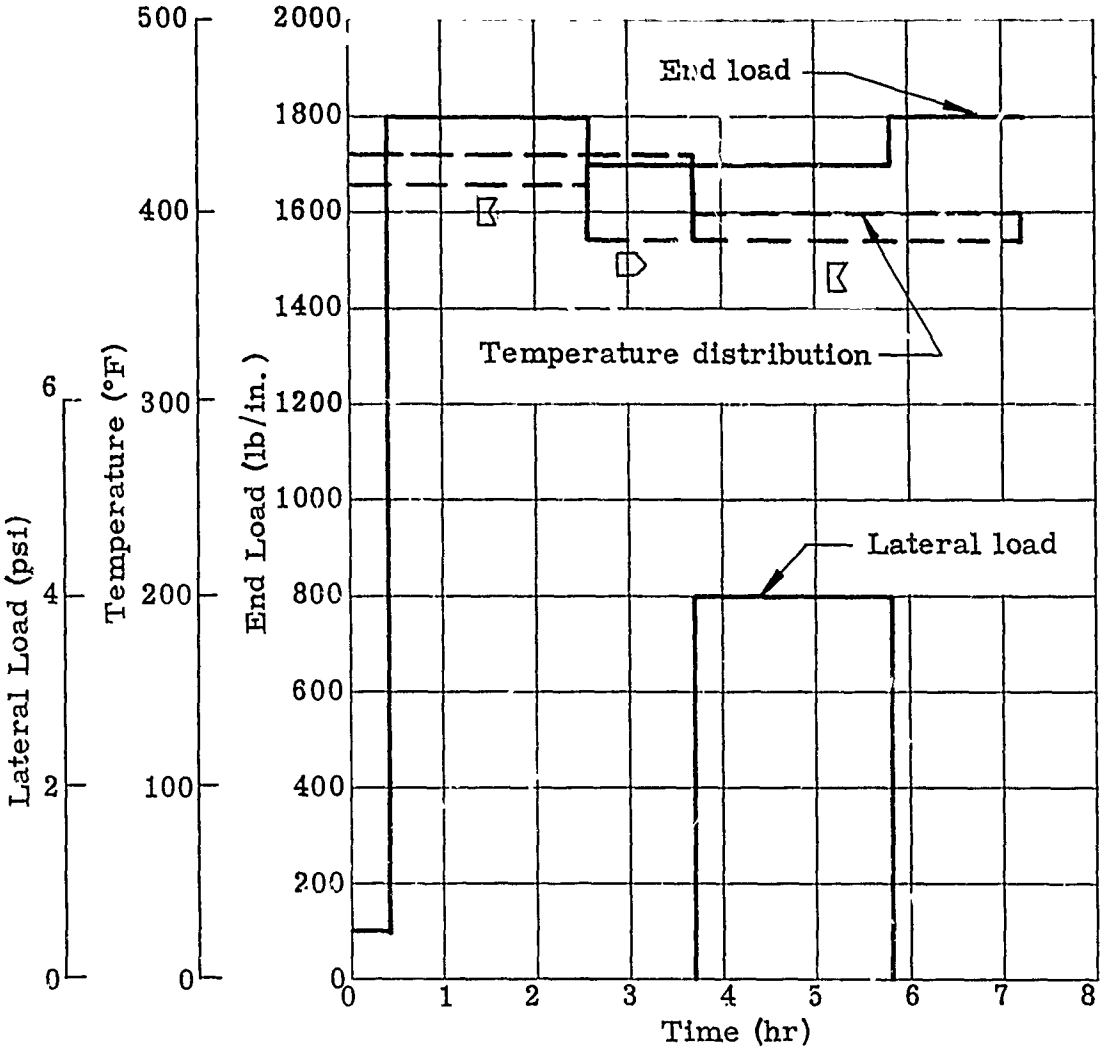


Fig. 6. Sample Plate Creep Analysis Problem, Applied Load and Temperature

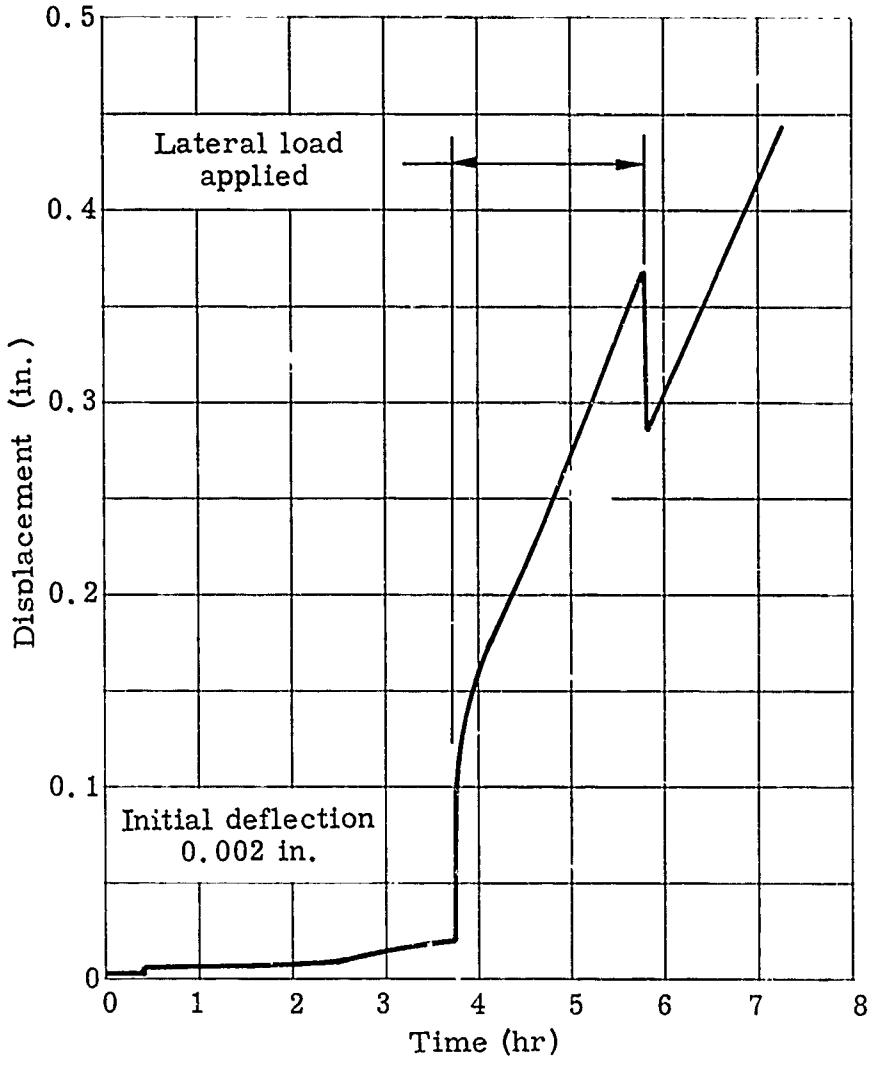
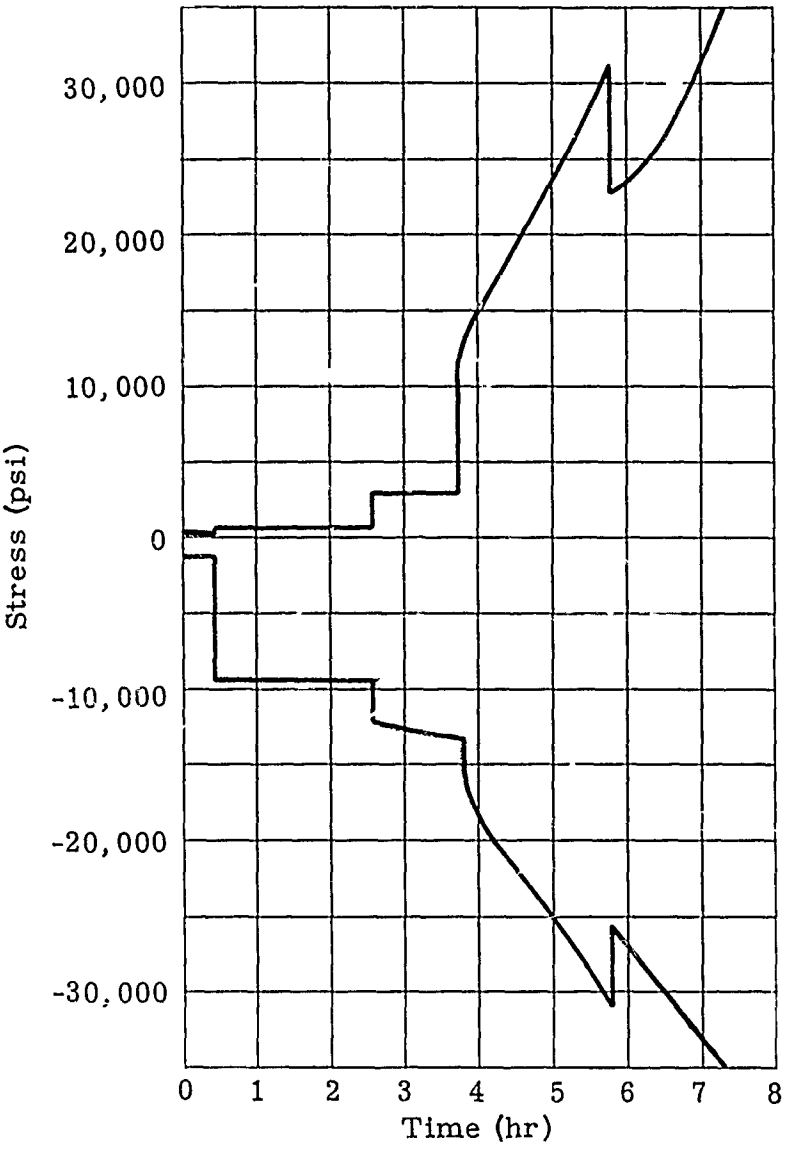


Fig. 7. Sample Plate Creep Analysis Problem, Displacement of Middle of Plate



NOTE: Maximum or minimum stresses do not always occur at the same point.

Fig. 8. Sample Plate Creep Analysis Problem, Maximum and Minimum Principal Stresses

4. Torsion Members

A solid shaft 3.0 inches in diameter is used. The time-dependent torque and temperature applied to the member are shown in Fig. 9.

Results are summarized in Fig. 10 (showing the angle of twist per unit length and the maximum stress as a function of time).

II. A LIMITED STUDY ON SEQUENTIAL EFFECTS OF LOAD-TEMPERATURE ENVIRONMENTS

The sequential effects of load and temperature on a particular structure will be investigated by means of this IBM-7090 program. Since a structure responds singularly under a specific load-temperature environment, the order of application of a group of loads and/or temperature will definitely influence the performance of the structure. It can be evaluated by the time-dependent stress distribution and deformation. In the problem, a group of tensile loads of 120,000, 90,000 and 60,000 pounds is employed to cover both elastic and plastic ranges. This group of loads will be applied slightly eccentrically to a long flat plate with approximate dimensions of 1/4 x 14 inches in cross section. Temperature distributions over the cross section comprise three main types: namely, a peaked type, T_p, which has 300° F along the top and bottom edge and 450° F at the center line of the plate; a recessed type, T_r, which has a 400° F along the top and bottom edges and 300° F along the center line; and a uniform type, T_u, which has 400° F over the cross section.

The analysis is divided into two parts. In the first part, or "P" series, six load functions are used under a fixed temperature function (shown in Fig. 11).

Keeping the temperature function fixed, the effects of load sequence on the plate may be determined.

A variation of temperature sequence will be treated likewise under a fixed load function. There are also six temperature functions in the second part, T-series, as shown in Fig. 12.

To measure the behavior of a structure, stress and strain or the deformation, which indicate the strength and the performance of the

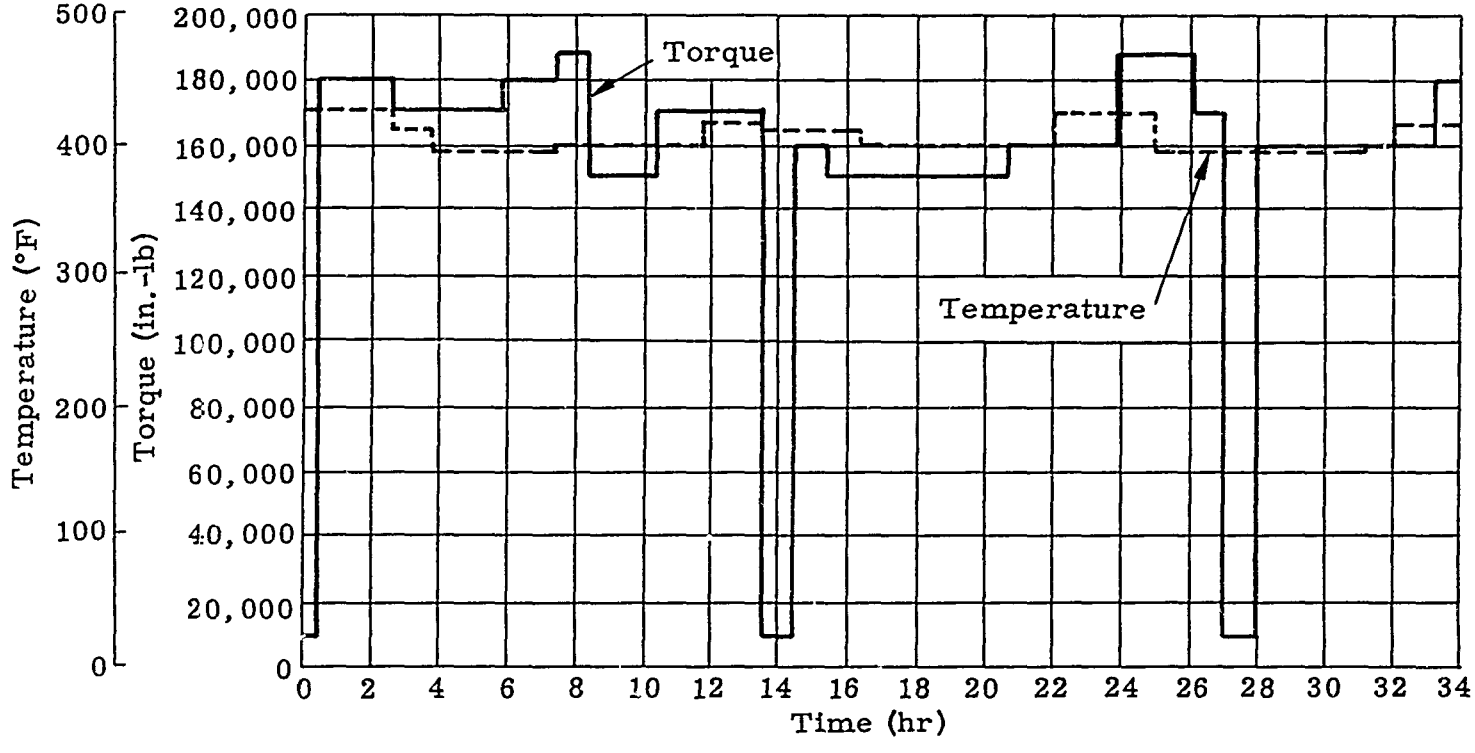


Fig. 9. Sample Torsional Member Creep Analysis Problem, Applied Torque and Temperature

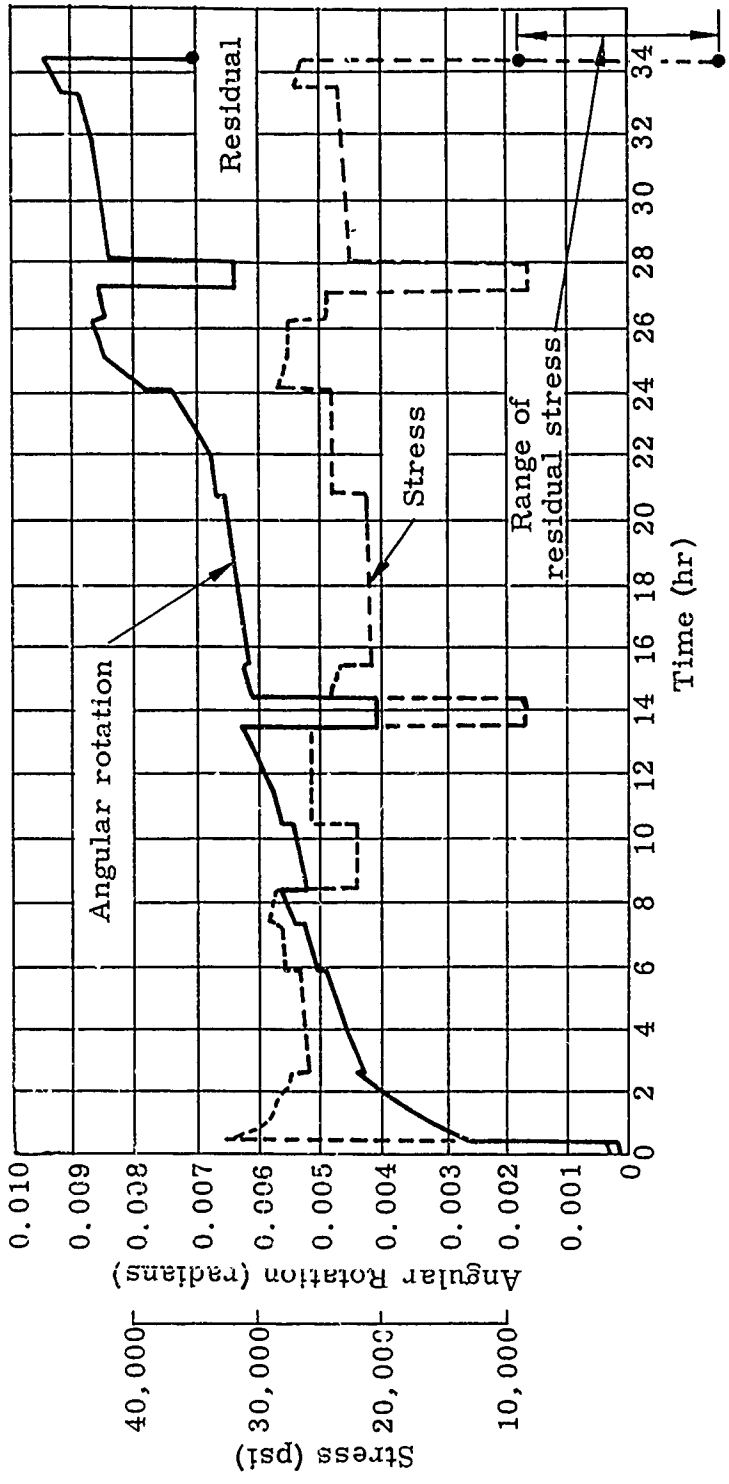


Fig. 10. Sample Torsional Member Creep Analysis Problem, Angular Displacement and Maximum Stress

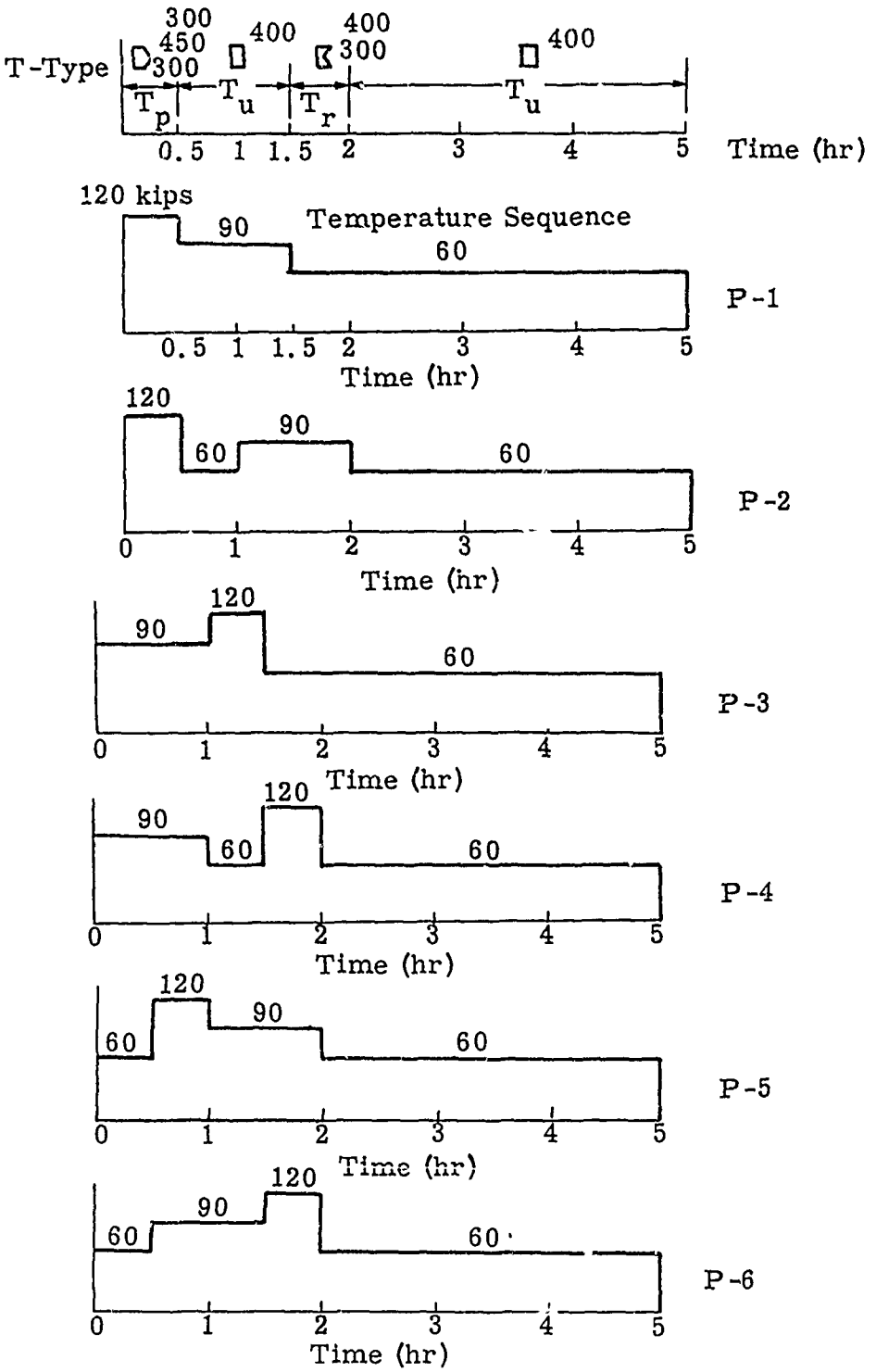


Fig. 11. P-Series

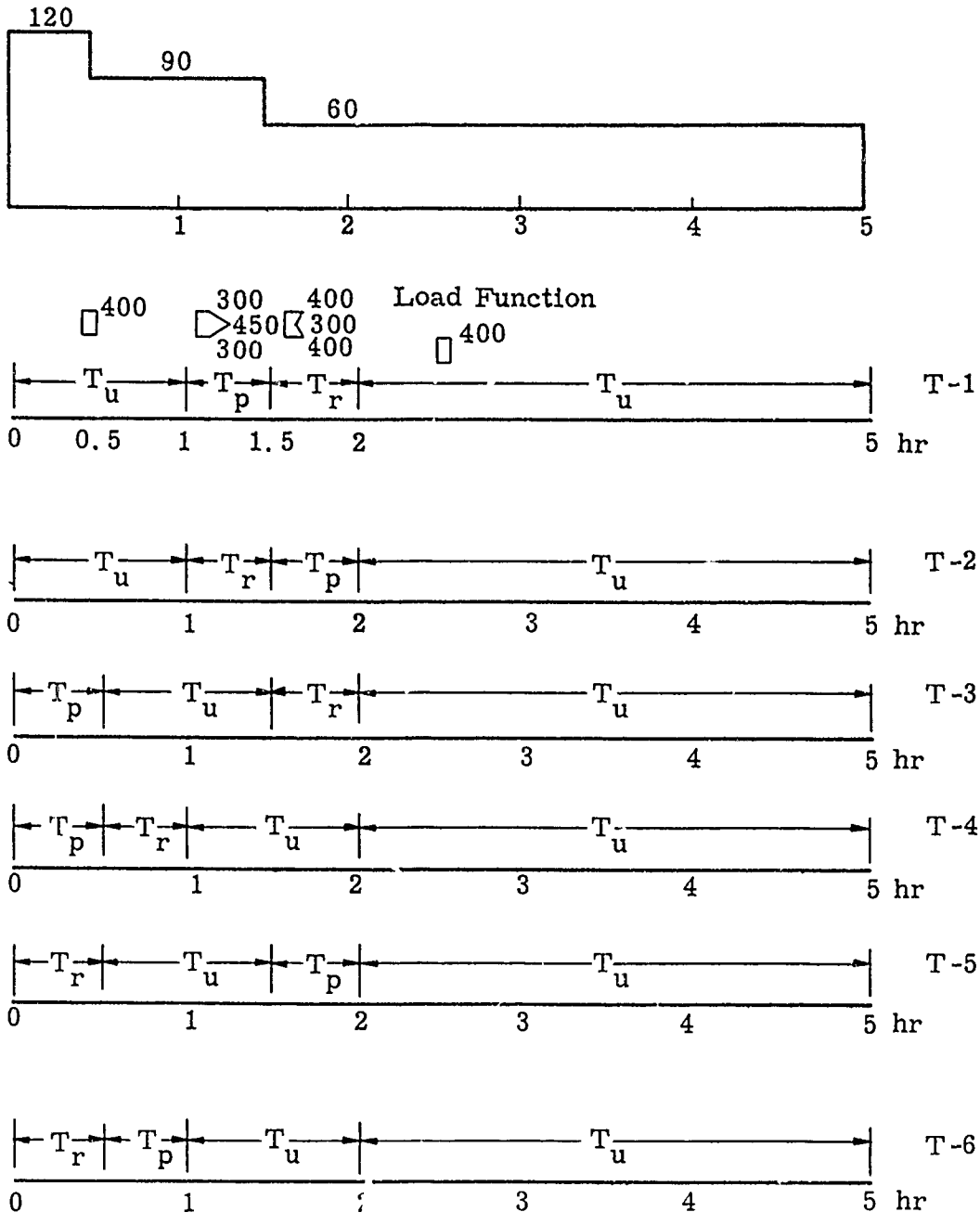


Fig. 12. T-Series

structure, will be adopted as criteria. Strain is further subdivided into two types, creep strain and total strain. Total strain, of course, is a parameter for structural performance. The creep strain will serve as a milestone to determine the expended life of the structure.

First, the degree of severity of the individual input elements must be established. Based on simple computations, the temperature patterns can be placed in the following order for both thermal expansion and creep:

$$T_u > T_p > T_r.$$

Also, it is obvious for the load functions to have an order of

$$P_{120} > P_{90} > P_{60}$$

in both static deformation and creep. The creep strains of both series are plotted with strain versus time (shown in Figs. 13 and 14).

Upper and lower bounds are provided by the P-1 and P-6 sequences, respectively. Similar bounds for the T-series are also obtained by T-1 and T-6.

At the end of 5 hours, P-1 gives a value of 0.0005736 inch/inch which is 224% higher than that of P-6. Similarly, T-1 gives 0.00083 inch/inch and is 221% over that of T-6. This wide area between the bounds indicates the serious effect of load and/or temperature sequences on the creep performance of the structure. The upper bound, of course, produces the most critical case while the lower bound gives the most optimum. P-1 and T-1 (both yield the upper bound) have a common character in their sequences. They are led off by P_{120} and T_u, the most critical elements, and the remainders of the sequences follow in descending order. On the other hand, P-6 and T-6, which yield the lower bound, have an ascending sequence. Thus, in this investigation, a stepping-down sequence should be considered as most critical, creep-wise, and used as a design criteria while a stepping-up function is a most optimum sequence which may be followed to restrict the flight procedure in favor of a prolonged service life of the aircraft.

The total deformation curves (Figs. 15 through 18) show no limits bound by any single sequence for the whole time span. However, by comparing the deflections at any instant, the values seem to follow the

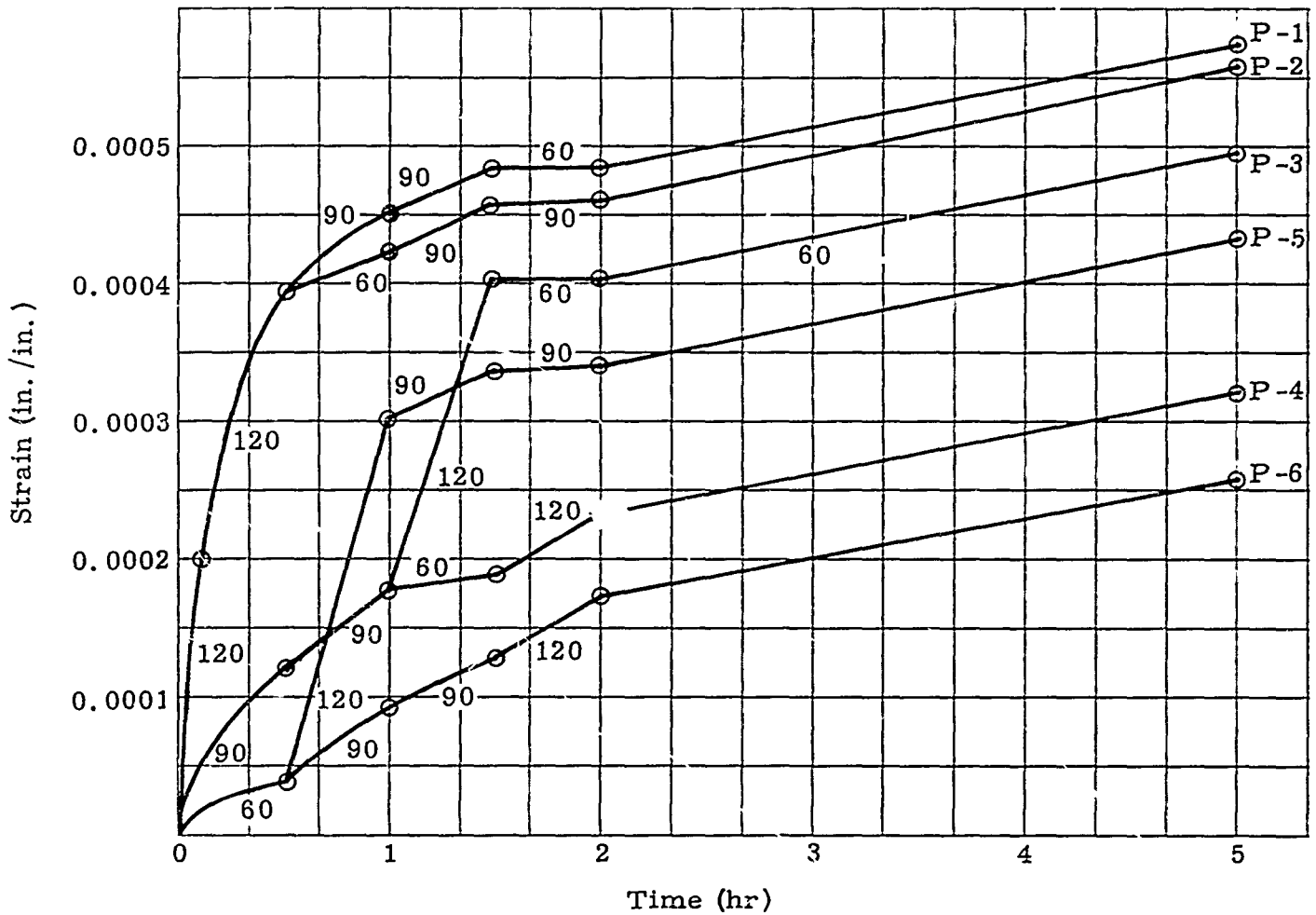


Fig. 13. Accumulated Creep Curves (P-series)

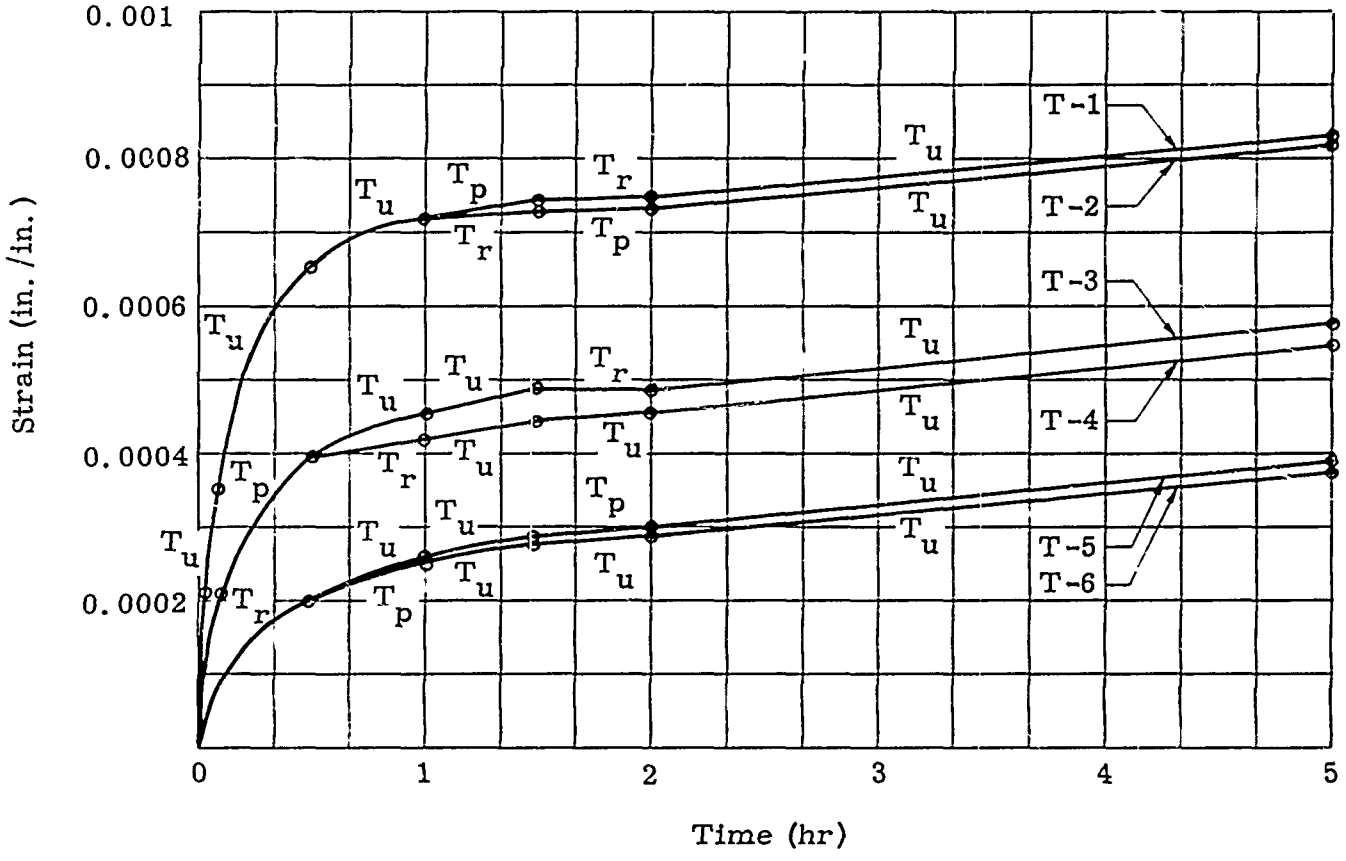


Fig. 14. Accumulated Creep Curves (T-series)

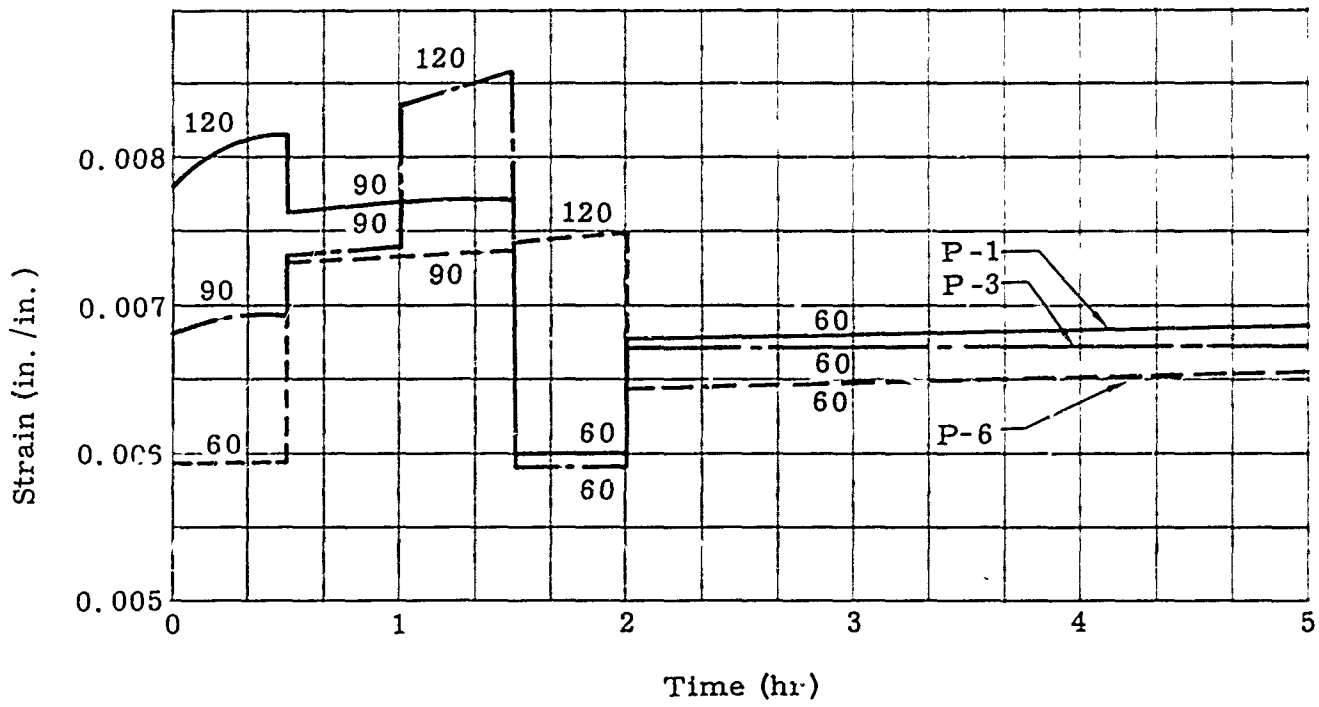


Fig. 15. Total Strain Curves (P-1, P-3, P-6)

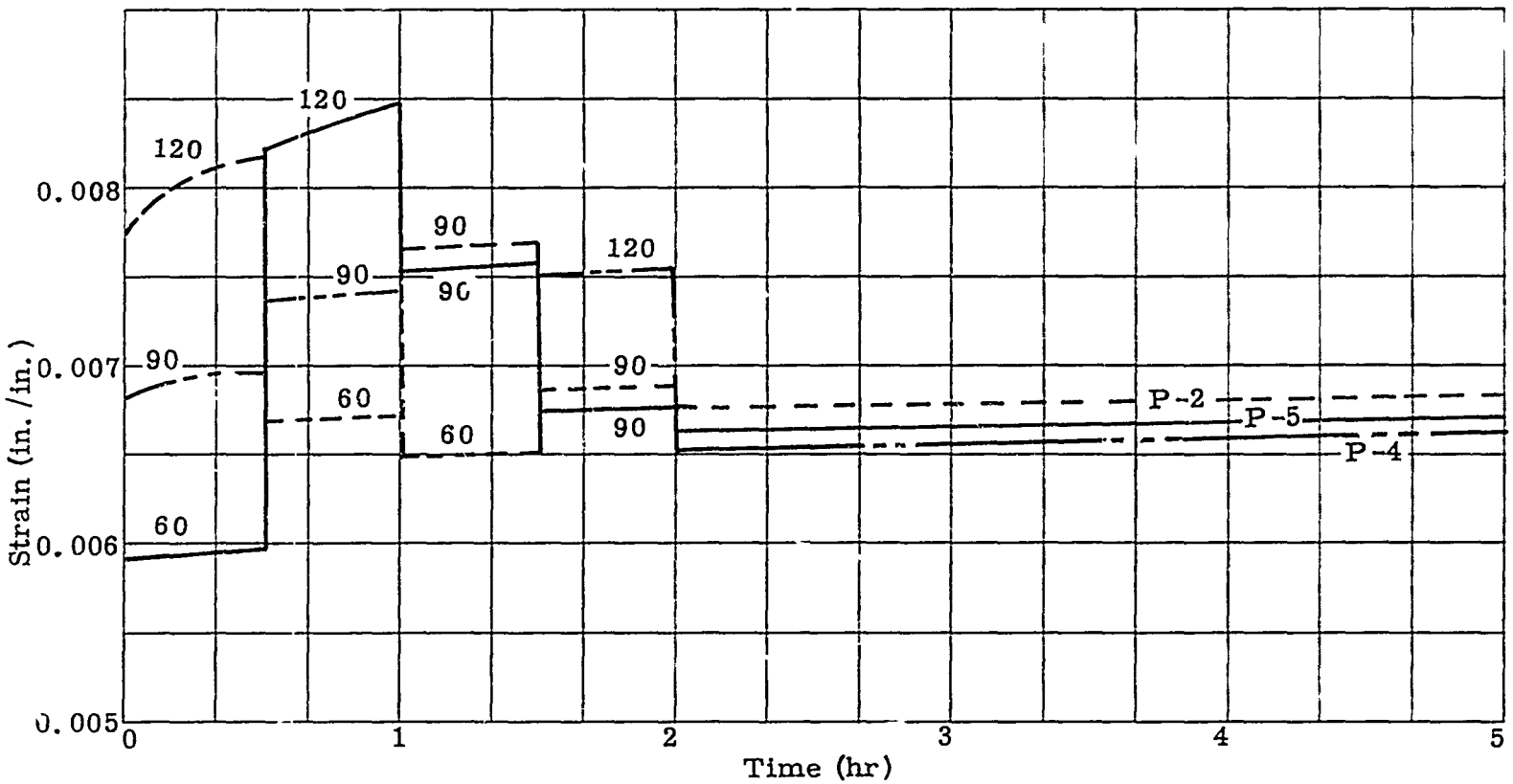


Fig. 16. Total Strain Curves (P-2, P-4, P-5)

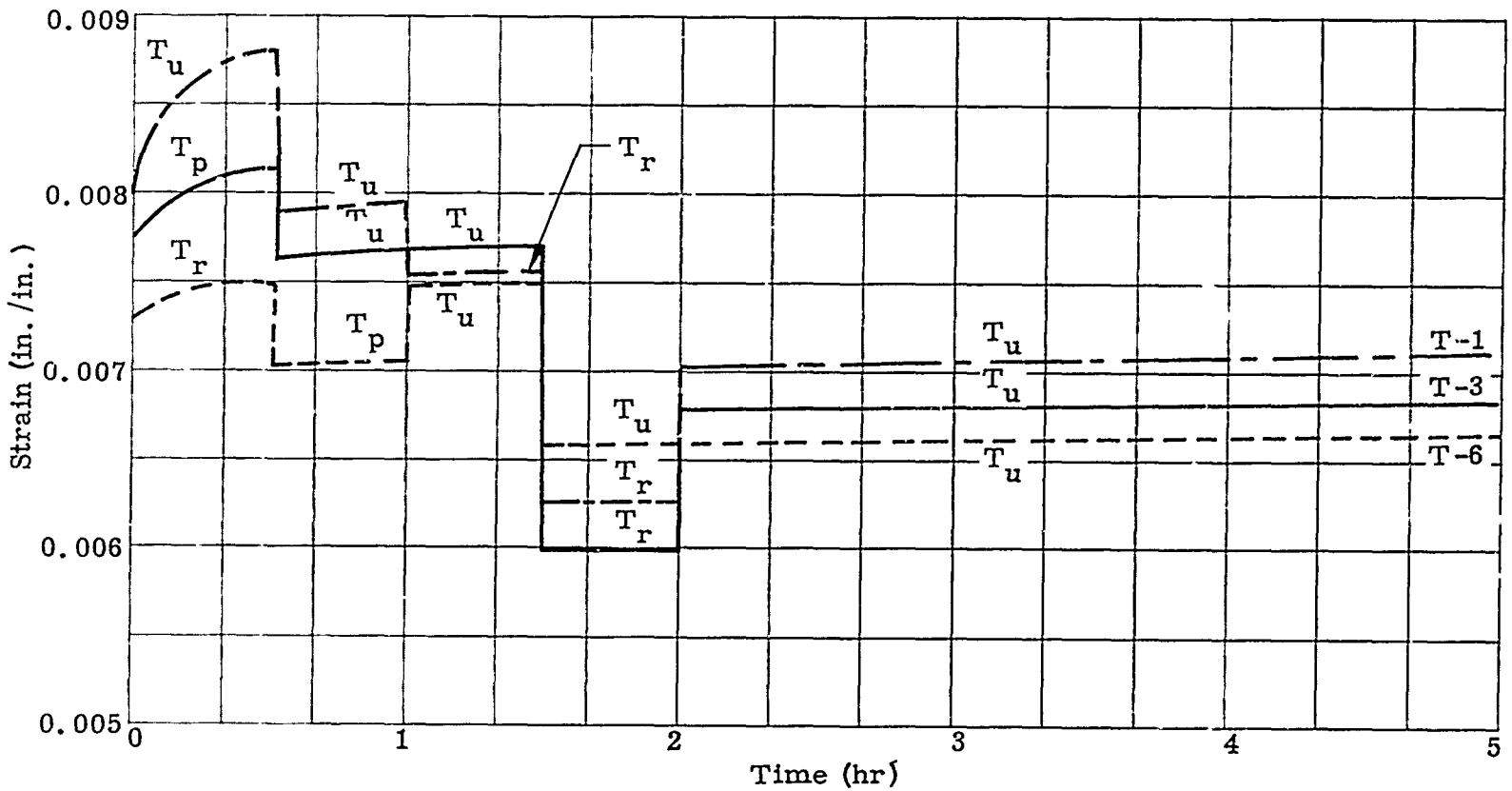


Fig. 17. Total Strain Curves (T-1, T-3, T-6)

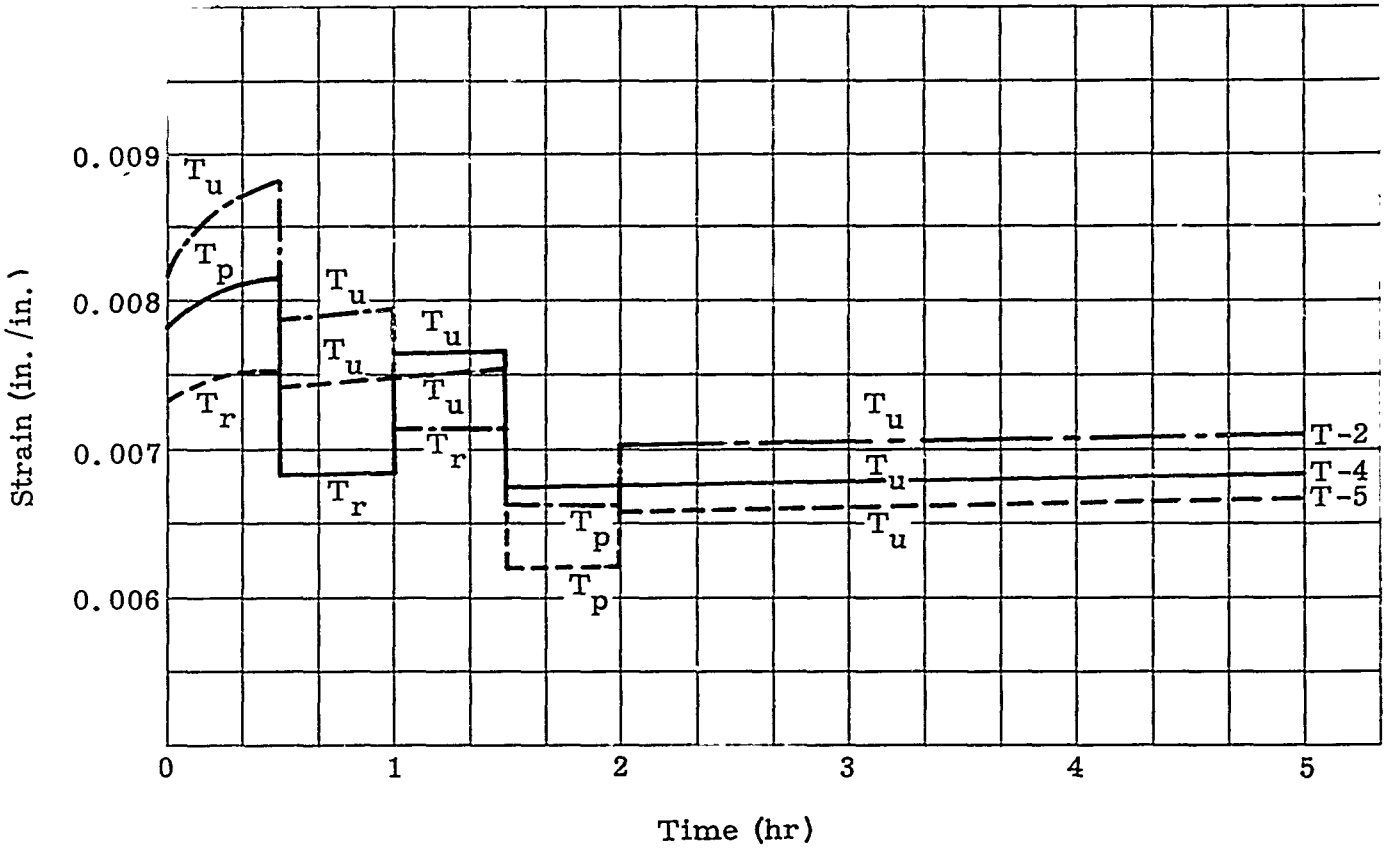


Fig. 18. Total Strain Curves (T-2, T-4, T-5)

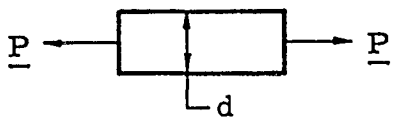
degree of severity in practically all cases. It suggests that an upper limit can be constructed by superimposing the static deflections of the most critical function on the upper bound of accumulated creep curve. This resulting curve should provide valuable information for design purposes. The values yielded by this combined curve are always conservative. Its degree of accuracy may be estimated approximately by the two creep bounds in some manner.

The stress distribution always consists of two parts (Fig. 19), the primary and the residual stress systems. The primary stress depends upon the acting loads and temperature distribution at that moment; the residual stress relies on the input function prior to that point. Thus, it is obvious that the residual stress system must be self-equilibrating and changing in form continuously. The self-equilibrating stress system does not affect the ultimate strength of the structure since it tends to diminish at large plastic strain. However, its actual distribution sometimes can be important in stability analyses and should be determined.

ACKNOWLEDGEMENTS

The work in this paper was performed in part under Air Force Contracts AF 33(616)-6436 and AF 33(616)-6904 augmented by Martin research programs of the Research and Development Department.

Mr. C. G. Swanson of The Martin Company contributed most of the theoretical development in the formulation of field equations for various structural components.



	P	Temp	Time
①	120	▷	0.0 hr
②	120	▷	0.5 hr
③	90	▯	0.5 hr
④	90	▯	1.5 hr
⑤	60	◸	1.5 hr
⑥	60	▯	2.0 hr

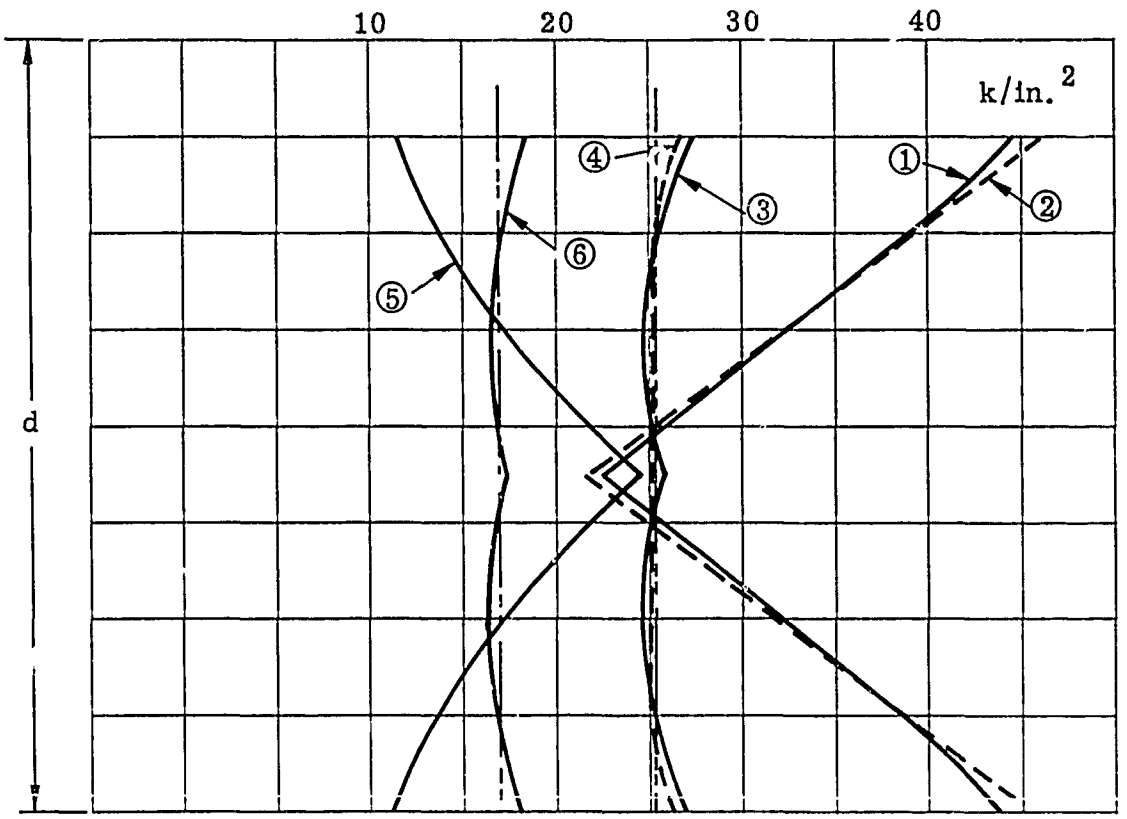


Fig. 19. Instantaneous Stress Distributions (load, thermal, creep, residual--P-1 or T-1)

III. REFERENCES

1. Padlog, J. and Schmitt, A., "A Study of Creep, Creep-Fatigue and Thermal-Stress-Fatigue in Airframes Subject to Aerodynamic Heating," WADC TR 58-294.

2. Huang, P. C., "Elasto-Plastic Bending Analysis for Structures Under Arbitrary Load-Temperature Environments--Part I, Analysis Development and Digital Program," WADD TR 60-541, 1960.

3. Van Der Maas, C. J., "Elasto-Plastic Bending Analysis for Structures Under Arbitrary Load-Temperature Environments--Part II, Experimental Verification," WADD TR 60-541, 1960.

4. Sprague, G. H. and Huang, P. C., "Behavior of Aircraft Structures Under Thermal Stresses," SAE Transactions, Vol. 66, 1958.

5. Parkes, E. W., "Wings Under Repeated Thermal Stress," Aircraft Engineering, Vol. 26, December 1954.

6. Heldenfels, R. R. and Vosteen, L. F., "Approximate Analysis of Effects of Large Deflections and Initial Twist or Torsional Stiffness of a Cantilever Plate Subjected to Thermal Stresses," NACA Report 1361.

7. Huang, P. C. and Van Der Maas, C. J., "Combined Effects of Axial Load, Thermal Stress and Creep in Flat Plates," WADC TR 57-442, March 1958.

8. Voorhees, H. R. and Freeman, J. W., "Notch Sensitivity of Heat-Resistant Alloys at Elevated Temperatures," WADC TR 54-175.

9. Hoff, N. J., "Stress Distribution in the Presence of Creep," PIBAL Report No. 362, September 1956.

10. Venkatraman, B., "Solution of Some Problems in Steady Creep," Polytechnic Institute of Brooklyn, PIBAL Report No. 402, July 1957.

11. Muvdi, B. B. and Giemza, C. J., "Primary Creep in Aircraft Design," SAE National Aeronautical Meeting, April 1958.

12. Smith, G. V., "Properties of Metals at Elevated Temperature," McGraw-Hill Book Company.

13. Giemza, C. J., "Experimentation, Analysis and Prediction for Environmental Creep," WADD TR 60-777, 1960.

14. Nadai, A., "Theory of Flow and Fracture of Solids," Second Edition, McGraw-Hill Book Company, 1950.

15. Sprague, G. H. and Huang, P. C., "Analytical and Experimental Investigation of Stress Distribution in a Long Flat Plate Subjected to Longitudinal Loads and Transverse Temperature Gradients," WADC TR 55-350.

16. Huang, P. C. and Van Der Maas, C. J., "Theoretical and Experimental Studies of the Stresses and Strains Around Cutouts in Loaded Unevenly Heated Plates," WADC TR 59-2.

17. Boley, B. A. and Weiner, J. H., "Theory of Thermal Stresses," John Wiley and Sons, Inc., 1960.

18. Gatewood, B. E., "Thermal Stresses with Application to Airplanes, Missiles, Turbines and Nuclear Reactors," McGraw-Hill Book Company, 1957.

19. Zender, G. W. and Pride, R. A., "The Combinations of Thermal and Load Stresses for the Onset of Permanent Buckling in Plates," NACA TN 4053.

20. Huang, P. C. and Van Der Maas, C. J., "Combined Effects of Axial Load, Thermal Stress and Creep in Flat Plates; Large Deflection Analysis of Buckled Plates Under Thermal Effects," WADC TR 57-442, Supplement 1, February 1959.

21. Lin, T. H., "Creep Stresses and Deflections of Columns," Journal of Applied Mechanics, Vol. 23, June 1956.

22. Libove, C., "Creep Buckling of Columns," Journal of the Aeronautical Sciences, Vol. 19, July 1952.

23. Gerard, G., "A Creep Buckling Hypothesis," Journal of the Aeronautical Sciences, Vol. 23, September 1956.

24. Patel, S. A. and Venkatraman, B., "Creep Behavior of Columns," PIBAL Report No. 422, May 1959.

25. Carlson, R. L. and Manning, G. K., "A Summary of Compressive Creep Characteristics of Metal Columns at Elevated Temperatures," WADC TR 57-96, April 1958.

26. Shanley, F. R., "Weight-Strength Analysis of Aircraft Structures," McGraw-Hill Book Company, 1952.

27. Bodine, E. G., Carlson, R. L. and Manning, G. K., "The Interaction of Bearing and Tensile Loads on the Creep Properties of Joints," NACA TN 3758.

28. Bodine, E. G., Carlson, R. L. and Manning, G. K., "Creep Deformation Patterns of Joints Under Bearing and Tensile Loads," NACA TN 4138.

29. Marin, J., "Creep Deformations in a Single Riveted Structural Joint Under Axial Tension," WADC TR 57-757, June 1959.

30. Mordfin, L. and Legate, A. C., "Creep Behavior of Structural Joints Under Constant Loads and Temperatures," NACA TN 3842, January 1957.

31. Swanson, C. G., Van Der Maas, C. J. and Huang, P. C., "Allowable Stresses for Elevated Temperature Structures," Martin Research Report-19, January 1961 (to be published as ASD TR 61-8).

32. Carlson, R. L., Breindel, W. W. W. and Manning, G. K., "An Investigation of Column Action During Creep Buckling," WADD TR 60-7, June 1960.

33. Hoff, N. J., "Creep Buckling," Aeronautical Quarterly, February 1956.

34. deVeubeke, F., "Creep Buckling," Chapter 13 of High Temperature Effects in Aircraft Structures, published for AGARD by Pergamon Press, 1958.

35. Libove, C., "Creep-Buckling Analysis of Rectangular-Section Columns," NACA TN 2956, June 1953.

36. Kemper, J., "Creep Bending and Buckling of Linearly Viscoelastic Columns," NACA TN 3136, January 1954.

37. Kemper, J., "Creep Bending and Buckling of Nonlinearly Viscoelastic Columns," NACA TN 3137, January 1954.

38. Kemper, J. and Patel, S. A., "Creep Buckling of Columns," NACA TN 3138, January 1954.

39. Hu, L. W. and Triner, N. H., "Bending Creep and Its Applications to Beam Columns," Journal of Applied Mechanics, March 1956.

40. Lin, T. H., "Creep Deflections and Stresses of Beam Columns," Journal of Applied Mechanics, March 1958.

41. Poritsky, H. and Fend, F. A., "Relief of Thermal Stresses Through Creep," Journal of Applied Mechanics, December 1958.

42. Patel, S. A. and Pandalai, K. A. V., "Torsion of Cylindrical and Prismatic Bars in the Presence of Primary Creep," PIBAL Report No. 417, April 1958.

43. Pandalai, K. A. V. and Patel, S. A., "Stress Distribution in Multi-Cellular Torque Boxes Due to Primary and Secondary Creep," PIBAL Report No. 480, December 1958.

44. Patel, S. A. and Pandalai, K. A. V., "Stress Distribution in Beams of Thin-Walled Sections in the Presence of Creep," PIBAL Report No. 486, February 1959.

45. French, F. W. and Patel, S. A., "Creep Buckling of Cylindrical Shells, Subjected to Uniform Axial Compression," PIBAL Report No. 489, May 1959.

46. Patel, S. A., Pandalai, K. A. V. and Venkatraman, B., "Creep-Stress Analysis of Thin-Walled Structures," PIBAL Report No. 497, July 1959.

METHODS AND ANALYSIS OF HEAT TRANSFER

Peter E. Grafton

The Boeing Company

ABSTRACT

The purpose of this paper is to review the significant modes of heat transfer and practical methods for their analysis to determine the thermal environment of structures for advanced flight vehicles. Emphasis is placed on maximum use of simplified analysis concepts and the range of their validity. Of particular interest is the strong damping of short period transient thermal inputs, resulting in a partial decoupling of the dynamic aerothermoelastic problem.

METHODS AND ANALYSIS OF HEAT TRANSFER

INTRODUCTION

The thermal analysis of structures for very high speed flight vehicles involves all the known modes of heat transfer. Forced convection from the surrounding airstream has received wide attention as the usually predominant source of heat input to the vehicle, and as flight speeds approach and exceed orbital velocity, hot gas radiation to the vehicle from the surrounding shock layer becomes significant. Surface radiation plays an important role in rejecting heat received by the vehicle as well as contributing to internal transfer of heat. Conduction is usually always present, and both forced and free convection may be involved in the operation of cooling systems and transfer of heat to fuel or propellants. Heat storage plays an important part in transient problems, and phase change may be an integral part of temperature control systems. The engineer is faced with quite a number of challenging problems in attempting to identify the significant modes of heat transfer in a given case, give quantitative expression to them, and include them within the framework of a mathematical model which can be used to predict temperature response with a satisfactory accuracy.

In view of the scope indicated above, it would be impractical if not impossible to present a detailed review of all aspects of the flight vehicle thermal analysis problem. Instead, it is the purpose of this paper to cover some of the more significant features of thermal behavior in flight structures, and the techniques which have been used successfully in their analysis. To accomplish this, the sources of heat input are reviewed briefly, followed by a survey of the more important modes of heat transfer within flight vehicles. Techniques which can be used to formulate the thermal response problem are then discussed, and the available tools for solution of the resulting equations are considered. Some simple examples are presented to illustrate the techniques and some of the more significant features of thermal response.

The literature of heat transfer is quite extensive and has been growing rapidly in recent years. A large portion

of it is applicable in some degree to the flight vehicle thermal response problem. However, due to the press of time in preparing this paper, it has not been possible to give references as completely as might be desired, and the indulgence of the reader in this regard is requested. The experience of the author and his associates in the practical thermal analysis of flight vehicle structures over the past few years has been used as a guide in selecting the topics covered.

Some preliminary remarks on the accuracy of thermal analyses are in order. Due to the significance of temperature in the behavior of flight structures, particularly when the structural materials are being used towards the upper limit of their temperature capability, the desired objective of thermal analysis would be to predict structural temperatures with a high accuracy of say $\pm 20^{\circ}F$. This sort of accuracy is not attainable today and is not likely to be achieved in the near future. The principal problems in achieving accuracy are the errors inherent in determining heating input rates, and the errors associated with the experimentally determined thermophysical properties which influence thermal response. Under the best of conditions, convective heat flux input can be predicted with an error of $\pm 20\%$ for high speed flight, and the accuracy of estimated heat fluxes from radiating hot gases is considerably poorer. For thermophysical properties, $\pm 10\%$ accuracy at the temperatures of interest is good by present standards. In view of this, attempts to achieve high accuracy by "exact" thermal response analyses cannot be justified, and simplified approximate techniques are satisfactory for engineering purposes.

SECTION I: SOURCES OF HEAT INPUT

By far the most predominant source of heat input to high speed flight vehicles is the exterior airstream. Since the major portion of the previous session was devoted to this subject of aerodynamic heating, consideration here will be limited to points pertinent to the thermal analysis problem.

Forced convection is the predominant mode of aerodynamic

heating for most of the flight regime of present interest. Figure 1 presents some approximate values of the heat fluxes encountered, based on data contained in reference 1, to illustrate the order of magnitude involved. By nature, forced convection is a boundary layer phenomenon, controlled by the fluid mechanics of both the boundary layer and the flow external to it around the vehicle. Techniques for predicting convective heating rates, experimentally, theoretically, or by a combination of both, will remain a fruitful area of research for some time. As mentioned previously, present techniques cannot provide estimates with a satisfactory degree of accuracy. It has been found useful to compile convective heating data in handbook form, such as ref. 1, applicable to simple shapes for preliminary estimates. For design values on practical configurations, the combination of extensive experimental measurements with theoretical analyses to account for incomplete simulation of flight conditions appears to be the most satisfactory solution at the present time.

One aspect of forced convection aerodynamic heating deserves special mention. Conventional practice is to express heating rates as the product of a heat transfer coefficient and the difference between recovery and surface temperatures (or enthalpies):

$$q = h(T_r - T_s) = H(i_r - i_s) \qquad (1)$$

For low speed flows and small to moderate temperature (or enthalpy) differences, the heat transfer coefficient is practically independent of surface temperature and Eq. 1 can be properly interpreted as expressing a linear dependence of heat flux on surface temperature. Under the conditions of high speed flight, the variation of the heat transfer coefficient with surface temperature is of the same order as the variation of the temperature (or enthalpy) difference. This is illustrated in figure 2 for a typical case. In most thermal analyses, the total variation of convective heat flux with surface temperature is small enough to be neglected entirely, and the heat flux can be evaluated at the start of a thermal analysis, based on a crude estimate (to within a few hundred degrees) of the surface temperature. This sort of treatment is used in the balance of this paper. If the heat flux variation with surface temperature is found to be significant, it can be properly included in most analyses by

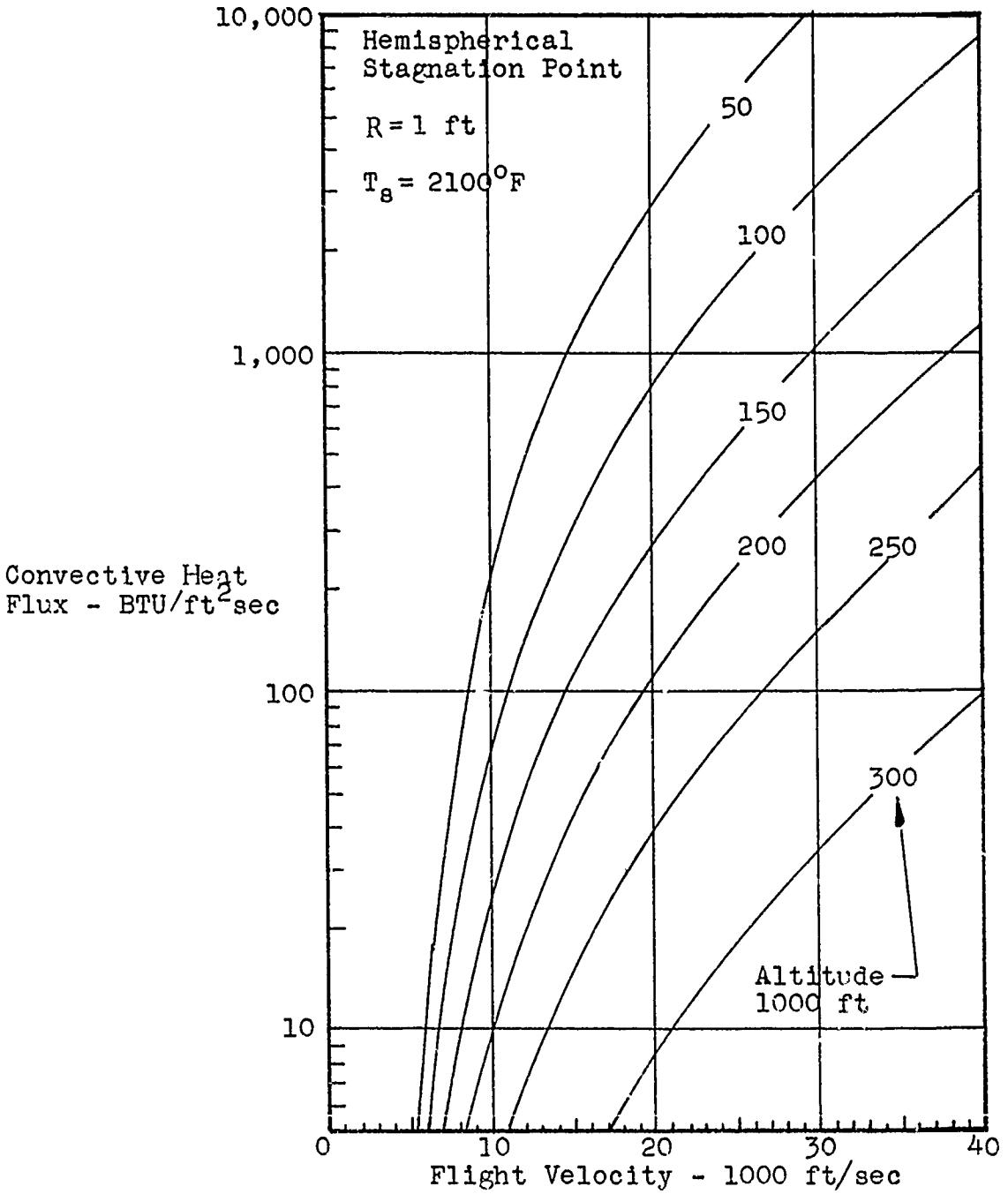


Figure 1(a)

Aerodynamic Heating by Forced Convection - Stagnation Point

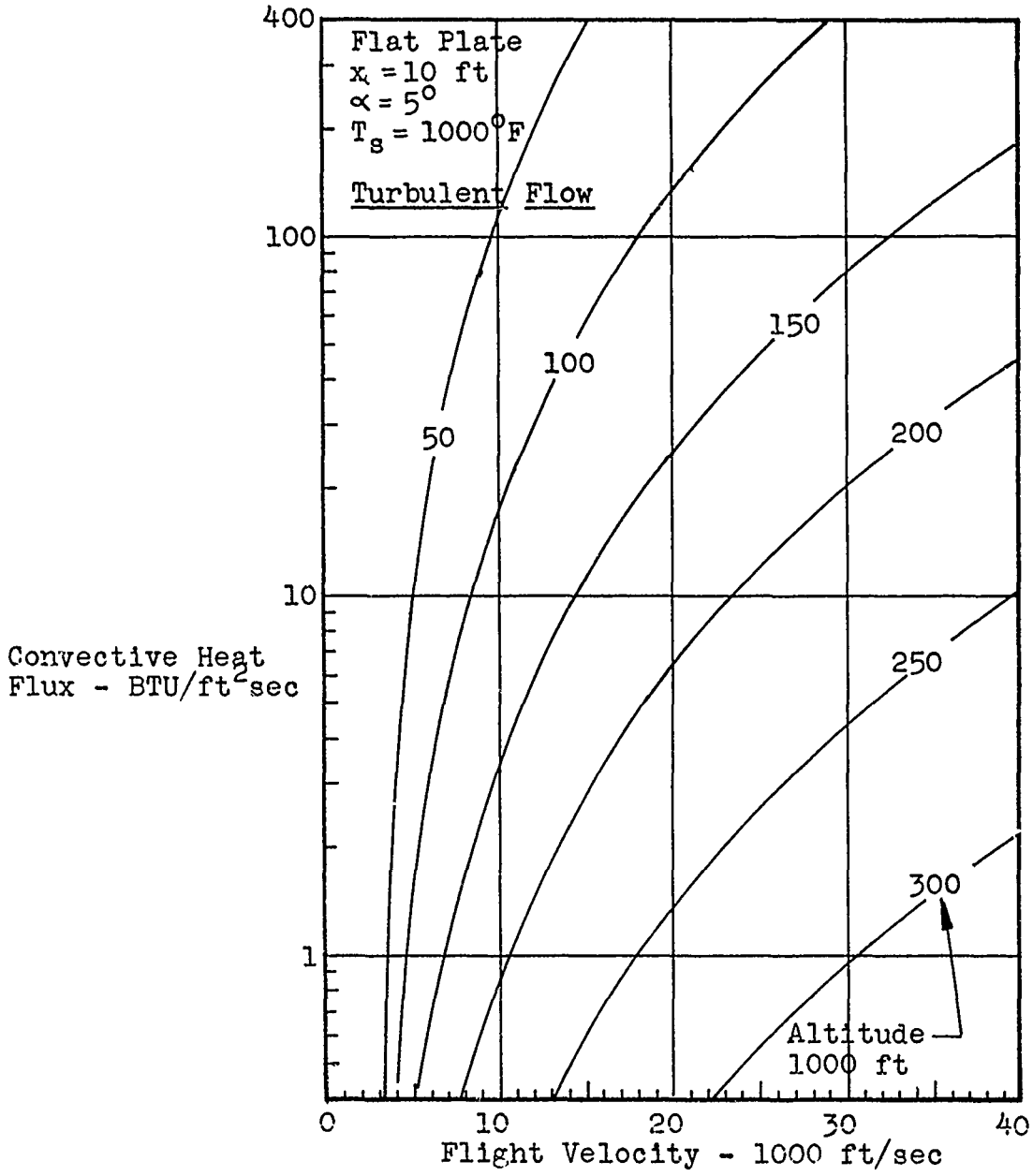


Figure 1(b)

Aerodynamic Heating by Forced Convection - Flat Plate

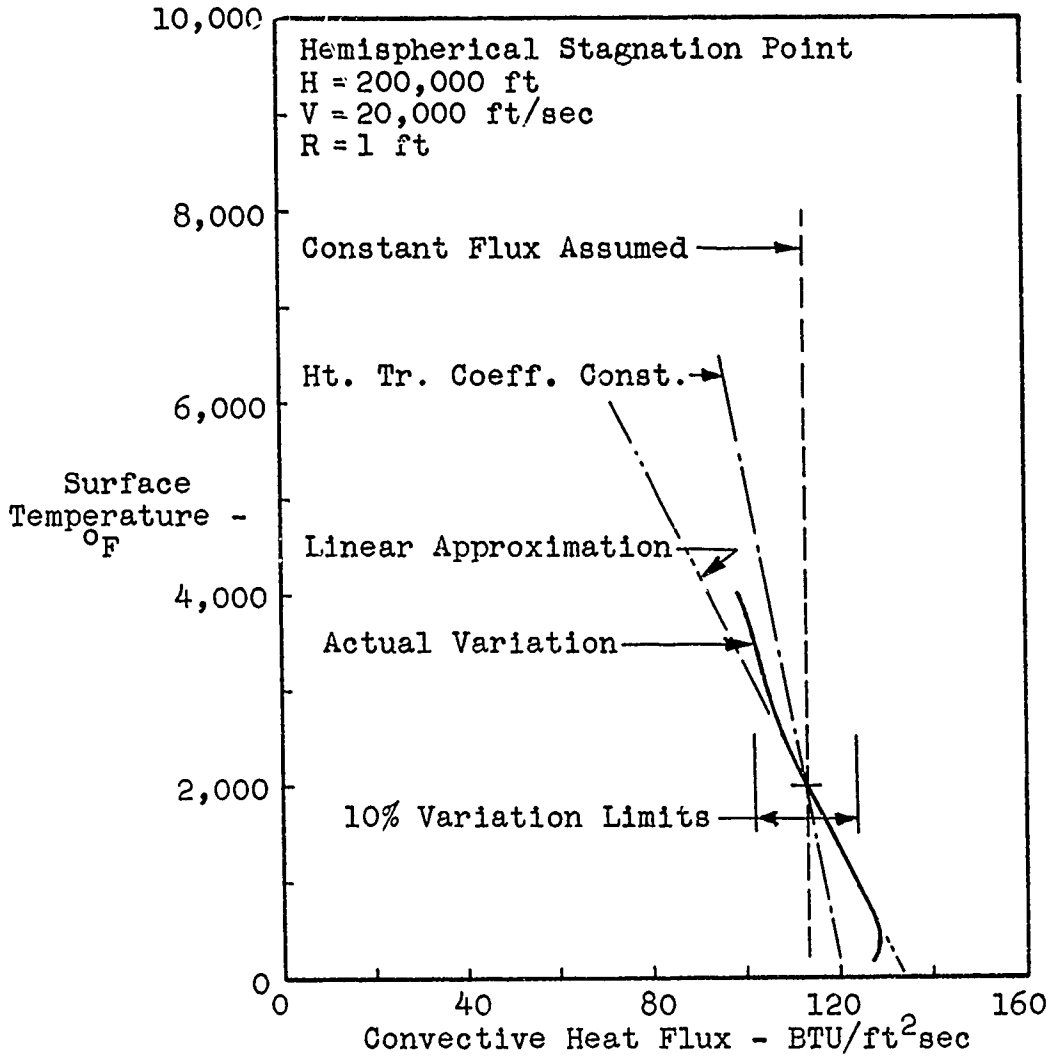


Figure 2

Surface Temperature Effect on Aerodynamic Forced Convection

approximating it with the linearized form:

$$q = h'(T_r' - T_s) \tag{2}$$

Where: $$h' = -\frac{\partial q}{\partial T_s} = h - (T_r - T_s)\frac{\partial h}{\partial T_s} = C_p H - (i_r - i_s)\frac{\partial H}{\partial T_s} \tag{3}$$

$$T_r' = T_{s_o} + \frac{q(T_{s_o})}{h'} \tag{4}$$

This is shown in figure 2, along with the other approximations.

Aerodynamic heat input by thermal radiation from hot gases in the shock layer surrounding the vehicle can become significant when flight velocities approach orbital speed and higher. Figure 3 illustrates the order of magnitude of heating rates from this source for a stagnation region, and can be compared to the convective heat rates of figure 1(a). Heating from this source is generally limited to the stagnation region and strongly windward facing surfaces of the vehicle, where the shock layer temperatures reach the very high values required to produce significant radiant emission. The accuracy of predicted radiation heating is considerably poorer than that associated with convective heating rates. This is due to the considerable uncertainty in the emission and absorption characteristics of high temperature air, and the difficulties in determining actual gas temperatures in the shock layer. An agressive program of both experimental and theorectical research will be required to improve this situation.

While aerodynamic heating is the predominant source of heat input for flight vehicles operating within the atmosphere, there are cases where other sources must be included in realistically evaluating the thermal response of the structure. These generally arise when considerable thermal protection has been provided to isolate interior structure from the effects of aerodynamic heating. The hot gases flowing in a conventional propulsion system are a prime source of heating to adjacent surfaces and structure. Both forced convection and hot gas radiation are again involved, with radiation having greater significance due to the higher emission rates of many combustion products, as compared to air. Fortunately, the engineer usually has access to valid

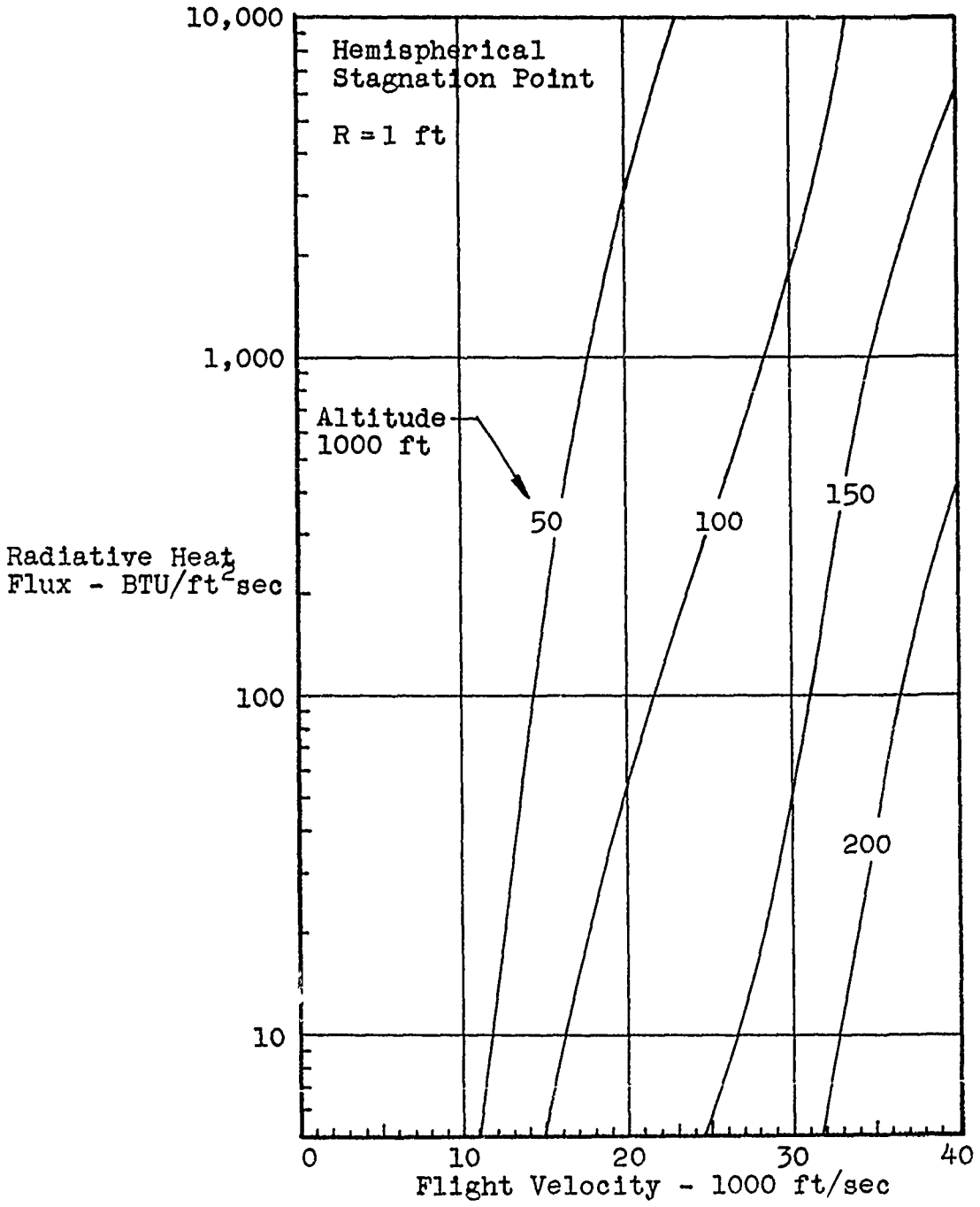


Figure 3

Aerodynamic Heating by Hot Gas Radiation - Stagnation Point

test measurements of propulsion system heating to assist him in estimating design heat inputs from this source. An exception is the case of heating from the expanding exhaust plume, involving an interaction with the exterior aerodynamics in the region of the exhaust nozzles. Vehicle equipment is a potential source of interior heating, but is generally negligible since those items generating a significant heat load usually have cooling systems to control the equipment operating environment. Solar and terrestial radiation is generally insignificant compared to aerodynamic heating and can be neglected for high speed vehicles in the atmosphere. Enemy weapons can provide a source of heat pulses of high magnitude and short duration which must be considered for military vehicles. Each of these potential sources must be evaluated, and if significant, the heating input rates to the structure determined, generally as a function of both spatial location and time.

SECTION II: MODES OF HEAT TRANSFER

Of all the modes of heat transfer, thermal radiation from surfaces, both exterior and interior, is most universally present and significant in the analysis of thermal response for structures of high speed vehicles. When the exterior surfaces reach a moderate to high temperature, this provides an extremely important mechanism of heat rejection from the vehicle. When moderate interior temperatures are reached, it also becomes a significant mechanism of transfer of heat energy from one portion of the vehicle to others at lower temperature.

Most materials are opaque to the transmission through them of radiation of the wavelengths associated with thermal energy, and their surfaces generally approximate grey body behaviour to a degree that makes this a satisfactory assumption for engineering purposes. Under these conditions, the heat flux emitted per unit surface area by radiation is expressed by the Stefan-Boltzmann Law:

$$q = \epsilon \sigma T^4 \qquad (5)$$

where T is the absolute surface temperature, σ is the Stefan-

Boltzmann Constant, and ϵ is the total hemispherical emissivity. This emissivity can vary over the range from zero to unity, depending on the material and surface condition. For most materials considered for high temperature applications, the variations is from approximately 0.5 to near unity. Figure 4 shows how this emitted heat flux varies with surface temperature over the range of interest.

For exterior surfaces, Eq. 5 expresses radiation heat transfer adequately. In interior heat transfer by radiation the combination of emission, absorption, and reflection of radiant energy flux must be considered, and the relative geometry of surface areas becomes an important factor. With the notation of figure 5, the radiative flux arriving at a unit area dA_2 from the area dA_1, for diffuse emission and reflection, can be expressed as:

$$q_{I_2} = \frac{1}{\pi}\left(q_{\epsilon_1} + q_{R_1}\right)\cos\theta_{12}\cos\theta_{21}\frac{dA_1}{r_{12}^2} \qquad (6)$$

where q_{ϵ_1} and q_{R_1} are the emitted and reflected fluxes per unit area from surface dA_1. For gray body surfaces, a fraction ϵ of the incident flux is absorbed, and a fraction $(1-\epsilon)$ is reflected. Generalizing to an enclosure with a large number of surface area elements dA_i, the heat flux per unit area absorbed by the ith element can be expressed in terms of the temperatures and absorbed heat fluxes of the other elements:

$$q_{A_i} = \frac{\epsilon_i}{\pi}\sum_{j\neq i}\left[\epsilon_j\sigma T_j^4 + \left(\frac{1}{\epsilon_j}-1\right)q_{A_j}\right]\cos\theta_{ij}\cos\theta_{ji}\frac{dA_j}{r_{ij}^2} \qquad (7)$$

Unfortunately, this represents a system of simultaneous equations for the absorbed heat fluxes which must be solved in order to find energy transfer rates between elements. In matrix notation, Eq. 7 becomes:

$$[A]\{q_A\} = [B]\{T^4\}\sigma \qquad (8)$$

where $A_{ij} = 1 \;;\; i=j$

$$= -\frac{\epsilon_i}{\pi}\left(\frac{1}{\epsilon_j}-1\right)\cos\theta_{ij}\cos\theta_{ji}\frac{dA_j}{r_{ij}^2} \;;\; i\neq j$$

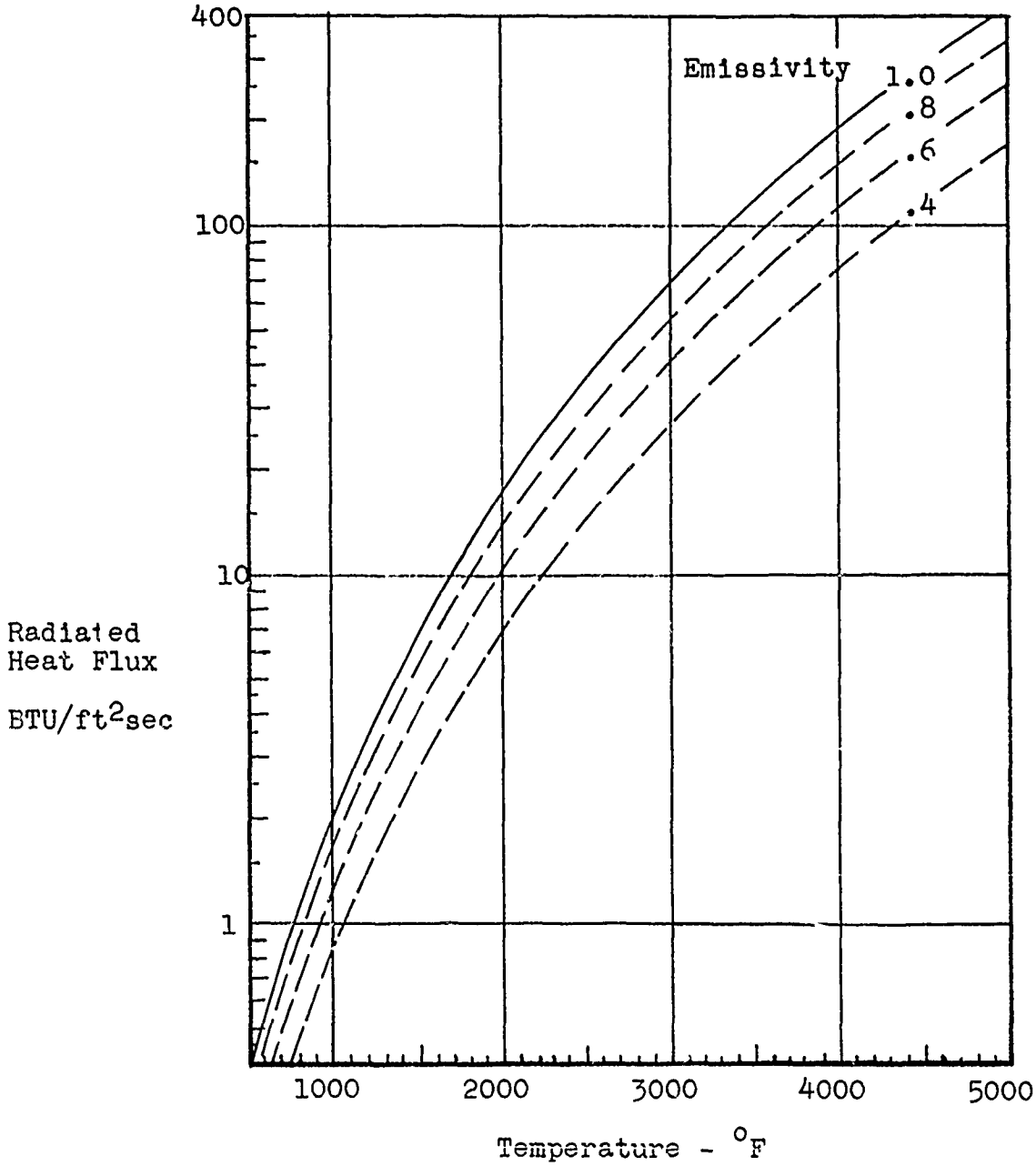


Figure 4

Heat Flux Emitted by Surface Radiation

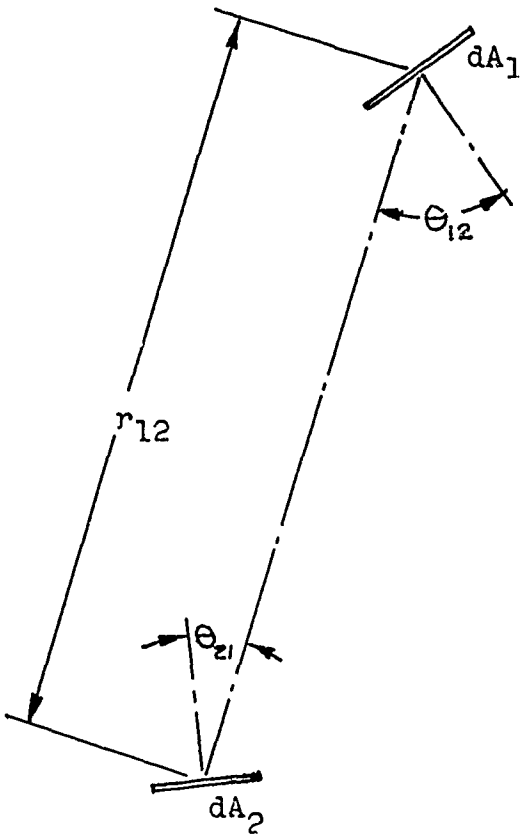


Figure 5

Geometry of Internal Radiation Transfer

$$B_{ij} = 0 \; ; \quad i = j$$

$$= \frac{\epsilon_i \epsilon_j}{\pi} \cos\theta_{ij} \cos\theta_{ji} \frac{dA_j}{r_{ij}^2} \; ; \quad i \neq j$$

The solution can then be represented by:

$$\{q_{/A}\} = [C]\{T^4\}\sigma \; ; \quad [C] = [A]^{-1}[B] \tag{9}$$

The inversion of a large order matrix may be involved, but it is facilitated by the small size of all terms not on the principal diagonal. When this absorbed heat flux is combined with the emitted heat flux, the net heat flux away from the ith element, per unit area, is found to be:

$$q_{/i} = \sum_j C_{ij}\sigma\left(T_i^4 - T_j^4\right) + \left[\epsilon_i - \sum_j C_{ij}\right]\sigma T_i^4 \tag{10}$$

If the space is completely enclosed, consideration of thermal equilibrium under uniform temperature conditions lead to the requirement that:

$$\sum_j C_{ij} = \epsilon_i \tag{11}$$

And the last term of Eq. 10 dissappears. For the special cases of radiant heat transfer between two infinite parallel planes, each at uniform temperature, the results simplify to:

$$q_{/12} = \frac{1}{\left(\frac{1}{\epsilon_1} + \frac{1}{\epsilon_2} - 1\right)}\sigma\left(T_1^4 - T_2^4\right) \tag{12}$$

This is a useful approximation in many practical problems when radiation takes place between surfaces that are closely spaced relative to the distances over which significant temperature changes occur laterally.

Thermal conduction through solid materials and the accompanying relation expressing heat flux as the product of the temperature gradient and a thermal conductivity are perhaps the best recognized of heat transfer modes. There

are a few points of particular interest in the analysis of flight vehicle structures. Thermal conductivity is usually always an experimentally determined quantity, and for many materials is found to vary significantly with temperature. For porous materials, such as many insulations, the measured apparent conductivity includes the effects of radiative transfer and gas conduction across the voids. This data can be used without difficulty in thermal analyses, provided it was determined under experimental conditions that duplicate operating conditions in regard to temperatures and ambient pressures. The inclusion of temperature variation of thermal conductivity in analyses may present severe practical problems due to the increased volume of computations required.

It is conventional to assume that the magnitude of the thermal conductivity is independent of the direction of the temperature gradient vector. While not strictly true for many materials, this assumption of isotropic behaviour is a reasonable approximation for most of them. For some, such as pyrolytic graphite, conductivities can differ by one to two orders of magnitude depending on the direction of the heat flux. This effect must be considered in a valid analysis, and can be readily included without complications if the coordinate system used in analysis coincides with the principal directions for orthotropic behaviour:

$$q_i = k_i(T) \cdot \frac{\partial T}{\partial x_i} \tag{13}$$

If this is not the case, considerable analytical complexity develops.

Internal heat transfer by convection is generally of secondary importance and limited to special cases, such as the use of fluid coolants. There is a considerable body of data available on heat transfer in channel flow, and heat transfer rates for forced convection can be expressed in the usual form:

$$q = h(T_s - T_f) \tag{14}$$

where T_s is the local temperature of the channel surface and T_f is the average temperature of the fluid. Evaluation of

the heat transfer coefficient requires a knowledge of the fluid flow rates, channel geometry, and fluid properties. A simultaneous thermal analysis of the fluid flow system is often required to establish fluid temperatures along the length of the channel.

Boiling heat transfer may be significant at the surfaces of propellant tanks, particularly when cryogenic fuels or oxidizers are involved. Here again, a non-linear dependence of heat transfer rates on temperature is encountered. In the nucleate boiling range:

$$q \sim (T_s - T_f)^n \qquad (15)$$

where T_s is the surface temperature, T_f is the saturation temperature of the fluid, and the exponent n ranges from 1.25 to 1.33. In many practical applications, large heat fluxes can be transferred to the fluid with very small temperature differences, so that the surface temperature can be assumed equal to the fluid saturation temperature.

When temperatures are changing with time, heat storage within the thermal system is as important as heat transfer from one part of the system to another. The time rate of energy storage in a volume element dV is given by:

$$\dot{dQ} = \rho c \dot{T} dV \qquad (16)$$

where ρ is the density and c is the specific heat of the material. The specific heat usually shows some dependence on the temperature, which may require inclusion in the analysis.

SECTION III: METHODS OF PROBLEM FORMULATION

Once the heat input rates have been established and the type of thermal system (structure plus thermal protection plus significant thermal masses of equipment, etc.) is known,

the analyst is faced with the problem of establishing a mathematical model for analysis. This is usually done on the physical basis of conservation of energy fluxes in the elements of the system, considering the significant modes of heat transfer and storage. This should be as simple as possible consistent with providing resultant temperature histories of reasonable accuracy, recognizing the inherent accuracy of the input data.

A significant feature of the thermal analysis of flight vehicles is that the great bulk of the available "classical" solutions for thermal response are of little or no use. The combination of a generally heterogeneous thermal system with multiple modes of heat transfer occurring simultaneously, and a heating input history which cannot be represented analytically, lead to an early consideration of numerical methods. In this respect, the situation is similiar to the relationship between the classical theory of elasticity and the practical analysis of structures.

Early in formulating the model, it must be decided whether the problem can be treated as essentially one dimensional heat flow, or if a more complete two or three dimensional system must be considered. Fortunately there are many cases in which a one dimensional solution provides adequate temperature predictions. The primary requirement is that the magnitude of the lateral heat fluxes, by any mode of significance, be small in comparison with the heat fluxes in the primary direction. As examples, the major portion of a thin wing could be adequately represented by a one dimensional model since lateral temperature gradients are small compared to gradients through the thickness. The leading edge region, however, may have significant lateral conduction and internal radiation which must be included in the analysis for realistic results.

Another problem is the substitution of a finite number of point or average local values of temperature for the more or less continuous temperature distribution occurring in the physical system. This is generally required to formulate the thermal response in terms of a set of first order simultaneous equations in the time derivatives of temperature. The lower limit on the number of elements is established by the requirements of accuracy in representation, while an upper limit is generally set by the computational capability that is available.

There are several approaches to this problem, each with their particular advantages and deficiencies. Perhaps the simplest and most widely used technique has been the direct formulation in terms of a lumped parameter system. Based on consideration of the geometry of the thermal system and the expected nature of the temperature distribution and gradients, the distributed thermal capacity of the system is replaced by "equivalent" lumped thermal masses. Heat flows between the masses, by the various significant mechanisms, are expressed in terms of the average temperatures of the masses, the geometry of the system, and the applicable thermal properties. This is a straightforward formulation which can be readily accomplished by anyone familiar with the basic principles of heat transfer. The primary disadvantage is in the interpretation of the resulting "average" temperatures of the elements, and what point within the lumped area on the original structure is at the average temperature. Errors also arise since convection and radiation depend on surface temperatures rather than average temperatures. These difficulties could be overcome by making each element small enough so that the temperature is essentially constant over it, but this is impractical in many problems.

A somewhat different approach is to take the temperatures at a set of specified points in the system as the dependent variables. The terms in the response equations are then evaluated using finite difference approximations for space derivatives (occurring for conduction) and numerical integration approximations for space integrals (occurring for internal radiation). While somewhat more difficult to formulate, this technique has the advantage of identifying temperatures at specific points in the thermal system. It is still subject to errors in regions of large temperature gradients unless a large number of closely spaced points are used.

A third and completely different approach is the use of variational techniques to formulate the response equations. An excellent exposition of the basic principles and techniques for application are contained in references 2 and 3. These will be easily recognized by those familiar with the formulation of dynamic response problems, involving many of the same concepts. The physical basis can be interpreted as a minimization of the errors of both temperature distribution and heat transfer. This leads to a general set of variational equations having the form:

$$\int_V \left(\rho c T \frac{\partial T}{\partial p_i} + \frac{\vec{q}}{k} \cdot \frac{\partial \vec{q}}{\partial \dot{p}_i}\right) dV + \int_S \frac{q_n}{K} \frac{\partial q_n}{\partial \dot{p}_i} dS = -\int_S T_e \frac{\partial q_n}{\partial \dot{p}_i} dS \qquad (17)$$

Here, p_i are the unknown functions of time which describe the temperature distribution in conjunction with an assumed spatial distribution. K is the thermal conductance, due to convection and/or radiation at surfaces between adjacent portions of the thermal system, or at external surfaces. The temperature and heat flux distributions must be derivable from a vector field function using space and time derivatives:

$$\rho c T = -\vec{\nabla} \cdot \vec{H} \qquad \vec{q} = \dot{\vec{H}} \qquad (18)$$

Application to one dimensional problems is straightforward, since assumed temperature distributions can be space integrated and time differentiated to determine heat flux distributions. Two and three dimensional problems pose greater difficulty, and the inclusion of internal radiation in such problems is not possible within the scope of present theory. The greatest advantage of this approach is that maximum advantage can be taken of any knowledge of the nature of the temperature distribution to reduce the number of functions p_i required to describe adequately the thermal response. Further development of these techniques is felt to be a fruitful area of research.

SECTION IV: METHODS OF SOLUTION

Once the thermal response problem has been reduced to a set of simultaneous first order differential equations with time as the independent variable and temperatures as the dependent variables, and the heat input forcing functions have been determined, the remaining task is to integrate the equations for transient response, or determine steady state solutions for relatively static conditions. This can be a formidable task when a large number of temperatures at different points are coupled by the effects of heat transfer, and computer assistance is a necessity.

The use of the high speed digital computer to carry out numerically the required integrations is quite common and both special purpose and general capability programs have been written to accomplish this. An attractive feature is the ease with which the non-linear terms arising from some modes of heat transfer are handled. There is a problem in choosing the time increment for numerical integration so that adverse error amplification characteristics do not develop, resulting in the requirement for extremely small intervals in some cases. These requirements can be relaxed by the use of more sophisticated numerical integration procedures, but this does not necessarily result in a saving in the time required for a given problem.

Both the differential analyzer and direct simulation types of analog computers have also been used to solve the thermal response equations. These avoid the difficulties of numerical integration at the cost of special equipment for input function generators and the simulation of non-linear heat transfer modes. The size of the problem that can be solved, in terms of the number of temperature responses, is severely limited by the size of the computer installation in most cases. The usual utility of the analog computer in allowing rapid parametric variations for preliminary investigations is of course present, but this can also be accomplished by multiple runs on a digital computer.

Reference 4 reports a study made to assess the relative merits of various methods of solving the thermal response problem to determine compartment heat loads on high speed vehicles, and the results provide a useful guide in handling the structural temperature response problem. It was found that a general purpose digital heat transfer program provided the best accuracy with least dollar cost, followed by differential analyzers, direct simulation analog computers, and hand calculations in order of decreasing merit.

Steady state temperature solutions are useful when the time variation of input heating rates is very slow, but when multiple modes of heat transfer, some of which are non-linear, are present, solving for steady state conditions is more difficult than determining transient response, except in the simplest of systems. The obvious solution is to put a steady state heat input into a transient response program and let it run until temperature changes become negligible, an unsophisticated but practically useful technique.

SECTION V: SOME EXAMPLES

Thin Skin Response: Perhaps the simplest example of considerable practical importance is the thermal response of "thin skin" surface structure thermally isolated from the rest of the vehicle, and not subject to significant lateral conduction effects. The term "thin skin" as used here indicates that the entire thickness of the skin is at an essentiallly uniform temperature. The thermal response is then governed by the differential equation:

$$(\rho c \delta)\dot{T} + \epsilon\sigma T^4 - q(t) = 0 \tag{19}$$

The terms are in order, the heat storage by the skin, the heat rejected by radiation, and the input aerodynamic heat flux rate (both convection and radiation). A specified initial temperature provides the required boundary condition. The coefficient (c) may be a function of temperature due to the variation of specific heat, but will be assumed constant for purposes of illustration.

When the first term is small in comparison with the remaining two, the radiation equilibrium temperature solution is valid:

$$T_E = \left(\frac{q}{\epsilon\sigma}\right)^{1/4} \tag{20}$$

This case arises when either the skin heat capacity is very small, or the rate of heat influx is varying slowly. A graphical representation of this solution is given by figure 4. The temperature error in assuming this solution valid can be expressed to a first approximation in terms of the equilibrium temperature and its time derivative as:

$$|\Theta| = \frac{(\rho c \delta)}{4\epsilon\sigma T_E^3} |\dot{T}_E| \tag{21}$$

Hence, errors are greatest for low equilibrium temperatures and high rates of equilibrium temperature change.

When the error of the equilibrium temperature approximation becomes excessive, the usual recourse is to numerical integration of Eq. 19. If a time interval for integration is chosen small enough so that linear variation of the temperature derivative with time over the interval is a good

approximation, and temperature variation is small enough so that the radiation term can be approximated by the linear form:

$$\epsilon\sigma T^4 = \epsilon\sigma T_o^3(4T-3T_o) \tag{22}$$

then the temperature T' at time t' t t is given in terms of the temperature T at time t and the two heat fluxes by:

$$T' = \frac{\left[1 + \frac{\epsilon\sigma T^3 \Delta t}{(\rho c\delta)}\right]T + \frac{\Delta t}{2(\rho c\delta)}(q_\dagger + q_\dagger')}{\left[1 + 2\frac{\epsilon\sigma T^3 \Delta t}{(\rho c\delta)}\right]} \tag{23}$$

In this case, the calculations can be readily carried out by hand or with the aid of a small digital computer. For the case of zero input heat flux, an analytic solution for radiation cooling is available:

$$T' = \frac{T}{\left[1+3\frac{\epsilon\sigma T^3 \Delta t}{(\rho c\delta)}\right]^{1/3}} \tag{24}$$

Comparison of the two indicates that the time interval should be limited to:

$$\Delta t \leq \frac{(\rho c\delta)}{2\epsilon\sigma T^3} \tag{25}$$

To limit the error involved in the radiation linearization, the time interval should also be limited to:

$$\Delta t \leq \frac{(\rho c\delta)T}{2(q_\dagger + q_\dagger')} \tag{26}$$

These are not absolute limits but are rather intended as a guide that will provide reasonably accurate results.

Typical results are shown in figure 6 for a heat flux history that might be representative of boost conditions. Response for several different values of skin heat capacity is shown. For the lowest value (0.02 BTU/ft^2°F), equilibrium temperatures would be a reasonable approximation for most of the time, while for the highest value (0.5 BTU/ft^2°F), the

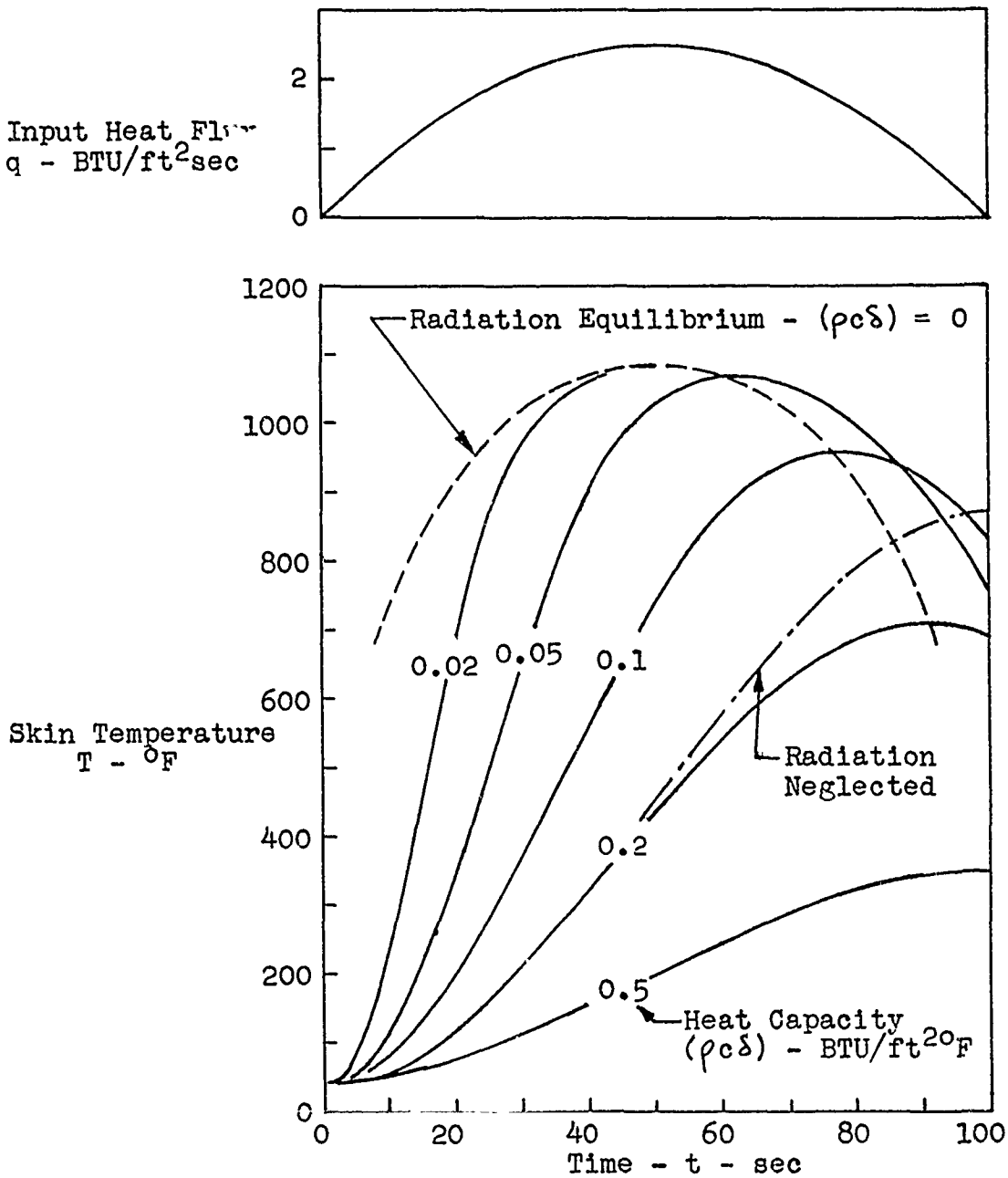


Figure 6

Thermal Response - Isolated Thin Skin

effects of radiation could be neglected.

A final item of interest for this simple response model is the transient response to small changes in heat input superimposed on steady state conditions. These might occur due to sudden maneuvers or dynamic motion of the vehicle. Representing the input heat flux and the resulting temperature by:

$$q = q_o + \Delta q(t) \qquad T = T_{E_o} + \Delta T(t) \tag{27}$$

The governing differential equation can then be linearized to:

$$(\rho c \delta)\Delta\dot{T} + 4\epsilon\sigma T_{E_o}^3 \Delta T - \Delta q = 0 \tag{28}$$

This can be readily solved for given heat flux variations and initial conditions. For a sinusoidal variation in the input heat flux:

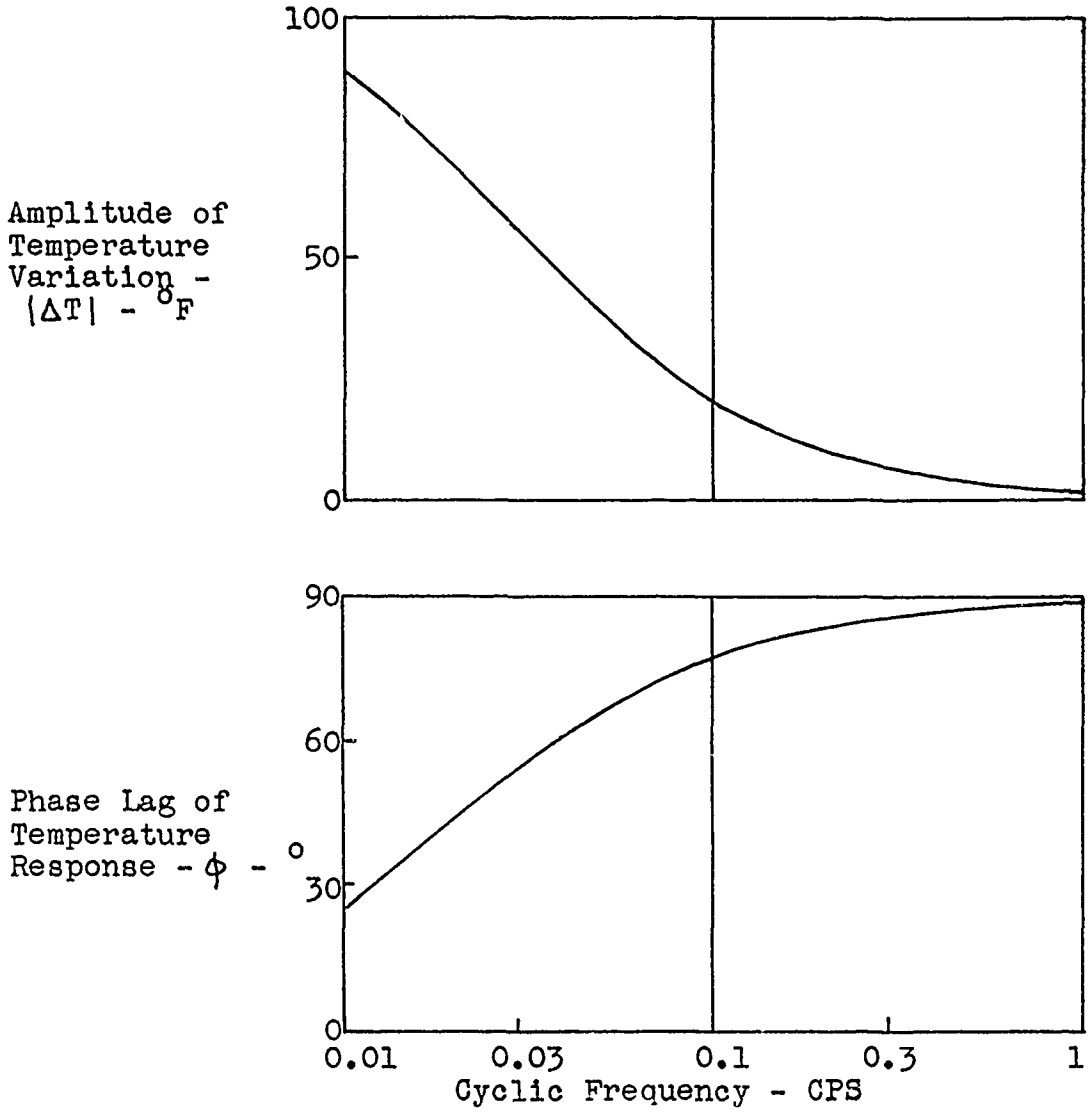
$$\Delta q = \bar{q} \sin\omega t \tag{29}$$

The temperature response is found to be:

$$\Delta T = \frac{\bar{q}}{4\epsilon\sigma T_{E_o}^3}\left[1 + \left(\frac{\rho c \delta \omega}{4\epsilon\sigma T_{E_o}^3}\right)^2\right]^{1/2} \sin(\omega t - \phi)\,; \quad \phi = \tan^{-1}\left(\frac{\rho c \delta \omega}{4\epsilon\sigma T_{E_o}^3}\right) \tag{30}$$

The interesting result here is the small amplitude of the temperature variation under most practical conditions for frequencies likely to be of dynamic interest. Figure 7 shows numerical results for a typical case, and from this it is obvious that the thermal response part of the dynamic aerothermoelastic problem is essentially decoupled. Since the isolated thin skin case has the highest amplitude of transient response of any thermal system, this result can be generalized to most practical flight structures.

The validity of the thin skin approximation can be tested by approximate calculation of the maximum difference in temperature across the thickness of the skin. This can be expressed in terms of the maximum rate of mean temperature



Steady State Conditions:
$T_o = 1500^\circ F$
$q_o = 6.4$ BTU/ft^{2}sec

Properties:
$(\rho c \delta) = 0.13 \frac{BTU}{ft^2 {}^\circ F}$
$\epsilon = 0.9$

Transient: $|\Delta q| = 1.28$ BTU/ft^{2}sec

Figure 7

Thin Skin Transient Response to Sinusoidal Heat Flux

change with time as:

$$\Theta = \frac{\rho c \delta^2}{2k} \dot{T} \tag{31}$$

If this is significantly large, the thin skin approximation is not valid, and the thick skin response must be investigated.

Thick Skin Response: This example retains all of the assumptions of the thin skin response example, except that temperature variation through the thickness is considered. With constant thermal conductivity, the thermal response must satisfy the partial differential equation:

$$\rho c \frac{\partial T}{\partial t} = k \frac{\partial^2 T}{\partial x^2} \tag{32}$$

Subject to the boundary conditions:

$$T(x,0) = T_0(x); \quad -k \frac{\partial T}{\partial x}_{0,t} = q_f(t) - \epsilon \sigma T^4; \quad \frac{\partial T}{\partial x}_{\delta,t} = 0 \tag{34}$$

The presence of the non-linear radiation term in the boundary conditions precludes simple analytic solution. Instead, two methods of approximate solution will be outlined, using only three temperatures in each for the sake of simplicity.

In a lumped parameter formulation, the total thickness is divided into three elements: a central element of width $\delta/2$; and two surface elements of width $\delta/4$. Assuming that the average element temperature is also the temperature at the midpoint of the element, heat conduction between elements can be readily expressed, leading to the following set of equations expressing the thermal balance at each element:

$$\begin{aligned}
&\frac{\rho c \delta}{4} \dot{T}_1 + \epsilon \sigma T_1^4 + \frac{8}{3} \frac{k}{\delta} (T_1 - T_2) - q_f = 0 \\
&\frac{\rho c \delta}{2} \dot{T}_2 - \frac{8}{3} \frac{k}{\delta} (T_1 - 2T_2 + T_3) = 0 \\
&\frac{\rho c \delta}{4} \dot{T}_3 - \frac{8}{3} \frac{k}{\delta} (T_2 - T_3) = 0
\end{aligned} \tag{35}$$

With appropriate initial values of temperatures and a given heat flux history, these equations can be integrated numerically to find the temperature response.

As an alternative, finite differences can be used to express the derivative on the right hand side of Eq. 32. Using the simplest possible difference expressions for points at the two surfaces and at the midpoint, and expressing the surface first derivatives in terms of the boundary conditions, a set of equations identical to Eqs. 35, except that the coefficient 8/3 becomes 2, result. Temperature histories were calculated for a typical example using both formulations and figure 8 shows the resulting temperature distributions at one point in time. The higher temperatures obtained from the lumped parameter formulation are due to the error associated with evaluation the surface radiation at a temperature which actually occurs in from the surface.

Thin Wing Response: As a final example, the thermal response of a thin wing structure with insulation on the highly heated side is considered. This model is shown conceptually in figure 9. One dimensional heatflow is assumed, by conduction through the insulation and by internal radiation between the two structural skins. Thermally thin skins are assumed, so the thermal response equations can be readily written as:

$$
\begin{aligned}
(\rho c\delta)_1 \dot{T}_1 + \epsilon_1 \sigma T_1^4 + \frac{k}{\Delta}(T_1 - T_2) - q_{f1} &= 0 \\
(\rho c\delta)_2 \dot{T}_2 + F_{23}\sigma(T_2^4 - T_3^4) - \frac{k}{\Delta}(T_1 - T_2) &= 0 \qquad (36) \\
(\rho c\delta)_3 \dot{T}_3 + \epsilon_3 \sigma T_3^4 - F_{23}\sigma(T_2^4 - T_3^4) - q_{f3} &= 0
\end{aligned}
$$

The steady state (constant heat flux) equilibrium solution for this and other configurations has been given in reference 5 and can be conveniently expressed in the following terms:

$$
r = \frac{q_3}{q_1} \; ; \; T_{E_0} = \left(\frac{q_1}{\sigma}\right)^{1/4} ; \; \theta_1 = \frac{T_{E1}}{T_{E_0}} \; ; \; \theta_2 = \frac{T_{E2}}{T_{E_0}} \; ; \; \theta_3 = \frac{T_{E3}}{T_{E_0}}
$$

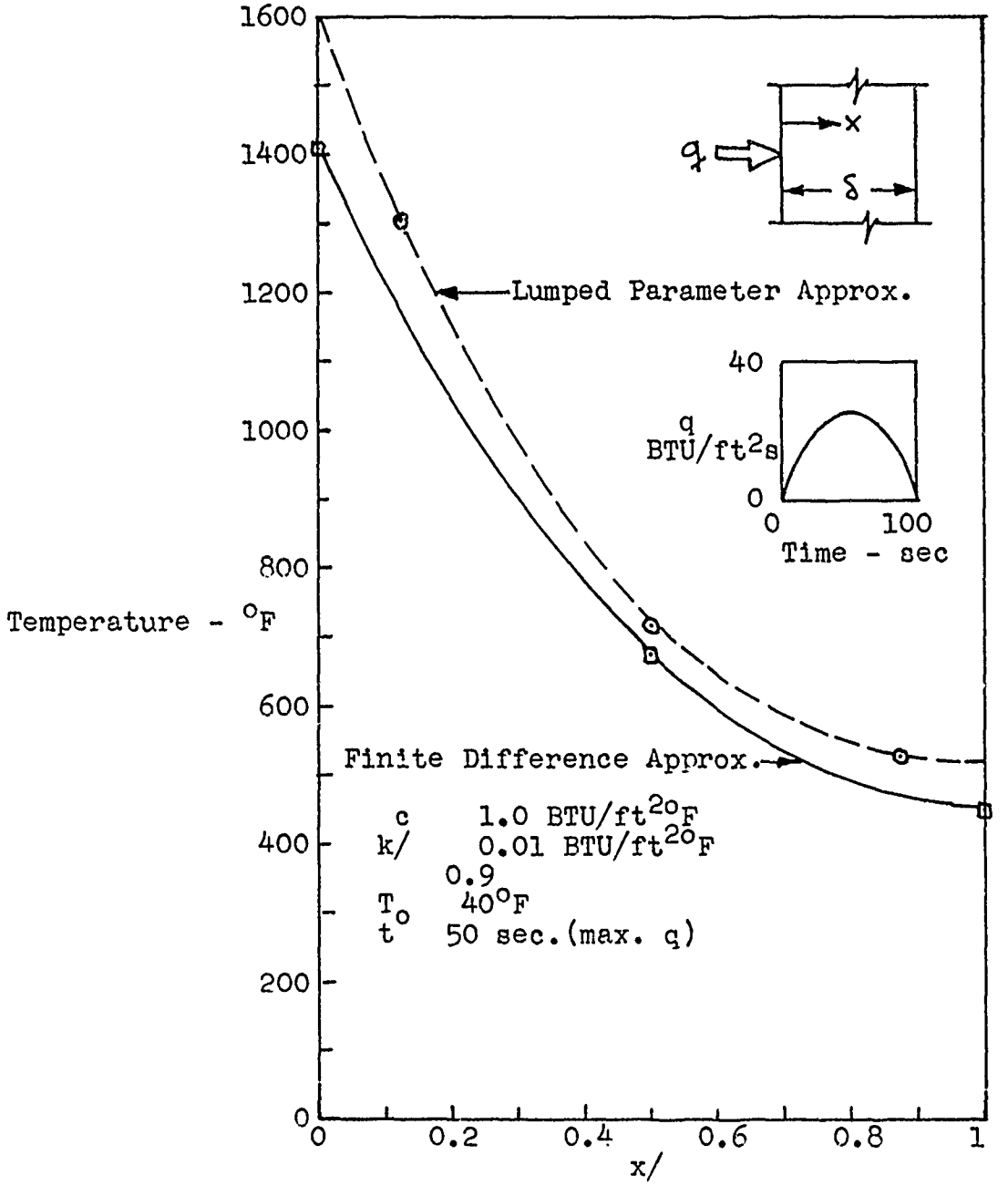


Figure 8

Thick Skin Transient Response

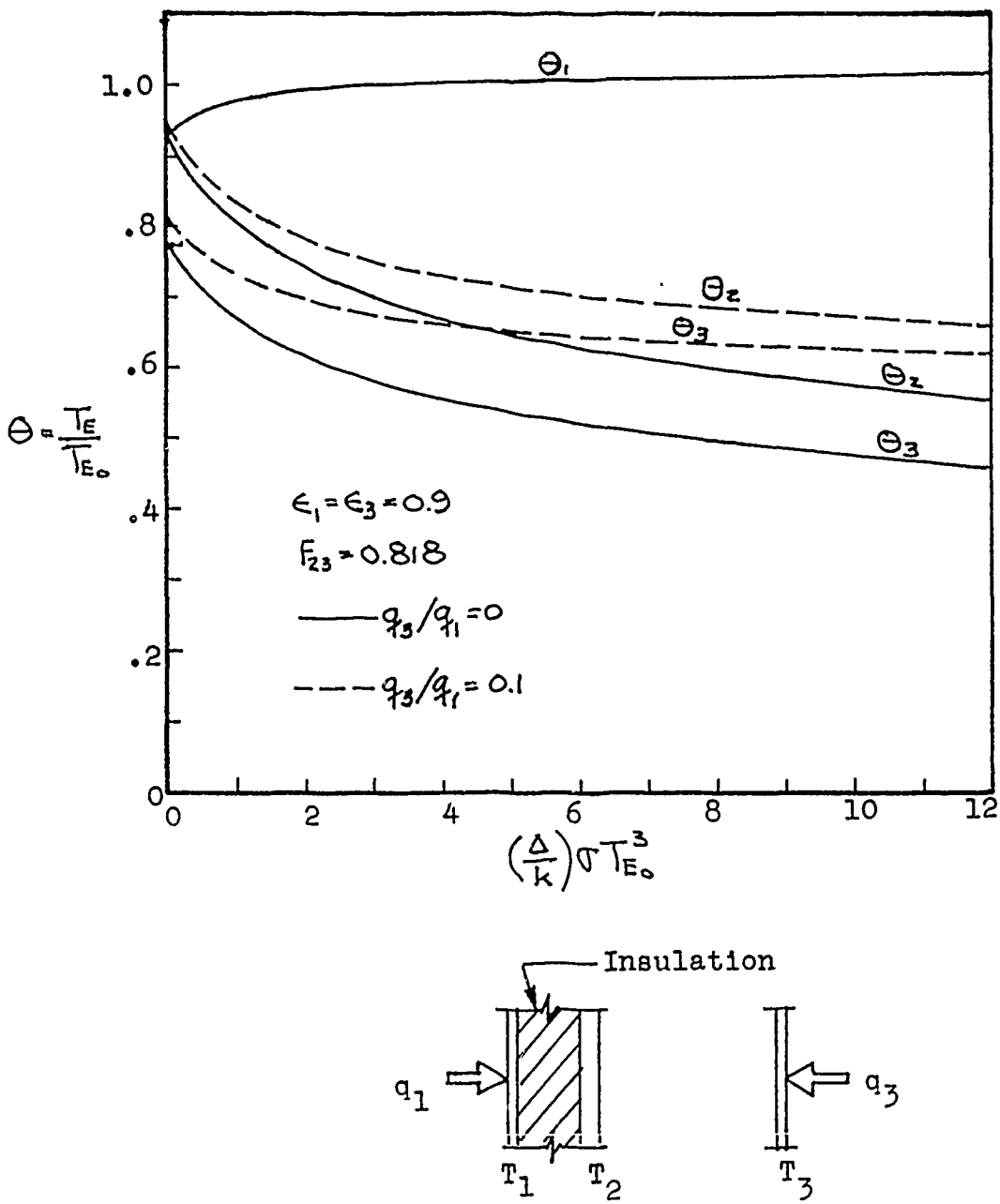


Figure 9

Steady State Response - Insulated Thin Wing

$$\theta_1 = \left\{\frac{1}{\epsilon_1}\left[1 + \frac{F_{23}}{(F_{23}+\epsilon_3)}\left(r - \epsilon_3\theta_2^4\right)\right]\right\}^{1/4} \qquad (37)$$

$$\theta_3 = \left[\frac{r + F_{23}\theta_2^4}{\epsilon_3 + F_{23}}\right]^{1/4} \qquad \frac{\Delta\sigma T_{E_0}^3}{k} = \frac{\theta_1 - \theta_2}{1 - \epsilon_1\theta_1^4}$$

Typical results are shown graphically in figure 9, for selected values of the governing parameters. This provides a convenient means of assessing the effectiveness of passive insulation protection for lifting surfaces subject to heating predominantly from one side.

From the results obtained in the analysis of thin skin response, it would be expected that serious errors could arise from neglect of the heat capacity terms in determining the transient response. However, the transient equations can be readily integrated by numerical techniques. Using the same approach as in the numerical integration of the thin skin equation, the following results are obtained:

$$\begin{aligned}
&\left[1 + 2\frac{\epsilon_1\sigma T_1^3\Delta t}{(\rho c\delta)_1} + \frac{(k/\Delta)\Delta t}{2(\rho c\delta)_1}\right]T_1' - \frac{(k/\Delta)\Delta t}{2(\rho c\delta)_1}T_2' = \left[1 + \frac{\epsilon_1\sigma T_1^3\Delta t}{(\rho c\delta)_1} - \frac{(k/\Delta)\Delta t}{2(\rho c\delta)_1}\right]T_1 \\
&\qquad + \frac{(k/\Delta)\Delta t}{2(\rho c\delta)_1}T_2 + \frac{\Delta t}{2(\rho c\delta)_1}(q_1 + q_1') \\
&-\frac{(k/\Delta)\Delta t}{2(\rho c\delta)_2}T_1' + \left[1 + 2\frac{F_{23}\sigma T_2^3\Delta t}{(\rho c\delta)_2} + \frac{(k/\Delta)\Delta t}{2(\rho c\delta)_2}\right]T_2' - 2\frac{F_{23}\sigma T_3^3\Delta t}{(\rho c\delta)_2}T_3' \\
&\qquad = \frac{(k/\Delta)\Delta t}{2(\rho c\delta)_2}T_1 + \left[1 + \frac{F_{23}\sigma T_2^3\Delta t}{(\rho c\delta)_2} - \frac{(k/\Delta)\Delta t}{2(\rho c\delta)_2}\right]T_2 - \frac{F_{23}\sigma T_3^3\Delta t}{(\rho c\delta)_2}T_3 \\
&-2\frac{F_{23}\sigma T_2^3\Delta t}{(\rho c\delta)_3}T_2' + \left[1 + 2\frac{(F_{23}+\epsilon_3)\sigma T_3^3\Delta t}{(\rho c\delta)_3}\right]T_3' = -\frac{F_{23}\sigma T_2^3\Delta t}{(\rho c\delta)_3}T_2 \\
&\qquad + \left[1 + \frac{(F_{23}+\epsilon_3)\sigma T_3^3\Delta t}{(\rho c\delta)_3}\right]T_3 + \frac{\Delta t}{2(\rho c\delta)_3}(q_3 + q_3')
\end{aligned} \qquad (38)$$

Hence, three simultaneous equations must be solved for each time interval, and the job becomes one suited for a small digital computer.

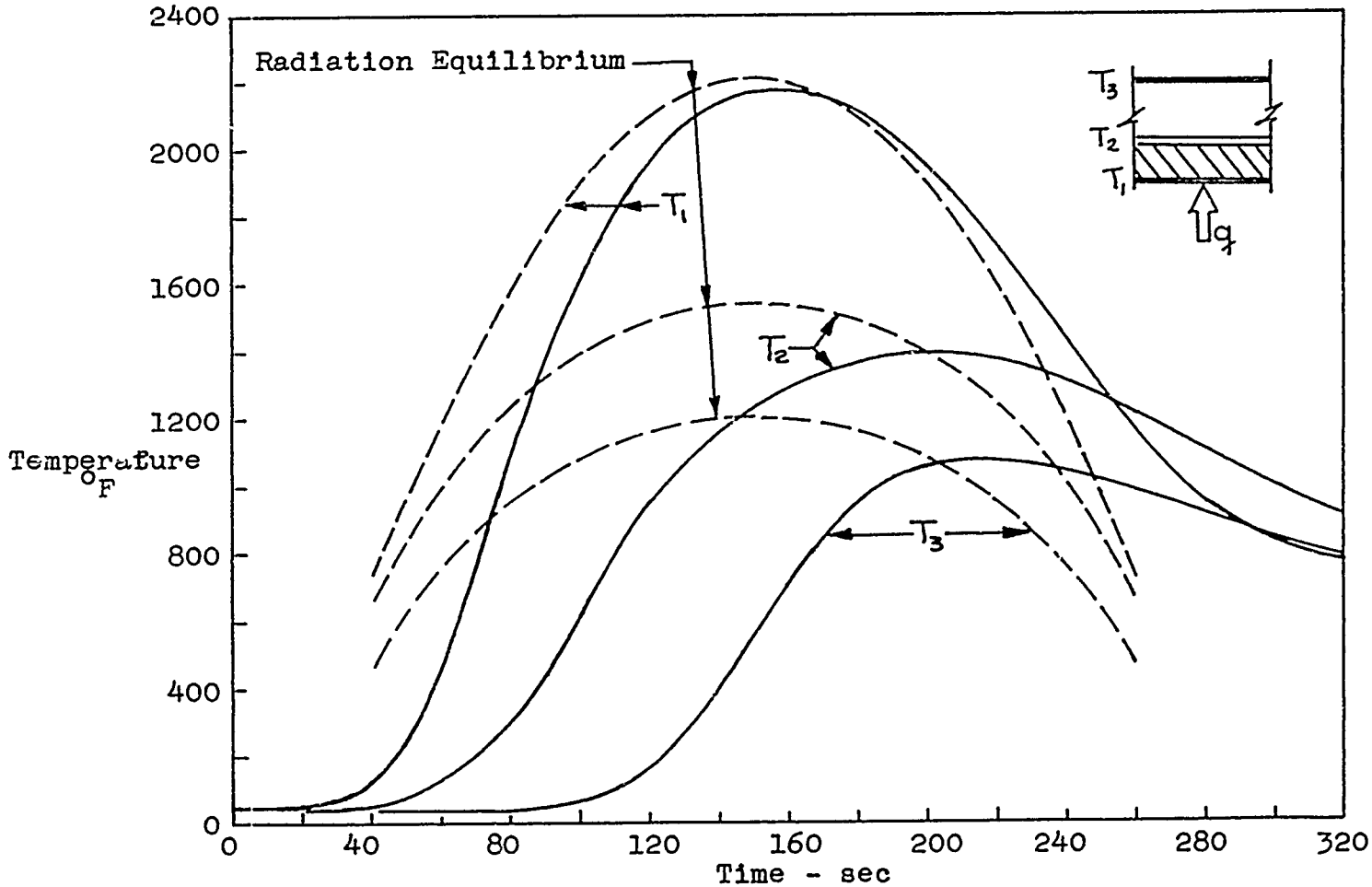


Figure 10

Transient Response - Insulated Thin Wing Structure

Computations were carried out for a typical thin wing structure and a heat flux history typical of a skip entry for a lifting vehicle. The resultant temperature histories are shown in figure 10. These illustrate the drastic departures from steady state equilibrium that can be encountered in practical problems. Of particular interest is the large temperature differences occurring between the two structural skins, since these would give rise either to large thermal stresses or large thermal distortions.

REFERENCES

1. Anon., Aerodynamic Heat Transfer Handbook, Boeing Doc. D2-9154, 1961

2. Biot, M. A., "New Methods in Heat Flow Analysis With Application to Flight Structures", Journal of the Aeronautical Sciences, Vol. 24. December 1957. pp 857-873

3. Biot, M. A., "Further Developments of New Methods in Heat Flow Analysis", Journal of the Aero/Space Sciences, Vol. 26. June 1959. p. 367

4. Malcolm, J. R. & Slack, R. L., Research of Thermal Analysis Methods Specifically Applicable to Compartments of Hypersonic Vehicles and Satellite Re-Entry Vehicles, (to be published as a WADD TR)

5. Anderson, R. A. & Brooks, W. A., "Effectiveness of Radiation as a Structural Cooling Technique for Hypersonic Vehicles", Journal of the Aero/Space Sciences, Vol. 27. January 1960. pp 41-48

WING LEADING EDGE OPTIMIZATION

FOR GLIDE RE-ENTRY VEHICLES

Wilbur L. Hankey
Dyna-Soar System Program Office
Aeronautical Systems Division

Richard E. Russell
Captain, USAF
Institute of Technology

ABSTRACT

A computer program was written to obtain the temperature distribution for a leading edge of arbitrary geometry. The program included the following mechanisms of heat transfer: convective aerodynamic heating, external radiation, conduction, and internal radiation. An investigation was made for a glide re-entry vehicle on the effect of external shape, reflector shape and orientation, and variation of material properties. The analysis demonstrated that a reduction in peak temperature of about 700°F could be obtained. The variation in temperature with angle of attack at critical heating equilibrium glide was also investigated.

WING LEADING EDGE OPTIMIZATION FOR GLIDE RE-ENTRY VEHICLES

INTRODUCTION

The topic under consideration in this paper is the optimization of the wing leading edge geometry of hypersonic glide re-entry vehicles. The object of the investigation was to analyze this problem and attempt to reduce the high temperatures encountered. Figure 1 presents a typical highly swept delta lifting re-entry vehicle similar to the Dyna Soar. The wing is shown, in profile, at an angle of attack, α, with respect to the free stream velocity, V_∞. The plan view depicts the high degree of wing sweep, denoted by the angle Λ. Section A-A is an enlarged view of the area under consideration in this study. This leading edge heating cap is considered to be a nonstructural member attached to the wing for the purpose of shielding the wing structure from the high temperatures of atmospheric re-entry. The heating cap is considered to be thermally insulated from the load carrying structure of the wing.

Past temperature prediction techniques have been conservative in ignoring conduction and internal radiation as modes of heat transfer. All energy entering the wing leading edge, under steady-state conditions, was assumed to be radiated externally to the atmosphere resulting in an "equilibrium temperature." For the investigation conducted, a computer program was developed which included the effects of internal radiation and conduction for an arbitrary two dimensional leading edge.

With this program available the optimization of a leading edge configuration was undertaken (Ref 1). The variables under consideration were exterior and reflector geometry, material thickness, conductivity, and emissivity. In addition, provisions were made to investigate the effect of variable flight conditions and angle of attack.

SECTION I. THEORY

A diagram of the mathematical model used in the analysis is shown in Figure 2. The leading edge was analyzed as a two-dimensional body of infinite length operating under steady-state, laminar flow conditions.

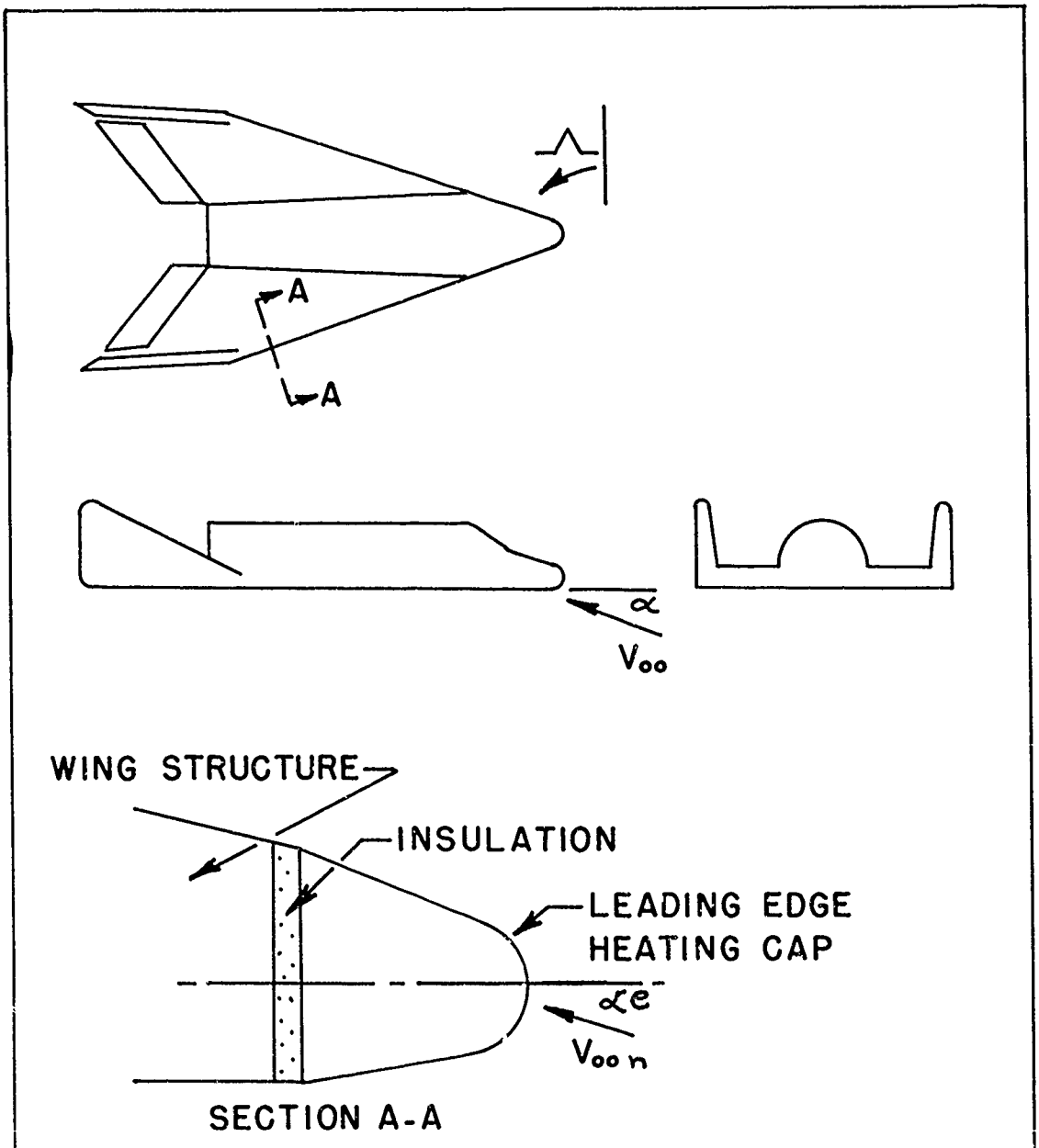


FIGURE 1

ORIENTATION OF THE WING LEADING EDGE

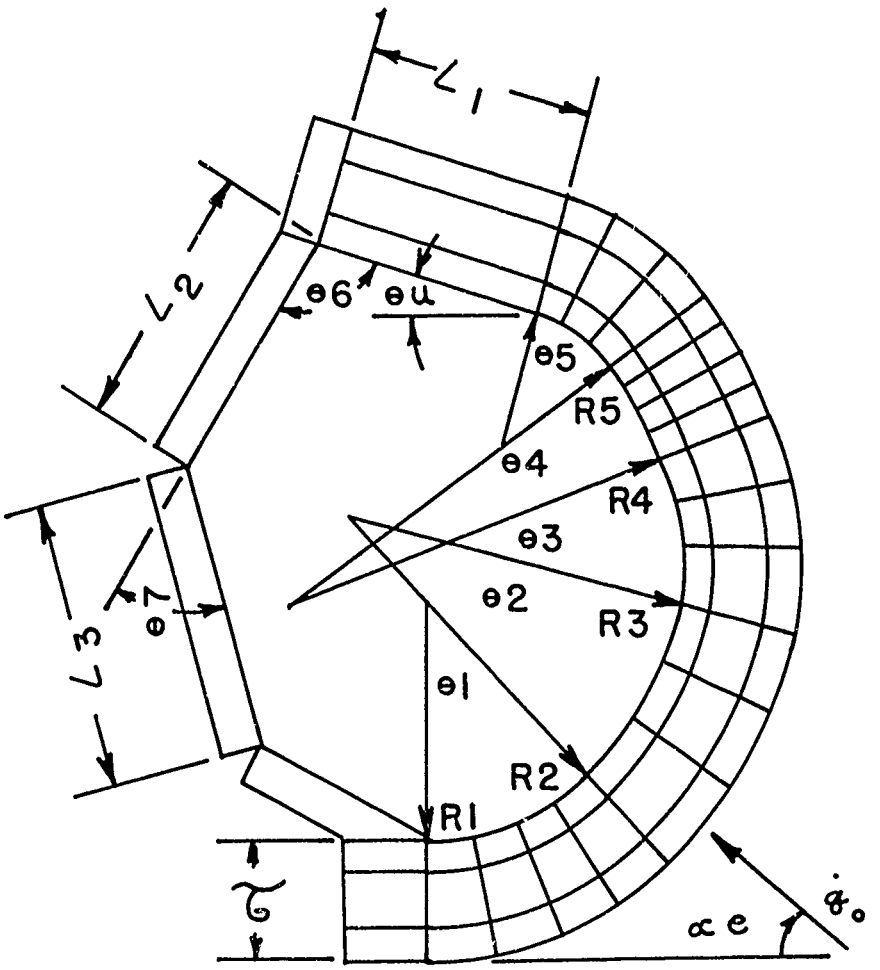


FIGURE 2

LEADING EDGE MATHEMATICAL MODEL

The model was subdivided into 71 elements for purposes of numerical solution. The method of analysis was to write a steady-state energy balance equation for each element, solve the set of 71 equations by trial and error, and iterate until adequate convergence was obtained.

Energy Balance Equation

The energy balance equation for the "i"th element may be expressed as follows (Ref 2):

$$\Delta S_i \left(\dot{q}_i - \epsilon_{ext}\, \sigma\, T_i^4\right) - \sum_{j=1}^{n} Ka_{i,j}\left(\frac{T_i - T_j}{b_{i,j}}\right) - \sum_{k=1}^{N} (A_i \mathcal{F}_{i,k})\sigma(T_i^4 - T_k^4) = 0 \quad (1)$$

where:

ΔS_i = external area of element "i"

$\dot{q}_i$ = external convective heating rate of element "i"

ϵ_{ext} = external emissivity of element "i"

σ = Stefan-Boltzmann radiation constant = 3.3402×10^{-15} $\frac{BTU}{in^2\text{-}^oR^4\text{-sec}}$

K = thermal conductivity

$a_{i,j}$ = conductive area between element "i" and an adjacent element "j"

T_i = unknown temperature of element "i"

$b_{i,j}$ = conductive length, center to center between element "i" and element "j"

$A_i \mathcal{F}_{i,k}$ = gray body view factor between interior elements, "i" and "k"; where n represents the number of elements adjacent to the "i"th element and N represents the number of interior elements engaged in mutual interior radiation when "i" is an interior element.

Stated in words, the energy balance reflects the fact that, under steady state conditions, all energy entering an element minus all energy leaving an element, by any mode, must equal zero. The equation was

written in its most general form, and it should be noted that any one element does not encounter all three modes of heat transfer. The equation will now be examined in detail.

Convective Heating

The first of the three expressions of Eq (1) is for external elements of area ΔS_i and contains the external convective heating rate.

A detailed study of current procedures for estimating the aerodynamic convective heating to a blunt nosed hypersonic vehicle has been conducted by the Hypersonic Flight Section of the Flight Dynamics Laboratory, ASD, Wright-Patterson AFB (Ref 2). From this study it was determined that for the heating rate distribution over the surface of a blunt, two-dimensional body, an equation expressed by Lees (Refs 3 and 4) would be most applicable.

$$\frac{\dot{q}_i}{\dot{q}_o} = \frac{\left(\frac{P_i}{P_o}\right)\left(\frac{V_\delta}{V_\infty}\right)_i}{\left[\frac{2\beta_o}{R_o}\int_o^{s_i}\left(\frac{P}{P_o}\right)\left(\frac{V_\delta}{V_\infty}\right)ds\right]^{\frac{1}{2}}} \qquad (2)$$

where $\frac{P_i}{P_o}$ = ratio of local static to stagnation pressure

$\left(\frac{V_\delta}{V_\infty}\right)_i$ = ratio of the velocity at the edge of the boundary layer to the free stream velocity

$\beta_o = \frac{R_o}{V_\infty}\frac{dV_\delta}{ds}$ non-dimensional stagnation point velocity gradient

s = streamline distance from the stagnation point to the center of the "i"th element

$\dot{q}_o$ = stagnation point heating rate = $\dot{q}_o\,(R_o, \rho_\infty, V_\infty, \Lambda_e)$

R_o = radius at stagnation point

External Radiation

Radiation of external elements to the atmosphere is treated by the standard radiation equation:

$$\dot{q}\Big)_{\substack{\text{radiation to}\\ \text{atmosphere}}} = \epsilon\sigma T_i^4 \qquad (3)$$

The temperature of the receiver has been assumed small compared to the temperature of the body surface and is therefore neglected.

Conduction

The second of the three expressions of Eq (1) represents the heat transfer by conduction between elements. This energy transfer between adjacent elements was accounted for by the Fourier heat-conduction law:

$$\dot{q} = KA \frac{\partial T}{\partial n} \tag{4}$$

In the finite difference form and symbology of Eq (1)

$$\dot{q}_{i,j} = K(a_{i,j}) \frac{(T_i - T_j)}{b_{i,j}} \tag{5}$$

Internal Radiation

The last expression in the energy balance equation represents radiation exchange between the 25 interior elements shown in Figure 2. The mathematical model used for this energy exchange was presented by Hottel (Ref 5). The interior enclosure was assumed to be composed of gray body elements which were diffuse reflecting with emissivity values less than unity. The net exchange of energy between any two interior elements is given by

$$\begin{aligned} \dot{q}_{i \rightleftharpoons k} &= A_i \mathcal{F}_{ik} (T_i^4 - T_k^4) \\ &= A_k \mathcal{F}_{ki} (T_i^4 - T_k^4) \end{aligned} \tag{6}$$

This determination of the gray body view factors, $A_i \mathcal{F}_{ik}$, requires a subroutine before the set of Eq (1) can be solved. This subroutine consists of an energy balance for the 25 interior elements and subsequent solution for the $A_i \mathcal{F}_{ik}$ factors. The method includes the simultaneous solution of 25 equations for each $A_i \mathcal{F}_{ik}$ factor, or, the solution of 625 equations.

SECTION II. COMPUTER PROGRAM

The major criteria under which the program was written were simplicity of input and the ability to solve for the temperature distribution of an arbitrary shape.

Provisions were made for a conductivity of the reflector, K_b, different from the main body conductivity, K. The consideration was for the possibility of a different material in the back plate from that in the main body.

The convective heating rate for the stagnation point was introduced into the problem as the heating rate parameter $\dot{q}_o\sqrt{R_o}$, which was a function of attitude, altitude and flight speed.

The effective angle of attack of the heating cap, α_e, obtained from cross flow theory, was included as a part of the computer input ($\tan\alpha_e = \tan\alpha\sec\Lambda$).

One of the major areas to be investigated in the study was thermal radiation. For this reason, three different possible values of emissivity were included as computer input: external, internal and reflector emissivity values.

Material thickness was introduced as two separate quantities: τ for the main body and τ_b for the back plate reflector. The main body was subdivided, in the τ direction, into three elements, with the outer and inner elements of 0.001τ in thickness while the center elements were 0.998τ thick. The purpose of this material division was to give more accurate skin surface temperature values, both exterior and interior, for radiation exchange of energy.

The above defined variables of the problem list the physical properties of the cap in question as well as the flight environment. A geometrical description of the cap is now required.

The leading edge configuration was approximated by five tangent circular arcs, a straight afterbody, and a 3 segment insulated reflector.

To summarize, the program was capable of calculating steady-state temperatures for any two-dimensional leading edge which could be approximated by five tangent circular arcs, a straight upper afterbody, and a curved insulated reflector. Provisions were available for variation in conductivity, emissivity, thickness, heating rate, and angle of attack.

III. INVESTIGATION

With the problem formulated on the IBM 7090 digital computer, the investigation of shapes was now possible.

The computer program contained the following list of variables: two values of conductivity, three emissivities, two thicknesses, a heating rate parameter, the angle of attack, eight lengths and eight angles. It was proposed to first study the geometric quantities (eight lengths and eight angles) while constraining the other parameters to reasonable design values. Once an optimum geometry was obtained the influence of the material properties and flight conditions would then be studied.

Typical refractory metal property values and critical heating flight conditions (V_∞ = 21 kilofeet/sec, L/D_{max}) were selected for the design point. A value of 45° for the effective angle of attack was taken as one representative for high sweep angles.

To obtain an efficient glide vehicle, the upper surface aft of the leading edge must be unexposed at the attitude for $(L/D)_{max}$. Thus the upper angle (Θ_u) was constrained at α_e.

The design point for the physical variables is shown below:

TABLE I

DESIGN POINT VALUE

$K = K_b = 0.000833$ Btu/sec-in-°R

$\epsilon = 0.8$

$\epsilon_b = 0.10$

$\tau = 0.040$ in.

$\tau_b = 0.015$ in.

$\dot{q}_e\sqrt{R_o} = 0.6944$ Btu/in$^{3/2}$-sec

$\alpha_e = 45°$

$\theta_u = 45°$

Exterior Shape

A simple cylindrical shape with a 45° upper surface was selected for the standard basis of comparison. First a computer solution was obtained neglecting conductivity and internal radiation to ascertain the simple "equilibrium temperature." In addition, a straight back plate reflector was taken which closed from the two points of tangency

of the cylinder and the flat surfaces (Fig 3a). The results of the temperature analysis, in which a maximum temperature of 3411°F was obtained, is shown in Figure 3.

Next, the same configuration was run with all internal emissivity values at zero, while conductivity was maintained at the design point value. It was observed that internal conduction has a relatively small effect on maximum temperature in this thickness range in that only a 19°F reduction in maximum temperature was obtained for this case (Fig 3).

A run was then made to include both internal conduction and internal cross radiation. A reduction in temperature of 182°F was observed due to internal radiation for this simple cylindrical shape. Thus it is apparent that considerable temperature relief is available through internal radiation (Fig 3).

Optimum Exterior Shape

In searching for an improved exterior configuration that would minimize with temperature without increasing frontal area, the constant heating surface was examined. For a given quantity of heat flux entering a surface, the peak equilibrium temperature is minimum for a constant temperature configuration. For this reason Lees equation (Eq 2) was solved for constant convective heating and the resultant shape obtained by numerical integration (Ref 6).

$$\frac{\dot{q}_i}{\dot{q}_o} = f(\phi_i, R_i) = 1 \qquad (7)$$

It was found that a constant heating rate could be maintained up to but not past about 38° (near the sonic point) either side of the stagnation point. Past this point, the heating rate diminishes rapidly and cannot be held constant. Figure 4 shows the derived optimum shape and the geometrical approximation of the optimum shape that was used for the computer solution.

This near optimum was then used, rather than the cylinder, to meet the constraints of the investigation. Figure 5 shows the effect of this constant heating rate on temperature distribution over the nose. The exterior surface skin temperature distribution for the cylinder and optimum shape were plotted for the design point. Note how the optimum shape reduces the higher peak temperature of the cylindrical shape nose into a generally constant temperature distribution on either side of the stagnation point. A sizeable reduction in peak temperature of 184°F was obtained with this configuration. Also, from Figure 5, it may be seen that the variation of temperature on either side of the stagnation point for the optimum is small. Because of the finite

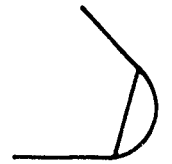
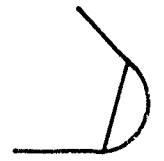
$\epsilon_{EXT} = 0.8$ $K = 0$ $\epsilon_{INT} = 0$	 CYLINDER	$T_{MAX} = 3411°F$
$\epsilon_{EXT} = 0.8$ $K = 0.00833$ $\epsilon_{INT} = 0$	 CYLINDER	$\Delta T_{MAX} = -19°F$
$\epsilon_{EXT} = 0.8$ $K = 0.00833$ $\epsilon_{INT} = 0.8$	 CYLINDER	$\Delta T_{MAX} = -182°F$
$\epsilon_{EXT} = 0.8$ $K = 0.00833$ $\epsilon_{INT} = 0.8$	 OPTIMUM	$\Delta T_{MAX} = -184°F$
		TOTAL $\Delta T_{MAX} = -385°F$

FIGURE 3

EFFECT OF CONDUCTION, EMISSIVITY, AND GEOMETRY ON TEMPERATURE

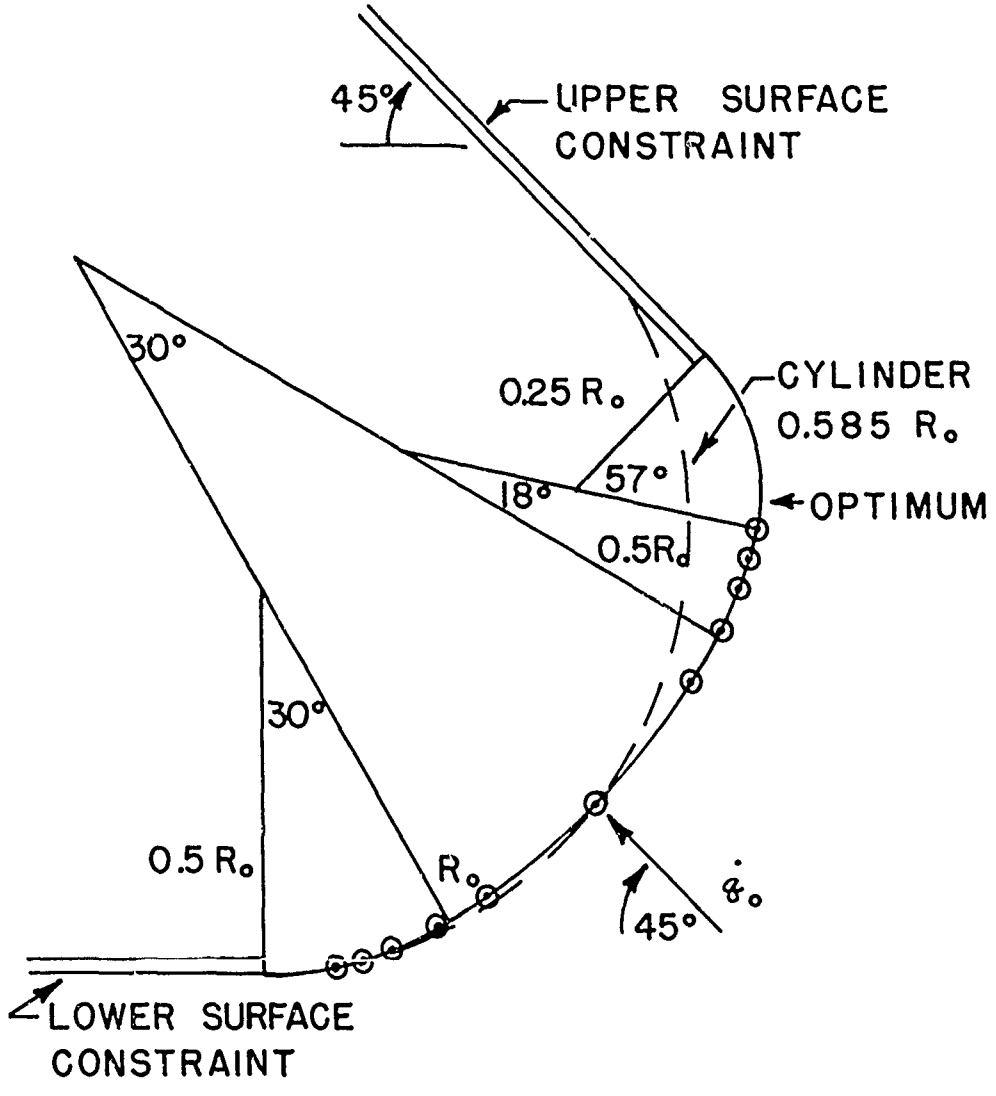


FIGURE 4

CONSTANT HEATING SURFACE GEOMETRY

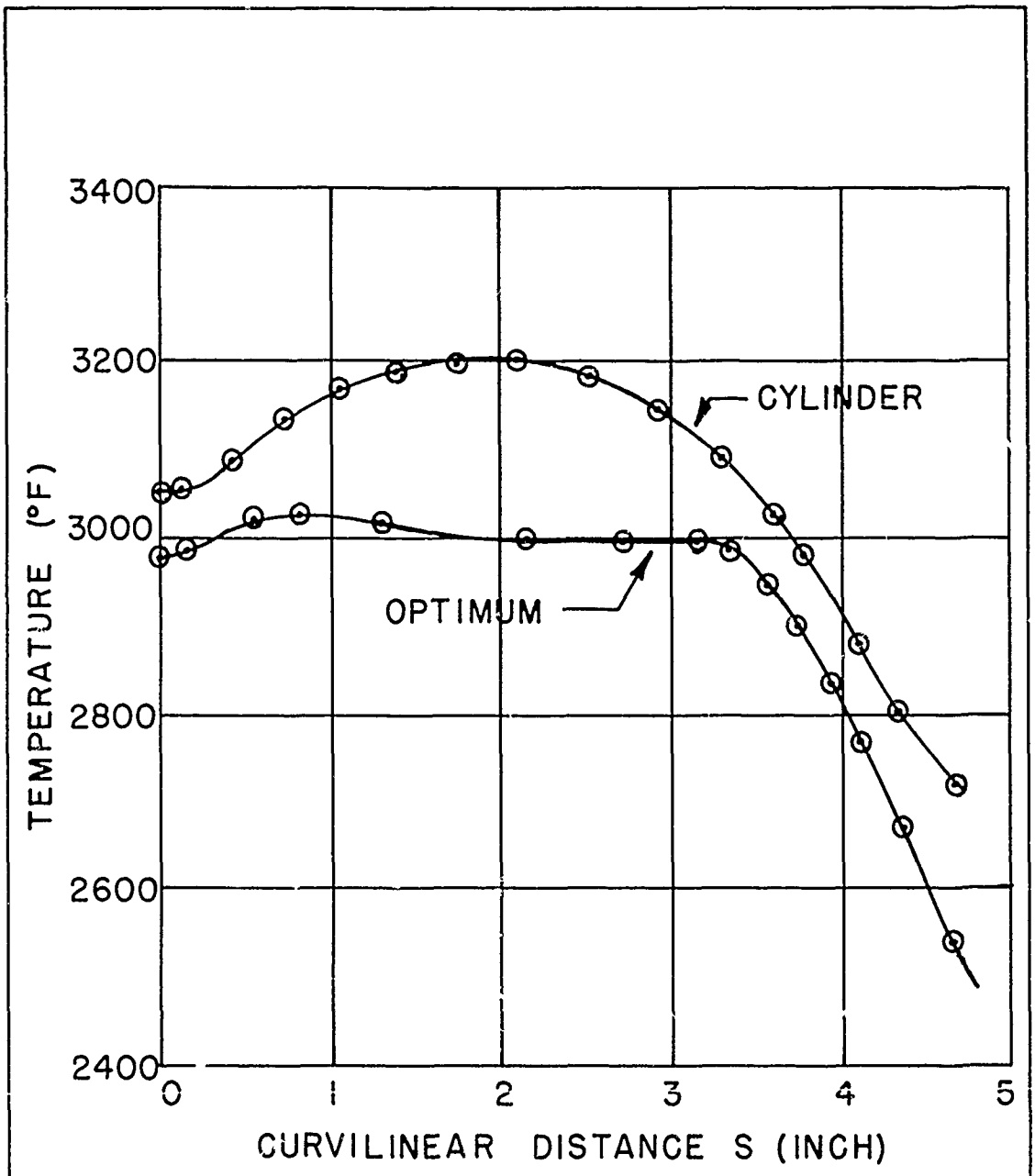


FIGURE 5

COMPARISON OF OPTIMUM AND CYLINDER TEMPERATURE DISTRIBUTIONS

difference method of solution and because the optimum shape must be described by only five radii and five angles in the computer program, this small variation in temperature was accepted as negligible and no attempt was made to further refine the optimum shape to a more constant temperature distribution. Thus, the constant heating shape was considered to be a practical optimum from the results of this investigation. With the exterior shape defined, the investigation was extended to examine the interior configuration.

Back Plate Reflector

Straight Reflector

The question was raised as to what effect rotation of the reflector, about the origin, would have on the peak temperature.

A series of runs for several angles of rotation of the straight reflector was conducted. A plot of the peak temperature against angular rotation of the back plate is shown in Figure 6. The angle of rotation is measured counterclockwise with respect to a vertical reflector position. The change in temperature as a function of angular rotation is seen to be nearly linear. For the design point, 6.1°F per degree of rotation may be taken as a constant within one per cent accuracy. The decrease in temperature was brought about by the addition of radiative area to the upper surface where the convective heat input is negligible. However, a limit exists for the rotation of the reflector due to structural constraints, and therefore a vertical reflector was adopted as practical. For this case, a temperature reduction of 226°F was evidenced as compared with the case in which the reflector was located between the tangency points. One of the best reflector shapes investigated in Reference 1, produced only an 18°F reduction in temperature.

Curved Reflector

With the knowledge thus gained of the effect of rotation of a straight reflector, an investigation of the effects of a curved reflector was made.

Several systematic variations of reflector shape with fixed end points were conducted but little benefit was derived. One of the best reflector shapes which possessed a 15 per cent concavity contributed only an 18°F reduction in temperature (Ref 1). Thus, it appears that little temperature reduction is possible for the added complexity of curving the reflector.

Physical Variables

Adopting the vertical straight reflector as a practical optimum completes the investigation of configuration geometry. The remainder

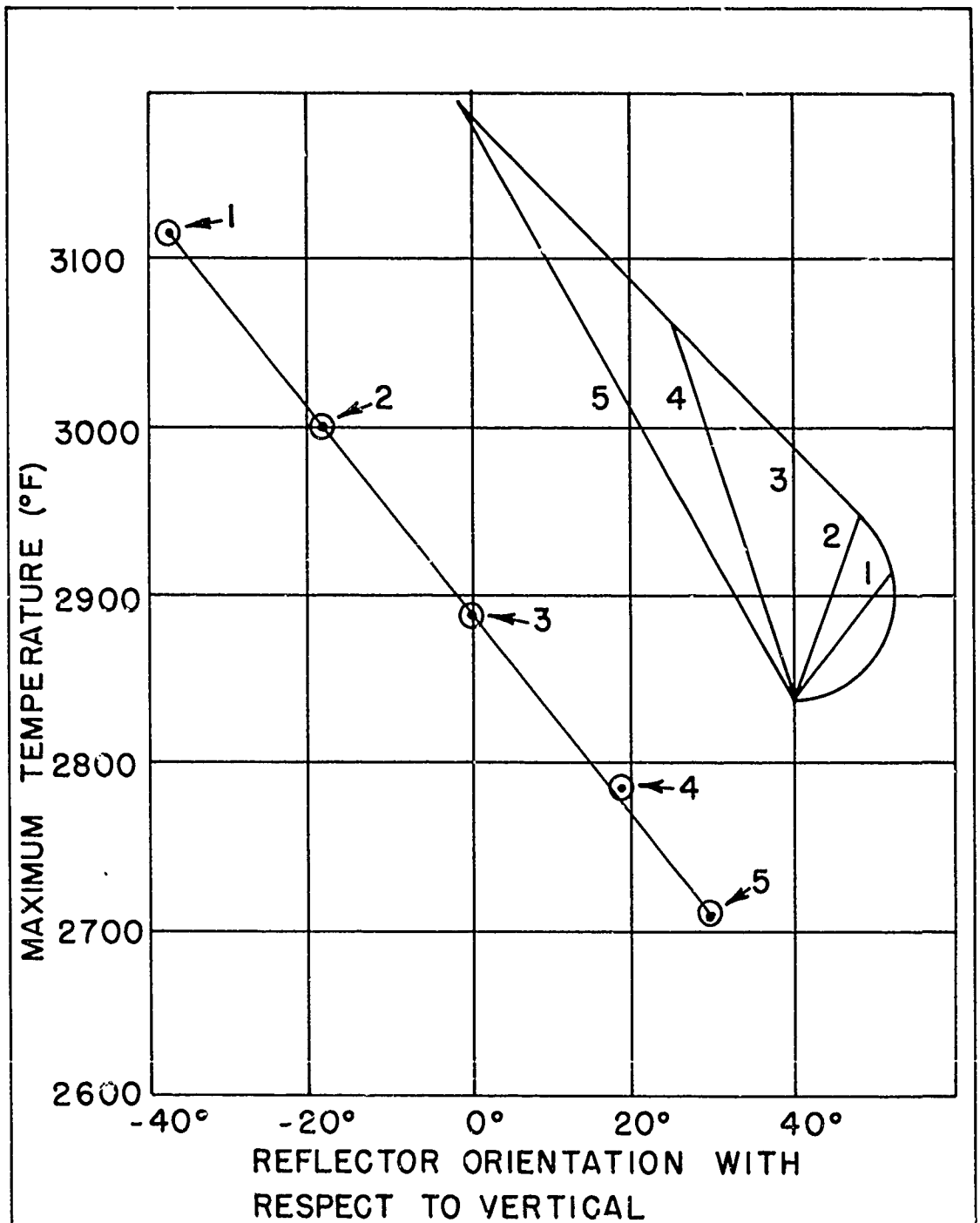


FIGURE 6

TEMPERATURE VARIATION WITH REFLECTOR ROTATION

of the investigation was devoted to analyzing the effect of the physical properties on the peak temperature. An investigation of the physical variables was made on the now optimum exterior shape and optimum reflector orientation. The method used for the investigation was to vary one variable through its practical range about its design point while holding all other variables at fixed values. The following table indicates the insensitivity of conductivity, thickness and reflector emissivity.

TABLE II

Variable Change	Peak Temperature Change
1/10 K	+24°F
10 K	-16°F
1/10 K_b	1°F
10 K_b	- 1°F
10 τ	+3°F
10 τ_b	- 2°F
$\epsilon_b = 1$	0°F
$\epsilon_b = 0$	1°F

Angle of Attack Variation

For a leading edge configuration to be a valid optimum, it must possess sufficient flexibility to operate throughout a wide angle of attack region without exceeding the critical temperature. For this reason a study was undertaken to determine the peak temperature for equilibrium glide at various angles of attack.

For equilibrium flight, the stagnation heating rate obeys the following proportionality (Ref 2):

$$\dot{q}_o \propto \frac{\cos\Lambda_e}{\sqrt{R_o C_L}} = \sqrt{\frac{1-\sin^2\Lambda\cos^2\alpha}{2\,R_o \sin^2\alpha\cos\Lambda}}$$

where Newtonian lift has been assumed and $R_o = R_o(\alpha_e)$. From the above equation it is apparent that higher angles of attack may produce higher stagnation heating rates, since the radius at the stagnation point decreases with angle of attack for the optimum configuration.

For this reason several angles of attack were investigated, the results of which are shown in Figure 7. For over a 25° increase in α_e the peak temperature variation is only $\pm$ 8°F. The variation in "equilibrium temperature" neglecting conduction and internal radiation was 250°F however (Fig 8). Hence the temperature invariance is due to the improved internal "view" counteracting the increased convective heating as the stagnation point rotates about the leading edge. This effect is indeed fortuitous since no attempt was made to incorporate this desirable feature in the leading edge design. It is this feature of successful operation throughout a wide angle of attack region that makes this configuration a true optimum.

SECTION IV. CONCLUSIONS

The conclusions reached below are a result of the investigation conducted in this study on a representative glide re-entry vehicle configuration. The numerical results apply to leading edges operating in the 3000°F range.

1. An analysis for the peak temperature on a leading edge cap neglecting internal radiation and conduction can be conservative by about 200°F when compared to an analysis which does include these mechanisms of heat transfer.

2. About a 200°F reduction in peak temperature may be obtained by tailoring of the external shape to a constant heating rate surface.

3. The orientation of the back plate reflector will have a large influence on the nose temperature (6°F per degree of angular rotation). The temperature reduction demonstrated in this study was a result of the improved radiation "view factor" and the addition of top area for radiative cooling.

4. A curved reflector will, based on the diffuse reflection assumption, have a minor influence on the magnitude of the peak temperature (approximately 20°F).

5. Of the three emissivity material properties involved, external emissivity is the main variable of importance. Internal emissivity is the next most important variable while variation of back plate emissivity has no effect on the peak temperature. High values of internal and external emissivities are desirable.

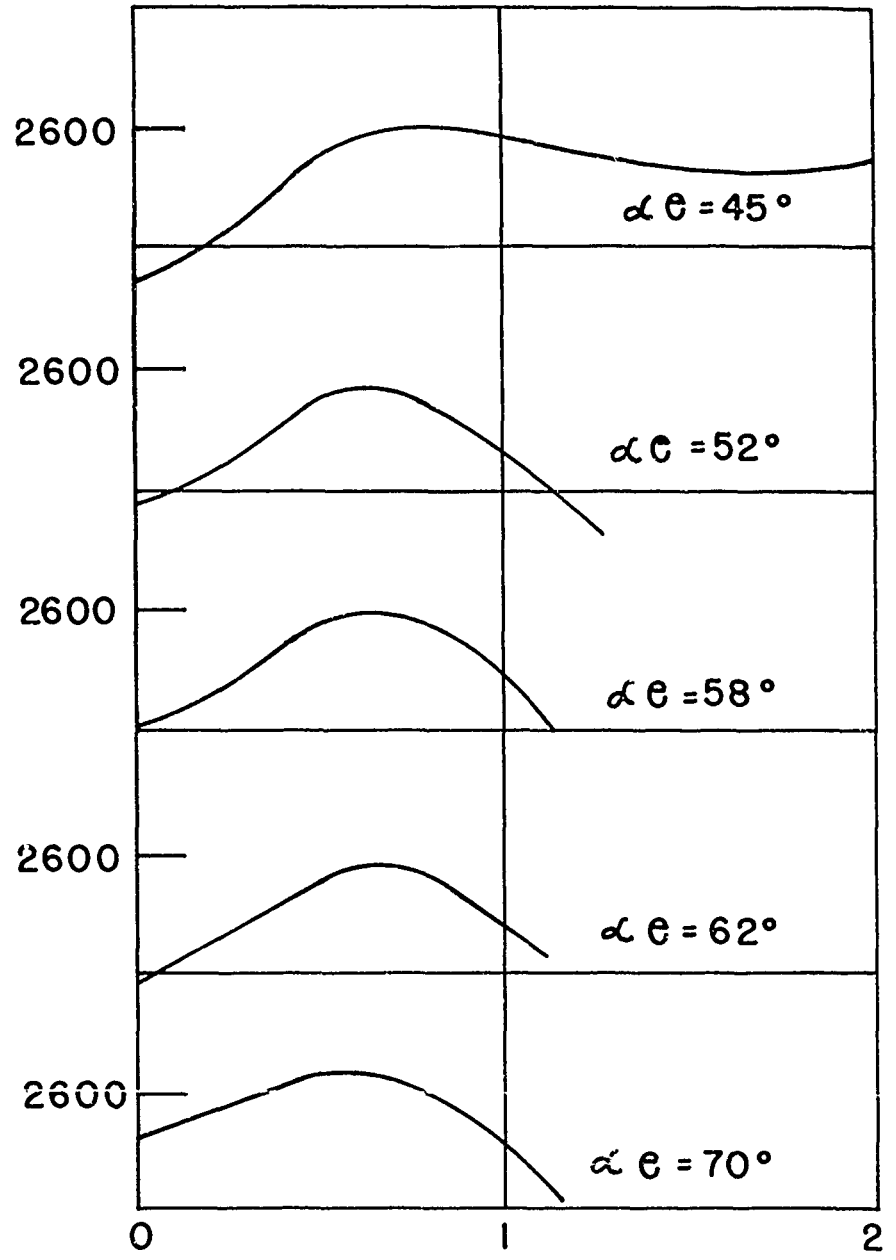


FIGURE 7

TEMPERATURE DISTRIBUTIONS FOR VARIOUS ANGLES OF ATTACK

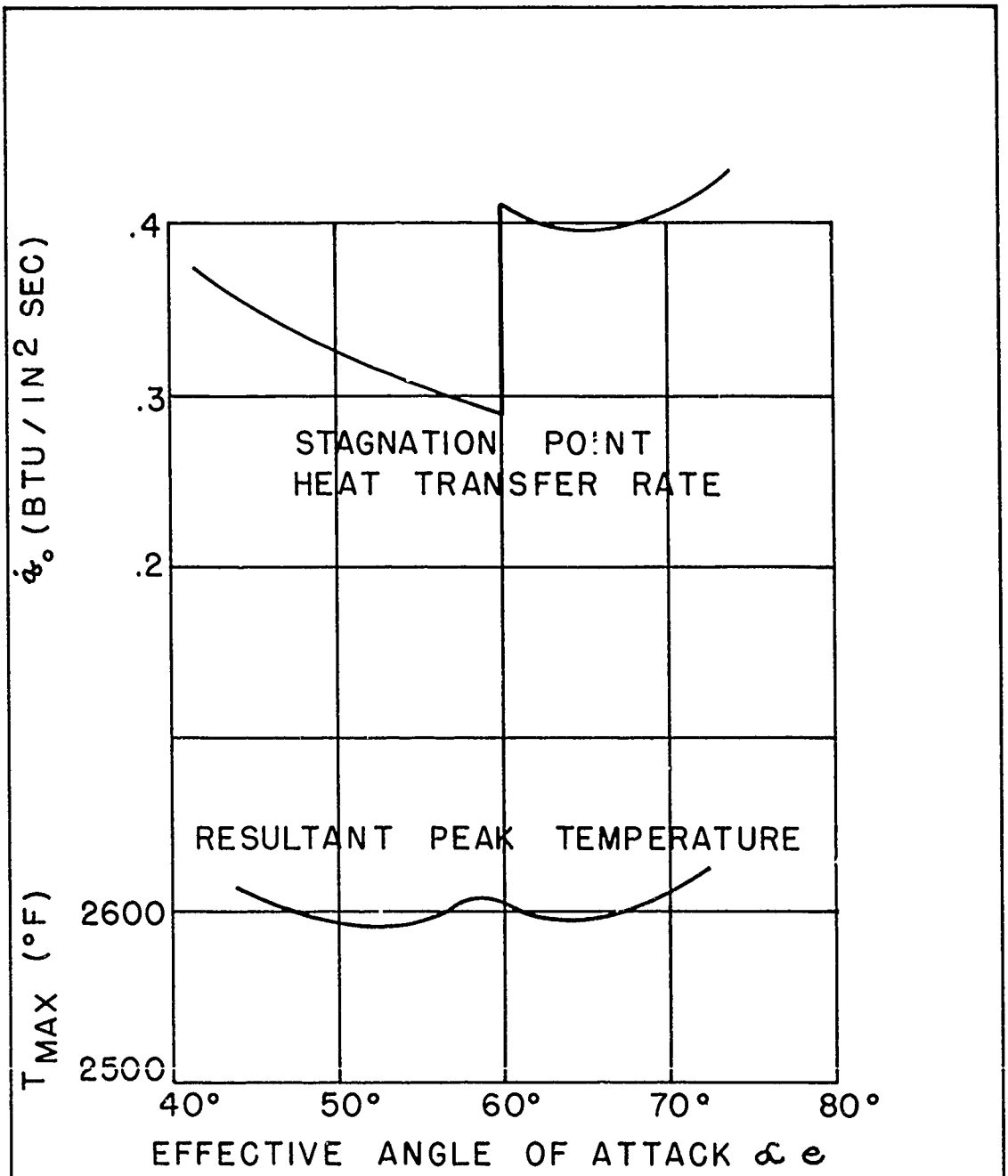


FIGURE 8

PEAK TEMPERATURE VARIATION WITH ANGLE OF ATTACK

6. The effects of conductivity and material thickness are negligible for the thin refractory metal thickness values which are dictated by weight considerations.

7. By including internal radiation and conduction in the analysis, the constant heating leading edge configuration possesses the capability of large angle of attack variation without exceeding a prescribed critical temperature.

SECTION V. References

1. Russell, Richard E., Wing Leading Edge Optimization for Aerodynamic Heating of Glide Re-Entry Vehicles, M.S. Thesis, USAF Institute of Technology, 1961

2. Hankey, W.L.; Neumann, R.D.; Flinn, E.H.; Design Procedures for Computing Aerodynamics Heating at Hypersonic Speeds, WADC Technical Report 59-610, Armed Services Technical Information Agency (ASTIA), Arlington Hall Station, Arlington 12, Virginia, June 1960

3. Lees, Lester, "Laminar Heat Transfer Over Blunt-Nosed Bodies at Hypersonic Flight Speeds," Jet Propulsion, Vol 26, Nr:4 - 259-269 ?74, April 1956

4. Wagner Richard D., et al, Laminar Heat — Transfer and Pressure — Distribution Studies on a Series of Re-Entry Nose Shapes at a Mach Number of 19.4 in Helium, NASA TN D-891, Washington D.C., NASA, June 1961

5. Hottel, Hoyt C., "Radiant-Heat Transmissions" in Heat Transmission (Third Edition), by William H. McAdams, New York; McGraw-Hill Book Company, Inc., 1954, pp. 55-125

6. Hankey, W.L.; Hooks, L.; Knott, P.; Constant Heating Rate Configurations for Hypersonic Vehicles, Flight Dynamic Laboratory Technical Memo 61-15, ASD, 1961

CLOSING REMARKS

by

Colonel A. L. Wallace, Jr.
Deputy for Technology
Aeronautical Systems Division

Good afternoon, ladies and gentlemen. We are surely greatly pleased with the group assembled here and the presentations by all the speakers. I am sure your attendance really justifies the efforts we put into organizing, planning, and getting this symposium underway. We wish to thank the session chairmen and our speakers, all of whom were selected because of their outstanding contributions in one or several of the technical areas.

You who are involved with research and development of the Air Force weapon systems are naturally concerned with the problems of optimization, safety, and reliability. Answers cannot be provided without an accurate definition of the environment for new designs--an environment including heating. Thus an accurate means must be available to account for thermodynamic as well as aerodynamic effects. We must avoid or live with the detrimental effects of severe heating in a structurally efficient manner. For example, we have to design around a situation. We found out awhile back that we were never going to be able to produce 1400-degree hydraulic fluids, so we decided we had better have some kind of a new flight-control system. So we designed around it by developing a hot-gas flight-control system. Now we might be involved in the same kind of solution to the problem here. We must design around it and solve the weapons systems problem.

You have reviewed with us the state-of-the-art and have seen the additional complexities and problems introduced by this kinetic heating. The severe limitations imposed by such heating on vehicle performance due to material and structural physical properties have been described. Clearly, we have a big job to do. There is no question about it, gentlemen, but the Government plays a part in this role in providing a symposium of this sort. I would like to quote from a speech Dr. Brown,

who is the Director of R & D in DOD, made a couple of weeks ago to a Naval research lab:

> "In-house Government research establishments must spearhead efforts to investigate the changing fields of science and engineering to find materials, techniques, and ideas with military significance and present these needs to the technical community in scientific terms."

Gentlemen, we, awhile back here, had a symposium in this same room which for the first time I think got the medical scientists, the physical scientists, and the mathematicians together. This was what we call "Bionics." And so I think we have to play a part here. It is our role and we must give you some feel for our requirements. You have helped us in developing these requirements. You have helped to bring us up to date on the state-of-the-art problems. We hope that you will go away from here today with the feeling that we have accomplished something. If you have, we surely feel that our efforts in getting this symposium together, with your help, have been beneficial.

I would like to recognize some of the people from ASD. If they will just stand--they are supposed to be in the front row. Will you please stand up? These are the people that were involved in getting this symposium together. Thank you very much for a job well done.

We surely appreciate your attendance these last three days and as far as the symposium is concerned, it is now adjourned.